NUCLEAR PHYSICS

JOURNAL DEVOTED TO THE EXPERIMENTAL AND THEORETICAL STUDY OF THE FUNDAMENTAL CONSTITUENTS OF MATTER AND THEIR INTERACTIONS

EDITOR: L. ROSENFELD - COPENHAGEN
ASSOCIATE EDITOR: O. NATHAN - COPENHAGEN

VOLUME XVII

NORTH-HOLLAND PUBLISHING COMPANY - AMSTERDAM

NUCLEAR PHYSICS

EDTIORIAL BOARD

AUSTRALIA & NEW ZEALAND:	H. Messel (Sydney), M. L. Oliphant (Canberra)
AUSTRIA:	B. Karlik, (Vienna), H. Thirring (Vienna)
BELGIUM:	M. de Hemptinne (Louvain), J. Verhaeghe (Ghent)
CANADA:	G. Volkoff (Vancouver)
DENMARK:	C. Møller (Copenhagen), S. Rozental (Copenhagen), G. E. Brown (Copenhagen)
FINLAND:	L. Simons (Helsinki)
FRANCE:	A. Berthelot (Saclay), S. Gorodetzky (Strasbourg)
GERMANY (DEM. REP.):	G. Hertz (Leipzig)
GERMANY (FED. REP.):	W. Gentner (Freiburg i. B.), J. H. D. Jensen (Heidelberg)
GREAT BRITAIN:	S. Devons (Manchester), T. H. R. Skyrme (Harwell)
HUNGARY:	L. Janossy (Budapest)
INDIA:	H. Bhabha (Bombay), R. Ramanna (Trombay)
IRISH REPUBLIC:	J. McConnell (Maynooth)
ISRAEL:	G. Racah (Jerusalem)
ITALY:	E. Amaldi (Rome)
JAPAN:	S. Kikuchi (Tokyo), S. Tomonaga (Tokyo)
MEXICO:	M. Moshinsky (Mexico)
NETHERLANDS:	H. Brinkman (Groningen), S. R. de Groot (Leiden)
NORWAY:	E. Hylleraas (Oslo), A. Lundby (Oslo), H. Wergeland (Trondheim)
POLAND:	L. Infeld (Warsaw)
PORTUGAL:	J. M. Araújo (Porto), J. R. de Almeida Santos (Coimbra)
SOUTH AMERICA:	G. Beck (Saõ Paulo), J. Leite Lopes (Rio de Janeiro)
SPAIN:	J. M. Otero (Madrid), C. Sanchez del Rio (Madrid)
SWEDEN:	O. Klein (Stockholm), K. Siegbahn (Uppsala), I. Waller (Uppsala)
SWITZERLAND:	P. Huber (Basel), P. Scherrer (Zürich)
U.A.R. & ARAB COUNTRIES:	F. El Bedewi (Alexandria), M. G. Nooh (Cairo)
U.S.A.	H. H. Barschall (Madison, Wisconsin), V. Weisskopf (Cambridge, Mass.)
U.S.S.R.:	M. A. Markov (Moscow), I. S. Shapiro (Moscow), D .V. Skobeltzyn (Moscow)
YUGOSLAVIA:	I. Supek (Zagreb)

NUCLEAR PHYSICS

JOURNAL DEVOTED TO THE EXPERIMENTAL AND THEORETICAL STUDY OF THE FUNDAMENTAL CONSTITUENTS OF MATTER AND THEIR INTERACTIONS

EDITOR: L. ROSENFELD - COPENHAGEN

VOLUME XVII

JUNE 1960—JULY 1960

NORTH-HOLLAND PUBLISHING COMPANY-AMSTERDAM

PRINTED IN THE NETHERLANDS

1.D.2:
1.E.4

Nuclear Physics **17** (1960) 1—8; © *North-Holland Publishing Co., Amsterdam*
Not to be reproduced by photoprint or microfilm without written permission from the publisher

LIFETIME MEASUREMENTS ON THE FIRST EXCITED STATES OF Mg^{25} AND Al^{25}

A. T. G. FERGUSON, M. A. GRACE † and J. O. NEWTON ††
Atomic Energy Research Establishment, Harwell, Berks.

Received 28 January 1960

Abstract: The lifetimes of the first excited states of the nuclei Mg^{25} and Al^{25} have been measured using both γ—γ coincidences and pulsed beam methods. The values obtained are

$$\tau_{\frac{1}{2}}(Mg^{25}) = 3.5 \pm 0.2 \times 10^{-9}$$
$$\tau_{\frac{1}{2}}(Al^{25}) = 1.8 \pm 0.3 \times 10^{-9}.$$

The difference between the reduced transition probabilities for these two which amounts to a factor of 10 is attributed to the fact that one is an odd proton and the other an odd neutron transition.

1. Introduction

The nuclei Mg^{25} and Al^{25} have been the subjects of exhaustive investigations by the Chalk River Group, Litherland *et al.* [1]), Gove *et al.* [2]), and many features of their level scheme are well understood. Litherland *et al.* [3]), have also shown that the spins and level energies togheter with relative transition probabilities can be understood in terms of the Nilsson model [4]), using a single value for the deformation parameter. Since such a model makes definite predictions as to the absolute radiative transition probabilities it seemed worthwhile to see whether any of these was likely to be measurable by direct methods. This survey suggested that the E2 transition from the first excited state to the ground state, which is a transition between the $K = \frac{1}{2}$ and $K = \frac{5}{2}$ bands, would lie in the 10^{-9} s range and could therefore be measured by conventional techniques, using nuclear reactions to excite these states. In the present experiments these states have been excited by bombardment with a pulsed beam of protons and their half life determined by methods closely related to the delayed coincidence technique.

2. Experimental Details

A pulsed beam of protons was supplied by the Harwell 5 MeV electrostatic generator. The physical arrangement is shown in fig. 1. The large distance from the resolving magnet to the target and the heavy shielding wall, result in a very

† Clarendon Laboratory, Oxford.
†† Now at the Physical Laboratories, The University, Manchester.

low background near the detector. The beam pulses of duration about 2×10^{-9} s are produced by sweeping the beam across the slit S by applying a 5 MHz R.F. voltage to the deflecting plates P. The distribution of time intervals between the arrival of the proton pulseand emission of γ-rays was measured using a time-to-amplitude converter, (Wells and Barlow [5])), the time interval distribution being displayed on a 100-channel pulse height analyser. A NaI crystal (3.81 cm $\times$ 2.54 cm) was used as detector and an auxiliary slow amplifier and single channel analyser were used to select only the photopeak that was of interest. The selection was performed by gating the 100-channel analyser.

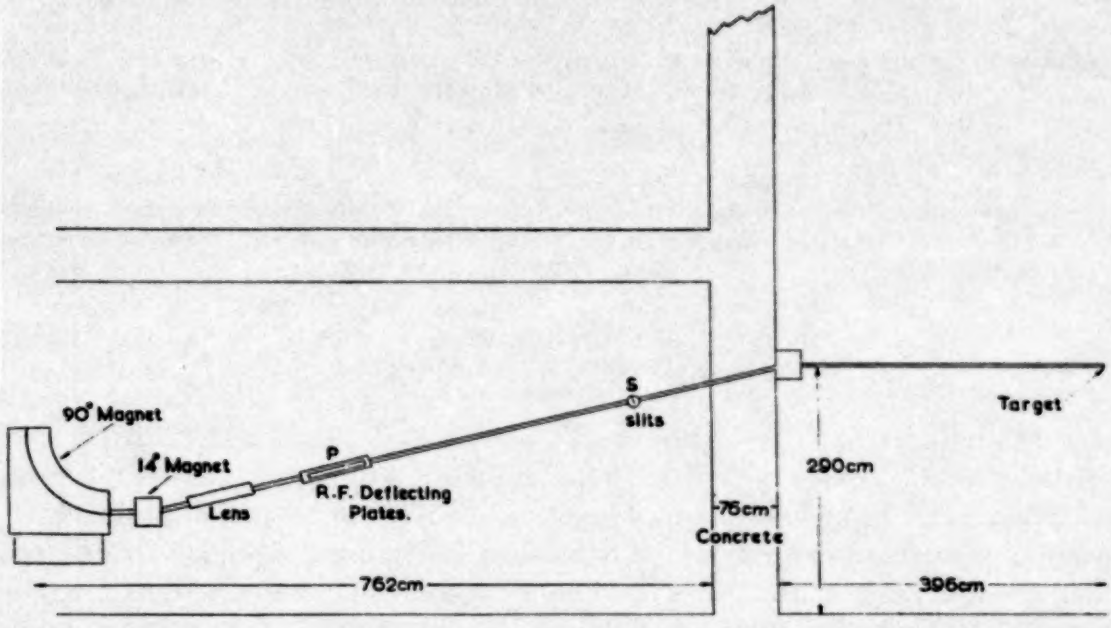

Fig. 1. The layout of the pulsed beam apparatus on the Harwell 5 MeV electro-static generator.

3. The 580 keV State in Mg^{25}

The 580 keV state in Mg^{25} was excited in the reaction $Mg^{25}(p, p')$ at the 1.96 MeV resonance. At this resonance Gove *et al.* [2]) had shown that inelastic scattering proceeded almost entirely through the first excited state at 580 keV (see fig. 2). The target consisted of 95 $\mu g/cm^2$ of magnesium metal isotopically enriched to greater than 90 % in Mg^{25}, evaporated on to a tantalum backing. The γ-ray energy spectrum observed with the NaI crystal showed a single photopeak at an energy of 580 keV with a negligible background. Selecting only pulses in the 580 keV photopeak the distribution of time intervals between the proton pulse and the γ-rays was observed; this is shown in fig. 3. To show that the shape of the curve is not purely instrumental a "prompt" distribution was obtained by replacing the target with Na^{23} and observing the 440 keV γ-rays from the reaction $Na^{23}(p, p')$ at a proton bombarding energy of about

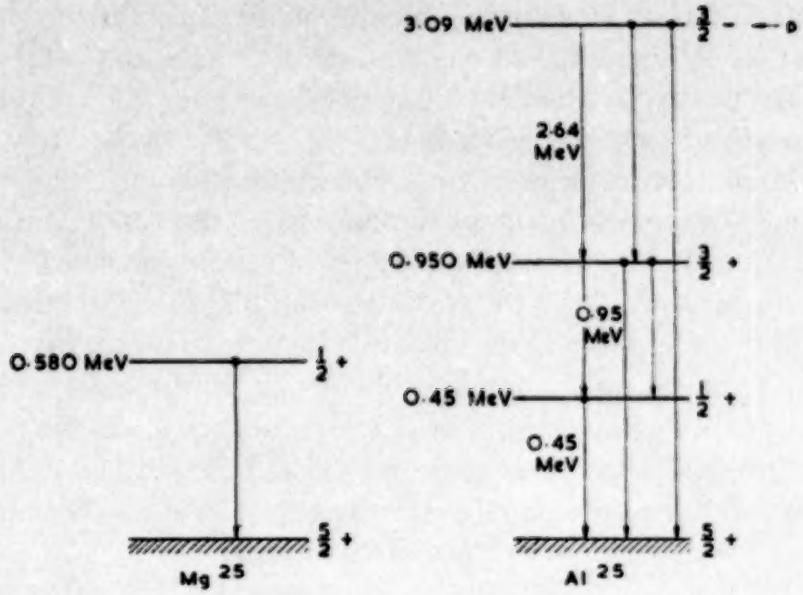

Fig. 2. Simplified level structures of Mg^{25} and Al^{25}.

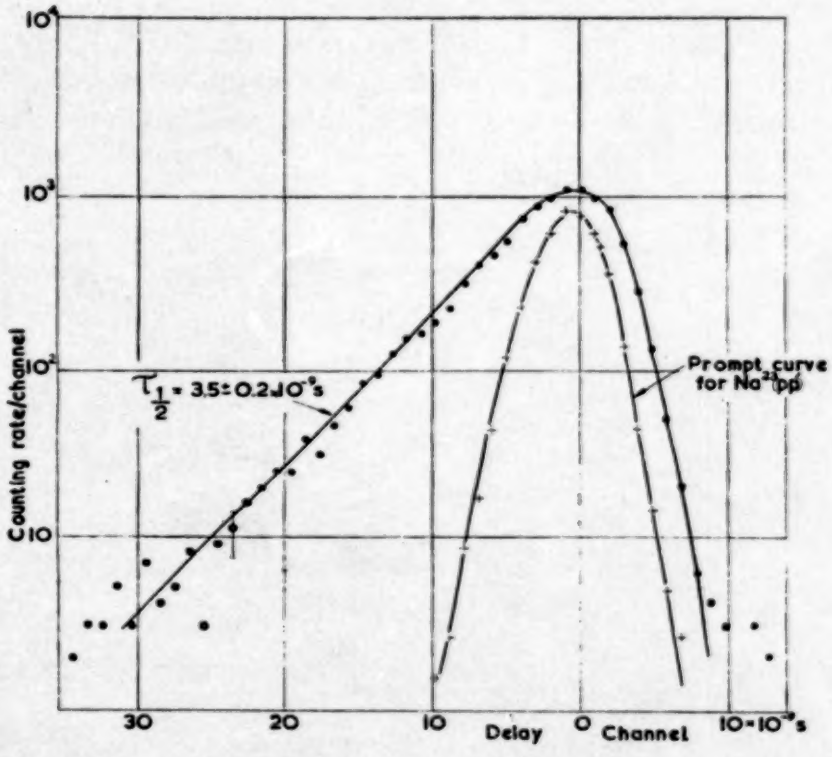

Fig. 3. Time interval spectrum of 580 keV γ-radiation from Mg^{25}(p, p′) at 1.96 MeV together with prompt spectrum from Na^{23} (p, p′).

2.1 MeV; the half life of this state is small ($\tau_{\frac{1}{2}} \leqq 10^{-12}$ s). The time distribution obtained in this experiment also appears in fig. 3. Comparison of the two curves shows that the tail in the time distribution of γ-rays from Mg^{25} is due to a finite lifetime. From the slope of the tail the half life is estimated to be $3.5 \pm 0.2 \times 10^{-9}$ s. The error quoted arises chiefly from the calibration.

Measurements were also made of the lifetime of the 930 keV state of Mg^{25} by observing the $Mg^{25}(p, p')$ reaction at the 2.9 MeV resonance. In order to make the comparison with Na^{23} valid, the scintillation counter voltage was lowered until the pulses due to the 980 keV photopeak had the same amplitude as was formerly given by the 440 keV photopeak. Under these conditions the delay curve was indistinguishable in shape from that given by the 440 keV γ-ray from Na^{23}, and it was concluded that the half-life was less than 1×10^{-9} s. For all these runs the background was negligible and the results shown in fig. 3 have had no background subtracted from them.

4. The 450 keV State in Al^{25}

The lifetime of the 450 keV state in Al^{25} was measured using the reaction $Mg^{24}(p, \gamma)Al^{25}$ at the 825 keV resonance using methods very similar to those described above. Litherland *et al.* [1]) had shown that at this resonance 83 % of the decays proceeded through the 450 keV level and that the only important source of background radiation arose from the annihilation of Al^{25} positons. The pulse amplitude spectrum observed with the scintillation counter is shown in fig. 4.

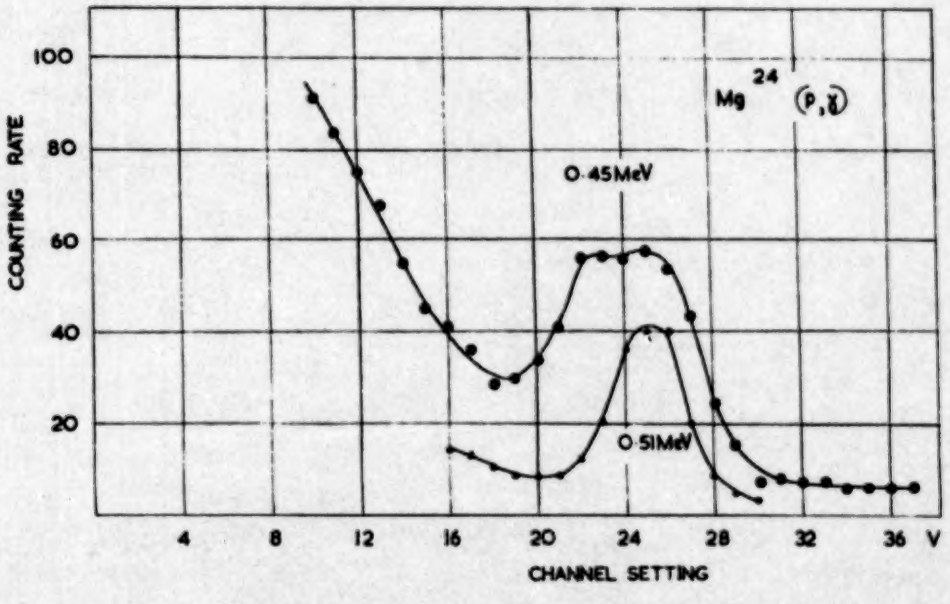

Fig. 4. Scintillation counter spectrum of γ-radiation from $Mg^{24}(p, \gamma)$ at 825 keV bombarding energy.

This can easily be analysed into components at 450 keV and 511 keV. It was confirmed that this radiation was associated with the 825 keV resonance and that the yield of 450 keV radiation was consistent with the level width reported by Litherland *et al.* [1]).

Selecting pulses in the complex γ-ray peak round 500 keV the time distribution was measured as before (fig. 5) together with a prompt curve obtained from

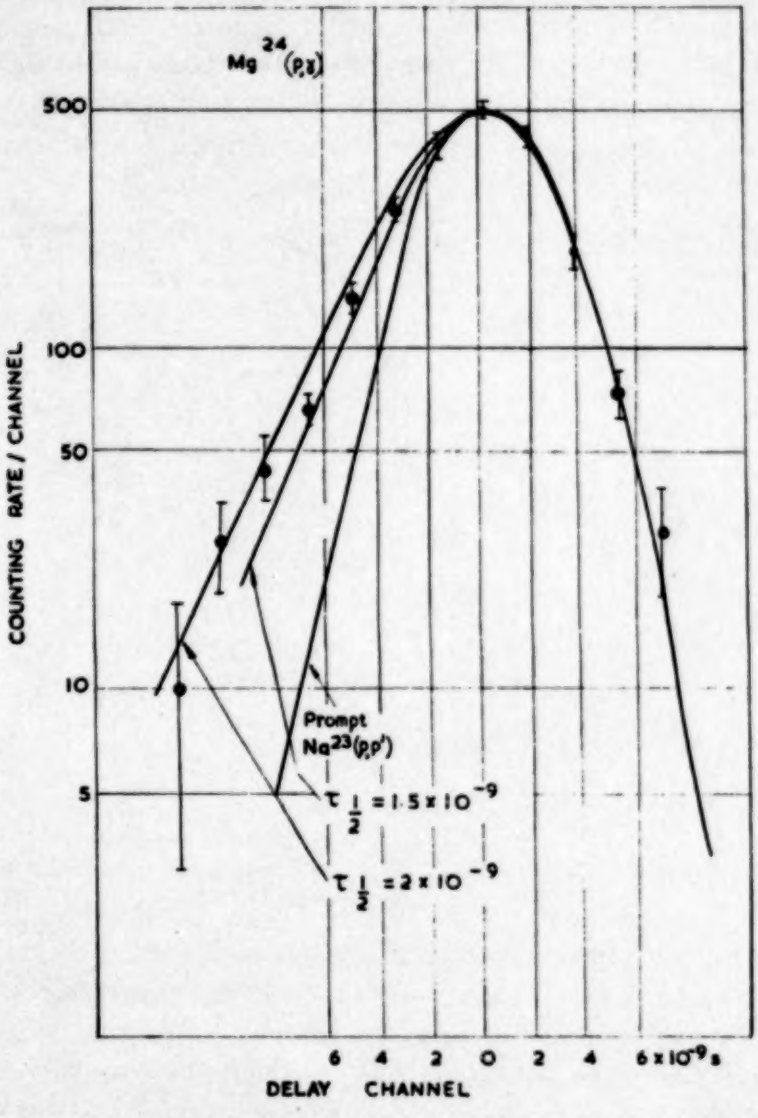

Fig. 5. Time interval spectrum of 450 keV γ-radiation from $Mg^{24}(p, \gamma)$ at 825 keV together with prompt spectrum from $Na^{23}(p, p')$

the $Na^{23}(p, p')$ reaction at the 1.29 MeV resonance. Since the proton burst width ($\approx 2\times10^{-9}$ s) makes only a small contribution to the full width of the delay curve (5×10^{-9} s) it is believed that the prompt curve obtained at this energy will be insignificantly different from that at 825 keV. The slope of the tail of the curve due to the γ-rays from Al^{25} was significantly greater than that

due to the Na^{23} γ-ray, but was too steep to give a reliable estimate of the lifetime by measuring its slope. If a number of finite lifetimes are folded into a prompt curve this may be compared with the shape of the delayed curve. If one does this one obtains $\tau_{\frac{1}{2}} = 1.8 \pm 0.3 \times 10^{-9}$ s.

In order to be certain that this delay distribution was due to the 450 keV γ-ray (and not to Compton electrons, for instance, from higher energy γ-rays) the pulse height spectrum corresponding to pulses under the peak of the delay distribution was observed. The pulse height spectrum due to the background which was random in time was also measured and subtracted from that due to pulses under the peak. The result is shown in fig. 6. It is clear that this is principally 450 keV radiation and shows convincingly that the γ-radiation responsible for the delay curve is the 450 keV transition.

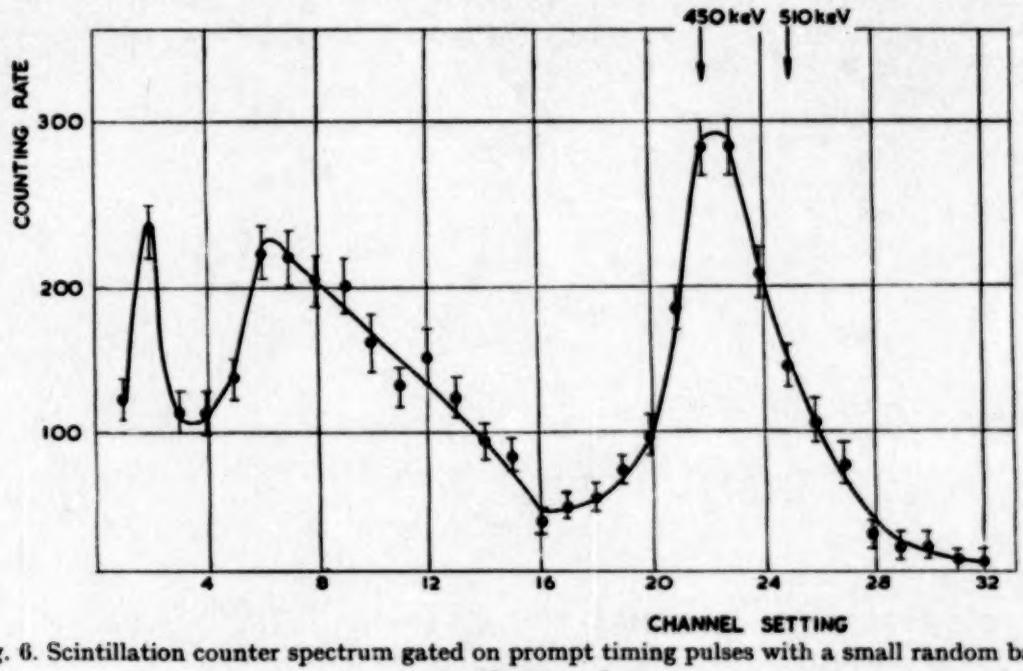

Fig. 6. Scintillation counter spectrum gated on prompt timing pulses with a small random background removed.

From energy considerations alone it had been expected that this transition would have a half-life longer than that of the corresponding mirror state in Mg^{25} and a further measurement was made in order to confirm that the lifetime was short. Using an uninterrupted beam, γ—γ coincidences were recorded between the 2.64 MeV and 450 keV γ-rays using two 5.1 cm $\times$ 5.1 cm NaI detectors and the distribution of delays was measured as before. Slow electronics was used to select coincidences between the 450 keV photopeak in one counter and the total capture and first escape peaks in the other. A prompt curve for comparison was obtained using the 0.58—2.62 MeV cascade in Pb^{208} where the lifetime is less than 10^{-10} s. With the geometry used a fraction of the coincidences could have been due to the escaping annihilation radiation following the 2.62 MeV radiation. This would have the effect of giving too low a value for $\tau_{\frac{1}{2}}$. Making

the maximum possible allowance for this effect the coincidence experiment gives $\tau_{\frac{1}{2}} < 2.0 \pm 0.3 \times 10^{-9}$ s. This is consistent with the value of $(1.8 \pm 0.3) \times 10^{-9}$ and confirms that the lifetime of the first excited state in Al^{25} is significantly less than that of the corresponding state in Mg^{25}.

5. Discussion

For purposes of discussion it is convenient to transform these lifetimes to the reduced transition probabilities $B(E2)$ for the upward transitions $\frac{5}{2} \rightarrow \frac{1}{2}$. For Mg^{25} this is $8.1 \pm 0.5 \times 10^{-53}$ e^2 cm^4 and for Al^{25}, $57 \pm 10 \times 10^{-53}$ e^2 cm^4. On the Nilsson model the predicted value is 5.6×10^{-53}, if we take for the deformation parameter the value $\eta = 4$ used by Litherland *et al.* [3]) to account for the observed data on these levels. This agrees fairly well with the Mg^{25} figure; in fact by altering the deformation parameter from 4 to 3.4 the transition probability can be increased to 8.1 without seriously affecting the level structure. On the other hand there is a rather large discrepancy between Al^{25} and the Nilsson predictions. The different behaviour of the two nuclei is presumably associated with the fact that in Mg^{25} the transition is due to an odd neutron whereas in Al^{25} it is due to an odd proton. On the strong coupling model of Nilsson odd neutron transitions between intrinsic states only take place through recoil effects and are therefore of the order of 1000 times slower than single particle. The fact that the neutron transition takes place at all with an intensity comparable with the odd proton transition implies a breakdown of this extreme condition and hence to some residual effect through core polarization. Nilsson and Mottelson [6]) have suggested that the effective charge of the radiating system be of the order of $(e_p + Ze/A)$ where e_p is the charge of the odd particle. Since $B(E2)$ involves e^2_{eff} this implies that the odd neutron transition should be a quarter of the Nilsson value while the odd proton should be about twice the Nilsson value. Such a term could therefore account satisfactorily for the difference between two probabilities, but the agreement between the experimental value and the Nilsson model is now rather poorer: for instance for Mg^{25} we observe 8.1×10^{-53} and on this model using this correction we expect 1.4×10^{-53}.

We thus conclude that the difference between the transition probabilities for this mirror pair is consistent with the transition in one case being odd neutron and in the other odd proton with core polarization being responsible for the speed of the odd neutron transition. Both transitions are of about the magnitude predicted by the Nilsson model.

We gratefully acknowledge all the help and stimulating discussion provided by the other members of the Van de Graaff Group and especially by Dr. E. B. Paul. We are indebted to the E.M. Separator Group for the supply of the enriched targets.

References

1) A. E. Litherland, E. B. Paul, A. G. Bartholomew and H. E. Gove, Phys. Rev. **102** (1956) 208
2) H. E. Gove, G. A. Bartholomew, E. B. Paul and A. E. Litherland, Nuclear Physics **2** (1956) 132
3) A. E. Litherland, H. McManus, E. B. Paul, D. A. Bromley and H. E. Gove, Can. J. Phys. **36** (1958) 378
4) S. G. Nilsson, Mat. Fys. Medd. Dan. Vid. Selsk. **29**, (1955) No. 16,
5) F. H. Wells and A. K. Barlow, A.E.R.E. Report R/2903 (1959)
6) B. R. Mottelson and S. G. Nilsson, Dan. Mat. Fys. Skr. **1**, No. 8 (1959)

1.E.4:
2.H.

Nuclear Physics **17** (1960) 9—15; © *North-Holland Publishing Co., Amsterdam*
Not to be reproduced by photoprint or microfilm without written permission from the publisher

THE DECAY OF THE 136 keV LEVEL IN Fe^{57}

A. T. G. FERGUSON, M. A. GRACE † and J. O. NEWTON ††

Atomic Energy Research Establishment, Harwell, Berkshire

Received 28 January 1960

Abstract: Coulomb excitation of the 136 keV state in Fe^{57} has been made using 2 MeV helium ions and a number of its properties have been studied. The angular distributions of the γ-rays from this state have been measured. Considerable perturbation of the state is required to explain these results. For the intensity of the 122 keV gamma ray relative to that of the 136 keV gamma ray a value of 8.6 ± 0.2 has been obtained. The half life of the state has been measured and found to be $(8.6 \pm 0.8) \times 10^{-9}$ s. A measurement of the Coulomb excitation cross section leads to a value for the upward $B(E2)$ of $(0.043 \pm 0.005) \times 10^{-48}$ $e^2 cm^4$. This is consistent within the errors of measurement with the lifetime result if we assume that the spin of the 136 keV level is $\frac{5}{2}$.

1. Introduction

The essential features of the low-lying levels in Fe^{57} which are excited in the decay of Co^{57} are well established (see for instance Lemmer, Segaert and Grace [1]) and are shown in fig. 1. The angular distribution of the γ-radiations

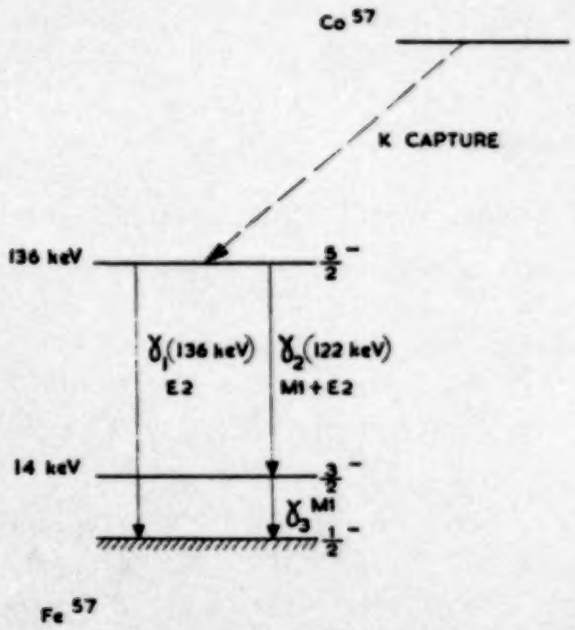

Fig. 1. Low-lying energy levels of Fe^{57}.

† Clarendon Laboratory, Oxford.
†† The Physical Laboratories, Manchester.

from the second excited state has been studied (Bishop *et al.* [2])) using the method of nuclear orientation and has led to the identifation of the strong γ-ray γ_2 as a mixture of M1 and E2 radiations with $\delta(E2/M1) = +0.19 \pm 0.02$. This same γ-ray can also be excited by Coulomb excitation as has been demonstrated by Temmer and Heydenburg [3]). Since the theory of this process now appears to be well understood it seemed worthwhile to study the angular distribution of the Coulomb excited radiation in order to try to obtain an independent determination of the multipole mixing ratio. In addition, since the Coulomb excitation data indicated that the half life of the 136 keV state was of order of 10^{-8} s, which is in the region of values which can be measured with considerable precision by conventional electronic techniques, it was decided both to remeasure the Coulomb excitation cross section and to measure the half life of the state. Such measurements give a check on the consistency of the theoretical probabilities for excitation by the Coulomb process and decay by gamma ray emission.

Four experiments were carried out. In the first a pair of scintillation counters were used to compare the angular distribution of the Coulomb excited raidation from the target with that from a radioactive source of Co^{57} emitting the same γ-radiation isotropically and mounted in the same position. In this measurement γ_1 and γ_2 were not resolved. In the second experiment a single proportional counter was used to resolve these γ-rays and to determine the angular distribution of the ratio of their intensities. From these results the anisotropies of γ_1 and γ_2 separately can be determined. The third experiment was a measurement of the half life of the 136 keV state using pulsed beam equipment. In the fourth experiment a measurement of the Coulomb excitation cross section was made.

2. Experimental Method and Results

The iron targets which were used had been electromagnetically enriched in Fe^{57} and were effectively thick (4 mg cm^{-2}) to the He^+ beam which was used to induce Coulomb excitation. They were electroplated on to copper discs. Magnetically resolved beams of up to 10 μA of He^+ ions from the A.E.R.E. Van de Graaff accelerator were used at energies between 1.9 and 2.5 MeV.

2.1. ANGULAR DISTRIBUTION OF $\gamma_1+\gamma_2$

The two scintillation counters (NaI(Tl)) were mounted approximately equidistant from the target, one along the beam axis (axial counter) and the other perpendicular to this (equatorial counter). Single channel pulse height analysers were set to straddle the 122 keV peaks and runs were made alternately with the Coulomb excited radiation and with the γ-radiation from the Co^{57} source. The target chamber had previously been adjusted so that the Co^{57} source and the beam spot on the target coincided to within 0.5 mm. The accuracy of

replacement of the Co^{57} source was also about 0.5 mm. In order to avoid any spurious directional effects arising from changes in geometry (such as fluctuation in the position of maximum beam intensity within its 3 mm diameter spot) the target was inclined at 45° to the beam so that it contained the internal bisector of the angle between the two counters. The target tube was thinned down to about 1 mm so that the radiation travelling to the two counters had approximately equal thicknesses of material to traverse. The solid angles subtended by the counters at the target 10 cm away were 0.12 sr. The background counting rate due to γ-radiation arising from places other than the target itself was assessed by replacing the iron target by one of copper. The background counting rate above the 122 keV peak, which amounted to 10 % of that in the peak, was sensibly the same for copper as for iron and gave confidence in this method of background assessment.

The ratios of the equatorial to axial counting rates for the Fe^{57} and the Co^{57} were respectively 1.579 ± 0.004 and 1.551 ± 0.004, giving a value of 0.982 ± 0.004 for the ratio $I(0)/I(\frac{1}{2}\pi)$ of the intensities at angles 0 and $\frac{1}{2}\pi$ for Fe^{57}. When account is taken of errors in source replacement etc., this value becomes 0.982 ± 0.014.

2.2. GAMMA RAY TRANSITION γ_1

In order to study the angular distribution of the weak ground state γ-ray γ_1 of 136 keV it was necessary to use a proportional counter of the type described by West [4]) to obtain sufficient energy resolution to separate this γ-ray from the intense 122 keV radiation. The counter was 5 cm in diameter and was filled to 2.5 atm pressure with xenon. It had a resolution of 5.4 % (full width at half-height) at 122 keV. The counter was enclosed in a lead box 2 mm thick with a 2.5 cm diameter hole which gave the counter an aperture of 0.3 sr.

Since the 122 keV γ-ray is emitted approximately isotropically this may be used to self monitor the 136 keV radiation. Thus it was only necessary to measure the spectrum with the one counter alternately in the axial and equatorial positions. Four runs were made and the pulse height distributions were recorded on a 30-channel pulse height analyser. A typical pulse height spectrum is shown in fig. 2. The background was again obtained by substituting a dummy target of natural copper. It was assumed that the shape of this background curve was the same as that when the Fe^{57} target was bombarded. Thus the background for the Fe^{57} experiment was obtained by normalising to the counting rate above the 136 keV peak. This was done because there was a small difference of about 20 % between the absolute yields from the two targets in this region of energy. The background counting rate under the 136 keV full energy peak amounted to about 30 % of the peak rate; that under the 122 keV peak amounted to about 2 % of the peak rate. A total of 10 runs was made, 5 at each angle, and a value for $I(0)/I(\frac{1}{2}\pi)$ of 1.10 ± 0.04 obtained for γ_2 relative to γ_1.

With the superior resolution available with this counter compared with that of earlier measurements (Alburger and Grace [5])) a better value for the branching ratio of 8.6 ± 0.2 for the relative intensities of the 122 and 136 keV γ-rays was obtained; this figure takes no account of internal conversion. In these measurements, greatest weight was attached to the full energy peaks since nelgigible background correction was necessary. After correcting for the relative detection efficiencies of the two γ-rays the above value was obtained.

2.3. THE HALF LIFE OF THE 136 keV STATE

In this experiment a pulsed beam of 2 MeV helium ions was used. These pulses with an approximate pulse width of 2×10^{-9} s and a repetition rate of 10^7 per s,

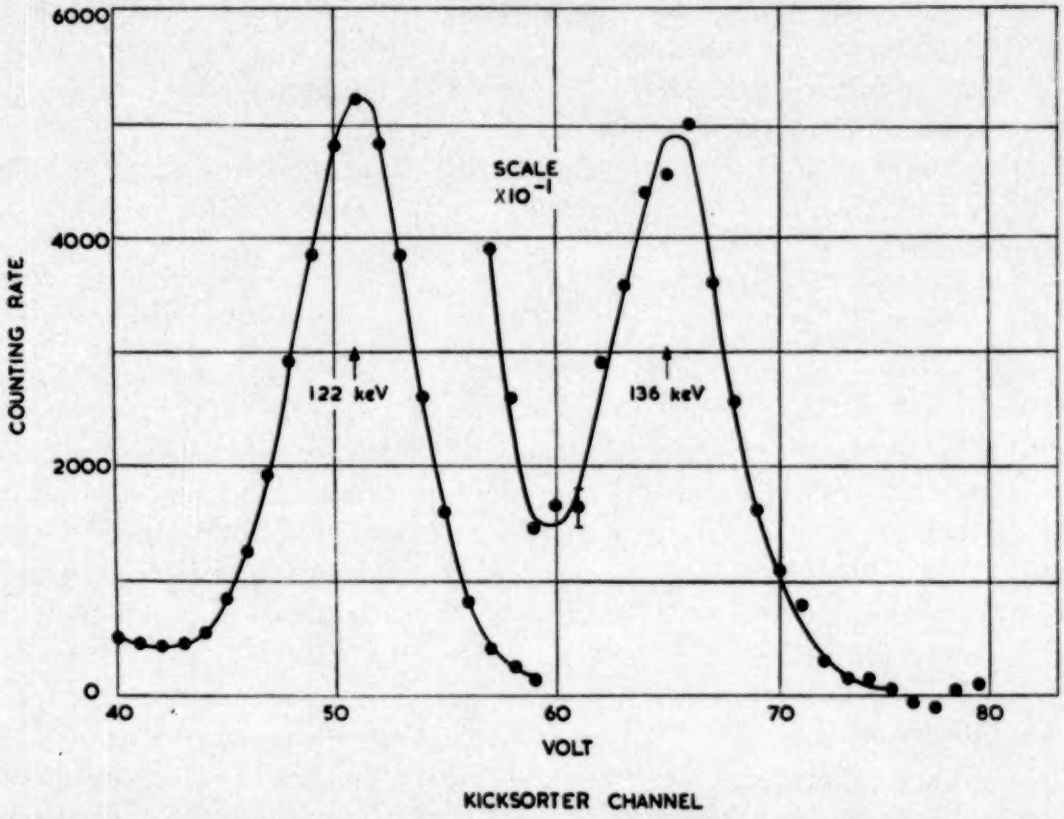

Fig. 2. Pulse height spectrum of the gamma rays from the Coulomb excitation of Fe^{57} taken in a proportional counter filled with Xe to 2.5 atm pressure.

were produced by sweeping the beam across a vertical slit. Gamma rays were detected in a 3.8 cm diameter $\times$ 2.5 cm thick NaI(Tl) crystal placed close to the target and shielded from extraneous radiation by 5 cm of lead; a single channel kicksorter was used to select pulses of the desired amplitude. The time interval between the arrival of a gamma ray pulse and a pulse derived from the sweep waveform was displayed on a 100-channel kicksorter with the aid of a time to pulse height converter. The width at half height of the delay spectrum for a prompt gamma ray is greater than 2×10^{-9} s mainly due to the relatively slow

decay time of the NaI(Tl) phosphor. In this experiment the width at half maximum for prompt curves obtained with gamma rays of approximately 130 keV was about 7×10^{-9} s. Such 'prompt' curves were obtained from the Coulomb excitation of Mn^{55} and Ta^{181} which give gamma rays of energy 128 keV and 136 keV respectively. The experimental delay spectra for Fe^{57} and Mn^{55} are shown in fig. 3, the backgrounds having been subtracted. A flat background spectrum was assumed for Fe^{57} since this was observed for Mn^{55}. The background counting rate was approximately one per cent of the counting

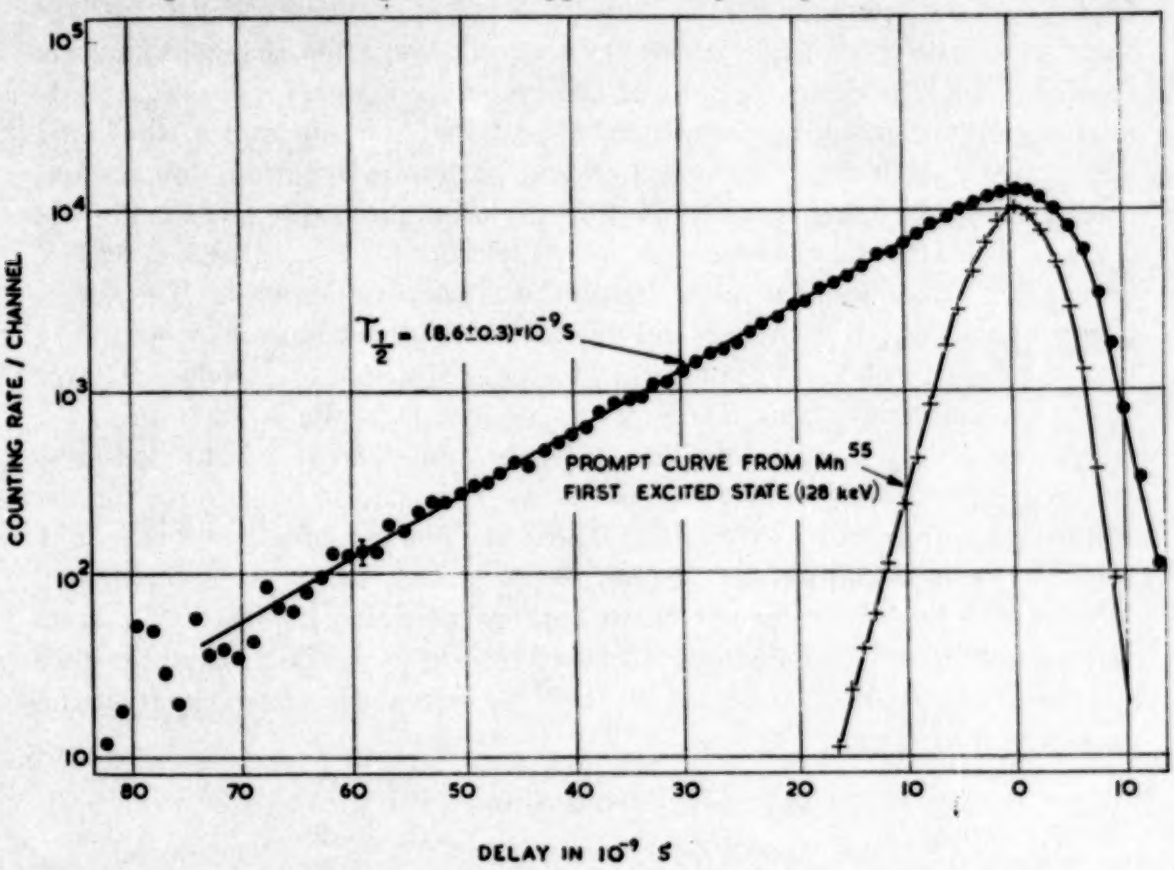

Fig. 3. Delay spectra for gamma rays from the Coulomb excitation of the 136 keV state in Fe^{57} and from the 128 keV level in Mn^{55}.

rate in the peak and therefore errors in its estimation have a negligible effect in the measured half life.

The relationship between pulse height and delay was measured by delaying either set of pulses with calibrated lengths of delay cable and observing the peak shift. There was a slight fluctuation in peak position at a fixed delay presumably owing to small shifts in the beam position. This was the largest source of error in the calibration. From the slope of the tail of the delay spectrum the value obtained for the half-life of the 136 keV state was $(8.6\pm0.8)\times10^{-9}$ s. Whilst this experiment was being set up another measurement of this half life was reported at an American Physical Society Meeting by Lynch and

Holland [6]). It was nevertheless decided to continue the experiment. Their value of $(8.0\pm0.7)\times10^{-9}$ s for the half-life is in satisfactory agreement with ours.

2.4. COULOMB EXCITATION CROSS SECTION

A target enriched to 81 % in Fe^{57} (4 mg cm^{-2} thick deposited on 0.025 cm copper foil) was bombarded with 2.5 MeV He^+ ions and the yield of Coulomb excited radiation from the 136 keV level was observed in a scintillation counter. This was set up in good geometry with the solid angle ($\approx$ 0.05 sr) being defined by a Pb+Cd diaphragm. In this way Pb X-radiation was excluded from the counter and the pulse height distribution recorded on a 100-channel kicksorter showed a single peak centred at 122 keV, together with a small escape peak. A background, amounting to about 10 % of the counting rate in the peak, which arose partly from the machine and partly from natural sources was readily assessed by taking runs with the γ-ray beam interrupted with a Pb+Cd disc and also with the machine switched off. Except for a small peak at 88 keV when the machine was on, the background was approximately flat. The uncertainty in assessing this background together with other counting errors arising from the finite resolving time of the kicksorter is estimated to introduce an error of ±3 %. Corrections were made for the absorption of the γ-radiation in the target and finally a figure of 5.52×10^4 excitations per μC of He^+ ions was reached. From the treatment of Alder *et al.* [7]) we can derive a value for the upward transition probability $B(E2)$ if we know the stopping power dE/dx at 2.5 MeV. From Whaling's survey [8]) of stopping cross sections it seems that a value of 660 keV $\cdot$ mg^{-1} would be an appropriate value for our Fe^{57} target: the probable error in the figure is estimated to be ±10 %. Combining these we find $B(E2) = (0.043\pm0.005)\times10^{-48}e^2\text{cm}^4$ the errors arising largely from the stopping cross section.

3. Discussion

3.1. THE ANGULAR DISTRIBUTIONS

The angular distribution of Coulomb excited radiation can in general be expressed in the form (Alder *et al.* [7]))

$$W(\theta) = 1+a_2A_2G_2P_2(\cos\theta)+a_4A_4G_4P_4(\cos\theta)$$

where A_2, A_4 are the coefficients for a hypothetical gamma-gamma correlation between the states, a_2, a_4 are coefficients depending on the Coulomb excitation process and G_2, G_4 are coefficients giving the attenuation of the correlation by external fields; G_2, G_4 are less than or equal to unity. Since from conversion electron data the 122 keV transition must be largely M1 and since also the coefficient a_4 is small the $P_4(\cos\theta)$ term can be neglected. The quantity $a_2A_2G_2$ can then be derived from the experiment and is found to be -0.020 ± 0.016. This result is consistent with the value $+0.19\pm0.02$ of δ, obtained from the alignment experiment whether or not considerable attenu-

ation is taking place. The results on the 136 keV γ-ray show that considerable disturbance must in fact be taking place if we assume, as is very likely, that the 136 keV state has spin $\frac{5}{2}$. The predicted thick target angular distribution gives $a_2A_2 = 0.22$ and $a_4A_4 = -0.015$. After correcting for geometry this gives $I(0)/I\frac{1}{2}\pi = 1.33$ and this is to be compared with the observed value of 1.08 ± 0.04. If this attenuated angular distribution arises from coupling with an extra-nuclear field, then the value of G_2 turns out to be 0.2 ± 0.1. Such a large perturbation requires $\omega\tau > 1$, where $\hbar\omega$ is the hyperfine structure splitting and τ the lifetime of the 136 keV state (Abragam and Pound [9]). Thus from our measured lifetime we find that the hfs must be greater than 0.0005 cm^{-1}. Measurements on the hfs of iron have not been made. It seems probable however from known values of the hfs of neighbouring elements both in metallic form and in hydrated crystals that the hfs could well be larger than this and hence that the attenuation could arise from this cause.

3.2. LIFETIME AND COULOMB EXCITATION MEASUREMENTS

It is interesting to compare the values of $B(E2)$ from the lifetime and Coulomb excitation measurements. A value for the downward transition probability can be calculated from the half life measurement, the branching ratio from the 136 keV state and the conversion data for the γ-radiation. The radiative transition probabilities upward and downward are simply related by a statistical factor depending only on the spins of the two states. Previous work has established that the ground state of Fe^{57} has spin $\frac{1}{2}$ and the 136 keV state almost certainly has spin $\frac{5}{2}$. When these two values for the spins are assumed the value we obtain for the upward $B(E2)$ is $(0.041 \pm 0.002) \times 10^{-48}$ e^2 cm^4 which is in excellent agreement with that of $(0.043 \pm 0.005) \times 10^{-48}$ e^2 cm^4 obtained from the Coulomb excitation data. This result can either be taken as a confirmation of the value of $\frac{5}{2}$ for the spin of the 136 keV state, if we assume the correctness of the theoretical electromagnetic analysis, or as confirmation of the electromagnetic analysis if we assume the correctness of the spin value.

We are indebted to the E. M. Separator Group at A.E.R.E., Harwell, for the supply of the enriched targets.

References

1) H. R. Lemmer, O. J. A. Segaert and M. A. Grace, Proc. Phys. Soc. **A 68** (1955) 701
2) G. R. Bishop, M. A. Grace, C. E. Johnson, A. C. Knipper, H. R. Lemmer, J. Perez y Jorba and R. G. Scurlock, Phil. Mag. **46** (1955) 951
3) G. M. Temmer and N. P. Heydenburg, Phys. Rev. **96** (1954) 426
4) D. West, Progress in Nuclear Physics (Pergamon Press) **3** (1958] 18
5) D. E. Alburger and M. A. Grace, Proc. Phys. Soc. A **67** (1954) 280
6) F. J. Lynch and R. E. Holland, Bull. Am. Phys. Soc. **3** (1958) 380
7) K. Alder, A. Bohr, T. Huus, B. Mottelson and A. Winther, Revs. Mod. Phys. **28** (1956) 432
8) W. Whaling, Handbuch der Physik **34** (1958) 193
9) A. Abragam and R. V. Pound, Phys. Rev. **92** (1953) 943

1.D.1:6.D *Nuclear Physics* **17** (1960) 16—29; © *North-Holland Publishing Co., Amsterdam*
Not to be reproduced by photoprint or microfilm without written premission from the publisher

MATRIX ELEMENTS IN NUCLEAR SHELL THEORY

T. A. BRODY, G. JACOB † and M. MOSHINSKY ††
Instituto de Física, Universidad de México, México, D.F.

Received 4 January 1960

Abstract: In a previous paper, transformation brackets for harmonic oscillator function were defined and used for the evaluation of matrix elements for nuclear forces. Numerical tables for the transformation brackets are now available. The purpose of this paper is to show how these tables, combined with those given in the present note, can be used to evaluate the matrix elements of nuclear shell theory directly in terms of Talmi integrals. For comparison between present methods and those used previously, a relation between Slater coefficients and Talmi integrals is also obtained.

1. Introduction

In a recent paper [1]) (to be referred to as I), one of us (M.M.) defined and gave explicit expressions for the transformation brackets for harmonic oscillator functions. These transformation brackets have been tabulated numerically [2]) by one of us (T.A.B.). The purpose of this paper is to show how these tables, combined with those given in the present note, can be used to evaluate the matrix elements of nuclear shell theory directly in terms of Talmi [3]) integrals.

We start by giving the definition of the transformation brackets. If we have a particle in an harmonic oscillator potential, its wave function is

$$\Re_{nl}(r)Y_{lm}(\theta, \varphi), \tag{1}$$

where $Y_{lm}(\theta, \varphi)$ is a spherical harmonic and $\Re_{nl}(r)$ is the radial function. Taking, as in I, r in units of $(\hbar/m\omega)^{\frac{1}{2}}$, the radial function has the form

$$\Re_{nl}(r) = r^l \exp\left(-\tfrac{1}{2}r^2\right) \sum_{k=0}^{n} (a_{nlk} r^{2k}), \tag{2}$$

where

$$a_{nlk} = \left[\frac{2(n!)}{\Gamma(n+l+\frac{3}{2})}\right]^{\frac{1}{2}} \binom{n+l+\frac{1}{2}}{n-k} \frac{(-1)^k}{k!}, \tag{3}$$

and Γ stands for a gamma function. The two-particle wave function with total angular momentum λ is then given by

† On leave of absence from Faculdade de Filosofía e Instituto de Física, Universidade do Rio Grande do Sul, Pôrto Alegre, Brasil.

†† Member of the Instituto Nacional de la Investigación Científica México, D.F.

$$|n_1 l_1, n_2 l_2, \lambda\mu\rangle = \sum_{m_1 m_2} \{\langle l_1 l_2 m_1 m_2|\lambda\mu\rangle \Re_{n_1 l_1}(r_1) Y_{l_1 m_1}(\theta_1, \varphi_1) \Re_{n_2 l_2}(r_2) Y_{l_2 m_2}(\theta_2, \varphi_2)\}, \tag{4}$$

where $\langle l_1 l_2 m_1 m_2|\lambda\mu\rangle$ is a Clebsch-Gordan coefficient. If we now introduce the relative and centre-of-mass coordinates by the definition

$$\mathbf{r} = \frac{1}{\sqrt{2}}(\mathbf{r}_1 - \mathbf{r}_2), \qquad \mathbf{R} = \frac{1}{\sqrt{2}}(\mathbf{r}_1 + \mathbf{r}_2), \tag{5}$$

we can construct a wave function of the same total angular momentum λ by

$$|nl, NL, \lambda\mu\rangle = \sum_{mM} \{\langle lLmM|\lambda\mu\rangle \Re_{nl}(r) Y_{lm}(\theta, \varphi) \Re_{NL}(R) Y_{LM}(\Theta, \Phi)\}. \tag{6}$$

The transformation brackets we referred to are those connecting (6) and (4), i.e.

$$|n_1 l_1, n_2 l_2, \lambda\mu\rangle = \sum_{nlNL} |nl, NL, \lambda\mu\rangle\langle nl, NL, \lambda|n_1 l_1, n_2 l_2, \lambda\rangle. \tag{7}$$

Because both kets must correspond to the same energy, $nlNL$ are restricted to those non-negative integers for which

$$2n + l + 2N + L = 2n_1 + l_1 + 2n_2 + l_2. \tag{8}$$

With the help of the brackets defined in (7), it was shown that all matrix elements of nuclear shell theory for central, spin-orbit coupling and tensor forces, could be given in terms of the reduced matrix elements

$$\langle nl||V(r)||n'l'\rangle = \int_0^\infty \Re_{nl}(r) V(r) \Re_{n'l'}(r) r^2 \mathrm{d}r, \tag{9}$$

where $V(r)$ is the radial part of the force between the particles and $\Re_{nl}$ is given by (2).

The transformation brackets

$$\langle nl, NL, \lambda|n_1 l_1, n_2 l_2, \lambda\rangle \tag{10}$$

have been tabulated [2]) for $n_1 = n_2 = 0$ and for all values of l_1, l_2 up to 6, i.e. the i-shell†. The values of the brackets for n_1, $n_2 \neq 0$ can be obtained by recurrence [1]) relations from those in which $n_1 = n_2 = 0$, and a general table will be available by the time this article is in print.

The tables published so far [2]) ($n_1 = n_2 = 0$) are arranged to give for each value of the set $l_1 l_2 \lambda$, all compatible values of $nlNL$, taking into account (8) and that

$$|l - L| \leqq \lambda \leqq l + L. \tag{11}$$

† The tables are available upon request from Instituto de Física, Apdo. Postal 31364, México 20, D.F.

An example, for $l_1=1$, $l_2=2$, $\lambda=1$, is given by table 1. In this table, ρ stands for the total energy (8) of the state in units of $\hbar\omega$, and the number

TABLE 1

l_1	l_2	λ	n	l	N	L	ρ	$\langle nl, NL, \lambda \vert 0l_1, 0l_2, \lambda\rangle$		p
1	2	1	0	0	1	1	3	0.408 248 29		0
			0	1	0	2		0.235 702 26		1
			0	1	1	0		−0.527 046 28		1
			0	2	0	1		0.235 702 26		2
			1	0	0	1		−0.527 046 28		0, 1, 2
			1	1	0	0		0.408 248 29	6	1, 2, 3

in the lower right corner, before the vertical line, gives the number of brackets in the set. The number was shown to have the value [2])

$$\begin{aligned} &\tfrac{1}{8}(\lambda+1)(\rho-\lambda+2)(\rho-\lambda+4), && \text{if } \rho-\lambda \text{ even},\\ &\tfrac{1}{8}\lambda(\rho-\lambda+1)(\rho-\lambda+3), && \text{if } \rho-\lambda \text{ odd}. \end{aligned} \tag{12}$$

The column marked p in table 1, which is separated from the table by a vertical line, indicates the index of the Talmi integrals compatible with each bracket, as discussed in the following sections.

To express the matrix elements of nuclear shell theory in terms of the Talmi integrals

$$I_p = 2[\Gamma(p+\tfrac{3}{2})]^{-1}\int_0^\infty r^{2p}\exp(-r^2)V(r)r^2\,dr, \tag{13}$$

we must first give the reduced matrix elements (9) in terms of I_p. From the definition (2, 3) of the radial functions it is clear that we can write

$$\langle nl||V(r)||n'l'\rangle = \sum_p B(nl, n'l', p)I_p, \tag{14}$$

where $B(nl, n'l', p)$ are certain coefficients whose explicit expression is given in the next section.

2. The coefficients $B(nl, n'l', p)$

From (9) and (2, 3) we see that

$$\begin{aligned}\langle nl||V(r)||n'l'\rangle = \sum_{k=-\infty}^{\infty}\sum_{k'=-\infty}^{\infty} a_{nlk}a_{n'l'k'}f(0, k, n)f(0, k', n')\\ \int_0^\infty r^{l+l'+2k+2k'}\exp(-r^2)V(r^2)r^2\,dr,\end{aligned} \tag{15}$$

where to extend the summations from $-\infty$ to $+\infty$, we introduce the step function $f(a, x, b)$ defined for $a \leqq b$ as follows:

$$f(a,x,b)=\begin{cases}0, & \text{if } x<a,\\ 1, & \text{if } a\leqq x\leqq b,\\ 0, & \text{if } x>b.\end{cases} \tag{16}$$

We now express k' in terms of a new variable p by †

$$k'=p-\tfrac{1}{2}(l+l')-k. \tag{17}$$

From (15) we obtain

$$\langle nl||V(r)||n'l'\rangle=\sum_{p=-\infty}^{\infty}\Big\{\sum_{k=-\infty}^{\infty}a_{nlk}a_{n'l'\,p-\frac{1}{2}(l+l')-k} f(0,k,n)f(0,p-\tfrac{1}{2}l-\tfrac{1}{2}l'-k,n')\tfrac{1}{2}\Gamma(p+\tfrac{3}{2})I_p\Big\}, \tag{18}$$

where I_p is given by (13). Using the properties (16) of the step function $f(a,x,b)$, we can write (18) as

$$\langle nl||V(r)||n'l'\rangle=\sum_{p=\frac{1}{2}(l+l')}^{\frac{1}{2}(l+l')+n+n'}B(nl,n'l',p)I_p, \tag{19}$$

where

$$B(nl,n'l',p)=\tfrac{1}{2}\Gamma(p+\tfrac{3}{2})\sum_{k=\alpha}^{\beta}a_{nlk}a_{n'l'\,p-\frac{1}{2}(l+l')-k}. \tag{20}$$

The limits of the summation in (20) are given by

$$\alpha\equiv\max\,[0,(p-\tfrac{1}{2}l-\tfrac{1}{2}l'-n')]=\begin{cases}0 & \text{if } p-\tfrac{1}{2}(l+l')-n'\leqq 0,\\ p-\tfrac{1}{2}(l+l')-n' & \text{if } p-\tfrac{1}{2}(l+l')-n'>0.\end{cases} \tag{21}$$

$$\beta\equiv\min\,[n,(p-\tfrac{1}{2}l-\tfrac{1}{2}l')]=\begin{cases}p-\tfrac{1}{2}(l+l') & \text{if } p-\tfrac{1}{2}(l+l')\leqq n\\ n & \text{if } p-\tfrac{1}{2}(l+l')>n.\end{cases} \tag{22}$$

From the explicit expression (3) of the a_{nlk} we obtain finally

$$B(nl,n'l',p)=\frac{(-1)^{p-\frac{1}{2}l-\frac{1}{2}l'}(2p+1)!}{2^{n+n'}p!}\left[\frac{n!n'!(2n+2l+1)!\,(2n'+2l'+1)!}{(n+l)!\,(n'+l')!}\right]^{\frac{1}{2}} \sum_{k=\alpha}^{\beta}\frac{(l+k)!(p-\frac{1}{2}l+\frac{1}{2}l'-k)!}{k!(2l+1+2k)!(n-k)!(2p-l+l'+1-2k)!(n'-p+\frac{1}{2}l+\frac{1}{2}l'+k)!(p-\frac{1}{2}l-\frac{1}{2}l'-k)!} \tag{23}$$

It will be shown in the next section that for diagonal matrix elements for all types of forces, we need to know only $B(nl,nl,p)$ and $B(nl,n-1\,l+2,p)$. These coefficients are tabulated at the end of the paper for all values of interest of n, l, p.

† As shown in I, $l+l'$ is even for all types of forces, so p remains an integer.

3. The Diagonal Matrix Elements for Nuclear Forces

With the help of the coefficient $B(nl, n'l', p)$ and the transformation brackets (10), we can give the matrix elements for nuclear forces directly in terms of Talmi integrals. We outline the procedure here only for the diagonal two particle matrix elements, but from the discussion in I, it is clear that the results can be generalized to any type of matrix element.

3.1. CENTRAL FORCES

Let us consider the diagonal matrix element for a central force $V(r)$, where r is the relative coordinate between two nucleons in a state $|n_1 l_1, n_2 l_2, \lambda\mu\rangle$ given by (4). It was shown in I, eq. (19), that

$$\langle n_1 l_1, n_2 l_2, \lambda\mu|V(r)|n_1 l_1, n_2 l_2, \lambda\mu\rangle = \sum_{nlNL} \{[\langle nl, NL, \lambda|n_1 l_1, n_2 l_2, \lambda\rangle]^2 \langle nl||V(r)||nl\rangle \delta_{\rho\varepsilon}\}, \quad (24)$$

where we introduce the Kronecker delta $\delta_{\rho\varepsilon}$,

$$\rho = 2n_1+l_1+2n_2+l_2, \qquad \varepsilon = 2n+l+2N+L, \quad (25)$$

to indicate explicitly that the transformation brackets vanish if $\rho \neq \varepsilon$, i.e. unless the energy conservation rule (8) is satisfied. From (24, 25) it is clear that none of the integers $nlNL$ can exceed ρ.

From (19) we can write

$$\langle nl||V(r)||nl\rangle = \sum_{p=0}^{\rho} [B(nl, nl, p) f(l, p, 2n+l) I_p], \quad (26)$$

where we again introduce the step function $f(a, x, b)$ of (16) so that the summation can be extended from 0 to ρ, as from (25) it is clear that $0 \leqq l \leqq 2n+l \leqq \rho$. Substituting (26) in (24), and interchanging the summation order, we obtain

$$\langle n_1 l_1, n_2 l_2, \lambda\mu|V(r)|n_1 l_1, n_2 l_2, \lambda\mu\rangle = \sum_{p=0}^{\rho} C_\varepsilon(n_1 l_1, n_2 l_2, \lambda, p) I_p, \quad (27)$$

where

$$C_\varepsilon(n_1 l_1, n_2 l_2, \lambda, p) = \sum_{nlNL=0}^{\rho} \{[\langle nl, NL, \lambda|n_1 l_1, n_2 l_2, \lambda\rangle]^2 \times B(nl, nl, p) \delta_{\rho\varepsilon} f(l, p, 2n+l)\}. \quad (28)$$

The matrix element (27) is then given directly in terms of Talmi integrals I_p, whose coefficients C_ε are determined by (28) in terms of the transformation brackets (10) and the coefficients (23). An illustrative example is given in the next section.

3.2. SPIN ORBIT COUPLING FORCES

As shown [1,5]) in I, for a spin orbit coupling force in LS coupling, it is enough to consider the reduced matrix element $V(r)\mathbf{l}$ where $\mathbf{r}$ and $\mathbf{l}$ are the relative coordinate and angular momentum respectively. Following a procedure entirely similar to the previous subsection, we obtain

$$\langle n_1 l_1, n_2 l_2, \lambda||V(r)\mathbf{l}||n_1 l_1, n_2 l_2, \lambda\rangle = \sum_{p=0}^{\rho} C_{LS}(n_1 l_1, n_2 l_2, \lambda, p) I_p \tag{29}$$

where, W being a Racah coefficient,

$$\begin{aligned} C_{LS}(n_1 l_1, n_2 l_2, \lambda, p) = \sum_{nlNL=0}^{\rho} &\{[l(l+1)(2l+1)(2\lambda+1)^2]^{\frac{1}{2}} \\ &\times (-1)^{L+1-l-\lambda} W(ll\lambda\lambda;\, 1L)[\langle nl, NL, \lambda|n_1 l_1, n_2 l_2, \lambda\rangle]^2 \\ &\times B(nl, nl, p)\delta_{\rho\varepsilon} f(l, p, 2n+l)\}. \end{aligned} \tag{30}$$

3.3. TENSOR FORCES

As shown [1,5]) in I, for a tensor force in LS coupling, it is enough to consider the reduced matrix element of the potential $V(r)Y_{2\mu}(\theta, \varphi)$, where (r, θ, φ) are the polar components of the relative coordinate. As this potential does not commute with $\mathbf{l}$, we have that for diagonal matrix elements there are coefficients $B(nl, n'l', p)$ with $n' \neq n$, $l' \neq l$ but satisfying the relation

$$2n'+l' = 2n+l, \qquad l' = l \pm 2, l. \tag{31}$$

Following the same procedure as in previous subsections, we have

$$\langle n_1 l_1, n_2 l_2, \lambda||V(r)Y_2(\theta, \varphi)||n_1 l_1, n_2 l_2, \lambda\rangle = \sum_{p=0}^{\rho} C_T(n_1 l_1, n_2 l_2, \lambda, p) I_p \tag{32}$$

where

$$\begin{aligned} C_T(n_1 l_1, n_2 l_2, \lambda, p) = \sum_{nlNL=0}^{\rho} \sum_{n'=0}^{\rho} \sum_{l'=|l-2|}^{l+2} &\{\tfrac{1}{2}[1+(-1)^{l-l'}] \\ &\times \langle nl, NL, \lambda|n_1 l_1, n_2 l_2, \lambda\rangle\langle n'l', NL, \lambda|n_1 l_1, n_2 l_2, \lambda\rangle(-1)^{L-\lambda-l'} \\ &\times [(2\lambda+1)^2(2l+1)(5/4\pi)]^{\frac{1}{2}}\langle l200|l'0\rangle W(ll'\lambda\lambda;\, 2L) \\ &\times B(nl, n'l', p)\delta_{n', n+\frac{1}{2}l-\frac{1}{2}l'}\delta_{\rho\varepsilon} f(\tfrac{1}{2}l+\tfrac{1}{2}l', p, \tfrac{1}{2}l+\tfrac{1}{2}l'+n+n')\}. \end{aligned} \tag{33}$$

For the diagonal matrix elements for the three types of forces, we need therefore the coefficients

$$B(nl, nl, p),\ B(nl, n-1l+2, p) \quad \text{and} \quad B(nl, n+1l-2, p).$$

But from the definition (9), (19) of $B(nl, n'l', p)$ we see that

$$B(nl, n+1l-2, p) = B(n+1l-2, nl, p) = [B(n'l', n'-1l'+2, p)]_{\substack{n'=n \\ l'=l-2}} \tag{34}$$

so that actually we only need to tabulate the coefficients $B(nl, nl, p)$ and

$B(nl, n-1l+2, p)$. These coefficients are given at the end of this paper in tables 2 and 3 for all values of n, l, p such that †

$$2n+l \leqq 12, \qquad \tfrac{1}{2}(l+l') \leqq p \leqq 2n+l. \tag{35}$$

These values of the parameters will correspond to all levels of interest in nuclear shell theory, for a system of two particles in the i-shell or lower, as then

$$2n_1+l_1 \leqq 6, \qquad 2n_2+l_2 \leqq 6, \qquad \text{and} \quad \rho \leqq 12. \tag{36}$$

For convenient use, the tables are arranged in order of increasing p and there is a blank line between the sets of values corresponding to different p's. For a fixed p the tables are arranged in order of increasing l first and then of increasing n.

4. An Example: the (0p)(0d) Configuration

To illustrate the systematic procedure to be followed when we want to express the matrix elements in terms of Talmi integrals, we take the simple configuration (0p)(0d) i.e. $n_1=0$, $l_1=1$, $n_2=0$, $l_2=2$, and then discuss the matrix element for a central force when the total angular momentum $\lambda=1$, i.e.

$$\langle 01, 02, 1||V(r)||01, 02, 1\rangle = \sum_{p=0}^{3} C_e(01, 02, 1, p) I_p \tag{37}$$

The values of $nlNL$ compatible with $\rho=3$, $\lambda=1$, are given in table 1. For each set of values $nlNL$ there is a corresponding set of p's that from (26) satisfies the inequality

$$l \leqq p \leqq 2n+l. \tag{38}$$

In table 1, in the column marked p, we give the values of p that satisfy (38) corresponding to the n, l in the same row. We see, for example, that $p=0$ appears in the first and fifth rows of the table, and therefore from (28) we have

$$\begin{aligned} C_e(01, 02, 1, 0) = {} & [\langle 00, 11, 1|01, 02, 1\rangle]^2 B(00, 00, 0) \\ & +[\langle 10, 01, 1\,|\,01, 02, 1\rangle]^2 B(10, 10, 0). \end{aligned} \tag{39}$$

From table 1 and table 2 we immediately obtain ††

$$C_e(01, 02, 1, 0) = \tfrac{7}{12}. \tag{40}$$

† The lower bound of p is $l+1$ if $l' = l+2$ and l if $l' = l$.

†† The coefficients C_e are clearly rational numbers, so in simple cases such as this example, the decimal fraction can be replaced by the corresponding simple fraction.

TABLE 2

n	l	p	$B(nl, nl, p)$	n	l	p	$B(nl, nl, p)$
0	0	0	1.000 000 0	2	2	3	−31.500 001
1	0	0	1.500 000 0	3	2	3	−86.625 000
2	0	0	1.875 000 0	4	2	3	−187.687 51
3	0	0	2.187 500 0	5	2	3	−351.914 08
4	0	0	2.460 937 4	0	3	3	1.000 000 0
5	0	0	2.707 031 2	1	3	3	4.500 000 1
6	0	0	2.932 617 1	2	3	3	12.375 000
				3	3	3	26.812 500
1	0	1	−3.000 000 1	4	3	3	50.273 440
2	0	1	−7.500 000 0				
3	0	1	−13.125 000	2	0	4	7.875 000 0
4	0	1	−19.687 499	3	0	4	122.062 50
5	0	1	−27.070 313	4	0	4	613.265 60
6	0	1	−35.191 406	5	0	4	1 976.132 8
0	1	1	1.000 000 0	6	0	4	4 970.786 1
1	1	1	2.500 000 0	2	1	4	−31.500 000
2	1	1	4.375 000 1	3	1	4	−225.749 98
3	1	1	6.562 500 0	4	1	4	−851.812 50
4	1	1	9.023 437 8	5	1	4	−2 346.093 8
5	1	1	11.730 469	1	2	4	4.500 000 1
				2	2	4	56.250 003
1	0	2	2.500 000 1	3	2	4	253.687 50
2	0	2	16.250 002	4	2	4	764.156 22
3	0	2	45.937 501	5	2	4	1 834.980 6
4	0	2	95.156 252	1	3	4	−9.000 000 6
5	0	2	166.933 60	2	3	4	−49.500 000
6	0	2	263.935 56	3	3	4	−160.875 00
1	1	2	−5.000 000 0	4	3	4	−402.187 52
2	1	2	−17.500 000	0	4	4	0.999 999 99
3	1	2	−39.375 000	1	4	4	5.500 000 2
4	1	2	−72.187 499	2	4	4	17.875 000
5	1	2	−117.304 69	3	4	4	44.687 504
0	2	2	1.000 000 0	4	4	4	94.960 939
1	2	2	3.500 000 0				
2	2	2	7.875 000 0	3	0	5	−86.625 004
3	2	2	14.437 500	4	0	5	−851.812 50
4	2	2	23.460 938	5	0	5	−4 074.984 8
5	2	2	35.191 409	6	0	5	−13 583.883
				2	1	5	12.375 000
2	0	3	−17.500 000	3	1	5	253.687 50
3	0	3	−96.250 004	4	1	5	1 572.140 6
4	0	3	−295.312 49	5	1	5	6 016.054 5
5	0	3	−685.781 26	2	2	5	−49.500 001
6	0	3	−1 349.003 9	3	2	5	−437.250 02
1	1	3	3.500 000 0	4	2	5	−1 957.312 5
2	1	3	33.250 000	5	2	5	−6 233.906 4
3	1	3	122.062 51	1	3	5	5.500 000 2
4	1	3	310.406 24	2	3	5	85.249 998
5	1	3	645.175 79	3	3	5	455.812 49
1	2	3	−7.000 000 1	4	3	5	1 586.406 3
				1	4	5	−11.000 000
				2	4	5	−71.499 998

TABLE 2

n	l	p	$B(nl, nl, p)$	n	l	p	$B(nl, nl, p)$
3	4	5	−268.125 01	2	6	7	−127.500 00
4	4	5	−759.687 52	3	6	7	−605.624 98
0	5	5	0.999 999 98	0	7	7	1.000 000 0
1	5	5	6.499 999 8	1	7	7	8.500 000 0
2	5	5	24.375 002	2	7	7	40.374 999
3	5	5	69.062 499				
				4	0	8	94.960 936
3	0	6	26.812 500	5	0	8	4 320.722 7
4	0	6	764.156 21	6	0	8	49 177.895
5	0	6	6 016.054 8	4	1	8	− 759.687 49
6	0	6	27 879.972	5	1	8	−14 054.218
3	1	6	− 160.875 00	3	2	8	69.062 498
4	1	6	−1 957.312 5	4	2	8	2 935.156 3
5	1	6	−11 133.892	5	2	8	31 932.776
2	2	6	17.874 999	3	3	8	− 414.375 00
3	2	6	455.812 51	4	3	8	−6 975.312 9
4	2	6	3 358.265 5	2	4	8	31.874 998
5	2	6	14 875.352	3	4	8	1 131.562 5
2	3	6	−71.499 998	4	4	8	10 982.266
3	3	6	− 750.749 99	2	5	8	− 127.500 00
4	3	6	−3 887.812 7	3	5	8	−1 763.750 1
1	4	6	6.500 000 3	1	6	8	8.500 000 2
2	4	6	120.250 00	2	6	8	208.250 01
3	4	6	743.437 47	3	6	8	1 635.187 4
4	4	6	2 935.156 2	1	7	8	−16.999 999
1	5	6	−13.000 001	2	7	8	− 161.499 99
2	5	6	−97.500 002	0	8	8	0.999 999 99
3	5	6	− 414.375 00	1	8	8	9.499 999 7
0	6	6	1.000 000 1	2	8	8	49.875 004
1	6	6	7.500 000 7				
2	6	6	31.875 000	5	0	9	−1 804.257 8
3	6	6	100.937 50	6	0	9	−40 595.799
				4	1	9	164.023 43
4	0	7	− 402.187 49	5	1	9	8 939.277 0
5	0	7	−6 233.906 7	4	2	9	−1 312.187 5
6	0	7	−42 983.790	5	2	9	−28 212.033
3	1	7	44.687 502	3	3	9	100.937 50
4	1	7	1 586.406 2	4	3	9	4 996.406 4
5	1	7	14 875.352	3	4	9	−605.624 96
3	2	7	− 268.125 02	4	4	9	−11 607.813
4	2	7	−3 887.812 6	2	5	9	40.375 000
5	2	7	−25 626.048	3	5	9	1 635.187 5
2	3	7	24.375 000	2	6	9	−161.500 00
3	3	7	743.437 55	3	6	9	−2 503.249 8
4	3	7	6 346.640 8	1	7	9	9.499 999 7
2	4	7	−97.499 999	2	7	9	261.249 99
3	4	7	−1 186.250 0	1	8	9	−19.000 00
4	4	7	−6 975.312 8	2	8	9	−199.500 00
1	5	7	7.500 000 4	0	9	9	0.999 999 97
2	5	7	161.250 02	1	9	9	10.500 000
3	5	7	1 131.562 6				
1	6	7	−15.000 001				

TABLE 2

n	l	p	$B(nl, nl, p)$	n	l	p	$B(nl, nl, p)$
5	0	10	344.449 21	6	0	11	−7 922.331 9
6	0	10	22 905.872	5	1	11	609.410 12
5	1	10	−3 444.492 3	5	2	11	−6 094.101 4
4	2	10	264.960 93	4	3	11	406.273 40
5	2	10	16 825.019	4	4	11	−3 250.187 3
4	3	10	−2 119.687 5	3	5	11	191.187 50
3	4	10	141.312 49	3	6	11	−1 147.125 0
4	4	10	7 984.156 2	2	7	11	60.375 000
3	5	10	−847.874 98	2	8	11	−241.500 00
2	6	10	49.875 002	1	9	11	11.500 000
3	6	10	2 269.312 5	1	10	11	−23.000 000
2	7	10	−199.500 00	0	11	11	1.000 000 0
1	8	10	10.500 000				
2	8	10	320.250 01	6	0	12	1 269.604 5
1	9	10	−21.000 000	5	2	12	1 015.683 5
0	10	10	1.000 000 0	4	4	12	597.460 94
1	10	10	11.500 000	3	6	12	251.562 49
				2	8	12	71.875 003
				1	10	12	12.500 001
				0	12	12	0.999 999 98

In a similar fashion we obtain

$$C_c(01,\ 02,\ 1,\ 1) = -\tfrac{1}{12}, \quad C_c(01,\ 02,\ 1,\ 2) = -\tfrac{1}{12},$$
$$C_c(01,\ 02,\ 1,\ 3) = \tfrac{7}{12}. \tag{41}$$

Thus the matrix element (37) can be written in terms of Talmi integrals as

$$\langle 01,\ 02,\ 1||V(r)||01,\ 02,\ 1\rangle = \tfrac{1}{12}(7I_0 - I_1 - I_2 + 7I_3) \tag{42}$$

We can now give the general procedure for the calculation of the matrix elements:

1. Given a definite state $|n_1l_1,\ n_2l_2,\ \lambda\mu\rangle$ we look in the table[2]) of the transformation brackets to get all values of $nlNL$ compatible with (8) and (11). These values are immediately available, as shown in table 1.

2. For each set $nlNL$ we determine all values of p compatible with the inequality (38).

3. We then take the brackets corresponding to a definite p, square them and multiply by the corresponding B's of table 2, and add them to obtain the coefficients $C_c(n_1l_1,\ n_2l_2,\ \lambda,\ p)$. For spin orbit coupling and tensor forces, one follows a similar procedure as indicated in Section 3.

The analysis outlined above is particularly suitable for machine computation. It is planned to give tables of coefficients C at some future date.

TABLE 3

n	l	p	$B(nl, n-1\,l+2, p)$	n	l	p	$B(nl, n-1\,l+2, p)$
1	0	1	0.948 683 34	2	3	4	8.112 490 1
2	0	1	1.984 313 6	3	3	4	23.124 156
3	0	1	3.214 955 2	4	3	4	53.298 544
4	0	1	4.617 128 0				
5	0	1	6.172 981 2	3	0	5	65.676 943
6	0	1	7.869 037 8	4	0	5	613.638 33
				5	0	5	2 843.415 3
1	0	2	−1.581 138 8	6	0	5	9 272.493 8
2	0	2	−8.031 745 1	2	1	5	−8.249 999 8
3	0	2	−20.667 570	3	1	5	−149.279 20
4	0	2	−40.674 700	4	1	5	−864.191 85
5	0	2	−69.078 598	5	1	5	−3 163.860 4
6	0	2	−106.794 08	2	2	5	24.045 529
1	1	2	1.336 306 2	3	2	5	185.891 58
2	1	2	3.750 000 0	4	2	5	769.122 29
3	1	2	7.616 286 4	5	2	5	2 323.892 0
4	1	2	13.145 910	1	3	5	−2.345 207 9
5	1	2	20.524 045	2	3	5	−26.694 946
				3	3	5	−123.921 76
2	0	3	11.244 443	4	3	5	−395.866 95
3	0	3	56.440 324	1	4	5	2.157 277 5
4	0	3	164.677 56	2	4	5	10.650 704
5	0	3	370.378 87	3	4	5	34.717 049
6	0	3	712.585 09	4	4	5	90.058 236
1	1	3	−1.870 828 7				
2	1	3	−13.416 667	3	0	6	−21.892 314
3	1	3	−43.835 958	4	0	6	−591.652 01
4	1	3	−104.290 89	5	0	6	−4 510.979 3
5	1	3	−207.520 90	6	0	6	−20 451.255
1	2	3	1.649 915 9	3	1	6	107.812 76
2	2	3	5.804 093 2	4	1	6	1 224.322 4
3	2	3	14.167 616	5	1	6	6 661.648 8
4	2	3	28.555 744	2	2	6	−10.779 030
5	2	3	50.982 201	3	2	6	−238.825 55
				4	2	6	−1 624.414 0
2	0	4	−5.952 940 4	5	2	6	−6 822.875 7
3	0	4	−83.588 838	2	3	6	31.548 572
4	0	4	−399.171 70	3	3	6	286.739 53
5	0	4	−1 245.819 8	4	3	6	1 360.889 6
6	0	4	−3 065.348 0	1	4	6	−2.549 509 8
2	1	4	17.250 000	2	4	6	−34.405 004
3	1	4	109.951 47	3	4	6	−183.263 94
4	1	4	387.923 84	4	4	6	−659.881 25
5	1	4	1 022.470 6	1	5	6	2.373 464 5
1	2	4	−2.121 320 3	2	5	6	13.400 094
2	2	4	−19.673 615	3	5	6	49.159 048
3	2	4	−77.829 893				
4	2	4	−216.949 50	4	0	7	328.695 55
5	2	4	−494.593 57	5	0	7	4 932.506 0
1	3	4	1.918 806 4	6	0	7	33 271.041

TABLE 3

n	l	p	$B(nl, n-1\,l+2, p)$	n	l	p	$B(nl, n-1\,l+2, p)$
3	1	7	−33.003 905	2	6	9	57.755 410
4	1	7	−1 091.110 5	3	6	9	760.425 04
5	1	7	−9 783.128 0	1	7	9	−3.082 207 1
3	2	7	162.835 59	2	7	9	−61.155 563
4	2	7	2 177.282 8	1	8	9	2.931 763 6
5	2	7	13 603.484	2	8	9	22.780 199
2	3	7	−13.520 817				
3	3	7	−354.570 41	5	0	10	−302.101 95
4	3	7	−2 770.479 1	6	0	10	−19 640.402
2	4	7	39.698 080	5	1	10	2 704.246 2
3	4	7	414.748 08	4	2	10	−193.500 11
4	4	7	2 220.634 0	5	2	10	−11 623.941
1	5	7	−2.738 612 8	4	3	10	1 345.036 5
2	5	7	−42.746 905	3	4	10	− 83.952 135
3	5	7	−256.917 21	4	4	10	−4 298.233 7
1	6	7	2.572 478 9	3	5	10	415.738 74
2	6	7	16.345 871	2	6	10	−22.884 219
3	6	7	66.648 271	3	6	10	−879.757 15
				2	7	10	67.592 989
4	0	8	−80.982 960	1	8	10	−3.240 370 2
5	0	8	−3 564.651 8	2	8	10	−71.155 540
6	0	8	−39 686.181	1	9	10	3.096 281 1
4	1	8	562.087 23				
5	1	8	9 938.613 2	6	0	11	6 949.680 9
3	2	8	−46.918 729	5	1	11	−497.581 27
4	2	8	−1 834.613 8	5	2	11	4 455.844 2
5	2	8	−18 911.085	4	3	11	−278.701 25
3	3	8	231.834 49	4	4	11	1 938.419 1
4	3	8	3 567.358 2	3	5	11	−107.438 09
2	4	8	−16.460 178	3	6	11	532.484 60
3	4	8	−498.663 04	2	7	11	−26.349 809
4	4	8	−4 400.787 9	2	8	11	77.932 257
2	5	8	48.446 492	1	9	11	−3.391 164 8
3	5	8	571.996 36	1	10	11	3.252 691 1
1	6	8	−2.915 475 9				
2	6	8	−51.675 895	6	0	12	−1 135.568 8
3	6	8	−345.869 45	5	2	12	−778.993 70
1	7	8	2.757 764 3	4	4	12	−387.683 85
2	7	8	19.475 947	3	6	12	−134.465 82
				2	8	12	−29.973 948
5	0	9	1 539.281 4	1	10	12	−3.535 533 8
6	0	9	33 870.982				
4	1	9	− 128.670 57				
5	1	9	−6 696.228 8				
4	2	9	893.786 22				
5	2	9	18 196.521				
3	3	9	−63.838 480				
4	3	9	−2 882.221 3				
3	4	9	315.819 94				
4	4	9	5 496.827 0				
2	5	9	−19.584 752				
3	5	9	−673.100 80				

5. Transformation Brackets and the Relation between Slater Coefficients and Talmi Integrals

The usual method of calculating matrix elements for nuclear forces is based on the reduction of the matrix elements to Slater coefficients[3,6,7]). For the sake of comparison we shall derive in this section a relation between Slater coefficients and Talmi integrals, using the coefficients $C_c(n_1l_1, n_2l_2, \lambda, p)$ discussed in the previous sections.

Using the well known methods of Racah, we can write the matrix elements for a central force

$$\langle n_1l_1, n_2l_2, \lambda\mu|V(|\mathbf{r}_1-\mathbf{r}_2|)|n_1l_1, n_2l_2, \lambda\mu\rangle = \sum_k \Big\{F^k(n_1l_1, n_2l_2)(-1)^\lambda \frac{(2l_1+1)(2l_2+1)}{2k+1} W(l_1l_1l_2l_2; k\lambda)\langle l_1l_1 00|k0\rangle\langle l_2l_2 00|k0\rangle\Big\}, \tag{43}$$

where $W(l_1l_1l_2l_2; k\lambda)$ is a Racah coefficient[8]) and F^k stands for the Slater coefficient

$$F^k(n_1l_1, n_2l_2) = \tfrac{1}{2}(2k+1)\int_0^\infty\int_0^\infty\int_{-1}^1 R^2_{n_1l_1}(r_1)R^2_{n_2l_2}(r_2)V(|\mathbf{r}_1-\mathbf{r}_2|)P_k(\cos\omega)r_1^2\,dr_1\,r_2^2\,dr_2\,d\cos\omega \tag{44}$$

where ω is the angle between $\mathbf{r}_1$ and $\mathbf{r}_2$.

Comparing (43) with (27), and using the orthogonality relation[8]) for Racah coefficients, we obtain

$$F^k(n_1l_1, n_2l_2) = (2k+1)^2[(2l_1+1)(2l_2+1)\langle l_1l_1 00|k0\rangle\langle l_2l_2 00|k0\rangle]^{-1} \sum_\lambda\{(2\lambda+1)(-1)^\lambda W(l_1l_1l_2l_2; k\lambda)\sum_{p=0}^{\rho}[C_c(n_1l_1, n_2l_2, \lambda, p)I_p]\}. \tag{45}$$

In (45) we have a closed expression for the Slater coefficients in terms of Talmi integrals.

In using tables 2 and 3, it is to be noted that though all values are given to eight significant digits, the last of these may be out by several units, due to the accumulation of rounding-off errors in the calculations. Thus $B(04, 04, 4)$ in table 2 can be taken as equal to 1.

Within the limits of rounding-off errors, all values in tables 2 and 3 obey the sum rules

$$\sum_p (p+\tfrac{3}{2})B(nl, n-1\,l+2, p) = -2\sqrt{n(n+l+\tfrac{3}{2})}, \quad \sum_p B(nl, nl, p) = 1, \tag{46}$$

which are easily obtained from the definition (14) together with (9) and (13).

One of us (G. J.) is indebted to the University of Rio Grande do Sul, Pôrto Alegre, Brasil, and to the Comisión Nacional de Energía Nuclear (México), for financial support during his stay in Mexico as a participant in the Latin American School of Physics.

The tabulation of the coefficients $B(nl, n'l', p)$, as well as the tabulation of the transformation brackets, was done with the 650 IBM machine at the University of Mexico. We are indebted to Ing. S. Beltran for making available the machine for the present calculations and to Raúl Ortega for help in carrying them out.

References

1) M. Moshinsky, Nuclear Physics **13** (1959) 104
2) T. A. Brody, Rev. Mexicana de Fisica **8** (1959) 139
3) I. Talmi, Helv. Phys. Acta **25** (1952) 185
4) W. Magnus and F. Oberhettinger, Special Functions of Mathematical Physics (Chelsea Publishing Co., New York 1949) pp. 84, 85
5) M. Moshinsky, Nuclear Physics **8** (1958) 19
6) R. Thieberger, Nuclear Physics **2** (1956/57) 533
7) K. W. Ford and E. J. Konopinski, Nuclear Physics **9** (1958/59) 218
8) G. Racah, Phys. Rev. **62** (1942) 438

Note added in proof: The transformation brackets have also been discussed recently by R. D. Lawson and M. Goeppert-Mayer, Phys. Rev. **117** (1960) 174;
A. Arima and T. Terasawa, Progr. Theor. Phys. **23** (1960) 115

1.B

Nuclear Physics **17** (1960) 30—43; © *North-Holland Publishing Co., Amsterdam*

Not to be reproduced by photoprint or microfilm without written permission from the publisher

UPPER BOUND ON THE NEUTRON-DEUTERON DOUBLET SCATTERING LENGTH

LARRY SPRUCH

Physics Department, Washington Square College, New York University, New York and Physics Department, University of Washington, Seattle, Washington †

and

LEONARD ROSENBERG

Institute of Mathematical Sciences, New York University, New York ††

Received 13 January 1960

Abstract: The method of obtaining upper bounds on scattering lengths is applied to the determination of the n—d doublet scattering length A_D. A new calculation is unnecessary; an analysis of the trial function used by Efimov in a variational estimate of A_D shows that that calculation effectively provides a bound. (The Efimov trial function has the 'inappropriate' normalization for present purposes, but it is exceedingly unlikely that this will alter the character of the present results. This question can be readily resolved in any case.) We find that the potentials assumed by Efimov imply $A_D < 1.1 \times 10^{-13}$ cm. If these potentials are accurate (this question is still an open one), it follows that of the two experimentally allowed sets, namely $A_D = 0.7 \times 10^{-13}$ cm and $A_Q = 6.4 \times 10^{-13}$ cm (Set I), or $A_D = 8.3 \times 10^{-13}$ cm and $A_Q = 2.6 \times 10^{-13}$ cm (Set II), Set I is correct, a conclusion consistent with some recent variational estimates of about 6×10^{-13} cm for the quartet scattering length A_Q. It is also shown, for the general problem, that the exact numerically determined value of the 'static' scattering length lies above the true value if the number of bound state solutions for the static and true problems are the same.

1. Introduction

It has been known for almost ten years on the basis of experimental data [1]) that the neutron—deuteron (n—d) quartet (A_Q) and doublet (A_D) scattering lengths are given by one of the following two sets

$$\begin{aligned} &\text{I.}\quad A_D = (0.7 \pm 0.3)f, \quad A_Q = (6.38 \pm 0.06)f, \\ &\text{II.}\quad A_D = (8.26 \pm 0.12)f, \quad A_Q = (2.6 \pm 0.2)f, \end{aligned} \tag{1}$$

where the length $f = 10^{-13}$ cm. However, in spite of the great difference between the two sets (the two values of A_D differ by an order of magnitude), previous

† Permanent address, New York University.

†† Sponsored by the Geophysics Research Directorate of the Air Force Cambridge Research Center, Air Research and Development Command, and by the Office of Ordinance Research, U. S. Army.

attempts to resolve the ambiguity have not, in our opinion, been conclusive.

The difficulties in arriving at an unambiguous decision are two-fold in origin:

(1) The two-body potential has been rather poorly known until recently, and it is of course by no means clear that it is well known now. (It will be assumed throughout that three-body interactions are negligible. There is no really strong evidence that this is so, and the assumption is made for purposes of simplicity.) It is true that the parameters which are chosen to characterize the two-body potential are chosen to fit the two-body data so that there is presumably some compensation for the incorrect form of the potential which is used, but it is anything but clear what the degree of compensation thereby afforded may be in the three-body n—d calculation under consideration.

(2) The fact that the n—d system contains more than 2 particles makes the calculation of the scattering lengths extremely difficult, so much so that the tensor character and the repulsive core of the interaction have in almost all cases been deliberately ignored. Further, and this is an essential point, it was not in the past possible to make any reliable estimates whatever of the errors introduced into the calculation by the various approximations which were used.

The second difficulty remains for all approximations not based on a variational approach. For a variational approach, however, it has recently been shown [2–4]) that it is possible for a wide variety of cases to obtain one bound, the upper one, on the scattering length. The calculations which determine the upper bound are no more difficult than a standard variational calculation, though for some cases the trial function must satisfy, not simply the usual boundary conditions, but also a relatively slight subsidiary condition.

The ability to obtain even one bound very much alters the character of the problem; while the first difficulty noted above is unaffected, the second is greatly reduced. Thus, if the upper bound on either the doublet or quartet scattering length lies below the larger of the two possible values for that scattering length, then to the extent that the potential used is a reasonable representation of the true potential, but *independently* of the accuracy of the trial function, the smaller of the two possible values must be the correct one. (Clearly, if the bound lies below the smaller of the two possible values, the potential must be in error.)

The method of obtaining a bound has previously been applied to n—d quartet scattering [3]). That case is somewhat simpler than n—d doublet scattering since the incident neutron cannot be bound to the deuteron. The formulation which was given includes the possibility of tensor forces and spin-orbit couplings, but for purposes of simplicity we will here confine ourselves to the case of central forces. One then finds

$$A_Q \leqq A_{Qt} + \left(\frac{2\mu}{\hbar^2}\right) \int \Psi_{Qt}(H - E_d)\Psi_{Qt}\,d\tau. \qquad (2)$$

In this expression, H is the effective Hamiltonian for $L = 0$ and takes the form

$$H = -\left(\frac{\hbar^2}{2\mu}\right)\left[\frac{1}{r^2}\frac{\partial}{\partial r}r^2\frac{\partial}{\partial r}+\frac{1}{q^2}\frac{\partial}{\partial q}q^2\frac{\partial}{\partial q}+\left(\frac{1}{r^2}+\frac{1}{q^2}\right)\frac{\partial}{\partial p}(1-p^2)\frac{\partial}{\partial p}\right] \tag{3}$$
$$+V_{12}+V_{13}+V_{23}.$$

Here the V_{ij} are the (central) interparticle potentials. With the proton labelled by 1 and the neutrons by 2 and 3, the coordinates are defined by

$$\mathbf{r} = \left(\frac{3^{\frac{1}{2}}}{2}\right)(\mathbf{r}_2-\mathbf{r}_1), \quad r = |\mathbf{r}|;$$

$$\mathbf{q} = \mathbf{r}_3-\tfrac{1}{2}(\mathbf{r}_1+\mathbf{r}_2), \quad q = |\mathbf{q}|;$$

q is the distance of neutron 3 from the centre of mass of the remaining two particles; p is the cosine of the angle between $\mathbf{q}$ and $\mathbf{r}$. The ground state energy of the deuteron is denoted by $E_d (E_d = -2.2\ \text{MeV})$, and the reduced mass is given by $\mu = \frac{2}{3}M$, where M is the nucleon mass. The volume element is $d\tau = r^2 dr q^2 dq\, dp$. The trial function, Ψ_{Qt}, may be represented as

$$\Psi_{Qt} = \psi_{Q3t}-\psi_{Q2t},$$

where ψ_{Q2t} is obtained from ψ_{Q3t} by interchanging the neutron coordinates (space and spin); ψ_{Q3t} represents that portion of the trial function which remains finite when neutron 3 goes off to infinity. The boundary conditions satisfied by ψ_{Q3t} are

$$\begin{aligned} &\psi_{Q3t} \to 2^{-\frac{1}{2}}\chi_Q R_d(r)\frac{A_{Qt}-q}{q} && \text{for } q \to \infty, \\ &\psi_{Q3t} \to 0 && \text{for } r \to \infty, \end{aligned} \tag{4}$$

where χ_Q is one of the four totally symmetric quartet spin functions, $R_d(r)$ is the (exact) spatial part of the deuteron ground state function, normalized such that

$$2\int_0^\infty r^2 R_d^2(r)dr = 1,$$

and A_{Qt} represents a trial value for the quartet scattering length.

It follows from the above discussion that the Kohn variational principle represents not only a variational estimate of but an upper bound on A_Q. As one particular consequence, we have that the numerical solution of the static approximation (sometimes also referred to as the exchange approximation), in which the deuteron is considered unaffected by the incident neutron, though the Pauli principle is taken into account, provides an upper bound on A_Q. More generally, most of the variational calculations that have been performed can be utilized to provide an upper bound on A_Q.

The above method was used to deduce an upper bound on A_Q [3,5]); it turned out to be close to the larger of the two possible values. Even assuming that the potential used is rather good, this does *not* prove that the larger of the two possible values of A_Q, that associated with set I, is correct; it is conceivable that the trial function is a rather poor one and that the use of a better trial function could lower the upper bound to the smaller value of A_Q associated with set II. It is in fact clear that if one has only an upper bound expression, a calculation of A_Q cannot possibly rigorously prove the correctness of set I, however much it may indicate the preference for that set, though it might conceivably have proved the correctness of set II. On the contrary, a calculation of A_D could hope to prove rigorously the correctness of set I. We will therefore turn our attention to the calculation of A_D.

In section 2 the general method for obtaining an upper bound will be utilized to show that, if the assumed two-body potentials are reasonably accurate, set I is correct. In section 3, with the hope that it may be useful for problems still more difficult than n—d scattering, the possibility of the utilization of the simpler static approximation for the determination of an upper bound will be discussed. Section 4 includes a discussion of a number of previous calculations of n—d scattering lengths.

2. n—d Doublet Scattering

In the determination of an upper bound on A_D, we must take into account in the formalism the existence of a bound state of a neutron and a deuteron with a total angular momentum of $\frac{1}{2}$, *i.e.*, the existence of a stable H^3 nucleus. (The possibility of the actual capture of the neutron with the emission of a gamma ray is neglected.) The general approach for a problem of this type has recently been given [4]). Once again, for ease of exposition only, we assume central potentials. As applied to the problem at hand, the general result then reduces to

$$A_D \leqq A_{Dt} + \frac{2\mu}{\hbar^2}\int \Psi_{Dt}(H-E_d)\Psi_{Dt}\,d\tau - \frac{2\mu}{\hbar^2}\frac{[\int \Psi_{Bt}(H-E_d)\Psi_{Dt}\,d\tau]^2}{E_{Bt}-E_d}; \qquad (5)$$

H is given by (3), and Ψ_{Bt} is a triton trial wave function, normalized to unity, which must be sufficiently accurate to give binding, *i.e.*, we must have

$$E_{Bt} \equiv \int \Psi_{Bt} H \Psi_{Bt}\,d\tau < E_d.$$

Ψ_{Bt} is otherwise arbitrary. The trial scattering function may be represented as

$$\Psi_{Dt} = \psi_{D3t} - \psi_{D2t}, \qquad (6)$$

where ψ_{D3t} and ψ_{D2t} differ by an interchange of neutron coordinates; ψ_{D3t} is that portion of the trial function which remains finite when neutron 3 goes off to infinity. We may write ψ_{D3t} in the form

$$\psi_{D3t} = u_t \chi^{(S)}_{D12} + v_t \chi^{(A)}_{D12}. \tag{7}$$

Here $\chi^{(S)}_{D12}$ and $\chi^{(A)}_{D12}$ are doublet spin functions which are, respectively, symmetric and antisymmetric in the spin coordinates of particle 1, the proton, and particle 2, a neutron. The boundary conditions satisfied by u_t and v_t are

$$\left.\begin{aligned} u_t &\to 2^{-\frac{1}{2}} R_d(r)(A_{Dt}-q)/q \\ v_t &\to 0 \end{aligned}\right\} \quad \text{for } q \to \infty,$$
$$\left.\begin{aligned} u_t &\to 0 \\ v_t &\to 0 \end{aligned}\right\} \quad \text{for } r \to \infty, \tag{8}$$

where A_{Dt} is the trial doublet scattering length.

It has been shown [4]) that the above approach is entirely equivalent to a variational calculation in which a restriction is placed on the form of the trial function. Thus, if one writes

$$\Psi_{Dt} = \Psi_{Dt'} + b\Psi_{Bt}, \tag{9}$$

where b is a variational parameter which appears nowhere else, and where Ψ_{Bt} satisfies the conditions previously stated, the substitution of Ψ_{Dt} into the Kohn variational principle, with a variation of b, leads to a variational estimate of A_D which is precisely the right hand side of (5). In other words, the Kohn variational principle with the above form of trial function gives a bound on A_D.

We consider now the variational calculation of A_D performed by Efimov [6]). We ignore for the moment the fact that his trial function does not satisfy the required boundary conditions given in (8). (His trial function has what we have described as 'inappropriate normalization' for the purposes of obtaining a bound [7]).) His most complicated doublet trial function is of the form

$$\Psi_{Dt} = \Psi_{Dt'} + \sum_{m=1}^{3} b_m \exp[-\tfrac{1}{2}m\lambda^2(r^2+q^2)]\chi^{(A)}_{D23}, \tag{10}$$

where $\chi^{(A)}_{D23}$ is a doublet function antisymmetric in the neutron spin coordinates and where λ^{-1} is equal to $1.332\,f$, the range of the Gaussian potentials assumed by Efimov. (A Serber force mixture was chosen.) A simple calculation shows that the term in (10) corresponding to $m = 1$ gives a value of -8 MeV for the expectation value of the Hamiltonian. (No binding is obtained for the terms corresponding to $m = 2$ or 3.) It therefore follows that an upper bound on A_D will be obtained if, in the calculation performed by Efimov, the data are converted so that they correspond to the use of the 'appropriate' normalization, given by (8) †. A conversion procedure of this type, for the case where no bound states exist, has been described previously [2]). In the present case there is the

† It is necessary, at this point, to recognize the formal equivalence between the Rubinow variational principle, which Efimov used, and the Kato variational principle with $\theta = 0$ normalization (see ref. [2])).

additional requirement that the converted variational expression should have a vanishing derivative with respect to the parameter b. The necessary rearrangement of the various integrals which appear in the variational calculation, such that this condition is satisfied, is easily determined and we shall omit the details here.

Now it has been shown that if the scattering length is positive, as it is in the present case, and if the calculation is sufficiently accurate (this is defined more precisely in ref. [2])) this conversion will provide a lower, and therefore improved, estimate of the scattering length †. We therefore conclude that the value obtained by Efimov is itself an upper bound on A_D, *i.e.*,

$$A_D < 1.1\, f. \tag{11}$$

(Similarly, we expect that the estimate of A_Q obtained by Efimov is an upper bound. Of course, a final verification should be made for both the doublet and the quartet cases by actually performing the conversion to the appropriate normalization of the Efimov data.) Thus we have the result that either Set I gives the correct values of the n—d scattering lengths, or else the assumed potentials so poorly represent the actual situation that they imply a value of A_D which is too small by a factor $\gtrsim 8$. The latter alternative seems to us to be rather unlikely, particularly since variational estimates of the quartet scattering length, based on the same potentials, turn out to be quite close to the value corresponding to Set I (see table 1). In any event the issue has been freed of the ambiguity usually present due to inaccuracies in the approximate solution of the three-body Schroedinger equation.

3. The Static Approximation

The methods we have developed for obtaining an upper bound on the scattering length when the total number of bound states which exist is known may be applied to more complicated problems, such as n—t or n—α scattering, where no bound states exist, or p—H^3 scattering, in which case a bound state does exist for one of the spin states. [In the last case, account must be taken of the presence of a Coulomb interaction between the scattered particle and the scattering system, but this is, at least in principle, a straightforward matter [7]).] However, it may be some time before it will be reasonable for such cases to attempt a realistic variational calculation of the type performed for n—d scattering by a number of people [6, 8, 9]). For the more complicated cases, it would be desirable to be able to extract a bound from the still difficult but

† This conversion procedure, in the form appropriate to the case where no bound states exist, has been applied in the n—d quartet problem, as discussed in ref. [3]). In that case the conversion *did* provide a slightly lower estimate of the scattering length; there is no reason to suspect a different behaviour in the doublet case.

relatively simpler problem of scattering in the static approximation. We will now show how this may be possible for these cases. For simplicity, we consider in detail the particular example of the static approximation in n—d doublet scattering. The treatment for other problems would be similar in character.

Consider the trial function Ψ_{Dst}, in which we choose (see (6) and (7))

$$\begin{aligned} v_{\mathrm{st}} &= 0, \\ u_{\mathrm{st}} &= 2^{-\frac{1}{2}} R_{\mathrm{d}}(r) f_{\mathrm{t}}(q)/q. \end{aligned} \tag{12}$$

From (8) we see that $f_{\mathrm{t}}(q)$ satisfies the boundary conditions

$$\begin{aligned} &f_{\mathrm{t}}(0) = 0, \\ &f_{\mathrm{t}}(q) \to A_{\mathrm{Dst}} - q \quad \text{for } q \to \infty. \end{aligned} \tag{13}$$

With this form of trial function the first integral which appears in (5) may be written

$$\begin{aligned} \int \Psi_{\mathrm{Dst}}(H-E_{\mathrm{d}})\Psi_{\mathrm{Dst}}\,\mathrm{d}\tau &= 2\times 2^{-\frac{1}{2}} \int [f_{\mathrm{t}}(q)/q] R_{\mathrm{d}}(r) \chi^{(\mathrm{S})}_{\mathrm{D}12}(H-E_{\mathrm{d}})\Psi_{\mathrm{Dst}}\,\mathrm{d}\tau \\ &= \int_0^\infty f_{\mathrm{t}}(q)\bar{H}(q) f_{\mathrm{t}}(q)\,\mathrm{d}q. \end{aligned} \tag{14}$$

The operator $\bar{H}(q)$ thus defined is just the integro-differential operator originally considered by Buckingham and Massey [10]) in their application of the static approximation to n—d scattering. The static approximation was also studied by Motz and Schwinger [11]); their formulation involved the use of a Green's function.

A considerable amount of work has been performed in finding exact numerical solutions of the static (or one-body) equation

$$\bar{H}(q) f(q) = 0 \tag{15}$$

with boundary conditions

$$\begin{aligned} &f(0) = 0, \\ &f(q) \to A_{\mathrm{Ds}} - q \quad \text{for } q \to \infty \end{aligned} \tag{16}$$

for a variety of assumed potentials [12–15]). It has been pointed out previously that a calculation based on the static approximation is variational in character. We will now show that we can in fact say more than that, namely, that the exact static scattering length A_{Ds} provides an upper bound on the true scattering length A_{D}, provided that a bound state exists for the operator $\bar{H}(q)$. More precisely, the condition that a bound be obtained is that it must be possible to find a trial triton wave function Ψ_{Bt} of the form

$$\Psi_{\mathrm{Bt}} = 2^{-\frac{1}{2}} R_{\mathrm{d}}(r)[f_{\mathrm{Bt}}(q)/q]\chi^{(\mathrm{S})}_{\mathrm{D}12} - (2 \leftrightarrow 3) \tag{17}$$

with

$$f_{Bt}(0) = 0, \qquad f_{Bt}(q) \to 0 \quad \text{for } q \to \infty, \tag{18}$$

such that

$$\int \Psi_{Bt}(H - E_d)\Psi_{Bt}\,d\tau = \int_0^\infty f_{Bt}\bar{H}f_{Bt}\,dq < 0.$$

If such a function Ψ_{Bt} can be shown in some fashion to exist (we need not actually exhibit it) we may formally substitute it in the expression (5) for the bound on A_D. If, further, we choose the trial scattering function as the exact solution of the static problem, we see that each of the integrals in (5) contains the vanishing factor $\bar{H}(q)f(q)$ in the integrand. Therefore, the inequality

$$A_D \leqq A_{Ds}$$

is established.

We note that in general, if one bound state exists in the static problem, as well as in the true problem, the exact static scattering length represents the best (i.e., lowest) value that can be determined from the Kohn variational principle with a trial function which is of the static form, and which contains as one of its terms a trial bound state function sufficiently accurate to give binding. The analogous result in the case when no bound state exists for the true problem, namely, that a Kohn variational calculation in which a static trial function is employed gives a result lying above the exact static scattering length was proved in the Appendix of ref. [3]).

The existence of a negative energy state for the static operator $\bar{H}(q)$ can be established by numerical methods similar to those used in solving the static scattering problem. We wish to point out, however, that the existence of a bound state is strongly suggested by data already available, namely that the static zero energy scattering function $f(q)$ has a node. The following argument, though not entirely rigorous, is offered in support of the statement that a node in the zero energy scattering function implies that a bound state exists.

Consider the integro-differential equation [10])

$$\bar{H}_\lambda g_\lambda(q) = \left[-\frac{3\hbar^2}{4M}\frac{d^2}{dq^2} + \lambda V\right] g_\lambda(q) = 0 \tag{19}$$

with boundary conditions

$$g_\lambda(0) = 0, \qquad \left.\frac{dg_\lambda(q)}{dq}\right|_{q=0} = 1. \tag{20}$$

[These boundary conditions differ from those previously placed on $f(q)$. However, since the two solutions, for a given potential strength λ, will differ only by a numerical factor, the proof may be carried through in terms of $g_\lambda(q)$]. For the actual potential, corresponding to $\lambda = 1$, we know from various numerical calculations that $g_1(q)$ has one node and will therefore have, asymp-

totically, a negative slope. On the other hand $g_0(q)$ is simply q, and therefore has a positive slope everywhere. If we assume that the asymptotic slope is a continuous function of λ, there exists some value of λ, to be denoted by λ_0, where $0 < \lambda_0 < 1$, for which the asymptotic slope of $g_{\lambda_0}(q)$ is zero. Since $g_{\lambda_0}(q)$ is a zero energy solution, the expectation value of $\bar{H}_{\lambda_0}(q)$ with respect to $g_{\lambda_0}(q)$ vanishes, *i.e.*,

$$\langle \bar{H}_{\lambda_0} \rangle_0 = \langle T \rangle_0 + \lambda_0 \langle \mathscr{V} \rangle_0 = 0. \tag{21}$$

Now from (21) and from the fact that $\langle T \rangle_0 > 0$ (as may be seen from an integration by parts, using the asymptotic form of g_{λ_0}) we have that $\langle \mathscr{V} \rangle_0 < 0$ and therefore that $\langle \bar{H}_1(q) \rangle_0 < 0$. This would imply the existence of a bound state for $\bar{H}_1(q)$ were it not for the fact that $g_{\lambda_0}(q)$ is not quadratically integrable and hence is not an admissible trial function. This offers no real difficulty since the function $g_{\lambda_0}(q)e^{-\tau q}$ *is* quadratically integrable, and the expectation value of $\bar{H}_\lambda(q)$ is a continuous function of τ at $\tau = 0$.

The proof as given above, while suggestive, is incomplete (*e.g.*, the assumed continuity of the asymptotic slope of the wave function with respect to λ, as well as the uniqueness of the solution of (19) with boundary conditions given by (20), have not been verified). In the case when the potential is a function, not an integral operator, the result we seek (indeed, a much more general result) can be obtained rigorously provided the potential falls off rapidly enough [16]). It seems very likely that the result is valid for the present problem as well, in spite of the weaknesses in the proof that we have pointed out. Thus, on the one hand, even though it includes an integral operator component, the potential is effectively short ranged in the sense that the wave function rapidly achieves its asymptotic form, as can be seen from the numerical calculations. Further, we are here concerned with the case in which the spatial part of the wave function is of mixed symmetry, and the lack of uniqueness which is found in the static quartet problem seems to arise specifically from the fact that there the wave function is spatially antisymmetric †.

If it is in fact true that a bound state exists for the static n—d problem, then the static calculations (see table 1), which provide values of A_{Ds} lying between the two experimentally allowed values of A_D, prove, to the extent that the assumed potentials are accurate, that Set I is correct. Of course, we had already

† See ref. [27]). In the quartet case the solution $f(q)$ of the integro-differential equation is determined only up to an arbitrary multiple of an 'energy-independent' solution $\phi(q)$. Swan [27]) shows that if this lack of uniqueness in $f(q)$ is removed by imposing a certain orthogonality condition on $f(q)$ [see (68) in ref. [27])] then $f(q)$ has one, and only one, node. This is shown to follow from the existence of the non-physical solution of the static equation $\phi(q)$, and the fact that no physical bound states exist for the static quartet problem. Since $\phi(q)$ vanishes asymptotically, the asymptotic form of $f(q)$ is unique; the question of nodes can be disregarded in an exact numerical determination of the scattering length. (Actually, an energy-independent solution is displayed by Swan only for the particular case when the deuteron wave function is assumed to be a Gaussian and there is some question, at least in our minds, whether the argument has general validity.)

TABLE 1

A survey of some n—d scattering length calculations

Approach	References and Notes	Doublet result	Quartet result	Implied Set
static approximation, numerically	ref. [13])	$A_{Ds} = 1.52\,f$	$A_{Qs} = 5.33\,f$	I
	[a])	$A_{Ds} = 2.72\,f$	$A_{Qs} = 5.24\,f$	I
variational calculation, polarization considered	ref. [8])	$A_D \approx 5.5\ f$	$A_Q \approx 6.5\ f$	I
	[b])	—	$A_Q < 5.7\ f$	I
	[c])	$A_D < 1.1\ f$	$A_Q < 6.3\ f$	I
	[d])	$A_D \approx 2.97\,f$	$A_Q < 5.72\,f$	I
zero range approximation	ref. [22])	$A_D \approx 3.0\ f$	$A_Q \approx 5.1\ f$	I
exclusion principle	ref. [23])	—	$A_Q >$ radius of deuteron $\approx 4.3\,f$	I
effective range expansion	ref. [18])	Theory excludes Set I		II
equivalent n—d potential	[e])	Theory excludes Set I		II

[a]) Burke and Robertson, ref. [14]). Results of a similar character are obtained in refs. [12]) and [15]).

[b]) Spruch and Rosenberg, ref. [3]). This bound was calculated from the numerical data determined by Sartori and Rubinow in obtaining the result given in ref. [8]). Additional numerical results, based on the method of the present authors and the data of ref. [8]), have been given by Rubinow and Sartori, ref. [5]).

[c]) Bounds deduced with the method of the present authors, ref. [3]), and the result for A_D of the present paper, from the variational calculation of Efimov, ref. [6]). The question of inappropriate normalization remains.

[d]) Burke and Haas, ref. [9]). We have expressed the quartet result as an inequality, according to the general result of ref. [3]). Here and in some other cases, the implication for set I follows from the approximate value of A_Q, not from the inequality for A_Q.

[e]) Delves and Brown, ref. [19]). Tensor forces were included in this calculation.

arrived at this conclusion using a different and essentially rigorous argument (see section 2); the validity of our conclusions is then *not* dependent on the existence of a static bound state, and the present section has been included only because of its possible utility for problems more complicated than n—d scattering.

4. Discussion

We have shown that on the basis of the central potentials assumed by Efimov and others, the scattering lengths given by Set II (see (1)] may be unambiguously excluded. The following discussion will be based on the tentative

assumption that the central potentials are sufficiently accurate to determine the correct scattering lengths. We are of course aware of the fallibility of this assumption, particularly since these same potentials give too much binding for the triton. It seems, nevertheless, a reasonable one to make since the variational estimates of *each* scattering length is quite close to the value associated with Set I.

It is of some interest at this point to survey briefly some of the rather large number of calculations in which attempts were made, with a variety of approximations, to decide on the correct set of n—d scattering lengths (see table 1). We will here somewhat arbitrarily consider only calculations performed within the past decade. We do this partly because many of the earlier calculations were performed with potentials which are no longer considered sufficiently accurate, and because some of the later calculations encompass much of the earlier material. Review material on n—d scattering is contained in an article by Verde [17]).

The calculations of Prohammer and Welton [18]), Delves and Brown [19]), Gordon [20]) and Troesch and Verde [21]) (we have referred to only the first two of these in table 1) lead to what we believe to be the erroneous conclusion that Set II is correct. It is then worthwhile to attempt to understand the reasons for the apparent failure of the methods used in these calculations. (It should be remarked that in most cases the authors stressed the fact that by virtue of the approximations which had been made their conclusions were tentative; in one case the result was never published.)

To begin with we note, as we have previously [3]), that there exist Kohn type variational calculations, in which polarization was ignored, whose predictions of the quartet scattering length A_Q is less than A_{Qs}, the exact (numerically determined) value of the scattering length in the static approximation. Such results violate the minimum property of A_{Qs} with respect to all Kohn variational estimates of A_Q in which the trial function is restricted according to the static approximation [3]). The explanation of this violation is almost certainly the crudity of the representation of the deuteron wave function. Since in these cases the same poor deuteron wave function was used in the doublet calculation as used for A_Q, it follows that the extimate of A_D can be quite far off.

We now turn to some of the other, non-variational, calculations which predict Set II. Here the analysis cannot be expected to be so simple since there are no rigorous criteria whatever with regard to the errors introduced by the approximation.

The unpublished but oft quoted calculation of Prohammer and Welton [18]) was based on the shape-independent approximation, which relates the binding energy, the scattering length, and the effective range. More serious than the (necessarily) somewhat arbitrary choice of the effective range is the question of the validity of the approximation itself, since it involves the replacement of

the doublet n—d scattering wave function, for zero incident kinetic energy, by the ground state function of H^3, whose energy eigenvalue lies about 6.3 (*i.e.*, 8.5—2.2) MeV lower. The presence of the threshold for deuteron disintegration only 2.2 MeV above zero incident kinetic energy may well make significant the difference between these two wave functions even in the relevant region of small interparticle distances. Clearly, no definite conclusions can be reached on the basis of the effective range expansion until the contributions of the higher order terms have at least been estimated.

The recent calculation of Delves and Brown [19]) is notable in that tensor forces (though not repulsive cores) were retained. This was done, however, at the expense of having had to make several rather severe simplifications, including the complete neglect of the Pauli principle and the imposition of certain restrictions on the form of the scattering function. Therefore, despite the fact that they are able, on the basis of these approximations, to account qualitatively for some low energy angular distributions and neutron polarization data, we feel justified in maintaining serious reservations with regard to their conclusion that Set II is correct.

With regard to the calculations which led to Set I, it would seem that the approximations used to obtain this presumably *correct* result may now be used with somewhat greater confidence in other scattering problems. These include the static approximation [12–15]), the zero range approximation of Skorniakov and Ter-Martirosian [22]) and the primarily qualitative argument, based on the use of the exclusion principle, of Davydov and Filippov [23]).

The dispersion-theory approach which has recently come into being would seem to be very promising for the present poblem, and in fact just complements the variational method we have described, since one can hope to deduce certain results without a detailed knowledge of the potential. Dispersion theory has already been applied to the n—d problem [24]) but no conclusive results have as yet been obtained. Other approaches, which are of special interest because they too, do not require a detailed knowledge of the potential, lie in a comparison of experimental data with theoretical calculations for those processes for which the theoretical calculations can be based on a knowledge of n—d scattering data. Such processes include the $d+d \rightarrow p+H^3$ reaction [25]), and the photodisintegration process, $\gamma+H^3 \rightarrow n+d$, and its inverse [26]). If it should turn out, on the basis of analyses of the above type, or directly from experiment, that Set II is actually correct, the n—d variational calculation would take on added interest since the three-body problem would then appear to provide a much more sensitive check on the two-body potentials than has hitherto been suspected.

We should like to return our attention now to the more general problem. The method used here to obtain the upper bound on the scattering length is valid under rather general circumstances [3, 7]). For example, it may be used if

one desires to base the analysis of the scattering problem on the assumption of more realistic interparticle forces, i.e., those which include the tensor force and the repulsive core. The p—d problem may also be treated, in a quite similar way, though the numerical calculations would be very much more cumbersome owing to the presence of the Coulomb field. Further, more complicated systems, involving more than three particles, can be studied. It would probably be reasonable at the present time, owing to the tremendous complexity of such problems, to restrict attempts to the static approximation, which could be attacked either by an exact numerical analysis or by a variational calculation. In these cases the generalization, which we will now sketch, of the result of section 3 to the situation in which many bound states exist may be extremely useful. If there are N composite bound states, the last term in (5) is replaced by a sum of N such terms, involving a set of N orthonormal trial bound state functions [4]). If each of these functions can be chosen to be of the form prescribed by the static approximation, and still give binding, *i.e.*, if the total number of composite bound states is the same in the static problem as in the true problem, a straightforward extension of the proof given in section 3 shows that the static scattering length is an upper bound to the true scattering length.

One of us (L. S.) would like to thank the members of the Physics Department of the University of Washington for the many courtesies extended to him during his recent brief summer stay there.

References

1) D. G. Hurst and J. Alcock, Can. J. Phys. **29** (1951) 36;
E. O. Wollan, C. G. Shull and W. C. Koehler, Phys. Rev. **83** (1951) 700
2) L. Spruch and L. Rosenberg, Phys. Rev. **116** (1959) 1034
3) L. Spruch and L. Rosenberg, Phys. Rev. **117** (1960) 1095
4) L. Rosenberg, L. Spruch and T. F. O'Malley, Phys. Rev. in print
5) S. I. Rubinow and L. Sartori, Proceedings of the International Conference on Nuclear Forces and the Few Nucleon Problem, London, July 1959 (to be published by Pergamon Press)
6) Y. N. Efimov, JETP **35** (1959) 98
7) L. Spruch and L. Rosenberg, Proceedings of the Internal Conference on Nuclear Forces and the Few Nucleon Problem, July 1959 (to be published by Pergamon Press)
8) L. Sartori and S. I. Rubinow, Phys. Rev. **112** (1958) 214
9) P. G. Burke and F. A. Haas, Proc. Roy. Soc. A **252** (1959) 177
10) R. A. Buckingham and H. S. W. Massey, Proc. Roy. Soc. A **179** (1941) 123
11) L. Motz and J. Schwinger, Phys. Rev. **58** (1940) 26
12) R. A. Buckingham, S. J. Hubbard and H. S. W. Massey, Proc. Roy. Soc. A **211** (1952) 183
13) R. A. Christian and J. L. Gammel, Phys. Rev. **91** (1953) 100
14) P. G. Burke and H. H. Robertson, Proc. Phys. Soc. **70** (1957) 777
15) F. A. Haas and H. H. Robertson, Proc. Phys. Soc. **73** (1959) 160
16) N. Levinson, Mat. Fys. Medd. Dan. Vid. Selsk. **25**, No. 9 (1949)
17) M. Verde, Handbuch der Physik, Vol. **39** (Springer-Verlag, Berlin, 1957) p. 144
18) F. G. Prohammer and T. A. Welton, Quarterly Report ORNL 1005
19) L. M. Delves and D. Brown, Nuclear Physics **11** (1959) 432

20) M. M. Gordon, Phys. Rev. **80** (1950) 1111
21) A. Troesche and M. Verde, Helv. Phys. Acta **24** (1951) 39
22) G. V. Skorniakov and K. A. Ter-Martirosian, JETP **4** (1957) 648;
G. V. Skorniakov, Proceedings of the International Conference on Nuclear Forces and the Few Nucleon Problem, London, July 1959 (to be published by Pergamon Press)
23) A. S. Davydov and G. T. Filippov, JETP **4** (1957) 267
24) R. Blankenbecler, M. L. Goldberger and F. R. Halpern, Nuclear Physics **12** (1959) 629
25) R. Blankenbecler and R. Amado, private communication
26) L. M. Delves, private communication
27) P. Swan, Proc. Roy. Soc. A **228** (1955) 10

2.F

Nuclear Physics **17** (1960) 44—53; © *North-Holland Publishing Co., Amsterdam*

Not to be reproduced by photoprint or microfilm without written permission from the publisher

THE EXCHANGE TRANSFER REACTION $Al^{27}(N^{14}, Mg^{27})O^{14}$

J. J. PINAJIAN

Oak Ridge National Laboratory †, *Oak Ridge, Tennessee*

Received 15 February 1960

Abstract: The thick target yield was measured for the reaction $Al^{27}(N^{14}, Mg^{27})O^{14}$, which may be described as a simultaneous transfer of a neutron from one nucleus and a proton from the other. Mg^{27} was chemically separated and thick target yields were measured by absolute γ-counting. A second aluminium foil behind the target was used to determine the amount of Mg^{27} produced by neutrons in the target. The ratio of front to back foil Mg^{27} yield was 1.54: 1.00. Thick targets of ZnO were used to measure the yield of $O^{16}(N^{14}, 3p)Mg^{27}$. The cross section at 27.6 MeV was found to be 110 μb. The yield of Mg^{27} in the 10 Å oxide layer of the special aluminium foil targets was estimated to be 1.5 % of the total yield. The thick target yield of 9.45 min Mg^{27}, in aluminium, measured at 27.6 MeV incident energy, was found to be 13.6×10^{-13} per incident nitrogen ion after correction for neutron-induced Mg^{27}. The cross section is estimated to be 2.2 ± 1.0 μb. Mg^{27} cannot be produced by the evaporation of light particles as in Al^{27} $(N^{14}, 3\alpha 2p)Mg^{27}$. Other possible mechanisms for the production of Mg^{27} are examined and their cross sections are estimated.

1. Introduction

At the energies available at this laboratory (27.6 MeV), nitrogen-induced nuclear reactions may proceed by two major reaction mechanisms: one is the formation of some sort of compound nucleus and its subsequent de-excitation by light particles, and the other is a transfer of nucleons from one nucleus to another. In the past, transfer studies at the Oak Ridge National Laboratory have been confined to single particle transfers: (1) the transfer of a neutron from the incident nitrogen ion to the target nucleus in several light target-elements from Be to S[1–5]) and (2) the transfer of a proton in two light elements [1,2]). Neutron transfer was observed by the yield of 10.1 min N^{13}. Proton transfer was detected by the presence of 121 s O^{15}. The former process has also been observed in aluminium [6]), in aluminium and nickel [7]) and recently in copper and tin [8]). Neutron transfer in aluminium, copper and tin induced by O^{16} ions was also observed. Alpha-particle transfer yielding 112 m F^{18} has been reported [9]) from the bombardment of lithium chloride by N^{14}. Recently two-neutron transfer, yielding 7.4 s N^{16}, has been reported from the bombardment of lithium fluoride, copper and aluminium by nitrogen ions [10]). The cross section for two-neutron transfer with nitrogen ions on to aluminium is estimated to be ≈ 15 μb for an integrated energy spectrum from 92 to 55 MeV. A contact transfer mechanism

† Operated for the U. S. Atomic Energy Commission by Union Carbide Corporation.

has been suggested for the observation of (p, 2n) and (2p, 3n) transfer reactions in the N^{14} and O^{16} bombardment of aluminium, copper and tin [8]). At least part of the cross sections in these reactions may be due to single transfers and subsequent de-excitations [11]).

Breit and co-workers have studied theoretically the nucleon transfer process in heavy-ion reactions [12]). Recently, Goldansky [13]) has calculated the cross section for the exchange of neutrons between complex nuclei near the Coulomb barrier energy. He estimates the magnitude of this cross section to be between 1 and 10 μb.

It is the purpose of the present work to measure the cross section for the simultaneous transfer of a proton and a neutron: the proton is transferred from the aluminium nucleus to the nitrogen and the neutron is transferred from the nitrogen to the aluminium. The reaction is

$$Al^{27}+N^{14} \rightarrow Mg^{27}+O^{14}$$

and would be evidenced by the presence of 9.45 min Mg^{27}. The Q-value for this reaction, calculated for the ground state for both residual nuclei, is † -7.76 MeV. The residual nucleus Mg^{27} can be formed in other ways: (1) fission of the compound nucleus; (2) the evaporation of particles from the compound nucleus formed in the interaction of N^{14} and Al^{27}; (3) (n, p) reactions on Al^{27}, where the neutrons are produced in the target itself from (N^{14}, xn) reactions; (4) $O^{16}(N^{14}$, 3p)Mg^{27} reactions on the oxide layer of the aluminium foil; and (5) the production of an excited state in Al^{28} by neutron transfer and its subsequent de-excitation by proton emission. Although (1) is not ruled out, it is unlikely. Fission has not been observed in light elements by other processes of excitation than such as light-particle-induced reactions [15]) or photo reactions. At the incident nitrogen energy, the evaporation of enough particles from the compound nucleus Ca^{41} to give Mg^{27} is energetically forbidden. Spectrographic

TABLE 1

Spectrographic analysis † of $-$H19 temper 99.99 % Alcoa aluminium foil

Element	Cu	Fe	Mg	Mn	Na	Ni	Ti	V
Concentration (in %)	<0.02	<0.02	0.002 ††	<0.003	<0.01	<0.05	<0.003	<0.002

† The author is indebted to J. A. Norris of the Y-12 Spectrochemical Laboratory, Oak Ridge National Laboratory, for the spectrographic analysis.

†† Value reported obtained by densitometric analysis with precision of the order of ± 10 % or better.

analysis (see table 1) shows that the impurities are not present in quantities sufficient to yield Mg^{27} by evaporation reactions. Processes (3) and (4) were

† The Q-values are calculated from tables given by Wapstra [14]).

evaluated experimentally. Process (5) was estimated from the systematics of the cross section for neutron transfer in Al^{27} and de-excitation probabilities based on the statistical theory of nuclear reactions. Table 2 lists the nuclear reactions in aluminium foil which will yield Mg^{27} or radioactive residuals with half-lives of about 9.45 min.

TABLE 2

Possible reactions in the 27.6 MeV (lab) nitrogen bombardment of natural aluminium foil which lead to Mg^{27} or radio-active residuals with half-lives of about 9.45 min. See also sect. 2

Activity	Half-Life (min)	Reaction	σ at 24.5 MeV N^{14}
Mg^{27}	9.45	$Al^{27}(N^{14}, O^{14})Mg^{27}$ $O^{16}(N^{14}, 3p)Mg^{27}$ $Al^{27}(n, p)Mg^{27}$	
K^{38}	7.64	$Al^{27}(N^{14}, p2n)K^{38}$	3310 μb [3])
N^{13}	10.1	$Al^{27}(N^{14}, N^{13})Al^{28}$ $O^{16}(N^{14}, N^{13})O^{17}$	184 μb [3]) $<$120 μb [4])

A preliminary report [16]) of the search for this exchange transfer utilizing the $\approx$ 1.7 μA internal beam of the 160 cm ORNL cyclotron with 23.6 MeV (4.4 MeV full width at half maximum) nitrogen ions has been published. The uncertainties in the method of beam intensity measurement, the low average energy and the wide energy spread of the beam suggested use of the well-defined deflected beam with a concomitant energy increase of about 4 MeV. It also became apparent that with such a small cross section for the exchange transfer, the contribution of the oxygen in the oxide layer on the surface of the aluminium foil and the production of Mg^{27} by $O^{16}(N^{14}, 3p)Mg^{27}$ would have to be evaluated more carefully.

2. Experimental

High purity 6.2 mg/cm^2 aluminium foils † (99.99 %) with an oxide film of approximately 10 Å were bombarded with 27.6 MeV nitrogen ions in the deflected beam of the 160 cm ORNL cyclotron. The targets were 12 mm by 27 mm.

The foils were bombarded directly in a Faraday cup. The beam energy was determined by measurement of the range in nuclear emulsion of protons scattered at 0° from a hydrogen target [17]). The beam current was measured and

† The —H19 temper Al foils were preprared by F. Keller. The instructive discussions of F. Keller and L. M. Foster, Alcoa Research Laboratories, Aluminum Company of America, concerning the properties of oxide films of aluminium foils, is gratefully acknowledged.

integrated with an electrometer and was usually about 0.5 μA. Bombardments lasted 20 minutes.

The Mg^{27} was chemically separated (see sect. 2.6) and identified by its 9.45 min half-life † and by its characteristic gamma rays of 0.84 MeV ($\approx$ 70 %) and 1.02 MeV ($\approx$ 30 %).

Experimentally, there were two main problems: (1) to distinguish the Mg^{27} produced by exchange transfer from that produced in $Al^{27}(n, p)Mg^{27}$ and $O^{16}(N^{14}, 3p)Mg^{27}$ reactions and (2) to make sure that the 9 min activity is Mg^{27} and not 7.64 min K^{38} or 10.1 min N^{13}.

2.1. $Al^{27}(n, p)Mg^{27}$

The principal source of the fast neutrons is from (N^{14}, xn) reactions in the target. Two 0.0025 cm aluminium foils were used in the bombardments. The front foil was sufficiently thick to stop all the N^{+3} ions [3]). The ratio of the neutron flux in the first and second foils was calculated to be 1 : 0.81 assuming an isotropic distribution of neutrons. Correction for the forward motion of the centre-of-mass is negligible. From the knowledge of the Mg^{27} activity in the second foil, the contribution of neutron-induced Mg^{27} in the first foil reactions could be calculated. The only activity found in the second foil, aside from negligible amounts of K^{38} contamination introduced when the two foils were mechanically separated, was 9.45 min Mg^{27}; hence this foil could be counted directly. A third aluminium foil, of the same thickness, was placed directly behind the second foil. The neutron flux in the second and third foils was approximately the same. The counting rates of the second and third foils were, within the experimental error, the same. This served to demonstrate that there was no separation or buckling of the foils during the bombardments.

2.2. $O^{16}(N^{14}, 3p)Mg^{27}$

The oxygen is present on aluminium as an oxide layer. The Q-value for this reaction is -9.11 MeV. The excitation function was measured in a manner reported previously [19]). Thick target yields were obtained for O^{16} by bombarding thick ZnO targets containing oxygen in its natural abundance. No nuclear reactions were expected with Zn because of the high Coulomb barrier. Thin nickel foils varying from 0.59 to 2.4 mg/cm^2 were placed before the targets so that yields could be measured at various incident energies. Chemical separation of Mg^{27} was followed by beta counting (with γ-monitoring to detect possible K^{38} contamination). The yield per incident particle and the cross section for this reaction as a function of nitrogen energy are shown in figs. 1 and 2.

† The half-lives and branching ratios used in this work are based on the values given in ref. [18]).

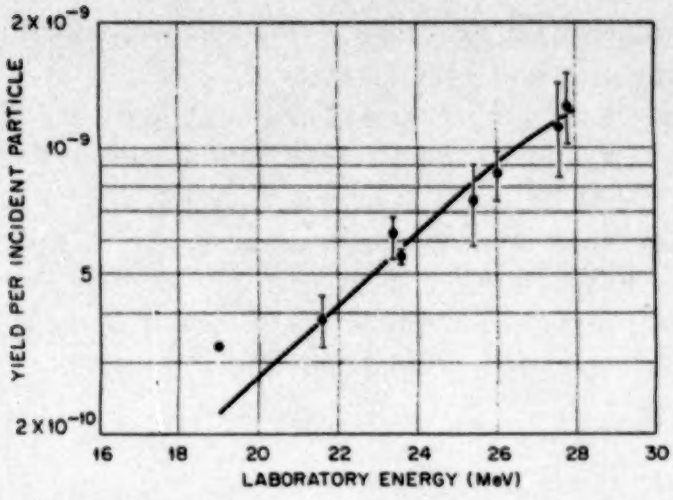

Fig. 1. The thick target yield of Mg^{27} produced by N^{14} bombardment of natural ZnO.

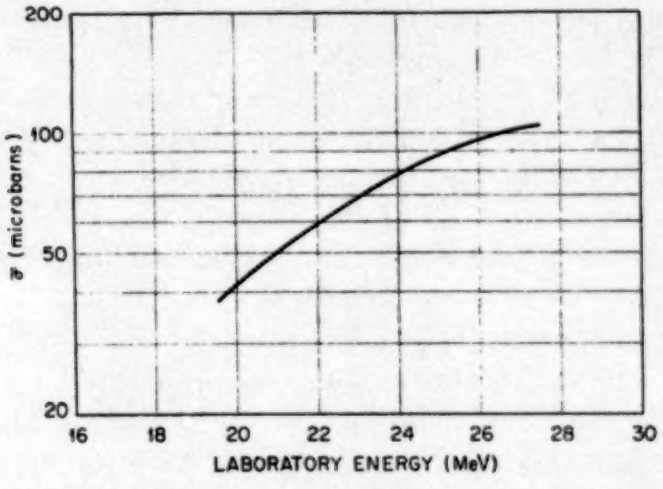

Fig. 2. Cross section for the production of Mg^{27} by N^{14} on O^{16}.

2.3. $Al^{27}(N^{14}, N^{13})Al^{28}$ AND $O^{16}(N^{14}, N^{13})O^{17}$

The interference of 10.1 min N^{13} activity was minimized by the chemical separation procedure. Selective gamma counting eliminated the possibility of its interference.

2.4. $Al^{27}(N^{14}, p2n)K^{38}$

The 7.64 min K^{38} activity is a problem because of its large production cross section [3]), gamma radiation and half-life. The radioactive decay of K^{38} is characterized by β^+ emission followed by a 2.16 MeV gamma ray. In the regions of interest for γ-counting of Mg^{27}, i.e. 0.84 MeV and 1.02 MeV, there existed the possibility that Compton electrons from the 2.16 MeV K^{38} gamma ray would be observed and mask the Mg^{27} lines. Therefore, bombardments of Al^{27} were made in which chemically separated K^{38} (see appendix) was analyzed under the same conditions (range of gamma spectrum, absorber and geometry). The ratio

of the peak height of the annihilation radiation to the Compton continuum between 0.84 and 1.02 MeV was found to be 35 to 1. In the course of Mg^{27} counting, the 0.51 MeV annihilation quanta were included in the analysis in order to demonstrate the absence of objectionable quantities of K^{38}.

2.5. GAMMA-COUNTING

The wet $MgC_2O_4 \cdot 2H_2O$ samples, in stainless steel counting cups, were covered with masking tape to reduce geometry changes due to moisture loss and placed over a 2.5×3.8 cm NaI(Tl) crystal. Care was taken to select a crystal with low Cs^{137} background. For Cs^{137}, the resolution of the NaI(Tl) crystal was 7.38 % and the peak to valley ratio was 23 : 1. A 0.47 cm brass absorber, placed between the sample and the detector, prevented the 1.75 MeV β^- of Mg^{27} from entering the crystal. The gamma spectrum from 0.20 to 2.35 MeV was measured with a 256-channel pulse height analyzer. The total counting rate in the region from 0.775 to 1.15 MeV was plotted as a function of time and a graphic analysis was made of the decay curve. To reduce uncertainties of calibration, the second foil was gamma counted with the same crystal, while the first foil was being chemically processed.

The efficiency of the NaI(Tl) crystal was measured by gamma counting Sc^{46} samples and beta counting the same samples with helium-filled end-window Geiger counters. The Geiger counter absolute efficiences were measured, in a manner described previously [19]), with a calibrated RaDEF source obtained from the National Bureau of Standards. The gamma radiation associated with Sc^{46} decay is 0.885 MeV and 1.119 MeV. Thus, it was possible to arrive at an efficiency of the NaI(Tl) crystal for the mixture of 0.84 and 1.02 MeV quanta associated with Mg^{27} decay.

3. Calculations and Results

The counting rate obtained from the graphical analysis of the decay curves was corrected for the scintillation crystal efficiency, chemical yield and decay during bombardment, and the yield of Mg^{27} per incident particle was calculated from the integrated beam current. The front-foil yields were about 50×10^{-12} per incident nitrogen ion. The average ratio of the front-foil yield to the back-foil yield was 1.54 : 1.00. The contribution of the neutron induced activity in the front-foil yields was determined from the knowledge of the back foil yields and geometry considerations. At 27.6 MeV, the cross section for the production of Mg^{27} by $O^{16}(N^{14}, 3p)Mg^{27}$ is 110 μb. The yield per incident particle in the 10 Å oxide layer was calculated to be 0.7×10^{-12}. Of the front foil Mg^{27} activity, approximately 67 % was due to neutron-induced Mg^{27} activity and approximately 1.5 % was due to the Mg^{27} activity produced in the oxide layer. The net Mg^{27} yield presumably is due to exchange transfer, and averaged 13.6×10^{-12}.

To obtain the cross section from thick target data, normally a smooth line is drawn to fit the experimental yield points as a function of energy. This curve is then differentiated in order to obtain the cross section as a function of energy. The relation can be expressed as

$$\bar{\sigma} = \frac{\Delta Y}{I \Delta E} \frac{M}{N_0} \frac{I}{\rho} \frac{\mathrm{d}E}{\mathrm{d}x},$$

where $\Delta Y/I\Delta E$ is the change in thick target yield per incident particle and per increment of energy ΔE of the incident nitrogen ions, M is the molecular weight of aluminium, N_0 is Avogadro's number and $\mathrm{d}E/\rho \mathrm{d}x$ is the stopping power of aluminium for nitrogen ions averaged over the energy interval E to $E+\Delta E$.

In this experiment the yield was measured at one energy only. If one assumes that at 27.6 MeV the shape of the yield curve for the exchange transfer is the same as the shapes of the yield curves for neutron transfer in Mg^{24}, Mg^{25}, Mg^{26} and Na^{23}, the average reduction in thick target yield per incident particle will be ≈ 34 %, i.e. $\Delta Y/I\Delta E = 0.34Y/I\Delta E$, where $\Delta E = 2$ MeV. The cross section for the nitrogen-induced Mg^{27} in aluminium may then be calculated using an extrapolation of the experimentally known stopping power of aluminium for nitrogen ions [3]). The cross section obtained in this fashion is found to be 2.2 ± 1.0 μb.

The error given is an estimated error. The uncertainties reflect on the error in two ways: (I) is there, in the aluminium matrix of the front foil, any nitrogen-induced Mg^{27} and (II) if so, how much? Uncertainties in (1) poor counting statistics, (2) chemical yield determinations and (3) impurities in the target contribute to (I) and (II), while (4) possible variations in the beam energy and (5) uncertainties in Geiger counter calibration, (6) scintillation crystal calibration (7) the stopping power of aluminium for nitrogen ions, and (8) the shape of the yield curve contribute to (II).

The errors associated with the poor counting statistics and the chemical yield determinations are estimated to be ≈ 20 %. Actually this is felt to be a conservative estimate since the consistency of the front foil to back foil ratios was good; the standard deviation was less then 5 %.

The results of a spectrographic analysis of the aluminium foil used in the bombardments are shown in table 1. Neutron transfer on Mg^{26} should be considered. About 11 % of the magnesium impurity is Mg^{26}. The neutron-transfer cross section for $Mg^{26}(N^{14}, N^{13})Mg^{27}$ has been measured [4]). At this energy, the yield of Mg^{27} per incident particle in the first 0.2 mg of the aluminium foil (i.e. a thickness equivalent to 3 MeV where more than 90 % of the yield is produced) would amount to 0.9×10^{-13}, a factor of 100 smaller than the yield for the reaction of interest.

Items (4) through (7) will make the absolute magnitude of the cross section uncertain by about 30 %. It is difficult to estimate the error associated with

the shape of the yield curve. The limits, of course, are that the curve falls off sharply or does not fall off at all. The former situation would yield a cross section approaching 6.6 μb as an upper limit. The latter would reduce the cross section. However, the Coulomb barrier is what influences the shape of the curve and this will cause the yield to fall off with energy. In the absence of any real information, it is felt that the assumption made is the most reasonable.

While there is considerable error in the magnitude of the cross section, there can be little doubt that Mg^{27} is produced by N^{14} on Al^{27}.

4. Discussion

More than 30 % of the total front foil Mg^{27} activity is induced by nitrogen in aluminium. We consider the following reactions:

(1) $Al^{27}(N^{14}, Mg^{27})O^{14}$ ($Q = -7.8$ MeV),
(2) $Al^{27}(N^{14}, Mg^{27})pN^{13}$ ($Q = -12.4$ MeV),
(3) $Al^{27}(N^{14}, Mg^{27})3\alpha 2p$ ($Q = -21.6$ MeV).

The first is the simplest and has the most favourable Q-value. The third is energetically forbidden since the available energy in the centre-of-mass system is only 16.8 MeV.

The second reaction can be either a three-body disintegration or the formation of Al^{28} in an excited state by neutron transfer, and its subsequent de-excitation by proton evaporation [10,11]). In the latter case, the threshold for proton emission by Al^{28} is 9.5 MeV and the exit barrier for the proton is 2.9 MeV, so that an excitation of about 13 MeV in the Al^{28} is needed for an appreciable yield of Mg^{27}. The "universal curve" for the neutron transfer cross section [4]) may be used to estimate its cross section. From such an estimation the cross section is less than 0.5 μb. Certainly not more than 10 % of these states in Al^{28} de-excite by proton emission since the threshold for neutron emission is at 7.7 MeV. Thus, probably less than 0.05 μb can be attributed to this mechanism.

Nothing is known about three-body disintegration in this type of reaction. However, since the cross section of transfer reactions are strongly Q-dependent, it is likely that reaction (1) is favoured over (2).

The cross section for the exchange transfer (neutron in, neutron out) reaction near the barrier, according to the quasi-classical calculations of Goldansky [13]) is estimated to be 1 to 10 μb. Since proton and neutron single transfer have about the same cross section at low atomic number, one would expect the calculation of the cross-section for (p, n) exchange transfer reaction to predict the same value. In spite of the very approximate nature of the calculations it is interesting to note that it agrees with the results of this experiment.

The author wishes to thank A. Zucker for his suggestions, help and interest during the experiment. He would also like to thank M. L. Halbert for help and many discussions. The help of J. G. Harris in the construction of the apparatus and of G. A. Palmer, H. L. Dickerson and A. W. J. Riikola for cyclotron bombardments is gratefully acknowledged. R. H. Bassel and R. M. Drisko are to be thanked for their calculations of the neutron flux.

Appendix

MAGNESIUM CHEMISTRY

The front foil was dissolved in 6*N* NaOH with K and Mg carrier. Potassium fluoride carrier was added and 12*N* HCl was added to dissolve the $Mg(OH)_2$. Boric acid was added to complex the fluorine activity present. The Mg was precipitated by the addition of NaOH pellets, heated, cooled and centrifuged. The $Mg(OH)_2$ was dissolved in HCl, KCl, KF and $AlCl_3$; and then H_3BO_3 was added and the Mg again precipitated. The $Mg(OH)_2$ was dissolved in warm glacial acetic acid with a minimum amount of 12*N* HCl, brought to a volume of 40 ml with 17.4*N* $HC_2H_3O_2$, and the Mg precipitated with 5 ml of a hot saturated solution of $(NH_4)_2C_2O_4$. The $MgC_2O_4 \cdot 2H_2O$ was washed with glacial acetic acid containing H_3BO_3, transferred to a counting cup, covered and gamma-counted. The time required was 20 to 25 min. The chemical yield was determined, after counting, by titration with disodium dihydrogen ethylenediamine tetraacetate with Eriochrome Black-T as the indicator. Chemical yields varied between 60 % and 80 %.

POTASSIUM CHEMISTRY

The supernatant from the first hydroxide precipitation (see above) was used to separate K^{38}. The solution was adjusted to pH $\approx$ 4 with HCl with methyl orange as the indicator. Then 10 ml of a citrate buffer (pH = 2.9) was added and 50 ml of 0.6 % sodium tetraphenylboron was used to precipitate the potassium. The $K(C_4H_5)_4B$ was washed with water containing HF, transferred to a tared counting cup, dried and counted.

References

1) H. L Reynolds and A. Zucker, Phys. Rev. **101** (1956) 166
2) H. L. Reynolds, D. W. Scott and A. Zucker, Phys. Rev. **102** (1956) 237
3) W. H. Webb, H. L. Reynolds and A. Zucker, Phys. Rev. **102** (1956) 749
4) M. L. Halbert, T. H. Handley, J. J. Pinajian, W. H. Webb and A. Zucker, Phys. Rev. **106** (1957) 251
5) D. E. Fisher, A. Zucker and A. Gropp, Phys. Rev. **113** (1959) 542
6) K. F. Chackett and J. H. Fremlin, Phil. Mag. **45** (1954) 735;
G. A. Chackett, K. F. Chackett and J. H. Fremlin, Phil. Mag. **46** (1955) 1
7) V. V. Volkov, A. S. Pasiuk and G. N. Flerov, JETP **33** (1957) 595

8) R. Kaufmann and R. Wolfgang, Phys. Rev. Letters **3** (1959) 232
9) D. G. Alkhazov, Iu. P. Gangrskii and I. Kh. Lemberg, JETP **33** (1957) 1160
10) V. A. Karnaukhov, G. M. Ter-Akopian and V. I. Khalizov, JETP **36** (1959) 748
11) A. Zucker, Phys. Rev. Letters (in press)
12) G. Breit, Phys. Rev. **102** (1956) 549;
G. Breit and M. E. Ebel, Phys. Rev. **103** (1956) 679; **104** (1956) 1030
13) V. I. Goldansky, Nuclear Physics **9** (1958/1959) 551
14) A. H. Wapstra, Physica **21** (1955) 367
15) B. L. Cohen, Phys. Rev. **102** (1956) 453
16) J. J. Pinajian, Bull. Am. Phys. Soc. **4** (1959) 219
17) H. L. Reynolds, D. W. Scott and A. Zucker, Phys. Rev. **95** (1954) 671
18) D. Strominger, J. M. Hollander and G. T. Seaborg, Rev. Mod. Phys. **30** (1958) 585
19) J. J. Pinajian and M. L. Halbert, Phys. Rev. **113** (1959) 589

9.B.

Nuclear Physics 17 (1960) 54—66; © North-Holland Publishing Co., Amsterdam

Not to be reproduced by photoprint or microfilm without written permission from the publisher

ENERGY LOSS OF HEAVY IONS IN NICKEL, OXYGEN, AND NUCLEAR EMULSION

P. G. ROLL † and F. E. STEIGERT

Sloane Physics Laboratory, Yale University, New Haven, Connecticut ††

Received 12 Febuary 1960

Abstract: Range-energy relations for He^4, B^{10}, B^{11}, C^{12}, N^{14}, O^{16}, F^{19} and Ne^{20} ions in oxygen and nickel have been measured in the energy range 2 to 10 MeV per amu (atomic mass unit). Together with similar relations for heavy ions in nuclear emulsions, reported in an earlier paper [2]), these have been differentiated numerically to obtain specific energy loss relations. The effective charge of heavy ions passing through matter, as well as the relative stopping power per atom of oxygen, nickel and emulsion, have been computed from these and compared with theoretical predictions. From this comparison, it has been concluded that fairly reliable calculations of specific energy losses and/or range-energy relations can be made for various heavy ion species in different stopping media.

1. Introduction

In performing experiments with beams of accelerated heavy ions, it is necessary to know the energy loss of the ions in the various materials through which they pass. Nickel foil is one of the more useful and readily available materials for constructing high-strength windows for use with high-current ion beams. The interest in oxygen stems from experiments currently in progress at this laboratory, using gaseous oxygen targets. Consequently, it was of paramount interest to carry out measurements of the range-energy relations for He^4, B^{10}, B^{11}, C^{12}, N^{14}, O^{16}, F^{19} and Ne^{20} ions in both of these materials. By differentiating these relations to obtain the specific energy loss $-\mathrm{d}E/\rho\mathrm{d}x$, two other useful types of information can be obtained; the effective charge of a heavy ion passing through matter, and the relative stopping power of different materials. This information is presented for nuclear emulsion as well as nickel and oxygen, since the measurements in emulsion, reported in an earlier paper [2]), are considerably more accurate.

A few determinations of the energy loss of heavy ions in various metal foils [3, 4]) and gases [5, 6]) have been made at energies less than 2 MeV per amu. It is only recently that these have been extended to higher energies. In conjunction with his work on the luminescent response of a KI crystal to energetic C^{12} ions, Burcham [7]) has determined the range-energy relation for C^{12} in aluminium up

† General Electric Edwin W. Rice, Jr. Fellow, 1958—59.

†† This work has been supported by the Office of Naval Research and the U. S. Atomic Energy Commission. A preliminary report of it appears in ref. [1]).

to 114 MeV. Oganesyan [8]) has published some data on the range-energy relations for C^{12}, N^{14} and O^{16} ions in aluminium, as well as C^{12} and O^{16} in copper and gold, for energies between 50 and 110 MeV. Finally, Dr. L. C. Northcliffe of this laboratory has recently completed precise and comprehensive determinations of the range-energy relations of He^4, B^{10}, B^{11}, C^{12}, N^{14}, O^{16}, F^{19} and Ne^{20} ions in aluminium [9]), for energies up to 10 MeV per amu. Because of the paucity of experimental data, reliance in the past has been placed on theoretical or semi-empirical calculations of energy losses. Using a semi-empirical method of estimating the effective ion charge z^* as a function of ion velocity, Papineau[10, 11]) has computed range-energy relations for various heavy ions in aluminium, copper and lead. Grinberg and Lemberg [12]) have recently reviewed some of the possible methods of obtaining specific energy loss relations in cases where measurements are not available.

2. Apparatus and Procedure

The apparatus used in this work is the same as that described in ref. [2]) and is shown in fig. 1. To reduce its intensity, the analysed beam from the Yale

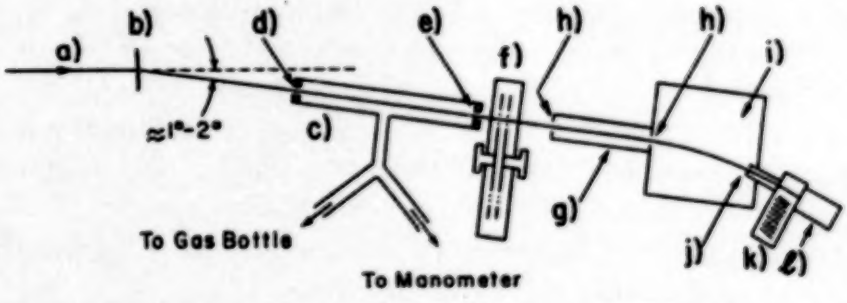

Fig. 1. Schematic diagram of apparatus. a) Analysed heavy ion beam; b) thin scattering foil; c) gas range cell; d) nickel window (5 μm); e) nickel window (2.5 μm); f) foil changer; g) laminated iron magnetic shield; h) collimating slits (0.013 cm); i) magnet pole face; j) exit slit (0.015 cm); k) nuclear emulsion plate magazine (not used here); l) scintillation counter.

Heavy Ion Linear Accelerator is scattered at a small angle from a thin foil. After energy degradation in either the gas range cell or the foil changer, the ions pass through two 0.013 cm collimating slits mounted on the ends of a laminated iron tube. This tube serves to shield the ions from the fringing field of the magnet until they emerge from the second slit, which is positioned close to the edge of the magnet pole faces. Following a circular trajectory of known radius in the field, the ions then pass through a 0.015 cm detector slit located inside the pole faces, and are detected in a scintillation counter. By using a counting rate meter, as well as observing the pulse rate on an oscilloscope screen, the magnetic field could be adjusted to maximize the counting rate. The energy of ions emerging from the gas range cell or the foils in the changer could then be determined from the measured magnetic field and the

known radius of curvature. During a run, the beam analyser magnet (not shown in fig. 1) maintained the initial beam energy constant to within ± 1 %.

The nickel foils used were cut with a punch of accurately known area and weighed on an analytical balance, resulting in an average foil thickness accurate to better than ± 1 %. Similar foils are reported to have a thickness variation averaging about ± 1.4 % from point to point [13]). Uniformity of the foils used here was checked on a larger scale by weighing pieces cut from different parts of a 15×20 cm sheet. The thickness of such pieces proved to be constant to within 2 or 3 %.

A mercury manometer was used to measure gas pressure in the range cell. This, together with the temperature and the length of the cell (about 1 m), was sufficient to determine the thickness of gas with a precision ranging from better than ± 1 % for thicknesses greater than 15 mg $\cdot$ cm^{-2}, to about 2 % for the smallest thicknesses. The gas used was U.S.P. tank oxygen, guaranteed better than 99 % pure.

Magnetic field measurements were made to a precision of a few tenths of a per cent, using both a commercial nuclear magnetic resonance gaussmeter and a calibrated series resistance in the magnet circuit. Finally, the radius of curvature of ions passing through the centers of the collimating and detector slits was determined optically to an accuracy of about 0.3 %. Details of this measurement are discussed in ref. [2]).

It should be remarked that, because of the severe collimation of the ion beam, the maximum angle through which an ion can be scattered in the absorbing material and still be detected is less than 2 minutes of arc. Hence, the contribution of nuclear scattering to the stopping power of the absorber is not likely to be measured in these experiments.

3. Results

The range-energy relations obtained for heavy ions in oxygen and nickel are graphed in figs. 2 and 3, respectively. All data have been normalized to an initial energy of 10 MeV per amu. The curves displayed are best fits to the data. Typical experimental points are indicated for O^{16} ions, and in the case of nickel, also for He^4. The curve which has been used to fit the He^4 data is that compiled by Whaling [14]).

As pointed out above, the foil or gas thickness, magnetic field and radius of curvature can all be determined to an accuracy of about ± 1 %. The principle source of possible error is the precision with which the collimated beam of ions can be centered on the detector slit. At higher energies, this can be accomplished with reasonable accuracy, but as the energy decreases, straggling in the absorber broadens the energy distributions of ions entering the magnetic field. At the same time, more of the ions will begin to pick up electrons, so that the popula-

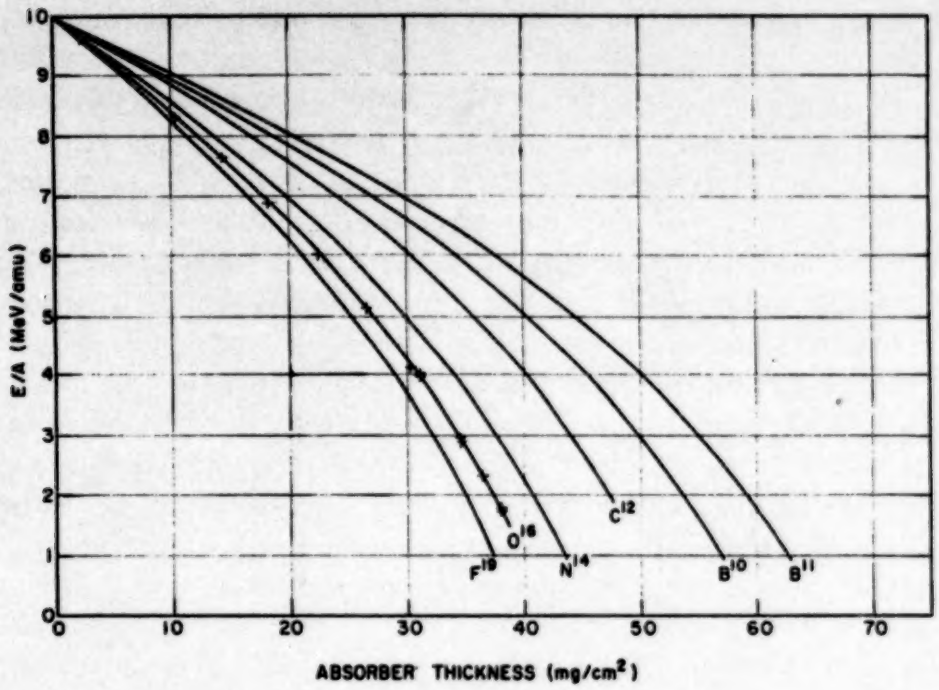

Fig. 2. Range-energy relations for heavy ions in oxygen gas. Typical experimental points are shown for O^{16} ions.

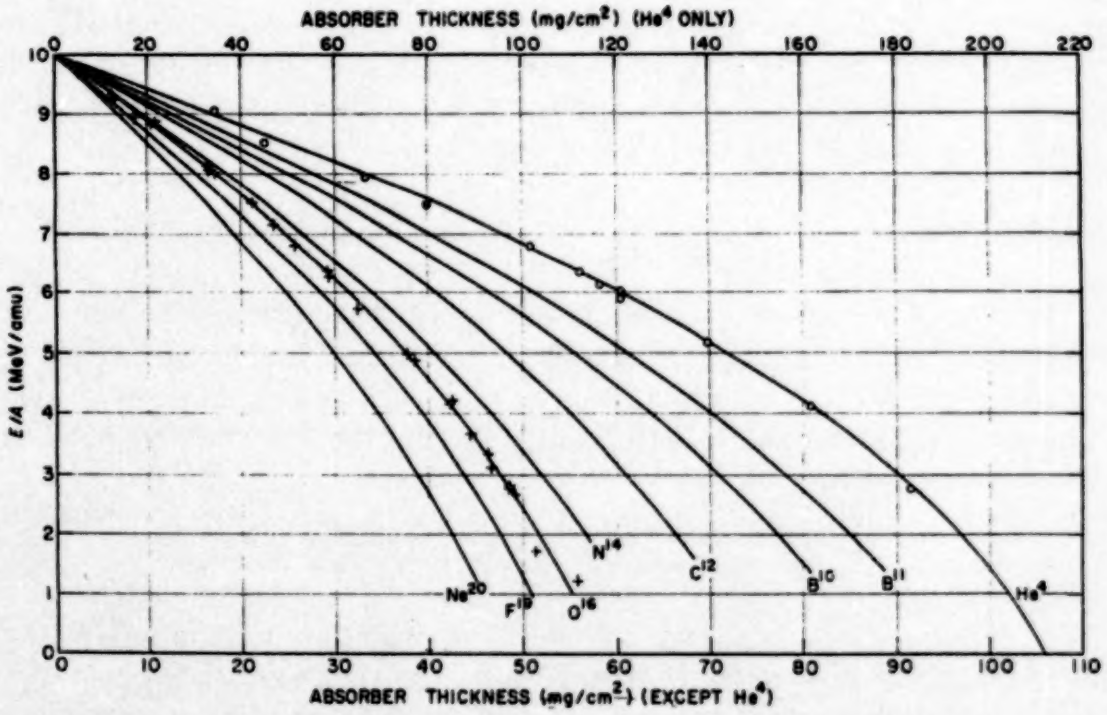

Fig. 3. Range-energy relations for heavy ions in nickel. To avoid confusion on the curves, typical experimental points are shown only for O^{16} and He^4 ions below about 9.3 MeV per amu. The solid curve with which the He^4 data have been fitted is that given by Whaling [14]).

tions of charge states $z-1$ and, eventually, $z-2$ will become comparable in magnitude with the maximum charge state z. Finally, an increase in multiple scattering in the thicker absorber, together with the broadening of the energy and charge distributions, seriously reduce the counting rate at energies below about 4 MeV per amu. Hence, as the energy is reduced, the counting rate becomes a less sharply peaked function of magnetic field, and the counting rate distributions from different charge states begin to overlap. Observation of these effects during the course of the experiments has led to the conclusion that the maximum possible experimental error in the energy, as given by the curves of figs. 2 and 3, is ± 0.2 MeV per amu. It is expected that the energies may be considerably more accurate than this. The good agreement between Whaling's results [14]) and the experimental data shown for He^4 in fig. 2 tend to support this expectation. In addition the few range-energy points measured by Oganesyan [8]) for C^{12} and O^{16} in copper agree quite well with the present work for nickel. (The range-energy relations for copper and nickel should be identical to within 1 % or so; cf. ref. [14]).)

For use in computing effective charge z^* and relative stopping power, the curves of figs. 2 and 3 have been differentiated numerically to obtain the specific energy loss relations $-\mathrm{d}(E/A)/\rho\mathrm{d}x$ versus E/A, shown in figs. 4 and 5. Similar curves for heavy ions in nuclear emulsion are shown in fig. 6. These have obtained by differentiating the more accurate range-energy relations presented in ref. [2]). The increased accuracy of the emulsion data is evident particularly at low energies, where the decrease in $-\mathrm{d}(E/A)/\rho\mathrm{d}x$ due to electron capture is marked. It must be emphasized that, because small differences have been taken in the process of differentiation, the accuracy of the specific energy losses may be considerably less than that of the range-energy relations themselves.

4. Effective Charge

The principle difference between the passage of heavy ions and protons or α particles through matter is the variation in the charge of the heavy ion due to electron capture and loss. The usual equation for specific energy loss, if it is to be valid for heavy ions, must be written with the effective ion charge z^* in place of the nuclear charge z:

$$-\frac{\mathrm{d}E}{\rho\mathrm{d}x} = \frac{4\pi z^2 e^4}{m_e v^2}\left(\frac{z^*}{z}\right)^2 \frac{NZ'}{A'} \ln\left(\frac{2m_e v^2}{I}\right), \qquad (1)$$

where v refers to the velocity of the incident ion, and Z', A', ρ, and I refer to the nuclear charge, atomic number, mass density and average excitation potential of the stopping material [15]) †. For protons or α particles of energy greater than

† Eq. (1) is valid theoretically only if the parameter $ze^2/\hbar v \ll 1$. This assumption is of course violated by the heavy ions under investigation here.

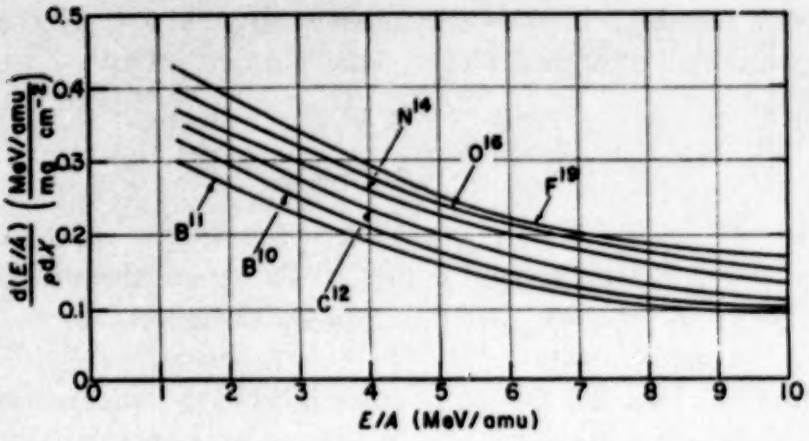

Fig. 4. Specific energy loss relations for heavy ions in oxygen gas. Curves obtained by numerical differentiation of range-energy relations shown in fig. 2.

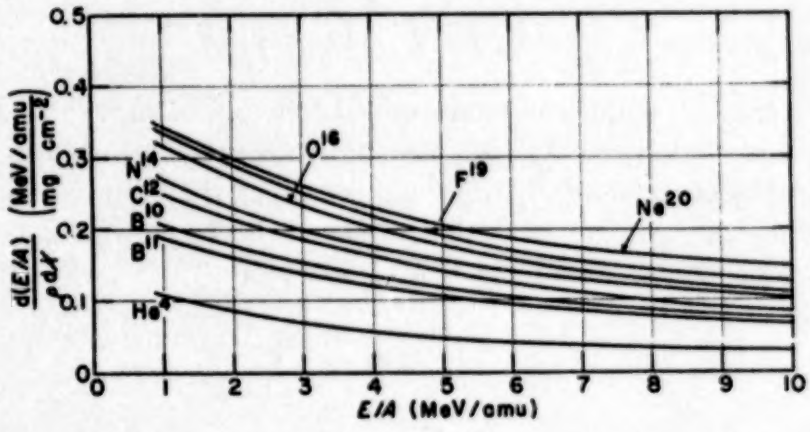

Fig. 5. Specific energy loss relations for heavy ions in nickel. Curves obtained by numerical differentiation of range-energy relations shown in fig. 3.

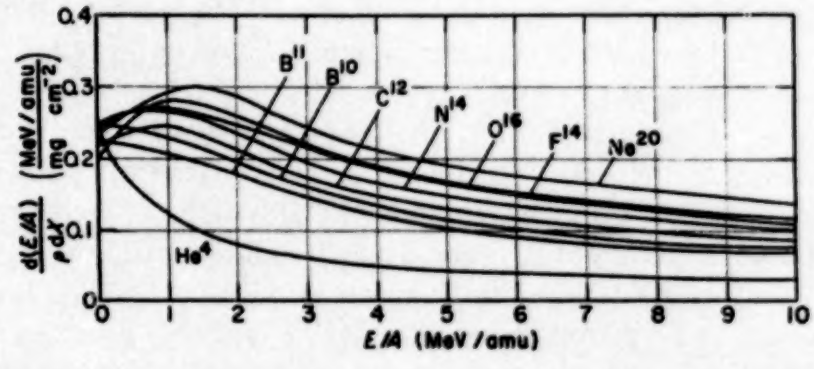

Fig. 6. Specific energy loss relations for heavy ions in nuclear emulsion. Curves obtained by numerical differentiation of curves shown in fig. 3 of ref. [1]).

about 1.0 MeV per amu, the ratio z^*/z is essentially unity [15]). Hence, the effective charge of an ion of nuclear charge z may be defined as

$$\left(\frac{z^*}{z}\right)^2 = \frac{(\mathrm{d}E/z^2\rho\mathrm{d}x)_z}{(\mathrm{d}E/z^2\rho\mathrm{d}x)_{p,\alpha}}, \tag{2}$$

where the specific energy losses of heavy ion and proton or α particle are evaluated at the same velocity, or, equivalently, at the same value of E/A. It is not intended here to ascribe any particular physical significance to z^* beyond defining it in terms of a ratio of specific energy losses.

It is customarily assumed that a nucleus will begin to capture electrons when its velocity v decreases to about the velocity v_e of an orbital electron in its atom. In the earliest work on fission fragment range-energy, Knipp and Teller[16]) and others computed orbital electron velocities using the Fermi-Thomas model of the atom. This predicted the effective charge as a numerical function of the form

$$\frac{z^*}{z} = f\left(\frac{v_e}{v}\right) = f\left(\frac{\beta}{z^{\frac{2}{3}}}\right), \quad \beta = \frac{v}{c}. \tag{3}$$

Papineau [10]) used an empirically-determined function of such form to compute his range-energy relations. As has been most recently mentioned by Northcliffe [9]) and Heckman *et al.* [17]), one might expect that, for heavy ions with velocities somewhat greater than that of the highest velocity K electron, the functional dependence should approach the form

$$\frac{z^*}{z} = f\left(\frac{v_K}{v}\right) = f\left(\frac{\beta}{z}\right), \tag{4}$$

where v_K is the velocity of the K electron.

Using eq. (2) and the specific energy losses from figs. 4, 5 and 6, $(z^*/z)^2$ has been computed as a function of both Fermi-Thomas and K-electron velocities. In the cases of nickel and emulsion, the He^4 data from figs. 5 and 6 has been used in the denominator of eq. (2). Since He^4 data was not obtained for oxygen gas, the range-energy relation given by Whaling [14]) for protons in oxygen was differentiated and used in this equation. The results are displayed in figs. 7—10. A comparison between the two velocity dependences has been made for the most accurate data (nuclear emulsion) in figs. 7 and 8. While the energy loss curves are not sufficiently accurate to permit precise quantitative conclusions, a general trend is noticeable. At lower velocities, the scatter of points is less when $(z^*/z)^2$ is plotted in terms of the Fermi-Thomas velocity, while at higher velocities, the scatter is less in terms of the K-electron velocity. This is just the type of behaviour suggested by Northcliffe and Heckman. Since data for nickel and oxygen are available and accurate only for higher velocities, $(z^*/z)^2$ has been graphed only as a function of K-electron velocity β/z for these materials

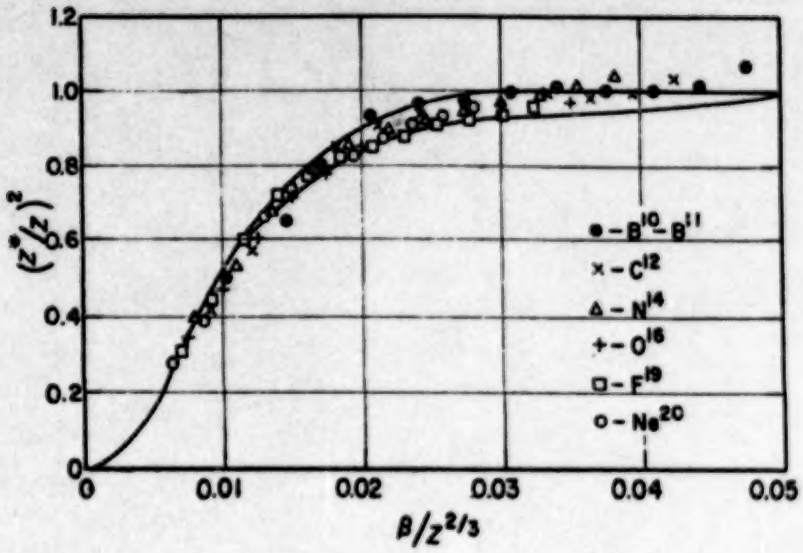

Fig. 7. Effective charge of heavy ions in nuclear emulsion, as a function of the ratio of ion velocity to Fermi-Thomas electron velocity. The solid curves shown are those used by Papineau [10, 11]).

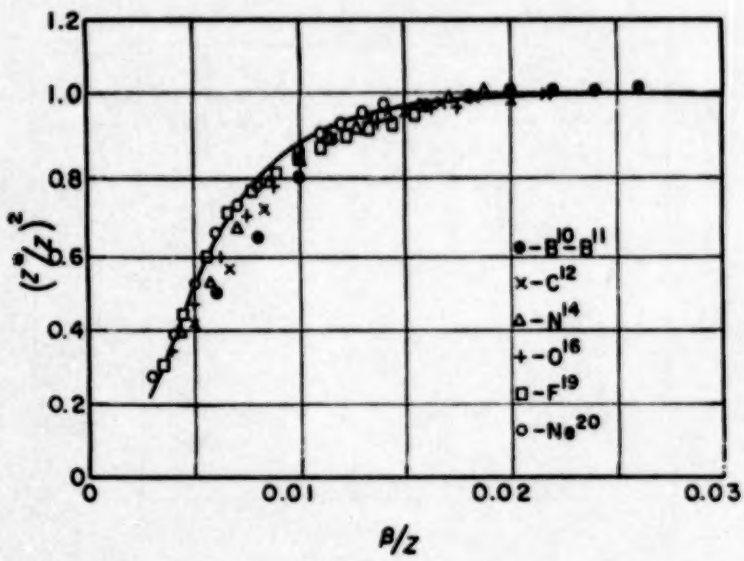

Fig. 8. Effective charge of heavy ions in nuclear emulsion, as a function of the ratio of ion velocity to K-electron velocity. The solid curve shown is that obtained by Northcliffe [9]) for heavy ions in aluminium.

(figs. 9 and 10). The decreased accuracy of the nickel and oxygen measurements is evidenced here by the greater scatter of points, as compared to the results for emulsion.

The solid curve on figs. 8, 9, and 10 is a best fit to a similar analysis for $(z^*/z)^2$ carried out by Northcliffe [9]) for his accurate aluminium range-energy measurements. Due to the limited accuracy of such an analysis, no significant differences in $(z^*/z)^2$ are apparent for emulsion, nickel, oxygen and aluminium. However, definite systematic trends are noticeable. The $(z^*/z)^2$ curve for heavy

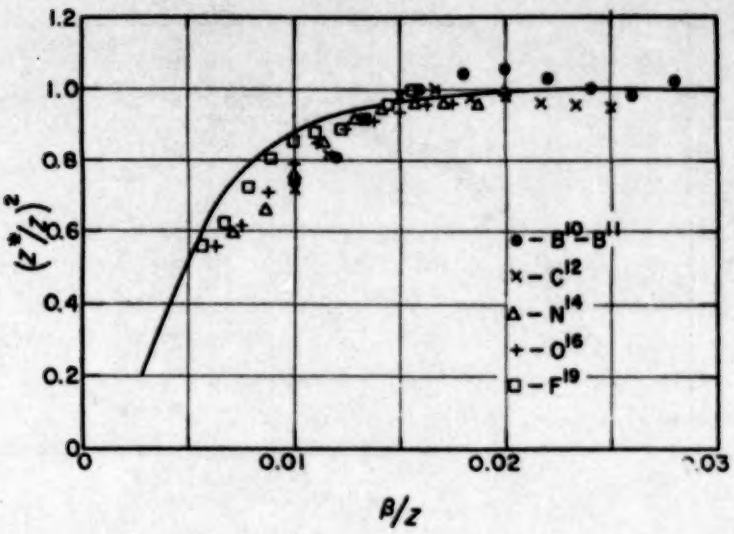

Fig. 9. Effective charge of heavy ions in oxygen gas, as a function of the ratio of ion velocity to K-electron velocity. The solid curve shown is that obtained by Northcliffe [9]) for heavy ions in aluminium.

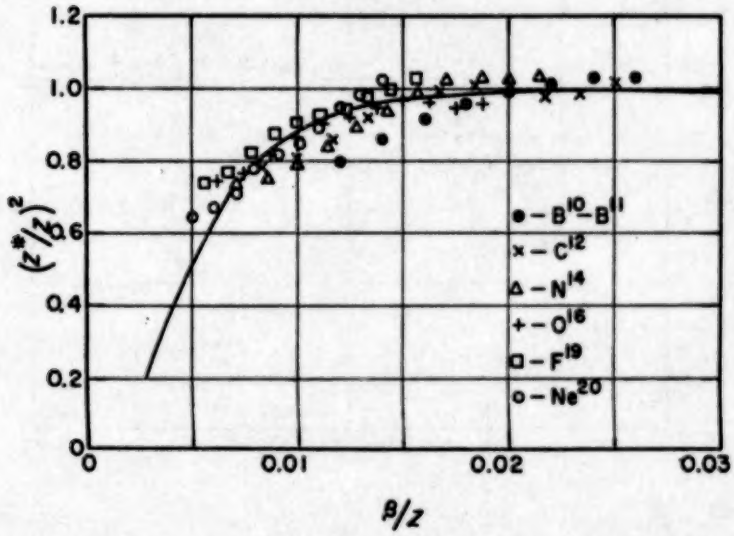

Fig. 10. Effective charge of heavy ions in nickel, as a function of the ratio of ion velocity to K-electron velocity. The solid curve shown is that obtained by Northcliffe [9]) for heavy ions in aluminium.

ions in oxygen is systematically low (fig. 10). In contrast, the scatter of points for nickel seems to straddle the solid curve for aluminium (fig. 9). Such systematic dependences of effective charge on stopping material have been discussed theoretically by Bohr and Lindhard [18]), and observed for fission fragments by Lassen [19]). Bohr and Lindhard propose that electron capture and loss from excited states of the ion will contribute to an increased effective charge in dense materials. In gases, the time between collisions will be sufficient for the excitation to spread itself over other electrons in the ion, as well as for radiative

de-excitation to occur. Collisions occur so frequently in solids, however, that an electron captured into an excited state will be more likely lost in a subsequent collision, due to its weaker binding, before it can lose its high excitation by radiation or sharing. Furthermore, these effects are likely to be more serious for highly charged (i.e., fast, light) heavy ions, with which the present work is concerned. In such cases, there will be more unoccupied quantum states of high excitation available, and fewer or no additional captured electrons with which excitation energy can be shared.

The effective charge in emulsion (fig. 9) also would appear to be slightly less than that in the metal foils. However, the complex composition of emulsion, as well as contributions to the rate of energy loss by nuclear elastic scattering, would render any comparison of doubtful value.

The utility of having available relations between effective charge and ion velocity is in computing heavy ion range-energy relations which have not been measured experimentally. Using a procedure such as that of Papineau [10]), together with proton or α-particle range-energy relations in a particular material, the evidence is that such calculations can be carried out with some degree of confidence. Some improvement might be noted by using different effective charge relations for gases and solids, as indicated, for instance, by figs. 8, 9 and 10.

5. Relative Stopping Power per Atom

Another quantity which is useful for determining the energy loss of heavy ions in matter is the relative stopping power. If the specific energy loss per atom of stopping material is denoted by the stopping cross-section [14])

$$\varepsilon = -\frac{1}{N}\frac{\mathrm{d}E}{\mathrm{d}x}, \tag{5}$$

where N is the number of stopping atoms per cm^3, then the stopping power of a substance relative to some standard material is defined as [20])

$$S = \frac{\varepsilon}{\varepsilon_0}, \tag{6}$$

where ε_0 is the stopping cross-section of the standard material. Assuming eq. (1) to be valid for heavy ions, the relative stopping power per atom is given theoretically by

$$S = \frac{Z'[\ln\,(2m_e c^2\beta^2) - \ln \bar{I}] - C_K(\beta, Z')}{Z'_0[\ln\,(2m_e c^2\beta^2) - \ln \bar{I}_0] - C_K(\beta, Z'_0)}. \tag{7}$$

An additional term $C_K(\beta, Z')$ has been included to correct for non-participation of K electrons in the energy loss processes [15, 20]). The average excitation

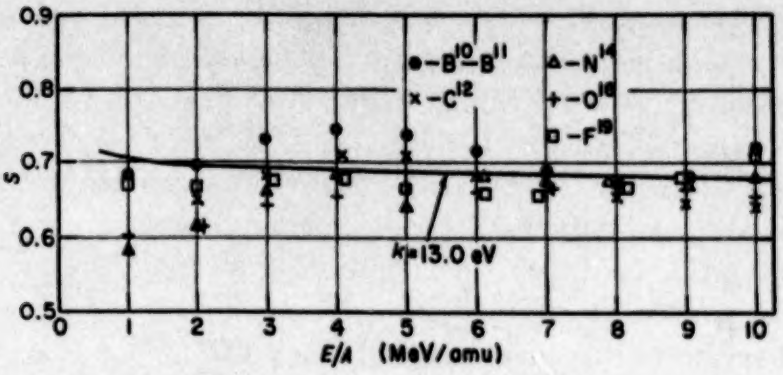

Fig. 11. Relative stopping power per atom for heavy ions in oxygen gas. Data are relative to the range-energy measurements for heavy ions in aluminium of Northcliffe [9]). The solid curve has been computed from eq. (7).

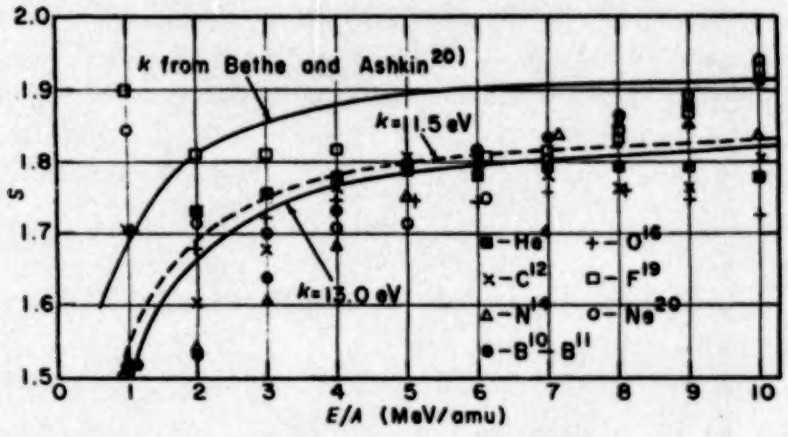

Fig. 12. Relative stopping power per atom for heavy ions in nickel. Data are relative to the range-energy measurements for heavy ions in aluminium of Northcliffe [9]). The solid curves have been computed from eq. (7).

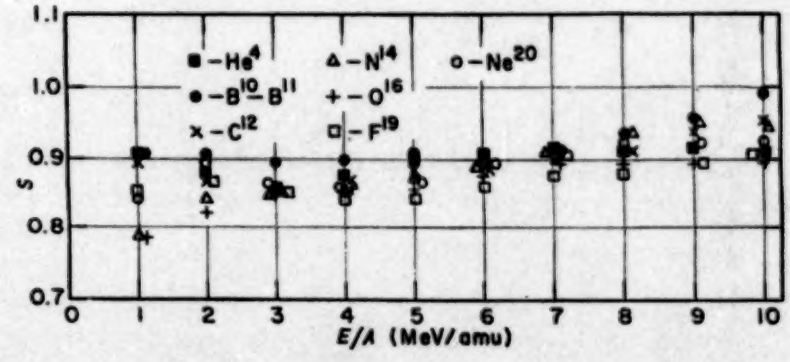

Fig. 13. Relative stopping power per atom for heavy ions in nuclear emulsion. Data are relative to the range-energy measurements for heavy ions in aluminium of Northcliffe [9]). A mass density of 4.00 g/cm³ has been assumed for the nuclear emulsion [3]).

potential $\bar{I}$ may be written in the form

$$\bar{I} = kZ', \tag{8}$$

where k is a rather poorly-known, slowly-varying function [15,20]) of Z'.

Figs. 11, 12 and 13 display values of the stopping power of oxygen, nickel and nuclear emulsion relative to aluminium, determined both from the experimentally-derived curves of figs. 4, 5 and 6 (points) and by computation (nickel and oxygen only) from eqs. (7) and (8) (solid lines). Experimental values of the specific energy loss of heavy ions in aluminium were obtained from Northcliffe's range-energy relations [9]).

Use of the value $k = 13.0$ eV in eq. (8), as recently suggested by Sternheimer [21]), results in considerably better agreement with the heavy ion data than the previous values tabulated by Bethe and Ashkin [20]). The K-shell corrections C_K have been taken from graphs presented by Evans [15]).

Down to 3 or 4 MeV per amu, the spread in experimental values of S is $\pm$ 5%. or less. There does not seem to be any systematic variation of relative stopping power with the mass or charge of the heavy ion. Finally, the discrepancy between experimental and calculated values of S, as shown in figs. 11 and 12, cannot be considered significant. Hence, if the specific energy loss of a heavy ion is known for one substance, it can be calculated for some other substance with an accuracy of a few per cent, using eq. (7). The accuracy of the present data does not permit the extension of these conclusions to energies less than about 3 MeV per amu.

The completion of this work was greatly facilitated by the cooperation and assistance of the staff and operators of the Yale Heavy Ion Linear Accelerator. Mr. E. Newman, Jr. provided invaluable assistance during the experimental work. In addition, we are most grateful to Dr. L. C. Northcliffe for furnishing his results prior to publication, for assisting in early phases of the work, and for many valuable discussions.

References

1) P. G. Roll, F. E. Steigert and A. M. Smith, Bull. Am. Phys. Soc. **4** (1959) 270
2) P. G. Roll and F. E. Steigert, Nuclear Physics **16** (1960) 534
3) H. L. Reynolds, D. W. Scott and A. Zucker, Phys. Rev. **95** (1954) 671
4) W. H. Webb, H. L. Reynolds and A. Zucker, Phys. Rev. **102** (1956) 749
5) D. L. Livesey, Can. J. Phys. **34** (1956) 203
6) Ia. A. Teplova, I. S. Dimitriev, V. S. Nikolaev and L. N. Fateeva, JETP **32** (1957) 974; translation: Sov. Phys. JETP **5** (1957) 797
7) W. E. Burcham, Proc. Phys. Soc. A **70** (1957) 309
8) Yu. Ts. Oganesyan, JETP **36** (1959) 936; translation: Sov. Phys. JETP **9** (1959) 661
9) L. C. Northcliffe, private communication (to be published)
10) A. Papineau, Comptes rend. **242** (1956) 2933
11) A. Papineau, private communication

12) A. P. Grinberg and I. X. Lemberg, Izvest. Akad. Nauk SSSR (Ser. Fiz.) **23** (1959) 887
13) A. B. Chilton, J. N. Cooper and J. C. Harris, Phys. Rev. **93** (1954) 413
14) W. Whaling, The Energy Loss of Charged Particles in Matter, Handbuch der Physik **34**, Editor Flügge (Springer, 1958) 193
15) R. D. Evans, The Atomic Nucleus (McGraw-Hill, 1955) Ch. 22
16) J. Knipp and E. Teller, Phys. Rev. **59** (1941) 659
17) H. H. Heckman, B. L. Perkins, W. G. Simon, F. M. Smith and W. H. Barkas, Phys. Rev. **117** (1960) 544
18) N. Bohr and J. Lindhard, Mat. Fys. Medd. Dan. Vid. Selsk. **28**, No. 7 (1954)
19) N. O. Lassen, Mat. Fys. Medd. Dan. Vid. Selsk. **26**, No. 5, No. 12 (1951)
20) H. A. Bethe and J. Ashkin, Passage of Radiations through Matter, Experimental Nuclear Physics **1**, Editor Segrè (Wiley, 1953) 166
21) R. M. Sternheimer, Phys. Rev. **115** (1959) 137

1.B

Nuclear Physics **17** (1960) 67—73; © *North-Holland Publishing Co., Amsterdam*

Not to be reproduced by photoprint or microfilm without written permission from the publisher

TENSOR AND $L \cdot S$ FORCES IN THE TRITON

G. H. DERRICK

Institute for Advanced Study, Princeton, New Jersey

and

J. M. BLATT

Applied Mathematics Department, University of New South Wales

Received 8 February 1960

Abstract: A variational estimate is made of the triton binding energy for a potential developed by Gammel, Christian and Thaler, modified to include $\mathbf{L} \cdot \mathbf{S}$ forces. This potential, which is similar in many respects to potentials based in part on meson theory, is found to be too weak to bind the triton at all; the state of lowest energy is a deuteron and a free neutron. The proportion of P-states coupled in by the $\mathbf{L} \cdot \mathbf{S}$ forces is less than 0.001 per cent.

1. Introduction

In two previous papers [1, 2]) a classification by the methods of group theory was made of the possible total-angular-momentum and isobaric-spin functions of the triton ground state. It was there shown that there are 16 such functions, of which only 10 are independent with respect to permutations of particles. The total wave function for the triton is then given by the sum of products of these total-angular-momentum and isobaric-spin functions with 16 radial wave functions. The latter depend only on the 3 interparticle distances r_{23}, r_{31} and r_{12}; again, only 10 of these radial wave functions are independent under permutations of the particles.

If we now substitute the above form of the triton wave function in the Schrödinger equation $H\psi = E\psi$, all angle, spin and isobaric-spin variables can be eliminated from the problem. We are then left with a set of coupled differential equations in only 3 variables r_{23}, r_{31} and r_{12}, for the 16 radial wave functions.

The present paper reports the results of some preliminary variational estimates of the triton binding energy made with this formalism.

2. The Potential

We have used one of the potentials given by Gammel, Christian and Thaler [3]) modified to include $\mathbf{L} \cdot \mathbf{S}$ forces [4, 5]). The interaction between particles i and j is given by

$$V_{ij} = V_{\mathrm{C}}(r_{ij}) + V_{\mathrm{T}}(r_{ij}) S_{ij} + V_{\mathrm{LS}}(r_{ij}) \mathbf{L}_{ij} \cdot (\mathbf{s}_i + \mathbf{s}_j); \qquad (1)$$

S_{ij} is the tensor operator for particles i and j, $\mathbf{L}_{ij}$ the angular momentum of these particles relative to their mutual centre of mass, and $\mathbf{s}_i$ and $\mathbf{s}_j$ the two spin vectors. The central, tensor and $\mathbf{L}\cdot\mathbf{S}$ radial potential functions, $V_C(r_{ij})$, $V_T(r_{ij})$ and $V_{LS}(r_{ij})$ respectively, are each cut-off Yukawa wells of the form

$$V(r_{ij}) = \begin{cases} \dfrac{-V_0 e^{-\mu r_{ij}}}{\mu r_{ij}} & \text{for } r_{ij} > r_0 \\ \infty & \text{for } r_{ij} < r_0. \end{cases}$$

The constants V_0, μ and r_0 depend on the various two-particle states; the values adopted are the final "best" values of ref. [5]) (p. 1339, 1340). Gammel *et al.* fitted the central and tensor part of the potential (1) to the low and medium energy two-body data. The spin-orbit terms were then added to improve the fit to the high energy scattering data, without, however, readjusting the central and tensor triplet parameters.

The main features of the potential (1) are:

(i) The central forces are much weaker than the tensor forces †, e.g. in the triplet even state the non-dimensional central well depth [6]) is only 0.35 compared with a tensor well depth of 0.96. The intrinsic ranges [6]) of these forces are about 2.0×10^{-13} cm.

(ii) The $\mathbf{L}\cdot\mathbf{S}$ forces are quite strong, but of very short range. Thus in the even state the well depth is 0.45 with an intrinsic range of only 0.8×10^{-13} cm. ††

3. Mathematical Method

The triton binding energy is the greatest lower bound of $(\psi, H\psi)/(\psi, \psi)$ for all quadratically integrable functions ψ for which the Hamiltonian H is Hermitian. With the aid of the matrix elements given in ref. [2]) this expectation value can be written entirely in terms of the radial wave functions, with all angle, spin and isobaric-spin variables eliminated.

3.1. THE TRIAL WAVE FUNCTION

Since the triton is predominately in the space-symmetric S-state, we need include, for a first survey, only those states which have non-zero matrix elements to the main S-state. In the notation of ref. [2]) these are states nos. 1, 3, 6, 7, 8, 9, 10. The predominant S-state no. 1 is connected directly to the mixed-symmetry S-state no. 3 by spin exchange forces, to P-states nos. 6 and 7 by the $\mathbf{L}\cdot\mathbf{S}$ forces, and to the D-states nos. 8, 9 and 10 by the tensor forces. (State no. 5 is also coupled in to first order by the $\mathbf{L}\cdot\mathbf{S}$ forces, but its kinetic energy is so high that it may be omitted [1, 2]).

† The potential we have used should be distinguished from that of Brueckner and Gammel [14]); their potential has central and tensor components of roughly equal strength.

†† We are grateful to Mr. T. Hamada for calculating these well depths and intrinsic ranges. The non-dimensional well-depth is the ratio of the actual well-depth to that just necessary to bind a 1S state.

Let us introduce the following notation:

$$u_i(r) = \frac{e^{-\gamma_i(r-r_0)}}{r}[1-e^{-\delta_i(r-r_0)}] \quad (i = 1, 3, 6, 7, 8, 9, 10),$$

$$v_i(r) = e^{-\varepsilon_i(r-r_0)}u_i(r),$$

$$S_i = u_i(r_{23})u_i(r_{31})u_i(r_{12}),$$

$$S'_i = u_i(r_{23})u_i(r_{31})v_i(r_{12})+u_i(r_{23})v_i(r_{31})u_i(r_{12})+v_i(r_{23})u_i(r_{31})u_i(r_{12}),$$

$$P_i = 3^{-\frac{1}{2}}[\{v_i(r_{23})u_i(r_{31})+u_i(r_{23})v_i(r_{31})\}u_i(r_{12})-2u_i(r_{23})u_i(r_{31})v_i(r_{12})],$$

$$Q_i = \{v_i(r_{23})u_i(r_{31})-u_i(r_{23})v_i(r_{31})\}u_i(r_{12}),$$

Δ = area of triangle

$$= \tfrac{1}{4}[(r_{23}+r_{31}+r_{12})(-r_{23}+r_{31}+r_{12})(r_{23}-r_{31}+r_{12})(r_{23}+r_{31}-r_{12})]^{\frac{1}{2}},$$

$$R^2 = r_{23}^2+r_{31}^2+r_{12}^2, \qquad \cos\lambda = \frac{4.3^{\frac{1}{2}}\Delta}{R^2},$$

$$F = 3^{-\frac{1}{2}}(r_{23}^2+r_{31}^2-2r_{12}^2), \qquad G = r_{23}^2-r_{31}^2.$$

Here, r_0 is the core radius, and γ_i, δ_i and ε_i variation parameters; the subscript i refers to the different triton states.

Using the notation of ref. [2]) our trial radial wave functions were

$$\begin{aligned}
f_1 &= \alpha_1 S_1+\alpha'_1 S'_1, \\
f_{3,1} &= \alpha_3 P_3, & f_{3,2} &= \alpha_3 Q_3, \\
f_{6,1} &= \alpha_6 \Delta P_6, & f_{6,2} &= \alpha_6 \Delta Q_6, \\
f_{7,1} &= \alpha_7 \Delta P_7, & f_{7,2} &= \alpha_7 \Delta Q_7, \\
f_{8,1}+3^{-\frac{1}{2}}\sin\lambda f_{9,1} &= \alpha_8 \cos^2\lambda P_8, \\
f_{8,2}+3^{-\frac{1}{2}}\sin\lambda f_{9,2} &= \alpha_8 \cos^2\lambda Q_8, \\
\cos\lambda f_{9,1}+f_{10,1} &= \alpha_9 S_9 F\cot\lambda, \\
\cos\lambda f_{9,2}+f_{10,2} &= \alpha_9 S_9 G\cot\lambda, \\
\cos\lambda f_{9,1}-f_{10,1} &= \alpha_{10}(GQ_{10}-FP_{10})\cot\lambda, \\
\cos\lambda f_{9,2}-f_{10,2} &= \alpha_{10}(GP_{10}+FQ_{10})\cot\lambda.
\end{aligned} \tag{2}$$

The amplitudes α_i are additional variation parameters. The radial wave functions (2) have the correct asymptotic behaviour near the two triangle configurations at which our specification of the Euler angles fails, viz. all three particles in a straight line, and the particles at the vertices of an equilateral triangle [2]).

3.2. NUMERICAL TECHNIQUES AND APPROXIMATIONS

The quantities $(\psi, H\psi)$ and (ψ, ψ) are given by triple integrals over all permissible values of r_{23}, r_{31} and r_{12} of quadratic expressions in the radial wave functions and their first derivatives [2]). Those integrals involved in the matrix elements of the main S-state to itself were calculated numerically using Simpson's integration formula [7]). All the other integrals were estimated to lower accuracy by a Monte Carlo method [8]). The following approximations were made:

(i) The hard core radius was taken to be the even-state value of $r_0 = 0.4 \times 10^{-13}$ cm in both even and odd two-particle states; in the odd states, where the core is actually slightly larger, the potentials were taken as zero for interparticle distances between $r_0 = 0.4 \times 10^{-13}$ cm and the actual core radius. Since the odd potentials have no direct matrix elements to the space-symmetric S-state, the error introduced thereby is negligible.

(ii) All P-state to D-state matrix elements were set to zero, since the proportion of P and D states is small.

(iii) All D-state to D-state matrix elements of the $\mathbf{L} \cdot \mathbf{S}$ force were taken as zero. †

4. Results

The potential (1) *was found to be too weak to bind the triton at all*; the minimum value of the energy $(\psi, H\psi)/(\psi, \psi)$ occurs for parameter values which simulate a deuteron with a neutron infinitely distant. With the wave function (2) there is no minimum of energy at all when all three particles are within range of one another's forces; as the parameters $\gamma_i \to 0$ the energy decreases steadily and finally becomes negative only at very small values of these parameters, corresponding to a deuteron and a free neutron.

To estimate by how much the potential fails to bind the triton, let us introduce the "force factor" i.e. the factor by which the potential must be multiplied to lead to the observed binding energy of 8.49 MeV. We have the following variation principle:

$$\text{force factor} \leqq \frac{(\psi, (T+B)\psi)}{(\psi, -V\psi)}$$

for all functions ψ for which $-V$ is a positive operator; T denotes the kinetic energy operator, and B the triton binding energy 8.49 MeV. Taking ψ given by (2) this variation principle yields the results listed in table 1.

The binding energy is a small difference of two large quantities (potential

† In a more recent calculation, to be published shortly, we have included these D-D elements of the $\mathbf{L} \cdot \mathbf{S}$ force. Their inclusion effectively increases the D-state kinetic energy, and *reduces* the triton binding.

TABLE 1

Calculated values of force factor, probabilities of contributing states, Coulomb energy, binding energy and optimum parameters

		Optimum parameters (10^{13} cm^{-1})			
		State	γ	δ	ε
Force factor	$<1.172 \pm 0.023$	1	0.18	1.1	0.4
Percent. S states, No. 1	89.5 ± 3.4	3	0.20	1.1	0.3
No. 3	0.59 ± 0.16	6,7	1.0	2.0	1.0
Percent. P states, No. 6	0.00008 ± 0.00003	8	0.22	0.9	1.0
No. 7	0.00072 ± 0.00024	9	0.65	0.9	irrelevant
Percent. D states, Nos. 8, 9, 10	9.9 ± 3.5	10	0.85	1.15	-0.5
Coulomb energy	0.83 ± 0.03 MeV				
Energy $(\psi, H\psi)/(\psi, \psi)$	4.0 ± 1.4 MeV				

The errors quoted arise from the Monte Carlo evaluation of the matrix elements. They are *not* estimates of the errors due to the use of the variation method, which errors could well be larger. The parameters γ, δ and ε were taken the same for the two P-states, nos. 6 and 7.

energy and kinetic energy), and the force factor applies to the potential energy only. Thus, the excess of the force factor over unity, namely 17 % is a very appreciable amount indeed. Furthermore, much of the potential energy comes from the tensor force, which enters quadratically; hence a significant fraction of the force factor is effectively squared.

5. Discussion

The question arises, whether the lack of binding might be due to a poor choice of trial wave function. To investigate this possibility we have estimated the triton binding energy with the function (2) for one of the potentials used by Pease and Feshbach [9]). We obtained a binding energy of 7.0 ± 1.1 MeV and a D-state probability of 4.6 ± 1.6 %; Pease and Feshbach's values were 7.63 MeV and 3.5 %. These two sets of results are quite consistent within our large statistical errors.

The lack of binding for the Gammel-Thaler force appears to stem from the weakness of the central part of the potential (1), compared with its tensor part. Thus the ratio of the central to tensor force non-dimensional well depths in the triplet even state is only 0.36. This contrasts with potentials used previously in triton energy calculations [9, 10]), where the central and tensor forces are roughly equal in strength, e.g. the corresponding central to tensor force ratio for the Pease-Feshbach potential is 0.78. Tensor forces are less effective in binding the triton than the deuteron [11]). Hence it follows that of two potentials which both bind the deuteron with the correct energy †, that with the higher

† Strictly, it was the potential (1) with $\mathbf{L} \cdot \mathbf{S}$ forces omitted which was fitted to the deuteron binding energy. However, if we omit the $\mathbf{L} \cdot \mathbf{S}$ forces from our triton calculation, our results are unaltered to the accuracy of the calculation.

proportion of central forces gives the more binding for the triton. This feature of the potential (1) (weak central forces, strong tensor forces) is shared by those potentials which are based in part on meson theory [12]).

A remarkable feature is the almost complete absence of P-states coupled in by the $\mathbf{L}\cdot\mathbf{S}$ force. The immediate reason for this is the smallness of the S-state to P-state matrix elements of the $\mathbf{L}\cdot\mathbf{S}$ force †. These elements are only 0.04 times the magnitude of the S-state to D-state elements of the tensor force. In addition the diagonal P-state matrix elements of the $\mathbf{L}\cdot\mathbf{S}$ force are strongly repulsive. A further inhibitory feature is the very high P-state kinetic energy, caused by the concentration at small distances of the P-state wave functions to take advantage of the very short ranged $\mathbf{L}\cdot\mathbf{S}$ force. However, the ineffectiveness of the $\mathbf{L}\cdot\mathbf{S}$ force can *not* be attributed solely to its very short range. Even if we take a fictitious $\mathbf{L}\cdot\mathbf{S}$ potential equal in range and strength to the tensor even potential, the proportion of P-states is still less than 0.002 %.

We can make a rough estimate of the importance of $\mathbf{L}\cdot\mathbf{S}$ forces from second order perturbation theory, using closure. For this estimate we include only the central part of the potential in the unperturbed Hamiltonian. We shall assume that the central forces alone suffice to bind the triton, and shall ignore tensor forces altogether. Let $|0\rangle$ denote the unperturbed triton ground state wave function with energy $-B$, and $|\alpha\rangle$ a three-nucleon scattering state with positive energy E_α. We shall assume that the first order perturbation $\langle 0|H'|0\rangle$ vanishes, and shall use closure. Then the increase in triton binding energy produced by a perturbation H' is given to second order by

$$\delta B = \sum_\alpha \frac{\langle 0|H'|\alpha\rangle\langle\alpha|H'|0\rangle}{E_\alpha + B} < \frac{1}{B}\sum_\alpha \langle 0|H'|\alpha\rangle\langle\alpha|H'|0\rangle < \frac{\langle 0|H'^2|0\rangle}{B}.$$

Taking H' as the $\mathbf{L}\cdot\mathbf{S}$ force and $|0\rangle$ as a pure space-symmetric S-state with the radial wave function $f_1(r_{23}, r_{31}, r_{12})$, we obtain

$$\delta B < \frac{1}{B}\int r_{23}r_{31}r_{12}\,dr_{23}\,dr_{31}\,dr_{12}\left[\Delta\left(\frac{1}{r_{23}}\frac{\partial f_1}{\partial r_{23}} - \frac{1}{r_{31}}\frac{\partial f_1}{\partial r_{31}}\right)V_{LS}(r_{12})\right]^2. \qquad (3)$$

As before Δ denotes the area of the triangle formed by the three particles; f_1^2 has been normalized to give unity when integrated over all permissible r_{23}, r_{31} and r_{12} with the weight factor $r_{23}r_{31}r_{12}$.

The integrand of the integral in eq. (3) has a second order zero on the surface $r_{23} = r_{31}$. In addition it vanishes everywhere on the bounding surface of the domain of integration ($\Delta = 0$). Thus we would expect δB to be very small. On the other hand the analogous closure estimate for tensor forces yields an integral whose integrand cannot vanish for *any* finite values of r_{23}, r_{31} and r_{12}

† The numerical values of the normalization, kinetic energy and potential energy matrix elements have been published elsewhere [13]).

outside the hard core (assuming f_1 itself has no zeros, which is always true for the lowest S state).

Qualitatively, one can look at the result as follows. The P-state angle-function $Y_M^{(1)}$ is essentially $\mathbf{r}_{12} \times \mathbf{r}_{23}$, and is thus anti-symmetric under exchange of particles (although of positive parity). The "natural" P-state is the one with exchange symmetric internal wave-function $f_P(r_{23}, r_{31}, r_{12})$, i.e., state no. 4 in our classification. However, since this function gets multiplied by $\mathbf{r}_{12} \times \mathbf{r}_{23}$, it is exchange-antisymmetric and hence is not coupled in at all, to lowest order. The states which *are* coupled in, states 5, 6 and 7, have lower exchange symmetry in their internal wave functions, hence have more nodes, and lead to extremely small matrix elements. The fact that the P-states are completely unimportant in the triton ground state is therefore a result of basic symmetries, not merely an accident of our particular calculation.

We have much pleasure in thanking Professor H. Messel for the excellent research facilities afforded us in the School of Physics, University of Sydney, where most of this work was carried out. We are also indebted to Dr. J. M. Bennett and the members of the Adolf Basser Computing Laboratories for a very generous allocation of Silliac computing time. One of us (G. H. D.) would like to acknowledge receipt of a research grant from the University of Sydney during 1959. He also wishes to thank Professor J. R. Oppenheimer for the hospitality extended to him, and for a grant-in-aid, at the Institute for Advanced Study.

References

1) G. Derrick and J. M. Blatt, Nuclear Physics **8** (1958) 310
2) G. H. Derrick, Nuclear Physics, **16** (1960) 405
3) J. L. Gammel, R. S. Christian and R. M. Thaler, Phys. Rev. **105** (1957) 311
4) J. L. Gammel and R. M. Thaler, Phys. Rev. **107** (1957) 291
5) J. L. Gammel and R. M. Thaler, Phys. Rev. **107** (1957) 1337
6) J. M. Blatt and J. D. Jackson, Phys. Rev. **76** (1949) 18
7) D. R. Hartree, Numerical Analysis (Oxford University Press, 1952)
8) A. S. Householder, Principles of Numerical Analysis (McGraw Hill, New York, 1953)
9) R. L. Pease, Thesis, M.I.T. (1950); R. L. Pease and H. Feshbach, Phys. Rev. **81** (1951) 142L
10) E. Gerjuoy and J. S. Schwinger, Phys. Rev. **61** (1942) 138;
H. Feshbach and W. Rarita, Phys. Rev. **73** (1948) 1272A;
75 (1949) 1384;
R. E. Clapp, Phys. Rev. **76** (1949) 873L
Thesis, Harvard University (1949);
T-M. Hu and K-N. Hsu, Phys. Rev. **78** (1950) 633L; Proc. Roy. Soc. A **204** (1951) 476;
G. Abraham, L. Cohen and A. S. Roberts, Proc. Roy. Soc. A **68** (1955) 265
11) R. D. Inglis, Phys. Rev. **55** (1939) 988;
J. M. Blatt and V. F. Weisskopf, Theoretical Nuclear Physics (John Wiley, New York, 1952)
12) J. Iwadare, S. Otsuki, R. Tamagaki and W. Watari, supplement to Prog. Theor. Phys., no. 3 (1956)
S. Gartenhaus, Phys. Rev. **100** (1955) 900;
P. S. Signell and R. E. Marshak, Phys. Rev. **109** (1958) 1229
13) G. H. Derrick, Thesis, University of Sydney (1959)
14) K. A. Brueckner and J. L. Gammel, Phys. Rev. **109** (1958) 1023

2.J

Nuclear Physics **17** (1960) 74—88; © *North-Holland Publishing Co., Amsterdam*

Not to be reproduced by photoprint or microfilm without written permission from the publisher

THE FISSION OF GOLD BY OXYGEN NUCLEI

A. R. QUINTON, H. C. BRITT, W. J. KNOX and C. E. ANDERSON

Sloane Physics Laboratory, Yale University, New Haven, Connecticut, U.S.A. †

Received 30 January 1960

Abstract: The angular distribution and the energies of the fission fragments, emitted in the bombardment of a thin gold foil by 160 MeV oxygen nuclei, have been experimentally determined by the use of a proportional counter detector. By a comparison with the theory of Halpern and Strutinski an estimate has been made of the shape of the fissioning nucleus at the saddle point. The total kinetic energy released was determined to be 150 MeV. It is claimed that the fissioning nucleus has typically a mass of 204 mass units. The possibility of the emission of charged particles, as well as neutrons, in some of the evaporation chains preceding fission, is discussed. A fission cross section of 1.8 ± 0.2 b was obtained.

1. Introduction

In the last few years interest has developed in fission studies in the angular distribution of the fragments with respect to the direction of the incident projectiles. On the theoretical side this interest stems from the attempt of A. Bohr [1]) to explain the then existing experimental data [2]) in terms of the collective model of the nucleus.

In the work referred to above the emphasis was on the state of the fissioning nucleus when excited just above threshold. Later treatments due to Strutinski [3]), and Halpern and Strutinski [4]) have concentrated on removing this energy restriction by resorting to statistical model considerations. According to Bohr the fission fragments leave one another along the line of the nuclear symmetry axis and the relevant quantum number is K, the projection of the total angular momentum I on this same axis. In the statistical treatments the same postulates hold but now one is dealing with distributions in K and I. However, at high excitation energies, K is not a good quantum number but is to be regarded as the mean moment of the nucleons about the nuclear axis.

Since the mean square value of K is related to the effective moment of inertia of the nucleus, which is in its turn determined by the shape of the nucleus, it follows that angular distribution measurements could perhaps become a powerful technique for fission investigations. This would be especially true if, as expected, it is the mean value of K^2 at the saddle point shape which controls the angular distribution.

Heavy ions would appear to be suitable projectiles for these investigations

†) This work was supported by the U. S. Atomic Energy Commission.

and this paper describes an attempt to exploit this promising new tool using 160 MeV oxygen ions. The requirements of the statistical treatment are met rather well, the fission cross section with a gold target is a large fraction of the geometrical cross section [5]) and the anisotropy is large.

Measurements of the energy spectra and angular distributions of the alpha particles [6]) and protons [7]) from the oxygen bombardment of a nickel target strongly suggest the influence of the high angular momentum characteristic of high energy heavy ion reactions. This influence is expected to appear in the fissioning of heavy nuclei [8]). Presumably it is just this effect which is responsible for the large anisotropy observed in the experiment under discussion, because the angular distribution is proportional to $1/\sin\theta$ in the classical limit, when I is large and K zero. This merely expresses the fact that fission fragments would be centrifuged off from a classical system, with constant probability in any direction in a plane perpendicular to I. Since the spin of Au^{197} is $\frac{3}{2}$ and the maximum orbital angular momentum contributed by the oxygen projectile is $\approx 85\hbar$, there is justification for the approximation that the projection M of the total angular momentum vector I is zero along the beam direction.

One of the less satisfactory features of heavy ion bombardment for bringing about fission is that the A and the Z of the fissioning nucleus are not known. It is expected that the principal competing processes are neutron evaporation and fission, after compound nucleus formation, although the possibility of some charged particle evaporation cannot be ruled out completely. Hence the reaction can be symbolized, perhaps, as Au (0; xn, f) but the range of values of x and their relative probabilities are not known. Since evaporation cools a nucleus down it means that the temperature of the fissioning nucleus takes on a range of values. It is reasonable to assume, however, that most of the nuclei fission from states of high excitation and of high angular momentum, so that the statistical considerations [3, 4]) should apply.

2. Method

A detailed description has been given elsewhere [9]) of the equipment used in this experiment. The full energy 160 MeV O^{16} beam was magnetically analysed and collimated to about 1° onto a thin self-supported gold target, 360 $\mu g/cm^2$ thickness. Occasionally 180 $\mu g/cm^2$ targets, supported by 40 $\mu g/cm^2$ formvar, were used. The beam current was collected in a Faraday cup and integrated, and the number of incident particles calculated on the assumption of completely stripped oxygen nuclei. Monitoring was also done by using a fixed cesium iodide scintillation counter at 20° with respect to the beam, and operating it so that only the elastically scattered oxygen ions were counted. Other measurements in this laboratory [10]) have shown that the scattering follows closely the Rutherford scattering law at such an angle. Usually the two systems of moni-

toring agreed to within 5 % and angular distributions from day to day never differed by more than 10 %.

The fission fragments were detected in a simple proportional counter, through a 500 $\mu g/cm^2$ nickel window, with the counter operated at a pressure of 60 cm of mercury which provided a maximum gas path equivalent to 4 mg/cm^2 of aluminium. At angles of observation less than 40° the low energy side of the fission spectrum was contaminated by elastically scattered oxygen nuclei and by particles of rather low mass emitted probably in direct interactions. They were rejected on the basis of their range. Since they could pass through the proportional counter they would be counted by the cesium iodide scintillation counter which forms the back wall of the gas counter. Pulses from both counters were fed, after passing through amplifiers and discriminating circuits, to an anticoincidence circuit, the output of which was used to open the gate of a 20 channel analyser. The observed energy spectra of particles stopping in the proportional counter were independent of counting rate except at the extreme forward angles. At these later angles, where elastic scattering predominates, the counting rate was lowered to a safer level but the energy spectra were less reliable in this range [9]).

3. Calibration

A Cf^{252} spontaneous fission source was used for the energy calibration of the proportional counter detector. Such a source proves to be extremely convenient for the following reasons: 1) the 6.1 MeV alpha particles allow the system to be checked for gain drifts very quickly; 2) the upper energy peak corresponds to a fission fragment mass close to that of the fragments expected in the experiment; 3) the energy resolution can be checked from the peak to valley ratio.

Fig. 1 shows a pulse height spectrum taken in three pieces with a 20 channel analyser. The pulse heights are relative to that of a 6.1 MeV alpha particle passing through the counter and depositing 2.5 MeV. A similar curve displaced on the average 2 channels to the left was obtained when the gold foil, later used for a target, was put between source and counter window. In this way "half target thickness" corrections could be applied to the data.

The results of Milton and Fraser [11]) were used for calibration purposes. Their curve for the single fragment energy spectrum, obtained by the time of flight method, was first normalised to the same total number of counts as the proportional counter spectrum. There was no significant disagreement in the shapes of the spectra obtained by the two methods, time of flight and proportional counter ionization. Then, after assuming that there was a direct correspondence in the energies at the peaks of the two curves, a detailed point by point energy calibration was obtained by measuring off, away from the peaks, equal increments of area under the two curves. Such a procedure gave an energy calibra-

tion from 55 MeV up to 115 MeV, sufficiently linear so that it could be extrapolated to higher energies if necessary.

Heavy ion induced reactions involve, of course, a large centre of mass velocity. As a consequence the fission fragments emitted at backward angles in the laboratory frame can well be of such low energy that calibrations below 55 MeV are needed. The procedure used depends for its validity on the following assumptions: 1) a windowless proportional counter would have a linear pulse

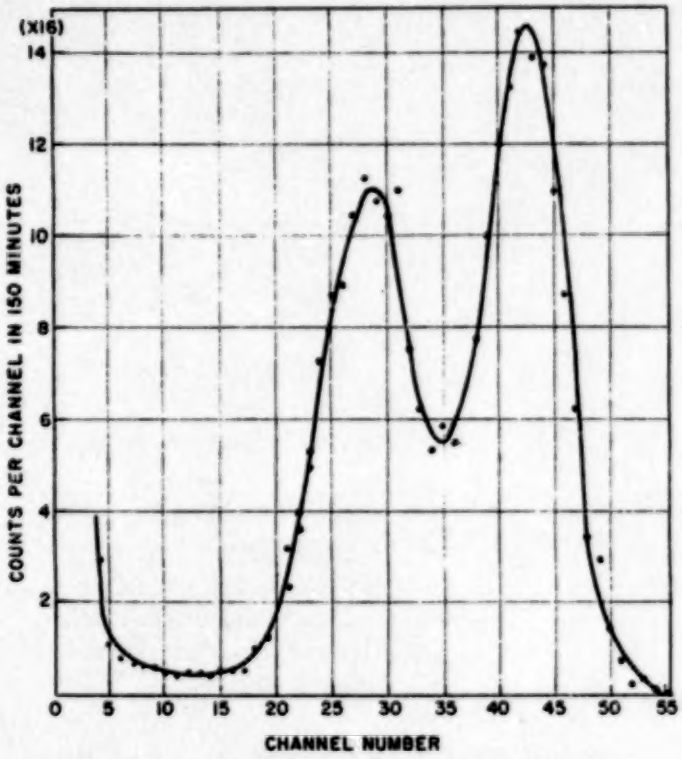

Fig. 1. The spectrum of pulse heights from the detection of Cf^{252} fission fragments in the proportional counter.

height versus energy response with a small intercept; 2) dE/dx is a constant for the fragments at the higher energies, say greater than 80 MeV. First a curve of pulse height versus air absorber thickness was determined for the upper peak of the spectrum, that is for the mass 100 fragment. The shape of this absorption curve indicated that dE/dx is a constant at the higher energies but decreases substantially at low energies. Then, by using a nickel foil of the same thickness as the counter window as an absorber it was possible to deduce the energy loss of a high energy fragment in the window. Hence the calibration from 80 MeV up could be corrected to give the windowless counter calibration. This curve when extrapolated to lower energies gave a small intercept of about 8 MeV corresponding probably, to our accuracy, to the ionization defect. Next, examination of the slope of the pulse height versus absorber curve at various

pulse heights indicated the correction to apply for an absorber of the thickness of the window. Then the assumed linear windowless curve could be moved back to give the final calibration curve (fig. 2) from 20 MeV upwards. The intercept on this curve corresponds to the most energetic particle which after passing through 160 $\mu g/cm^2$ of gold and 500 $\mu g/cm^2$ of nickel could enter the gas of the counter but not produce a detectable number of ion pairs.

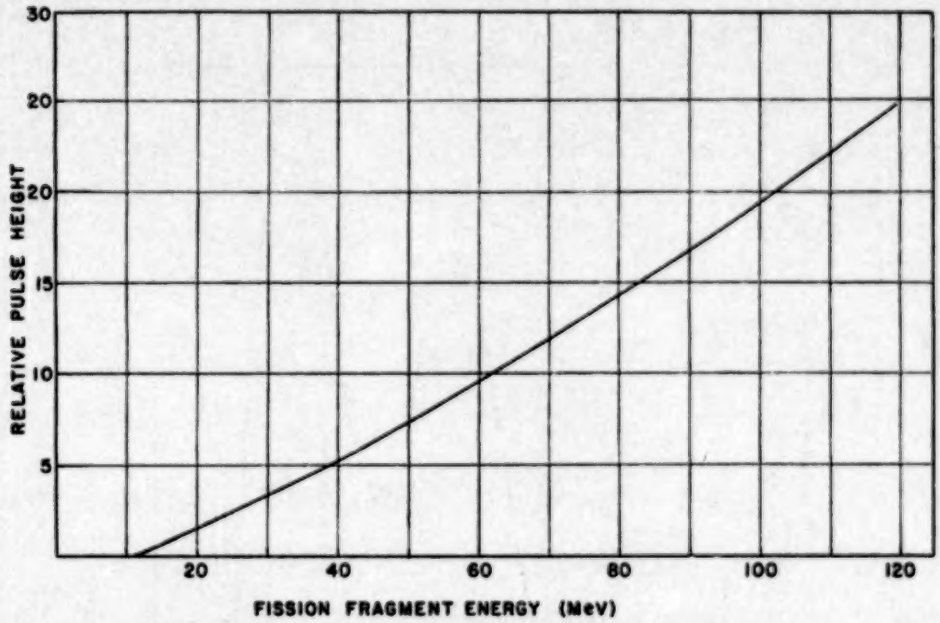

Fig. 2. The proportional counter energy calibration curve for fission fragments of A ≈ 100. The energy scale refers to the fragment kinetic energy outside the counter window. The pulse heights are relative to the pulse height produced by a 6.1 MeV alpha particle depositing 2.5 MeV in the counter.

4. Results and Transformations

In fig. 3 is shown the angular distribution in the laboratory frame of reference, illustrating the rather striking preference for emission of fragments along or against the beam direction. Each point represents a summation of the number of particles of all energies for a selected laboratory angle. Typical spectra for three angles are presented in fig. 4(a). These curves, which are, of course, normalised to the same number of incident oxygen ions, also demonstrate the large centre of mass velocity of the collision as evidenced by the lowering of the peak energy as the angle of observation increases in the backward direction.

In order to make a transformation to the collision centre of mass coordinate system it is necessary to know the velocity of the fragment whose energy has been measured, or in other words, the fragment mass has to be known. In this respect we surmise that the reaction under consideration is similar to that studied radiochemically by Tarantin *et al.* [12]). The result of that investigation was that the fissioning of gold by 115 MeV nitrogen ions proceeded by symmetric

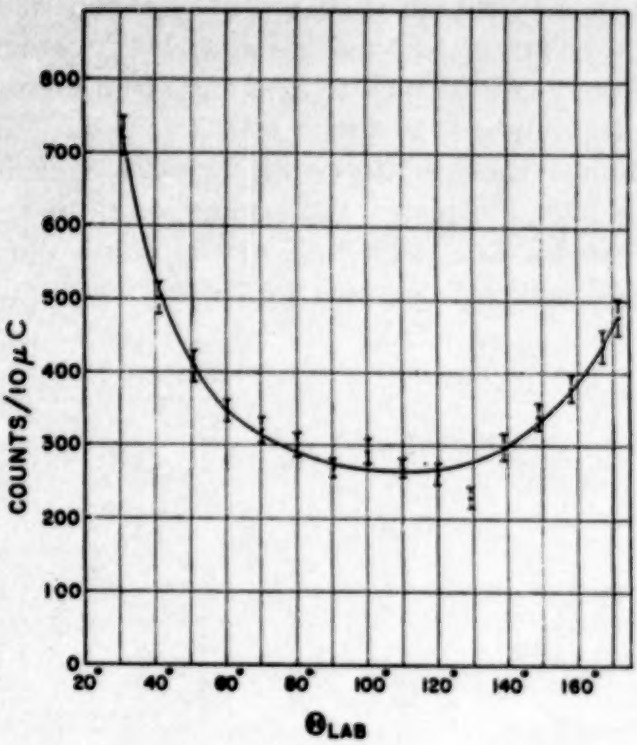

Fig. 3. The angular distribution of fission fragments in the laboratory frame of reference.

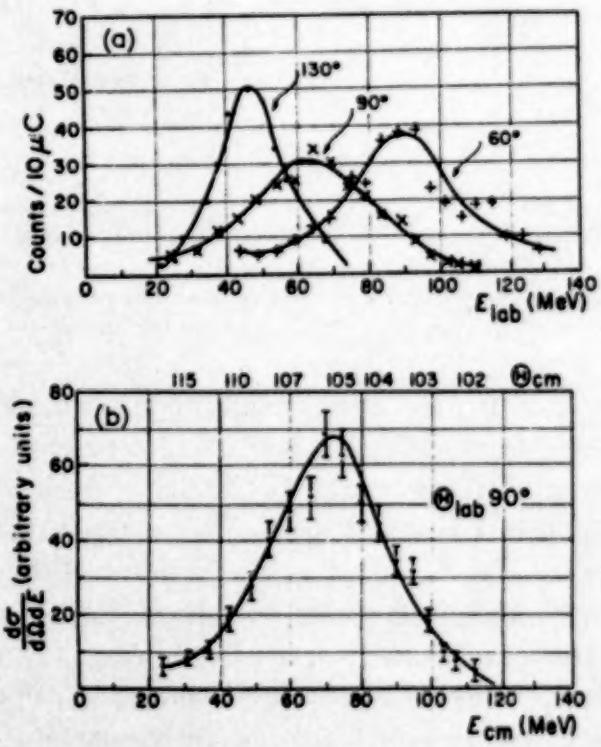

Fig. 4. (a) Typical fission fragment energy spectra at 60°, 90° and 130° in the laboratory frame.
(b) The 90° data transformed to the centre of mass energy.

division with the mass yield curve peaked at $A \approx 100$, and about 20 mass units wide at the points of half maximum yield. Accordingly, the energy spectra for this system of gold plus oxygen were transformed assuming that the detected fragment always had a mass of 100 units but was emitted from a system moving through the laboratory with the velocity of the centre of mass of the collision system. Inherently, the assumption is that, on the average, the evaporated particles leave behind a fissioning nucleus of net undisturbed velocity. In fig. 4(b) is shown the result for the 90° labortory spectrum, as an

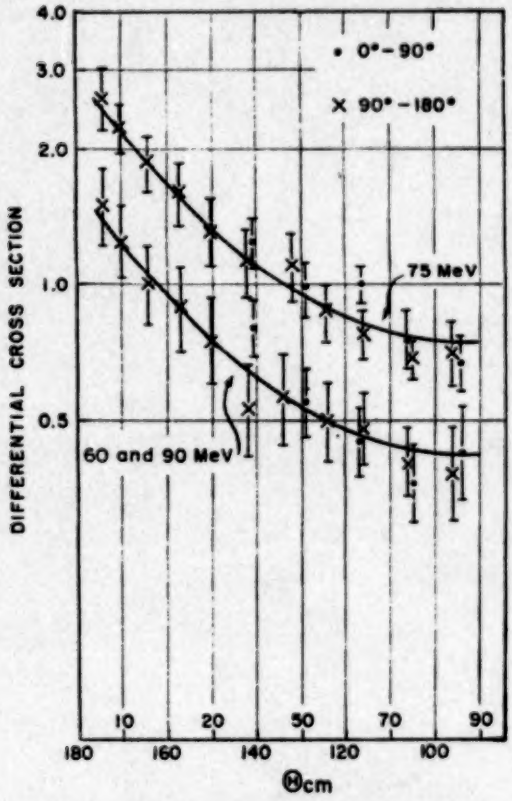

Fig. 5. Centre of mass angular distributions for 75, 60 and 90 MeV fragments.

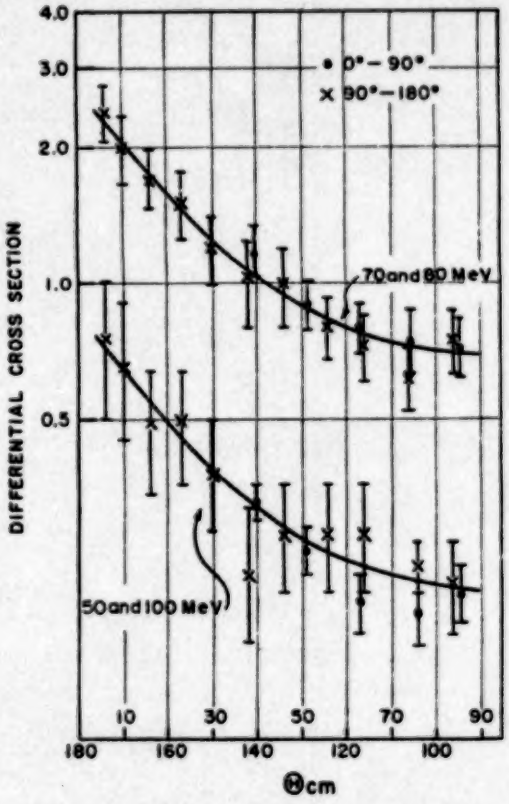

Fig. 6. Centre of mass angular distributions for 50, 70, 80 and 100 MeV fragments.

illustration, with centre of mass energy and angle scales. From sixteen such curves one can proceed to unfold the laboratory spectra and construct curves of the centre of mass angular distributions. This has been done for fragment energies from 50 to 100 MeV in 5 MeV steps. The results demonstrate symmetry of the angular distributions about 90°, and symmetry of the energy spectrum, at any angle, about 75 MeV. The second symmetry follows because, to within the accuracy of the data points, one curve can be drawn through the 70 and 80 MeV points, one through the 65 and 85 MeV points, etc. For this reason such pairs of energies have been coupled together in the presentation of the data (figs. 5—7). The error shown for each point is estimated from the error of the nearest point on the smooth curve from which it was extracted.

At this stage of the analysis it is possible to construct, from the angular distributions for various fragment energies, a centre of mass spectrum at any desired centre of mass angle. Actually closer inspection shows that, for each curve in figs. 5—7, a factor can be found which, within the experimental statistics, makes each curve coincide with the 75 MeV curve. In other words the angular distributions are not dependent upon fragment energy. The reciprocal of each factor has been plotted in fig. 8 to yield the centre of mass energy spectrum and so this plot represents a best determination of the energy spectrum, taking into account the data at all angles.

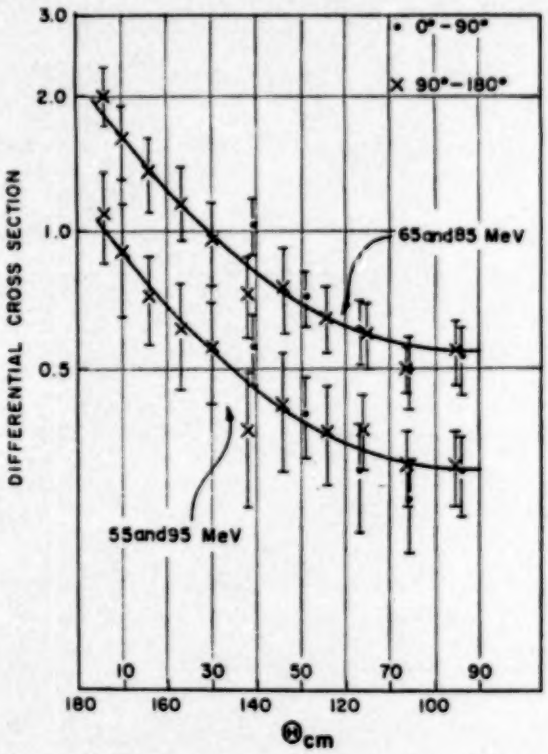

Fig. 7. Centre of mass angular distributions for 55, 65, 85 and 95 MeV fragments.

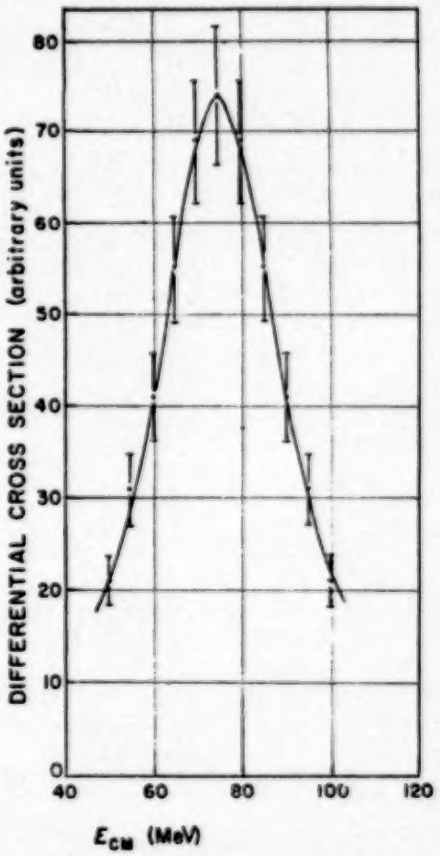

Fig. 8. The best determination of the centre of mass energy spectrum (see text).

As a check some of the data has been transformed assuming, first of all, a fragment mass of 90 units and secondly a mass of 110. In the first case the resulting spectra decrease in energy as the angle of observation increases. For the transformation assuming a mass of 110 units the reverse trend is seen, namely an increase in energy at the backward angles relative to the forward. Now it is certainly to be expected that the fission takes place from a compound system and hence that the centre of mass spectra should not be angle dependent. Furthermore if a laboratory spectrum contained fragments of say mass 90 and

mass 110, with the same shape of the spectrum for the two masses, then the transformed spectrum would show a tendency to double hump. But as one proceeded from small to large angles the two peaks would merge and cross over. So the spectrum shape would be angle dependent and, most significantly of all, linear momentum would not be conserved in the reconstructed fission events. The claim is made therefore that the fission process observed in this experiment is symmetric with a rather narrow range of masses around mass number 100. Actually the procedure outlined above can give crudely the most probable fragment mass emitted in symmetric fission, if one demands a unique centre of mass energy spectrum. Some slight trends in our transformed data would

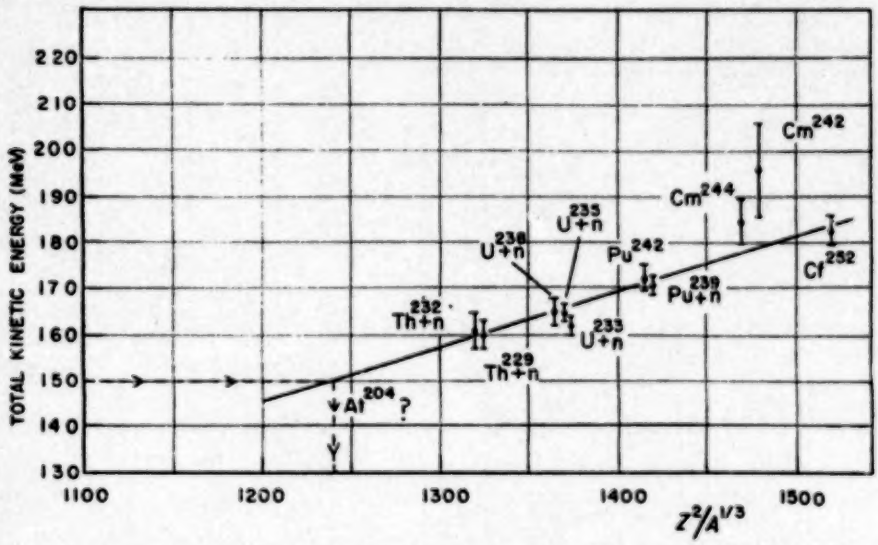

Fig. 9. The total kinetic energy released in fission as a function of $Z^2/A^{\frac{1}{3}}$. see ref. [13]).

suggest that a mass of 101 units would fit this criterion better than the trial value of 100 mass units. If an allowance is made for the liberation of 2 neutrons at fission, then the conclusion is reached that the fissioning system has an $A \approx 204$.

A useful empirical curve is available [13]), which correlates the kinetic energy released in fission with the parameter $Z^2/A^{\frac{1}{3}}$. If the assumptions are made that this relation is valid when extrapolated to 150 MeV total kinetic energy released and that the parent nucleus has a mass of 204, then it follows that the most probable fissioning nucleus is an astatine isotope (fig. 9). This in its turn would mean that some charged particle emission was competing with the neutron evaporation before fission. Some preliminary investigations of the alpha particle spectra and angular distributions have been made. It is rather clear that most of these particles came from the compound system prior to fission (or as an alternative to fission) because the peak energy corresponds closely to the barrier of a $Z \approx 80$ nucleus rather than a $Z \approx 40$ nucleus. The ratio of alpha particles to fission events is roughly 2 : 3. Proton emission is expected to

be at least equally significant. Another possibility is that some stripping reactions can leave a system with a fragment of the oxygen projectile amalgamated with a gold target nucleus and this system subsequently fissions. Such a mechanism tends to lower the average Z and A of the parent suggested by the experimental results presented here. However without the elaboration of coincident counters it is difficult to see how these "stripping plus fission" reactions could be measured in sufficient detail to permit a valid centre of mass transformation.

The cross section for fission was determined by a direct comparison, using the same proportional counter, target and geometry, of the elastic scattering counting rate of oxygen ions at a few forward angles with the fission counting rate, and allowing for the presence of two fragments in the later case. McIntyre and co-workers [10]) have measured the differential scattering cross section for 160 MeV oxygen ions on a gold target and hence the laboratory angular distribution of fig. 3 is calibrated in this fashion. A cross section of 1.8 ± 0.2 b is the result. The fraction of the total compound nucleus cross section represented by this value is not known. Polikanov and Druin [5]) report that the formula

$$\sigma_{\text{fission}} = \pi r_0^2 (A^{\frac{1}{3}} + A_2^{\frac{1}{3}})^2 \left(1 - \frac{B}{E}\right),$$

where B is the Coulomb barrier and E the available kinetic energy in the centre of mass system, fits the measured cross sections with $r_0 = 1.5 \times 10^{-13}$ cm. This same formula would give a fission cross section of 2.3 b and so it is seen that the agreement between formula and experimental result, at this higher bombarding energy, is only fair. The quoted probable error comes mainly from the uncertainty in the value of the scattering angle of the elastically scattered oxygen nuclei, which are counted by the fixed monitor.

5. Discussion

In this section we attempt an interpretation of the angular distribution of the fragments of all energies. Fig. 10 shows this distribution with a plot of $1/\sin\theta$ for comparison and it is clear that from 40° to 140° the curves are coincident to within the accuracy of the measurement. Beyond 140°, and presumably further forward than 40°, the observed distribution is significantly lower than $1/\sin\theta$.

Following the analysis of ref. [4]), the claim is made that the data enable the mean square value of K to be obtained. At the saddle point shape of the fissioning nucleus the projection K of the total angular momentum I along the symmetry axis is "frozen in". Fission is achieved a short time later and no other parameters other than I and this particular value of K affect the direction of

fragment emission. For a given K and I the angular distribution is found to be, from an elementary geometrical averaging procedure,

$$W(\theta) \approx \frac{1}{\left(\sin^2\theta - \frac{K^2}{I^2}\right)^{\frac{1}{2}}}.$$

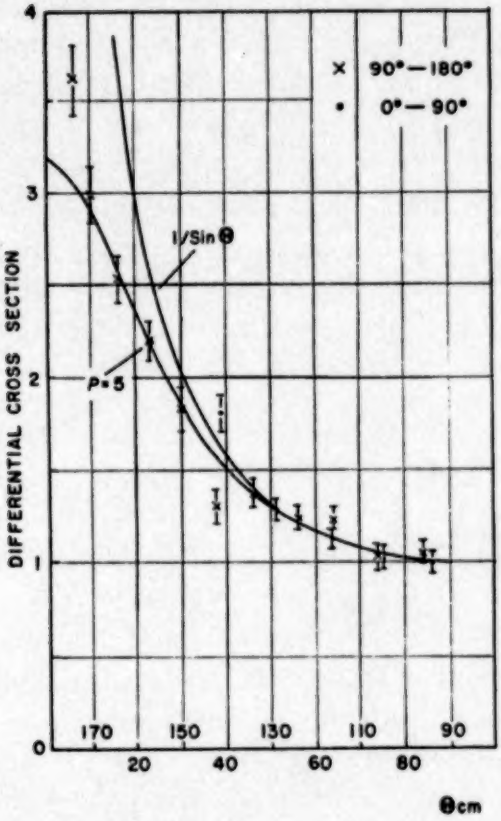

Fig. 10. The angular distribution of fission fragments emitted in the reaction $Au^{197}+O^{16}$. The departure from $1/\sin\tau$ and the fit to the curve $p = 5$ are illustrated.

Hence the distributions in K and I determine the angular distribution. The usual classical treatment of impact parameters leads to an I distribution, linear in $2I+1$, up to a maximum I_m given by

$$I_m\hbar = \mu V_{lab}(r_1+r_2)\left(1-\frac{B}{E}\right)^{\frac{1}{2}}.$$

In this formula μ is the reduced mass of the system, (r_1+r_2) the sum of the radii of the target and projectile nuclei, B the Coulomb barrier energy and E the kinetic energy in the centre of mass. If a formula $r = r_0A^{\frac{1}{3}}$ is assumed with $r_0 = 1.5\times10^{-13}$ cm and distortions of the nuclei are ignored, $I_m = 87\hbar$ for the reaction under consideration.

The distribution $P(K)$ in K will be governed by a Boltzmann-factor $\exp(-E_{\mathrm{rot}}/T)$, leading to the expression

$$P(K) \propto \exp\left\{-\frac{K^2\hbar^2}{2T}\left(\frac{1}{j_\parallel}-\frac{1}{j_\perp}\right)\right\},$$

where T is the nuclear temperature and $j_\parallel$ and $j_\perp$ are the moments of inertia of the nucleus, about axes parallel and perpendicular respectively to the nuclear symmetry axis.

Then defining

$$K_0^2 = \frac{Tj_{\mathrm{eff}}}{\hbar^2} \quad \text{with} \quad \frac{1}{j_{\mathrm{eff}}} = \frac{1}{j_\parallel} - \frac{1}{j_\perp},$$

the fission angular distribution is determined by the parameter $\not{p}$ where [4])

$$\not{p} = \left(\frac{I_{\mathrm{m}}}{2K_0}\right)^2.$$

For example if $\not{p} = \infty$ the distribution follows the relation $1/\sin\theta$, but as $\not{p} \to 0$ the distribution becomes increasingly isotropic.

In the use of this relation allowance should be made for the change in angular momentum of the nucleus brought about by the departure of evaporation products. It is expected that the plane of emission of these particles is strongly correlated with the angular momentum. Furthermore, because of the increase in level density with decreasing spin, the tendency will be for the emerging particles to lower I. Consider four possible chains of evaporation prior to fission: 1) 9n; 2) 8n+p; 3) 7n+2p; 4) 5n+α. At the prevailing excitation energies and potential barriers an evaporation neutron could carry off a maximum of $3\hbar$, a proton $4\hbar$ and an alpha particle $12\hbar$. These values correspond to emission with the maximum impact parameter but with the average particle energy. In making these estimates for the neutron case, twice the nuclear temperature was taken for the average energy with the nuclear temperature averaged along a chain of evaporation; in the case of charged particles, quantal penetration was considered and the classical barrier was taken for the average energy. This last consideration is in more accord with our experience than to regard the barrier energy as the most probable particle energy. Using these values one might guess that the 87 units of angular momentum are reduced to $67\hbar$.

As shown in fig. 10 the data can be fitted satisfactorily with $\not{p} = 5$ and suggest that the root mean square deviation in the Gaussian K distribution is given by $K_0 = 15.0$.

In carrying out the nuclear temperature calculations above the assumption was made that the Fermi gas model is applicable and hence that

$$E_{\mathrm{exc}} \approx \frac{A}{10} T^2 \approx 20\, T^2$$

For calculating excitation energies (E_{exc}), published tables of atomic masses [14]) were used. Again, with the same assumptions about the energy removed by an evaporated particle as above, the excitation energy of the nucleus at the end of each of the postulated evaporation chains can be estimated. The results are shown in table 1. The same table lists the final nuclear temperature, the

TABLE 1

Nuclear temperatures and other quantities for different evaporation chains

Evaporation Chain	E_{exc} (MeV)	T (MeV)	$x = \frac{(Z^2/A)}{(Z^2/A)_{crit}}$	$f(x)$	E_f (MeV)
9n	8.9	0.66	0.805	0.0054	2.8
8n+p	8.2	0.63	0.788	0.0070	3.6
7n+2p	4.2	0.14	0.770	0.0091	4.7
5n+α	38.4	1.36	0.770	0.0091	4.7

values of the fission parameter x and the corresponding function [15]) $f(x)$ together with the fission barrier. For these purposes $(Z^2/A)_{crit} = 46$ and $4\pi r_0^2\sigma = 15$ MeV were used with

$$E_f = 4\pi r_0^2 \sigma A^{\frac{2}{3}} f(x).$$

It should be remarked that the theory leading to this result is for nuclei which are spherical in their equilibrium forms and that rotation is not considered. As shown by Pik-Pichak [16]) the fission barrier is lowered by rotation. His analysis when applied to the cases under consideration predicts that E_f would be close to 1 MeV. It should also be mentioned that for the typical fissioning nucleus some 6.5 MeV of energy is in the rotational form if it is assumed that the saddle point shape can be approximated by a rigid ellipsoid with a 2 : 1 axis ratio.

An examination of the table suggests that the nucleus formed by the evaporation of 5 neutrons and an alpha particle might still continue to evaporate neutrons, or other particles, rather than fission. In other words 8n+α is an extreme possibility. It is possible to suggest then that evaporation to around $A = 204$ with $Z = 85$—87 is feasible since at that point the excitation energies left to the nuclei are greater than the fission barriers but not enough energy is available to evaporate particles.

Recently calculations of the Monte Carlo type have been carried out by Dostrovsky *et al.* [17]) on fission-spallation competition. These calculations apply to high energy proton bombardment of heavy nuclei so the initially excited nuclei are not the same as in this experiment. However the energy ranges are similar, and an examination of the theoretical predictions shows them to be qualitatively in accord with the suggestion here of the evaporation of about 9

nucleons prior to fission, including some charged particles. The expectation is also that the charged particles are emitted early in the evaporation chain.

Now combining the K_0 estimate of 15.0 with an estimated temperature of $T = 0.66$ MeV there results a value of 2.30×10^{-46} g · cm² for j_{eff}. Presumably also the nucleus can be considered to be behaving as a rigid body at the prevailing excitation energies so that the corresponding nuclear dimensions can be estimated. Let us assume that the nucleus can be represented by a prolate ellipsoid at the saddle point shape with $a > b = c$, and further that the distortion from spherical shape takes place at constant volume with no thermal expansion. Then

$$j_{eff} = \tfrac{2}{5} M b^2 \frac{a^2+b^2}{a^2-b^2}$$

and

$$ab^2 = r^3 = r_0^3 A.$$

Calculation shows that, if $a = 9.1 \times 10^{-13}$ cm and $b = c = 6.8 \times 10^{-13}$ cm, the value of j_{eff} estimated from the experimental results is obtained. This axes ratio of 1.35 : 1 can be compared with the saddle point shape calculations of Swiatecki [15]). When x is approximately equal to 0.8, he predicts a 1.90 : 1 at the saddle. Qualitatively then there is fair agreement between theory and experiment. The theory however ignores the effects of rotation. Considerations of the energy of a uniformly charged liquid droplet, including a rotational energy term, show that a rotating drop can reach the saddle point shape with less distortion (i.e. a/b smaller) than a non-rotating drop, under otherwise the same conditions.

References

1) A. Bohr, Proceedings of the International Conference on the Peaceful Uses of Atomic Energy, Geneva, 1955, Vol. 2 (United Nations 1956) 151
2) J. E. Brolley and W. C. Dickinson, Phys. Rev. **90** (1953) 388;
94 (1954) 640;
R. L. Henkel and J. E. Brolley, Phys. Rev. **103** (1956) 1292
3) V. M. Strutinski, J. Nuclear Energy **7** (1958) 239
4) I. Halpern and V. M. Strutinski, Second United Nations' Conference on the Peaceful Uses of Atomic Energy, Geneva, 1958, Vol. 15, 398
5) S. M. Polikanov and V. A. Druin, JETP **36** (1959) 522
6) W. J. Knox, A. R. Quinton and C. E. Anderson, Phys. Rev. Letters **2** (1959) 402
7) W. J. Knox, A. R. Quinton and C. E. Anderson, to be published
8) Proceedings of the Conference on Reactions between Complex Nuclei, Gatlinburg, Tennessee, 5–7 May, 1958, ORNL-2606, p. 159
9) C. E. Anderson, A. R. Quinton, W. J. Knox and R. Long, Nuclear Instruments and Methods, to be published
10) J. A. McIntyre, private communication
11) J. C. D. Milton and J. S. Fraser, Phys. Rev. **111** (1958) 877
12) N. I. Tarantin, Iu. B. Gerlit, L. I. Guseva, B. F. Miasoedov, K. V. Fillippova and G. N. Flerov, JETP **34** (1958) 220

13) J. Terrell, as presented by R. B. Leachman, Second United Nations' Conference, Geneva, 1958, Vol. 15, p. 331
14) A. G. W. Cameron, A Revised Semi-Empirical Atomic Mass Formula, Chalk River, Ontario, CRP-690, A.E.C.L. 433, December 1958
15) W. J. Swiatecki, Phys. Rev. **104** (1956) 993
16) G. A. Pik-Pichak, JETP **34** (1958) 238
17) I. Dostrovsky, Z. Fraenkel and P. Rabinowitz, Second United Nations' Conference on the Peaceful Uses of Atomic Energy, Geneva, 1958, Vol. 15, p. 301

2.E

Nuclear Physics **17** (1960) 89—95; © *North-Holland Publishing Co., Amsterdam*

Not to be reproduced by photoprint or microfilm without written permission from the publisher

NOTE ON THE SPIN-ORBIT PART OF THE OPTICAL MODEL POTENTIAL

J. SAWICKI

Department of Physics, University of California, Berkeley, California

Received 18 January 1960

Abstract: The spin-orbit part of the optical model potential is calculated using a modified, more accurate form of the impulse approximation model of Riesenfeld and Watson. In contrast to the usual model the integrations over the target particle momentum are performed. Comparison with the usual theories is discussed and the polarization of nucleons elastically scattered from carbon nuclei with the use of the Signell-Marshak nucleon-nucleon scattering phase shifts.

1. Introduction

In order to explain all the polarization phenomena in the elastic scattering of nucleons from complex nuclei it has been necessary to introduce the spin-orbit part of the optical model potential. This spin-orbit potential corresponds to the single particle shell model spin-orbit potential responsible for the j-splittings of nuclear levels. Recently the spin-orbit part of the shell model potential has been related to the spin-dependent two-body nuclear forces consistent with the nucleon-nucleon scattering data (see refs. [1-2]), referred to further as I and II, respectively, and other references listed in I and II). The spin-orbit potential can be expressed in terms of the derivatives of the nuclear density and it is zero for the case of nuclear matter (infinite nucleus). In the optical model case the real reaction matrix K_{LS} of Brueckner has to be replaced by the complex t_{LS} matrix. As a result the spin-orbit potential is complex. In the asymptotic region of high energies Riesenfeld and Watson [3]) (RW) have given approximate expressions for the spin-orbit part of the optical potential in terms of nucleon-nucleon phase shifts. Their potential is just proportional to the nucleon-nucleon scattering amplitude in the forward direction. This theory has been applied to the proton-carbon scattering data by Ohnuma [4]) with the use of the Gammel-Thaler and Signell-Marshak phase shifts. A somewhat similar theory has been developed by Bethe [5]), Cromer [6]), and Saperstein and Feldman [7]).

The purpose of the present note is to discuss a somewhat more general form of the potential and to extend the practical expression for the potential to the energy range where the momentum of the struck target particle is not negligible as compared with the momentum of the incoming nucleon. As the off-energy-shell propagation of t_{LS} is unfortunately unknown, the usual on-energy-shell

approximation is used. A numerical example with the Signell-Marshak phase shifts is given.

2. Calculation

Using Watson's theory one arrives [8]) at the following expression for the generally non-local kernel playing the role of the optical potential operator:

$$\langle \mathbf{k}'_0|U|\mathbf{k}_0\rangle = \int d\mathbf{k}_1 d\mathbf{k}'_1 \langle \mathbf{k}'_{01}|\bar{t}_{01}|\mathbf{k}_{01}\rangle \delta(\mathbf{K}_{01}-\mathbf{K}'_{01})(2\pi)^{-3} \cdot \int d\mathbf{r}_a d\mathbf{r}_b e^{i\mathbf{k}_1\cdot\mathbf{r}_b - i\mathbf{k}'_1\cdot\mathbf{r}_a}\rho(\mathbf{r}_a, \mathbf{r}_b), \tag{1}$$

where $\mathbf{k}_0$, $\mathbf{k}'_0$ and $\mathbf{k}_1$, $\mathbf{k}'_1$ are the initial and final momenta of the projectile and the target particle, respectively, and $\mathbf{k}_{01} = \frac{1}{2}(\mathbf{k}_0-\mathbf{k}_1)$, $\mathbf{k}'_{01} = \frac{1}{2}(\mathbf{k}'_0-\mathbf{k}'_1)$, $\mathbf{K}_{01} = \mathbf{k}_0+\mathbf{k}_1$, $\mathbf{K}'_{01} = \mathbf{k}'_0+\mathbf{k}'_1$; $\bar{t}_{01}$ is the "effective "antisymmetrized average t-matrix †, and $\rho(\mathbf{r}_a, \mathbf{r}_b)$ is the single particle mixed density:

$$\rho(\mathbf{r}_a, \mathbf{r}_b) = A\int d\sigma_1 d\tau_1 d(2)\ldots d(A)\Psi_0^*(\mathbf{r}_a, \sigma_1, \tau_1, 2\ldots A)\Psi_0(\mathbf{r}_b\sigma_1, \tau_1, 2\ldots A) \tag{2}$$

where Ψ_0 is the exact wave function of the target nucleus. The spin-orbit part of U is given by t_{LS}, which can be written as

$$\langle \mathbf{k}'_{01}|\bar{t}|\mathbf{k}_{01}\rangle_{LS} = -\frac{4\pi\hbar^2}{(2\pi)^3 M}\tfrac{3}{4}\bar{C}(k^2_{01}, \vartheta)(\boldsymbol{\sigma}_0+\boldsymbol{\sigma}_1)\cdot\frac{\mathbf{k}_{01}\times\mathbf{k}'_{01}}{|\mathbf{k}_{01}\times\mathbf{k}'_{01}|} \tag{3}$$

where $\vartheta = \sphericalangle(\mathbf{k}_{01}, \mathbf{k}'_{01})$ and the factor $\frac{3}{4}$ stands for the fact that only triplet spin states are included. If we use the on-energy shell ($k^2_{01} = k'^2_{01}$) free nucleon-nucleon scattering t-matrix we can express (3) in terms of nucleon-nucleon phase shifts from

$$\bar{C}(k^2_{01}, \vartheta) = i\frac{\sqrt{2}}{4}(\tilde{M}_{10}-\tilde{M}_{01}) \tag{4}$$

in the notation of Stapp *et al.* [9]), where, as previously, the symbol ã stands for the iso-spin averaging. In the following we shall omit the Coulomb phase shifts and amplitudes which can be easily included in the usual way (we treat the neutron-nucleus scattering). We find explicitly (with $\mathbf{k}_{01}=\mathbf{k}$, $\mathbf{k}'_{01}=\mathbf{k}'$, $k=k'$)

$$\begin{aligned}\mathrm{Re}\,\bar{C}(k^2, \vartheta) = \frac{1}{16k}\Bigg\{&(3\sum_{l\,\mathrm{odd}}+\sum_{l\,\mathrm{even}})\Bigg[\frac{2l+1}{l(l+1)}2\sin^2\eta_l P_l^1(\vartheta)\\ &+(2l+3)[-(\cos^2\varepsilon_{l+1}\sin^2\eta_{l,l+1}+\sin^2\varepsilon_{l+1}\sin^2\eta_{l+2,l+1})\frac{2}{l+1}P_l^1(\vartheta)\\ &+(\cos^2\varepsilon_{l+1}\sin^2\eta_{l+2,l+1}+\sin^2\varepsilon_{l+1}\sin^2\eta_{l,l+1})\frac{2}{l+2}P_{l+2}^1(\vartheta)]\Bigg]\\ &+6\sin^2\eta(^3\mathrm{P}_0)P_1^1(\vartheta)\Bigg\},\end{aligned} \tag{5}$$

† The averaging over the iso-spin states for a standard $2Z = A$ nucleus gives $\bar{t} = \frac{1}{2}t(T=1)+\frac{1}{2}t(T=0)$.

where η_l, $\eta_{l',l+1}$ are the uncoupled ($j = l$), and coupled Blatt and Biederharn triplet states phase shifts; $\eta(^3P_0)$ is the $^3P_0$-phase shift, ε_{l+1} is a tensor coupling coefficient. The imaginary part of $\bar{C}(k^2, \vartheta)$ is obtained from (6) by replacing $2\sin^2\eta$ by $\sin 2\eta$ everywhere and by changing sign of the whole expression †.

On introducing the coordinates $\mathbf{R} = \frac{1}{2}(\mathbf{r}_a + \mathbf{r}_b)$, $\mathbf{r} = \mathbf{r}_a - \mathbf{r}_b$ we finally obtain for the spin-saturated core, in analogy with eq. (31) of I,

$$\langle \mathbf{k}'_0|U|\mathbf{k}_0\rangle_{LS} = -\tfrac{3}{4}\frac{\hbar^2}{2\pi^2 M}\int \mathrm{d}\mathbf{R}\mathrm{d}\mathbf{r}(2\pi)^{-3}\int \mathrm{d}\mathbf{k}_1 \frac{\bar{C}(k^2,\vartheta)}{k^2\sin\vartheta} \cdot \boldsymbol{\sigma}_0 \cdot (\mathbf{k}\times\mathbf{k}')\,\rho(\mathbf{R},\mathbf{r})\mathrm{e}^{i\mathbf{p}\cdot\mathbf{R}}\mathrm{e}^{-i(\mathbf{k}_1-\frac{1}{2}\mathbf{p})\cdot\mathbf{r}} \tag{6}$$

where $\mathbf{p} = \mathbf{k}'_0 - \mathbf{k}_0$. One can change the variable $\mathbf{k}_1$ to $\mathbf{k}(\mathrm{d}\mathbf{k}_1 = -8\mathrm{d}\mathbf{k})$. An equation analogous to eq. (9) of II is then easily obtained. In deriving eq. (9) of II the function $f_X(|2\mathbf{k}+\mathbf{p}|)$ of II was replaced by $f_X(2k)$ and then, in going to eq. (10) of II, the exponent $\frac{1}{2}\mathbf{p}\cdot\mathbf{r}$ was dropped, as the terms of the type $\nabla_R{}^2\rho(\mathbf{R}, 0)$ were omitted as rather small in comparison with the other terms. Similarly we drop the exponent $\frac{1}{2}\mathbf{p}\cdot\mathbf{r}$. In addition, the terms involving $\cos\vartheta = 1+\mathbf{k}\cdot\mathbf{p}/k^2$ occurring in $\bar{C}/k^2\sin\vartheta$ can be replaced by their average values in order to simplify the $\mathbf{k}$-angular integration. In fact, it was found in I that e.g., the $\cos\vartheta$-term of the reaction matrix gives a rather small contribution, anyway. We arrive at an expression analogous to eq. (10) of II:

$$\langle \mathbf{k}'_0|U|\mathbf{k}_0\rangle_{LS} = \frac{6\hbar^2}{\pi^3 M}\int \mathrm{d}\mathbf{R}\mathrm{e}^{i\mathbf{p}\mathbf{R}}\boldsymbol{\sigma}_0\cdot(\mathbf{k}_0\times\mathbf{k}'_0)\int_0^\infty \mathrm{d}r\, r^2\rho(\mathbf{R},r) \cdot j_1(k_0 r)/k_0 \int_0^\infty \mathrm{d}k\, k^3 j_1(2kr)\frac{-\bar{C}}{k^2\sin\vartheta} \tag{7}$$

where the $\mathbf{r}$-angular dependence has been suppressed. In the following practical application we shall use Kisslinger's approximation [10]: $\rho(\mathbf{R}, \mathbf{r}) \approx \rho(\mathbf{R}, r) = \rho(R)\mathrm{e}^{-\gamma r^2}$ as discussed in II. On introducing the notation $(-\bar{C}/k^2\sin\vartheta) = \mathscr{R}(k)+i\mathscr{I}(k)$ and $\mathbf{n} = \mathbf{k}_0\times\mathbf{k}'_0/k^2{}_0\sin\theta$, where $\theta = \sphericalangle(\mathbf{k}_0, \mathbf{k}'_0)$, we can rewrite

† Similarly the central part of $\bar{t}$ is

$$\langle \mathbf{k}'_{01}|\bar{t}|\mathbf{k}_{01}\rangle_c = -\frac{4\pi\hbar^2}{(2\pi)^3 M}\bar{a}(k^2,\vartheta) = \frac{\hbar^2}{2\pi^2 M}\tfrac{1}{4}(2\bar{M}_{11}+\bar{M}_{00}+\bar{M}_{ss}),$$

$$\mathrm{Re}\,\bar{a}(k^2,\vartheta) = \frac{1}{16k}\{(\sum_{l\,\mathrm{odd}} + 3\sum_{l\,\mathrm{even}})(2l+1)\sin 2\delta_l P_l(\vartheta) + (\sum_{l\,\mathrm{even}} + 3\sum_{l\,\mathrm{odd}})[(2l+1)\sin 2\eta_l + (2l+3)[(\cos^2\varepsilon_{l+1}\sin 2\eta_{l,\,l+1} + \sin^2\varepsilon_{l+1}\sin 2\eta_{l+2,\,l+1})P_l(\vartheta) + (\cos^2\varepsilon_{l+1}\sin 2\eta_{l+2,\,l+1} \sin^2\varepsilon_{l+1}\sin 2\eta_{l,\,l+1})P_{l+2}(\vartheta)]] + 3\sin 2\eta(^3P_0)P_1(\vartheta)\}$$

where δ_l's are the singlet states phase shifts. The imaginary part is obtained by replacing $\sin 2\delta(\eta)$ by $2\sin^2\delta(\eta)$ everywhere.

eq. (7) in the form

$$\langle \mathbf{k}'_0|U|\mathbf{k}_0\rangle_{LS} = i\sigma_0 \cdot \mathbf{n} k_0^2 \sin\theta\left(U_{SR}(\mathbf{k}_0, \mathbf{k}'_0)+iU_{SI}(\mathbf{k}_0, \mathbf{k}'_0)\right) \tag{8}$$

where

$$U_{SR}(\mathbf{k}_0, \mathbf{k}'_0) = 48\frac{\hbar^2}{M}\rho(\mathbf{p})\int_0^\infty \mathrm{d}r\, r^2 \mathrm{e}^{-\gamma r^2}\frac{j_1(k_0 r)}{k_0}\int_0^\infty \mathrm{d}k\, k^3 j_1(2kr)\mathscr{I}(k) \tag{8a}$$

and the same for U_{SI} with $\mathscr{I}(k)$ replaced by $(-\mathscr{R}(k))$. Here Kisslinger's approximation has been used, and $\rho(\mathbf{p}) = (2\pi)^{-3}\int \mathrm{d}\mathbf{R}\mathrm{e}^{i\mathbf{p}\cdot\mathbf{R}}\rho(\mathbf{R})$ is the familiar density form factor known from refs. [3-4]). In configuration space the non-local $\langle U\rangle_{LS}$ can be replaced by a diagonal (local) U_{LS}, but involving an infinite series of derivatives of $\rho(\mathbf{R})$.

Another simplified formula for the spin-orbit kernel can be obtained using the "straight lines" approximation of eq. (33) of I which seems to be not unreasonable in the medium and low energy range. We write

$$\frac{i\bar{C}}{k^2\sin\vartheta} \approx a+4bk^2+4ck^2\cos\vartheta \tag{9}$$

where a, b, c are complex constants. Furthermore, similarly as in I, we confine ourselves to $\rho(R, r)$ satisfying the conditions

$$\left.\frac{\partial\rho}{\partial r}\right|_{r=0} = 0,\ \left.\left(r^2\frac{\partial}{\partial r}\left(\frac{1}{r}\frac{\partial\rho}{\partial r}\right)\right)\right|_{r=0} = 0,\quad \left.\frac{\partial}{\partial r}(\nabla_r^2\rho)\right|_{r=0} = 0.$$

These conditions are satisfied by a great variety of realistic densities, in particular, in Kisslinger's approximation and for the harmonic oscillator functions. Following I we obtain the expression

$$\begin{aligned}\langle \mathbf{k}'_0|U|\mathbf{k}_0\rangle_{LS} = i\frac{3}{8}\frac{\hbar^2}{2\pi^2 M}\int \mathrm{d}\mathbf{R}\,\mathrm{e}^{i\mathbf{p}\cdot\mathbf{R}}\sigma_0\cdot(\mathbf{k}_0\times\mathbf{k}'_0)\\ \cdot\{Z(\mathbf{R})+\rho(\mathbf{R})(\nu k_0^2+\nu' k_0'^2+2\mu\mathbf{k}_0\cdot\mathbf{k}'_0)\},\end{aligned} \tag{10}$$

where

$$Z(\mathbf{R}) = a\rho(\mathbf{R})-(b+c)\frac{\partial^2}{\partial r^2}\rho(\mathbf{R}, r)|_{r=0},$$

$$\nu = \tfrac{1}{4}(9b-3c),\quad \nu' = \tfrac{1}{4}(b-3c),\quad 2\mu = \tfrac{1}{2}(5c-3b).$$

The function $Z(\mathbf{R})$ is given in I for the shell model wave function of the O^{16} nucleus; the analogous expression for Ca^{40} is

$$Z(\mathbf{R}) = N\left[\tfrac{1}{2}a\left(5+\left(\frac{R}{r_0}\right)^4\right)+\frac{b+c}{2r_0^2}\left(\frac{13}{4}+\left(\frac{R}{r_0}\right)^2+\frac{R^4}{4r_0^4}\right)\right]\mathrm{e}^{-R^2/2r_0^2}$$

where N is normalization constant, $r_0 = 1/\sqrt{2\nu}$ and ν is the usual shell model

harmonic oscillator parameter. In Kisslinger's approximation,

$$Z(\mathbf{R}) = [a+2\gamma(b+c)]\rho(\mathbf{R}). \tag{11}$$

It is rather easy to establish the correspondence between eqs. (10) and (7) which provides a useful check of the formulae. Using eq. (11) we can rewrite eq. (10) in the form of eq. (8), where

$$U_{SR}(\mathbf{k}_0, \mathbf{k}'_0)+iU_{SI}(\mathbf{k}_0, \mathbf{k}'_0) = \frac{3}{8}\frac{4\pi\hbar^2}{M}[a+2\gamma(b+c)+\nu k_0^2+\nu' k_0'^2+2\mu\mathbf{k}_0\cdot\mathbf{k}'_0]\rho(\mathbf{p}) \tag{12}$$

where $\rho(\mathbf{p})$ is as defined previously. We shall also assume that the density is central, i.e., that the nucleus is spherical. It is then easy to find the corresponding operator in the configuration space in the simple form

$$\begin{aligned}\langle \mathbf{r}'_0|U|\mathbf{r}_0\rangle_{LS} &= (2\pi)^{-3}\int d\mathbf{k}_0 d\mathbf{k}'_0 e^{-i\mathbf{k}'_0\cdot\mathbf{r}'_0}\langle \mathbf{k}'_0|U|\mathbf{k}_0\rangle_{LS} e^{i\mathbf{k}_0\cdot\mathbf{r}_0} \\ &= \delta(\mathbf{r}_0-\mathbf{r}'_0)V_{LS}(r_0)\boldsymbol{\sigma}_0\cdot\mathbf{L},\end{aligned} \tag{13}$$

$$\begin{aligned}V_{LS}(r_0) = -\frac{3}{8}\frac{4\pi\hbar^2}{M}\Big[&\frac{1}{r_0}\frac{d}{dr_0}Z(r_0)+\frac{\mu}{r_0}\frac{d}{dr_0}(\nabla^2_{\mathbf{r}_0}(\rho(r_0)) \\ &-(\nu+\nu'+2\mu)\frac{1}{r_0}\frac{d}{dr_0}\rho(r_0)\nabla^2_{\mathbf{r}_0}\Big].\end{aligned} \tag{13a}$$

With $Z(r_0)$ given by eq. (11) the leading term in eq. (13a) has the familiar Thomas form. We see that in the approximation of eq. (9) or a similar one the spin-orbit kernel is local and we obtain the effective local spin-orbit potential $V_{LS}(r)\boldsymbol{\sigma}_0\cdot\mathbf{L}$.

3. Numerical Results and Comparison with Previous Work

In order to have comparison with the work of Riesenfeld and Watson [3]) and Ohnuma [4]) we have to introduce their well depth normalization of the spin-orbit potential for elastic scattering ($k_0 = k'_0$). We write

$$V_{SR} = -\frac{\rho_0}{\rho(p)}\left(\frac{m_\pi c}{\hbar^2}\right)^2 U_{SR}(\mathbf{k}_0, \mathbf{k}'_0)|_{k_0=k'_0} \tag{14}$$

and similarly for the imaginary part V_{SI}, where $\rho_0 = 3A/4\pi R^3$, R is the nuclear radius, and m_π is the pion rest mass. In eq. (14) the relativistic kinematic correction factor has been omitted. The inclusion of that factor in the fashion of refs. [3–4]) is straightforward. In refs. [3–4]) comparison with experiment is given for the elastic scattering of protons from the C^{12} target nucleus. Recently Meyer-Berkhout *et al.* [11]) have given the density of C^{12} in a rather convenient form: $\rho(R) = N(1+\alpha R^2/r_s^2)e^{-R^2/r_s^2}$, where N is normalization constant,

$\alpha = 1.12$, $r_s = 1.71 \times 10^{-13}$ cm. For this density the density form factor can be written in the form

$$\rho(p) = \frac{3}{2\pi^3} e^{-(k_0 r_s)^2 \sin^2 \frac{1}{2}\theta} \left(1 - \frac{4\alpha}{2+3\alpha} (k_0 r_s)^2 \sin^2 \tfrac{1}{2}\theta\right). \tag{15}$$

Following refs. [3-4]) we shall introduce the central potential well depths in their notation and with their normalization as $V_{CR} + iV_{CI}$.

Koehler [12]) and Levintov [13]) have shown that the polarization of the high energy nucleons scattered at small scattering angles from nuclei can be calculated to a good accuracy by the Born approximation. In Born approximation the polarization of the scattered particles is obtained in the form

$$P(\theta)\mathbf{n} = \frac{2(V_{CI}V_{SR} - V_{CR}V_{SI})(\hbar k_0/m_\pi c)^2 \sin\theta}{V_{CR}^2 + V_{CI}^2 + (V_{SR}^2 + V_{SI}^2)(\hbar k_0/m_\pi c)^4 \sin^2\theta} \mathbf{n} \tag{16}$$

which shows that $P(\theta)$ is independent of the density form factor $\rho(p)$ and the normalization constant ρ_0 of eq. (14) occurring also in the expressions for V_{CR} and V_{CI} (cf. ref. [4])) provided the approximations of eq. (8a) or (12) are valid. Our formulae apply essentially to the neutron scattering only; however, at energies $E_L \gtrsim 100$ MeV the Coulomb effects are important only at very small scattering angles.

The Signell-Marshak [14]) nuclear phase-shifts and tensor coupling parameters were used for the comparison of $\bar{C}$ of eq. (5). The parameter $\gamma = 4.61/R_0^2$, $R_0 = 1.18A^{\frac{1}{3}} \times 10^{-13}$ cm has been used as in II. The quantities V_{SR} and V_{SI} were then computed with $A = 12$ and $R = 3.06 \times 10^{-13}$ cm taken from ref. [4]) using the approximations of eq. (8a) and (12) for the incoming particle energies $E_L = 100$ and 200 MeV. Using the rather crude form of eq. (12) the seemingly best fit gives $V_{SR} + iV_{SI} \approx (2.0 + i0.5)$ MeV at $E_L = 100$ MeV. If the values of the parameters V_{CR} and V_{CI} are taken somewhat inconsistently from ref. [4]) for the same S-M phase-shifts, we obtain rather too small polarizations (e.g., $P(\theta = 20°) \approx 15.6\ \%$) in comparison with the data by Dickson and Salter [15]). In fact, the values of V_{SR} and V_{SI} given in ref. [4]) are significantly larger. The result of ref. [4]), that V_{SI} is much smaller than V_{SR}, is confirmed.

The more accurate approximation of eq. (8a) with the same S-M phase shifts and the same parameters γ, A and R gives at $E_L = 100$ MeV the result $V_{SR} + iV_{SI} \approx (3.1 - i0.8)$ MeV, and at $E_L = 200$ MeV: $(2.2 - i0.6)$ MeV. The double integrations of eq. (8a) were performed numerically. These numbers are a little smaller than the numbers obtained by Ohnuma [4]) using the RW theory, probably owing to the fact that the integrations over the momentum of the target particle generally tend to reduce the calculated well depths; e.g., Ohnuma's $V_{SR} + iV_{SI} \approx (3.8 - i1.1)$ MeV at $E_L = 100$ MeV. However, both the order of magnitude and the variation with the incoming particle energy of the parameters V_{SR} and V_{SI} are in essential agreement with the RW theory even at

energies as low as 100 MeV. In order to illustrate the effect of the r-dependent factor of the density we considered the unrealistic limiting case of $\gamma = 0$. In this case we find $V_{SR} = 4.9$ MeV at $E_L = 100$ MeV.

The above quoted numbers obtained from eq. (8a) together with Ohnuma's V_{CR} and V_{CI} give an even slightly better fit to the 95 MeV polarization data [15]) than the fit of fig. 2 of ref. [4]). However, in order to have realistic results for the polarization, one should first calculate V_{CR} and V_{CI} from the same approximation consistently.

References

1) J. Sawicki and R. Folk, Nuclear Physics **11** (1959) 368
2) J. Sawicki, Nuclear Physics **13** (1959) 350
3) W. B. Riesenfeld and K. M. Watson, Phys. Rev. **102** (1956) 1157
4) S. Ohnuma, Phys. Rev. **111** (1958) 1173
5) H. A. Bethe, Annals of Phys. **3** (1958) 190
6) A. H. Cromer, preprint
7) A. M. Saperstein and D. Feldman, Nuovo Cimento **14** (1959) 457
8) J. Dabrowski and J. Sawicki, Nuclear Physics **13** (1959) 621
9) H. P. Stapp, T. J. Ypsilantis and N. Metropolis, Phys. Rev. **105** (1957) 302
10) L. S. Kisslinger, Phys. Rev. **104** (1956) 1077
11) U. Meyer-Berkhout, K. W. Ford and A. E. Green, Annals of Phys. **8** (1959) 119
12) H. S. Koehler, Nuclear Physics **1** (1956) 433
13) I. I. Levintev, Soviet Phys. JETP **1** (1956) 175
14) P. S. Signell and R. E. Marshak, Phys. Rev. **109** (1958) 1229
15) J. M. Dickson and D. C. Salter, Nuovo Cimento **7** (1957) 235

1.C:8.B

Nuclear Physics **17** (1960) 96—108; © *North-Holland Publishing Co., Amsterdam*

Not to be reproduced by photoprint or microfilm without written permission from the publisher

A MODEL FOR THE INTERPRETATION OF K⁻-MESON CAPTURES AT REST IN COMPLEX NUCLEI

I. E. McCARTHY † and D. J. PROWSE

Department of Physics, University of California, Los Angeles 24, California ††

Received 8 February 1960

Abstract: A model for the interactions of K⁻-mesons in complex nuclei is proposed which combines the peripheral absorption ideas of Jones and to a limited extent the idea of volume absorption proposed by Gilbert, Violet and White. The model is capable of explaining the observed experimental effects without demanding momentum correlations in the nucleus and without the necessity of invoking the idea of nuclear surface clusters first proposed by Wilkinson.

The energy spectra of both the Σ^+- and Σ^--hyperons resulting from the single nucleon reactions in emulsion nuclei in which both pion and Σ-hyperon are observed to emerge from the interaction, are well fitted assuming that these reactions mainly occur at the nuclear surface. The energy spectrum of Σ-hyperons (> 60 MeV) unaccompanied by π-mesons which are assumed to result from the multi-nucleon reaction of the type $K^- + p + p \rightarrow \Sigma^+ + n$ and similar reactions, is consistent with the assumption that the nucleons involved are uncorrelated in momentum space. The relative cross sections for the two processes are also consistent with this assumption, hence the nucleon cluster interpretation of these events is open to doubt.

1. Introduction

A number of emulsion groups (e.g., European Collaboration [1]), Eisenberg *et al.* [2])) have made extensive studies of the K⁻-meson capture process in nuclear emulsion and have reached the conclusion that the number of multi-nucleon absorption events is appreciable, representing some 15—25 % of the total, and that the single nucleon absorption events which occur are mainly peripheral.

The experimental evidence for the multi-nucleon fraction is based on the emission of an appreciable number of fast hyperons (> 60 MeV) always unaccompanied by a pion. The great majority of those with energy less than 60 MeV are accompanied by a pion and come from the well-known one-nucleon reaction

$$K^- + p \rightarrow \Sigma^{\pm} + \pi^{\mp}.$$

The charged pion absorption probability has been determined by both the above groups to be quite small (0.12 for the negative pion). Such a low figure can only

† Permanent address: Department of Mathematical Physics, University of Adelaide, Adelaide, South Australia.

†† Partially supported by programs of the U. S. Atomic Energy Commission and the National Science Foundation.

arise if the one-nucleon reaction is mainly peripheral, although it must be borne in mind that this absorption ratio depends on events in which a Σ-hyperon is seen to emerge. If the hyperon is very strongly interacting in nuclear matter (as it is believed to be [3])), this restriction on the events for which the pion absorption probability is measured will heavily bias the experiment in favour of peripheral interactions *in any case*, when the pion absorption probability is expected to be low.

There is little evidence to suggest that the multi-nucleon reaction is peripheral, although Jones [4]) has shown that the K^--meson is likely to be captured in the periphery (i.e., outside the radius at which the density is less than 20 % of the maximum value) for any reasonable value of the absorption potential ($\approx$ 100 MeV) †, and it has been suggested by Wilkinson [6]) that both the one- and multi-nucleon reactions take place in particle clusters which may exist in the extreme nuclear surface. Eisenberg *et al.* [7]) have pointed out numerous differences in the reactions of K^--mesons at rest and in flight which suggest a different mechanism for each, namely a volume absorption for the interactions in flight and a peripheral absorption at rest.

The model proposed by Gilbert, Violet and White (GVW) [8]) to explain the absorption of K^--mesons at rest assumed that the K^--mesons interacted with single nucleons situated deep enough in the nucleus to feel a substantial nuclear potential. This model was used by GVW to explain the differences in the Σ^+ and Σ^--hyperon energy spectra as being due to the different Coulomb potentials seen by the Σ^+ and Σ^--hyperons. They also showed that the ratio of Σ^-/Σ^+ actually observed was likely to be smaller than that at production because of the Coulomb potential trapping a number of Σ^--hyperons in the nucleus. In addition an analysis of the Σ^+ and Σ^- spectra of GVW by Capps [9]) utilizing the same model was claimed to give a slight indication of an attractive potential of some 25 MeV for the Σ^+ and Σ^--hyperon. This conclusion was reinforced by a study of events giving a single pion by GVW. The energy spectrum of these pions was considerably different from that for pions accompanied by a Σ-hyperon. No pions above about 90 MeV would normally be possible from a reaction in which a Σ-hyperon is involved; if, however, the Σ-hyperon is trapped in a negative energy state in the potential well, additional energy becomes available for the pion. Observation of single pions at energies above 100 MeV is therefore evidence for trapping provided that these pions are produced accompanied by a hyperon. GVW concluded from the absence of single pions near 160 MeV that the $\Lambda^0+\pi^-$ reaction was very much unfavoured and that the pions above 100 MeV therefore did arise from the $\Sigma^\pm+\pi^\mp$ reactions.

† Optical model studies of the reaction cross section and the angular distribution of elastic scattering from emulsion nuclei confirm that this is the correct order of magnitude. The real part of the potential is probably 25 MeV attractive [5]), but this is not sufficient to invalidate the calculations of Jones.

A number of groups [1, 2]) have contested this conclusion and the model of Jones [4]) of peripheral capture seemed to support them. If one accepts peripheral interactions for all K^--mesons, the existence of these high energy pions can only be explained by the $\Lambda^0+\pi^-$ reaction because the nuclear potential experienced by the Σ-hyperons at 7×10^{-13} cm (the radius of the 5g orbit in silver from which Jones supposes capture) is likely to be very small and unable to account for these events; the Λ^0-reaction only gives rise to negative pions whereas the $\Sigma^\pm$-reactions can give rise to pions of both signs. A test for the trapping mechanism is thus provided by the existence or absence of positive pions above 100 MeV. Experiments at Livermore [10]) and at UCLA [11]), using emulsion stacks exposed to slow K^--mesons in a pulsed magnetic field in order that the charges of the particles produced could be determined by curvature measurements, have recently confirmed the existence of such high energy positive pions. It seems fairly clear therefore that some of the captures do take place in a region of the nucleus where the Σ-hyperon produced can feel an appreciable potential. The problem is therefore to reconcile the ideas of Jones with experimental facts which, although suggesting that a large number of reactions giving both Σ-hyperon and pion are peripheral, nevertheless show that an appreciable number of single nucleon reactions do proceed further inside the nucleus than suggested by Jones. It is the purpose of this paper to present a modified model for K^--meson capture which is based on the original ideas of GVW and of Jones, and which accounts for the experimental facts as known today. In addition the suggestion of Wilkinson that the multi-nucleon reaction events occur in peripheral nucleon clusters is critically examined.

2. Proposed Mechanism for K^--Nucleus Interactions at Rest

Following Jones, let us assume that the K^--meson is captured in a Coulomb orbit and cascades down in spherically symmetric states, which are greatly favoured statistically, by emitting γ-rays until it is in a 6h or 5g state in a heavy nucleus. In such a state, according to the potential measured in elastic scattering experiments, the probability of nuclear capture is about equal to the probability for the K-mesic atom to decay into the next state. The capture occurs in about 10^{-17} s.

If a reaction with a nucleon occurred within this time, the reaction products would come from far out in the nuclear surface (region A of fig. 1), where their nuclear potential is small, in violation of the experimental evidence of the effect of this potential on the pion spectrum mentioned in the introduction. Also, as suggested by Wilkinson, multi-nucleon reactions could not occur unless at least two nucleons, closely correlated in momentum, were likely to be found at this distance.

A way out of the dilemma, which is consistent with elastic scattering and

absorption measurements, and which does not require nucleon correlations, is as follows. Let us assume that rather than being captured by the first nucleon it sees, the K⁻-meson is likely to undergo an elastic scattering. That is, it is absorbed from the entrance channel by transferring some of its angular momentum to a nucleon. Such transfer must increase the angular momentum of the nucleon so as not to violate the Pauli exclusion principle. Hence the angular momentum of the K⁻-meson is reduced and it drops into a part of the nucleus (region B of fig. 1) where it is much more likely to collide with a nucleon or group of nucleons and to react catastrophically.

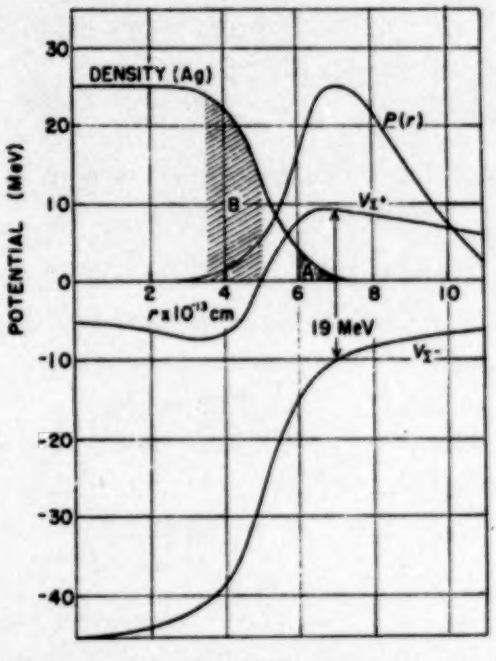

Fig. 1. Diagram of the potentials seen by Σ^-- and Σ^+-hyperons in the nucleus. A nuclear potential following the density distribution and of maximum value 25 MeV (attractive) has been chosen. Region A is the region where the K⁻-meson is removed from the entrance channel and in region B the K⁻-meson reacts with several nucleons or with single nucleons to produce π^+-mesons of more than 100 MeV. $P(r)$ represents the probability of absorption.

The relative number of reactions actually occurring where the K⁻-meson is removed from the entrance channel and in a region of higher density will be given by the relative cross section for scattering compared with that for catastrophic absorption. This is difficult to estimate because the free K⁻ — (p or n) cross section will be reduced by the inhibiting factor of the Pauli principle; in addition, experimental data are not very precise at the energies involved. The Coulomb energy of the K⁻-meson at 7×10^{-13} cm from the centre of the nucleus is about 10 MeV which corresponds to a momentum of 100 MeV/c. Such a momentum would be expected for a particle in a g state. Emulsion and bubble chamber results [12]) for free protons give a cross section of about 50 mb for each process. The inhibition due to the Pauli principle will modify the ratio

in favour of the reaction occurring in region A by a factor of roughly 2. In section 4 it will be shown that surface reactions lead to the observed hyperon spectra from the one-nucleon process.

The multi-nucleon process is expected to occur in a region of the nucleus where the density is near maximum. It is easily seen that the average nucleon spacing is such that more than one nucleon is likely to react with the K^--meson. The multi-nucleon process is known to occur with high probability in the case of π^--nucleus reactions [13]). Since the Compton wave-length of the K^--meson is much less than that of the pion, it is to be expected that the K^--meson is unlikely to react with more than two nucleons. In section 5 it will be shown that the momenta involved in our model are sufficient to lead to the observed Σ-hyperon energy spectra (> 60 MeV).

3. Effective Momentum Distribution of the K^-—p Centre of Mass in the Periphery of the Nucleus

The spectrum of the Σ-hyperons observed from the one-nucleon reaction has often been considered to reflect the momentum distribution of the nucleons involved in the reaction. The volume-interaction theories of Capps and GVW have used the volume momentum distribution $\exp(-p^2/15\ \text{MeV})$ observed in high energy (p, d) reactions [14]). Although expressing the opinion that the interactions are peripheral, Chadwick *et al.* [15]) have used the volume momentum distribution for calculating the Σ-hyperon-pion angular correlation. Capps made some assumptions about the potential seen by Σ-hyperons in the nucleus, and although the low energy ends of the spectra are fitted quite well, the number of high energy particles is overestimated.

Estimates of the negative pion absorption from bound proton reactions are in severe conflict with the volume absorption idea for this type of reaction in which both pion and hyperon are observed to emerge from the interaction. Indeed the experimental evidence is overwhelming that this type of event occurs on the periphery of the nucleus. There is therefore considerable doubt whether the volume momentum distribution for the protons is relevant to the experiment. In addition it would be surprising if the potential seen by the majority of Σ-hyperons is anything other than that due to their electric charge.

It has been stated [6]) that the 60 MeV cut-off in the observed spectra reflects the 250 MeV/c Fermi momentum of saturated nuclear matter. If the nucleon density in the surface is really small, the K^--meson does not sense saturated nuclear matter at all. The Fermi momentum would be much lower on the Fermi-Thomas model.

A possible explanation is that the nuclear surface consists of saturated nuclear matter such as α-particles whose time average density is small. It has been suggested by Wilkinson [6]) in support of this idea that the high energy

Σ-hyperons (> 60 MeV) which appear unaccompanied by pions are produced by absorption of the K^--mesons by two nucleons in such a cluster, which would have momentum components higher than the Fermi momentum for dilute nuclear matter. We have shown that this assumption is not necessary to explain the large cross section for multi-nucleon absorption and we shall show later that both the low- and high-energy Σ-hyperon spectra are consistent with the idea that the nucleon wave functions are uncorrelated.

It is clear that the Fermi-Thomas model is not good for the nuclear surface, and that the concept of a Fermi distribution for nucleon momenta is approximately meaningful only in the case when the whole nucleus is observed.

In previous calculations it was assumed that the K^--mesons were at rest relative to the nucleons. That this is not the case is seen by considering the tangential momentum of a particle in a g state at 6×10^{-13} cm. A semi-classical approximation gives an average momentum of 130 MeV/c. In quantal language, the K^--meson wave function varies more sharply than the proton wave function in the inner part of the interaction region and less sharply in the outer part. We would expect the momentum components to be comparable. The momentum distribution of partially localized particles is discussed more fully by Baker, McCarthy and Porter [16]).

In this paper we use the momentum distribution of the $K^- - p$ centre-of-mass characteristic of the surface. This concept will be discussed more fully in another publication [16]), but in the case of a plane-wave approximation it is familiar from direct interaction theory [17]). One of the major sources of error in the usual plane-wave direct interaction theory, namely the fact that a plane-wave entrance channel does not allow for the anisotropy of the region of interaction [18]). is not present in this case because the entrance channel is spherically symmetric owing to the random nature of the motion of the K^--meson just before capture.

In addition to the plane-wave assumption, we assume that the absorption of Σ-hyperons is not strongly energy-dependent, that the Σ and π-particles are produced isotropically in the centre-of-mass system by a δ-function interaction, and that the interaction is not strongly dependent on the relative momentum.

The latter approximation does not appear to be a good one at first sight, considering the fact that the cross section for the production of Σ^--hyperons in $K^- - p$ interactions is about 100 mb for relative momenta less than 100 MeV/c and 25 mb for greater relative momenta. The cross section for Σ^+-hyperons is about 25 mb at all relative momenta. If the K^--meson and the nucleon are moving isotropically with respect to each other, the relative momentum will be less than 100 MeV/c in only about 10 % of the cases and these events will be widely spread over the spectrum of the momentum of the centre-of-mass. Hence this approximation is expected to be a very good one for Σ^+-hyperons and not a bad one of the Σ^--hyperons.

In the above approximation the matrix element for the one-nucleon reaction is

$$M_1 = \text{const.} \int d^3\mathbf{r}\, e^{-i\mathbf{p}\cdot\mathbf{r}} \varphi_p(\mathbf{r})\varphi_K(\mathbf{r}), \tag{1}$$

where $\mathbf{p}$ is the final state momentum, which is also the momentum of the $K^- - p$ centre-of-mass; the functions $\varphi_p(\mathbf{r})$ and $\varphi_K(\mathbf{r})$ are the proton and K-meson wave functions. For the accuracy of this work it will be sufficient to assume that the radial part of $\varphi_K(\mathbf{r})$ is proportional to a factor $\rho(r)$ which is constant outside a radius $R \times 10^{-13}$ cm and drops sharply inside. This is justified by the fact that the proton wave function drops sharply outside R and becomes the dominant factor in the integrand. We shall use a shell model wave function for $\varphi_p(\mathbf{r})$. The momentum distribution is proportional to

$$f(p) = p^2 \sum_L C_L \left| \int dr r^2 j_L(pr)\rho(r)R_p(r) \right|^2, \tag{2}$$

where $R_p(r)$ is the radial proton wave function, C_L are coefficients obtained [17]) by the vector addition of the proton and K^--meson angular momenta L_p and L_K. We have

$$|L_p - L_K| \leqq L \leqq L_p + L_K. \tag{3}$$

The values of L are not distinguished by the experiment. The coefficients C_L favour intermediate values of L.

The general features of the distribution for a given L are as follows. If the interaction is completely localized at R, the momentum distribution is

$$f_L(p) = p^2[j_L(pR)]^2. \tag{4}$$

If the region of interaction is roughly the nuclear surface, peaks in the distribution after the first are almost completely suppressed, and this is not strongly dependent on the detailed shape of $\rho(r)$. The position of the first peak is given by L/R, but is only weakly dependent on this parameter.

In the next section it will be shown that the hyperon spectrum, which is given by an integral over the momentum distribution, is even less sensitive.

In fig. 2 the momentum distributions for $L = 2$ and 3 and $R = 5 \times 10^{-13}$ cm are compared with the distribution $\exp(-p^2/15\ \text{MeV})$. The form of $\rho(r)$ used is consistent with the model of section 2. The important general fact about surface momentum distributions is that they contain relatively fewer high and low momentum components than the Gaussian.

4. The Energy Spectra of the Σ-Hyperons

The hyperon spectra can be obtained from the momentum distribution of the $K^- - p$ system using the relativistic kinematics outlined by GVW. Some of the unknowns in the calculation are the excitation energy of the nucleus and the

nuclear potentials felt by the Σ- and π-particles. The nuclear and Coulomb potentials felt by the Σ-hyperon have the effect of shifting the high energy end of the spectrum along the energy axis. The high energy end of the unshifted spectrum is insensitive to these unknown factors [8]) and they will be neglected.

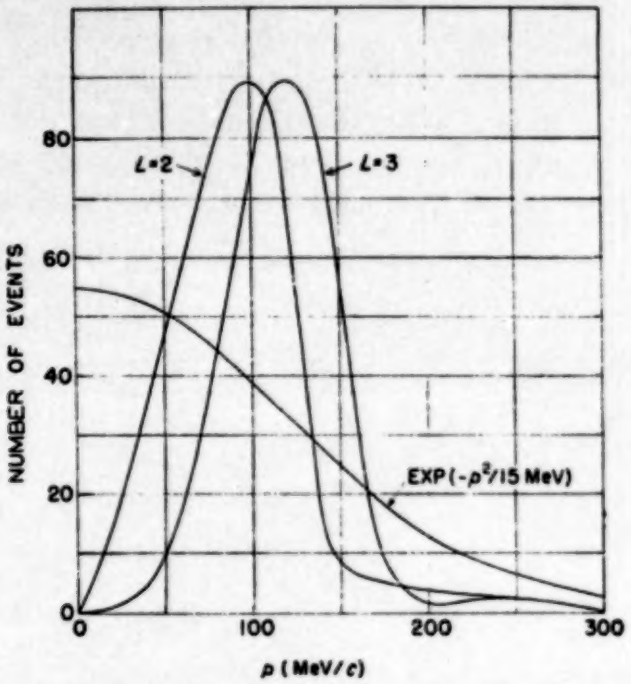

Fig. 2. The momentum distribution of the centre-of-mass of the $K^- - p$ system (omitting the phase space factor p^2) assuming that $L = 2$ and $L = 3$, in comparison with the Gaussian momentum distribution obtained from the nucleon distribution in high-energy (p, d) reactions assuming that the K^--meson is relatively stationary.

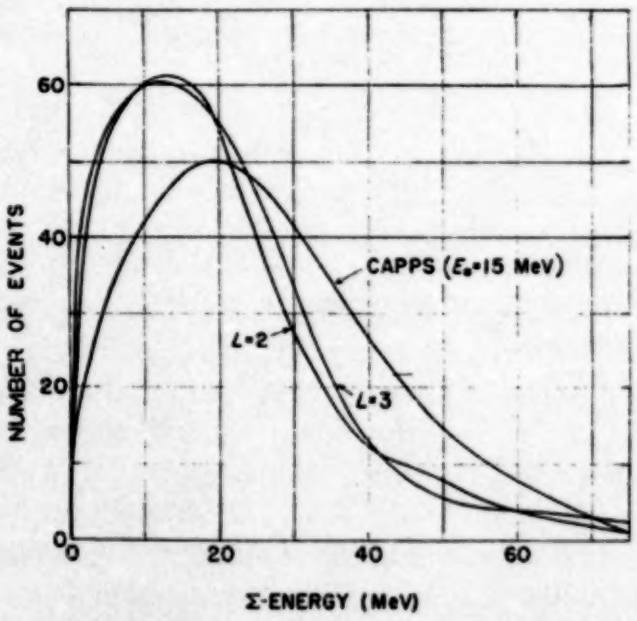

Fig. 3. Σ-hyperon energy spectra obtained from the momentum distributions of fig. 2.

The Coulomb potential will shift the Σ^+-spectrum to the right and the Σ^--spectrum to the left by an amount ΔE. Unshifted spectra are illustrated in fig. 3.

The insensitivity of the result to the assumptions for L/R is shown by the fact that a change of 50 % in L/R shifts the high-energy part of the curve by only 2 MeV and does not change its slope. The number of hyperons in the high energy tail (> 60 MeV in the Σ^+ case) of the distribution is increased by sharp localization of the reaction. The fact that the cut-off at 60 MeV is experimentally abrupt is a strong argument against more severe localization. The few events in the tail can be regarded as fluctuations due to the uncertainty principle.

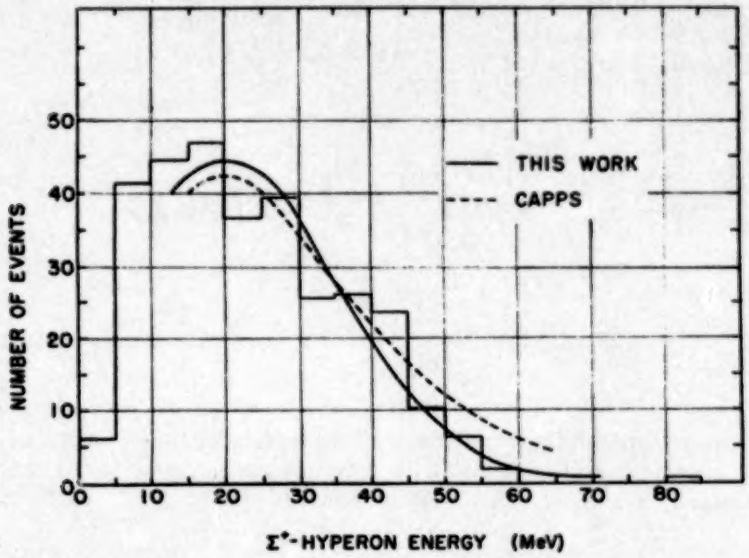

Fig. 4. Σ^+-hyperon energy spectrum obtained by shifting the $L = 3$ spectrum of fig. 3 to the right by 9 MeV, compared with an experimental spectrum obtained by adding the results of various groups [1, 2, 8, 15, 20]).

Since we expect the high-energy part of the spectrum to be sensitive only to the momentum distribution and the Coulomb potential, we shall only attempt to fit the experimental results for $E > 15$ MeV in the Σ^+-hyperon case. In the Σ^--hyperon case, the part of the spectrum that is sensitive to more detailed assumptions is shifted out of the positive energy region. We have made the calculation for silver which is representative of large emulsion nuclei. The ratio of captures by light nuclei to those by heavy nuclei is thought to be 25 % [19]). Since L/R is roughly the same for both, the Coulomb potential is the only distinguishing factor. The difference in the energy shift expected between ratios 0 and 0.25 is 0.5 MeV. In fig. 4, the fit obtained for Σ^+-hyperons using $L = 3$ is illustrated. The curve was fitted by adjusting the ordinate scale and shifting the abscissa by 9 MeV towards higher energies. This is consistent with Coulomb repulsion. To test whether the assumptions of small nuclear potentials

are valid, the same ordinate scale was used and the curve was shifted 9 MeV to the left in an attempt to fit the Σ^--spectrum. The result is illustrated in fig. 5.

There is obviously a deficiency of low energy Σ^--hyperons. It may be seen from the potentials illustrated in fig. 1 that low energy Σ^--hyperons can be refracted and reflected into a part of the nucleus where a second interaction is likely to occur and thus remove such an event from the $\Sigma+\pi$ category. Low energy Σ^+-hyperons will be refracted away from the nucleus and not reflected so much since they are crossing a boundary from a region of high refractive index to one of lower refractive index. Thus there is no deficiency of Σ^+-hyperons.

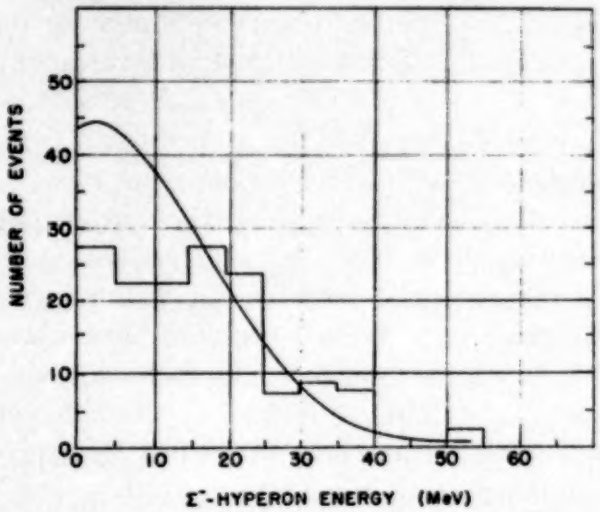

Fig. 5. Σ^--hyperon energy spectrum obtained by shifting the $L = 3$ spectrum of fig. 3 to the left by 9 MeV, compared with an experimental spectrum obtained by adding the results of various groups [1, 2, 6,15, 20]).

The fact that we do not have to shift both spectra in the same direction is evidence that the nuclear attraction is negligible as would be expected from the surface reaction assumption. In the model of Capps, such a shift must be made. He attributes it to an attractive nuclear potential. If the present model is correct, it is seen from the unshifted spectra in fig. 3 that the model of Capps, which is based on a Gaussian momentum distribution, predicts too many high momentum components. This fact is consistent with the surface reaction picture. The Gaussian was originally found necessary in order to reproduce the effects of high momentum components which are found in nuclear matter of maximum density [21]).

The relative number of Σ^+ and Σ^--hyperons actually derived experimentally has not been in accord with that expected from the hydrogen bubble chamber results [12]) which favour Σ^--hyperon production in the ratio 2 : 1. In events in which both Σ-hyperon and pion emerge the ratio observed in emulsion should

therefore be 1 : 2 if we neglect the motion of the particles. Above a relative momentum of 100 MeV/c, the ratio at production from protons is about 1 : 1. More than 90 % of the interactions in the periphery will have such a relative momentum, considering the average proton and K^--meson momenta already estimated. It is justifiable to neglect the energy dependence below 100 MeV/c. From fig. 3, it is clear that about 70 % of the Σ^--hyperons produced would actually escape the Coulomb potential if it were not for refraction and reflection effects which strongly modify the spectrum at low energies as mentioned above. A comparison between the curves in fig. 5 indicates that this mechanism is responsible for a further diminution of 20 % in the number of Σ^--hyperons finally emerging.

Thus the fraction of Σ^--hyperons observed should be only 50 % of those produced, which leads to a $\Sigma^+ : \Sigma^-$ ratio of 2 : 1, in agreement with that observed experimentally [1]).

It is important to note that the Σ-hyperon spectra are by far the best experimental data for comparison with a semi-classical theory since, as we have seen, they are so insensitive to assumptions about the various potentials. The pion, being a much lighter particle, is sensitive to such assumptions and its spectrum gives a measure of the potential between the Σ-hyperons and the nucleus. Measurements of the final state momentum distribution have been made, but they are not suitable for comparison with a semiclassical theory owing to their extreme dependence on the initial direction of the Σ-hyperon and the pion. If these particles are initially travelling in a tangential direction, the nucleus will transfer considerably more momentum to them for the same energy transfer than if they started radially. Owing to the size of the region of interaction, a semi-classical calculation involving vector momenta is completely invalidated by the uncertainty principle. A quantal calculation of the type given in section 3 is capable of giving only the distribution of the absolute value of the momentum of the centre-of-mass under the assumption of isotropy which, in this case, is justified.

5. The Spectrum of Hyperons from Multi-Nucleon Interactions

Consider the case in which the K^--meson reacts with two nucleons. Using the same assumptions as in section 3, and uncorrelated proton wave functions, the momentum distribution for the centre-of-mass of the K^--two-nucleon system is given by the square of the matrix element

$$M_2 = \text{const.} \int \mathrm{d}^3\mathbf{r} \mathrm{e}^{-\mathrm{i}\mathbf{p}\cdot\mathbf{r}} \varphi_K(\mathbf{r}) \varphi_{p1}(\mathbf{r}) \varphi_{p2}(\mathbf{r}), \tag{5}$$

where the definition of the wave functions is analogous to that of eq. (1). Since the data are not extensive enough for an attempt at fitting, we shall be

content to point out the general features of the spectrum. Since the product of three radial wave functions appears in the integration, the integrand will be slightly better localized leading to some higher momentum components; however, we may see approximately what happens by considering the first peak in the momentum distribution. This will be spread more than in the one-nucleon reaction case because L can take more values. We would expect the distribution to be shifted towards somewhat higher momentum values since R is smaller than in the one-nucleon case. However, the momentum distribution will have roughly the same character as before, that is a peaked distribution centered at about 150 MeV/c with a spread somewhat less than 100 MeV/c. Similar considerations apply when more than two nucleons are concerned in the hyperon production.

The centre-of-mass momentum of the Σ-hyperon is about 500 MeV/c in the two-nucleon case, so we would expect the spectrum to be spread from about 20 MeV to 200 MeV in agreement with the experimental data.

6. Conclusions

K^--mesons at rest are absorbed by the nucleus at the extreme surface where the meson is likely to interact with a nucleon once in about 10^{-17} s. The absorption mechanism consists either of a reaction with the nucleon in which a Σ-hyperon and a π-meson is produced, or of a transfer of angular momentum to the nucleon in such a way that the K^--meson drops into a much denser part of the nuclear surface. Here it may again react with one nucleon, but it is also very likely to react with two or more nucleons so that a π-meson is not produced.

It is thus possible for the interaction to occur at such a depth that the hyperon is trapped in a nuclear potential. Hence π-mesons with energy greater than the maximum for a reaction in the Coulomb potential alone may be observed in the one-nucleon process. This energy difference gives an estimate of the potential between the Σ-hyperon and the nucleus. It is attractive.

The energy spectra of the hyperons in the one-nucleon events are better fitted with the assumption of a surface rather than a volume interaction. In the case of the multi-nucleon reaction it is unnecessary to assume nucleon correlations to explain the observed spectra.

The results obtained here have an important bearing on the many-body problem of the finite nucleus, since they throw light on the nature of dilute nuclear matter. It has been proved possible [22]) to calculate the wave functions for a finite nucleus with the assumption that the correlations in dilute nuclear matter are the same as those in infinite nuclear matter of the same density. Such a calculation would be invalid if dilute nuclear matter consisted of nucleon clusters. Since the wave functions in the finite nucleus calculations of Brueckner *et al.* [22]) are almost indistinguishable from single-particle wave functions in a

local potential, it is significant that such wave functions are adequate to describe K^--meson interactions, as well as other direct interactions. The K^--meson interactions at rest have been thought to provide evidence for such clusters; however, it is now seen that this is not the case.

There is strong evidence that direct (p, α) reactions occur frequently [23]). However, it can be shown [24]) that α-particle clusters can be excited in nuclear matter when the nucleon correlations are of the weak long-range type which are well-known to produce nuclear quadrupole moments and α-particle model effects. It is not difficult to believe that protons can penetrate the nucleus to a sufficient depth to excite such clusters directly.

We are grateful to Dr. G. B. Chadwick, Professor D. H. Stork, Professor H. K. Ticho and Dr. R. S. White for many discussions, and Dr. White for sending us pre-publication results.

References

1) K^--collaboration, Nuov. Cim. **13** (1959) 690; **14** (1959) 315
2) Y. Eisenberg, W. Koch, M. Nikolić, M. Schneeburger and H. Winzeler, Nuov. Cim. **11** (1959) 351
3) H. K. Ticho, private communication
4) P. B. Jones, Phil. Mag. **3** (1958) 33
5) M. A. Melkanoff, D. J. Prowse and D. H. Stork, Phys. Rev. Letters **4** (1960) 183
6) D. H. Wilkinson, Phil. Mag. **4** (1959) 215
7) Y. Eisenberg, W. Koch, E. Lohrmann, M. Nikolić, M. Schneeburger and H. Winzeler, Nuov. Cim. **9** (1958) 745
8) F. C. Gilbert, C. E. Violet and R. S. White, Phys. Rev. **107** (1957) 228
9) R. H. Capps, Phys. Rev. **107** (1957) 239
10) R. S. White, private communication
11) D. J. Prowse and D. H. Stork, private communication
12) M. F. Kaplon, Proc. Ann. Int. Conf. High En. Phys. CERN (1958) 171
13) M. G. K. Menon, H. Muirhead and O. Rochar, Phil. Mag. **41** (1950) 583
14) K. R. Greider, Phys. Rev. **114** (1959) 786
15) G. B. Chadwick, S. A. Durrani, P. B. Jones, J. W. G. Wignall and D. H. Wilkinson, Phil. Mag. **3** (1958) 1193
16) I. E. McCarthy and D. L. Pursey, to be published;
G. A. Baker Jr., I. E. McCarthy and C. E. Porter, to be published
17) N. Austern, S. T. Butler and H. McManus, Phys. Rev. **92** (1956) 350
18) I. E. McCarthy, Nuclear Physics **11** (1959) 574
19) C. Carote, I. Hauser, U. Kundt, U. Krecker, K. Lanius, K. Lewin and H. W. Meier, Nuov. Cim. **16** (1959) 432
20) S. Nilsson and A. Frisk, Ark. Fys. **14** (1958) 303
21) K. A. Brueckner, R. J. Eden and N. C. Francis, Phys. Rev. **98** (1955) 1445
22) K. A. Brueckner, Proc. Int. Conf. Nucl. Optic. Model (1959) 145
23) P. E. Hodgson, Phil. Mag. **44** (1953) 1113
24) K. Wildermuth and Th. Kanellopoulos, Nuclear Physics **7** (1958) 150

2.A.1

Nuclear Physics **17** (1960) 109—115; © *North-Holland Publishing Co., Amsterdam*

Not to be reproduced by photoprint or microfilm without written permission from the publisher

TOTAL NEUTRON CROSS SECTION OF B^{10} IN THE THERMAL NEUTRON ENERGY RANGE

H. W. SCHMITT, R. C. BLOCK and R. L. BAILEY

Oak Ridge National Laboratory, Oak Ridge, Tennessee

Received 2 November 1959

Abstract: A precise determination of the total neutron cross section of B^{10} has been made by means of transmission measurements of boron samples highly enriched in B^{10}. The ORNL fast chopper time-of-flight spectrometer was used to obtain results in the neutron energy range $0.018 \leqq E \leqq 0.4$ eV. It is found that the total cross section of B^{10} in this energy range follows the relation $\sigma_t(b) = (612 \pm 6)/\sqrt{E(eV)}$. The total cross section of B^{10} for neutrons of energy 0.0253 eV (velocity = 2200 m/sec) is found to be 3848 ± 38 b.

1. Introduction

The total neutron cross section of B^{10} in the thermal and low-eV energy range has in general been derived from measurements [1–7]) of the total cross section of natural boron together with measurements [8–13]) of the isotopic abundances of B^{10} and B^{11} in the samples. There have been discrepancies of the order of five per cent in the reported values [14]) of σ_t for B^{10} in recent years, arising primarily from discrepancies in measurements of isotopic abundance. Because of a specific need [15]) for more precise knowledge of the B^{10} cross section, and for clarification of the above situation, the present direct total cross section measurement using boron samples highly enriched in B^{10} has been made.

2. Experimental Method

Experimentally, a straightforward neutron transmission measurement was made using the ORNL fast chopper time-of-flight spectrometer [16]) installed at the Oak Ridge Research Reactor. The M-I rotor, a 45.7-cm diameter stainless steel rotor with 0.076-cm wide parallel slits, was used in conjunction with a 44.6-m flight path. A bank of six BF_3 proportional counters was used to detect the neutrons. The data were collected in a 2048-channel time-of-flight analyzer, used here in two sections of 1024 channels each to store sample-in and sample-out counts. The rotor was spun at 130 or 220 r.p. min to allow low energy neutrons to pass through; the resultant resolution was about 2 μsec/m. The energy range covered in a single run was $0.018 \leqq E \leqq 0.04$ eV, $0.03 \leqq E \leqq 0.1$ eV, or $0.1 \leqq E \leqq 0.4$ eV. A sample of B_2O_3 dissolved in D_2O and a compensating sample of pure D_2O were alternately placed in the neutron beam at intervals of

5 to 10 minutes to average out the effects of slowly varying pile power and long-term electronic drifts.

The B_2O_3 was prepared as follows: The original boron metal powder was dissolved in nitric acid, and boric acid was then crystalized out of solution. The boric acid was thoroughly dehydrated to B_2O_3 which in turn was fused in a platinum dish. The amount of fused B_2O_3 was carefully determined by weight. The B_2O_3 was immediately dissolved in D_2O. One of more aliquots were taken and diluted volumetrically with D_2O to known concentrations of B_2O_3 in solution. After all cross section measurements were completed, titrations of some of the samples were carried out to determine the B_2O_3 concentrations. Titration results agreed with the original weight determinations within 0.7 per cent for these samples. Spectrochemical analysis of the solutions indicated less than 0.1 per cent metallic and rare earth impurities in the samples. Pertinent sample data are given in table 1.

TABLE 1
Sample data for total cross section measurement of B^{10}

Sample No.	Isotopic Composition (per cent B^{10})	B^2O^3 Concentration (mg/cm^2)	Sample Thickness (B^{10} atoms/$cm^2 \times 10^{-20}$)
IA–1	96.64±0.05	8.01	2.787±0.014
IA–2	96.64±0.05	25.03	8.705±0.061
IA–3	96.64±0.05	5.43	1.891±0.010
IIA	99.89±0.05	8.41	3.308±0.024
IIB	99.89±0.05	8.09	3.183±0.027
IIIA	96.39±0.05	8.48	3.215±0.026

In Column 1, the Roman numerals indicate initial boron samples obtained from the ORNL Isotopes Division; the letters and Arabic numerals indicate chemical preparation. For example, a single concentrated solution of Sample I was used in preparing transmission samples of three different concentrations; in the case of Sample II, two complete and independent chemical preparations were made. Estimated uncertainties in sample thickness are included in Column 4.

Matched aluminium sample holders were used for the compensating D_2O sample and the B_2O_3—D_2O sample; thus the liquid thicknesses were identical. All of the D_2O used in a given solution and compensator was taken from the same original D_2O sample. Since the total cross section of the D_2O enters into the B^{10} total cross section determination, as discussed below, this cross section was directly measured with the chopper. A comparison of this measurement with previously reported results for H_2O [17]) and D_2O [18]) total cross sections indicates an H_2O content of less than 0.9 per cent in each case, as expected for these D_2O samples.

An additional measurement was made of the relative transmissions of the two empty aluminium sample containers used respectively for the boron solutions and the D_2O compensator. These two transmissions agreed within 0.1 per cent, indicating no detectable deposition of boron on the aluminum walls.

3. Analysis of Data

In the determination of B^{10} total cross section values as a function of energy, it was necessary to apply only three corrections to the transmission data. These will be discussed in turn.

1) Correction due to background in the BF_3 counters. The neutron backgrounds which inherently affect this type of measurement arise from (a) ambient room background, (b) high energy neutrons which leak through the chopper rotor, (c) neutrons which are scattered by the rotor only to be rescattered into the direction of the counters, and (d) neutrons scattered near the detector which arrive at the detector with an incorrect time of flight. The last of these backgrounds, (d), called the "spurious" background, was negligible in this experiment as the detector was almost completely surrounded by a 1.5-mm thickness of cadmium backed by a 5-cm thickness of boron carbide. Backgrounds from the other three sources were determined by two separate measurements as follows: (1) the background counting rate was measured with the rotor displaced to cut off the neutron beam, and (2) with the rotor in its normal aligned position, the background counting rate was measured with a 1.5-mm thick cadmium absorber in the beam. Results of these two measurements agreed within 10 per cent, indicating that the third source of background, (c) mentioned above, was negligible. Thus the background may be attributed to (a) and (b) and was accurately determined by routine transmission measurements with a 1.5-mm thickness of cadmium in the neutron beam. The total effect of background was quite small; the correction in the determination of σ_t for B^{10} amounted to no more than one per cent in any of the measurements.

2) Correction due to displacement of D_2O. Although the D_2O thickness in the sample-out measurement was identical to the solution thickness in the sample-in measurement, a small correction has been included for the fact that the D_2O content in molecules per cm^2 was not identical for the two cases. The correction was applied using the known B_2O_3 concentration together with the measured solution density, the measured density of the D_2O, and the measured total cross section of the D_2O sample. The magnitude of the correction is less than 0.4 per cent.

3) Correction due to the presence of oxygen and B^{11}. This correction is straightforward and simply corrects the measured cross section for the presence of oxygen and B^{11} to obtain the B^{10} total cross section. Total cross sections of oxygen and B^{11} for this purpose were taken from the literature [17, 14a]); the magnitude of the correction is less than 0.5 per cent.

The background correction was applied directly to the transmission data, and from these background-corrected transmission data the "effective total cross section" vs. energy for a given sample in a given run was obtained. The effective total cross section, σ_{eff}, is defined according to the equation

$$N_{B^{10}}\sigma_{eff} = -\ln T = N_{B^{10}}\sigma_{B^{10}}+N_{B^{11}}\sigma_{B^{11}}+N_{oxy}\sigma_{oxy}-(\Delta N)\sigma_{D_2O} \qquad (1)$$

where T is the background-corrected transmission, N_x is the thickness of material x in atoms per cm², ΔN is the difference in D_2O content in atoms per cm² between the sample solution and the compensating D_2O sample, and σ_x is the total cross section of element x (except σ_{D_2O} which is the measured total cross section of the D_2O sample of this experiment). In solving for the B^{10} total cross section from eq. (1), it is seen that the corrections for oxygen and B^{11} and for the difference in D_2O content between the sample solution and compensator sample tend to cancel; the net correction is less than about 0.2 per cent of σ_{eff}, and the uncertainty is of the order of 0.1 per cent. (As pointed out by Egelstaff [2]), the effect of chemical binding on the scattering cross sections introduces an error in σ_t for B^{10} of less than 2 barns per boron atom, or less than 0.1 per cent in this experiment.) Table 2, which contains a summary

TABLE 2
Summary of Results

Sample No. (Table 1)	Energy Range (eV)	Mean $\sigma_{eff}\sqrt{E}$ (b · eV½)	Corrections (b · eV½)		Mean $\sigma_t\sqrt{E}$ for B^{10} (b · eV½)	Mean $\sigma_t\sqrt{E}$ for B^{10} for each sample (b · eV½)
			D_2O	Oxygen $+B^{11}$		
IA−1	0.03 −0.1	641	+0.8	−1.7	641	
IA−1	0.018−0.04	640	+0.6	−1.3	639	
IA−2	0.03 −0.1	635	+1.5	−1.7	635	639±5
IA−2	0.1 −0.4	630	+2.5	−2.9	630	
IA−3	0.018−0.04	644	+0.4	−1.3	643	
IIA	0.018−0.04	611	+0.6	−1.2	611	610±6
IIA	0.03 −0.1	610	+0.8	−1.7	609	
IIB	0.018−0.04	610	+0.6	−1.2	610	610±6
IIB	0.03 −0.1	611	+0.8	−1.7	610	
IIIA	0.03 −0.1	617	+0.8	−1.7	616	616±6
IIIA	0.018−0.04	618	+0.6	−1.3	617	

Uncertainty in the mean value of $\sigma_t\sqrt{E}$ for each sample includes uncertainty in sample thickness and B^{10} concentration. (See text for further details.)

of results, gives for each run the weighted mean value of $\sigma_{eff}\sqrt{E}$, the corrections applied, and the mean value of $\sigma_t\sqrt{E}$ for B^{10}. Fig. 1 shows a plot of $\sigma_{eff}\sqrt{E}$ vs. $\sqrt{E}$ for a typical run.

In order to check the $1/v$ (v = neutron velocity) dependence of the sample cross section, a second analysis was done as follows: the curves of $\sigma_{eff}\sqrt{E}$ vs. $\sqrt{E}$ were fitted by the method of least squares to the equation

$$\sigma\sqrt{E} = a+b\sqrt{E} \qquad (2)$$

where $b \neq 0$ indicates non-$1/v$ behaviour of the cross section. For every run

the values of a and b together with the associated statistical uncertainties were obtained. In all cases except one, the value of b was within two standard deviations of zero. A weighted mean value of the constant a for all runs of a given sample (IA, IIA, IIB or IIIA) was obtained; this value agreed within 0.8 per cent with the mean value of $\sigma_{eff}\sqrt{E}$ obtained from the corresponding runs. Thus it is indicated that any non-$1/v$ term in the measured total cross

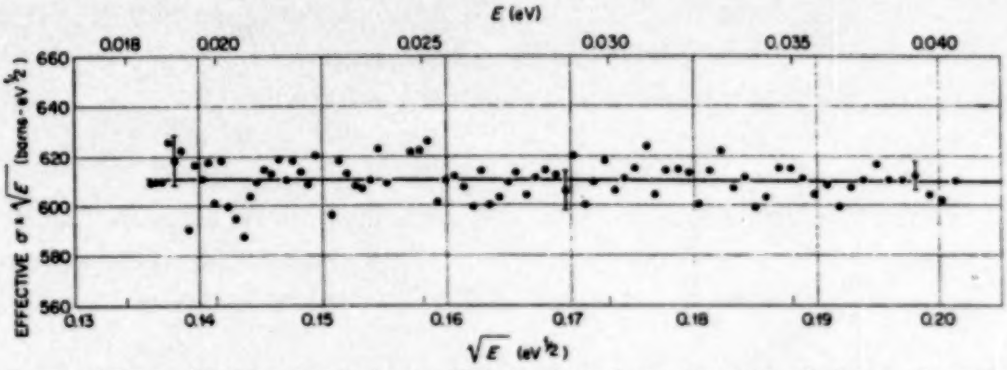

Fig. 1. $\sigma_{eff}\sqrt{E}$ vs. $\sqrt{E}$ for a typical run. Points plotted are averages of eleven channels; the entire neutron energy range is covered by 1024 channels. Flags indicate typical statistical uncertainties only.

section is negligible, and that indeed the total cross section for B^{10} follows the $1/v$ law to quite good accuracy in the energy range of the present experiment. This particular result is not surprising inasmuch as, for example, the scattering cross section of B^{10} is of the order of 4 barns [14a]), compared with measured total cross sections greater than 2000 barns for this experiment.

4. Results and Discussion

A summary of results is given in table 2. Fifteen runs were made using four independent chemical preparations of samples and various combinations of boron concentration and energy range. Results are reported according to sample and energy range; see table 1 caption for explanation of sample designation. Weighted mean values of $\sigma_{eff}\sqrt{E}$ are tabulated, and the corrections are indicated. Finally, the weighted mean values of $\sigma_t\sqrt{E}$ for B^{10} for all cases are tabulated in column 6, and the weighted mean value of $\sigma_t\sqrt{E}$ for B^{10} for each independently prepared sample is given in column 7.

A sufficient number of counts was accumulated in each transmission measurement so that the effect of counting statistics on the mean value of $\sigma_{eff}\sqrt{E}$, and hence $\sigma_t\sqrt{E}$ for B^{10}, for each run was of the order of ± 0.3 per cent or less. The fluctuations which occurred for runs on the same sample were not inconsistent with such a variation; thus, the effect of small pile power changes, small changes in electronic circuit characteristics, etc., appears to be negligible. It is evident that the dominant uncertainty in the mean value of $\sigma_t\sqrt{E}$ for B^{10} obtained from a single sample is the uncertainty in the sample content itself.

All uncertainties are taken into account in the combined uncertainties given in column 7, table 2.

It is seen in table 2 that the result obtained for sample IA [19]) differs markedly from the results obtained for samples IIA, IIB, and IIIA. Since the discrepancy is more than four standard deviations, it is concluded that a systematic error, whose source is unknown, occurred. All calibrations and other tests in all transmission measurements indicated valid measurements were made; titration of the samples after completion of the measurements yielded results which agreed within 0.7 per cent with the original quantitative preparations based on weights. Also the quantity $\sigma_t\sqrt{E}$ for B^{10} appeared to be constant over the entire energy range of the experiment. While it is difficult to designate the source of such a systematic error, two possibilities may be suggested: (1) high cross section impurities whose presence was not detected in spectrochemical tests, (2) errors at some point in the determination of boron content in the sample in question.

In view of the considerations of the preceding paragraph, the result obtained with Sample IA is disregarded in arriving at a final mean value of $\sigma_t\sqrt{E}$ for B^{10}. The total cross section of B^{10} in the neutron energy range $0.018 \leqq E \leqq 0.4$ eV, obtained from the present experiment, is then

$$\sigma_t = \frac{612 \pm 6}{\sqrt{E(\text{eV})}} \text{ b.} \tag{3}$$

The total cross section for neutrons of energy 0.0253 eV (velocity = 2200 m/sec) is

$$\sigma_t(0.0253 \text{ eV}) = 3848 \pm 38 \text{ b.} \tag{4}$$

Since, as pointed out in the previous section, the scattering cross section of B^{10} is negligible compared to the total cross section, the absorption cross section for B^{10} in the present energy range is essentially given by eqs. (3) and (4).

This result is thus far the only published measurement of the total cross section of B^{10} in which a sample highly enriched in B^{10} has been used. Measurements of the total cross section of the Argonne-Brookhaven standard of California natural boron have been made by a number of groups [1, 2, 4, 6, 7]); the average of all results given by Hughes and Schwartz [14a]) is 755 b for $E = 0.0253$ eV (2200 m/sec). Using this cross section together with that obtained for B^{10} in this experiment, we compute the isotopic abundance of B^{10} in the Argonne-Brookhaven boron sample to be 19.6 ± 0.2 per cent. This value is in agreement with recent measurements of Sites and Spitzer [20]) and Haas *et al.* [21]), giving 19.8 ± 0.1 per cent, but in disagreement with earlier measurements of Thode *et al.* [12]) and Inghram [13]).

Further discussion added in proof:

An experiment identical with that reported in this paper has been carried out using a sample of the Argonne-Brookhaven standard natural boron, graciously provided by G. R. Ringo of Argonne National Laboratory. The sample solution was prepared exactly as described for the B^{10} samples, and used in a sample holder similar to that of the above experiment; the concentration and sample thickness were respectively 8.62 ± 0.04 mg B_2O_3 per cm^3 and $6.08\pm0.03\times10^{20}$ atoms B per cm^2. Transmission measurements were carried out as above, using the $B_2O_3-D_2O$ solution and a D_2O compensator. Two separate runs were made covering the energy range 0.022 to 0.042 eV; data were analyzed and corrections applied as described in text. Results of the two runs agreed within ±0.7 per cent. The weighted average of these runs gives the result $\sigma_t(0.0253\text{ eV}) = 757\pm6$ b for the Argonne-Brookhaven standard natural boron. Using the scattering cross sections for B^{10} and B^{11} given in ref. [14a]), we obtain $\sigma_{abs}(0.0253\text{ eV}) = 753\pm6$ b, in excellent agreement with other measurements [7, 14, 14a]) in which samples of the same boron were used.

The authors wish to thank J. R. Sites of the ORNL Analytical Chemistry Division for the mass spectrometric analyses and Mrs. Jacqueline Blackwood for her assistance in many of the calculations. Helpful discussions with J. A. Harvey and G. G. Slaughter are gratefully acknowledged.

References

1) W. W. Havens, Jr., E. Melkonian and B. M. Rustad, Columbia University Report CU-160, 1957 (unpublished)
2) P. A. Egelstaff, J. Nucl. Energy **5** (1957) 41
3) Collie, Meads and Lockett, Proc. Phys. Soc. A **69** (1956) 464
4) G. von Dardel and N. G. Sjostrand, Phys. Rev. **96** (1954) 1566
5) Scott, Thompson and Wright, Phys. Rev. **95** (1954) 582
6) Green, Littler, Lockett, Small, Spurway and Bowell, J. Nucl. Energy **1** (1954) 144
7) Carter, Palevsky, Myers and Hughes, Phys. Rev. **92** (1953) 716
8) Melton, Gilpatrick, Baldock and Healy ,Anal. Chem. **28** (1956) 1049
9) V. Shiuttse, J. Exp. and Theor. Phys. **2** (1956) 402
10) G. M. Panchenkov and B. D. Moisseev, Zh. Fiz. Khim. **30** (1956) 1118
11) O. Osberghaus, Z. Physik **128** (1950) 366
12) Thode, Macnamara, Lossing and Collins, J. Am. Chem. Soc. **70** (1948) 3008
13) M. G. Inghram, Phys. Rev. **70** (1946) 653
14) See for example values given (a) by D. J. Hughes and R. B. Schwartz, Report BNL-325, 2nd Ed. (Supt. of Documents, U. S. Printing Office, Washington, D. C. 1958), and (b) by Hughes and Harvey in the same report, first edition (1955)
15) H. W. Schmitt, Nuclear Physics, to be published
16) R. C. Block, J. A. Harvey and G. G. Slaughter, Bull. Am. Phys. Soc. **4** (1959) 270
17) E. Melkonian, Phys. Rev. **76** (1949) 1750
18) Rainwater, Havens, Dunning and Wu, Phys. Rev. **73** (1948) 733
19) H. W. Schmitt, R. C. Block and R. L. Bailey, Bull. Am. Phys. Soc. **4** (1959) 415
20) J. R. Sites and E. J. Spitzer (1959) (unpublished)
21) Haas, Rourke, Mewherter and McDonald, Knolls Atomic Power Laboratory Report KAPL-2062 (1959) (unpublished)

1.E.1:
2.A.1

Nuclear Physics **17** (1960) 116—128; © *North-Holland Publishing Co., Amsterdam*
Not to be reproduced by photoprint or microfilm without written permission from the publisher

A STUDY OF ENERGY LEVELS IN Sc^{43}, Ti^{45}, V^{47}, V^{49}, V^{50} AND Zn^{65}

G. J. McCALLUM †, A. T. G. FERGUSON and G. S. MANI ††

Atomic Energy Research Establishment, Harwell, Berkshire

Received 28 January 1960

Abstract: Thresholds for neutron emission following the proton bombardment of Ca^{43}, Ca^{44}, Sc^{45}, Ti^{47}, Ti^{49}, Ti^{50} and Cu^{65} have been studied up to a proton energy of 4.9 MeV. The positions of excited states in Sc^{43}, Ti^{45}, V^{47}, V^{49}, V^{50} and Zn^{65} have been determined.

1. Introduction

Nuclei with incomplete $1f_{\frac{7}{2}}$ shells are of great theoretical interest as they lie in a region where the j-j coupling shell model is thought to apply and where collective excitations are expected to be unimportant. In recent years much experimental information has been obtained on the excited states of nuclei in this region, the majority on neutron rich nuclei. The experiments reported here were carried out to augment these data through a study of (p, n) reactions. Apart from those in Zn^{65}, the levels reported here are in nuclei with incomplete $1f_{\frac{7}{2}}$ proton and neutron shells.

The following reactions have been studied using the Harwell Electrostatic Generator as a source of protons of energy up to 4.9 MeV:
Ca^{43}(p, n)Sc^{43}, Ca^{44}(p, n)Sc^{44}, Sc^{45}(p, n)Ti^{45}, Ti^{47}(p, n)V^{47}, Ti^{49}(p, n)V^{49}, Ti^{50} (p, n)V^{50}, Cu^{65}(p, n)Zn^{65}.
From these the positions of energy levels in the final nuclei have been determined. Where other measurements exist our results are in good agreement and in addition a number of new levels are reported.

2. Experimental Techniques

The threshold detector which was used in our experiments has been described by Evans, Kinsey and Whitmore [1]) and by Ferguson and Paul [2]). A similar detector has been developed at the Argonne National Laboratory by Lee [3, 4]).

Briefly, the detector (illustrated schematically in fig. 1) operates in the following way. Use is made of the scattering resonance [5]) in Li^7 at 258 ± 3 keV.

† Nuclear Sciences Institute, New Zealand Department of Scientific and Industrial Research; present address: Atomic Energy of Canada Limited, Chalk River, Ontario, Canada.

†† Indian Atomic Energy Commission, Atomic Energy Establishment, Trombay, Bombay, India. Present address: Rice Institute, Houston, Texas.

A disc of lithium metal of normal isotopic constitution is surrounded by an annulus of BF_3 counters embedded in paraffin wax (referred to as A counters) and a short distance behind this on the axis of the annulus another array of BF_3 counters (B counters) is mounted. The whole assembly is heavily shielded and mounted with the axis of the annulus perpendicular to the proton beam. When neutrons of $\approx$ 258 keV pass through the lithium block the number of counts in the A counters rises and the number in the B counters decreases as a result of resonant scattering in the block. By determining the energies at which peaks in the ratio A/B occur, the positions of levels in the nucleus formed following a (p, n) reaction can be deduced by a simple computation.

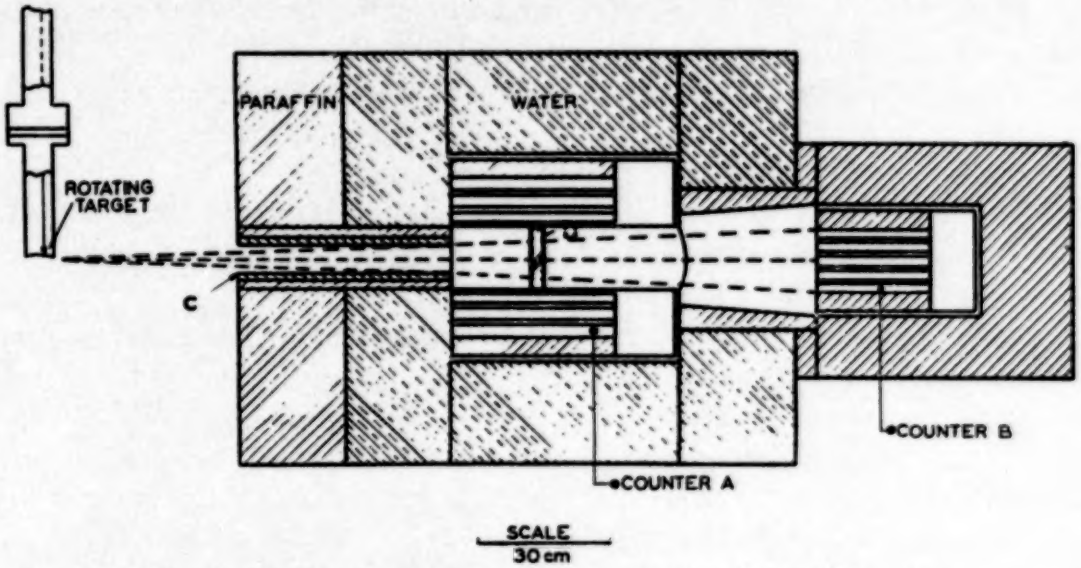

Fig. 1. General arrangement of the target and threshold detector.

The peak width is made up predominantly from two contributions, the target thickness and the finite width of the lithium resonance. For the thickness of lithium used in our experiments the expected full width at half height (above background) is $\approx$ 30 keV. That this resolution is achieved can be seen in fig. 3 where a level 25 keV above the ground state is clearly resolved.

For most measurements the following techniques were used. Counting was automatically stopped after a predetermined number of counts had been accumulated in the B counters (typically 1000 to 10 000 counts) and the ratio A/B determined. In this way the statistics on each experimental point are relatively constant but with a slightly increased accuracy in the regions where the ratio is high. A preliminary run was usually made with lower statistical accuracy and then more precise measurements made where the ratio showed pronounced peaks. In early experiments counting was automatically stopped after a fixed charge had been accumulated on the target. In this way an approximate yield curve was obtained. As changes in yield corresponding to resonances in the compound nucleus did not appear to alter the shape of our curves in any

way, in later measurements the former counting procedure described was adopted. It should however be noted that Lee †, studying [4]) the reaction $Mn^{55}(p, n)Fe^{55}$, has observed spurious peaks in his A/B ratio associated with resonances in the compound nucleus. His detecting equipment was similar in design to that described above but could also be rotated with respect to the incident beam direction. The possibility therefore exists that some of the low peaks reported here may be spurious although the heavier shielding around our detector should reduce this possible source of error.

For most samples, repeat measurements were made on different days and the energy calibration of the beam analysing magnet made in one of two ways. (i) The thresholds of the $Li^7(p, n)Be^7$ and $T(p, n)He^3$ reactions [6]) were determined using a BF_3 counter surrounded with wax as the neutron detector. For the latter reaction an additional magnetometer calibration was obtained by using a mass 2 beam. (ii) The experimentally determined positions of the ground state peaks arising from the reactions [6]) $F^{19}(p, n)Ne^{19}$ and $Sc^{45}(p, n)Ti^{45}$ in the resonant scattering detector were taken as standards; the value of 258 keV was used for the energy of the scattering resonance in lithium.

It should be noted that determination of ground state thresholds using our equipment gives results which are inherently less accurate than those obtainable using the counter ratio method described by Bonner and Cook [7]). This arises because of our additional uncertainties in determining target thickness, the uncertainty in the position of the lithium resonance and the difficulty of accurately measuring the centre of a peak which is at least 30 keV broad. However, for locating closely spaced levels in the residual nucleus the resonant scattering detector is certainly superior. The uncertainties in determining the target thickness and the position of the lithium resonance do not contribute to the error in deducing level positions. Another advantage of the resonant scattering threshold detector is the fact that it examines the residual nucleus at $\approx$ 260 keV higher excitation energy than the counter ratio detector. This is an advantage owing to the increased penetrability for the outgoing neutrons at the higher energy and may be important if the compound nucleus shows marked resonance structure. For example, the neutron yield from the $Si^{30}(p, n)P^{30}$ reaction is very low up to 20 keV above the threshold at 5.174 ± 0.030 MeV for this latter reason and the counter ratio method cannot be used directly to measure the threshold [8]).

3. Results

3.1. $Ca^{43}(p, n)Sc^{43}$

A target of CaF_2, thickness 95 $\mu g/cm^2$, evaporated onto a gold backing was used for the measurements shown in fig. 2. Measurements were also made using

† The authors wish to thank Dr. Lee for transmitting details of this work [4]) prior to publication.

a thick ($\approx$ 500 μg/cm^2) CaO target. The isotopic composition of the calcium in both targets is given in table 1.

In the last column of table 1 the ground state Q values for the various Ca(p, n)Sc reactions are listed; these values have been calculated from the recent compilation of atomic mass data by Kravtsov [9]). It will be seen that the

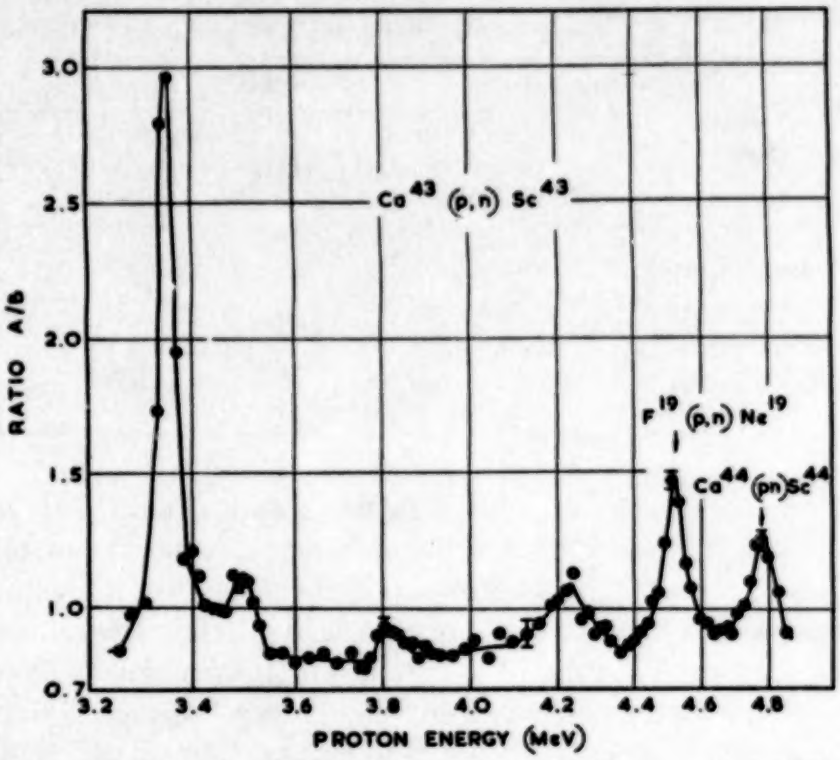

Fig. 2. The ratio A/B as a function of proton energy for the reaction Ca^{43}(p, n)Sc^{43}.

TABLE 1

Isotopic Composition of calcium targets

Isotope	Natural Abundance (%)	Abundance in Target (%)	Ground state Q value for (p, n) reaction (MeV)
Ca^{40}	96.9	41.54	−14.59
Ca^{42}	0.64	2.17	−6.67
Ca^{43}	0.14	43.66	−3.003
Ca^{44}	2.1	12.62	−4.433
Ca^{46}	0.0032	—	−2.163
Ca^{48}	0.18	0.012	−0.513 †

† The value of $Q_0 = -660 \pm 30$ keV has been found for this reaction by Elwyn *et al.* [10]). There is thus a large discrepancy between the mass data and experiment for this reaction, as has already been noted by Elwyn. This value has been confirmed by direct observation of the neutron yield as a function of energy by Johnson [11]) using protons from a Cockcroft-Walton cascade generator. He obtains the value $Q_0 = -660 \pm 10$ keV.

only reactions which would be observed within the range of energies available (up to ≈ 4.9 MeV) are $Ca^{43}(p, n)Sc^{43}$ and $Ca^{44}(p, n)Sc^{44}$. When the CaF_2 target is used the reaction $F^{19}(p, n)Ne^{19}$ with a threshold [8]) at 4.229 ± 0.005 MeV is energetically possible.

TABLE 2

Energy levels of Sc^{43} and Q values for the reaction $Ca^{43}(p, n)Sc^{43}$

Q value (MeV)	Levels in Sc^{43}	
	Results of present experiment (MeV)	Results of Ferguson and Morrison [12]) (MeV)
-3.005 ± 0.010		
-3.143 ± 0.010	0.138 ± 0.008	
-3.467 ± 0.011	0.456 ± 0.010	0.490 ± 0.020
-3.879 ± 0.011	0.874 ± 0.010	0.880 ± 0.020

The experimental results are shown in fig. 2 with typical counting errors (± 1 standard deviation) indicated. In obtaining the results in table 2 an allowance has been made for the estimated mean energy loss in the target. The results obtained by Ferguson and Morrison using a He^3 spectrometer [12]) are shown for comparison. The value of Q_0 obtained for the reaction (-3.005 ± 0.010 MeV) agrees well with the value (-3.003 ± 0.011 MeV) calculated from Kravtsov's compilation [9]). The peak at ≈ 4.2 MeV is very broad and may include some unresolved levels. A run made with a thick $Ca^{43}O$ target revealed no peaks between 4.4 and 4.7 MeV; above that energy the $Ca^{44}(p, n)Sc^{44}$ threshold is reached.

3.2. $Ca^{44}(p, n)Sc^{44}$

The peak at 4.8 MeV in fig. 2 is ascribed to the reaction $Ca^{44}(p, n)Sc^{44}$ in which Sc^{44} is left in its ground state. The Q value obtained, $Q_0 = -4.412 \pm 0.015$ MeV is in reasonable agreement with the value -4.43 ± 0.011 MeV calculated from mass data. That this peak is indeed due to the reaction $Ca^{44}(p, n)Sc^{44}$ rather than $Ca^{43}(p, n)Sc^{43*}$ in which the Sc^{43} is left in an excited state could be confirmed by repeating the measurement with a target of different isotopic composition. The only evidence in favour of our identification (apart from the obvious one of agreeing with mass data predictions) is that the peak is a very strong one in spite of the high neutron background arising from competing processes; ground state peaks are commonly strong. The amount of Ca^{44} in the target is sufficient to account for such a peak. As the peak was present when the CaO target was used it does not arise from the $F^{19}(p, n)Ne^{19}$ reaction.

3.3. $Sc^{45}(p, n)Ti^{45}$

For these measurements a target of Sc_2O_3 of thickness 105 $\mu g/cm^2$ evaporated onto a gold backing was used. The experimental results are shown in fig. 3 and

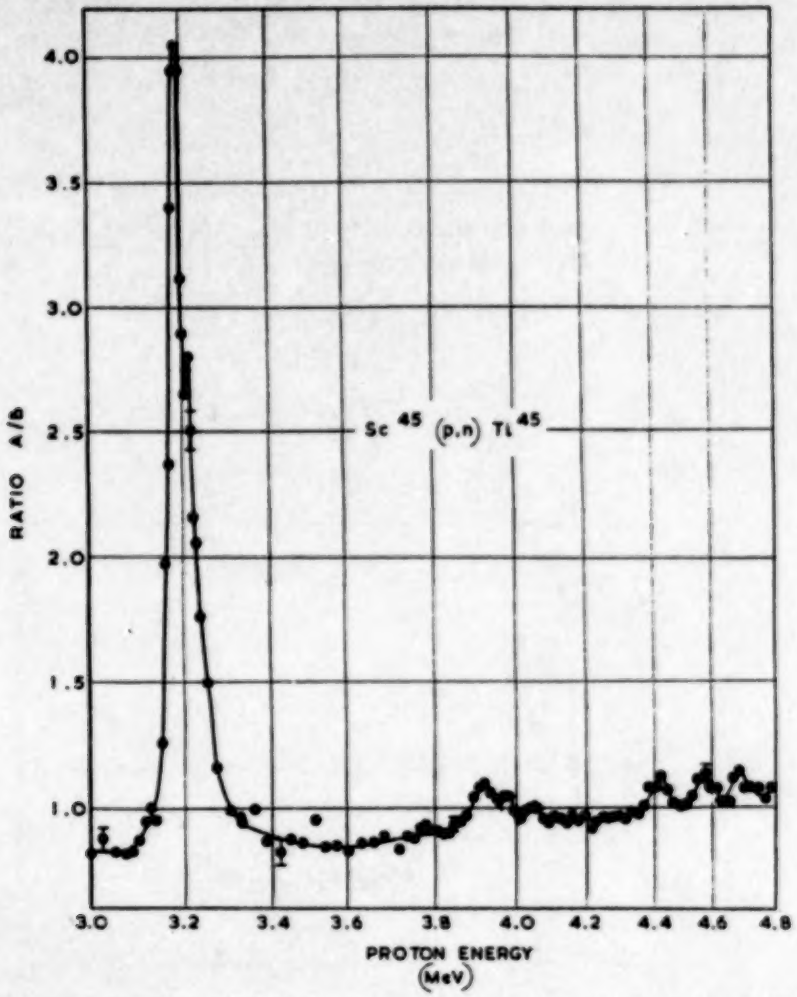

Fig. 3. The ratio A/B as a function of proton energy for the reaction $Sc^{45}(p, n)Ti^{45}$.

TABLE 3
Energy levels of Ti^{45} and Q values for the reaction $Sc^{45}(p, n)Ti^{45}$

Q value (MeV)	Levels in Ti^{45}	
	Present experiment (MeV)	Results of Brugger *et al.* [13]) (MeV)
-2.844 ± 0.004		
-2.869 ± 0.006	0.025 ± 0.004	
-3.584 ± 0.009	0.740 ± 0.008	0.743 ± 0.011
(-3.630 ± 0.011)	(0.786 ± 0.010)	
(-3.703 ± 0.011)	(0.859 ± 0.010)	
-4.076 ± 0.013	1.232 ± 0.012	1.194 ± 0.010
-4.176 ± 0.013	1.332 ± 0.012	1.347 ± 0.010
-4.289 ± 0.013	1.445 ± 0.012	1.460 ± 0.011

tabulated in table 3 together with those of Brugger *et al.* [13]). Except for the level at 1.230 MeV the agreement is excellent. Three additional levels are shown. The existence of the 25 keV level was shown on several repeat runs and could be considered definitely established. The 785 and 859 keV levels, however, are shown bracketed as the peaks are barely above the statistical fluctuations in background; their existence must be considered doubtful.

3.4. $Ti^{47}(p, n)V^{47}$

The target used in these experiments was formed by evaporating a sample of isotopically enriched Ti powder onto a weighed gold blank; a thickness of 160 $\mu g/cm^2$ was obtained. The isotopic composition of the target is given below:

Ti^{46}	4.49 %
Ti^{47}	60.9 %
Ti^{48}	30.7 %
Ti^{49}	1.94 %
Ti^{50}	1.96 %.

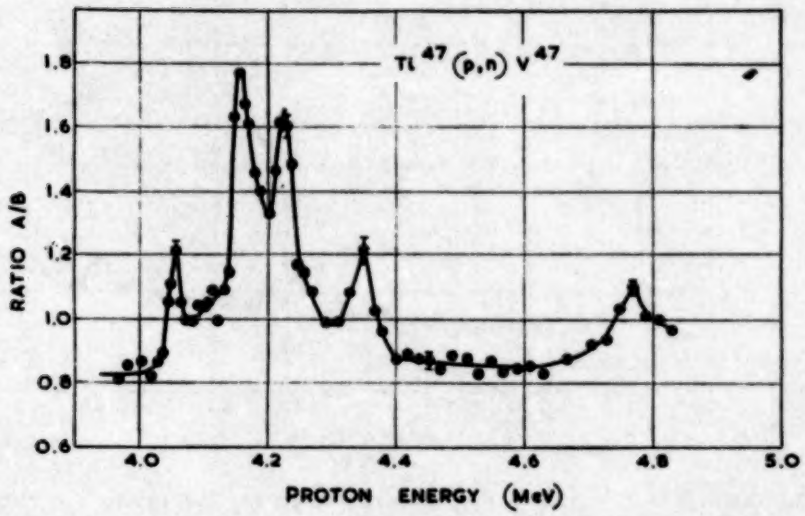

Fig. 4. The ratio A/B as a function of proton energy for the reaction $Ti^{47}(p, n)V^{47}$.

TABLE 4

Energy levels of V^{47} and Q values for the reaction $Ti^{47}(p, n)V^{47}$

Q value (MeV)	Levels in V^{47} (MeV)
-3.707 ± 0.013	
-3.800 ± 0.014	0.093 ± 0.007
-3.862 ± 0.014	0.155 ± 0.007
-3.983 ± 0.014	0.276 ± 0.007
-4.400 ± 0.018	0.693 ± 0.012

The results obtained are shown on table 4 and the ratio A/B as a function of energy plotted in fig. 4. The ground state threshold, corresponding to

$Q_0 = -3.707 \pm 0.013$ MeV is higher than the value calculated from Kravtsov's masses (-3.664 ± 0.056 MeV), but well within his quoted errors; from our values a nuclear binding energy of 403.347 ± 0.027 MeV and a mass of $46.969\,826 \pm 0.000\,015$ a.m.u. are indicated for V^{47}.

3.5. $Ti^{49}(p, n)V^{49}$

A 220 $\mu g/cm^2$ thick target of Ti evaporated directly onto a gold backing was used for these measurements. The target had the following isotopic composition:

Ti^{46}	2.87 %
Ti^{47}	3.21 %
Ti^{48}	29.4 %
Ti^{49}	62.1 %
Ti^{50}	2.39 %.

The A/B ratios are plotted in fig. 5 and the Q values and level positions deduced therefrom, listed in table 5 and compared with the results of other workers. The ground state value $Q = -1.383 \pm 0.009$ MeV agrees well with the value

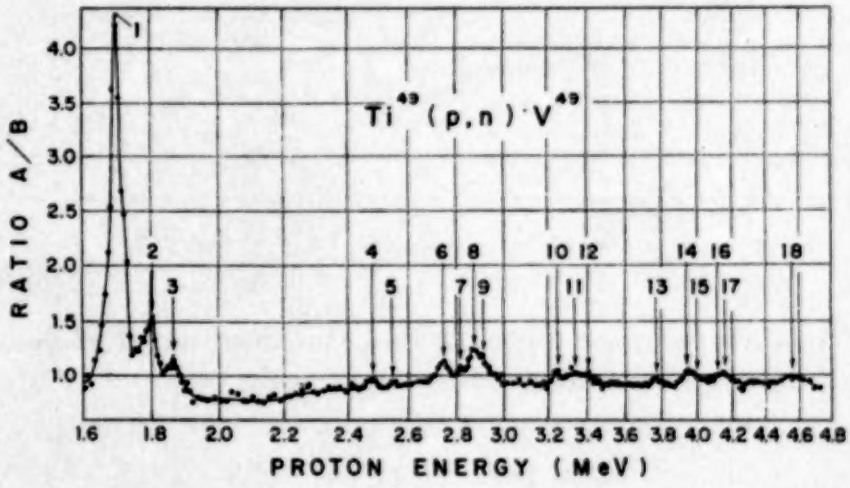

Fig. 5. The ratio A/B as a function of proton energy for the reaction $Ti^{49}(p, n)V^{49}$.

-1.392 ± 0.005 MeV obtained by Trail and Johnson [14]). As an aid to identification only the peaks in fig. 5 are numbered. Where other measurements exist they are in good agreement with the results presented here except for the level at 1.029 ± 0.012 MeV which is higher than the 0.97 ± 0.02 MeV obtained by Elwyn *et al.* [10]) using a neutron time-of-flight technique. The two peaks 5 and 7 are statistically barely significant and the existence of the corresponding reported levels at 0.835 and 1.098 MeV therefore need further confirmation. The peaks 14—15 and 16—17 have been drawn as doublets although the counting

statistics barely warrant this assignment; the base width of the peaks however suggest this interpretation. The broad peak marked 11—12 could well be more than two unresolved levels.

TABLE 5

Energy levels of V^{49} and Q values for the reaction $Ti^{49}(p, n)V^{49}$

Peak number	Q value (MeV)	Levels in V^{49} (MeV)			
		Present results	Elwyn *et al.* [10])	Craseman and Easterday [15])	Nuclear level Schemes [16])
1	−1.383±0.009				
2	−1.468±0.010	0.085±0.008	0.086±0.010		0.089
3	−1.533±0.010	0.150±0.008	0.145±0.010	0.153	0.150
4	−2.141±0.012	0.758±0.010	0.73 ±0.02	0.762	
5	(−2.218±0.012)	(0.835±0.010)			
6	−2.412±0.012	1.029±0.012	0.97 ±0.02		
7	(−2.482±0.012)	(1.099±0.012)			
8	−2.533±0.012	1.150±0.012			
9	−2.561±0.012	1.178±0.012			
10	−2.904±0.013	1.521±0.013			
11	−3.003±0.020	1.620±0.020			
12	−3.085±0.020	1.702±0.020			
13	−3.424±0.015	2.041±0.015			
14	−3.577±0.015	2.194±0.015			
15	−3.616±0.015	2.233±0.015			
16	−3.765±0.015	2.382±0.015			
17	−3.824±0.015	2.441±0.015			
18	−4.180±0.020	2.797±0.020			

3.6. $Ti^{50}(p, n)V^{50}$

Measurements were made using a 200 $\mu g/cm^2$ thick target of Ti evaporated onto a gold backing. The isotopic composition of the target used was as follows:

Ti^{46}	2.34 %
Ti^{47}	2.63 %
Ti^{48}	25.81 %
Ti^{49}	2.33 %
Ti^{50}	65.88 %.

The neutron yield below $\approx$ 3.5 MeV was extremely low. Since the spins of Ti^{50} and V^{50} are 0^+ and 6^+ respectively the (p, n) reaction leading to the ground state would be expected to compete unfavourably with compound elastic and inelastic proton scattering. It is therefore not possible to identify unambiguously the two lowest peaks shown in fig. 6 with the $Ti^{50}(p, n)V^{50}$ reaction. Accordingly two possible level schemes for V^{50} are presented in table 6. The arguments in favour of level scheme A are the following:

(i) The ground state Q value obtained (-2.991 ± 0.010 MeV) agrees well with that calculated from Kravtsov's masses (-2.996 ± 0.003 MeV). Since Kravtsov's value is based on the masses of Ti^{50} and V^{50} which have both been determined directly by mass spectroscopy the actual value is most unlikely to be more than 10 keV different from that quoted.

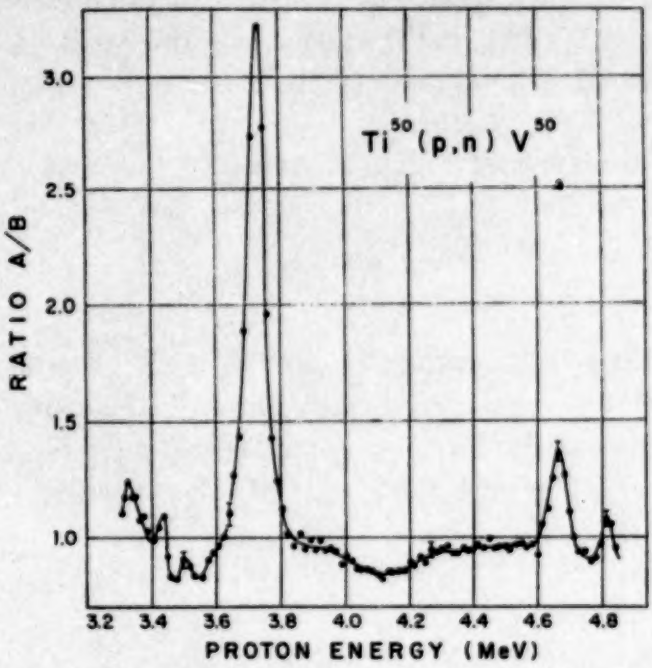

Fig. 6. The ratio A/B as a function of proton energy for the reaction $Ti^{50}(p, n)V^{50}$.

TABLE 6

Energy levels of V^{50} and Q values for the reacton $Ti^{50}(p, n)V^{50}$

Q value (MeV)	Levels in V^{50} (MeV)	
	A	B
-2.991 ± 0.010		
-3.086 ± 0.010	0.095 ± 0.012	
-3.151 ± 0.010	0.160 ± 0.012	
-3.370 ± 0.007	0.379 ± 0.010	0.219 ± 0.010
-4.301 ± 0.009	1.310 ± 0.011	1.150 ± 0.011
-4.477 ± 0.010	1.486 ± 0.012	1.326 ± 0.012

(ii) The total neutron yield which was very low at threshold rose with energy at a rate which indicated that the neutrons observed were from the $Ti^{50}(p, n)V^{50}$ reaction rather than from the $Ti^{49}(p, n)V^{49}$ reaction; the (p, n) thresholds of the other titanium isotopes are at higher energies than those under discussion.

The evidence for level scheme B is supported by the Coulomb excitation studies of Temmer and Heydenburg [17]), and Fagg *et al.* [17]) on V^{50}. A thick

target excitation function showed that the 225 keV radiation which they observed was emitted from a level whose excitation energy was considerably less than 320 keV. They therefore concluded that the first excited state was at 225 keV. It is however possible that level scheme A is correct and that there is also a level at 225 keV which was not detected in the present experiment. The Coulomb excitation experiments would tend to emphasize levels of high spin whereas in the $Ti^{50}(p, n)V^{50}$ experiment the yield to any such levels > 160 keV above the ground state could be masked by the high yield to the 160 keV level.

In view of the mass spectrographic evidence the authors are inclined to favour level scheme A.

3.7. $Cu^{65}(p, n)Zn^{65}$

A 370 $\mu g/cm^2$ thick target enriched to 99.4 % in Cu^{65} was used for the measurements; the Cu^{65} was evaporated directly onto a gold backing. The experimental results are shown in fig. 7 and the Q values and energy levels calculated are given in table 7 together with the results of other workers. Owing to the low

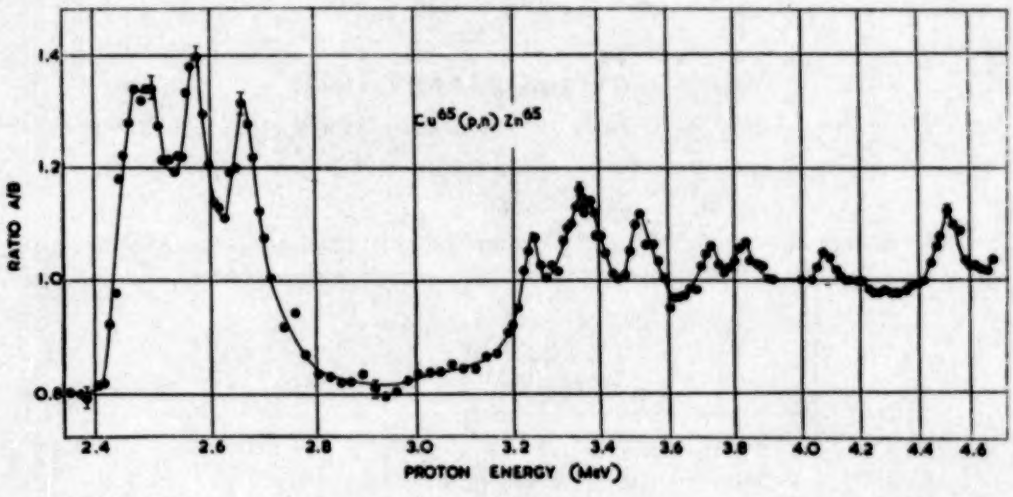

Fig. 7. The ratio A/B as a function of proton energy for the reaction $Cu^{65}(p, n)Zn^{65}$.

neutron yield near the threshold (it is not suggested that there is any strong inhibition in the population of the ground state in the (p, n) reaction; the low yield here results from the increasing height of the Coulomb barrier) and the close spacing of the ground state and first excited state it was not possible to obtain an accurate value for the ground state threshold. In deducing the position of the levels in Zn^{65} (column 2 of table 7) Marion and Kavanagh's [18]) more accurate value $Q_0 = -2.1325 \pm 0.0015$ MeV has been used rather than our value of -2.145 ± 0.010 MeV.

TABLE 7

Energy levels of Zn^{65} and Q values for the reaction $Cu^{65}(p, n)Zn^{65}$

Q value (MeV)	Levels in Zn^{65} (MeV)			
	Present experiment ($Q_0 = -2.132$)	Brugger *et al.* [13])	Bernstein and Lewis [19])	Cook and Bonner [20])
-2.145 ± 0.010				
-2.181 ± 0.013	0.049 ± 0.013		0.054 ± 0.002	
-2.259 ± 0.010	0.127 ± 0.010		0.119 ± 0.002	
-2.330 ± 0.010	0.198 ± 0.010		0.209 ± 0.003	
-2.908 ± 0.013	0.776 ± 0.013	0.78 ± 0.03		
-3.025 ± 0.013	0.893 ± 0.013			0.86
-3.051 ± 0.013	0.919 ± 0.013			
-3.173 ± 0.013	1.041 ± 0.013			
-3.405 ± 0.013	1.273 ± 0.013	1.26 ± 0.03		
-3.484 ± 0.014	1.352 ± 0.014			
-3.715 ± 0.014	1.583 ± 0.014			
-4.095 ± 0.014	1.963 ± 0.014	1.93 ± 0.02		

4. Discussion of Results

The comparison of the energy level schemes of pairs of nuclei whose external nucleons may be represented respectively by $(1f_{\frac{7}{2}})^n$ and $(1f_{\frac{7}{2}})^{-n}$ forms a good test of the simpler forms of the j-j coupling shell model. This predicts identical level schemes for such nuclei. The only previous comparison was between Ca^{43} and Ca^{45}, which showed poor agreement. The data from this work allows comparison to be made of Ti^{45} and Ti^{47}, and of Sc^{43} and Sc^{47}. These comparisons are made in table 8. It is clear that there is no obvious relationship between these level schemes and that some more complex form of nuclear model will be required for their detailed description.

TABLE 8

Comparison of low lying energy levels of nuclei with configurations $(1f_{\frac{7}{2}})^n$ and $(1f_{\frac{7}{2}})^{-n}$

Nucleus	Configuration		Level position (experimental) (keV)	Reference
	protons	neutrons		
Ca^{43}		$(1f_{\frac{7}{2}})^3$	380, 610, 1000	[18])
Ca^{35}		$(1f_{\frac{7}{2}})^{-3}$	180, 1430, 1690	[18])
Ti^{45}	$(1f_{\frac{7}{2}})^2$	$(1f_{\frac{7}{2}})^3$	25, 740, 859, 1230	This work
Ti^{47}	$(1f_{\frac{7}{2}})^2$	$(1f_{\frac{7}{2}})^{-3}$	160, 1400, 2390, 2640	[18])
Sc^{43}	$(1f_{\frac{7}{2}})^1$	$(1f_{\frac{7}{2}})^2$	138, 456, 874	This work
Sc^{47}	$(1f_{\frac{7}{2}})^1$	$(1f_{\frac{7}{2}})^{-2}$	480, 1310	[18])

Two of the authors (G. J. M. and G. S. M.) are particularly indebted to Dr. E. Bretscher and Dr. E. B. Paul for use of the excellent facilities of the Van de Graaff group during their stay. Thanks are due to the Electromagnetic Separator Group for supplying all the isotopically enriched targets used in the experiments and to the Mass Spectroscopy Group for the mass analyses. Finally, the unfailing cooperation of the Van de Graaff operating personnel during many long hours of operation is gratefully acknowledged.

References

1) J. E. Evans, B. B. Kinsy and B. G. Whitmore, Can. J. Phys. **37** (1959) 396
2) A. T. G. Ferguson and E. B. Paul, Nuclear Physics **12** (1959) 426
3) F. P. Mooring, L. L. Lee, Bull. Am. Phys. Soc. **1** (1956) 327
4) L. L. Lee and F. P. Mooring, Phys. Rev. **115** (1959) 969
5) D. J. Hughes and J. A. Harvey, Neutron Cross Sections, U.S.A.E.C. Report BNL-325
6) J. B. Marion and T. W. Bonner, Fast Neutron Physics (Interscience), to be published
7) T. W. Bonner and C. F. Cook, Phys. Rev. **96** (1954) 122
8) D. A. Bromley *et al.*, Can. J. Phys., to be published
9) V. A. Kravtsov, Uspekhi Fiz. Nauk. **65** (1958) 451
10) Elwyn, Landon, Oleksa and Glasoe, Phys. Rev. **112** (1958) 1200
11) C. M. P. Johnson, private communication
12) A. T. G. Ferguson and G. C. Morrison, Proc. of the Int. Conf. on the Neutron Interactions with the Nucleus, U.S.A.E.C. Report TID-7547 (1957)
13) Brugger, Bonner and Marion, Phys. Rev. **100** (1955) 84
14) C. C. Trail and C. H. Johnson, Phys. Rev. **91** (1953) 474
15) B. Craseman and H. T. Easterday, Phys. Rev. **90** (1953) 1124
16) Way, King, McGinnis and van Lieshout, Nuclear Level Schemes, $A = 40$ to $A = 92$, U.S.A.A.E.C. Report TID-5300 (1955)
17) G. M. Temmer and N. P. Heydenburg. Phys. Rev. **104** (1956) 967;
Fagg, Geer, and Wolicki, Phys. Rev. **104** (1956) 1073
18) J. B. Marion and R. W. Kavanagh, Phys. Rev. **104** (1956) 107
19) E. M. Bernstein and H. W. Lewis, Phys. Rev. **107** (1957) 737
20) C. F. Cook and T. W. Bonner, Phys. Rev. **94** (1954) 807A

1.D.1:
2.G

Nuclear Physics **17** (1960) 129—140; © *North-Holland Publishing Co., Amsterdam*
Not to be reproduced by photoprint or microfilm without written permission from the publisher

LOCATION OF THE $3s_{\frac{1}{2}}$ SINGLE PARTICLE NEUTRON LEVEL IN VARIOUS NUCLEI

BERNARD L. COHEN and ROBERT E. PRICE

University of Pittsburgh, Pittsburgh, Pa. †

Received 12 January 1960

Abstract: The $3s_{\frac{1}{2}}$ neutron levels in nuclei of mass 85—135 are located by angular distributions of protons from (d, p) reactions on nuclei with even neutron numbers. Where the proton number is even, almost all of the single particle level is in one nuclear level, and where there is an odd proton of low j, it is in two levels with spin $j+\frac{1}{2}$ and $j-\frac{1}{2}$ which are separated by about 60 keV. Both of these cases are in agreement with the simple single particle model with negligible configuration mixing, but where there is an odd proton of large j, the single particle level has many components, indicating strong configuration mixing. The binding energy of the $3s_{\frac{1}{2}}$ neutron varies very smoothly from isotope to isotope of the same element, and when corrected for symmetry energy, its variation with A is very smooth. The variation with A decreases about by half when its major shell begins filling, and becomes negligible when ground states of odd-mass nuclei are $s_{\frac{1}{2}}$. This is explained as due to the fact that the levels become partially "hole" states, and since the energy of particle and hole states shift in opposite directions as a function of mass number, the two effects tend to cancel. Since, according to pairing theory and experimental observations, all subshells in a major shell begin to fill when the major shell begins to fill, energy shifting of a single particle level decreases rapidly once its major shell begins to fill. The observed shifting is in at least semi-quantitative agreement with the theory. Some difficulties with the Wilkinson theory of the photonuclear giant resonance are pointed out, and strong evidence against reduced mass effects in excited states of nuclei are presented.

1. Introduction

The manner in which the location of given single particle levels varies with mass number has been studied by Bergstrom and Andersson [1]) in the Pb region using results from radioactive decay scheme work, and by Schiffer and Lee [2]) in the Fe region using (d, p) reactions. However, both these studies covered only a small mass range, and their principal value is in demonstrating the fluctuations from nucleus to nucleus rather than the overall variation of the location with mass.

From the standpoint of basic nuclear theory, however, this overall variation is of considerable importance. A very simple rough calculation of it may be made from the optical model, and more complete optical model calculations have been made by Schröder [3]), and by Ross, Mark, and Lawson [4]). Wilkinson [5]) has pointed out that the reduced mass would have an important effect on this variation.

† Assisted by the National Science Foundation and the joint program of the Office of Naval Research and the U. S. Atomic Energy Commission.

In a previous paper [6]), we reported the regular occurrence of peaks in low resolution measurements of the energy distributions of protons from (d, p) reactions; these peaks were presumed to be due to the conglomeration of single particle levels comprising a single major shell, but there was no very direct proof for this presumption. In the work reported here, we identify the $3s_{\frac{1}{2}}$ single particle level by angular distribution studies, and follow its binding energy from nucleus to nucleus in the mass range 85—135. The results confirm the above mentioned presumption of ref. [6]), but suggest an explanation for some of the anomalous conclusions of that paper. In addition, they shed light on the manner in which these levels are split up, the effect of symmetry energy on them, etc.

2. Experimental

It is well known that angular distributions of protons from (d, p) reactions are characterized by relatively strong structure which depend on the orbital

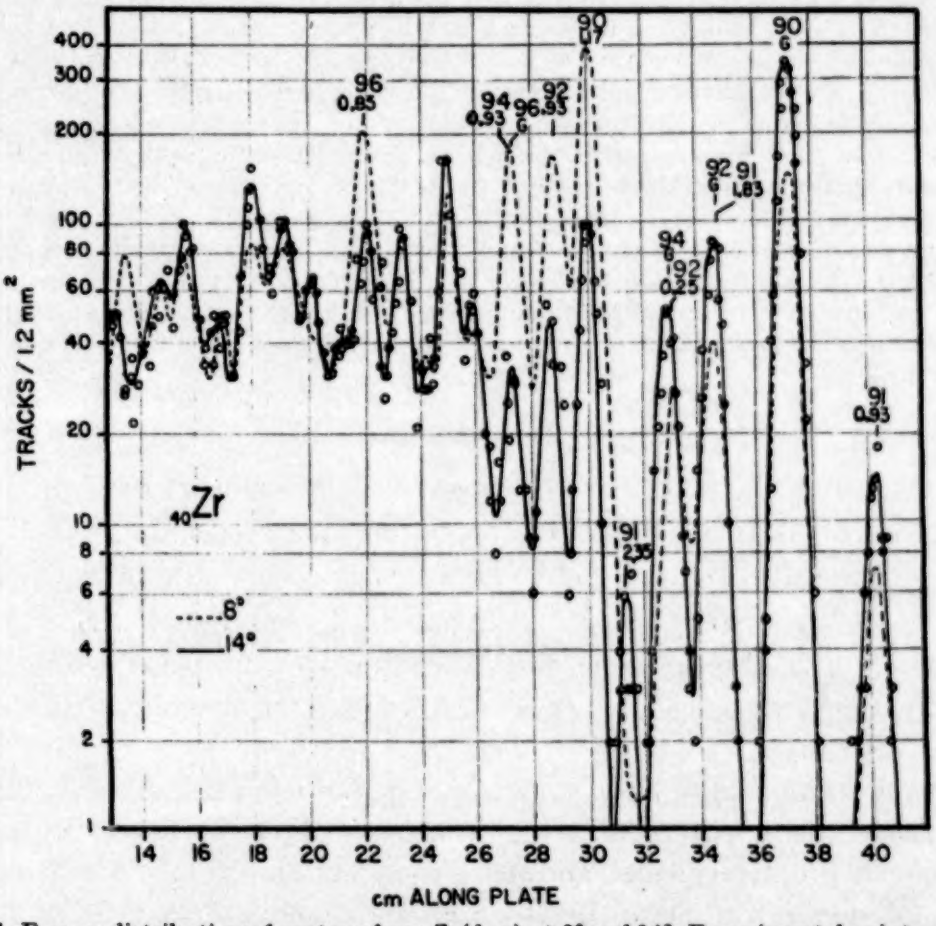

Fig. 1. Energy distribution of protons from Zr(d, p) at 8° and 14°. Experimental points are shown for 14° data; these are typical of all data obtained in this experiment. Levels are labelled by the mass number of the target isotope in larger letters and the excitation energy (in MeV) in the final nucleus in smaller letters (G denotes ground states). Note that ordinate scale is logarithmic; this explains scatter of data points at small ordinates. Energy dispersion is about 170 keV per cm. Target was natural Zirconium metal foil.

angular momentum l_n with which the stripped neutron enters the nucleus In light elements, these angular distributions are well fitted by Butler theory [7]), whereas in heavier elements, an empirical systematics must be used. The empirical systematics for 15 MeV deuterons induced (d, p) reactions in the region centered about mass 110 indicates [8]) that for $l_n = 0$ the intensity decreases sharply (by at least a factor of 2) from 8° to 14°, whereas for all other values of l_n it increases. Several checks on this qualitative feature are available through-

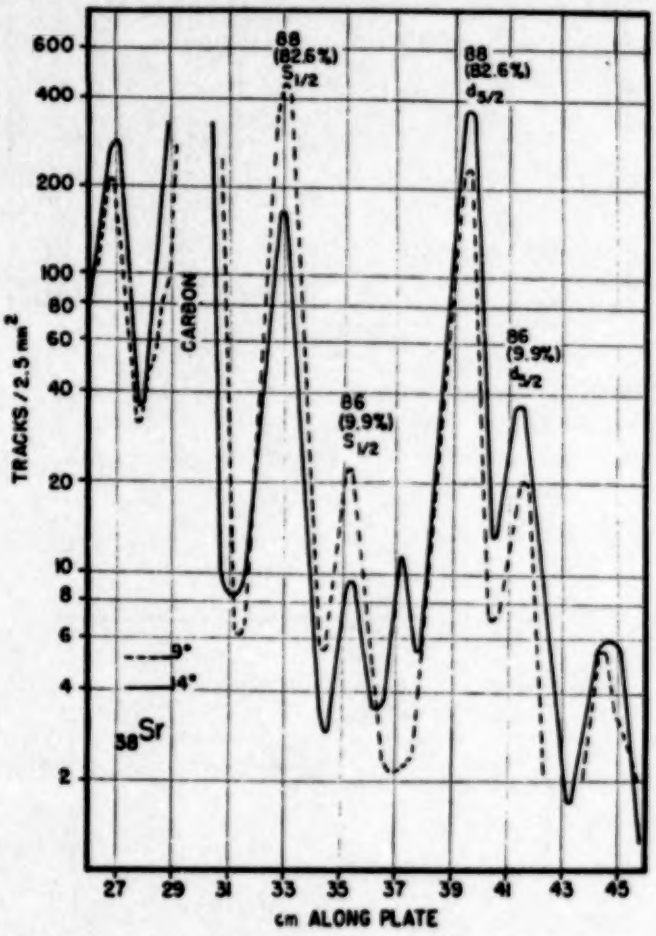

Fig. 2. Energy distribution of protons from Sr(d, p) at 9° and 14°. Peaks are labelled with mass number of target isotope and its isotopic abundance, and the single particle neutron configuration assignment. Target was SrO on Mylar, so that peaks from C and O are very strong. Energy dispersion is about 160 keV per cm.

out the region from transitions between known levels. Thus, by comparing energy spectra obtained at 8° and 14°, the $l_n = 0$ transitions may readily be picked out. Examples of this are shown in fig. 1 to 7.

In cases when the target nuclei have an even number of neutrons, the levels excited by $l_n = 0$ transitions are the single particle $3s_{\frac{1}{2}}$ levels. This is the case in all odd-Z nuclei, and in even isotopes of even-Z nuclei. Since separated isotopes were not generally used, the interpretation of the data from even-Z targets is somewhat complicated. Firstly, there are many $l_n = 0$ transitions from the

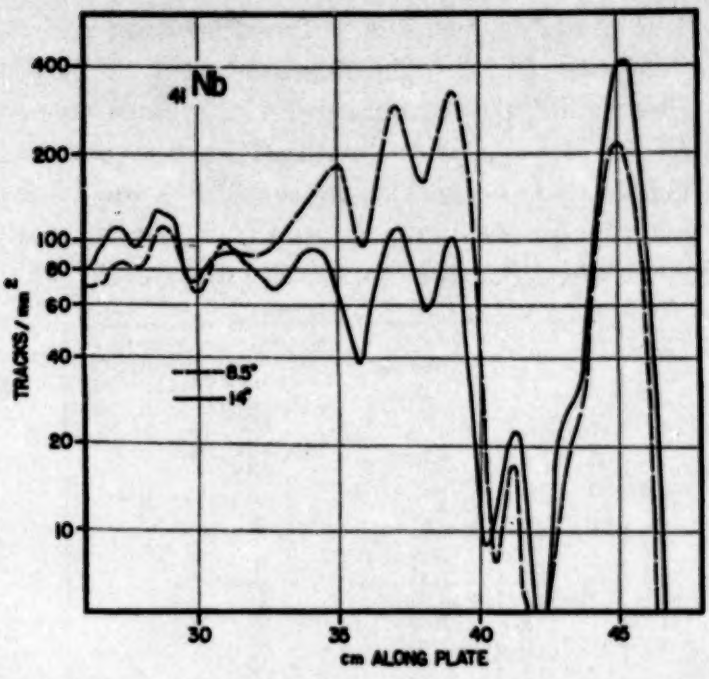

Fig. 3. Energy distribution of protons from Nb(d, p) at 8.5° and 14°. Target was Nb metal foil and energy dispersion is about 160 keV per cm. Experimental energy resolution is about 90 keV which is considerably less than the widths of the peaks.

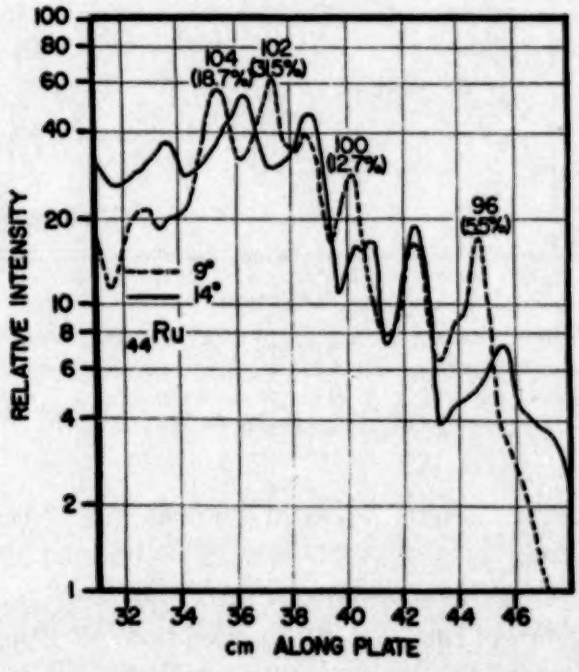

Fig. 4. Energy distribution of protons from Ru(d, p) at 9° and 14°. Peaks which are larger at 9° than at 14° are labelled with the mass number of the target isotope. Note that heights of peaks are roughly proportional to isotopic abundances and that the position of the various peaks shifts uniformly with mass number. These properties were used to assign target isotopes. Target was RuO on Mylar, and energy dispersion is about 160 keV per mm.

odd-mass isotopes, but the intensity of these is always quite small because: (1) the cross section is proportional to[9]) the factor $(2I_f+1)/(2I_i+1)$, which is larger for $0 \rightarrow \frac{1}{2}$ transitions than for $\frac{1}{2} \rightarrow 0$ or $\frac{5}{2} \rightarrow 2$ transitions which are those expected in odd-mass isotopes, (2) the reduced widths are generally smaller than those for even isotopes, as the latter have essentially single particle reduced

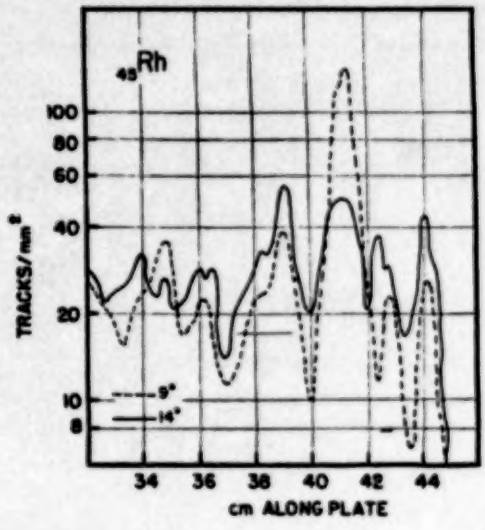

Fig. 5. Energy distribution of protons from Rh(d, p) at 9° and 14°. Target was Rh metal foil; energy dispersion is 160 keV per cm. Cf. caption for fig. 3.

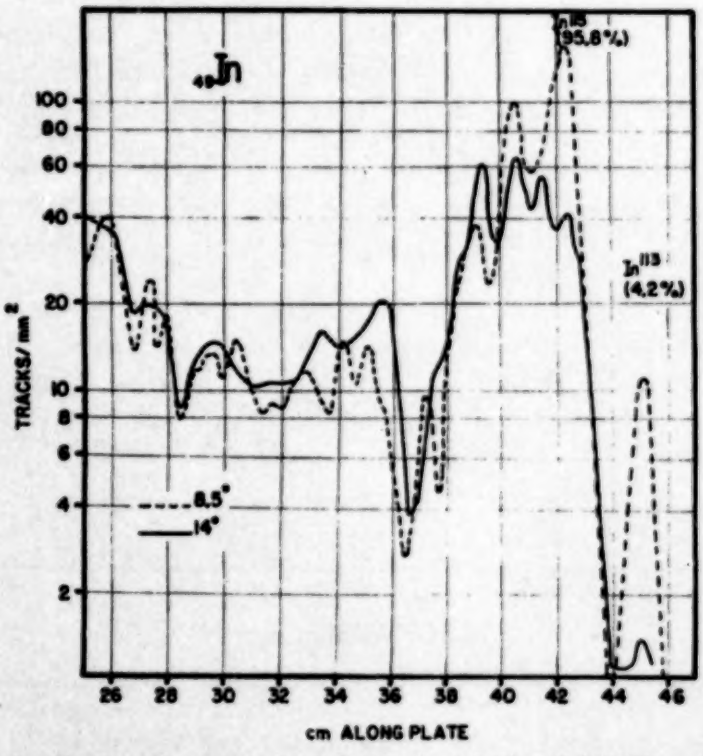

Fig. 6. Energy distribution of protons from In(d, p) at 8.5° and 14°. Target was In metal foil; energy dispersion is 160 keV per cm. Cf. caption for fig. 3.

widths, and (3) the isotopic abundance of odd-mass isotopes is generally small. Secondly, there are $l_n = 0$ transitions from each even isotope, so that mass assignments are not obvious. These were made by use of systematics, i.e. assigning the most weakly bound state to the most neutron-rich isotope (neglecting those of very low abundance), etc. The relative abundances served as a check on this procedure, and in no case was there an inconsistency; i.e.,

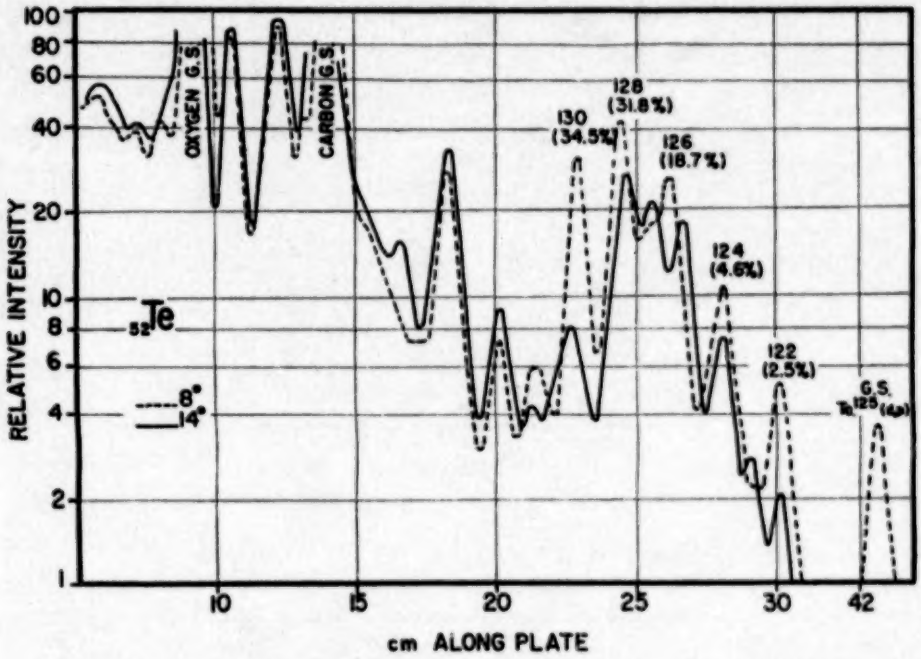

Fig. 7. Energy distribution of protons for Te(d, p) at 8° and 14°. Target was TeO_2 on a Mylar backing; energy dispersion is about 178 keV per cm. Cf. caption for fig. 4.

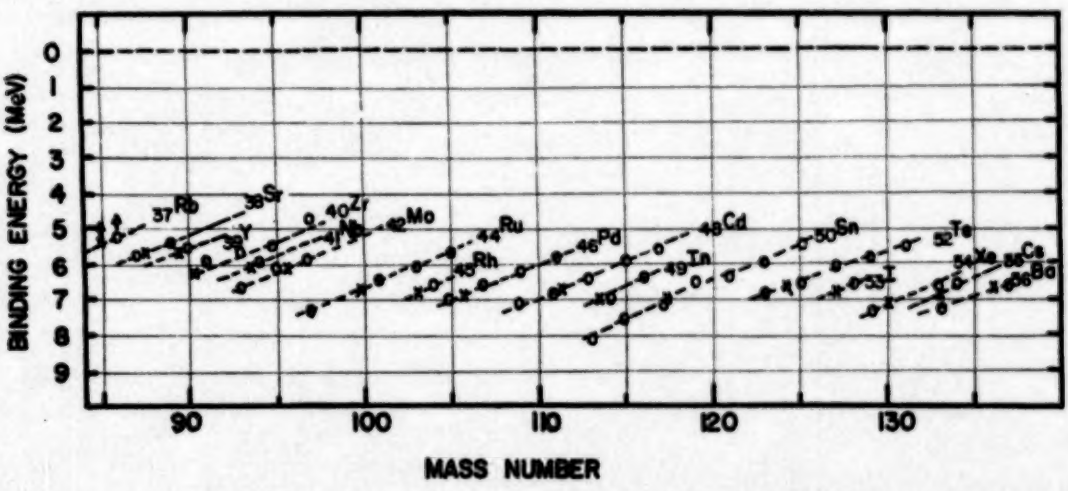

Fig. 8. Binding energy of $3s_{\frac{1}{2}}$ levels as a function of mass number. Dashed lines connect points for a single atomic number. The crosses on the dashed lines indicate the mass number where the line of maximum beta stability intersects the atomic number of the latter. Data for Xe and Ba are from known levels; all others were measured in the experiment reported here. Points for odd atomic number elements represent "centre of gravity" of $3s_{\frac{1}{2}}$ levels.

there was always one peak for each isotope; it always occurred at about the expected energy and with about the expected intensity. The systematics works very well for the isotopes of Sn and Cd where separated isotopes were used, and the excellent regularity in the results (fig. 8) gives strong support to the method.

3. Results

3.1. MULTIPLICITY OF LEVELS

In all cases where targets are even isotopes, there is one and only one strong $l_n = 0$ peak for each isotope. This result is just the prediction of the simple single particle model, according to which the states of the final odd-neutron nucleus are composed of the states of the target even nucleus plus a neutron.

For cases when the target has an odd number of protons, the single particle model predicts two states corresponding to the two possible couplings between the spin of the odd proton and the spin of the added odd neutron. In some cases, the experiments indicate that there are more than two levels involved: in $_{49}$In (cf. fig. 6), there are two peaks, but each is wider than the experimental resolution; and in $_{41}$Nb (cf. Fig. 3), there are several peaks all of which are wider than the experimental resolution. In $_{45}$Rh (cf. Fig. 5) and $_{39}$Y, the data are indicative of only two strong peaks (actually one peak which is wider than the experimental resolution and is thus presumably double). For $_{53}$I, the experimental resolution is not good enough to be certain, but there seem to be more than two peaks.

It is interesting to speculate on the explanation for these differences. In Nb and In, one expects the proton configuration to be pure $g_{\frac{9}{2}}$ and $(g_{\frac{9}{2}})^{-1}$ respectively. The states excited by adding an $s_{\frac{1}{2}}$ neutron would then have spins 4 or 5. Excited states with these spins would also be expected from coupling the $g_{\frac{9}{2}}$ proton to various other neutron configurations. The experimental results here indicate that there is strong configuration mixing among these states, causing appreciable amount of $g_{\frac{9}{2}}s_{\frac{1}{2}}$ configuration to be present in several of them. In Rh and Y, on the other hand, where the proton configuration is $p_{\frac{1}{2}}$, the simpe $p_{\frac{1}{2}}s_{\frac{1}{2}}$ configuration does not get mixed with other 0^- and 1^- states. The conclusion suggested by this and the aforementioned results on even target nuclei is that there is little mixing of the neutron configurations in odd neutron nuclei if the proton number is even, or if there is an odd proton with a small angular momentum, but that this mixing becomes quite important if there is an odd proton with large angular momentum. This mixing may be due to the odd proton of high angular momentum polarizing the neutron core †.

Another interesting observation from the data for odd proton target nuclei is that the peaks always seem to be wider than the experimental resolution and are therefore presumed to be double. This suggests that the corresponding

† This explanation was suggested by S. Meshkov.

states in which the odd proton and odd neutron angular momenta are parallel and antiparallel lie about 60 keV apart. This must certainly be true of the 0^- and 1^- states formed in Rh and Y, and is very probably true of the 4^+ and 5^+ states formed in Nb and In.

3.2. VARIATION OF BINDING ENERGY WITH MASS NUMBER

A most interesting correlation is obtained if the binding energy of the $3s_{\frac{1}{2}}$ neutron state is plotted against mass number as in fig. 8. For the odd-mass nuclei when several peaks are observed, the "centre of gravity" of these peaks is plotted. The known $s_{\frac{1}{2}}$ levels in Xe and Ba are also shown. The data for various isotopes of a given element are connected by dashed lines which to a good approximation appear to be straight and parallel to one another, so that interpolations and extrapolations may be made quite easily. On each dashed line in fig. 8, a cross is shown at the mass number at which the line of maximum beta stability [10]) passes through its atomic number. These crosses then give the binding energy of a $3s_{\frac{1}{2}}$ neutron to even-neutron nuclei corrected for symmetry energy to the centre of beta stability; this is essentially the quantity calculated from nuclear models as discussed in the introduction.

From fig. 8, it is straightforward to determine the dependence of well depth on symmetry energy which is an interesting quantity for some purposes. Another interesting observation from fig. 8 is the regularity between odd and even proton number elements. Evidently the binding energy of a $3s_{\frac{1}{2}}$ neutron is essentially unaffected by the proton configuration.

The dashed lines and crosses of fig. 8 are shown in fig. 9. That figure also shows where the $3s_{\frac{1}{2}}$ levels goes through zero binding energy as evidenced by the neutron giant resonance [11]). With reasonable interpolation, the binding energy of the $3s_{\frac{1}{2}}$ level can thus be followed from mass 55 to 135. The results of Schiffer and Lee [2]) in the mass 49—64 region are also shown in fig. 10; the fact that they fall well below the energy indicated by the neutron giant resonance may be explained by assuming that the level becomes very broad when it reaches high excitation, and that in ref. [2]) only the lowest component of it is observed.

If one accepts the line in fig. 10 as representing the location of the $3s_{\frac{1}{2}}$ level, it apparently behaves very differently in the region where it is in the major shell that is filling ($90 < A < 135$), and in the region where the previous major shell is filling ($55 < A < 90$). In the latter region, its energy dependence is approximately $S = 12$ MeV, where S is defined as

$$S = A \frac{\mathrm{d}E}{\mathrm{d}A};$$

E is the binding energy, and A is the mass number.

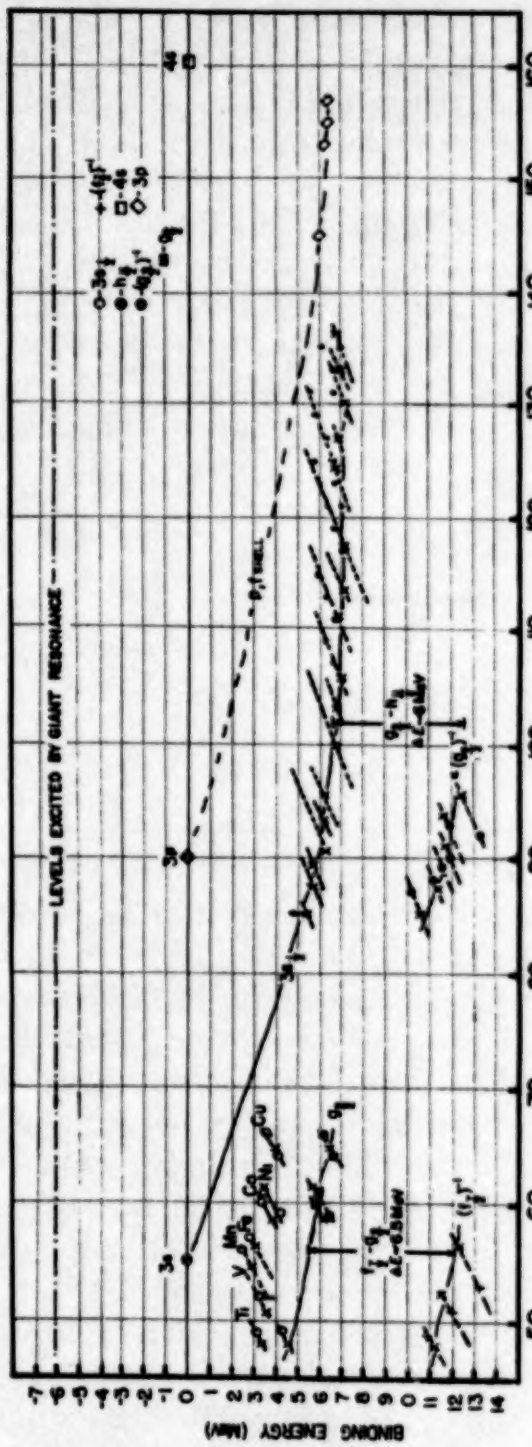

Fig. 9. Binding energy of various levels as a function of mass number. The dashed lines and crosses from fig. 8 are reproduced here and the line labelled $3s_{\frac{1}{2}}$ is drawn through the crosses. It is extrapolated to pass through the neutron giant resonance which is at zero binding energy for mass 55. The location of the 3p and 4s giant resonances are also shown. Other data points are the $3s_{\frac{1}{2}}$ and $g_{\frac{7}{2}}$ from ref. [2]); some $h_{\frac{9}{2}}$ and some 3p levels known from decay scheme studies; the energy required to remove a $g_{\frac{7}{2}}$ neutron from the closed shell, designated at $(g_{\frac{7}{2}})^{-1}$; and the same quantity for an $f_{\frac{7}{2}}$ neutron, designated $(f_{\frac{7}{2}})^{-1}$. The dot-dash line near the top shows the positions of the levels excited by the photonuclear giant resonance according to the Wilkinson theory.

In the region where its major shell is filling, the binding energy of the $3s_{\frac{1}{2}}$ level changes very slowly with A. For $90 < A < 105$, where the $d_{\frac{3}{2}}$ and $g_{\frac{7}{2}}$ subshells are supposedly filling, $S \approx 6$ MeV, and for $105 < A < 135$, where the $s_{\frac{1}{2}}$ subshell itself is supposedly filling (along with the $g_{\frac{7}{2}}$, $h_{\frac{11}{2}}$ and $d_{\frac{3}{2}}$ subshells), no shift is detectable; it might be expressed as $S = 0 \pm 3$ MeV.

The dependence on mass of the location of the $3s_{\frac{1}{2}}$ single particle and single hole states in the strict single particle theory is shown in fig. 10. The particle states shift with A at a rate corresponding to $S \approx 13$ MeV according to ref. [3]), and cease to exist when their binding energy reaches the top of the Fermi sea. The hole states begin at this point and they follow a line which is a reflection of an extension of the particle state curve about the top of the Fermi sea, since their excitation energy is just the difference between the binding energy of a $3s_{\frac{1}{2}}$ particle and the top of the Fermi sea. In this model, only the particle states are excited by (d, p) reactions and only the hole states are excited by (p, d) reactions.

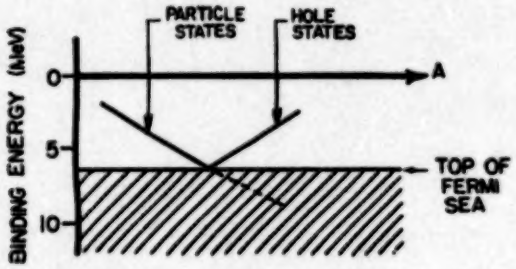

Fig. 10. Binding energy of $3s_{\frac{1}{2}}$ level as a function of mass number according to simple theory.

However, when pairing interactions are introduced, the location of the top of the Fermi sea relative to the single particle states becomes fuzzy. In particular, ground states consist of mixtures of configurations in which several single particle states are partly filled, whereas in the simple theory some of these should lie below the top of the Fermi sea and thus be completely filled, and others should lie above the top of the Fermi sea and thus be completely empty. As a result of this fuzziness, each of the states of fig. 10 becomes partly a particle state and partly a hole state, so that all of them can be excited either by (d, p) or (p, d) reactions but with less than the single particle width in each case. Moreover, the dependence of binding energy on mass is modified from the simple form shown in fig. 10. Since hole states and particle states shift in opposite directions with increasing mass, the two effects tend to cancel and the total shift is decreased when states become mixtures of particle and hole states.

This then explains the difference between the experimental results of fig. 9 and the single particle model prediction of fig. 10. Whereas from the single particle model one might assume that the $3s_{\frac{1}{2}}$ particle state reaches the top of the Fermi sea at $A \approx 120$, where the ground state of odd-neutron nuclei is $s_{\frac{1}{2}}$,

it may be expected [12]) that the pairing interaction causes the ground states of even nuclei to contain appreciable amounts of $(s_{\frac{1}{2}})^2$ in their configurations very shortly after the major shell begins filling at $A = 90$. There is direct experimental evidence for this in masses as low as 97 from the large cross section for excitation of the 2^+ first excited state of Mo^{96} by the Mo^{97}(d, t) reaction [13]); it indicates that the reaction proceeds by the pick-up of an $s_{\frac{1}{2}}$ neutron from the ground state of Mo^{97}, and that the ground state of Mo^{97} contains $(s_{\frac{1}{2}})^2$ in at least 20 percent of its configuration. Thus the point at which the $3s_{\frac{1}{2}}$ level reaches the top of the Fermi sea is not sharply defined but is spread through the entire region where its major shell is filling.

The observed shift of binding energy with A in the region $A < 90$ ($S \approx 12$ MeV) is in reasonable agreement with the calculation of Schröder [3]) which gives $S \approx 13$ MeV for a diffuse edge well. The shift in the region $90 < A < 110$ is in reasonable agreement with the above cited evidence that $(s_{\frac{1}{2}})^2$ is about 25 per cent full in this region. The levels are thus about 75 per cent "particle" and 25 per cent "hole" which would give a rate of shift about half as large as if the levels were 100 per cent particle. The observed shift is $S \approx 6$ MeV, which is just half the shift in the region $A < 90$ where the levels are 100 per cent "particle" levels.

It may be noted here that most of the discrepancies in shift of binding energy with A pointed out in ref. [6]) may be explained by the above methods. For example, the overall shift in the 3p level may be estimated. The binding energy is zero at $A = 90$ (neutron giant resonance) and in line with the above considerations it reaches about 5 MeV at $A = 140$ where its major shell begins to fill. This gives $S \approx 12$ MeV in agreement with the theory. The discrepancies in the overall shift discussed in ref. [6]) arose from taking a linear interpolation between the neutron giant resonance and the mass number at which the states in question are ground states of odd-neutron nuclei. They were further aggravated by comparing these values with the theoretical calculations for a square well rather than for a diffuse edge well.

3.3. APPLICATION TO THE WILKINSON THEORY OF THE PHOTONUCLEAR GIANT RESONANCE

In the mass 100 region, the Wilkinson theory of the photonuclear giant resonance [5]) explains that resonance as an excitation of a $g_{\frac{7}{2}}$ neutron to an $h_{\frac{11}{2}}$ state. The location of known $h_{\frac{11}{2}}$ states in this region is shown by the solid circles in fig. 9. It is abundantly clear that they lie very close to the dashed lines which represent the positions of the $3s_{\frac{1}{2}}$ states. The energy required to remove a $g_{\frac{7}{2}}$ neutron, designated as the binding energy of $(g_{\frac{7}{2}})^{-1}$, is shown in fig. 9 for several nuclei. The data were obtained from mass differences between isotopes with 49 and 50 neutrons, and from (d, t) reaction studies [14]). While the regions where the positions of the $h_{\frac{11}{2}}$ and $(g_{\frac{7}{2}})^{-1}$ states are well determined do not

quite overlap, there is little error possible in the small extrapolation required to determine their energy difference. This energy difference is readily seen to be about 6 MeV, in contrast to the observed energy of 17 MeV for the photonuclear giant resonance. The position of the next major shell as estimated from the neutron giant resonance and the location of known $f_{\frac{7}{2}}$, $f_{\frac{5}{2}}$, $p_{\frac{3}{2}}$ and $p_{\frac{1}{2}}$ levels is also shown in fig. 9. It is clear that for the $h_{\frac{11}{2}}$ level to be responsible for the photonuclear giant resonance, it would have to lie well above the position of the next major shell.

A similar determination is shown in fig. 9 for the transition from the $f_{\frac{7}{2}}$ to the $g_{\frac{9}{2}}$ level in the mass 50—60 region. The energy required to remove an $f_{\frac{7}{2}}$ neutron, designated as the binding energy of $(f_{\frac{7}{2}})^{-1}$, is determined from mass differences between isotopes with 27 and 28 neutrons, and binding energies of $g_{\frac{9}{2}}$ levels are taken from ref. [2]). The energy of the transition is found to be about 6.5 MeV, essentially the same as for the $g_{\frac{9}{2}} \rightarrow h_{\frac{11}{2}}$ transition in the mass 100 region, and similarly in disagreement with the energy of the photonuclear giant resonance.

A possible explanation for this large discrepancy has been proposed by G. E. Brown [15]) based on co-operative effects in particle-hole interactions. It is abundantly clear, however, that these difficulties of reconciling the Wilkinson theory of the photonuclear giant resonance with the behaviour of shell model states are not due to reduced mass effects as was originally proposed [5]). This would not only be in disagreement with the distance between major shells shown in fig. 9, but would require the binding energy to shift as a function of A with $S \approx 25$ MeV, contrary to the conclusions of section 3.2 above.

The authors are greatly indebted to J. R. Cameron for initiating the photographic plate program, to the plate reading group headed by Mrs. A. Trent for its vital services, to S. Meshkov and N. Austern for valuable discussion, and to A. J. Allen for his support and encouragement.

References

1) I. Bergstrom and G. Andersson, Arkiv för Fysik **12**, No. 19 (1957) 415
2) J. P. Schiffer, L. L. Lee and B. Zeidman, Phys. Rev. **115** (1959) 427
3) Schröder, Nuovo Cimento **10** (1958) 461
4) Ross, Mark and Lawson, Phys. Rev. **102** (1956) 1613; **104** (1956) 401
5) D. H. Wilkinson, Physica **23** (1956) 1039
6) Cohen, Mead, Price, Quisenberry and Martz, Phys. Rev., in print
7) S. T. Butler, Deuteron Stripping
8) B. L. Cohen and R. E. Price, to be published
9) See, for example, T. Auerback and J. B. French, Phys. Rev. **98** (1955) 1276
10) W. H. Sullivan, Trilinear Chart of Nuclides (U. S. Gov't Printing Office, Washington, D.C.)
11) H. Feshbach, C. E. Porter and V. F. Weisskopf, Phys. Rev. **96** (1954) 448
12) L. Kisslinger and R. Sorenson, private communication
13) B. L. Cohen and R. E. Price, Phys. Rev., in print
14) J. B. Hay, B. L. Cohen and R. E. Price, Bull. Am. Phys. Soc. **4** (1958) 287
15) G. E. Brown, private communication

1.E.5

Nuclear Physics **17** (1960) 141—152; © *North-Holland Publishing Co., Amsterdam*

Not to be reproduced by photoprint or microfilm without written permission from the publisher

MESURES DE DIFFUSION ÉLASTIQUE D'ÉLECTRONS DE 28 MeV PAR LES NOYAUX LOURDS

J. B. BELLICARD et P. BARREAU

Section de Physique Nucléaire à Moyenne Energie, C.E.N. Saclay

Reçu le 21 janvier 1960

Abstract: We have made measurements on 28 MeV electron scattering by gold and bismuth nucleus. Angular distributions of scattered electrons have allowed us to determine the root mean square radius of the charge distribution of the two nuclei with a precision of two percent. For the parameter r_0 entering into the expression for the radius $R = r_0 A^{\frac{1}{3}}$ of the homogeneous sphere adopted as charge distribution model, we found (in units of 10^{-13} cm) $r_0 = 1.17 \pm 0.02$ for gold, $r_0 = 1.15 \pm 0.03$ for bismuth. These results are in agreement with high-energy electron scattering results.

1. Introduction

Le grand développement des mesures de diffusion élastique des électrons par le noyau a montré l'intérêt de ces expériences pour la détermination précise de la distribution de charge des noyaux. Les mesures de diffusion élastique effectuées par Hofstadter [1,2]) sur les noyaux lourds avec des électrons d'énergies relativement élevées ($E > 150$ MeV) ont permis de déterminer avec une bonne précision les paramètres principaux des distributions de charge: rayon quadratique moyen $\langle r^2 \rangle$ et épaisseur de surface. Par contre, d'autres mesures effectuées avec des électrons d'énergies moyennes [3,4]) (30 MeV $< E <$ 60 MeV) ont non seulement abouti à des résultats moins précis sur la mesure de $\langle r^2 \rangle$, mais indiquaient des valeurs de ce paramètre inférieures de 5 à 10 % à celles trouvées par Hofstadter.

Les analyses théoriques de la diffusion élastique d'électrons par les noyaux lourds reposent sur la résolution par la méthode des ondes partielles de l'équation de Dirac relative à la diffusion d'électrons par un noyau dont la distribution de charge statique est de symétrie sphérique [5,6,7]). Si l'énergie des électrons est inférieure à 30 MeV, l'analyse mathématique du problème démontre que la distribution angulaire des électrons diffusés ne dépend en première approximation que du rayon quadratique moyen de la distribution de charge.

Ces considérations nous ont conduits à effectuer une nouvelle série d'expériences sur la diffusion d'électrons par des noyaux lourds tels que l'or et le bismuth. La comparaison de nos résultats avec les distributions angulaires théoriques obtenues pour diverses valeurs du rayon quadratique moyen nous ont permis de déterminer ce paramètre avec une précision meilleure que 2 %.

Dans cette limite, nos résultats sont compatibles avec ceux obtenus par Hofstadter *et al.* [1,2]).

2. Appareillage et méthodes expérimentales

2.1. PRODUCTION DU FAISCEAU

Le faisceau d'électrons utilisé pour nos expériences de diffusion est celui de l'accélérateur linéaire d'électrons de 28 MeV du Centre d'Études Nucléaires de Saclay. A la sortie de l'accélérateur, un analyseur magnétique [10]) formé de deux secteurs magnétiques de 60° permet d'obtenir un faisceau utile d'électrons d'énergie E connue avec une précision de $2\,{}^0/_{00}$; ces électrons sont groupés dans une bande d'énergie ΔE telle que $\Delta E/E \approx 2\,{}^0/_{00}$. Ce faisceau est resserré sur la cible de diffusion par un système de deux lentilles quadrupolaires; ses dimensions atteignent alors 2 mm $\times$ 6 mm.

2.2. ANALYSE DU FAISCEAU DIFFUSÉ

L'analyse du faisceau diffusé est assurée par un spectromètre magnétique à double focalisation formé par un secteur de 162°. L'angle du secteur et sa disposition par rapport à la chambre des cibles ont été choisis pour assurer une analyse des électrons diffusés sous des angles variant continûment de 19° à 161°.

Le secteur magnétique, la partie inférieure de la chambre de diffusion, le système de détection et sa protection sont montés sur une plateforme tournante dont l'axe de rotation passe par le centre de la cible (fig. 1). La partie supérieure de la chambre des cibles est maintenue fixe pendant la rotation de cet ensemble; un chemin de roulement assure sa liaison mécanique avec la partie inférieure, l'étanchéité de la chambre étant assurée par un seul joint de néoprène. Le changement de l'angle d'analyse peut ainsi être effectué en gardant un bon vide dans tout l'ensemble des canalisations.

Pour un angle solide d'acceptance maximum $\Omega/4\pi = 0.5\times10^{-3}$, les qualités optiques du spectromètre, étudiées avec une source d'électrons monocinétiques, permettent d'obtenir un pouvoir de résolution $\Delta E/E = 2.2\,{}^0/_{00}$; ΔE désigne ici la largeur à mi-hauteur de la raie enregistrée. La stabilité du champ magnétique du spectromètre était assurée par la régulation de la tension d'alimentation des bobines d'excitation à mieux que 0.5×10^{-3}. L'étalonnage du champ magnétique, effectué avec une sonde à effet Hall, nous donne, par mesure du courant circulant dans les bobines, la valeur du champ magnétique avec une précision de 2×10^{-3}.

La détection des électrons diffusés est effectuée au moyen de scintillateurs plastiques. Les électrons traversent successivement deux scintillateurs de 0.5 mm d'épaisseur; le premier est situé dans le plan focal du spectromètre; sa largeur (2 mm) est voisine de celle du faisceau; le second scintillateur, situé à 10 cm du premier, sur le trajet du faisceau, a des dimensions plus larges,

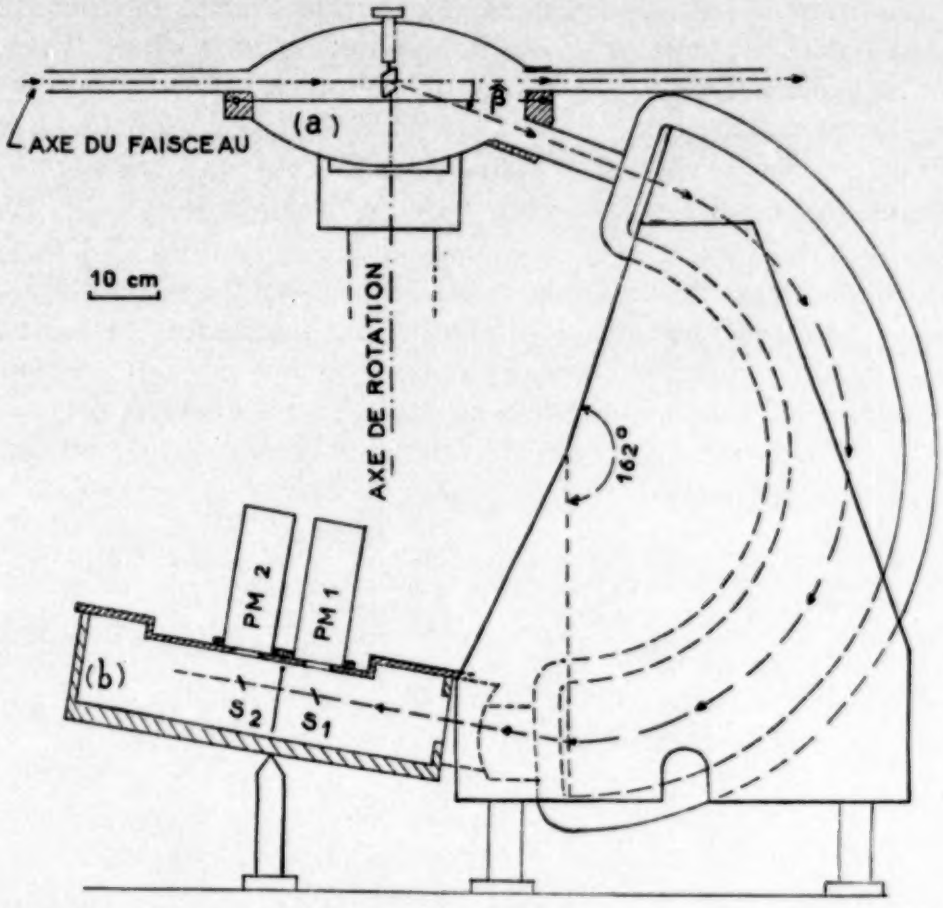

Fig. 1. Schéma de l'installation du spectromètre placé dans la position d'analyse des électrons diffusés sous l'angle minimum $\theta_{min} = \beta$. On notera: (a) la chambre de cibles: (b) le dispositif de comptage adopté pour la détection en coïncidence des électrons diffusés: les deux scintillateurs S_1 et S_2 placés sur le trajet des électrons sont vus par deux photomultiplicateurs.

notamment pour tenir compte de la diffusion multiple des électrons dans le premier. Les deux scintillateurs sont vus par des photomultiplicateurs 56 AVP qui commandent un circuit à coincidence, dont le temps de résolution est de 10^{-8} s. Ce système a l'avantage de réduire considérablement le bruit de fond.

2.3. PROCÉDURE EXPÉRIMENTALE

Le monitorage des expériences est effectué au moyen d'un cylindre de Faraday dont les dimensions permettent d'arrêter complètement le faisceau d'électrons et de contrôler constamment son intensité au cours de l'expérience [11]).

La direction et la concentration du faisceau sur la cible ont été contrôlées au moyen de lames de verre impressionnées par le passage du faisceau.

En raison de la grande variation de la section efficace de diffusion $d\sigma/d\Omega$ en fonction de θ,

$$\left(\frac{d\sigma}{d\Omega}\right)_{\theta=30^\circ} \Big/ \left(\frac{d\sigma}{d\Omega}\right)_{\theta=160^\circ} \approx 10^4,$$

nous avons utilisé, pour chaque distribution angulaire, deux cibles dont l'épaisseur variait dans un rapport 10 environ. Pour l'or, nos cibles avaient des densités superficielles de 109 $\mu g/cm^2$ et de 920 $\mu g/cm^2$. Pour le bismuth, ces densités étaient de 120 $\mu g/cm^2$ et de 1230 $\mu g/cm^2$. Le raccordement des mesures effectuées avec chaque cible était réalisé pour $\theta = 90°$; au cours des mesures, les cibles étaient orientées de façon à faire un angle de 45° avec le faisceau incident.

Pour chaque angle de diffusion, le relevé complet du pic élastique était effectué cinq fois en moyenne. Les distributions angulaires ont été établies avec les comptages relevés au sommet du pic; ces comptages sont fonction de la résolution du spectromètre qui reste constante au cours d'une série d'expériences. Cette méthode nous a permis de vérifier le recoupement statistique de chaque série de mesures.

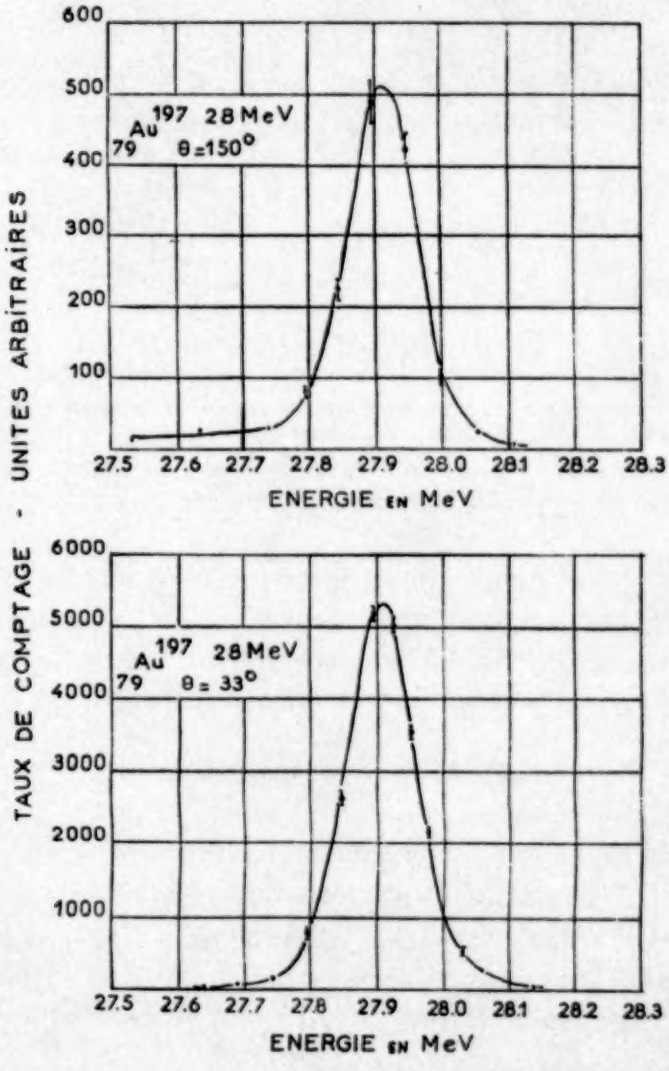

Fig. 2. Diffusion des électrons par l'or. Courbes typiques donnant les taux de comptage en fonction de l'énergie des électrons diffusés pour $\theta = 33°$ et $\theta = 150°$.

Nous donnons le relevé typique de deux pics élastiques pour l'or à 33° et à 150°. La résolution obtenue $\Delta E/E = 4.5\,{}^0/_{00}$ tient compte de l'optique du spectromètre et de la définition en énergie du faisceau incident (fig. 2).

3. Analyse théorique

La distribution angulaire des électrons diffusés par le noyau est donnée par

$$\frac{\mathrm{d}\sigma}{\mathrm{d}\Omega} = \sec^2 \tfrac{1}{2}\theta |f(\theta)|^2, \tag{1}$$

$$f(\theta) = \frac{1}{2ik} \sum_j \mathrm{e}^{2i\eta_j} (j+\tfrac{1}{2}) \left(P_{j-\frac{1}{2}}(\cos\theta) + P_{j+\frac{1}{2}}(\cos\theta)\right), \tag{2}$$

où

$$\eta_j = \eta_{jc} + \delta_j, \tag{3}$$

j est le moment angulaire total de l'onde partielle, et k le nombre d'onde de l'électron.

Le déphasage η_j de chaque onde partielle est la somme de deux termes: η_{jc} représente la partie purement Coulombienne de la diffusion (c'est-à-dire la diffusion par un noyau ponctuel de charge Ze); le déphasage supplémentaire δ_j dépend de l'énergie et de la répartition de charge envisagée par la valeur prise par la fonction $\gamma_j(kR)$ à la surface du noyau:

$$\gamma_j(kR) = \frac{\phi_{1,j}(kR)}{\phi_{2,j}(kR)}, \tag{4}$$

où ϕ_1, ϕ_2 sont les solutions des équations radiales de Dirac pour l'électron dans le champ du noyau.

Seules les premières ondes partielles sont affectées par l'extension des charges; pour des énergies $\leqq 30$ MeV, la valeur $\delta_{\frac{1}{2}}$ est prépondérante pour décrire cet effet: à 28 MeV nous avons déjà $\delta_{\frac{3}{2}} \leqq 0.02\ \delta_{\frac{1}{2}}$.

Pour le même domaine d'énergies, plusieurs auteurs, Elton [12]), Bodmer [8]), Glassgold [6]), utilisant des méthodes approchées pour le calcul de $\gamma_j(kR)$, ont tenté de montrer que, dans la limite de précision des expériences, la distribution angulaire des électrons diffusés était indépendante du modèle de distribution de charges pourvu que le rayon quadratique moyen $\langle r^2 \rangle$ soit le même pour deux types de distribution de charge considérés. Cela conduit par exemple à donner au rayon R_s d'une sphère creuse chargée superficiellement une valeur

$$R_s = (\tfrac{3}{5})^{\frac{1}{2}} R_H,$$

R_H désignant le rayon de la sphère pleine équivalente; Reignier [9]) a démontré que deux distributions de charge sont équivalentes „du point de vue de l'onde partielle j et de l'énergie E "si elles donnent la même valeur à la valeur moyenne

d'une certaine fonction $\mathcal{J}_j(kr)$ prise sur l'étendue du noyau. Aux basses énergies $\langle \mathcal{J}_j(kr) \rangle$ s'exprime au moyen des moments des charges; par exemple,

$$\langle \mathcal{J}_{\frac{1}{2}}(kr) \rangle = \langle r^2 \rangle - \frac{b^2(0)}{15} \langle r^4 \rangle, \tag{5}$$

où $b(0) = V(0) - E$ est l'énergie cinétique de l'électron prise au centre du noyau. Cette analyse nous conduit à

$$\langle r^2 \rangle_H = \alpha \langle r^2 \rangle_s, \quad \alpha > 1 \quad (\alpha = 1.02 \quad \text{pour} \quad E = 28 \text{ MeV}).$$

La sphère creuse équivalente à la sphère pleine du point de vue de l'onde partielle $j = \frac{1}{2}$ doit avoir un rayon quadratique moyen $\langle r^2 \rangle_s$ plus petit que celui de la sphère pleine $\langle r^2 \rangle_H$, si l'on veut que le déphasage supplémentaire $\delta_{\frac{1}{2}}$ soit le même pour les deux distributions. Le calcul exact de $\delta_{\frac{1}{2}}$ pour les deux types de distributions de charge confirme cette appréciation. Si l'on veut déterminer $\langle r^2 \rangle$ à une précision supérieure de 2 %, il faut adopter un modèle de charge aussi voisin que possible de la distribution de charge réelle; c'est pourquoi nous avons adopté un modèle de sphère pleine pour calculer les distributions angulaires des électrons diffusés pour différentes valeurs de $\langle r^2 \rangle = 0.6 R_H^2$.

Pour se conformer aux notations habituelles,

$$R_H = r_0 A^{\frac{1}{3}} \times 10^{-13} \text{ cm};$$

c'est entre différentes courbes reliées à des valeurs définies de r_0 que nous opterons.

4. Analyse des expériences

Les résultats bruts recueillis au cours de l'expérience doivent subir des corrections qui tiendront compte de la géométrie de l'expérience (angle solide du spectromètre, direction moyenne, dimensions et ouverture du faisceau), des phénomènes secondaires subis par les électrons dans la cible (diffusion multiple, pertes radiatives).

4.1. CORRECTIONS DE GÉOMÉTRIE

L'angle minimum sous lequel la diffusion des électrons peut être observée est $\beta = 19°$. Le spectromètre étant en place pour cette observation, une rotation d'un angle φ de la plateforme qui le supporte permet d'observer la diffusion sous l'angle θ tel que

$$\cos \theta = \cos \beta \cos \varphi.$$

Une variation $\Delta\theta$ de θ s'exprime linéairement en fonction des variations $\Delta\varphi$ et $\Delta\beta$ qui en sont l'origine:

$$\Delta\theta = \operatorname{cotg} \theta \, (\Delta\varphi \operatorname{tg} \varphi + \Delta\beta \operatorname{tg} \beta).$$

L'angle solide d'acceptance du spectromètre est délimité par un diaphragme d'ouverture rectangulaire S qui permet de recevoir sur le détecteur des électrons diffusés sous des angles $\theta_0+\Delta\theta$; les valeurs extrêmes de $\Delta\theta$ sont définies par

$$\Delta\varphi = \pm 1.6°, \quad \Delta\beta = \pm 2.8°.$$

Il en résulte que la section efficace moyenne des électrons diffusés dans l'angle d'acceptance du spectromètre est

$$\bar{\sigma}_1 = \int_S \frac{\sigma(\theta)\,\mathrm{d}\Delta\varphi\,\mathrm{d}\Delta\varphi}{S}$$

où $\sigma(\theta)$ au voisinage de θ_0 peut s'exprimer par

$$\sigma = \sigma(\theta_0)\mathrm{e}^{-\Delta\theta/G}, \qquad G = \text{cte}. \tag{6}$$

La connaissance de $\bar{\sigma}_1$ permet de corriger l'intensité reçue sur le détecteur et de la rapporter à $\sigma(\theta_0)$: cette correction atteint 1 % à 30°; 0.3 % à 150°; elle est à peu près négligeable.

La dimension et l'ouverture angulaires du faisceau pourraient introduire d'autres corrections sur la mesure de σ. Si l'on admet que ces deux effets sont représentés par une distribution gaussienne, la section efficace moyenne mesurée à θ_0 est

$$\overline{\sigma_2(\theta)} = (\pi^{\frac{1}{2}}\Delta)^{-1}\int_{-\infty}^{+\infty}\sigma(\theta')\exp\frac{(\theta-\theta')^2}{\Delta^2}\,\mathrm{d}\theta' = \sigma(\theta)_0\mathrm{e}^{-(\Delta^2/4G^2)}$$

avec $\Delta \leqq 1°$; $\sigma(\theta')$ est donné par (6).

Cette valeur moyenne de la section efficace mesurée donne une nouvelle correction de l'intensité reçue par le détecteur; elle est inférieure à la précédente et négligeable.

4.2. PHÉNOMÈNES SECONDAIRES DANS LES CIBLES

La diffusion multiple des électrons dans les cibles est négligeable: pour la cible de bismuth la plus épaisse (1230 μg/cm^2) l'angle moyen $\langle u\rangle$ de diffusion multiple est inférieur à 18'.

Les électrons diffusés qui subissent des pertes radiatives supérieures à l'intervalle d'énergie ΔE accepté par les détecteurs ne sont pas comptés dans le pic élastique. L'intensité $I = I_0\mathrm{e}^{-\delta}$ reçue par le cristal est inférieure à celle, I_0, qu'il recevrait en l'absence de pertes radiatives. Schwinger et Suura [13,14]) ont étudié l'interaction de l'électron avec le champ de radiation et calculé le coefficient δ qui permet d'évaluer les pertes radiatives en fonction de la résolution du spectromètre et de l'angle θ de diffusion:

$$\delta = \frac{4}{137\pi}\left(\left(\log\frac{E}{\Delta E} - \tfrac{13}{12}\right)\left(\log\left(\frac{2E}{mc^2}\sin\tfrac{1}{2}\theta\right) - \tfrac{1}{2}\right) + \tfrac{17}{72}\right). \tag{7}$$

Dans le cas de l'or, si $\Delta E/E = 3\times 10^{-3}$, le pourcentage d'électrons perdus dans le comptage par effet radiatif passe de 12 % à 30° à 17 % à 150°. Il est donc nécessaire d'en tenir compte dans l'estimation de I_0.

4.3. CONFRONTATION DES RÉSULTATS EXPÉRIMENTAUX ET THÉORIQUES

L'expérience nous délivre la distribution angulaire des électrons diffusés en valeur relative. La diffusion des électrons sous des angles faibles, $\theta \leqq 30°$, est très peu dépendante de la distribution de charge et nous permettrait à la rigueur d'ajuster nos résultats expérimentaux à une courbe de distribution angulaire théorique. Cette méthode ne donne qu'un résultat préliminaire qui peut être utilisé ensuite dans l'emploi de la méthode des moindres carrés pour ajuster avec précision notre courbe de distribution angulaire expérimentale à une courbe théorique.

La méthode des moindres carrés indique que l'expression

$$\sum_{i=1}^{n} N_i \left(\frac{\sigma_i}{\lambda\Omega_i} - 1\right)^2 \tag{8}$$

doit être rendue minimum par le choix d'une courbe théorique appropriée; σ_i et $\lambda\Omega_i$ sont les sections de choc de diffusion théorique et expérimentale à l'angle θ_i, N_i désigne le nombre total de coups comptés dans l'expérience pour l'angle θ_i. Le paramètre λ est introduit pour tenir compte du fait que Ω_i n'est connu qu'en valeur relative. Pour chaque courbe théorique, le paramètre λ sera choisi de façon à rendre minimum l'expression (8):

$$\lambda = \frac{\sum_i \left(\frac{\sigma_i}{\Omega_i}\right)^2 N_i}{\sum_i \left(\frac{\sigma_i}{\Omega_i}\right) N_i}. \tag{9}$$

5. Résultats

5.1. DIFFUSION ÉLASTIQUE SUR L'OR

L'or est un noyau très peu déformé, comme le montre la valeur de son moment quadrupolaire; la valeur μ de son moment magnétique n'est pas nulle. L'étude théorique a montré que la contribution magnétique dipolaire qui en résulte dépend de la même façon que la charge de la taille finie du noyau. Le rapport de ces deux contributions est de l'ordre de $(\mu/Z)^2$ et n'est appréciable que pour les noyaux légers [1,15]). Le noyau d'or peut donc être considéré dans nos expériences de diffusion comme une distribution de charge statique à symétrie

sphérique; les mêmes conclusions seront valables pour le bismuth.

L'or présente deux niveaux à 77 et 268 keV; ceux-ci ne donnent pas de contribution appréciable à la diffusion [16]); le pic correspondant au niveau de 268 keV qui pourrait être séparé facilement du pic élastique n'a pas été vu, même à grand angle (160°) avec une cible plus épaisse (8 mg/cm²); l'examen des pics élastiques relevés aux grands angles montre qu'ils ne présentent pas de déformation susceptible d'indiquer une contribution du niveau de 77 keV.

La méthode des moindres carrés appliquée à la distribution angulaire expérimentale (fig. 3) des électrons diffusés par l'or sous des angles θ tels que $33° \leqq \theta \leqq 150°$ nous indique que le meilleur accord est obtenu pour la courbe

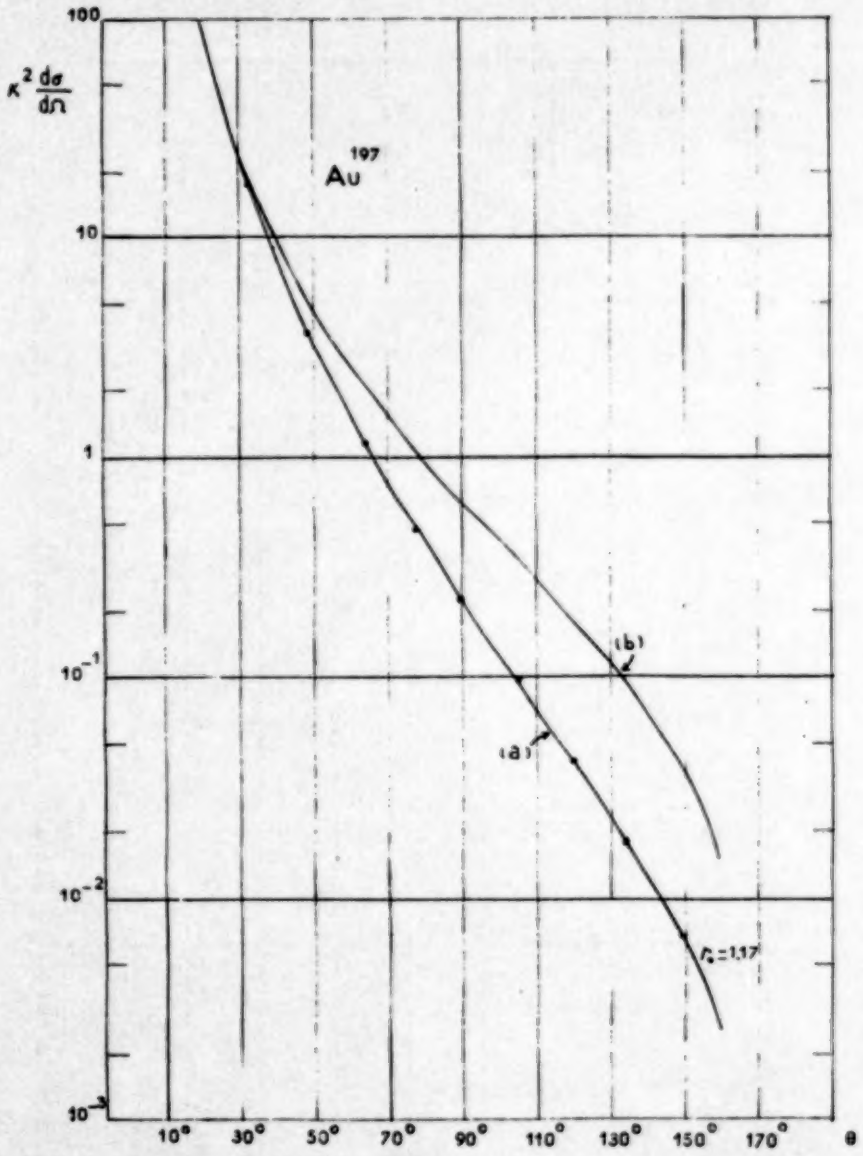

Fig. 3. ^{197}Au. (a) Distribution angulaire des électrons diffusés. Les points expérimentaux sont distribués sur la courbe théorique $r_0 = 1.17$. Les fluctuations statistiques sont beaucoup trop faibles pour y figurer. (b) Courbe théorique correspondant au noyau ponctuel.

de distribution angulaire théorique qui correspond à la diffusion par un noyau sphérique homogène de rayon $R = r_0 A^{\frac{1}{3}} \times 10^{-13}$ cm $= 6.81 \times 10^{-13}$ cm. La précision obtenue sur la mesure des paramètres expérimentaux (angle de diffusion, énergie des électrons incidents), leurs légères fluctuations au cours des mesures, nous ont amenés à conclure que la précision obtenue sur r_0 est meilleure que 2 %; pratiquement $r_0 = 1.17 \pm 0.02$.

5.2. DIFFUSION ÉLASTIQUE SUR LE BISMUTH

La distribution angulaire experimentale des électrons diffusés (fig. 4) par le noyau de bismuth s'étend sur un domaine angulaire plus faible que dans le cas du noyau d'or; elle est comprise dans des limites telles que $62°.5 < \theta < 150°$; la

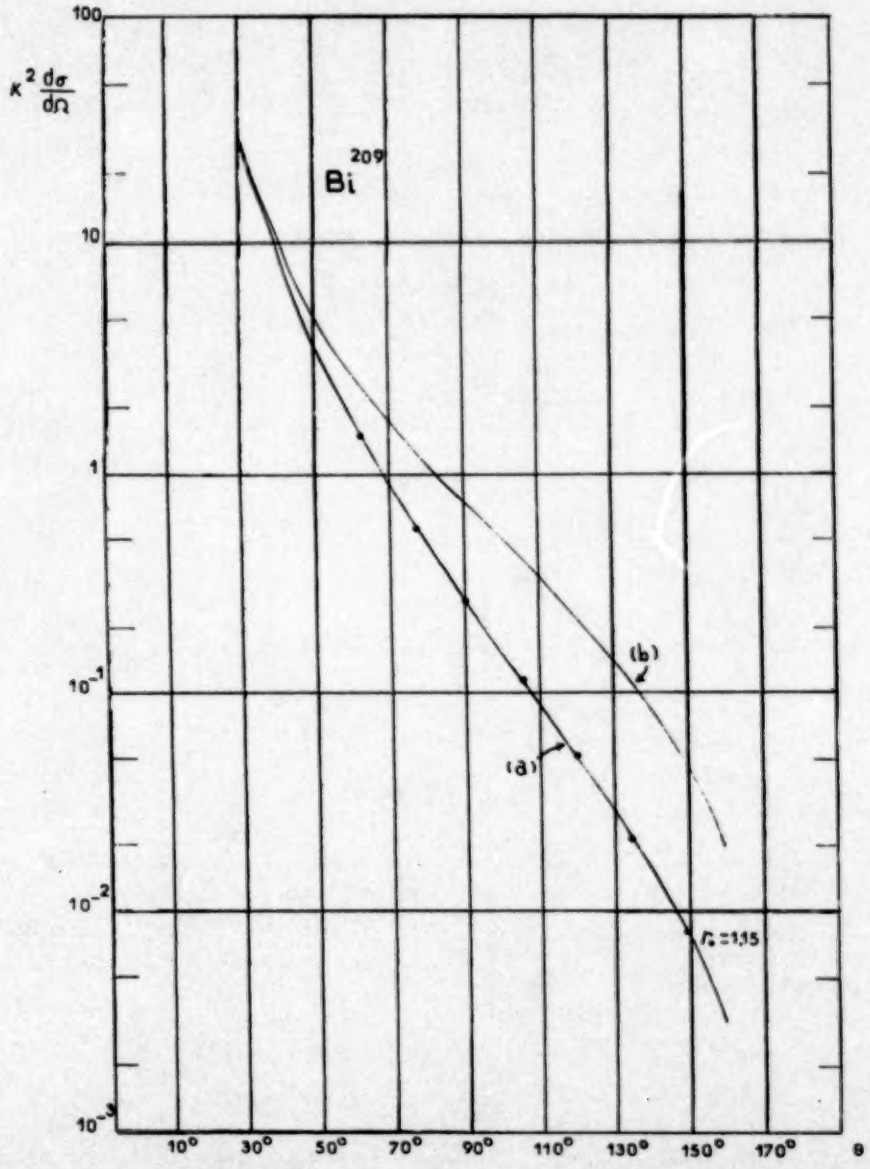

Fig. 4. ^{209}Bi. (a) Distribution angulaire des électrons diffusés. Les points expérimentaux sont portés sur la courbe théorique $r_0 = 1.15$. (b) Courbe théorique correspondant au noyau ponctuel.

précision statistique des points expérimentaux est également moins bonne. Il en résulte que la précision obtenue sur r_0 est sensiblement moindre que pour l'or: $r_0 = 1.15 \pm 0.03$.

6. Conclusions

La valeur du rayon quadratique moyen de la distribution de charge des noyaux lourds qui résulte des valeurs trouvées pour le paramètre r_0 est en accord avec celle donnée par les expériences de Stanford réalisées avec des électrons d'énergies plus élevées (150 MeV $< E <$ 185 MeV). Ces expériences donnaient pour l'or $r_0 = 1.18 \pm 0.01$ et pour le bismuth $r_0 = 1.20 \pm 0.025$ [2]). Les valeurs plus faibles du paramètre r_0 trouvées par Pidd et Hammer [4]) ne sont pas confirmées: elles semblent résulter de la faible précision des mesures (r_0 est connu avec une précision de 10 %) et d'un dispositif expérimental moins avantageux que le nôtre.

Dans la limite de précision des expériences, la comparaison de nos résultats avec ceux obtenus par Hofstadter et ses collaborateurs indique que les distributions angulaires des électrons diffusés sont expliquées par des distributions de charge dont le rayon quadratique moyen ne semble pas varier avec l'énergie. Ils soulignent qu'il n'y a pas d'interaction non électromagnétique dans les expériences de diffusion électron-noyau. Pour préciser ce point déjà soulevé par Hofstadter *et al.* [2]), il faudrait, non seulement obtenir une précision très supérieure dans la mesure des paramètres définissant le modèle, mais encore vérifier expérimentalement la distribution angulaire des pertes radiatives.

L'intérêt de la diffusion élastique des électrons de basse énergie par les noyaux a été souligné par les travaux théoriques de J. Reignier [9]) et confirmé par nos expériences pour les noyaux lourds. Les derniers travaux réalisés à l'Université de Stanford par U. Meyer-Berkhout *et al.* sur la diffusion élastique des électrons par les noyaux 1p [17]) ont également démontré que des données expérimentales obtenues à basse énergie (80 à 160 MeV pour les noyaux considérés) étaient indispensables pour décrire complètement un modèle de répartition de charge.

Nous tenons à remercier MM. J. Thirion et C. Tzara pour l'intérêt et l'aide qu'ils nous ont apportés en vue de la réalisation de ce travail. Nous voulons exprimer également notre reconnaissance à M. J. Reignier, de l'Université Libre de Bruxelles, pour les conseils qu'il nous a donnés au cours de discussions théoriques sur le problème examiné. Nous remercions également M[lle] Wahl et le Bureau de Calcul du Centre d'Études Nucléaires de Saclay de leur assistance technique pour le calcul des sections efficaces de diffusion, ainsi que l'équipe de fonctionnement de l'accélérateur linéaire pour son dévouement au cours de nos expériences.

Bibliographie

1) R. Hofstadter, Ann. Rev. of Nucl. Sc. **7** (1957)
2) B. Hahn, D. G. Ravenhall et R. Hofstadter, Phys. Rev. **101** (1956) 1131
3) E. M. Lyman, A. O. Hanson et M. B. Scott, Phys. Rev. **84** (1951) 626
4) R. W. Pidd et C. L. Hammer, Phys. Rev. **99** (1955) 1396
5) D. R. Yennie, D. G. Ravenhall et R. N. Wilson, Phys. Rev. **95** (1954) 500
6) A. E. Glassgold, Phys. Rev. **98** (1955) 1360
7) A. E. Glassgold et E. W. Mack, M.I.T. Technical Report no. 65 (1954)
8) A. R. Bodmer, Proc. Phys. Soc. A **66** (1953) 1041
9) J. Reignier, Nuclear Physics **7** (1958) 526
10) C. Schuhl et J. Miller, Rapport S.R.N.M.E. no. 1 (1959)
11) K. L. Brown et G. W. Tautfest, Rev. Sc. Instr. **27** (1956) 696
12) L. R. B. Elton, Proc. Phys. Soc. A **66** (1953) 806
13) J. Schwinger, Phys. Rev. **76** (1949) 780
14) H. Suura, Phys. Rev. **99** (1955) 1020
15) M. N. Rosenbluth, Phys. Rev. **79** (1950) 615
16) L. I. Schiff, Phys. Rev. **96** (1954) 765
17) U. L. Meyer-Berkhout, K. W. Ford et A. E. S. Green, Ann. of Physics **8** (1959) 119

1.E.4

Nuclear Physics **17** (1960) 153—162; © *North-Holland Publishing Co., Amsterdam*

Not to be reproduced by photoprint or microfilm without written permission from the publisher

ERZEUGUNG KURZLEBIGER ISOMERE DURCH IMPULSAKTIVIERUNG MIT THERMISCHEN NEUTRONEN

K. F. ALEXANDER und V. BREDEL

Zentralinstitut für Kernphysik, Rossendorf bei Dresden

Eingegangen am 30. Dezember 1959

Abstract: An external neutron beam from the Rossendorf Research Reactor was periodically interrupted by a steel rotor. By placing a sample in the modulated neutron beam it was possible to observe short-lived isomeric states produced by thermal neutron capture. The spectra of the delayed γ-radiation were measured with a scintillation spectrometer. In this way a number of isomeric transitions were found and their half-lives were obtained by means of a 5 channel time analyser. The energies and half-lives of the following isomers were measured: Na^{24m} (475±10 keV, 20±1 msec); Ga^{m} (99±5 keV, 38±2 msec); In ^{116m} (160±8 keV, 2460±80 msec); Ho^{166m} (131±5 keV, 0.214±0.010 msec). The newly discovered Ho^{166m} has a K-conversion coefficient of about 0.4. Therefore the transition is probably of the type E2.

1. Einleitung

Die Beobachtung von Aktivitäten mit Lebensdauern im msec-Gebiet stößt auf spezifische experimentelle Schwierigkeiten. Die bei längeren Halbwertszeiten übliche Methode der räumlichen Trennung zwischen Erzeugung und Messung der interessierenden Aktivität ist u.a. wegen der notwendigen hohen Transportgeschwindigkeiten schlecht anwendbar. Die für sehr kurze Lebensdauern gut geeignete Methode der verzögerten Koinzidenzen versagt oberhalb ca. 10^{-4} sec wegen der rapiden Zunahme der zufälligen Koinzidenzen. Diese experimentellen Schwierigkeiten dürften mit ein Grund dafür sein, daß bis vor wenigen Jahren keine isomeren Kernzustände mit Lebensdauern im msec-Gebiet bekannt waren (siehe z.B. Ref. [1])) und auch heute noch eine auffällige Lücke in der empirischen Halbwertszeit-Verteilung der bekannten Isomere existiert.

Neue Möglichkeiten zur Untersuchung von Isomeren mit Halbwertszeiten zwischen 10^{-4} und 10^{-1} sec ergaben sich durch die Methode der impulsweisen Aktivierung, die zuerst von Jampolski *et al.* [2]) und Softky [3]) im Jahre 1955 angewandt wurde. Bei dieser Methode wird die Probe nicht bewegt. Die Aktivität wird durch impulsweise Bestrahlung erzeugt und ihr Abklingen in den Pausen zwischen den Bestrahlungen gemessen. Bisher wurden derartige Arbeiten nur an Beschleunigern durchgeführt, und zwar durch Aktivierung mit Protonen, schnellen Neutronen und Bremsstrahlung. Auf diese Weise wurde in den letzten Jahren eine größere Anzahl von isomeren Niveaus gefunden und identifiziert.

Eine Impulsaktivierung mit thermischen Neutronen wurde bisher nicht versucht, obwohl dadurch die Zahl der zugänglichen Kerne wesentlich vergrößert werden kann und außerdem bei der Aktivierung durch thermische Neutronen die Identifizierung der gebildeten isomeren Kerne im allgemeinen leichter sein sollte.

Durch periodische Unterbrechung eines Strahls von Reaktorneutronen mit Hilfe eines Rotors läßt sich eine Impulsaktivierung dieser Art durchführen. Im folgenden werden erste Resultate, die mit einer nach diesem Prinzip arbeitenden Apparatur erhalten wurden, mitgeteilt.

2. Versuchsanordnung

Das kollimierte Strahlungsbündel von ca. 1 cm Durchmesser aus einem horizontalen Kanal des Rossendorfer Forschungsreaktors wird periodisch durch einen Rotor unterbrochen, der unmittelbar am Kanalausgang angeordnet ist (Fig. 1). Der Rotor stellt einen 13 cm langen Stahlzylinder von 18 cm Durch-

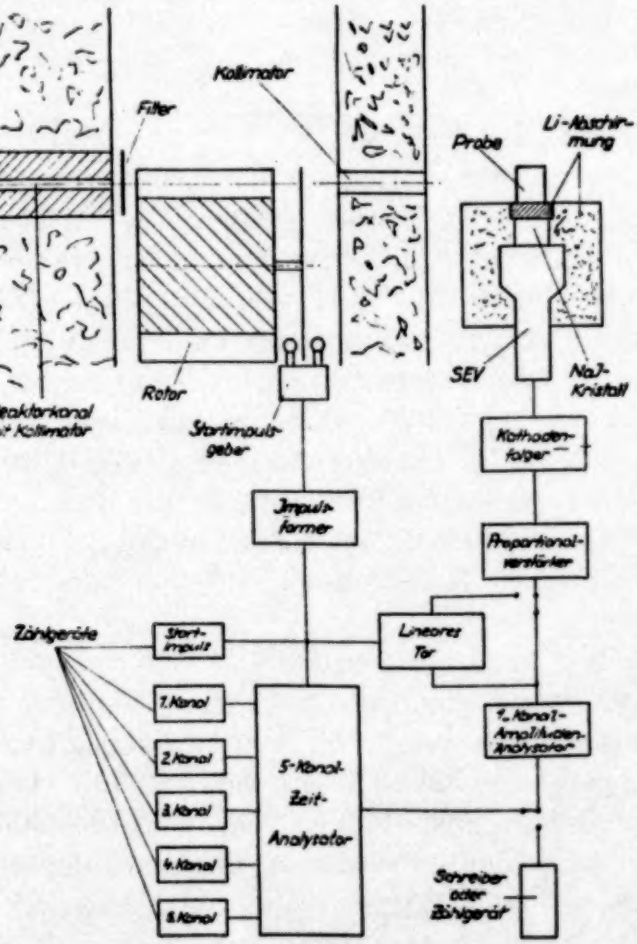

Fig. 1. Schema der Versuchsanordnung.

messer dar, dessen Achse parallel zum Strahl liegt. Er besitzt an seiner Peripherie zwei sektorförmige Ausfräsungen, so daß der Strahl zweimal je Umdrehung jeweils für eine Vierteldrehung frei passieren kann. Die dem Reaktor zugewandte Stirnfläche des Rotors ist mit Cd-Blech bedeckt. Die Drehzahl des Rotors kann zwischen 4 und 1800 Umdrehungen/min beliebig gewählt werden. Die Probe ist hinter dem Rotor im Strahlengang angeordnet. Dazwischen befindet sich noch eine aus Beton- und Bleiziegeln errichtete Abschirmwand mit Kollimator, die Probe und Detektor vor Streustrahlung schützen soll.

Die von der Probe emittierte γ-Strahlung wird mit einem Einkanal-Szintillationsspektrometer registriert. Der NaJ-Kristal (3×2.5 cm) und der SEV sind gegen Streuneutronen mit Lithium abgeschirmt, und zwar befindet sich zwischen Probe und Szintillator eine 1.6 cm dicke Platte aus LiF, während die seitliche Abschirmung aus mehreren cm Li_2CO_3 besteht. Als SEV wurde der Typ M 12 FS (VEB Carl Zeiß, Jena) verwendet.

Auf der Achse des Rotors befindet sich eine Scheibe aus dünnem Aluminiumblech mit zwei um 180° versetzten Schlitzen, durch die mit Hilfe einer Lichtquelle und einer Photozelle jeweils kurz nach dem Abdecken des Neutronenstrahls ein elektrischer Startimpuls erzeugt wird.

Zur Aufnahme des Spektrums der durch den Zerfall eines isomeren Niveaus verzögert auftretenden γ-Strahlung wird durch den Start-impuls ein Tor für eine einstellbare Zeit geöffnet. Die vom Tor durchgelassenen Impulse gelangen auf einen Einkanal-Impulshöhenanalysator, dessen Ausgangsimpulse entweder von einem Zählgerät oder über eine Integrierstufe mit einem Schreiber registriert werden.

Zur Messung der Abklingzeit wird der Einkanalanalysator auf die dem isomeren Übergang entsprechende Linie eingestellt. Die Ausgangsimpulse werden einem 5-Kanal-Zeitanalysator zugeführt, der nach Eintreffen des Startimpulses nacheinander fünf Zählkanäle einstellbarer Zeitdauer freigibt. Dieses Gerät ist quarzgesteuert und ermöglicht Kanalbreiten zwischen 10 μsec und 10 sec mit großer Genauigkeit einzustellen [4]).

Da keine Vorkehrungen getroffen waren, die Drehzahl des Rotors sehr genau konstant zu halten, wurden die Messungen jeweils auf die gleiche Anzahl von Startimpulsen bezogen, die mit einem besonderen Gerät gezählt wurden.

Um den durch Einfang thermischer Neutronen allein hervorgerufenen Effekt zu erhalten, wurden Cd-Differenzmessungen sowohl für das verzögerte Spektrum, als auch für die Abklingzeit durchgeführt. Da das Cd-Filter neben der Absorption thermischer Neutronen auch eine gewisse Schwächung der Untergrund-γ-Strahlung hervorruft, wurde es bei Effektmessungen durch ein für thermische Neutronen transparentes Filter ersetzt, dessen Dicke so bemessen war, daß sich bei Verwendung einer Graphitprobe keine Differenz zwischen den mit beiden Filtern gemessenen Zählraten ergab. Für die an Na, Ga und In durchgeführten Messungen wurde als Kompensationsfilter ein Pb-Blech verwendet. Im Gebiet

zwischen der K-Kante des Bleis und der des Cadmiums ändert sich jedoch die Kompensationswirkung, so daß die Cd-Differenzmessung bei kleinen Energien gestört werden (siehe Fig. 4). Beim Ho, wo auch die Röntgenlinie beobachtet werden konnte, wurde daher ein Sn-Filter zur Kompensation verwendet, dessen K-Kante in der Nähe der K-Kante des Cd liegt und das daher auch in diesem Gebiet eine gute Kompensation gewährleistet.

Die Energieeichung des Spektrometers wurde mit Hilfe von Eichpräparaten während der Messung des verzögerten Spektrums unter den gleichen Versuchsbedingungen durchgeführt, wie sie bei der Aufnahme des Spektrums selbst herrschten. Dies war deswegen notwendig, weil die starke Belastung des Spektrometers während der Aktivierungsperiode eine einige Prozent betragende Erhöhung des Verstärkungsgrades in den dazwischenliegenden Meßperioden bewirkt.

3. Versuchsergebnisse

3.1. NATRIUM

Die ersten Messungen mit der beschriebenen Apparatur wurden mit Natrium durchgeführt. Dieses Element war für uns deswegen von Interesse, weil bereits von Dropesky und Schardt [5]) ein isomerer Zustand beim Na^{24} gefunden worden war, dessen Lebensdauer aber von diesen Autoren wegen experimenteller Schwierigkeiten nur grob abgeschätzt werden konnte (5 bis 50 msec). Na^{24m} wurde hier beim Zerfall des Ne^{24} beobachtet. Die Energie des isomeren Übergangs wurde zu 472 keV bestimmt. Da in dem γ-Spektrum, das beim Einfang thermischer Neutronen im Na^{23} entsteht, eine intensive Linie bei 472 keV auftritt [6]) war zu vermuten, daß das von Dropesky und Schardt beobachtete Isomer auch durch Neutroneneinfang erzeugt werden kann.

Für die Untersuchung des Na^{24m} wurde als Probe ein mit 45 g NaF gefüllter dünnwandiger Aluminiumbehälter verwendet. Das mit dem Schreiber aufgenommene verzögerte Spektrum zeigt Fig. 2. Wird das Bleifilter durch das Cadmiumfilter ersetzt, so verschwindet die starke Linie fast vollständig. Die Energie der γ-Linie liegt nach unseren Messungen bei 475 ± 10 keV.

Fig. 3 zeigt das Ergebnis einer Abklingmessung mit einer Zeitkanalbreite von 10 msec. Als Halbwertszeit ergibt sich der Wert von 20.0 ± 1 msec. Der gleiche Wert wurde auch mit einer Zeitkanalbreite von 4 msec gefunden. Er befindet sich in guter Übereinstimmung mit den Angaben anderer Autoren (Tab. 1).

3.2. GALLIUM

Bisher wurde nur der obere Teil (> 4 MeV) des beim Einfang thermischer Neutronen im Ga emittierten γ-Spektrums gemessen [6, 10]). Über die Existenz von Ga-Isomeren gibt es bisher folgende Beobachtungen.

Facing p. 156

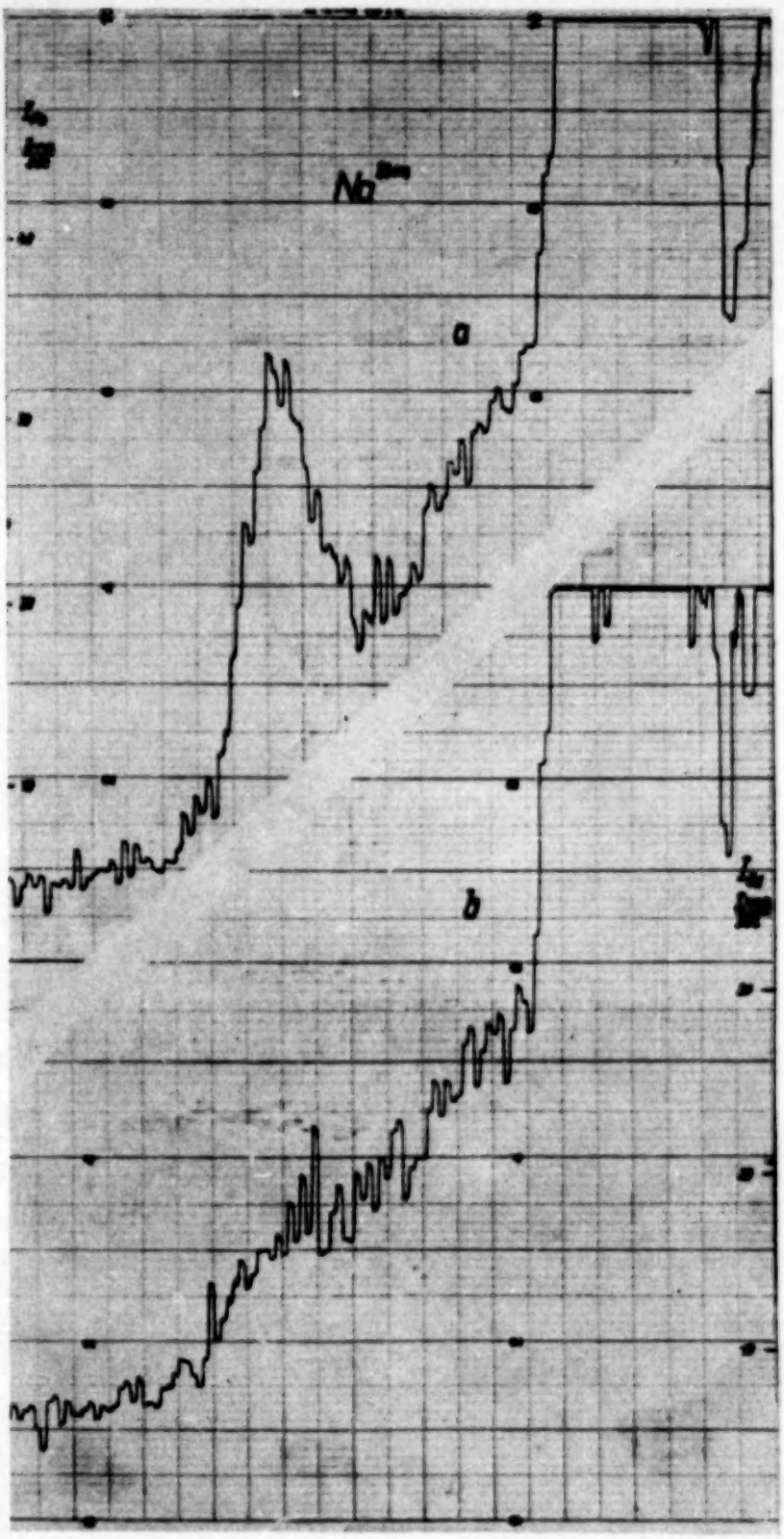

Fig. 2. Das mit Schreiber registrierte verzögerte Na^{24m}-Spektrum.
a) mit Pb-Filter, b) mit Cd-Filter.

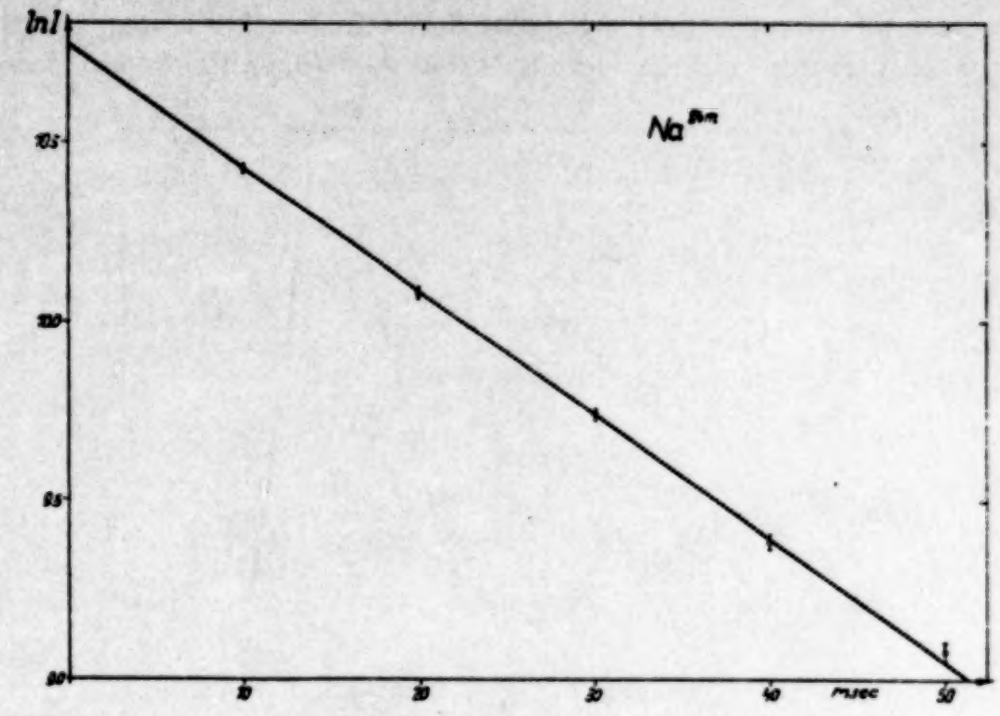

Fig. 3. Abklingkurve für Na^{24m}.

TABELLE 1

Kurzlebige Isomere bei Na, Ga, In und Ho

Element	Reaktion	$T_{\frac{1}{2}}$ (msec)	E_γ (keV)	Literatur
Na	$Ne^{24} \xrightarrow{\beta} Na^{24m}$	5 ÷ 50	472 ± 5	[5])
	$Na^{23}(d, p)Na^{24m}$	19.9 ± 0.7		[8])
	$Mg^{24}(n, p)Na^{24m}$	20 ± 1	470 ± 10	[9])
	$Al^{27}(n, \alpha)Na^{24m}$	20 ± 1	470 ± 10	[9])
	$Na^{23}(n, \gamma)Na^{24m}$	20 ± 2		[7])
	$Na^{23}(n, \gamma)Na^{24m}$	20 ± 1	475 ± 10	Diese Arbeit
Ga	$Ga^{71}(p, pn)Ga^{70m}$	19 ± 1	190 ± 10	[11])
	$Ge^{70}(n, p)Ga^{70m}$	16 ± 1	170 ± 10	[9])
	$Ga^{71}(n, \gamma)Ga^{72m}$	40 ± 2	≈ 90	[7])
	$Ga(n, \gamma)Ga^{m}$	38 ± 2	99 ± 5	Diese Arbeit
In	$Cd^{114}(p, n)In^{114m}$	47 ± 10	312 ± 10	[12])
	$In^{115}(n, 2n)In^{114m}$	42 ± 2	320 ± 10	[9])
	$In^{115}(\gamma, n)In^{114m}$	42 ± 5	311 ± 5	[14])
	$In^{113}(n, \gamma)In^{114m}$	2500	150	[7])
	$In^{115}(n, \gamma)In^{116m}$	2460 ± 80	160 ± 8	Diese Arbeit
Ho	$Ho^{165}(n, \gamma)Ho^{166m}$	0.214 ± 0.010	131 ± 5	Diese Arbeit

Morosow und Jampolski [11]) erzeugten durch Impulsaktivierung von Ga^{71} mit 10 MeV-Protonen nach der Reaktion $Ga^{71}(p, pn)Ga^{70m}$ ein Isomer

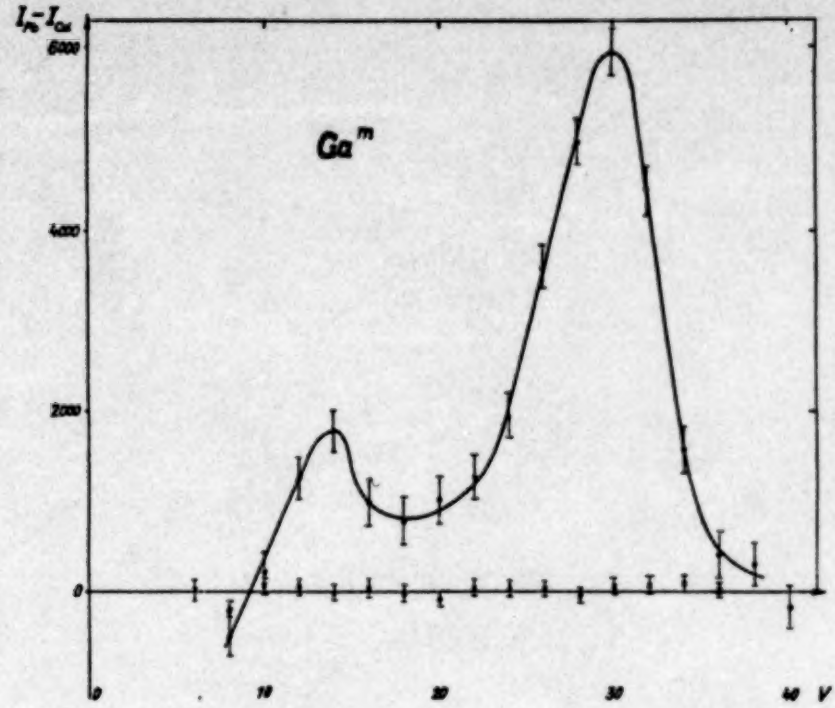

Fig. 4. Das punktweise aufgenommene verzögerte Ga^m-Spektrum (Pb—Cd-Differenzmessung). × Messung mit Graphitprobe.

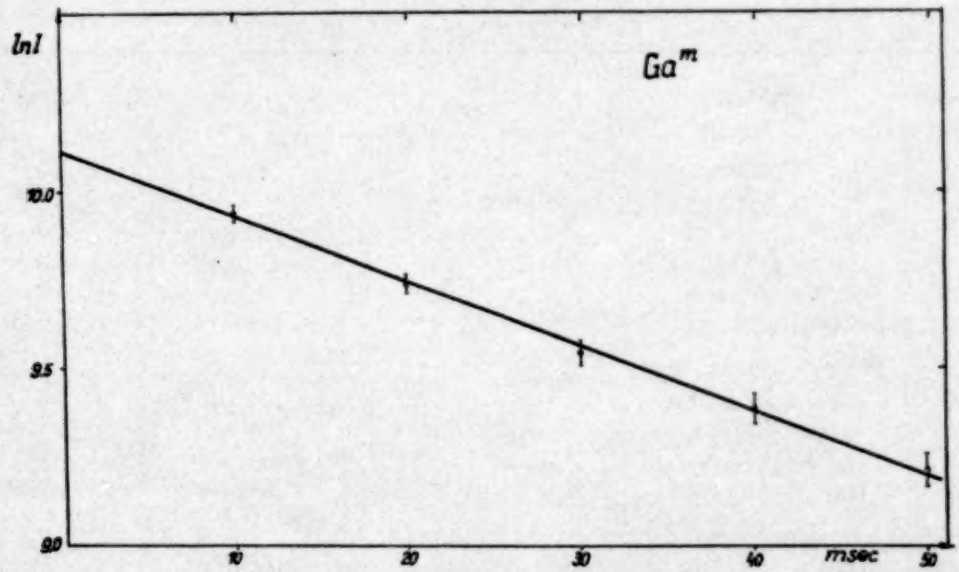

Fig. 5. Abklingkurve für Ga^m.

($E = 190$ keV, $T_{\frac{1}{2}} = 19$ msec), das ebenfalls mit der Reaktion $Ga^{70}(n, p)Ga^{70m}$ hergestellt wurde [9]). Bei der Aktivierung von Gallium mit thermischen Neutronen wurde von Campbell und Fettweis [7]) ein anderes Isomer ($E = 90$ keV, $T_{\frac{1}{2}} = 40$ msec) gefunden, das von diesen Autoren dem Ga^{72} zugeordnet wird.

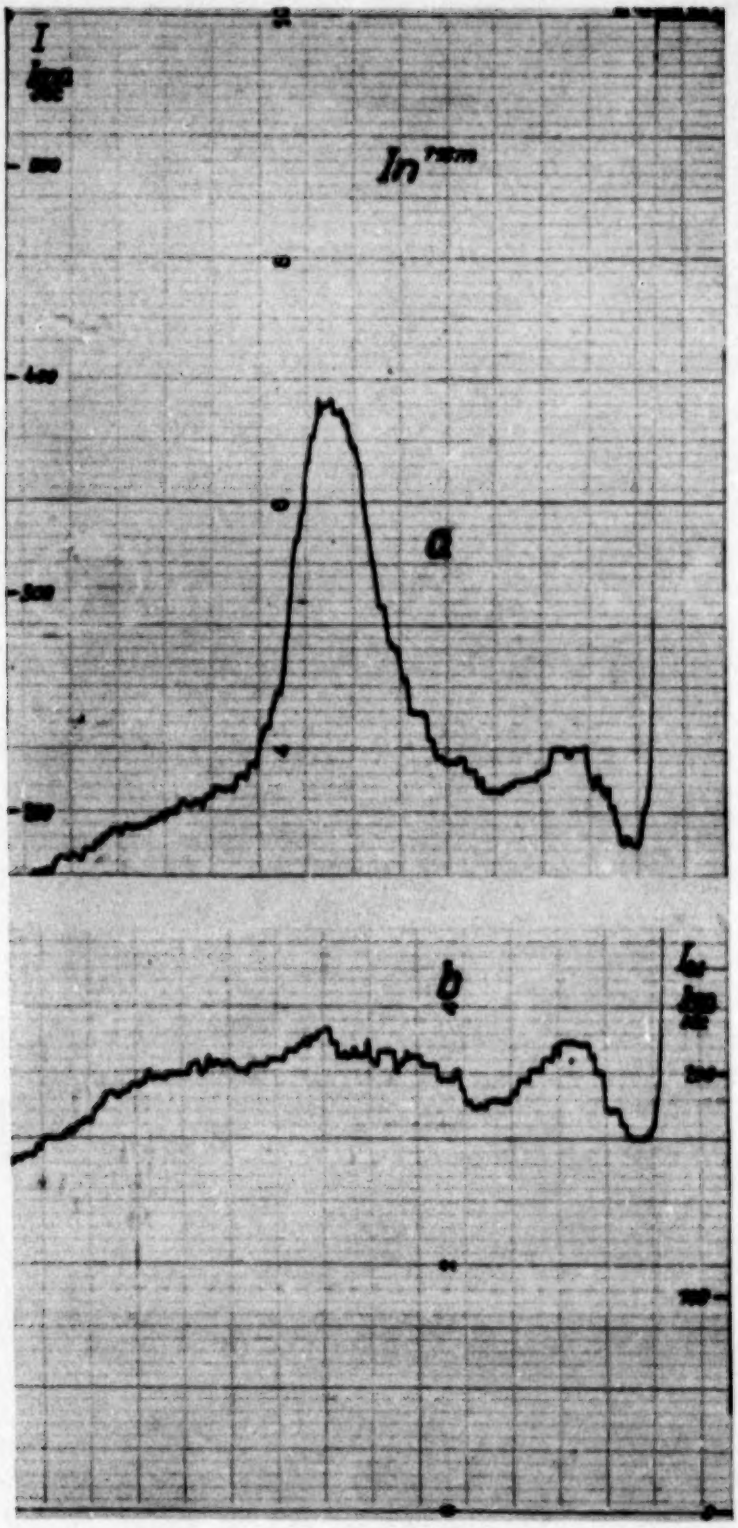

Fig. 6. Das mit Schreiber registrierte verzögerte In^{116m}-Spektrum.
a) mit Pb-Filter, b) mit Cd-Filter.

Bei unseren Messungen wurde als Probe 35 g metallisches Gallium verwendet. Das punktweise aufgenommene verzögerte Spektrum (Cd-Differenzmessung) zeigt Fig. 4. Die Energie der Photolinie liegt bei 99 ± 5 keV. Aus der Abklingmessung (Fig. 5) ergibt sich $T_{\frac{1}{2}} = 38 \pm 2$ msec. Diese Daten sind in guter Übereinstimmung mit den von Campbell und Fettweis [7]) gemessenen Werten.

Die in Ref. [9]) und [11]) gefundene Aktivität wurde von uns nicht beobachtet. Eine Zuordnung des 38 msec-Isomers ist nach unseren Messungen nicht möglich, da beim Neutroneneinfang im Ga natürlicher Isotopenzusammensetzung zu 60 % Ga^{70} und zu 40 % Ga^{72} entsteht und keine getrennten Isotope zur Verfügung standen.

3.3. INDIUM

Beim Einfang thermischer Neutronen im In natürlicher Isotopenzusammensetzung entsteht zu ca. 1 % In^{114} und zu 99 % In^{116}. Beide Nukleide besitzen ein langlebiges Isomer [In^{114m}(49 d), In^{116m}(54 min)]. Ein dem In^{114} zugeordnetes weiteres Isomer mit einer Halbwertszeit von 42 msec wurde von mehreren Autoren beobachtet (Tab. 1).

Bei der Aktivierung von In mit thermischen Neutronen tritt eine Aktivität mit $T_{\frac{1}{2}} = 2.5$ sec auf, die bereits 1951 von Kahn [12]) beobachtet wurde, und die in den "Nuclear Data Sheets" dem In^{116} zugeordnet wird. Von Campbell und Fettweis [7]) wurde dieses Isomer jedoch durch Verwendung getrennter Isotope ebenfalls dem In^{114} zugeordnet.

Bei unseren Messungen wurde ein In-Blech von 0.5 mm Dicke als Probe verwendet. Das mit dem Schreiber aufgenommene verzögerte Spektrum (Fig. 6) enthält eine sehr starke Linie, deren Energie durch Eichung mit

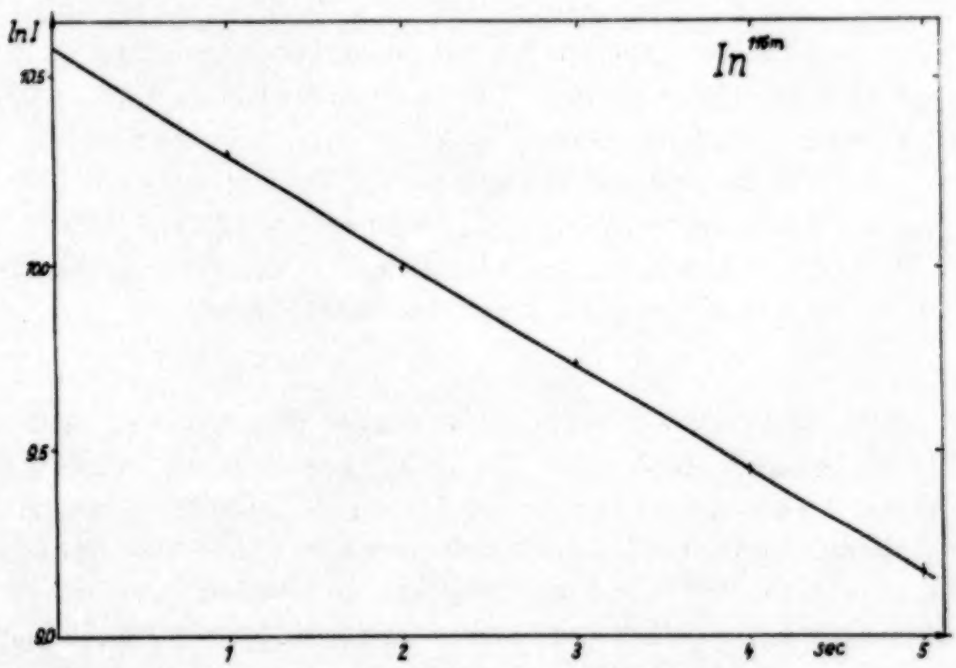

Fig. 7. Abklingkurve für In^{116m}.

In^{114m}(49 d) zu 160±8 keV bestimmt wurde. Die Abklingmessungen ergaben als Halbwertszeit $T_{\frac{1}{2}} = 2.46 \pm 0.08$ sec (Fig. 7). Es handelt sich also offenbar um die gleiche Aktivität, die in Ref. [7]) und [12]) beobachtet wurde. Trotz intensiver Suche wurde ebenso wie in Ref. [7]) keine dem 42 msec-Isomer entsprechende Aktivität gefunden.

Aus einer Intensitätsabschätzung kommen wir im Gegensatz zu Ref. [7]) zu dem Schluß, daß die 2.5 sec-Aktivität dem In^{116} zuzuordnen ist. Unter der Voraussetzung, daß maximal 1 % der in der Probe absorbierten Neutronen ein In^{114}-Isomer erzeugen kann, ist eine mindestens um den Faktor 6 kleinere Zählrate zu erwarten, als tatsächlich von uns beobachtet wurde.

Interessant ist ein Vergleich mit den vorliegenden Messungen der weichen Komponente des prompten In-Einfangsspektrums (Tab. 2).

TABELLE 2

Promptes Einfangsspektrum von In (weiche Komponente)

Hamermesh [15])		Skljarewski [16])		Draper [17])	
E_γ	I_γ	E_γ	I_γ	E_γ	I_γ
256±10	–	285±10	42 %	280±14	24 %
160±10	–	175± 5	31 %	188±10	16 %
		102± 3	18 %	98± 6	16 %
		70± 5	5 %	67± 6	5 %

Die verzögerte Linie liegt etwas unterhalb der von Skljarewski und Draper gefundenen zweiten γ-Linie. Während Skljarewski kontinuierlich mißt und daher das prompte und das verzögerte Spektrum gleichzeitig erhält, war die Versuchsanordnung von Draper so beschaffen, daß die verzögert auftretende γ-Strahlung je nach der Lebensdauer mit wesentlich vermindeter Intensität registriert wird. Die Unterschiede in den Angaben der beiden Autoren könnten so erklärt werden, daß im Einfangsspektrums des In^{116} zwei Linien etwa gleicher Intensität bei 160 und 188 keV vorhanden sind, wobei die 160 keV-Linie dem 2.5 sec-Isomer zuzuordnen ist, während die 188 keV-Linie prompt auftritt. Bei Skljarewski wurden wahrscheinlich die beiden Linien nicht getremt, während Draper nur die prompte Linie beobachten konnte.

3.4. HOLMIUM

Das weiche Einfangsspektrum von Ho wurde ebenfalls von Skljarewski *et al.* [16]) und Draper [17]) beobachtet. Da die 125 keV-Linie bei Draper in ihrer Intensität stark reduziert ist, wurde von ihm die Vermutung geäußert, daß es sich hier um einen isomeren Übergang mit einer Lebensdauer von der Größenordnung msec handelt. Diese Vermutung konnte von uns bestätigt werden.

Als Probe wurden 2 g Holmiumoxyd in einem dünnwandigen Aluminiumbehälter verwendet. Das punktweise aufgenommene verzögerte Spektrum

(Cd-Sn-Differenzmessung) zeigt Fig. 8. Die dem isomeren Übergang entsprechende γ-Linie liegt bei 131 ± 5 keV. Die Röntgenlinie bei 46 keV ist im Spektrum stark ausgeprägt. Abklingmessungen wurden sowohl bei der Röntgenlinie als auch bei der γ-Linie durchgeführt (Fig. 9). In beiden Fällen ergab sich die gleiche Halbwertszeit $T_{\frac{1}{2}} = 0.214 \pm 0.010$ msec.

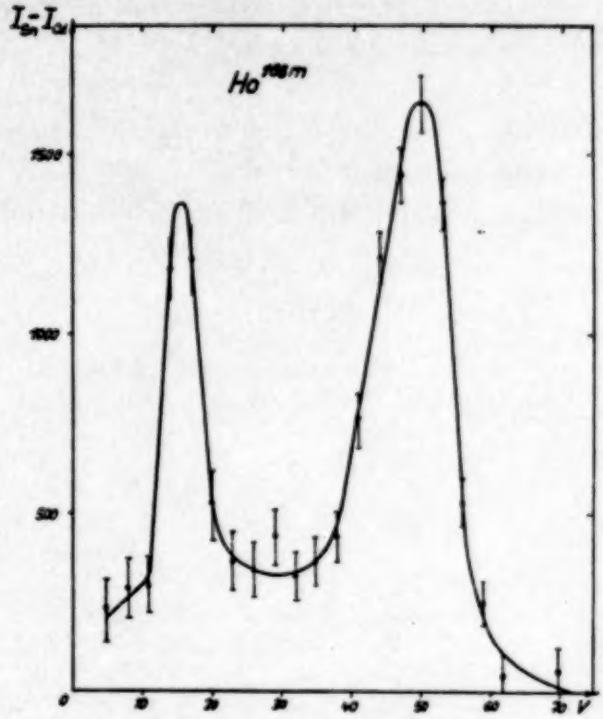

Fig. 8. Das punktweise aufgenommene verzögerte Ho^{166m}-Spektrum (Sn-Cd-Differenzmessung).

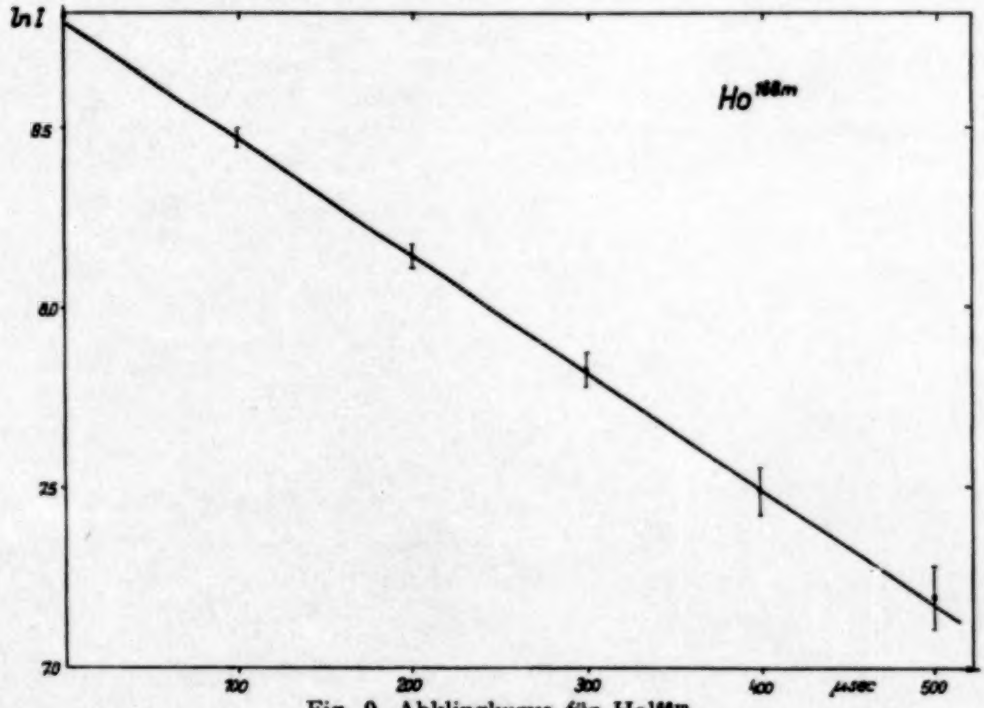

Fig. 9. Abklingkurve für Ho^{166m}.

Aus der relativen Intensität der Röntgenlinie kann unter Berücksichtigung der unterschiedlichen Absorption in der Szintillatorabschirmung der K-Konversionskoeffizient grob abgeschätzt werden. Wir erhalten $\alpha_K \approx 0.4$. Diese Abschätzung wurde durch Vergleichsmessungen mit In^{114m}(49 d), dessen Konversionskoeffizient bekannt ist, bestätigt. Sowohl die Lebensdauer als auch der Wert von α_K lassen darauf schließen, daß es sich bei dem 0.2 msec-Isomer um einen behinderten E2-Übergang handelt.

Herrn H. Flöter danken wir für seine wertvolle Unterstützung bei der Durchführung und Auswertung der Messungen. Die Herren H. Döhler und S. Plato haben wesentlichen Anteil am Aufbau der elektronischen Apparatur.

Literatur

1) M. Goldhaber and A. W. Sunyar, Phys. Rev. **83** (1951) 906
2) P. A. Yampolsky, O. I. Leipunsky, M. Ya. Gen and A. M. Tichomirov, Izv, Akad. Nauk SSSR., ser. fiz. **19** (1955) 338
3) S. D. Softky, Phys. Rev. **98** (1955) 736
4) H. Döhler, Kernenergie (im Druck)
5) B. J. Dropesky and A. W. Schardt, Phys. Rev. **102** (1956) 426
6) L. V. Groshev, A. M. Demidov, V. N. Lutzenko and V. I. Pelechov, Atlas spektrov γ-luchei (Moskau, 1958) (translation: Pergamon Press, 1959)
7) E. C. Campbell and P. F. Fettweiss, Nuclear Physics **13** (1959) 92
8) A. W. Schardt and A. Goodman, Bull. Amer. Phys. Soc. **4** (1959) 56
9) V. L. Glagolev, O. M. Kovryzhnych, Yu. V. Makarov, P. A. Yampolsky, JETP **36** (1959) 1046
10) P. J. Campion and G. A. Bartholomew, Can. J. Phys. **35** (1957) 1361
11) A. M. Morozov and P. A. Yampolsky, JETP **36** (1959) 950
12) J. Kahn, ORNL-1089 (1951)
13) O. I. Leipunsky, A. M. Morozov, Yu. V. Makarov, P. A. Yampolsky, JETP **32** (1957) 393
14) R. B. Duffield and S. H. Vegors, Phys. Rev. **112** (1958) 1958
15) B. Hamermesh and V. Hummel, Phys. Rev. **88** (1952) 916
16) V. V. Sklyarevsky, E. P. Stepanov and B. A. Obinyakov, Atomn. Energ. **5** (1958) 454
17) V. E. Draper, Phys. Rev. **114** (1959) 269

7.B

Nuclear Physics **17** (1960) 163—168; © *North-Holland Publishing Co., Amsterdam*

Not to be reproduced by photoprint or microfilm without written permission from the publisher

HIGH ENERGY THEOREM IN QUANTUM ELECTRODYNAMICS

LAWRENCE E. EVANS

The Johns Hopkins University, Baltimore, Maryland †

Received 28 December 1959

Abstract: A theorem of Lehmann, Symanzik and Zimmermann on the high energy behaviour of the meson-nucleon vertex is extended to quantum electrodynamics. It is shown that the vertex function in quantum electro-dynamics vanishes in the limit of infinite momentum transfer. This theorem does not necessarily imply the vanishing of the conventional electromagnetic form factors in this limit.

1. Introduction

Electromagnetic form-factors have recently been the object of considerable investigation. In the case of the electron-photon interaction (quantum electrodynamics), Drell and Zachariasen [1]) have analysed these form-factors by means of the dispersion relation. They assumed, in particular, form-factors which vanish when the momentum-transfer is infinite. Within the framework of their approximations, they were unable to obtain results consistent with their assumption. An analysis of the behaviour of the electromagnetic vertex at infinite momentum-transfer, using only exact methods, is therefore of interest.

The purpose of this note is to exhibit the extension to quantum electrodynamics of such a high energy theorem, which was proved for the meson-nucleon vertex by Lehmann, Symanzik and Zimmermann [2]). The present theorem is essentially the same as that of ref. [2]), namely that the vertex-function must vanish at infinite momentum transfer, if the spectral representations given by Lehmann [3]) and Källén [4]) for the exact photon propagator are valid. Since the proof is quite similar to that of ref. [2]), many technical details which are discussed in that paper will be omitted here.

2. Integral Equation for the Spectral Function

First we shall obtain an integral equation for the spectral function ††, similar to that obtained in ref. [2]). The necessary condition for the existence of a solution to this equation forms the basis of the proof.

We introduce the following definitions:

† Supported in part by the National Science Foundation.

†† We shall use Källén's [4]) spectral representation, which is more suited to electrodynamics than that of Lehmann [3]).

$$\langle 0|\mathrm{T}\psi(x)\bar{\psi}(y)|0\rangle = -\tfrac{1}{2}S^F(x-y),$$
$$\langle 0|\overline{\mathrm{T}}\psi(x)\bar{\psi}(y)|0\rangle = -\tfrac{1}{2}\bar{S}^F(x-y),$$
$$\langle 0|\mathrm{T}A_\mu(x)A_\lambda(y)|0\rangle = \tfrac{1}{2}D^{F'}_{\mu\lambda}(x-y),$$
$$\langle 0|\overline{\mathrm{T}}A_\mu(x)A_\lambda(y)|0\rangle = \tfrac{1}{2}\bar{D}^{F'}_{\mu\lambda}(x-y), \tag{1}$$
$$\langle 0|\mathrm{T}\psi(x)A_\mu(y)\bar{\psi}(z)|0\rangle = \int \mathrm{d}\xi\,\mathrm{d}\eta\,\mathrm{d}\zeta\, D^{F'}_{\mu\lambda}(y-\eta)S^F(x-\xi)\Gamma_\lambda(\xi\eta\zeta)S^{F'}(\zeta-z),$$
$$\langle 0|\overline{\mathrm{T}}\psi(x)A_\mu(y)\bar{\psi}(z)|0\rangle = \int \mathrm{d}\xi\,\mathrm{d}\eta\,\mathrm{d}\zeta\, \bar{D}^{F'}_{\mu\lambda}(\eta-y)\bar{S}^F(x-\xi)\bar{\Gamma}_\lambda(\xi\eta\zeta)\bar{S}^F(\zeta-z).$$

The chronological and anti-chronological Wick products are denoted in (1) by T and $\overline{\mathrm{T}}$, respectively.

For later reference we note here that with these definitions and familiar reduction formulas one obtains

$$\langle p'|j_\mu(0)|p\rangle = k^2 D^{F'}_{\mu\lambda}(k)\bar{u}(p')\Gamma_\lambda(p',p)u(p), \tag{2}$$

where $k = p'-p$, $j_\mu(x) = -\Box A_\mu(x)$, $\langle p'|$ and $|p\rangle$ are single electron states, and spinor normalization is $u^\dagger u = 1$. This establishes that the function Γ_μ defined by (1) is equivalent to the usual vertex function defined, for example by Dyson [5]).

Our analysis will concern the $D^{+'}$-function, defined by

$$\langle 0|A_\mu(x)A_\lambda(y)|0\rangle = iD^{+'}_{\mu\lambda}(x-y). \tag{3}$$

In momentum space, we can represent this function by means of the spectral function of Källén [4]):

$$D^{+'}_{\mu\lambda}(k) = -2\pi i\theta(k)\int_0^\infty \mathrm{d}a\,\delta(a+k^2)\left\{\delta_{\mu\lambda}\left[\delta(a)+\frac{\Pi(-a)}{a}\right] + k_\mu k_\lambda\left[\frac{\Pi(-a)}{a^2}-2M\delta(a)\right]\right\}. \tag{4}$$

Definitions, given in ref. [4]), are

$$\Pi(k^2) = -\frac{1}{3k^2}\sum_{p_n=k}\langle 0|j_\mu|n\rangle\langle n|j_\mu|0\rangle \tag{5}$$

and

$$\langle 0|A_\mu|k\rangle = (\delta_{\mu\lambda}-k_\mu k_\lambda M)\langle 0|A^{(\mathrm{in})}_\lambda|k\rangle. \tag{6}$$

$\sum_{p_n=k}$ is a sum over states with total momentum k, and in (6), $|k\rangle$ means a state of a single photon with momentum k. The exact value of the constant M does not concern us here.

From (4) and (1) we can obtain

$$\left.\begin{matrix} D^{F'}_{\mu\lambda}(k) \\ \bar{D}^{F'}_{\mu\lambda}(k) \end{matrix}\right\} = \mp 2i \int_0^\infty da \, \frac{1}{k^2 + a \mp i\varepsilon} \left\{ \delta_{\mu\lambda} \left[\delta(a) + \frac{\Pi(-a)}{a} \right] + k_\mu k_\lambda \left[\frac{\Pi(-a)}{a^2} - 2M\delta(a) \right] \right\}. \tag{7}$$

Following ref. [2]), we analyze $D^{+'}$ in another way by introducing a complete set of "in"-states:

$$\langle 0|A_\mu(x)A_\lambda(y)|0\rangle = \sum_n \langle 0|A_\mu(x)|n^{(\mathrm{in})}\rangle \langle {}^{(\mathrm{in})}n|A_\lambda(y)|0\rangle. \tag{8}$$

The contribution of states of a single photon can easily be shown to be

$$\langle 0|A_\mu(x)A_\lambda(y)|0\rangle^{(1)} = i(\delta_{\mu\lambda} + 2M\partial_\mu\partial_\lambda)D^+(x-y),$$
$$D^+(x-y) = -\frac{i}{(2\pi)^3} \int dk \, e^{ik(x-y)} \theta(k)\delta(k^2). \tag{9}$$

For later reference, we give the contribution of states of an electron pair:

$$\langle 0|A_\mu(x)A_\lambda(y)|0\rangle^{(2)} = \int d\xi \, d\eta \, D^{F'}_{\mu\nu}(x-\xi) F^{(2)}_{\nu\tau}(\xi-\eta) \bar{D}^{F'}_{\tau\lambda}(\eta-y),$$
$$F^{(2)}_{\nu\tau}(\xi-\eta) = -\int dx_1 dx_2 dy_1 dy_2 \, \mathrm{Tr}\,[\Gamma_\nu(x_1 \xi x_2) S^+(x_2-y_1) \bar{\Gamma}_\tau(y_1 \eta y_2) S^-(y_2-x_1)]. \tag{10}$$

The general contribution (excepting the one-photon states) can be written, as is argued in ref. [2]), in the form used in (10). That is,

$$\langle 0|A_\mu(x)A_\lambda(y)|0\rangle = \langle 0|A_\mu(x)A_\lambda(y)|0\rangle^{(1)} + \int d\xi \, d\eta \, D^{F'}_{\mu\nu}(x-\xi) F_{\nu\tau}(\xi-\eta) \bar{D}^{F'}_{\tau\lambda}(\eta-y) \tag{11}$$

and we can write

$$F_{\nu\tau}(\xi-\eta) = \sum_{(n)} F^{(n)}_{\nu\tau}(\xi-\eta)$$

where (n) denotes the contribution from states with a particular particle composition. Writing (11) in momentum space, we have from (9), (3), and (4)

$$-2\pi\theta(k) \frac{\Pi(k^2)}{k^2} \left[\delta_{\mu\lambda} - \frac{k_\mu k_\lambda}{k^2} \right] = D^{F'}_{\mu\nu}(k) F_{\nu\tau}(k) \bar{D}^{F'}_{\tau\lambda}(k). \tag{12}$$

Now one can obtain, without difficulty, from (11) and the current conservation equation $\partial_\mu j_\mu = 0$, the condition

$$k_\mu F_{\mu\nu}(k) = F_{\mu\nu}(k) k_\nu = 0. \tag{13}$$

This condition has considerable importance, because it means that the part of the propagator $D^{F'}_{\mu\nu}(k)$ which is proportional to $k_\mu k_\nu$ does not contribute in (12).

This, in turn, removes the chief difficulties which arise out of the vector nature of the electromagnetic field.

The right-hand side of (12) can thus be written as $|Q(k)|^2 F_{\mu\lambda}(k)$, where

$$\tfrac{1}{4}|Q(k)|^2 = \pi^2 \left(\frac{\Pi(k^2)}{k^2}\right)^2 + \left[\frac{1}{k^2} + \mathrm{P}\int_0^\infty \mathrm{d}s\, \frac{\Pi(-s)}{s(s+k^2)}\right]^2 \tag{14}$$

(P means principal value.) We know that $F_{\mu\lambda}(k)$ contains only positive frequencies, and we accordingly define

$$F(k) \equiv F_{\mu\mu}(k) = \tfrac{3}{2}\pi\theta(k)R(-k^2).$$

Finally, with $\phi(t) \equiv \Pi(-t)/t^2$, $t \equiv -k^2$ we obtain from (13) and (14) the desired integral equation

$$\phi(t) = R(t)\left[\pi^2\phi(t) + \left\{\frac{1}{t} + \mathrm{P}\int_0^\infty \mathrm{d}t'\, \frac{\phi(t')}{t-t'}\right\}^2\right]. \tag{15}$$

Eq. (15) contains as a parameter the unknown function $R(t)$, and the solution, which can be obtained by the method of ref. [2]), is therefore of no particular interest. The important property for our purposes is the existence of a necessary condition for existence of a regular † solution. This condition, which is obtained just as in ref. [2]), is

$$\int_0^\infty \mathrm{d}t\, \frac{R(t)}{t^2} \leqq 1. \tag{16}$$

It is the restriction on $R(t)$ for large t implied by this condition that gives us the desired theorem.

3. Lower Bound for $R(t)$; Completion of the Proof

We shall see that a lower bound for $R(t)$ is the contribution from the intermediate state of a pair. To show this, we shall show that all the $F^{(n)}(k)$ are positive or zero. In the present case, unlike that discussed in ref. [2]), the use of the indefinite metric requires a close examination of this point.

From (11), (7), (13), and (14) it follows that

$$2\pi\theta(k) \sum_{p_n=k}{}' \langle 0|A_\mu|n\rangle\langle n|A_\lambda|0\rangle = |Q(k)|^2 F_{\mu\lambda}(k) \tag{17}$$

where Σ' denotes a sum over all states except those of a single photon. By (13), each contribution to $F_{\mu\lambda}(k)$ must have the form

$$F^{(n)}_{\mu\lambda}(k) = \theta(k)\left[\delta_{\mu\lambda} - \frac{k_\mu k_\lambda}{k^2}\right] f^{(n)}(-k^2),$$

† That is, a solution such that the integral in (15) converges uniformly.

so that we can write, choosing $\mu = \nu = 1$, the contribution of states (n) to (17) in the form

$$2\pi \sum_{\substack{\text{spins} \\ p_n = k}} \langle 0|A_1|(n)\rangle \langle (n)|A_1|0\rangle = |Q|^2 \left(1 - \frac{k_1^2}{k^2}\right) f^{(n)}(-k^2). \tag{18}$$

In view of the indefinite metric, the left-hand side of (18) is

$$\frac{1}{2\pi} \sum_{\substack{\text{spins} \\ p_n = k}} |\langle 0|A_1|(n)\rangle|^2 (-1)^{N_4(n)}, \tag{18'}$$

where $N_4(n)$ is the number of scalar photons in the states (n). Now by an argument based on current conservation, just as given in ref. [4]), one can show that the only non-vanishing contribution to (18') comes from states containing no longitudinal or scalar photons. Consequently (18') is positive or zero, and we have $f^{(n)}(-k^2) \geqq 0$; from this follows $R(t) \geqq R^{(2)}(t)$, the contribution of the pair states to R. Hence we can use $R^{(2)}(t)$ as a lower bound for $R(t)$.

Introducing form-factors for Γ_μ as follows:

$$\bar{v}(p)\Gamma_\lambda(-p, q)u(q) = \bar{v}(p)[g_1(-k^2)\gamma_\lambda + g_2(-k^2)\sigma_{\lambda\tau}k_\tau]u(q)$$

(where $k = p+q$), we can obtain from the second of eqs. (10)

$$\begin{aligned} R^{(2)}(t) &= \frac{1}{(2\pi)^2}\,\theta(t-4m^2)\sqrt{t(t-4m^2)}\,S(t), \\ S(t) &= |g_1(t)+2mg_2(t)|^2 - \tfrac{1}{3}\left(1 - \frac{4m^2}{t}\right)[|g_1(t)|^2 - t|g_2(t)|^2]. \end{aligned} \tag{19}$$

Clearly, in order to satisfy (16) we must have $S(\infty) = 0$, which leads to

$$\lim_{t\to\infty} \begin{Bmatrix} |g_1|^2 \\ t|g_2|^2 \end{Bmatrix} = 0. \tag{20}$$

This completes the proof.

4. Discussion

The hypothesis under which (20) was proved is, essentially, that the integral in (15) should converge uniformly. The convergence of this integral is required for the validity of the spectral representation (7). We know that (7) gives correct results in perturbation theory. In addition, the vacuum polarization, which is proportional to the integral in (15), has been calculated [6]) to fourth order directly from expansion of $\Pi(k^2)$ in powers of e^2, and the results are in agreement with present experimental knowledge. Thus the information we have at present, while admittedly meager, is certainly consistent with the assumption we have made about the integral in (15).

Finally we note that if we assumed $k^2 D^{F'}(k)$ to remain bounded as $-k^2 \to \infty$ we should obtain from (2)

$$\lim_{-k^2 \to \infty} \langle p'|j_\mu|p\rangle = 0. \tag{21}$$

This would imply that the conventional electromagnetic form-factors, which are defined in terms of the matrix element in (21), do indeed vanish in this limit, as is assumed in ref. [1]). However, from (7) we obtain

$$\lim_{-k^2 \to \infty} k^2 D^{F'}(k) = 1 + \int_0^\infty \mathrm{d}a \, \frac{\Pi(-a)}{a} = \frac{1}{1-L} \tag{22}$$

in the notation of ref. [4]) Källén's proof of the divergence of at least one of the renormalization constants consists in showing that the right-hand side of (21) is in fact not zero, and that (22) is infinite. Thus, while the vertex-function form factors vanish in the limit, the same cannot be said for the usual electromagnetic form-factors. It should be emphasized that the divergence of (22) in no way invalidates our theorem.

I should like to acknowledge the generous support of the National Science Foundation, and the assistance and encouragement of Dr. G. Feldman, Dr. T. Fulton, and Messrs. P. De Celles and S. Edwards, Jr.

References

1) S. Drell and F. Zachariasen, Phys. Rev. **111** (1958) 1727
2) H. Lehmann, K. Symanzik and W. Zimmermann, Nuovo Cimento **2** (1955) 425
3) H. Lehmann, Nuovo Cimento **11** (1954) 342
4) G. Källén, Helv. Phys. Acta **25** (1952) 417;
see also Handbuch der Physik, Vol. 5, Pt. 1 (Springer-Verlag, Berlin, 1958) pp. 109–364
5) F. J. Dyson, Phys. Rev. **75** (1949) 1736
6) G. Källén and A. Sabry, Mat. Fys. Medd. Dan. Vid. Selsk. **29**, No. 17 (1955)

1.D.2

Nuclear Physics **17** (1960) 169—174; © *North-Holland Publishing Co., Amsterdam*

Not to be reproduced by photoprint or microfilm without written permission from the publisher

ROTATIONAL ENERGIES AND MOMENTS OF INERTIA OF NON-AXIAL NUCLEI

A. S. DAVYDOV, N. S. RABOTNOV and A. A. CHABAN

Moscow State University, Moscow

Received 18 November 1959

Abstract: It is shown that the ratios of rotational energies of a non-axial nucleus depending on the ratios of energies of two rotational states with spin 2 change but little with the deviation of nuclear moments of inertia from their hydrodynamic values.

1. Introduction

In the papers of Davydov and Filippov [1]) and of Davydov and Rostovsky [2]) a theory of the rotational states was developed for nuclei which do not possess axial symmetry. It was shown that the ratio of the energy of all the rotational levels to the energy of the first excited state with spin 2 is uniquely determined if the experimental value of the corresponding ratio for the second spin 2 state is available. It was further shown that the relative probabilities for quadrupole electric transitions between rotational levels are also determined uniquely through the same ratio of energies.

These simple results are obtained if one makes two simplifying assumptions: a) the internal nuclear state does not change with its rotation (adiabatic approximation), b) the principal nuclear angular momenta are expressed only through two parameters A and γ with the help of the equalities

$$I_i = A \sin^2 (\gamma - \tfrac{2}{3}\pi i), \quad i = 1, 2, 3. \tag{1}$$

Such dependence of angular momenta on γ is, in particular, obtained in the hydrodynamic nuclear model and therefore we shall call this approximation a hydrodynamical one.

It seems natural to inquire to what extent the results of refs. [1, 2]) are to be affected if one abandons both simplifying assumptions. MacDonald † has used the expression for the moments of inertia in the form

$$I_i = I_i^{\mathrm{H}} \left[\left(\frac{I_i^{\mathrm{H}}}{I_i^{\mathrm{R}}} \right)^{\frac{1}{2}} + p \right]^{-2}, \tag{2}$$

where I_i^{R} are the moments of inertia of a solid body, I_i^{H} are the moments of inertia coinciding with I_i of formula (1) at $A = 4B\beta^2$, and p is a new parameter which

† The authors wish to thank N. MacDonald for kindly sending the preprint of his work.

was taken to be equal to 0.1 and 0.2. The peculiar feature of expression (2) is that $I_i \to I^R_i$ for $p \to 0$; for $p \neq 0$ and $\gamma \to 0$, the moment of inertia $I_3 \to 0$; for $p \neq 0$ and $\beta \to 0$, all the values $I_i \to 0$. Formula (2) can be considered as an empirical formula which takes into account the deviations of the nuclear moments of inertia from their hydrodynamical values. MacDonald has investigated only rotational levels of spin 2. We shall show below that in this case it is impossible to determine which of the corrections is more important: non-adiabatic conditions or deviation of the moments of inertia from their hydrodynamical values.

The present work attempts to investigate in adiabatic approximation the rotational states of non-axial nuclei with three arbitrary principal moments of inertia. We shall show that in the general case the ratio of the rotational energies is expressed in terms of the following two parameters: ξ, which is the energy ratio of two levels with spin 2, and η, which is a parameter depending on the character of collective motions responsible for the rotation of the nucleus. Comparison of the results with experiment allows us to establish that the hydrodynamical approximation is sufficient for calculating energy ratios of the rotational levels. The reason for deviations of the theoretical results from experiment is to be sought in the interaction of rotation with the internal nuclear states.

2. Calculation of the Rotational Energies

Let us write down the operator of the rotational energy of a non-axial even nucleus in adiabatic approximation

$$H = \tfrac{1}{2}\sum_{i=1}^{3} a_i J_i^2,$$

where $a_i = \hbar^2/I_i$ and J_i are the projections of the angular momentum on the principal directions of the nucleus; I_i are the principal moments of inertia of the nucleus.

It has been pointed out in ref. [2]) that the rotational states of even nuclei belong to the total symmetry representation of group D_2. In the present article we shall consider only such states. It is easy to show that the energies of the rotational states of spin 2 is determined by the equation

$$E^2 - 2(a_1+a_2+a_3)E + 3(a_1a_2+a_1a_3+a_2a_3) = 0.$$

If we express the roots of this equation by $E_1(2)$ and $E_2(2)$, and use the properties of the coefficients of a quadratic equation, we shall be able to write

$$\frac{\sum a_i}{E_1(2)} = \tfrac{1}{2}(1+\xi), \quad \frac{a_1a_2+a_1a_3+a_2a_3}{E_1^2(2)} = \tfrac{1}{3}\xi, \tag{3}$$

where

$$\xi = \frac{E_2(2)}{E_1(2)} > 1.$$

The energies of all rotational states will be expressed in dimensionless units $\mathscr{E} = E/E_1(2)$. Then the energies of the rotational states with spins 3 and 5 will be directly expressed through the experimentally determinable ratio ξ with the help of the formulae

$$\mathscr{E}(3) = 1+\xi, \quad \mathscr{E}_1(5) = 4+\xi, \quad \mathscr{E}_2(5) = 1+4\xi.$$

The energy of the rotational levels of other spin values depends not only on the parameter ξ but also on the other parameter

$$\eta = \frac{a_1 a_2 a_3}{E_1^3(2)}. \tag{4}$$

Thus, for instance, the energy levels of spin 4 and 6 are defined by the respective equations

$$\mathscr{E}^3 - 5(1+\xi)\mathscr{E}^2 + 4[\xi^2 + \tfrac{19}{3}\xi + 1]\mathscr{E} - 40[\tfrac{1}{3}\xi(1+\xi) + 7\eta] = 0,$$

$$\mathscr{E}^4 - 14(1+\xi)\mathscr{E}^3 + 49(1+4\xi+\xi^2)\mathscr{E}^2 - [36(\xi^3+1) + 578\xi(1+\xi) + 3888\eta]\mathscr{E}$$
$$+ [252\xi(1+\xi^2) + 889\xi^2 + 13608(1+\xi)\eta] = 0.$$

If the moments of inertia are determined by formula (1), then

$$\eta = \eta_H = \xi^2[18(1+\xi)]^{-1}$$

and the energies of all the rotational states will be functions of only one parameter ξ, which in this case equals or exceeds 2, while in the general case η is a second parameter, whose possible values lie in a certain interval which can be determined through the value of ξ. In order to determine the limits of this parameter variation depending on ξ, we have to take into account that according to eqs. (3) and (4) the values $a_i/E_1(2)$ $(i = 1, 2, 3)$ are the roots of the equation of the third degree

$$x^3 - \tfrac{1}{2}(1+\xi)x^2 + \tfrac{1}{3}\xi x - \eta = 0.$$

In conformity with the requirement that the roots of this equation should be real and positive, we find that the value η can lie in the following intervals, determinable through the value of ξ:

$$\begin{aligned} \xi^2(3-\xi) \leqq 54\eta \leqq 3\xi - 1 \quad &\text{if} \quad 1 < \xi \leqq 3; \\ 0 \leqq 54\eta \leqq 3\xi - 1 \quad &\text{if} \quad \xi \geqq 3. \end{aligned} \tag{5}$$

The ratios $\mathscr{E}_1(4)$ and $\mathscr{E}_2(4)$, as functions of ξ for different values of η satisfying the inequalities (5), are represented in fig. 1. The shaded area lies between the

curve corresponding to the hydrodynamical approximation (designated by η_H) and the curve corresponding to the moments of inertia determined with the help of eq. (2) at $\beta = p = 0.2$ (designated by η_{HD}). Fig. 2 shows the possible values of $\mathscr{E}_1(6)$ ratios for different values of ξ and the values of η that satisfy the inequalities (5).

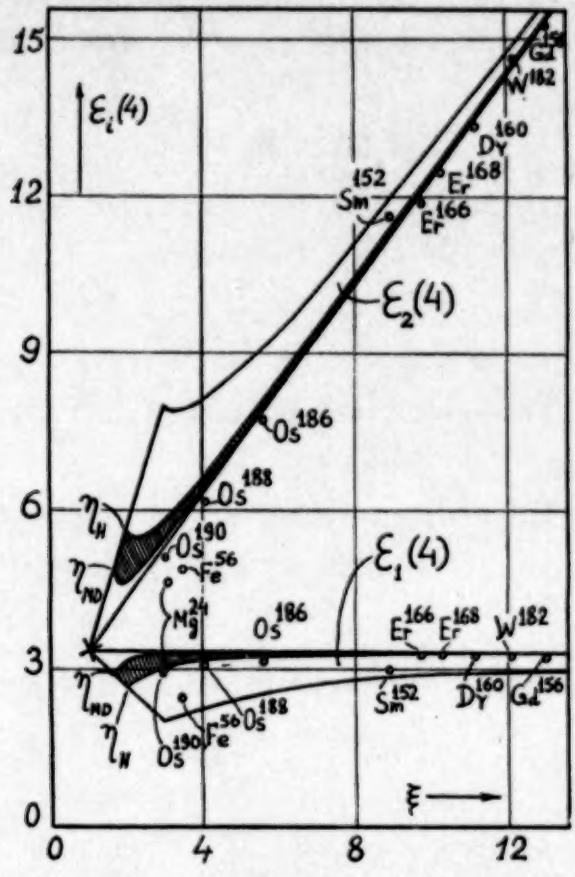

Fig. 1. The possible theoretical values of the ratios $\mathscr{E}_1(4)$ and $\mathscr{E}_2(4)$ for different values of ξ and η.

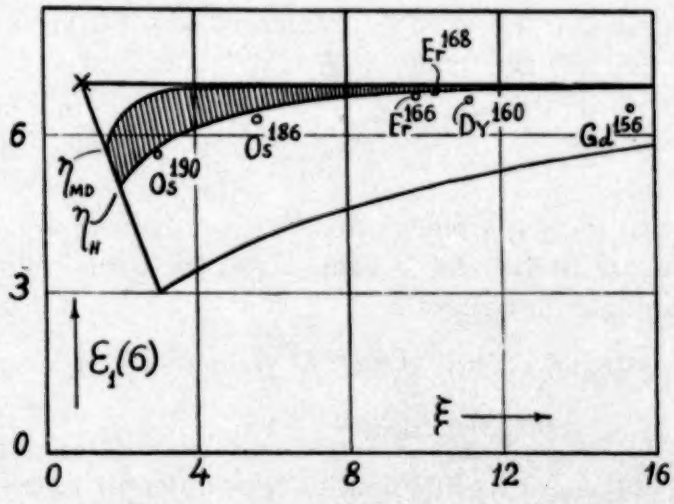

Fig. 2. The possible theoretical values of $\mathscr{E}_1(6)$ for different values of ξ and η.

One should certainly keep in mind that the values of η satisfying the inequalities (5) correspond to all possible relations between the principal angular momenta and in particular to some which obviously cannot be realized in a nucleus. Such is, for instance, the case of a solid-body rotation of a spherical body ($I_1 = I_2 = I_3$, $\xi = 1$) marked by a cross in figs. 1 and 2. Similar are the cases for which η is near to or equals zero.

3. Comparison with Experiment and Discussion

Recently it has become customary to consider that in nuclei the moments of inertia have values which are intermediate between those given by a hydrodynamical model and by a solid-body rotation model. Therefore, the real relation between the principal moments of inertia of a nucleus apparently corresponds to those values of η for which the energy ratios $\mathscr{E}_i(J)$ are shifted from the hydrodynamical values in the direction of the shaded area. This being taken into account, the energy ratios $\mathscr{E}_i(J)$ will only slightly change with the change of η values tolerated for atomic nuclei. This dependence becomes particularly slight for $\xi \geqq 4$. Almost all the experimental ratios of $\mathscr{E}_1(4)$ and $\mathscr{E}_1(6)$ available at the present moment (see table 1) lie lower than the possible theoretical

TABLE 1

Experimental ratios

Nucleus	$E_1(2)$ (keV)	ξ	$\mathscr{E}(3)$	$\mathscr{E}_1(4)$	$\mathscr{E}_2(6)$	$\mathscr{E}_1(4)$	Ref.
Os^{190}	186.7	2.99	4.04	2.94	5.12	5.61	[3, 5]
Mg^{24}	1368	3.09	3.82	3.01	4.61	—	[3]
Fe^{56}	845	3.49	4.54	2.47	4.85	—	[6]
Os^{188}	155	4.09	5.10	3.08	6.17	—	[4]
Os^{186}	137.2	5.60	6.63	3.16	7.73	6.33	[4]
Sm^{152}	122.3	8.92	10.14	3.01	11.68	—	[4]
Er^{166}	80.7	9.76	10.67	3.29	11.87	6.76	[7]
Er^{168}	79.9	10.29	11.22	3.31	12.47	6.86	[7]
Dy^{160}	87.0	11.16	12.11	3.27	13.35	6.70	[8]
Gd^{156}	89.0	13.01	14.0	3.24	15.34	6.56	[3, 4]
W^{182}	100.9	12.11	13.20	3.26	14.68	—	[4]

values calculated in adiabatic approximation (the shaded areas in figs. 1 and 2), while the experimental energy ratios $\mathscr{E}_2(4)$ lie lower than the theoretical ones at any η satisfying inequalities (5). This indicates that the agreement of the theory with experiment cannot be improved by passing from the hydrodynamical moments of inertia to values intermediate between these and the moments of inertia obtained in a solid-body model. Moreover, it follows from fig. 1 that if we formally choose those relations between the three principal moments of inertia which improve the agreement with the experimental $\mathscr{E}_1(4)$ ratios, we shall at the same time make this agreement worse for the

$\mathscr{E}_2(4)$ ratios. Thus, it may be stated that the disagreement of the theory with experiment is occasioned by the adiabatic approximation used in the calculations.

The results obtained in the present article permit to expect that a theory which will take into account the coupling between rotation and the internal excited states of a nucleus can be developed on the basis of the dependence of the angular momenta in the hydrodynamical model on the parameter γ responsible for the deviation of the shape of the nucleus from axial symmetry. The dependence of the relative energies $\mathscr{E}_1(4)$, $\mathscr{E}_2(4)$ and $\mathscr{E}_1(6)$ on the deviation of the parameter η from its hydrodynamical value η_H is less than the corrections due to the violation of the adiabatic conditions.

References

1) A. S. Davydov and G. F. Filippov, JETP **35** (1958) 440; Nuclear Physics **8** (1958) 237
2) A. S. Davydov and V. S. Kostovsky, JETP **36** (1959) 1788; Nuclear Physics **12** (1959) 58
3) B. S. Dželepov and L. K. Peker, Decay Schemes of Radioactive Nuclei (Moscow, 1958)
4) B. S. Dželepov and L. K. Peker, Excited States of Radioactive Nuclei, UINR, Dubna, p. 218
5) O. Nielson, N. Roy Poulson, R. Sheline and B. S. Jensen, Nuclear Physics **10** (1959) 475
6) S. Cook, Nuclear Physics **7** (1958) 480
7) K. P. Jacob, J. W. Mihelich, R. Hantz and T. Handey, Bull. Am. Phys. Soc. **3** (1958) 558
8) B. Bitterlikh, E. P. Grigoriev, B. S. Dželepov, A. P. Zolotavin and B. Kratzik, Izv. Acad. Nauk SSSR, Ser. Fiz. **23** (1959) 868

10.A *Nuclear Physics* **16** (1960) 888—888; © *North-Holland Publishing Co., Amsterdam*

BOOK REVIEWS

1. M. DEMEUR, *Aspects théoriques de la systématique des noyaux atomiques* (1957)
2. G. GUÉBEN et J. GOVAERTS, *La méthode d'analyse par activation en utilisant les neutrons d'une source Ra—Be* (sans date)
3. J. SERPE, *Les lois de conservation en physique des particules élémentaires* (1959)
4. J. GÉHÉNIAU (Éditeur), *Particules élémentaires (feuilles d'information)* (1959)
5. M. DEMEUR, *Développements théoriques récents en spectroscopie nucléaire* (1959)

(Institut Interuniversitaire des Sciences Nucléaires, Bruxelles)

Il convient de signaler cette excellente série de monographies éditées par l'Institut Interuniversitaire des Sciences Nucléaires de Bruxelles. C'est là le genre de mises au point succinctes, mais précises qui convient à une science en état de développement rapide comme la physique nucléaire. L'une des monographies (no 4) est même imprimée sur feuilles détachées, assemblées dans un classeur prévoyant des additions futures. Chaque monographie, illustrée de nombreux diagrammes et graphiques (le plus souvent reproduits tels quels des publications originales), ne présente pas seulement une compilation de travaux récents, mais contient aussi l'apport personnel des auteurs, et acquiert de ce chef la valeur d'une contribution originale au sujet.

Le côté matériel de l'édition mérite quelques critiques. On peut se demander si une présentation aussi luxueuse est vraiment de mise pour des brochures qui sont essentiellement des instruments de travail: il est difficile de les maintenir ouvertes à une page déterminée sans abîmer le brochage, et elles tiennent beaucoup de place. De plus, chaque monographie devrait être clairement datée, et le titre (au moins en abrégé) devrait être imprimé sur le dos. Aucune indication n'est donnée sur le moyen de se les procurer, sauf l'adresse de l'Institut, qui est 11 rue d'Egmont, Bruxelles.

L. R.

P. H. MARGEN, *Nuclear reactor optimization* (The Nuclear Engineering Monographs No. 9) (Temple Press, London 1959. 81 pages. 12s6d)

The purpose of optimization is to determine, from the possible combinations of the relatively many independent variables of a nuclear reactor, that combination which gives the lowest cost of electricity.

It is, as the author also points out, impossible in such a small book to cover all the problems of optimization. However, the book gives an excellent idea of many of the difficult problems in optimization and shows in an excellent way how far one can succeed even with relatively simple methods.

The principles of optimization are first demonstrated on a simple problem: the classic Kelvin Law equating cable losses with annual charges. The next chapter deals with the variables in a nuclear reactor considered from both a physical and a thermal viewpoint. The following chapter treats the sequence of design and optimization calculations, the number of independent variables and some practical limitations. Three chapters are devoted to optimization of the physics design, heat transfer and thermodynamics.

A typical design of a heavy water moderated and gas-cooled reactor is used as an example. The designer's original guess and the result of the "first round" are compared in appendix two. Other appendices give some cost formulae and tabulated data. A bibliography is included.

H. Abel-Larsen

L. V. GROSHEV, A. M. DEMIDOV, V. N. LUTSENKO and V. I. PELEKHOV, *Atlas of spectra of gamma rays from radiative capture of thermal neutrons* (Pergamon Press 1959. 198 p. £7)

The tremendous pace in the accumulation of new nuclear data, and the great variety in these data are, of course, vital elements in the excitement and challenge associated with work in nuclear physics. However, this pace and variety often makes it difficult to assemble and assess the available facts. Well organized reviews and compilations are badly needed. The present collection of the γ-ray spectra observed following neutron capture will thus be welcomed both by physicists interested in nuclear spectra and also by those interested in the practical uses of nuclear radiation.

The Atlas contains a systematic survey of the literature up to about the beginning of 1958, including a considerable amount of work by the Russian physicists which was not published at that time. This corresponds roughly to the same period covered in a recent Canadian compilation (Compilation of Thermal Capture Gamma Rays (CRGP-784) by G. A. Bartholomew and L. A. Higgs, Chalk River, Ontario). The two compilations follow a similar form, the Canadians relying somewhat more on Canadian work while the Russians rely somewhat more on Russian work. Thus, each of the two groups, who, taken together, have contributed the overwhelming majority of the available measurements in this field, have now presented systematic surveys of the present states of the measured capture γ-ray spectra.

The Russian compilatior goes somewhat further than the Canadian, in that it contains an attempt to interpret the observed γ lines in a nuclear level diagram wherever that is possible and it also contains a very useful table of the stable elements, their thermal capture cross-sections and the binding energies of the neutron in the resulting nuclei. One must be warned, however, that the table includes some binding energies obtained from measured mass differences and some estimated from empirical systematics of nuclear masses without indicating the rather essential difference in the quality of these two types of determination.

The edition of the Russian Atlas under review represents a translation of the text and photographic reproduction of the approximately 140 level diagrams and energy spectra contained in the Russian original (published by The Atomic Energy Commission of the U.S.S.R., Moscow 1958). The text and tables are clear and attractively printed; the photographic process is very successful but is unable to correct the rather numerous minor imperfections that mar a number of the diagrams published in the original.

B. R. Mottelson

10.C

Nuclear Physics **17** (1960) 177—180; © *North-Holland Publishing Co., Amsterdam*

Not to be reproduced by photoprint or microfilm without written permission from the publisher

I. V. KURCHATOV
(1903—1960)

I. P. ALEXANDROV and I. K. KIKOIN

Academy of Sciences of the U.S.S.R., Moscow

Received 28 March 1960

On the 7th of February the sudden death occurred of I. V. Kurchatov, an outstanding experimental physicist. Intense scientific and organizational activities had undermined the health of this man who had been so full of vitality and optimism. I. V. Kurchatov died at the height of his vigorous scientific activities, replete with stimulating ideas and far-reaching plans. As a result of his death we lost not only the greatest scientist, but also an outstanding organizer of scientific investigations, the man whose name is closely associated with all developments and major achievements in the field of atomic energy in the USSR.

I. V. Kurchatov was born on January 12, 1903 in the settlement "Simsky Zavod" in the Urals. Having graduated from the Crimean University in 1923 he was soon engaged in research.

In 1925 he started his scientific career at the Leningrad Physical-Technical Institute under Academician A. F. Ioffe and was justly reputed one of his most gifted pupils. His first papers were concerned with the physics of dielectrics predominating in A. F. Ioffe's laboratory at that time.

Then I. V. Kurchatov turned to a phenomenon which had been little studied and seemed quite enigmatic at that time: the anomaly of the electric properties of Rochelle salt. Whereas only a few physicists had been investigating properties of Rochelle salt, the anomaly itself being of little interest to scientists, the fundamental work of I. V. Kurchatov and his colleagues gave rise to a new major field in the physics of dielectrics: ferro-electricity. Before long I. V. Kurchatov found an analogy between the electric properties of Rochelle salt and the magnetic properties of ferromagnetics.

In connection with this he embarked on an extensive research programme which by its scope and significance could be compared with the studies of the principal properties of ferromagnetics which had been conducted for many years by a very large number of scientists throughout the world.

The scope of I. V. Kurchatov's study of ferro-electricity was exceptionally wide. Within a comparatively short time it yielded abundant fruit. A thorough

June (3) 1960

study was made of the dependence of Rochelle salt polarization in an electric field as well as of the processes of hysteresis. The electro-caloric effect (similar to the magneto-caloric effect) and a jump of the heat capacity at the Curie point were discovered. In fact, this substance was found to have two Curie points. Under I. V. Kurchatov's guidance the piezo-electric properties of Rochelle salt were investigated. These new major experimental data made it possible to develop a quantitative theory of ferro-electricity, whose underlying idea was the domain structure of crystals. Thus it was shown that the analogy between the electric properties of Rochelle salt and the magnetic properties of ferromagnetics is not superficial but implies a profound analogy of causes bringing forth both categories of phenomena. Thereby Kurchatov's inquiry into ferroelectrics far extended the category of substances with domain structure.

I. V. Kurchatov did not confine himself to pure laboratory research in this fascinating field of dielectrics. He realized that some phenomena he observed could have important technical applications, and having attracted a number of prominent engineers he worked out, with his characteristic energy, the measures required for an industrial use of ferroelectrics. There is hardly any need to mention how widely they are used nowadays.

Despite the impressive results accomplished by I. V. Kurchatov and his colleagues in a field of physics new at that time and offering alluring prospects, in the early thirties he became aware of the particular significance of nuclear physics and radically changed the direction of research in his laboratory, concentrating his efforts on nuclear research. It is amazing in how short a time I. V. Kurchatov was able to master this field of physics entirely new to him.

After a number of experiments on artificial radioactivity, in 1935 he discovered the phenomenon of nuclear isomerism in artificially radioactive bromine. This discovery was a starting point for further research conducted by the scientist himself as well as other physicists.

Anxious to extend the range of his investigations, I. V. Kurchatov had also undertaken some work at the Leningrad Radium Institute, where a small cyclotron, with magnetic poles of about 1 m diameter, had been constructed by that time.

At the same time, together with other physicists of the Leningrad Physical Technical Institute, he started on the construction of a large cyclotron. This work took much of his time and attention. The construction of the cyclotron was completed shortly before the war, but the blockade of Leningrad interrupted the research on this cyclotron.

In 1940, soon after the discovery of the fission of the uranium nucleus, his laboratory conducted, under his direct guidance, a series of investigations which led to the discovery of the spontaneous fission of uranium.

During the second world war I. V. Kurchatov used his energy and experience for the defence of his country.

Having returned to nuclear research, I. V. Kurchatov soon became the scientific head of all Soviet research concerned with the use of nuclear power. I. V. Kurchatov persistently and unavailingly worked in developing and perfecting atomic and hydrogen weapons in order to strengthen the defence of his country. The first Soviet nuclear reactors were constructed under his guidance and with his direct participation. It is well known that Kurchatov's efforts in this field met with a complete success.

At the same time I. V. Kurchatov strove to extend the scope of research concerned with the peaceful uses of nuclear power. Drawing on his experience and knowledge in the building of reactors, he actively contributed to the construction of the world's first industrial nuclear power plant.

These investigations provided the basis for the construction of large-scale industrial nuclear power plants, one of which (Byeloyarskaya) now bears his name. The construction of the first reactors was naturally preceded by an enormous experimental work concerned with the investigations of nuclear reactions and measurements of nuclear constants of both fissile and construction materials. I. V. Kurchatov had directed all this work and personally participated in it. At this suggestion scientists undertook an extensive number of fundamental investigations and calculations which ensured the successful operation and maintainance of industrial reactors.

It should be remembered that the secrecy shrouding this problem prevented any contacts of Soviet physicists with physicists of other countries. As a result all scientific and technical problems in practical applications of nuclear energy had to be solved by the physicists of the USSR entirely by their own efforts.

In the early fifties the Institute headed by I. V. Kurchatov embarked on an extensive research programme in controlled thermo-nuclear reactions. This field of physics attracted the particular interest of I. V. Kurchatov in his last years. His lecture in Great Britain in 1956 was responsible for lifting the secrecy shrouding thermonuclear work in many countries and thus paved the way for extensive scientific contacts among the physicists of various countries working in this field.

Subsequently, the bulk of Soviet research in controlled thermo-nuclear reactions was conducted under his guidance. It was due to his suggestion and incessant interest that the "Ogra", one of the largest installations for obtaining and studying high-temperature plasmas, was constructed. A few days before his sudden death I. V. Kurchatov together with his colleagues participated in measurements undertaken with this installation. During the last months I. V. Kurchatov outlined an extensive programme for the development of research in controlled thermo-nuclear reactions. Merciless death bore down upon him when he was discussing one of the projects with his close associates.

Despite his enormous scientific engagements I. V. Kurchatov found time for active social activities. He strove to establish peace and friendship between

the peoples of the world and actively worked for establishing the international collaboration of scientists. In his public speeches he urged the prohibition of nuclear weapons and the use of nuclear power exclusively for peaceful purposes.

I. V. Kurchatov permanently headed the Institute of Atomic Power which he had founded. Owing to his personal qualities, he succeeded in enlisting and inspiring a large body of scientists and enjoyed a well-deserved prestige and affection. Within a comparatively short time the Institute became one of the most prominent centres of physical research.

The influence of his personality was not, however, confined to his Institute. A number of scientific and industrial organizations were constantly drawing on his scientific and technical ideas.

I. V. Kurchatov was very popular among the Soviet people and was repeatedly elected a member of the Supreme Soviet of the USSR. The Soviet government highly valued his exceptional qualities and awarded him all highest orders of the country. The Academy of Sciences elected him as a member in 1943.

His death is an irretrievable loss to the Soviet people, the scientists of the Soviet Union and, indeed, of all the world.

List of principal publications

On electrical strength of dielectrics [with A. F. Ioffe and K. D. Sinelnikov] (C. R. Ac. Sci. USSR **1** (1927) 65).

Dielektrische Eigenschaften der Seignettesalzkristalle [with P. P. Kobeko] (Zs. f. Physik **66** (1930) 192).

Investigations of the dielectric constant of Rochelle salt in different cristallographic directions [with G. Shchepkin] (JETP **1** (1931) 164).

Der untere Curie-Punkt im Seignettesalz (Phys. Zs. Sow. **3** (1933) 321).

Das Seignettesalz im Gebiete der spontanen Orientierung (Phys. Zs. Sow. **5** (1935) 200).

Dependence of the polarisation upon the field strengths in ferro-electrics outside the spontaneous orientation region (JETP **3** (1933) 181).

Le champ moléculaire dans les diélectriques (Les sels de Seignette) (Hermann, Paris, 1936).

Sur un cas de radioactivité artifiecille provoquée par un bombardement de neutrons, sans capture du neutron [with L. Mysovsky and L. Rusinov] (C. R. Ac. Sci. **200** (1935) 1201).

Fission of heavy nuclei (Proc. Ac. Sci. USSR **5** (1941) 578).

Isomery of atomic nuclei [with L. Rusinov] (Proc. Ac. Sci. USSR **1** (1947) 285).

On the possibility of the development of thermonuclear reactions in gaseous discharge (Atomnaya Energiya **3** (1956) 65).

Some problems concerning the development of atomic power in the USSR (lecture delivered at Harwell on 25 April, 1956) (Atomnaya Energiya **3** (1956) 1).

Some investigations in the field of thermonuclear reactions made at the Institute of Atomic Energy of the Academy of Sciences of the USSR (Atomnaya Energiya **5** (1958) 105).

7.B

Nuclear Physics **17** (19 0) 181—217; © *North-Holland Publishing Co., Amsterdam*

Not to be reproduced by photoprint or microfilm without written permission from the publisher

COLLISION OF NUCLEONS WITH LARGE ANGULAR MOMENTA

A. D. GALANIN, A. F. GRASHIN, B. L. IOFFE and I. Ya. POMERANCHUK

Institute of Theoretical and Experimental Physics, Moscow

Received 13 June 1959

Abstract: That part of the nucleon-nucleon scattering amplitude for large orbital angular momenta $l \gg 1$ which involves two-meson exchange is calculated in the present paper. The connection between this amplitude and the scattering of real mesons by nucleons is determined with the aid of dispersion relations. The method thus evolved is valid if the inequality $l\mu/p \gg 1$ holds (μ is the meson mass and p the nucleon momentum in the centre-of-mass system), apart from the condition $l \gg 1$.

Specific calculations are performed for a singlet amplitude in non-relativistic approximation for not very large orbital angular momenta $1 \ll l \ll 4m^2/\mu^2$ (m is the mass of a nucleon and μ that of a meson). Calculations show that already F and G phases at nucleon energies in the laboratory system $E_l \lesssim 150$ MeV may be obtained from one-meson approximation with adequate accuracy. This conclusion may prove to be essential for the phase shift analysis of nucleon scattering.

1. Introduction

It was shown in the paper of Okun and Pomeranchuk [1]) that only interactions involving one-meson exchange are of importance in collisions of nucleons with large angular momenta, and the relevant scattering amplitude therefore may be computed theoretically †. In this general form this statement is beyond argument since it is based on the general premise that increasingly larger impact parameters come into play as the angular momenta increase. Yet to make this purely theoretical proposition of practical value it has to be shown that even with comparatively small angular momenta the scattering phases may be derived from the one-meson approximation with satisfactory accuracy. Evaluation of accuracy of one-meson approximation may be arrived at by computing the next approximation with respect to a "collision periphery range," i.e., two-meson approximation when the colliding nucleons exchange two mesons. In the present paper these computations are performed under the following assumptions:

1. The values of the orbital angular momenta for which the phases are calculated are large ($l \gg 1$).

2. For a given l the nucleon energies are limited from above by the inequality $l\xi \gg 1$ where $\xi = \mu/p$, μ is the mass of π-meson, p the nucleon momentum in the centre-of-mass system.

† Cf. the previous papers cited in ref. [1]).

The second assumption has a simple physical meaning: the quasi-classic impact parameter $r_0 = l\xi/\mu \gg 1/\mu$. Thus, this assumption is a condition for the collision periphery. In other words, unless this condition holds the classification of interactions with respect to a "periphery range" with a small expansion parameter is pointless.

The methods set down in the present paper make it possible to obtain, for two-meson phases, the main part of the asymptotic expansion with respect to the small parameter $1/L(l, \xi)$ which equals $1/l$ at low energies ($\xi^2 \gtrsim 1$), and increases up to $1/l\xi$ (for $\xi^2 \ll 1$) as the energy increases. The idea of the computation is that under the above assumptions the mesons with the physical relation between energy and momentum $\omega^2 - \mathbf{k}^2 = \mu^2$, and not with the physical energy $\omega = 0$ and the momentum transfer $q^2 = 4\mu^2$, play the main role among the virtual mesons which the nucleons exchange. The nucleon-nucleon scattering amplitude is expressed through the scattering amplitude of these π-mesons on nucleons while the latter amplitude may be calculated exactly through the dispersion relations for scattering of π-mesons on nucleons if the momentum transfer is fixed †. Apart from this amplitude, the terms which correspond to the first approximation of the perturbation theory (with renormalized constant g^2) in meson-nucleon scattering are taken into consideration. Though these terms vanish at $\omega = 0$ their contribution is comparable in magnitude with, and opposite in sign to, the contribution of the terms calculated by dispersion relations, owing to the presence of a pole at small values of $\omega = \mu^2/2m$.

2. Scattering Phases for Large Angular Momenta

The matrix and the phases of nucleon-nucleon scattering may be expressed through the integrals of the amplitudes $M(E, \cos\theta)$ corresponding to various spin states ($E = \sqrt{m^2+p^2}$ is the total energy, θ the scattering angle in the centre-of-mass system; the spin and charge indices are not written):

$$I_{l,m}(E) = \int_{-1}^{+1} P_l^{(m)}(\cos\theta) M(E, \cos\theta) \mathrm{d}\cos\theta, \qquad m = 0, 1, 2 \qquad (2.1)$$

where $P_l^{(m)}$ are the associated Legendre polynomials. Let us confine ourselves to the integral (2.1) with $m = 0$ (for $m = 1$ and 2 the arguments are similar).

In calculating the integral (2.1) for large l it is convenient to make use of the analytic properties of the scattering amplitude with respect to $\cos\theta$ (or with respect to the square of the momentum transfer, which is the same) at a fixed energy in the centre-of-mass system. The dispersion relations with respect to the square of the momentum transfer may be derived by a method quite similar to that employed by Mandelstam [2]) for meson-nucleon scattering. For nucleon-

† A similar method was used by Chew *et al.* [23]) and Federbush *et al.* [24]) in dealing with the problem of the electromagnetic nucleon form factor.

nucleon scattering this method is less justifiable than for π-meson-nucleon scattering and is supported merely by an analysis of the first approximations of the perturbation theory, apart from pure surmises. It will be noted, however, that to arrive at our conclusions there is no need for a complete dispersion formula (as will be clear from the following), but what is important is the location of the first (nearest) singularity, which can hardly raise any doubt. Using a method similar to that of ref. [2]) we write the nucleon-nucleon scattering amplitude in the following form (cf. ref. [3])):

$$(2\pi)^4 T(p_1, p'_1; p_2, p'_2)\delta(p_1+p_2-p'_1-p'_2)$$
$$= i\frac{m^2}{8\pi E}\int \mathrm{d}^4x\mathrm{d}^4y\, \mathrm{e}^{i(p'_1x+p'_2y)}\bar{u}_\mu(p'_1)\bar{u}_\nu(p'_2)\cdot\langle -p_1|T(\eta_\mu(x), \eta_\nu(y))|p_2\rangle$$

or

$$T(p_1, p'_1; p_2, p'_2) = i\frac{m^2}{8\pi E}\int \mathrm{d}^4x\, \mathrm{e}^{\frac{1}{2}i(p'_1-p'_2)x}\bar{u}_\mu(p'_1)\bar{u}_\nu(p'_2)$$
$$\cdot\langle -p_1|T(\eta_\mu(\tfrac{1}{2}x), \eta_\nu(-\tfrac{1}{2}x))|p_2\rangle. \quad (2.2)$$

Here p_1, p_2, p'_1, p'_2 are the four-momenta of the nucleons before and after collision, $u(p'_1)$, $u(p'_2)$ the spinors for outgoing nucleon, and $\eta(x)$ is the right part of the Dirac equation for nucleons (metric $+1, -1, -1, -1$). As usual [4, 5]) we introduce the function $M(p_1, p'_1; p_2, p'_2)$ determined by the delayed anti-commutator in lieu of the scattering amplitude:

$$M(p_1, p'_1; p_2, p'_2) = i\frac{m^2}{8\pi E}\int \mathrm{d}^4x\, \mathrm{e}^{\frac{1}{2}i(p'_1-p'_2)x}\theta(x_0)$$
$$\cdot\bar{u}_\mu(p'_1)\bar{u}_\nu(p'_2)\langle -p_1|\{\eta_\mu(\tfrac{1}{2}x), \eta_\nu(-\tfrac{1}{2}x)\}|p_2\rangle. \quad (2.3)$$

The function $M(p_1, p'_1; p_2, p'_2)$ is divided into a dispersive part $D(p_1, p'_1; p_2, p'_2)$ and absorptive part $A(p_1, p'_1; p_2, p'_2)$:

$$M(p_1, p'_1; p_2, p'_2) = D(p_1, p'_1; p_2, p'_2)+iA(p_1, p'_1; p_2, p'_2), \quad (2.4)$$

by expressing $\theta(x_0)$ in (2.3) in the form $\theta(x_0) = \frac{1}{2}(\varepsilon(x_0)+1)$. The absorptive part may be expressed as

$$A(p_1, p'_1; p_2, p'_2) = A_1(p_1, p'_1; p_2, p'_2)+A_2(p_1, p'_1; p_2, p'_2), \quad (2.5)$$

$$A_1(p_1, p'_1; p_2, p'_2) = \pi^3\frac{m^2}{E}\sum_n \bar{u}_\mu(p'_1)\bar{u}_\nu(p'_2)\langle -p_1|\eta_\mu(0)|n\rangle$$
$$\cdot\langle n|\eta_\nu(0)|p_2\rangle\delta(p_n-p'_1+p_1),$$
$$A_2(p_1, p'_1; p_2, p'_2) = \pi^3\frac{m^2}{E}\sum_n \bar{u}_\mu(p'_1)\bar{u}_\nu(p'_2)\langle -p_1|\eta_\nu(0)|n\rangle \quad (2.6)$$
$$\cdot\langle n|\eta_\mu(0)|p_2\rangle\delta(p_n-p'_2+p_1),$$

where $|n\rangle$ is a physical state with the four-momenta p_n and summation is performed with respect to the full system of states for which the four-momenta are given and the number of heavy particles are equal to 0. The scattering amplitude $T(p_1, p'_1; p_2, p'_2)$ expressed through the dispersive and the absorptive parts assumes the same shape (2.4) with the only difference that A_2 is multiplied by (-1). For real nucleon-nucleon scattering in the centre-of mass system, $E'_1-E_1 = 0$, $E'_2-E_1 = 0$, whereas $E_n > 0$. Hence it follows that for a real process the absorptive part is equal to 0 and the function $M(p_1, p'_1; p_2, p'_2)$ coincides with the scattering amplitude. It will be noted that A_2 differs from A_1 in that the variables of the first and second nucleons are interchanged after scattering. As for $M(p_1, p'_1; p_2, p'_2)$ it is a function of the two invariants $(p_1+p_2)^2 = 4E^2$ and $q^2 = (p'_1-p_1)^2 = -2p^2(1-\cos\theta)$, apart from spin and charge variables. The dispersion relations with respect to q^2 at constant E^2 may be obtained using Goldberger's method [4]) and integrating an expression for the absorptive part which may be derived from (2.3) with respect to q^2. This yields †

$$M(E, q^2) = \frac{1}{\pi}\int_{-\infty}^{+\infty} \frac{A(E, q'^2)}{q'^2-q^2-i\varepsilon}\,dq'^2 \tag{2.7}$$

if $\operatorname{Im} q^2 \geqq 0$. Eq. (2.7) is written symbolically: actually, (2.7) should hold for every independent spin (charge) amplitude.

It is convenient to set aside a one-meson state in the summation with respect to intermediate states (2.6). Then the residual terms of the sum will begin with a two-meson state since $p_n^2 > 4\mu^2$ for them. Taking this into account (2.7) may be re-written

$$M(E,q^2) = M^{(1)}(E,q^2) + \frac{1}{\pi}\int_{4\mu^2}^{\infty} \frac{A_1(E, q'^2)}{q'^2-q^2-i\varepsilon}\,dq'^2 - \frac{1}{\pi}\int_{4\mu^2}^{\infty} \frac{A_2(E, r'^2)}{r'^2-r^2+i\varepsilon}\,dr'^2 \tag{2.8}$$

where $r^2 = (p'_2-p_1)^2 = -2p^2(1+\cos\theta)$, $\tau_\alpha^{(1)}$ and $\tau_\alpha^{(2)}$ are the matrices of the isobaric spin of the first and second nucleons, g^2 is the renormalized π-meson-nucleon coupling constant $g^2 = 14.5$. In (2.8) the functions $A_1(E, q^2)$ and $A_2(E, r^2)$ are determined by the relations (2.6) in which the summation with respect to intermediate states begins with a two-meson state. In integrating $A_2(E, q^2)$ we expressed q^2 through $r^2 = 4m^2-4E^2-q^2$; in this form the antisymmetry of the scattering amplitude is quite explicit.

The term $2iA_1(E, q^2)$ (and $2iA_2(E, q^2)$ respectively) may be determined as a discontinuity in the scattering amplitude arising when q^2 crosses the real axis

† The dispersion relations are written without additional subtraction. The subtraction term in our case is of no significance since at $l > 0$ it will vanish after substituting (2.7) in (2.1) and integrating with respect to $\cos\theta$.

from above at a point which lies to the right (to the left) of the point $q^2 = 4\mu^2 (q^2 = -4\mu^2 - 4p^2)$. This assertion directly follows from (2.8) if one considers that (2.8) or (2.7) determine the scattering amplitude in the upper semi-plane of the complex plane q^2. An analytic continuation into tne lower semi-plane should be drawn by crossing the segment of the real axis $-4(\mu^2+p^2) < q^2 < 4\mu^2$ where the amplitude has no singularities (except for the poles).

To calculate the scattering phases let us substitute (2.8) into (2.1). The integration of the pole term in (2.8) will determine the contribution of one-meson approximation to the scattering phases. For the singlet amplitude the one-meson approximation yields (the index $m = 0$ will be omitted)

$$I_l^{(1)} = \frac{g^2 \xi^2}{2E} \lambda_\tau Q_l(1+\tfrac{1}{2}\xi^2) \tag{2.9}$$

where $\lambda_\tau = 1$ for even l (isobaric spin $T = 1$) and $\lambda_\tau = -3$ for odd $l (T = 0)$ and $Q_l(t)$ is the Legendre function of second kind

$$Q_l(t) = \tfrac{1}{2} \int_{-1}^{1} \frac{P_l(t')}{t-t'} \mathrm{d}t'. \tag{2.10}$$

Corrections for one-meson approximation arise from the substitution of the two last terms of (2.8) into (2.1) and in virtue of the relation $Q_l(t) = (-1)^{l+1} Q_l(-t)$ prove to be equal †:

$$I_l^{(2)} = \frac{1}{\pi p^2} \int_{4\mu^2}^{\infty} Q_l\left(1+\frac{q'^2}{2p^2}\right) [A_1(E, q'^2) + (-1)^{l+1} A_2(E, q'^2)] \mathrm{d}q'^2. \tag{2.11}$$

The contribution of the term A_2 to (2.11) is equal to the contribution of A_1. This conclusion directly follows from the fact that for the singlet state $A_2 = A_1$ at $T = 0$ and the amplitude contains only odd l, whereas $A_2 = -A_1$ and the amplitude contains only even l for $T = 1$. Therefore,

$$I_l^{(2)} = \frac{2}{\pi p^2} \int_{4\mu^2}^{\infty} Q_l\left(1+\frac{q'^2}{2p^2}\right) A_1(E, q'^2) \mathrm{d}q'^2. \tag{2.12}$$

Let us make use of the condition $l \gg 1$. At large l the function $Q_l(1+\frac{1}{2}z^2)$ steeply falls as z increases: if $z \gg 1$, $Q_l(1+\frac{1}{2}z^2) \sim z^{-2(l+1)}$, and if $z \ll 1$, but $lz \gg 1$,

† The calculation of the integrals $I_{l,m}(E)$ for $m = 1$ and 2 leads to expressions similar to (2.9) and (2.11) with the only difference that the functions $\sqrt{t^2-1}\,Q_l^{(1)}$ and $(t^2-1)Q_l^{(2)}$ occur instead of the functions $Q_l(t)$. To verify this it suffices to substitute (2.8) into (2.1) and consider the equations (we assume that $l > 1$)

$$\tfrac{1}{2} \int_{-1}^{1} \frac{\sqrt{1-t^2}}{t-t'} P_l^{(1)}(t') \mathrm{d}t' = -\sqrt{t^2-1}\, Q_l^{(1)}(t),$$

$$\tfrac{1}{2} \int_{-1}^{1} \frac{1-t'^2}{t-t'} P_l^{(2)}(t') \mathrm{d}t' = (t^2-1) Q_l^{(2)}(t).$$

then $Q_l(1+\frac{1}{2}z^2) \approx e^{-lz}$. Let us assume the condition $l\xi \gg 1$, $\xi = \mu/p$ (for $\xi < 1$), apart from the condition $l \gg 1$. Then a small region of integration close to the lower limit will be predominant in the integral (2.12). Let us make use of the following expression for the function $Q_l(t)$ (cf. ref. [6]), eq. (6.777)):

$$Q_l(t) = \sqrt{\pi}\frac{\Gamma(l+1)}{\Gamma(l+\frac{3}{2})} e^{-(l+1)\ln(t+\sqrt{t^2-1})} \cdot F(\tfrac{1}{2}, l+1, l+\tfrac{3}{2}, (t+\sqrt{t^2-1})^{-2}), \quad (2.13)$$

and expand the exponent and hypergeometrical function into a series in the neighbourhood of $t_0 = 1+2\xi^2$, $(\Delta t = t-t_0)$:

$$Q_l(t) = Q_l(t_0)e^{-\frac{\Delta t(l+1)}{\sqrt{t_0^2-1}}}\left[1+\frac{(l+1)t_0}{(t_0^2-1)^{\frac{1}{2}}}\frac{(\Delta t)^2}{2}\right]\cdot\left[1-\frac{\Delta t}{2(t_0^2-1)(t_0+\sqrt{t_0^2-1})}\right]. \quad (2.14)$$

After substituting (2.14) into (2.12), the integral $I_l^{(2)}$ will be reduced to

$$I_l^{(2)} = \frac{8}{\pi}\xi^2 Q_l(t_0)\int_0^\infty d\left(\frac{q'^2-4\mu^2}{4\mu^2}\right) e^{-\frac{L(q'^2-4\mu^2)}{4\mu^2}} A_1(E, q'^2),$$

$$A_1(E, q^2) = \frac{1}{2i}[M(E, q^2+i0)-M(E, q^2-i0)], \quad (2.15)$$

where

$$L = (l+1)\frac{\xi}{\sqrt{1+\xi^2}} \approx \begin{cases} (l+1)\xi & \text{if } \xi \ll 1 \\ l+1 & \text{if } \xi \gg 1. \end{cases} \quad (2.16)$$

It is not difficult to verify that the terms of the expansion in square brackets in (2.14) at large L make a small contribution to integral (2.12) (of the order $1/L$); our expansion is therefore justified and (2.15) has an accuracy of the order $1/L$.

Now let us show that at large L there is no need of using the full dispersion relation (2.7) for obtaining (2.15), but it is sufficient if on the complex plane q^2, inside the ellipse passing through the point $q^2 = 4\mu^2+\kappa^2$ (the constant $\kappa^2 \gg 4\mu^2/L$) and having its foci at the points $q^2 = 0$ and $q^2 = -4\mu^2/\xi^2$, there are no other singularities besides the poles and the singularities on the real axis at $q^2 \geqq 4\mu^2$ and $q^2 \leqq -4\mu^2(1+\xi^{-2})$. To prove this, let us transform integral (2.1) using the relation

$$I_l = \frac{1}{2p^2}\int_{-4p^2}^{0} P_l\left(1+\frac{q^2}{2p^2}\right)M(E, q^2)dq^2 = \frac{1}{2p^2\pi i}\oint_C Q_l\left(1+\frac{q^2}{2p^2}\right)M(E, q^2)dq^2, \quad (2.1')$$

and then deform the contour C (which is shown as a dotted line in fig. 1) into the contour $C_1+C'_1+C_2$. We shall select an arc in the complex plane in the shape of the above-mentioned ellipse, extending the latter until it reaches the nearest singular point in the complex plane. If the ellipse reaches the point on the right semi-axis $q^2 = 4\mu^2+\kappa^2$, (2.1) may be written

$$I_l = -\frac{1}{p^2} Q_l(1+\tfrac{1}{2}\xi^2)\ \mathrm{res}\,[M(E,\mu^2)+(-1)^l M(E,-\mu^2-4p^2)]$$

$$+\frac{1}{2p^2\pi i}\int_{4\mu^2}^{\infty} Q_l\left(1+\frac{q^2}{2p^2}\right)[\Delta M(E,q^2)-(-1)^l \Delta M(E,-q^2-4p^2)]\,dq^2 \quad (2.11')$$

$$+ f Q_l\left(1+\frac{4\mu^2+\kappa^2}{2p^2}\right),$$

$$\Delta M(E,q^2) = M(E,q^2+i0)-M(E,q^2-i0) = 2iA(E,q^2),$$

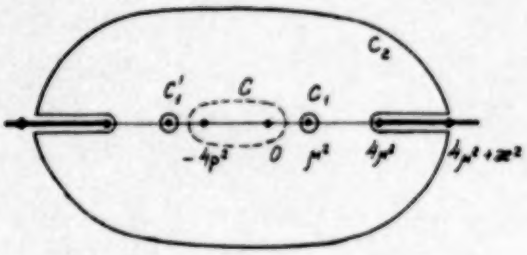

Fig. 1. The contour of integration in the complex plane q^2.

which is equivalent to (2.9), (2.11) to the accuracy of the last term (f is a certain smooth function of p^2 and l). As compared with the integral along both sides of the cut $q^2 \geqq 4\mu^2$ this term has the additional small factor

$$\frac{Q_l\left(1+\frac{4\mu^2+\kappa^2}{2p^2}\right)}{Q_l\left(1+\frac{4\mu^2}{2p^2}\right)} \ll 1, \quad \text{if} \quad l \gg 1,$$

and at large l it may be neglected.

As follows from (2.15) the values of the amplitude $A_1(E,q^2)$ at $q^2-4\mu^2 \approx 4\mu^2/L \ll 4\mu^2$ must be of interest to us. This being the case only a two-meson state remains in the summation with respect to intermediary states (2.6) since the next (3-meson) state corresponds to a minimum q^2 equal to $9\mu^2$, while the state corresponding to a nucleon-antinucleon pair lies still further. Thus the expression for $A_1(E,q^2)$ assumes the form

$$A_1(E,q^2) = \frac{1}{8(2\pi)^3}\frac{m^2}{E}\sum_{\alpha,\beta}\int d\mathbf{k}_1 d\mathbf{k}_2 \bar{u}_\mu(p'_1)\,\bar{u}_\nu(p'_2)$$

$$\cdot \langle -p_1|\eta_\mu(0)|k_1,\alpha_1;k_2,\beta\rangle\langle k_1,\alpha;k_2,\beta|\eta_\nu(0)|p_2\rangle \cdot \delta(k_1+k_2-q), \quad (2.17)$$

where k_1 and k_2 are the 4-momenta of two π-mesons in the charged states α and β, $q = p'_1-p_1$. The matrix elements which enter (2.17) are simply related to the invariant matrix element $f_{\alpha\beta}(p_1,p'_1;k,k')$ of meson-nucleon

scattering (ω being the energy of the meson):

$$\bar{u}_\mu(p'_1)\langle -p_1|\eta_\mu(0)|k_1, \alpha; k_2, \beta\rangle = \frac{2\pi}{\sqrt{\omega_1\omega_2}} f_{\alpha\beta}(p_1, p'_1; k_1, -k_2),$$
$$\bar{u}_\nu(p'_2)\langle k_1, \alpha; k_2, \beta|\eta_\nu(0)|p_2\rangle = \frac{2\pi}{\sqrt{\omega_1\omega_2}} f_{\alpha\beta}(p_2, p'_2; -k_1, k_2). \tag{2.18}$$

Here [7-10],

$$f_{\alpha\beta}(p, p'; -k_1, k_2) = f^*_{\alpha\beta}(p', p; k_1, -k_2). \tag{2.19}$$

Substituting (2.18) into (2.17), we obtain

$$A_1(E, q^2) = \frac{1}{16\pi}\frac{m^2}{E}\sum_{\alpha,\beta}\int\frac{d\mathbf{k}_1 d\mathbf{k}_2}{\omega_1\omega_2} f_{\alpha\beta}(p_1, p'_1; k_1, -k_2) \cdot f_{\alpha\beta}(p_2, p'_2; -k_1, k_2)\delta(k_1+k_2-q). \tag{2.20}$$

The integral in (2.20) is written in an invariant form (since $d\mathbf{k}/\omega$ is an invariant). It is convenient to analyse it in that system of co-ordinates in which the time-like 4-vector q has only a non-vanishing time component. In this system $\omega_1 = \omega_2 = \frac{1}{2}q$; $\mathbf{k}_1 = -\mathbf{k}_2 = \mathbf{k}$; $k = \sqrt{\frac{1}{4}q^2-\mu^2} \approx \mu/\sqrt{L}$ so that the components of the vector $\mathbf{k}$ are small. It is easy to see that if we put $k_1 = \frac{1}{2}q+k$, $k_2 = \frac{1}{2}q-k$, the components of the vector $\mathbf{k}$ are also of the order $\mu/\sqrt{L}$ in other systems of co-ordinates which are of interest to us — in the system of the centre of nucleon mass, for example. Therefore, in calculating $f_{\alpha\beta}$ to the first approximation with respect to $1/L$ †, one may neglect k, simply putting $k_1 = k_2 = \frac{1}{2}q$. This approximation is unjustifiable only for those terms in $f_{\alpha\beta}$ which undergo sharp changes in the interval $0 < k \lesssim \mu/\sqrt{L}$. The matrix element $f_{\alpha\beta}(p_1, p'_1; k+\frac{1}{2}q, k-\frac{1}{2}q)$ may be regarded as a function of the two invariants $\nu = \frac{1}{2}(p_1+p_1')(k+\frac{1}{2}q)$, q^2 and written

$$f_{\alpha\beta}(p_1, p'_1; k+\tfrac{1}{2}q, k-\tfrac{1}{2}q) = \bar{u}(p'_1)[L_{\alpha\beta}(\nu, q^2)+(\mathbf{k}+\tfrac{1}{2}q)M_{\alpha\beta}(\nu, q^2)]u(p_1), \tag{2.21}$$

where $L_{\alpha\beta}$ and $M_{\alpha\beta}$ are scalar functions of their arguments. A similar expression holds for $f_{\alpha\beta}(p_2, p'_2; -(k+\frac{1}{2}q), -(k-\frac{1}{2}q))$.

The term proportional to q may be discarded in virtue of the equation

$$\bar{u}(p'_1)qu(p_1) = \bar{u}(p'_1)(p'_1-p_1)u(p_1) = 0. \tag{2.22}$$

Let us first assume that $f_{\alpha\beta}$ is a sufficiently slow function of k so that one may neglect k and put $k_1 = k_2 = \frac{1}{2}q$. Then $\nu = \nu_0 = \frac{1}{2}(2p_1+q)\frac{1}{2}q = 0$, $q^2 = 4\mu^2$, and

$$f_{\alpha\beta}(p_1, p'_1; \tfrac{1}{2}q, -\tfrac{1}{2}q) = \bar{u}(p'_1)L_{\alpha\beta}(0, 4\mu^2)u(p_1); \tag{2.23}$$

† Though the components of the vector $\mathbf{k}$ are as small as $1/\sqrt{L}$, the error which arises if they are neglected will be of the order $1/L$, since the terms linear with respect to $\mathbf{k}$ will vanish in integrating over the angles.

and as follows from (2.19), $L_{\alpha\beta}(0, 4\mu^2)$ is real. Substituting (2.23) into (2.20) and integrating with respect to $\mathbf{k}_1$ and $\mathbf{k}_2$ (in the system of co-ordinates in which $\mathbf{q} = 0$), we obtain

$$A_1(E, q^2) = \frac{m^2}{8E}\sqrt{\frac{q^2}{4\mu^2}-1}\,\bar{u}(p'_1)L_{\alpha\beta}(0, 4\mu^2)u(p_1)\bar{u}(p'_2)L_{\alpha\beta}(0, 4\mu^2)u(p_2). \quad (2.24)$$

We have thus obtained a well-known result [11]), namely, that the absorptive part of the amplitude, which in the present case coincides with the imaginary part †, is proportional to $\sqrt{q^2-4\mu^2}$ at the branching point. Apart from terms which vary sufficiently slowly in the neighbourhood of the point $\nu = 0$, $q^2 = 4\mu^2$, the function $f_{\alpha\beta}$ has terms in which one may put $\nu = 0$, $q^2 = 4\mu^2$ only at very large values of L which are of no practical interest. These pole terms correspond to the one-nucleon intermediate state in the meson-nucleon scattering amplitude and are described by the first approximation of the perturbation theory with the re-normalized constant g^2. The pole term in $f_{\alpha\beta}$ has the form ††

$$\begin{aligned} &f_{p\alpha\beta}(p_1, p'_1; k_1, -k_2) \\ &\quad = g^2\bar{u}(p'_1)[\gamma_5(p_1+k_1-m)^{-1}\gamma_5\tau_\alpha\tau_\beta+\gamma_5(p_1+k_2-m)^{-1}\gamma_5\tau_\beta\tau_\alpha]u(p_1), \quad (2.25)\\ &\quad = -g^2\bar{u}(p'_1)[(2p_1k_1+\mu^2)^{-1}\tau_\alpha\tau_\beta-(2p_1k_2+\mu^2)^{-1}\tau_\beta\tau_\alpha]ku(p_1). \end{aligned}$$

Since $f_{p\alpha\beta}$ contains a small factor k in the numerator, one might think that this term could be omitted. Yet (2.25) has a pole situated rather close to the point $k = 0$ (at a distance of $\mu^2/2m$ from it; cf. (2.27)). The integrals with pole terms therefore require exact calculation. To verify this let us consider the interference term when the pole is term taken in one amplitude and a constant of the form (2.23) in the other. In this case both terms in square brackets in (2.25) yield equal contributions and the interference term will be

$$-\frac{1}{16\pi}\frac{m^2}{E}g^2\int\frac{d\mathbf{k}_1 d\mathbf{k}_2}{\omega_1\omega_2}\bar{u}(p'_1)ku(p_1)\frac{1}{2p_1k_1+\mu^2}\bar{u}(p'_2) \cdot L_{\alpha\alpha}(0, 4\mu^2)u(p_2)\delta(k_1+k_2-q). \quad (2.26)$$

In the system of co-ordinates in which $\mathbf{q} = 0$, the singlet part (2.26) may be written (the spinors being normalized by $\bar{u}u = 1$ and the terms $q^2/4m^2$ discarded)

$$\frac{1}{16\pi}\frac{m}{E}g^2\int\frac{d\mathbf{k}}{\omega^2}\frac{\mathbf{k}\cdot\mathbf{p}_1}{\mu^2-\frac{1}{2}q^2-2\mathbf{k}\cdot\mathbf{p}_1}\delta(q-2\omega)\bar{u}(p'_2)L_{\alpha\alpha}(0, 4\mu^2)u(p_2). \quad (2.27)$$

Changing over from (2.26) to (2.27) we have taken into account that the

† The absorptive part ceases to coincide with the imaginary one when we cross the line of singular points (except for the line $q^2 = 4\mu^2$) as the arguments E, q^2 vary. The line $q^2 = 4\mu^2 + \mu^4/p^2$ which corresponds to the vanishing of all four denominators in the simplest four-vertex graph will be the nearest line of this kind (see ref. [12])).

†† In our notations we follow ref. [13]), $\gamma_5^2 = 1$.

energies of the first nucleon in the selected system of the co-ordinates are equal to $E_1 = -\frac{1}{2}q$, $E'_1 = \frac{1}{2}q$ before and after the collision, respectively. The components of the momentum $\mathbf{p}_1$ in the integrand (2.27) are purly imaginary when $\frac{1}{2}q < m$. If the z-axis is directed along the purely imaginary vector $\mathbf{p}_1$, therefore, the scalar product $\mathbf{k} \cdot \mathbf{p}_1$ will be $\mathbf{k} \cdot \mathbf{p}_1 = k_z p_1 = i\sqrt{m^2 - \frac{1}{4}q^2}\sqrt{\frac{1}{4}q^2 - \mu^2}\cos\theta \approx im\sqrt{\frac{1}{4}q^2 - \mu^2}\cos\theta$ and after the elimination of the δ-function integral, (2.27) will assume the shape

$$\int \frac{d\mathbf{k}}{\omega^2} \frac{\mathbf{k} \cdot \mathbf{p}_1}{\mu^2 - \frac{1}{2}q^2 - 2\mathbf{p}_1 \cdot \mathbf{k}} \delta(q - 2\omega)$$

$$= \tfrac{2}{9}\pi\sqrt{\tfrac{1}{4}q^2 - \mu^2}\int_{-1}^{+1} dx \frac{im\sqrt{\frac{1}{4}q^2 - \mu^2}\,x}{\mu^2 - \frac{1}{2}q^2 - 2im\sqrt{\frac{1}{4}q^2 - \mu^2}\,x} \qquad (2.28)$$

$$\approx -\tfrac{2}{9}\pi\sqrt{\tfrac{1}{4}q^2 - \mu^2}\left[1 - \frac{\mu^2}{2m\sqrt{\frac{1}{4}q^2 - \mu^2}} \operatorname{arctg} \frac{2m\sqrt{\frac{1}{4}q^2 - \mu^2}}{\mu^2}\right].$$

From (2.28) it is clear that the contribution of the polar term will be proportional to $(\frac{1}{4}q^2 - \mu^2)^{\frac{3}{2}}$ for sufficiently small $\frac{1}{4}q^2 - \mu^2 \ll (\mu/2m)^2\mu^2$ and as may well be expected proves to be $1/L$ of the contribution of the leading term of (2.24) after substitution into (2.15). But in (2.15) so small values of $\frac{1}{4}q^2 - \mu^2$ predominate only for very large angular momenta when $L \gtrsim (2m/\mu)^2$. It stands to reason that this case is of no practical interest. The case $L \ll (2m/\mu)^2$ is, on the contrary, of interest to us. Then $\frac{1}{4}q^2 - \mu^2 \gg (\mu/2m)^2\mu^2$ for the effective region of integration in (2.15), the term (2.28) being reduced to $-\frac{2}{9}\pi\sqrt{(\frac{1}{4}q^2 - \mu^2)}$. Using (2.27) and (2.28) we arrive at the conclusion that for $L \ll (2m/\mu)^2$ the interference term (2.26), after substitution in (2.15), yields a contribution of the same order with respect to $1/L$ as the leading term (2.24), and will differ from it merely by a factor of the order $g^2\mu/m \approx 1$ (if we assume that $L_{\alpha\alpha}(0, 4\mu^2) \approx 1/\mu$).

Thus, to calculate $A_1(E, q^2)$ the matrix element $f_{\alpha\beta}$ should be represented as a sum of the pole term (2.25) and of the residual part of the matrix element $\tilde{f}_{\alpha\beta} = f_{\alpha\beta} - f_{p\alpha\beta}$, which it is sufficient to calculate at the point $\nu = 0$ and $q^2 = 4\mu^2$. To obtain more accurate results in $\tilde{f}_{\alpha\beta}$ we also take into account the first term of the expansion in ν and k †.

We shall perform calculations in four-dimensional form, computing the discontinuity in the scattering amplitude $\Delta M(E, q^2) = 2iA_1(E, q^2)$ directly and substituting it into (2.15). Let us therefore translate the conclusions we have reached into the conventional graphic terms.

In two-meson approximation the nucleon-nucleon scattering amplitudes are calculated by the graphs of figs. 2a, b. The hatched areas in these graphs corre-

† The result of integrating the product of this term and the pole term will be as small as $\approx \mu/m$, not as $1/L$, and may prove to be essential numerically.

spond to an aggregate of all graphs with two external nucleon lines and two meson lines. The scattering amplitude corresponding to the graphs of fig. 2

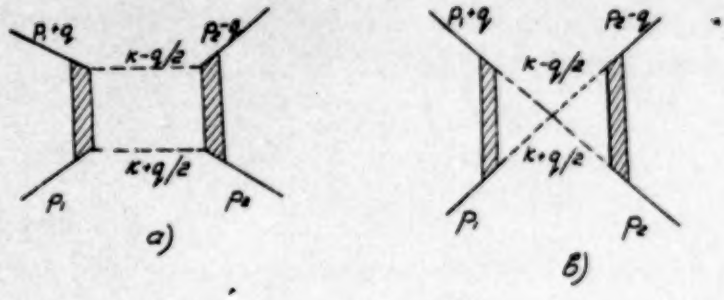

Fig. 2. The Feynman graphs corresponding to the N−N scattering amplitude in two-meson approximation.

may be written, excluding the terms which have no discontinuity when $q^2 \geqq 4\mu^2$ (i.e. which are non-singular in the neighbourhood of $q^2 \approx 4\mu^2$)

$$M(E, \cos\theta) = \frac{m}{2\pi i}\int \mathrm{d}^4 k f_{\alpha\beta}(p_1, p_1+q; k+\tfrac{1}{2}q, k-\tfrac{1}{2}q)$$

$$\cdot f_{\alpha\beta}(p_2, p_2-q; -k-\tfrac{1}{2}q, -k+\tfrac{1}{2}q)\frac{1}{(k+\frac{1}{2}q)^2-\mu^2}\,\frac{1}{(k-\frac{1}{2}q)^2-\mu^2}, \quad (2.29)$$

where the meson-nucleon scattering amplitude $f_{\alpha\beta}$ should be calculated as was stated above. A coefficient $\frac{1}{2}$ is introduced in (2.29) because in the meson-nucleon scattering amplitude $f_{\alpha\beta}$ we consider the graphs in which the meson of momentum $k+\frac{1}{2}q$ is first absorbed in a state α and then the meson of momentum $k-\frac{1}{2}q$ is emitted in a state β, as well as the graphs with the inverse order of absorption and emission, which results in doubling all graphs for nucleon-nucleon scattering. As follows from eq. (2.20), M should include the values of Green's functions on the mass surface $k_1^2 = k_2^2 = \mu^2$: instead of Green's functions for mesons, therefore, we have substituted their free values.

Fig. 3. The graph for $\pi-$N scattering, taking account of $\pi-\pi$ scattering.

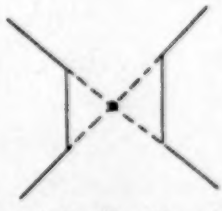

Fig. 4. The graph for N−N scattering, taking account of $\pi-\pi$ scattering.

Let us now proceed to the role of meson-meson scattering. As follows from (2.20) $f_{\alpha\beta}$ is an exact amplitude of nucleon-meson scattering, taking account of meson-meson scattering, so that the graphs of the type shown in fig. 3, for example, enter $f_{\alpha\beta}$. At first glance it might seem that if we substitute this graph

in the right and left parts of fig. 2 we should make the mistake of considering the graph of fig. 4 twice. In point of fact the contribution of the graph of fig. 4 close to the singularity $q^2 = 4\mu^2$ really doubles, since the singularity may arise (i.e. the meson lines may become real) both to the left and to the right of the point of meson-meson scattering †.

3. Use of Dispersion Relations for Meson-Nucleon Scattering

In the present section we calculate the amplitude of meson-nucleon scattering $f_{\alpha\beta}(p_1, p_1+q; k+\frac{1}{2}q, k-\frac{1}{2}q)$ for small values of k and $q^2 = 4\mu^2$ through its analytic continuation beyond the physical region. Let us consider the difference of the scattering amplitude and the polar term $\tilde{f}_{\alpha\beta} = f_{\alpha\beta} - f_{p\alpha\beta}$. Let us write $\tilde{f}_{\alpha\beta}$ in the form (2.21) and expand it in powers of k, confining ourselves to the terms linear with respect to k:

$$\tilde{f}_{\alpha\beta}(p_1, p_1+q; k+\tfrac{1}{2}q, k-\tfrac{1}{2}q) = \tilde{L}_{\alpha\beta}(0, 4\mu^2) + \left.\frac{\partial \tilde{L}_{\alpha\beta}(\nu, 4\mu^2)}{\partial \nu}\right|_{\nu=0} [p_1 k + \tfrac{1}{2}(kq)] + k\tilde{M}_{\alpha\beta}(0, 4\mu^2). \quad (3.1)$$

The terms proportional to the invariant kq vanish when integrating with respect to k, since $kq = 0$ in the system of co-ordinates where $\mathbf{q} = 0$ ††. Therefore, (3.1) assumes the shape

$$\tilde{f}_{\alpha\beta} = \tilde{L}_{\alpha\beta}(0, 4\mu^2) + p_1 k \left.\frac{\partial \tilde{L}_{\alpha\beta}(\nu, 4\mu^2)}{\partial \nu}\right|_{\nu=0} + k\tilde{M}_{\alpha\beta}(0, 4\mu^2). \quad (3.2)$$

The squares of all external four momenta entering (3.1) are equal to their values for free motion: $p_1^2 = p_1'^2 = m^2$, $k_1^2 = k_2^2 = \mu^2$; and in this sense $f_{\alpha\beta}$ is a matrix element of scattering of real mesons on nucleons. Yet the energies of these mesons and the momentum transfer are not physical in the physical systems of co-ordinates. Indeed, it follows from the equation $\nu_0 = 0$ that the total energy of the meson $\omega = 0$ in the Breit system of co-ordinates, in which the sum of the nucleon momenta before and after scattering is equal to 0: $\mathbf{p}_1 + \mathbf{p}_2 = 0$. On the other hand, the square of the momentum transfer $q^2 = q_0^2 - \mathbf{q}^2 = 4\mu^2$ is positive, whereas in real processes of scattering it is always negative. This means that the meson-nucleon scattering amplitude which is of interest to us cannot be obtained directly with the help of experimental data on meson-nucleon scattering and we have to use an analytic continuation of the amplitude onto the values $\omega = 0$, $q^2 = 4\mu^2$.

† Owing to meson-meson scattering the amplitude of nucleon-meson scattering has a singularity at $q^2 = 4\mu^2$ and is proportional to $a + ib\sqrt{(q^2 - 4\mu^2)}$ close to this point (when $k = 0$). This singularity may, it seems, result in corrective terms of the order L^{-1}. Yet it may be seen that such corrections do not actually arise in the perturbation theory. The same result may be obtained from (2.20) if one considers (2.19) and the reality of the coefficients a and b.

†† This conclusion has been confirmed by direct calculation.

First of all let us determine the dependence of (3.2) on the isobaric variables. The functions $L_{\alpha\beta}(\nu, q^2)$ and $M_{\alpha\beta}(\nu, q^2)$ may be represented as follows:

$$\begin{aligned} L_{\alpha\beta}(\nu, q^2) &= \delta_{\alpha\beta}L^{(1)}(\nu, q^2) - i\varepsilon_{\alpha\beta\gamma}\tau_\gamma L^{(2)}(\nu, q^2), \\ M_{\alpha\beta}(\nu, q^2) &= \delta_{\alpha\beta}M^{(1)}(\nu, q^2) - i\varepsilon_{\alpha\beta\gamma}\tau_\gamma M^{(2)}(\nu, q^2), \end{aligned} \tag{3.3}$$

where

$$\begin{aligned} L^{(1)} &= \tfrac{1}{2}(L_+ + L_-) = \tfrac{1}{3}(L_1 + 2L_3), & L^{(2)} &= \tfrac{1}{2}(L_+ - L_-) = \tfrac{1}{3}(L_3 - L_1); \\ M^{(1)} &= \tfrac{1}{2}(M_+ + M_-) = \tfrac{1}{3}(M_1 + 2M_3), & M^{(2)} &= \tfrac{1}{2}(M_+ - M_-) = \tfrac{1}{3}(M_3 - M_1), \end{aligned} \tag{3.4}$$

and L_+, $M_+(L_-, M_-)$ are the matrix elements of scattering of $\pi^+(\pi^-)$ mesons on protons, while L_1, M_1 and L_3, M_3 are the matrix elements of scattering of mesons on nucleons in states with total isobaric spins $\frac{1}{2}$ and $\frac{3}{2}$ respectively.

As follows from (2.19) the quantities $L^{(1)}$, $M^{(1)}$, $L^{(2)}$, $M^{(2)}$ possess simple properties of symmetry with respect to the substitution $\nu \to -\nu$:

$$\begin{aligned} L^{(1)}(\nu, q^2) &= L^{(1)*}(-\nu, q^2), & L^{(2)}(\nu, q^2) &= -L^{(2)*}(-\nu, q^2); \\ M^{(1)}(\nu, q^2) &= -M^{(1)*}(-\nu, q^2), & M^{(2)}(\nu, q^2) &= M^{(2)*}(-\nu, q^2). \end{aligned} \tag{3.5}$$

The general expression for the imaginary part of the scattering amplitude obviously shows that the imaginary part of the functions $L^{(i)}$ and $M^{(i)}$ must vanish when $\nu = 0$ and $q^2 \leqq 4\mu^2$. † Hence, and from (3.5), it follows that

$$\tilde{f}_{\alpha\beta} = \tilde{L}^{(1)}(0, 4\mu^2)\delta_{\alpha\beta} - i\varepsilon_{\alpha\beta\gamma}\tau_\gamma \left\{ p_1 k \frac{\partial \tilde{L}^{(2)}(\nu, 4\mu^2)}{\partial \nu}\bigg|_{\nu=0} + k\tilde{M}^{(2)}(0, 4\mu^2) \right\}. \tag{3.6}$$

The quantities on the right hand side of (3.6) may be expressed through their values at physical energies with the aid of dispersion relations with respect to energy for a fixed value of the square of the momentum transfer q^2. The problem of determining for which values of q^2 such dispersion relations hold has been investigated in a number of papers [14, 15, 16]). The authors of these papers, however, were concerned with the merely negative q^2 involved in real processes. A justification of dispersion relations when $q^2 > 0$ and, in particular, at the point $q^2 = 4\mu^2$ of interest to us may be obtained easily enough. Let us write the matrix element of meson-nucleon scattering in the Breit system of co-ordinates as a function of the meson energy ω in this system and the momentum transfer q^2 [17]):

$$f_{\alpha\beta}(\omega, q^2) = i\int \mathrm{d}^4x\, \mathrm{e}^{i[\omega t - \mathbf{n}\cdot\mathbf{r}\sqrt{\omega^2 - \mu^2 + \frac{1}{4}q^2}]}\, \theta(x_0)\langle p'_1|[j_\beta(\tfrac{1}{2}x), j_\alpha(-\tfrac{1}{2}x)]|p_1\rangle. \tag{3.7}$$

† The imaginary part of the amplitude of scattering of meson on nucleon proves to be different from 0 only for such meson energies for which there may exist a real state of the meson-nucleon system (this corresponds to energies $\omega > \omega_1 = (m\mu + \frac{1}{4}q^2)/(m^2 + \frac{1}{4}q^2)^{\frac{1}{2}}$ in the Breit system of co-ordinates) or a real state of the system of two mesons. As can easily be seen, the latter results in the occurrence of an imaginary part of the scattering amplitude when $q^2 > 4\mu^2$, the imaginary part vanishing proportionally to $\sqrt{(q^2 - 4\mu^2)}$ when $q^2 \to 4\mu^2$.

Here $j_\alpha(x)$ is the nucleon current, and $\mathbf{n}$ is a certain unit vector †. As is well known, the difficulty of justifying dispersion relations on the basis of eq. (3.7) lies in that the root in the exponent of (3.7) proves to be imaginary and the entire expression divergent when integrating with respect to $\mathbf{r}$ when $f_{\alpha\beta}(\omega, q^2)$ is continued analytically into the complex plane for values $\omega^2 < \mu^2 - \frac{1}{4}q^2$. It is obvious that when $q^2 > 0$ (which is equivalent to a decrease in the mass of the meson, as it were) proof is even easier than for forward scattering. In particular, when $q^2 = 4\mu^2$, the exponent in (3.7) assumes quite a simple form: $\exp\{-i\omega(t - \mathbf{n}\cdot\mathbf{r})\}$, as well as the analyticity of $f_{\alpha\beta}(\omega, q^2)$ in the upper semi-plane ω, and, consequently, the existence of dispersion relations follows directly from the vanishing of the delayed current commutator when $t^2 - r^2 < 0$ and $t < 0$.

It is convenient to write dispersion relations not for L and M but for the matrix element of meson-nucleon scattering without spin flip $f(\omega, q^2)$ and with spin flip $\varphi(\omega, q^2)$. The relation of f and φ to L and M is obtained through the expression

$$\bar{u}(p')[L^{(i)}(\omega, q^2) + k_1 M^{(i)}(\omega, q^2)]u(p)$$
$$\equiv v'^{*}[f^{(i)}(\omega, q^2) + i\boldsymbol{\sigma}\cdot(\mathbf{k}_1 \times \mathbf{k}'_1)\varphi^{(i)}(\omega, q^2)]v \qquad (i = 1,2), \quad (3.8)$$

where v' and v are the 2-component spinors describing the spin states of the initial and final nucleons, respectively, in their rest system, and $\boldsymbol{\sigma}$ are two-column Pauli matrixes. Expressing $\bar{u}(p')$ and $u(p)$ through two-component spinors v', v we obtain the relation between L, M and f, φ in the Breit system:

$$f^{(i)}(\omega, q^2) = \frac{E}{m} L^{(i)}(\omega, q^2) + \omega M^{(i)}(\omega, q^2),$$
$$\varphi^{(i)}(\omega, q^2) = -\frac{1}{2m} M^{(i)}(\omega, q^2), \quad (3.9)$$

where E is the nucleon energy in the Breit system $E = \sqrt{(m^2 + \frac{1}{4}\mathbf{q}^2)}$, $\mathbf{q}^2 = -q^2$. The matrix elements $f^{(i)}(\omega, q^2)$, $\varphi^{(i)}(\omega, q^2)$ may be expressed through the scattering amplitudes (with and without spin flip) in the centre-of-mass system of meson and nucleon. If one writes invariant matrix element (3.8) in the centre-of-mass system as ††

† The components of the nucleon and meson momenta in the Breit system generally have the form

$$\mathbf{p}_1 = \{0, 0, \tfrac{1}{2}\sqrt{\mathbf{q}^2}\}, \quad \mathbf{p}'_1 = \{0, 0, -\tfrac{1}{2}\sqrt{\mathbf{q}^2}\}, \quad \mathbf{k}_1 = \{k_x, k_y, -\tfrac{1}{2}\sqrt{\mathbf{q}^2}\}, \quad \mathbf{k}'_1 = \{k_x, k_y, \tfrac{1}{2}\sqrt{\mathbf{q}^2}\},$$

or, if one introduces a unit vector $\mathbf{n}$ in the (x, y) plane

$$\mathbf{n} = \{k_x, k_y\}(k_x^2 + k_y^2)^{-\frac{1}{2}}, \quad \mathbf{k}_1 = \{\mathbf{n}\sqrt{\omega^2 - \mu^2 - \tfrac{1}{4}\mathbf{q}^2}, -\tfrac{1}{2}\sqrt{\mathbf{q}^2}\}, \quad \mathbf{k}'_1 = \{\mathbf{n}\sqrt{\omega^2 - \mu^2 - \tfrac{1}{4}\mathbf{q}^2}, \tfrac{1}{2}\sqrt{\mathbf{q}^2}\}$$

($\mathbf{k}_1$ is an incident meson momentum, $\mathbf{k}'_1$ a scattered meson momentum, $k'_1 = -k_2$). The quantity $\nu = \frac{1}{2}(p + p')k_1$ is related with the energy ω through $\nu = \omega\sqrt{m^2 - \frac{1}{4}q^2}$.

†† The factor $(E_c + \omega_c)/m$ in the right hand side of (3.10) is introduced to make f_c and φ_c exactly equal to the scattering amplitudes.

$$\bar{u}_c(p'_c)[L^{(i)}(\omega_c, q^2)+k_{1c}M^{(i)}(\omega_c, q^2)]u_c(p_c)$$

$$=\frac{E_c+\omega_c}{m}v'^*[f_c^{(i)}(\omega_c, q^2)+i\sigma\cdot\mathbf{k}_{1c}\times\mathbf{k}'_{1c}\varphi_c^{(i)}(\omega_c, q^2)]v \quad (3.10)$$

(the index c denotes the centre-of-mass system), and considers the fact that $L^{(i)}$ and $M^{(i)}$ are invariant, a relation between f_c, φ_c and f, φ may easily be found after we express f_c and φ_c through L and M and use (3.9). As a result we obtain [10])

$$f^{(i)}(\omega, q^2)=\frac{E_c+\omega_c}{m}\left\{\frac{E^2+mE}{E(E_c+m)}f_c^{(i)}(\omega_c, q^2)-\tfrac{1}{2}\mathbf{q}^2\frac{E^2-E_c^2}{E(E_c+m)}\varphi_c^{(i)}(\omega_c, q^2)\right\},$$

$$\varphi^{(i)}(\omega, q^2)=-\frac{1}{2m}\frac{1}{E_c+m}f_c^{(i)}(\omega_c, q^2)+\left[1+\frac{\mathbf{q}^2}{4m(E_c+m)}\right]\varphi_c^{(i)}(\omega_c, q^2), \quad (3.11)$$

the meson energy in the centre-of-mass system E_c being related to the energy in the Breit system through †

$$E\omega=(E_c+\omega_c)\omega_c-\mu^2-\tfrac{1}{4}\mathbf{q}^2, \quad (3.12)$$

The energies of the mesons which are of importance in dispersion relations being of the order of 2μ or 3μ in the centre-of-mass system, we may within a satisfactory accuracy ($\approx(\mu/m)^2$) replace (3.11) by the approximate expressions

$$f^{(i)}(\omega, q^2)=\frac{E_c+\omega_c}{m}f_c^{(i)}(\omega_c, q^2), \qquad \varphi^{(i)}(\omega, q^2)=\varphi_c^{(i)}(\omega_c, q^2). \quad (3.13)$$

For the amplitudes $f_{c,T}(\omega_c, q^2)$, $\varphi_{c,T}(\omega_c, q^2)$ corresponding to the given values of the total isobaric spin $T=\frac{1}{2}$, $T=\frac{3}{2}$, the well-known expansions in Legendre polynomials [10]) apply:

$$f_{c,T}(\omega_c, q^2)=\frac{1}{2ik_c}\sum_l[(l+1)e^{2i\delta_{l+}^T(\omega_c)}+le^{2i\delta_{l-}^T(\omega_c)}-(2l+1)]P_l\left(1-\frac{\mathbf{q}^2}{2k_c^2}\right),$$

$$\varphi_{c,T}(\omega_c, q^2)=\frac{1}{2ik_c^3}\sum_l[e^{2i\delta_{l+}^T(\omega_c)}-e^{2i\delta_{l-}^T(\omega_c)}]\dot{P}_l\left(1-\frac{\mathbf{q}^2}{2k_c^2}\right), \quad (3.14)$$

where $\delta_{l+}^T(\omega_c)$ and $\delta_{l-}^T(\omega_c)$ are the scattering phases for isobaric spin T and total angular momenta $j=l+\frac{1}{2}$ and $j=l-\frac{1}{2}$, respectively, and $\dot{P}_l(x)=\mathrm{d}P_l(x)/\mathrm{d}x$. The dispersion relations for the functions $\tilde{f}^{(i)}(\omega, q^2)$ and $\tilde{\varphi}^{(i)}(\omega, q^2)$ have the form

† As follows from (3.12) $\omega_c=0$ at the point $\omega=0$, $q^2=-4\mu^2$ of interest to us, i.e., the Breit system coincides with the centre-of-mass system. This fact may, of course, be seen directly from an explicit expression for the components of nucleon and meson momenta in the Breit system.

$$\mathrm{Re}\,[\tilde{f}^{(1)}(\omega, q^2)]-\mathrm{Re}[\tilde{f}^{(1)}(\omega_0, q^2)]=\frac{2}{\pi}(\omega^2-\omega_0^2)\int_{\omega_1}^{\infty}\omega'\,\mathrm{d}\omega'\,\frac{\mathrm{Im}\,f^{(1)}(\omega', q^2)}{(\omega'^2-\omega^2)(\omega'^2-\omega_0^2)},$$

$$\mathrm{Re}\,[\tilde{f}^{(2)}(\omega, q^2)]-\frac{\omega}{\omega_0}\mathrm{Re}[f^{(2)}(\omega_0, q^2)-f_{\mathrm{p}}{}^{(2)}(\omega_0, q^2)]$$

$$=\frac{2}{\pi}\omega(\omega^2-\omega_0^2)\int_{\omega_1}^{\infty}\mathrm{d}\omega'\,\frac{\mathrm{Im}\,f^{(2)}(\omega', q^2)}{(\omega'^2-\omega^2)(\omega'^2-\omega_0^2)}, \qquad (3.15)$$

$$\mathrm{Re}\,[\tilde{\varphi}^{(1)}(\omega, q^2)]=\frac{2\omega}{\pi}\int_{\omega_1}^{\infty}\mathrm{d}\omega'\,\frac{\mathrm{Im}\,\varphi^{(1)}(\omega', q^2)}{\omega'^2-\omega^2},$$

$$\mathrm{Re}\,[\tilde{\varphi}^{(2)}(\omega, q^2)]=\frac{2}{\pi}\int_{\omega_1}^{\infty}\omega'\,\mathrm{d}\omega'\,\frac{\mathrm{Im}\,\varphi^{(2)}(\omega', q^2)}{\omega'^2-\omega^2},$$

where ω_1 is the minimum energy at which the meson+nucleon states become possible:

$$\omega_1=\frac{m\mu-\frac{1}{4}\mathbf{q}^2}{(m^2+\frac{1}{4}\mathbf{q}^2)^{\frac{1}{2}}}$$

(the energy which corresponds to ω_1 in the centre-of-mass system of meson and nucleon being equal to μ), and ω_0 is a certain fixed energy. There is no need to perform subtraction in the latter two relations (3.15). Indeed, the scattering amplitude with spin-flip should decrease with energy as any amplitude of a inelastic process [18]). Hence it follows that when energy increases, the function φ_{c} decreases sufficiently rapidly and the integral converges without any additional subtraction.

The values $f_{\mathrm{p}}{}^{(1)}$ and $f_{\mathrm{p}}{}^{(2)}$ which enter (3.15) are easily calculated if the expression for the polar term (2.25) is written

$$\begin{aligned}
&g^2v'^*\Bigg\{-\omega\left[\frac{1}{2E\omega+\mu^2+\frac{1}{2}\mathbf{q}^2}+\frac{1}{2E\omega-\mu^2-\frac{1}{2}\mathbf{q}^2}\right]\delta_{\alpha\beta}\\
&\quad-i\varepsilon_{\alpha\beta\gamma}\tau_\gamma\left[-\frac{\omega}{2E\omega-\mu^2-\frac{1}{2}\mathbf{q}^2}+\frac{\omega}{2E\omega+\mu^2+\frac{1}{2}\mathbf{q}^2}\right]\\
&\quad+\frac{i}{2m}\boldsymbol{\sigma}\cdot(\mathbf{k}_1\times\mathbf{k}'_1)\left[\left(\frac{1}{2E\omega+\mu^2+\frac{1}{2}\mathbf{q}^2}+\frac{1}{2E\omega-\mu^2-\frac{1}{2}\mathbf{q}^2}\right)\delta_{\alpha\beta}\right.\\
&\quad\left.-i\varepsilon_{\alpha\beta\gamma}\tau_\gamma\left(\frac{1}{2E\omega-\mu^2-\frac{1}{2}\mathbf{q}^2}-\frac{1}{2E\omega^2+\mu+\frac{1}{2}\mathbf{q}^2}\right)\right]\Bigg\}v\\
&\equiv v'^*\{f_{\mathrm{p}}{}^{(1)}(\omega, q^2)\delta_{\alpha\beta}-i\varepsilon_{\alpha\beta\gamma}\tau_\gamma f_{\mathrm{p}}{}^{(2)}(\omega, q^2)+i\boldsymbol{\sigma}\cdot\mathbf{k}_1\times\mathbf{k}'_1[\varphi_{\mathrm{p}}{}^{(1)}(\omega, q^2)\delta_{\alpha\beta}\\
&\qquad-i\varepsilon_{\alpha\beta\gamma}\tau_\gamma\varphi_{\mathrm{p}}{}^{(2)}(\omega, q^2)]\}v.
\end{aligned} \qquad (3.16)$$

Let us express f and φ in the subtraction and integral terms of (3.15) through scattering amplitudes in the centre-of-mass system and let us select the

threshold energy ω_0 as μ in this system (i.e., $\omega_0 = \omega_1$ in the Breit system). Then, after substituting $f_p^{(1)}$ and $f_p^{(2)}$ from (3.16), the dispersion relations for $f^{(1)}$, $f^{(2)}$ and $\varphi^{(2)}$ which are of interest to us will have the form

$$\tilde{f}^{(1)}(\omega, q^2) = \frac{m+\mu}{m} f_c^{(1)}(\mu, q^2) + \frac{g^2}{m} + \frac{2}{\pi}(\omega^2-\omega_1^2)\int_\mu^\infty \frac{d\omega'}{d\omega'_c} d\omega'_c \omega' \frac{E'_c+\omega'_c}{m} \frac{\operatorname{Im} f_c^{(1)}(\omega', q^2)}{(\omega'^2-\omega^2)(\omega'^2-\omega_1^2)},$$

$$\tilde{f}^{(2)}(\omega, q^2) = \frac{\omega}{\omega_1}\frac{m+\mu}{m} f_c^{(2)}(\mu, q^2) + \frac{g^2}{2m}\frac{\mu^2+\frac{1}{2}\mathbf{q}^2}{m\mu-\frac{1}{4}\mathbf{q}^2}\frac{\omega}{\omega_1} + \frac{2\omega}{\pi}(\omega^2-\omega_1^2)\int_\mu^\infty \frac{d\omega'}{d\omega'_c} d\omega'_c \frac{E'_c+\omega'_c}{m} \frac{\operatorname{Im} f_c^{(2)}(\omega', q^2)}{(\omega'^2-\omega^2)(\omega'^2-\omega_1^2)}, \tag{3.17}$$

$$\tilde{\varphi}^{(2)}(\omega, q^2) = \frac{2}{\pi}\int_\mu^\infty \frac{d\omega'}{d\omega'_c} d\omega'_c \omega' \frac{\operatorname{Im} \varphi_c^{(2)}(\omega', q^2)}{(\omega'^2-\omega^2)}.$$

We have neglected small corrections of the order $(\mu/m)^2$ in the polar terms in the right hand side of (3.17) and dropped the sign of Re in the left hand side of (3.17) since we are interested in the values of ω close to 0 and $q^2 = 4\mu^2$ where the amplitude is real. In the integral terms of (3.17) we have changed to integration with respect to meson energy in the centre-of-mass system ω'_c so that the lower limit of integration has proved to be equal to μ.

Calculation of the right hand side of (3.17), and, in particular, of the value of the amplitude in the non-physical region may be performed along these lines (cf. ref. [19]) and ref. [10])). If $\mathbf{q}^2$ is fixed, physically realizable states begin with $\omega_{c,\min} = \sqrt{(\mu^2+\frac{1}{4}\mathbf{q}^2)}$ so that a region from $\omega'_c = \mu$ to $\omega'_c = \omega_{c,\min}$ is non-physical. If, however, we make use of the expansion of the scattering amplitude in Legendre polynomial (3.14) it can easily be seen that the values of scattering phases $\delta_l(\omega_c)$ will always be reached for physical values $k_c > 0$, and non-physical elements will be contained only in non-physical values of $\cos\theta_c$: $|\cos\theta_c| > 1$. The analytic continuation of the Legendre polynomials $P_l(\cos\theta_c)$ for the values $|\cos\theta_c| > 1$ is well known and consequently the integral in the right hand side of (3.17) will be calculated with adequate accuracy, provided we do not go beyond the region in which the analytic continuation of $f_c(\omega_c, q^2)$ and $\varphi_c(\omega_c, q^2)$ with respect to q^2 is justified.

As for the problem of meson-nucleon scattering in the perturbation theory, it is shown [20]) that the singularity closest to the point $q^2 = 0$, where we begin to continue $f(\omega, q^2)$ and $\varphi(\omega, q^2)$ analytically, lies at $q^2 = 4\mu^2$, and it may well be expected that an analytic continuation is possible when $q^2 < 4\mu^2$. This singularity is related to meson-nucleon scattering through an intermediate two-meson state and has the nature of a branching point of the $\sqrt{4\mu^2-q^2}$ type.

As is well known, a power series in x for functions of the $(1-x)^{\frac{1}{2}}$ type is absolutely convergent at the point $x = 1$ and yields a correct (vanishing) value of the function. This makes it possible to extend the analytic continuation to the point $q^2 = 4\mu^2$ as well, and consequently the values $f_c(\omega_c, 4\mu^2)$, $\varphi_c(\omega_c, 4\mu^2)$ may be obtained through the analytic continuation of $f_c(\omega_c, q^2)$, $\varphi_c(\omega_c, q^2)$ from small values of q^2. The terms containing singularities in such analytic continuation are found to vanish. The latter result agrees with the observation in the footnote to sec. 2, where it was shown that the terms proportional to $\sqrt{4\mu^2-q^2}$ yield a small contribution of an order of $1/L$ which may be discarded in zero approximation †.

From all that has been stated above it follows that we can calculate the right hand side of (3.17) if we write the scattering amplitude as in (3.14), take scattering phases from experiment and analytically continue the Legendre polynomials $P_l(\cos\theta_c)$ to the values $\cos\theta_c = 1+2\mu^2/k_c^2$.

For practical purposes it is sufficient to consider only 3 phases δ_1, δ_3 and δ_{33} in expansion (3.14). The dependence of these phases on energy is taken according to Orear's phase analysis [21]):

$$\delta_1 = 0.16\frac{k_c}{\mu}, \quad \delta_3 = -0.11\frac{k_c}{\mu}, \quad \operatorname{ctg}\delta_{33} = \left(\frac{\mu}{k_c}\right)^3 (8.05-3.8\omega^*)\omega^*,$$

$$\mu\omega^* = E_c+\omega_c-m.$$

Calculation yields

$$\frac{m+\mu}{m} f_c^{(1)}(\mu, 4\mu^2) = \frac{0.70}{\mu},$$

$$-\frac{2}{\pi}\omega_1^2\int_\mu^\infty \frac{d\omega'}{d\omega'_c}d\omega'_c \frac{E'_c+\omega'_c}{m\omega'}\frac{\operatorname{Im} f_c^{(1)}(\omega'_c, 4\mu^2)}{\omega'^2-\omega_1^2} = -\frac{0.23}{\mu},$$

$$\frac{m+\mu}{m\omega_1} f_c^{(2)}(\mu, 4\mu^2) = \frac{0.23}{\mu^2}, \tag{3.18}$$

$$-\frac{2}{\pi}\omega_1^2\int_\mu^\infty \frac{d\omega'}{d\omega'_c}d\omega'_c \frac{E'_c+\omega'_c}{m\omega'^2}\frac{\operatorname{Im} f_c^{(2)}(\omega', 4\mu^2)}{\omega'^2-\omega_1^2} = -\frac{0.047}{\mu^2},$$

$$\frac{2}{\pi}\int_\mu^\infty \frac{d\omega'}{d\omega'}d\omega'_c \frac{1}{\omega'}\operatorname{Im}\varphi_c^{(2)}(\omega', 4\mu^2) = \frac{0.028}{\mu^2}.$$

Adding (3.18) and the values of polar terms (when $g^2 = 14.5$) we obtain

† It will be noted that since the terms having the branching point $q^2 = 4\mu^2$ in the imaginary part of the scattering amplitude are strictly equal to 0 when $q^2 < 4\mu^2$, these terms will have no effect at all on the analytic continuation of Im $f_c(\omega'_c q^2)$ (or Im $\varphi_c(\omega'_c, q^2)$ up to $q^2 = 4\mu^2$. The argument cited in the text is important only for the terms Re $f_c^{(1)}(\omega_0, q^2)$ in (3.17).

$$\tilde{f}^{(1)}(0, 4\mu^2) = \frac{g^2}{\mu}\left(\frac{\mu}{m} + \frac{0.70}{g^2} - \frac{0.23}{g^2}\right) = 0.18\frac{g^2}{\mu},$$

$$\frac{\partial}{\partial\omega}\tilde{f}^{(2)}(\omega, 4\mu^2)\,|_{\omega=0} = \frac{g^2}{\mu^3}\left(-0.0085 + \frac{0.23}{g^2} - \frac{0.047}{g^2}\right) = 0.0041\frac{g^2}{\mu^2}, \quad (3.19)$$

$$\tilde{\varphi}^{(2)}(0, 4\mu^2) = 0.0126\frac{g^2}{m\mu^2}.$$

Hence, using (3.9), we obtain for the values in (3.6)

$$\tilde{L}^{(1)}(0, 4\mu^2) = 1.2\frac{g^2}{m}, \quad \left.\frac{\partial\tilde{L}^{(2)}(\nu, 4\mu^2)}{\partial\nu}\right|_{\nu=0} = 0.029\frac{g^2}{m\mu^2},$$
$$\tilde{M}^{(2)}(0, 4\mu^2) = -0.025\frac{g^2}{\mu^2}. \quad (3.20)$$

Let us discuss the accuracy of the results thus obtained. As follows from (3.19) and (3.17), the main contribution (over 80 %) to the computation of the principal term $\tilde{L}^{(1)}(0, 4\mu^2)$ is made by the subtraction of the polar term $f_p^{(1)}(\omega_0, 4\mu^2)$ which is calculated exactly. The contribution of the integral term in $f^{(1)}$ (3.17) is below 10 %, and therefore any uncertainty which may arise through inaccurate calculation at large energies does not exceed 1 % in $\tilde{L}^{(1)}$ (actually the integral converges already at energies $\omega_c \approx 2.5\mu$ and uncertainty in its value does not apparently exceed 10 %). The contribution of the subtraction term $f_c^{(1)}(\mu, 4\mu^2)$ to $L^{(1)}$ is about 25 %. In its computation the p-phase is of principal importance since the terms conditioned by the p-phase do not vanish at the fixed q^2 and $k_c \to 0$. The calculation of D phases, according to the data of Mukhin and Pontecorvo [22]), changes $f_c^{(1)}(\mu, 4\mu^2)$ by 7 % in the most unfavourable case ($\delta_{3,\,j=\frac{1}{2}} = -0.21(\pi/180)(k_c/\mu)^5$, $\delta_{3,\,j=\frac{1}{2}} = 0$). The inaccuracy in $f^{(1)}(\mu, 4\mu^2)$ occurs largely because the function $f_c^{(1)}(\mu, q^2)$ has a singularity of $\sqrt{(4\mu^2-q^2)}$ type (cf. the footnote to p. 192), and the computation of $f_c^{(1)}(\mu, 4\mu^2)$ through analytic continuation of merely S, P and D amplitudes with respect to q^2 is not adequate. It may be supposed that $f_c^{(1)}(\mu, 4\mu^2)$ may contain an error of 25 % and consequently the value $\tilde{L}^{(1)}(0,4\,\mu^2)$ is determined within an accuracy of 5 to 7 %. It is assumed that meson-meson scattering is not abnormally large and the singular part $\tilde{f}_c^{(1)}(\mu, q^2)$ does not contain a large coefficient. This assumption may be wrong if meson-meson scattering has a resonance at small energies. In this case higher phases should be drawn upon to evaluate the accuracy of $\tilde{f}_c^{(1)}(\mu, 4\mu^2)$. An appraisal obtained on the basis of the D phase may prove not to be sufficiently accurate, since data on higher phases are absent and information on the inaccuracy of the experiments [22]) is not available.

The terms $\partial L^{(2)}/\partial\nu$ and $M^{(2)}$ are considerably less than $L^{(1)}$ and therefore an

error in calculating the former will have no practical effect on further results. The main error occurs due to an inaccurate calculation of the integral of the imaginary part $\varphi_c^{(2)}(\omega', q^2)$ at large energies and may apparently reach 15 to 20 %.

Substitution of $f_{\alpha\beta}$ in (2.29) as $f_{p,\alpha\beta}+\tilde{f}_{\alpha\beta}$ leads to a sum of several terms among which heavy cancellation occurs, as is shown in the following sections. In other words, if $f_{\alpha\beta}$ is replaced by the first approximation of the perturbation theory the result will be grossly in error). This compensation of $f_{p,\alpha\beta}$ and $\tilde{f}_{\alpha\beta}$ greatly increases errors in determining the value of $\tilde{L}^{(1)}(0, 4\mu^2)$. Concrete computation of two-meson phases and their comparison with one-meson phases will be performed in the following sections.

4. Calculation of Two-Meson Amplitude

According to formulas (2.25), (3.1), (3.6) and (3.20), the meson-nucleon scattering amplitude $f_{\alpha\beta}$ may be written as follows:

$$f_{\alpha\beta}(p_1, p_1+q; k+\tfrac{1}{2}q, k-\tfrac{1}{2}q) = f_{p,\alpha\beta}+\tilde{f}'_{\alpha\beta}+\tilde{f}''_{\alpha\beta},$$

$$f_{p,\alpha\beta} = g^2\tau_\alpha\tau_\beta \frac{-k}{(k+\frac{1}{2}q)^2+2p_1(k+\frac{1}{2}q)} + g^2\tau_\beta\tau_\alpha \frac{k}{(k-\frac{1}{2}q)^2-2p_1(k-\frac{1}{2}q)}, \tag{4.1}$$

$$\tilde{f}'_{\alpha\beta} = \frac{g^2}{m}\alpha\delta_{\alpha\beta}, \quad \tilde{f}''_{\alpha\beta} = \frac{g^2}{\mu^2} i\varepsilon_{\alpha\beta\gamma}\tau_\gamma\left(\beta_1 k+\beta_2\frac{p_1 k}{m}\right)$$

$$(\alpha = 1,2; \quad \beta_1 = 0.025, \quad \beta_2 = -0.029).$$

Substituting (4.1) in (2.29) and discarding the quadratic term in $\tilde{f}''_{\alpha\beta}$ (the contribution to the phases from this term contains an additional factor $1/L$), we obtain

$$M^{(2)}(q^2) = \frac{g^4}{\pi m}\left[\frac{3\alpha^2}{4}B_0 - \frac{3\alpha}{2}B_1+\tau_\alpha^{(1)}\tau_\alpha^{(2)}B_2+(3+2\tau_\alpha^{(1)}\tau_\alpha^{(2)})B_3+(3-2\tau_\alpha^{(1)}\tau_\alpha^{(2)})B_4\right],$$

$$B_0 = \frac{2}{i}\int \Delta(k, q)\mathrm{d}^4k(\bar{u}_{p_1+q}u_{p_1})(\bar{u}_{p_2-q}u_{p_2}),$$

$$B_1 = \frac{2m}{i}\int\left[\frac{(\bar{u}_{p_1+q}|k|u_{p_1})(\bar{u}_{p_2-q}u_{p_2})}{(k+\frac{1}{2}q)^2+2p_1(k+\frac{1}{2}q)} + \frac{(\bar{u}_{p_2-q}|k|u_{p_2})(\bar{u}_{p_1+q}u_{p_1})}{(k-\frac{1}{2}q)^2+2p_2(k-\frac{1}{2}q)}\right]\Delta(k, q)\mathrm{d}^4k, \tag{4.2}$$

$$B_2 = -\frac{2m^2}{i\mu^2}\int\left[\frac{\left(\bar{u}_{p_1+q}\left|\beta_1 k+\beta_2\frac{p_1 k}{m}\right|u_{p_1}\right)(\bar{u}_{p_2-q}|k|u_{p_2})}{(k-\frac{1}{2}q)^2+2p_2(k-\frac{1}{2}q)}\right.$$

$$\left. + \frac{(\bar{u}_{p_1+q}|k|u_{p_1})\left(\bar{u}_{p_2-q}\left|\beta_1 k+\beta_2\frac{p_2 k}{m}\right|u_{p_2}\right)}{(k+\frac{1}{2}q)^2+2p_1(k+\frac{1}{2}q)}\right]\Delta(k, q)\,\mathrm{d}^4k,$$

$$B_3 = = \frac{m^2}{i}\int \frac{(\bar{u}_{p_1+q}|k|u_{p_1})(\bar{u}_{p_2-q}|k|u_{p_2})\Delta(k,q)\mathrm{d}^4k}{[(k+\frac{1}{2}q)^2+2p_1(k+\frac{1}{2}q)][(k-\frac{1}{2}q)^2+2p_2(k-\frac{1}{2}q)]},$$

$$B_4 = -\frac{m^2}{i}\int \frac{(\bar{u}_{p_1+q}|k|u_{p_1})(\bar{u}_{p_2-q}|k|u_{p_2})\Delta(k,q)\mathrm{d}^4k}{[(k+\frac{1}{2}q)^2+2p_1(k+\frac{1}{2}q)][(k+\frac{1}{2}q)^2-2p_2(k+\frac{1}{2}q)]}, \tag{4.2}$$

$$\Delta(k,q) = [(k-\tfrac{1}{2}q)^2-\mu^2]^{-1}[(k+\tfrac{1}{2}q)^2-\mu^2]^{-1}.$$

Introducing the Feynman parameter x as usual we write B_0 in the form

$$B_0 = \frac{2w}{i}\int_0^1 \mathrm{d}x \int \mathrm{d}^4k[k^2-\mu^2+\tfrac{1}{4}q^2-qk(1-2x)]^{-2}, \tag{4.3}$$

$$w = (\bar{u}_{p_1+q}u_{p_1})(\bar{u}_{p_2-q}u_{p_2}). \tag{4.4}$$

The integral with respect to d^4k in (4.3) diverges at infinity, but the contribution from large momenta is an additive constant which generally does not depend on q^2 and may be omitted. We obtain the finite contribution by differentiating (4.3) with respect to μ^2, then integrating with respect to d^4k and again integrating with respect to μ^2. Finally, integrating over $\mathrm{d}x$, we obtain a singular part of the integral in the form

$$B_0 = -\frac{ws}{\sqrt{1-s^2}}\operatorname{arctg}\frac{\sqrt{1-s^2}}{s} \tag{4.5}$$

where

$$s = \sqrt{1-\frac{q^2}{4\mu^2}}. \tag{4.6}$$

Here we have chosen the branch which is positive in the physical region. In this case $s = -i|s|$ on the upper side of the cut.

Further on we shall confine ourselves to considering a singlet amplitude in non-relativistic approximation and shall calculate the matrix element of type (4.4) for this case alone (cf. (4.16) and (4.23)). Expanding w in powers of p^2/m^2 and substituting $\cos\theta = 1+2\xi^2$, we obtain, including the terms quadratic in p^2/m^2, †

$$w = 1+\frac{p^2}{2m^2}(1-\cos\theta) = 1-\varepsilon^2,\ \varepsilon^2 = \mu^2/m^2. \tag{4.7}$$

Expanding (4.5) in powers of s^2 and retaining the leading term, we finally obtain

$$B_0 = -\tfrac{1}{2}\pi(1-\varepsilon^2)s. \tag{4.8}$$

† It will be noted that there are no corrective terms closest to those written in (4.7) (p^4/m^4 in the present case). Similar cancellations take place in the matrix elements (4.16) and (4.23).

For the integration we introduce two Feynman parameters x_1 and x_2 into B_1 (noting that $2p_1q = -q^2$, $2p_2q = q^2$):

$$B_1 = \frac{4m}{i}\int_0^1 dx_2 \int_0^{1-x_2} dx_1 \int d^4k \left\{ \frac{(u_{p_1+q}|k|u_{p_1})(u_{p_2-q}u_{p_2})}{(k^2-2\bar{p}k-\Delta)^3} + \ldots \right\}, \tag{4.9}$$

$$\bar{p} = -\tfrac{1}{2}q+qx_1-p_1x_2, \qquad \Delta = -\tfrac{1}{4}q^2-p_1qx_2+\mu^2(1-x_2).$$

The dots denote a similar term in which p_1 is replaced by p_2. Integrating over to d^4k we obtain

$$B_1 = w\int_0^1 dx_2 \int_0^{1-x_2} \frac{x_2}{b^2}\, dx_1, \tag{4.10}$$

$$b^2 = x_2^2+\varepsilon^2(1-x_2)-4\varepsilon^2(1-s^2)x_1(1-x_1-x_2).$$

Making the variable substitution $x_1 = \frac{1}{2}(1-\varepsilon y-z)$, $x_2 = \varepsilon y$, and integrating over dz, we obtain

$$B_1 = \frac{w}{\sqrt{1-s^2}}\int_0^{1/\varepsilon} \frac{y}{a} \operatorname{arctg} \frac{(1-\varepsilon y)\sqrt{1-s^2}}{a}\, dy, \tag{4.11}$$

where

$$a^2 = s^2+\varepsilon(1-2s^2)y+[1-\varepsilon^2(1-s^2)]y^2. \tag{4.12}$$

For small s^2 small values of y are of importance in (4.11) and therefore arctg $[(1-\varepsilon y)\sqrt{(1-s^2)}/a]$ may be replaced by $\frac{1}{2}\pi$. (It is shown in the Appendix that we shall thereby obtain the exact value of the singular part of the integral (4.11)). After this the integral is easily calculated, the upper limit yielding a term, non-singular in the neighbourhood of $s^2 = 0$, which may be discarded. Expanding the integral in powers of s^2 and ε^2 and substituting (4.7) we obtain

$$B_1 = -\tfrac{1}{2}\pi(1+\tfrac{1}{2}\varepsilon^2)[s-\tfrac{1}{2}\varepsilon \ln(\varepsilon+2s)]. \tag{4.13}$$

The integral B_1 corresponds to the interference term which has already been considered in sec. 2, and its discontinuity across the cut coincides with (2.28).

As was stated above, in calculating phases we shall be concerned only with such cases when $|2s| \gg \varepsilon$ in the effective region of integration in (2.15) (which corresponds to $L \ll 4m^2/\mu^2$). We do not therefore expand the terms of type $\ln(\varepsilon+2s)$ in powers of s^2. Since $s > 0$ in the physical region the argument of the logarithm in (4.13) does not vanish. Yet this argument vanishes on another sheet of the Riemann surface where $s < 0$ and consequently there is a singularity on this sheet when $4s^2 = \mu^2/m^2$, or $q^2 = 4\mu^2-\mu^4/m^2$.

The integral B_2 is written in the form

$$B_2 = -\frac{4}{\varepsilon^2}\int_0^1 dx_2 \int_0^{1-x_2} dx_1\, F,$$

$$F = \frac{1}{i}\int d^4k \left[\frac{(\bar{u}_{p_1+q}|k|u_{p_1})\left(\bar{u}_{p_2-q}\left|\beta_1 k+\beta_2\frac{\hat{p}_2 k}{m}\right|u_{p_2}\right)}{(k^2-2\bar{p}k-\Delta)^3} + \ldots \right] \tag{4.14}$$

where the values $\bar{p}$ and Δ are determined in (4.9) and the dots denote a similar term where p_1 is replaced by p_2. Differentiating F with respect to μ^2 and integrating over d^4k we obtain

$$\frac{dF}{d\mu^2} = \frac{1-x_2}{4}\left\{\frac{m^2x_2^2\beta_1 w_1 + x_2[x_2(m^2+2p^2)+\frac{1}{4}q^2(1-2x_1)]\beta_2 w}{(\bar{p}^2+\Delta)^2} - \frac{1}{2}\frac{\beta_1 w_2+\beta_2 w_1}{\bar{p}^2+\Delta}\right\}, \tag{4.15}$$

where

$$w_1 = \frac{1}{2m}\left[(\bar{u}_{p_2-q}u_{p_2})(\bar{u}_{p_1+q}|p_2|u_{p_1}) + (\bar{u}_{p_2-q}|p_1|u_{p_2})(\bar{u}_{p_1-q}u_{p_1})\right],$$

$$w_2 = (\bar{u}_{p_1+q}|\gamma_\alpha|u_{p_1})(\bar{u}_{p_2-q}|\gamma_\alpha|u_{p_2}).$$

Including the terms quadratic in p^2/m^2 and ε^2,

$$w_1 = 1 + \left(\frac{p^2}{m^2}\right)[2-\tfrac{1}{2}(1-\cos\theta)] = 1 + \frac{2p^2}{m^2} + \varepsilon^2,$$
$$w_2 = 1 + \frac{2p^2}{m^2}. \tag{4.16}$$

Further calculations do not offer any difficulty. Discarding the terms non-singular in the neighbourhood of $s^2 = 0$, using (4.7) and (4.16), and introducing the notation

$$\beta = -(\beta_1+\beta_2)\left(1 + \frac{2p^2}{m^2} + \tfrac{5}{2}\varepsilon^2\right) - 2\varepsilon^2\beta_1 \tag{4.17}$$

we obtain

$$B_2 = -\tfrac{1}{4}\pi\beta[s - \tfrac{1}{2}\varepsilon \ln(\varepsilon+2s)]. \tag{4.18}$$

We proceed to the calculation of the integrals B_3 and B_4 which correspond to the contributions of the fourth order of the perturbation theory. Introducing four Feynman parameters and integrating over d^4k we obtain

$$B_3 = \tfrac{1}{4}m^2\int dx_1\,dx_2\,dx_3\,dx_4\,\delta(\textstyle\sum x_i - 1)\left[\frac{(\bar{u}_{p_2-q}|h|u_{p_2})(\bar{u}_{p_1+q}|h|u_{p_1})}{(h^2+\Delta)^2} - \frac{1}{2}\frac{w_2}{h^2+\Delta}\right], \tag{4.19}$$

$$B_4 = -\tfrac{1}{4}m^2\int dx_1\,dx_2\,dx_3\,dx_4\,\delta(\textstyle\sum x_i - 1)\left[\frac{(\bar{u}_{p_2-q}|h'|u_{p_2})(\bar{u}_{p_1+q}|h'|u_{p_1})}{(h'^2+\Delta)^2} - \frac{1}{2}\frac{w_2}{h'^2+\Delta}\right], \tag{4.20}$$

where

$$h = p_2x_1 + p_1x_2 - \tfrac{1}{2}q(x_1 - x_2 + x_3 - x_4),$$
$$h' = p_2x_1 - p_1x_2 - \tfrac{1}{2}q(x_1 + x_2 + x_3 - x_4),$$
$$\Delta = \mu^2(x_3+x_4) - \tfrac{1}{4}q^2(1-2x_1-2x_2).$$

Noting that the numerator in (4.19) may be, written within an accuracy p^2/m^2, ε^2, in the form (cf. (4.22))

$$(\bar{u}_{p_2-q}|h|u_{p_2})(\bar{u}_{p_1+q}|h|u_{p_1}) = m^2(x_1+x_2)^2 w_1,$$

we transform B_3 as follows:

$$B_3 = -\tfrac{1}{4}\left(\tfrac{1}{2}w_2+w_1\frac{\partial}{\partial\gamma}\right)_{\gamma=1}\int \mathrm{d}x_1\mathrm{d}x_2\mathrm{d}x_3\mathrm{d}x_4\,\delta(\textstyle\sum x_i-1)$$
$$\cdot\left\{\gamma(x_1+x_2)^2+\varepsilon^2[x_3+x_4-4(1-s^2)x_3x_4]+4\left[\frac{p^2}{m^2}+\varepsilon^2(1-s^2)\right]x_1x_2\right\}^{-1}.$$

Making the variable substitution $x_1 = \frac{1}{2}\varepsilon(x+y)$, $x_2 = -x_1+\varepsilon y$, $x_3 = \frac{1}{2}(1-x_1-x_2-z)$ and integrating over $\mathrm{d}z$ we obtain

$$B_3 = -\frac{1}{4\sqrt{1-s^2}}\left(\tfrac{1}{2}w_2+w_1\frac{\partial}{\partial E^2}\right)\int_0^{1/\varepsilon}\mathrm{d}y\int_0^{v}\frac{\mathrm{d}x}{b_1}\,\mathrm{arctg}\,\frac{(1-\varepsilon y)\sqrt{1-s^2}}{b_1},$$

$$b_1^2 = s^2+\varepsilon(1-2s^2)y+E^2y^2-\left[\frac{p^2}{m^2}+\varepsilon^2(1-s^2)\right]x^2,\quad E^2 = 1+\frac{p^2}{m^2}.$$

Just as in calculating B_1 and B_2, we substitute $\frac{1}{2}\pi$ for arctg in the integrand and integrate the result over $\mathrm{d}x$:

$$B_3 = -\frac{\pi}{8\sqrt{1-s^2}}\left(\tfrac{1}{2}\omega_2+\omega_1\frac{\partial}{\partial E^2}\right)$$
$$\cdot\int_0^{1/\varepsilon}\frac{\mathrm{d}y}{\sqrt{\frac{p^2}{m^2}+\varepsilon^2(1-s^2)}}\,\arcsin\left(\frac{y}{a_1}\sqrt{\frac{p^2}{m^2}+\varepsilon^2(1-s^2)}\right),$$

$$a_1^2 = s^2+\varepsilon(1-2s^2)y+E^2y^2.$$

When p^2/m^2, $\varepsilon^2 \ll 1$, the arcsin may be expanded into a series (of which we keep two terms), after which integration over $\mathrm{d}y$ and then differentiation with respect to E^2 yield, for $|s|^2 \ll 1$,

$$B_3 = -\frac{\pi}{16}\left\{(1+4\varepsilon^2)s-\varepsilon(1+\tfrac{5}{2}\varepsilon^2)\ln(\varepsilon+2s)+(1+\varepsilon^2)\frac{\varepsilon s}{\varepsilon+2s}\right\}. \qquad (4.21)$$

For calculating B_4 we must know the numerator in (4.20) more accurately:

$$(\bar{u}_{p_2-q}|h'|u_{p_2})(\bar{u}_{p_1+q}|h'|u_{p_1}) = m^2(x_1-x_2)^2w_1+m^2x_1x_2w_3, \qquad (4.22)$$

$$w_3 = -\frac{4p^4}{m^4}\left[1-\tfrac{1}{2}(1-\cos\theta)\right] = -\frac{4p^2}{m^2}\left(\frac{p^2}{m^2}+\varepsilon^2\right). \qquad (4.23)$$

Making the variable substitution $x_2 = \frac{1}{2}(1-x_3-x_4-\varepsilon z)$, $x_3 = \frac{1}{2}(1-\varepsilon y-x)$, $x_4 = 1-\varepsilon y-x_3$ and integrating the result over dz, we obtain

$$B_4 = \tfrac{1}{4}\mathscr{L}\frac{1}{E}\int_0^{1/\varepsilon} dy \int_0^{1-\varepsilon v} dx \frac{1}{b_2} \operatorname{arctg} \frac{yE}{b_2},$$

$$\mathscr{L} = \tfrac{1}{2}w_2 + (w_1 - \tfrac{1}{4}w_3)\frac{\partial}{\partial E^2} - \tfrac{1}{4}w_3 \frac{\partial}{\partial (p^2/m^2)}, \qquad E^2 = 1 + \frac{p^2}{m^2}, \tag{4.24}$$

$$b_2^2 = s^2 + \varepsilon(1-2s^2)y - \left[\frac{p^2}{m^2} + \varepsilon^2(1-s^2)\right] y^2 + (1-s^2)x^2.$$

Calculation of B_4 (cf. the Appendix) yields the following result in non-relativistic approximation:

$$B_4 = -\tfrac{1}{16}\pi \left\{(1+3\varepsilon^2)s - \varepsilon(1+\tfrac{3}{2}\varepsilon^2)\ln(\varepsilon+2s) + \frac{\varepsilon}{2Ev}\ln\frac{2Es+\varepsilon v}{\xi E(1+v)} - i\pi\frac{\varepsilon}{4v\sqrt{1-s^2}}\right\}, \tag{4.25}$$

$$v = \sqrt{1+\frac{4s^2}{\xi^2}}. \tag{4.26}$$

The branch of the root (4.26) is determined similarly to (4.6) with the cut from $s^2 = -\frac{1}{4}\xi^2$ to $-\infty$. A characteristic of this part of the amplitude is the second singularity when $v = 0$, which corresponds to $q^2 = 4\mu^2(1+\frac{1}{4}\xi^2)$ with a singularity of the $[4\mu^2(1+\frac{1}{4}\xi^2)-q^2]^{-\frac{1}{2}}$ type. When $\frac{1}{4}\xi^2 \ll 1$ the second point is in the neighbourhood of the first point ($s^2 = 0$) and when $\xi^2 \to \infty$ it recedes from the first point ($s^2 = 0$) and when $\xi^2 \to \infty$ it recedes from the first one to an infinitely large distance; therefore the terms in (4.25) singular only at the second point will contribute to the phases only for the case $\frac{1}{4}\xi^2 \lesssim 1/L$. As a result, expansion is performed in powers of ξ^2 when such terms are calculated, which ensures the calculation of phases with errors $\lesssim 1/L$ (cf. the Appendix). The last term in (4.25) is the only term in the entire two-meson amplitude which yields any contribution to $\operatorname{Im} I_l^{(2)}$, and therefore it is calculated accurately for any $s^2 \leqq 0$, since the neighbourhood of the second singular point $|s| \approx \frac{1}{2}\xi$ is an effective region of integration over $|s|$ for $\operatorname{Im} I_l^{(2)}$.

Substituting the results (4.8), (4.13), (4.18), (4.21) and (4.25) in (4.2) we obtain the following expression for the singular part of the singlet amplitude ($|s|^2 \ll 1$ and $|v|^2 \ll 1$):

$$M^{(2)}(s^2) = -\tfrac{3}{8}\frac{g^4}{m}\left\{c_0 s + \varepsilon c_1 \ln(\varepsilon+2s) + \varepsilon c_2 \frac{s}{\varepsilon+2s} + \varepsilon\frac{3-2\lambda_\tau}{12}\left[\frac{1}{Ev}\ln\frac{2Es+\varepsilon v}{\xi E(1+v)} - \frac{i\pi}{2v\sqrt{1-s^2}}\right]\right\}, \tag{4.27}$$

$$c_0 = (\alpha-1)^2+(\tfrac{7}{2}-\alpha-\alpha^2)\varepsilon^2+\tfrac{1}{3}\lambda_\tau(\varepsilon^2+2\beta),$$
$$c_1 = \alpha-1+(\tfrac{1}{2}\alpha-2)\varepsilon^2-\tfrac{1}{3}\lambda_\tau(\varepsilon^2+\beta), \qquad (4.27)$$
$$c_2 = \frac{3+2\lambda_\tau}{6}(1+\varepsilon^2)$$

where λ_τ is the eigenvalue of the operator $\tau_a^{(1)}\tau_a^{(2)}$. In calculating the amplitude the corrections of the first order of the power expansion in ε^2 and $p^2/m^2 = \varepsilon^2/\xi^2$ are taken into account.

5. Calculation of Two-Meson Phases

To calculate two-meson singlet phases we have only to integrate the scattering amplitude over $|s|$ along the cut, using relation (2.15) for every function in (4.27).

Noting that the discontinuity across the cut for the function s has the form $\Delta s = -2i|s|$ we obtain, for the contribution of this function to I_l,

$$[s]_l = -\frac{4\xi^2}{\sqrt{\pi}} L^{-\frac{1}{2}} Q_l(1+2\xi^2). \qquad (5.1)$$

Substituting the discontinuity of the function $\ln(\varepsilon+2s)$, equal to $-2i$ arctg $(2|s|/\varepsilon)$, in (2.15) we obtain, for the relevant contribution to I_l,

$$[\ln(\varepsilon+2s)]_l = -\frac{16\xi^2}{\pi} Q_l(1+2\xi^2)\int_0^\infty e^{-L|s|^2} \operatorname{arctg}\frac{2|s|}{\varepsilon}\cdot|s|\mathrm{d}|s|. \qquad (5.2)$$

We calculate the integral (5.2) by first differentiating it with respect to ε:

$$\frac{\partial}{\partial\varepsilon}\int_0^\infty e^{-L|s|^2} \operatorname{arctg}\frac{2|s|}{\varepsilon}|s|\mathrm{d}|s| = -\tfrac{1}{4}\sqrt{\frac{\pi}{L}}+\tfrac{1}{8}\varepsilon\pi\, e^{\frac{1}{4}\varepsilon^2 L}[1-\Phi(\tfrac{1}{2}\varepsilon\sqrt{L})], \qquad (5.3)$$

where $\Phi(\frac{1}{2}\varepsilon\sqrt{L})$ is a probability integral.

If we confine ourselves to considering not very large angular momenta, the parameter $\zeta = \frac{1}{2}\varepsilon\sqrt{L} \ll 1$. At any energy it is sufficient for this to limit l by the inequality

$$l \ll \frac{4}{\varepsilon^2} = 180. \qquad (5.4)$$

Now expanding (5.3) in powers of ζ we obtain, after integration with respect to ε (taking account of the values of (5.2) at $\varepsilon = 0$),

$$[\ln(\varepsilon+2s)]_l = -4\xi^2 Q_l(1+2\xi^2)L^{-1}\left[1-\frac{2}{\sqrt{\pi}}\zeta+\ldots\right]. \qquad (5.5)$$

It will be noted that both terms written in (5.5) may be easily obtained directly from (5.2) by expanding arctg $(2|s|/\varepsilon)$ in powers of $\varepsilon/2|s|$, yet the next terms of the expansion in ζ cannot be obtained in this way, since the integrals, of each individual term will diverge, nor can the residue of the series be integrated term by term. The expansion in $\varepsilon/2|s|$ is possible because $2|s| \gg \varepsilon$ in the effective region of integration if the condition (5.4) is fulfilled.

For the term $s/(\varepsilon+2s)$ we obtain, after expanding in powers of $\varepsilon/2|s|$,

$$\Delta \frac{s}{\varepsilon+2s} = -\frac{2i\varepsilon|s|}{\varepsilon^2+4|s|^2} = -\frac{i\varepsilon}{2|s|} + \dots$$
$$\left[\frac{s}{\varepsilon+2s}\right]_l = -\frac{2}{\sqrt{\pi}}\xi^2\varepsilon L^{-\frac{1}{2}}Q_l(1+2\xi^2). \tag{5.6}$$

As in the previous case we obtain the first term of the power expansion in ζ.

In integrating the remaining terms we shall consider two regions of integration separately: $0 \leqq |s| \leqq \frac{1}{2}\xi$ (from the first singular point to the second) and $\frac{1}{2}\xi \leqq |s|$ (beyond the second point). For the function $[\ln(2Es+\varepsilon v) - \ln E\xi(1+v)]/Ev$ we have in the first region

$$\Delta \frac{1}{Ev}\ln\frac{2Es+\varepsilon v}{E\xi(1+v)} = -\frac{2i}{Ev}\operatorname{arctg}\frac{2E|s|}{\varepsilon v} = -\frac{2i}{Ev}\left(\frac{\pi}{2} - \frac{\varepsilon v}{2E|s|} + \dots\right) \tag{5.7}$$

The first term of the expansion in $\varepsilon/2|s|$ yields the contribution to I_l:

$$-\frac{8\xi^2}{E}Q_l(1+2\xi^2)\int_0^{\frac{1}{2}\xi} e^{-L|s|^2}\frac{|s|\mathrm{d}|s|}{\sqrt{1-4|s|^2/\xi^2}} = -\frac{4\xi^3}{E\sqrt{L}}Q_l e^{-\frac{1}{4}L\xi^2}\int_0^{\frac{1}{2}\sqrt{L}\,\xi} e^{x^2}\mathrm{d}x. \tag{5.8}$$

In the second region,

$$\Delta \frac{1}{Ev}\ln\frac{2E|s|+\varepsilon v}{E\xi(1+v)} = \frac{2i}{Ev}\left[\ln(\varepsilon|v|+2E|s|) - \ln 2E|s|\right] = \frac{i\varepsilon}{E^2|s|} + \dots. \tag{5.9}$$

Uniting the contributions of the first term of the expansion (5.9) and of the second term in (5.7) we obtain

$$\frac{4\xi^2}{\sqrt{\pi}}\varepsilon L^{-\frac{1}{2}}\left(1-\frac{p^2}{m^2}\right)Q_l(1+2\xi^2). \tag{5.10}$$

We have substituted $E^2 = 1+p^2/m^2$ in (5.10) and considered the terms of the first order in p^2/m^2.

The last term in the amplitude of (4.27), proportional to $i/v\sqrt{(1-s^2)}$, is the only one contributing to Im $I_l^{(2)}$. The cut for this term begins only at the second point † and therefore we cannot use eq. (2.15) obtained for the initial point

† It is worthwhile to note that this result has no bearing on the approximation we have used (expansion in $1/L$) and holds good even for the exact scattering amplitude, i.e., the contribution to Im I_l yield the values $t \geqq t_\xi$.

$t = 1+2\xi^2$. In a perfectly similar way we can obtain for the initial point $t_\xi = 1+2\xi^2(1+\frac{1}{4}\xi^2)$ which corresponds to $v = 0$ $(q^2 = 4\mu^2(1+\frac{1}{4}\xi^2))$:

$$I_l = \frac{\xi^4}{\pi i} Q_l(t_\xi) \int_0^\infty e^{-L_\xi |v|^2} \Delta M(v^2) d|v|^2,$$
$$L_\xi = (l+1) \frac{\xi^3}{4\sqrt{(1+\frac{1}{4}\xi^2)[1+\xi^2(1+\frac{1}{4}\xi^2)}} \approx \frac{\xi^2}{4(1+\frac{1}{4}\xi^2)} L. \tag{5.11}$$

Substituting $i/v\sqrt{(1-s^2)} \approx i/v\sqrt{(1+\frac{1}{4}\xi^2)}$ in (5.11), we obtain, for the relevant contribution to I_l,

$$\left[\frac{i}{v\sqrt{1-s^2}}\right]_l = i2\xi^3(\pi L)^{-\frac{1}{2}} Q_l(t_\xi). \tag{5.12}$$

Collecting the results (5.1), (5.5), (5.6), (5.10) and (5.12) we obtain for the two-meson singlet integral

$$I_l^{(2)} = \frac{3g^4\xi^2}{2mE\sqrt{\pi}L^{\frac{3}{2}}} \left\{ Q_l(1+2\xi^2)[c_0+\zeta d_1+\zeta^2 d_2] + i\pi \frac{\lambda_\tau^2}{12\varepsilon} \xi\zeta^2 Q_l(t_\xi) \right\},$$
$$d_1 = 2\sqrt{\pi}\left[c_1 + \frac{3-2\lambda_\tau}{6}\left(1-\frac{p^2}{2m^2}\right)\psi(z)\right], \quad \psi(z) = z e^{-z^2}\int_0^z e^{x^2} dx, \quad z^2 = \tfrac{1}{4}L\xi^2,$$
$$d_2 = 2c_2 - 4c_1 - (1-\tfrac{2}{3}\lambda_\tau)\left(1-\frac{p^2}{m^2}\right), \quad \zeta = \tfrac{1}{2}\varepsilon\sqrt{L}. \tag{5.13}$$

Substituting numerical values for α and β, as well as the value $\varepsilon^2 = 0.022$ we have

$$c_0 = 0.06+0.01\lambda_\tau$$
$$d_1 = 0.6-0.03\lambda_\tau+0.6\lambda_\tau^2\psi(z)\left(1-\frac{p^2}{2m^2}\right), \tag{5.14}$$
$$d_2 = -0.7+\frac{p^2}{m^2}+\lambda_\tau\left(1.4-\frac{2}{3}\frac{p^2}{m^2}\right).$$

The scattering singlet phases are related to the integrals I_l in the following manner:

$$p \operatorname{Re} I_l = 2\sin 2\delta_l \approx 4\delta_l, \qquad p \operatorname{Im} I_l = 2(1-\cos 2\delta_l) \approx 4\delta_l^2.$$

Hence it follows that the two-meson phase $\delta_l^{(2)} = \varepsilon m \operatorname{Re} I_l^{(2)}/4\xi$ for large angular momenta (when $|\delta_l| \ll 1$), and $\operatorname{Im} I_l^{(2)}$ is proportional to the square of the one-meson phase $\delta_l^{(1)}$, whereas $\operatorname{Im} I_l^{(1)} = 0$ and the square of the "full"

phase $(\delta_l)^2 \approx (\delta_l^{(1)})^2$. The results obtained, (5.13) and (5.14), show that there is evidence of a heavy compensation of the contribution due to the perturbation theory (the graphs of the fourth order) and the terms obtained through dispersion relations (containing α and β). Besides, the terms containing β_1 and β_2 are cancelled (only the linear combination $\beta \ll \beta_1, \beta_2$ enters the final result), and consequently the part of the meson-nucleon scattering amplitude $\tilde{f}''_{\alpha\beta}$ (cf. (4.1)) makes a negligible contribution to (5.13).

Eq. (5.13) is the main part of the asymptotic expansion in the parameter $1/L$ (cf. sec. 2) and therefore its accuracy must in general be of the order $1/L$. As a consequence of the above-mentioned compensation in the main term the role of the next term of the asymptotic expansion may increase. For rough estimates the formula thus obtained may be used also in those cases when the expansion parameter $1/L$ is not very small.

TABLE 1

Relation between two-meson and one-meson phases

E_{lab} (MeV)	2.5	10	40	90	160	360	650
ζ	4	2	1	$\frac{3}{4}$	$\frac{1}{2}$	$\frac{1}{3}$	$\frac{1}{4}$
^1P	-0.08	-0.15	-0.2				
^1D	0.02	0.04	0.1	0.25			
^1F	-3×10^{-3}	-6×10^{-3}	-0.02	-0.04	-0.05	-0.1	
^1G	10^{-3}	3×10^{-3}	0.01	0.04	0.1	0.25	
^1H	-10^{-4}	-4×10^{-4}	-3×10^{-3}	-7×10^{-3}	-0.015	-0.035	-0.08

The table shows the values $\delta_l^{(2)}/\delta_l^{(1)}$ calculated for some l and ξ according to eqs. (5.13) and (2.9). It is clear that the one-meson ^1D phase for energies $E_{\text{lab}} \lesssim 40$ MeV, and the one-meson ^1F and ^1G phases for $E_{\text{lab}} \lesssim 150$ MeV may be used with a satisfactory degree of accuracy. These estimates are valid in order of magnitude for triplet phases as well. Hence it follows that in phase shift analyses for nucleon scattering all phases corresponding to $l \geqq 3$ may be regarded as one-meson phases for $E_{\text{lab}} \lesssim 150$ MeV and only S, P and D phases have to be determined from experiment.

6. Conclusion

The results we have obtained show that the nucleon-nucleon elastic scattering phases are determined by one-meson interaction even when angular momenta are not large. This fact may be essential in a phase shift analysis of nucleon-nucleon collisions, since there is no need to regard all included phases as

arbitrarily varied parameters, as has been already pointed out in refs. [25, 26]). If the two-meson amplitudes (5.13) prove to be considerably less than the one-meson amplitudes (2.9) for the given l and E, there is a sufficient reason to consider the relevant phases in one-meson approximation. Lack of full experimental data on nucleon-nucleon scattering apparently precludes the possibility to perform a unique phase-shift analysis of experimental data. Of all data on p—p scattering the best result (with an energy of 310 MeV) is yielded by 8 sets of phases [27]) out of which only two have phases with large l coinciding with one-meson phases. There is no doubt that the one-meson "tail" used within the limits pointed out in the present paper is bound to facilitate a phase-shift analysis.

The results of the present paper were essentially based on the use of dispersion relations for values of momentum transfer close to $4\mu^2$. Though there are no grounds to question the applicability of these relations under these conditions, an experimental check-up of the results thus obtained may throw some light on the problem of applicability of dispersion relations. Since we have discussed only singlet amplitude we naturally have not obtained a complete spin matrix scattering operator corresponding to two-meson exchange. Yet calculations for triplet states offer no essential difficulties and have been performed by one of us (A. F. G.) and I. Yu. Kobsarev.

Throughout the above discussion we expanded in powers of $1/L$, retaining only the first non-vanishing term and so the accuracy of our result should be within $1/L$. It is not difficult, however, to see that the basic formulas (2.12) and (2.20) will hold for considerably smaller limitations on the magnitude of the angular momentum. For their applicability it is sufficient for the following inequality to hold:

$$1 \gg \frac{Q_l(1+\frac{9}{2}\xi^2)}{Q_l(1+2\xi^2)} \approx \begin{cases} e^{-(l+\frac{1}{2})\xi} & \text{for} \quad \xi^2 \ll 1 \\ (\frac{4}{9})^{l+1} & \text{for} \quad \xi^2 \gg 1, \end{cases}$$

making it possible to neglect three-meson states in summation with respect to intermediate states in $A_1(E, q^2)$, eq. (2.20) holding as well. In this case, however, it is not permissible to confine oneself to calculation of $\tilde{f}_{\alpha\beta}$ at the point $\omega = 0$ and $q^2 = 4\mu^2$, but it is necessary to know the meson-nucleon scattering amplitude in a certain region close to this point. The problem of analytic continuation of the meson-nucleon scattering amplitude may therefore become much more complex. If, however, this analytic continuation were performed, it would yield sufficiently accurate expressions for two-meson phase nucleon-nucleon scattering even at smaller l. It should be emphasised that such inclusion of smaller l is essentially based on the results of Mandelstam [2]), while the results obtained in this paper are in fact based merely on the following: 1) the nearest singular point (except for the one-meson pole) lies at $q^2 = 4\mu^2$; 2) there are no other singular points close to $q^2 = 4\mu^2$. As a result of the above-mentioned heavy compensations of the main terms, inaccuracies in determining $\tilde{L}^{(1)}(0, 4\mu^2) = \alpha$

(cf. sec. 3) can radically change (by a factor 2, for example) the final data on the two-meson phases given in the table. If, on the other hand, the ratio $\delta_l^{(2)}/\delta_l^{(1)}$ for example, is below 10 %, these inaccuracies cannot alter the conclusion that the scattering phases are basically determined in the present case by one-meson interaction.

It has proved to be possible to express the nucleon-nucleon scattering due to two-meson exchange through π-meson-nucleon scattering and thus to establish a relation between these processes. This fact is no accident. If calculation for small l proves to be possible, the nucleon-nucleon scattering will be expressed through the meson-nucleon scattering amplitude, the $\pi+N\to 2\pi+N$ amplitude, etc.

The authors are indebted to L. D. Landau for numerous discussions, as well as to V. B. Berestestsky, L. B. Okun, A. P. Rudik, Ya. A. Smorodinsky, K. A. Ter-Martirosian and I. M. Shmushkevitch for a number of useful comments.

Appendix

1. CALCULATION OF B_1

To calculate the integral B_1 we introduce the auxiliary function

$$B_1(u)=\frac{1}{\sqrt{1-s^2}}\int_0^{1/\varepsilon}\frac{y}{a}\operatorname{arctg}\frac{(1-\varepsilon y)\sqrt{1-s^2}+u}{a}\,dy, \tag{A.1}$$

$$a^2=s^2+\varepsilon(1-2s^2)y+\left(1-\varepsilon^2(1-s^2)\right)y^2.$$

The wanted integral is equal to the value of this function at $u=0$, which may be written as

$$B_1(0)=B_1(\infty)-\int_0^\infty du\,\frac{\partial B_1(u)}{\partial u}, \tag{A.2}$$

$$B_1(\infty)=\frac{\pi}{2\sqrt{1-s^2}}\int_0^{1/\varepsilon}\frac{y\,dy}{a}, \tag{A.3}$$

$$\frac{\partial B_1(u)}{\partial u}=\frac{1}{\sqrt{1-s^2}}\int_0^{1/\varepsilon}\frac{y\,dy}{1-\varepsilon y+y^2+u^2+2(1-\varepsilon y)\sqrt{1-s^2}}, \quad u\geqq 0. \tag{A.4}$$

Let us consider the analytic properties of the functions (A.2), (A.3), (A.4) with respect to the variable s^2. The initial integral was an analytic function throughout the plane with a cut from $s^2=0$ to $-\infty$ (which corresponds to $q^2\geqq 4\mu^2$, $t\geqq 1+2\xi^2$). Since an additional singular point $s^2=1$ ($q^2=0$) appeared in the integral (A.3) it is necessary to make a second cut from $s^2=1$ to $+\infty$ ($q^2\leqq 0$, $t\leqq 1$) for (A.3). Integral (A.4) is analytical in the right

semi-plane as a function of the variable $\sqrt{(1-s^2)}$ and throughout the plane with a cut from $s^2=1$ to $+\infty$ as a function of s^2, since we put $\sqrt{(1-s^2)}>0$ when $s^2<1$. Since in calculating the phases it is necessary to integrate over the cut $s^2 \leqq 0$ ($q^2 \geqq 4\mu^2$), the contribution from the second term in (A.2) identically vanishes and this term may be discarded. The calculation of the remaining part is trivial enough. Thus, the above-stated method enabled us to obtain a singular term contributing to (2.15) out of the initial integral (4.11), thereby "spoiling" the behaviour of the function in another region which does not enter subsequent integration (2.15).

2. CALCULATION OF B_4

The integral B_4 corresponding to the Feynman graph of the fourth order shown in fig. 5, in contrast to the previous integrals, possesses this peculiarity:

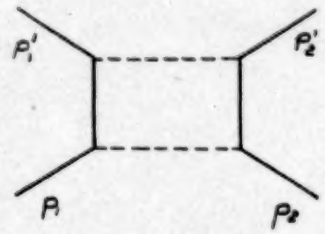

Fig. 5. The Feynman graph corresponding to the integral B_4.

the integrand of its parametric representation (4.23) is singular for any real q^2. This results in the real axis for the integral $B_4(q^2)$, formally considered for any complex q^2, being a singular line.

We show by direct calculation, however, that the function $B_4(q^2)$ may be continued analytically from the physical region throughout the entire plane with a cut from $q^2=4\mu^2$ to $+\infty$, which corresponds to the analytic continuation of the amplitude employed in sec. 2, this amplitude coinciding with the initial Feynman integral only in the upper semi-plane. It is precisely this function that we need for the calculation of the phases and we shall not introduce any special notation for it.

To compute the remaining integral in (4.24) over two parameters we introduce the function

$$f(u)=\int_0^{1/\varepsilon} dy \int_0^{1-\varepsilon y} dx \frac{1}{b_2} \operatorname{arctg} \frac{yE+u}{b_2}, \qquad (A.5)$$

$$b_2^2 = s^2+\varepsilon(1-2s^2)y-\left(\frac{p^2}{m^2}+\varepsilon^2(1-s^2)\right)y^2+(1-s^2)x^2-i0.$$

The infinitesimal addition $-i0$ is preserved for the correct selection of the (Feynman) amplitude. The wanted integral is equal to the value of $f(u)$ for $u=0$:

$$f(0) = f(\infty) - \int_0^\infty du\, \frac{\partial f(u)}{\partial u},$$

$$f(\infty) = \tfrac{1}{2}\pi \int_0^{1/\varepsilon} dy \int_0^{1-\varepsilon y} \frac{dx}{b_2} = \frac{\pi}{2\sqrt{1-s^2}} \int_0^{1/\varepsilon} [\ln (R_1 + \sqrt{1-s^2}(1-\varepsilon y)) - \ln R] dy, \tag{A.6}$$

$$R^2 = s^2 + \varepsilon(1-2s^2)y - \left(\frac{p^2}{m^2} + \varepsilon^2(1-s^2)\right) y^2 - i0,$$

$$R_1^2 = 1 - \varepsilon y - \frac{p^2}{m^2} y^2 - i0, \tag{A.7}$$

$$\frac{\partial f(u)}{\partial u} = \int_0^{1/\varepsilon} dy \int_0^{1-\varepsilon y} dx\, \frac{1}{s^2 + \varepsilon(1-2s^2)y + \left[E^2 - \frac{p^2}{m^2} - \varepsilon^2(1-s^2)\right] y^2 + (1-s^2)x^2 + 2Eyu + u^2},$$

$$u \geqq 0. \tag{A.8}$$

The integrand in (A.7) is still singular all along the real axis and therefore s^2 should be regarded as real in subsequent integration over dy and the result of integration should be analytically continued into a non-physical region. The integrand (A.8) is singular only for $s^2 \leqq 0 (q^2 \geqq 4\mu^2)$, i.e., the second term (A.6) is an analytic function throughout the plane with a cut from $s^2 = 0$ to $-\infty$. After integrating over dx, (A.8) has the form

$$\frac{\partial f(u)}{\partial u} = \frac{1}{\sqrt{1-s^2}} \int_0^{1/\varepsilon} \frac{dy}{q^2} \operatorname{arctg} \frac{\sqrt{1-s^2}(1-\varepsilon y)}{a_2},$$

$$a_2^2 = s^2 + \varepsilon y(1-2s^2) + \left[E^2 - \left(\frac{p_2}{m^2} + \varepsilon(1-s^2)\right)\right] y^2 + 2Eyu + u^2. \tag{A.9}$$

Out of this integral let us obtain the term singular on the cut by introducing another auxiliary parameter, just as has been done in (A.1) and (A.2):

$$\frac{\partial f(u)}{\partial u} = \frac{\partial f(u, \infty)}{\partial u} - \int_0^\infty dv\, \frac{\partial^2 f(u, v)}{\partial u\, \partial v}, \tag{A.10}$$

$$\frac{\partial f(u, \infty)}{\partial u} = \frac{\pi}{2\sqrt{1-s^2}} \int_0^{1/\varepsilon} \frac{dy}{a_2}, \tag{A.11}$$

$$\frac{\partial^2 f(u, v)}{\partial u \partial v} = \int_0^{1/\varepsilon} \frac{1}{1 - \varepsilon y + \left[E^2 - \frac{p^2}{m^2}\right] y^2 + 2Eyu + u^2 + v^2 + 2(1-\varepsilon y)v\sqrt{1-s^2}},$$

$$u, v \geqq 0. \tag{A.12}$$

The second term in (A.10) may be discarded since it is an analytic function for $\mathrm{Re}\, s^2 < 1$ ($\mathrm{Re}\, q^2 > 0$). An additional singular point $s^2 = 1$ and a second cut from $s^2 = 1$ to $+\infty (q^2 \leqq 0)$ appears in the remaining singular part (A.11). Let us substitute (A.10) and (A.11) in (A.6) and integrate over du. At the upper limit the integral diverges but the dependence on s^2 vanishes and therefore it is necessary to retain only the contribution from the lower limit †. Thus the singular part contributing to (2.15) has the form

$$f = f(\infty) + \frac{\pi}{2\sqrt{1-s^2}} \int_0^{1/\varepsilon} dy \ln [R_2 + Ey],$$
$$R_2^2 = s^2 + \varepsilon y(1-2s^2) + \left[E^2 - \left(\frac{\hat{p}^2}{m^2} + \varepsilon^2(1-s^2)\right)\right] y^2 - i0. \tag{A.13}$$

The integrals over dy which remain in (A.13) are calculated exactly, since after integration by parts and elimination of irrationalities in the denominator the integrals are reduced to elementary integrals:

$$f(\infty) = i\pi \frac{2\frac{\hat{p}^2}{m^2} + \varepsilon^2}{4P^2 \frac{\hat{p}}{m}} \ln \frac{\varepsilon - 2i\frac{\hat{p}}{m}}{\varepsilon} - \frac{\pi K_1}{4\sqrt{1-s^2}} \ln(-K_1) + \frac{\pi K_2}{4\sqrt{1-s^2}} \ln K_2$$
$$+ i\pi^2 \frac{\varepsilon(1-2s^2)}{8P^2\sqrt{1-s^2}} - \pi \frac{\varepsilon(1-2s^2)}{8P^2\sqrt{1-s^2}} \ln\left(4\frac{\hat{p}^2}{m^2} + \varepsilon^2\right) - \frac{\pi K}{8P^2\sqrt{1-s^2}} \ln \frac{2\sqrt{1-s^2}\frac{\hat{p}}{m} - iK}{2\sqrt{1-s^2}\frac{\hat{p}}{m} + iK}$$
$$+ \frac{\pi\varepsilon(1-2s^2)}{8P^2\sqrt{1-s^2}} \ln\left\{\frac{1}{4P^2}(F_1 - KF_2)(F_1 + KF_2)\right\} + \frac{\pi K}{8P^2\sqrt{1-s^2}} \ln \frac{F_1 - KF_2}{F_1 + KF_2},$$
$$F_1 = 2\left(2\frac{\hat{p}^2}{m^2} + \varepsilon^2\right)(\sqrt{1-s^2} + 1 - s^2) + K^2, \tag{A.14}$$
$$F_2 = \varepsilon(1 + 2\sqrt{1-s^2}).$$

Here the notations are

$$P^2 = \frac{\hat{p}^2}{m^2} + \varepsilon^2(1-2s^2), \qquad K = \sqrt{4s^2\frac{\hat{p}^2}{m^2} + \varepsilon^2},$$
$$K_1 = \frac{1}{2P^2}(K + \varepsilon(1-2s^2)) - i0, \qquad K_2 = \frac{1}{2P^2}(K - \varepsilon(1-2s^2)).$$

† This can easily be seen if (A.6) is differentiated with respect to s^2 then integrated over du and again integrated over s^2.

The root K is selected so that it is positive in the physical region and the cut is directed from $s^2 = -\frac{1}{4}\xi^2$ to $-\infty(q^2 \geqq 4\mu^2(1+\frac{1}{4}\xi^2))$, the function (A.14) being analytic throughout the plane with the above-mentioned cut. Retaining only the terms singular for $s^2 < 1$ $(q^2 > 0)$, we obtain

$$f(\infty) = \frac{\pi}{4\sqrt{1-s^2}}\{-K_1 \ln(-K_1) + K_2 \ln K_2\}. \tag{A.15}$$

The second term in (A.13) is calculated in a similar way:

$$\int_0^{1/\varepsilon} dy \ln[R_2+Ey] = \frac{1}{\varepsilon}\left[\ln\left(\sqrt{E^2-\frac{p^2}{m^2}}+E\right)-1\right]+\tfrac{1}{2}K_1\ln(-K_1)$$

$$-\tfrac{1}{2}K_2\ln K_2+K_2\ln\left(\frac{1}{\varepsilon}+K_2\right)-\tfrac{1}{2}i\pi K_1+\frac{K}{2P^2}\ln(2Es+K)$$

$$-\frac{E\varepsilon(1-2s^2)}{2WP^2}\ln[2Ws+\varepsilon(1-2s^2)]+\tfrac{1}{2}(K_1+K_2)\ln(2P^2\varepsilon)$$

$$-\tfrac{1}{2}K_1\ln\left\{2\left(E+\sqrt{E^2-\frac{p^2}{m^2}}\right)\left[K\sqrt{E^2-\frac{p^2}{m^2}}+\varepsilon E(1-2s^2)\right]+\varepsilon K(K-\varepsilon)\right\}$$

$$-\tfrac{1}{2}K_2\ln\left\{2\left(E-\sqrt{E^2-\frac{p^2}{m^2}}\right)\left[K\sqrt{E^2-\frac{p^2}{m^2}}+\varepsilon E(1-2s^2)\right]+\varepsilon K(K+\varepsilon)\right\}$$

$$+\frac{\varepsilon E(1-2s^2)}{2WP^2}\ln\left(2W\frac{\sqrt{E^2-\frac{p^2}{m^2}}}{\varepsilon}+2\frac{E^2-\frac{p^2}{m^2}}{\varepsilon}-\varepsilon\right)$$

where $W^2 = E^2-P^2$. Discarding the terms non-singular for $s^2 < 1$, as well as the last term singular for $W = 0$ (which correspond to $q^2 = 4M^2$), and adding to (A.15), we obtain the exact singular part of the initial integral (for $4\mu^2 \leqq q^2 < 4M^2$):

$$f = \frac{\pi}{2\sqrt{1-s^2}}\left\{-\frac{E\varepsilon(1-2s^2)}{2WP^2}\ln[2Ws+\varepsilon(1-2s^2)]\right.$$

$$+\frac{K}{2P^2}\ln(2Es+K)-\frac{i\pi K}{4P^2}+K_2\ln\left(2\frac{p^2}{m^2}+\varepsilon^2+\varepsilon K\right) \tag{A.16}$$

$$-\tfrac{1}{2}K_1\ln\left\{2\left(E+\sqrt{E^2-\frac{p^2}{m^2}}\right)\left[K\sqrt{E^2-\frac{p^2}{m^2}}+\varepsilon E(1-2s^2)\right]+\varepsilon K(K-\varepsilon)\right\}$$

$$\left.-\tfrac{1}{2}K_2\ln\left\{2\left(E-\sqrt{E^2-\frac{p^2}{m^2}}\right)\left[K\sqrt{E^2-\frac{p^2}{m^2}}+\varepsilon E(1-2s^2)\right]+\varepsilon K(K+\varepsilon)\right\}\right\}.$$

A characteristic of the functions $f(s^2)$ and $B_4(s^2)$ derived from $f(s^2)$ through application of a certain differential operator (see (4.24)) is the presence of two singular points: $s^2 = 0$ ($q^2 = 4\mu^2$) and $s^2 = -\frac{1}{4}\xi^2$ (the second point corresponding to the value $K = 0, q^2 = 4\mu^2(1+\frac{1}{4}\xi^2)$). For $\frac{1}{4}\xi^2 \ll 1$ the second point is in the neighbourhood of the first and for $\xi^2 \to \infty$ it is removed from the first to an infinitely great distance. It stands to reason that the terms singular only at the second point will contribute to (5.15) in integration only when $\frac{1}{4}\xi^2 \lesssim 1/L$, since for them the cut begins at $|s|^2 = \frac{1}{4}\xi^2$ and they will have an additional factor $\exp(-\frac{1}{4}L\xi^2)$, after integration, as compared with the terms singular at the first point. For this reason such terms in (A.16) may be expanded in powers of ξ^2, the main terms of the expansion being retained. The accuracy of the phases will be determined by the parameter $\xi^2 \exp(-\frac{1}{4}L\xi^2)$, vanishing at $\xi^2 \to 0$ (high energies) and at $\xi^2 \to \infty$ (low energies). The greatest error will be in the intermediate region $\frac{1}{4}\xi^2 \approx 1/L$ where this parameter reaches the maximum value $4/2.7L \approx 1/L$. But even in this region the expansion in ξ^2 ensures as great accuracy as the asymptotic expansion in $1/L$ we have used. Thus the corrections stemming from the next terms of the expansion in ξ^2 should be considered only in the next terms of the asymptotic expansion, which have the additional factor $1/L$. Besides, only the leading term of the power expansion in K^2 should be considered, just as we have considered only the leading term of the power expansion in s^2. Noting these considerations, let us simplify the last three terms in (A.16), after which we obtain, for $|s|^2 \ll 1$, $|K|^2 \ll \varepsilon^2$, in non-relativistic approximation,

$$f = \frac{\pi}{4P^2}\left\{-\frac{E\varepsilon}{W}\ln(2Ws+\varepsilon(1-2s^2))+K\ln\left(\frac{p}{m}\frac{2Es+K}{E(\varepsilon+K)}\right)-\frac{i\pi K}{2\sqrt{1-s^2}}\right\}. \quad \text{(A.17)}$$

The nearest correction terms of (A.17) vanish while the greatest of the remaining terms have the form $K\xi^4/P^2$, $(K/P^2)(p/m)^4$ and may be neglected. Treating (A.17) by the differential operator $\mathscr{L}(1/4E)$ (cf. (4.24)) we obtain the function $B_4(s^2)$ for $|s|^2 \ll 1$, $|K|^2 \ll \varepsilon^2$:

$$B_4 = \tfrac{1}{16}\pi\left\{(1+3\varepsilon^2)s-\varepsilon(1+\tfrac{3}{2}\varepsilon^2)\ln(\varepsilon+2s)\right.$$
$$\left.+\frac{\varepsilon^2}{2EK}\ln\left(\frac{p}{m}\frac{2Es+K}{E(\varepsilon+K)}\right)-\frac{i\pi\varepsilon^2}{4K\sqrt{1-s^2}}\right\}. \quad \text{(A.18)}$$

The last term in (A.18) is the only one contributing to $\operatorname{Im} I_t^{(2)}$, i.e., the cut begins at the second point $|s|^2 = \frac{1}{4}\xi^2$ ($q^2 = q_\xi^2 = 4\mu^2(1+\frac{1}{4}\xi^2)$) in computing $\operatorname{Im} I_t^{(2)}$. For this reason the conditions $|s|^2 \ll 1$, $|K|^2 \ll \varepsilon^2$ were not used in computing this term, which makes it possible to calculate $\operatorname{Im} I_t^{(2)}$ for any energy: the main contribution to the integration with respect to q^2 will now be made by the neighbourhood of $q^2 \approx q_\xi^2$.

References

1) L. B. Okun and I. Ya. Pomeranchuk, JETP **36** (1959) 300
2) S. Mandelstam, Phys. Rev. **112** (1958) 1344
3) H. Lehmann, K. Symanzik and W. Zimmermann, Nuovo Cimento **1** (1955) 205
4) M. Goldberger, Phys. Rev. **99** (1955) 979
5) V. Ya. Fainberg and Ye. S. Fradkin, DAN **109** (1956) 507
6) I. M. Ryzhik and I. S. Gradstein, Table of Integrals (Moscow 1951)
7) A. Salam, Nuovo Cimento **3** (1956) 424;
   A. Salam and W. Gilbert, Nuovo Cimento **3** (1956) 607
8) B. L. Ioffe, JETP **31** (1956) 583
9) Ye. S. Fradkin, JETP **31** (1956) 515
10) R. H. Gapps and G. Takeda, Phys. Rev. **103** (1956) 1877
11) R. I. Eden, Proc. Roy. Soc. A **210** (1952) 388
12) R. Karplus, S. M. Sommerfield and E. H. Wichman, Phys. Rev. **114** (1959) 376;
   L. D. Landau, Nuclear Physics **13** (1959) 181
13) R. P. Feynman, Phys. Rev. **76** (1949) 749, 769
14) N. N. Bogolyubov, B. V. Medvedev and M. K. Polivanov, Questions of Dispersion Relations (Moscow, 1959)
15) H. J. Bremerman, R. Oehme and J. E. Taylor, Phys. Rev. **109** (1958) 2178
16) H. Lehman, Nuovo Cimento **10** (1958) 579
17) N. N. Bogolyubov and D. V. Shirkov, Introduction to the Theory of Quantum Fields (Gostekhizdat, 1957) 404
18) I. Ya. Pomeranchuk, JETP **30** (1956) 423;
   L. B. Okun and I. Ya. Pomeranchuk, JETP **30** (1956) 424
19) M. L. Goldberger, Proc. Sixth Ann. Rochester Conf., 1956
20) K. Simanzik, Progr. Theor. Phys. **20** (1958) 690
21) J. Orear, Phys. Rev. **100** (1955) 288
22) A. I. Mukhin and B. M. Pontecorvo, JETP **31** (1956) 550
23) G. F. Chew, R. Karplus, S. Gasiorowicz and F. Zachariasen, Phys. Rev. **110** (1958) 265
24) P. Federbush, M. L. Goldberger and S. B. Treiman, Phys. Rev. **112** (1958) 642
25) A. F. Grashin, JETP **36** (1959) 1717
26) M. Morvavcsik, P. Cziffra, M. Mac Gregor and H. Stapp, Bull. Am. Phys. Soc. **4** (1959) 49
27) H. Stapp, T. Ypsilantis and N. Metropolis, Phys. Rev. **105** (1957) 302

1.B:7.C

Nuclear Physics **17** (1960) 218—226; © *North-Holland Publishing Co., Amsterdam*

Not to be reproduced by photoprint or microfilm without written permission from the publisher

ON PERIPHERAL NUCLEON-NUCLEON INTERACTION IN THE TWO-MESON APPROXIMATION

A. F. GRASHIN and I. Yu. KOBSAREV

The Institute of Theoretical and Experimental Physics of the Academy of Sciences of the USSR, Moscow

Received 18 January 1960

Abstract: Triplet nucleon-nucleon scattering phase shifts for non-relativistic energies are calculated in the two-meson approximation and compared with the one-meson phase shifts. The one-meson approximation is found to be accurate for all mixing parameters (beginning from $^3S-{}^3D$) and this permits one to use them in phase shifts analysis for selection of unique solution. The peripheral part of the effective two-meson potential corresponding to the derived scattering amplitude is also found in this paper.

1. Introduction

A method for calculation in the two-meson approximation of nucleon-nucleon scattering phase shifts for large orbital angular momenta has been proposed in ref. [1]). This method yields the leading terms of the expansion in the parameter $1/L = \sqrt{1+p^2/\mu^2}/(l+1)$ where μ is the π-meson mass and p is the nucleon momentum in the c.m.s. Concrete calculations were carried out for the singlet state [1]) in non-relativistic approximation, including the corrections $\propto p^2/m^2$, and the expansion in powers of a second parameter $\zeta = \frac{1}{2}\varepsilon\sqrt{L}(\varepsilon = \mu/m$, m is the nucleon mass) being also carried out. Thus the singlet phase shift is expressed as a double series in the parameters $1/L$ (leading term) and ζ (first three terms). The method proposed is therefore valid only in the intermediate region $1 \ll L \ll 4/\varepsilon^2$ and passage to the limit $l \to \infty$ cannot be carried out in the final formulas.

Calculations for the triplet state can be performed in the approximation described above in a similar way and this permits one to determine the scattering operator in the two-meson approximation. For comparison with various theoretical investigations and phenomenological models of nucleon interaction we have also computed the nucleon-nucleon potential corresponding to the derived two-meson scattering operator. The expansion into $1/x$ of the potential (x is the distance between the nucleons in units of $1/\mu$) corresponds to an expansion in $1/L$ of the phase shifts. This means that the present method permits one to obtain the peripheral part of the potential for distances $x > 1$ with an accuracy $\propto 1/x$.

2. Scattering Amplitudes and Phase Shifts

The only difference between the calculation of the scattering operator $M^{(2)}(q^2)$ in the vicinity of the first singularity † $q^2 = -4\mu^2$ and the calculation of the singlet amplitude performed in ref. [1]) is that the singlet matrix elements w, w_1, w_2, w_3 (see formulas (4.7), (4.16), (4.23) in ref. [1])) are replaced by the corresponding spin operators. Furthermore, when calculating the terms from the perturbation theory graphs, the terms $\propto s^2$ where $s^2 = 1+q^2/4\mu^2$ must be considered. Including the corrections $\propto p^2/m^2$ the non-exchange part of the scattering operator can be written in the form

$$M^{(2)}(q^2) = M_s(q^2)+i\mathbf{S}\cdot\frac{\mathbf{p}'\times\mathbf{p}}{m^2}M_{LS}(q^2)+\frac{(\boldsymbol{\sigma}^{(1)}\cdot\mathbf{q})(\boldsymbol{\sigma}^{(2)}\cdot\mathbf{q})}{m^2}M_T(q^2), \quad (1.1)$$

where

$$M_s = -\frac{3g^4}{8mE}\left\{c_{0s}s+c_{1s}\varepsilon\ln(\varepsilon+2s)+\tfrac{1}{8}(3+2\lambda_\tau)\frac{\varepsilon s}{\varepsilon+2s}\right.$$
$$\left.+\frac{3-2\lambda_\tau}{12E}\frac{\varepsilon}{v}\left[\ln\frac{2Es+\varepsilon v}{E(1+v)\mu/p}-\frac{i\pi}{2\sqrt{1-s^2}}\right]\right\},$$

$$c_{0s} = (\alpha-1)^2, \quad c_{1s} = \alpha-1;$$

$$M_{LS} = -\frac{3g^4}{8mE}\left\{c_{0(LS)}s+c_{1(LS)}\varepsilon\ln(\varepsilon+2s)+\frac{3+2\lambda_\tau}{12}\frac{\varepsilon s}{\varepsilon+2s}\right.$$
$$\left.+\frac{3-2\lambda_\tau}{12E}\frac{\varepsilon m^2}{p^2}\left(\frac{1}{v}-v\frac{\mu^2}{\mu^2+p^2}\right)\left[\ln\frac{2Es+\varepsilon v}{E(1+v)\mu/p}-\frac{i\pi}{2\sqrt{1-s^2}}\right]\right\},$$

$$c_{0(LS)} = -\tfrac{1}{2}(\alpha-1)^2+\frac{3-2\lambda_\tau}{12}\frac{\mu^2}{\mu^2+p^2}+\tfrac{2}{3}\lambda_\tau\beta_2,$$

$$c_{1(LS)} = -\tfrac{1}{2}\alpha-(1-2s^2)\frac{3-2\lambda_\tau}{12E}\frac{m^2}{\mu^2+p^2}-\tfrac{1}{3}\lambda_\tau\left(\beta_2+2\beta\frac{s^2}{\varepsilon^2}\right);$$

$$M_T = -\frac{3g^4}{8mE}\left\{c_{0T}s+c_{1T}\varepsilon\ln(\varepsilon+2s)\right.$$
$$\left.-\frac{3-2\lambda_\tau}{48E}\frac{\varepsilon v m^2}{\mu^2+p^2}\left[\ln\frac{2Es+\varepsilon v}{E(1+v)\mu/p}-\frac{i\pi}{2\sqrt{1-s^2}}\right]\right\},$$

$$c_{0T} = -\tfrac{1}{8}\left(1+\tfrac{1}{2}\frac{\mu^2}{\mu^2+p^2}\right)-\tfrac{1}{12}\lambda_\tau\left(1-\beta_1-\tfrac{1}{2}\frac{\mu^2}{\mu^2+p^2}\right),$$

† The notations introduced in ref. [1]) are employed in the present paper. However the square of the momentum transfer q^2 differs in sign from that adopted in ref. [1]). Our choice of sign is convenient since then $q^2 = \mathbf{q}^2$.

$$c_{1T}=\frac{3+2\lambda_\tau}{48}+(1-2s^2)\frac{3-2\lambda_\tau}{48}\frac{m^2+\frac{1}{2}\mu^2}{\mu^2+p^2}-\tfrac{1}{24}\lambda_\tau\beta_1\left(1-4\frac{s^2}{\varepsilon^2}\right);$$

$$E^2=1+\frac{p^2}{m^2},\quad \mathbf{S}=\tfrac{1}{2}(\boldsymbol{\sigma}^{(1)}+\boldsymbol{\sigma}^{(2)}),\quad v=\frac{\sqrt{4s^2p^2+\mu^2}}{\mu};$$

$$\alpha=1.2,\quad \beta_1=0.025,\quad \beta_2=-0.029,\quad \beta=-\beta_1-\beta_2;$$

λ_τ is the eigenvalue of the operator $\boldsymbol{\tau}^{(1)}\cdot\boldsymbol{\tau}^{(2)}$. By calculating in the total spin representation the matrix elements $M(S, S'_z, S_z, T)$ of the operator (1.1) and integrating over $|s|$ as in ref. [1]) one can obtain the coefficients of the expansion of the amplitudes in associated Legendre polynomials $a_l(S, S'_z, S_z, T)$. Triplet amplitudes corresponding to changes of the spin projection $|\Delta S_z|=1$ and 2 are expanded in the polynomials $P_l^{(1)}$ and $P_l^{(2)}$ and the expansion coefficients are expressed in terms of integrals over the cut with associated functions of the second kind $Q_l^{(1)}$ and $Q_l^{(2)}$. Replacing the associated functions by Q_l we obtain, with an accuracy $\propto 1/L$,

$$a_l(1,1,0,T)=-p\frac{4(\mu/p)^3}{i\pi l}\sqrt{1+\frac{\mu^2}{p^2}}\,Q_l\left(1+\frac{2\mu^2}{p^2}\right)\cdot\int_0^\infty e^{-L|s|^2}\Delta\left[\frac{M(1,1,0,T)}{\sin\theta}\right]|s|\mathrm{d}|s|,$$

$$a_l(1,1,-1,T)=-p\frac{2(\mu/p)^2}{i\pi l^2}\,Q_l\left(1+\frac{2\mu^2}{p^2}\right)\cdot\int_0^\infty e^{-L|s|^2}\Delta M(1,1,-1,T)|s|\mathrm{d}|s|,$$

where Δf is the discontinuity of the function f across the cut $q^2\leqq -4\mu^2$.

Finally, expressing the various phase shifts † in terms of the coefficients $a_l(S, S'_z, S_z, T)$ we can write them in the following form:

$$\eta_l^J=\frac{3g^4\varepsilon\mu/p}{8E\sqrt{\pi}L^{\frac{1}{2}}}\,Q_l\left(1+\frac{2\mu^2}{p^2}\right)\{d_0^J+2\sqrt{\pi}\zeta d_1^J+\zeta^2 d_2^J\}. \tag{1.2}$$

It is implied here that the upper index J for the singlet state must be dropped. For the coefficients of the ζ powers entering into (1.2) we obtain

$$d_0=(\alpha-1)^2,\quad d_1=\alpha-1+\tfrac{1}{6}(3-2\lambda_\tau)\left(1-\frac{p^2}{2m^2}\right)\psi(z),$$

$$d_2=-4(\alpha-1)+\frac{p^2}{m^2}+\tfrac{1}{3}\lambda_\tau\left(4-\frac{2p^2}{m^2}\right),$$

† Formulas (6) of ref. [2]) can be used for this purpose with an accuracy to terms $\infty 1/l$. The notations for phase shifts and amplitude expansion coefficients are identical to those introduced in ref. [2]) but only the real parts are of interest to us.

$$z^2 = \frac{L\mu^2}{4p^2}, \quad \psi(z) = z\exp(-z^2)\int_0^z \exp(x^2)\mathrm{d}x;$$

$$d_i^{\,l} = d_i, \quad d_i^{\,l\pm1} = d_i \pm \varepsilon\sqrt{\varepsilon^2 + \frac{p^2}{m^2}}\,D_i \quad (i = 0, 1, 2);$$

$$D_0 = (\alpha-1)^2 - \tfrac{4}{3}\lambda_\tau(\beta_2 - \tfrac{1}{2}\beta), \quad D_2 = -2(2\alpha+1),$$

$$D_1 = \alpha - (3-2\lambda_\tau)\left(1-\frac{p^2}{2m^2}\right)\frac{m^2}{3p^2}(\psi(z)-\tfrac{1}{2}) - \tfrac{1}{3}\lambda_\tau\frac{\beta}{\zeta^2}.$$

A triplet phase with $J = l$ and a singlet phase coincide and the triplet phases $\eta_l^{\,l\pm1}$ (with $J = l\pm1$) differ by the additional terms arising from the spin-orbit interaction.

The mixing parameter has the form

$$\xi_J = \frac{3g^4\varepsilon^3\mu/p}{8E\sqrt{\pi}L_J^{\frac{3}{2}}}\left(1+2\frac{\mu^2}{p^2}+2\frac{\mu}{p}\sqrt{1+\frac{\mu^2}{p^2}}\right)\cdot Q_{J+1}\left(1+2\frac{\mu^2}{p^2}\right)\{h_0+2\sqrt{\pi}\zeta h_1\}, \quad (1.3)$$

$$h_0 = 1-\tfrac{2}{3}\lambda_\tau\beta_1,$$

$$h_1 = -\frac{9+2\lambda_\tau}{24} - \frac{(3-2\lambda_\tau)(1-p^2/2m^2)m^2}{12(\mu^2+p^2)}\cdot\frac{\psi(z_J)}{z_J^{\,2}} + \frac{\lambda_\tau\beta_1}{6\zeta_J^{\,2}};$$

$$L_J = \frac{J+2}{\sqrt{1+p^2/\mu^2}}, \quad \zeta_J = \tfrac{1}{2}\varepsilon\sqrt{L_J}, \quad z_J^{\,2} = \frac{L_J\mu^2}{4p^2}.$$

Formulas (1.2) and (1.3) are the first terms of the expansion in $1/L$ and ζ. Corrections of the order of ε^2 have been neglected in the amplitude and phase shift calculations since their order of magnitude is the same as that of corrections $\propto 1/L$ to the subsequent terms of the expansion in ζ (note that $\varepsilon^2 = 4\zeta^2/L$). The interesting result is the strong compensation of contributions from perturbation theory in the $\eta_l^{\,J}$ phases and from the "smooth" part of the meson-nucleon amplitude containing the coefficient α (in the main terms there enters $\alpha-1 \ll \alpha, 1$). Contributions from terms of the meson-nucleon amplitude containing β_1 and β_2 are small and for rough estimates can be neglected.

An important result is the disappearance of the coefficient α from the mixing parameter ξ_J. This is due to the fact that the corresponding part of the meson-nucleon amplitude is independent of the spin variables and does not contribute to tensor forces. Since the coefficient β_1 in ξ_J yields a relatively small contribution, the mixing parameter can be described by perturbation theory with a

good accuracy. This permits one to derive for it formulas which are more accurate than (1.3) by considering the next terms of the expansion in $1/L$ †.

The ratios of the two-meson shifts (1.2), (1.3) to the corresponding one-meson phase shifts computed in ref. [2]) are presented in tables 1 and 2. The zero values in the tables signify that the phase shift ratios are less than 1 %; for the mixing parameters, ratios which were smaller than 0.1 % were replaced by zero. Phase

TABLE 1

Ratios of two-meson phases to one-meson phases for isospin $T = 1$.

E_{lab} (MeV)	10	40	100	200	300	400	670
$^1D_2$	0.04	0.1	0.25	0.5			
$^1G_4$	0	0.01	0.04	0.1	0.2	0.25	
$^3P_0$	0.06	0.03	0.02				
$^3P_1$	−0.07	−0.1	−0.15				
$^3P_2$	1	2	2				
ξ_2	−0.001	−0.003	−0.01	−0.02	−0.04	−0.05	
$^3F_2$	0.02	0.04	0.06	0.07	0.08	0.07	
$^3F_3$	−0.01	−0.02	−0.04	−0.08	−0.1	−0.15	
$^3F_4$	0.05	0.25	0.4	0.7	1	1	
ξ_4	0	0	−0.002	−0.008	−0.01	−0.02	−0.04
$^3H_4$	0	0.01	0.03	0.06	0.07	0.08	0.09
$^3H_5$	0	0.	−0.01	−0.03	−0.05	−0.07	−0.1
$^3H_6$	0.01	0.02	0.1	0.3	0.4	0.5	0.8

TABLE 2

Ratios of two-meson phases to one-meson phases for isospin $T = 0$.

E_{lab} (MeV)	10	40	100	200	300	400	670
$^1P_1$	−0.15	−0.2	−0.2				
$^1F_3$	−0.01	−0.02	−0.04	−0.07	−0.1	−0.1	
$^1H_5$	0	0	−0.01	−0.02	−0.03	−0.04	−0.08
ξ_1	−0.004	−0.02	−0.02	−0.015			
$^3D_1$	−0.07	−0.01	0.05	0.07			
$^3D_2$	0.02	0.03	0.03	0.04			
$^3D_3$	0.3	−0.6	−0.8	−0.8			
ξ_3	−0.001	−0.003	−0.006	−0.006	−0.005	−0.002	
$^3G_3$	−0.01	−0.02	0.01	0.03	0.05	0.06	
$^3G_4$	0	0.01	0.01	0.02	0.02	0.02	
$^3G_5$	0.02	−0.08	−0.2	−0.3	−0.3	−0.4	

shift ratios were not calculated in those cases when the parameter $1/L \geqq 1$. However, comparatively large values of the parameter $1/L\,(0.4-0.8)$ correspond to the ratios presented in the table and hence our results can be considered only

† For this purpose the exact singular part of the perturbation theory amplitudes should be used. For one of the perturbation theory graphs giving the anomal large contribution in (1.3) the exact singular part has been computed in ref. [1]).

as rough estimates and may be used only to determine the limits of applicability of the one-meson approximation.

It can be seen from the tables that the ratios for triplet phase shifts with $J = l+1$ are very large. As noted in ref. [2]) this is connected with the fact that the one-meson approximation yields an anomalous energy dependence p^{2l+3} for these phases. An interesting result is the high accuracy of all one-meson mixing parameters (beginning from ξ_1). This circumstance is important for comparison of the theoretical results with the experimental ones, since from the polarization data one can derive with a high degree of accuracy the experimental values of the mixing parameters. Thus comparison of the theoretical ξ_2 for p−p scattering at 310 MeV with the experimental values [3]) is sufficient to choose, only on the basis of this single parameter, two solutions from the eight found by Stapp *et al.* (the second and fourth solutions). A subsequent, more accurate analysis taking account of higher phase shifts in the one-meson approximation shows [4]) that these two solutions fuse into one (the second solution). The application of "peripheral" one-meson phase shifts (for which tables 1 and 2 yield ratios below, for example, 10 %) in the phase shift analysis may also permit one to obtain unique solutions for other energies.

Let us consider the analytical properties of the two-meson phase shifts in p^2. All the calculations in this paper as well as in ref. [1]) were performed for the physical energies. However, the method applied can be used as well for the case of unphysical energies. Therefore the formulas (1.2), (1.3) are also valid for the complex values of p^2 with an accuracy $\propto 1/|L|, |\zeta|^2$. In the unphysical region the two-meson phases have a branch point with a cut from $p^2 = -\mu^2$ to $-\infty$. The function $Q_l(1+2\mu^2/p^2)$ is uniquely determined on the whole plane with the cut, and for the analytical continuation of the function $\psi(z)$ occurring in (1.2), (1.3) it is convenient to use the expansion near $p^2 = 0 (z = \infty) \psi(z) = = \frac{1}{2}+\frac{1}{4}z^{-2}+ \ldots$ However, the integration over dq^2 by the method of steepest descent, as well as the expansion in s^2 for one of the graphs of the perturbation theory in the calculation of the two-meson phase shifts, is valid only if $|p^2+\mu^2| \gg \mu^2/|L|$. Thus, the formulas (1.2), (1.3) are not valid near the singular point $p^2 = -\mu^2$.

3. Nucleon-Nucleon Potential

The calculated two-meson phase shifts are determined by the interaction in the peripheral region $x > 1$ where it may be considered weak. This permits one to use the Born approximation for the construction of the potential † corresponding to the calculated amplitudes.

† It should be noted that, strictly speaking, there exists no potential in the usual sense describing nucleon-nucleon scattering. A reflection of this is that the equivalent potential derived by us depends on p^2 and is thus non-local. Moreover, for higher terms of our expansion the operation of construction of the potential is in general not unique.

Inverting the usual Born formula we obtain for the potential

$$U = -\frac{1}{2\pi^2 m}\int e^{i\mathbf{q}\cdot\mathbf{r}} M(q^2)\mathrm{d}\mathbf{q}. \tag{2.1}$$

Inserting the scattering operator (1.1) in (2.1) we obtain the potential in the form

$$U = U_s + \mathbf{L}\cdot\mathbf{S}U_{LS} + (\boldsymbol{\sigma}^{(1)}\cdot\boldsymbol{\nabla}_x)(\boldsymbol{\sigma}^{(2)}\cdot\boldsymbol{\nabla}_x)U_T, \tag{2.2}$$

where $\mathbf{L}\cdot\mathbf{S}$ is a spin-orbit operator with the eigenvalues $\frac{1}{2}[J(J+1)-l(l+1)+-S(S+1)]$; and the functions U_s, U_{LS}, U_T, after integration over the directions of vector $\mathbf{q}$, assume the form

$$\begin{aligned} U_s &= \frac{i}{\pi m r}\int_{-\infty}^{+\infty} e^{iqr} M_s(q^2) q\mathrm{d}q, \\ U_{LS} &= \frac{i}{\pi m^3 r}\frac{\partial}{\partial r}\frac{1}{r}\int_{-\infty}^{+\infty} e^{iqr} M_{LS}(q^2) q\mathrm{d}q, \\ U_T &= -\frac{i\mu^2}{\pi m^3 r}\int_{-\infty}^{+\infty} e^{iqr} M_T(q^2) q\mathrm{d}q. \end{aligned} \tag{2.3}$$

In order to integrate over $\mathrm{d}q$ we close the contour in the upper half-plane by circumventing the cut along the imaginary axis $\mathrm{Im}\, q \geqq 2\mu$. The integral over the infinite arc can yield a contribution only of the δ-like type when $M(q^2)$ does not decrease rapidly enough for $|q|^2 \to \infty$. Thus, the peripheral part of the potential is specified only by the integral over the cut, only a small region near the singularity $q = 2i\mu$ playing a role for $x \gg 1$. Changing to the variable s^2 and using the steepest descent method we obtain, with an accuracy to $1/x$,

$$\int_{-\infty}^{+\infty} e^{iqr} M(q^2)\cdot q\mathrm{d}q = 4\mu^2 e^{-2x}\int_0^{\infty} e^{-x|s|^2}\Delta M(s^2)\cdot|s|\mathrm{d}|s|. \tag{2.4}$$

The remaining integration over $\mathrm{d}|s|$ in (2.4) is identical to the integration of the discontinuity $\Delta M(s^2)$ performed during calculation of the phase shifts and differs from it only by formal replacement of the parameter L by x. Employing the results of the previous calculations and denoting by $d_1(x)$, $D_1(x)$, $h_1(x)$ the functions obtained by formal substitution $L \to x$ from the coefficients d_1, D_1, h_1 (see (1.2), (1.3)) we have, for $1 \ll x \ll 4/\varepsilon^2$,

$$U_s = -\frac{3g^4\varepsilon^2\mu}{4\sqrt{\pi}}\frac{e^{-2x}}{x^{\frac{1}{2}}}\{d_0+\varepsilon\sqrt{\pi x}\,d_1(x)+\tfrac{1}{4}\varepsilon^2 x\,d_2\}, \tag{2.5}$$

$$U_{LS} = -\frac{3g^4\varepsilon^4\mu}{4\sqrt{\pi}}\frac{e^{-2x}}{x^{\frac{1}{2}}}\{D_0+\varepsilon\sqrt{\pi x}\,D_1(x)+\tfrac{1}{4}\varepsilon^2 x\,D_2\}, \tag{2.6}$$

$$U_T = -\frac{3g^4\varepsilon^4\mu}{16\sqrt{\pi}}\frac{e^{-2x}}{x^{\frac{1}{2}}}\{h_0+\varepsilon\sqrt{\pi x}\,h_1(x)\}. \tag{2.7}$$

In accordance with the expansion of the phase shifts in $1/L$ and ζ the pre-exponential factors in the potentials are the leading terms of the expansion in $1/x$ and $\frac{1}{2}\varepsilon\sqrt{x}$. Therefore, in differentiating with respect to x in the tensor part of potential (2.2) and in the spin-orbit part (see (2.3)), only lowest order terms in $1/x$ should be retained.

The two-meson potential (2.2), (2.5), (2.6), (2.7), which is the next correction to the well-known one-meson potential (see for example ref. [5])) consists of central, spin-orbit and tensor parts. The interactions of the $\boldsymbol{\sigma}^{(1)} \cdot \boldsymbol{\sigma}^{(2)}$ and $(\boldsymbol{\sigma}^{(1)} \cdot \mathbf{L})(\boldsymbol{\sigma}^{(2)} \cdot \mathbf{L})$ types give corrections to the phases η_l^J of the order $1/L$, ε^2, which are not considered in our approximation. The tensor interaction gives corrections of the same order to the phases η_l^J, but, on the contrary, determine completely the mixing parameters. Therefore, we keep the tensor terms in the scattering operator (1.1) and in the potential (2.2) while dropping the interactions of the $\boldsymbol{\sigma}^{(1)} \cdot \boldsymbol{\sigma}^{(2)}$ and $(\boldsymbol{\sigma}^{(1)} \cdot \mathbf{L})(\boldsymbol{\sigma}^{(2)} \cdot \mathbf{L})$ types. The important feature of the two-meson potential is the essential energy dependence contained in the $\psi(\mu\sqrt{x}/2p)$ function. The ψ function can be replaced by a constant for $p^2/\mu^2 \ll \frac{1}{4}x$. Hence it follows that the region where the local potential exists is determined, not by the condition $p^2/m^2 \ll 1$ (non-relativistic region), but by the more stringent condition $p^2/\mu^2 \ll 1$.

The spin-orbit forces being absent in the one-meson approximation are of special interest. Some authors (Gammel and Thaler [8]) and Signell, Zinn and Marshak [6])) come to the conclusion that a strong spin-orbit interaction must be introduced to explain the experimental data on nucleon-nucleon scattering [6, 7, 8]) On the other hand, Otsuki *et al.* [9]) assert that the experimental data on nucleon-nucleon scattering at $E_{\text{lab}} \leqq 150$ MeV may be explained without the introduction of strong spin-orbit forces. In this connection it is interesting to compare the two-meson spin-orbit potential with the phenomenological potentials proposed by Gammel-Thaler [8]) and Signell-Zinn-Marshak [6]). The potential of Signell *et al.* [6]) has the form

$$U_{LS} = -(42 \text{ MeV})\frac{e^{-2x}}{x^2}. \tag{2.8}$$

The spin-orbit part of the Gammel-Thaler's potential [8]) in the intermediate region $x \approx 1$ coincides approximately with (2.8), but falls off much more rapidly in the peripherical region $x \gg 1$.

The two-meson LS-interaction has for $p^2/\mu^2 \ll \frac{1}{4}x$ the following form:

$$U_{LS}^{(2)} \approx \tfrac{1}{4}g^4\varepsilon^3\mu(3-2\lambda_\tau)\frac{e^{-2x}}{x^4}. \tag{2.9}$$

The spin-orbit interaction for $p^2/\mu^2 \gg \frac{1}{4}x$ is much weaker and has the opposite sign:

$$U_{LS}^{(2)} \approx -\tfrac{1}{8}g^4\varepsilon^5\mu\frac{e^{-2x}}{x^3}\left(6\alpha+(3-2\lambda_\tau)\frac{m^2}{p^2}\right). \tag{2.10}$$

For the iso-spin $T = 1$, and an energy of, for example, $E_{\text{lab}} = 200$ MeV, this gives

$$U_{LS}^{(2)} \approx -(5 \text{ MeV}) \frac{e^{-2x}}{x^3}.$$

The authors are indebted to L. B. Okun and I. Ya. Pomeranchuk for useful discussions.

Note added in proof: The potential obtained above is equivalent to the peripheral two-meson amplitude only in the first Born approximation (pseudo-potential). It was found that a 'true' potential with a wide region of locality $p^2/m^2 \ll 1$ may be obtained if one makes use of a correct method of construction taking into account higher Born approximations (A. F. Grashin and Yu. P. Nikitin, JETP, in press).

References

1) A. D. Galanin, A. F. Grashin, B. L. Ioffe and I. Ya. Pomeranchuk, Nuclear Physics **17** (1960) 181 ; JETP **37** (1959) 1663; **38** (1960) 475
2) A. F. Grashin, JETP **36** (1959) 1717
3) H. Stapp, T. Ypsilantis and N. Metropolis, Phys. Rev. **105** (1957) 302
4) P. Cziffra, M. MacGregor, M. Moravcsik and H. Stapp, Phys. Rev. **114** (1959) 880; M. Mac Gregor, M. Moravcsik and H. Stapp, Phys. Rev. **116** (1959) 1248
5) H. Bethe and F. Hofman, Mesons and Fields, vol. II.
6) P. Signell, R. Zinn and R. Marshak, Phys. Rev. Letters **1** (1959) 416
7) S. Ohnuma and D. Feldman, Phys. Rev. **102** (1956) 1641
8) J. Gammel and R. Thaler, Phys. Rev. **107** (1957) 291
9) S. Otsuki, Progr. Theor. Phys. **20** (1958) 171
10) W. Watari, Progr. Theor. Phys. **20** (1958) 181; R. Tomagaki, Progr. Theor. Phys. **20** (1958) 503

8.B

Nuclear Physics **17** (1960) 227—237; © *North-Holland Publishing Co., Amsterdam*

Not to be reproduced by photoprint or microfilm without written permission from the publisher

ON THE INTERACTION HAMILTONIAN FOR THE DECAY OF Σ-HYPERONS

SHOICHI HORI

Instituttet for Teoretisk Fysik, Copenhagen, Denmark †

Received 1 February 1960

Abstract: The interaction Hamiltonian for the decay of Σ-hyperons is phenomenologically constructed under the assumptions that: 1) the spin of the Σ-hyperon is $\frac{1}{2}$, 2) the CP-invariance holds, 3) the effects of the final state interactions are negligible, 4) $\tau(\Sigma_-) = 2\tau(\Sigma_+)$, 5) the branching ratio $w(\Sigma_+ \to p+\pi_0)/w(\Sigma_+ \to n+\pi_+) \approx 1$, 6) the $\Delta I = \frac{1}{2}$ rule is valid, 7) $\alpha_+ = \alpha_- = 0$. These assumptions are sufficient to determine the interaction Hamiltonian uniquely if the coupling type (derivative or direct) of the Hamiltonian is prescribed, and from the Hamiltonian we obtain the result $\alpha_0 = \pm 1$ not inconsistent with the experiment. Conversely, when we replace the assumption 6) by $\alpha_0 = \pm 1$, we cannot conclude that the $\Delta I = \frac{1}{2}$ rule holds. If we assume $\alpha_0 = \pm 1$, $\alpha_+ = 0$, and leave α_- arbitrary, taking into account the fact that the polarization of the Σ_--hyperon may be small, we obtain two kinds of solutions, one of which coincides with the result under the assumption $\alpha_- = 0$; the other yields $|\alpha_-| = 0.8$.

1. Introduction

Recently it has been observed that the asymmetry factors α_+ and α_- for the decays $\Sigma_+ \to n+\pi_+$ and $\Sigma_- \to n+\pi_-$ are small, while the asymmetry factor α_0 for the decay $\Sigma_+ \to p+\pi_0$ is large [1]). As is well known, this experimental fact cannot be explained with recourse to the hypothesis of the universal V-A interaction [2, 3]) which so far has been believed to be valid in every weak interaction. Therefore, it seems desirable to find out the restrictions which should be imposed on the interaction Hamiltonian to explain all existing experimental data or to make the Hamiltonian as simple as possible.

The problem of the Σ-decays has already been of interest to many physicists and has been treated by several authors in similar but somewhat varying manners, or from slightly different standpoints [4–7]).

Here, we start by assuming that:

1) the spin of the Σ-hyperon is $\frac{1}{2}$;

2) the $\Delta I = \frac{1}{2}$ rule is valid [8]) (we shall include later also the $\Delta I = \frac{3}{2}$ and $\Delta I = \frac{5}{2}$ interactions);

3) the CP-invariance does hold;

4) the effects of the final state interactions are negligible. (Even if the spin of the Σ-hyperon is $\frac{3}{2}$, the phase shifts due to the final state interaction turn out to

† On leave of absence from Kanazawa University, Kanazawa, Japan.

be too small to affect the asymmetry factors appreciably. We shall also neglect entirely the radiative corrections due to strong interactions. If they are taken into consideration, the restrictions obtained here should be imposed not on the Hamiltonian, but on the matrix element itself. Then, the interaction Hamiltonian which will be obtained in this paper should be regarded as the effective interaction Hamiltonian);

5) $\tau(\Sigma_-)/\tau(\Sigma_+) = 2$, where $\tau(\Sigma_\pm)$ is the lifetime of the $\Sigma_\pm$ hyperon;

6) the branching ratio $w(\Sigma_+ \to \mathrm{p}+\pi_0)/w(\Sigma_+ \to \mathrm{n}+\pi_+) = 1$;

7) $\alpha_+ = \alpha_- = 0$.

With these assumptions, an interaction Hamiltonian will be derived uniquely if the coupling type (the derivative or direct coupling) of the Hamiltonian is given. From the Hamiltonian we shall obtain the result $|\alpha_0| = 1$. On the other hand, if we assume $|\alpha_0| = 1$ together with $\alpha_+ = \alpha_- = 0$ instead of $\Delta I = \frac{1}{2}$, we cannot conclude that the resulting Hamiltonian satisfies the $\Delta I = \frac{1}{2}$ rule. When we relax the condition $\Delta I = \frac{1}{2}$, fairly wide ranges of Hamiltonians can satisfy the presumptions $|\alpha_0| = 1$ and $\alpha_+ = \alpha_- = 0$. The only difference would occur in Σ_0-decays ($\Sigma_0 \to \mathrm{p}+\pi_-$, $\mathrm{n}+\pi_0$) which we could never observe.

A question may arise: since, in experiments on the asymmetry factors, the Σ_+-hyperon and the Σ_- hyperon have been produced through different reactions,

$$\pi_+ + \mathrm{p} \to \Sigma_+ + \mathrm{K}_+ \tag{1}$$

and

$$\pi_- + \mathrm{p} \to \Sigma_- + \mathrm{K}_+, \tag{2}$$

and the reaction (2) contains both $I = \frac{1}{2}$ and $\frac{3}{2}$ states while the reaction (1) contains only the $I = \frac{3}{2}$ state, the degree of polarization of the Σ_--hyperon actually might be small. Therefore we examine, in section 4, the possibility that $|\alpha_0| = 1$ and $\alpha_+ = 0$, but that α_- may be different from zero. Then we obtain the two types of solution; the first will coincide with that obtained in sections 2 and 3 and the second will be valid only if the $\Delta I = \frac{1}{2}$ rule does not hold and will lead to the result $|\alpha_-| = \frac{4}{5}$ instead of $\alpha_- = 0$. The form of the Hamiltonian will not be so simple in this last case.

The experimental values of the asymmetry factors [1]) are

$$\left.\begin{aligned} \bar{P}_+\alpha_0 &= 0.70 \pm 0.30 \\ \bar{P}_+\alpha_+ &= 0.02 \pm 0.07 \end{aligned}\right\} \text{for } \Sigma_+ \text{ produced by 1.0 GeV } \pi_+,$$
$$\bar{P}_-\alpha_- = \begin{cases} 0.02 \pm 0.05 & \text{for } \Sigma_- \text{ from 1.0 GeV } \pi_- \\ -0.06 \pm 0.05 & \text{for } \Sigma_- \text{ from 1.1 GeV } \pi_-, \end{cases} \tag{3}$$

where $\bar{P}_\pm$ are the initial polarizations of the $\Sigma_\pm$-hyperon, averaged over the production angle. The experimental values of the lifetimes [9]) are

$$\tau(\Sigma_+) = (0.86 \pm 0.17) \times 10^{-10}\,\mathrm{s}$$

and

$$\tau(\Sigma_-) = (1.83 \pm 0.26) \times 10^{-10}\,\mathrm{s},$$

so that

$$\frac{\tau(\Sigma_-)}{\tau(\Sigma_+)} = 2.2 \pm 0.5. \tag{4}$$

The experimental branching ratio [9]) is

$$\frac{w(\Sigma_+ \to \mathrm{p} + \pi_0)}{w(\Sigma_+ \to \mathrm{p} + \pi_+)} = 1.0 \pm 0.2. \tag{5}$$

2. Construction of the Interaction Hamiltonian with the $\Delta I = \frac{1}{2}$ Rule

The $\Delta I = \frac{1}{2}$ rule also seems to hold in almost all weak interactions [8]). Thus, we begin with the construction of the Hamiltonian which is consistent with the rule $\Delta I = \frac{1}{2}$.

Let $\chi(j, m)$ be a final state which corresponds to the isospin j and its third component m. Then, the complex conjugate of this function will be transformed as $(-1)^{j-m}\chi(j, -m)$, which we shall denote as

$$\chi^*(j, m) \sim (-1)^{j-m}\chi(j, -m). \tag{6}$$

This can be proved by means of mathematical induction. If eq. (6) holds for $\chi_1(j_1, m_1)$, $\chi_2(j_2, m_2)$ and if $\chi(j, m) \sim \Sigma \langle j_1 j_2 m_1 m_2 | j_1 j_2 j m \rangle \chi_1(j_1, m_1)\chi_2(j_2, m_2)$, we can easily show that eq. (6) holds also for $\chi(j, m)$. We know that eq. (6) holds for $j = \frac{1}{2}$, i.e. $\xi^* \sim i\tau_2\xi$ for a 3-dimensional spinor ξ. (We may define the transformation property of a spinor in an alternative way as $\xi^* \sim -i\tau_2\xi$; in this case we have $\chi^*(j, m) \sim (-1)^{j+m}\chi(j, -m)$, which can be proved in entirely the same way and which is the expression described in ref. [10])).

The interaction Hamiltonian which satisfies the $\Delta I = \frac{1}{2}$ rule and produces the final state with isospin j can be constructed in the following way:

$$\mathscr{H}_{2j}(\tfrac{1}{2}, M) = \sum_{m, m'} (j1 - mm' | j1\tfrac{1}{2}M)(-1)^{j+m}\chi^*(j, m)\Sigma(1, m') \tag{7}$$

with

$$\chi(j, m) = \sum_{\mu, \mu'} (\tfrac{1}{2}1\mu\mu' | \tfrac{1}{2}1jm)\mathrm{N}(\tfrac{1}{2}\mu)\pi(1\mu'), \tag{8}$$

where $\mathrm{N}(\frac{1}{2}\mu)$, $\pi(1\mu')$ and $\Sigma(1m')$ denote the nucleon, pion and Σ-hyperon wave functions. Here we have taken into consideration the relation (6) and the law of charge conservation and have omitted the spatial property of the Hamiltonian. The conservation of charge requires $M = \frac{1}{2}$. Thus, the other component $M = -\frac{1}{2}$ should be given up.

On writing down the components explictly,

$$N(\tfrac{1}{2},\tfrac{1}{2}) = p, \quad N(\tfrac{1}{2},-\tfrac{1}{2}) = n,$$

$$\pi(1,1) = \pi_+, \quad \pi(1,0) = \pi_0, \quad \pi(1,-1) = \pi_-,$$

we obtain

$$\mathscr{H}_1(\tfrac{1}{2}) = \sqrt{\tfrac{2}{3}}(\sqrt{\tfrac{1}{3}}\bar{p}\pi_0{}^* - \sqrt{\tfrac{2}{3}}\bar{n}\pi_+{}^*)\Sigma_+ + \sqrt{\tfrac{1}{3}}(\sqrt{\tfrac{2}{3}}\bar{p}\pi_-{}^* - \sqrt{\tfrac{1}{3}}\bar{n}\pi_0)\Sigma_0, \tag{9}$$

$$\mathscr{H}_3(\tfrac{1}{2}) = \sqrt{\tfrac{1}{6}}(\sqrt{\tfrac{2}{3}}\bar{p}\pi_0{}^* + \sqrt{\tfrac{1}{3}}\bar{n}\pi_+{}^*)\Sigma_+ + \sqrt{\tfrac{1}{3}}(\sqrt{\tfrac{1}{3}}\bar{p}\pi_-{}^* + \sqrt{\tfrac{2}{3}}\bar{n}\pi_0)\Sigma_0 + \sqrt{\tfrac{1}{2}}\bar{n}\pi_-{}^*\Sigma_-. \tag{10}$$

Or, if we introduce the following vector and spinor components:

$$\pi_+ = -\frac{1}{\sqrt{2}}(\pi_1 + i\pi_2) = -\pi_-{}^*, \quad \pi_- = \frac{1}{\sqrt{2}}(\pi_1 - i\pi_2) = -\pi_+{}^*, \quad \pi_0 = \pi_3 = \pi_0{}^*,$$

$$\Sigma_+ = -\frac{1}{\sqrt{2}}(\Sigma_1 + i\Sigma_2), \quad \Sigma_- = \frac{1}{\sqrt{2}}(\Sigma_1 - i\Sigma_2), \quad \Sigma_0 = \Sigma_3,$$

$$\bar{N} = (\bar{p}, \bar{n}), \quad \hat{N} = \bar{N}i\tau_2 = (-\bar{n}, \bar{p}),$$

we can rewrite the Hamiltonian as

$$\mathscr{H}_1(\tfrac{1}{2}) = \tfrac{1}{3}[\hat{N}\boldsymbol{\pi}\cdot\boldsymbol{\Sigma} + i\hat{N}\boldsymbol{\tau}\cdot\boldsymbol{\pi}\times\boldsymbol{\Sigma}], \tag{11}$$

$$\mathscr{H}_3(\tfrac{1}{2}) = \frac{1}{3\sqrt{2}}[-2\hat{N}\boldsymbol{\pi}\cdot\boldsymbol{\Sigma} + i\hat{N}\boldsymbol{\tau}\cdot\boldsymbol{\pi}\times\boldsymbol{\Sigma}]. \tag{12}$$

In accordance with the $\Delta I = \frac{1}{2}$ rule, the most general interaction Hamiltonian is a linear combination of $\mathscr{H}_1(\frac{1}{2})$ and $\mathscr{H}_3(\frac{1}{2})$,

$$\mathscr{H} = f\mathscr{H}_1(\tfrac{1}{2}) + g\mathscr{H}_3(\tfrac{1}{2}), \tag{13}$$

where f and g are coupling constants. Using this interaction Hamiltonian we can calculate the transition amplitude M_0, M_+ and M_- for the decays $\Sigma_+ \to p+\pi_0$, $\Sigma_+ \to n+\pi_+$ and $\Sigma_- \to n+\pi_-$. They are

$$\begin{aligned} M_0 &= \frac{\sqrt{2}}{3} f\mathscr{M}_1 + \frac{1}{3} g\mathscr{M}_3, \\ M_+ &= -\frac{2}{3} f\mathscr{M}_1 + \frac{1}{3\sqrt{2}} g\mathscr{M}_3, \\ M_- &= \frac{1}{\sqrt{2}} g\mathscr{M}_3, \end{aligned} \tag{14}$$

where a common constant factor only depending on the masses is omitted and where

$$\mathscr{M}_1 = \begin{pmatrix} s_1 \\ p_1 \end{pmatrix}, \quad \mathscr{M}_3 = \begin{pmatrix} s_3 \\ p_3 \end{pmatrix}. \tag{15}$$

Here s and p denote the amplitudes of s and p waves, normalized as

$$|\mathscr{M}_1|^2 = |s_1|^2 + |p_1|^2 = 1, \quad |\mathscr{M}_3|^2 = |s_3|^2 + |p_3|^2 = 1. \tag{16}$$

The expression (15) is an abbreviated notation for $\mathcal{M} = P_s s + P_p p$, where P_s and P_p are the projection operators to the s and p states. All the suffixes 1 and 3 in the above formulae stand for $2j$, twice the isospin of the final state. The transition amplitudes (14) satisfy the well-known Gell-Mann and Rosenfeld relation [3])

$$\sqrt{2}M_0 = M_- - M_+.$$

The assumptions 5) and 6) in section 1 state that

$$|M_0|^2 = |M_+|^2 = |M_-|^2,$$

from which we obtain

$$g = \varepsilon_1 \frac{2}{\sqrt{5}} f, \tag{17}$$

and

$$\mathcal{M}_1 \cdot \mathcal{M}_3 = \varepsilon_1 \frac{1}{\sqrt{10}}, \tag{18}$$

where $\varepsilon_1 = \pm 1$; hereafter we shall always use ε to denote ± 1. The assumptions 3) and 4) in section 1 assure us that the amplitude may be regarded to be real. Therefore we obtain the following expressions for the asymmetry factors:

$$\begin{aligned}
\alpha_- &= \frac{2 s_3 p_3}{|s_3|^2 + |p_3|^2}, \\
\alpha_+ &= \frac{2\left(-\frac{2}{3} f s_1 + \frac{1}{3\sqrt{2}} g s_3\right) \cdot \left(-\frac{2}{3} f p_1 + \frac{1}{3\sqrt{2}} g p_3\right)}{\left|-\frac{2}{3} f s_1 + \frac{1}{3\sqrt{2}} g s_3\right|^2 + \left|-\frac{2}{3} f p_1 + \frac{1}{3\sqrt{2}} g p_3\right|^2}, \\
\alpha_0 &= \frac{2\left(\frac{\sqrt{2}}{3} f s_1 + \frac{1}{3} g s_3\right) \cdot \left(\frac{\sqrt{2}}{3} f p_1 + \frac{1}{3} g p_3\right)}{\left|\frac{\sqrt{2}}{3} f s_1 + \frac{1}{3} g s_3\right|^2 + \left|\frac{\sqrt{2}}{3} f p_1 + \frac{1}{3} g p_3\right|^2}.
\end{aligned} \tag{19}$$

From the assumption $\alpha_- = 0$, we have either $p_3 = 0$ or $s_3 = 0$. Let us first examine the case $p_3 = 0$. Another solution will be obtained by exchanging the s amplitudes for the p amplitudes, because the equations are symmetric with respect to s and p. The normalization condition (16) yields

$$s_3 = \varepsilon_2 (\equiv \pm 1). \tag{20}$$

The amplitude s_1 can be determined from the condition $\alpha_+ = 0$, which gives

$$s_1 = \frac{1}{2\sqrt{2}} \frac{g}{f} \varepsilon_2 = \varepsilon_1 \varepsilon_2 \frac{1}{\sqrt{10}}, \tag{21}$$

where use has been made of eq. (17). Taking into account the normalization condition (16) we have

$$p_1 = \varepsilon_3 \frac{3}{\sqrt{10}}. \tag{22}$$

Inserting these values into the third of eqs. (19) we get automatically

$$\alpha_0 = \varepsilon_1 \varepsilon_2 \varepsilon_3. \tag{23}$$

Now we consider the coupling type of the Hamiltonian. Every term in the Hamiltonians of eqs. (9) and (10) may be either the derivative coupling of the form

$$m_\pi^{-1} \bar{\mathrm{N}} \gamma_\mu (a + b\gamma_5) \Sigma \partial_\mu \pi, \tag{24}$$

or the direct coupling of the form

$$\bar{\mathrm{N}} (a + b\gamma_5) \Sigma \pi. \tag{25}$$

If we take the normalization condition as

$$a^2 + x^{-2} b^2 = 1, \tag{26}$$

we may put

$$a = \mathrm{s}, \quad b = x\mathrm{p}, \tag{27}$$

where

$$x^{-1} = \frac{M+m}{M-m} \frac{E+m}{p} = 0.85 \quad \text{for the derivative coupling}$$

and

$$x^{-1} = \frac{E+m}{p} = 0.1 \text{ for the direct coupling;}$$

here M and m are the masses of the Σ-hyperon and the nucleon, p is the momentum of the nucleon or the meson in the rest system of the hyperon and $E = (p^2 + m^2)^{\frac{1}{2}}$.

Incorporating all these results into eq. (13), we obtain several solutions, one of which is

$$\begin{aligned} \mathscr{H} = \frac{2}{3\sqrt{5}} f [& \tfrac{1}{2} \bar{\mathrm{p}} \gamma_\mu \{ \quad (1+3x\gamma_5) + \quad 2 \} \Sigma_+ \partial_\mu \pi_0^* \\ & + \frac{1}{\sqrt{2}} \bar{\mathrm{n}} \gamma_\mu \{ - \quad (1+3x\gamma_5) + \quad 1 \} \Sigma_+ \partial_\mu \pi_+^* \\ & + \tfrac{1}{2} \bar{\mathrm{p}} \gamma_\mu \{ \quad (1+3x\gamma_5) + \sqrt{2} \} \Sigma_0 \partial_\mu \pi_-^* \\ & + \frac{1}{\sqrt{2}} \bar{\mathrm{n}} \gamma_\mu \{ -\tfrac{1}{2} (1+3x\gamma_5) + \quad 2 \} \Sigma_0 \partial_\mu \pi_0^* \\ & + \frac{3}{\sqrt{2}} \bar{\mathrm{n}} \gamma_\mu \Sigma_- \partial_\mu \pi_-^*]. \end{aligned} \tag{28}$$

Other solutions will be derived either by the interchange of s and p or by changing the sign of γ_5 or f (in the following, we shall omit this kind of remark). When expressed in the form of eqs. (11) and (12), the Hamiltonian (28) assumes an especially simple form,

$$\mathscr{H} = \frac{1}{\sqrt{10}} f [\bar{\mathrm{N}} \gamma_\mu (1 - x\gamma_5) \boldsymbol{\Sigma} \cdot \partial_\mu \boldsymbol{\pi} - i \bar{\mathrm{N}} \boldsymbol{\tau} \gamma_\mu (1 + x\gamma_5) \boldsymbol{\Sigma} \times \partial_\mu \boldsymbol{\pi}]. \tag{29}$$

If we put $x = 1$ in eq. (29), the result is essentially the same as the Hamiltonian derived by K. Nakagawa [11]), based on the assumption of the "one to one" law. In this case, we have $\alpha_+ = \alpha_- = 0$, as is easily seen from eq. (28); on the other hand,

$$\alpha_0 = \frac{2x}{1+x^2} = 0.985, \quad \frac{\tau(\Sigma_-)}{\tau(\Sigma_+)} = \frac{3+x^2}{2x^2} = 2.07,$$

$$\frac{w(\Sigma_+ \to \mathrm{p}+\pi_0)}{w(\Sigma_+ \to \mathrm{n}+\pi_+)} = \tfrac{1}{2}(1+x^2) = 0.86.$$

These values deviate somewhat from our original assumptions, but they are still permissible owing to the experimental uncertainties.

3. The Inclusion of Hamiltonians with $\Delta I = \frac{3}{2}$ and $\Delta I = \frac{5}{2}$

The interaction Hamiltonian with $\Delta I = \frac{3}{2}$ and $\Delta I = \frac{5}{2}$ can be constructed in a way similar to eq. (7):

$$\mathscr{H}_{2I}(\Delta I, M) = \sum_{m,m'} (j1-m\cdot m'|j1\Delta I M)(-1)^{j+m}\chi^*(j,m)\Sigma(1,m'). \quad (30)$$

Here again only the component $M = \frac{1}{2}$ is compatible with the law of charge conservation. We shall write down explicitly

$$\mathscr{H}_1(\tfrac{3}{2}) = -\tfrac{1}{3}(\bar{\mathrm{p}}\pi_0{}^* - \sqrt{2}\bar{\mathrm{n}}\pi_+{}^*)\Sigma_+ + \tfrac{1}{3}(2\bar{\mathrm{p}}\pi_-{}^* - \sqrt{2}\bar{\mathrm{n}}\pi_0)\Sigma_0,$$

$$\mathscr{H}_3(\tfrac{3}{2}) = -\frac{2}{3\sqrt{5}}(2\bar{\mathrm{p}}\pi_0{}^* + \sqrt{2}\bar{\mathrm{n}}\pi_+{}^*)\Sigma_+ - \frac{1}{3\sqrt{5}}(\bar{\mathrm{p}}\pi_-{}^* + \sqrt{2}\bar{\mathrm{n}}\pi_0{}^*)\Sigma_0 - \sqrt{\tfrac{2}{5}}\bar{\mathrm{n}}\pi_-{}^*\Sigma_-,$$

$$\mathscr{H}_1(\tfrac{5}{2}) = 0,$$

$$\mathscr{H}_3(\tfrac{5}{2}) = \frac{1}{\sqrt{10}}(\sqrt{2}\bar{\mathrm{p}}\pi_0{}^* + \bar{\mathrm{n}}\pi_+{}^*)\Sigma_+ - \frac{1}{\sqrt{5}}(\bar{\mathrm{p}}\pi_-{}^* + \sqrt{2}\bar{\mathrm{n}}\pi_0{}^*)\Sigma_0 + \frac{1}{\sqrt{10}}\bar{\mathrm{n}}\pi_-{}^*\Sigma_-.$$

Then the most general interaction Hamiltonian for the decay of the Σ-hyperon is

$$\mathscr{H} = f\mathscr{H}_1(\tfrac{1}{2}) + f'\mathscr{H}_1(\tfrac{3}{2}) + g\mathscr{H}_3(\tfrac{1}{2}) + g'\mathscr{H}_3(\tfrac{3}{2}) + g''\mathscr{H}_3(\tfrac{5}{2}). \quad (31)$$

In this case, the transition amplitudes can be expressed as

$$M_0 = \frac{\sqrt{2}}{3}F\mathscr{M}_1 + \tfrac{1}{3}G\mathscr{M}_3,$$

$$M_+ = -\tfrac{2}{3}F\mathscr{M}_1 + \frac{1}{3\sqrt{2}}G\mathscr{M}_3,$$

$$M_- = \frac{1}{\sqrt{2}}G'\mathscr{M}_3,$$

where

$$F = f - \frac{1}{\sqrt{2}} f',$$
$$G = g - \frac{4}{\sqrt{5}} g' + \frac{3}{\sqrt{5}} g'', \tag{32}$$
$$G' = g - \frac{2}{\sqrt{5}} g' + \frac{1}{\sqrt{5}} g''.$$

It can easily be seen that, if $G = G'$ (then $g' = g''$) or $G = -G'$ (then $g - \frac{3}{\sqrt{5}} g' + \frac{2}{\sqrt{5}} g'' = 0$), we obtain exactly the same results as we had in the of $\Delta I = \frac{1}{2}$ in section 2.

To examine more general cases, we put

$$G = \varepsilon_1 \frac{2}{\sqrt{5}} Fy \tag{33}$$

and obtain

$$s_3 = 0, \quad p_3 = \varepsilon_2; \quad s_1 = \varepsilon_1 \varepsilon_2 \frac{1}{\sqrt{10}} y, \quad p_1 = \varepsilon_1 \sqrt{1 - \tfrac{1}{10} y^2}. \tag{34}$$

By inserting these values into the expression for α_0, we get

$$\alpha_0 = \varepsilon_1 \varepsilon_2 \varepsilon_3 \frac{3y\sqrt{10 - y^2}}{5 + 4y^2}. \tag{35}$$

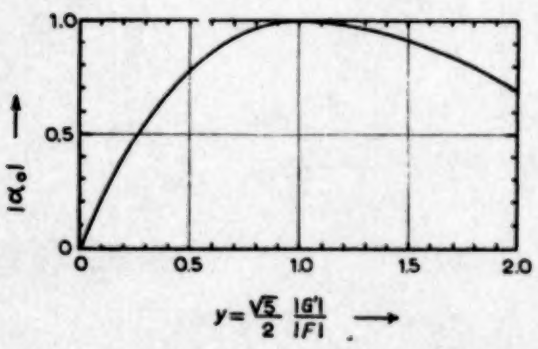

Fig. 1. The asymmetry factor α_0 as a function of the parameter y.

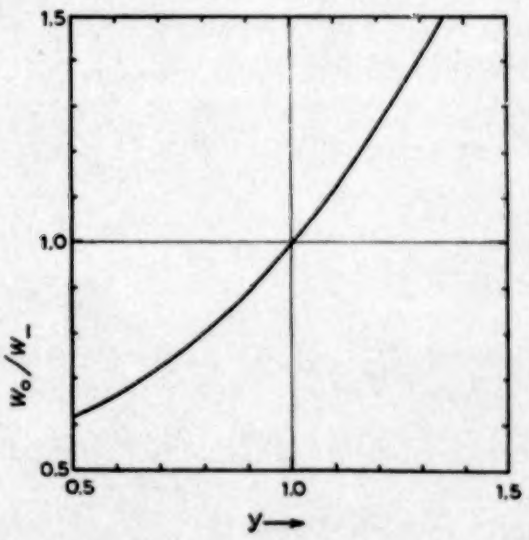

Fig. 2. The branching ratio $w(\Sigma_+ \to p + \pi_0)/w(\Sigma_+ \to n + \pi_+)$ as a function of the parameter y.

Fig. 1 gives α_0 as a function of y. We have not yet made use of the relation $|M_0|^2 = |M_+|^2 = |M_-|^2$. We have

$$\frac{w(\Sigma_+ \to p + \pi_0)}{w(\Sigma_+ \to n + \pi_+)} = \frac{(5 + 4y^2)}{(10 - y^2)} \tag{36}$$

for the branching ratio (fig. 2). This equation is more suitable to determine the value of y than eq. (35). Comparing eq. (36) with the experimental value given by form. (5), we obtain

$$y = 1.0 \pm 0.2.$$

The ratio of the lifetimes is more or less arbitrary because it contains G':

$$\frac{\tau(\Sigma_-)}{\tau(\Sigma_+)} = (\tfrac{4}{3})(1+\tfrac{1}{5}y^2)\,\frac{F^2}{G'^2}. \tag{37}$$

We may express G' in terms of F by inserting the experimental value of τ_-/τ_+. If the value of y is fixed, say, to 1, we obtain

$$G' = \pm(0.95^{+0.13}_{-0.09})\,\frac{2}{\sqrt{5}}\,F.$$

Even if we could obtain the ratio $F : G : G'$ in this way, the five individual coupling constants in eq. (26) would remain undetermined. To fix them completely, we should have to have some information of the N$-\pi$ mode of the Σ_0-hyperon decay. This is impossible in practice, because this decay mode is always masked by the more frequent mode $\Sigma_0 \to \Lambda+\gamma$. The situation is worse than the case of the Λ-hyperon decay, in which we have to examine the decay mode $\Lambda \to \mathrm{n}+\pi_0$ in order to confirm the $\Delta I = \frac{1}{2}$ rule [12]). This decay mode does occur, although it is difficult to detect.

4. Vanishing Initial Polarization of the Σ-Hyperon

As was stated in section 1, the Σ_- and Σ_+-hyperons have been created through different reactions. Therefore, the initial polarization of the Σ_--hyperon might be small, whereas the polarization of the Σ_+-hyperon is doubtlessly large, because the experimental value of $\bar{P}_+\alpha_0$ is large.

In this case, we abandon the assumption $\alpha_- = 0$ and assume nothing about the value of α_-, however, we want to construct an interaction Hamiltonian which satisfies the assumptions

$$|M_0|^2 = |M_+|^2 = |M_-|^2 \tag{38}$$

and

$$|\alpha_0| = 1, \quad \alpha_+ = 0. \tag{39}$$

Here again we put

$$G = \varepsilon_1\,\frac{2}{\sqrt{5}}\,Fy.$$

Then we have

$$G'^2 = (\tfrac{2}{3})(1+\tfrac{1}{5}y^2)F^2, \tag{40}$$

and

$$s_1 s_3 + p_1 p_3 = \varepsilon_1 \frac{\sqrt{10}}{8y}\left(1-\tfrac{1}{5}y^2\right) \tag{41}$$

from the relation (38). Next, we put

$$\alpha_0 = \varepsilon_1 \varepsilon_2 \varepsilon_3 . \tag{42}$$

Let us choose ε_3 as the sign of p_1 and ε_2 as an arbitrary sign factor. We make use of the condition $\alpha_+ = 0$ to get

$$s_1 = \varepsilon_1 \frac{1}{\sqrt{10}} y\, s_3 \quad \text{or} \qquad p_1 = \varepsilon_1 \frac{1}{\sqrt{10}} y\, p_3 . \tag{43}$$

Then we can solve eq. (41), (42) and (43) together with the normalization condition (16) to obtain

$$\begin{aligned} s_1 &= \varepsilon_1 \varepsilon_2 \frac{\sqrt{15}}{20} \frac{5-y^2}{\sqrt{5+y^2}}, & p_1 &= \varepsilon_3 \frac{\sqrt{15}}{60} \frac{35+y^2}{\sqrt{5+y^2}}, \\ s_3 &= \varepsilon_2 \frac{3}{2y} \frac{5-y^2}{\sqrt{5+y^2}}, & p_3 &= \varepsilon_1 \varepsilon_3 \frac{5\sqrt{6}}{12y} \frac{1-y^2}{\sqrt{5+y^2}}, \end{aligned} \tag{44}$$

where y should be a root of the equation

$$(y^2-1)(y^2-25) = 0.$$

This equation can be derived, for instance, by substituting the first and second of eqs. (44) into $s_1^2 + p_1^2 = 1$.

The result obtained for $y^2 = 1$ is equivalent to what was already discussed in the previous sections. For $y^2 = 25$ we have $\alpha_- = 0.8\, \varepsilon_1 \varepsilon_2 \varepsilon_3$. This means that α_- has the same sign as α_0 and is as large as $0.8\alpha_0$. If this is the case, $\bar{P}_-$ should be of the order of $\frac{1}{10}\bar{P}_+$ or smaller. This would be testified, if we could measure the polarization of the decay neutron [13]) or if we could use the Σ_--hyperon from the reaction $\pi_- + n \to \Sigma_- + K_0$.

A form of the interaction Hamiltonian in this case is

$$\begin{aligned} \mathcal{H} = \pm F[&\bar{p}\gamma_\mu(1+\varepsilon x\gamma_5)\Sigma_+ \partial_\mu \pi_0^* + \varepsilon x \bar{n}\gamma_\mu\gamma_5\Sigma_+ \partial_\mu \pi_+^* \\ &\pm \sqrt{\tfrac{2}{5}}\bar{n}\gamma_\mu(1+2\varepsilon x\gamma_5)\Sigma_- \partial_\mu \pi_-^* \\ &+\alpha\{\sqrt{2}\bar{p}\gamma_\mu(1-\varepsilon x\gamma_5)\Sigma_0 \partial_\mu \pi_-^* - \bar{n}\gamma_\mu(1-\varepsilon x\gamma_5)\Sigma_0 \partial_\mu \pi_0^*\} \\ &-\beta\{\bar{p}\gamma_\mu(1+2\varepsilon x\gamma_5)\Sigma_0 \partial_\mu \pi_-^* + \sqrt{2}\bar{n}\gamma_\mu(1+2\varepsilon x\gamma_5)\Sigma_0 \partial_\mu \pi_0^*\}], \end{aligned} \tag{45}$$

where $\varepsilon = \varepsilon_1\varepsilon_2\varepsilon_3$, $\alpha = \frac{1}{3}(1+\xi)$, $\beta = 1/3\sqrt{5}(\sqrt{5}\mp 1+\eta)$ and $\xi = 3/\sqrt{2}\ f'/F$,

$\eta = \varepsilon_1 \varepsilon_2 3/\sqrt{5} g''/F$. We cannot further simplify this Hamiltonian as we did in eq. (29) for the case of $\Delta I = \frac{1}{2}$.

The author is indebted to Professor L. Rosenfeld for his interest in this work. He likes to thank Professor Niels Bohr and Professor Aage Bohr for their kind hospitality.

References

1) R. L. Cool, B. Cork, J. W. Cronin and W. A. Wenzel, Phys. Rev. **114** (1959) 912
2) M. Gell-Mann and A. H. Rosenfeld, Ann. Rev. Nucl. Sc. **7** (1957) 407
3) R. H. Dalitz, Revs. Mod. Phys. **31** (1959) 823
4) Y. Yamaguchi, Prog. Theor. Phys. **19** (1958) 485
5) K. Itabashi, Prog. Theor. Phys. **19** (1958) 747
6) T. Eguchi and S. Nagata, Prog. Theor. Phys. **20** (1958) 44
7) B. d'Espagnat and J. Prentki, Phys. Rev. **114** (1959) 1366
8) F. S. Crawford *et al.*, Phys. Rev. Lett. **2** (1959) 226
9) L. W. Alvarez *et al.*, Nuov. Cim. **5** (1957) 1026;
see also the articles by G. A. Snow and A. Rosenfeld, Proc. 7th Roch. Conf. on High En. Phys. (1957)
10) A. R. Edmonds, Angular Momentum in Quantum Mechanics (Princeton University Press, Princeton, 1958)
11) K. Nakagawa, Nuclear Physics **10** (1959) 20
12) S. Okubo *et al.*, Phys. Rev. **112** (1958) 665
13) T. D. Lee and C. N. Yang, Phys. Rev. **108** (1957) 1645

2.I:3.C

Nuclear Physics **17** (1960) 238—249; © *North-Holland Publishing Co., Amsterdam*

Not to be reproduced by photoprint or microfilm without written permission from the publisher

GESAMTABSORPTION VON γ-STRAHLEN ZWISCHEN 10 UND 30 MeV IN LEICHTEN KERNEN

B. ZIEGLER

Physikalisches Institut der Technischen Hochschule Karlsruhe

und

Kernphysikalische Abteilung des Max-Planck-Instituts für Chemie (Otto-Hahn-Institut), Mainz

Eingegangen am 18. Januar 1960

Abstract: Absorption cross sections in carbon, oxygen and aluminium have been determined with a 32 MeV betatron and a magnetic pair spectrometer in the energy interval between 10 and 30 MeV. In this region, where the nuclear absorption is unimportant, the measured total electronic absorption cross section agrees within 1 % with the theoretical value based on the theories of Klein and Nishina for the Compton effect, of Bethe and Heitler for the pair production in the field of the nucleus, and of Borsellino for the pair production in the field of the electron. The total nuclear absorption shows the giant resonance peak well known in photonuclear reactions. The peak cross section was found to be 18 mb at 22.5 MeV for carbon, and 50 mb at 20 MeV for Al. The oxygen and aluminium data suggest a smoothly varying nuclear absorption cross section.

1. Einleitung

In letzter Zeit wurde verschiedentlich der Versuch unternommen, γ-Spektren und Absorptionskoeffizienten im gesamten Energiebereich von 10—30 MeV zu messen. Solange noch keine monochromatischen γ-Strahlen zur Verfügung stehen, muß man sich dabei mit einem Bremsspektrum als Strahlenquelle begnügen und einen Detektor verwenden, der nur auf Quanten in einem schmalen Energieintervall anspricht. Hierzu wurden verschiedene Spektrometerprinzipien benutzt: Totalabsorption in NaJ-Kristallen [1, 2]), magnetische Analyse von Comptonelektronen [3]), magnetische Analyse von Paarteilchen [4]).

Die Experimente zeigen, daß der nur langsam mit der Quantenenergie sich ändernden Absorption durch Comptoneffekt und Paarbildung (Wirkungsquerschnitte $\sigma_c(E)$ und $\sigma_p(E)$) bei etwa 20 MeV eine viel schwächerere Absorptions-„Linie" überlagert ist. Sie entsteht durch Anregung von Dipolschwingungen im Atomkern (Riesenresonanz). In den oben zitierten und in der vorliegenden Arbeit sollen 1) die theoretischen Werte für $(\sigma_c(E)+\sigma_p(E))$ experimentell geprüft und 2) Lage, Höhe und Breite der Riesenresonanz $(\sigma_k(E))$ bestimmt werden. Das Experiment kann stets nur die Summe $\sigma_{exp} = (\sigma_p+\sigma_c+\sigma_k)$ liefern. Für die Prüfung von $(\sigma_p+\sigma_c)$ ist man deswegen auf den Energiebereich angewiesen, wo σ_k gegen $(\sigma_p+\sigma_c)$ zu vernachlässigen ist. Setzt man willkürlich „außerhalb der Riesenresonanz" den experimentellen Absorptionsquerschnitt σ_{exp} gleich der Summe der berechneten Werte $(\sigma_p+\sigma_c)$, so braucht

man nur die Energievariation, nicht den absoluten Wert von σ_{exp} zu bestimmen, um die im Gebiete der Riesenresonanz gefundene Differenz $\sigma_{exp}-(\sigma_p+\sigma_e)$ der Kernabsorption (σ_k) zuschreiben zu können. Dieser in einer früheren Arbeit [4]) der Einfachheit halber praktizierte Vorgang enthält natürlich die Möglichkeit eines systematischen Fehlers, da man nicht sicher weiß, wo man σ_k nullsetzen darf. Die mit dieser Methode gefundenen integrierten Wirkungsquerschnitte waren kleiner, als nach der Summenregel für Dipolübergänge [5]) zu erwarten war. Zur Klärung dieser Unstimmigkeit wurden die Versuche mit einer Apparatur wiederholt, die frei von dem oben erwähnten systematischen Fehler war und eine bessere Statistik zu erzielen erlaubte. Nach wie vor muß man jedoch σ_p und σ_e im betrachteten Energiebereich genau kennen, um σ_k richtig bestimmen zu können.

Bei einigen leichten Elementen wurde berichtet [6, 7]), daß der Reaktionsquerschnitt für Kernphotoeffekt im Gebiet der Riesenresonanz in einzelne schmale Linien zerfällt. Dasselbe sollte dann auch für den totalen Absorptionsquerschnitt gelten. In diesem Fall würde die Absorption als Funktion der Länge keinem Exponentialgesetz folgen, zumindest solange die Absorptionslinie schmäler als die Breite der Detektornachweisfunktion ist. Daher wurde die Absorption verschieden langer Sauerstoff-Absorber gemessen, um daraus eine Aussage über mögliche Strukturen im Kernabsorptionsquerschnitt zu erhalten.

2. Experimentelle Anordnung

Die Versuchsanordnung ist ähnlich der früher [4]) verwendeten, mit dem Betatron als Strahlenquelle und dem Paarspektrometer als Detektor. Fig. 1 zeigt einen waagrechten Schnitt in Strahlhöhe. Größere Kristall- und Konverterfolienfläche erhöhen die Lichtstärke gegenüber der früheren Anordnung ohne wesentliche Verschlechterung des Auflösungsvermögens. Bei einem Abstand von 3 m zwischen Betatron-Antikathode und Konverterfolie können nunmehr biz zu 1.20 cm lange Absorber verwendet werden. Dabei bleibt die Compton-Korrektur (s.u.) unter 2 %. Die Kammer Ik_1 mißt den primären Quantenfluß in relativen Einheiten. Sie ist gegen Streuelektronen aus dem Betatronrohr gut abgeschirmt. Der Einfluß der am Absorberanfang rückgestreuten Elektronen auf die Anzeige der Kammer Ik_1 ist nicht nachweisbar.

Bei der Messung ohne Absorber mußte die Intensität des γ-Strahls etwa um einen Faktor 10 reduziert werden, da sonst die Zahl der zufälligen Koinzidenzen zu groß geworden wäre. Dies konnte durch Ändern der Einschußbedingungen ohne wesentliche Auswirkung auf die Form der γ-Blitze und des Bremsspektrums erreicht werden †. Der Betatronexpansionsstrom, normalerweise eine halbe Sinuswelle, erhielt durch Einschalten eines abstimmbaren LC-Gliedes eine

† Den Herren der Heidelberger Betatrongruppe verdanken wir einen sorgsamen Vergleich der Bremsspektren bei großer und kleiner Intensität. Die dabei gefundene 1 %-Differenz im Verhältnis der Cu- zu C-Aktivierung gibt eine unerhebliche Vergrößerung des in der Hauptsache statistisch bedingten Gesamtfehlers in σ_k.

Komponente der 3. Oberwelle, wodurch ein mehr rechteckiger Stromverlauf erzielt wurde, die γ-Blitzdauer von 50 auf 120 μs anstieg und im selben Verhältnis die Zahl der zufälligen Koinzidenzen abnahm.

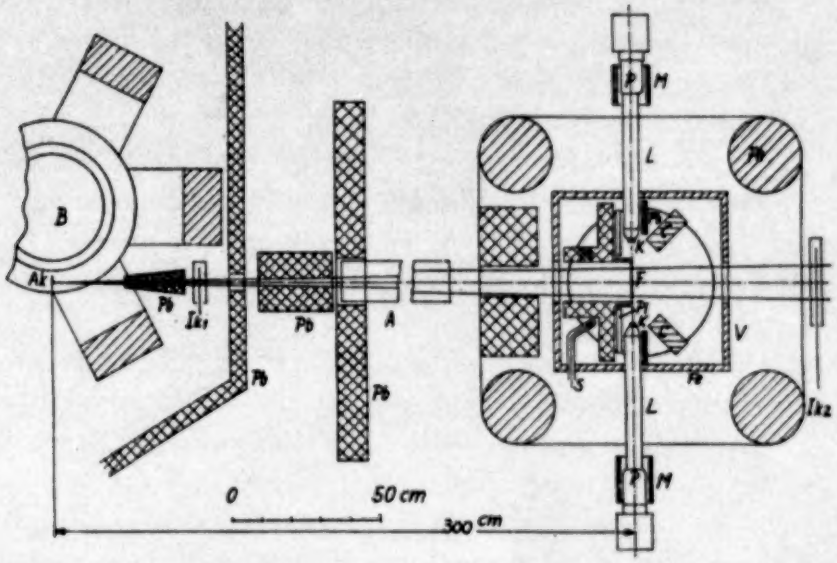

Fig. 1. Horizontaler Schnitt durch Betatron B und Paarspektrometer. AK Antikathode des Betatrons; Pb Bleiblenden und Abschirmung; F Konverterfolie (Breite × Höhe = 12×8 cm²); K org. Szintillations-Kristalle (Breite × Dicke × Höhe=0.2×0.3×7 cm³); L Plexiglaslichtleiter (4,3 cm ø); P Multiplier 6810A; M doppelte μ-Metall-Abschirmung; Ik_1, Ik_2 Ionisationskammern zur Dosierung des γ-Strahls (mit Elektrometer, bzw. Elektrometerschreiber verbunden); S Protonenresonanz und HALL-Sonde zur Magnetfeldmessung; A Absorber; Pl Plexiglasplatten zur Reduzierung der Rückstreuung aus den Pb-Blenden; C Graphitblenden.

Die Koinzidenzkreise [8]) blieben im Wesentlichen ungeändert. Multiplier mit großem Ausgangsstrom (RCA 6810A) machen die Kettenverstärker überflüssig. Eine Regelschaltung hält die beiden Stufen für die direkten und verzögerten Koinzidenzen automatisch auf gleicher Trennzeit. Eine detaillierte Beschreibung dieser Schaltung wird vorbereitet.

3. Messung und Auswertung

Der Quotient aus der Zahl der echten Koinzidenzen n_e und der in der Kammer Ik_1 gesammelten Ladung werde mit I, bei einer Messung ohne Absorber mit I_0 bezeichnet. I_0 ist in Fig. 2 über der Quantenenergie aufgetragen. Die eingetragenen Fehler sind einfache mittlere statistische Fehler:

$$\frac{\Delta I_0}{I_0} = \frac{\sqrt{(n_e+n_z)+n_z}}{(n_e+n_z)-n_z}; \qquad (1)$$

n_z ist die Zahl der während der Meßzeit registrierten zufälligen Koinzidenzen. Die Meßwerte wurden durch eine glatte Kurve möglichst gut angenähert, für die ein χ^2-Test die Wahrscheinlichkeit $P = 0.22$ ergibt.

Die zu erwartenden Schwächungen durch Paarbildung im Kernfeld und Comptoneffekt wurden mit tabellierten Absorptionskoeffizienten [9]) berechnet. Für die Paarbildung im Feld der Hüllenelektronen wurden die von Borsellino [10]) angegebenen Werte benützt. Sie passen am besten zu neueren Messungen [11, 12]) und sind in Fig. 3 zusammen mit Ergebnissen anderer Theorien eingezeichnet.

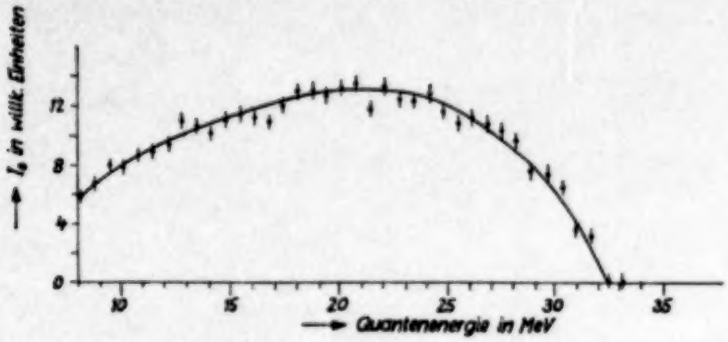

Fig. 2. Meßkurve, im Wesentlichen Produkt aus Bremsspektrum und Paarbildungsquerschnitt, ohne Absorber.

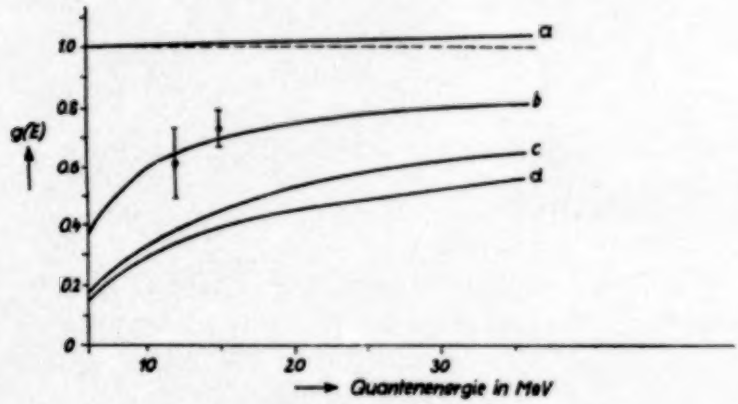

Fig. 3. Paarbildungsquerschnitt im Feld der Z Hüllenelektronen $\sigma_{p\ el} = g(E)\sigma_{p\ Kern}/Z$ nach: a) Wheeler und Lamb [13]); b) Borsellino [10]); c) Joseph und Rohrlich [14]); d) Votruba [15]) (tabelliert in Ref. [9])). Zur Auswertung wurde Kurve b) benutzt.
Die Meßpunkte stammen aus der Kohlenstoffabsorber-Messung, wobei Paarbildung im Kernfeld nach Bethe und Heitler, Comptoneffekt nach Klein und Nishina berechnet wurde.

Der Meßwert I bedarf einer kleinen Korrektur, weil einige der Quanten, die von höheren Energien in das gerade eingestellte Energieintervall hineingestreut werden, die Konverterfolie noch treffen können. Für das Verhältnis der Zahl dieser Streuquanten zur Zahl der im eingestellten Energieintervall liegenden Quanten, die den Absorber ungehindert passieren, findet man [4])

$$f = NZr_0^2 ab\left(\frac{1}{d-l} - \frac{1}{d}\right). \tag{2}$$

Dabei ist N die Atomzahldichte; Z die Ordnungszahl des Absorbers; $r_0 =$

$= 2.82 \times 10^{-13}$ cm der klassische Elektronenradius; a und b Breite und Höhe der Konverterfolie; l die Länge des Absorbers; d der Abstand vom Absorberanfang zur Konverterfolie. Die in Fig. 4 eingezeichnete Kurve I'_0 entstand aus der in Fig. 2 durch Multiplizieren mit den theoretischen Schwächungsfaktoren für Comptoneffekt und Paarbildung und dem Faktor $(1+f)$ für den Kohlenstoff-Absorber. Sie ist zu vergleichen mit den eingezeichneten Meßwerten I.

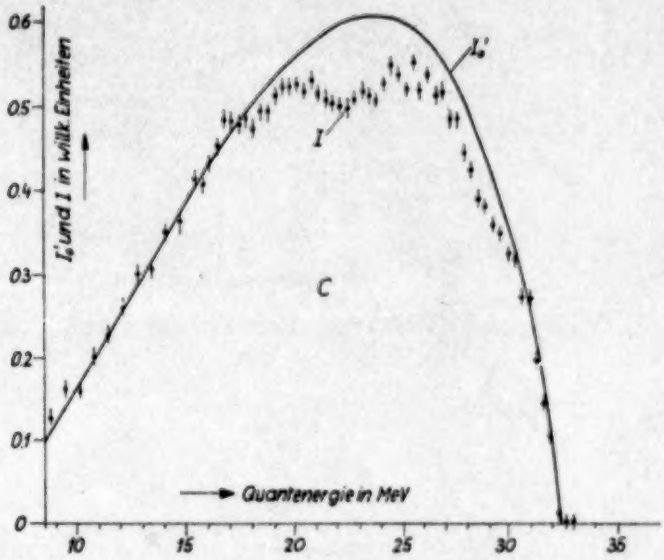

Fig. 4. I'_0 entsteht aus I_0 durch Multiplizieren mit den theoretischen Schwächungsfaktoren $e^{-N(\sigma_p+\sigma_e)l}$ (für Comptoneffekt und Paarbildung) und dem Faktor $(1+f)$. I sind die Meßwerte für den Graphitabsorber ($l = 97.4$ cm; Dichte $\rho = 2.11$ g/cm³) †.

Die sehr deutliche Abweichung der Meßpunkte von der Kurve im Bereich der Riesenresonanz wird der Absorption durch die Atomkerne zugeschrieben:

$$\sigma_k = \frac{1}{Nl} \ln \frac{I'_0}{I}. \tag{3}$$

Diese einfache Deutung versagt in dem Fall, daß sich $\sigma_k(E)$ über die Nachweisbreite des Detektors hinweg ändert. An ihre Stelle tritt die kompliziertere Beziehung (7), die im folgenden abgeleitet werden soll.

In Fig. 5 ist der Fall skizziert (wie er nach Penfold und Spicer [6]) und Garwin und Penfold [7]) qualitativ für O^{16} zu erwarten ist), daß σ_k sich aus einzelnen, getrennten Resonanzen zusammensetzt, die schmäler als die Halbwertsbreite der Detektornachweisfunktion $A(E, E')$ sind. Letztere soll so definiert sein, daß sie die relative Wahrscheinlichkeit angibt, mit der Quanten der Energie E zur Zählrate beitragen, wenn das Spektrometer (d.h. das Magnetfeld) auf die Energie E' eingestellt ist. Da zur experimentellen Ermittlung keine monochromatischen γ-Strahlen ausreichender Intensität zur Verfügung standen,

† Das besonders reine und homogene Material wurde von der Kernreaktor Bau- und Betriebsgesellschaft, Karlsruhe, dankenswerterweise zur Verfügung gestellt.

wurde $A(E, E')$ berechnet. Die dazu außer der geometrischen Anordnung der Zähler benötigten Daten, im Wesentlichen die Winkel- und Energieverteilung der Paarteilchen beim Austritt aus der Konverterfolie, wurden experimentell bestimmt und mit den Theorien der Paarbildung [16]) und Vielfachstreuung [17]) verglichen. Die dabei gefundenen Ergebnisse stimmen gut mit den Voraussagen der Theorie überein [18]).

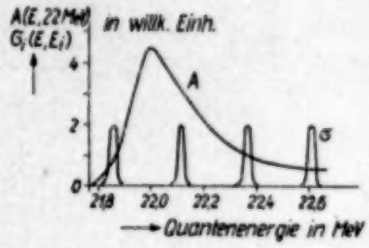

Fig. 5. Berechnete Detektor-Nachweisfunktion $A(E, E')$ bei $E' = 22$ MeV; angenommene schmale Resonanzen des Kernabsorptionsquerschnittes σ_k im Abstand $\frac{1}{4}$ MeV, entsprechend den Ergebnissen von Penfold und Spicer [6]) und Garwin und Penfold [7]).

Die Absorptionslinien sollen bei den Energien E_i liegen und Breit-Wigner-Verlauf haben:

$$\sigma_k(E, E_i) = \frac{\hat{\sigma}_i}{\left(\frac{E-E_i}{\frac{1}{2}\Gamma}\right)^2 + 1}; \tag{4}$$

$\hat{\sigma}$ ist der maximale Wirkungsquerschnitt; Γ die gesamte Halbwertsbreite. Ist $P(E, E_0)\mathrm{d}E$ das Quantenzahl-Spektrum mit der Grenzenergie E_0, so gilt allgemein (ohne Berücksichtigung des Compton-Korrekturfaktors f)

$$\frac{I}{I_0}(E') = \frac{\int_0^\infty P(E, E_0)A(E, E')\mathrm{e}^{-N(\sigma_p(E)+\sigma_e(E)+\sigma_k(E))l}\mathrm{d}E}{\int_0^\infty P(E, E_0)A(E, E')\mathrm{d}E}. \tag{5}$$

Für den in Fig. 5 skizzierten Fall von n schmalen Resonanzen läßt sich der Zähler zerlegen in einen „glatten" und n „Resonanzanteile" (s. z. Beisp. Ref. [19, 20])). Unter der Voraussetzung, daß $P(E, E_0)$ und $(\sigma_p+\sigma_e)$ sich über die Detektor-Breite nur wenig ändern und andererseits Γ klein ist gegen diese Breite (was beides für O^{16} nach [6, 7]) gut erfüllt ist), findet man

$$\frac{I}{I_0}(E') = \mathrm{e}^{-N(\sigma_p(E')+\sigma_e(E'))l}\left\{1 - \sum_{i=1}^{n} \frac{A(E_i, E')}{\int_0^\infty A(E, E')\mathrm{d}E} \int_0^\infty (1-\mathrm{e}^{-N\sigma_k(E, E_i)l})\mathrm{d}E\right\}. \tag{6}$$

Entwickelt man den Integranden bis zum quadratischen Glied einschließlich, so ergibt sich mit (4)

$$\frac{I}{I_0}(E') = \mathrm{e}^{-N(\sigma_p(E')+\sigma_e(E'))l}\left\{1 - \frac{Nl}{\int_0^\infty A(E, E')\mathrm{d}E} \sum_{i=1}^{n} [A(E_i, E')(1-\tfrac{1}{4}Nl\hat{\sigma}_i)\tilde{\sigma}_i]\right\}; \tag{7}$$

$\tilde{\sigma}_i$ ist der über die Energie integrierte Wirkungsquerschnitt der i'ten Resonanz.

4. Meßergebnisse und Diskussion

4.1. KOHLENSTOFF

Von 9 bis 17 MeV zeigt Fig. 4 recht gute Übereinstimmung zwischen den Meßpunkten I und der gerechneten Kurve I'_0. Die gemessene Schwächung stimmt mit der berechneten auf ± 3 %, der gemessene Wirkungsquerschnitt

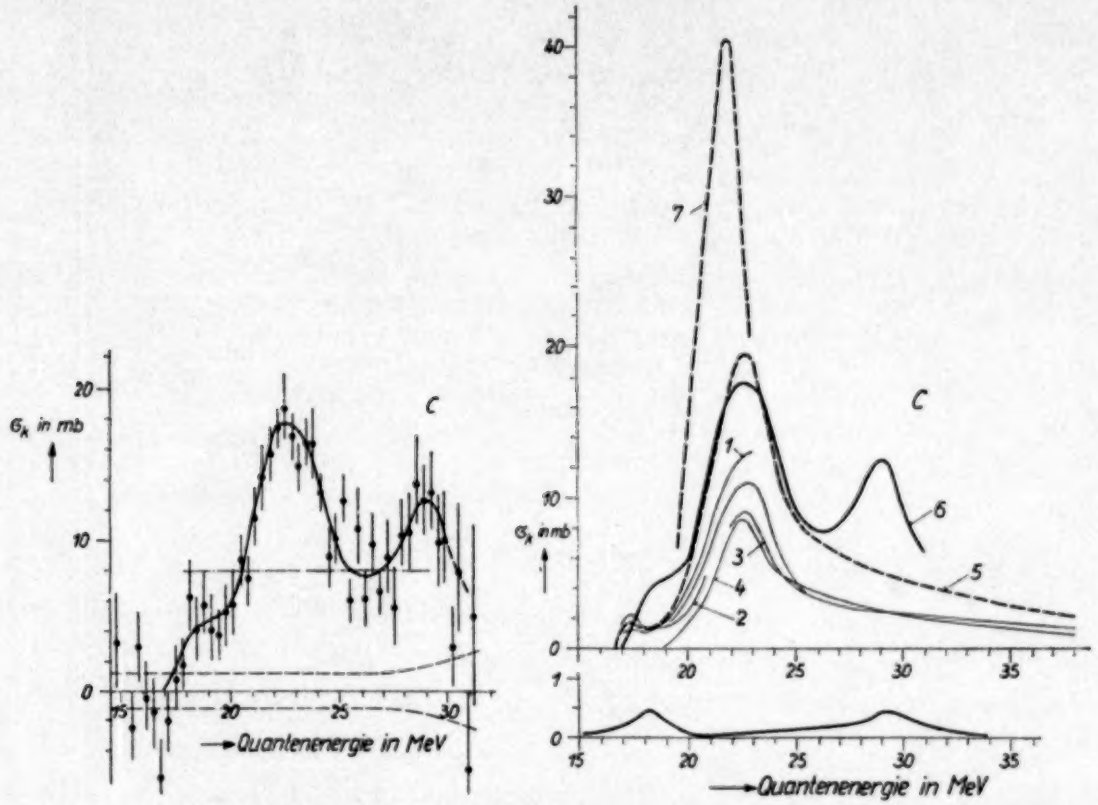

Fig. 6. Kernabsorptionsquerschnitt von Kohlenstoff. a) Berechnet nach (3). Die strichpunktierte Gerade gibt die bei einer früheren Messung [4]) (wobei nur der Gang mit der Energie, nicht der Absolutwert der Schwächung gemessen wurde) irrtümlich angenommene Lage der Nullinie von σ_k an, woraus ein zu kleiner Wert des maximalen Absorptionsquerschnittes resultierte.
b) 1. $\sigma(\gamma, p)$ nach Cohen *et al.* [21]); statt des dort angegebenen Wertes $4\pi(d\sigma/d\Omega)_{90°}$ wurde entsprechend der Winkelverteilung von Penner und Leiss [22]) ein um 20 % kleinerer Wert eingezeichnet.
2. $\sigma(\gamma, p)$ durch detailed balance aus $B^{11}(p, \gamma)$ gewonnen [21]);
3. $\sigma(\gamma, p)$ nach Penner und Leiss [22]).
4. $\sigma(\gamma, n)$ nach Barber *et al.* [23])
5. Mittelwerte aus 1, 2, 3 addiert zu Kurve 4;
6. Experimentelle Kurve aus Fig. 6a.
7. Riesenresonanz von C^{12} nach G. R. Bishop und R. Wilson im Handbuch der Physik, Bd. **42**, S. 337 (Springer Verlag 1957)
c) $\sigma(\gamma, 3\alpha)$ nach Goward und Wilkins [24]), ohne Feinstruktur.

$(\sigma_p+\sigma_c)$ mit dem bei der Rechnung angenommenen auf ± 1 % überein. Das Verhältnis σ_p/σ_c ist etwa $\frac{1}{2}$. Benutzt man für die Paarbildung im Kernfeld und den Comptoneffekt die theoretischen Werte, so erhält man für den Wirkungsquerschnitt der Paarbildung im Elektronenfeld aus den Kohlenstoffmessungen

zwischen 10 und 16 MeV die beiden in Fig. 3 eingezeichneten Meßpunkte.

Die Auswertung von Fig. 4 nach (3) liefert die in Fig. 6a gezeichneten Werte für den Kernabsorptionsquerschnitt σ_k. Die Fehlerbalken wurden aus Fig. 4 übertragen, enthalten also nur die einfachen mittleren statistischen Fehler der Messung I mit Absorber. Der Fehler der Meßkurve I_0 ergibt eine Unsicherheit in der Lage der Nullinie, angedeutet durch die gestrichelten Kurven. Zum Vergleich sind in Fig. 6b die Ergebnisse neuerer Messungen der Reaktionsquerschnitte $\sigma(\gamma, p)$ [21, 22]) und $\sigma(\gamma, n)$ [23]) eingezeichnet. Die Summenkurve $\sigma(\gamma, p)$ und $\sigma(\gamma, n)$ stimmt im Gebiet der Hauptresonanz bei 22.5 MeV gut mit der Meßkurve überein, während sie bei 18.5 MeV und 29 MeV deutlich darunter liegt.

Ein χ^2-Test für den Bereich 24—32 MeV liefert für die ausgezogene Kurve $P = 0.25$ und für eine horizontale Gerade in der Höhe 10 mb den Wert $P = 0.0025$. Man kann demnach ein Maximum bei 29 MeV als gesichert betrachten. Eine Messung mit etwas höherer Grenzenergie könnte allerdings diese Frage besser beantworten.

Immerhin ist auffallend, daß der Wirkungsquerschnitt der Reaktion C^{12} $(\gamma, 3\alpha)$ gerade bis 18 und 29 MeV resonanzartige Maxima durchläuft [24]). Ihr Betrag ist zu klein, um die Differenz zwischen Meß- und Summenkurve auszufüllen. Dazu könnte jedoch auch die (γ, d)-Reaktion (Schwelle bei 25 MeV) beitragen. Von ihr ist lediglich das Ausbeuteverhältnis bei 300 MeV Grenzenergie $Y(\gamma, d)/Y(\gamma, p) = 0.12$ bekannt [25]) †

Mit dem Summensatz für Dipolübergänge [27]), angewandt auf den Atomkern, finden Levinger und Bethe [5]) unter vereinfachten Annahmen

$$\int_0^\infty \sigma_k \mathrm{d}E = 60 \frac{NZ}{A} \alpha \qquad \text{(in MeV} \cdot \text{mb)}. \tag{8}$$

Im Faktor α stecken die wenig bekannten Parameter des Kernpotentials und Annahmen über die Art der Wechselwirkung der Nukleonen im Kern. Sein Zahlenwert dürfte bei etwa 1.3 liegen. Danach ist für Kohlenstoff $\int_0^\infty \sigma_k \mathrm{d}E = 230$ MeV · mb zu erwarten. Die ganze Fläche unter der Meßkurve bis 30 MeV ergibt (130 ± 20) MeV · mb. Die bisher bekannten (γ, n)- und (γ, p)-Querschnitte [22, 23]) liefern hierzu noch etwa 50 MeV · mb oberhalb 30 MeV. Die Summe 180 MeV · mb liegt immer noch 50 MeV · mb unterhalb des erwarteten Wertes, woraus man schließen kann, daß auch oberhalb 30 MeV andere Reaktionen noch zum totalen Absorptionsquerschnitt wesentlich beitragen.

4.2. ALUMINIUM

Zwischen 10 und 15 MeV liegen die Meßpunkte (s. Fig. 7) im Mittel um 3 % unter der mit den theoretischen Schwächungsfaktoren gerechneten Kurve.

† Bei S^{32} fanden Katz u. Penfold [26]) 6 MeV oberhalb der Schwelle ein Maximum des Wirkungsquerschnittes $\sigma(\gamma, d)$ von 6 mb (entsprechend etwa $\frac{1}{3}\sigma(\gamma, n)_{max}$).

Dies bedeutet, daß die Summe der theoretischen Wirkungsquerschnitte für Comptoneffekt und Paarbildung um 1 % zu klein berechnet wurden. Da bei Kohlenstoff keine derartige Differenz festgestellt wurde, kann man vermuten, daß die Diskrepanz hauptsächlich vom Paarbildungsquerschnitt herrührt. Das Verhältnis σ_p/σ_e ist hier etwa eins.

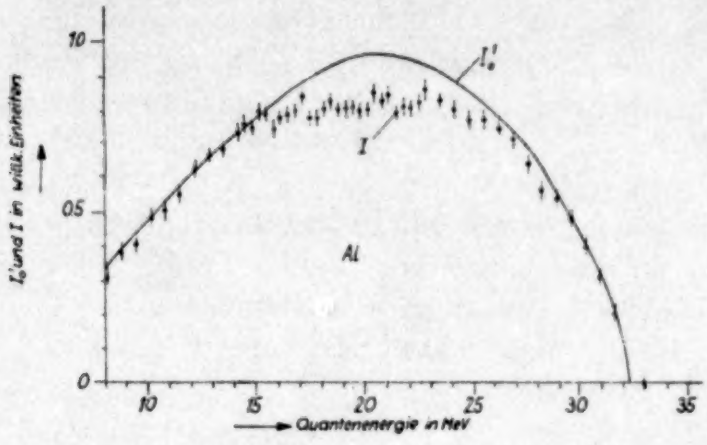

Fig. 7. Dieselbe Darstellung wie in Fig. 4 für den Aluminiumabsorber ($l = 45.5$ cm; Dichte $\rho = 2.7\,\mathrm{g/cm^3}$).

Von besonderem Interesse war, zu untersuchen, ob die sich früher[4]) andeutende und auch von anderen Autoren[3]) berichtete Struktur in der Riesenresonanzabsorption, die durch die Deformation des Al^{27}-Kernes hervorgerufen sein könnte[28, 29]), einer Prüfung mit besserer Statistik standhält. Fig. 8 zeigt das Ergebnis. Ein χ^2-Test für die nach Augenmaß eingezeichnete glatte Kurve

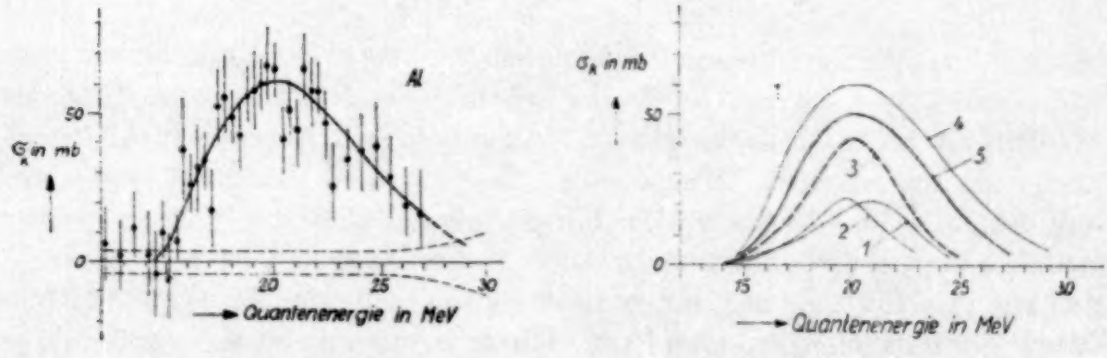

Fig. 8. Kernabsorptionsquerschnitt von Aluminium,
a) berechnet nach (3). Wird an der Summe $(\sigma_p+\sigma_e)$ eine Korrektur von +1 % angebracht, um zwischen 10 und 15 MeV bessere Übereinstimmung zwischen I'_0 und I zu erhalten (s. Fig. 7), so rückt die Nullinie für σ_k um 11 mb nach oben.
b) 1) $\sigma(\gamma, p)$ nach Halpern[30]) *et al.*;
2. $\sigma(\gamma, n)$ nach Montalbetti *et al.*[31]);
3. Summe $\sigma(\gamma, p)+\sigma(\gamma, n)$.
4. Kurve aus 8a;
5. Kurve aus 8a, verschoben um 11 mb.

gibt $P = 0.25$. Es besteht somit kein Grund, die Existenz irgendwelcher Strukturen anzunehmen †.

Fig. 8b zeigt für Aluminium einen Vergleich von Reaktionsquerschnitten (Kurven 1 und 2, Summenkurve 3) mit dem gemessenen Absorptionsquerschnitt (Kurve 4). Erhöht man die Summe von σ_p und σ_c um 1 % um zwischen 10 und 15 MeV bessere Übereinstimmung zwischen I'_0 und I zu erhalten (s. Fig. 7), so rückt die Nullinie für σ_k um 11 mb nach oben und man erhält Kurve 5 in Fig. 8b. Obwohl eine theoretische Begründung dieser 1 %-Differenz noch aussteht, ist diese Verschiebung experimentell gerechtfertigt. Kurve 5 in Fig. 8b soll als Endergebnis für Al angesehen werden.

Nach der Dipol-Summenregel ist bei Al ein integrierter Wirkungsquerschnitt von 530 MeV · mb zu erwarten (mit $\alpha = 1.3$). Kurve 5 in Fig. 8b ergibt (390 ± 100) (MeV · mb). Wegen des großen Fehlers hat es noch keinen Sinn, diese Messungen etwa zur experimentellen Ermittlung des Faktors α heranzuziehen.

4.3. SAUERSTOFF

Da aus den Ergebnissen verschiedener Experimente [6, 7]) gefolgert wird, daß der Wirkungsquerschnitt im Gebiet der Riesenresonanz bei O^{16} aus einzelnen, getrennten Absorptionslinien sich zusammensetzt, wurde versucht, die Dickenabhängigkeit der Absorption von γ-Quanten im Energiebereich 12 bis 26 MeV zu bestimmen. Aus zeitlichen Gründen konnte nur bei 6 Einstellungen des Spektrometers (11.6; 15.5; 19.5; 21.5; 23.5; 26.3 MeV) gemessen werden. Die größte verwendbare Absorberdicke war 120 cm H_2O.

Die Ergebnisse sind in Fig. 9 zusammengestellt. Die eingezeichneten Kurven wurden mit $(\sigma_p + \sigma_c)$ und der Comptonkorrektur $f(l)$ berechnet. Für $\sigma_k = 0$ sollten die Meßwerte auf diesen Kurven liegen. Für jede Energie ist ein Wirkungsquerschnitt angegeben, der sich aus der Differenz der Neigung einer durch die Meßpunkte gelegten Ausgleichskurve gegen die theoretische Kurve ergibt. Statistisch signifikante Abweichungen vom rein exponentiellen Verlauf konnten nicht beobachtet werden. Es sollen nun die Meßergebnisse mit den Angaben von Penfold und Spicer [6]) und Spicer und Garwin [7]) verglichen werden.

Die genannten Autoren leiten aus Knicken in der Anregungsfunktion für den (γ, n)-Prozeß folgende mittlere Parameterwerte der Resonanzstruktur des Wirkungsquerschnitts um 22 MeV herum ab: $\Gamma = 25$ keV; $\hat{\sigma}(\gamma, n) = 50$ mb; $\int_0^\infty \sigma dE = 2$ MeV · mb. Aus einem Selbstabsorptionsversuch im gleichen Energiebereich schließen sie auf Breiten einer Teilresonanz des totalen Absorptionsquerschnittes von kleiner als $\Gamma = 30$ keV und Spitzenwerte $\hat{\sigma} \geqq 106$ mb.

† Für die von Milhalovič [8]) eingezeichnete Kurve mit Resonanzstrukturen gibt ein χ^2-Test $P < 0.001$, während eine glatte Kurve (mit horizontalem Verlauf unter 17 MeV und über 25 MeV in 50 mb Höhe) den Wert $P = 0.35$ liefert.

Damit wird $\int_{\text{eine Res.}} \sigma dE \approx 5\,\text{MeV} \cdot \text{mb}$. Die beiden Angaben sind vereinbar, wenn man $\sigma(\gamma, \text{p})/\sigma(\gamma, \text{n})$ energieunabhängig etwa gleich $\frac{3}{2}$ setzt, was mit bisherigen Messungen verträglich ist. Im Intervall von 1 MeV bei 22 MeV fanden die genannten Autoren etwa 4 Resonanzen.

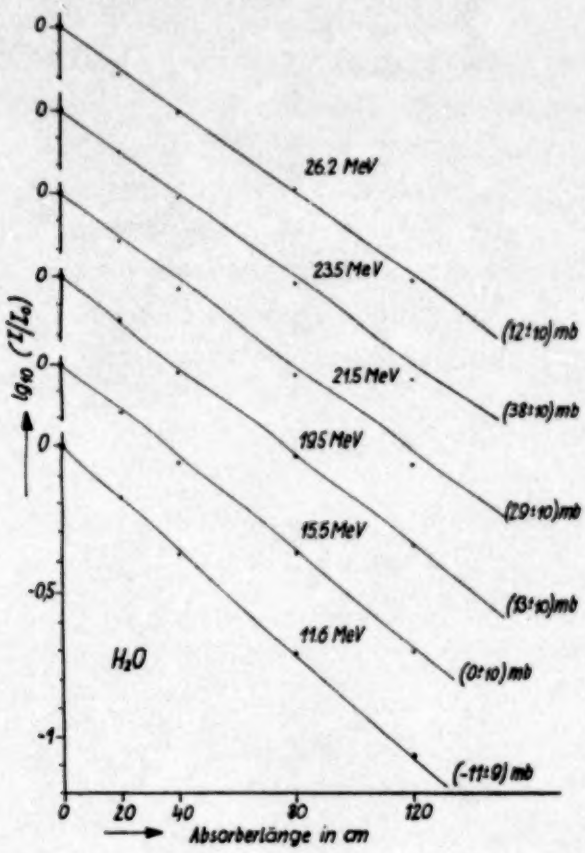

Fig. 9. Schwächung in H_2O bei den angegebenen γ-Energien. Die ausgezogenen Kurven wurden mit theoretischen Werten für $(\sigma_p + \sigma_c)$ berechnet, inkl. Comptonfaktor $f(l)$. Die angegebenen Wirkungsquerschnitte wurden mittels Ausgleichrechnung als Differenz zwischen den Neigungen der experimentellen und theoretischen Kurven ermittelt; einfacher mittlerer statistischer Fehler.

Mit diesen Werten und der in Fig. 5 dargestellten Spektrometernachweisfunktion lautet das Absorptionsgesetz (7) bei $E = 22$ MeV

$$\frac{I}{I_0}(E, l) = e^{-N(\sigma_p(E)+\sigma_c(E))l}\{1 - 5\times 10^{-4} l + 4\times 10^{-7} l^2\}. \tag{9}$$

Die Abweichung vom reinen Exponentialgesetz ist bei $l = 120$ cm nur etwa $3\,{}^0/_{00}$, ist also kleiner als der statistische Fehler dieses Experimentes.

Setzt man näherungsweise anstelle von (7)

$$\frac{I}{I_0}(l) = e^{-N(\sigma_p(E)+\sigma_c(E)+\sigma'_k(E))l} \quad \text{mit} \quad \sigma'_k = \frac{\sum_{i=1}^{n} A(E_i, 22\,\text{MeV})\,\tilde{\sigma}_i}{\int_0^\infty A(E, 22\,\text{MeV})dE}, \tag{10}$$

so wird σ'_k mit 17.5 mb deutlich kleiner als der hier gefundene Meßwert (33±7) mb (Mittelwert zwischen 21.5 und 23.5 MeV). Unter der Annahme schmaler Resonanzen ist demnach keine übereinstimmende Deutung der Ergebnisse beider Experimente möglich.

Nimmt man andererseits einen glatten Verlauf des Kernabsorptionsquerschnittes im Gebiet der Riesenresonanz an und benutzt anstelle eines aus (γ, n)- und (γ, p)-Messungen synthetisierten totalen Querschnitts zur Berechnung des beim Selbstabsorptionsversuch gemessenen [7]) Mittelwertes

$$\langle\sigma^0\rangle_0 = \frac{\int_0^\infty P(E, E_0)\sigma_k^2(E)\mathrm{d}E}{\int_0^\infty P(E, E_0)\sigma_k(E)\mathrm{d}E} \tag{11}$$

die in Fig. 9 angegebenen Wirkungsquerschnitte, so findet man im Rahmen der Meßfehler Übereinstimmung mit dem gemessenen $\langle\sigma^0\rangle_0$, also ein Verschwinden des „Resonanzeffektes". Damit braucht man auch zur Deutung des Ergebnisses beim Selbstabsorptionsversuch nicht mehr die Annahme schmaler Resonanzen.

Literatur

1) H. W. Koch und R. S. Foote, Rev. Sci. Instr. **25** (1954) 746
2) J. Kockum und N. Starfelt, Nucl. Instr. **5** (1959) 37
3) M. V. Milhalovič *et al.*, Phys. Rev. **114** (1959) 1621
4) B. Ziegler, Z. Phys. **152** (1958) 566
5) J. S. Levinger und H. A. Bethe, Phys. Rev. **78** (1950) 115
6) A. S. Penfold und B. M. Spicer, Phys. Rev. **100** (1955) 1377
7) A. S. Penfold und E. L. Garwin, Phys. Rev. **114** (1959) 1324
8) B. Ziegler, Z. angew. Phys. **10** (1958) 397
9) G. White Grodstein, N.B.S. Circular **583** (1957)
10) A. Borsellino, Helv. Phys. Acta **20** (1947) 136; Nuovo Cimento **4** (1947) 112
11) J. Moffat und G. C. Weeks, Proc. Phys. Soc. **73** (1959) 114
12) E. L. Hart, G. Cocconi, V. T. Cocconi und J. M. Sellen, Phys. Rev. in Druck
13) J. A. Wheeler und W. E. Lamb Jr., Phys. Rev. **55** (1939) 858
14) J. Joseph und F. Rohrlich, Revs. Mod. Phys. **30** (1958) 354
15) V. Votruba, Phys. Rev. **73** (1948) 1468
16) W. Heitler, The Quantum Theory of Radiation (Oxford, 1945)
17) G. Molière, Z. Naturforsch. **2a** (1947) 133
18) F. Kropf und W. Köhnlein, Dipl. Arbeiten, Karlsruhe 1958, unveröff.
19) C. Tzara, J. Phys. Rad. **17** (1956) 1001
20) A. K. M. Siddiq und R. N. H. Haslam, Can. J. Phys. **36** (1958) 963
21) L. Cohen *et al.*, Phys. Rev. **104** (1956) 108
22) S. Penner und J. E. Leiss, Phys. Rev. **114** (1959) 1101
23) W. C. Barber, W. D. George und D. D. Reagan, Phys. Rev. **98** (1955) 73
24) F. K. Goward und J. J. Wilkins, Proc. Roy. Soc. A **228** (1955) 376; Proc. Roy. Soc. A **217** (1953) 357
25) J. W. De Wire *et al.*, Phys. Rev. **95** (1954) 629
26) L. Katz und A. S. Penfold, Phys. Rev. **81** (1951) 816
27) H. A. Bethe, Handbuch der Physik **24/1** (1933) 434
28) K. Okamoto, Phys. Rev. **110** (1958) 142
29) M. Danos, Nuclear Physics **5** (1958) 23
30) J. Halpern und A. K. Mann, Phys. Rev. **83** (1951) 370
31) R. Montalbetti, L. Katz und J. Goldemberg, Phys. Rev. **91** (1953) 659

2.D

Nuclear Physics **17** (1960) 250—263; © *North-Holland Publishing Co., Amsterdam*

Not to be reproduced by photoprint or microfilm without written permission from the publisher

CLASSICAL THEORY OF COMPOUND NUCLEUS REACTIONS

TORLEIF ERICSON †

Department of Physics and Laboratory for Nuclear Science, Massachusetts Institute of Technology, Cambridge, Massachusetts ††

Received 15 January 1960

Abstract: The emission of particles from a compound system to individual states in the residual nucleus is studied in the classical limit of large angular momenta. Expressions are derived for total and differential cross-sections, when the target spin is polarized and unpolarized under different initial and final conditions. It is found that the angular distribution has a very simple classical limit, when the dependence on angular momentum of the penetrabilities of the emitted particle can be neglected.

1. Introduction

In spite of the great accuracy and generality of the description of angular momentum effects in nuclear reactions by Racah coefficients and Legendre polynomials, this formalism sometimes gives long and cumbersome expressions for results which become extremely simple in the classical limit of large angular momenta. In view of the fact that the classical study of a reaction provides a clearer insight into the dependence of cross-sections and angular distributions on various factors, and in some cases even a quite good quantitative description, we have investigated the emission of particles in the classical limit under the assumption of the existence of an intermediate compound state [1]). In a recent paper [2]) the angular distribution of particles emitted from a compound nucleus to many states in the residual nucleus has been shown to be equivalent to that resulting from evaporation of particles from a heated, rotating liquid drop. In the present paper we shall consider transitions to individual, isolated states of definite spin and parity in the residual nucleus. This paper can therefore in part be considered as a classical sequel to the quantal treatment of this problem by Wolfenstein [3]) and Hauser-Feshbach [4]). Our approach will, however, be entirely different and based on the classical approximation used by Ericson-Strutinski [2]) for the treatment of the rotating liquid drop. In the present case we cannot hope, however, to obtain results which permit an interpretation in a simple classical picture of this kind, owing to the fact that we study individual levels only. We shall consider the case of a reaction going

† On leave from Institute of Theoretical Physics, Lund, Sweden.

†† This work is supported in part through AEC Contract At-(30-1)-2098, by funds provided by the U. S. Atomic Energy Commission, the Office of Naval Research and the Air Force Office of Scientific Research.

from an initial state of the target of spin j_1, polarized or unpolarized, passing through a longlived intermediate compound state of angular momentum J from which a secondary particle is emitted by transition to a final state of spin j_f in the residual nucleus. We shall derive the general expressions for the total cross-section as well as the general formulas for the differential cross-sections with emphasis on the fundamental geometrical shapes of the angular distributions which obtain if the penetrabilities of the emitted particle are independent of its orbital angular momentum.

A definite assumption underlying our calculations is the hypothesis of an intermediate compound system for which the statistical assumption of matrix elements with random phases is valid. For lighter elements this approximation is doubtful even at fairly high excitation; not going into any detailed discussion of this point here we only point out that for a classical, spherical liquid drop in thermal equilibrium the rotation time must be long compared to the relaxation time for equilibrium. A liquid drop in equilibrium has the moment of inertia of a rigid body; a lower limit for the nuclear relaxation time is given by the time it takes for a nucleon to traverse the nucleus, but the actual relaxation time must be expected to be several times longer. By analogy with the liquid drop we shall therefore have an approximate condition for the existence of an intermediate system in equilibrium given by

$$\frac{5A^{4/3}}{I} \gg 1,$$

where I is the angular momentum of the absorbed incident particle measured in units of $\hbar$. The relation above has to be strictly fulfilled; indeed the left hand side must be expected to be at least an order of magnitude smaller in view of the too short relaxation time used. From its structure it is obvious that the condition is rather poorly fulfilled for light nuclei and high angular momenta (grazing collisions), i.e. for cases when direct interactions are known to be important †.

2. Theory

2.1. GENERAL FORMULAE

In the following we shall treat all angular momenta as classical, continuous vectors. The intrinsic spins of neutrons and protons both as projectiles and emitted particles will be neglected, because they are outside the classical description and because the orbital angular momenta are assumed to be large. We denote the spin of the target nucleus by $\mathbf{j}_1$, the orbital angular momentum of the incident particle by $\mathbf{I}$, the angular momentum of the intermediate compound state by $\mathbf{J} = \mathbf{I}+\mathbf{j}_1$, the orbital angular momentum of the emitted

† For a further discussion see forthcoming review article on statistical reactions by the author, to be published in *Advances in Physics*.

particle by $\mathbf{l}$ and the spin of the residual nucleus by $\mathbf{j}_f$, all measured in units of $\hbar$ †. The incident direction is the Z-axis, $\hat{\boldsymbol{Z}}$, and the direction of emission is $\mathbf{n}$.

The emission of a particle of angular momentum $\mathbf{l}$ in the direction $\mathbf{n}$ from the compound state $\mathbf{J}$ to the state j_f in the residual nucleus has a transition probability per unit time $P(\mathbf{J}, \mathbf{l}, j_f; \mathbf{n})$, which can be obtained by the principle of detailed balance [5]) in terms of the inverse cross-section, i.e. absorption of particles of angular momentum $-\mathbf{l}$ incident from the direction $-\mathbf{n}$. The classical inverse cross-section is expressed by Ericson-Strutinski [2]) in terms of the scalar product of the vectors $\mathbf{n}$ and $\mathbf{l}$, the Dirac delta-function and the volume element d^3l as

$$\mathrm{d}\sigma_l(\mathbf{n}, E) = \lambda\!\!\!^{-2}\delta(\mathbf{n}\cdot\mathbf{l})\mathsf{T}_l(E)\mathrm{d}^3l. \tag{1}$$

Here $\mathsf{T}_l(E)$ is the penetration factor of particles of angular momentum $\mathbf{l}$ and energy E neglecting deviations from nuclear sphericity ††. This factor depends on the actual model used for the nucleus, as it contains the entire dynamics of the process. The factor $\delta(\mathbf{n}\cdot\mathbf{l})$ in eq. (1) explicitly accounts for the perpendicularity of the orbital angular momentum of the particles to their direction of motion. The quantal expression for the cross-section for the l^{th} partial wave incident on a target is the well-known formula

$$\sigma_l(E) = (2l+1)\pi\lambda\!\!\!^{-2}\mathsf{T}_l(E). \tag{2}$$

The corresponding classical expression for continuous l is obtained from eq. (1) if we integrate over the solid angle of $\mathbf{l}$ and regard $\mathbf{n}$ as the Z-axis:

$$\sigma_l(E)\mathrm{d}l = \int_{\Omega_l} \lambda\!\!\!^{-2}\delta(\mathbf{n}\cdot\mathbf{l})\mathsf{T}_l(E)l^2\mathrm{d}l\mathrm{d}\Omega_l = 2l\pi\lambda\!\!\!^{-2}\mathsf{T}_l(E)\mathrm{d}l, \tag{2a}$$

which is exactly the classical analogue of eq. (2).

The principle of detailed balance including angular momentum conservation now permits us to write down the probability of emission per unit time. We denote by $\rho(\mathbf{J})$ the density of states of angular momentum $\mathbf{J}$ in the intermediate nucleus and by g the statistical factor of the emitted particle ($g = 2s+1$; s = spin of emitted particle). Then,

$$P(\mathbf{J}, \mathbf{l}, j_f; \mathbf{n}, E_f)\mathrm{d}^3l\mathrm{d}\Omega_n = \frac{1}{h}\,\frac{k^2\mathrm{d}\Omega_n g\mathrm{d}\sigma_l(\mathbf{n}, E_f)}{\rho(\mathbf{J})}\cdot\int C(\mathbf{j}; j_f)\delta^{(3)}(\mathbf{l}+\mathbf{j}-\mathbf{J})\mathrm{d}^{(3)}j \tag{3}$$

Here $\delta^{(3)}(\mathbf{r})$ is the 3-dimensional delta function which takes into account conservation of angular momentum and $C(\mathbf{j}; j_f)$ represents the phase space associated with the level of spin j_f due to the different possible orientations of its spin. This phase space factor is given by

$$C(\mathbf{j}; j_f) = \frac{1}{\pi}\,\frac{\delta(j-j_f)}{2j_f}. \tag{4}$$

† Wherever needed for clarity, we use indices i and f referring to initial and final states.

†† Particle energies are always supposed to refer to channel energy in centre of mass system.

The delta function fixes the length of $\mathbf{j}$ to j_t and we obtain the total phase space available to state j_t if we integrate this over all $\mathbf{j}$.

$$\int C(\mathbf{j}; j_t)\mathrm{d}^3 j = 2j_t,$$

which is the classical form of the quantal number of sub-states $(2j_t+1)$, as it should be.

The probability of emission from the compound state $\mathbf{J}$ to j_t is thus obtained from eq. (3) simply by introducing $\mathrm{d}\sigma_l(\mathbf{n}, E)$ and $C(\mathbf{j}; j_t)$ explicitly from eqs. (1) and (4) and integrating over $\mathbf{l}$

$$\begin{aligned} P(\mathbf{J}, j_t; \mathbf{n}, E_t) &= \frac{1}{h}\frac{k^2 g}{\rho(\mathbf{J})}\int \lambda^2 \delta(\mathbf{n}\cdot\mathbf{l})\mathsf{T}_l(E_t)\mathrm{d}^3\mathbf{l}\int\frac{1}{\pi}\frac{\delta(j-j_t)}{2j_t}\delta^{(3)}(\mathbf{l}+\mathbf{j}-\mathbf{J})\mathrm{d}^3 j \\ &= \frac{1}{h}\frac{g}{\rho(\mathbf{J})\pi 2j_t}\int \delta(\mathbf{n}\cdot\mathbf{l})\delta(|\mathbf{l}-\mathbf{J}|-j_t)\mathsf{T}_l(E_t)\mathrm{d}^3 l. \end{aligned} \tag{5}$$

If we instead ask for the total probability of emission from $\mathbf{J}$ to state j_t we have to integrate eq. (5) over total solid angle of $\mathbf{n}$.

$$\begin{aligned} P(\mathbf{J}, j_t; E_t) &= \frac{1}{h}\frac{g}{\rho(\mathbf{J})\pi 2j_t}\int \delta(|\mathbf{l}-\mathbf{J}|-j_t)\mathsf{T}_l(E_t)\mathrm{d}^3 l\int\delta(\mathbf{n}\cdot\mathbf{l})\mathrm{d}\Omega_n \\ &= \frac{1}{h}\frac{g}{\rho(\mathbf{J})\pi 2j_t}\iint\delta(|\mathbf{l}-\mathbf{J}|-j_t)\mathsf{T}_l(E_t)\frac{2\pi}{l}l^2\,\mathrm{d}l\mathrm{d}\Omega_l. \end{aligned} \tag{6}$$

This equation can be further simplified by carrying out the integration over the solid angle of $\mathbf{l}$. The pertinent integral is

$$\int\delta(|\mathbf{l}-\mathbf{J}|-j_t)\mathrm{d}\Omega_l = \frac{2j_t\pi}{lJ}\Delta^{(3)}(l, J, j_t). \tag{7}$$

We have expressed this integral in terms of the "triangular" function $\Delta^{(3)}(l, J, j_t)$ defined as

$$\Delta^{(3)}(l, J, j_t) = \begin{cases} 1 & \text{if } l, J, j_t \text{ can form a triangle} \\ 0 & \text{otherwise.} \end{cases}$$

Substituting eq. (7) back into eq. (6) we finally obtain

$$P(\mathbf{J}, j_t; E_t) = \frac{2\pi}{h}\frac{g}{J\rho(\mathbf{J})}\int_0^\infty \Delta^{(3)}(l, J, j_t)\mathsf{T}_l(E_t)\mathrm{d}l. \tag{8}$$

Practically all information needed about the decay of the compound system is contained in eqs. (5) and (8) and the probabilities of emission are there in a suitable form for further calculations. We shall therefore use these equations as the starting point for later discussions.

2.2. EMISSION CROSS-SECTION

The cross-section $\sigma(\mathbf{j}_1, j_t; \mathbf{n}, E_t)$ is obviously the cross-section for the formation of the compound state **J** times the relative probability of decay, which has to be integrated over all possible **J**. As the incident particles arrive along the Z-axis we can use eq. (1) and obtain in terms of the orbital angular momentum **I** of the projectile, remembering that angular momentum conservation requires $\mathbf{J} = \mathbf{I}+\mathbf{j}_1$,

$$\sigma(\mathbf{j}_1, j_t; \mathbf{n}, E_t) = \int \mathrm{d}\sigma_{\mathbf{I}}^{(1)}(\hat{Z}) \frac{P(\mathbf{J}, j_t; \mathbf{n}, E_t)}{\Sigma'_\nu P_\nu(\mathbf{J}, j'_t; E'_t)}. \tag{9}$$

The primed sum and the index ν in the denominator take into account all modes of decay of the state **J** by different kinds of emissions and to different states of the residual nucleus including compound elastic scattering.

The total cross-section for emission to the state j_t is thus obtained from eqs. (1), (8), and (9) to be

$$\sigma(\mathbf{j}_1, j_t; E_t) = \lambda_1^2 \int_0^\infty I \mathsf{T}_{\mathbf{I}}^{(\mathrm{i})} \mathrm{d}I \int_0^{2\pi} \mathrm{d}\varphi \frac{g \int_0^\infty \Delta^{(3)}(l, J, j_t) \mathsf{T}_l(E_t)\, \mathrm{d}l}{\Sigma'_\nu g_\nu \int_0^\infty \Delta^{(3)}(l, J, j'_t)\, \mathsf{T}_l^{(\nu)}(E'_t)\, \mathrm{d}l}, \tag{10}$$

where φ is the azimuthal angle of **I**, which describes its position in the plane perpendicular to the beam and $\mathsf{T}_l^{(\nu)}(E)$ the penetration factor of the particle ν incident on the corresponding residual nucleus. During the integration over the azimuthal angle φ the magnitude of the angular momentum J will vary with φ. This quantity enters both numerator and denominator in eq. (10) in a very complex manner in most cases and the integral over φ is therefore not suited for a general discussion. It simplifies, however, appreciably in two cases, namely:

a) when the target nucleus is unpolarized,

b) when the compound nuleus decays mostly by evaporation to levels in the statistical region and when angular momentum restrictions on the evaporated particles can be neglected. The first of these conditions implies that

$$P(\mathbf{J}, j_t; E_t) \ll P_{\text{total}}(\mathbf{J}).$$

This condition can usually be fulfilled in medium weight and heavy nuclei, where neutron evaporation becomes dominant at an excitation of a couple of MeV above the threshold for neutron emission. The second condition of no angular momentum restriction implies that the spins j'_t of the statistically populated levels must have a distribution of spins proportional to $2j'_t$ (i.e. quantally to $2j'_t+1$) for the effectively participating levels, because this is the geometrical phase space factor. This again implies that the effective values of j'_t must be smaller than the spin-cut-off factor [2]). Therefore the intermediate state cannot have arbitrarily large effective angular momentum for case (b) to be valid.

We obtain the result for unpolarized target by averaging over all directions of the target spin $\mathbf{j}_1$. Observing that

$$\frac{1}{4\pi}\int f(J)\,\mathrm{d}\Omega_{j_1} = \frac{1}{4j_1 I}\int_{|I-j_1|}^{I+j_1} 2Jf(J)\,\mathrm{d}J$$

because $J^2 = I^2+j_1^2-2\mathbf{j}_1\cdot\mathbf{I}$, we obtain

$$\sigma(j_1, j_t; E_t) = \frac{\pi\lambda_1^2}{2j_1}\int_0^\infty \mathsf{T}_I^{(1)}\,\mathrm{d}I \int_{|I-j_1|}^{I+j_1} 2J\mathrm{d}J\,\frac{g\int_0^\infty \Delta^{(3)}(l, J, j_t)\mathsf{T}_l(E_t)\mathrm{d}l}{\Sigma'_\nu g_\nu \int_0^\infty \Delta^{(3)}(l, J, j'_t)\mathsf{T}_l^{(\nu)}(E'_t)\mathrm{d}l} \tag{11}$$

Eq. (11) provides a useful form for the total cross-section when the emission from the intermediate state takes place to a few levels only in the residual nucleus. It should be noticed that this classical form of the total cross-section exhibits a strong similarity to the corresponding quantal form (cf. eq. (9) of ref. [4])).

Eq. (11) simplifies still further in the case of a low spin of the initial state, i.e. for $j_1 \ll I$ for the important values of I and becomes

$$\sigma(j_1 \approx 0, j_t; E_t) = \int_0^\infty \sigma_I^{(1)}\,\mathrm{d}I\,\frac{g\int_0^\infty \Delta^{(3)}(l, I, j_t)\mathsf{T}_l(E_t)\mathrm{d}l}{\Sigma'_\nu g_\nu \int_0^\infty \Delta^{(3)}(l, I, j'_t)\mathsf{T}_l^{(\nu)}(E'_t)\mathrm{d}l} \tag{11a}$$

When the number of states populated from the intermediate compound state increases eq. (11) rapidly becomes cumbersome owing to the great complexity of the sum in the denominator.

In case (b) of dominating statistical decay with no angular momentum restrictions on the **l** of the emitted particles, the denominator again takes on a simple form even in the case of polarized targets. In this case the quantal density of states of spin j'_t is $(2j'_t+1)\rho_0(E^*)$ in terms of the density of levels of spin 0 at excitation energy E^* for the states which have a high probability of being populated. We can thus write classically

$$\begin{aligned}
&\Sigma'_\nu g_\nu \int_0^\infty \Delta^{(3)}(l, J, j'_t)\mathsf{T}_l^{(\nu)}(E'_\nu)\mathrm{d}l \\
&\quad\approx \Sigma_\nu g_\nu \int_0^\infty \rho_{0\nu}(E_\nu{}^*)\mathrm{d}E_\nu \int_0^\infty \mathsf{T}_l^{(\nu)}(E_\nu)\mathrm{d}l \int_0^\infty 2j'_t\Delta^{(3)}(l, J, j'_t)\mathrm{d}j'_t \\
&\quad= 2J\Sigma_\nu g_\nu \int_0^\infty \rho_{0\nu}(E_\nu{}^*)\mathrm{d}E_\nu \int_0^\infty 2l\mathsf{T}_l^{(\nu)}(E_\nu)\mathrm{d}l \\
&\quad= \frac{2}{\pi}J\Sigma_\nu \int_0^\infty \rho_{0\nu}(E_\nu{}^*)k_\nu{}^2\sigma^{(\nu)}(E_\nu)\mathrm{d}E_\nu .
\end{aligned} \tag{12}$$

Here we have written $\sigma^{(\nu)}(E_\nu) = \pi\lambda_\nu{}^2\int_0^\infty 2l\mathsf{T}_l^{(\nu)}(E_\nu)\mathrm{d}l$. Substituting eq. (12) into eq. (10) we obtain

$$\sigma(\mathbf{j}_1, j_t; E_t) = \int_0^\infty \sigma_I^{(1)}\,\mathrm{d}I\,\frac{\pi g\int_0^\infty \mathsf{T}_l(E_t)\mathrm{d}l\,\frac{1}{2\pi}\int_0^{2\pi}\frac{\mathrm{d}\varphi}{2J}\Delta^{(3)}(l, J, j_t)}{\Sigma_\nu g_\nu \int_0^\infty k_\nu{}^2\sigma^{(\nu)}(E_\nu)\rho_{0\nu}(E_\nu{}^*)\mathrm{d}E_\nu}. \tag{13}$$

While the result of eq. (13) still has a very simple structure, we shall also re-express it in terms independent of the angle φ for the benefit of the reader who is particularly interested in a comparison with quantum mechanics, where this angle of course has no place in the answer. The result is fairly complicated and involves the elliptic integrals $F(\psi, k)$ and the real part of arcsin x. If α is the angle between the Z-direction and the direction of polarization the cross-section can be written

$$\sigma(\mathbf{j}_1, j_t; E_t) = \int_0^\infty \sigma_I^{(1)} \mathrm{d}I \frac{g \int_0^\infty \mathsf{T}_l(E_t) f(l, j_t; I, j_1, \sin\alpha)\mathrm{d}l}{\Sigma_\nu g_\nu \int_0^\infty k_\nu^2 \sigma^{(\nu)}(E_\nu)\rho_{0\nu}(E_\nu^*)\mathrm{d}E_\nu} \tag{13a}$$

Here the function $f(l, j_t; I, j_1, \sin\alpha)$ is given by

$$\begin{aligned} f(l, j_t; I, j_1, \sin\alpha) = (J_{\max}^{\frac{1}{2}} + J_{\min}^{\frac{1}{2}})^{-2} \Bigg\{ & [1 - \Delta^{(3)}(l, J_{\max}, j_t)] \\ & \times F\left(\mathrm{Re}\arcsin \frac{J_{\max}^{\frac{1}{2}} + J_{\min}^{\frac{1}{2}}}{J_{\max}^{\frac{1}{2}} - J_{\min}^{\frac{1}{2}}} \cdot \frac{l + j_t - J_{\max}^{\frac{1}{2}} J_{\min}^{\frac{1}{2}}}{l + j_t + J_{\max}^{\frac{1}{2}} J_{\min}^{\frac{1}{2}}} ; \left(\frac{J_{\max}^{\frac{1}{2}} - J_{\min}^{\frac{1}{2}}}{J_{\max}^{\frac{1}{2}} + J_{\min}^{\frac{1}{2}}}\right)^2\right) \\ & - [1 - \Delta^{(3)}(l, J_{\min}, j_t)] \\ & \times F\left(\mathrm{Re}\arcsin \frac{J_{\max}^{\frac{1}{2}} + J_{\min}^{\frac{1}{2}}}{J_{\max}^{\frac{1}{2}} - J_{\min}^{\frac{1}{2}}} \cdot \frac{|l - j_t| - J_{\max}^{\frac{1}{2}} J_{\min}^{\frac{1}{2}}}{|l - j_t| + J_{\max}^{\frac{1}{2}} J_{\min}^{\frac{1}{2}}} ; \left(\frac{J_{\max}^{\frac{1}{2}} - J_{\min}^{\frac{1}{2}}}{J_{\max}^{\frac{1}{2}} + J_{\min}^{\frac{1}{2}}}\right)^2\right) \\ & + 2F\left(\tfrac{1}{2}\pi; \left(\frac{J_{\max}^{\frac{1}{2}} - J_{\min}^{\frac{1}{2}}}{J_{\max}^{\frac{1}{2}} + J_{\min}^{\frac{1}{2}}}\right)^2\right)\Bigg\}. \end{aligned}$$

The numbers $J_{\max}$ and $J_{\min}$ above are the maximum and minimum values of the length of $\mathbf{J}$ and are given by

$$\begin{aligned} J_{\max} &= (I^2 + j_1^2 + 2Ij_1 \sin\alpha)^{\frac{1}{2}}, \\ J_{\min} &= (I^2 + j_1^2 - 2Ij_1 \sin\alpha)^{\frac{1}{2}}. \end{aligned}$$

The eq. (13a) will contain some obvious simplifications when $\sin\alpha = 0$ or 1.

Returning to eq. (13), the cross-section will simplify in the case of unpolarized target, similarly as eq. (11), into

$$\sigma(j_1, j_t; E_t) = \frac{\pi^2}{2j_1} \lambda_1^2 \int_0^\infty \mathsf{T}_I^{(1)} \mathrm{d}I \frac{g \int_{|I-j_1|}^{I+j_1} \mathrm{d}J \int_0^\infty \Delta^{(3)}(l, J, j_t)\mathsf{T}_l(E_t)\mathrm{d}l}{\Sigma_\nu g_\nu \int_0^\infty k_\nu^2 \sigma^{(\nu)}(E_\nu)\rho_{0\nu}(E_\nu^*)\mathrm{d}E_\nu}. \tag{14}$$

The cross-section for a target of low spin, polarized or unpolarized, becomes in analogy with eq. (11a)

$$\sigma(\mathbf{j}_1 \approx 0, j_t; E_t) = \pi^2 \lambda_1^2 \int_0^\infty \mathsf{T}_I^{(1)} \mathrm{d}I \frac{g \int_0^\infty \Delta^{(3)}(l, I, j_t)\mathsf{T}_l(E_t)\mathrm{d}l}{\Sigma_\nu g_\nu \int_0^\infty k_\nu^2 \sigma^{(\nu)}(E_\nu)\rho_{0\nu}(E_\nu^*)\mathrm{d}E_\nu}. \tag{14a}$$

2.3. ANGULAR DISTRIBUTION OF EMITTED PARTICLES

In this subsection we shall discuss the angular distribution of the emitted particles in different cases. It will turn out that the most useful classical ex-

pressions for the angular distributions are the geometrical ones which arise when the penetrability of the emitted particle is independent of orbital angular momentum. These expressions are clearly also the most important, as their general form, owing to their geometrical origin, will tend to persist even when penetration factors cannot be regarded as constant.

Using eqs. (5) and (8) together with eq. (1) we can immediately write

$$\sigma(\mathbf{j}_1, j_t; \mathbf{n}, E_t) = \lambda_1^2 \int_0^\infty I \mathsf{T}_I^{(1)} \mathrm{d}I \int_0^{2\pi} \mathrm{d}\varphi \frac{J}{(2\pi)^2 j_t} \frac{\int \delta(\mathbf{n}\cdot\mathbf{l})\delta(|\mathbf{l}-\mathbf{J}|-j_t)\mathsf{T}_l(E_t)\mathrm{d}^3 l}{\Sigma_\nu' g_\nu \int_0^\infty \Delta^{(3)}(l, J, j_t')\mathsf{T}_l^{(\nu)}(E_\nu')\mathrm{d}l}. \quad (15)$$

Though further integrations of eq. (15) can be performed under different assumptions about the initial spin without further specifying the dynamics of the process, the formulae which thus arise are not particularly useful. An important special case is, however, that of penetration factors for transition to the residual level independent or l so that they can be written $\mathsf{T}(E_t)$. Thus, the resulting angular distribution in this case is that inherent in the problem when there are no dynamical restrictions on the length of the angular momentum vector of the emitted particle. Introducing the step function $\theta(x)$, which is 0 for $x < 0$ and 1 for $x > 0$, we can then write the geometrical angular distribution as

$$\sigma_g(\mathbf{j}_1, j_t; \mathbf{n}, E_t) = \mathsf{T}(E_t)\lambda_1^2 \int_0^\infty I \mathsf{T}_I^{(1)} \mathrm{d}I \int_0^{2\pi} \frac{\mathrm{d}\varphi}{2\pi} \frac{gJ[\theta(\mathbf{J}\cdot\mathbf{n}+j_t)-\theta(\mathbf{J}\cdot\mathbf{n}-j_t)]}{\Sigma'_\nu g_\nu \int_0^\infty \Delta^{(3)}(l, J, j_t')\mathsf{T}_l^{(\nu)}(E'_\nu)\mathrm{d}l}. \quad (16)$$

Thus the differential cross-section for $\mathbf{j}_1 \approx 0$ is given by (cf. fig. 1)

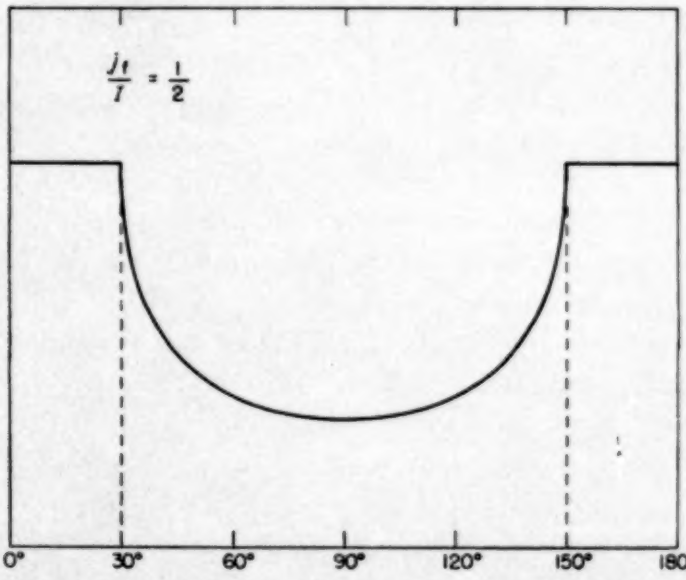

Fig. 1. Classical angular distribution for penetration factors independent of the angular momentum of the emitted particle in the case of a 0 spin target. The ratio between the spin of the level j_t in the residual nucleus and the angular momentum I of the incident particle is $\frac{1}{2}$. In the quantal case the angular distribution will be more smeared out, particularly in the neighbourhood of the critical angle.

$$\sigma_g(\mathbf{j}_1 \approx 0, j_t; \mathbf{n}, E_t) = \mathsf{T}(E_t) \int_0^\infty \sigma_I^{(1)} \mathrm{d}I \frac{\dfrac{gI}{\pi^2} \operatorname{Re} \arcsin \dfrac{j_t}{I \sin\theta}}{\Sigma'_\nu g_\nu \int_0^\infty \Delta^{(3)}(l, I, j'_t) \mathsf{T}_l^{(\nu)}(E'_\nu) \mathrm{d}l}. \quad (17)$$

Here θ is the angle between $\mathbf{n}$ and the beam direction. For compactness we have introduced the real part of arcsin x which has the property

$$\operatorname{Re} \arcsin x = \begin{cases} \arcsin x & (|x| < 1) \\ \frac{1}{2}\pi & (x > 1) \\ -\frac{1}{2}\pi & (x < -1). \end{cases}$$

As in the case of the total cross-section, closed expressions can be obtained when the intermediate state decays mainly to levels in the statistical region, corresponding to case (b) for the total cross-section. In the case of a polarized target the geometrical cross-section is obtained from eqs. (12) and (16):

$$\sigma_g(\mathbf{j}_1, j_t; \mathbf{n}, E_t) = \mathsf{T}(E_t) \int \sigma_I^{(1)} \mathrm{d}I \frac{\dfrac{g}{4\pi} \operatorname{Re} \left\{ \arcsin \dfrac{j_t + \mathbf{j}_1 \cdot \mathbf{n}}{I \sin\theta} + \arcsin \dfrac{j_t - \mathbf{j}_1 \cdot \mathbf{n}}{I \sin\theta} \right\}}{\Sigma'_\nu g_\nu \int_0^\infty k_\nu^2 \sigma^{(\nu)}(E_\nu) \rho_{0\nu}(E_\nu^*) \mathrm{d}E_\nu}. \quad (18)$$

It is immediately apparent that the same angular distribution results from aligned and polarized nuclei because the result is invariant under the substitution $\mathbf{j}_1 \to -\mathbf{j}_1$. It is not difficult to see that the more general eqs. (15) and (16) have the same property. This result obtains because the angular distribution from a classical rotating system of angular momentum $\mathbf{J}$ is only dependent on the magnitude of $\mathbf{J}$ and the direction of the axis, thus being the same for $\mathbf{J}$ and $-\mathbf{J}$. In our case $\mathbf{J} = \mathbf{I} + \mathbf{j}_1$, where $\mathbf{I}$ has to be averaged over its directions. The simultaneous change of $\mathbf{I}$ to $-\mathbf{I}$ and $\mathbf{j}_1$ to $-\mathbf{j}_1$ will thus only change $\mathbf{J}$ into $-\mathbf{J}$ with no change in angular distribution. As $-\mathbf{I}$ appears in the average on an equal basis as $\mathbf{I}$ the resultant angular distribution is thus the same for polarized and aligned targets.

The differential cross-section for unpolarized target results from eq. (18) by averaging over the directions of $\mathbf{j}_1$:

$$\begin{aligned} &\sigma_g(j_1, j_t; \mathbf{n}, E_t) \\ &= \mathsf{T}(E_t) \int_0^\infty \sigma_I^{(1)} \mathrm{d}I \frac{g}{2\pi} \frac{1}{2j_1} \Big\{ (j_1 + j_t) \operatorname{Re} \arcsin \frac{j_1 + j_t}{I \sin\theta} - |j_1 - j_t| \operatorname{Re} \arcsin \frac{|j_1 - j_t|}{I \sin\theta} \\ &+ \operatorname{Re} \sqrt{I^2 \sin^2\theta - (j_1 + j_t)^2} - \operatorname{Re} \sqrt{I^2 \sin^2\theta - (j_1 - j_t)^2} \Big\} \quad (19) \\ &\times \left[\Sigma_\nu g_\nu \int_0^\infty k_\nu^2 \sigma^{(\nu)}(E_\nu) \rho_{0\nu}(E_\nu^*) \mathrm{d}E_\nu \right]^{-1}. \end{aligned}$$

The real part of the square root is introduced to express conveniently

$$\operatorname{Re}\sqrt{x} = \begin{cases} \sqrt{x} & (x > 0) \\ 0 & (x < 0). \end{cases}$$

In the case of $j_1 \approx 0$ eq. (19) simplifies into

$$\sigma_g(j_1 \approx 0, j_f; \mathbf{n}, E_f) = \mathsf{T}(E_f) \int_0^\infty \sigma_I^{(1)} \mathrm{d}I \frac{\frac{g}{2\pi} \operatorname{Re} \arcsin \frac{j_f}{I \sin\theta}}{\Sigma_\nu g_\nu \int_0^\infty k_\nu^2 \sigma^{(\nu)}(E_\nu) \rho_{0\nu}(E_\nu^*) \mathrm{d}E_\nu}. \quad (19a)$$

3. Discussion

In the previous section we have mathematically derived a number of expressions for total and differential cross-sections in different cases. This section will discuss these results from a qualitative point of view, so as to expose the underlying physical mechanism and to get a clearer insight into the formulas. We shall do this in detail for the angular distributions which lend themselves readily to such a discussion.

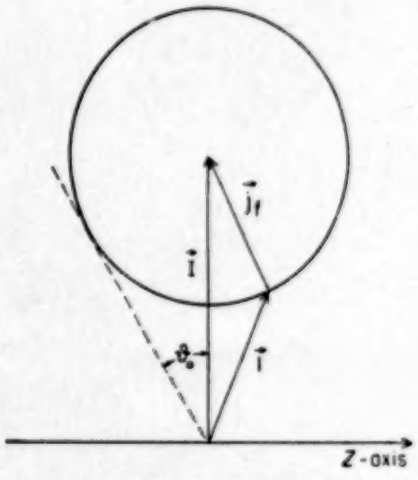

Fig. 2. Coupling of angular momentum vectors in the case of a 0 spin target. The angular momentum **l** of the emitted particle is restricted to lie on a sphere of radius j_f around the end point of the angular momentum **I** of the incident particle. The critical angle ϑ_0 is the angle between **I** and a tangent to the sphere.

Consider first the case of a zero spin target. The angular momentum of the intermediate state is thus entirely due to the orbital angular momentum of the projectile and is therefore in the plane perpendicular to the beam direction. On the other hand, there are no restrictions on the direction of the spin of the residual nucleus $\mathbf{j}_f$; only the length of this vector is specified. From conservation of angular momentum, the angular momentum **l** of the emitted particle is restricted to its direction by the condition $\mathbf{l} = \mathbf{I} - \mathbf{j}_f$ (see fig. 2). This means that the vector is restricted to end on a sphere of radius j_f around the end of **I**. We can

therefore regard **l** as being aligned with **I** but for the decoupling due to the fact that $j_t \neq 0$. The maximum angle of decoupling between **l** and **I** is given by

$$\sin \vartheta_0 = \frac{j_t}{I}. \tag{20}$$

If **l** and **I** are completely aligned the angular distribution of the emitted particles becomes $1/\sin\theta$ when the average over the direction of **I** perpendicular to the beam is taken. This is the form of the average mass distribution in space which arises when a homogeneous disk is rotating around a diameter. The place of the disk is in our case taken by the plane perpendicular to **l** in which the particles are emitted and which is being averaged over the directions of **I**. The large values of the differential cross-section for small values of $\sin\theta$ are thus due to a piling up of contributions from the different planes due to the complete perpendicularity of **l** to the beam direction at complete alignment. Therefore

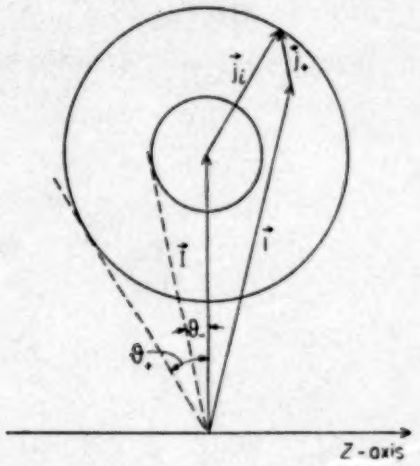

Fig. 3. Coupling of angular momentum vectors in the case of an unpolarized target of spin $\mathbf{j}_1$. The angular momentum **l** of the emitted particle is restricted to lie within the spherical shell determined by the radii j_1+j_t and $|j_1-j_t|$ around the end point of the angular momentum **I** of the incident particle. The two critical angles ϑ_+ and ϑ_- are the angles between **I** and a tangent to the corresponding sphere.

when **l** is decoupled from **I** by an angle $\approx \vartheta_0$ we expect a smearing out of the angular distribution in an angle of this magnitude around the beam; for angles far from this direction we expect an essentially unchanged angular distribution, similar to that of complete alignment. This result shows up clearly in eqs. (17) and (19a), if we take $j_t \ll I$. For $\sin\theta < j_t/I$ the angular distribution is so smeared out as to be isotropic, for $\sin\theta \gg j_t/I$ it has the behaviour $1/\sin\theta$ characteristic of complete alignment (see fig. 1). It is interesting to note that the ratio between the 90° and 0° cross-sections in the case of only one participating I-value is given by eq. (17) as $(2/\pi)\vartheta_0$. In the more general case of many participating I-values the ratio can be expressed by the average critical angle as $(2/\pi)\bar{\vartheta}_0$. While eq. (17) is derived for penetration factors not dependent on l, it is obvious that the general

characteristics of this angular distribution, i.e. a smearing-out region, a critical decoupling angle and a $1/\sin\theta$ region with a minimum at 90° have a considerably larger range of validity, and apply to all angular distributions from compound nuclei, if the angular momenta are fairly large. If there is no critical angle, or if the critical angle is close to 90°, the influence of the penetration factors as a function of l becomes dominant and the angular distribution should be calculated from eq. (15). In this case the angular distribution may even have a maximum at 90°.

This can be seen as follows. In the case of constant penetrabilities the angular distribution is isotropic if there is no decoupling angle. The large values of l are of the order of $I+j_t$ corresponding to a good alignment of **l** with **I**. When these are suppressed by the penetrabilities, this gives a relatively larger weight to those **l** which are approximately perpendicular to **I**, giving rise to a forced non-alignment instead of an alignment. The angular distribution is therefore in this case typical of that of the non-aligned case with a maximum at 90°, the opposite of that of the aligned case. This situation is only possible if the geometrical angular distribution is isotropic or very close to isotropic.

If we generalize our discussion to include the case of a target spin different from zero, we notice that the only difference is that angular momentum conservation now requires that $\mathbf{l} = \mathbf{I}+(\mathbf{j}_1-\mathbf{j}_t)$. This means that **l** now can end anywhere within the spherical shell determined by the two spheres with centres at the end point of **I** and with radii j_1+j_t and $|j_1-j_t|$, the target being assumed unpolarized (see fig. 3). From the geometry of the problem there must be two angles of special significance, ϑ_+ and ϑ_-, corresponding to the maximum and minimum angles that **l** can make with **I** while being located on the two limiting spheres. Thus,

$$\sin\vartheta_\pm = \frac{|j_1 \pm j_t|}{I}\,. \tag{21}$$

By the same reasoning as earlier the angular distribution will be typical of the aligned case and will have the character of $1/\sin\theta$ for $\sin\theta > \sin\vartheta_+$. Similarly the angular distribution must be just as smeared out as in the case of a zero spin target, i.e. again isotropic for $\sin\theta < \sin\vartheta_-$ (cf. eq. (19)). In the intermediate region of $\sin\vartheta_- < \sin\theta < \sin\vartheta_+$ there will still be an influence of the directional correlation though smearing-out effects will operate. This region will therefore give rise to a smooth joining between the isotropic and $1/\sin\theta$ regions.

In the case of total cross-sections, in eqs. (10), (11) and (12) the introduction of the "triangular" function $\Delta^{(3)}(l, J, j_t)$ corresponds exactly to the well-known quantal result that only l-values with the property $|J-j_t| \leqq l \leqq J+j_t$ can contribute to the cross-section. The exact comparison of eq. (11) to its known quantal form shows that the only essential difference consists of changing sums

into integrals and substituting $l+\frac{1}{2}, I+\frac{1}{2}$, etc. for l, I, etc., according to Kramers' rule. We may thus expect the classical expressions to reproduce closely the quantal ones if this replacement is introduced even in more complicated cases.

We want to point out two peculiarities of the classical description. Firstly, it should be noticed that the entire classical derivation has been performed without mentioning parity, which has no place in the classical description. Parity should have entered the different probabilities of decay and will give rise to a factor $\frac{1}{2}$ multiplying each decay probability. From eq. (9) we conclude, however, that the final result will remain unchanged because only the *ratio* of decay probabilities enters the final result and the common factor $\frac{1}{2}$ will drop out. As a consequence of this the level density $\rho_{0\nu}(E_\nu{}^*)$ which enters eq. (12) and following, always refers to the density of states of *both* parities. The second peculiarity is exemplified by the angular distribution of fig. 1. It results if the angular momentum vectors are assumed to have sharp values, $j_1 = 0, I$ and j_t. The angular distribution will then have infinite slope at the critical angle ϑ_0 in spite of the fact that is is impossible to obtain this with a finite number of Legendre-polynomials if the angular distribution is expanded in this way. On the other hand the quantal description always contains a finite number of Legendre-polynomials. The discrepancy is, however, entirely spurious; we are classically never allowed to use angular momentum vectors better defined than to one unit of $\hbar$ in length; the angular distribution has therefore to be averaged over this region of values for the classical vectors, and the apparent discontinuity in slope disappears.

Eqs. (14) and (14a) indicate the possibility of making an absolute determination of nuclear level densities by measuring the total cross-section to an individual state, when most of the decay goes to the statistical region. To make such a measurement a knowledge of the variation of the level density with energy is to some extent necessary. We illustrate the method in a case when the main part of the cross-section is due to neutron evaporation. With the idealized assumptions of geometric inverse cross-section for the neutron, πR^2, and a level density in the residual nucleus which varies exponentially in the region of excitation energy corresponding to the major part of the neutrons, $\rho_{0n}(E_n{}^*) = \rho_{0n}(U_n)e^{-E_n/T_n}$, where T_n denotes the nuclear temperature and U_n the maximum excitation energy of the residual nucleus, we have from eq. (14a), for target spin $j_1 \approx 0$,

$$\sigma(j_1 \approx 0, j_t; E_t) = \frac{\pi \dfrac{\hbar^2}{2M_n} \lambda_1{}^2 \displaystyle\int_0^\infty \mathsf{T}_I{}^{(1)} \mathrm{d}I \quad g \int_{|I-j_t|}^{I+j_t} \mathsf{T}_l(E_t)\mathrm{d}l}{\rho_{0n}(U_n) g_n R^2 T_n{}^2}. \tag{22}$$

Direct values of level densities are not easily obtained except from studies of neutron resonances. It should be possible to obtain level densities to at least within a factor two by the method outlined above. We want to emphasize that

the level density measured pertains to the residual nucleus corresponding to the neutron emission even if the level j_t has arisen from charged particle emission. The condition for the applicability of this method is that the cross-section is not dominated by direct interactions.

As a final conclusion we want to stress the basic simplicity of the classical results for cross-sections and in particular for angular distributions, which result from compound nucleus decay. The characteristic, geometrical, features of the angular distributions are the *minimum at* 90°, which is purely a result of angular momentum conservation and random phases, and the *critical decoupling angle*, within which the angular distribution is essentially isotropic. The fact that angular distributions determined experimentally usually have this form when they are symmetric around 90° and are thought to be due to compound nucleus formation seems to show that the influence of penetration factors does not change this basic structure of the distribution.

It is a pleasure to thank Professor H. Feshbach for several interesting discussions.

References

1) N. Bohr and F. Kalckar, Mat. Fys. Medd. Dan. Vid. Selsk. **14**, No. 10 (1937)
2) T. Ericson and V. Strutinski, Nuclear Physics **8** (1958) 284; **9** (1958/59) 689
3) L. Wolfenstein, Phys. Rev. **82** (1951) 690
4) W. Hauser and H. Feshbach, Phys. Rev. **87** (1952) 366
5) V. Weisskopf, Phys. Rev. **52** (1937) 295

1.D.1

Nuclear Physics **17** (1960) 264—270; © *North-Holland Publishing Co., Amsterdam*

Not to be reproduced by photoprint or microfilm without written permission from the publisher

NEUTRON ENERGY LEVELS IN A DIFFUSE POTENTIAL

ARUNDHATI GHOSH and N. C. SIL

Indian Association for the Cultivation of Science, Department of Theoretical Physics, Jadavpur, Calcutta 32

Received 15 February 1960

Abstract: The energy eigenvalues of neutrons within the nucleus for a spherically symmetrical potential $V(r) = -V_0[1+\exp\{(r-R)/a\}^{-1}$ are investigated by following a new method due to Lanczos for solving the differential equation. The s- and p-state energy levels have been calculated for atomic mass 200 with the values of parameters adopted by Feshbach, Porter and Weisskopf in their calculation of the neutron strength function with a similar potential. The results of our calculation agree closely with those of Malenka, whose potential is nearly, though not exactly, the same as ours.

1. Introduction

It has been pointed out by several authors [1]) that the true level sequence of nucleus for the shell model may be obtained from a diffuse potential which lies somewhere between that of harmonic oscillator and square well. Investigations have been made by many authors [2, 3]) to determine the bound states of neutrons moving in a spherically symmetric potential with an exponentially diffuse boundary. The success of the diffuse potential due to Woods and Saxon [4]) in nucleon-nucleus scattering problems has stimulated a number of authors [5, 6]) to apply the same for the investigation of the bound states of nucleons. The analytic solution of the Schrödinger equation for the bound s-states of neutrons with the potential $V(r) = -V_0[1+\exp\{(r-R)/a\}]^{-1}$, where R is the nuclear radius and a is the diffusivity parameter, has been given by Lawson[7]) in the form of an infinite Taylor series. Because of slow convergence of his series, the practical difficulties for evaluation of observable quantities are considerable. Following Lanczos [8]), we modify the above equation by equating it to an error term instead of to zero. The error term is proportional to a Tshebysheff polynomial of a given order. As a result, the differential equation becomes soluble by a finite power series. The right side of the equation, i.e. the error term, vanishes at the zero points of the Tshebysheff polynomial and the power series solution thus obtained is an interpolating one. The superiority of this method lies in the fact that a fixed number of terms gives a much more accurate result than what is possible with the same number of terms in the Taylor series. When considering higher angular momentum states, we have replaced the centrifugal potential term by its mean values at the two short ranges on both sides of the nuclear

boundary and solved the differential equation in these ranges by the method described above; analytic solutions have been used in regions other than these two ranges.

2. Mathematical Formulation

The Schrödinger equation for the neutron bound states in the potential $V(r) = -V_0[1+\exp\{(r-R)/a\}]^{-1}$ may be written as

$$\frac{d^2u_l}{dx^2} + \left\{\frac{\lambda^2}{1+\beta e^x} - k^2 - \frac{l(l+1)}{x^2}\right\} u_l(x) = 0, \tag{1}$$

where

$$x = \frac{r}{a}, \qquad \lambda^2 = \frac{2M}{\hbar^2} V_0 a^2, \qquad k^2 = \frac{2M}{\hbar^2} |E| a^2, \quad \beta = e^{-R/a}.$$

The function u, which is r times the radial wave function, should satisfy the boundary condition $u(0) = 0$ and $u(x \to \infty) \to 0$. For s-states the term due to centrifugal potential energy is absent.

To solve equation (1) in the region $R \leqq r < \infty$ we write [7]) $u = \exp(-kx)$ (the other solution $\exp(+kx)F$ does not satisfy the boundary condition); the equation becomes

$$z(z+\beta)\frac{d^2F}{dz^2} + (z+\beta)(1+2k)\frac{dF}{dz} + \lambda^2 F = 0, \tag{2}$$

with the substitution $z = e^{-x}$ (z varies from β to 0). Now we put $z = \beta p$ and, applying the suggestion of Lanczos [8]), modify the above differential equation by putting on the right side a term proportional to Tshebysheff's polynomial $T_n(p)$ of order n:

$$D(\bar{F}) = \tau T_n(p), \qquad D(\bar{F}) \equiv p(p+1)\frac{d^2\bar{F}}{dp^2} + (p+1)(1+2k)\frac{d\bar{F}}{dp} + \lambda^2 \bar{F}. \tag{3}$$

This artificial modification of the given differential equation can be considered as introducing an error which becomes negligible if τ is made sufficiently small. This simple modification, as shown by Lanczos, transforms the extrapolating power series to an interpolating one. To take advantage of the table given by Lanczos, we have made the transformation such that the new independent variable always varies from 0 to 1. Let

$$T_n(p) = B_0 + B_1 p + B_2 p^2 + \ldots + B_r p^r + \ldots + B_n p^n. \tag{4}$$

We now put the finite series

$$\bar{F} = a_0 + a_1 p + a_2 p^2 + \ldots + a_r p^r + \ldots + a_n p^n \tag{5}$$

in the differential equation (3) and comparing the coefficients of the same power of ρ on both sides of the equation, we get the recursion formulae

$$\tau B_r = a_r[\lambda^2+r(2k+r)]+a_{r+1}[(r+1)(1+2k+r)], \tag{6a}$$

$$\tau B_n = [n^2+2kn+\lambda^2]a_n. \tag{6b}$$

These relations will determine the coefficients a_r of the approximate solution and the factor τ which estimates the error of the approximation in terms of a_0.

The solution in the region $0 < r \leqq R$ is written as

$$u^{\pm}(x) = e^{\pm i\gamma x} F^{\pm},$$

where $\gamma = \sqrt{\lambda^2-k^2}$. Now with the substitution $t = e^x$ we get from equation (1)

$$t(1+\beta t)\frac{d^2F^{\pm}}{dt^2}+(1\pm 2i\gamma)(1+\beta t)\frac{dF^{\pm}}{dt}-\lambda^2\beta F^{\pm} = 0, \tag{7}$$

where t varies from 1 to $1/\beta$. With the substitution $q = \beta(t-1)/(1-\beta)$, the range of q becomes 0 to 1, and eq. (7) becomes

$$q(q+1)\frac{d^2F}{dq^2}+(q+1)(1\pm 2i\gamma)\frac{dF}{dq}-\lambda^2 F = 0, \tag{8}$$

neglecting terms involving $\beta \approx 10^{-6}$. Taking

$$F^{\pm} = a_0+a_1^{\pm}q+a_2^{\pm}q^2+\ldots+a_r^{\pm}q^r+\ldots+a_n^{\pm}q^n, \tag{9}$$

we get as before the recursion formulae

$$\tau B_r = [-\lambda^2+r(r\pm 2i\gamma)]a_r^{\pm}+[(r+1)(1\pm 2i\gamma+r)]a_{r+1}^{\pm}, \tag{10a}$$

$$\tau B_n = [-\lambda^2+n(n\pm 2i\gamma)]a_n^{\pm}. \tag{10b}$$

Following Lawson [7]) we take the solution which will satisfy the boundary and reality conditions as a linear combination of u^+ and u^-. The eigenvalues are obtained by matching the logarithmic derivative of the inner and outer solutions at $r = R$.

For the calculation of p and higher angular momentum states, the centrifugal potential term offers difficulty for an exact solution of the equation. Considering the relative importance of the centrifugal potential with respect to the nuclear potential and the appropriate transformation of the independent variable we divide the entire range of r from 0 to ∞ into four subranges (cf. fig. 1):

(I) $0 < r \leqq r_1$ (the nuclear potential remains practically constant),

(II) $r_1 \leqq r \leqq R$

(III) $R \leqq r \leqq r_2$ } (the nuclear potential varies considerably),

(IV) $r_2 \leqq r < \infty$ (the nuclear potential is practically zero).

In range (I), the nuclear potential, which practically remains constant, is replaced by a constant term and the centrifugal term is taken exactly. In range (IV), the nuclear potential practically falls to zero and we take only the centrifugal term. The analytic solutions fitting the boundary condition at $r = 0$ and $r = \infty$ are then easily obtained. In ranges (II) and (III), the centrifugal term is approximated by half the sum of its values at the two extreme points of the ranges. For our calculation we have divided the range in such a way that at

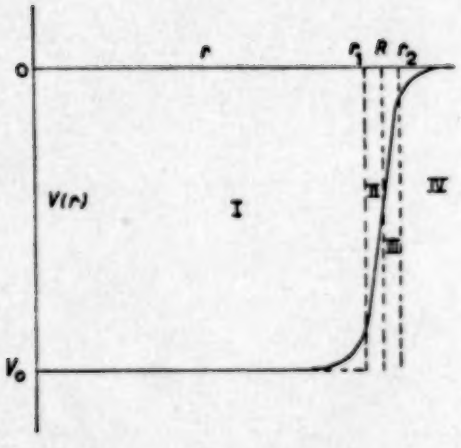

Fig. 1. Shape of the nuclear potential $V(r) = -V_0[1+\exp\{(r-R)/a\}]^{-1}$ with $V_0 = 52$ MeV, $R = (1.15A^{\frac{1}{3}}+0.4)\times 10^{-13}$ cm, $a = 0.57\times 10^{-13}$ cm. The entire range of r is divided into four subranges: (I) 0 to r_1, (II) r_1 to R, (III) R to r_2 and (IV) r_2 to ∞.

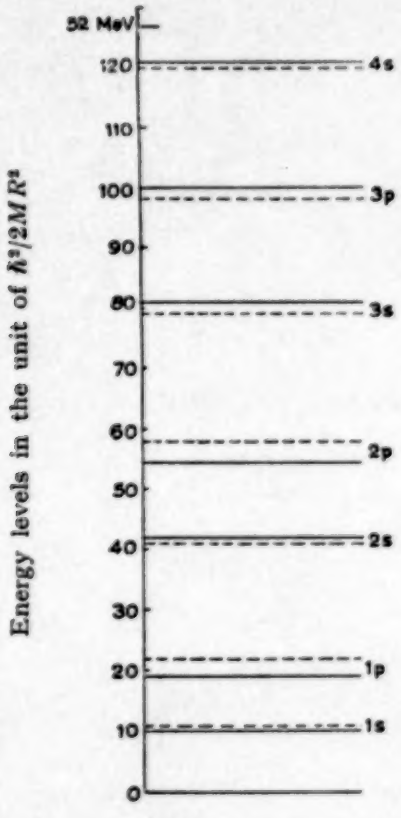

Fig. 2. Neutron energy levels for atomic mass 200. The continuous lines correspond to the present calculations and the broken lines to those of Malenka.

$r_1 = R-a\log_e 9$ the nuclear potential drops only to $\frac{9}{10}$ of the value V_0. Thus, from $r = 0$ to $r = r_1$ the nuclear potential may be taken as constant. At $r_2 = R+a\log_e 9$ the nuclear potential drops to $\frac{1}{10}V_0$; thus, beyond this range it may be neglected. Thus, the variation of nuclear potential may be considered to be confined only in the region $r_1 = R-a\log_e 9$ to $r_2 = R+a\log_e 9$. In this short range it is justified to take the centrifugal potential term as linear, in which case it may be replaced by its mean values. Now in the range (III), we

write

$$u_l^{\pm}(x) = e^{\pm k'x} F^{\pm},$$

where

$$k'^2 = k^2 + \tfrac{1}{2}l(l+1)\left[\left(\frac{a}{R}\right)^2 + \left(\frac{1}{\frac{R}{a} + \log_e 9}\right)^2\right]$$

and change the independent variable from x to z as before; z varies from $\frac{1}{9}\beta$ to β. The resulting equation for $F^{\pm}$ is

$$z(z+\beta)\frac{d^2F^{\pm}}{dz^2} + (z+\beta)(1 \mp 2k')\frac{dF^{\pm}}{dz} + \lambda^2 F^{\pm} = 0.$$

We normalize the range of z by putting $p = \frac{1}{8}(9z-\beta)/\beta$ and proceeding as before, we get the recursion formulae

$$\tau B_n = [\lambda^2 + n(n \mp 2k')]a_n, \tag{11a}$$

$$64\tau B_{n-1} = 64[\lambda^2 + (n-1)(n-1 \mp 2k')]a_{n-1} + n[88(n-1) + 80(1 \mp 2k')]a_n, \tag{11b}$$

$$64\tau B_r = 64[\lambda^2 + r(r \mp 2k')]a_r + (r+1)[80(1 \mp 2k') + 88r]a_{r+1} + 10(r+2)(r+1)a_{r+2}. \tag{11c}$$

In the range (II), we write

$$u^{\pm}(x) = e^{\pm i\gamma' x} F^{\pm} \quad \text{with} \quad \gamma' = \sqrt{\lambda^2 - k''^2},$$

where

$$k''^2 = k^2 + \tfrac{1}{2}l(l+1)\left[\left(\frac{a}{R}\right)^2 + \left(\frac{1}{\frac{R}{a} - \log_e 9}\right)^2\right].$$

Taking $t = e^x$ as our independent variable, varying from $1/\beta$ to $1/9\beta$, we get the following equation for $F^{\pm}$:

$$t(1+\beta t)\frac{d^2F^{\pm}}{dt^2} + (1 \pm 2i\gamma')(1+\beta t)\frac{dF^{\pm}}{dt} - \lambda^2\beta F^{\pm} = 0.$$

The range of t is next normalized by putting $q = \frac{1}{8}(9\beta t - 1)$ and proceeding as before we get the recursion formulae

$$\tau B_n = [-\lambda^2 + n(n \pm 2i\gamma')]a_n, \tag{13a}$$

$$64\tau B_{n-1} = 64[-\lambda^2 + (n-1)(n-1 \pm 2i\gamma')]a_{n-1} + n[88(n-1) + 80(1 \pm 2i\gamma')]a_n, \tag{13b}$$

$$64\tau B_r = 64[-\lambda^2 + r(r \pm 2i\gamma')]a_r + (r+1)[80(1 \pm 2i\gamma') + 88r]a_{r+1} + 10(r+2)(r+1)a_{r+2}. \tag{13c}$$

In the range (III), the solution is written as

$$A^+ e^{+k'x} F^+ + A^- e^{-k'x} F^-.$$

In the range (IV), the solution is taken as $x h_l^{(1)}(ikx)$. The constants A^+ and A^- are determined by matching the two solutions and their derivatives at $r = r_2$. In the range (II), we take the solution as

$$A e^{i\gamma' x} F^+ + A^* e^{-i\gamma' x} F^-.$$

In the range (I), the solution is given as $x j_l(\gamma x)$. The constants A and A^* are determined by the usual matching at $r = r_1$. The eigenvalues are determined by matching the logarithmic derivative of the solutions in the ranges (II) and (III) at $r = R$.

3. Results and Discussion

In fig. 2, we give the results of our calculation for atomic mass 200. The values of the parameters in the potential function are $V_0 = 52$ MeV, $R = (1.15A^{\frac{1}{3}} + 0.4) \times 10^{-13}$ cm $= 7.12 \times 10^{-13}$ cm for $A = 200$, and $a = 0.57 \times 10^{-13}$ cm. These are the same as taken by Feshbach *et al.* [9]) in their calculation of the neutron strength function. The results of our calculation agree with those of Malenka [2]) who has taken the nuclear potential to be of the form

$$V(r) = -V_0 \quad \text{for} \quad r < R,$$

$$V(r) = -\tfrac{3}{4} V_0 e^{-(r-R)/a} \quad \text{for} \quad r > R,$$

where the values of the parameters are $V_0 = 34.1$ MeV, $R = r_0 A^{\frac{1}{3}} = 8.77 \times 10^{-13}$ cm for $A = 200$, and $a = 0.71 \times 10^{-13}$ cm.

In discussing the practical importance of our method, we may mention that it yields with the same number of terms a much more accurate approximation than the Taylor series. For the ranges $0 < r < R$ and $R < r < \infty$ Lawson [7]) has given a solution in the form of a Taylor series in powers of $e^{+r/a}$ and $e^{-r/a}$ respectively. Both series solutions converge rather badly at the point corresponding to $r = R$, which lies on the circles of convergence in the complex plane. The economy of our method can be easily seen from the calculation of the outer wave functions evaluated at $r = R$ for $k = 0.20$; in our method when we want to approximate the solution by a polynomial of order 6, i.e. $F = a_0 + a_1 p + \ldots a_4 p^4 + \ldots a_6 p^6$, the error to be introduced in the differential equation is of the order of $a_0 \times 10^{-4}$; this also gives roughly an estimate of the error in the solution; whereas the Taylor series solution evaluated up to the 12th term gives an error in the solution of the order of $a_0 \times 10^{-2}$. The truncated Taylor series gives good approximation only in the neighbourhood of the point of expansion but it fails to yield satisfactory approximation as we move far

away from this point. The method used here, on the other hand, gives good approximation throughout the range, the maximum error at any point of the range can be made sufficiently small.

If we take the spin-orbit interaction into account, the radial Schrödinger equation for the two states $j = l+\frac{1}{2}$ and $j = l-\frac{1}{2}$ may be obtained in the form given by Ross *et al.* [5]). Since the spin-orbit interaction is only a surface effect, it has appreciable value only in the ranges (II) and (III) where we may replace the term dV/rdr (occurring in the spin-orbit coupling energy) by dV/Rdr as maximum weight at $r = R$. In the ranges (II) and (III) the differential equation may be solved by applying the method of Lanczos when analytic solutions are known for the range (I) and (IV). As an alternative the spin-orbit coupling energy may also be considered as a simple perturbation energy when we can use as the unperturbed wave functions the solutions we have obtained without considering the spin-orbit term.

We wish to thank Professor D. Basu for his kind interest in the problem and for helpful discussions during the progress of the work.

References

1) M. G. Mayer and J. Hans D. Jensen, Elementary Theory of Nuclear Shell Structure (1955)
2) B. J. Malenka, Phys. Rev. **86** (1952) 68
3) A. E. S. Green and K. Lee, Phys. Rev. **99** (1955) 772
4) R. D. Woods and D. S. Saxon, Phys. Rev. **95** (1954) 577
5) A. A. Ross, Hans Mark and R. D. Lawson, Phys. Rev. **102** (1956) 1613
6) P. E. Nemirovskii, Soviet Physics, JETP, **6** (1958) 573
7) R. D. Lawson, Phys. Rev. **101** (1956) 311
8) C. Lanczos, Journal of Mathematics and Physics **17** (1938)
9) H. Feshbach, Annual Rev. of Nuclear Science **8** (1958) 88

2.A.1

Nuclear Physics **17** (1960) 271—278; © *North-Holland Publishing Co., Amsterdam*

Not to be reproduced by photoprint or microfilm without vritten permission from the publisher

ABSOLUTBESTIMMUNG DES SCHWELLENWERTES DER REAKTION $Li^7(p, n)Be^7$

HANS H. STAUB und HUBERT WINKLER

Physik-Institut der Universität Zürich

Eingegangen am 30. Januar 1960

Abstract: The threshold proton energy of the reaction $Li^7(p, n)Be^7$ is measured, using the magnetic deflection technique in a homogeneous 180° field. The procedure of extrapolation of the yield curve is presented. The final value obtained is $E_S = 1880.3 \pm 0.5$ keV. A summary of all recent values of this threshold energy is presented. Furthermore, revised values of resonance energies, measured previously by Bumiller and collaborators, are given as the present measurements allow an accurate correction for the permeability of the vacuum chamber.

1. Einleitung

Die Kernreaktion $Li^7(p, n)Be^7$ mit einem Schwellenwert von 1881 keV ist der wichtigste Standard für die Energieeichung niederenergetischer Partikelbeschleuniger. Dieser Schwellenwert ist deshalb einige Male sowohl absolut als auch relativ zu anderen absolut gemessenen Energiewerten bestimmt worden. Herb, Snowden und Sala [1]), und Bondelid und Kennedy [2]) benutzten für ihre Absolutmessungen die Ablenkung der Protonen im elektrostatischen Zylinderfeld. Die Energie der Protonen ergibt sich dabei aus geometrischen Messungen, Korrekturen für den Feldverlauf am Anfang und Ende des elektrischen Feldes und aus dem Vergleich einer Hochspannung von ca. 20 kV mit einem Normalelement. Shoupp, Jennings und Jones [3]) haben die Geschwindigkeit der Protonen mit einer Laufzeitmethode absolut gemessen, wobei zur Energiebestimmung eine Frequenz und eine Länge gemessen werden müssen. Mit einem elektrostatischen Analysator sind Relativmessungen der $Li^7(p, n)$ Schwellenenergie zur Energie der Alphateilchen des RaC′ und des Po von Sturm und Johnson [4]) ausgeführt worden, wobei für den Absolutwert die Energiewerte von Briggs bzw. Rosenblum und Dupouy benutzt wurden. Eine weitere Relativmessung liegt von Jones, Douglas, McEllistrem und Richards [5]) vor, bei der der Schwellenwert im elektrostatischen Analysator mit dem Q-Wert der inelastischen Protonstreuung an Mg^{24} verglichen wurde. Die Vergleichsenergie, d.h. die Energie des dem β-Zerfall des Na^{24} folgenden γ-Strahls, wurde an die absolut gemessenen γ-Energiewerte des Co^{60} (magnetisches Photoelektronspektrometer), bzw. des Au^{198} (Kristallspektrometer) angeschlossen.

Die Wünschbarkeit weiterer unabhängiger Absolutmessungen des $Li^7(p, n)$-

Schwellenwertes wurde insbesondere an der Sitzung vom 29. April 1959 des Subcommittee on Nuclear Constants des National Research Councils in Washington festgestellt.

2. Meßmethode

Wir haben nach einer schon von Bumiller, Staub und Weaver [6]) für die Messung von (p, γ)-Resonanzen benützten Absolutmethode den Schwellenwert der Reaktion $Li^7(p, n)Be^7$ neu bestimmt. Bei dieser Methode wird der Impuls der Protonen durch Ablenkung über 180° in einem homogenen Magnetfeld gemessen. Ein- und Austrittsspalt, welche den Krümmungsradius der Protonen bestimmen, befinden sich dabei im homogenen Feld. Das Magnetfeld wird mit der Methode der magnetischen Kernresonanz von Protonen gemessen. Man erhält also den Impuls der beschleunigten Protonen durch Messung einer Länge (Spaltabstand) und einer Frequenz. Bei der Berechnung der Energie in Elektronenvolt werden dann außer einer sehr kleinen relativistischen Korrektur nur noch zwei absolut gemessenene Größen benutzt, nämlich das gyromagnetische Verhältnis γ_p des Protons und das Verhältnis ν_C/ν_K der Zyklotronfrequenz des Protons zu seiner Kernresonanzfrequenz bei gleichem Magnetfeld. Diese beiden atomaren Konstanten sind von Driscoll und Bender [7]) bzw. Sommer, Thomas und Hipple [8]) sehr genau absolut bestimmt worden. Bei der Ablenkung im homogenen Magnetfeld tritt nach 180° eine Richtungsfokussierung der Protonen gleicher Energie auf. Eine genaue Kenntnis der Protonenbahn zwischen den Spalten ist deshalb nicht notwendig. Es genügt, die möglichen Bahnen im Magnetfeld durch einen ziemlich breiten Spalt als Aperturblende etwa bei 90° einzuschränken.

3. Ausbeutekurve

Als Neutronendetektor diente ein mit ca. 0.5 atm BF_3 gefüllter Proportionalzähler von 40 mm Durchmesser und etwa 200 mm Länge, der mit seiner Achse in Richtung des einfallenden Protonenstrahls hinter dem Target angebracht war. Der Zähler war mit 3 cm Paraffin umgeben, auch befand sich zwischen dem Target und dem Zähler eine Paraffinschicht von 1 cm. Der Nulleffekt betrug ca. 2 % der höchsten in diesem Experiment gemessenen Zählraten und wurde durch Auswechseln des Li-Targets gegen ein Ag-Target gleicher Geometrie bestimmt. Bei abgestelltem Van de Graaff-Generator war der Nulleffekt etwa 20 % kleiner. Wir benutzten nur dicke Targets. Abb. 1 und 2 zeigen die Zahl der registrierten Neutronen Y (Impulse des BF_3-Zählers pro Coulomb, Nulleffekt abgezogen) als Funktion des Magnetfeldes für die 2. und 4. Meßreihe. Die Halbwertsbreite ΔE der dreieckförmigen Energieverteilung der Protonen hinter dem Ausgangsspalt betrug bei beiden Meßreihen ca. 1/5000. Der Wirkungs-

querschnitt $\sigma(E_p)$ der Reaktion als Funktion der Protonenenergie, E_p ist gegeben durch die Breit-Wigner-Formel

$$\sigma = \frac{2J+1}{(2s+1)(2I+1)}\,\pi\lambda^{\bar{2}}\,\frac{\Gamma_n\Gamma_p}{(E_p-E_0)^2+\frac{1}{4}(\Gamma_n+\Gamma_p)^2},$$

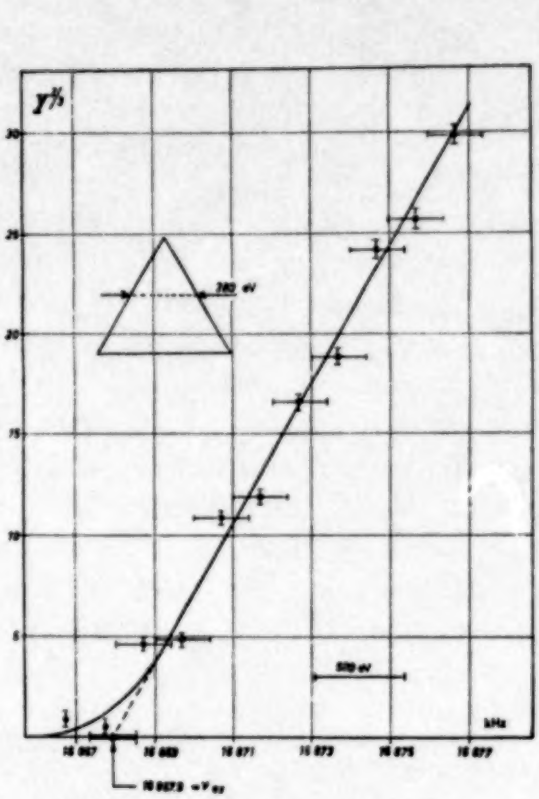

Abb. 1. (2. Meßreihe)

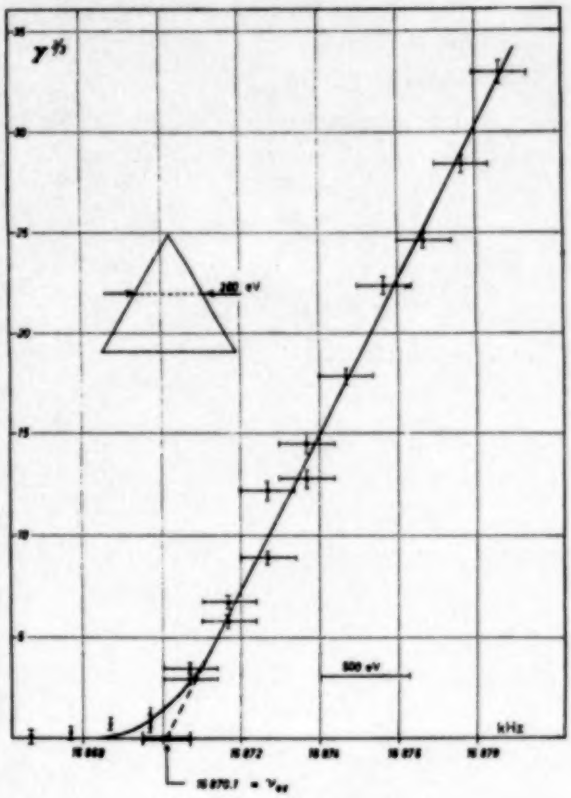

Abb. 2. (4. Meßreihe)

Die Neutronenzahl Y als Funktion des Magnetfeldes. Die Ordinatenfehler sind die statistischen Fehler der einzelnen Messung, während die Abszissenfehler die Unsicherheit im stabilisierten Feldwert darstellen (siehe Tabelle 3, Einstellung der zeitlichen Stabilisierung).

in welcher $E_0 = 1.90\,\mathrm{MeV}$ [9,10]) die Protonenergie des dicht über dem Schwellenwert E_s liegenden Niveaus 2^-, $\Gamma_n = C_n\sqrt{(E_p-E_s)}$ die Neutronenbreite und $\Gamma_p = C_p\sqrt{E_p}$ die Protonenbreite darstellt ($C = C_n/C_p \approx 5$).
In dem von uns gemessenen kleinen Energiebereich von ca. 2 keV oberhalb E_s ist dann, da $E_p-E_0/\Gamma_p \ll 1$,

$$\sigma \approx \frac{x}{(1+Cx)^2} \approx x \equiv \sqrt{\frac{E_p-E_s}{E_p}} \approx \sqrt{\frac{E_p-E_s}{E_s}} \propto \sqrt{E_p-E_s}.$$

Damit ergibt sich die Neutronenausbeute eines dicken Targets (Energieverlust im Target groß gegen E_p-E_s) für monoenergetische Protonen proportional zu $(E_p-E_s)^{\frac{1}{2}}$. Der Nenner $(1+Cx)^2$ des Wirkungsquerschnittes verursacht in dem benutzten kleinen Energieintervall nur eine unmerkliche Abweichung von der Proportionalität der Neutronenausbeute mit $(E_p-E_s)^{\frac{1}{2}}$. Die dreieckförmige

Energieverteilung der Protonen macht sich nur in der Nähe des Schwellenwertes, so lange $(E_p - E_s) \leqq \Delta E$, bemerkbar. Es ist bisher üblich gewesen, die gemessenen Ausbeutekurven der Reaktion linear auf Ausbeute Null zu extrapolieren und so einen von der Energieverteilung der Protonen unabhängigen Schwellenwert zu bestimmen. Da die Ausbeute Y jedoch nicht linear, sondern mit der Potenz $\frac{3}{2}$ von $(E_p - E_s)$ abhängt, haben wir die Punkte $Y^{\frac{2}{3}}$ aufgetragen und diese linear extrapoliert. Die Fehler unserer Meßpunkte sind jedoch so groß, daß sie eine experimentelle Unterscheidung zwischen

$$Y \propto (E_p - E_s) \text{ und } Y \propto (E_p - E_s)^{\frac{3}{2}}$$

nicht gestatten. Bei einer direkten linearen Extrapolation von Y würden sich die von uns in den einzelnen Meßreihen bestimmten extrapolierten Schwellenwerte um 350 ± 50 eV erhöhen. Die experimentelle Ausbeutekurve kann ihre Form ändern, sobald in dem gemessenen Bereich von E_p der Bruchteil der vom Zähler tatsächlich registrierten Neutronen sich ändert. Bei $E_p - E_s = 2$ keV, dem größten von uns benutzten Wert, liegt die Neutronenenergie zwischen 18 und 45 keV und der Emissionswinkel der Neutronen zwischen 0° und 13°, gegenüber 29.7 keV und 0° am Schwellenwert. Da im Schwerpunktssystem die Neutronen isotrop emittiert werden [9]), ist ihre Energieverteilung im Laborsystem isotrop und die mittlere Energie variiert nur sehr wenig. Der vom Detektor erfaßte räumliche Winkel ist genügend groß, um bei jedem Wert von E_p den gesamten Emissionswinkel zu erfassen.

4. Apparatur und Korrekturen

Wir verwendeten die von Bumiller *et al.* [6]) beschriebene Apparatur mit einem Radius der Protonenbahn von 500 mm. Der Eintritts- und Austrittsspalt sind an den Enden eines wassergekühlten Stabes befestigt und dadurch in ihrem Abstand unabhängig vom Magneten und von der Vakuumkammer. Der Abstand D_0 der Spalte wurde durch Vergleich mit einem Normalmeter mittels eines Kathetometers gemessen. Die Spaltbreiten wurden mit einem Komparator bestimmt. Das Magnetfeld wurde mit einer zylindrischen Kerninduktionsprobe von 5 mm Durchmesser und 8 mm Länge, deren Achse tangential zur Protonenbahn steht, gemessen. Das Feld mußte punktweise ausgemessen werden, da es entlang der Protonenbahn kleine Inhomogenitäten von höchstens 3×10^{-4} aufweist und senkrecht zur Bahn einen radialen Gradienten von ca. 3×10^{-5} pro mm besitzt, welcher durch die Konstruktion des Magneten bedingt ist. Das gemessene mittlere Feld wurde dann für die Berechnung des Impulses der Protonen noch mit der von Hartree [9]) angegebenen Korrektur erster Näherung

$$\tfrac{1}{2} \int_0^{\pi} \Delta B(\theta) \sin\theta \, d\theta$$

für die Feldabweichung längs der Bahn korrigiert ($\Delta\nu_1$, siehe Tabelle 1). Der

Wert dieser Korrektur war bei unseren Messungen stets kleiner als 2.5×10^{-4}. Mit einer Kerninduktionsprobe gleicher Form und Größe wie die Meßprobe, die sich in einer Einbuchtung der Vakuumkammer befand, wurde das Feld über eine Regeleinrichtung auf $\pm 3 \times 10^{-5}$ zeitlich stabil gehalten. Diese Probe diente gleichzeitig zur Messung des Magnetfeldes während der Aufnahme der Ausbeutekurve der Reaktion. Da die Probe dann nicht auf der Protonenbahn, sondern 10 mm radial nach innen verschoben stand, mußte auch für den radialen Gradienten des Magnetfeldes korrigiert werden ($\Delta\nu_2$, Tabelle 1). Der Mittelspalt bei 90° hatte eine Breite von 0.25 mm. Er stabilisierte mit isolierten Spaltbacken über ein gittergesteuerte Coronaentladung den Van de Graaf-Generator.

TABELLE 1

Frequenzkorrekturen (in kHz) für die 4. Meßreihe; wahrer Schwellenwert
$\nu_0 = \nu_{ex} + \Delta\nu_1 + \Delta\nu_2 + \Delta\nu_3 + \Delta\nu_3$

Unkorrigierter Schwellenwert, aus der Ausbeutekurve extrapoliert	$\nu_{ex} = 16870.1$
Hartree-Korrektur für inhomogenes Feld längs des Sollkreises der Protonen	$\Delta\nu_1 = +0.3$
Korrektur für Messung des Feldes bei der Aufnahme der Ausbeutekurve 10 mm vom Sollkreis der Protonen radial nach innen	$\Delta\nu_2 = +5.8$
Abweichung der Protonenbahn vom Sollkreis, auf dem das Feld gemessen wurde (Korrektur nach Hartree)	$\Delta\nu_3 = -1.0$
Änderung des Feldes beim Einbau der Kammer	$\Delta\nu_4 = +2.4$

Die Lage des Mittelspaltes wurde zu 2.2 mm innerhalb des durch Ein-und Austrittsspalt und deren Verbindungslinie bestimmten Kreises gefunden. Das bedeutet, daß der einfallende Protonenstrahl beim Eintrittsspalt nicht genau in Richtung der Tangente dieses Kreises (des Sollkreises der Protonen) stand. So lange der Winkel α der Abweichung des einfallenden Strahles von dieser Tangente klein ist, verschiebt sich bei gleicher Energie das Bild des Eintrittsspaltes am Austrittsspalt um $\frac{1}{4}D_0\alpha^2$ (D_0 = Spaltabstand) nach innen. Für unseren Winkel α ist diese Verschiebung kleiner als 0.5×10^{-2} mm und wurde deshalb nicht berücksichtigt. Infolge des schwachen radialen Gradienten des Magnetfeldes bewegt sich jedoch in diesem Falle der Strahl nicht in gleichem Feld wie auf dem ausgemessenen Sollkreis. Die dafür unter Benutzung der Formel von Hartree angebrachte kleine zusätzliche Korrektur beträgt ca. 0.6×10^{-4} ($\Delta\nu_3$, Tabelle 1). Schließlich ergibt sich eine letzte Korrektur dadurch, daß das Magnetfeld bei ausgebauter Vakuumkammer gemessen wird. Ein Einfluß mechanischer Kräfte von der Vakuumkammer auf die Magnetpole ist zwar nicht vorhanden, da die Kammer mechanisch unabhängig vom Magneten befestigt ist, jedoch erhöhen die sehr geringen ferromagnetischen Verunreinigungen im Messing der Kammer das Feld um 1.4×10^{-4}, wie mit Kerninduktionsproben innerhalb der Kammer gemessen wurde ($\Delta\nu_4$, Tabelle 1). Die Targetkammer und die Vakuumkammer im Magneten waren über eine mit

flüssiger Luft beschickte Kühlfalle und eine wassergekühlte Baffle an eine Oeldiffusionspumpe angeschlossen. Die Targets wurden durch Aufdampfen einer Lithiumschicht von ca. 0.1 mm Dicke auf Silberblech hergestellt. Das Lithium wurde dann entweder gesättigtem Wasserdampf ausgesetzt, bis es vollständig in Lithiumhydroxyd übergegangen war, oder aber etwa 1 Minute an Luft gebracht, wobei wahrscheinlich Lithiumnitrid, Lithiumoxyd und Lithiumhydroxyd entstanden. Die Targets wurden während der Messungen teilweise geheizt, um die Bildung von Oel- bzw. Kohlenstoffschichten darauf zu verhindern. Es wurden vier Meßreihen zur Bestimmung des extrapolierten Schwellenwertes ν_{ex} aufgenommen. Dabei wurden verschiedene Targets, Spaltabstände und Spaltbreiten verwendet. Tabelle 2 gibt eine Übersicht über die Messungen. Magnetfelder sind in Frequenzen ausgedrückt, wobei

TABELLE 2

Uebersicht der Messungen

Meßreihe	1	2	3	4
Target	mit Wasserdampf in LiOH verwandelt	wie unter Meßreihe 1	wie unter Meßreihe 1	1 Min. der Luft ausgesetzt
Temperatur des Targets (°C)	ca. 30°	ca. 200°	ca. 200°	ca. 200°
Spaltabstand D_0 (mm)	1 001.15	1 000.16	1 000.17	1 000.17
Breite Eintrittsspalt (mm)	0.16	0.10	0.10	0.10
Breite Austrittsspalt (mm)	0.12	0.10	0.10	0.10
ν_{ex} (kHz)	16 850.7	16 867.9	16 868.8	16 870.1
Hartree-Korrektur (kHz)	+3.8	+2.5	+1.5	+0.3
Schwellenwert (keV)	1 880.46	1 880.28	1 880.31	1 880.32

$B = 2\pi\nu/\gamma_p$. Tabelle 1 gibt als Beispiel die Meßwerte und Korrekturen für die vierte Meßreihe. Die letzten drei Korrekturen sind für alle Meßreihen gleich. Die Beschleunigungsspannung der Protonen an den korrigierten Schwellenwerten ν_0 ergibt sich in absoluten Volt als

$$V = \frac{\pi^2}{2\gamma_p}\frac{\nu_C}{\nu_K} D_0^2 \nu_0^2 (1-\delta) \times 10^{-8}$$

wobei $\delta = \frac{1}{2}eV/M_0c^2$ die relativistische Korrektur erster Ordnung der Beziehung zwischen Energie und Impuls ist. Für die beiden Konstanten benutzten wir die Werte [7, 8])

$$\gamma_p = 26751.3 \pm 0.2\ s^{-1}G^{-1}$$

$$\nu_K/\nu_C = 2.79268 \pm 0.00006.$$

Die absoluten mittleren Fehler der gemessenen Größen und Korrekturen sind für die verschiedenen Meßreihen gleich und in Tabelle 3 aufgeführt. Die Frequenz der Kerninduktionsproben wurden mit einem elektronischen Zählgerät Hewlett-Packard Typ 524 B gemessen, das durch Vergleich mit einer Normalfrequenz auf besser als 5×10^{-6} geeicht wurde. Die Konstanz der Frequenz der Kerninduktionsprobe zur Stabilisierung des Magneten wurde

TABELLE 3

Absolute mittlere Fehler, ausgedrückt in Frequenz (kHz)

ν_{ex}	±0.6
Mögliche Verschiebung des Zentrums der trapezförmigen bzw. dreieckförmigen Energieverteilung der Protonen hinter dem Ausgangsspalt infolge unsymmetrischer Stabilisierung des Van de Graaf-Generators	±0.7
Feldkorrektur † $\Delta\nu_1$	±0.7
Einstellung der zeitlichen Stabilisierung des Magneten auf die Mitte des Kernresonanzsignals bei der Aufnahme der Ausbeutekurve	±0.7
Feldkorrektur † $\Delta\nu_2$	±1.2
Feldkorrektur † $\Delta\nu_3$	±0.7
Feldkorrektur † $\Delta\nu_4$	±0.6
Abstand der Spalte, umgerechnet auf Feld (einschließlich Unsicherheit in der Temperatur des Spaltträgers)	±0.8
Konstanten γ_p und ν_K/ν_C, umgerechnet auf Feld	±0.4
Quadratische Addition ergibt $\pm\sqrt{4.9}$ kHz, entsprechend 500 eV.	

† Einschließlich Ablesegenauigkeit des Kernresonanzsignals auf dem Kathodenstrahl-Oszillographen und Unsicherheit der Lage der Kerninduktionsprobe im Magnet).

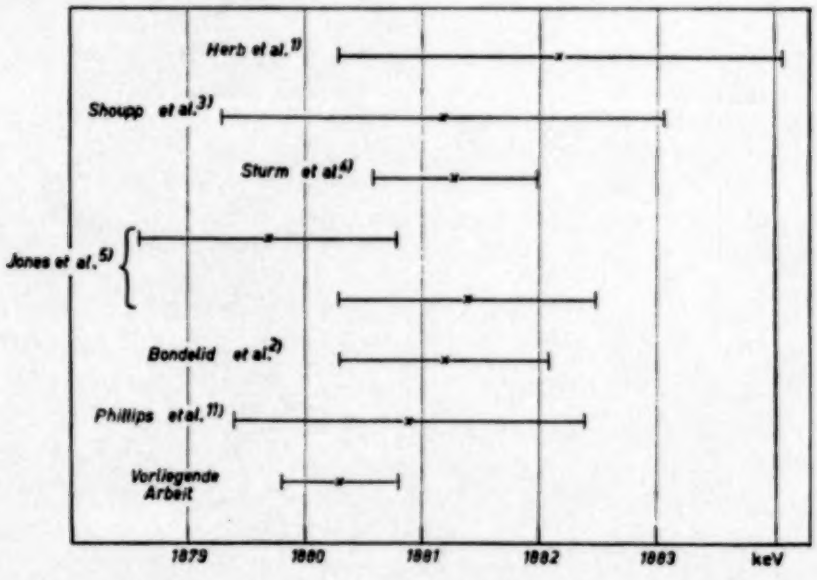

Abb. 3. Bisherige Absolutmessungen des Schwellenwertes der Reaktion $Li^7(p, n)Be^7$ (nach Jones *et al.* [5]).

während der Aufnahme der Ausbeutekurve ständig mit dem gleichen Gerät überwacht. Das von der SIP hergestellte Normalmeter wurde 1955 im Eidgenössischen Amt für Maß und Gewicht in Bern geeicht.

Als Mittel ergibt sich für die lineare Extrapolation der mit $\frac{2}{3}$ potenzierten experimentellen Ausbeutekurve der Wert 1880.3 ± 0.5 keV als Schwellenwert der Reaktion $Li^7(p, n)Be^7$. Abb. 3 zeigt in graphischer Darstellung die bis heute publizierten Werte des $Li^7(p, n)$-Schwellenwertes.

Durch die nunmehr erfolgte genauere Messung der Feldänderungen infolge des Kammermaterials müssen die von Bumiller *et al.* [6]) angegebenen Resonanzwerte relativ um 2.8×10^{-4} erhöht werden. Die relative Felderhöhung von 1.4×10^{-4} liegt innerhalb der von diesen Autoren angegebenen obersten Grenze von 2×10^{-4}. Die Korrektur ergibt damit die folgenden Werte:

$F^{19}(p, \gamma)$: 340.6 ± 0.5 keV,
$Li^7(p, \gamma)$: 441.3 ± 0.6 keV,
$F^{19}(p, \gamma)$: 871.5 ± 0.4 keV,
$Al^{27}(p, \gamma)$: 991.1 ± 0.2 keV.

Wir danken Herrn Ch. Gerber für seine tatkräftige Mithilfe bei den Messungen. Der Kommission für Atomwissenschaft des Schweizerischen Nationalfonds danken wir für die uns gewährte großzügige finanzielle Hilfe.

Literatur

1) Herb, Snowden und Sala, Phys. Rev. **75** (1949) 246
2) Bondelid und Kennedey, NRL Report 5083 (1958)
3) Shoupp, Jennings und Jones, Phys. Rev. **76** (1949) 502
4) Sturm und Johnson, Phys. Rev. **83** (1951) 542
5) Jones, Douglas, McEllistrem und Richards, Phys. Rev. **94** (1954) 947
6) Bumiller, Staub und Weaver, Helv. Phys. Acta **29** (1956) 83
7) Driscoll und Bender, Phys. Rev. Letters **1** (1958) 413
8) Sommer, Thomas und Hipple, Phys. Rev. **82** (1951) 699
9) Newson, Williamson, Jones, Gibbons und Marshak, Phys. Rev. **108** (1957) 1294
10) Macklin und Gibbons, Phys. Rev. **109** (1958) 105
11) Phillips, National Research Council, Report of Subcommittee on Nuclear Constants (1959)

7.B

Nuclear Physics **17** (1960) 279—288; © *North-Holland Publishing Co., Amsterdam*

Not to be reproduced by photoprint or microfilm without written permission from the publisher

ANNIHILATION OF POLARIZED POSITONS IN MAGNETIZED MATERIAL

I. LOVAS

Central Research Institute for Physics, Budapest

Received 12 February 1960

Abstract: The dependence of angular correlation of annihilation radiation on the polarization of negatons and positons has been analyzed and measured. The contribution of the bound negatons to the annihilation process is about 5 %.

1. Introduction

Studies of positon annihilation in magnetized material seem to be interesting for two reasons. Firstly, it is possible in this way to investigate the longitudinal polarization of positons resulting from beta decay [1]); secondly, useful information can be gained concerning the negatons involved in the annihilation process[2]).

By magnetization the negatons of magnetic materials can be polarized in an arbitrary direction. If the positons have a definite polarization, the relative spin orientations of negatons and positons, that is the relative probability of singlet and triplet states in the negaton-positon system can be influenced by magnetization. Since 2-photon annihilation occurs only from the singlet state, the conditions of this annihilation, among others its angular correlation, can be changed by varying the probability of the singlet state.

Of course, this assumption holds only if the negatons of the 3d shell, which are subject to magnetization, participate in the interaction leading to annihilation.

Thus, if there exists a dependence between the angular correlation of the annihilation radiation and the magnetization of the studied magnetic material, two qualitative conclusions may be drawn: (1) the positons are polarized, (2) in contrast to the prevailing theory [5]), not only the free negatons but also the core negatons are involved in the annihilation process. A theoretical analysis and detailed measurements of the variation in the angular correlation will even lead to quantitative results as to the degree of polarization of the positons as well as to the relative probability of annihilation with bound negatons.

This problem was examined for the first time by S. S. Hanna and R. S. Preston [1]). With their experimental arrangement, however, it was not possible to measure unambiguously the dependence of the differential angular correlation on polarization, and therefore the contribution of bound negatons to the annihilation process was not obtained.

In the following we shall first determine theoretically the dependence of the angular correlation of the annihilation radiation on negaton and positon polarization and then describe the measurements performed to investigate the problem in question.

2. Theory

The slowing down of positons in solids is very fast so that in about 10^{-12} s their energies are reduced to a thermal level of 0.025 eV [3]). With decreasing energy the annihilation probability rapidly increases [4]). Therefore most of the positons slow down prior to annihilation.

Energies and momenta of positons in the state prior to annihilation may be neglected as compared with energies and momenta of negatons of metals (apart from the small number of free negatons of the lower part in the Fermi distribution). In 2-photon annihilation, owing to the energy conservation law, the energy of the gamma rays is about mc^2, since the kinetic energy of the negaton is negligible as compared with its rest energy. It follows from the above that the resultant momentum $\hbar\mathbf{k} = \hbar\mathbf{k}_1 + \hbar\mathbf{k}_2$ of the photons resulting from the annihilation of the negaton-positon pair is equal to the momentum $\hbar\mathbf{p}$ of the negaton involved in the process.

From fig. 1 which illustrates the momentum conservation it can be seen that

$$\hbar p \approx \hbar k_2 \sin\vartheta \approx mc\vartheta, \tag{1}$$

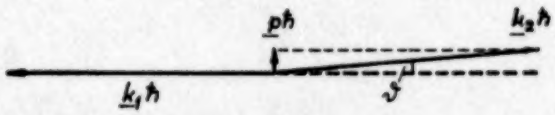

Fig. 1. Conservation of momentum.

since $\hbar p \ll mc$. Thus it is obvious that if we want to determine the angular correlation of the annihilation radiation, it is sufficient to compute the annihilation probability in terms of negaton momentum and by substituting $p = mc\vartheta/\hbar$ the angular correlation function is immediately obtained.

Indicating now by indices l the different free and bound states of negatons the wave function of the l-th type negaton is given by the Fourier series

$$\Psi_l(\mathbf{r}) = \frac{1}{\sqrt{V}} \sum_{\mathbf{p}} a_l(\mathbf{p}) u \, e^{i\mathbf{p}\cdot\mathbf{r}}, \tag{2a}$$

where the spinor u, by means of the approximation $u(\mathbf{p}) \approx u(0) \equiv u$, is considered to be independent of the wave vector; V is the volume of normalization.

Representing the positon state by a negative energy state, the wave function

of the positon is obtained by similar considerations as

$$\Phi(\mathbf{r}) = \frac{1}{\sqrt{V}} \sum_{\mathbf{q}} b(\mathbf{q}) v e^{-i\mathbf{q}\cdot\mathbf{r}}. \tag{2b}$$

The negaton-positon system is annihilated in consequence of interaction with the electromagnetic field. The matrix element of the interaction Hamiltonian corresponding to the emission of two photons having momenta $\hbar\mathbf{k}_1$, $\hbar\mathbf{k}_2$ and polarizations $\mathbf{e}_1$, $\mathbf{e}_2$ is

$$\begin{aligned}\langle |H| \rangle = \sum_{w} \frac{2\pi\hbar e^2 c}{V\sqrt{k_1 k_2}} \sum_{\mathbf{p},\mathbf{q}} a_l(\mathbf{p}) b(\mathbf{q}) \delta_{\mathbf{p}-\mathbf{q},\mathbf{k}_1+\mathbf{k}_2} \\ \cdot \left[\frac{\langle v|(\boldsymbol{\alpha}\cdot\mathbf{e}_2)|w(-\mathbf{k}_1)\rangle\langle w(-\mathbf{k}_1)|(\boldsymbol{\alpha}\cdot\mathbf{e}_1)|u\rangle}{mc^2 - k_1\hbar c - \sqrt{m^2c^4 + k_1^2\hbar^2c^2}} \right. \\ \left. + \frac{\langle v|(\boldsymbol{\alpha}\cdot\mathbf{e}_1|w(-\mathbf{k}_2)\rangle\langle w(-\mathbf{k}_2)|(\boldsymbol{\alpha}\cdot\mathbf{e}_2)|u\rangle}{mc^2 - k_2\hbar c - \sqrt{m^2c^4 + k_2^2\hbar^2c^2}} \right].\end{aligned} \tag{3}$$

The spinor of intermediate state is denoted by w. In calculating the quantity in brackets, we have, in conformity with the previous assumptions, neglected the momenta of negaton and positon as compared with those of the photons.

Introducing now the symbols

$$\psi_l(\mathbf{r}) = \langle u|\Psi_l(\mathbf{r})\rangle, \quad \varphi(\mathbf{r}) = \langle v|\Phi(\mathbf{r})\rangle \tag{4}$$

the Fourier amplitudes are derived as

$$\begin{aligned} a_l(\mathbf{p}) &= \frac{1}{\sqrt{V}} \int \psi_l(\mathbf{r}_1) e^{-i\mathbf{p}\cdot\mathbf{r}_1} d\tau_1, \\ b(\mathbf{q}) &= \frac{1}{\sqrt{V}} \int \varphi(\mathbf{r}_2) e^{i\mathbf{q}\cdot\mathbf{r}_2} d\tau_2. \end{aligned} \tag{5}$$

Making use of these expressions the sum in the interaction matrix element can be transformed as follows:

$$\sum_{\mathbf{p},\mathbf{q}} a_l(\mathbf{p}) b(\mathbf{q}) \delta_{\mathbf{p}-\mathbf{q},\mathbf{k}_1+\mathbf{k}_2} = \int \psi_l(\mathbf{r}) \varphi(\mathbf{r}) e^{-i\mathbf{k}\cdot\mathbf{r}} \, d\tau \equiv f_l(\mathbf{k}). \tag{6}$$

Thus it can be seen that the interaction matrix element contains the Fourier transform of the product of the wave functions of the negaton and the positon.

The transition probability corresponding to the interaction matrix element is then

$$dW(\mathbf{k}, P_n^{\,l}, P_p) = C \sum_{l} |f_l(\mathbf{k})|^2 (1 - P_n^{\,l} P_p) k^2 dk d\Omega_k, \tag{7}$$

where C is a quantity containing only universal constants, P_n^l and P_p are the degrees of polarization of the l-th type negaton and positon.

The degree of polarization is zero except for the 3d shell negatons:

$$P_n^l = \begin{cases} P_n & \text{for 3d shell negatons,} \\ 0 & \text{for other negatons;} \end{cases}$$

therefore we have

$$dW(\mathbf{k}, P_n, P_p) = C[\sum_l |f_l(\mathbf{k})|^2 - P_n P_p |f_{3d}(\mathbf{k})|^2] k^2 dk d\Omega_k. \tag{8}$$

In the following we shall determine the function $f_{3d}(\mathbf{k})$, which is given by

$$f_{3d}(\mathbf{k}) = \int \psi_{3d}(\mathbf{r}) \varphi(\mathbf{r}) e^{-i\mathbf{k}\cdot\mathbf{r}} d\tau. \tag{9}$$

We know very little about the positon wave function $\varphi(\mathbf{r})$. In any case at energies of 0.025 eV it has probably a "Swiss cheese" character, since it extends over the volume of several atoms, but in the place of the positive ions there are "holes" due to Coulomb repulsion, that is the wave function becomes zero within the ions. From this picture we may assume the positon wave function to have spherical symmetry and to vanish suddenly in the neighbourhood of the ion radius, whereas in the interionic volume it is supposed to remain approximately at a constant value.

The wave function of a 3d negaton is given by

$$\psi_{3d}(\mathbf{r}) = R(r) Y_{2m}(\theta_r, \phi_r), \tag{10}$$

where $R(r)$ is the radial wave function of the 3d negaton. Using now the Rayleigh expansion

$$e^{i\mathbf{k}\cdot\mathbf{r}} = 4\pi \sum_{l'm'} i^{l'} j_{l'}(kr) Y^*_{l'm'}(\theta_r, \phi_r) Y_{l'm'}(\theta_k, \phi_k) \tag{11}$$

we have

$$f_{3d}(\mathbf{k}) = 4\pi Y_{2m}(\theta_k, \phi_k) \int R(r) \varphi(r) j_2(kr) r^2 dr. \tag{12}$$

Since $R(r)$ is zero outside and $\varphi(r)$ is zero inside the atomic volume, the product $R(r)\varphi(r)$ is a function with a sharp peak close to the ion radius a and anywhere else equal to zero. Thus for mathematical simplicity it is convenient to use the approximation $R(r)\varphi(r) \propto \delta(r-a)$. Of course, actually the function product in question has no singularity at all at a. The error due to the approximation by the δ function can be corrected by a cut-off of the integral at high values of k. This procedure is equivalent to that of substituting for the product $R(r)\varphi(r)$ a function of finite width without singularity.

In this way we have

$$\int R(r)\varphi(r) j_2(kr) r^2 dr \propto \int \delta(r-a) j_2(kr) r^2 dr = a^2 j_2(ka). \tag{13}$$

For high values of k the integral can be cut off by using instead of $j_2(ka)$ the function

$$[(ka)^4 e^{-b(ka)^2}]^{\frac{1}{2}} \quad (b = 0.19), \tag{14}$$

which reproduces fairly well the first maximum of the Bessel function, but for higher k values tends rapidly to zero [5]). Integrating now with respect to solid angle Ω_k, the expression for the transition probability becomes

$$\frac{dW(k, P_n, P_p)}{dk} = A_2(k) - P_n P_p B_2(k),$$

where

$$B_2(k) \propto k^6 e^{-ba^2k^2} \tag{15}$$

As it will be seen later, in our experiments it is not $\mathbf{k}$ but one of its components which will be measured. Therefore, instead of $dW(k)/dk$ we have to know the function $dW(k_z)/dk_z$. The latter is readily obtained by a simple transformation of $dW(k)/dk$ with the use of the following general procedure. Let $\rho(r)$ be the arbitrary density function of the probability variable r which is the absolute value of the vector $\mathbf{r}$, and $\rho_z(z)$ that of the probability variable z which is one component of $\mathbf{r}$; we then find

$$\rho_z(z)\,dz = \int_0^{2\pi}\int_0^{\frac{1}{2}\pi}\int_{\frac{z}{\cos\vartheta}}^{\frac{z+dz}{\cos\vartheta}} \rho(r)dr \sin\vartheta\, d\vartheta\, d\varphi = 2\pi\int_0^{\frac{1}{2}\pi} \rho\left(\frac{z}{\cos\vartheta}\right)\frac{dz}{\cos\vartheta}\sin\vartheta\, d\vartheta. \tag{16}$$

Upon substitution of $\cos\vartheta = 1/\gamma$ we have

$$\rho_z(z) = 2\pi\int_1^\infty \rho(z\gamma)\frac{d\gamma}{\gamma} \tag{17}$$

and this leads to

$$\frac{dW(k_z, P_n, P_p)}{dk_z} = A_1(k_z) - P_n P_p B_1(k_z),$$

where

$$B_1(k_z) \propto [1 + ba^2k_z^2 + \tfrac{1}{2}b^2a^4k_z^4]e^{-ba^2k_z^2}. \tag{18}$$

On the basis of the relationship $k_z = mc\vartheta/\hbar$ we may substitute for k_z the value of the angle ϑ formed by the direction of the two photons and we obtain

$$\frac{dW(\vartheta, P_n, P_p)}{d\vartheta} \equiv S(\vartheta, P_n, P_p) = A(\vartheta) - P_n P_p \eta B(\vartheta)$$

where

$$B(\vartheta) = (1 + 0.13a^2\vartheta^2 + 0.0085\,a^4\vartheta^4)e^{-0.13a^2\vartheta^2} \tag{19}$$

(a is given in Å and ϑ in milliradians); under the normalized conditions $A(0) = 1$, $B(0) = 1$, η gives the probability of annihilation with 3d negatons.

The shape of the function $B(\vartheta)$ is shown in fig. 2 for various values of the ion radius.

The function $A(\vartheta)$ is precisely the angular correlation function for the unpolarized case. The calculation of $A(\vartheta)$ being rather complicated and subject to some uncertainties it was found more convenient to determine it experimentally.

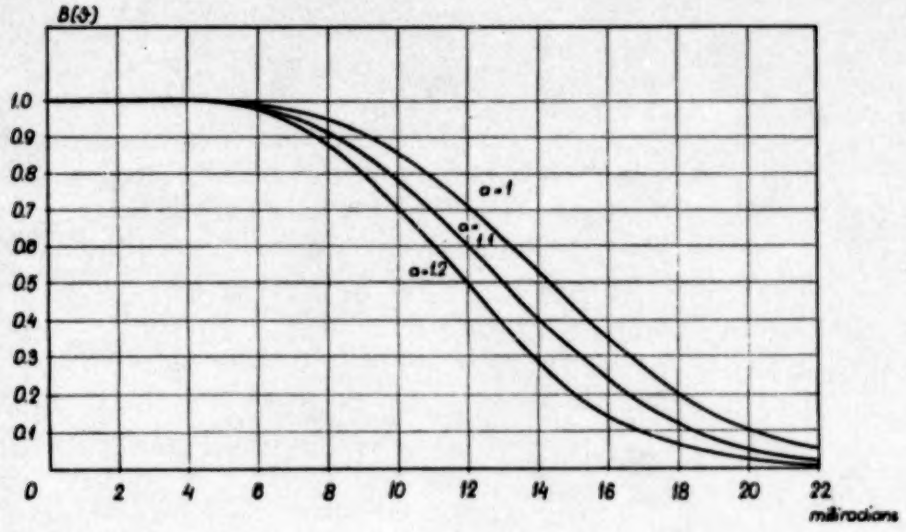

Fig. 2. 3d shell two-photon angular correlation.

3. Experiments

Our first experiments were performed in order to determine the angular correlation of the γ particles emitted in positon annihilation, and to this end $\gamma-\gamma$ coincidences were recorded at various angular positions.

Upon determination of the angular correlation we counted the number of $\gamma-\gamma$ coincidences in such a way that the magnetization of the sample was first parallel, then opposite to the positon momentum. The ratio $(n_+-n_-)/(n_++n_-)$ was determined for all angular positions; n_+ and n_- represent the number of coincidences for the positon momentum parallel and opposite to the direction of the magnetic field.

In our measurements the direction of the magnetic field was alternated every 5 minutes in order to restrict the error due to possible instabilities in the recording apparatus, and no correction was required for the decay of the Cu^{64} positon source.

The measurement of the angular correlation was carried out in the usual way. The experimental arrangement is shown in fig. 3.

On both sides of the annihilator, each at a distance of 1 m, there is a fixed and a movable scintillation counter and before the counters lead absorbers are mounted to form a vertical slit of 5 mm width.

The 2 mm thick and 5 mm diam. disc shaped annihilator (iron, magnetite or copper) is attached to one of the poles of a 7 mm pole space magnet. The magnetic field intensity at the annihilator was about 10.000 G.

The Cu^{64} positon source is mounted on the other pole of the magnet. The 0.3 mm thick, 5 mm diam. copper disc after having been activated for 6 hours in the core of the Hungarian Research Reactor gives a 0.18 c activity source. The positon activity was about 19 % of the overall activity, thus about 34 mc[6]).

The γ radiation emitted by positons annihilated close to the source was absorbed by a collimating system. The photomultipliers were screened against

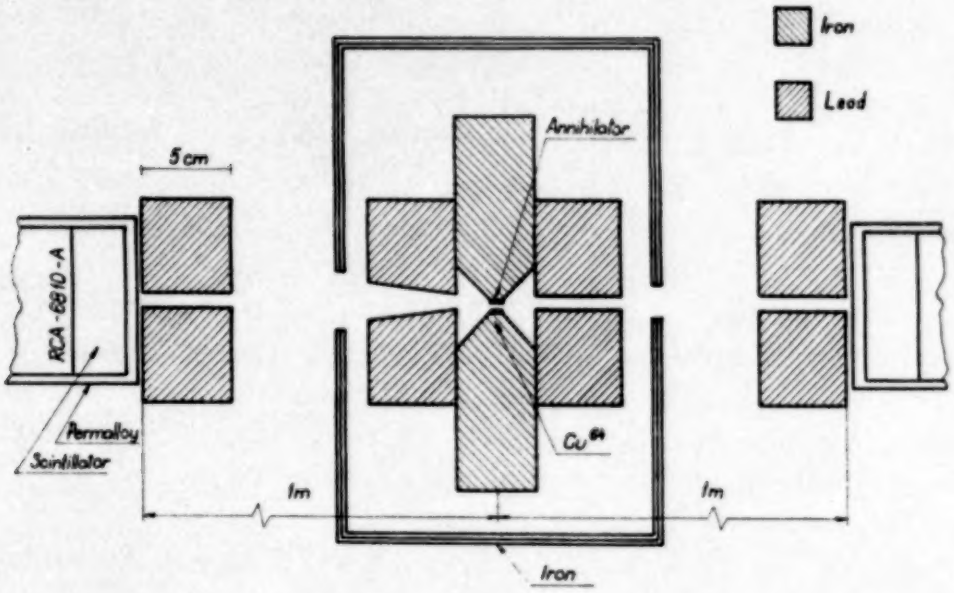

Fig. 3. Experimental arrangement.

the effect of the magnetic field by a permalloy cylinder, an additional shielding was provided by a plated iron shield. The scintillation counter pulses were detected by a fast-slow coincidence arrangement with a resolving power of $(3\pm1)\times10^{-9}$ s. Plastic phosphors were used as scintillators which were connected to RCA 6810—A photomultipliers.

The inhomogeneous magnetic field produced around the poles has a focussing effect on the positons emerging from the positon source. Therefore the number of annihilated positons increases with the magnetic field turned on. The focussing effect, however, does not depend on the direction of the field if the geometry has a cylindrical symmetry. Using the fixed counter as monitor it could be established in the experiment that the alternation of the field direction did not affect the number of positons annihilated in the annihilator. In determining the polarization of positons thus annihilated the depolarization occurring in the inhomogeneous field had to be taken into account.

4. Results

In our measurements three kinds of annihilator were applied:
1) Ferromagnetic iron (Armco),
2) Ferrimagnetic magnetite (natural single crystal),
3) Copper.

In the last two cases no polarization dependence has been observed. This is obvious for copper, since its negatons cannot be polarized by magnetization. Actually the measurement on copper served only to check the experimental arrangement.

In principle the angular correlation could be expected to be dependent on polarization for magnetite. Actually no such dependence was found. The magnetite was chosen because as a semiconductor it contains only a few free negatons so that positon annihilation with bound negatons is here more probable than in the case of metals. This is probably true, but the result obtained in our experiments shows that in magnetite, having the structure $Fe^{++}\,Fe_2^{+++}O_4^{--}$, the positons annihilate with the negatons of the negative oxygen ions and not with negatons bound to the positive Fe ions.

Furthermore, the negative result can be explained also by the fact that even for saturation magnetization the magnetic moment per magnetite molecule is only 4.2 Bohr magneton, which is associated with the ferro-ion, since the magnetic moments of the ferri-ions compensate each other in consequence of the ferrimagnetic structure. Thus only every seventh out of all the atoms has a resultant magnetic moment.

For iron a definite polarization dependence was observed. The coincidence ratio $(n_+-n_-)/(n_++n_-)$ was markedly positive for certain angles.

In order to compare the experimental and theoretical results, the angular correlation function is written in the form

$$\frac{S(\vartheta+P_n,\ P_p)-S(\vartheta-P_n,\ P_p)}{S(\vartheta+P_n,\ P_p)+S(\vartheta-P_n,\ P_p)}=-P_nP_p\eta\frac{B(\vartheta)}{A(\vartheta)}. \tag{20}$$

The above expression is equal to $(n_+-n_-)/n_++n_-$. The function $A(\vartheta)$ can be obtained directly by angular correlation measurement; $B(\vartheta)$ has been computed above.

When the values for P_n and P_p have been calculated by taking into account the experimental conditions, then with a suitable choice of η the function $P_nP_p\eta B(\vartheta)/A(\vartheta)$ can be fitted to the experimental points.

In determining the degree of polarization P_n of negatons, we have to consider that in the atomic state the 3d shell contains 6 and the 4s shell 2 negatons. In a metallic structure, however, there is a probability of 0.7 that the 4s electrons will go over into the 3d shell. At room temperature and exposed to a magnetic field of 10000 G, an iron atom has a magnetic moment of about 2.1

Bohr magnetons. Thus the degree of polarization of the 3d negatons is $P_n = 0.28$. Only a very rough estimation can be made of the polarization degree of positons. The longitudinal polarization of positons resulting from beta decay is equal to the mean value of v/c. The maximum energy of positons emitted by a Cu^{64} source being 656 keV, the degree of polarization becomes $P_p = \langle v/c \rangle = 0.88$. Now, allowing for self absorption occurring in the source, for geometry and for the depolarizing and focussing effect of the inhomogeneous field, in a crude approximation we obtain for the degree of polarization of positons annihilated in the annihilator ≈ 0.6.

The experimental values and the calculated function $P_n P_p \eta B(\vartheta)/A(\vartheta)$ are shown in figs. 4 and 5.

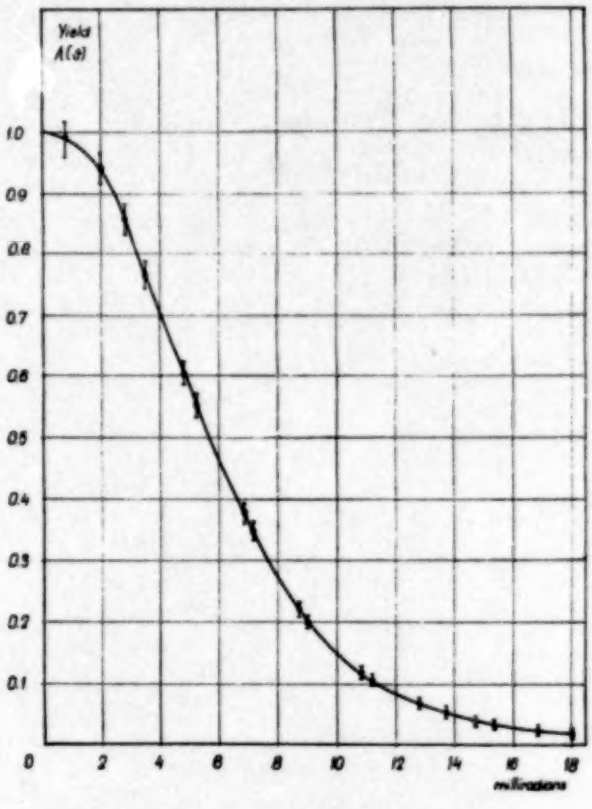

Fig. 4. Two-photon angular correlation of the positon annihilation in iron.

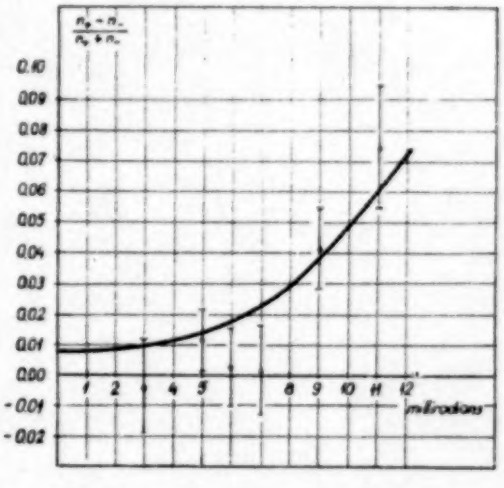

Fig. 5. Dependence of angular correlation on polarization.

The best agreement is obtained with η chosen to be about 0.05 and the ion radius 1 Å. Taking into consideration that in the crystal lattice of iron the half interatomic spacing is 1.28 Å, the value 1 Å for the ion radius seems quite reasonable. Incidentally, in the calculations made by Ferrel [5]) the wave function of the positon was found to be zero in a sphere with a radius of 0.98 Å.

The results obtained for η show that the probability of 3d negatons participating in the annihilation process is 5 %.

Summarizing our results, the following conclusions can be drawn:
1) positons resulting from beta decay are polarized longitudinally, that is parallel to the direction of momentum;
2) also core negatons are involved in the annihilation process;
3) the fraction of 3d negatons participating in the process is about 5 %;
4) the ion radius of iron is 1 Å.

I am very much indebted to my colleague Z. Zámori whose help made it possible to carry out the required measurement and who designed, built and checked the electronical apparatus for the experiments. Thanks are due also to D. Kiss, B. Kardon and others for useful advice and assistance during the experiments.

References

1) S. S. Hanna and R. S. Preston, Phys. Rev. **106** (1957) 1363; **109** (1958) 716
2) I. Lovas, Acta Physica Hung. VIII (1958) 441
3) R. L. Garwin, Phys. Rev. **91** (1953) 1571;
G. E. Lee-Whiting, Phys. Rev. **97** (1955) 1557
4) W. Heitler, The Quantum Theory of Radiations, 2nd ed. (Oxford, 1944) p. 204
5) R. A. Ferrel, Rev. Mod. Phys. **28** (1956) 308
6) B. S. Dželepow and L. K. Peker, Decay Schemes of Radioactive Nuclei (Moscow, 1958) p. 146

8.C

Nuclear Physics **17** (1960) 289—316; © *North-Holland Publishing Co., Amsterdam*

Not to be reproduced by photoprint or microfilm without written permission from the publisher

INTERPRETATION OF ELECTRODYNAMICS AND BARYON THEORY WITHIN A SIX-DIMENSIONAL MANIFOLD

JERZY RAYSKI

Physical Institute of the Jagellonian University
and
Physical Institute of the Polish Academy of Science, Kraków

Received 14 December 1959

Abstract: Assuming a six-dimensional world with a singular metric, a unitary theory of gravitation and electromagnetic field is formulated. Electric charge is interpreted as angular momentum in the fifth and sixth dimensions. Sommerfeld's constant is closely connected with the degree of singularity of the metric tensor. Isobaric spin and its connection with the electric charge as well as the pseudo-scalar character of pions are easily interpretable. The hypothesis of a six-dimensional world enables a systematization of elementary particles. In particular, it is shown that the baryon family fits quite naturally into the six-dimensional framework.

1. Introduction

The present status of the theory of fields and elementary particles is unsatisfactory. We do not know why Nature "prefers" some types of fields and particles and "rejects" some others, apparently equally possible. The exact form of field equations (linear, or non-linear?) is not known. The interaction terms have been introduced purely phenomenologically. The concepts of iso-spin and strangeness are purely formal, and we do not understand why the third component of iso-spin is unavoidably connected with the electric charge.

In the contemporary field theory the gravitational field plays a distinguished role: it is the only field fitting quite naturally into the geometrical (riemannian) framework, and therefore we have confidence in the (non-linear) form of the gravitational field equations as well as in the general form T_{jk} of the interaction term appearing in these equations. In order to construct a more satisfactory theory of other fields and particles, a new methodology, as powerful as Einstein's geometrical method, is badly needed. But do we really need a new methodology? The aim of this paper is to show that some progress may be achieved by using exactly the same methodology. The essentially new ideas introduced by relativity have been: (i) increasing the number of dimensions by fusing space and time into a four-dimensional space-time, and (ii) a subsequent generalization of the flat manifold to a riemannian one. A straightforward continuation of the same programme is to look for a further extension of the number of dimensions. This programme is not new. Several authors considered

a 5- or 6-dimensional manifold in order to construct a unitary theory of the gravito-electromagnetic field. Their results were promising, though not free from objection. We shall take up once more the same programme but shall extend it to include such problems as the structure of baryons, the concept of isospin, etc.

2. Electric Space

The contemporary theory of fields and particles is built up of several heterogeneous assumptions. In particular, we can distinguish two heterogeneous types of conservation laws: some of them are intimately connected with geometry, the others reach beyond geometry. The laws of conservation of energy-momentum and of angular momentum express nothing else but homogeneity and isotropy of space-time and therefore belong to geometry, some others, e.g. conservation of charge or of the baryon number, have not yet acquired any geometrical interpretation. In other words, some of the groups of transformation (translations, rotations, and inversions in space-time) possess a geometrical meaning, but some others (gauge transformations, charge conjugation, etc. . . .) possess none. This situation seems unsatisfactory from a methodological point of view and shows that the contemporary "fundamental theory" is very far from a uniform and closed conceptual system. Therefore, we shall concentrate our attention upon the possibility of a geometrical interpretation of the electric charge, and shall try to ascribe a geometrical meaning to such transformations as gauge transformations, charge conjugation, etc.

Charged bosons are usually described by non-hermitian field quantities ψ. Their hermitian parts ψ_1, ψ_2, given by the decomposition

$$\psi = \psi_1 + i\psi_2, \quad \psi^* = \psi_1 - i\psi_2, \tag{1}$$

can be interpreted as components of a vector in a two-dimensional space to be called *electric space*. Gauge transformations of the first kind,

$$\psi \to e^{if}\psi, \quad \psi^* \to e^{-if}\psi^*, \tag{2}$$

mean rotations in this space. Charge conjugation,

$$\psi \to \psi^*, \quad \psi^* \to \psi, \tag{3}$$

is interpretable as inversion of the second axis in the electric space. Here the second axis is by no means privileged, since one can supplement the inversion by a gauge transformation: a rotation through the angle π.

The same geometrical interpretation is applicable to fermions described by four-component complex spinors. Such spinors admit gauge transformations of exactly the same form (2). Moreover, they transform under charge conjugation in exactly the same way (3) as bosons provided a Majorana representation of the

γ^k-matrices is used (the elements of the γ^k-matrices are real for $k = 1, 2, 3$, and imaginary for $k = 4$). Thus, the components ψ_1, ψ_2 of a spinor given by the decomposition (1) in a Majorana representation can also be interpreted as components of a vector in the electric space.

Now, the question arises as to the mutual relation between the two-dimensional electric space and the four-dimensional space-time.

3. The Basic Geometrical Structure

Let us discuss the hypothesis that the four-dimensional space-time together with the two-dimensional electric space form a six-dimensional riemannian space. As we shall see later, this assumption will enable us to construct a unitary theory of the gravitational and electromagnetic field and to get some insight into the geometrical meaning of both the electromagnetic and the gravitational coupling constants. The same hypothesis of a six-dimensional world will be useful for a discussion of the structure of baryons, mesons and leptons, and will enable us to interpret isobaric spin, the connection of its "third component" with the electric charge, and the pseudo-scalar character of the nucleon-pion interaction.

Of course, the usual four-dimensional space-time must be distinguished in one way or another within the six-dimensional manifold, otherwise we could not account for the fact that the fifth and sixth dimensions are not directly perceptible. The most natural way to account for the distinguished role of some dimensions, without going beyond the traditional framework of riemannian geometry, is to postulate a suitable metric tensor $g_{\mu\nu}$ (greek indices run from 1 to 6, latin ones from 1 to 4). Assume that the six-dimensional manifold is not flat even if we neglect the gravitational effects. The absence of gravitation manifests itself only in the fact that a four-dimensional subspace is flat so that we can introduce a system of coordinates such that

$$g_{11} = g_{22} = g_{33} = -g_{44} = 1, \quad g_{jk} = 0 \quad \text{for} \quad j \neq k; \tag{4}$$

but it implies nothing as regards the remaining $g_{\mu\nu}$ components. These are still free at our disposal. By choosing them to be different from $\pm\delta_{\mu\nu}$ our aim of distinguishing the fifth and sixth dimension will be attained.

In order to be able to interpret the subspace (x^5, x^6) as the electric space we have to guarantee invariance under rotations in (x^5, x^6). This can be secured by putting

$$g_{55} = g_{66} = \varphi(r), \quad g_{k5} = g_{k6} = g_{56} = 0, \tag{5}$$

where

$$r = [(x^5)^2 + (x^6)^2]^{\frac{1}{2}}. \tag{6}$$

In this way we distinguish a point $r = 0$ in the electric space and a four-dimensional flat hypersurface given by the equations

$$x^5 = x^6 = 0, \quad \text{or} \quad r = 0, \tag{7}$$

within the six-dimensional world. This hypersurface is to be interpreted as the Minkowski space.

The form of the function $\varphi(r)$ appearing in (5) is to a great extent arbitrary. We have only to know its behaviour in the immediate neighbourhood of the point $r = 0$. As will be seen from section 5, we would not be able to account for the fact that the elementary charge ($e = 137^{-\frac{1}{2}}$) is smaller than unity unless we assume that $\varphi(r)$ is singular for $r \to 0$. Therefore we assume

$$\varphi(r) \to \pm l^a r^{-a} \quad \text{for} \quad r \to 0 \tag{8}$$

where $a > 0$ is a parameter and l is a constant with the dimension of a length. For definiteness let us work e.g. with a function

$$\varphi(r) = -(1+l^a r^{-a}). \tag{8'}$$

The metrical structure of the six-dimensional manifold given by (4) and (5) together with (6) and (8) defines a "playground" for physical phenomena †.

The singularity of the metric tensor components cannot be too strong. In order to secure that the distance between two points, one of them characterized by $r = 0$ the other by $r \neq 0$, be finite, it is necessary to assume

$$a < 2. \tag{9}$$

Let us compute the scalar curvature $R^{(0)}$ of our manifold in the limit of small values of r. The superscript (0) attached to R means that gravitational and electromagnetic effects are neglected, or equivalently, that we compute only the curvature of the electric subspace

$$R^{(0)} = R_{55}\, g^{55} + 2R_{56}\, g^{56} + R_{66}\, g^{66}.$$

The result is

$$R^{(0)} = -a^2 l^{-2a} r^{2(a-1)}, \quad r \approx 0. \tag{10}$$

Hence it is seen that, in spite of the singular character of the metric tensor, we can secure a singularity-free curvature if $a \geqq 1$. Let us assume a quasi-regular metric where the curvature is of class C_1 and vanishes for $r = 0$ together with first derivatives. This necessitates

$$\tfrac{3}{2} < a. \tag{11}$$

The metric characterized by (9) and (11) may be called quasi-regular. In a quasi-regular world the metric tensor $g_{\mu\nu}$ as well as the curvature tensor $R_{\mu\nu}$ are

† The above assumptions secure a full symmetry of the manifold ($g_{11} = g_{22} = g_{33} = -g_{44} = -g_{55} = -g_{66} = 1$, $g_{\mu\nu} = 0$ for $\mu \neq \nu$) only in the domains far apart from the singular hypersurface (7). The inhomogeneity and anisotropy of the manifold in the neighbourhood of the Minkowski hypersurface can be understood as a consequence of the existence and special distribution of matter in a broad sense of this word: *Urmaterie*.

singular, but the curvature $\tilde{\mathcal{R}}$ together with its first derivatives is regular, and the distances are finite.

Since the six-dimensional manifold is inhomogeneous and anisotropic, the invariance under translations of the variables x^5 and x^6 is violated, so that we cannot expect the existence of new conservation laws for a fifth and sixth component of an "energy-momentum six-vector". The groups of rotations in the subspaces (x^k, x^5) and (x^k, x^6) cannot play the same role we are accustomed to from considerations of isotropic spaces either. On the other hand, the dimensions 5 and 6 are quite equivalent, whence the laws of physics have to be invariant under rotations in (x^5, x^6) around the point $x^5 = x^6 = 0$. This invariance will constitute the geometrical basis for electrodynamics.

4. A Geometrical Interpretation of the Electromagnetic Field

In order to realize that our procedure of geometrizing the electromagnetic field is quite similar to the well known procedure of geometrizing the gravitational field, let us recall briefly the essential steps of the latter. First of all one used to extend the Lorentz group to that of all (sufficiently regular) non-linear transformations

$$x^k = f^k(\overset{\circ}{x}{}^1, \ldots \overset{\circ}{x}{}^4) \tag{12}$$

where $\overset{\circ}{x}{}^k$ mean the cartesian coordinates. Under this transformation the metric tensor components cease to be of the simple form (4) but are still subjected to restrictions whose meaning is that space-time remained as it was beforehand, i.e. flat. In this case the g_{jk} describe only fictitious gravitational potentials. Then comes the decisive step: while preserving the generalized form $ds^2 = g_{jk}dx^j dx^k$, the restrictions upon g_{jk} are dropped, which means an encroachment upon the geometry: space-time acquires an x^k-dependent curvature and the g_{jk} characterize genuine gravitational effects. In the case of a gravitational field in vacuo the field equations follow from the variational principle

$$\delta W = \delta \int R\sqrt{-\mathrm{Det}\, g_{jk}}\, d^4x = 0. \tag{13}$$

Then, the case of the gravitational field in vacuo can be generalized by adding to the lagrangian R covariant lagrangians $\mathcal{L}(\psi)$ for the other fields ψ playing the role of sources of the gravitational field. The total lagrangian is

$$\mathcal{L}(g_{jk}, \psi) = \frac{1}{g} R(g_{jk}) + \mathcal{L}(\psi), \tag{14}$$

where g is a constant with dimension [cm^2]. It is nothing else but the gravitational coupling constant.

The above procedure can be closely imitated for the case of electrodynamics. First of all there is the group of rotations in the subspace (x^5, x^6) around the

origin $x^5 = x^6 = 0$ that do not influence the form of the metric tensor components (4), (5). This group of transformations is analogous to the Lorentz group. Then, similarly as was the case with the Lorentz group, we extend the group of rotations in (x^5, x^6) to a group of non-linear transformations by assuming an x^k-dependent angle of rotation

$$\alpha = \underset{\circ}{\alpha} + f(x^k). \tag{15}$$

In other words, we admit different rotations in (x^5, x^6) for different points in the Minkowski subspace. Owing to the symmetry with respect to such rotations physical laws must remain covariant also under the group of transformations (15). This group is to be identified with the gauge group. Since (15) is a non-linear transformation, it changes the form of the metric tensor components. A straightforward computation yields

$$\begin{gathered} g_{jk} = \delta_{jk} + r^2\varphi(r) f_j f_k, \quad g_{k\alpha} = -r^2\varphi(r) f_k, \quad g_{\alpha\alpha} = r^2\varphi(r), \quad g_{rr} = \varphi(r), \\ g_{kr} = g_{\alpha r} = 0, \end{gathered} \tag{16}$$

where f_k is the gradient of the phase introduced by (15):

$$f_k = \partial_k f. \tag{17}$$

The variables r, α are connected with x^5, x^6 by

$$x^5 = r\cos\alpha, \quad x^6 = r\sin\alpha, \tag{18}$$

and we have used an imaginary time coordinate

$$x^4 = it \tag{19}$$

in order to simplify the notation.

Of course, the metric properties of our manifold have not been influenced by the above transformation, and the appearance of the functions f_k defined by (17) does not introduce any new physical contents into the theory. However, closely imitating the procedure of general relativity, a decisive step will be made by dropping the restriction (17) while preserving the form (16) of the metric tensor. This constitutes an encroachment upon the geometry whereby the manifold acquires an x^k-dependent curvature and the quantities f_k involved in it will represent the electromagnetic potentials.

Let us compute the curvature of the manifold with the metric (16) in the limit of very small values of r, i.e. neglecting all powers of r except the lowest. We get †

$$R = \tfrac{1}{2} l^a r^{2-a} f_{kj} f_{kj} \tag{20}$$

where

$$f_{kj} = \partial_j f_k - \partial_k f_j. \tag{21}$$

† The term $R^{(0)}$ disappears in this approximation since it is proportional to a higher power of r.

Owing to (9) the curvature vanishes in the limit $r = 0$, but we notice a remarkable fact: for small but non-vanishing values of r it is proportional to the lagrangian of the electromagnetic field

$$\mathscr{L}(f_{jk}) = \tfrac{1}{2} f_{jk} f_{jk} \tag{22}$$

if f_k are interpreted as electromagnetic potentials. By comparing (20) with (14) it is seen that the desirable result will be obtained by replacing $l^a r^{2-a}$ by the gravitational coupling constant. This means that, instead of going over to the limit $r = 0$, we have to average over a very small region around $r = 0$ in the subspace (x^5, x^6) to obtain

$$g = l^a \langle r^{2-a} \rangle. \tag{23}$$

In other words, we have to assume that physical phenomena are not confined strictly to the four-dimensional hypersurface $r = 0$ (Minkowski world) but reach microscopically beyond it into the fifth and sixth dimensions.

For small values of r the coefficient $l^a r^{2-a}$ is equal to

$$g(r) = -a^2 (R^{(0)} \sqrt{\operatorname{Det} g^{(0)}_{\mu\nu}})^{-1} \tag{24}$$

where $R^{(0)}$ and $g^{(0)}_{\mu\nu}$ denote the curvature and the metric tensor of the subspace (x^5, x^6) alone, or equivalently, of the six-dimensional world with neglected gravitational and electromagnetic effects. This expression possesses an invariant meaning with respect to the groups of transformations (12) and (15), and is a scalar density with respect to arbitrary transformations in (x^5, x^6). The formula (23) can be written in the form

$$g = \langle g(r) \rangle. \tag{25}$$

This gives us some insight into the geometrical meaning of the gravitational coupling constant †.

Limiting ourselves to the lowest power of r when computing the curvature and making the substitution (23) means a first approximation. In this approximation the usual variational principle yields Maxwell equations

$$\partial_k f_{kj} = 0 \tag{26}$$

with neglected gravitational corrections.

† The question arises whether the necessity of averaging in (x^5, x^6) over a very small domain in the neighbourhood of $r = 0$ can be made intuitively clear. From (8′) and (10) it is seen that the curvature $R^{(0)}$ possesses the property of a barrier (it vanishes for $r = 0$ but is different from zero in the neighbourhood of $r = 0$). We can imagine this curvature to play the role of a potential wall for the position in the subspace (x^5, x^6). The probability that the event takes place at a point (x^5, x^6) might be given by a probability amplitude $\Phi(x^5, x^6)$ being a solution of an eigenvalue problem, e.g.

$$\sum_{\mu,\nu=5}^{6} g^{(0)\mu\nu} \Phi_{\mu;\nu} + \varepsilon R^{(0)} \Phi = \lambda \Phi.$$

The lowest state should be symmetric and the solution $\Phi = \Phi(r)$ would differ from zero only in the immediate neighbourhood of $r = 0$.

In this way it is proved that the electromagnetic field is interpretable geometrically on very similar lines to those well known from Einstein's theory of gravitation. Both the gravitational and the electromagnetic field are intrinsically geometrical concepts: both are interpretable in terms of the curvature of the manifold and both satisfy field equations derivable from the same lagrangian R/g. The main difference is that in the case of gravitation only the components R_{jk} of the contracted curvature tensor contribute to the total curvature of the six-dimensional manifold, whereas in the case of the electromagnetic field only the components R_{k5} and R_{k6} (or rather only $R_{k\alpha}$) contribute to the total curvature. It is interesting to notice that neither the gravitational nor the electromagnetic field influence the components R_{55}, R_{56} and R_{66}.

The analogy between gravitation and electromagnetism may be traced still further. Owing to the arbitrariness in choosing the coordinate system we have, in the theory of gravitation, four arbitrary functions, so that only six among the g_{jk} are "physical". Similarly, in the geometrical theory of the electromagnetic field, there is an arbitrariness in choosing the coordinate system, providing one arbitrary function f (introduced by (15)). Therefore only three among the f_k are "physical". We can perform a transformation (15), i.e. replace f_k by $f_k+\partial_k f$ without influencing the physical contents of the theory. We can choose the function f so that the new quantity $A_k = f_k+\partial_k f$ satisfies the Lorentz condition Thus, the arbitrariness in the choice of the electromagnetic potentials is not only formally analogous to, but exactly of the same nature as the arbitrariness in the choice of g_{jk} in the theory of gravitation.

5. Interaction with Charged Fields

Consider a field transforming like a vector under rotations in the subspace (x^5, x^6) around the point $x^5 = x^6 = 0$. This field possesses two non-vanishing components ψ^5 and ψ^6. (It can be looked upon as a six-vector whose components ψ^k vanish.) Let us compute the covariant derivatives of this vector field with the metric defined by (16). Christoffel symbols (computed in the limit of very small r) that are of interest for our present purpose are

$$\Gamma^k_{ij} = \Gamma^5_{k5} = \Gamma^6_{k6} = 0, \quad \Gamma^5_{k6} = -\Gamma^6_{k5} = \tfrac{1}{2}(2-a)f_k, \tag{27}$$

whence we get the covariant derivatives

$$\psi^5_{;k} = \partial_k\psi^5+\tfrac{1}{2}(2-a)f_k\psi^6, \quad \psi^6_{;k} = \partial_k\psi^6-\tfrac{1}{2}(2-a)f_k\psi^5. \tag{28}$$

Combining the components ψ^5 and ψ^6 into a complex field

$$\psi = \frac{1}{\sqrt{2}}(\psi^5+i\psi^6), \quad \psi^\dagger = \frac{1}{\sqrt{2}}(\psi_5-i\psi_6) = \frac{1}{\sqrt{2}}\varphi(r)(\psi^5-i\psi^6) \tag{29}$$

we find

$$\psi_{;k} = (\partial_k - ief_k)\psi, \quad \psi^\dagger_{;k} = (\partial_k + ief_k)\psi^\dagger \tag{30}$$

where

$$e = \tfrac{1}{2}(2-a). \tag{31}$$

We recognize in (30) the well known expressions occurring in the theories of electrically charged fields. This discovery enables us to complete a geometrical interpretation of electrodynamics.

Let us consider the usual Lagrangian for a free complex field ψ. This Lagrangian is to be reinterpreted, according to (29), as a Lagrangian for a vector field $L(\psi^5, \psi^6, \partial_k\psi^5, \partial_j\psi^6)$, covariant with respect to rotations in (x^5, x^6). Taking the electromagnetic field into account we have not only to add the two lagrangians together, but, at the same time, to replace the derivatives $\partial_k\psi$ and $\partial_k\psi^\dagger$ by the covariant derivatives according to (30) because the manifold is no longer flat in the presence of the electromagnetic field. Thus, we have to assume the following lagrangian:

$$L = L(f_{jk}) + L(\psi, \psi^\dagger, \psi_{;j}, \psi^\dagger_{;k}) \tag{32}$$

with $L(f_{jk})$ given by (22) and $\psi_{;k}$ given by (30).

The usual variational principle applied to (32) yields the usual equations for the complex field ψ including its interaction with the electromagnetic field according to the rules

$$\partial_k\psi \to (\partial^k - ief_k)\psi, \quad \psi^* \to \psi^\dagger, \quad \partial_k\psi^* \to (\partial_k + ief_k)\psi^\dagger, \tag{33}$$

and the Maxwell equations in the presence of a charge and current four-vector j_k

$$\partial_j f_{jk} = -ej_k, \tag{34}$$

where j_k differs from the traditional charge and current density (constructed from $\psi, \psi^*, \partial_k\psi, \partial_k\psi^*$) merely by a change of notation $\psi^* \to \psi^\dagger$.

From the above derivation it is seen that the electromagnetic interaction is of closely analogous (geometric) origin to the gravitational interaction.

The whole scheme of electrodynamics has acquired a simple geometrical interpretation. The charged field, being a vector field with respect to rotations in (x^5, x^6), describes particles with a unit spin in this subspace. Therefore the electric charge is nothing else but angular momentum in the electric subspace. The charged particle possesses an angular momentum of absolute value 1 (in units $c = \hbar = 1$) in (x^5, x^6). However, owing to the metric properties of our manifold, this spin does not come forth with its full "strength" 1, but diminished by the factor (31). This factor is the root of the Sommerfeld constant. Its experimental value $e = 137^{-\frac{1}{2}}$ lies within the limits (9) and (11) defining the quasi-regular manifold †. Expressed in terms of the electric charge the restrictions (9) and(11) are

† As is seen from (31) we could not get the desired result $e < 1$ with the help of a regular metric: $a \leqq 0$.

$$\tfrac{1}{4} > e > 0. \tag{35}$$

Our formalism cannot predict the exact experimental value $e = 137^{-1}$, but still, we can understand the reasons why this value must be significantly smaller than unity.

As regards the problem of the exact value $e = 137^{-1}$ we should like to add the following remark. This value can be either "accidental" (we can even imagine that it changes slowly during centuries for some unknown cosmological reasons) or it is distinguished by some requirement of stability. We should like to mention some investigations [1]) showing that divergent self-masses can be avoided by assuming a suitable mixture of fields and couplings. When all sorts of fields and their couplings will be known, it can well happen that only for some special values of the coupling constants will it be possible to avoid divergences of the self-energy type and get a minimum rest mass of the particle dressed in all possible types of self-fields.

Let us consider the problem of charge conjugation. This transformation is equivalent to the substitution

$$\psi \to \psi^{\dagger}, \quad \psi^{\dagger} \to \psi, \tag{36}$$

valid for bosons as well as for fermions described by four-component spinors in the Majorana representation. As is seen from (29) charge conjugation is still interpretable as an inversion in (x^5, x^6), in view of the fact that it is immaterial which of the two, ψ or $\psi^{\dagger}$, is built up of vector components with upper or lower indices. In this way charge conjugation acquires a simple geometrical interpretation. It is interesting to notice that the famous transformation CP is a transformation with determinant 1 if looked upon from the six-dimensional viewpoint.

With the aid of (27) one can compute the second covariant derivatives of the charged field and check their commutability. The result is

$$\psi_{;jk} - \psi_{;kj} = e f_{jk} \psi, \tag{37}$$

whence it is seen once more that the existence of the electromagnetic field f_{jk} means a change of geometry: the field f_{jk} introduces an x^k-dependent curvature of the six-dimensional manifold.

Concluding, it may be stated that not only gravitation but also electrodynamics is expressible entirely in a geometrical language. This can be done in a riemannian six-dimensional space embedding the usual space-time. This last is distinguished as a hypersurface where the metric tensor $g_{\mu\nu}$ and the curvature tensor $R_{\mu\nu}$ are singular, Gauge transformations are identical with rotations in the electric subspace (x^5, x^6) around the singular point. Electric charge is essentially identical with the angular momentum in this subspace, and charge conjugation is interpretable as inversion. The conservation law for the electric

charge is a consequence of the isotropic character of the electric subspace. The electromagnetic field is equivalent to an x^k-dependent curvature of the six-dimensional manifold. Electromagnetic and gravitational field equations follow from the same lagrangian $(1/g)R$, whereby the part $g^{jk}R_{jk}$ is responsible for gravitation and the part $g^{5k}R_{5k}+g^{6k}R_{6k}$ is responsible for electromagnetic field. The constant a involved in the definition of the geometrical "background" is closely connected with the electromagnetic coupling constant. The gravitational coupling constant is interpretable in terms of an ultramicroscopic spread of events in the fifth and the sixth dimension.

6. A Cosmological Digression

One of the aims of this paper: to show the usefulness of the hypothesis of a six-dimensional manifold, is already attained by showing the possibility of formulating a unitary theory of the gravito-electromagnetic field. In order to account for the facts that (i) the fifth and the sixth dimension are not directly perceptible, and that (ii) the Sommerfeld constant is small in comparison with unity, we were compelled to assume that — even in the absence of gravitation and electromagnetic field — the manifold is not flat but is characterized by a metric given by the formulae (4), (5), (6) and (8). At the first sight such a particular type of metric seems quite arbitrary and looks artificial, but its consequences proved to be so promising that we feel entitled to take it seriously: perhaps such a structure of the geometrical background is not at all artificial but quite natural and intelligible?

The relativistic trend in physics has shown that the physical space is intimately connected with matter. We can say even that the two notions are inseparable, or that matter creates its own space. From this point of view the concept of a flat (i.e. empty) space is only a mathematical abstraction and cannot possess any physical meaning. Physical space must be a riemannian space. Now, the simplest case of a riemannian space is a two-dimensional space. In a two-dimensional space the components of the curvature tensor are interrelated

$$R_{\mu\nu\rho\sigma} = \tfrac{1}{2}(g_{\mu\rho}g_{\nu\sigma}-g_{\mu\sigma}g_{\nu\rho})R \qquad (\mu, \nu, \rho, \sigma = 1,2), \tag{38}$$

so that only one of them is independent. As the independent quantity one can choose the scalar curvature R. By contracting (38) we get

$$R_{\mu\nu}-\tfrac{1}{2}g_{\mu\nu}R = 0, \qquad (\mu, \nu = 1,2). \tag{39}$$

This relation is identically satisfied in a two-dimensional space but we notice a remarkable fact: it is exactly of the form of the gravitational field equations in the absence of external sources: a tensor field $T_{\mu\nu}$, contrast to the theory of Einstein, does not appear on the right hand side. Thus, in a two-dimensional

space there can exist only a primitive (quasi-gravitational) field, described completely by a single field quantity. This field is autonomous in the following sense: it cannot possess any external cause of its existence (in form of a source $T_{\mu\nu}$). Thus, a two-dimensional, quasi-gravitational field has a truly elementary character (Urmaterie). In view of the intimate connection between space and matter, we can also invert our argument and say that the elementary (quasi-gravitational) field creates a two-dimensional space.

Now, we can understand why the physical space is six-dimensional: since the time-like and the space-like characters mean two distinct (though in principle equivalent) possibilities, there should exist three types of elementary fields, and consequently three types of elementary (i.e. two-dimensional) space Σ_1, Σ_2, Σ_3 with the signatures $(++)$, $(+-)$, and $(--)$ respectively. For reasons of completeness all three types of quasi-gravitational fields and spaces should coexist in Nature, just spanning a six-dimensional space with the signature $(+++---)$ †.

For reasons of symmetry and simplicity we may assume that the three elementary fields involve the same function φ with the properties

$$\varphi(|r^2|) \to \infty \quad \text{for} \quad r^2 \to 0, \quad \varphi(|r^2|) \to 1 \quad \text{for} \quad |r^2| \to \infty, \tag{40}$$

so that, in a certain coordinate system, we have

$$g_{11} = g_{22} = \varphi(|p^2|), \quad g_{33} = -g_{44} = \varphi(|q^2|), \quad g_{55} = g_{66} = -\varphi(|r^2|), \quad g_{\mu\nu} = 0 \quad \text{for} \quad \mu \neq \nu, \tag{41}$$

where

$$p^2 = (x^1)^2 + (x^2)^2, \quad q^2 = (x^3)^2 - (x^4)^2, \quad r^2 = -(x^5)^2 - (x^6)^2. \tag{41'}$$

Hereby the three subspaces (1,2), (3,4), and (5,6) have acquired a concrete physical contents: they are formed by means of some special solutions for the three-types of quasi-gravitational fields. In each of the three subspaces there exists a singular point (in the subspace (3,4) there exist also two singular lines crossing at a singular point). The manifold characterized by (41) is invariant under the transformations $x^1 \rightleftarrows x^6$, $x^2 \rightleftarrows x^5$, $x^3 \rightleftarrows x^4$ and the change of signature.

In order to restore the situation assumed beforehand and described by (4), (5), (6) and (8) we have only to assume that our galaxy is situated very far from the singular points in the subspaces (1,2) and (3,4) but very close to the singular point in the subspace (5,6), i.e. outside the "curvature barrier" in (1,2) and (3,4) but inside the "curvature barrier" in (5,6) (cf. footnote on page 295).

† The six-dimensional point space can be regarded as an elementary space, say Σ_1, whose elements are not points, but other elementary spaces, say Σ_2. Thus, Σ_1 is a two-parametric family, not of points, but of elementary spaces Σ_2. The space Σ_2 is in turn a two-parametric family of elementary spaces Σ_3. Since only the three types of elementary spaces exist, the third should be a two-parametric family of ordinary points. Hereby Σ_3 is by no means privileged since we can as well change the order of hierarchy of the three spaces.

7. Isospin

The purpose of this section is to show that the idea of a six-dimensional manifold is not only useful for formulating a unitary theory of the gravito-electro-magnetic field, but is also of some methodological value for the theory of nuclear forces.

Let us start by pointing out the remarkable fact that (in contradistinction to electrodynamics, where bosons as well as fermions serve as sources of the electromagnetic field) only fermions (baryons), but not bosons, constitute the sources of nuclear forces. This gives us a hint that the problem of nuclear interactions must be intimately connected with the theory of spinors.

The well known theorem of Cartan [2]) states that spinors with $2^{E(\frac{1}{2}n)}$ components are adequate for the case of n-dimensional spaces. The proof of the theorem is based upon the possibility of constructing bilinear expressions $\psi_\alpha^* A_{\alpha\beta}\psi_\beta$ transforming like scalar, vector, and skew-symmetric tensors of rank $2, 3 \ldots, n$. Thus, for the case of a six-dimensional space, eight-component spinors, and a Clifford algebra realizable by means of γ-matrices with eight rows and columns, should play a particularly important role. (Four-or two-component spinors can also play some role in the six-dimensional world but should be regarded rather as exceptional degenerate cases.)

Let us consider Dirac matrices Γ^μ with eight rows and columns. There exist seven and only seven hermitian matrices (determined up to a common unitary transformation) satisfying the relations

$$\Gamma^\mu\Gamma^\nu+\Gamma^\nu\Gamma^\mu = 2\delta_{\mu\nu}. \tag{42}$$

Six of them are independent, the seventh is essentially the product of the remaining six:

$$\Gamma^7 = -i\Gamma^1\Gamma^2\ldots\Gamma^6. \tag{43}$$

Six of them play the same role in the six-dimensional space as the usual Dirac matrices γ^k with four rows and columns in the four-dimensional space, while the seventh plays the same role as γ^5. A particularly simple realization of the set of Γ^μ is

$$\Gamma^k = \begin{pmatrix} \gamma^k & \\ & \gamma^k \end{pmatrix}, \quad \Gamma^5 = \begin{pmatrix} & \gamma^5 \\ \gamma^5 & \end{pmatrix}, \quad \Gamma^6 = \begin{pmatrix} & -i\gamma^5 \\ i\gamma^5 & \end{pmatrix}, \quad \Gamma^7 = \begin{pmatrix} \gamma^5 & \\ & -\gamma^5 \end{pmatrix}. \tag{44}$$

Let us consider the equation for the nucleon coupled to the pion field:

$$(\gamma^k\partial_k+M+iG\gamma^5\boldsymbol{\tau}\cdot\boldsymbol{\varphi})\psi = 0, \tag{45}$$

where G is the coupling constant, τ_1, τ_2, τ_3 are Pauli matrices in the space of isobaric spin (iso-space) and φ_1, φ_2, φ_3 denote the components of the pionic field. This equation can be reinterpreted from a six-dimensional point of view. To this end we replace the two indices attached to the nucleonic field quantity

$\psi_{\alpha,\rho}$, and connected with the ordinary spin ($\alpha = 1, \ldots 4$) and isospin ($\rho = 1, 2$), by a single index, i.e. put

$$\begin{aligned} \Psi_1 &= \psi_{1,1}, \quad \Psi_2 = \psi_{2,1}, \quad \Psi_3 = \psi_{3,1}, \quad \Psi_4 = \psi_{4,1}, \\ \Psi_5 &= \psi_{1,2}, \quad \Psi_6 = \psi_{2,2}, \quad \Psi_7 = \psi_{3,2}, \quad \Psi_8 = \psi_{4,2}. \end{aligned} \tag{46}$$

In this notation the eq. (45) assumes an interesting form:

$$(\Gamma^k \partial_k + i(\Gamma^5\phi_5 + \Gamma^6\phi_6 + \Gamma^7\phi_7) + M)\Psi = 0, \tag{47}$$

where the Γ_μ are given by (44) and

$$\phi_5 = G\varphi_1, \quad \phi_6 = G\varphi_2, \quad \phi_7 = G\varphi_3. \tag{48}$$

In our opinion this transcription reveals the deeper meaning of the structure of nuclear forces. The eq. (47) is more elegant than (45) and is intelligible from the six-dimensional point of view. First of all, the two components φ_1 and φ_2 of the pionic field actually denote a vector field ϕ_5, ϕ_6 with respect to rotations in the electric subspace (x^5, x^6) of the six-dimensional world. According to our geometrical electrodynamics these components must describe a charged field. Indeed, a field which is a vector in the subspace (x^5, x^6) describes particles with a spin of magnitude 1 in this subspace and consequently with a charge of magnitude e. Since there are only two possible orientations of spin 1 in a two-dimensional space, there are two charge eigenvalues $\pm e$. On the other hand, the field ϕ_7 (i.e. the "third component" φ_3) is a scalar with respect to rotations in the whole six-dimensional space (as is seen from (47)) so that it must describe neutral particles †. In this way it is seen that the electromagnetic properties of the pionic field follow quite automatically from (47).

We can also draw directly some conclusions with regard to the nucleonic charge: Since the nucleon is described by means of a spinor field quantity describing particles with spin $\frac{1}{2}$ in the six-dimensional world, its spin possesses two orientations $\pm\frac{1}{2}$ with respect to any two-dimensional subspace of the six-dimensional space. In particular, it has two orientations $\pm\frac{1}{2}$ with respect to the subspace (x^5, x^6) so that the difference of the two spin projections upon the electric subspace must be unity, and consequently, the difference of the two charge eigenvalues must be equal to one unit of the electric charge e ††.

The six-dimensional formalism enables us to understand the meaning of iso-spin and iso-space. Iso-space is not a genuine space but is an imitation brought about by the fact that in the six-dimensional space embedding the Minkowski space there exist three Dirac matrices Γ^5, Γ^6, Γ^7 that appear as superfluous from the point of view of an observer confined to stay for ever in

† The covariant derivative of a scalar field is $\phi_{/k} = \partial_k\phi$, so that no interaction with the electromagnetic field can arise.

†† On the other hand, it is not yet explained why the "centre of charge" of the nucleon is $\frac{1}{2}e$. We shall come back to this question in the next section.

the Minkowski subspace. These three matrices are algebraically equivalent and therefore it is possible to perform transformations isomorphic to rotations in a three-dimensional space. This abstract space may be denoted as a (5, 6, 7)-space. The equation (47) is invariant under rotations in this space.

Of course, the above mentioned invariance breaks down if we take electromagnetic interactions into account. The electromagnetic phenomena just enable us to discover that only two of the dimensions (5, 6, 7) are genuine, namely (5, 6), whereas 7 is a fictitious dimension feigned by the algebraic fact that, if there exist six Dirac matrices satisfying (42), there must also exist a seventh in the form of the product of the remaining six, and also satisfying (42).

Thus, iso-spin and "iso-space", as well as a violation of the rotational symmetry in iso-space by electromagnetic interactions, and the connection of the "third component" of iso-spin with the electric charge, find a very simple and natural explanation with the help of the hypothesis of a six-dimensional universe.

We can also understand why a pseudo-scalar form of the pion-nucleon interaction is simpler and more natural than, e.g., a scalar interaction with scalar mesons. This is directly connected with the fact that γ^5 is automatically involved in the matrices Γ^5, Γ^6, and Γ^7 spanning the "iso-space". This implies a pseudo-scalar character for pions, of course under the assumption of invariance of strong interactions with respect to inversions.

In the above considerations we disregarded, for the sake of simplicity, the fact that — even when neglecting gravitational and electromagnetic fields — our six-dimensional manifold is not flat. In order to account for the curvature brought about by the "rigid background" (*Urmaterie*) we have to put

$$\tilde{\Gamma}^\mu \tilde{\Gamma}^\nu + \tilde{\Gamma}^\nu \tilde{\Gamma}^\mu = 2g^{\mu\nu} \qquad (\mu, \nu = 1, \ldots, 6) \tag{49}$$

with

$$g^{11} = g^{22} = g^{33} = -g^{44} = 1, \quad g^{55} = g^{66} = \frac{1}{\varphi(r)}, \quad g^{\mu\nu} = 0 \quad \text{for} \quad \mu \neq \nu, \tag{50}$$

where $\varphi(r)$ is the function occurring in the formulae (5)—(8). In order to satisfy (49) we have to use an antihermitian γ^4 (and γ^5) and put

$$\tilde{\Gamma}^k = \begin{pmatrix} \gamma^k & \\ & \gamma^k \end{pmatrix}, \quad \tilde{\Gamma}^5 = \frac{1}{\sqrt{|\varphi(r)|}} \begin{pmatrix} & \gamma^5 \\ \gamma^5 & \end{pmatrix}, \quad \tilde{\Gamma}^6 = \frac{1}{\sqrt{|\varphi(r)|}} \begin{pmatrix} & -i\gamma^5 \\ i\gamma^5 & \end{pmatrix}, \tag{51}$$

differing from (44) mainly by the factor $|\varphi(r)|^{-\frac{1}{2}}$. However, this factor can be absorbed by a suitable change of the definition (48):

$$\tilde{\phi}_5 = G\varphi_1 \sqrt{|\varphi(r)|}, \quad \tilde{\phi}_6 = G\varphi_1 \sqrt{|\varphi(r)|} \tag{52}$$

so that we get again the same equation (47).

8. The Nucleon

In the foregoing section it was proved that the difference between the two charge eigenstates of the nucleon must be equal to unity, but we were unable to prove that they should be exactly 1.0. If isospin constituted the only cause of the electric charge, the charge eigenvalues of the nucleon would be $\pm\frac{1}{2}$. But there is also another cause: the fact that the nucleon is described by a complex spinor. We have pointed out before that four-component complex spinors can be regarded as vectors under rotations in the electric space. If it were the same with eight-component complex spinors, the two constituents of the charge would correspond to $\frac{3}{2}$, $\frac{1}{2}$. However, half-integral charge makes no sense: it was possible to formulate a geometrical theory of electrodynamics only under the assumption that the charged field behaves like a vector under rotations in (x^5, x^6) which means that the resultant angular momentum component M_{56} of charged particle must be ± 1.

The way out of this dilemma is as follows: besides the possibility of defining the transformation character of a complex field quantity by decomposing it into a real and an imaginary part (in a Majorana representation) and regarding these parts as components of a vector in (x^5, x^6),

$$\psi = \psi^5 + i\psi^6, \tag{53}$$

there exists also another possibility: to assume ψ and ψ^* to transform like components of a two-component spinor $\psi_{(\zeta)}$ under rotations in (x^5, x^6) †. Thus we put

$$\begin{pmatrix} \psi \\ \psi^* \end{pmatrix} = \begin{pmatrix} \psi_{(1)} \\ \psi_{(2)} \end{pmatrix}. \tag{54}$$

If we perform a rotation in (x^5, x^6) through the angle f, the first alternative yields

$$\psi' = e^{if}\psi, \quad \psi^{*\prime} = e^{-if}\psi^*, \tag{55}$$

whereas the second alternative yields

$$\begin{pmatrix} \psi'_{(1)} \\ \psi'_{(2)} \end{pmatrix} = \begin{pmatrix} e^{\frac{1}{2}if}\psi_{(1)} \\ e^{-\frac{1}{2}if}\psi_{(2)} \end{pmatrix}, \tag{56}$$

i.e.

$$\psi' = e^{\frac{1}{2}if}\psi, \quad \psi^{*\prime} = e^{-\frac{1}{2}if}\psi^*. \tag{56'}$$

Both alternatives obey the same transformation law under inversions:

$$\psi' = \pm\psi^*, \quad \psi^{*\prime} = \pm\psi. \tag{57}$$

For the second alternative, this agrees with the fact that the two-component

† We put this new spinor index into parenthesis in order not to confuse it with the usual spinor index.

spinors should transform under inversions like

$$\begin{pmatrix} \psi'_{(1)} \\ \psi'_{(2)} \end{pmatrix} = \pm \begin{pmatrix} & 1 \\ 1 & \end{pmatrix} \begin{pmatrix} \psi_{(1)} \\ \psi_{(2)} \end{pmatrix} \tag{57}$$

in order to secure that the eigenstate of the spin projection $\frac{1}{2}$ described by $\binom{1}{0}$ goes over into an eigenstate of the spin projection $-\frac{1}{2}$ described by $\binom{0}{1}$ and vice versa.

In view of the existence of the two possibilities of transformation laws for complex field quantities under rotations and inversions in the electric subspace, we can secure integral values of the electric charge by associating the alternative (53) with four-component complex spinors, and the alternative (54) with eight-component complex spinors. Consequently, ψ stands in (54) and (56) for any component of the spinor Ψ describing the nucleon.

Thus, in contradistinction to the case of four-component spinors, for eight-component complex spinors we have to do simultaneously with two half-integral spins with respect to the electric subspace. One of them is the projection $I_{(3)} = I_{56}$ of the isospin, the other is a new spin, to be called co-spin and denoted by J_{56}. These two half-integral spins either give a resultant spin of magnitude 1 or cancel each other.

It could be argued that, in view of (54), the co-spin cannot have a definite eigenvalue since both components $\Psi_{(1)} = \Psi$, $\Psi_{(2)} = \Psi^*$ must be different from zero simultaneously. This argument holds true only in the non-quantized form of the theory. In the quantized form, Ψ and Ψ^* are operators and there exist states where $\Psi|\rangle = 0$ and $\Psi^*|\rangle \neq 0$, or vice versa.

The charge and current density j^k of the nucleon is

$$\frac{1}{e} j^k = \tfrac{1}{4} i[\overline{\Psi}, \Gamma^k(1+\Gamma^{[5,6]})\Psi] \tag{58}$$

where

$$\overline{\Psi} = \Psi^* \Gamma^4 \quad \text{and} \quad \Gamma^{[5,6]} = \frac{1}{2i}(\Gamma^5\Gamma^6 - \Gamma^6\Gamma^5). \tag{58'}$$

Hence, the electric charge q, which is the operator of infinitesimal rotation in the subspace (x^5, x^6), has the form

$$\frac{1}{e} q = \tfrac{1}{4} \int \mathrm{d}^3x[\Psi^*, (1+\Gamma^{[5,6]})\Psi]. \tag{59}$$

Its two constituent parts

$$J_{56} = \tfrac{1}{4} \int \mathrm{d}^3x[\Psi^*, \Psi], \quad I_{56} = \tfrac{1}{4} \int \mathrm{d}^3x[\Psi^*, \Gamma^{[5,6]}\Psi] \tag{60}$$

are nothing else but co-spin and iso-spin projection, respectively. The expressions (58)—(60) behave correctly under charge conjugation because they have been properly antisymmetrized.

Besides the charge and current density (58) there exists an infinity of other (normalized) four-vectors

$$\tfrac{1}{2}i[\overline{\Psi}, \Gamma^k(\alpha+\beta\Gamma^{[5,6]})\Psi] \quad \text{with} \quad \alpha+\beta = 1, \tag{61}$$

also satisfying the continuity equation. One of them ($\alpha = 1$, $\beta = 0$) is distinguished by the fact that it is invariant under the transformation exchanging proton with neutron:

$$\Psi' = \begin{pmatrix} & 1 \\ 1 & \end{pmatrix} \Psi \tag{62}$$

(in which 1 means a unit matrix with four rows and columns). The corresponding integrated quantity

$$b = 2J_{56} \tag{63}$$

is the nucleonic (baryonic) number. It is remarkable that, in contradistinction to the iso-spin, the change of orientation of the co-spin of the nucleon is necessarily connected with a change of sign of the nucleonic number.

It is also interesting that the charge and current (58) involves a projection operator $\frac{1}{2}(1+\Gamma^{[5,6]})$. This resembles the situation in the theory of weak interactions involving another projection operator $\frac{1}{2}(1+\gamma^5)$. We suspect this analogy not to be purely formal.

9. The (N, Ξ)-System

The assumption (54) is not the only alternative: the roles of ψ and ψ^* can also be interchanged, so that

$$\begin{pmatrix} \psi^* \\ \psi \end{pmatrix} = \begin{pmatrix} \psi_{(1)} \\ \psi_{(2)} \end{pmatrix}. \tag{64}$$

Denoting the eight-component spinor of the type (54) by N, and that of the type (64) by Ξ, it is easily seen that they transform under rotation in the electric subspace through the angle f according to

$$N' = e^{\frac{1}{2}if} e^{\frac{1}{2}if\Gamma^{[5,6]}} N, \quad \Xi' = e^{-\frac{1}{2}if} e^{\frac{1}{2}if\Gamma^{[5,6]}} \Xi, \tag{65}$$

where the first exponential factor arises from the assumed spinor-like character of ψ together with ψ^*, as indicated by (54) and (64), and is connected with the co-spin, while the second exponential factor arises from the fact that, being eight-component spinors, they describe particles with a half-integral iso-spin. Eq. (64), or the second formula (65), implies the opposite connection between co-spin and baryonic number

$$b = -2J_{56}. \tag{66}$$

At first sight this seems to yield no new alternative in comparison with (63),

since it is immaterial whether the nucleon is called "particle" or "antiparticle". But we shall get something new by combining both alternatives formally into a spinor with 16 components:

$$\Psi_\rho = N_\rho, \quad \Psi_{\rho+8} = \Xi_\rho \qquad (\rho = 1, \ldots 8). \quad (67)$$

In this case the charge is

$$\frac{q}{e} = \tfrac{1}{4}\int \mathrm{d}^3x \left[\Psi^*, \left(\begin{pmatrix} 1 & \\ & -1 \end{pmatrix} + \begin{pmatrix} \Gamma^{[5,6]} & \\ & \Gamma^{[5,6]} \end{pmatrix}\right)\Psi\right], \quad (68)$$

where 1 means a unit matrix with eight rows and columns. The baryonic number is again

$$b = \tfrac{1}{2}\int \mathrm{d}^3x[\Psi^*, \Psi]. \quad (69)$$

Such a spinor field describes simultaneously the nucleon and the cascade hyperon.

10. The (N, Λ, Σ, Ξ)-System

The above mentioned alternatives (54) and (64) of regarding the field quantity with its conjugate as a two-component spinor with respect to the group of rotations and inversions in the electric subspace do not exhaust all the possibilities. Besides (54) and (64), valid for any component of the spinor, there are "mixed" alternatives

$$\begin{pmatrix} \psi^* \\ \psi \end{pmatrix} = \begin{pmatrix} \psi_{(1)} \\ \psi_{(2)} \end{pmatrix} \quad \text{for} \quad \alpha = 1, \ldots 4, \quad \begin{pmatrix} \psi \\ \psi^* \end{pmatrix} = \begin{pmatrix} \psi_{(1)} \\ \psi_{(2)} \end{pmatrix} \quad \text{for} \quad \alpha = 5, \ldots 8, \quad (70)$$

or

$$\begin{pmatrix} \psi \\ \psi^* \end{pmatrix} = \begin{pmatrix} \psi_{(1)} \\ \psi_{(2)} \end{pmatrix} \quad \text{for} \quad \alpha = 1, \ldots 4, \quad \begin{pmatrix} \psi^* \\ \psi \end{pmatrix} = \begin{pmatrix} \psi_{(1)} \\ \psi_{(2)} \end{pmatrix} \quad \text{for} \quad \alpha = 5, \ldots 8. \quad (71)$$

Eight-component spinors of the types (70) and (71) possess again two causes for the appearance of the electric charge: one part of the charge results from the complex character of the spinor and the assumed spinor-like character indicated by (70) or (71), the other part of the charge results, as usually, from the fact that — being eight-component spinors — they describe particles with a half-integral iso-spin.

Denoting the eight-component spinors of the type (70) and (71) by Z and Σ respectively, and combining them — together with N and Ξ — into a 32-component spinor

$$N_\rho = \Psi_\rho, \quad Z_\rho = \Psi_{\rho+8}, \quad \Sigma_\rho = \Psi_{\rho+16}, \quad \Xi_\rho = \Psi_{\rho+24} \quad (\rho = 1, \ldots 8), \quad (72)$$

we get the following expression for the electric charge

$$\frac{q}{e} = \tfrac{1}{2}\int \mathrm{d}^3x[\Psi^*, (j_{56}+i_{56})\Psi] \tag{73}$$

where

$$j_{56} = \tfrac{1}{2}\begin{pmatrix} 1 & & & \\ & -\Gamma^{[5,6]} & & \\ & & \Gamma^{[5,6]} & \\ & & & -1 \end{pmatrix}, \quad i_{56} = \tfrac{1}{2}\begin{pmatrix} \Gamma^{[5,6]} & & & \\ & \Gamma^{[5,6]} & & \\ & & \Gamma^{[5,6]} & \\ & & & \Gamma^{[5,6]} \end{pmatrix}, \tag{74}$$

or

$$j_{56}+i_{56} = \tfrac{1}{2}\begin{pmatrix} 1+\Gamma^{[5,6]} & & & \\ & 0 & & \\ & & 2\Gamma^{[5,6]} & \\ & & & -1+\Gamma^{[5,6]} \end{pmatrix}. \tag{75}$$

Hence it is seen that in the middle part of the 32×32 matrix ($\rho = 9, \ldots, 24$) the distinction between co-spin and iso-spin has disappeared. Or, better to say, by assuming the transformation laws (70) and (71) co-spin turned over into isospin. Both half-integral iso-spins either sum up or cancel each other. If they sum up, we get the hyperons $\Sigma^{\pm}$ (for $\rho = 17, \ldots, 24$). If they cancel, we have to do with a mixture of Σ^0 and Λ (for $\rho = 9, \ldots, 16$). The (Z, Σ)-system, being a composition of two half-integral iso-spins, can be reduced into irreducible parts: iso-spin of magnitude 1 with the projections 1, 0, -1, and iso-spin zero. They correspond to the hyperons Σ^+, Σ^0, Σ^- and Λ respectively. In all these cases one may say that the co-spin disappears.

In this way we get an explanation of the baryon family. The characteristics of baryons are summarized in table 1. The particles characterized by co-spin $\frac{1}{2}$,

TABLE 1

The baryon family

b	1				-1			
J_{56}	$-\frac{1}{2}$	0		$\frac{1}{2}$	$-\frac{1}{2}$	0		$\frac{1}{2}$
I	$\frac{1}{2}$	1	0	$\frac{1}{2}$	$\frac{1}{2}$	0	1	$\frac{1}{2}$
name	Ξ	Σ	Λ	N	$\bar{\mathrm{N}}$	$\bar{\Lambda}$	$\bar{\Sigma}$	$\bar{\Xi}$

0, $-\frac{1}{2}$ are called "isofermions", "isobosons", "anti-isofermions", respectively. In strong interactions iso-spin as well as co-spin are conserved separately (whence follows the conservation of the number of isofermions). Weak interactions violate iso-spin conservation and are characterized by

$$|\Delta I_{56}|+|\Delta J_{56}| = 1. \tag{76}$$

11. The Rest-Mass Problem

It is usually believed that the rest mass is a consequence of the interaction of the particle with the surrounding self-field. Therefore, it cannot be predicted theoretically unless a satisfactory, divergence-free theory of all types of interactions is known. However, since the baryons form a family, the types of interaction between them should be closely analogous, so that it is plausible that the ratios of their masses are connected by a simple rule and depend upon the quantum numbers b, J_{56}, I, I_{56}. Therefore we ask: is there a feature, within the scheme of baryons, that could justify the fact that Ξ is much heavier, and N much lighter, than Λ and Σ?

Let us define the quantity

$$T_{56} = J_{56} - b. \tag{77}$$

This quantity can be written also in the form

$$T_{56} = \tfrac{1}{4}\rho \int \mathrm{d}^3x[\Psi^*, \Psi] \tag{78}$$

where

$$\rho = -1 \text{ for } N, \quad \rho = -2 \text{ for } \Lambda \text{ and } \Sigma, \quad \rho = -3 \text{ for } \Xi. \tag{78'}$$

The absolute value of the factor ρ (resembling somewhat the g-factor of Landé) can be regarded as responsible for the inequalities of the baryon masses.

The quantity T_{56} is also remarkable for the following reason: together with iso-spin, it characterizes unambiguously the particle. Indeed, if T_{56} is given, the remaining quantum numbers are

$$b = -\operatorname{sgn} T_{56}, \quad J_{56} = T_{56} - \operatorname{sgn} T_{56} \tag{79}$$

for one-particle states. Therefore, we can use it to characterize the particles and to construct table 2. This table has been constructed according to the following

TABLE 2

Other classification of baryon family

T_{56}	$-\frac{3}{2}$		-1				$-\frac{1}{2}$		$\frac{1}{2}$		1				$\frac{3}{2}$	
I	$\frac{1}{2}$		1			0	$\frac{1}{2}$		$\frac{1}{2}$		0	1			$\frac{1}{2}$	
I_{56}	$-\frac{1}{2}$	$\frac{1}{2}$	-1	0	1	0	$-\frac{1}{2}$	$\frac{1}{2}$	$-\frac{1}{2}$	$\frac{1}{2}$	0	-1	0	1	$-\frac{1}{2}$	$\frac{1}{2}$
	Ξ^-	Ξ^0	Σ^-	Σ^0	Σ^+	Λ	n	p	$\bar{\mathrm{p}}$	$\bar{\mathrm{n}}$	$\bar{\Lambda}$	$\bar{\Sigma}^-$	$\bar{\Sigma}^0$	$\bar{\Sigma}^+$	$\bar{\Xi}^0$	$\bar{\Xi}^+$

rules: first of all we arranged the particles from the left to the right according to the ascending values of T_{56}. In this way we get a table with reflection symmetry: the particles and their antiparticles are situated symmetrically with respect to the centre of the table. Then we arrange the particles according to

iso-spin. We put Σ further away from the centre than Λ since the magnitude of its iso-spin is larger (also particles with larger $T = |T_{56}|$ are situated further away from the centre). Finally, we arrange the members of each charge multiple according to the same rule: from the left to the right with increasing I_{56}.

The most striking regularity of the table 2 is that the particles arranged themselves, quite automatically, in an ascending sequence of their masses according to their distances from the centre of the table: the lightest baryon, the proton, is situated close to the centre, next comes the neutron which is a little heavier, etc. It is hard to believe such a regularity to be purely accidental. Most probably the final result of a satisfactory computation of self-masses will be simple and "anschaulich" in contradistinction to what seems to be suggested by the awkward methods of self-mass computation applied nowadays.

12. Leptons

In the foregoing sections, the baryons have been interpreted in terms of eight-component complex spinors constituting the most natural type of spinors within the six-dimensional manifold. Indeed, it was possible to establish a one-to-one correspondence between different theoretical possibilities of transformation laws and the baryons known from experiment. However, the degenerate cases of four- or two-component spinors can also play some role in the six-dimensional world (similarly as the two-component spinors play some role in the four-dimensional world: neutrino). The aim of this section is to show that these degenerate cases can be put in a one-to-one correspondence with leptons.

The four-component spinors can be regarded as eight-component spinors with the supplementary condition $\Psi_{\alpha+4} = \Psi_\alpha$. In view of (46) this means that the corresponding particles possess no iso-spin:

$$I = 0. \tag{80}$$

Nevertheless, it is possible to construct a charge and current density four-vector also in this case. This fact can be expressed in the terminology of the six-dimensional world as follows: the real and the imaginary part of the four-component spinor (expressed in a Majorana representation) transform like components of a vector

$$\psi = \psi^5 + i\psi^6, \quad \psi^* = \psi^5 - i\psi^6 \tag{81}$$

under rotations and inversions in the electric subspace (x^5, x^6) around the origin. However, there exists an alternative possibility:

$$\psi = \psi^5 - i\psi^6, \quad \psi^* = \psi^5 + i\psi^6. \tag{82}$$

Defining the electric charge q/e as the operator of infinitesimal rotation in the electric subspace we get

$$\frac{q}{e} = f \quad \text{or} \quad \frac{q}{e} = -f \tag{83}$$

for the cases (81) and (82), respectively, where

$$f = \tfrac{1}{2}\int \mathrm{d}^3x[\psi^*, \psi] \tag{84}$$

may be called the number of (light) fermions.

Now, similarly as in the case of baryons, where all the alternatives of transformation characters with respect to rotations in (x^5, x^6) could be combined formally into a 32-component spinor, we can combine formally the two alternatives (81) and (82) into an eight-component spinor Ψ, so that

$$f = \tfrac{1}{2}\int \mathrm{d}^3x[\Psi^*, \Psi], \quad \frac{q}{e} = \tfrac{1}{2}\int \mathrm{d}^3x \left[\Psi^*, \begin{pmatrix} 1 & \\ & -1 \end{pmatrix} \Psi\right]. \tag{85}$$

Comparing (85) with (68) one may say that particles described by four-component spinors possess no iso-spin but an integral co-spin, so that

$$\frac{q}{e} = J_{56}. \tag{86}$$

The alternatives of four-component spinors being already exhausted by (85), they should correspond to the two types of charged fermions: muon and electron.

TABLE 3

The charged leptons

f	1		−1	
J_{56}	−1	1	−1	1
I	0	0	0	0
	μ^-	e^+	e^-	μ^+

TABLE 4

Other classification of charged leptons

T_{56}	−2	0	0	2
	μ^-	e^+	e^-	μ^+

Let us construct the tables 3 and 4, closely corresponding to the tables 1 and 2 of baryons, where T_{56} is defined, in close analogy with (77), by

$$T_{56} = J_{56} - f. \tag{87}$$

The same regularities hold as in the case of baryons: the particles situated symmetrically with respect to the centre of the table form particle-antiparticle

pairs, and the mass increases according to the distance from the centre of the table.

It is to be noticed that the concept of number of fermions does not coincide with that of the number of leptons. This last is determined by the co-spin

$$l = J_{56} \tag{88}$$

and corresponds rather to the concept of the number of iso-fermions, whereas f corresponds to the number of baryons b.

The quantity T_{56} (or $-\frac{1}{2}T_{56}$ to be called "muonic load") can be regarded as responsible for the mass difference between muon and electron. Introduce e.g. a coupling between leptons and baryons of the type

$$G_1(\bar{p}e)(\bar{e}p)+G'_1(\bar{n}e)(\bar{e}n)+G_2(\bar{\Xi}^+\mu)(\bar{\mu}\Xi^-)+G'_2(\bar{\Xi}^0\mu)(\bar{\mu}\Xi^0), \tag{89}$$

conserving the numbers of heavy and light fermions, as well as the electric charge, parity, the number of isofermions and that of leptons. This interaction is charge-independent if $G_1 = G'_1$ and $G_2 = G'_2$. Thus, it can be a strong interaction. However, G_1 does not need to be equal to G_2, The coupling constant can be proportional to the muonic load, so that $G_1 = G'_1 = 0$. In this way we are left with a strong coupling only between muon and the cascade hyperon, which accounts, at least qualitatively, for the mass difference between muon and electron as well as between cascade hyperon and nucleon.

Besides the degenerate cases of four-component spinors describing electron and muon, there is a degenerate case of two-component spinor. As is well known, it is possible to secure Lorentz invariance only if the rest mass of the corresponding particles vanishes. It is impossible to secure in this case invariance under inversions or to construct a charge and current density. Therefore, the two-component spinor describes the neutrino. No other alternative of two-component spinor exist.

In this way all fermions known from experiment have found a theoretical interpretation. They split into three classes: baryons (N, Λ, Σ, Ξ) described by eight-component spinors, light fermions (e, μ) described by four-component spinors, and neutrino (ν) described by a two-component spinor.

13. Mesons

The problem of mesons is more complicated than that of baryons or leptons since it is not sure whether they can be regarded as elementary particles. It is not excluded that mesons are clusters of fermions and antifermions. Nevertheless, one can try to classify them on similar lines as baryons. The simplest way of doing this is to reduce the number of possibilities known in the case of fermions to one half because bosons do not possess antiparticles in the usual sense of this word. Thus, we are left with the following alternatives:

$K^{+,0}$: a particle with iso-spin $I = \frac{1}{2}$, co-spin $J_{56} = \frac{1}{2}$ (corresponding to $N^{+,0}$ and $\bar{\Xi}^{+,0}$);

$K^{-,0}$: a particle with iso-spin $I = \frac{1}{2}$, co-spin $J_{56} = -\frac{1}{2}$ (corresponding to $\bar{N}^{-,0}$ and $\Xi^{-,0}$);

$\pi^{\pm,0}$: a particle with iso-spin $I = 1$, co-spin $J_{56} = 0$ (corresponding to $\Sigma^{\pm,0}$ and $\bar{\Sigma}^{\pm,0}$);

$\pi_0{}^0$: a particle with iso-spin $I = 0$, co-spin $J_{56} = 0$ (corresponding to Λ and $\bar{\Lambda}$).

In this scheme there appears an unknown particle $\pi_0{}^0$. This hypothetical particle is distinguished, in comparison with the remaining mesons, by $I+J=0$, where $J = |J_{56}|$, whereas in the other cases $I+J = 1$. Under this circumstance we may suppose that the coupling constant G is proportional to $I+J$ so that it vanishes for the case of $\pi_0{}^0$. Thus, this particle can exist but is not involved in strong interactions and therefore will not easily be detectable.

The question arises whether the above list exhausts all the possibilities? This does not seem to be the case. There still exist the following theoretical possibilities:

W^-: a particle with iso-spin $I = 0$ and co-spin $J_{56} = -1$ (corresponding to e^- and μ^-);

W^+: a particle with iso-spin $I = 0$ and co-spin $J_{56} = +1$ (corresponding to e^+ and μ^+).

These hypothetical particles, corresponding to leptons, seem — at first sight — to have nothing to do with strong interactions. However, this does not need to be so. A coupling of the type

$$(\bar{N}\Xi)W^* + (\bar{\Xi}N)W, \tag{90}$$

where W is a field quantity involving annihilation operators for W^- and creation operators for the antiparticles W^+, possesses all the features of strong interactions: it is charge independent and conserves co-spin.

The meson W will be created in the reactions

$$p + \pi^- \to \Xi^- + W^+ \tag{91'}$$

and

$$p + n \to p + n + W^+ + W^-. \tag{91''}$$

The decays $\Xi^0 \to p + W^-$ or $\Xi^- \to n + W^-$ would not take place if the rest mass of W is sufficiently large. These mesons would decay, with a long life time, through the chain of virtual processes

$$W \to (\bar{N} + \Xi) \to (\bar{N} + \Lambda + K^*) \to \pi + K^*, \tag{92}$$

where K^* denotes the antiparticle to $K^{+,0}$. In this way there is a possibility of explaining the heavy meson reported by Wang-Kan-Chang [3]).

All the well-known mesons, including the hypothetical meson of Wang-Kan-Chang, can be arranged into a table similar to the table 2 of baryons and the table 4 of charged leptons. To this end let us introduce an auxiliary quantum number T_{56}, of course not by (77) which is specialized for baryons, but by the alternative form (79). We get $T_{56} = 0$ for the pion, $T_{56} = -\frac{1}{2}$ for the K-meson, and $T_{56} = -2$ for the hypothetical W-meson. Arranging the particles from the left to the right, according to the same rules as those applied formerly to fermions, we get the table 5. We notice again the same regularities as before:

TABLE 5

The mesons

T_{56}	-2	$-\frac{1}{2}$		0			$\frac{1}{2}$		2
J_{56}	-1	$\frac{1}{2}$		0			$-\frac{1}{2}$		1
I_{56}	0	$-\frac{1}{2}$	$\frac{1}{2}$	-1	0	1	$-\frac{1}{2}$	$\frac{1}{2}$	0
	W^-	K^0	K^+	π^-	π^0	π^+	$\bar{K}^-$	$\bar{K}^0$	$\bar{W}^+$

particles situated symmetrically with respect to the centre of the table are charge-conjugate to each other (π^0 is charge-conjugate to itself) and the masses increase according to the distance from the centre of the table: the lightest meson π^0 is situated at the centre, then comes the charged pion which is a little heavier, then the charged K-meson which was proved recently to be lighter than its neutral counterpart, and finally we have the heaviest meson W. It is hard to believe that the regularities exhibited by the tables 2, 4, and 5 should be purely accidental.

14. The Question of Global Symmetry†

The appearance of γ^5 in the nucleon-pion interaction term has been explained in section 7. It constitutes the simplest and the most natural possibility in view of the fact that the products $\gamma^5\tau_1$, $\gamma^5\tau_2$, $\gamma^5\tau_3$ appear to be nothing else but the "superfluous" matrices Γ^5, Γ^6, Γ^7 in a transcription into eight-component spinor notation. It is quite natural to extend this rule to all strong interactions involving pions, i.e. assume that γ^5 always appears in the combination $\gamma^5\boldsymbol{\tau}$, but that γ^5 or $\boldsymbol{\tau}$ never appear alone. This rule leads to the following coupling terms:

$$iG_{\mathrm{NN}\pi}\bar{\mathrm{N}}\gamma^5\boldsymbol{\tau}\mathrm{N}\cdot\boldsymbol{\pi} \quad iG_{\Xi\Xi\pi}\bar{\Xi}\gamma^5\boldsymbol{\tau}\cdot\Xi\boldsymbol{\pi}, \quad iG_{\Lambda\Sigma\pi}\Lambda\boldsymbol{\Sigma}\cdot\boldsymbol{\pi}, \tag{93}$$

but is inconsistent with a coupling of the type $G_{\Sigma\Sigma\pi}\bar{\boldsymbol{\Sigma}}\gamma^5\cdot(\boldsymbol{\Sigma}\times\boldsymbol{\pi})$ necessitating the appearance of a γ^5 without a $\boldsymbol{\tau}$ to secure parity conservation. In this way it is seen that the requirement of global symmetry is inconsistent with the hypothesis of a six-dimensional world.

† The contents of this chapter have been prepared in collaboration with Dr. K. Wohlrab.

There are several semi-empirical hints against global symmetry [4]), and in favour of $G_{\Sigma\Sigma\pi} = 0$. If these facts become firmly established, they will constitute a support for our theory.

From (93) it follows that the relative parity of Λ is opposite to that of Σ. This is consistent with the fact that Λ is a scalar and Σ is a vector in isospace (i.e. in the abstract space induced by the matrices Γ^5, Γ^6, Γ^7). Indeed, inversions in the six-dimensional world change the sign of expressions of the type $\overline{\Psi}\Gamma^7\Psi$, i.e. reverse the "direction of the axis 7". Hereby Λ is not influenced but Σ^0 (that is Σ^7) changes sign. Therefore the relative parities of these hyperons should be opposite.

15. The Other Strong Interactions

Extending the above-mentioned rule (γ^5 and $\boldsymbol{\tau}$ always to appear in the combination $\gamma^5\boldsymbol{\tau}$) to the remaining strong interactions between mesons and baryons we get the following coupling terms:

$$iG_{N\Sigma K}\bar{N}\gamma^5\boldsymbol{\tau}\cdot\boldsymbol{\Sigma}K, \quad iG_{\Xi\Sigma K}\bar{\Xi}\gamma^5\boldsymbol{\tau}\cdot\boldsymbol{\Sigma}K^*, \quad iG_{N\Lambda K}\bar{N}\Lambda K, \quad iG_{\Xi\Lambda K}\bar{\Xi}\Lambda K^*, \quad iG_{N\Xi W}\bar{N}\Xi W^*, \tag{94}$$

whence it follows that (i) the relative parities of N and Ξ are the same, (ii) the W meson is scalar. This scheme agrees with the former finding that the relative parities of Λ and Σ are opposite. On the other hand, it does not presume anything about the character of the K-meson. It is seen from (94) that if K is pseudo-scalar (scalar), the relative parities of N and Σ are the same (opposite).

The above types of interaction terms involving a K-meson seem to be in disagreement with the present experimental evidence [5]). This evidence not being conclusive, it may finally turn out that our proposal (94) is correct. If not, we shall have to admit that strong interactions with the K-meson necessarily involve an "extra" factor γ^5 i.e. a product of the matrices $\Gamma^5\Gamma^6\Gamma^7$. However, we do not yet see any natural reason for the appearance of such a factor.

The interaction terms (93) and (94) involve N and Ξ symmetrically. Therefore they cannot explain the Ξ—N mass difference. Thus, either the coupling constants in (93) and (94) are different, or there are other causes for the inequalities of the rest masses, e.g. a coupling of the type (89) with $G_1 = G'_1 = 0$.

16. Concluding Remarks

In the theory sketched above the gravitational and the electromagnetic field appear to be closely related: both are metrical fields. Since the electromagnetic field is quantizable, also the gravitational field should be subjected

to a procedure of quantization, so that gravitons would acquire the same amount of physical reality as photons.

The remaining fields are of a different origin and constitute sources of the gravito-electromagnetic field. The different possible types of eight-component spinor fields correspond exactly to the different types of baryons, those of four-component spinor fields to charged leptons, and that of two-component spinor field to the neutrino. In this way not only photons and gravitons but also all fermions known from experiment find a natural place in our six-dimensional framework. Also mesons seem to fit quite well into the same framework. Iso-spin including its unavoidable connection with the electric charge has found a natural explanation. Besides iso-spin, particles are characterized by another important quantity: the co-spin. A remarkable regularity of the particle masses follows from our tables of elementary particles.

The electromagnetic interaction has been determined from purely geometrical considerations, closely corresponding to those used in the general relativity to determine the gravitational interaction. The other types of interactions (strong and weak) do not follow unavoidably from the theory but still, some types of couplings are favoured: in particular, a global symmetry of strong interactions seems rather unnatural.

Part of this investigation was pursued during author's stay at the Joint Institute for Nuclear Research in Dubna. The author would like to express his thanks to the Director of the Joint Institute, Professor Blochinzev, for the kind hospitality.

References

1) Rayski *et al.*, Helv. phys. Acta **23** (1950) 287; Acta phys. Polon. **10** (1950) 159;
H. Enatsu, Nuovo Cimento Suppl. **3** (1956) 526
2) E. Cartan, Leçons sur la théorie des spineurs (Hermann, Paris, 1938)
3) Wang-Kan-Chang *et al.*, Reports at the Kiev Conference, 1959
4) B. d'Espagnat and J. Prentki, preprint (1959);
H. Umezawa, private information
5) Dalitz, Kiev Conference, 1959

2.C

Nuclear Physics **17** (1960) 317—328; © *North-Holland Publishing Co., Amsterdam*

Not to be reproduced by photoprint or microfilm without written permission from the publisher

RESONANCE REACTIONS WITH GENERALIZED ONE-LEVEL APPROXIMATION

HARRY LUSTIG †

Department of Physics, University of Illinois, Urbana, Illinois ††

Received 22 January 1960

Abstract: A formalism is developed for the analysis of nuclear reactions which involve partially overlapping resonance levels. The Wigner R matrix, for each value of the total angular momentum and of the parity, is divided into a single-level matrix and an energy-dependent background matrix. The collision matrix, in the form defined by Blatt and Biedenharn, may then be expressed, for an N-channel reaction, in terms of the N partial widths of the tagged level, N "potential" phase shifts, and the $\frac{1}{2}N(N+1)$ parameters of the unitary and symmetric background matrix. By invoking the unitarity and symmetry of the collision matrix itself, the number of independent parameters in the background matrix is then reduced to $\frac{1}{2}N(N-1)$. An explicit recipe is given for the construction of the collision matrix, and is illustrated for $N = 2$ and $N = 3$. In this formalism, the separation between the strongly energy-dependent single-level part and the contributions from the background matrix is preserved throughout; the formalism will thus be practically useful when the latter varies slowly with energy in the region of the tagged resonance. The further simplifications which occur when the background matrix is diagonal, or nearly diagonal, are discussed.

1. Introduction

Although the R matrix theory of nuclear reactions [1]) is rigorously valid for all non-relativistic reactions of the type a+b → c+d, it has, in general, been applied only, on the one hand, to treat cases of isolated levels for which the Breit-Wigner formula [2]) is expected to hold rigorously, and, on the other hand, to provide a foundation for phenomenological theories of average cross sections [3]) (continuum model [4]) and optical model [5])) which are of interest when many levels overlap. The use of the theory in the analysis of cross sections involving *partially* overlapping levels (and indeed such analyses themselves) have generally been eschewed, perhaps, because the attendant difficulty and tedium were thought to exceed the amount of basic knowledge to be gained. Exceptions to this situation include the two-level approximation of Wigner [6]) and the division of the R matrix into a single-level matrix and a background matrix described in the review article of Lane and Thomas [3]). However, the former is of somewhat limited usefulness and the latter only goes part of the

† On sabbatical leave from The City College of New York.

†† Supported, in part, by the joint program of the U. S. Atomic Energy Commission and the Office of Naval Research.

way in facilitating the analysis of reactions in which a single resonance predominates, although it does not monopolize the cross section.

That there are occasions on which the analysis of partially overlapping levels needs to be undertaken is evident. Knowledge of the quantum numbers of fairly closely spaced nuclear levels is often of theoretical interest. Resonances have been observed in the scattering of pions by nucleons, and as the experimental work in elementary particle physics proceeds, it is not unlikely that interesting cases of interfering resonances will be found. In the practical realm, the demands of reactor physicists for cross sections are becoming ever more voracious, and there is no moratorium for energies in between the domain of the single-level formula and the region of applicability of statistical models. Frequently experimenters are able to measure one cross section (say, the total), and the analyst is called upon to determine the parameters required to predict another cross section (say, the angular distribution).

The analysis of data which involve overlapping resonances is complicated by three effects. 1) Because of the energy spread of the particles, the actually observed cross sections, near a resonance, will differ from those given in the literature. While there is generally little difficulty in making the required correction for well isolated levels, the matter becomes more complicated for overlapping resonances. 2) The interference of levels of different spin and/or parity introduces additional terms into the cross section formulas. While this complicates the analysis, at least the number of level parameters is not increased beyond the sum of the numbers of parameters of the individual levels. 3) The interaction for a given total angular momentum and parity cannot be fully ascribed to a single level plus hard sphere scattering. Because additional parameters are introduced into the cross section formulas, this is the most serious of the complications. If, at a given energy, several resonances contribute in more or less equal measure, a true multilevel formalism should be employed. If, on the other hand, there is physical evidence that one resonance predominates and that the unattributed effects are due to the tails of relatively far away levels, the analysis is most readily carried out with the aid of the introduction of a background matrix. We call this approach the generalized one-level approximation, although, as we shall see, it is rigorously valid in a formal sense.

Points 1) and 2) have been treated by the author in a previous paper [7]) and the generalized one-level approximation was carried out there for the single channel case, i.e. the case where the R matrix is one-dimensional. It is the purpose of this note to develop a useful generalized one-level formalism for the case in which the reaction has an arbitrary number of channels.

The work proceeds in two stages. First, the collision matrix must be divided so as to separate the background matrix from the strongly energy-dependent single-level contribution. This has been done by Lane and Thomas and, as we shall see, was in a sense already accomplished by Wigner and Eisenbud [1]);

a variation of the procedure which is more useful for our purpose is given in ref. [7]). For the sake of completeness as well as for the sake of greater generality the derivation is outlined in section 2 of this paper. In order to facilitate the analysis of experimental data, it is essential that the collision matrix be parametrized in terms of a minimum number of parameters consistent with maintaining the separation between the slowly varying ("potential") contribution and the strongly energy dependent resonance part. This is accomplished in section 3 and constitutes the main result of this paper. An explicit recipe is given for the construction of the collision matrix and illustrated for the cases $N = 2$ and $N = 3$. Section 4 is devoted to examining simplifications in the background matrix under various physically reasonable approximations, in descending order of stringency.

Inasmuch as our work is based on the results of Wigner and Eisenbud, we shall preserve their notation for the quantities introduced by them. An exception to this rule is that for the collision matrix we shall use the $\mathbf{S}$ matrix of Blatt and Biedenharn [8]) rather than the slightly different $\mathbf{u}$ matrix of Wigner and Eisenbud (or the $\mathbf{U}$ of Lane and Thomas). The reason for this is that Blatt and Biedenharn give explicit formulas for the cross sections in terms of the elements of the $\mathbf{S}$ matrix and that we consider these formulas particularly well suited for calculation and comparison with experiments. The relationship between $\mathbf{S}$ and $\mathbf{u}$ is given immediately below in section 2.

2. Separation of the Collision Matrix into a Background Matrix and a Single-Level Matrix

In the Blatt-Biedenharn formalism, cross sections are given as sums of terms involving the elements of collision matrices $\mathbf{S}^{J\Pi}$ (called scattering matrices by the authors). The element $S^{J\Pi}_{\alpha' s' l'}$ of the matrix $S^{J\Pi}$ stands for the probability amplitude for a reaction with total angular momentum J and parity Π going from channel $\alpha s l$ into $\alpha' s' l'$. The channel index α defines the type of incoming particle and the quantum state of the struck nucleus; the channel spin s is the total spin angular momentum in the channel; l is the incoming orbital angular momentum. The primed indices refer to the corresponding after-collision quantities. The total number of channels (called alternatives by Wigner and Eisenbud) and hence the dimensionality of the $\mathbf{S}^{J\Pi}$ matrix are given by the number of possible combinations $\alpha s l$. The cross section formulas contain an $\mathbf{S}$ matrix for each combination of J and Π which enters into the reaction. The matrix $\mathbf{S}^{J\Pi}$ is related to Wigner and Eisenbud's $\mathbf{u}^J$ by $S^{J\Pi}_{\alpha' s' l';\, \alpha s l} = i^{l+l'} u_{s' l';\, s l}$; their index s includes both our α and s.

According to Wigner and Eisenbud the $\mathbf{S}$ matrix may be related to the derivative matrix $\mathbf{R}$ by

$$\mathbf{S}^{J\Pi} = \boldsymbol{\omega} \frac{\mathbf{1} + i\mathbf{B}\mathbf{R}^{J\Pi}\mathbf{B} + i\mathbf{C}}{\mathbf{1} - i\mathbf{B}\mathbf{R}^{J\Pi}\mathbf{B} - i\mathbf{C}} \boldsymbol{\omega}. \tag{1}$$

In this expression ω, $\mathbf{B}$, and $\mathbf{C}$ are diagonal matrices; $\mathbf{B}$ and $\mathbf{C}$ are real, ω (whose element ω_{asl} equals i^l-times the Wigner-Eisenbud matrix element ω_{sl}) is of modulus 1, and all three can be readily calculated once the energy, channel radius, and non-nuclear interactions (centrifugal and Coulomb forces) are specified. For the physical significance of these quantities as well as their detailed specification, the reader is referred to the work of Wigner and Eisenbud or, if he is willing to undertake the required translation of notation, to the review of Lane and Thomas. In our work these matrices will be inextricably mixed up with empirical parameters and there is no need to know how to calculate them explicitly. Their general mathematical properties, which limit the number of parameters necessary for their specification, will, however, be of importance.

The real and symmetric matrix $\mathbf{R}$ is wholly determined by the wave function in the interior region (i.e. by the nuclear interactions) and by the boundary conditions which relate the wave function to its derivative on the surface of that region. The $\mathbf{R}$ matrix may be expressed in terms of a set of eigenvalues $E_\lambda{}^{J\Pi}$ of the nuclear system by

$$\mathbf{R}^{J\Pi} = \sum_\lambda \frac{\boldsymbol{\gamma}_\lambda{}^{J\Pi}\boldsymbol{\gamma}_\lambda{}^{J\Pi t}}{E_\lambda{}^{J\Pi} - E}. \tag{2}$$

The αsl components of the column matrix (vector) $\boldsymbol{\gamma}_\lambda{}^{J\Pi}$ are energy independent coefficients ("reduced widths" amplitudes) which depend on the size of the λ^{th} eigenfunction at the entrance to channel αsl. We denote by $\boldsymbol{\gamma}_\lambda{}^{J\Pi t}$ the row matrix which is the transpose of $\boldsymbol{\gamma}_\lambda{}^{J\Pi}$. Since we shall only be concerned with the $\mathbf{S}$ matrix for a given value of J and Π we shall drop these superscripts; the reader should, however, keep in mind for later reference which of the quantities in eq. (1) depend on J and Π and which do not.

The "true" one-level approximation consists of replacing the sum in eq. (2) by a single term:

$$\mathbf{R} = \frac{\boldsymbol{\gamma}\boldsymbol{\gamma}^t}{E_\lambda - E}. \tag{3}$$

This approximation leads to the Breit-Wigner formula and also to the various cross section formulas of Blatt and Biedenharn.

Instead of making this approximation we divide the infinite sum in expression (2) into a single level contribution and a background matrix $\mathbf{R}_b(E)$,

$$\mathbf{R} = \frac{\boldsymbol{\gamma}\boldsymbol{\gamma}^t}{E_\lambda - E} + \mathbf{R}_b(E). \tag{4}$$

While this choice and everything that follows in this and the following section are completely general and do not depend on any assumptions regarding $\mathbf{R}_b$,

our formulation will be most useful when R_b varies slowly with energy, at least over the width of the single resonance.

We must now substitute expression (4) for the R matrix into expression (1) for the S matrix and attempt to isolate from S the term with the explicit energy dependence $1/(E_\lambda - E)$. It turns out that this has essentially been done for us, by Wigner and Eisenbud. In an earlier, more intuitive formulation [6]), Wigner had arrived at a single level expression for R which included an additional energy independent matrix, R_∞. This term was retained by Wigner and Eisenbud when they made the single-level approximation to their rigorous expression [our formula (2)] and obtained the collision matrix, only to be discarded at the very end. Since the mathematics do not make use of the fact that R_∞ is independent of E, we may follow the same procedure as Wigner and Eisenbud, merely by replacing R_∞ by $\mathsf{R}_b(E)$. We need to write down only the result:

$$\mathsf{S} = \boldsymbol{\omega}\left[\frac{(\mathsf{1}+i\mathsf{C}')}{(\mathsf{1}-i\mathsf{C}')} + \frac{2i\mathbf{a}\mathbf{a}^{\mathrm{t}}}{E_\lambda+\Delta-E-\frac{1}{2}i\Gamma}\right]\boldsymbol{\omega}, \tag{5}$$

and to define the new quantities which appear in this result: C' is given by

$$\mathsf{C}' = \mathsf{B}\mathsf{R}_b\mathsf{B}+\mathsf{C}, \tag{6}$$

and thus is seen to be a symmetric and real matrix. The complex vectors $\mathbf{a}$ are defined by

$$\mathbf{a} = (\mathsf{1}-i\mathsf{C}')^{-1}\mathsf{B}\boldsymbol{\gamma}, \tag{7}$$

and the total width Γ is given by

$$\Gamma = 2(\mathbf{a}, \mathbf{a}) = \sum_{\alpha s l}\Gamma_{\alpha s l}, \tag{8}$$

where the partial widths $\Gamma_{\alpha s l}$ are defined by

$$\Gamma_{\alpha s l} = 2a^*_{\alpha s l}a_{\alpha s l}. \tag{9}$$

Finally, the level shift Δ is defined by

$$\Delta = (\mathbf{a}, \mathsf{C}'\mathbf{a}). \tag{10}$$

All the quantities we have defined are energy dependent, but only weakly so, if R_b is slowly varying function of E. As Lane and Thomas point out, Δ may be made zero at the centre of the resonance by a judicious choice of boundary conditions, and in most cases this result will then hold approximately over the width of the resonance. We note further that from (7) and the reality of B, $\boldsymbol{\gamma}$, and C it follows that

$$\mathbf{a} = (\mathsf{1}-i\mathsf{C}')^{-1}(\mathsf{1}+i\mathsf{C}')\mathbf{a}^*, \tag{11}$$

Except for slight changes in notation and for the different meaning of the C' matrix, expression (5) is identical to formula (56) of Wigner and Eisenbud.

It is desirable to replace the complex vectors a in (5) by real quantities which are directly related to the observed partial widths. This is done by introducing the square roots of the partial widths

$$g_{\alpha sl} = (2a^*_{\alpha sl}a_{\alpha sl})^{\frac{1}{2}} = \Gamma^{\frac{1}{2}}_{\alpha sl}. \tag{12}$$

After some factoring, formula (5) for the S matrix may then be written

$$\mathsf{S} = \exp i\mathbf{\Omega}\left(\mathsf{T} + \frac{i\mathbf{g}\mathbf{g}^{\dagger}}{E_\lambda + \Delta - E - \frac{1}{2}i\Gamma}\right)\exp i\mathbf{\Omega}. \tag{13}$$

In this expression $\exp i\mathbf{\Omega}$ is a diagonal matrix, whose components $\exp i\Omega_{\alpha sl}$ are given by

$$\exp i\Omega_{\alpha sl} = a^{\frac{1}{2}}_{\alpha sl}a^{*-\frac{1}{2}}_{\alpha sl}\omega_{\alpha sl}, \tag{14}$$

noting that $a^{\frac{1}{2}}_{\alpha sl}a^{-\frac{1}{2}}_{\alpha sl}$ as well as $\omega_{\alpha sl}$ is complex and of absolute value 1. The matrix T is defined by

$$T_{\alpha' s' l';\,\alpha sl} = a^{*\frac{1}{2}}_{\alpha' s' l'}a^{-\frac{1}{2}}_{\alpha' s' l'}[(1-iC')^{-1}(1+iC')]_{\alpha' s' l';\,\alpha sl}a^{*\frac{1}{2}}_{\alpha sl}a^{-\frac{1}{2}}_{\alpha sl}, \tag{15}$$

and $\mathbf{g}$ is a column matrix whose components are the $g_{\alpha sl}$, defined in eq. (12). The matrices $\exp i\mathbf{\Omega}$ and T will vary slowly with energy as long as the background matrix R_b does.

3. Parametrization of the T Matrix

It is clear that the more parameters are in the collision matrix, the more complicated will be the cross section formulas and the more ambiguous and uninformative will be the matching of the parameters to the experimental data. We must therefore minimize the number of parameters in S. If this were all that was required, it would be a trivial task. For we know [9]) that the S matrix must be symmetric and unitary, which means that for N dimensions it may be formally represented by $\frac{1}{2}N(N+1)$ independent parameters instead of the $2N^2$ required for a general complex matrix †. The parametrization of the S matrix in terms of these parameters would, however, be a self-defeating step, for it would completely mix up the slowly varying parameters with the strongly energy-dependent term, thus preventing us from exploiting the existence of the resonance in our analysis. What we must do is to reduce the number of parameters

† The task of expressing these $\frac{1}{2}N(N+1)$ "eigenphase shift" parameters explicitly in terms of the, in general, more numerous resonance parameters is, however, not trivial. A procedure for doing so, for the non-potential part of the S matrix, in the case of an n-level, N-channel reaction ($n < N$) has been given by Biedenharn and Willard [10]). The results for the two-level situation are already so complicated as to require special assumptions in order to be applicable in practice. The usefulness of the eigenphase shift representation of the S matrix lies in the fact that certain cross-section formulas take on a relatively simple form. The forte of the Biedenharn-Willard procedure would seem to be the possibility of rapid calculation of cross sections when the resonance parameters are known, rather than the determination of resonance parameters from experimental data.

in the S matrix without destroying the separation between background and resonance terms, even at the risk of not achieving the minimum parametrization permitted by the general properties of S. This task requires that we work on the T matrix.

Before turning to the general case we note immediately that for a single-channel reaction (i.e. elastic scattering without change of channel spin or orbital angular momentum) eq. (11) loses its matrix character, whence its substitution into (15) shows that $\mathsf{T} = 1$. In this case T involves no additional parameters at all and the single element of the S matrix is given by

$$S = \exp 2i\Omega \left(1 + \frac{i\Gamma}{E_\lambda + \Delta - E - \frac{1}{2}i\Gamma}\right). \tag{16}$$

This expression looks similar to the single channel case for the "true" single-level approximation (as given, say, by Blatt and Biedenharn). We should note, however, that in the latter case the potential phase shift which appears in the exponential is the calculable hard sphere phase shift which depends on l but not on J. In our case Ω is an empirical parameter which contains not only the hard sphere shift but also R_b; it is J-dependent and may thus be considered a potential phase shift in the presence of spin-orbit coupling.

The first step in parametrizing T for the general case of N dimensions is to note that T is itself symmetric and unitary. This is evident from eq. (15), and the fact that C′ is real and symmetric and that the diagonal matrix, whose components are $a_{\alpha\beta}^{*\frac{1}{2}} a_{\alpha\beta}^{-\frac{1}{2}}$, is unitary. Therefore T has $\frac{1}{2}N(N+1)$ parameters, to which must be added the $2N+1$ other parameters which appear in S (N Ω's, N g's, and E_λ, assuming that Δ can be neglected). We now proceed to reduce the number of parameters in T.

We introduce the angle

$$\beta = \arctan \frac{\frac{1}{2}\Gamma}{E - E_\lambda - \Delta} \tag{17}$$

and rewrite (13)

$$\mathsf{S} = \exp i\mathbf{\Omega} \left(\mathsf{T} - \frac{i \sin\beta \exp(-i\beta)\mathbf{g}\mathbf{g}^{\mathrm{t}}}{\frac{1}{2}\Gamma}\right) \exp i\mathbf{\Omega}. \tag{18}$$

We now take the product

$$[\exp(-i\mathbf{\Omega})\mathsf{S}\exp(-i\mathbf{\Omega})][\exp(-i\mathbf{\Omega})\mathsf{S}\exp(-i\mathbf{\Omega})]^\dagger \tag{19}$$

where † denotes the adjoint. This gives

$$\mathsf{S}\mathsf{S}^\dagger = \mathsf{1}$$

$$= \mathsf{1} + \frac{\sin^2\beta\ \mathbf{g}\mathbf{g}^{\mathrm{t}}\mathbf{g}\mathbf{g}^{\mathrm{t}}}{(\frac{1}{2}\Gamma)^2} + \frac{i\sin\beta\exp(i\beta)\mathsf{T}\mathbf{g}\mathbf{g}^{\mathrm{t}}}{\frac{1}{2}\Gamma} - \frac{i\sin\beta\exp(-i\beta)\mathbf{g}\mathbf{g}^{\mathrm{t}}\mathsf{T}^{\mathrm{t}}}{\frac{1}{2}\Gamma}. \tag{20}$$

Using the fact that $\mathsf{g}(\mathsf{g}^\dagger\mathsf{g})\mathsf{g}^\dagger = \mathsf{g}\mathsf{g}^\dagger(\mathsf{g},\mathsf{g}) = \Gamma\mathsf{g}\mathsf{g}^\dagger$ and introducing the complex but symmetric matrix $\mathsf{V} = (\exp i\beta)\mathsf{T}$, eq. (20) becomes

$$0 = -2i\sin\beta\ \mathsf{g}\mathsf{g}^\dagger + \mathsf{V}\mathsf{g}\mathsf{g}^\dagger - \mathsf{g}\mathsf{g}^\dagger\mathsf{V}^*. \tag{21}$$

With $\mathsf{V}_\mathscr{R}$ and $\mathsf{V}_\mathscr{I}$ standing for the real and imaginary parts of V, respectively, this yields the two equations

$$\mathsf{V}_\mathscr{R}\mathsf{g}\mathsf{g}^\dagger - \mathsf{g}\mathsf{g}^\dagger\mathsf{V}_\mathscr{R} = 0, \tag{22}$$

and

$$\mathsf{V}_\mathscr{I}\mathsf{g}\mathsf{g}^\dagger + \mathsf{g}\mathsf{g}^\dagger\mathsf{V}_\mathscr{I} - 2\sin\beta\ \mathsf{g}\mathsf{g}^\dagger = 0. \tag{23}$$

The first of these equations states that $\mathsf{V}_\mathscr{R}$ commutes with $\mathsf{g}\mathsf{g}^\dagger$. This implies that $\mathsf{V}_\mathscr{R}$ and $\mathsf{g}\mathsf{g}^\dagger$ must be simultaneously diagonalizable. By virtue of its symmetry and unitarity, the diagonal form of T and hence of $\mathsf{V}_\mathscr{R}$, in terms of its independent parameters, is well known. It is $\mathsf{T} = \mathsf{U}^{-1}\exp 2i\boldsymbol{\delta}\,\mathsf{U}$, with N real eigenvalues δ, and U being an orthogonal matrix of $\frac{1}{2}N(N-1)$ real parameters, corresponding to a rotation in N-dimensional space. The matrix $\mathsf{V}_\mathscr{R}$ may then be written $\mathsf{V}_\mathscr{R} = \mathsf{U}^{-1}\cos(2\boldsymbol{\delta}+\beta)\mathsf{U}$.

By bringing $\mathsf{g}\mathsf{g}^\dagger$ to diagonal form and examining its eigenvectors we will be able to impose restrictions on the parameters of U. Since $\mathsf{g}\mathsf{g}^\dagger$ is a matrix of rank 1 it is easily diagonalized. Calling the eigenvalues μ and using a single subscript i or j to stand for the triples αsl, $\alpha' s' l'$, we write

$$\sum_{j=1}^{N} g_i g_j u_j = \mu u_i, \tag{24}$$

and letting the scalar product $\sum_j g_j u_j = f$, we have

$$u_i = \frac{f g_i}{\mu}. \tag{25}$$

Substituting this into (24), we obtain

$$\mu = \sum_j g_j g_j = \Gamma. \tag{26}$$

This gives one of the eigenvalues, say μ_N. The corresponding eigenvector is

$$\mathsf{u}_N = \frac{f}{\Gamma}\mathsf{g}. \tag{27}$$

The other eigenvalues μ_k, $(k = 1, 2, \ldots N-1)$, are zero. From (24) the corresponding eigenvectors must then obey the restriction

$$\mathsf{g}^\dagger\mathsf{u}_k = 0, \quad k = 1, 2, \ldots N-1. \tag{28}$$

With f arbitrary, eqs. (27) and (28) together give $2(N-1)$ restrictions on the number of independent parameters in U. It would be a mistake, however, to

attempt to subtract the number $2(N-1)$ from $\frac{1}{2}N(N-1)$ to arrive at the number of independent parameters in U. To see what the true situation is we start from a real, but otherwise unrestricted U matrix of N^2 parameters. We now impose the $\frac{1}{2}N(N+1)$ orthogonality relations

$$\sum_{j=1}^{N} u_{kj}u_{ij} = \delta_{ki}, \quad i, k = 1, 2, \ldots N. \tag{29}$$

Of these, the relation $\sum_j u_{Nj}u_{Nj} = 1$, together with (27), serves to fix the value of f and of u_{Nj}:

$$f = \sqrt{\Gamma}, \tag{30}$$

and

$$u_{Nj} = \frac{g_j}{\sqrt{\Gamma}}, \quad j = 1, 2, \ldots N. \tag{31}$$

Keeping a count, we have used up one orthogonality relation and gained the N relations (31), i.e. we are left with $\frac{1}{2}N(N+1)-1+N$ restrictions on U. The $N-1$ orthogonality relations $\sum_{j=1}^{N} u_{kj}u_{Nj} = 0$, $(k = 1, 2, \ldots N-1)$, upon substitution of (27) yield only the relations (28). Thus no new restrictions are added by the latter. The matrix U is left with $\frac{1}{2}N^2-\frac{3}{2}N+1$ independent parameters.

With U properly particularized we are now assured that the imaginary part $\mathsf{V}_\mathscr{I} = \mathsf{U}^{-1} \sin(2\delta+\beta)\mathsf{U}$ also commutes with gg^t. We have $\mathsf{V}_\mathscr{I}\mathsf{gg}^t+\mathsf{gg}^t\mathsf{V}_\mathscr{I} = 2\mathsf{V}_\mathscr{I}\mathsf{gg}^t$, and eq. (23) becomes

$$\{\mathsf{U}^{-1}[\sin(2\delta+\beta)-\sin\beta]\mathsf{U}\}\mathsf{gg}^t = 0. \tag{32}$$

If the product of two square matrices, neither of which is null, is to be zero, it is necessary that both matrices be singular and that the sum of the ranks of the two matrices do not exceed their dimension. Applying this theorem to eq. (32), the matrix $\mathsf{U}^{-1}[\sin(2\delta+\beta)-\sin\beta]\mathsf{U}$ must be singular and, since gg^t is of rank 1, at most of rank $N-1$. Since U can obviously not be singular, the diagonal matrix $\sin(2\delta+\beta)-\sin\beta$ must be, and if its rank is not to be more than $N-1$, at least one of its elements, say $\sin(2\delta_N+\beta)-\sin\beta$ must be zero. This means that $\delta_N = 0$. [We may exclude the other solution $\delta_N = \frac{1}{2}\pi-\beta$ on the ground that we wish the T matrix to be independent of β. By working with the otherwise undesirable representation of S in terms of complex resonance parameters (eq. (5)] it may, however, be shown, without any assumptions regarding the energy dependence of the background matrix, that this second solution is truly spurious]. Thus, at most $N-1$ parameters survive in the diagonal part of $\mathsf{V}_\mathscr{I}$ and hence in the diagonal part of T; the N^{th} element of the latter is 1.

The theorem of the preceding paragraph states a necessary but not a sufficient condition for satisfying eq. (32). To see what else is required we rewrite (32) with $\mathsf{U}^{-1}[\sin(2\delta+\beta)-\sin\beta]\,\mathsf{U}$ in spectral form, and with the knowledge

that $\delta_N = 0$:

$$\sum_{k=1}^{N-1} [\sin(2\delta_k+\beta)-\sin\beta]\mathsf{u}_k\,\mathsf{u}_k{}^t\mathsf{g}\mathsf{g}^t = 0. \tag{33}$$

The least restrictive way of satisfying this equation is to require that $\mathsf{u}_k{}^t\mathsf{g} = 0$, $(k = 1, 2, \ldots N-1)$. This requirement is, however, exactly the same as eq. (28). Thus no new restrictions are added †.

We see therefore that the matrix T has $\frac{1}{2}N(N-1)$ independent parameters, $\frac{1}{2}N^2-\frac{3}{2}N+1$ from U and $N-1$ from $\exp 2i\boldsymbol{\delta}$, instead of the $\frac{1}{2}N(N+1)$ to which, as a symmetric and unitary matrix it would ordinarily be entitled. If we add to these the N Ω's, the N g's and E_λ, we see that we have only $N+1$ more than if we had refused to take cognizance and advantage of the presence of the resonance.

We now illustrate, explicitly, the procedure for the parametrization of the collision matrix for a two-channel reaction. The most general two-by-two unitary and symmetric matrix may be written

$$\mathsf{T} = \mathsf{U}^{-1}\exp 2i\boldsymbol{\delta}\,\mathsf{U} = \begin{pmatrix}\cos\varepsilon & -\sin\varepsilon\\ \sin\varepsilon & \cos\varepsilon\end{pmatrix}\begin{pmatrix}\exp 2i\delta_1 & 0\\ 0 & \exp 2i\delta_2\end{pmatrix}\begin{pmatrix}\cos\varepsilon & \sin\varepsilon\\ -\sin\varepsilon & \cos\varepsilon\end{pmatrix}. \tag{34}$$

The elements of U may be read off directly from (31): $\sin\varepsilon = -g_1/\sqrt{\Gamma}$, $\cos\varepsilon = g_2/\sqrt{\Gamma}$. The matrix T will contain only one free parameter δ. Hence T is given by

$$\mathsf{T} = \frac{1}{\sqrt{\Gamma}}\begin{pmatrix}g_2 & g_1\\ -g_1 & g_2\end{pmatrix}\begin{pmatrix}\exp 2i\delta & 0\\ 0 & 1\end{pmatrix}\begin{pmatrix}g_2 & -g_1\\ g_1 & g_2\end{pmatrix}\frac{1}{\sqrt{\Gamma}} = \exp 2i\delta\left(1-\frac{\mathsf{g}\mathsf{g}^t}{\Gamma}\right)+\frac{\mathsf{g}\mathsf{g}^t}{\Gamma}. \tag{35}$$

From (18) the complete S matrix may then be written

$$\mathsf{S} = \exp i\boldsymbol{\Omega}\left[\exp 2i\delta\left(1-\frac{\mathsf{g}\mathsf{g}^t}{\Gamma}\right)+\exp(-2i\beta)\frac{\mathsf{g}\mathsf{g}^t}{\Gamma}\right]\exp i\boldsymbol{\Omega}. \tag{36}$$

A similar procedure should be followed to obtain the T matrix for $N > 2$. One should always begin by writing down U in its explicitly orthogonal representation. For $N = 3$ this may be done in terms of the Euler angles; for larger values of N, the Cayley transform supplies a convenient representation (unless one or more of the eigenvalues of U are equal to $+1$). Eq. (31) will always provide $N-1$ additional independent constraints to reduce the number of parameters in U to $\frac{1}{2}N^2-\frac{3}{2}N+1$.

For $N = 3$, the U matrix is, in terms of the Euler angles as defined by Goldstein [11],

† It is easy to show that if $\delta_k = 0$, the corresponding vector u_k does not appear in S. It might therefore appear that we could have eliminated additional parameters by not choosing the same row $k = N$ for the assignment $\delta_k = 0$ and for the specification of u_k [eq. (31)]. However, if we had not made this "redundant" choice, the vector u_k would have been included in the sum (33), and the condition $\mathsf{u}_k{}^t\mathsf{g} = 0$ would have contradicted (31).

$$\begin{pmatrix} \cos\psi\cos\phi-\cos\theta\sin\phi\sin\psi & \cos\psi\sin\phi+\cos\theta\cos\phi\sin\psi & \sin\psi\sin\theta \\ -\sin\psi\cos\phi-\cos\theta\sin\phi\cos\psi & -\sin\psi\sin\phi+\cos\theta\cos\phi\cos\psi & \cos\psi\sin\theta \\ \sin\theta\sin\phi & -\sin\theta\cos\phi & \cos\theta \end{pmatrix}. \tag{37}$$

Eq. (31) tells us immediately that $\cos\theta = g_3/\sqrt{\Gamma}$, and that $\cos\varphi = -g_2/(g_1^2+g_2^2)^{\frac{1}{2}}$.

4. Approximations

We wish to stress again that all expressions given so far are exact. They are practically useful if R_b is a slowly varying function of energy and if N is not excessively large. Further simplifications occur if further assumptions can be made regarding the nature of the R_b matrix. We shall discuss three types of approximation.

4.1. FIRST APPROXIMATION: $\mathsf{R}_b = 0$

This is the most drastic approximation and corresponds to a "true" single-level situation, which leads to the Breit-Wigner formula and to Blatt and Biedenharn's expression for the S matrix [their formula (5.6)]. The latter may easily be obtained from our formula (13) by noting that because of the diagonality of $\mathsf{C}' = \mathsf{C}$, (11) states that $\mathsf{T} = \mathsf{1}$. By combining (14) with (11), we note that the phase shifts $\boldsymbol{\Omega}$ now depends only on $\boldsymbol{\omega}$ and C and are independent of the total angular momentum J. Furthermore, if it is assumed that the channel radius is independent of the channel spin s (although it may vary for different channels α) the definitions of $\boldsymbol{\omega}$ and of C show [1]) that the $\boldsymbol{\Omega}$ are the known, spin independent "hard sphere" phase shifts, including appropriate Coulomb factors for charged particle reactions. Leaving the channel radius out of the count, there are now only $N+1$ parameters needed to specify an N-channel reaction.

4.2. SECOND APPROXIMATION: R_b IS DIAGONAL

The next approximation which should be tried if the "true" single level approximation fails is to assume that R_b is diagonal. This assumption is physically reasonable because the contributions of the individual distant levels to the nondiagonal elements of R_b can be either positive or negative, and thus tend to cancel, whereas the diagonal components are all proportional to the positive widths; cf. eq. (2). It leads to mathematically simple results because once again C' is diagonal and $\mathsf{T} = \mathsf{1}$. The potential phase shifts $\boldsymbol{\Omega}$, however, now include unknown, J dependent contributions from R_b, and must be considered empirical parameters. There are now altogether $2N+1$ parameters for each matrix S^{JII}.

4.3. THIRD APPROXIMATION: THE OFF-DIAGONAL ELEMENTS OF R_b ARE SMALL COMPARED TO THE DIAGONAL ELEMENTS

For the reason stated above, this is the next natural approximation to make, if the assumption of approximation 2 must be relaxed. We should like to be able to write the T matrix as $\mathsf{T} = \mathsf{1}+\mathsf{X}$, where X is small. We can show that the smallness of the non-diagonal elements of R_b compared to the diagonal elements is indeed a necessary condition for the validity of this approximation, but the complete quantitative criteria are complicated and will not be discussed here. If T may be written in this way, the unitarity of T and the assumption that $\mathsf{X}\mathsf{X}^\dagger \approx 0$ show that X is pure imaginary. It may then easily be shown that in the parametrization of T, the U matrix remains unchanged from before, while the diagonal matrix $\exp 2i\boldsymbol{\delta}$ goes over into $\mathsf{1}+2i \sin \boldsymbol{\delta}$, with δ_N of course again being equal to zero. Our approximation allows us to put $\sin^2 \boldsymbol{\delta} \approx 0$, and this will lead to simplifications in the cross section formulas which involve squares of the S matrix †.

I should like to thank Dr. H. S. Wilf and Dr. D. G. Ravenhall for interesting discussions.

† Another approximation, which amounts to requiring that *all* the elements of R_b be small, is made in the appendix of the "optical model" paper of Feshbach, Porter and Weisskopf [5]). The authors introduce their approximation directly into the Wigner-Eisenbud formalism for $l = 0$ and obtain certain "gross structure" cross-section formulas for the low-energy case.

Editor's note: Another method leading to the separation of a background matrix is outlined in my lectures at the Summer Meeting of Physicists at Hercegnovi (Yugoslavia) (1959). The text of these lectures is also available as a NORDITA publication (on request from the NORDITA office).

References

1) E. P. Wigner and L. Eisenbud, Phys. Rev. **72** (1947) 29
2) G. Breit and E. P. Wigner, Phys. Rev. **49** (1936) 519; and 642
3) A. M. Lane and R. G. Thomas, Revs. Mod. Phys. **30** (1958) 257
4) Feshbach, Peaslee and Weisskopf, Phys. Rev. **71** (1947) 145
5) Feshbach, Porter and Weisskopf, Phys. Rev. **90** (1953) 166; **96** (1954) 448
6) E. P. Wigner, Phys. Rev. **70** (1946) 606
7) H. Lustig, Phys. Rev. **114** (1960) 1317
8) J. M. Blatt and L. C. Biedenharn, Revs. Mod. Phys. **24** (1952) 258
9) See, e.g., J. M. Blatt and V. F. Weisskopf, Theoretical Nuclear Physics (John Wiley and Sons, New York, 1952) Ch. X
10) L. C. Biedenharn and H. B. Willard, Proc. Phys. Soc. **12** (1958) 874
11) H. Goldstein, Classical Mechanics (Addison-Wesley Pub. Co., Reading, Mass., 1950) p. 107

7.B

Nuclear Physics **17** (1960) 329—338; © *North-Holland Publishing Co., Amsterdam*

Not to be reproduced by photoprint or microfilm without written permission from the publisher

POLARISATION NUCLÉAIRE DANS L'ATOME MÉSIQUE DE DEUTÉRIUM

M. DEMEUR et Ch. JOACHAIN †

Université Libre de Bruxelles

Reçu le 13 janvier 1960

Abstract: The energy-shift due to polarisation of the deuteron by a bound mu-meson has been evaluated. This effect compensates nearly the energy-shift caused by the finite extension of the nucleus. Finite extension of the nucleons and D-state of the deuteron have been neglected.

1. Introduction

Foldy et Eriksen ont examiné les possibilités de mise en évidence de la polarisation du vide par des expériences où ce phénomène est indépendant de la présence d'électrons [1]). L'étude de l'effet Lamb dans les atomes mésiques mu très légers semble convenir à ce but, la masse du méson réduisant considérablement la contribution de la correction radiative qui constitue la majeure partie de l'effet Lamb électronique. Pour $Z < 6$ la polarisation du vide l'emporte en valeur absolue sur l'effet de volume; au-delà du carbone l'effet de volume croît rapidement et masque le phénomène recherché. Foldy et Eriksen examinent brièvement d'autres corrections présentes et concluent qu'elles peuvent être raisonnablement négligées. Parmi celles-ci une seule semble demander une évaluation détaillée: il s'agit de la polarisation du noyau par le méson μ^-.

Dans le cas des noyaux lourds cet effet a été calculé par Cooper et Henley [2]), et par Lakin et Kohn [3]). Dans le cas des noyaux légers, Foldy et Eriksen estiment que le déplacement dû à la polarisation nucléaire est relativement petit devant l'effet de volume.

Le deutéron nous a semblé être le noyau léger dont la polarisation est à la fois la plus aisée et la plus intéressante à étudier. C'est d'abord comme correction à la diffusion de Rutherford que la polarisation du deutéron a retenu l'attention [4–9]). Elle est ensuite apparue comme correction à la diffusion élastique des électrons de grande énergie par les deutérons [10–12]). Récemment Krall et Salpeter [13]) ont étudié les effets dispersifs induits dans le deutéron, l'hélium et le carbone par des électrons de grande énergie et par des électrons liés.

2. Extension finie du deutéron

Le proton, le neutron et le méson étant repérés par $\mathbf{r}_p$, $\mathbf{r}_n$ et $\mathbf{r}_m$, nous utilisons les vecteurs $\mathbf{R} = \mathbf{r}_p - \mathbf{r}_n$ et $\mathbf{r} = \mathbf{r}_m - \frac{1}{2}(\mathbf{r}_p + \mathbf{r}_n)$. L'hamiltonien débarrassé du

† Stagiaire de Recherches du Fonds National de la Recherche Scientifique.

mouvement du centre de masse s'écrit

$$H = -\frac{\hbar^2}{2\mu}\Delta_r - \frac{\hbar^2}{M}\Delta_R - \frac{e^2}{|\mathbf{r}-\frac{1}{2}\mathbf{R}|} + V(\mathbf{R})$$

où μ est la masse réduite du méson par rapport à celle du deutéron, M la masse du proton, prise égale à celle du neutron, et $V(\mathbf{R})$ l'énergie potentielle du deutéron. Nous récrivons l'hamiltonien sous la forme

$$H = H_0 + H_1, \quad H_0 = H_r + H_R,$$

$$H_r = -\frac{\hbar^2}{2\mu}\Delta_r - \frac{e^2}{r}, \quad H_R = -\frac{\hbar^2}{M}\Delta_R + V(\mathbf{R}),$$

$$H_1 = \frac{e^2}{r} - \frac{e^2}{|\mathbf{r}-\frac{1}{2}\mathbf{R}|},$$

où H_0 et H_1 conduiront à un calcul de perturbation, H_0 étant séparable en $H_r(\mathbf{r})$ et $H_R(\mathbf{R})$.

Les fonctions d'onde d'ordre zéro étant définies par

$$\Psi^{(0)}_{\mathrm{mN}} = \psi_{\mathrm{m}}(\mathbf{r})\varphi_{\mathrm{N}}(\mathbf{R}),$$

$$H_0\Psi^{(0)}_{\mathrm{mN}} = E^{(0)}_{\mathrm{mN}}\Psi^{(0)}_{\mathrm{mN}} = (\varepsilon_{\mathrm{m}} + E_{\mathrm{N}})\Psi^{(0)}_{\mathrm{mN}},$$

l'effet d'extension finie du deutéron est donné, au premier ordre, par

$$E^{(1)}_{\mathrm{mN}} = \langle \mathrm{mN}|H_1|\mathrm{mN}\rangle.$$

Pratiquement, nous sommes intéressés par l'état fondamental du deutéron que nous décrivons ici par la fonction d'onde de Hulthén:

$$\varphi_0(\mathbf{R}) = \left(\frac{\alpha\beta(\alpha+\beta)}{2\pi(\alpha-\beta)^2}\right)^{\frac{1}{2}} \frac{\mathrm{e}^{-\alpha R} - \mathrm{e}^{-\beta R}}{R},$$

en négligeant la composante D. On a

$$E^{(1)}_{\mathrm{m0}} = \langle \mathrm{m}|\bar{V}(r)|\mathrm{m}\rangle,$$

où

$$\bar{V}(r) = -e^2\frac{4\alpha\beta(\alpha+\beta)}{(\alpha-\beta)^2}\int_1^\infty \left(\frac{1}{u} - 1\right)(\mathrm{e}^{-2\alpha r u} - \mathrm{e}^{-2\beta r u})^2\,\mathrm{d}u$$

est un potentiel moyen qui est central parce que nous n'avons retenu que la composante S du deutéron. Ce potentiel moyen n'agissant que dans la région occupée par les nucléons, une approximation excellente est fournie par

$$E^{(1)}_{\mathrm{m0}} = 4\pi|\psi_{\mathrm{m}}(0)|^2\int_0^\infty r^2\bar{V}(r)\,\mathrm{d}r,$$

dont la validité se limite aux états électroniques s. Nous obtenons ainsi

$$E^{(1)}_{\mathrm{ns},0} = \frac{1}{n^3}\,\frac{e^2\beta(\alpha+\beta)}{12\,a^3\alpha^2(\alpha-\beta)^2}, \tag{1}$$

où

$$a = \hbar^2/\mu e^2,$$

$$\alpha = 2.31\times 10^{12}\,\mathrm{cm}^{-1}, \quad \beta = 7\alpha.$$

Pour l'état hydrogénoïde 1s nous avons

$$\Delta E/h = 4.3\times 10^7\ \mathrm{MHz} \text{ pour un méson } \mu^-,$$

$$\Delta E/h = 5.7\ \mathrm{MHz} \text{ pour un électron.}$$

La formule (1) fournit pour un électron dans l'état 2s

$$\Delta E/h = 0.7\ \mathrm{MHz}$$

en bon accord avec l'évaluation de Salpeter [14])

$$\Delta E/h = (0.733\pm 0.025)\ \mathrm{MHz}.$$

3. Polarisation du deutéron

3.1. CORRECTION DU SECOND ORDRE

La correction du second ordre à l'état fondamental est donnée par

$$E^{(2)}_{1s,0} = \sum_{\substack{N,m\\ \neq 1s,0}} \frac{|\langle 1s,0|H_1|m,N\rangle|^2}{E^{(0)}_{1s,0} - E^{(0)}_{m,N}}$$

et est donc négative. Sa contribution est opposée à celle de l'effet d'extension finie.

Le déplacement d'énergie $E^{(2)}_{1s,0}$ se décompose en deux termes:

a) la correction statique, obtenue en maintenant le deutéron dans son état fondamental:

$$(E^{(2)}_{1s,0})_{\mathrm{statique}} = \sum_{m\neq 1s} \frac{|\langle 1s,0|H_1|m,0\rangle|^2}{\varepsilon_{1s} - \varepsilon_m},$$

b) la correction dispersive obtenue en sommant sur les états continus du deutéron

$$(E^{(2)}_{1s,0})_{\mathrm{dispersive}} = \sum_{m,N\neq 0} \frac{|\langle 1s,0|H_1|m,N\rangle|^2}{E^{(0)}_{1s,0} - E^{(0)}_{m,N}}. \tag{2}$$

A proprement parler la polarisation du deutéron est constituée par la correction dispersive.

3.2. CORRECTION STATIQUE

On a

$$(E^{(2)}_{1s,0})_{\text{statique}} = \sum_{m \neq 1s} \frac{|\langle 1s|\bar{V}|m\rangle|^2}{\varepsilon_{1s}-\varepsilon_m}.$$

Du fait que l'état fondamental du système a été supposé à symétrie sphérique les états intermédiaires m sont des états s.

Il est utile de considérer séparément la correction statique due aux états liés et celle due aux états continus du méson. La première se présente comme une série de puissances de $(a\alpha)^{-1}$, expression dont l'ordre de grandeur est obtenu en prenant le rapport des dimensions nucléaires aux dimensions atomiques (mésiques). Le premier terme de cette série constitue une bonne approximation et est donné par

$$(E^{(2)}_{1s,0})_{\text{statique, méson lié}} = \sum_{n \neq 1} \frac{|\langle 1s|\bar{V}|ns\rangle|^2}{\varepsilon_{1s}-\varepsilon_{ns}} = -\frac{e^2\beta^2(\alpha+\beta)^2}{288\, a^5\alpha^4(\alpha-\beta)^4}$$

$$= \begin{cases} -7.1\times 10^2 \text{ MHz pour le méson } \mu^- \\ -2.4\times 10^{-9} \text{ MHz pour l'électron.} \end{cases}$$

Cette correction est petite car le recouvrement des fonctions d'onde du deutéron et du méson est particulièrement faible.

La correction statique due aux états continus du méson est sensiblement plus grande car l'intégration sur les longueurs d'onde contient des termes qui recouvrent bien la fonction d'onde du deutéron. Une intégration graphique conduit aux résultats suivants:

$$(E^{(2)}_{1s,0}) \text{ statique méson continu} = \begin{cases} -1.8\times 10^5 \text{ MHz pour le méson } \mu^- \\ -1.3\times 10^{-2} \text{ MHz pour l'électron.} \end{cases}$$

3.3. CORRECTION DISPERSIVE

La correction dispersive (2) est utilement décomposée en trois contributions:

$$A = \sum_{N \neq 0} \frac{|\langle 1s, 0|H_1|1s, N\rangle|^2}{E_0-E_N},$$

$$B = \sum_{N \neq 0} \sum_{\substack{m \text{ liés} \\ \neq 1s}} \frac{|\langle 1s, 0|H_1|m, N\rangle|^2}{(\varepsilon_{1s}-\varepsilon_m)+(E_0-E_N)},$$

$$C = \sum_{N \neq 0} \sum_{m \text{ continus}} \frac{|\langle 1s, 0|H_1|m, N\rangle|^2}{(\varepsilon_{1s}-\varepsilon_m)+(E_0-E_N)}.$$

Ces trois expressions seront évaluées en supposant que les états excités du deutéron peuvent être représentés par des ondes planes.

On a d'abord

$$A = \sum_{N \neq 0} \frac{|\langle 0|\bar{\bar{V}}|N\rangle|^2}{E_0 - E_N}$$

avec

$$\bar{\bar{V}}(R) = \frac{2e^2}{a}\left[e^{-R/a}\left(\tfrac{1}{2} + \frac{a}{R}\right) + \left(\tfrac{1}{2} - \frac{a}{R}\right)\right].$$

Etant donné l'ordre de grandeur de a par rapport aux dimensions nucléaires, le potentiel moyen $\bar{\bar{V}}$ ne peut conduire qu'à une contribution petite. Les longueurs d'onde des ondes planes $|N\rangle$ qui contribuent à A correspondent à des nucléons non relativistes. Dans ces conditions, A peut être évalué aisément au moyen de la fonction de Green d'une particule libre et l'on obtient

$$A = -\frac{10\, Me^4\beta(\alpha+\beta)}{9\hbar^2 a^6 \alpha^6(\alpha-\beta)^2},$$

d'où

$$A/h = \begin{cases} -1.8\times 10^2 & \text{MHz pour le méson } \mu^- \\ -3.2\times 10^{-12} & \text{MHz pour l'électron,} \end{cases}$$

ce qui est négligeable devant la correction statique.

Le terme B peut être simplifié en utilisant le fait que $(\alpha a)^{-1}$ est petit devant l'unité. Il se présente alors sous la forme d'une série dont il est aisé de trouver une majorante:

$$B < \sum_{N \neq 0} \sum_{n=2}^{\infty} \frac{1}{n^3} \frac{|\langle 0|\bar{\bar{V}}|N\rangle|^2}{E_0 - E_N},$$

qui fournit $B < A$ puisque la sommation sur n vaut 0.202.

Le terme C fournira la contribution la plus importante par le fait qu'il somme tous les recouvrements possibles de l'onde plane décrivant le méson et de celle décrivant les nucléons. Notre attention a été attirée sur ce point à la lecture du preprint [13]) que E. E. Salpeter nous avait aimablement envoyé. Notre traitement dans l'espace de configuration conduit rapidement à l'expression obtenue par Krall et Salpeter dans l'espace des moments:

$$C = -8e^4|\psi_{1s}(0)|^2 \int_0^\infty \frac{dk}{k}\left(\frac{1}{k}\sum_{N\neq 0}\frac{|\langle 0|e^{i\mathbf{k}\cdot\frac{1}{2}\mathbf{R}}|N\rangle|^2}{\varepsilon(k) - \varepsilon_{1s} + E_N - E_0}\right).$$

L'étude de $g(k)$ a été faite par Krall et Salpeter dans le cas de l'électron. Nous l'avons reprise dans le cas du méson μ^-. Nous retrouvons d'abord que la contribution la plus importante de g se fait dans le domaine $(E_0/\hbar c,\ R_0^{-1})$ où E_0 est l'énergie de liaison du deutéron et où R_0 provient de la relation

$$R_0^2 = \langle 0|(\tfrac{1}{2}R)^2|0\rangle.$$

Ce résultat était prévisible puisque ce domaine est défini indépendamment de la masse de la particule négative. Par contre cet intervalle recouvre la région des énergies semi-relativistes du méson alors que dans le cas de l'électron [13]), les énergies de ce domaine sont „extrême-relativistes". Alors que Krall et Salpeter évaluent C à l'aide de $\varepsilon(k) = \hbar ck$, il faut utiliser ici $\varepsilon(k) = c(\mu^2c^2+\hbar^2k^2)^{\frac{1}{2}}-\mu c^2$. On a alors

$$C = -8e^4|\psi_{1s}(0)|^2 \frac{R_0^2}{3\hbar c}\left[\log\frac{k_0+u_1+v_1}{k_0+u_0+v_0} - \frac{v_1}{u_1} + \frac{v_0}{u_0}\right]$$

avec

$$u_1 = (R_0^{-2}+k_0^2)^{\frac{1}{2}}-k_0, \qquad v_1 = (u_1^2+2k_0u_1)^{\frac{1}{2}},$$
$$u_0 = (E_0^2/\hbar^2c^2+k_0^2)^{\frac{1}{2}}-k_0, \quad v_0 = (u_0^2+2k_0u_0)^{\frac{1}{2}},$$
$$k_0 = \mu c/\hbar.$$

La formule (3) est valable quelle que soit la masse de la particule négative. Le cas de l'électron est obtenu en faisant $k_0 = 0$:

$$u_0 = v_0 = E_0/\hbar c, \quad u_1 = v_1 = R_0^{-1},$$

ce qui donne

$$C = -8e^4|\psi_{1s}(0)|^2 \frac{R_0^2}{3\hbar c}\log\frac{\hbar c}{R_0E_0},$$

qui est bien la formule de Krall et Salpeter.

L'évaluation numérique fournit finalement

$$C/h = \begin{cases} -3.6\times10^7 \text{ MHz pour le méson } \mu^- \\ -2.1\times10^{-1} \text{ MHz pour l'électron.} \end{cases}$$

Ce terme constitue donc l'essentiel de la correction du second ordre.

4. Discussion

Le résultat obtenu indique que dans l'atome mésique mu de deutérium les deux corrections nucléaires d'extension finie et de polarisation se compensent à peu près. Les déplacements de raies sont donc approximativement égaux dans le cas du proton et du deutéron et sont constitués en ordre principal par la polarisation du vide. Le deutéron étant le noyau le plus aisé à polariser étant donné son énergie de liaison faible, il faut s'attendre à ce que dans les autres atomes mésiques, la polarisation nucléaire ne soit qu'une fraction (en valeur absolue) de l'effet de volume.

Par une modification de la masse dans nos formules il est possible de calculer la polarisation nucléaire par différentes particules négatives n'ayant avec le deutéron que des interactions faibles. Deux remarques peuvent encore être

faites sur la formule (3): d'une part la fonction d'onde de l'état fondamental du deutéron n'intervient que par la valeur moyenne de R^2; d'autre part la fonction d'onde de l'état fondamental du méson n'intervient que par sa valeur à l'origine. Dans le cas non-relativiste on a donc immédiatement

$$E^{(2)}_{ns,0} = \frac{1}{n^3} E^{(2)}_{1s,0}.$$

Le tableau 1 résume nos résultats. Les résultats relatifs au méson mu sont présentés dans le tableau 2 sous une forme analogue à celle de Foldy et Eriksen.

TABLEAU 1

Déplacements des niveaux dus à la polarisation et à l'effet de volume nucléaires (en MHz)

Effets	Electron		Méson μ^-	
	1s	2s	1s	2s
Effet de volume	5.7	0.7	4.3×10^{7}	5.4×10^{6}
Correction statique	-1.3×10^{-2}	-1.6×10^{-3}	-1.8×10^{5}	-2.2×10^{4}
Correction dispersive	-2.1×10^{-1}	-2.6×10^{-2}	-3.6×10^{7}	-4.5×10^{6}

Dans ce qui précède les nucléons ont été traités comme des points. La méthode de calcul que nous avons choisie ici diffère de celles utilisées par d'autres auteurs [2, 4]): nous justifions maintenant notre choix.

TABLEAU 2

Déplacements des raies dans les atomes mésiques d'hydrogène et de deutérium

Atome mésique $\frac{\Delta E_{2s,\frac{1}{2}} - \Delta E_{1s,\frac{1}{2}}}{E_2 - E_1} \times 10^3$	Hydrogène	Deutérium
Polarisation du vide	0.89	0.89
Relativité	0.01	0.01
Effet de volume	—	-0.07_8
Effet de polarisation	—	$+0.06_8$

5. Remarques sur la méthode de calcul

5.1. CHOIX DU SYSTÈME DE COORDONNÉES

Le système de coordonnées suivant permet d'obtenir une limite inférieure de l'effet de polarisation du deutéron lorsque le système deutéron-méson est dans l'état fondamental. Nous utilisons les vecteurs

$$\mathbf{r}' = \mathbf{r}_m - \mathbf{r}_p, \quad \mathbf{R}' = \mathbf{r}_n - \mathbf{r}_p,$$

qui conduisent après élimination du mouvement du centre de masse à l'hamiltonien

$$H = -\frac{\hbar^2}{2\mu'}\Delta_{r'} - \frac{\hbar^2}{M}\Delta_{R'} - \frac{e^2}{r'} + V(\mathbf{R}') - \frac{\hbar^2}{M}\nabla_{r'}\cdot\nabla_{R'}, \tag{1}$$

où μ' est la masse réduite du méson par rapport au proton et M la masse d'un nucléon.

L'hamiltonien de perturbation est ici

$$H' = -\frac{\hbar^2}{M}\nabla_{r'}\cdot\nabla_{R'}.$$

A l'ordre zéro, on a

$$\Psi^{(0)}_{k_1k_2} = \varphi_{k_1}(\mathbf{r}')\varphi_{k_2}(\mathbf{R}')$$

et

$$E^{(0)}_{k_1k_2} = \varepsilon_{k_1} + E_{k_2},$$

où ε_{k_1} désigne l'énergie du méson dans l'état k_1 et E_{k_2} l'énergie du deutéron dans l'état k_2.

Au premier ordre, il vient

$$E^{(1)}_{k_1k_2} = \langle k_1k_2|H'|k_1k_2\rangle = 0, \tag{2}$$

car H' est de parité impaire.

Au second ordre, et pour l'état fondamental du système on démontre aisément que

$$E^{(2)}_{1s,0} = A + B$$

où

$$A = \frac{1}{E^{(0)}_{1s,0}}\langle 1s, 0|H'^2|1s, 0\rangle$$

et

$$B = \frac{1}{E^{(0)}_{1s,0}}\sum_{\substack{l_1\neq 1s\\ l_2\neq 0}} E^{(0)}_{l_1l_2}\frac{|\langle 1s, 0|H'|l_1, l_2\rangle|^2}{E^{(0)}_{1s,0} - E^{(0)}_{l_1,l_2}}.$$

On calcule sans peine

$$A = \frac{e_4\,\mu'^2\,\alpha\beta}{E^{(0)}_{1s,0}M^2},$$

d'où

$$\mathrm{A/h} = \begin{cases} -1.1\times 10^{12}\ \mathrm{MHz\ pour\ un\ méson}\ \mu^- \\ -2.6\times 10^{7}\ \ \mathrm{MHz\ pour\ un\ électron.} \end{cases}$$

Pour améliorer la limite inférieure ainsi obtenue il faut évaluer le terme B dont le calcul même approché n'est pas aisé. D'autre part, l'hamiltonien (1)

s'exprime en fonction de la masse réduite du méson par rapport au proton et non par rapport au deutéron. Des corrections de masse supplémentaires s'introduisent donc dans les calculs.

Observons enfin que la correction $E^{(1)}_{1s,0}$ étant nulle dans ce système de coordonnées en vertu de la relation (2), l'effet de volume est rejeté au second ordre ce qui complique l'interprétation des résultats fournis par le calcul des perturbations. Ces divers inconvénients ne sont pas présents lorsqu'on utilise le système de coordonnées défini au § 2 et dont le choix se trouve ainsi justifié.

5.2. CHOIX DE L'HAMILTONIEN NON PERTURBÉ

Il est possible, en utilisant le système de coordonnées défini au § 2, de calculer la polarisation du deutéron au second ordre du calcul des perturbations après avoir annulé la correction énergétique du premier ordre. A cet effet, nous ajoutons et retranchons à l'hamiltonien du problème le potentiel moyen $\bar{V}(r)$ défini au § 2, ce qui nous conduit à écrire

$$H = H_0 + H_1$$

avec

$$H_0 = H_m + H_d,$$

$$H_m = \left[-\frac{\hbar^2}{2\mu} \Delta_r + \bar{V}(r) - \frac{e^2}{r} \right],$$

$$H_d = \left[-\frac{\hbar^2}{M} \Delta_R + V(\mathbf{R}) \right],$$

$$H_1 = \frac{e^2}{r} - \frac{e^2}{|\mathbf{r} - \frac{1}{2}\mathbf{R}|} - \bar{V}(r).$$

C'est une méthode de ce type qui a été utilisée par Cooper et Henley [2]) pour étudier la polarisation nucléaire des atomes mésiques lourds. A l'ordre zéro, l'hamiltonien mésique H_m tient déjà compte de l'extension finie du noyau par suite de la présence de $\bar{V}(r)$.

Les fonctions propres de H_0 s'écrivent

$$\Psi^{(0)}_{l_1 l_2} = \psi_{l_1}(\mathbf{r}) \phi_{l_2}(\mathbf{R})$$

où les $\psi_{l_1}(\mathbf{r})$ ne sont pas hydrogénoïdes. Au premier ordre du calcul des perturbations, et pour l'état fondamental du deutéron ($l_2 = 0$)

$$E^{(1)}_{l_1,0} = \langle l_1, 0 | H_1 | l_1, 0 \rangle = 0$$

en vertu de la définition de $\bar{V}(r)$.

Bibliographie

1) L. L. Foldy et E. Eriksen, Phys. Rev. **95** (1954) 1048
2) L. N. Cooper et E. Henley, Phys. Rev. **92** (1953) 801
3) W. Lakin et W. Kohn, Phys. Rev. **94** (1954) 787
4) H. S. W. Massey et C. B. O. Mohr, Proc. Camb. Phil. Soc. **34** (1938) 498
5) J. B. French et M. L. Goldberger, Phys. Rev. **87** (1952) 899
6) Malenka, Kruse et Ramsey, Phys. Rev. **91** (1953) 1165
7) Ramsey, Malenka et Kruse, Phys. Rev. **91** (1953) 1162
8) B. W. Downs, Phys. Rev. **98** (1955) 194
9) J. Sawicki, Acta Phys. Polon. **13** (1954) 225
10) L. I. Schiff, Phys. Rev. **98** (1955) 756
11) R. R. Lewis, Jr. Phys. Rev. **102** (1956) 544
12) H. S. Valk et B. J. Malenka, Phys. Rev. **104** (1956) 800
13) N. A. Krall et E. E. Salpeter, Phys. Rev. **115** (1959) 457
14) E. E. Salpeter, Phys. Rev. **89** (1953) 92

10.D *Nuclear Physics* **17** (1960) 339—340; © *North-Holland Publishing Co., Amsterdam*

BOOK REVIEWS

R. C. EXTERMANN (Editor), *Radioisotopes in scientific research*, vol. 1 (Research with radioisotopes in physics and industry (Pergamon Press, 1958. xxi—761 pages. £ 7)

This volume is the first of a series of four, embodying the proceedings of the first international conference on radioisotopes, sponsored by Unesco. It comprises the papers dealing with radioisotopes in physics and industry. Many of these communications either summarize research published elsewhere, or give a preliminary account calling for more detailed documentation. For this reason, this collection has become outdated just as quickly as the comprehensive proceedings of other huge conferences, including those held in Geneva.

It cannot be questioned that the great value of such conferences lies in the personal contacts established where so many scientists from different parts of the world meet. However, in view of the fact that all papers read at the conference were available in large numbers both as abstracts and as complete preprints, it can be questioned whether the costly edition of these proceedings does not drain both the sponsoring agency and the potential buyers of funds that might profitably be spent on more lasting and more informative publications.

Hilde Levi

FRIEDRICH MÜNZINGER, *Atomkraft*. Der Bau ortsfester und beweglicher Atomantriebe und seine technischen und wirtschaftlichen Probleme. Eine kritische Einführung für Ingenieure, Volkswirte und Politiker. 3. Aufl. (Springer 1960. xii—304 pages. DM 42)

New material has been added in this third edition, and a considerable amount of information is contained in its more than 300 pages, but often with some lack of precision. Maybe the author has tried to do too many things in one book, e.g. to write for readers with too widely different backgrounds in basic knowledge. Vertical lines indicate the sections which the author deem of principal interest to the non-engineer.

Alice in Wonderland might have liked this book because she detests books without pictures and conversation. There is a lot of pictures and the text is mainly conversation.

There is a chapter called 'Atomic energy' and another 'Atomic revolution'. The latter contains one subsection only, entitled 'Allgemeines', which I would translate as 'Generalities'. Let me quote from this section: "Reaktoren sind gewissermassen ein Nebenprodukt oder, wenn man so sagen will, ein illegitimes aber vielversprechendes Kind der Atombombe". This entire chapter carries a vertical line and illustrates the fact that the presentation is argumentative.

The book must be a best-seller since it has been of interest to produce a third edition within a short period of time. Editions have appeared † in 1955, 1957 and 1960. It is sad that many persons acquire their knowledge of atomic energy from a book of this kind.

O. Kofoed-Hansen

S. T. BUTLER and H. MESSEL, Editors, *From nucleus to universe*, A course of selected lectures in physics and astronomy (Shakespeare Head Press, Sydney, 1960. 335 pages. 84 s.)

These twelve lectures are aimed at science teachers in an attempt to keep them in touch with the recent developments in nuclear science, astronomy and cosmology. Each lecture is given by a different author, starting with a résumé of elementary nuclear properties by Prof. Butler; they are on the whole lucid expositions of advances in specialised fields. Unfortunately, a certain lack of co-ordination has caused different authors to assume different levels of knowledge for their starting point, and it is difficult to see who could derive equal benefit from all lectures.

The book is well illustrated and neatly printed.

J. R.

† Reviewed in this journal **1** (1956) 229 and **4** (1957) 492.

RALPH T. OVERMAN and HERBERT M. CLARK *Radioisotope techniques* (McGraw-Hill, 1960. xiv—476 pages. 77s. 6d.)

This book should undoubtedly prove useful for many research workers in the field of applied radioactivity, for teachers who want to set up laboratory courses in radioisotope work, and for students who want to familiarize themselves with this subject.

The book is unusual in its scope. It gives simultaneously a description of the background material in elementary physics, mathematics and chemistry for radioactivity work and an excellent set of laboratory experiments appended to each chapter. Thus, the book is like an old-fashioned textbook for experimentalists, but dealing with a modern topic.

A complete chapter is devoted to radiological safety, including safe methods for radioactivity work, decontamination and waste disposal.

Anybody who reviews a book feels that there are some points which he personally would have chosen to treat differently, but often such points are those where the reviewer might wish to call himself a specialist, and for this reason his objections are often of minor consequence since most textbooks are not meant to be very useful to the specialist. The present book is undoubtedly intended mainly for scientists in non-nuclear fields who want to use radioisotope techniques as a tool. Thus it is excellent that difficulties and sources of errors are emphasized and a careful reader who follows the instructions in this book should be able to avoid most of the embarrassing mistakes which one is so easily led into in radioactivity work. Furthermore, an excellent collection of references is given so that a reader who wants to know more about a specific subject will easily find his way to the proper source.

A few of the chapters appear slightly oldfashioned. Thus, the chapter on standardization and calibration places too much emphasis on the simple GM counter and too little on 4π beta counting and coincidence counting. Thus Campion's 4π beta-gamma coincidence method is not mentioned at all. Incidentally, in the discussion of the coincidence method one possible source of error, namely angular correlations between the two radiations, is not mentioned. But perhaps I am now heading towards the special pitfall for reviewers which I mentioned above and ought instead to remember the goal of the book which is to be a guide for students, teachers and those who wish to apply radioisotope techniques. For this purpose the book should be excellent.

O. Kofoed-Hansen

Maritime organic moderated and cooled reactor (United States Atomic Energy Commission, Technical Information Service, 1959. xi—198 pages. $ 3.50)

The report describes the results of a conceptual design study of an organic moderated and cooled reactor (OMCR) power plant adapted to a Class T-7 tanker (dead weight 60 840 t). It has been prepared for the Maritime Reactors Branch of the Atomic Energy Commission by Atomics International, a division of North American Aviation, Inc.

The design study encompassed the ship's power plant including the reactor, primary loops, reactor auxiliary equipment, turbine system, and standby power equipment. The purpose of the study was to develop preliminary design data in sufficient detail to estimate among other things preliminary hazards review, capital costs and operating costs.

Part of the report is devoted to a general description of the organic moderated reactor system. This description is found in a number of the reports prepared by the Atomics International.

The report gives an excellent and instructive description of the entire reactor system which includes a reactor capable of developing a total of 30 000 SHP. This part of the report is accompanied by excellent drawings, etc.

A substantial part of the report is taken up by a survey of problems relating to operation and dependability.

The report draws the conclusion that the cost of construction for the tanker in question propelled by an OMCR will be 28.5 million $, i.e. that it is approximately 50 per cent dearer than the corresponding tanker equipped with a conventional boiler-turbine plant. In consequence of the lower fuel cost and the larger carrying capacity of the reactor driven ship, the difference between cost per ton of cargo will be considerably lower, namely 11.3 against 9.55 $.

Jens J. Thiel

2.G

Nuclear Physics **17** (1960) 341—358; © *North-Holland Publishing Co., Amsterdam*

Not to be reproduced by photoprint or microfilm without written permission from the publisher

EXCHANGE EFFECTS IN STRIPPING REACTIONS

M. A. NAGARAJAN and M. K. BANERJEE

Saha Institute of Nuclear Physics, Calcutta, India

Received 12 February 1960

Abstract: The necessity of considering exchange effects in stripping reactions is now well established. We have calculated the relative phases and amplitudes of the direct and exchange terms by taking anti-symmetrized wave functions. Shell model wave functions have been used for the nuclear wave functions. Calculations of the angular distributions for the reactions Be^{9}(d, p)Be^{10}, F^{19}(d, p)F^{20} and O^{16}(d, p)O^{17} have been made and these are seen to agree very well with the experimental angular distributions in these reactions. The interactions responsible for the knock out reaction and the heavy particle stripping reaction have been discussed.

1. Introduction

In the theory of the angular distribution in the deuteron stripping reaction, as developed by Butler [1]) and Bhatia and Huang [2]), the following mechanism was assumed for the reaction. In a (d, p) or a (d, n) reaction, the neutron or proton is stripped off the deuteron and captured by the target and the proton or neutron is released with the appropriate energy. A characteristic prediction of such a mechanism is that the angular distribution is peaked in the forward hemisphere. In fact, the angular distribution is then approximately represented by the form $|j_L(qR)|^2$, where [3]) $j_L(Z)$ is the spherical Bessel function or order L, q is the momentum change of the target nucleus, R is the mean radius of the region of interaction and L is the angular momentum of the orbital state in which the neutron or proton is captured. This distribution is now commonly termed as the Butler distribution. In a large number of cases, the experimental angular distribution in the forward hemisphere could be satisfactorily explained as a Butler distribution. However, when the measurement of the angular distribution was extended to the backward hemisphere it was found that in many instances the differential cross section shows an increase with increasing angle.

Owen and Madansky [4]) were the first to recognise the observed rise of the differential cross section in the backward hemisphere as the effect of exchange in stripping reactions. In order to see the different effects clearly let us consider the reaction O^{17}(d, n)F^{18}. Let us label the neutrons of the deuteron and O^{17} as 1 and 2 respectively. The proton will be labelled by the symbol p and the double closed shell core O^{16} common to the target and the final nucleus will be referred to by the symbol c. The state of affair before the start of the reaction is represented

in fig. 1(a). Here 1 and p are bound together to form the projectile deuteron and 2 and c are bound together to form the target nucleus. The mechanism of the reaction which was outlined in the beginning of the section leads to a state

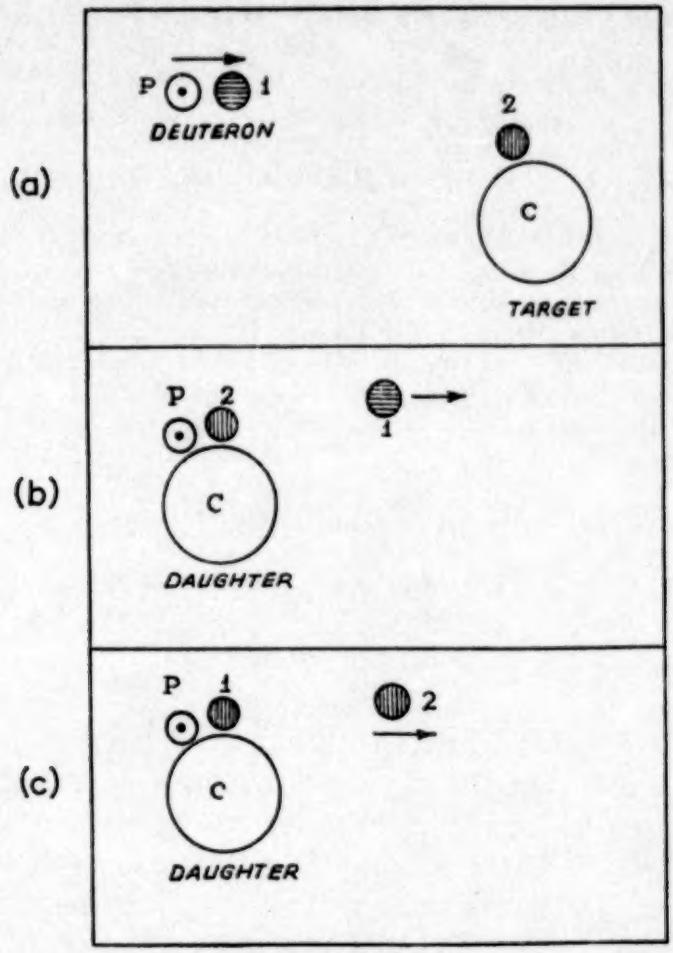

Fig. 1. (a) The initial state of the system before the reaction. (b) The mechanism of direct stripping. (c) The mechanism of exchange stripping.

of affair after the reaction shown in fig. 1(b). Here p is captured by the target nucleus and 1 goes out. But since the neutrons 1 and 2 are indistinguishable, the mechanism in which the roles of 1 and 2 are interchanged should also contribute to the reaction. This has been shown in fig. 1(c). Usually the mechanism represented by 1(b) is called the direct stripping and that represented by 1(c) is called the exchange stripping.

By integrating over suitably chosen internal co-ordinates both direct and exchange processes may be approximated by three-body processes. The three particles may be denoted by the symbols A, B and C and the processes may be symbolically represented by the equation

$$(A+B)+C \rightarrow A+(B+C).$$

Thus, in the present example, for the direct process we may integrate over the internal co-ordinates of O^{17}, which will yield an average over the intrinsic state of O^{17}. Then we may consider O^{17} as a structureless particle and assign it the symbol C. The neutron 1 and the proton p may be called A and B respectively. For the exchange amplitude, we should integrate over the internal co-ordinate of the deuteron composed of the neutron 2 and the proton p and also over the internal co-ordinates of the core O^{16}. Then the deuteron and the core may be considered as structureless particles and these may be assigned the symbols C and B respectively, while the neutron 1 may be assigned the symbol A. It may also be shown that in each case the interactions responsible for the transition are the binding interaction V_{AB} (or V_{BC}) and the unbound pair interaction V_{AC}. The contribution of the latter is always very small compared to the former. The ratio of the two types of contribution is somewhat larger for the exchange process than for the direct process. There is at least one known example [5]), B^{10}(d, p)B^{11*}($Q = 7.10$ MeV), where the reaction is a purely exchange process and the unbound pair interaction contributes more strongly than the binding interaction.

The contribution of the binding interaction to the exchange process which is usually the most important exchange effect is called the "heavy particle stripping". The significance of this name becomes clear when one goes over to a system which is moving with the deuteron. In this system, the target approaches the deuteron. The target is thought of as composed of the core and the neutron. The core is stripped off the target and is captured by the deuteron, while the neutron is released. Since the binding interaction is responsible for the process, which is also the case in direct stripping, it is given the name heavy particle stripping.

When the interaction between the captured particle and the released particle, which is known as the unbound pair interaction, is responsible for the reaction, the description that the latter is knocked out by the former seems appropriate. Hence this is called the knock out interaction. It is clear from the description of the heavy particle stripping process that the neutrons will tend to move in the original direction of the target, which corresponds to the backward direction. Thus the amplitude for the heavy particle stripping increases in the backward direction. On the other hand the knock out amplitude is peaked essentially in the forward direction. The total amplitude for the reaction will be a sum of the direct and exchange amplitudes. The relative phase between the two amplitudes is determined by the nature of space symmetry of the relative motion of the two neutrons.

Madansky and Owen [4]) suggested the heavy particle stripping mechanism to account for the large backward component observed in the reaction B^{11}(d, n)C^{12}. They used the ratio of the amplitudes of heavy particle stripping to the direct process as a parameter to be determined by matching the theoreti-

cal predictions with the observed angular distribution. In addition, they have chosen different quantization axes for the description of the direct and exchange processes, and have omitted the consideration of the term $P_L(\cos\theta)$ in the interference term, where θ is the angle between the quantization axes [20]). French [6]) proposed a formalism wherein he considered only targets with one exchangeable nucleon outside a closed shell. A serious setback of the formalisms of the above authors is that the direct and the heavy particle stripping amplitudes have to be normalized independently and their ratio treated as a parameter [7]).

In our work reported here, we have tried to formulate the problem in a manner that would enable us, in principle, to determine the relative phases of the direct and exchange amplitudes as well as their relative magnitudes. The magnitudes of the two amplitudes depend on a number of factors, chiefly the strengths of the interactions and the widths. In the plane wave approximation, the strengths of the interactions appear through the binding energies, which are experimentally known. The widths contain geometrical factors, determined by the angular momentum coupling in the nuclear wave functions, and their radial widths. The relative phase of the two amplitudes is essentially determined by the angular momentum coupling and the symmetries of the nuclear wave functions. The appearance of the radial widths is a consequence of the use of a "cut off" in the radial integration. It is difficult to locate the cut off radius with great certainty. As a result the radial widths obtained from the experiment are not precise numbers.

In sect. 2 we have dealt with the problem of antisymmetrization in a pick-up reaction. Sections 4, 5 and 6 deal with the evaluation of the exchange and direct amplitudes and the interference term. In sect. 7, we discuss how we can parametrize the problem. The method of evaluation of these parameters has also been discussed. Our calculations for the reactions $Be^9(d, p)Be^{10}$, $O^{16}(d, p)O^{17}$ and $F^{19}(d, p)F^{20}$ have been discussed in sect. 8.

2. Antisymmetrization in a (n, d) reaction

For the sake of convenience, we shall consider the (n, d) reaction. It will be obvious, however, that the formalism presented here is applicable to all pick-up and stripping reactions.

In the Born approximation, the (n, d) cross section is given by the expression

$$\sigma(\mathbf{k}_f) = \frac{v_f}{v_i}\left(\frac{\mu_f}{2\pi}\right)^2 \cdot S\left|\langle \mathbf{k}_f; \mathrm{pn}|\langle 1, 2, \ldots, A|\sum_{i=1}^{A}(V_{ni}+V_{pi})\left(1-\sum_{j=1}^{A}P_{jn}-P_{np}\right)|1, 2, \ldots, A; \mathrm{p}\rangle|\mathbf{k}_i; \mathrm{n}\rangle\right|^2. \tag{1}$$

Here n denotes the incoming neutron, and (pn) denotes the outgoing deuteron

composed of the neutron n and the picked up proton p. The quantities $\mathbf{k}_i$ and $\mathbf{k}_f$ are the momenta of the neutron and the deuteron in the centre of mass system. The ket $|\mathbf{k}_i; \mathrm{n}\rangle$ describes, in addition to the motion of the neutron relative to the target nucleus, its intrinsic spin state. Similarly, the ket $|\mathbf{k}_f; \mathrm{pn}\rangle$ describes the motion of the centre of mass of the deuteron relative to the final nucleus as well as its internal state. The state of the final nucleus, composed of the particles $1, 2, \ldots, A$, is designated by the ket $|1, 2, \ldots, A\rangle$. The state of the target nucleus, which contains the proton p in addition to the particles $1, 2, \ldots, A$ is designated by the ket $|1, 2, \ldots, A; \mathrm{p}\rangle$. Further, v_i and v_f are the velocities of the neutron and proton in the centre of mass system, while μ_f is the reduced mass of the deuteron and the final nucleus. The symbol S denotes the summation and averaging over the orientations of the spins of the final and initial states. We have used the isobaric spin formalism which enables us to treat the neutron and proton on the same footing. The operator P_{jn} exchanges the particles j and n. The operator $(1-\sum_{j=1}^{A} P_{jn}-P_{np})$ antisymmetrizes the neutron n with the particles $1, 2, \ldots, A$, p of the target nucleus.

The expression for the (n, d) cross section can be separated into two parts; we may write

$$\sigma(\mathbf{k}_f) = \frac{v_f}{v_i}\left(\frac{\mu_f}{2\pi}\right)^2 \mathrm{S}|D-E|^2, \tag{2}$$

where

$$\mathrm{D} = \langle \mathbf{k}_f; \mathrm{pn}|\langle 1, 2, \ldots, A|\sum_{i=1}^{A}(V_{ni}+V_{pi})(1-P_{np})|1, 2, \ldots, A; \mathrm{p}\rangle|\mathbf{k}_i; \mathrm{n}) \tag{2a}$$

$$E = \langle \mathbf{k}_f; \mathrm{pn}|\langle 1, 2, \ldots, A|\sum_{i=1}^{A}(V_{ni}+V_{pi})\sum_{j=1}^{A}P_{jn}|1, 2, \ldots, A; \mathrm{p}\rangle|\mathbf{k}_i; \mathrm{n}\rangle \tag{2b}$$

Here D and E are the direct and exchange amplitudes. In view of the fact that the target wave function and the final nucleus (composed of particles $1, 2, \ldots, A$) wave function are antisymmetrical over the particles $1, 2, \ldots, A$ each one of the exchange operators in the sum $\sum_{j+1}^{A} P_{jn}$ will make the same contribution to E. Hence, we may write E as

$$E = A\langle \mathbf{k}_f; \mathrm{pn}|\langle 1, 2, \ldots A|\sum_{i=1}^{A}(V_{ni}+V_{pi})P_{An}|1, 2, \ldots, A; \mathrm{p}\rangle|\mathbf{k}_i; \mathrm{n}\rangle. \tag{2b'}$$

After exchanging A and n, we write

$$E = A\langle \mathbf{k}_f; \mathrm{pn}|\langle 1, 2, \ldots, A|\sum_{i=1}^{A-1}(V_{ni}+V_{pi})+(V_{nA}+V_{pA})|1, 2, \ldots, A-1, \mathrm{n}; \mathrm{p}\rangle|\mathbf{k}_i; A\rangle. \tag{2b''}$$

Here we have rearranged the interaction potential to appear like the sum of the binding and the unbound pair potential.

In the expression for D, the factor 2 appears as a result of the operation of $(1-P_{np})$ on the deuteron wave function. Since this factor appears because we have used the isobaric spin formalism, it is evident that it will be taken care of when we calculate the overlap of the initial and final state isobaric spin wave functions. Similarly, it can be shown that, in the case of exchange stripping, after we take into account the factors that appear as a result of integration over the isobaric spin variables, the multiplying factor that appears in E is replaced by the number of neutrons in the target nucleus that can exchange places with the incident neutron.

3. Unbound Pair Interaction

In the previous section we have seen how the interaction potential causing stripping can be classified into the binding and the unbound pair potentials. We shall, from naive considerations, try to estimate the contribution from the unbound pair interaction. Let us consider the (d, n) reaction. In the case of the direct stripping process, the unbound pair is the neutron of the deuteron and the target nucleus. Though these two are not bound together at any time during the reaction, both the neutron and the target nucleus are bound to a common centre, namely the proton, at least part of the time. For this reason, the neutron may come within the range of interaction of the target nucleus. The probability that the neutron may come within the range of interaction of the target nucleus would only be large if the wave functions describing the bound state of the neutron with the proton, and that of the target nucleus with the proton were similar. However, we know that the two wave functions are widely dissimilar in extension, and would therefore except a small contribution from the unbound pair interaction. Estimates of the contribution from the unbound pair interaction have been made by Fulton and Owen [8]) by assuming specific forms for the interaction potential. These estimates indicate that the contribution from the unbound pair interaction is less than 4 % of the contribution from the binding potential.

In the case of exchange stripping, it was mentioned in sect. 1 that the unbound pair interaction is the interaction that causes the knock out reaction. The effective knock out interaction is obtained after averaging this unbound pair interaction over the internal co-ordinates of the deuteron. We have assumed a δ-function form for the knock out potential that gives the correct scattering length. The pseudo potential taken was

$$V_{nd} = 14\delta(\mathbf{r}_n - \mathbf{r}_d).$$

The angular distribution in the knock out process is similar to that in the direct stripping process. Hence, a comparison of the amplitudes of the direct and knock out processes would be sufficient to determine the importance of

the knock out process. Rough estimates of the knock out amplitudes were made for the reactions $B^{11}(d, n)C^{12}$ and $O^{16}(d, p)O^{17}$ by choosing the initial and final nucleus wave functions as produced by a square well. These estimates show that the amplitude increases in the case of the reaction $O^{16}(d, p)O^{17}$ since the orbital angular momenta of the two wave functions is the same. However, the knock out amplitude is truly small compared with the direct amplitude, and in reactions where the direct stripping mechanism is allowed, one may neglect the contributions from the knock out process [6]). In our formulation we have considered only the direct and heavy particle stripping processes.

4. Evaluation of the Exchange Amplitude

In the evaluation of the direct and exchange amplitudes, we have used the channel spin formalism. The channel spin is obtained by a vector addition of the intrinsic spins of the two constituents of the channel. The formulation has been done for a (d, n) reaction. We make the following assumptions:

1) the motion of the incident deuteron relative to the target nucleus, and that of the outgoing neutron relative to the final nucleus are described by plane waves;

2) the effect of the unbound pair interaction is neglected;

3) cut off radii have been assumed for the capture of the deuteron and the emission of the neutron.

We shall use the following notation. The ket $|\alpha JTMM_T\rangle$ denotes the state of the nucleus, where J and T are respectively the total angular momentum and the isobaric spin of the state, and M and M_T are their respective Z-components; α denotes all other quantum numbers necessary to specify the state uniquely. The suffixes i, f and c denote respectively the target nucleus, the final nucleus and the core. We neglect the small D-state admixture in the ground state of deuteron and write $S_d T_d \mu_d M_{Td}$ for the ground state of deuteron, where S_d and T_d denote the spin and isobaric spin of the deuteron respectively, μ_d and M_{Td} being their respective Z-components. The channel spins for the initial and final channels I_i and I_f are given by the expressions

$$\mathbf{I}_i = \mathbf{J}_i + \mathbf{S}_d$$

$$\mathbf{I}_f = \mathbf{J}_f + \boldsymbol{\sigma}_n$$

N_i and N_f are the respective z-components of I_i and I_f. Y_{lm} is a spherical harmonic, and z_{lm} is the unnormalized spherical harmonic related to Y_{lm} through the relation

$$z_{lm} = \left(\frac{4\pi}{2l+1}\right)^{\frac{1}{2}} Y_{lm}.$$

Further, $\left[\begin{smallmatrix} j_1 & j_2 & j \\ m_1 & m_2 & m \end{smallmatrix}\right]$ is the vector addition coefficient, $U(abcd; ef)$ is the modi-

fied Racah coefficient as defined by Jahn [9]), and finally, $\begin{bmatrix} l_1 & s_1 & j_1 \\ l_2 & s_2 & j_2 \\ L & S & J \end{bmatrix}$ is a $LS-jj$ transformation coefficient.

In the LS-coupling scheme, we replace α by $[\lambda]LS$ where $[\lambda]$ is the symmetry quantum number and L and S are the orbital and spin angular momenta. We write for the vectorially coupled channel wave function for the initial channel

$$|([\lambda_1]L_1S_1J_1T_1M_{T_1}); (S_dT_dM_{T_d}); I_1N_1\rangle = \sum_{M_1\mu_d} \begin{bmatrix} J_1 & S_d & I_1 \\ M_1 & \mu_d & N_1 \end{bmatrix} |[\lambda_1]L_1S_1J_1T_1M_1M_{T_1}\rangle |S_dT_d\mu_dM_{T_d}\rangle. \tag{3}$$

The target nucleus wave function is expressed as a linear combination of the product of the wave function of the core and that of a neutron as follows:

$$\begin{aligned} &|[\lambda_1]L_1S_1J_1T_1M_1M_{T_1}\rangle \\ &= \sum \langle [\lambda_c]L_cS_cT_c; l_n|\}[\lambda_1]L_1S_1J_1\rangle \begin{bmatrix} L_c & l_n & L_1 \\ S_c & \sigma_n & S_1 \\ J_c & j_n & J_1 \end{bmatrix} \begin{bmatrix} l_n & \sigma_n & j_n \\ m_n & \mu_n & M_n \end{bmatrix} \\ &\times \begin{bmatrix} J_c & j_n & J_1 \\ M_c & M_n & M_1 \end{bmatrix} \begin{bmatrix} T_c & T_n & T_1 \\ M_{T_c} & M_{T_n} & M_{T_1} \end{bmatrix} |[\lambda_c]L_cS_cJ_cT_cM_cM_{T_c}\rangle |\sigma_nT_n\mu_nM_{T_n}\rangle \\ &\times U_{l_n}(r_{nc})Y_{l_nm_n}(\Omega_{nc}), \end{aligned} \tag{4}$$

where the first factor in the summation is a singe particle coefficient of fractional parentage. The $LS-jj$ transformation coefficient, which is the second factor, appears when we recouple the angular momenta L_c and S_c of the core to form the total angular momentum J_c. The quantity $U_{l_n}(r_{nc})$ is the radial part of the wave function that describes the motion of the neutron relative to the centre of mass of the core.

Similarly, we write for the vectorially coupled final channel wave function

$$|([\lambda_f]L_fS_fJ_fT_fM_{T_f}); (\sigma_nT_nM_{T_n}); I_fN_f\rangle = \sum_{M_f\mu_n} \begin{bmatrix} I_f & \sigma_n & I_f \\ M_f & \mu_n & N_f \end{bmatrix} |[\lambda_f]L_fS_fJ_fT_fM_fM_{T_f}\rangle |\sigma_nT_n\mu_nM_{T_n}\rangle. \tag{5}$$

We expand the final nucleus wave function as a linear combination of the product of the wave functions of the core and that of the deuteron:

$$\begin{aligned} |[\lambda_f]L_fS_fJ_fT_fM_fM_{T_f}\rangle &= \sum F(L_cS_cT_c; l^2L_dS_dT_d; L_fS_fT_f) \\ &\times \begin{bmatrix} L_c & L_d & L_f \\ S_c & S_d & S_f \\ J_c & J_d & J_f \end{bmatrix} \begin{bmatrix} L_d & \mu_d & J_d \\ m_d & S_d & M_d \end{bmatrix} \begin{bmatrix} J_c & J_d & J_f \\ M_c & M_d & M_f \end{bmatrix} \\ &\times \begin{bmatrix} T_c & T_d & T_f \\ M_{T_c} & M_{T_d} & M_{T_f} \end{bmatrix} |[\lambda_c]L_cS_cJ_cT_cM_cM_{T_c}\rangle \\ &\times |S_dT_d\mu_dM_{T_d}\rangle U_{L_d}(r_{dc})Y_{L_dm_d}(\Omega_{dc}). \end{aligned} \tag{6}$$

Here the square of $F(L_c S_c T_c; L^2 L_d S_d T_d; L_f S_f T_f)$ is a measure of the probability that the final nucleus will appear as a core consiting of $A-1$ particles and a deuteron, with the angular momenta specified. The quantity $U_{L_d}(r_{dc})$ is the radial part of the wave function that describes the motion of the centre of mass of the deuteron relative to the centre of mass of the core.

After averaging over the internal co-ordinates of the core and the deuteron, we write the exchange term as

$$E = G_E R_{E1} R_{E2}, \tag{7}$$

where R_{E1} and R_{E2} are radial integrals given by

$$\begin{aligned} R_{E1} &= \int_{R_1}^{\infty} U_{L_d}(r_{dc}) V_{dc} j_{L_d}(q_d r_{dc}) r_{dc}^2 \mathrm{d}r_{dc} \\ R_{E2} &= \int_{R_2}^{\infty} U_{l_n}(r_{nc}) j_{l_n}(q_n r_{nc}) r_{nc}^2 \mathrm{d}r_{nc}; \end{aligned} \tag{8}$$

these integrals are independent of the mode of angular momentum coupling. The quantity G_E in eq. (7) contains all the geometrical factors and is given by

$$\begin{aligned} G_E = \sum (-i)^{l_n+L_d} 4\pi (2l_n+1)(2L_d+1)\}^{\frac{1}{2}} & Z_{l_n m_n}(\mathbf{q}_d) Z^*_{L_d m_d}(\mathbf{q}_n) \\ \times \langle [\lambda_c] L_c S_c T_c; l_n | \} [\lambda_1] L_1 S_1 J_1 \rangle & F(L_c S_c T_c; l^2 L_d S_d T_d; L_f S_f T_f) \\ \times \begin{bmatrix} L_c & l_n & L_1 \\ S_c & \sigma_n & S_1 \\ J_c & j_n & J_1 \end{bmatrix} & \begin{bmatrix} L_c & L_d & L_f \\ S_c & S_d & S_f \\ J_c & J_d & J_f \end{bmatrix} \begin{bmatrix} J_1 & S_d & I_1 \\ M_1 & \mu_d & N_1 \end{bmatrix} \begin{bmatrix} J_f & \sigma_n & I_f \\ M_f & \mu_n & N_f \end{bmatrix} \begin{bmatrix} l_n & \sigma_n & j_n \\ m_n & \mu_n & M_n \end{bmatrix} \\ \times \begin{bmatrix} L_d & S_d & J_d \\ m_d & \mu_d & M_d \end{bmatrix} & \begin{bmatrix} J_c & j_n & J_1 \\ M_c & M_n & M_1 \end{bmatrix} \begin{bmatrix} J_c & J_d & J_f \\ M_c & M_d & M_f \end{bmatrix} \begin{bmatrix} T_c & T_n & T_1 \\ M_c & M_{T_n} & M_{T_1} \end{bmatrix} \\ \times \begin{bmatrix} T_c & T_d & T_1 \\ M_c & M_{T_d} & M_{T_1} \end{bmatrix}. & \end{aligned} \tag{9}$$

In the actual evaluation, we have assumed definite values for the angular momenta of the core, and as such the summation over these is only formal. After summing over all the projections indicated we obtain

$$\begin{aligned} G_E = \sum (-i)^{l_n+L_d} 4\pi \{[2l_n+1)(2L_d+1)\}^{\frac{1}{2}} & Z_{l_n m_n}(\mathbf{q}_n) Z^*_{L_d m_d}(\mathbf{q}_d) \begin{bmatrix} l_n & L_d & \lambda_d \\ m_n & \mu_d & \mu_d \end{bmatrix} \\ \times (-)^{S_d+l_n+\sigma_n+I_1+\lambda_1-J_c-\lambda_3+m_n} & \left\{ \frac{(2I_1+1)(2\lambda_2+1)}{(2J_c+1)(2L_d+1)} \right\}^{\frac{1}{2}} \begin{bmatrix} I_1 & \lambda_4 & I_f \\ N_1 & \mu_4 & N_f \end{bmatrix} \\ \times \begin{bmatrix} L_c & l_n & L_1 \\ S_c & \sigma_n & S_1 \\ J_c & j_n & J_1 \end{bmatrix} & \begin{bmatrix} L_c & L_d & L_f \\ S_c & S_d & S_f \\ J_c & J_d & J_f \end{bmatrix} U(J_c j_n I_1 S_d; J_1 \lambda_1) U(J_c J_d I_f \sigma_n; J_f \lambda_2) \\ \times U(l_n \sigma_n \lambda_1 S_d; j_n \lambda_3) & U(L_d S_d \lambda_2 \sigma_n; J_d \lambda_3) U(I_1 \lambda_1 I_f \lambda_2; J_c \lambda) \\ \times U(l_n \lambda_3 \lambda_4 \lambda_2; \lambda_1 L_d) & \begin{bmatrix} T_c & T_n & T_1 \\ M_{T_c} & M_{T_n} & M_{T_1} \end{bmatrix} \begin{bmatrix} T_c & T_d & T_f \\ M_{T_c} & M_{T_d} & M_{T_f} \end{bmatrix} \\ \times \langle [\lambda_c] L_c S_c T_c; l_n | \} [\lambda_1] L_1 S_1 T_1 \rangle & F(L_c S_c T_c; l^2 L_d S_d T_d; L_f S_f T_f). \end{aligned} \tag{10}$$

For the case when the deuteron is captured in a S-state by the core, the expression for G_E considerably simplifies:

$$G_E = \sum (-i)^{l_n} 4\pi (2l_n+1)^{\frac{1}{2}} Z_{l_n m_n}(\mathbf{q}_n) \begin{bmatrix} I_1 & l_n & I_f \\ N_1 & -m_n & N_f \end{bmatrix} \begin{bmatrix} T_c & T_n & T_1 \\ M_{T_c} & M_{T_n} & M_{T_1} \end{bmatrix}$$
$$\times \begin{bmatrix} T_c & T_d & T_f \\ M_{T_c} & M_{T_d} & M_{T_f} \end{bmatrix} (-)^{J_c I + I_1 - J_1 - J_f - l_n + m_n} \left\{ \frac{(2j_n+1)}{(2l_n+1)} \right\}^{\frac{1}{2}} \begin{bmatrix} L_c & l_n & L_1 \\ S_c & \sigma_n & S_1 \\ J_c & j_n & J_1 \end{bmatrix} \quad (11)$$
$$\times U(J_c j_n S_d I_1; J_1 J_f) U(l_n I_f j_n I_f; I_1 \sigma_n) U(L_c S_c J_f S_d; J_c S_f)$$
$$\times \langle [\lambda_c] L_c S_c T_c; l_n | \} [\lambda_1] L_1 S_1 T_1 \rangle F(L_c S_c T_c; l^2 0 S_d T_d; L_f S_f T_f).$$

The evaluation of G_E in jj-coupling is done in the same manner and gives

$$G_E = \sum (-i)^{l_n L_d} 4\pi \{(2l_n+1)(2L_d+1)\}^{\frac{1}{2}} Z_{l_n m_n}(\mathbf{q}_n) Z_{l_d m_d}(\mathbf{q}_d)$$
$$\times \begin{bmatrix} l_n & L_d & \lambda_4 \\ -m_n & m_d & \mu_4 \end{bmatrix} \begin{bmatrix} I_1 & \lambda_4 & I_f \\ N_1 & \mu_4 & N_f \end{bmatrix} \begin{bmatrix} T_c & T_d & T_1 \\ M_{T_c} & M_{T_d} & M_{T_1} \end{bmatrix} \begin{bmatrix} T_c & T_d & T_f \\ M_{T_c} & M_{T_d} & M_{T_f} \end{bmatrix} \left\{ \frac{(2I_1+1)(2\lambda_2+1)}{(2J_c+1)(2L_d+1)} \right\}^{\frac{1}{2}}$$
$$\times \begin{bmatrix} l_n & l_p & L_d \\ \sigma_n & \sigma_p & S_d \\ j_n & j_p & J_d \end{bmatrix} U(J_c j_n I_1 S_d; J_1 \lambda_1) U(J_c J_d I_f \sigma_n; J_f \lambda_2) \quad (12)$$
$$\times U(l_n \sigma_n \lambda_1 S_d; j_n \lambda_3) U(L_d S_d \lambda_2 \sigma_n; J_d \lambda_3) U(I_1 \lambda_1 I_f \lambda_2; J_c \lambda_4)$$
$$\times U(l_n \lambda_3 \lambda_4 \lambda_2; \lambda_1 L_d) \langle [\lambda_c] J_c T_c; j_n | \} [\lambda_1] J_1 T_1 \rangle$$
$$\times F(J_c T_c; j^2 J_d T_d; J_f T_f).$$

For $L_d = 0$, the expression becomes

$$G_E = \sum (-i)^{l_n} 4\pi \{(2l_n+1)\}^{\frac{1}{2}} Z_{l_n m_n}(\mathbf{q}_n) \begin{bmatrix} I_1 & l_n & I_f \\ N_1 & -m_n & N_f \end{bmatrix} \begin{bmatrix} T_c & T_n & T_1 \\ M_{T_c} & M_{T_n} & M_{T_1} \end{bmatrix}$$
$$\times \begin{bmatrix} T_c & T_d & T_f \\ M_{T_c} & M_{T_d} & M_{T_f} \end{bmatrix} (-)^{J_c + I_1 - J_c - j_p - j_n - l_n + 2\sigma_n + m_n} \frac{(2j_n+1)^2}{(2l_n+1)(2\sigma_n+1)} \Bigg\}^{\frac{1}{2}} \quad (13)$$
$$\times U(J_c j_n S_d I_1; J_1 J_f) U(l_n I_f j_n J_f; I_1 \sigma_n) U(S_d \sigma_n j_p l_n; \sigma_p j_n)$$
$$\cdot \langle [\lambda_c] J_c T_c; j_n | \} [\lambda_1] J_1 T_1) F(J_c T_c; j^2 J_d T_d; J_f T_f).$$

Let us now return to eqs. (7) and (8). The radial integrals R_{E1} and R_{E2} are measures of the probability amplitude for the core to capture the deuteron in a state with orbital angular momentum L_d, and of that for the emission of the neutron by the target nucleus from an orbit of angular momentum l_n. In eqs. (8), R_1 and R_2 are the cut-off radii at which the capture of the deuteron and the emission of the neutron have taken place. The integrals are evaluated using the equations of motion for U_l and j_l; we obtain the expressions [10])

$$R_{E1} = -\frac{\nu_{L_d} R_1^{\frac{1}{2}}}{2M_{dc}} W(R_1 \Lambda_1 q_d L_d),$$
$$R_{c2} = \frac{\nu_{l_n} R_2^{\frac{1}{2}}}{(q_d^2 + 2M_{dc} E_{dc})} W(R_2 \Lambda_2 q_n l_n), \tag{14}$$

where

$$\nu_{L_d} = R_1^{\frac{1}{2}} |U_{L_d}(r_{dc})|_{r_{dc}=R_1}, \quad \nu_{l_n} = R_2^{\frac{1}{2}} |U_{l_n}(r_{nc})|_{r_{nc}=R_2},$$

are dimensionless quantities related to the reduced width γ_l through the equation

$$\nu_l^2 = \frac{2mR^2}{\hbar^2} \gamma_l^2. \tag{15}$$

The functions $W(R_1 \Lambda_1 q_d L_d)$ and $W(R_2 \Lambda_2 q_n l_n)$ are defined as follows:

$$W(R_1 \Lambda_1 q_d L_d) = \left[\frac{\mathrm{d}}{\mathrm{d}r_{dc}} j_{L_d}(q_d r_{dc}) - \Lambda_1 j_{L_d}(q_d r_{dc})\right]_{r_{dc}=R_1}$$
$$W(R_2 \Lambda_2 q_n l_n) = \left[\frac{\mathrm{d}}{\mathrm{d}r_{nc}} j_{l_n}(q_n r_{nc}) - \Lambda_2 j_{l_n}(q_n r_{nc})\right]_{r_{nc}=R_2}. \tag{16}$$

In eqs. (14), M_{dc} is the reduced mass of the deuteron and the core, and E_{dc} is the binding energy of the deuteron in the final nucleus.

The quantities Λ_1 and Λ_2 used in eqs. (14) and (16) denote the logarithmic derivatives of U_{L_d} and U_{l_n}. The quantities W were evaluated using square well wave functions for $U_{L_d}(r_{dc})$ and $U_{l_n}(r_{nc})$.

The expression for the heavy particle stripping amplitude contains the term $F(L_c S_c T_c; l^2 L_d S_d T_d; L_t S_t T_t)$ which is a measure of the probability that the deuteron is captured by the core with a relative orbital angular momentum L_d to form the final nucleus. This capture probability will be larger the lower the value of L_d, becoming maximum for $L_d = 0$. The lowest value of L_d is also determined by the parity selection rule. If the parity of the state of the core and that of the final nucleus are different, the p-capture will contribute most, whereas if the parity of the state of the core is the same as that of the final nucleus, the S-cpature contributes most to the heavy particle stripping cross section. In our evaluation, we have used this fact and have considered the contribution only from the lowest L_d.

5. Evaluation of the Direct Amplitude

Expressions for the direct stripping amplitude have been given by several authors [11]). We shall only give the expressions for D in the LS- and jj-coupling schemes. We write

$$D = G_D R_D \tag{17}$$

where G_D contains all the geometrical factors and depends upon the mode of angular momentum coupling. In the LS-coupling scheme G_D is given by

$$G_D = \sum (-i)^{l_p} 4\pi \{(2l_p+1)\}^{\frac{1}{2}} Z^*_{l_p m_p}(\mathbf{q}_t)(-)^{L_i - L_f + I_i - I_f + 1} \begin{bmatrix} I_i & l_p & I_f \\ N_i & m_p & N_f \end{bmatrix}$$
$$\times \langle [\lambda_i] L_i S_i T_i; l_p | \} [\lambda_f] L_f S_f T_f \rangle U(\sigma_n \sigma_p I_i J_i; S_d Z) U(l_p Z I_f \sigma_n; J_f I_i) \quad (18)$$
$$\times U(l_p L_i J_f S_f; L_f Z) U(S_i L_i \sigma_p Z; J_i S_f) \begin{bmatrix} T_i & T_p & T_f \\ M_{T_i} & M_{T_p} & M_{T_f} \end{bmatrix} \begin{bmatrix} T_n & T_p & T_d \\ M_{T_n} & M_{T_p} & M_{T_d} \end{bmatrix}$$

where l_p is the angular momentum of the orbit in which the proton has been captured, and $\langle [\lambda_i] L_i S_i T_i; l_p | \} [\lambda_f] L_f S_f T_f \rangle$ is a single particle coefficient of fractional parentage. The quantity

$$\mathbf{q}_t = \mathbf{K}_i - \frac{A}{A+1} \mathbf{K}_f$$

is the change in the momentum of the target nucleus.

In the jj-coupling scheme, G_D becomes

$$G_D = \sum (-i)^{l_p} 4\pi (2l_p+1)^{\frac{1}{2}} Z^*_{l_p m_p}(\mathbf{q}_t)(-)^{l_p + \sigma_p - j_p} \begin{bmatrix} I_i & l_p & I_f \\ N_i & m_p & N_f \end{bmatrix}$$
$$\times \left\{ \frac{(2J_f+1)(2S_d+1)}{(2I_f+1)(2\sigma_p+1)} \right\}^{\frac{1}{2}} \langle [\lambda_i] J_i T_i; j_p | \} [\lambda_f] J_f T_f \rangle \begin{bmatrix} J_f & J_i & j_p \\ \sigma_n & S_d & \sigma_p \\ I_f & I_i & l_p \end{bmatrix} \quad (19)$$
$$\times \begin{bmatrix} T_i & T_p & T_f \\ M_{T_i} & M_{T_p} & M_{T_f} \end{bmatrix} \begin{bmatrix} T_n & T_p & T_d \\ M_{T_n} & M_{T_p} & M_{T_d} \end{bmatrix}.$$

The radial integral is separated into two parts and is written as

$$R_D = R_{D1} R_{D2}$$

where

$$R_{D1} = \int_0^\infty U_0(r_{pn}) j_0(q_n r_{pn}) r_{pn}^2 \, dr_{pn},$$
$$R_{D2} = \int_{R_2}^\infty U_{l_p}(r_{pt}) V_{pt} j_{l_p}(q_t r_{pt}) r_{pt}^2 \, dr_{pt}. \quad (20)$$

Here, $\mathbf{q}_n = \mathbf{K}_f - \frac{1}{2}\mathbf{K}_i$ is the momentum change of the outgoing neutron. The integral R_{D1} was calculated using for the deuteron wave function a Hulthén function of the form

$$U_0(r_{pn}) = N \left\{ \frac{e^{-\alpha r_{pn}} - e^{-\beta r_{pn}}}{r_{pn}} \right\}, \quad (21)$$

where N is the normalization factor and $\beta = 7\alpha = 2.2736$ mesic units. We obtain

$$R_{D1} = N\left\{\frac{1}{\alpha^2+q_n^2} - \frac{1}{\beta^2+q_n^2}\right\}. \tag{22}$$

The integral R_{D2} was evaluated as a cut-off integral, and we write

$$R_{D2} = -\frac{\nu_{lp} R_3^{\frac{1}{2}}}{2M_{pT}} W(R_3 \Lambda_3 q_t l_p), \tag{21}$$

where ν_{lp} and $W(R_3\Lambda_3 q_t l_p)$ are defined as in eqs. (15) and (16).

6. Interference Term

The interference term is DE^*+ED^*. For the case when L_d is zero, the expressions for the interference term in the LS- and jj-coupling schemes are given below.

LS-coupling

$$\begin{aligned} G_I = \sum & 4\pi \langle [\lambda_1] L_1 S_1 T_1; l_p | \} [\lambda_t] L_t S_t T_t \rangle \langle [\lambda_c] L_c S_c T_c; l_n | \} [\lambda_1] L_1 S_1 T_1 \rangle \\ & \times F(L_c S_c T_c; l^2 0 S_d T_d; L_t S_t T_t) P_{l_p}(q_t q_n)(-)^{J_1+l_p+j_n-J_c-1} \\ & \times U(L_c S_c J_t S_d; J_c S_t) U(\sigma_n S_d l_p j_p; \sigma_p j_n) U(J_1 J_t j_n S_d; j_p J_c) \\ & \times \begin{bmatrix} L_1 & l_p & L_t \\ S_1 & \sigma_p & S_t \\ J_1 & j_p & J_t \end{bmatrix} \begin{bmatrix} L_c & l_n & L_1 \\ S_c & \sigma_n & S_1 \\ J_c & j_n & J_1 \end{bmatrix} \begin{bmatrix} T_1 & T_p & T_t \\ M_{T_1} & M_{T_p} & M_{T_t} \end{bmatrix} \begin{bmatrix} T_n & T_p & T_d \\ M_{T_n} & M_{T_p} & M_{T_d} \end{bmatrix} \begin{bmatrix} T_c & T_n & T_1 \\ M_{T_c} & M_{T^n} & M_{T_1} \end{bmatrix} \\ & \times \begin{bmatrix} T_c & T_d & T_t \\ M_{T_c} & M_{T_d} & M_{T_t} \end{bmatrix} \times \left\{\frac{(2J_1+1)(2J_t+1)^2(2S_d+1)}{(2J_c+1)(2\sigma_p+1)}\right\}^{\frac{1}{2}} \times R_D R_E. \end{aligned} \tag{24}$$

jj-coupling

$$\begin{aligned} G_I = \sum & 4\pi \langle [\lambda_1] J_1 T_1; j_p | \{ [\lambda_t] J_t T_t \rangle \langle [\lambda_c] J_c T_c; j_n | \} [\lambda_1] J_1 T_1 \rangle \\ & \times F(J_c T_c; j^2 S_d T_d; J_t T_t) P_{l_p}(q_t q_n)(-)^{J_1+j_n+l_p-J_c-1} \\ & \times U(J_1 j_n J_t S_d; J_c j_p) |U(j_n j_p \sigma_n \sigma_p; S_d l_p)|^2 \begin{bmatrix} T_1 & T_p & T_t \\ M_{T_1} & M_{T_p} & M_{T_t} \end{bmatrix} \\ & \times \begin{bmatrix} T_c & T_n & T_1 \\ M_{T_c} & M_{T_n} & M_{T_1} \end{bmatrix} \begin{bmatrix} T_n & T_p & T_d \\ M_{T_n} & M_{T_p} & M_{T_d} \end{bmatrix} \begin{bmatrix} T_c & T_d & T_t \\ M_{T_c} & M_{T_d} & M_{T_t} \end{bmatrix} \\ & \times \left\{\frac{(2J_1+1)(2J_t+1)(2j_n+1)^2}{(2S_d+1)(2l_p+1)(2J_c+1)}\right\}^{\frac{1}{2}} R_D R_E. \end{aligned} \tag{25}$$

For the case $L_d = 0$, the interference term is non-vanishing only for $l_p = l_n$, because of the orthogonality of the Clebsch-Gordan coefficients

$$\begin{bmatrix} I_1 & l_p & I_t \\ N_1 & m_p & N_t \end{bmatrix} \quad \text{and} \quad \begin{bmatrix} I_1 & l_n & I_t \\ N_1 & -m_n & N_t \end{bmatrix}.$$

Thus only in cases when the captured proton enters the same orbit as that of the emerging proton is the interference term non-vanishing [6]). The phase of the interference term depends upon the spatial antisymmetry of the two exchanging neutrons. In the case of the reaction O^{16}(d, p)O^{17} for instance, the two exchanging protons must have the same spin projections, and hence must be spatially antisymmetric. The above arguments regarding the phase of the interference term would be true if strictly LS-coupling is valid. In case of a departure from the LS-coupling scheme, the phase of the interference term becomes dependent on the mode of angular momentum coupling in the nuclear wave functions in a more complicated manner.

7. Reduced Widths

For the sake of convenience in the calculation of angular distributions, we write the total differential cross section as

$$\sigma(\mathbf{K}_f) = (D - \lambda E)^2$$

where D and E are the direct and exchange amplitudes, and the parameter λ contains the coefficients of fractional parentage and the radial widths. It is explicitly given by

$$\lambda = \frac{\langle [\lambda_c] L_c S_c T_c; l_n | \} [\lambda_i] L_i S_i T_i \rangle F(L_c S_c T_c; \lambda^2 L_d S_d T_d; L_f S_f T_f) \nu_{l_n} \nu_{L_d}}{\langle [\lambda_i] L_i S_i T_i; l_p | \} [\lambda_f] L_f S_f T_f \rangle \nu_{l_p}} \tag{26}$$

in the LS-coupling scheme. A similar expression is obtained for λ in the jj-coupling scheme.

The coefficients of fractional parentage have been evaluated by Jahn [12]) in the LS-coupling scheme and by Flowers [13]) in the jj-coupling scheme. The dimensionless quantities ν_{l_n}, ν_{L_d} and ν_{l_p} were calculated by assuming a square well of radius which gives the correct binding energy. The quantity $F(L_c S_c T_c; l^2 L_d S_d T_d; L_f S_f T_f)$ will also depend upon the fact that the two particles of the core find a deuteron correlation. The probability that the two particles can form a deuteron was calculated by calculating the overlap of the deuteron wave function with the product of the two single particle wave functions.

The parameter λ was calculated by fitting the theoretically obtained angular distribution with the experimental one. This value of λ was compared with the value obtained by a theoretical calculation made in the manner outlined above. For the reaction O^{16}(d, p)O^{17}, the theoretically calculated value of λ was 0.0368 and the value obtained from least square fitting was 0.05.

8. Comparison of the Theory with Experiments

Comparisons were made with experimentally obtained angular distributions in the case of the following reactions:

$Be^9(d, p)Be^{10}$, $O^{16}(d, p)O^{17}$ and $F^{19}(d, p)F^{20}$.

In all the cases the calculations were made for the case when the final nucleus is left in its ground state. For the second reaction a pure jj-coupling calculation was made, while a configuration mixing calculation was made in the case of the third reaction.

8.1. THE REACTION $Be^9(d, p)Be^{10}$

It was observed by De Jong and Endt [14]) that at low deuteron energies, the angular distribution of outgoing protons in the reaction $Be^9(d, p)Be^{10}$ shows a maximum in the backward hemisphere. The differential cross section is very small at forward angles increasing in the backward direction. There is no maximum observed in the forward hemisphere. To explain this feature of the angular distribution, we assumed a pure exchange mechanism for the reaction. The ground state spin of Be^9 is $\frac{3}{2}^-$ while that of Be^{10} is 0^+. The core Li^8, was assumed to be in a 1^+ state. In the LS-coupling scheme, this assignment of the state of Li^8 would completely forbid the exchange reaction because of the vanishing of the coefficient of fractional parentage $\langle p^4[22]\ L = 0, S = 1, T = 1; p|\}p^5[41] L = 1, S = \frac{1}{2}, T = \frac{1}{2}\rangle$. In the jj-coupling scheme, a calculation of the ratio of the exchange to direct amplitudes made in the manner outlined in the previous section yields a ratio 1 : 4. In the exchange stripping case the proton is emitted from the p-orbit and the deuteron captured in a s-orbit by Li^8 to form Be^{10}. It is the $|j_0^2|$distribution corresponding to the capture of the deuteron in a S-state by Li^8 which produces the desired shape of the angular distribution. We obtained a good agreement with experiment for a deuteron energy of 520 keV, assuming a radius of interaction of 3.1 mesic units (fig. 2).

Our comment regarding the exchange nature of the angular distribution

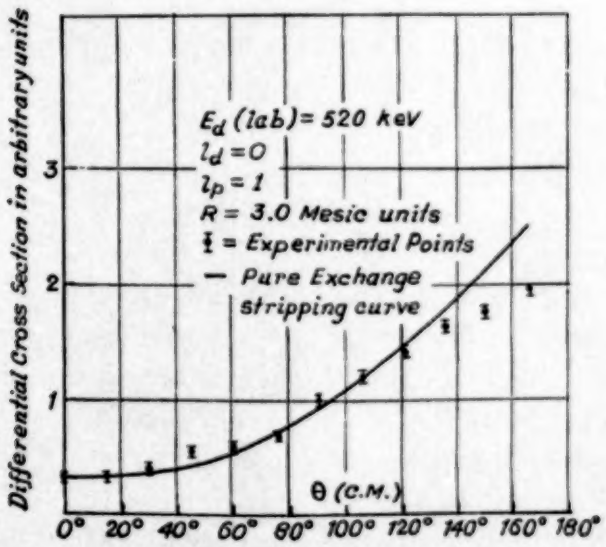

Fig. 2. The angular distribution of ground state protons in the reaction $Be^9(d, p)Be^{10}$.

would be that the wave functions for Li^8, Be^8 and Be^{10} are intermediate coupling wave functions and that there is an accidental cancellation of the direct amplitude.

8.2. THE REACTION $O^{16}(d, p)O^{17}$

Calculations were made for the angular distribution of the ground state protons in the reaction $O^{16}(d, p)O^{17}$ (see ref. [15])), for a deuteron energy of 3.49 MeV. The core N^{15} has a ground state spin of $\frac{1}{2}^-$. The ground state spin of O^{16} is 0^+ and that of O^{17} is $\frac{5}{2}^+$. Hence, in the direct stripping, the neutron is captured in a $l_n = 2$ orbit. In the exchange stripping the proton is emitted from a p-orbit and the deuteron is captured by N^{15} in a p-orbit.

A good agreement is obtained between theory and experiment for a radius of interaction of 3.6 mesic units (fig. 3).

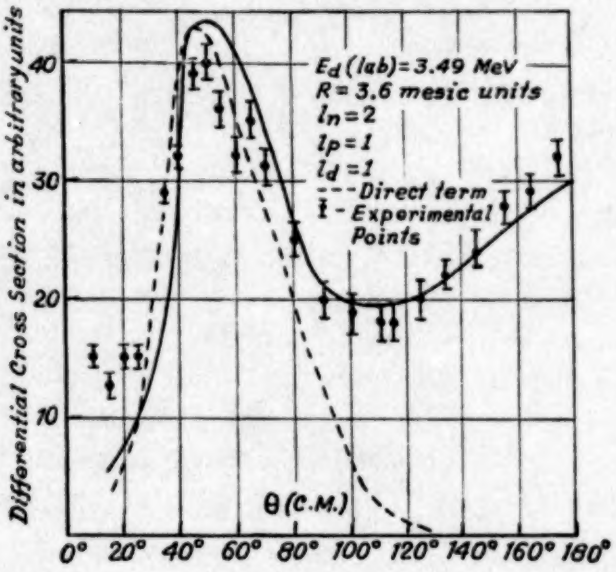

Fig. 3. The angular distribution of ground state protons in the reaction $O^{16}(d, p)O^{17}$.

8.3. THE REACTION $F^{19}(d, p)F^{20}$

It is known that there is a considerable amount of configuration mixing in the region where the 1d-shell begins. Redlich [16]) and Elliott and Flowers [17]) have made configuration mixing calculations for nuclei of masses 18 and 19. Bromley, Bruner and Fulbright [18]) have studied the reaction $F^{19}(d, p)F^{20}$ in the region of angles $5° \leqq \theta \leqq 95°$. They observed two maxima, one at small angles and the other at 50°. They concluded that there is a mixture of $l_n = 0$ and $l_n = 2$ stripping. From the magnitudes of these two maxima it comes out that the probability of a neutron capture in the d-orbit must be about 10 times that of a neutron capture in a S-orbit.

We made a configuration mixing calculation for the ground state of F^{20} using the Hamiltonian of Redlich. In order to make this problem amenable to

calculation, we made the following assumptions:

1) configurations containing more than one $d_{\frac{3}{2}}$ particle may be neglected (this assumption is justified because of the large energy difference in the $d_{\frac{3}{2}}$ and $d_{\frac{5}{2}}$ levels);

2) we have considered as parents of the ground state of F^{20} only the ground state ($J = \frac{1}{2}, T = \frac{1}{2}$) and the first excited state ($J = \frac{5}{2}, T = \frac{1}{2}$) of F^{19}.

These two assumptions reduced the energy matrix to a 13×13 matrix. The ground state wave function of F^{20} obtained after diagonalizing the energy matrix was

$$\begin{aligned}\Psi(J = 1^+, T = 1) &= 0.42|1d_{\frac{5}{2}}^4[211](200)\, J = 1, T = 1\rangle + 0.44|1d_{\frac{5}{2}}^4[211](211)\, J = 1, T = 1\rangle \\ &+ 0.62|1d_{\frac{5}{2}}^3([21](210)\, J = \tfrac{1}{2}, T = \tfrac{1}{2})2s_{\frac{1}{2}};\ J = 1, T = 1\rangle \\ &+ 0.21|1d_{\frac{5}{2}}^3([21](210)\, J = \tfrac{1}{2}, T = \tfrac{1}{2}]1d_{\frac{3}{2}};\ J = 1, T = 1\rangle \\ &+ 0.15|1d_{\frac{5}{2}}2s_{\frac{1}{2}}^3\, J = 1, T = 1\rangle + 0.28|1d_{\frac{5}{2}}^2(J = 1, T = 0)2s_{\frac{1}{2}}^2;\ J = 1, T = 1\rangle \\ &+ 0.32|1d_{\frac{5}{2}}^2(J = 0, T = 1)2s_{\frac{1}{2}}^2;\ J = 1, T = 1\rangle.\end{aligned}$$

The study of the angular distribution in the reaction F^{19}(d, p)F^{20} was extended to angles beyond 90° by Seward, Slaus and Fulbright [19]). The angular distribution was found to be flattish in the forward direction and starts rising beyond 90°.

Our calculations were made including the contribution from heavy particle stripping. The core is O^{18}, taken to be in a 0^+ state. The wave functions for O^{18} and F^{19} were taken from Redlich's calculations. The deuteron is captured in a s-state by O^{18}, while the proton can be emitted from either the s or d state by F^{19}. The probability for an emission from the d-state was found to be negligible.

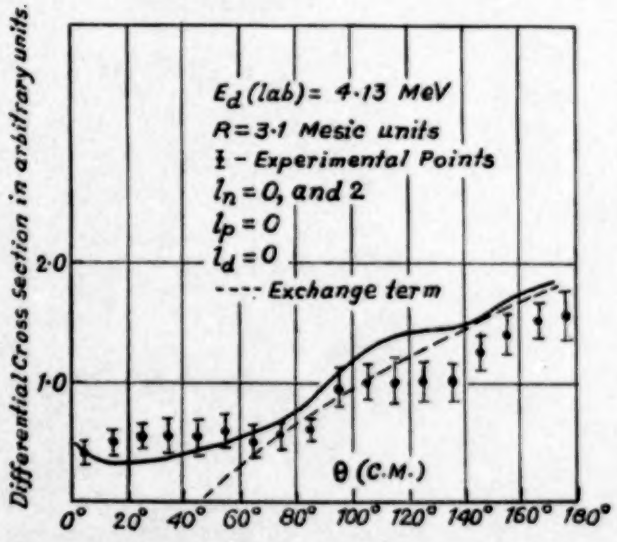
Differential Cross section in arbitrary units.
E_d (lab) = 4·13 MeV
R = 3·1 Mesic units
± - Experimental Points
l_n = 0, and 2
l_p = 0
l_d = 0
---- Exchange term
2·0
1·0
θ (C.M.)
0° 20° 40° 60° 80° 100° 120° 140° 160° 180°

Fig. 4. The angular distribution of ground state protons in the reaction F^{19}(d, p)F^{20}.

The calculated wave function of the ground state of F^{20} was not able to reproduce the desired feature of a larger d-state capture of the neutron in the direct stripping case. We can only conclude that the Hamiltonian assumed is not the correct Hamiltonian.

Assuming that the probability of a d-state capture of the neutron is 10 times larger than its capture in a b-state calculations were made and a good agreement has been obtained (fig. 4).

The authors are indebted to Professor A. K. Saha for many helpful discussions.

References

1) S. T. Butler, Proc. Roy. Soc. A **208** (1951) 559
2) A. B. Bhatia, K. Huang, R. Huby and H. C. Newns, Phil. Mag. **43** (1952) 485
3) L. I. Schiff, Quantum Mechanics (McGraw-Hill, 1948) 77
4) L. Madansky and G. E. Owen, Phys. Rev. **99** (1955) 1608; **105** (1957) 1766
5) N. T. S. Evans and A. P. French, Phys. Rev. **109** (1958) 1272
6) A. P. French, Phys. Rev. **107** (1957) 1655
7) T. Kamamuri, R. Nakasima and S. Takagi, Theor. Phys. (Japan) **17** (1957) 306
8) T. Fulton and G. E. Owen, On stripping Type Nuclear Reactions, AEC contract AT (30-1), 2028, Appendix A
9) H. A. Jahn, Proc. Roy. Soc. A **205** (1951) 192
10) P. B. Daitch and J. B. French, Phys. Rev. **87** (1952) 900 (L)
11) See for instance T. Auerbach and J. B. French, Phys. Rev. **98** (1955) 1276 or R. Huby, Prog. Nucl. Phys. **3** (1953); the latter contains all the relevant references.
12) H. A. Jahn, Proc. Roy. Soc. A **205** (1951) 192;
H. A. Jahn and H. van Wierengen, Proc. Roy. Soc. A **209** (1951) 502
13) B. H. Flowers, Proc. Roy. Soc. A **214** (1952) 515
14) D. de Jong, P. M. Endt and L. J. G. Simons, Physica **18** (1952) 676
15) E. Baumgartner and H. W. Fulbright, Phys. Rev. **107** (1957) 219
16) M. G. Redlich, Phys. Rev. **95** (1954) 448
17) J. P. Elliott and B. H. Flowers, Proc. Roy. Soc. A **229** (1955) 536
18) D. A. Bromley, J. A. Bruner and H. W. Fulbright, Phys. Rev. **107** (1957) 159
19) F. D. Seward, I. Slaus and H. W. Fulbright, Phys. Rev. **107** (1957) 159
20) Hasegawa and Ichikawa, Progr. Theor. Phys. **21** (1959) 569

7.A:8.B

Nuclear Physics **17** (1960) 359—376; © *North-Holland Publishing Co., Amsterdam*

Not to be reproduced by photoprint or microfilm without written permission from the publisher

NON-ADIABATIC TREATMENT OF THE SCATTERING OF K^+ MESONS BY NUCLEONS

GRZEGORZ BIAŁKOWSKI and ANDRZEJ JUREWICZ

Institute for Theoretical Physics, Warsaw University, Warsaw, Poland

Received 8 February 1960

Abstract: Assuming pseudoscalar Yukawa coupling between K mesons and baryons, calculations of the K^+ nucleon phase shifts have been performed. The method used is the three-dimensional Tamm-Dancoff approximation. Calculations have been performed for the $S_{\frac{1}{2}}$, $P_{\frac{1}{2}}$ and $P_{\frac{3}{2}}$ waves in the $T = 1$ and $T = 0$ states. The corresponding phase shifts and the total cross sections for K^+ on p and K^+ on n, elastic and charge exchange scattering are presented. The only parameters to be determined from experimental data are the coupling constants G^2 and $\mathcal{G}^2$. A discussion of the values of these quantities is given.

1. Introduction

Recent experimental results [1]) concerning the scattering of K mesons by nucleons show the following features of this process:

a) K^+ *on* p *scattering*

In this case we have the best information. The total cross section remains nearly constant over the wide energy region from 0 up to about 1.5 GeV of K^+ kinetic energy in the laboratory frame. It changes from nearly 14 mb at low energies up top a maximum value of 20 mb at about 800 MeV and then falls down. The experimental data show the interaction to be repulsive. The angular distribution is isotropic in the c.m. system at low energies. The phase analysis leads us to the conclusion that the best fit to the experimental data can be obtained with a large negative S phase shift and the P phase shifts nearly vanishing.

b) K^+ *on* n *scattering*

In this case both elastic and charge exchange scattering are allowed. The experimental data come from K^+ scattering on nuclei and till now are not conclusive to such an extent as the previously discussed K^+-p data.

At low energies the total cross section for elastic K^+-n scattering is smaller by several mb than that for the K^+-p process, whereas at high energies they are presumably of the same value approximately.

The charge exchange ($K^+ + n \rightarrow K^0 + p$) scattering is much smaller than the elastic one, especially in the low energy region. The angular distribution probably is not isotropic. This fact can be explained in terms of strong P wave interaction in the $T = 0$ state.

The problem of scattering of K mesons by nucleons has been discussed theoretically by several authors [2]). Since their results are not in good agreement with the present experimental data, we have attempted to calculate K^+ nucleon phase shifts in a perhaps more accurate manner.

The method we used is the three-dimensional Tamm-Dancoff approximation[3]) It is well known that this method has not been fully successful in the probem of scattering of pions by nucleons. It has seemed to us, however, that the case of K^+ mesons shows some features which perhaps enable us to apply this method. The main difference between K^+-N and π-N interaction is the principle of associated production which in the first case excludes just these graphs which in the second case (see sect. 2) lead to well-known difficulties. Further, in accordance with conclusions of Morpurgo and Touschek [4]), we may expect in our case better agreement of theoretical results with the experimental data than in the case of π-N scattering because of the repulsive character of our interaction.

It should be noted that in our case the fixed source theory is not expected to fit experimental data because of the fact that it favours P states. We now believe that the parity of K^+ is odd with respect to the YN pair (Y denotes Λ or Σ hyperon), which seems to be confirmed, among others, by recent results concerning the photoproduction of K^+.

In our previous paper [5]) we have given preliminary results for the scattering in the $T = 1$ state. Now, more extensive data on this process will be presented, including also the $T = 0$ state.

2. The Derivation of the Integral Equation

In order to derive the integral equation for the process under consideration, we may use the formalism given by Królikowski and Rzewuski [6]). In this formalism the equation of state in momentum space is

$$(H_0 - E)|\Phi_1\rangle = U(E)|\Phi_1\rangle, \tag{1}$$

where H_0 denotes the hamiltonian of free fields, E the total energy of the system $|\Phi_1\rangle$ a projection of the state vector on the subspace of states containing 1 K meson and 1 nucleon with arbitrary momenta, isospins and spins.

In the lowest approximation we get

$$U(E) = P_1 H_1 P_\perp \left(\frac{\mathrm{P}}{E - H_0}\right) P_\perp H_1 P_1, \tag{2}$$

where

$$P_1 = |\Phi_1\rangle\langle\Phi_1|, \qquad P_\perp = 1 - P_1.$$

Further, H_1 is the interaction Hamiltonian in the well known form

$$H_1 = G\int \bar{\psi}_\Lambda \gamma_5 \psi_N \varphi_K^* \, \mathrm{d}v + \mathscr{G}\int \bar{\psi}_\Sigma{}^a \gamma_5 \psi_N \tau_a \varphi_K^* \, \mathrm{d}v + \mathrm{H.c.} \tag{3}$$

We assume that the spin of K is 0 and its parity odd with respect to ΛN and ΣN pairs. The symbol P in eq. (2), denoting the Cauchy principal value, means that we have assumed the standing wave boundary condititon. No attempt has been made to include interaction with other particles, in particular 3- or 4-boson interactions.

Proceeding in the usual way, we obtain in the centre of mass system the following integral equation for the scattering amplitude $f^{\alpha\beta}(\mathbf{p})$ (in the units $\hbar = c = 1$):

$$[E-E(p)-\Omega(p)]f^{\beta\alpha}(\mathbf{p}) = \frac{G^2}{4\pi}\int \mathrm{d}_3 q L_\Lambda(\mathbf{p},\mathbf{q}) f^{\alpha\beta}(\mathbf{q}) + \frac{G^2}{4\pi} S_\Lambda(\mathbf{p}) f^{\beta\alpha}(\mathbf{p})$$

$$+ \frac{\mathscr{G}^2}{4\pi}\int \mathrm{d}_3 q L_\Sigma(\mathbf{p},\mathbf{q}) \tau_\rho{}^{\mu\alpha}\tau_\rho{}^{\sigma\beta} f^{\mu\sigma}(\mathbf{q}) + \frac{\mathscr{G}^2}{4\pi} S_\Sigma(\mathbf{p}) \tau_\rho{}^{\mu\beta}\tau_\rho{}^{\sigma\alpha} f^{\sigma\alpha}(\mathbf{q}), \quad (4)$$

where

$$L_\Lambda(\mathbf{p},\mathbf{q}) = (4\pi^2)^{-1} mM\Lambda^+(\mathbf{p})[\mathscr{E}(\mathbf{p}+\mathbf{q})]^{-1}[E(p)E(q)\Omega(p)\Omega(q)]^{-\frac{1}{2}}$$

$$\times\left[\Pi^+(-\mathbf{p}-\mathbf{q})\frac{\mathrm{P}}{E(p)+E(q)+\mathscr{E}(\mathbf{p}+\mathbf{q})-E} + \Pi^-(\mathbf{p}+\mathbf{q})\frac{\mathrm{P}}{\Omega(p)+\Omega(q)+\mathscr{E}(\mathbf{p}+\mathbf{q})-E}\right], \quad (5)$$

and

$$(4\pi^2)S_\Lambda(\mathbf{p}) = \int \mathrm{d}_3 q mM[\mathscr{E}(\mathbf{p}+\mathbf{q})]^{-1}\Big\{[E(q)\Omega(p)]^{-1}\,\mathrm{Tr}\,(\Pi^-(-\mathbf{p}-\mathbf{q})\Lambda^-(\mathbf{q}))$$

$$\cdot\frac{\mathrm{P}}{E-E(p)-E(q)-\mathscr{E}(\mathbf{p}+\mathbf{q})} - [E(p)\Omega(q)]^{-1}\Lambda^+(\mathbf{q})\Pi^-(\mathbf{p}+\mathbf{q})\frac{\mathrm{P}}{E-\mathscr{E}(\mathbf{p}+\mathbf{q})-\Omega(p)-\Omega(q)}\Big\}$$

$$+\int \mathrm{d}_3 q mM[\mathscr{E}(\mathbf{p}+\mathbf{q})]^{-1} \quad (6)$$

$$\cdot\Big\{[E(q)\Omega(p)]^{-1}\,\mathrm{Tr}\,(\Lambda^-(-\mathbf{q})\Pi^-(\mathbf{p}+\mathbf{q}))\frac{\mathrm{P}}{E-E(p)-E(q)-2\Omega(p)-\mathscr{E}(\mathbf{p}+\mathbf{q})}$$

$$-[E(p)\Omega(q)]^{-1}\Lambda^+(\mathbf{p})\Pi^+(-\mathbf{p}-\mathbf{q})\frac{\mathrm{P}}{E-2E(p)-\Omega(p)-\Omega(q)-\mathscr{E}(\mathbf{p}+\mathbf{q})}\Big\}$$

$$+2\int \mathrm{d}_3 q\mathrm{d}_3 q' mM\delta(0)[E(q')\Omega(q)\mathscr{E}(\mathbf{q}+\mathbf{q}')]^{-1}\frac{\mathrm{P}}{E-E(p)-\Omega(p)-E(q')-\Omega(q)-\mathscr{E}(\mathbf{q}'+\mathbf{q})}$$

$$\cdot[\mathrm{Tr}(\Pi^+(-\mathbf{q}-\mathbf{q}')\Lambda^+(\mathbf{q}')) + \mathrm{Tr}\,(\Lambda^-(\mathbf{q}')\Pi^-(-\mathbf{q}-\mathbf{q}'))].$$

Here, m, $E(p)$; μ, $\Omega(p)$; M, $\mathscr{E}(p)$ are the masses and relativistic energies of N, K and Λ, respectively; $\Lambda^\pm(\mathbf{p})$ and $\Pi^\pm(\mathbf{p})$ are the projection operators for N and Λ; for example, $\Lambda^\pm(\mathbf{p}) = (2m)^{-1}(\pm\gamma_0 E(p)\pm\mathbf{p}\cdot\boldsymbol{\gamma}+m)$. One can obtain L_Σ and S_Σ from eqs. (5) and (6) respectively, by replacing M by $\mathscr{M}$ (the mass of Σ) everywhere. The Greek indices denote isobaric states and the convention

of summation has been adopted for them. We should note that in the scattering amplitude $f^{\alpha\beta}(\mathbf{p})$ the summation over directions of the nucleon spin has been performed.

In eq. (5) the two terms of the sum correspond to the processes of figs. 1a and 1b.

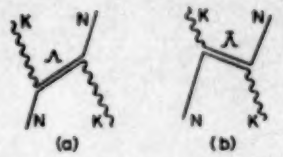

Fig. 1. Graphs of the processes contributing to eq. (5).

In eq. (6) we have the self energy processes of figs. 2a—2f.

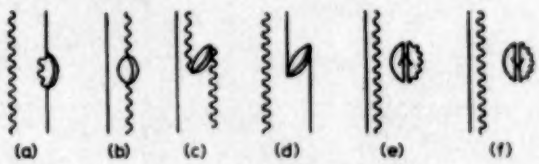

Fig. 2. Graphs of the self energy processes of eq. (6).

Notice that in eq. (5) there are no processes of the type of figs. 3a, 3b leading to self energy parts when iterated. This means that $L_A(\mathbf{p}, \mathbf{q})$ contains convergent terms only. The divergent terms arising in the equation are those appearing in eq. (6).

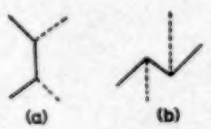

Fig. 3. Graphs of processes not contributing to eq. (5).

Eq. (5) contains just the same terms as those which arise when the new Tamm-Dancoff method is applied to the K^+N scattering (cf. ref.[7])). It is well-known that in the NTD method no vacuum self energy terms (those of figs. 2e and 2f) would appear. On the other hand, we might renormalize the remaining self energy terms if we believe in the renormalization of the new Tamm-Dancoff method. However, we shall omit the resulting corrections, considering all the masses and coupling constants as renormalized ones. In this case the difference between the processes corresponding to figs. 2a, . . ., 2d in the old and new Tamm-Dancoff method is of no importance. In consequence we shall only take into account the terms of the integral equation defined by eq. (5). The absence of processes corresponding to figs. 3a and 3b has also the consequence that no difficulty arises in our case with respect to the crossing symmetry, in contradistinction to the case of π-N scattering.

3. Separation of Angular Variables and Isospin States

The separation of angular variables has been performed just in the same manner as in the paper by Dyson *et al.* [3]). Finally, we obtain a one-dimensional integral equation for the scattering amplitude $f^{\alpha\beta}(p)$ with definite total angular momentum and parity. In this case, any state with definite total angular momentum and parity has also its orbital momentum well defined.

Since the amplitude $f^{\alpha\beta}(p)$ is labelled by the isospins of the nucleon and K meson, it is not in general an eigenfunction of the total isospin of the system. In our case this quantity has two eigenvalues, namely 0 and 1. Corresponding eigenfunctions are antisymmetric and symmetric combinations of $f^{\alpha\beta}(p)$, respectively. As is well known, the matrix $\tau_\rho{}^\beta \tau_\rho{}^\gamma$ is diagonal in the eigenstates of the total isospin and has eigenvalues 1 for $T = 1$ and -3 for $T = 0$.

Thus, by simple addition and subtraction of integral equation (4) we may obtain the equation for amplitudes with definite total isospin ($f_0(p)$ and $f_1(p)$). Then, the amplitudes for the three observed processes are

$$\begin{aligned} &\text{for} \quad K^+ + p \to K^+ + p : f_1(p) \\ &\text{for} \quad K^+ + n \to K^+ + n : \tfrac{1}{2}(f_1(p) + f_0(p)) \\ &\text{for} \quad K^+ + n \to K^0 + p : \tfrac{1}{2}(f_1(p) - f_0(p)). \end{aligned} \tag{7}$$

The resulting integral equations are

$$[E - E(p) - \Omega(p)] f_1(p) = \frac{G^2}{4\pi} \mathrm{P} \int K_A(p, q) f_1(q) \mathrm{d}q + \frac{\mathscr{G}^2}{4\pi} \mathrm{P} \int K_\Sigma(p, q) f_1(q) \mathrm{d}q \tag{8}$$

and

$$[E - E(p) - \Omega(p)] f_0(p) = -\frac{G^2}{4\pi} \mathrm{P} \int K_A(p, q) f_0(q) \mathrm{d}q + \frac{3\mathscr{G}^2}{4\pi} \mathrm{P} \int K_\Sigma(p, q) f_0(q) \mathrm{d}q, \tag{9}$$

where

$$\begin{aligned} K_A(p, q) &= (4\pi)^{-1} q^2 [E(p) E(q) \Omega(p) \Omega(q)]^{-\frac{1}{2}} \\ &\times \Big\{ [E(p) + m][(M - 2m + E) N_\beta(b) + (E(p) + E(q) + \Omega(p) + \Omega(q) + M - 2m - E) N_\beta(d)] \\ &+ \frac{pq}{E(q) + m} [(2m - M + E) N_\gamma(b) + (E(p) + E(q) + \Omega(p) + \Omega(q) + 2m - M - E) N_\gamma(d)] \Big\}. \end{aligned} \tag{10}$$

Here $b = E(p) + E(q) - E$, $d = \Omega(p) + \Omega(q) - E$, and $\beta = 0$, $\gamma = 1$; $\beta = 1$, $\gamma = 0$; $\beta = 1$, $\gamma = 2$ in the $S_{\frac{1}{2}}$, $P_{\frac{1}{2}}$ and $P_{\frac{3}{2}}$ states, respectively. Further,

$$N_0(b) = (2pq)^{-1} \ln \frac{\mathscr{E}(p+q) + b}{\mathscr{E}(p-q) + b}, \tag{11a}$$

$$\begin{aligned} N_1(b) = &-(2pq)^{-1}(M^2 + p^2 + q^2 - b^2) N_0(b) \\ &+ (2pq)^{-1}\{1 - 2b[\mathscr{E}(p+q) + \mathscr{E}(p-q)]^{-1}\} \end{aligned} \tag{11b}$$

$$N_2(b) = -3(4pq)^{-1}(M^2+p^2+q^2-b^2)N_1(b) \\ -2^{-1}N_0(b)+2b[\mathscr{E}(p+q)+\mathscr{E}(p-q)]^{-3}. \quad (11c)$$

We remind that $K_\Sigma(p, q)$ may be obtained from $K_\Sigma(p, q)$ by replacing M by $\mathscr{M}$ everywhere.

4. Non-Singular Amplitude

If $f(p)$ were a regular function, the left sides of the equations (8) and (9) would vanish for $p = p_0$, where p_0 is a root of the equation $E(p_0)+\Omega(p_0) = E$. Since the right side in general does not vanish identically for $p = p_0$, the amplitude must be singular for $p = p_0$. The amplitude has to be of the form

$$f(p) = \delta(E-E(p)-\Omega(p))+\mathrm{P}\frac{\varphi(p)}{E-E(p)-\Omega(p)}, \quad (12)$$

according to the previously assumed standing wave boundary condition; $\varphi(p)$ denotes here the non-singular amplitude connected with the phase shift in the following way:

$$\varphi(p_0) = -\frac{1}{\pi}\operatorname{tg}\delta. \quad (13)$$

In this way we obtain from eq. (8) the integral equation for $\varphi(p)$ in a $T = 1$ state:

$$\varphi(p) = \frac{G^2}{4\pi}\varphi_{0\Lambda}(p)+\frac{\mathscr{G}^2}{4\pi}\varphi_{0\Sigma}(p) \\ +\mathrm{P}\int dq[E-E(q)-\Omega(q)]^{-1}\left[\frac{G^2}{4\pi}K_\Lambda(p, q)+\frac{\mathscr{G}^2}{4\pi}K_\Sigma(p, q)\right]\varphi(q). \quad (14)$$

The form of the equation for the $T = 0$ state is obvious:

$$\varphi_{0\Lambda}(p) = K_\Lambda(p, p_0)\frac{E(p_0)\Omega(p_0)}{Ep_0}. \quad (15)$$

In the same way $\varphi_{0\Sigma}$ may be obtained from K_Σ. The physical meaning of $\varphi_0(p)$ consists in describing the process in the first Born approximation.

5. General Properties of the Integral Equation

The kernel of the integral equation (14) may have singularities of two kinds. The first is connected to the denominator

$$M(q) = E(q)+\Omega(q)-E. \quad (16)$$

This singularity appears in the kernel independently of the value of E. In the further calculations this singularity has been taken into account exactly.

Singularities of the second kind arise from the logarithms contained in the functions N of eqs. (11). The typical singular factor is

$$\ln \frac{\mathscr{E}(p+q)+\Omega(p)+\Omega(q)-E}{\mathscr{E}(p-q)+\Omega(p)+\Omega(q)-E}.$$

This logarithm may have two kinds of singular points, arising when the numerator or the denominator vanishes. As may readily be seen, there are no singularities in the energy region up to $E = M+2\mu$. In a similar way we may see that also the other logarithms are not singular in this region, since their singularities arise for energies $E \geqq M+2m$, $E \geqq \mathscr{M}+2\mu$ and $E \geqq \mathscr{M}+2m$. We notice that for $E = M+2\mu$ the production of an additional K meson becomes possible: $\mathrm{K}+\mathrm{N} \to \mathrm{K}+\Lambda+\bar{\mathrm{K}}$. In the region above $E = M+2\mu$ the kernel of the equation has an imaginary part. This fact should be interpreted as indicating a decrease of the amplitude $f(p)$ in favour of three-particle amplitudes. The energy $E = M+2\mu$ corresponds to the kinetic energy of the K meson in the lab. system of about 1260 MeV (Notice that in the case of π mesons this energy was about 170 MeV). Since this region is large enough, we may confine ourselves to the energies which do not exceed this value.

We may also study the behaviour of the kernel in the neighbourhood of 0 and ∞ with respect to p and q. This behaviour will be important when we shall choose the best approximation for the kernel. One obtains the results of table 1 for the three lowest orbital states. The function $K(p,q)$ is positive in the quadrant $p > 0$, $q > 0$, for the $S_{\frac{1}{2}}$ and $P_{\frac{1}{2}}$ states, whereas for the $P_{\frac{3}{2}}$ state it changes sign, being positive in the neighbourhood of 0 and negative elsewhere.

TABLE 1

Behaviour of the kernel in eq. (14)

	$p \to 0$	$p \to \infty$	$q \to 0$	$q \to \infty$
The kernel in the $S_{\frac{1}{2}}$ state behaves as	constant	$\frac{1}{p}$	q^2	$\frac{1}{q}$
The kernels in the $P_{\frac{1}{2}}$ and $P_{\frac{3}{2}}$ states behave as	$\frac{1}{p}$	$\frac{1}{p}$	q	constant

We may conclude that in the $S_{\frac{1}{2}}$ and $P_{\frac{1}{2}}$ states the interaction is repulsive, and the solution $\varphi(p)$ of the equation lies below the $\varphi_0(p)$ function. This means that (for the same value of the coupling constant) we obtain smaller cross sections than in the Born approximation. Thus, we may expect that it will be necessary to increase the coupling constant in comparison with the result obtained in a perturbation calculation, in order to obtain a good fit to the experimental data.

In the $P_{\frac{1}{2}}$ state the situation is quite different. The attractive character of the interaction causes the participation of this state to be increased.

Finally, we give in table 2 the behaviour of $\varphi_0(p)$ in the neighbourhood of 0 and ∞.

TABLE 2

Behaviour of the Born-amplitude $\varphi_0(p)$

	$p \to 0$	$p \to \infty$
In the $S_{\frac{1}{2}}$ state $\varphi_0(p)$ behaves as	constant	$\frac{1}{p}$
In the $P_{\frac{1}{2}}$ and $P_{\frac{3}{2}}$ states $\varphi_0(p)$ behaves as	$\frac{1}{p}$	$\frac{1}{p}$

6. Semi-Numerical Solution of the Equation

An exact solution of the equation (14) does not seem to be available because of the complicated structure of the kernel and $\varphi_0(p)$. We must therefore choose an approximate method, which has to fulfil the following conditions: (1) it should lead to integrals analytically performable; (2) it should be correct enough, namely it should be able to preserve the exact behaviour of the kernel and $\varphi_0(p)$ in the neighbourhood of 0 and ∞ and in the neighbourhood of the only singularity occurring at the point where $M(q) = 0$.

For this purpose we approximate the kernel of the equation by a degenerate one (of the Pincherle-Goursat type). This approximation has been performed by a semi-numerical method which will be presented later. In order to simplify these calculations, our equation has been slightly transformed in an exact manner .We shall deal with the equation in the $T = 1$ state only (all the transformations given below can be performed in the $T = 0$ state as well). We have

$$\psi(p) = \psi_0(p) + \mathrm{P}\int \mathrm{d}q[E - E(q) - \Omega(q)]^{-1} \left\{\frac{G^2}{4\pi}\bar{K}_\Lambda(p, q) + \frac{\mathscr{G}^2}{4\pi}\bar{K}_\Sigma(p, q)\right\}\psi(q), \quad (16)$$

where

$$\psi(p) = \frac{p}{E(p)}\varphi(p) \quad \text{and} \quad \psi_0(p) = \frac{p}{E(p)}\left[\varphi_{0\Lambda}(p)\frac{G^2}{4\pi} + \frac{\mathscr{G}^2}{4\pi}\varphi_{0\Sigma}(p)\right], \quad (17, 18)$$

whereas

$$\bar{K}(p, q) = \frac{pE(q)}{qE(p)}K(p, q) \text{ for the } S_{\frac{1}{2}} \text{ state,} \quad (19)$$

and

$$\bar{K}(p, q) = \frac{mp}{qE(p)}K(p, q) \text{ for the } P_{\frac{1}{2}} \text{ and } P_{\frac{3}{2}} \text{ states.} \quad (20)$$

The behaviour of $\bar{K}$ and $\psi_0(p)$ is then as listed in table 3.

TABLE 3

Behaviour of $\bar{K}(p, q)$ and $\psi_0(p)$

	$p \to 0$ $(q \to 0)$	$p \to \infty$ $(q \to 0)$
$\bar{K}$ in the $S_{\frac{1}{2}}$ state behaves as	$p(q)$	$\frac{1}{p}$ $\left(\frac{1}{q}\right)$
$\bar{K}$ in the $P_{\frac{1}{2}}$ and $P_{\frac{3}{2}}$ states behaves as	constant	$\frac{1}{p}$ $\left(\frac{1}{q}\right)$
$\psi_0(p)$ in the $S_{\frac{1}{2}}$ state behaves as	p	$\frac{1}{p}$
$\psi_0(p)$ in the $P_{\frac{1}{2}}$ and $P_{\frac{3}{2}}$ states behaves as	constant	$\frac{1}{p}$

With a suitable change of variables:

$$x = \frac{p}{E(p)}, \quad y = \frac{q}{E(q)}, \tag{21}$$

we transform our integral equation from the interval $\langle 0, \infty)$ to the interval $\langle 0, 1)$. In the new variables the equation has the form

$$u(x) = u_0(x) + \mathrm{P}\int_0^1 \mathrm{d}y \left\{ \frac{G^2}{4\pi} H_\Lambda(x, y) + \frac{\mathscr{G}^2}{4\pi} H_\Sigma(x, y) \right\} u(y), \tag{22}$$

where

$$u_0(x) = \frac{G^2}{4\pi} u_{0\Lambda}(x) + \frac{\mathscr{G}^2}{4\pi} u_{0\Sigma}(x), \quad u_0(x) = \psi_0(p(x)), \tag{23}$$

$$H_\Lambda(x, y) = m(1-y^2)^{-\frac{3}{2}}[E(1-y^2)^{\frac{1}{2}} - m - \{y^2(m^2-\mu^2)+\mu^2\}^{\frac{1}{2}}]^{-1} \bar{K}_\Lambda(p(x), q(y)), \tag{24}$$

$$u(x) = \psi(p(x)). \tag{25}$$

Taking into account the behaviour of the kernel H in the neighbourhood of 0 and 1 we approximate it in such a way that

$$\bar{K}_\Lambda(p(x), q(y)) \approx Q(x)Q(y) \sum_{i,j=0}^{3} C_{\Lambda ij} x^i y^j, \tag{26}$$

where

$$Q(x) = \begin{cases} x(1-x^2)^{\frac{1}{2}} & \text{for the } S_{\frac{1}{2}} \text{ state} \\ (1-x^2)^{\frac{1}{2}} & \text{for both P states.} \end{cases} \tag{27}$$

($\bar{K}_\Sigma$ has been approximated in a similar way). In eq. (26), the C_{ij} are numerical coefficients depending on the energy E. They have of course different values for different states.

Notice that vanishing as p in 0 or as p^{-1} in ∞ in the (p, q) plane corresponds to vanishing as x in 0 or as $(1-x)^{\frac{1}{2}}$ in the neighbourhood of 1 in (x, y) plane. In eq. (27) $(1-x^2)^{\frac{1}{2}}$ instead of $(1-x)^{\frac{1}{2}}$ is taken since the resulting integrals are more easy to calculate.

The above approximation is in principle sufficient to solve the equation, but as the integrals to be performed are complicated, we have decided to approximate $u_0(x)$ in a similar way as the kernel:

$$u_{0A}(x) \approx Q(x) \sum_{i=0}^{3} B_{Ai} x^i, \tag{28}$$

where the B_i are numerical coefficients C_{ij}.

The numbers C_{ij} we determine from the condition that the approximate kernel equals the exact one in 16 points lying in the square $0 \leqq x < 1$, $0 \leqq y < 1$; these points have been chosen so as to obtain the best approximation. The coefficients B_i have been calculated in a quite similar manner.

Such an approximation leads to the following form of the solution:

$$u(x) = Q(x) \sum_{i=0}^{3} N_i x^i. \tag{29}$$

The coefficients N depend on E, G^2 and $\mathscr{G}^2$. We have

$$N_i = \frac{G^2}{(4\pi)^2} B_{Ai} + \frac{\mathscr{G}^2}{(4\pi)^2} B_{\Sigma i} + \sum_{k,j=0}^{3} J_{j+k+2-2l} \left\{ \frac{G^2}{(4\pi)^2} C_{Aij} + \frac{\mathscr{G}^2}{(4\pi)^2} C_{\Sigma ij} \right\} N_k \quad (i = 0, 1, 2, 3), \tag{30}$$

where l is the orbital number. In eq. (30) we introduced

$$J_r = \mathrm{P} \int_0^1 \frac{m y^r \, \mathrm{d}y}{(1-y^2)^{\frac{1}{2}} [E(1-y^2)^{\frac{1}{2}} - m - \{y^2(m^2-\mu^2)+\mu^2\}^{\frac{1}{2}}]}. \tag{31}$$

For our purposes we had to calculate J_r with $r = 0, 1, \ldots 8$.

The above integrals have been expressed exactly by a sum of rational and elliptic integrals (of all 3 kinds). The latter have been calculated effectively with the help of expansions given by B. Radon [9]) and A. Erdelyi [10]).

When N_i is calculated, we may obtain the phase shift from the transformed formula (13):

$$\operatorname{tg} \delta = -\pi x_0^{-1} Q(x_0) u(x_0). \tag{32}$$

We remind that the above formulae correspond to the $T = 1$ state. For the $T = 0$ state all the calculations are quite similar.

7. Results

The only parameters still undetermined are the coupling constants G^2 and $\mathscr{G}^2$.

In our preliminary calculations [5]) we have put the masses of Λ and Σ both numerically equal to the mass of Λ. In this case $K_\Lambda = K_\Sigma$ and we deal only with the joint coupling constant $(G^2 + \mathscr{G}^2)/4\pi$ in the $T = 1$ state and $(3\mathscr{G}^2 - G^2)/4\pi$ in the $T = 0$ state.

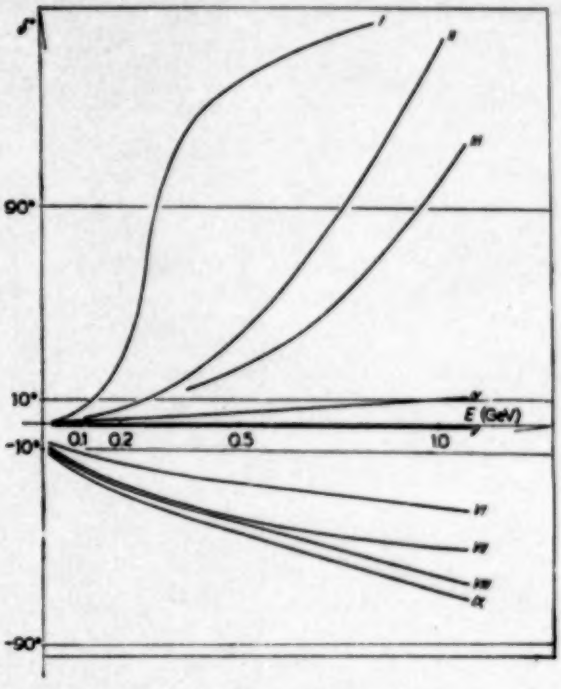

Fig. 4. Calculated phase shifts for $K^+ - p$ scattering vs. kinetic energy of K^+ in the lab. system.
$P_{\frac{1}{2}}$ state: the curves I, II, IV correspond to the masses of Λ and Σ equal to M and to the coupling constants $(G^2+\mathscr{G}^2)/4\pi = 17,\ 12.5,\ 4$; the curve III corresponds to masses of Λ and Σ equal to $\mathscr{M}$ and $(G^2+\mathscr{G}^2)/4\pi = 12.5$.
$P_{\frac{3}{2}}$ state: we give only one example (curve V), corresponding to $(G^2+\mathscr{G}^2)/4\pi = 17$; for the smaller coupling constants the curves would lie between the curve V and the energy axis.
$S_{\frac{1}{2}}$ state: the curves VI, VII, VIII and IX correspond to the same values of the coupling constants and the masses of the hyperons as the curves IV, III, II, I, respectively.

The results in this case (for $T = 1$) are presented in fig. 4. The best fit to the experimental data can be obtained for $(G^2+\mathscr{G}^2)/4\pi = 15$ in the lowest energies up to 300 MeV. In this region the $S_{\frac{1}{2}}$ wave strongly predominates in agreement with the experimental results. However, such a large coupling constant gives wrong results for higher energies, since the $P_{\frac{3}{2}}$ wave contribution increases too rapidly, and a resonance arises at the energy of about 500 MeV. The position of the resonant energy strongly depends on the magnitude of the coupling constant. When it decreases the resonance moves to higher energies. The contribution from the $P_{\frac{1}{2}}$ wave is practically of no importance.

If we put the masses of Λ and Σ both equal to $\mathscr{M}$, the only important changes

when compared with the above results appear in the behaviour of the $P_{\frac{1}{2}}$ phase shift. In this case the resonance is always situated at a higher energy than the resonance discussed above.

Notice that the perturbational coupling constant $(G^2+\mathscr{G}^2)/4\pi \approx 4$ gives too low values for the phase shifts. Finally we should mention that the approximation $M = \mathscr{M}$ would give no charge exchange scattering if we additionally required $G^2 = \mathscr{G}^2$.

Now, the assumption $M = \mathscr{M}$ will be rejected. In this case we have obtained phase shifts in the $T = 1$ and $T = 0$ states for $S_{\frac{1}{2}}$ and $P_{\frac{1}{2}}$ waves. Results for $G^2 = \mathscr{G}^2$ are presented in fig. 5. One can see that even taking into account the

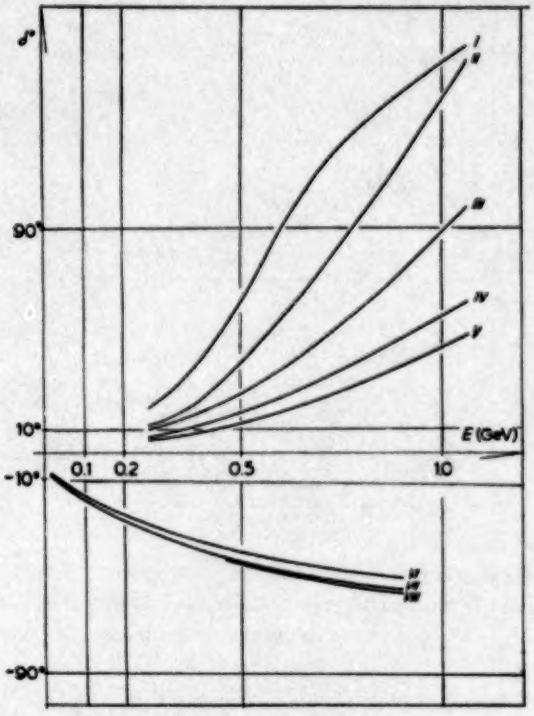

Fig. 5. Calculated phase shifts for $T = 0$ and $T = 1$ states ($M \neq \mathscr{M}$, $G^2 = \mathscr{G}^2$).
$P_{\frac{1}{2}}$ state. $T = 1$: (I) $G^2/4\pi = 7.4$; (II) $G^2/4\pi = 6.8$; (IV) $G^2/4\pi = 5$.
$T = 0$: (III) $G^2/4\pi = 6.8$; (V) $G^2/4\pi = 5$.
$S_{\frac{1}{2}}$ state. $T = 1$: (VI) $G^2/4\pi = 5$; (VII) $G^2/4\pi = 6.8$.
$T = 0$: the curves in this state differ only slightly from those in the $T = 1$ state with the same coupling constants; we give but one example: (VIII) $G^2/4\pi = 6.8$.

difference between the hyperon masses, the charge exchange scattering is in this case small. This is caused by the fact that phase shifts for $T = 1$ and $T = 0$ states are but slightly changed with respect to the results presented in fig. 4. In order to fit the charge exchange data we have taken into account various ratios $G^2/\mathscr{G}^2$. The results for an energy of 100 MeV and $(G^2+\mathscr{G}^2)/4\pi = 13.5$ are given in fig. 6. In our opinion the best result is obtained for $G^2/\mathscr{G}^2 = \frac{8}{3}$. The resulting phase shifts are presented in fig. 7.

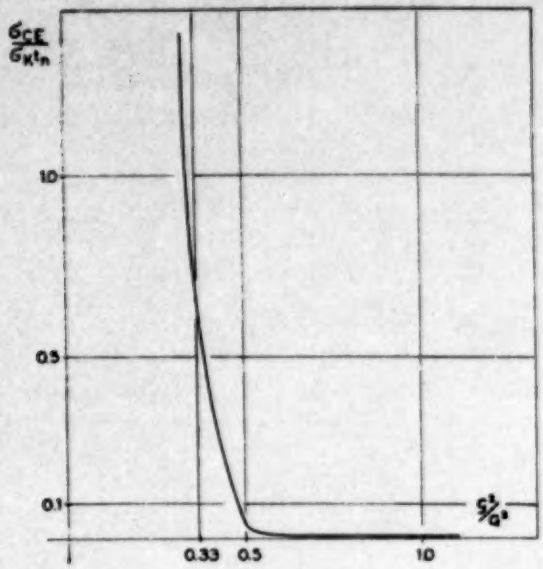

Fig. 6. The ratio $\sigma_{CE}/\sigma_{K^+n}$ vs. $\mathscr{G}^2/G^2$ for a kinetic energy of K+ in the lab. system of 100 MeV and $(G^2+\mathscr{G}^2)/4\pi = 12.5$.

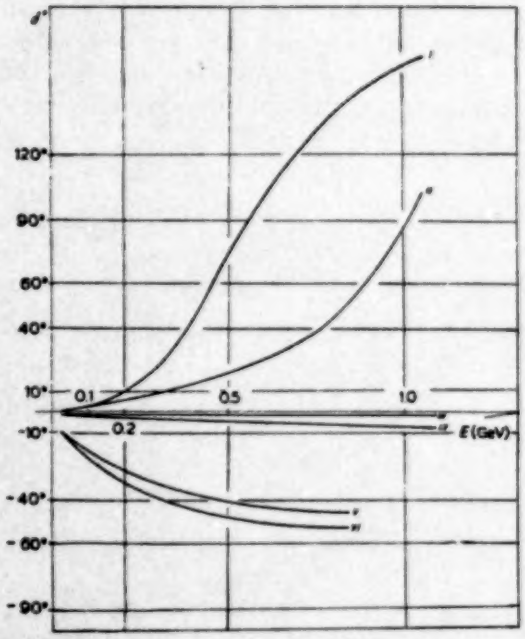

Fig. 7. Calculated phase shifts for $T = 0$ and $T = 1$ states ($M \neq \mathscr{M}$, $3G^2 = 8\mathscr{G}^2$).
$P_{\frac{1}{2}}$ state. $T = 1$: (I) $G^2/4\pi = 10.8$; (II) $G^2/4\pi = 7.3$.
$T = 0$: (III) $G^2/4\pi = 10.8$.
$S_{\frac{1}{2}}$ state. $T = 1$: (V) $G^2/4\pi = 7.3$; (VI) $G^2/4\pi = 10.8$.
$T = 0$: (IV) $G^2/4\pi = 10.8$.

when compared with the above results appear in the behaviour of the $P_{\frac{1}{2}}$ phase shift. In this case the resonance is always situated at a higher energy than the resonance discussed above.

Notice that the perturbational coupling constant $(G^2+\mathscr{G}^2)/4\pi \approx 4$ gives too low values for the phase shifts. Finally we should mention that the approximation $M = \mathscr{M}$ would give no charge exchange scattering if we additionally required $G^2 = \mathscr{G}^2$.

Now, the assumption $M = \mathscr{M}$ will be rejected. In this case we have obtained phase shifts in the $T = 1$ and $T = 0$ states for $S_{\frac{1}{2}}$ and $P_{\frac{1}{2}}$ waves. Results for $G^2 = \mathscr{G}^2$ are presented in fig. 5. One can see that even taking into account the

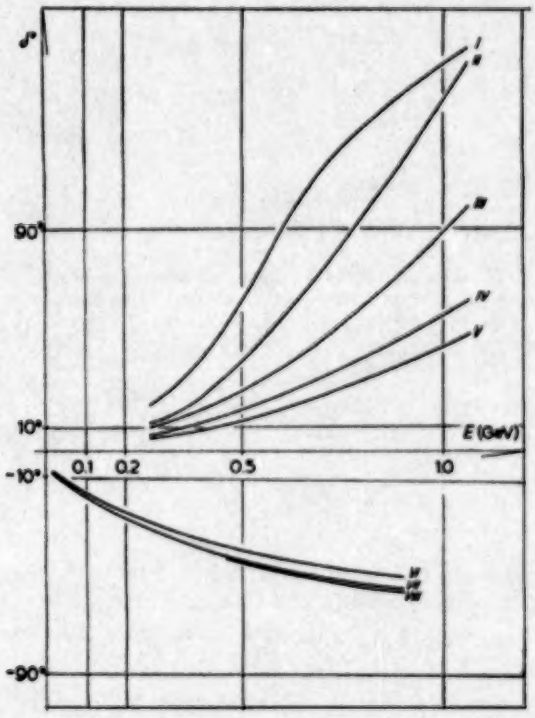

Fig. 5. Calculated phase shifts for $T = 0$ and $T = 1$ states ($M \neq \mathscr{M}$, $G^2 = \mathscr{G}^2$).
$P_{\frac{1}{2}}$ state. $T = 1$: (I) $G^2/4\pi = 7.4$; (II) $G^2/4\pi = 6.8$; (IV) $G^2/4\pi = 5$.
$T = 0$: (III) $G^2/4\pi = 6.8$; (V) $G^2/4\pi = 5$.
$S_{\frac{1}{2}}$ state. $T = 1$: (VI) $G^2/4\pi = 5$; (VII) $G^2/4\pi = 6.8$.
$T = 0$: the curves in this state differ only slightly from those in the $T = 1$ state with the same coupling constants; we give but one example: (VIII) $G^2/4\pi = 6.8$.

difference between the hyperon masses, the charge exchange scattering is in this case small. This is caused by the fact that phase shifts for $T = 1$ and $T = 0$ states are but slightly changed with respect to the results presented in fig. 4. In order to fit the charge exchange data we have taken into account various ratios $G^2/\mathscr{G}^2$. The results for an energy of 100 MeV and $(G^2+\mathscr{G}^2)/4\pi = 13.5$ are given in fig. 6. In our opinion the best result is obtained for $G^2/\mathscr{G}^2 = \frac{8}{3}$. The resulting phase shifts are presented in fig. 7.

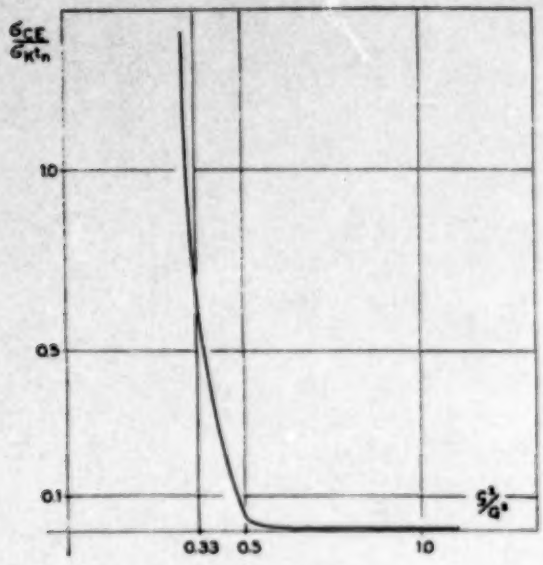

Fig. 6. The ratio $\sigma_{CE}/\sigma_{K^+n}$ vs. $\mathcal{G}^2/G^2$ for a kinetic energy of K+ in the lab. system of 100 MeV and $(G^2+\mathcal{G}^2)/4\pi = 12.5$.

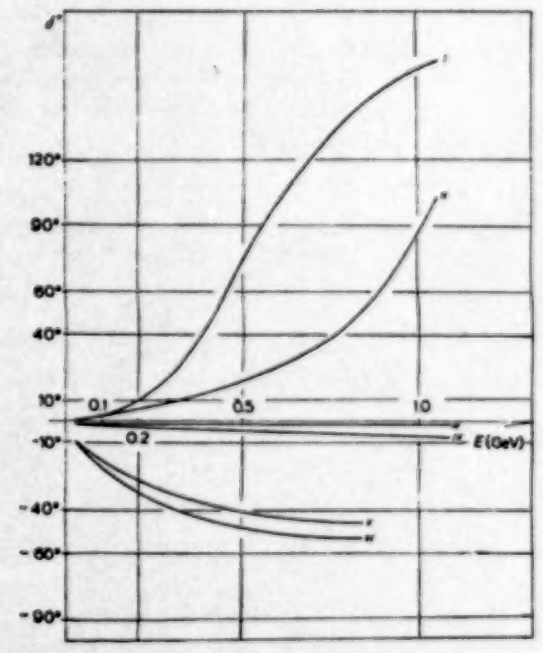

Fig. 7. Calculated phase shifts for $T = 0$ and $T = 1$ states ($M \neq \mathcal{M}$, $3G^2 = 8\mathcal{G}^2$).

$P_{\frac{1}{2}}$ state. $T = 1$: (I) $G^2/4\pi = 10.8$; (II) $G^2/4\pi = 7.3$.
$T = 0$: (III) $G^2/4\pi = 10.8$.

$S_{\frac{1}{2}}$ state. $T = 1$: (V) $G^2/4\pi = 7.3$; (VI) $G^2/4\pi = 10.8$.
$T = 0$: (IV) $G^2/4\pi = 10.8$.

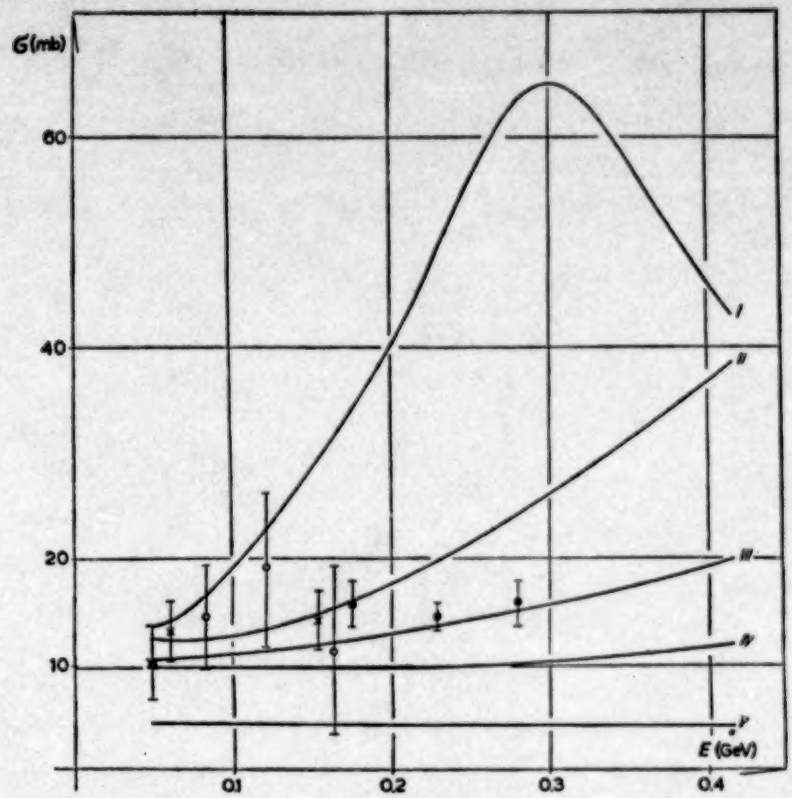

Fig. 8. Calculated and experimental total cross sections in the low energy region for the K^+-p scattering.

I and V. The masses of Λ and Σ both equal to M; (I) $(G^2+\mathcal{G}^2)/4\pi = 17$; (V) $(G^2+\mathcal{G}^2)/4\pi = 4$. II and IV. $M \neq \mathcal{M}$, $3G^2 = 8\mathcal{G}^2$; (II) $G^2/4\pi = 10.8$; (IV) $G^2/4\pi = 7.3$. III. $\mathcal{M} \neq M$, $G^2/4\pi = \mathcal{G}^2/4\pi = 6.8$.

⊖ — Lanutti *et al.* ⊗ — UCLA (Stork *et al.*), ⊕ — Kerth, △ — Meyer *et al.* The best fit to the experimental data observed in case III is in principle not connected to the ratio of the coupling constants but only to their sum, equal to 13.5. It may seem, however, that for the lowest energies this agreement is better for slightly larger coupling constants.

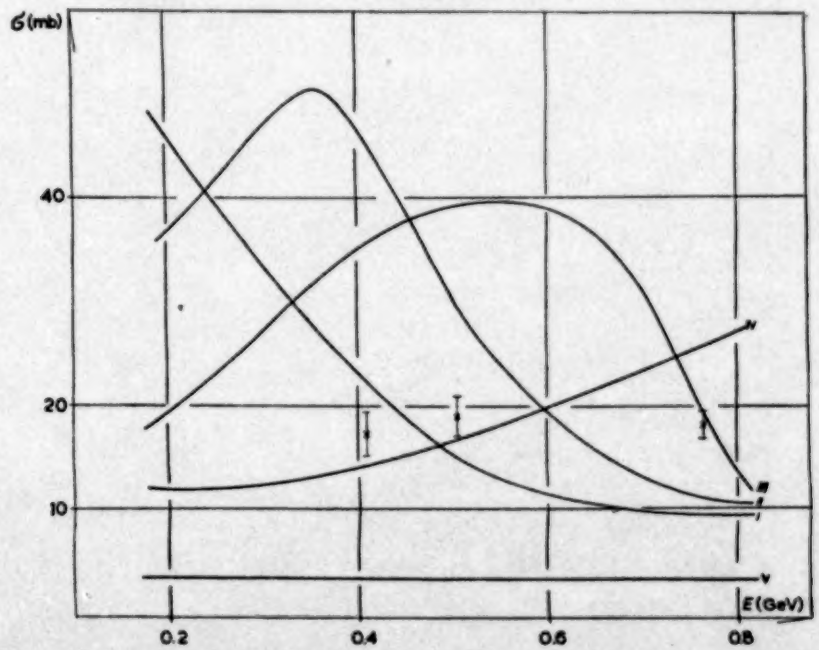

Fig. 9. Calculated and experimental total cross sections in the high energy region for the K^+-p scattering. For the explanation see fig. 8.

⊗ — Burrowes *et al.* No agreement seems to be possible for a definite choice of coupling constant. This may be caused among others by disregard of (a) the production of additional pions, (b) higher orbital states (see also sect. 8).

In fig. 8 we present calculated total cross sections for K+—p scattering compared with experimental data at low energies. In fig. 9, the same results are given for the high energy region. We did not succeed in fitting the experimental data for both regions with the same coupling constants G^2 and $\mathscr{G}^2$.

Calculated total cross sections for K+—n elastic and charge exchange scattering, also compared with experimental data, are given in fig. 10.

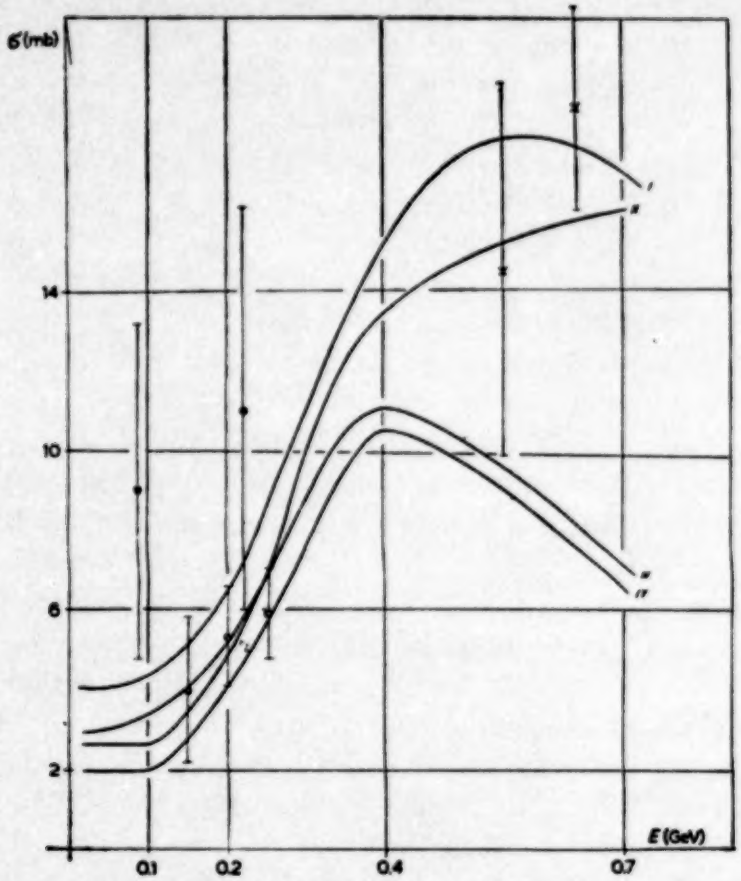

Fig. 10. Calculated and experimental total cross sections vs. kinetic energy of K+ in the lab. system for the K+—n elastic and charge exchange scattering ($\mathscr{M} \neq M$, $8\mathscr{G}^2 = 3G^2$).

K+—n elastic: (I) $G^2/4\pi = 10.8$; (III) $G^2/4\pi = 7.3$.
K+—n charge exchange: (II) $G^2/4\pi = 10.8$; (IV) $G^2/4\pi = 7.3$.
I — UCLA (Stork *et al.*), computed average; } K+—n elastic.
X — Burrowes *et al.* }
O — UCLA (Stork *et al.*), K+—n charge exchange.

8. Discussion

There are, perhaps, the following main sources of errors:

(a) numerical and semi-numerical mistakes (a bad approximation, a wrong method of solving of the equation etc.);

(b) the omission of the renormalization corrections;

(c) a slow convergence of the Tamm-Dancoff method causing the higher order terms in $U(E)$, eq. (2), to be important (in writing down such terms we must also take into account some new interactions, namely N-N π, Σ-Λ-π, Σ-Σ-π, Σ-Ξ-K, Λ-Ξ-K);

(d) the incorrectness of the Tamm-Dancoff method as such;

(e) wrong physical assumptions concerning e.g. the pseudoscalar character of the K—N interaction and the disregarding of the other possible interactions such as K-K-π (or K-K-π-π).

As far as (c) and (d) are concerned no conclusive remarks can be made because of our poor knowledge of the non-adiabatic methods. We believe, however, that they lead to less incorrect results than e.g. the perturbation method, even in their lowest approximation. We shall now deal with the remaining points only. We should just like to remark that in our case the better results seem to be connected with the repulsive interaction in the $S_{\frac{1}{2}}$ state, whereas the results in the attractive interaction in the $P_{\frac{3}{2}}$ state are worse. This might be explained e.g. by the better convergence of the Tamm-Dancoff method when a repulsive interaction is considered (see ref. [4])).

The problem of possible numerical mistakes can be solved in principle. Following one of the well-known methods of evaluating the error in the approximate solution of an integral equation with regular kernel, we have been able to get some information concerning this error in our case (when the kernel is singular with the Cauchy principal value of the integral). We mention that the approximation obtained for the kernel and for $\varphi_0(p)$ is very good and that the relative difference between the correct and approximate functions does not exceed 0.1 %. Further, the behaviour of these functions in the neighbourhood of 0 and 1 (x, y plane) and in the neighbourhood of the singularity of the kernel is reproduced exactly. Then, the relative error in the solution is a few percent. It depends of course on the total energy, becoming larger when the energy increase Thus, we do not think that the main cause of the observed discrordance between the experimental data and the results of the calculations is (a).

Now, we should like to draw attention to some facts, which perhaps might suggest that the cause is the omission of the renormalization corrections. First, we mention that one can notice a good agreement between our results and the experimental data in the low energy region at least for the $T = 1$ state. In this region we have obtained, first, the correct dependence of the total cross section on energy and, second, the correct (isotropic) differential cross section. (We see, however, that any appreciable anisotropy of the differential cross section for the scattering in the $T = 0$ state for the lowest energies, could not be reconciled with our results.) In order to get this agreement with experiment we must take the rather unusual coupling constants $(G^2+\mathscr{G}^2)/4\pi = g^2/4\pi \approx 15$. We should like to mention, however, that speculations based on the idea of the global symmetry of the strong interactions may lead to a similar conclusion: $2\frac{1}{2}G$

must equal $2\frac{1}{2}\mathscr{G}$ and must equal g (when g denotes the N-N-π coupling constant). These relations between the coupling constants are valid for the bare constants, whereas the "physical" ones may be different. Now, let us call some results given by Visscher [7]) concerning the π-N scattering here, the difference between π-N and K-N scattering is of no importance): thre is an effective coupling "constant" depending on energy (and, of course on the state to which the scattering leads), which is equal to the bare constant when the kinetic energy vanishes. This fact led in Visscher's paper [7]) to serious difficulties connected with a non-physical pole in the coupling "constant". On the other hand, the dependence of the coupling "constant" on the energy can be used to explain the behaviour of the cross sections for K-N scattering with energy. According to this hypothesis the effective coupling constant varies slightly with energy (and some other observables) from its bare value when $E_{\text{kin}} = 0$. Unfortunately this fact cannot be checked by means of the calculation technique. Slightly changing the coupling constant we should be able to get a good agreement with the experimental data in a very wide energy region, say, up to 1200 MeV. Notice that if the hypothesis in question is true, the dispersion relations might serve in the main to find some average coupling constant over a wide energy region.

As far as (e) is concerned we should like to remark that the possibility of the scalar character of the coupling N-Y-K is not very likely now because of some arguments based on the analysis of the photoproduction of K mesons and some conclusions from the analysis of K-N scattering by dispersion relations. Now, Święcki and Szalek checked that the Tamm-Dancoff method leads in the case of the scalar coupling to unreasonable conclusions for the K-N scattering (one obtains a very strong attractive interaction in the $S_{\frac{1}{2}}$ state at the lowest energies, where the P states are of less importance).

The hypothesis concerning the new four and three boson interactions (K-K-π or K-K-π-π) [11]) must also be taken into account. In this case the whole cross section might originate from two different virtual processes. Thus we should probably diminish the N-K-Y coupling constants and obtain the agreement with observational data on account of the new interaction. This situation seems to be possible, but if the new interaction is to give an (almost) constant contribution to the total cross section, at least for low energies, the N-K-Y interaction must be rather strong. Otherwise we cannot get the observed rapid increase of the total cross section from about 300 MeV. This increase is closely connected with the contribution of the $P_{\frac{1}{2}}$ state.

In order to discuss this possibility, we have performed the calculation also for the smaller coupling constant $(G^2+\mathscr{G}^2)/4\pi \approx 10$. Our results seem to point out that agreement with experiments is possible if we assume that the "new" interaction gives a contribution of the order of magnitude of 4—5 mb.

The authors wish to express their gratitude to Professor W. Królikowski for his interest and numerous discussions. The authors are also much indebted to M. Święcki and M. Szalek for performing a part of the numerical calculations.

References

1) D. I. Meyer *et al.*, Phys. Rev. **107** (1958) 278;
J. E. Lanutti *et al.*, Phys. Rev. **109** (1958) 2121;
H. C. Burrowes *et al.*, Phys. Rev. Letters **2** (1959) 118;
L. W. Alvarez, Report in the Proceedings of the Kiev Conference (1959)
2) C. Ceolin and L. Taffara, Nuov. Cim. **5** (1957) 435;
D. Amati and B. Vitale, Nuov. Cim. **5** (1957) 1533;
C. Ceolin and L. Taffara, Report of the Padua-Venice Conference (1957);
P. T. Matthews and A. Salam, Phys. Rev. **110** (1958) 569;
C. Ceolin *et al.*, Nuov. Cim. **12** (1959) 502
3) F. J. Dyson *et al.*, Phys. Rev. **95** (1954) 1644
4) G. Morpurgo and B. F. Touschek, Nuov. Cim. **10** (1953) 1681;
G. Morpurgo, Nuov. Cim. **11** (1954) 103
5) G. Białkowski and A. Jurewicz, Phys. Rev. **116** (1959) 1269
6) W. Królikowski and J. Rzewuski, Nuov. Cim. **3** (1956) 260
7) W. M. Visscher, Phys. Rev. **96** (1954) 788
8) M. Gell-Mann and M. Goldberger, Proceedings of the Fourth Rochester Conf., p. 29
9) B. Radon, Atti Accad. Naz. Lincei, Mem. Cl. Fis. Mat. Nat. **2** (1950) 69–109
10) A. Erdelyi *et al.*, Higher Transcendental Functions, Vol. 2, p. 249
11) S. Barshay, Phys. Rev. **110** (1958) 743

7.C

Nuclear Physics **17** (1960) 377—387; © *North-Holland Publishing Co., Amsterdam*

Not to be reproduced by photoprint or microfilm without written permission from the publisher

CENTRAL AND PERIPHERAL COLLISIONS OF FAST NUCLEONS (II)

V. S. BARASHENKOV and V. M. MALTSEV

Joint Institute of Nuclear Research, Laboratory of Theoretical Physics, Dubna, USSR

Received 25 December 1959

Abstract: Theoretical momentum spectra of particles produced in nucleon collisions are compared with the experimental data obtained at $T = 9$ GeV. Energy losses in inelastic nucleon collisions are calculated. Cases of central and peripheral collisions are treated separately.

1. Introduction

Previous papers [1]) have dealt with a model of central and peripheral collisions of fast nucleons. On the basis of p—p and p—n collisions at $T = 9$ GeV it was shown that the experimental angular distributions of the produced particles can be explained if the cross-section of peripheral collisions constitutes no less than 20 % of the cross-section of all the inelastic N—N collisions:

$$\sigma_p \geqq 0.2\, \sigma_{in}. \tag{1}$$

Now on the basis of the same model we shall consider energy characteristics of inelastic nucleon collisions. The results of the calculation will again be compared with the experimental data obtained in Dubna at the energy $T = 9$ GeV.

Particular attention will be paid to the average energy loss of a nucleon in a single N—N collision ΔE. This value has attracted the attention of many researchers and has been the subject of repeated measurements and discussions (see, for instance, refs. [2–10]). After the work in ref. [1]) was completed, the accuracy of the experimental values of ΔE has been considerably improved and the average experimental values of ΔE have been found to be lower than their previous estimates.

It is natural that on the basis of the so far imperfect model one may expect only a rough agreement with experiment. Therefore, like in ref. [1]), our main task has been to establish in what way and in what direction the theoretical conclusions are affected by taking into account peripheral collisions of nucleons, and also to direct attention of experimenters to those points which first of all require more accurate measurements.

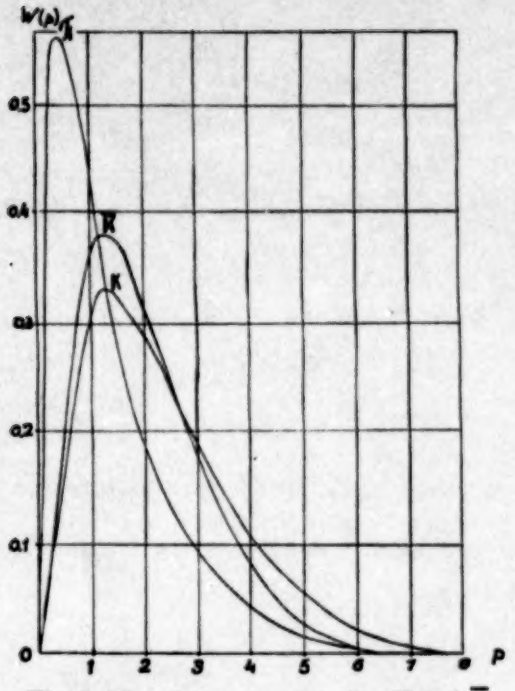

Fig. 1. Momentum spectra of π, K and $\overline{\mathrm{K}}$ mesons in the laboratory system of coordinates. The momenta are given in units of GeV/c.

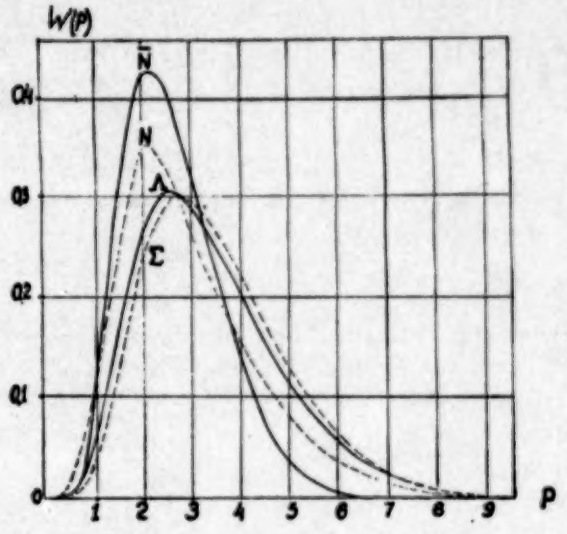

Fig. 2. Momentum spectra of nucleons, antinucleons, Λ and Σ hyperons in the laboratory system of coordinates. The dotted lines are the spectra of nucleons and Σ hyperons. The momenta are given in units of GeV/c.

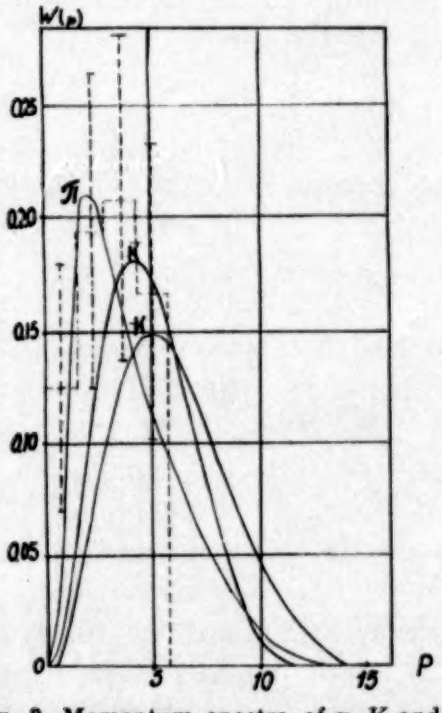

Fig. 3. Momentum spectra of π, K and $\overline{\mathrm{K}}$ mesons in the centre-of-mass system of the colliding nucleons. The dotted curve is an experimental histogram for π mesons. The momenta are given in units of $m_\pi c$, where m_π is the π meson mass.

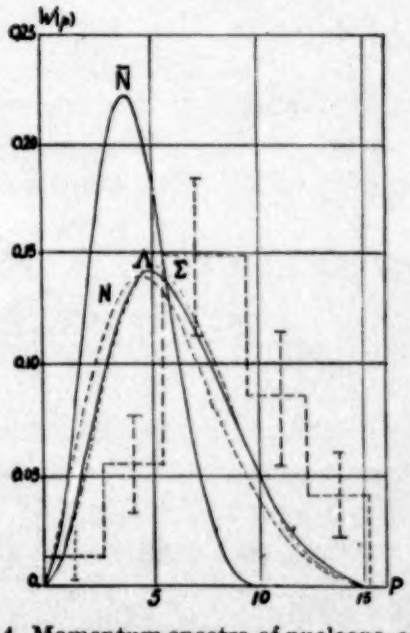

Fig. 4. Momentum spectra of nucleons, antinucleons, Λ and Σ hyperons in the centre-of-mass system of the colliding nucleons. In dots are the theoretical spectrum of nucleons and the corresponding experimental histogram, as well as the spectrum of Σ hyperons. The momenta are given in units of $m_\pi c$ where m_π is the π meson mass.

2. Momentum Distribution of Particles Produced in Central Collisions

Figs. 1—4 represent momentum spectra $W = W(p)$ of different kinds of particles produced in central N—N collisions and calculated in the statistical theory of multiple production. Momentum distributions for all the kinds of produced particles are given in the centre-of-mass system of the colliding nucleons and in the laboratory system, since in analysing the experimental data and in preparing new experiments it is necessary to know momentum distributions in both coordinate systems. A slight difference between the pion and nucleon momentum spectra and the similar spectra listed in ref. [7]) is due to a more accurate account of the reactions with strange particles and a more accurate method of calculations. In evaluating the spectra we used the method of calculating energy phase volumes worked out by L. G. Zastavenko [11]) in our laboratory. For comparison in figs. 3 and 4 we give experimental momentum distributions of charged π mesons and protons in p—p collisions taken from ref. [12]). (in this work 28 π meson tracks and 42 proton tracks were analysed). The average statistical errors of the measurements, $\Delta_n = (N_n)^{\frac{1}{2}}/\sum_m N_m$, are also given.

TABLE 1

Experimental and theoretical values of average nucleon and meson momenta

	π mesons		Protons	
	Experiment	Theory	Experiment	Theory
$\bar{p}$(GeV/c) Laboratory system	1.0±0.2	1.46	3.6 ±0.5	2.90
$\bar{p}$(GeV/c) Centre-of-mass system	0.4±0.1	0.57	1.24±0.25	0.79

Table 1 lists experimental and theoretical values of average momenta $\bar{p}$ of nucleons and π mesons. The theoretical values consider only central collisions of nucleons and are obtained with the help of the distributions plotted in figs. 1—4. Experimental values of $\bar{p}$ for the centre-of-mass system are calculated from experimental histograms in figs. 3—4. The dispersion of experimental values

$$\Delta\bar{p} = \sqrt{\frac{\Delta p \sum_n N_n (p_n - \bar{p})^2}{\sum_m N_m}}$$

is given. The experimental values of $\bar{p}$ for the laboratory system of coordinates are obtained by Lorentz transformation from the centre-of-mass system under the assumption that in p—p collisions the angular distributions of π mesons and nucleons in the centre-of-mass system are symmetrical with respect to the

angle $\theta = \frac{1}{2}\pi$ (this assumption is consistent with the theoretical and experimental results obtained in refs. [1, 6]):

$$\bar{p} \approx \gamma\varepsilon_c; \quad (\gamma^2\varepsilon_c^2 \gg m^2), \tag{2}$$

where ε_c is the average energy of the produced protons or π mesons in the centre-of-mass system of the colliding protons;

$$\gamma = E_c/M \tag{3}$$

is a coefficient of relativistic transformation (E_c is the primary proton energy in the centre-of-mass system, M is the nucleon mass); m is the mass of the particle under consideration.

The values of $\bar{p}$ thus obtained are close to the values derived in ref. [2]) from analysis of the interaction between emulsion nuclei and 9 GeV protons $\bar{p} \approx p_{sp} = 3.0 \pm 0.5$ GeV for protons and $\bar{p} \approx p_{s\pi} = 1.0 \pm 0.2$ GeV for charged π mesons. Similar results are also obtained in refs. [5, 8]).

It is seen from table 1 and fig. 3 that within the limits of experimental errors there are no sharp contradictions between the theoretical and experimental data for π mesons. However, the experimental momentum spectra are notably softer than the theoretical ones. The large statistical errors do not allow so far to draw more definite conclusions.

The experimental momentum spectrum of protons is found to be harder than the theoretical spectrum. The difference between the theoretical and experimental spectra can be qualitatively explained if one takes into account that neither in the spectrum measurements of ref. [12]) nor in those of refs. [5, 8–10]) were central and peripheral collisions separated. While it should be noted that a nucleon spectrum after a peripheral collision is harder than a spectrum of nucleons produced in a central collision, conversely, π mesons produced in peripheral collision are on the average softer than π mesons from central collisions. These problems will be treated in greater detail in sec. 5.

TABLE 2

Theoretical values of the average transverse momenta and energy losses in central collisions

Particle type	π	K^+	K^-	$\bar{N}$	Λ	Σ
$p_\perp$(GeV/c)	0.45	0.64	0.53	0.46	0.68	0.68
ΔE_i(%) (T = 100 %)	49	1.6	0.2	0.8	1.6	3.3

Table 2 lists theoretical values of the average transverse momenta $p_\perp$ of particles produced in central collisions (for nucleons $p_\perp = 0.6$ GeV/c; see ref. [2]). The corresponding measurements are not yet completed at present. There are

only rough estimates for protons and charged π mesons obtained in studying the interaction between emulsion nuclei and 9 GeV protons [2]). These estimates do not contradict the calculated values of $p_\perp$.

3. Energy Losses in Central Collisions

Table 2 gives the relative energy losses for production of the i-type particles in a single central N—N collision in the laboratory system of coordinates; those losses are

$$\Delta E_i = n_i \varepsilon_i / T.$$

Here ε_i is the average energy; n_i is the average number of i-type particles produced in a central collision of nucleons; T is the kinetic energy of a primary proton. Values of ε_i are calculated from the momentum spectra plotted in figs. 1 and 2; values of n_i are taken from ref. [13]).

Thus, the average energy spent by the incident proton in formation of *new* particles in a single central N—N collision is

$$\Delta E_c = \sum_i \Delta E_i \approx 0.58 \tag{5}$$

or about 58 % of its primary energy $T = 9$ GeV. The calculations did not take into account the energy loss for production of Ξ particles and anticiparticles $\tilde{\Lambda}$, $\tilde{\Sigma}$ and $\tilde{\Xi}$. The estimates have shown, however, that in this case only a small error $\lesssim 1$ % is introduced into ΔE_c. We have also assumed that $\varepsilon_{K^0} \approx \varepsilon_{K^+}$ and $\varepsilon_{\bar{K}^0} \approx \varepsilon_{K^-}$ (see table 3 in ref. [13])). The total energy loss of a primary proton in a single central collision is

$$\Delta E^c_{tot} = \Delta E_c + T_c/T \approx 0.79. \tag{6}$$

Here $T_c = 0.21\, T$ is the average kinetic energy of a nucleon after the central collision.

4. Energy Losses in Peripheral Collisions

In a single peripheral N—N collision the energy of new particle production is on the average

$$\Delta E_p = \tfrac{1}{2}(\Delta E'_p + \Delta E''_p), \tag{7}$$

where $\Delta E'_p$ is the average energy loss in collision of a peripheral meson of the incident nucleon with the nucleon at rest and $\Delta E''_p$ is the corresponding energy loss in collision of the incident nucleon with the meson cloud of the nucleon at rest (in the coordinate system where the incident nucleon is at rest, this energy is evidently equal to $\Delta E'_p$).

In the model of peripheral collisions without a residual isobar (see fig. 2 in ref. [1])) we have

$$\Delta E'_{\mathrm{p}} = \frac{2}{\sigma_{\mathrm{p}}}\int_{\mu}^{\varepsilon^*}[\varepsilon - t_{\mathrm{N}}(\varepsilon)]\sigma_{\pi\mathrm{N}}(\varepsilon)q(\varepsilon)\mathrm{d}\varepsilon \approx \bar{\varepsilon} - T_{\mathrm{N}}, \tag{8}$$

where

$$T_{\mathrm{N}} = \frac{2}{\sigma_{\mathrm{p}}}\int_{\mu}^{\varepsilon^*} t_{\mathrm{N}}(\varepsilon)\sigma_{\pi\mathrm{N}}(\varepsilon)q(\varepsilon)\mathrm{d}\varepsilon \tag{9}$$

is the average kinetic energy of a nucleon after a collision with the peripheral π meson and where

$$\bar{\varepsilon} = \int_{\mu}^{\varepsilon^*} \varepsilon q(\varepsilon)\mathrm{d}\varepsilon / n \tag{10}$$

is the average energy of peripheral mesons. Further, we have in eqs. (8) and (9)

$$\sigma_{\mathrm{p}} = 2\int_{\mu}^{\varepsilon^*}\sigma_{\pi\mathrm{N}}(\varepsilon)q(\varepsilon)\mathrm{d}\varepsilon \approx 2\sigma_{\pi\mathrm{N}}\cdot n, \tag{11}$$

n being the average number of peripheral mesons in a nucleon shell; and finally, in all these equations

$$\varepsilon^* = E - \sqrt{\tfrac{1}{2}M(E+M)} \tag{12}$$

is the upper limit of the peripheral meson spectrum $q(\varepsilon)$ ($E = T+M$ and M is the nucleon mass).

In the isobar model of peripheral collisions (see fig. 3 in ref. [1]) we have

$$\Delta E'_{\mathrm{p}} \approx \bar{\varepsilon} - T_{\mathrm{N}} + E_{\pi}, \tag{13}$$

where E_{π} is the average energy of π mesons produced in isobaric decay. Since in the rest system of an isobar the angular distribution of such mesons is isotropic, passing to the laboratory system of coordinates we get

$$E_{\pi} = \frac{2\varepsilon_{1s}}{\sigma_{\mathrm{p}}}\int_{\mu}^{\varepsilon^*}\gamma_{1s}(\varepsilon)\sigma_{\pi\mathrm{N}}(\varepsilon)q(\varepsilon)\mathrm{d}\varepsilon \approx \frac{\varepsilon_{1s}}{M'}(E-\bar{\varepsilon}), \tag{14}$$

where

$$\gamma_{1s}(\varepsilon) = \frac{(E-\varepsilon)}{M'} \tag{15}$$

is a modulus of relativistic transformation, $M' = 1.3\,M$ is the isobar mass, and $\varepsilon_{1s} \approx 0.3$ GeV is the average energy of a meson produced in isobaric decay in the coordinate system in which this isobar is at rest.

An expression for $\Delta E''_{\mathrm{p}}$ can be easily obtained by Lorentz transformation from the coordinate system in which the incident proton is at rest:

$$\Delta E''_{\mathrm{p}} = \gamma(\Delta E'_{\mathrm{p}} + \beta\Delta p'). \tag{17}$$

Here

$$\gamma = \frac{E}{M}, \quad \beta \approx 1 - \frac{M^2}{2E^2}. \tag{18}$$

The longitudinal component $\Delta p'$ of the momentum of newly-produced particles is given by

$$\Delta p' \approx -\frac{2}{\sigma_p}\int_\mu^{\varepsilon^*} [p(\varepsilon) - p_N(\varepsilon)]\sigma_{\pi N}(\varepsilon)q(\varepsilon)d\varepsilon \approx -\bar{\varepsilon} + \mathscr{P}_N \tag{19}$$

in the model of peripheral collisions without an isobar and by

$$\Delta p' \approx -\bar{\varepsilon} + \mathscr{P}_N + p_\pi \tag{20}$$

in the model with an isobar. Here, the quantity

$$\mathscr{P}_N = \frac{2}{\sigma_p}\int_\mu^{\varepsilon^*} p_N(\varepsilon)\sigma_{\pi N}(\varepsilon)q(\varepsilon)d\varepsilon \tag{21}$$

is the average momentum of a nucleon after a collision with a peripheral π meson; $p(\varepsilon) \approx \varepsilon$ is the momentum of a peripheral meson, and

$$p_\pi = -\frac{2\varepsilon_{is}}{\sigma_p}\int_\mu^{\varepsilon^*} \gamma_{is}(\varepsilon)\beta_{is}(\varepsilon)\sigma_{\pi N}(\varepsilon)q(\varepsilon)d\varepsilon = -E_\pi + \frac{M'\varepsilon_{is}}{2n}\int_\mu^{\varepsilon^*} \frac{q(\varepsilon)\,d\varepsilon}{E-\varepsilon} \tag{22}$$

is the average momentum of a π meson produced in isobaric decay.

Taking into account inaccuracy of values $p_N(\varepsilon)$ (see below) we have neglected the transverse component of momenta $p_\perp(\varepsilon)$ and $\mathscr{P}_{N\perp}$ in formulas (19) and (20).

Finally, for the energy ΔE_p spent in production of new particles we obtain the following expressions (respectively for versions with and without an isobar):

$$\Delta E_p = \tfrac{1}{2}\bar{\varepsilon}\left(1 + \tfrac{1}{2}\frac{M}{E}\right) + \tfrac{1}{2}\mathscr{P}_N\frac{E}{M} - \tfrac{1}{2}T_N\left(1 + \frac{E}{M}\right), \tag{23}$$

$$\Delta E_p = 0.12(3.1\bar{\varepsilon} + E)\left(1 + \tfrac{1}{2}\frac{E}{M}\right) + \tfrac{1}{2}\frac{E}{M}\left(\mathscr{P}_N + \frac{0.2\,M^2}{n}\int_\mu^{\varepsilon^*}\frac{q(\varepsilon)d\varepsilon}{E-\varepsilon}\right) - \tfrac{1}{2}T_N\left(1 + \frac{E}{M}\right). \tag{24}$$

Since the average energy of the recoil of a nucleon in peripheral collisions is not large ($T_{rec} \ll \Delta E_p$), the total energy loss of fast incident nucleons is close to the energy loss in production of new particles:

$$\Delta E^p_{tot} \approx \Delta E_p. \tag{25}$$

If, however, the conditions of the experiment are such that the average energy of a nucleon is measured after the collision,

$$\bar{T} = \tfrac{1}{2}(T - \Delta E_p), \tag{26}$$

then the total energy loss of a primary nucleon in a single peripheral collision is

$$\Delta E_{tot}^{p} \equiv T - \bar{T} = \tfrac{1}{2}(T + \Delta E_p). \tag{27}$$

5. Discussion

In order to calculate the values of ΔE_p at a given minimum impact parameter r_0 it is necessary to know the momentum spectrum $p_N(\varepsilon)$ of nucleons produced in peripheral π—N collisions. This spectrum can be calculated theoretically if one uses the statistical theory of multiple production (for greater detail see ref. [14]) for describing inelastic π—N collisions and the optical model (see ref. [15])) — for describing elastic π-N collisions. In this case

$$p_N = \frac{\sigma_{in} p_N^{in} + \sigma_{el} p_N^{el}}{\sigma_{in} + \sigma_{el}}, \tag{28}$$

where p_N^{in} and p_N^{el} are the values of nucleon momentum for inelastic and elastic collisions and where $\sigma_{el} \approx \frac{1}{3}\sigma_{in}$.

Values of $p_N(\varepsilon)$ may be also obtained by interpolation of the available experimental data. However the values thus obtained are not more accurate than the theoretical ones since the experimental data in the energy range $T \geqq 1$ GeV are known only in several points and with large statistical errors [16] †. Fig. 5 shows the values of $p_N(\varepsilon)$ momentum and the corresponding values of the kinetic energy

$$t_N = \frac{\sigma_{in} t_N^{in} + \sigma_{el} t_N^{el}}{\sigma_{in} + \sigma_{el}}, \tag{29}$$

used in calculating the energy losses ΔE_p.

On the other hand the calculations have shown that the value ΔE_p changes but little with the change of $\mathscr{P}_N$ and T_N in a wide range of their values.

Therefore it is to be expected that within our model the possible inaccuracy of $p_N(\varepsilon)$ cannot considerably affect the calculated values of energy losses ΔE_p.

Fig. 6 shows the calculated values of $\mathscr{P}_N$ and T_N for peripheral collisions of nucleons with the impact parameter $r \geqq r_0$ at $T = 9$ GeV. The same figure gives the average energy losses ΔE_p in peripheral collisions calculated for these

† We are thankful to R. M. Lebedev who acquainted us with his experimental spectra of nucleons from inelastic π^-p interactions at energy $T = 7$ GeV prior to publication.

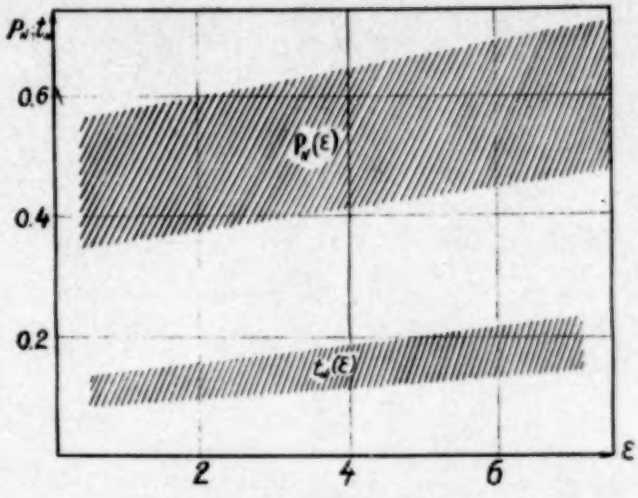

Fig. 5. The average kinetic energy t_N and nucleon momentum p_N after a collision with a peripheral π meson of energy ε. The shaded areas are the values of t_N and p_N tolerated by the statistical errors in measurements. The values t_N and ε are expressed in GeV, the values p_N in GeV/c, both in the laboratory system of coordinates.

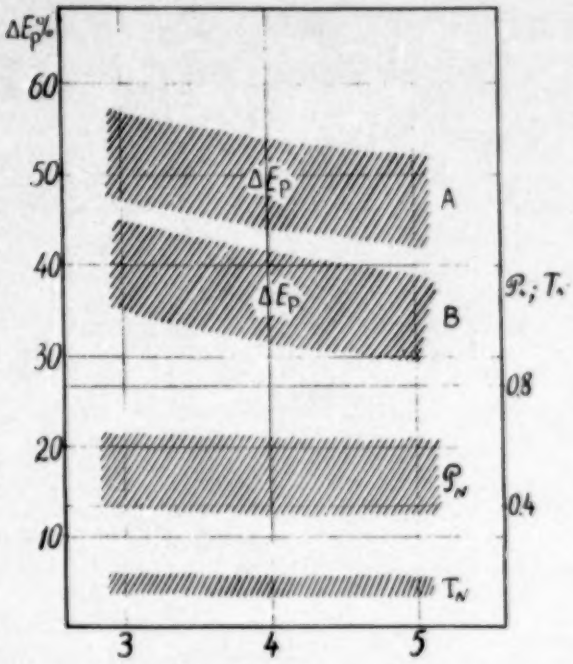

Fig. 6. Dependence of values T_N, $\mathcal{P}_N$ and ΔE_p on the minimum impact parameter: A is a model with an isobar, B is a model without it. The shaded areas are the values tolerated by the statistical errors in measurements. The values T_N are expressed in GeV; values $\mathcal{P}_N$ are in GeV/c and values of the minimum impact parameter are in units of $\hbar/Mc = 2.1 \times 10^{-14}$ cm.

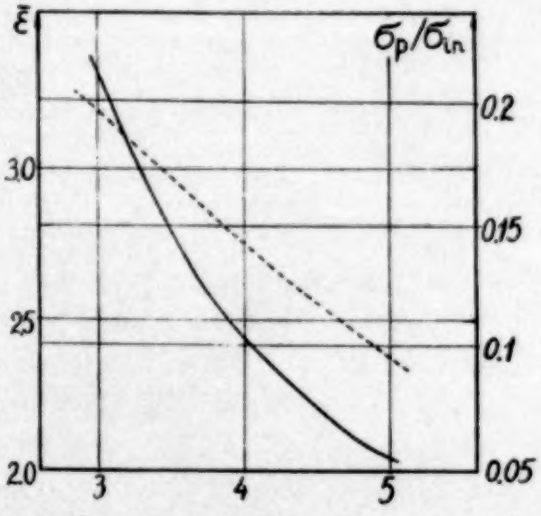

Fig. 7. Dependence of the peripheral meson average energy $\bar{\varepsilon}$ (dotted curve) and the peripheral collision cross-section σ_p (solid curve) on the value of the minimum impact parameter r_0. Values of $\bar{\varepsilon}$ are given in GeV, values of r_0 are in units of $\hbar/Mc = 2.1 \times 10^{-14}$ cm.

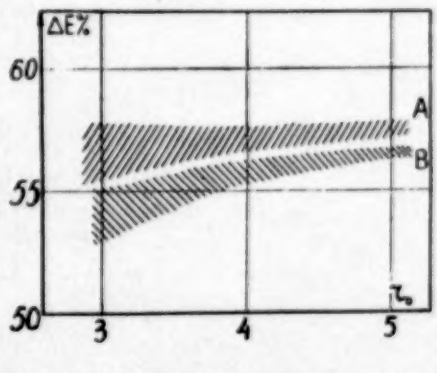

Fig. 8. Dependence of the total energy loss in N—N collisions on the value of the minimum impact parameter r_0: A is a model with an isobar, B is a model without it. The shaded areas are the values of ΔE tolerated by the statistical errors in measurements (the value of ΔE_0 being assumed to be accurate.) Values of r_0 are given in units of $\hbar/Mc = 2.1 \times 10^{-14}$ cm.

values of $\mathscr{P}_N$ and T_N. Fig. 8 represents the calculated values of the total energy loss in a single inelastic interaction

$$\Delta E = (1-\xi)\Delta E_c + \xi \Delta E_p, \tag{30}$$

where $\sigma_p \equiv \xi\sigma_{in}$ is a theoretical value of the cross-section of peripheral collisions; for different r_0 it is plotted in fig. 7.

It is seen from figs. 6 and 8 that the difference between a total energy loss ΔE and an energy loss in a central N—N collision ΔE_c is not great. The values of ΔE_p and ΔE_c are also found to be comparable in their magnitude.

The difference in energy losses ΔE for models with and without an isobar approximately constitutes only 5 % for $r_0 = 3\hbar/Mc$ and still less for greater values of r_0. It is evident that neither the experimental data nor the theoretical calculations are sufficiently accurate at present for separating the models of peripheral collisions.

The value of ΔE_c, and together with it the value of ΔE can be diminished by several per cent by decreasing the cross-sections of strange particles production † and by increasing the cross-section ratios ξ (within the limits of errors of measurements of σ_{in}).

TABLE 3

Experimental values of average energy losses in collisions

Ref.	3	5	9	2	6	8
ΔE(%)	30	30±10	33±9	≧40±10	≈30 (<45)	35±2

Table 3 lists the experimental values of average energy losses in N—N collisions obtained by different researchers. It is seen that the theoretical values ΔE notably exceed the average experimental ones.

The calculations have shown that by taking into account the peripheral collisions we improve the agreement between the experimental and theoretical values of the average momenta of nucleons and π mesons produced in N—N collisions, but still, as for ΔE, a complete quantitative agreement cannot be obtained.

However, the knowledge of experimental values is not yet sufficient at the present moment. The values of ΔE are obtained in the majority of cases from the analysis of the interaction of a primary proton with nuclei. These values are to be considered only as an approximate estimation of energy losses in N—N

† The cross-section of strange particles production σ_s is calculated in phenomenological theory [13]. However, the experimental data on the production of strange particles at $T > 1$ GeV admit of such decrease of these theory parameters that at $T \approx 9$ GeV the value σ_s is decreased by a factor of $\frac{3}{2}$ to 2.

collisions (usually as an estimation from below; cf. ref.[2])). The values of ΔE obtained from the analysis of interactions in stripped emulsions are also of a preliminary character. In particular, an estimate $\Delta E < 45\ \%$ based on proton momentum measurements may prove to be understated, since it does not take into account statistical errors of the measurements. The above said concerns as well the experimental values of average momenta of particles produced in N—N collisions. Therefore it is still difficult to determine the amount of difference between the experimental and theoretical values. Considerations offered in the present work, as well as in ref. [1]) allow only to assert that the agreement of angular and energy characteristics with experiment is improved by taking into account peripheral collisions of nucleons.

Further progress requires more accurate experimental data.

Note added in proof: As a result of recent measurements made by a group of experimentalists Wang Shu-fen, Gramenitsky *et al.*, the mean value of ΔE became larger again: the real value of ΔE lies within the values (0.39 ± 0.02) and (0.47 ± 0.02). These experimentalists think that the real value of ΔE lies closer to the lower than to the upper limit.

References

1) V. S. Barashenkov *et al.*, Nuclear Physics **13** (1959) 583;
   V. S. Barashenkov *et al.*, JETP **38** (1960) 650
2) V. S. Barashenkov *et al.*, Nuclear Physics **14** (1959/60) 522
3) N. L. Grigorov, Usp. Fiz. Nauk **58** (1956) 599
4) V. J. Veksler, Report at the High Energy Physics Conference, Kiev, July 1959
5) G. L. Baiatian *et al.*, JETP **36** (1959) 690
6) N. P. Bogachev *et al.*, JETP **37** (1959) 1225
7) V. S. Barashenkov *et al.*, Nuclear Physics **9** (1958) 74
8) N. P. Bogachev *et al.* (S. Buniatov's communication at the seminar in L.T.P. of the Joint Institute of Nuclear Research)
9) G. B. Zdanov *et al.*, JETP **37** (1959) 620
10) G. B. Zdanov *et al.*, JETP **37** (1959) 611
11) L. G. Zastavenko, JETP **37** (1959) 1319
12) N. P. Bogachev *et al.*, High Energy Physics Conference, Kiev, July 1959
13) V. S. Barashenkov *et al.*, Nuov. Cim. **7** Suppl. 1 (1958) 117
14) V. S. Barashenkov, Nuclear Physics **15** (1960) 486
15) D. I. Blokhintsev *et al.*, Usp. Fiz. Nauk. **68** (1959) 417;
    V. S. Barashenkov and Huan Nian-Nin, JETP (1959) 832
16) W. D. Walker *et al.*, Phys. Rev. **104** (1956) 526;
    R. S. Whitten and M. M. Block, Phys. Rev. **111** (1958) 1676;
    V. A. Beliakov *et al.*, (K. M. Lebedev's private communication);
    M. Chreatien *et al.*, Phys. Rev. **108** (1957) 850;
    G. Maenchen *et al.*, Phys. Rev. **108** (1957) 872;
    Van Gan-Chan *et al.*, High Energy Physics Conference, Kiev, July 1959

1.E.2:
1.E.5

Nuclear Physics **17** (1960) 388—420; © *North-Holland Publishing Co., Amsterdam*

Not to be reproduced by photoprint or microfilm without written permission from the publisher

NEUTRON AND PROTON DENSITIES IN NUCLEI AND THE SEMI-EMPIRICAL MASS FORMULA

A. R. BODMER

Department of Theoretical Physics, University of Manchester, Manchester, England

Received 8 February 1960

Abstract: The semi-empirical statistical method due to Wilets, with the use of trial nucleon densities, has been used to investigate the nucleon density distributions and their relation with the semi-empirical mass formula. In particular those features depending on the neutron excess have been isolated, especially the difference in extension δ between the neutron and proton densities and the surface symmetry energy $E_{s\tau}$. In addition to the usual Weiszäcker type gradient terms a new mixed gradient term has to be introduced. For both δ and $E_{s\tau}$ the density dependence of the symmetry energy density ε_τ plays an important role, while $E_{s\tau}$ also depends on δ. The variational solution for δ together with the empirical value of $E_{s\tau}$ then determine both δ and the density dependence of ε_τ in terms of the magnitudes of the gradient terms. The general conclusions are independent of these magnitudes if these are consistent with the empirical surface energy and thickness. For stable nuclei, $\delta \propto (N-Z)/A$ to a good approximation. δ is small ($\lesssim 0.3\times10^{-13}$ cm) even for the heaviest stable nuclei, the neutrons thus extending slightly beyond the protons. The density dependence of ε_τ is found, tentatively, to be considerably smaller than in the independent particle approximation for nuclear matter. The empirically used dependence for $E_{s\tau} \propto (N-Z)^2/A^{\frac{1}{3}}$ seems well justified for nuclei near the stable valley. The dependence of the total surface thickness on the neutron excess is found to be quite small.

1. Introduction

The calculation of nucleon densities for finite nuclei based on realistic forces requires an adequate self-consistent procedure. The Hartree-Fock method is known to be a poor approximation for nuclei because the nature of the nuclear forces implies dynamic correlations which are essential for understanding the saturation properties of nuclear matter. The Brueckner method [1–3]) which takes account of essentially two-body correlations seems much more promising and calculations made so far give good results for nuclear matter [1]). For finite nuclei the method [3–5]) is however difficult and tedious to apply, especially in a fully self-consistent manner, and general features of the density distributions of finite nuclei are difficult to study. For such problems a more amenable, although more approximate, self-consistent approach is the statistical method [6]) which works directly in terms of the nucleon densities and their spatial derivatives; an essential prerequisite being knowledge of the energy density in terms of these. The method has been applied to nuclei especially by Gombás and collaborators [7]) who used energy densities obtained essentially in the independent-

particle approximation and correspondingly rather unrealistic forces, together with the classical, but not well founded, value of the Weizsäcker gradient term[8]). A more satisfactory procedure would be to try to obtain the energy density, at least apart from the gradient terms, from the Brueckner method.

A way of circumventing such detailed knowledge in using the statistical method has been suggested by Wilets [9–11]). A similar approach to the problem of the nuclear surface has also been made by Skyrme [12]). In this semi-empirical statistical method the energy density is assumed to depend on the nucleon densities in a plausible way through, in the first place, unspecified parameters, which may then subsequently be related to nuclear matter calculations based on realistic nuclear forces. Thus in Wilets' treatment [9, 11]) of the distribution of the total nucleon density essentially two parameters enter: the nuclear compressibility which specifies the density dependence of the volume energy density and the magnitude of the Weizsäcker type gradient terms considered by Wilets as essentially unknown [13]). These two parameters may then be determined, through the method, by making use of the empirical surface energy term of the semi-empirical mass formula and the nuclear surface thickness as determined by the electron scattering experiments [14]). The large value of the compressibility coefficient obtained is in fair agreement with that calculated by Brueckner and Gammel [1]) for nuclear matter using realistic two-body forces. However, especially Naqvi [15]) has shown that in the Hartree-Fock approximation it is in general to be expected that the effective magnitudes of the Weizsäcker gradient terms will be different for the calculation of the energy and for the variational calculation. This implies that Wilets' results cannot be expected to be unique.

In the present paper, using the semi-empirical statistical method, the emphasis will be mainly on the difference between the neutron and proton densities and associated effects arising from a difference in the number of neutrons and protons. A calculation of the difference between the neutron and proton density distributions has been made by Wilets [10, 11]) who assumed a definite and essentially arbitrary form for the density dependence of the symmetry energy density. It will however be shown that the difference between the neutron and proton densities depends quite importantly on this density dependence and that, in the spirit of the semi-empirical statistical method, this density dependense must be introduced, in the first place, through undetermined parameters.

In addition to the well-known Weizsäcker type gradient terms it is also found necessary to introduce a mixed gradient term $\propto \nabla\rho_n \cdot \nabla\rho_p$. The magnitude of this new gradient term must then be considered as a further parameter. Also, as a result of Naqvi's investigation [15]), we shall not assume in general that the effective magnitudes of the gradient terms are the same for the calculation of the energy and the variational calculation. However, by making use of the empirical surface energy and thickness the permissible magnitudes of

the gradient terms are considerably restricted and the general conclusions become to a large extent independent of the uncertainties in the gradient terms.

In order to determine the difference in extension of the neutron and proton densities and thus also the density dependence of the symmetry energy density (within limits determined by the uncertainties due to the gradient terms) another piece of data is clearly required. This will be shown to be provided by the surface symmetry energy [16]) which has been determined in recent fits of the binding energies [17, 18]). Thus in general an important aim of this investigation is to obtain an understanding of the effects due to a difference in the number of neutrons and protons not only on the nucleon density distributions but also on the total binding energy.

2. The Semi-Empirical Statistical Method

2.1. THE ENERGY DENSITY AND THE VARIATIONAL PROBLEM

In the statistical method the neutron and proton densities, ρ_n and ρ_p, for a nucleus of N neutrons and Z protons are obtained from the condition $\delta\int\varepsilon(\rho_n, \rho_p)dv = 0$ with respect to independent variations of ρ_n and ρ_p together with the subsidiary conditions $\int\rho_n dv = N$, $\int\rho_p dv = Z$. Only spherically symmetric density distributions will be considered.

Here, $\varepsilon(\rho_n, \rho_p)$ is the energy density for which we take the following general form:

$$\varepsilon(\rho_n, \rho_p) = \varepsilon_v(\rho)+\varepsilon_\tau(\rho_n, \rho_p)+V_C\rho_p + K_0\left[\frac{(\nabla\rho_n)^2}{\rho_n}+\frac{(\nabla\rho_p)^2}{\rho_p}\right] + K_1\frac{4\nabla\rho_n\cdot\nabla\rho_p}{\rho_0}\left(\frac{\rho_0}{\rho}\right)^n, \quad (2.1)$$

where $\rho = \rho_n+\rho_p$ is the total nucleon density, and ρ_0 is the total central density of nuclei, assumed to be also to a good approximation the density of nuclear matter.

For the volume energy density $\varepsilon_v(\rho)$ we take the following convenient two-parameter (K and m) form

$$\varepsilon_v(\rho) = \rho\left\{-P+K_m\left[\left(\frac{\rho}{\rho_0}\right)^m-1\right]^2+k_m\left[\left(\frac{\rho}{\rho_0}\right)^m-1\right]^3\right\}, \quad (2.2a)$$

where P is the binding energy per particle of nuclear matter and $K_m = K/18m^2$; K is the usual compressibility coefficient and m is a further parameter. Further, $k_m = -P+K_m$ and is such that $[\varepsilon_v(\rho)/\rho]_{\rho=0} = 0$, i.e. that the energy per particle is zero for $\rho = 0$ as is physically required. This condition must be satisfied in order to obtain a reasonably realistic representation of $\varepsilon_v(\rho)$ for the whole range of values $0 \leqq \rho \leqq \rho_0$. The value $m = \frac{1}{3}$ corresponds to expanding $\varepsilon_v(\rho)$ in terms of the usual scale parameter $(\rho/\rho_0)^{\frac{1}{3}}$. We shall also consider the

one-parameter (K) form used by Wilets [11])

$$\varepsilon_v(\rho) = \rho P\left[-2\left(\frac{\rho}{\rho_0}\right)^k + \left(\frac{\rho}{\rho_0}\right)^{2k}\right], \tag{2.2b}$$

where k is determined by $K = 18Pk^2$. Eq. (2.2b) satisfies $[\varepsilon_v(\rho)/\rho]_{\rho=0} = 0$.

For the symmetry energy density $\varepsilon_\tau(\rho_n, \rho_p)$ we take

$$\varepsilon_\tau(\rho_n, \rho_p) = u_\tau \lambda^2 \rho F(\rho), \tag{2.3}$$

with

$$\lambda = \frac{\rho_n - \rho_p}{\rho} \tag{2.4}$$

and

$$F(\rho) = 1 + \alpha\frac{\rho-\rho_0}{\rho_0} + \beta\frac{(\rho-\rho_0)^2}{\rho_0^2}. \tag{2.5}$$

The coefficient u_τ specifies the magnitude of ε_τ at ρ_0, while $F(\rho)$ gives the density dependence of ε_τ in terms of two parameters α, β. Since physically for a given λ(given $(N-Z)/A$) the symmetry energy per particle must be zero for $\rho = 0$, i.e. $[\varepsilon_\tau(\rho_n, \rho_p)/\rho]_{\rho=0} = 0$, it is seen that α, β must satisfy $\alpha - \beta = 1$. This condition must be satisfied in order to obtain a reasonable representation of $F(\rho)$ for the whole range of values $0 \leqq \rho \leqq \rho_0$.

We denote by V_C the Coulomb potential, the small exchange contribution to the Coulomb energy having been neglected. The coefficients K_0, K_1 are defined by

$$K_i = \xi_i \frac{\hbar^2}{8M} \quad (i = 0,1); \tag{2.6}$$

M is the nucleon mass and

$$\frac{\hbar^2}{8M} = 2.6\ (r_e/f)^2\ \text{MeV}, \tag{2.7}$$

$r_e = 1.41\ f$ with $f = 10^{-13}$ cm. The parameter ξ_0 determines the magnitude of the well-known Weizsäcker type gradient terms. These arise in regions of varying density from the kinetic energy and from the potential energy due to the interactions between *like* nucleons. The parameter ξ_1 determines the magnitude of the mixed gradient term. This is new and arises from the interactions between *unlike* nucleons. This will be shown in a subsequent paper. It is found, in the independent-particle approximation, that $\xi_1 \approx 1$ for the conditions appropriate to nuclear matter. If the dynamic correlations are predominantly of two-body type and if these are of fairly short range compared with the internucleon distance — a condition necessary for the applicability of the Brueckner method [2]), — the estimate of the mixed gradient term obtained in the independ-

ent particle approximation should be not unreasonable, at least as regards order of magnitude. Two values of n will be considered: $n = 0, 1$. The value $n = 1$ corresponds to the same density dependence as that of the usual Weizsäcker terms. It may, however, be shown that $n = 0$ is more plausible. For a given ξ_1, the value $n = 0$ will give a smaller effective contribution than $n = 1$.

The above discussed magnitude of the mixed gradient term is essentially based on the value appropriate for the calculation of the energy from eq. (2.14). More fundamental investigations [15, 19–21]), especially that by Naqvi [15]), of the statistical method, based on the Hartree-Fock approximation, indicate, however, that the effective magnitude ξ_{0V} of the Weizsäcker type gradient terms entering into the variational condition may be different, possibly larger [15]), than the magnitude ξ_{0E} appropriate for the energy †. This difference may exist also for the mixed gradient term, although it may perhaps be expected to be less for this, there being no kinetic energy contribution. For the present we shall, merely for convenience, assume the values for both the variational condition and the energy to be the same. When these are to be distinguished we shall denote the appropriate value by a suffix $_V$ or $_E$.

It is convenient to use ρ and λ instead of ρ_n and ρ_p. Then ε separates into terms depending only on ρ and terms involving λ (the Coulomb energy is more conveniently left expressed in terms of ρ_p):

$$\begin{aligned}\varepsilon(\rho,\lambda) = {} & \varepsilon_V(\rho)+K_W\frac{(\nabla\rho)^2}{\rho}+V_C\rho_p \\ & +u_\tau\lambda^2\rho F(\rho)+K_0\frac{\rho(\nabla\lambda)^2}{1-\lambda^2} \\ & -K_1\left[\lambda^2\frac{(\nabla\rho)^2}{\rho}+2\lambda\nabla\rho\cdot\nabla\lambda+\rho(\nabla\lambda)^2\right]\left(\frac{\rho_0}{\rho}\right)^{n-1},\end{aligned} \tag{2.8}$$

where

$$K_W = \frac{\hbar^2}{8M}\xi_W = K_0+K_1\left(\frac{\rho_0}{\rho}\right)^{n-1} \tag{2.9}$$

determines the effective magnitude of the Weizsäcker term for ρ. For $n = 1$,

$$\xi_W = \xi_0+\xi_1 \quad (n = 1). \tag{2.10a}$$

For $n = 0$ it is still possible to use the usual form of the Weizsäcker term with K_W independent of ρ by taking a suitable average of eq. (2.9) over the nuclear surface. With the Gaussian surface eq. (3.1),

$$\xi_W = \xi_0+0.28\,\xi_1 \quad (n = 0), \tag{2.10b}$$

† See also ref. [13]) where an empirical investigation of the magnitude of the Weizsäcker gradient terms is given.

is a good approximation for all except very light nuclei. It is thus to be noted that ξ_W, i.e. the effective magnitude of the Weizsäcker gradient term for the total density, has an important contribution from the mixed gradient term.

The densities ρ_n and ρ_p are then obtained, for given N and Z, from the solutions ρ and λ of the variational condition

$$\delta \int \varepsilon(\rho, \lambda) \mathrm{d}v = 0, \tag{2.11}$$

with respect to independent variations of ρ and λ the variation being taken with the subsidiary conditions

$$\int \rho \, \mathrm{d}v = A, \tag{2.12}$$

$$\int \rho \, \lambda \mathrm{d}v = N - Z. \tag{2.13}$$

The pair of coupled Euler equations for ρ and λ appropriate to eq. (2.11) with ε given by eq. (2.8) will not be written down since the variational problem will be solved directly using trial densities. We may, however, mention that when $\xi_1 = 0$, the Coulomb forces are neglected, and $F(\rho) = 1$, then the exact solution of the Euler equations corresponds to $\lambda =$ constant, and thus using the subsidiary conditions to $\lambda = \lambda_0 = (N-Z)/A$ or $\rho_n/\rho_p = N/Z$. Thus, in this case, ρ_n and ρ_p are proportional to each other and in particular their extensions are the same. If now the Coulomb forces are switched on the Coulomb repulsion between the protons will cause these to extend further out than the neutrons. Also when $\xi_1 = \xi_0 = 0$ and the Coulomb forces are neglected it is possible to see some features of the exact solutions. Then, although in general λ is not constant, it is proportional to $N-Z$, and with a central region of constant ρ both ρ_n and ρ_p start to fall off together outside this central region.

The variational solution will be self-consistent within the limits of applicability of the statistical method. This of course cannot reproduce finer features of the density distributions arising from details of shell structure; in particular the tail of the wavefunction of an odd, loosely bound, nucleon may well extend somewhat beyond the bulk of the corresponding density distribution.

2.2. THE ENERGY AND THE SEMI-EMPIRICAL MASS FORMULA

The solution of the variational problem forms one aspect of the semi-empirical statistical approach. The other aspect is the relation of the energy

$$E = \int \varepsilon \, \mathrm{d}v, \tag{2.14}$$

obtained from eq. (2.8) and eqs. (2.12), (2.13) as a function of N and Z, with the semi-empirical mass formula (for shortness: mass formula). For a given ε, eq. (2.14) gives both volume and surface energy terms for a finite nucleus.

These terms as functions of N and Z may then be compared with the corresponding terms of the mass formula.

In considering differences between ρ_n and ρ_p (i.e. λ) the relevant terms in the mass formula are the symmetry energy terms. In addition to the well-known volume symmetry energy $E_{v\tau}$ more recent analyses [17, 18]) of the nuclear binding energies have also included a surface symmetry energy $E_{s\tau}$ [16]). With

$$\lambda_0 = \frac{N-Z}{A}, \tag{2.15}$$

the empirical symmetry energies are given by

$$E_{v\tau} = u_\tau \lambda_0^2 A, \tag{2.16}$$

$$E_{s\tau} = -u_{s\tau} \lambda_0^2 A^{\frac{2}{3}}. \tag{2.17}$$

However, also the volume energy $E_v = -AP$ and the surface energy $E_s = u_s A^{\frac{2}{3}}$ will enter when the theoretical expression for $E_{s\tau}$ is considered.

Two independent analyses including $E_{s\tau}$ have been made, the results being in reasonably good agreement with each other (all energies in MeV):

Green [17, 11]) : $P = 16.34$, $u_\tau = 30.34$, $u_s = 20.96$, $u_{s\tau} = 36.35$, (2.18a)

Cameron [18]): $P = 17.04$, $u_\tau = 31.45$, $u_s = 25.84$, $u_{s\tau} = 44.24$. (2.18b)

In relating eq. (2.8) to the mass formula, through eq. (2.14), P and u_τ in eq. (2.2) and eq. (2.3) will turn out to be just the constants which occur in E_v and $E_{v\tau}$, respectively, as has been implied above. The Coulomb energy E_C will be in agreement with the semi-empirical value by choosing the densities to be consistent with the nuclear charge distribution as determined by the electron scattering experiments [14]).

Since in the semi-empirical statistical method the values of the various energy terms obtained from eq. (2.14) are required to be in numerical agreement with the corresponding semi-empirical values, the nuclear stability conditions [22]) implied by the mass formula will be automatically satisfied. In particular the bottom of the mass valley, which is determined by competition between E_C and $E_{v\tau}$, $E_{s\tau}$, will be given by [23])

$$Z = A(1.981 + 0.01496\, A^{\frac{2}{3}})^{-1}$$

or

$$\lambda_0 = 1 - 2(1.981 + 0.01496\, A^{\frac{2}{3}})^{-1}. \tag{2.19}$$

It is seen that for the stable nuclei, approximately, $\lambda_0 \propto A^{\frac{2}{3}}$ ($\lambda_0 \approx 0.0075\, A^{\frac{2}{3}}$) and that λ_0 is rather small ($\lesssim 0.2$) even for the heaviest stable nuclei.

3. The Nucleon Densities

3.1. SEPARABILITY OF THE VARIATIONAL PROBLEM

We shall choose the trial densities ρ_n, ρ_p for the variational problem of eq. (2.11) to be such that the difference between ρ_n and ρ_p is specified by a single variational parameter which is essentially the difference $\delta = t_n - t_p$ between the surface thicknesses t_n, t_p of ρ_n, ρ_p. To achieve this and also to separate the variational problem for the difference between ρ_n and ρ_p (i.e. for λ) from that for ρ we shall choose ρ_n and ρ_p such that $\rho = \rho_n + \rho_p$ remains fixed — and essentially in agreement with the empirically determined density — when only δ is varied.

The justification for this procedure may be seen as follows: ρ will be specified in terms of various parameters (e.g. the central density and the surface thickness) which together with δ will be determined by the complete variational condition (2.11) for both ρ and λ. Since the conditions for ρ and λ are coupled, the complete solution would, schematically, be obtained in the form $\rho = \rho(\delta)$, $\delta = \delta(\rho)$, and ρ and δ (and therefore λ) are then obtained by solving these simultaneous equations. Besides contributions from the terms depending on both ρ and λ in eq. (2.8), the equation $\rho = \rho(\delta)$ will involve contributions from those terms of eq. (2.8) which depend only on ρ, i.e. $\varepsilon_v(\rho) + K_W(\nabla\rho)^2/\rho$, these not contributing to the equation $\delta = \delta(\rho)$. Thus for any given ρ the variational problem for δ is determined irrespective of ξ_W and $\varepsilon_v(\rho)$ †. Now, eventually the solution for ρ must be such as to agree with the empirical distribution and this may always be achieved to a very good approximation by a suitable choice of ξ_W and the dependence of ε_v on ρ. Strictly, the variational problem $\delta = \delta(\rho)$ will involve an implicit dependence on δ through $\rho = \rho(\delta)$, the latter manisfesting itself by a dependence of ρ on $(N-Z)/A$. However, this dependence of ρ is small (see sect. 6) and for $\delta = \delta(\rho)$ it is a very good approximation to use just the empirically determined distribution for ρ which, in fact, with the presently available data shows no significant dependence on $(N-Z)/A$. Thus for δ only the variational problem $\delta = \delta(\rho)$ need be considered, ρ being just such as to agree with the empirical distribution. However, when considering the total surface energy, $E_s + E_{s\tau}$, such a separation is no longer possible. This is because of the dependence of ρ on δ which, although small, implies that there are contributions to $E_{s\tau}$ which are of a similar order of magnitude as the contributions to $E_{s\tau}$ corresponding to $\delta = \delta(\rho)$. Thus for $E_{s\tau}$ we must also consider the problem for $\rho = \rho(\delta)$ which will involve $\varepsilon_v(\rho)$ and ξ_W.

3.2. THE TOTAL NUCLEON DENSITY

We shall take ρ to be constant in the nuclear interior and to have a Gaussian fall-off outside this:

† This type of separability for the variational problem for δ from that for ρ may also be seen from the two Euler equations for the problem. One of these in fact determines λ in terms of only ε_τ, ξ_0 and ξ_1, for any chosen ρ.

$$\begin{aligned} \rho &= \rho_0 \qquad \text{for} \quad r < R_0 \\ \rho &= \rho_0 e^{-x^2/t^2} \quad \text{for} \quad r > R_0, \end{aligned} \tag{3.1}$$

where $x = r - R_0$ and t determines the surface thickness. This distribution has the advantage that all the integrals subsequently occurring can be evaluated analytically, while at the same time being sufficiently realistic.

The electron scattering data [14]) indicate that the surface thickness of the nuclear charge distribution is remarkably constant for a wide range of nuclei, while an analysis by Elton [24]) of these data also shows them to be consistent with a central density which is the same for all nuclei. It will be assumed that the distribution of ρ is to a good approximation the same as that of ρ_p. This will be confirmed by the results of the present paper. In fact for not too large differences between the distributions of ρ and ρ_p this assumption affects the results only slightly. Then from Elton's results [24]) the parameters of eq. (3.1) are given by

$$r_0 = (\tfrac{4}{3}\pi\rho_0)^{-\frac{1}{3}} = 1.115\, f, \quad t = 2f, \tag{3.2}$$

the last value corresponding to a 90 %—10 % transition thickness of 2.38 f. With ρ given by eq. (3.1) the subsidiary condition (2.12) relates R_0 to ρ_0 and therefore to r_0. To a very good approximation

$$R_0 = \omega_A r_0 A^{\frac{1}{3}}, \tag{3.3}$$

with

$$\omega_A = 1 - 0.886\tau_0 - 0.214\tau_0^2 - 0.0213\tau_0^3, \tag{3.4}$$

where

$$\tau_0 = t/r_0 A^{\frac{1}{3}} \quad \text{and, from eq. (3.2),} \quad t/r_0 = 1.8. \tag{3.5}$$

Thus ω_A and therefore R_0 is readily obtained and eq. (3.1) is then fully known for any given A in terms of r_0 and t.

A quantity which will occur frequently is $4\pi\rho_0 R_0^3\tau$ which from eq. (3.3) is

$$4\pi\rho_0 R_0^3\tau = 3\frac{t}{r_0}\omega_A^2 A^{\frac{2}{3}}, \tag{3.6}$$

where

$$\tau = \frac{t}{R_0} = \frac{\tau_0}{\omega_A}. \tag{3.7}$$

The parameter τ determines the importance of the curvature of the surface. It is seen that, approximately, $4\pi\rho_0 R_0^3\tau \propto A^{\frac{2}{3}}$ and energy terms involving this expression are thus surface terms, the factor ω_A^2 arising from curvature corrections due to the finite nuclear size. Some numerical values are given in table 1.

3.3. THE NEUTRON AND PROTON TRIAL DENSITIES

We consider in the first instance Gaussian surfaces for both ρ_n and ρ_p with thicknesses t_n and t_p and central densities ρ_{0n} and ρ_{0p} both constant out to the

TABLE 1
Numerical values of nuclear surface parameters

A	64	125	216
τ_0	0.45	0.36	0.3
ω_A	0.556	0.652	0.714
τ	0.81	0.5515	0.42

same radius R_0 as for ρ. Then, with $\frac{1}{2}(t_n+t_p)=t+d$ and $t_n-t_p=\delta$, we have

$$e^{-x^2/t_n^2}=e^{-x^2/t^2}\left[1+\frac{x^2}{t^2}\left(2\frac{\Delta_n}{t}-3\left(\frac{\Delta_n}{t}\right)^2\right)+2\left(\frac{\Delta_n}{t}\right)^2\frac{x^4}{t^4}\right.$$
$$\left.+\text{terms involving higher powers of } \Delta_n/t \text{ and } x^2/t^2\right] \quad (3.8)$$

where $\Delta_n=t_n-t=d+\frac{1}{2}\delta$. We have a similar expression for $\exp(-x^2/t_p^2)$, with $\Delta_p=t_p-t=d-\frac{1}{2}\delta$. Now the requirement that

$$\rho_n+\rho_p=\rho_0 e^{-x^2/t^2}$$

for $r>R_0$ can only be satisfied if in eq. (3.8) terms involving x^4/t^4 and higher powers are not present. Thus to estimate the effects of terms in $(\delta/t)^2$ in the trial densities we must make some allowance for the third term, involving x^4/t^4, in eq. (3.8) and correspondingly for ρ_p. We do this by replacing x^4/t^4 by $(x^2/t^2)\overline{(x/t)^2}$ where $\overline{(x/t)^2}$ is the average of x^2/t^2 over the distribution (3.1) for $r>R_0$. The trial densities we use are then

$$\rho_n=\begin{cases}\rho_{0n}=\rho_0\dfrac{N'}{A} & (r<R_0) \quad (3.9a)\\ \rho\dfrac{N'}{A}\left[1+\dfrac{x^2}{t^2}\left(2\dfrac{d}{t}+\dfrac{\delta}{t}\right)\left\{1-\frac{1}{4}\mu\left(2\dfrac{d}{t}+\dfrac{\delta}{t}\right)\right\}\right] & (r>R_0) \quad (3.9b)\end{cases}$$

and

$$\rho_p=\begin{cases}\rho_{0p}=\rho_0\dfrac{Z'}{A} & (r<R_0) \quad (3.10a)\\ \rho\dfrac{Z'}{A}\left[1+\dfrac{x^2}{t^2}\left(2\dfrac{d}{t}-\dfrac{\delta}{t}\right)\left\{1-\frac{1}{4}\mu\left(2\dfrac{d}{t}-\dfrac{\delta}{t}\right)\right\}\right] & (r>R_0), \quad (3.10b)\end{cases}$$

with

$$\mu=3-2\frac{\overline{x^2}}{t^2}. \quad (3.11)$$

From eqs. (3.1) and (3.2,) $2\overline{(x/t)^2}\approx 1.5$ and thus $\mu\approx 1.5$, for all except rather light nuclei. Eqs. (3.9a) and (3.10a) define N' and Z'.

The condition that $\rho_n + \rho_p = \rho$, with ρ given by eq. (3.1), then gives

$$\rho_{0n}+\rho_{0p} = \rho_0 \quad \text{or} \quad N'+Z' = A, \tag{3.12}$$

and

$$\frac{d}{t} = \tfrac{1}{2}\left[-\lambda'_0\frac{\delta}{t} + \tfrac{1}{8}\mu\left(\frac{\delta}{t}\right)^2(1-\lambda_0'^2) + \tfrac{1}{32}\mu\left(\frac{\delta}{t}\right)^4(1-\lambda_0'^2)^2\right], \tag{3.13}$$

with

$$\lambda'_0 = \frac{N'-Z'}{A}. \tag{3.14}$$

Also, using eqs. (3.12) and (3.14),

$$\frac{N'}{A} = \frac{\rho_{0n}}{\rho_0} = \tfrac{1}{2}(1+\lambda'_0); \quad \frac{Z'}{A} = \frac{\rho_{0p}}{\rho_0} = \tfrac{1}{2}(1-\lambda'_0). \tag{3.15}$$

For a given ρ, ρ_n and ρ_p now depend only on δ; λ'_0 being determined in terms of δ by the subsidiary condition (2.13). Thus, from eqs. (3.9), (3.10), (3.12), (3.13) and (3.14),

$$\lambda = \frac{\rho_n-\rho_p}{\rho} = \begin{cases} \lambda'_0 & (r < R_0) \\ \lambda'_0 + \dfrac{x^2}{t^2}(1-\lambda_0'^2)\dfrac{\delta'}{t} & (r > R_0), \end{cases} \tag{3.16}$$

where

$$\frac{\delta'}{t} = \frac{\delta}{t}\left[1 + \tfrac{1}{2}\mu\lambda'_0\frac{\delta}{t} - \tfrac{1}{8}\mu(1-\lambda_0'^2)\left(\frac{\delta}{t}\right)^2\right]. \tag{3.17}$$

The subsidiary condition (2.13) then gives the following equation which determines λ'_0 in terms of δ/t:

$$\frac{B\mu}{2}(\lambda_0'^3-\lambda'_0)\left(\frac{\delta}{t}\right)^2 + \lambda_0'^2\frac{\delta}{t}B - \lambda'_0 + \left(\lambda_0 - \frac{\delta}{t}B\right) = 0, \tag{3.18}$$

where

$$B = \tfrac{3}{4}\sqrt{\pi}\,\tau b = \tfrac{3}{4}\sqrt{\pi}\tau(1+2.26\tau+1.5\tau^2)(1+2.66\tau+3\tau^2+1.33\tau^3). \tag{3.19}$$

The appropriate solution of eq. (3.18) is, to the third order in δ/t,

$$\Delta\lambda_0 = \lambda'_0-\lambda_0 = -B(1-\lambda_0^2)\frac{\delta'}{t} - 2B^2\lambda_0(1-\lambda_0^2)\left(\frac{\delta'}{t}\right)^2 + B^3(1-\lambda_0^2)(1-5\lambda_0^2)\left(\frac{\delta}{t}\right)^3, \tag{3.20}$$

where here δ'/t is just the value obtained from eq. (3.17) with λ'_0 from eq. (3.20) to the first order in δ/t, i.e.,

$$\frac{\delta'}{t} = \frac{\delta}{t}\left[1 + \tfrac{1}{2}\mu\lambda_0 \frac{\delta}{t} - \tfrac{1}{2}\mu\,(1-\lambda_0^2)\,(0.25+B)\left(\frac{\delta}{t}\right)^2\right]. \tag{3.21}$$

Thus for a given ρ the trial densities ρ_n and ρ_p are fully determined for given N and Z by the one parameter δ/t through eqs. (3.9)—(3.15), (3.19)—(3.21), while λ is given as a function of δ/t by eqs. (3.16), (3.19)—(3.21). The dependence of λ'_0 on δ/t in eq. (3.20), represents for fixed ρ the mutual compensation of ρ_n and ρ_p in the central region due to changing the relative extensions of ρ_n and ρ_p. From the way in which the trial densities have been obtained it is seen that these have very nearly Gaussian surfaces for small δ/t. Thus if δ/t is small, δ will, to a good approximation, just be the difference in the Gaussian surface thicknesses of ρ_n and ρ_p. The above trial densities are expected to give an adequate representation of the relevant physical features since they relate in a reasonable way the variation of the extensions of ρ_n and ρ_p with the mutual changes of these densities at each other's expense.

For much of the following work we may just put $\mu = 0$, i.e. retain only the first order terms in δ/t in the trial functions (3.9) and (3.10), and thus replace δ'/t by just δ/t in the expressions (3.16) and (3.20) for λ and λ'_0. To obtain the effects due to the second order terms involving μ one has then merely to replace, in all the expressions so obtained for the energy, δ/t by δ'/t as given by eq. (3.21). The second order terms in ρ_n, ρ_p can clearly only contribute to terms involving $(\delta/t)^2$ and higher powers of δ/t in the energy. These contributions, however, turn out to be only of order λ_0^2, and thus small, relative to the second order contributions due to the first-order terms in the trial densities. Thus the trial densities for $\mu = 0$ turn out to be rather satisfactory, even when they are used to obtain the energy to higher powers than the first in δ/t. Any uncertainty in the precise values of μ will thus be unimportant.

For $\mu = 0$, ρ_p which will be required for the Coulomb energy, is, from eqs. (3.10), (3.13) and (3.14),

$$\rho_p = \begin{cases} \rho_0 \dfrac{Z'}{A} & (r < R_0) \\ \rho \dfrac{Z'}{A}\left[1 - 2\dfrac{x^2}{t^2}\dfrac{\delta}{t}\dfrac{N'}{A}\right] & (r > R_0), \end{cases} \tag{3.22}$$

with N' and Z' determined in terms of δ/t by eqs. (3.15), (3.19) and (3.20).

The trial densities, as functions of N and Z, have thus been obtained in terms of three variational parameters: ρ_0 and t determining $\rho = \rho_n + \rho_p$ and δ determining the difference between ρ_n and ρ_p.

4. The Energy

With the trial densities of sections 3.2 and 3.3 and the energy density (2.8) the total energy may be calculated from eq. (2.14) in closed form. These calculations are straightforward but often tedious, especially for the Coulomb energy, and only the results will be given. In the expansion of the energy in powers of δ/t we shall not consider higher powers than $(\delta/t)^3$.

4.1. THE SURFACE ENERGY AND THE MAGNITUDE OF THE WEIZSÄCKER GRADIENT TERMS FOR ρ

As indicated in sect. 3.1 it is necessary to consider E_s in connection with the expression for $E_{s\tau}$. Consideration of E_s together with the surface thickness t will also give estimates for ξ_{WE} and ξ_{WV}. It will be adequate to consider E_s in the semi-infinite approximation, i.e. when the curvature of the nuclear surface is neglected (see sect. 4.2) †. E_s arises in addition to $E_v = -PA$ from the part of eq. (2.8) which depends only on ρ, i.e. from $\varepsilon_v(\rho)+K_W(\nabla\rho)^2/\rho$. Then from this and eqs. (2.2), (2.14), (3.1) and (3.6) (with $\omega_A = 1$ in the semi-infinite approximation) one obtains ††

$$E_s = \tfrac{3}{4}\sqrt{\pi}A^{\frac{2}{3}}\frac{t}{r_0}Q\left[T+10.4\left(\frac{r_e}{t}\right)^2\frac{\xi_{WE}}{Q}\right], \tag{4.1}$$

where for eq. (2.2a)

$$Q = K_m,\ T = 2\left[\left(\frac{1}{\sqrt{2m+1}}-\frac{2}{\sqrt{m+1}}+1\right)\right.$$
$$\left.+\frac{k_m}{K_m}\left(\frac{1}{\sqrt{3m+1}}-\frac{3}{\sqrt{2m+1}}+\frac{3}{\sqrt{m+1}}-1\right)\right] \tag{4.2a}$$

and for eq. (2.2b)

$$Q = P,\quad T = 2\left[\frac{1}{\sqrt{2k+1}}-\frac{2}{\sqrt{k+1}}+1\right]. \tag{4.2b}$$

The variational condition (2.11) for ρ then implies that, in the approximation when all the terms in eq. (2.8) except those depending only on ρ are neglected, t will be determined by $\mathrm{d}E_s(\xi_{WV})/\mathrm{d}t = 0$. The quantity ξ_{WE} in eq. (4.1) must be

† Since the effects of curvature turn out to be mainly due to the Coulomb energy, the semi-infinite approximation is in fact rather good for E_s.

†† Here, as elsewhere in this paper, we have ignored the difference between ρ_∞, the density of nuclear matter, and ρ_0, the central density. Such a difference will arise with a finite compressibility coefficient. Thus we have considered t as the only variational parameter for ρ, and not also ρ_0. The effect of compressibility on ρ_0 is rather easily included, but can be shown to be unimportant for the purposes of this paper. It is, however, of vital importance for changes of radius between nuclei see e.g. ref. [25]). We hope to return to this problem, for nuclei with a finite surface thickness in a later paper.

replaced by ξ_{WV}, appropriate to the variational condition, which then gives

$$t = 3.22\, r_e \sqrt{\frac{\xi_{WV}}{QT}}. \tag{4.3}$$

ξ_{WV} and ξ_{WE} may now be obtained as functions of K (and also of m for eq. (2.2a)) from eqs. (4.1), (4.2) and (4.3) by making use of the empirical values of u_s, P and t. Thus

$$\xi_{WV} = 0.0963\, QT \frac{t^2}{r_e^2}, \tag{4.4}$$

$$\xi_{WE} = 0.0723\, u_S \frac{t r_0}{r_e^2} - 0.0963\, QT \frac{t^2}{r_e^2}, \tag{4.5}$$

and thus

$$\chi = \frac{\xi_{WV} - \xi_{WE}}{\xi_{WV}} = 2\left(1 - 0.375 \frac{u_S}{QT} \frac{r_0}{t}\right). \tag{4.6}$$

As is expected, $\xi_{WV} = \xi_{WE} = 0$ when $t = 0$. Wilets [12]) assumed $\xi_{WV} = \xi_{WE}$ and thus, with eq. (2.2b) and by direct solution of the appropriate Euler equation, obtained $K = 218$ MeV for the values (2.18a) and $K = 302$ MeV for the values (2.18b). The values of K obtained from eq. (4.6), putting $\chi = 0$, are in good agreement with Wilets' values, as may be seen from inspection of table 2. However, we shall not assume $\xi_{WV} = \xi_{WE}$ but rather obtain these as functions of K (and m) from eqs. (4.4) and (4.5). Numerical values with $t = 2f$ are given in table 2. $K = 170$ MeV corresponds closely to the values obtained by Brueckner and Gammel [1]). σ' will be of importance later in connection with $E_{s\tau}$ and is defined by

$$\sigma' = \frac{\sigma}{1 - \frac{1}{2}\chi}, \quad \sigma = \frac{u_{s\tau}}{u_\tau}. \tag{4.7}$$

From table 2 it is seen that for a given K the different forms used for ε_v give similar results except for small m in conjunction with very large K †. This latter case must, however, be excluded because the expression (2.2a) changes sign (i.e. $\varepsilon_v(\rho)$ becomes positive) for $0 < \rho < \rho_0$ if K is sufficiently large. Thus for $m = \frac{1}{3}$ such a change in sign occurs for $K = 100$ MeV and for $K = 200$ MeV the expression (2.2a) becomes quite appreciably positive for a considerable range of values of ρ and can no longer be considered as giving a reasonable representation of $\varepsilon_v(\rho)$. For $m = 1$ this change of sign occurs only for $K \lesssim 300$ MeV, while for expression (2.2b) no such change of sign occurs. It is then seen from table 2 that for all reasonable $\varepsilon_v(\rho)$ both ξ_{WV} and ξ_{WE} are of the order of

† It may be remarked that, for $\rho_0/\rho > 1$, eq. (2.2a) with $m = 1$ gives a slightly better fit than either $m = \frac{1}{3}$ or eq. (2.2b), to the curves for $\varepsilon_v(\rho)/\rho$, given up to $(\rho_0/\rho)^{\frac{1}{3}} = 1.4$ by Brueckner and Gammel.

TABLE 2
Numerical values of the surface energy parameters

Parameters			Green, eq. (2.18a)				Cameron, eq. (2.18b)			
K (MeV)	eq.	m	ξ_{WV}	ξ_{WE}	χ	σ' ($\sigma = 1.2$)	ξ_{WV}	ξ_{WE}	χ	σ' ($\sigma = 1.4$)
100	(2.2a)	1	0.812	0.893	−0.10	1.144	0.844	1.266	−0.5	1.12
	(2.2a)	½	0.573	1.104	−0.926	0.820	0.589	1.519	−1.58	0.78
	(2.2b)		0.573	1.135	−0.98	0.805	0.605	1.502	−1.483	0.803
170	(2.2a)	1	0.892	0.815	0.086	1.25	0.923	1.181	−0.28	1.23
	(2.2a)	½	0.909	0.80	0.12	1.28	0.915	1.189	−0.30	1.22
	(2.2b)		0.777	0.932	−0.20	1.09	0.791	1.312	−0.66	1.05
200	(2.2a)	1	0.926	0.78	0.158	1.30	0.956	1.147	−0.20	1.27
	(2.2a)	½	1.05	0.662	0.37	1.47	1.053	1.053	0.00	1.40
	(2.2b)		0.86	0.846	0.015	1.21	0.857	1.252	−0.46	1.14
300	(2.2a)	1	0.913	0.794	0.13	1.285	1.071	1.038	0.032	1.42
	(2.2a)	½	1.515	0.194	0.872	2.13	1.52	0.59	0.612	2.02
	(2.2b)		1.04	0.67	0.355	1.45	1.078	1.032	0.04	1.43

unity and especially for presumably the more realistic values of $K \approx 200$ MeV do not differ very much. There seems no clear indication that $\xi_{WV} > \xi_{WE}$, although this is true for the larger values of K especially with eq. (2.18a). Naqvi's investigation [15]), based on the Hartree-Fock approximation, indicated that $\xi_{0V} > \xi_{0E}$ and that the difference may be quite appreciable. However, as Naqvi has emphasized, this conclusion is quite tentative since the difference he obtained between ξ_{0V} and ξ_{0E} depended quite sensitively on the detailed assumptions made about the form of the self-consistent potential. Additional uncertainties in making a direct comparison with our results arise from the contribution to ξ_W from ξ_1 (eq. (2.10)) and the inadequacy of the Hartree-Fock approximation †. It may also be noted that, in particular for $n = 0$, the results of table 2 are consistent with both ξ_0 and ξ_1 being of the order of unity.

Later on, when considering $E_{s\tau}$, we shall require the change in E_s due to the change Δt in t corresponding to the terms which were neglected in eq. (2.8) in obtaining the expression (4.3). The corresponding change in E_s is then from eq. (4.1), to the first order in Δt and making use of eq. (4.3):

$$\Delta E_s = \frac{\mathrm{d}E_s(\xi_{WE})}{\mathrm{d}t}\Delta t = \tfrac{3}{4}\sqrt{\pi}A^{\frac{1}{3}}QT\chi\Delta t. \tag{4.8}$$

Thus $\Delta E_s \neq 0$ only in virtue of $\xi_{WV} \neq \xi_{WE}$.

† Very tentatively, such a comparison seems to indicate that values of $K \lesssim 150$ MeV are not very likely and that for $K \approx 200$ MeV Green's values (2.18a) are slightly favoured as compared with Cameron's values (2.18b).

4.2. SYMMETRY AND δ-DEPENDENT ENERGY TERMS

For the variational problem for δ we require all the energy terms which depend on δ/t, while for the symmetry energy we shall in addition require the λ_0-dependent terms for $\delta = 0$ (i.e. when $\lambda = \lambda_0$). All the expressions for the energy given below are for $\mu = 0$. The bracketed superscripts indicate the relevant powers of δ/t.

The symmetry energy density (2.3) gives

$$E_{v\tau}+E_{s(\tau)}=u_\tau\left\{\lambda_0^2\int\rho F(\rho)\mathrm{d}v+2\lambda_0\int(\lambda-\lambda_0)\rho(F(\rho)-1)\mathrm{d}v + \int(\lambda-\lambda_0)^2\rho F(\rho)\mathrm{d}v\right\}, \quad (4.9)$$

with, using eqs. (3.1) and (2.5),

$$\rho F(\rho)=\begin{cases}\rho_0 & (r<R_0)\\ \rho_0 e^{-\frac{x^2}{t^2}}[(1-\alpha+\beta)+(\alpha-2\beta)e^{-\frac{x^2}{t^2}}+\beta e^{-\frac{2x^2}{t^2}}] & (r>R_0).\end{cases} \quad (4.10)$$

The subsidiary conditions (2.12), (2.13) have been used to replace F by $F-1$ in the second term of eq. (4.9). Since $\lambda \neq \lambda_0$ only when $\delta \neq 0$, the second and third terms in eq. (4.9) depend on δ/t, while the first term is independent of δ and gives rise to $E_{v\tau}$ as well as a contribution to $E_{s(\tau)}$ when $F(\rho) \neq 1$. Since $F(\rho_0) = 1$, the second term in eq. (4.9) arises only from the surface. We use $E_{s(\tau)}$ instead of $E_{s\tau}$ in order to distinguish the surface symmetry energy terms due to ε_τ from the total surface symmetry energy.

From eqs. (4.9), (4.10) and ρ and λ as given in sects. 3.1, 3.2, we have

$$E_{v\tau} = u_\tau\lambda_0^2 A, \quad (4.11)$$

$$E_{s(\tau)} = E^{(0)}_{s(\tau)}+\sum_{i=1}^{3}E^{(i)}_{s(\tau)}, \quad (4.12)$$

$$E^{(0)}_{s(\tau)} = -u_\tau\lambda_0^2(4\pi\rho_0 R_0^3\tau)\frac{\sqrt{\pi}}{4}S_0, \quad (4.13)$$

$$\sum_{i=1}^{3}E^{(i)}_{s(\tau)} = -u_\tau(4\pi\rho_0 R_0^3\tau)\frac{\sqrt{\pi}}{4}(1-\lambda_0^2) \times\left\{\lambda_0\frac{\delta}{t}S_1-\left(\frac{\delta}{t}\right)^2[(1-\lambda_0^2)S_2-2\lambda_0^2 BS_1]-\lambda_0\left(\frac{\delta}{t}\right)^3 2B[2(1-\lambda_0^2)S_2+\tfrac{1}{2}BS_1]\right\}, \quad (4.14)$$

where

$$S_0=\frac{4}{\sqrt{\pi}}s_0, \quad S_1=\frac{8}{\sqrt{\pi}}(s_1-s_0B), \quad S_2=\frac{4}{\sqrt{\pi}}\left[\left(s'_0+\frac{1}{3\tau}\right)B^2-2s'_1B+s'_2\right], \quad (4.15)$$

with

$$s_0 = -\frac{\sqrt{\pi}}{2}[(\beta-\alpha)(1+1.13\tau+0.5\tau^2)+(\alpha-2\beta)(0.707+0.564\tau+0.177\tau^2)$$
$$+\beta(0.578+0.376\tau+0.096\tau^2)],$$
$$s_1 = -\frac{\sqrt{\pi}}{4}[(\beta-\alpha)(1+2.26\tau+1.5\tau^2)+(\alpha-2\beta)(0.354+0.564\tau+0.265\tau^2)$$
$$+\beta(0.193+0.251\tau+0.096\tau^2)],$$
$$s'_0 = -s_0+\frac{\sqrt{\pi}}{2}(1+1.13\tau+0.5\tau^2),$$
$$s'_1 = -s_1+\frac{\sqrt{\pi}}{4}(1+2.26\tau+1.5\tau^2), \tag{4.16}$$
$$s'_2 = \frac{3\sqrt{\pi}}{8}[(1-\alpha+\beta)(1+3.009\tau+2.5\tau^2)+(\alpha-2\beta)(0.177+0.376\tau+0.221\tau^2)$$
$$+\beta(0.064+0.1115\tau+0.0535\tau^2)].$$

Thus from eq. (4.11), u_τ is seen to be just the coefficient of $E_{v\tau}$ in the mass formula. When $\alpha = \beta = 0 (F(\rho) = 1)$, $E_{s(\tau)}$ is seen to contain contributions only from terms involving $(\delta/t)^2$ or higher powers of δ/t, while when $\delta/t = 0$, $E_{s(\tau)} = E^{(0)}_{s(\tau)}$ and this is only different from zero when α, $\beta \neq 0$.

The Coulomb energy is

$$E_C = e\int V_C \rho_p \, dv, \quad V_C(r) = e\frac{4\pi}{r}\int_0^r \rho_p r'^2 \, dr', \tag{4.17}$$

ρ_p being given by eq. (3.22). We shall only give the results for the part of E_C depending on δ/t, this being the only part we require; we have

$$E_C^{(1)}+E_C^{(2)} = 0.1\,(4\pi\rho_0 R_0^3\tau)\frac{\sqrt{\pi}}{4}(1-\lambda_0^2)\left(e^2\frac{4\pi}{3}\rho_0 R_0^2\right)$$
$$\times\left[\frac{\delta}{t}\frac{Z}{A}C_1+\left(\frac{\delta}{t}\right)^2(1-\lambda_0^2)\,0.996\tau C_2\right], \tag{4.18}$$

where

$$C_1 = 6b+30\tau c_0 b-5c_1$$
$$C_2 = \left(6b^2+\frac{40}{9\pi}c_2+30\tau c_0 b^2-\tfrac{20}{3}c_1 b\right)-\frac{Z}{N}(4b^2-\tfrac{10}{3}c_1 b+20\tau c_0 b^2), \tag{4.19}$$

with

$$c_0 = 0.886+1.678\tau+1.715\tau^2+0.964\tau^3+0.235\tau^4,$$
$$c_1 = 1 \quad +3.785\tau+5.81\ \tau^2+4.36\ \tau^3+0.398\tau^4, \tag{4.20}$$
$$c_2 = 1.178+3.67\tau+4.018\ \tau^2+1.587\tau^3,$$

and b being given by eq. (3.19).

From eqs. (3.2), (3.3) we find

$$e^2\frac{4\pi}{3}\rho_0 R_0^2 = 1.292\,\omega_A^2 A^{\frac{1}{3}}\ \text{MeV}. \tag{4.21}$$

The second order term $E_C^{(2)}$ turns out to be of minor importance. The positive sign for $E_C^{(1)}+E_C^{(2)}$ expresses the fact that E_C is increased as the proton distribution is contracted (i.e. δ increased).

The energy due to the λ-dependent part of the Weizsäcker gradient term in eq. (2.8) (i.e. the term in K_0) is

$$\begin{aligned} E_{gW} &= E_{gW}^{(2)}+E_{gW}^{(3)} \\ &= (4\pi\rho_0 R_0^3\tau)\,\frac{\sqrt{\pi}}{4}\,(1-\lambda_0^2)10.4\frac{r_e^2}{t^2}\left[\left(\frac{\delta}{t}\right)^2 g_0+\left(\frac{\delta}{t}\right)^3\lambda_0 G_0\right]\xi_0\ (\text{MeV}), \end{aligned} \tag{4.22}$$

where

$$G_0 = 3g_1-2Bg_0,$$

with

$$\begin{aligned} g_0 &= 1+2.26\tau\ +1.5\tau^2, \\ g_1 &= 1+3.009\tau+2.5\tau^2. \end{aligned} \tag{4.23}$$

Thus $(\delta/t)^2$ is the lowest order in which the Weizsäcker gradient terms make a λ_0-dependent contribution.

The energy due to the λ-dependent part of the mixed gradient term in eq. (2.8) (i.e. the term in K_1) is

$$E_{gm} = E_{gm}^{(0)}+\sum_{i=1}^{3}E_{gm}^{(i)}, \tag{4.24}$$

$$E_{gm}^{(0)} = -(4\pi\rho_0 R_0^3\tau)\,\frac{\sqrt{\pi}}{4}\,\lambda_0^2\ 10.4\frac{r_e^2}{t^2}\,g_{0n}\xi_1\ (\text{MeV}), \tag{4.25}$$

$$\begin{aligned} \sum_{i=1}^{3}E_{gm}^{(i)} = -(4\pi\rho_0 R^3{}_0\tau)\,\frac{\sqrt{\pi}}{4}\,(1-\lambda_0^2)10.4\frac{r_e^2}{t^2} \\ \times\left[\frac{\delta}{t}\lambda_0 G_{1n}+\left(\frac{\delta}{t}\right)^2 G_{2n}+\left(\frac{\delta}{t}\right)^3\lambda_0 G_{3n}\right]\xi_1\ (\text{MeV}), \end{aligned} \tag{4.26}$$

where

$$\begin{aligned} G_{1n} &= 2[1.5g_{1n}-g_{0n}(1+B)], \\ G_{2n} &= (1-\lambda_0^2)[g_{0n}(1+B)^2-3g_{1n}(1+B)+3.75g_{2n}]+2\lambda_0^2 BG_{1n}, \\ G_{3n} &= 2B\{g_{0n}(1+B)[(3B+2)-\lambda_0^2(7B+2)]-1.5g_{1n}[(3B+4)+\lambda_0^2(B-4)] \\ &\qquad +7.5g_{2n}(1-\lambda_0^2)\}, \end{aligned} \tag{4.27}$$

with

$$g_{00} = \frac{1}{2\sqrt{2}}(1+1.6\tau+0.75\tau^2)$$

$$g_{10} = \frac{1}{4\sqrt{2}}(1+2.128\tau+1.25\tau^2) \quad (n=0),$$

$$g_{20} = \frac{1}{8\sqrt{2}}(1+2.551\tau+1.75\tau^2) \tag{4.28}$$

$$g_{01} = g_0,\ g_{11} = g_1$$

$$g_{21} = 1+3.61\tau+3.5\tau^2 \quad (n=1).$$

In contrast to the Weizsäcker gradient terms, the mixed gradient terms are seen to make a λ_0-dependent contribution already in zero'th and first order in δ/t.

4.3. CURVATURE EFFECTS

A frequently used approximation is to neglect effects due to the curvature of the nuclear surface. This semi-infinite approximation (limit of $\tau = 0$) is obtained by retaining only the leading terms in the expansions in powers of τ of the above expressions for the energy. Because the surface thickness is an appreciable fraction of the nuclear radius for actual nuclei it is not evident that the semi-infinite approximation will be a good one.

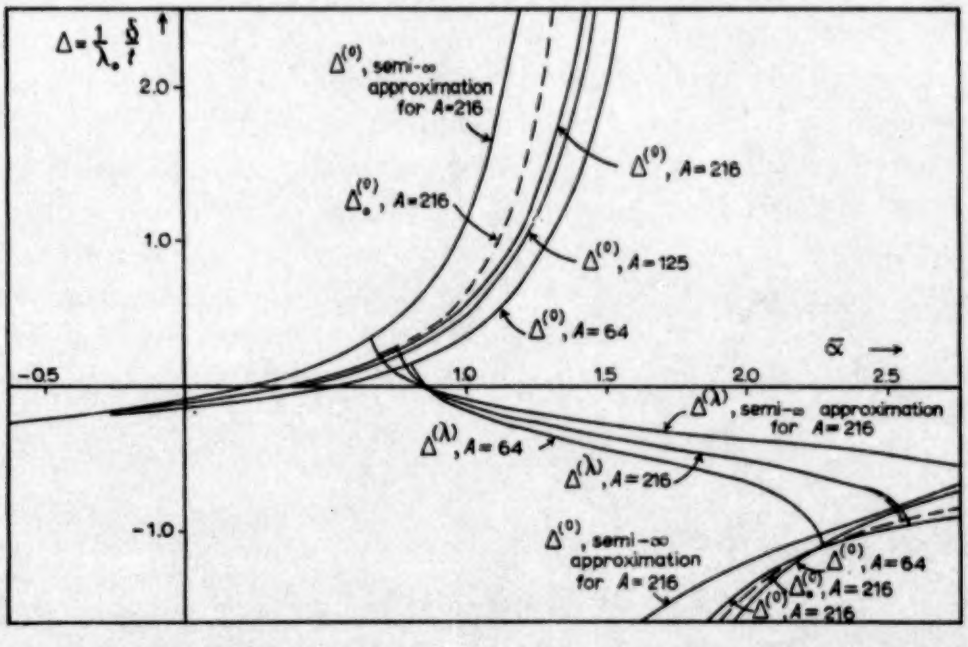

Fig. 1. $\Delta^{(0)}$ and $\Delta^{(\lambda)}$ as functions of $\bar{\alpha}$ for $A = 64, 125, 216$ and in the semi-infinite approximation for $A = 216$ with $\mu = 1.5, \xi_0 = 1, \xi_1 = \beta = 0$ and $\sigma' = 1.2$. The corresponding curves for $A = 216$, when $\mu = 0$ and the higher order terms in δ/t are neglected, are shown dashed.

Even for heavy nuclei the coefficients S, C, G are considerably larger than for $\tau = 0$. Thus, for $A = 216$, e.g.

$$S_1 = 2.09(\alpha - 0.88\beta), \quad C_1 = 5.12, \quad G_{11} = 1.70,$$

while the corresponding values for $\tau = 0$ are

$$S_1 = 1.29(\alpha - 0.75\beta), \quad C_1 = G_{11} = 1.$$

The large curvature dependence of these coefficients is, however, largely compensated in the corresponding energies by the curvature dependence of the factors depending on $\omega_A (< 1)$. The net effect of curvature on the various energy terms then results in only a slow variation of these with A, although even for heavy nuclei curvature effects are not negligible, as may be seen from fig. 1. Most of the curvature effects are due to the Coulomb energy since this depends considerably more strongly on τ than the other energies.

5. The Variational Calculation for δ

The difference in extension between ρ_n and ρ_p will be determined by the value of δ which minimizes the energy. Thus we require that part of the energy, $E_\delta(\delta/t)$, which depends on δ/t, i.e. all the energies calculated in sect. 4.2 except $E_{v\tau}$, $E^{(0)}_{s(\tau)}$ and $E^{(0)}_{gm}$. With δ'/t given by eq. (3.21) one has then †, to order $(\delta/t)^3$,

$$\frac{E_\delta\left(\frac{\delta}{t}\right)}{(4\pi\rho_0 R_0^3\tau)\,\frac{\sqrt{\pi}}{4}\,(1-\lambda_0^2)u_\tau} = -\lambda_0\frac{\delta'}{t}V_1 + \left(\frac{\delta'}{t}\right)^2 V_2 + \lambda_0\left(\frac{\delta}{t}\right)^3 V_3, \quad (5.1)$$

where

$$V_1 = S_1 + \frac{10.4}{u_\tau}\frac{r_e^2}{t^2}\,\xi_{1v}G_{1n} - \frac{0.129}{u_\tau}\,\omega_A{}^2 C_1\,\frac{Z}{\lambda_0 A^{\frac{1}{3}}}, \quad (5.2)$$

$$V_2 = [(1-\lambda_0^2)S_2 - 2\lambda_0^2 BS_1] + \frac{10.4}{u_\tau}\frac{r_e^2}{t^2}(g_0\xi_{0v} - G_{2n}\xi_{1v}) + \frac{0.129}{u_\tau}\,\omega_A{}^2 A^{\frac{1}{3}}(1-\lambda_0^2)\tau C_2, \quad (5.3)$$

$$V_3 = 2B[2(1-\lambda_0^2)S_2 + \tfrac{1}{2}BS_1] + \frac{10.4}{u_\tau}\frac{r_e^2}{t^2}(G_0\xi_{0v} - G_{3n}\xi_{1v}). \quad (5.4)$$

† The 3rd order Coulomb terms are negligible.

The variational condition for δ: $\mathrm{d}E_\delta(\delta/t)/\mathrm{d}(\delta/t) = 0$, then gives the following equation for δ/t:

$$\Delta^{(0)} = \frac{1}{\lambda_0}\frac{\delta}{t} = \frac{\Delta_0^{(0)} - \Delta^{(0)^2} 1.5\lambda_0^2 \left\{\frac{V_3}{V_2} + \mu[1+(1-\lambda_0^2)(0.25+B)\Delta_0^{(0)}]\right\}}{1-\mu\lambda_0^2\Delta_0^{(0)}}. \tag{5.5}$$

The superscript $^{(0)}$ emphasizes that this is the value obtained from the variational condition. With

$$\Delta_0^{(0)} = \frac{V_1}{2V_2} \tag{5.6}$$

we denote the value of $\Delta^{(0)}$ when $\mu = 0$ and only terms up to $(\delta/t)^2$ in eq. (5.1) are retained. The contributions of the terms in μ and in $\Delta^{(0)^2}$ in eq. (5.5) are seen to be only of order λ_0^2 relative to $\Delta_0^{(0)}$ which is then in general a good approximation to $\Delta^{(0)}$.

The following are a few general features of the variational solution (5.5), (5.6):

1) The effectiveness of the Coulomb repulsion between the protons in pushing these out relative to the neutrons, i.e. in decreasing δ, is determined by u_τ.

2) The effect on δ/t of only a neutron-proton difference, i.e. of $\lambda_0 \neq 0$ when the Coulomb forces are neglected, depends on u_τ only through the gradient terms and is otherwise determined by the dependence of ε_τ on ρ. In the absence of Coulomb forces, $\delta/t \propto \lambda_0$, almost exactly, apart from a slow dependence on A due to curvature effects. This is in agreement with deductions from the Euler equations. However, even with the Coulomb forces, for nuclei not too far from the bottom of the mass valley, i.e. essentially for stable nuclei, $\Delta^{(0)}$ depends approximately only on A and thus $\delta/t \propto \lambda_0$, approximately, apart from curvature effects. This may be seen from eq. (5.6) if for the Coulomb term occurring in V_1 one remembers that λ_0 is approximately proportional to $A^{\frac{1}{3}}$ for stable nuclei.

3) For light nuclei for which $N = Z$ ($\lambda_0 = 0$) one has from eqs. (5.5), (5.6) and (5.2),

$$\frac{\delta}{t} = -\frac{0.129}{u_\tau}\frac{\omega_A^2 C_1 \frac{Z}{A^{\frac{1}{3}}}}{2V_2}, \tag{5.7}$$

only the Coulomb term now contributing to the numerator. Thus $\delta/t < 0$ when $\lambda_0 = 0$ if $V_2 > 0$. Such an extension of the protons beyond the neutrons for $N = Z$ is to be expected if the nuclear forces are charge independent. The condition that $V_2 > 0$ implies a restriction on the values of α, β and thus also on the values of $\Delta^{(0)}$ for heavier nuclei for which $\lambda_0 > 0$. This restriction is discussed further below.

4) In agreement with the conclusion obtained from the Euler equations, $\delta/t = 0$ if $\alpha = \beta = \xi_1 = 0$ and the Coulomb forces are switched off. If these are then switched on, $\delta/t < 0$ and the protons will extend beyond the neutrons.

5) The mixed gradient term is the only one which contributes to first order in δ/t and thus only ξ_1, and not also ξ_0, occurs in the numerator of eq. (5.6).

The only parameter of the mass formula which occurs in $\Delta^{(0)}$ is u_τ. The two values of u_τ, expressions (2.18a) and (2.18b), are close to each other and give practically the same result for $\Delta^{(0)}$. Thus with Green's value of u_τ (expr. (2.18a)) and with $r_e^2/t^2 = 0.5$ ($t = 2f$) one obtains for $\Delta_0^{(0)}$ for $A = 216$:

$$\Delta_0^{(0)} = \begin{cases} \dfrac{0.456(\bar{\alpha}-0.374-0.06\xi_{1V})}{1.308-\bar{\alpha}-0.165(0.2\xi_{1V}-\xi_{0V})} & (n=0), \quad (5.8a) \\ \dfrac{0.456(\bar{\alpha}-0.374+0.14\xi_{1V})}{1.308-\bar{\alpha}-0.165(2\xi_{1V}-\xi_{0V})} & (n=1), \quad (5.8b) \end{cases}$$

where to a good approximation

$$\bar{\alpha} = \alpha - 0.9\beta. \tag{5.9}$$

Very nearly this combination of α, β also occurs for other values of A, while in the semi-infinite approximation $\bar{\alpha} = \alpha - 0.8\beta$.

Fig. 1 shows $\Delta_0^{(0)}$ and $\Delta^{(0)}$ as functions of $\bar{\alpha}$ and illustrates the effect of the second order corrections in λ_0^2 as well as the effects of curvature. The curves are quite typical also for other values of the parameters than those used for the figure. It is seen that mostly $\Delta^{(0)} = O(1)$ and thus that mostly $\delta/t = \lambda_0 \Delta^{(0)} \ll 1$. (The maximum value of $\Delta^{(0)}$ for $A = 216$, not reached on fig. 1, is ≈ 3.1 while the maximum value of $\Delta_0^{(0)} = \infty$). Since the energy is obtained as an expansion in powers of δ/t (and not of Δ) this implies, as in fact fig. 1 shows, that $\Delta_0^{(0)}$ is a rather good approximation to $\Delta^{(0)}$ except where $|\Delta_0^{(0)}| \gg 1$. Curvature effects are reasonably small and are mainly due to the Coulomb energy terms. In particular it is seen that differences between any two nuclei in the range $100 \lesssim A \lesssim 220$ are quite small and that correspondingly $\delta/t \propto \lambda_0$ almost exactly. Since physically it is required that $\alpha - \beta = 1$, the physically significant values of $\bar{\alpha}$ must be reasonably close to unity unless rather improbably $|\beta| \gg 1$. The reversal in sign of $\Delta^{(0)}$ in the neighbourhood of $\bar{\alpha} = 1$ occurs because $F(\rho)$, and therefore ε_τ, can become negative for some $\rho > 0$ if $\alpha - \beta > 1$. Thus it may be shown from the Euler equations that λ will then in general also change sign for a corresponding value of ρ in the surface. Thus, there is a range of values of $\bar{\alpha}$ near unity for which λ changes from being positive throughout the surface to being predominantly negative. In this region of $\bar{\alpha}$, where δ changes sign, the trial densities are thus expected to be rather poor and δ has only a very average significance. The parameter δ starts to decrease when $\bar{\alpha}$ is such

that in (2.8),

$$\bar{\varepsilon}_\tau = \varepsilon_\tau + (\text{the } \lambda\text{-dependent part of the gradient terms})$$

becomes negative for $\rho = 0$. Thus, with $\xi_0, \xi_1 > 0$, the quantity $\bar{\varepsilon}_\tau$ becomes negative for values of $\bar{\alpha}$ less than those for which $F(\rho) \leqq 0$ if the λ-dependent part of the mixed gradient term predominates over the λ-dependent part of the Weizsäcker term. This situation is only of importance for $n = 1$ and when ξ_0 and ξ_1 are of a similar order of magnitude; for $n = 0$, which is the more plausible value, the effectiveness of the mixed gradient terms is much reduced. However, quite generally it seems very doubtful whether $\bar{\varepsilon}_\tau < 0$ should be admitted as physically acceptable even if $\varepsilon_\tau > 0$. This is strongly supported by the consideration that $\delta/t < 0$ for $\lambda_0 = 0$, as must be physically expected, only if $V_2 > 0$, since this implies that values of $\bar{\alpha}$ greater than the value $\bar{\alpha}_0$ for which the denominator of eq. (5.8) becomes zero are excluded. This is, however, just equivalent to excluding values of α, β for which $\bar{\varepsilon}_\tau < 0$. Together with $\alpha - \beta = 1$ this then implies, as may be seen from eq. (5.8) or figs. 1 and 2, that $\delta > 0$ for not too light nuclei with $\lambda_0 > 0$, i.e. the neutrons extend beyond the protons, unless rather improbably $\beta \ll -1$.

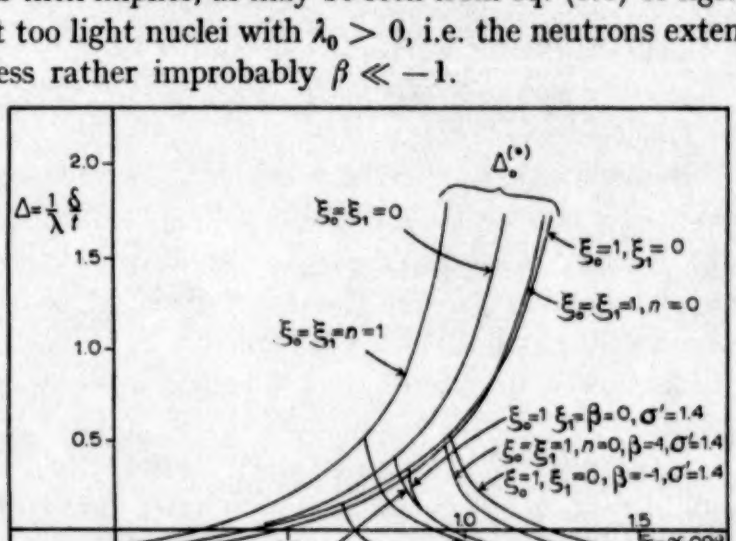

Fig. 2. $\Delta_0^{(0)}$ and $\Delta^{(\lambda)}$ (for $\mu = 0$ and when the higher order terms in $\Delta^{(\lambda)3}$ in eq. (6.11) are neglected) as functions of $\bar{\alpha} = \alpha - 0.9\beta$ for $A = 216$ and for some indicated values of ξ_0, ξ_1, σ', β and n.

Fig. 2 shows $\Delta_0^{(0)}$ as a function of $\bar{\alpha}$, up to $\bar{\alpha}_0$, for $A = 216$ and for a few representative values of ξ_0, ξ_1 and n.

6. The Surface Symmetry Energy

The surface symmetry energy is the sum of all surface terms (i.e. involving the factor $4\pi\rho_0 R_0^3 \tau$) which are proportional to λ_0^2 or more generally any power of λ_0. As already mentioned in sect. 3.1 there are two types of contributions to $E_{s\tau}$.

Firstly there are the explicit surface symmetry energy terms which will be denoted by $\hat{E}_{s\tau}$. These arise from the dependence of the calculated energy on λ_0 when any dependence of ρ on λ_0 is ignored. The terms $\hat{E}_{s\tau}$ include in addition to the terms $E_s(\delta/t)$ depending on δ/t already considered for the variational calculation for δ, also $E^{(0)}_{s(\tau)} + E^{(0)}_{gm} (\propto \lambda_0^2)$, i.e. the λ_0-dependent terms for $\delta = 0$. For the terms depending on δ/t it must be remembered that, as a result of the variational calculation, δ/t is approximately proportional to λ_0 for stable nuclei. Thus, apart from a slow dependence on A due to curvature effects, both $E^{(1)}_{s(\tau)}$ and $E^{(2)}_{s(\tau)} \propto \lambda_0^2 A^{\frac{2}{3}}$ and similarly $E^{(2)}_{gW}$, $E^{(1)}_{gm}$, $E^{(2)}_{gm} \propto \lambda_0^2 A^{\frac{2}{3}}$, while $E^{(3)}_{s(\tau)}$, $E^{(3)}_{gW}$, $E^{(3)}_{gm} \propto \lambda_0^4 A^{\frac{2}{3}}$. One then obtains (for $\mu = 0$):

$$\hat{E}_{s\tau} = \sum_{i=0}^{3} \hat{E}^{(i)}_{s\tau}, \tag{6.1}$$

$$\hat{E}^{(i)}_{s\tau} = -u_\tau \lambda_0^2 A^{\frac{2}{3}} \frac{3\sqrt{\pi}}{4} \frac{t}{r_0} \omega_A^2 \Lambda_i \left(\frac{1}{\lambda_0} \frac{\delta}{t}\right)^i \quad (i = 0, 1, 2, 3), \tag{6.2}$$

with

$$\begin{aligned} &\Lambda_0 = S_0 + \frac{10.4}{u_\tau} \frac{r_e^2}{t^2} g_{0n} \xi_{1E}, \quad \Lambda_1 = (1-\lambda_0^2) V_1(\xi_{1E}), \\ &\Lambda_2 = -(1-\lambda_0^2) V_2(\xi_{1E}, \xi_{0E}), \quad \Lambda_3 = -\lambda_0^2 V_3(\xi_{1E}, \xi_{0E}), \end{aligned} \tag{6.3}$$

and where V_1, V_2, V_3 are given by eqs. (5.2)—(5.4); ξ_{0V}, ξ_{1V} being replaced by ξ_{0E}, ξ_{1E} since the energy is being considered. It is seen that apart from the gradient and the Coulomb contributions the overall magnitude of $\hat{E}_{s\tau}$ is determined by u_τ; the remaining dependence on ε_τ occurring through α, β.

Secondly there are surface symmetry energy terms, denoted by $\hat{E}_{s\tau}$, due to the dependence of ρ on λ_0 referred to in sect. 3.1. This dependence arises from the dependence of ρ on δ which is a consequence of the complete variational condition for ρ. Thus in sect. 4.1 the variational condition for t was considered neglecting the symmetry and δ/t dependent terms in the energy. These, however, are just $\hat{E}_{s\tau}$ as given by eqs. (6.1)—(6.3). Thus the complete variational condition for t is

$$\frac{\mathrm{d}}{\mathrm{d}t} [E_s(\xi_{WV}) + \hat{E}_{s\tau}(\xi_{0V}, \xi_{1V})] = 0, \tag{6.4}$$

where E_s is given by eq. (4.1). Eq. (6.4) gives, in the semi-infinite approximation which will suffice for $\hat{E}_{s\tau}$ †,

$$t(\lambda_0) = t(\lambda_0 = 0) + t_\lambda, \tag{6.5}$$

† The following results are most easily obtained by considering t and δ/t as the independent variational parameters. If instead t and δ are used the same results are of course obtained but in this case the variational condition for δ must be used.

where, with $\Delta = (1/\lambda_0)(\delta/t)$, to the lowest order in λ_0^2

$$t_\lambda = \lambda_0^2 \tfrac{1}{2} \frac{t}{r_0} \frac{u_\tau}{QT} \left[S(\Delta) - \frac{QT}{u_\tau \xi_{WV}} \eta_V(\Delta) \right],$$

or, using eq. (4.4),

$$t_\lambda = \lambda_0^2 \tfrac{1}{2} \frac{t}{r_0} \frac{u_\tau}{QT} \left[S(\Delta) - \frac{5.13}{u_\tau} \eta_V(\Delta) \right], \tag{6.6}$$

with

$$S(\Delta) = S_0 + \Delta(1-\lambda_0^2) \left(S_1 - \frac{0.129}{u_\tau} \frac{Z}{\lambda_0 A^{\frac{1}{3}}} \right) - \Delta^2 (1-\lambda_0^2)^2 S_2, \tag{6.7}$$

$$\eta_V(\Delta) = g_{0n} \xi_{1V} + \Delta(1-\lambda_0^2) G_{1n} \xi_{1V} + \Delta^2 (1-\lambda_0^2)(G_{2n} \xi_{1V} - \xi_{0V}). \tag{6.8}$$

Thus the dependence of t on λ_0 is determined by t_λ which is seen to be approximately proportional to λ_0^2, for nuclei near the stable valley, since then δ/t is approximately proportional to λ_0 as a result of the variational calculation. Because $\lambda_0^2 \ll 1$ also $t_\lambda \ll t (\lambda_0 = 0)$. Thus from eqs. (6.6), (6.1)—(6.3), (6.9), (6.10) and the empirical value of $u_{s\tau}$ it may be shown that very approximately $t_\lambda \approx [6\lambda_0^2/(\xi_{WV} + \xi_{WE})]$. From table 2, $\xi_{WV} + \xi_{WE} \approx 2$ and is approximately independent of K. Thus $t_\lambda \approx 3\lambda_0^2 f$. Thus even for the heaviest nuclei t_λ is only $\approx 0.1\, f$. Thus although t is expected to increase slightly with λ_0, this variation is expected to be very slight and to be observable only with difficulty, especially as shell structure effects on t may be comparable. However, if the average dependence of t on $(N-Z)$ could be experimentally determined this would clearly be of considerable interest for the problem of the nucleon density distributions.

The contribution $\tilde{E}_{s\tau}$ due to t_λ is then given by eq. (4.8) (with $\Delta t = t_\lambda$) and is to the lowest order in λ_0^2

$$\tilde{E}_{s\tau} = u_\tau \lambda_0^2 \frac{3\sqrt{\pi}}{4} A^{\frac{1}{3}} \tfrac{1}{2} \frac{t}{r_0} \left(S(\Delta) - \frac{5.13}{u_\tau} \eta_V(\Delta) \right) \chi. \tag{6.9}$$

This depends on K only through $\chi = (\xi_{WV} - \xi_{WE})/\xi_{WV}$. It is to be noted that although $t_\lambda \ll t$, nevertheless the corresponding contribution $\tilde{E}_{s\tau}$ to $E_{s\tau}$ is of a similar order of magnitude as $\hat{E}_{s\tau}$. This corresponds to the fact that t_λ/t is of similar order of magnitude as $E_{s\tau}/E_s$. The total surface symmetry energy is then

$$E_{s\tau} = \hat{E}_{s\tau} + \tilde{E}_{s\tau}. \tag{6.10}$$

Since as a result of the variational calculation δ/t is approximately proportional to λ_0 for stable nuclei, only $E_{s\tau}^{(3)}$ being approximately proportional to $\lambda_0^4 A^{\frac{1}{3}}$ will have a different dependence on λ_0 than the semi-empirical term. However, because $\lambda_0^2 \ll 1$ and also $\delta/t \ll 1$ the contribution of $E_{s\tau}^{(3)}$ to $E_{s\tau}$ is quite small.

Thus the empirically used dependence $\lambda_0^2 A^{\frac{2}{3}}$ seems well justified; curvature effects causing only a slow additional dependence on A.

The *theoretically predicted* value of $E_{s\tau}$ is obtained by substituting in eqs. (6.1)—(6.3), (6.7)—(6.10) the appropriate value of δ/t given by the variational calculation. Because of curvature effects this predicted $E_{s\tau}$ will have a slow A dependence in addition to the empirical variation $\lambda_0^2 A^{\frac{2}{3}}$. Only in the semi-infinite approximation would this curvature dependence disappear; most of this coming from the Coulomb energy terms. Since the symmetry energy is relatively most important for heavier nuclei the empirical value of $u_{s\tau}$ will effectively be determined by the binding energies of the heavier nuclei. Thus these should be considered when comparing theoretical and empirical values of $E_{s\tau}$.

Equating formula (6.10) with the semi-empirical value $-u_{s\tau}\lambda_0^2 A^{\frac{2}{3}}$ gives a relation between δ/t and α, β (and also involving ξ_0, ξ_1, σ and χ). With eq. (3.21) and $(3\sqrt{\pi}/4)(t/r_0) = 2.384$ from expression (3.5), this surface symmetry condition is †

$$\begin{aligned} \Delta^{(\lambda)} = \Delta_0{}^{(\lambda)} + \Delta^{(\lambda)2}\left\{\frac{V_2}{V_1} - \lambda_0^2\frac{\mu}{2}\left[1-(1-\lambda_0^2)(0.25+B)\Delta^{(\lambda)}\right]\right\} \\ +\lambda_0^2\Delta^{(\lambda)3}\left\{\frac{V_3}{V_1} + \mu\frac{V_2}{V_1}\left[1-(1-\lambda_0^2)(0.25+B)\Delta^{(\lambda)}\right]\right\}, \end{aligned} \tag{6.11}$$

where

$$\Delta_0{}^{(\lambda)} = \frac{\dfrac{\sigma'}{2.384\,\omega_A{}^2} - \Lambda_0}{(1-\lambda_0^2)V_1}, \tag{6.12}$$

with σ' given by eq. (4.7). The quantities V_1, V_2 and V_3 are given by eqs. (5.2)—(5.4) but with ξ_{0V}, ξ_{1V} replaced by

$$\xi'_0 = \frac{\xi_{0E} + \dfrac{\chi}{2}\xi_{0V}}{1-\dfrac{\chi}{2}}, \quad \xi'_1 = \frac{\xi_{1E} + \dfrac{\chi}{2}\xi_{1V}}{1-\dfrac{\chi}{2}}. \tag{6.13}$$

The superscript $^{(\lambda)}$ emphasizes that $\Delta^{(\lambda)}$ is the value of $(1/\lambda_0)(\delta/t)$ occurring in the surface symmetry condition, i.e. the value of Δ consistent with the empirical value of $E_{s\tau}$. The effect of μ is small but, in contrast to $\Delta^{(0)}$, only the terms in $\Delta^{(\lambda)3}$ are of order λ_0^2. From eq. (5.6) the coefficient of the term in $\Delta^{(\lambda)2}$ in eq.

† Because of the similar structure of $\hat{E}_{s\tau}$ and $\tilde{E}_{s\tau}$ the curvature dependence of $\tilde{E}_{s\tau}$ is expected to be similar to that of $\hat{E}_{s\tau}$ and in (6.11) and (6.12) has been assumed to be the same. In any case any uncertainty due to curvature effects in $\tilde{E}_{s\tau}$, which has been obtained in the semi-infinite approximation, is expected to be absorbed by the uncertainty in σ'.

(6.11) is, for $\mu = 0$,

$$\frac{V_2}{V_1} = \frac{1}{2\Delta_0^{(0)}} \tag{6.14}$$

but with ξ'_0, ξ'_1 instead of ξ_{0V}, ξ_{1V} for $\Delta_0^{(0)}$.

The appropriate solution of (6.11) is that for which $\Delta^{(\lambda)} = 0$ when $\Delta_0^{(\lambda)} = 0$. † This is because from eq. (6.12) σ', i.e. essentially $\hat{E}_{s\tau}$, is then completely determined by just α, β, ξ'_1, and does not depend on δ/t and thus, from the general expression for $\hat{E}_{s\tau}$ in terms of an integral over the energy density, that $\lambda = \lambda_0$ (see e.g. eq. (4.9) and the discussion following this) implying that $\delta/t = 0$. It is to be noted that there is no solution of eq. (6.11) for all values of $\bar{\alpha}$. Thus with neglect of the unimportant terms in λ_0^2 there is no solution for $\Delta^{(\lambda)}$ if $\Delta_0^{(\lambda)} > V_1/4V_2$ (i.e. for $2\Delta_0^{(\lambda)} > \Delta_0^{(0)}$ if $\xi'_0 = \xi_0$, $\xi'_1 = \xi_1$).

It will be noted that the main effect of $\hat{E}_{s\tau}$ is to change the effective value of $\sigma = u_{s\tau}/u_\tau$ to $\sigma' = \sigma/(1-\frac{1}{2}\chi)$. From table 2 it is seen that σ' is almost the same for Green's and Cameron's values of $\sigma = 1.2$ and 1.4 respectively and depends mainly on K. Further for $150 \lesssim K \lesssim 300$ MeV (with small m in conjunction with larger K excluded) the differences between the possible values of σ' given in table 2 are not much more than that between $\sigma = 1.2$ and $\sigma = 1.4$. Also, as for $\Delta^{(0)}$, it makes almost no difference for $\Delta^{(\lambda)}$ whether Green's or Cameron's value of u_τ is used. Thus, for $A = 216$ and with Green's value of u_τ,

$$\Delta_0^{(\lambda)} = \frac{0.586\,(0.7\,\sigma' - \bar{\alpha} - 0.28\beta - 0.096\xi'_1)}{(\bar{\alpha} - 0.06\xi'_1 - 0.374)} \quad (n = 0), \tag{6.15a}$$

$$\Delta_0^{(\lambda)} = \frac{0.586\,(0.7\,\sigma' - \bar{\alpha} - 0.28\beta - 0.322\xi'_1)}{(\bar{\alpha} + 0.139\xi'_1 - 0.374)} \quad (n = 1), \tag{6.15b}$$

while, from eq. (6.14), V_2/V_1 is given in terms of $\Delta_0^{(0)}$ which is given by eq. (5.8). For $\Delta^{(\lambda)}$, in constrast to $\Delta^{(0)}$, β occurs also explicitly in addition to in $\bar{\alpha}$.

Fig. 1 shows $\Delta^{(\lambda)}$ as a function of $\bar{\alpha}$ for several values of A, the curves shown being again quite typical. As for $\Delta^{(0)}$, curvature effects as well as higher order effects due to the terms in λ_0^2 are seen to be small. Fig. 2 shows $\Delta^{(\lambda)}$ as a function of $\bar{\alpha}$ for $A = 216$ and for a few representative values of ξ_0, ξ_1, n, β and σ'.

7. The Consistency Problem and Discussion of Results

7.1. THE CONSISTENCY PROBLEM

Equating $\Delta^{(0)}$ and $\Delta^{(\lambda)}$ as given by eqs. (5.5), (5.6) and (6.11), (6.12) determines, as functions of ξ_0, ξ_1 and σ', the values of Δ (i.e. of δ) on the one hand and

† The other solution of eq. (6.11) (with neglect of the higher order corrections in λ_0^2) for which $\Delta^{(\lambda)} \neq 0$ when $\Delta_0^{(\lambda)} = 0$ intersects $\Delta^{(0)}$ at almost the same values of $\bar{\alpha}$ as the appropriate solution used. Since only these points of intersection will be of final interest both solutions in fact give essentially the same final results.

the values of α, β on the other which are consistent both with the variational condition for δ and with the empirical value of E_{sr}. Such values of δ/t and of α, β will be called acceptable values and correspond to the points where the curves of $\Delta^{(0)}$ and $\Delta^{(\lambda)}$ as functions of $\bar{\alpha}$, as e.g. shown in figs. 1 and 2, intersect. Numerical results for these acceptable values will be considered particularly for $A = 216$, since because of curvature effects the empirical values of u_{sr} will be most appropriate for heavier nuclei. † With $\xi'_0 = \xi_{0V}$, $\xi'_1 = \xi_{1V}$ the acceptable values of α, β are easily shown to be determined, to order λ_0^2, by the condition

$$\Delta_0^{(0)} = 2\Delta_0^{(\lambda)} + \lambda_0^2 \Delta_0^{(0)2} \frac{V_3}{V_2}. \tag{7.1}$$

The term in λ_0^2 is a small correction and is seen to be independent of μ. The corresponding acceptable values of Δ are obtained by substituting the acceptable values of α, β obtained from eq. (7.1) into eq. (5.5) (or to a sufficiently good approximation into eq. (5.6)). The only set of acceptable values of α, β determined by eq. (7.1) which is physically acceptable, i.e. for which $\bar{\alpha} < \bar{\alpha}_0$, corresponds to $\Delta > 0$ and is the one which corresponds to the intersections of $\Delta^{(0)}$ and $\Delta^{(\lambda)}$ shown in fig. 2. In the limit when the term in λ_0^2 in eq. (7.1) is neglected there is just one other set of acceptable values which corresponds to $\Delta < 0$ and $\bar{\alpha} \approx 2$. In table 3 the acceptable values of Δ, $\bar{\alpha}$ and α (for $\Delta > 0$) are given for $A = 216$ for some values of β, ξ_0, ξ_1, and σ', the range of values of ξ_0, ξ_1 and σ' having been taken so as to be roughly consistent with the results of table 2.

TABLE 3

Acceptable values of Δ, $\bar{\alpha}$ and α for $A = 216$

				$\sigma' = 1.0$				$\sigma' = 1.4$			
β	ξ_0	ξ_1	n	$\Delta^{(0)}$	$\bar{\alpha}$	α	$\alpha-\beta$	$\Delta^{(0)}$	$\bar{\alpha}$	α	$\alpha-\beta$
0	0	0	–	0.195	0.655	0.655	0.655	0.41	0.82	0.82	0.82
0	1	0	–	0.16	0.66	0.66	0.66	0.335	0.845	0.845	0.845
0	0	1	0	0.07	0.59	0.59	0.59	0.33	0.79	0.79	0.79
0	0	1	1	0.10	0.37	0.37	0.37	0.35	0.56	0.56	0.56
0	1	1	0	0.085	0.595	0.595	0.595	0.26	0.80	0.80	0.80
0	1	1	1	0.08	0.37	0.37	0.37	0.27	0.58	0.58	0.58
−1	0	0	–	0.415	0.825	−0.075	0.925	0.78	0.965	0.065	1.065
−1	1	0	–	0.335	0.845	−0.055	0.945	0.53	0.97	0.07	1.07
−1	0	1	0	0.33	0.79	−0.11	0.89	0.60	0.92	0.02	1.02
−1	0	1	1	0.35	0.56	−0.34	0.66	0.675	0.68	−0.22	0.78
−1	1	1	0	0.26	0.80	−0.10	0.90	0.475	0.95	0.05	1.05
−1	1	1	1	0.27	0.58	−0.32	0.68	0.52	0.72	−0.18	0.82

† The values of δ for lighter nuclei should thus strictly be obtained from the variational solution for δ for the value of A considered, but using the acceptable values of α, β obtained for heavier nuclei, since these acceptable values will, because of curvature effects, be the significant ones.

7.2. ACCEPTABLE VALUES OF α AND β

For a given β the corresponding acceptable value of $\bar{\alpha}$, and therefore also of α, is determined as a function of ξ_0, ξ_1 and σ'. The condition $\alpha-\beta = 1$ then limits the range of these acceptable values. From table 3 it is seen that $\alpha-\beta \approx 1$ only for $\beta < 0$ and ≈ -1, irrespective of the values of ξ_0, ξ_1 and σ' considered. This implies correspondingly small acceptable values for $\alpha : \alpha < 1$ and ≈ 0. The acceptable values of $\bar{\alpha}$ increase with σ', which, as may be seen from table 2, increases with K. Thus small values of $K \lesssim 100$ MeV will give even smaller acceptable values of α, β. The dependence of the acceptable values on ξ_0 is seen to be small. That on ξ_1 is considerably larger for $n = 1$ but is also small for $n = 0$ which is the more plausible value. Thus most of the uncertainty due to the gradient terms comes from the mixed gradient term and relatively little from the Weizsäcker term. The conclusion that β is appreciably negative and α small and considerably less than unity is independent of the assumption $\xi'_0 = \xi_{0V}$, $\xi'_1 = \xi_{1V}$ as may be seen from inspection of fig. 2. Thus the uncertainties in the magnitudes of the gradient terms do not affect this conclusion, although this is naturally somewhat tentative in view of the approximations implied by the use of trial densities. For the general consistency of the whole approach it is satisfactory that the empirical values of $u_{s\tau}$ give acceptable values of $\bar{\alpha}$ which are mostly not too different from unity as is to be expected from the condition $\alpha-\beta = 1$ for not too unreasonably large $|\beta|$.

It is of interest to consider briefly other evidence about α, β. Tentative evidence about α is provided by the isotope shift of heavier elements [25]). † With the approximate theory used in ref. [25]) for calculating changes of radius, the isotope shift indicates that α is probably considerably less than unity and possibly even negative, unless one is prepared to accept quite small values of $K(\lesssim 50$ MeV). This is in satisfactory agreement with the acceptable values obtained above.

Further, we also consider the theoretically expected values of α, β for nuclear matter. The relevant considerations will be given in a subsequent paper and only the results will be briefly mentioned here. In the independent particle approximation, with appropriate effective two-body interactions, α is found to be slightly less than unity (≈ 0.9) and β small and negative (≈ -0.1). Thus the acceptable values of α found above are significantly smaller than in the independent particle approximation while those of β are significantly more negative. Inclusion of dynamic correlations implies that the effective two-body

† In ref. [25]) the density dependence of $E_{V\tau}(E_{S\tau})$ was specified by $k_{V\tau}$, $K_{V\tau}(k_{S\tau}, K_{S\tau})$, these being the ratios relative to $E_{V\tau}(E_{S\tau})$ of respectively the first and second derivatives of $E_{V\tau}(E_{S\tau})$ with respect to the usual scale parameter $(\rho/\rho_0)^{\frac{1}{3}}$ at ρ_0. It is easy to show that $k_{V\tau} = 3\alpha$ and $K_{V\tau} = 6(\alpha+3\beta)$. Thus for a Fermi gas of free nucleons for which $\alpha = \frac{2}{3}$, $\beta = -\frac{1}{9}$, one has correspondingly $k_{V\tau} = K_{V\tau} = 2$. For $k_{S\tau}$ and $K_{S\tau}$, the corresponding relations are rather more difficult to obtain and will be considered in a subsequent paper where changes of radius will be treated more adequately than in ref. [25]).

interactions will have an additional dependence on ρ to that arising from the wavefunction normalization, which is the only one in the independent particle approximation. There are, then, strong indications that α can be much reduced below the independent-particle value while β can become considerably more negative. This theoretical conclusion is thus consistent with the acceptable values obtained above as well as with the conclusions obtained from the isotope shift data.

7.3. ACCEPTABLE VALUES OF δ

With $\beta \approx -1$ the range of acceptable values of Δ is seen from table 3 to be $0.25 \lesssim \Delta \lesssim 0.8$. If less negative β are admitted the lower limit will be somewhat smaller; ≈ 0.1. Remembering the smallness of λ_0 it is seen that the acceptable values of $\delta = \lambda_0 t\Delta$ will be quite small; thus even for heavy stable nuclei $\delta \lesssim 0.3\,f$. Thus we may conclude with some confidence that for all except light nuclei the neutrons extend slightly beyond the protons with, for medium and heavy nuclei, $0.2\lambda_0 f \lesssim \delta \lesssim 1.6\lambda_0 f$ (with $t = 2\,f$), while for lighter nuclei ($A \lesssim 100$) the corresponding values would be slightly smaller because of curvature effects (see e.g. fig. 1). For light nuclei with $N = Z$,

$$\frac{\delta}{t} \approx \frac{-0.0014A^{\frac{1}{3}}}{1.41-\bar{\alpha}-(0.29\xi_1-0.13\xi_0)}$$

from eq. (5.7) and thus, using the results of table 3, $\delta \approx -0.005\,A^{\frac{1}{3}}\,f$, the Coulomb repulsion between the protons causing these to extend very slightly beyond the neutrons. It is clear that a more precise determination of δ and thus also of α, β depends on the one hand on a more precise knowledge of principally the mixed gradient term and on the other hand on a more precise value of σ' and thus of K.

The difference between the 90 %—10 % surface thicknesses of ρ_n and ρ_p is slightly larger than δ, approximately in the ratio of 1.2. The difference between the *half-density radii* of ρ_n and ρ_p is $\approx 0.82\,\delta$ while the corresponding difference for ρ and ρ_p is $\approx 0.41(1+\lambda_0)\delta$.

The results for δ seem consistent with the empirical evidence. Thus a comparison of the π^+ and π^- absorption cross sections in the GeV region [26]) indicates essentially equal radii for the neutrons and protons. Further, the π^+ [27]) and neutron [28]) absorption cross sections in the GeV region indicate only a small difference between the half-density radii of the matter (ρ) and charge (essentially ρ_p) distributions, this difference lying between 0.0 and $0.4\,f$[29]). Also Drell [30]), and more recently Elton [24]), conclude from the electron scattering data in conjunction with the optical model potentials for low energy nucleons that the half-density radii of ρ_n and ρ_p do not differ by a significant amount (small compared with $1\,f$). A study [31]) of deuterons produced by nucleon pick-up suggests a surface layer of neutrons with a thickness $\approx 0.8\,f$ for heavy nuclei. This large value is, however, rather uncertain, since it has been obtained

assuming equal momentum distributions for the surface neutrons and protons, and a more detailed analysis may well result in a considerably smaller value.

8. Conclusion

The semi-empirical statistical method [9–11]), with the use of trial nucleon densities, has been used to investigate the nucleon density distributions and their relation with the various terms of the semi-empirical mass formula. It has been possible to isolate those features depending on a difference in the number of neutrons and protons, in particular the difference between ρ_n and ρ_p and the surface symmetry energy $E_{s\tau}$.

The energy $E_{s\tau}$ depends on δ (essentially the difference between the surface thicknesses of ρ_n and ρ_p) while both $E_{s\tau}$ and δ depend on the dependence on ρ of the symmetry energy density, ε_τ; this dependence being specified by α, β through eqs. (2.3) and (2.5). The magnitude u_τ of ε_τ is determined by the volume symmetry energy term $E_{v\tau}$. To a good approximation for stable nuclei: $\delta \propto \lambda_0 = (N-Z)/A$, effects due to the finite curvature of the nuclear surface causing only a slow additional dependence on A. The effectiveness of the Coulomb repulsion between the protons on δ is determined by u_τ, while that of $N-Z$ depends largely on α, β and thus is determined rather by the relative rate of variation of the symmetry energy density through the surface than just by its magnitude u_τ. The energy $E_{s\tau}$ is made up of two parts. One is due to the dependence of the calculated energy on λ_0 and δ when any dependence of ρ on λ_0 and δ is ignored. The other part arises from the dependence of ρ on λ_0 and δ and depends on the difference between the effective magnitudes of the Weizsäcker gradient terms for ρ for the energy and the variational calculation. With the empirical values of the surface energy E_s and of the surface thickness this difference is then essentially determined by only the compressibility K. The dependence of ρ on λ_0 is small; thus for the surface thickness $t = t(\lambda_0 = 0) + t_\lambda$, one has $t_\lambda \approx 3\lambda_0^2 f$ for nuclei near the stable valley and even for the heaviest stable nuclei this is only $\approx 0.1\ f$. However, both types of contributions to $E_{s\tau}$ are of a similar order of magnitude. The empirically used dependence $E_{s\tau} \propto \lambda_0^2 A^{\frac{2}{3}}$, seems well justified for nuclei near the stable valley. Thus a symmetry energy density having the form required to give $E_{v\tau} \propto \lambda_0^2 A$ implies a surface symmetry energy of the empirically used form (apart from slowly varying curvature corrections) as a result of the self-consistent adjustment of ρ_n and ρ_p to each other as reflected in the result of the variational calculation that δ is approximately proportional to λ_0 for nuclei near the stable valley. It is to be noted that the rather general energy density (2.1) gives essentially just *all* the terms used in the semi-empirical mass formula.

Since the calculated $E_{s\tau}$ depends on δ, the empirical value of $u_{s\tau}$ [17, 18]) provides a relation, the "surface symmetry condition", between the values of

δ and α, β consistent with $u_{s\tau}$. The surface symmetry condition together with the variational solution for δ determine the "acceptable" values of δ and α, β which are consistent with both the variational condition and the empirical value of $E_{s\tau}$. It is then found that, tentatively, $\alpha < 1$ and ≈ 0 while $\beta < 0$ and ≈ -1. These values are considerably smaller than in the independent particle approximation for nuclear matter but are consistent with the small value of α indicated by the isotope shift data [25]) as well as with theoretical expectations for nuclear matter when the effects of dynamic correlations are included. δ is found to be within the range of $0.2\,\lambda_0 f \lesssim \delta \lesssim 1.6\,\lambda_0 f$ for medium and heavy nuclei with slightly smaller values for lighter nuclei. This slight extension of the neutrons beyond the protons ($\delta \lesssim 0.3 f$ even for the heaviest stable nuclei) is consistent with a very slight extension of the protons beyond the neutrons for light nuclei with $N = Z$ for which $\delta \approx -0.005\,A^{\frac{1}{3}} f$. The general conclusions about δ and α, β are independent of the uncertainties in the magnitudes of the gradient terms if these are consistent with the empirical surface energy and surface thickness. A more precise determination of α, β and δ then depends mainly on a better knowledge of K and the mixed gradient term.

The small value of δ compared with that obtained by Johnson and Teller [32]) is due to the self-consistent treatment of the interactions between the neutrons and protons as already made evident by Wilets [10, 11]). Also it is clear that dynamic correlations are essential for the difference in extension between ρ_n and ρ_p, not only through u_τ [1]), but also through the dependence of ε_τ on ρ.

Any uncertainties in the statistical method due to this being an approximation to a more exact many-body theory, such as e.g. the Brueckner method for finite nuclei [3–5]), may be considered as residing in the gradient terms. To reduce the uncertainties in these thus requires more fundamental investigations, such as on the lines of that by Naqvi [15]), relating the statistical method in a satisfactory way to such a more fundamental many-body theory. Such investigations will have to take account of the mixed gradient term in addition to the usual Weizsäcker gradient terms and may perhaps offer almost as many difficulties as a fully self-consistent application of a more exact many-body theory.

The author would like to thank Dr. A. M. Naqvi for some stimulating discussions.

References

1) K. A. Brueckner and J. L. Gammel, Phys. Rev. **109** (1958) 1023, where also compəte references to earlier work are given.
2) L. G. Gomes, J. D. Walecka and V. F. Weisskopf, Ann. of Phys. **3** (1958) 241;
A. de Shalit and V. F. Weisskopf, Ann. of Phys. **5** (1958) 282
3) R. J. Eden, in Nuclear Reactions, ed. by P. M. Endt and M. Demeur (North-Holland Publishing Company-Amsterdam, 1959)

4) R. J. Eden and V. J. Emery, Proc. Roy. Soc. A **248** (1958) 266;
R. J. Eden, V. J. Emery and S. Sampanthar, Proc. Roy. Soc. A **253** (1959) 177, 186
5) K. A. Brueckner, J. L. Gammel and H. Weitzner, Phys. Rev. **110** (1958) 431
6) P. Gombás, Handbuch der Physik, Vol. **36** (Springer-Verlag, Berlin, 1956);
P. Gombás, Die Statistische Theorie des Atoms (Wien, 1949)
7) P. Gombás, Acta Phys. Hung. **1** (1951) 329; **2** (1952) 223; **5** (1956) 511;
P. Gombás *et al.*, Nuclear Physics **4** (1957) 448;
N. F. Findler, Nuclear Physics **8** (1958) 338
8) C. F. von Weiszäcker, Z. Physik **96** (1935) 431;
P. Gombás, Acta Phys. Hung. **3** (1954) 105
9) R. A. Berg and L. Wilets, Phys. Rev. **101** (1956) 201
10) L. Wilets, Phys. Rev. **101** (1956) 1805
11) L. Wilets, Revs. Mod. Phys. **30** (1958) 542
12) T. H. R. Skyrme, Phil. Mag. **1** (1956) 1043
13) R. A. Berg and L. Wilets, Proc. Phys. Soc. A **72** (1955) 182
14) R. Hofstadter, Revs. Mod. Phys. **28** (1956) 214;
Ann. Rev. Nucl. Sci. **7** (1957)
15) M. A. Naqvi, Nuclear Physics **10** (1959) 256
16) E. Feenberg, Revs. Mod. Phys. **19** (1947) 239
17) A. E. S. Green, Revs. Mod. Phys. **30** (1958) 569; Phys. Rev. **95** (1954) 1006; see also ref. [11])
18) A. G. W. Cameron, Can. J. Phys. **35** (1951) 1021
19) A. S. Kompaneiets and E. S. Pavlovsky, Soviet Physics **4** (1957) 328;
A. S. Kompaneiets, Comptes Rendus du Congrès International de Physique Nucléaire (Dunod, Paris, 1959) 808
20) N. H. March and W. H. Young, Proc. Phys. Soc. A **72** (1958) 182
21) W. R. Theis, Z. Physik **142** (1955) 503
22) J. M. Blatt and V. F. Weisskopf, Theoretical Nuclear Physics (John Wiley, New York, 1952)
23) E. Fermi, Nuclear Physics (Notes by Orear, Rosenfeld and Schluter, University of Chicago press, Chicago 1950)
24) L. R. B. Elton, Nuclear Physics **5** (1957) 173; **8** (1958) 396
25) A. R. Bodmer, Nuclear Physics **9** (1958/59) 371
26) A. Abashian, R. Cool and J. W. Cronin, Phys. Rev. **104** (1958) 855
27) J. W. Cronin, R. Cool and A. Abashian, Phys. Rev. **107** (1957) 1121
28) T. Coor, D. A. Hill, W. F. Hornyak, L. W. Smith and G. Snow, Phys. Rev. **98** (1955) 1369;
R. W. Williams, Phys. Rev. **98** (1955) 1387
29) L. R. B. Elton, Revs. Mod. Phys. **30** (1958) 557
30) S. D. Drell, Phys. Rev. **100** (1955) 97
31) W. H. Hess and B. J. Moyer, Phys. Rev. **101** (1956) 337
32) M. H. Johnson and E. Teller, Phys. Rev. **93** (1954) 357

9.C

Nuclear Physics **17** (1960) 421—423; © *North-Holland Publishing Co., Amsterdam*

Not to be reproduced by photoprint or microfilm without written permission from the publisher

ON THE INTRINSIC PAULI PRINCIPLE

W. KRÓLIKOWSKI

Institute of Theoretical Physics, University of Warsaw and
Institute for Nuclear Research, Polish Academy of Sciences, Warsaw

Received 8 February 1960

Abstract: It is pointed out that the absence of higher spins and multiple charges for elementary particles may be a consequence of a fundamental principle, which plays here a similar role as the Pauli principle in atomic physics. A realization of such an "intrinsic Pauli principle" for isobaric properties of elementary particles is given.

It is well known that in elementary particle physics there appears a number of intrinsic quantities, such as intrinsic angular momentum or spin, intrinsic parity, isospin, intrinsic charge parity, strangeness, electric charge, baryonic charge and so on. From the theoretical point of view those quantities can be described by assuming proper transformation properties of quantum fields. The problem of restricting the number of all possible fields to the observed ones is of much interest, and was, of course, extensively investigated. Especially the absence of higher spins and multiple charges for elementary particles is very striking and may be taken into account as a hint for the theory of elementary particles.

We should like to point out that the absence of higher spins and multiple charges might be a consequence of a fundamental principle, which would play a similar role in elementary particle physics as the Pauli principle in atomic physics. We might call it the "intrinsic Pauli principle", because it would be related to intrinsic quantities.

In a previous paper [1]) it was shown that the isobaric properties of baryons and leptons can be derived from a formulation of such an intrinsic Pauli principle and, especially, that the list of presently known baryons and leptons can be closed. In the present note we turn back to the formulation of the intrinsic Pauli principle for isobaric properties of baryons, leptons and mesons.

Let us consider the three-dimensional isospace. We denote by $\alpha = 1,2$ and $a = 1,2$ isospin indices corresponding to charges $+e$, 0 and 0, $-e$ respectively. We construct an "intrinsic Fock representation" obeying Fermi-Dirac statistics (Pauli principle):

$$\begin{aligned} &\langle 0| \\ &\langle a_1| = \langle 0|\xi_{a_1}, \qquad \text{where} \quad \{\xi_a, \xi_b^*\} = \delta_{ab}. \\ &\langle a_1 a_2| = \langle 0|\xi_{a_1}\xi_{a_2} \end{aligned} \tag{1}$$

(Further basis vectors do not appear the representation (1) because of the Pauli principle). We take into account three spinor fields $B_\alpha(x)$ ($\alpha = 1,2$) and $L(x)$ and one pseudoscalar field $M(x)$. We assume that $B_\alpha(x)$ ($\alpha = 1,2$) and $L(x)$ are abstract vectors in an "intrinsic configuration space" given by the basic vectors (1), whereas $M(x)$ is an abstract hermitian matrix in this space. Then in the representation (1) we have

$$B_\alpha = \begin{pmatrix} \langle 0|B_\alpha\rangle \\ \langle a_1|B_\alpha\rangle \\ \langle a_1 a_2|B_\alpha\rangle \end{pmatrix}, \quad L = \begin{pmatrix} \langle 0|L\rangle \\ \langle a_1|L\rangle| \\ \langle a_1 a_2|L\rangle \end{pmatrix} \tag{2}$$

and

$$M = \begin{pmatrix} \langle 0|M|0\rangle & \langle 0|M|b_1\rangle & \langle 0|M|b_1 b_2\rangle \\ \langle a_1|M|0\rangle & \langle a_1|M|b_1\rangle & \langle a_1|M|b_1 b_2\rangle \\ \langle a_1 a_2|M|0\rangle & \langle a_1 a_2|M|b_1\rangle & \langle a_1 a_2|M|b_1 b_2\rangle \end{pmatrix}. \tag{3}$$

Applying the vector addition of all individual isospins corresponding to indices α, a and b we can go over to new representations for fields $B = (B_\alpha)$, L and M, in which the total isospin squared $\mathbf{T}^2$ and its third component T_3 are defined.

Since the isospin indices ($\alpha = 1,2$), ($a = 1,2$) and ($b = 1,2$) in formulae (2) and (3) correspond to charges $(+e, 0)$, $(0, -e)$ and $(0, +e)$ respectively, the charges of the resulting B, L and M particles are given by (cf. ref. [1]):

$$\frac{Q^B}{e} = T_3 - \tfrac{1}{2}S^B + \tfrac{1}{2}N^B, \qquad \frac{Q^L}{e} = T_3 - \tfrac{1}{2}S^L \tag{4}$$

and

$$\frac{Q^M}{e} = T_3 - \tfrac{1}{2}S^M \tag{5}$$

respectively, where N^B is the baryonic number and the quantities S are in the case of the B and L fields the numbers of contributing a indices, and in the case of the M field the numbers of a indices minus the numbers of b indices. We can see that the quantities S are strangeness numbers (with opposite signs) and formulae (4) and (5) give Gell-Mann-Nishijima relations, if we identify B, L and M particles with baryons, leptons and mesons respectively.

The resulting B, L and M particles and their experimental counterparts are listed in table 1. Other components of B, L and M fields do not exist, because of the Pauli principle. The particles with the same S, T and T_3 are identified in table 1. The symbol D^- denotes here the heavy meson suggested recently by experiment [2]).

The new representations for fields B, L and M are given by formulae

$$B = \begin{pmatrix} (\mathrm{pn}) \\ \Lambda^0, (\Sigma^+ \Sigma^0 \Sigma^-) \\ (\Xi^0 \Xi^-) \end{pmatrix}, \qquad L = \begin{pmatrix} ?^0 \\ (\nu e^-) \\ \mu^- \end{pmatrix} \tag{6}$$

TABLE 1

Elementary particles of the fields B, L and M

Field	S	T	T_3	Q	Identification
B	0	$\frac{1}{2}$	$\pm\frac{1}{2}$	$+e$	p
				0	n
	1	0	0	0	Λ^0
			+1	$+e$	Σ^+
	1	1	0	0	Σ^0
			−1	$-e$	Σ^-
	2	$\frac{1}{2}$	$\pm\frac{1}{2}$	0	Ξ^0
				$-e$	Ξ^-
L	0	0	0	0	$?^0$ (second neutrino?)
	1	$\frac{1}{2}$	$\pm\frac{1}{2}$	0	ν
				$-e$	e^-
	2	0	0	$-e$	μ^-
M	0	0	0	0	$?^0$ (second neutral pion?)
			+1	$+e$	π^+
	0	1	0	0	π^0
			−1	$-e$	π^-
	1	$\frac{1}{2}$	$\pm\frac{1}{2}$	0	$\overline{\mathrm{K}}^0$
				$-e$	K^-
	2	0	0	$-e$	D^-

and

$$M = \begin{pmatrix} ?^0 & (\mathrm{K}^0\mathrm{K}^+) & \mathrm{D}^+ \\ (\overline{\mathrm{K}}^0\mathrm{K}^-) & ?^0,\ (\pi^+\pi^0\pi^-) & (\mathrm{K}^+\mathrm{K}^0) \\ \mathrm{D}^- & (\mathrm{K}^-\overline{\mathrm{K}}^0) & ?^0 \end{pmatrix}. \tag{7}$$

If we do not identify the particles with the same S, T and T_3, then we get in the case of mesons three different neutral isosinglets with $S^M = 0$ and two different isodoublets with $S^M = 1$ and $S^M = -1$ (and their conjugates).

The assumption that the meson field M has the character of an abstract matrix agrees with the spirit of Yukawa interactions, which are linear in meson fields and bilinear in baryon fields.

References

1) W. Królikowski, Nuclear Physics **10** (1959) 213, **11** (1959) 687

2) Wan-Gan-Chiang, communication at the International Conference on High Energy Physics (Kiev, 1959);
T. Yamanouchi and M. F. Kaplon, Phys. Rev. Letters **3** (1959) 283;
T. Yamanouchi, Phys. Rev. Letters **3** (1959) 480

2.B

Nuclear Physics **17** (1960) 424—434; © *North-Holland Publishing Co., Amsterdam*

Not to be reproduced by photoprint or microfilm without written permission from the publisher

POLARIZATION OF NEUTRONS FROM THE REACTIONS $Li^7(p, n)Be^7$ AND $D(d, n)He^3$

J. A. BAICKER † and K. W. JONES ††

Columbia University, New York, New York †††

Recieved 15 February 1960

Abstract: The polarization of neutrons has been measured for the $Li^7(p, n)^7Be$ reaction at a laboratory angle of 50° at bombarding energies from 3.0 to 6.0 MeV, and for the $D(d, n)He^3$ reaction at a laboratory angle of 40° at bombarding energies from 2.0 to 4.5 MeV. The polarization was determined from the left-right asymmetry in the scattering of the neutrons from liquid helium. A nanosecond time-of-flight system was used as a neutron spectrometer.

1. Introduction

Measurements of the polarization of neutrons produced in nuclear reactions are of interest as data which may help to identify reaction mechanisms, as an aid in the identification of the spins and parities of nuclear excited states and as a tool to use for the study of spin-orbit interactions in the scattering of neutrons by nuclei.

The present work on the $D(d, n)He^3$ and $Li^7(p, n)Be^7$ reactions was mainly motivated by a desire to extend the known polarized neutron sources to higher neutron energies than were previously available. Theoretical studies have been made of both reactions and additional data would be very useful for a detailed understanding of the mechanism. The $D(d, n)He^3$ reaction involves comparatively simple nuclei and might be well suited for such calculations.

Blin-Stoyle [1]) and Fierz [2]) have made theoretical studies of the polarization expected from the $D(d, n)He^3$ reaction. They were able to predict the angular dependence of the polarization, but were not able to calculate the energy dependence in detail for lack of information on two-body forces. If the $D(d, n)He^3$ reaction at higher energies is considered to proceed mainly by a surface interaction, the polarization might be calculated on the basis of a stripping model. In this case the polarization would be produced by the interaction of the outgoing neutron with the residual nucleus [3]).

Predictions of the $Li^7(p, n)Be^7$ polarization at about 2.2 MeV have been made by Adair [4]). His calculations assumed that the polarization was produced by the interference of known excited states in the compound nucleus Be^8. The

† Now at R. C. A. Laboratories, Princeton, New Jersey.

†† Now at The Ohio State University, Columbus, Ohio.

††† Work partially supported by the U. S. Atomic Energy Commission.

predicted energy variation of the polarization was not verified by later experimental results. Therefore, additional states in Be^8 should be considered, or perhaps, as suggested by Striebel *et al.* [5]), a direct interaction process should be considered.

A number of experimental investigations of both reactions have been made. The D(d, n)He^3 reaction has been measured at energies up to 1.8 MeV [6–10]) and at 8.2 MeV [11]), and the Li^7(p, n)Be^7 reaction has been measured to 4.95 MeV [5, 12–15]).

In the present work data were taken at a fixed angle as a function of bombarding energy. Alignment of the experimental equipment was so difficult that angular distributions were not attempted. The equipment used consisted of a time-of-flight neutron spectrometer and a liquid helium polarimeter. The time-of-flight spectrometer is capable of giving an excellent signal to background ratio and good energy resolution. The use of liquid helium gave a considerably larger number of scattering centers than could conveniently be obtained with a gas sample.

2. Method of Measuring Polarization

The polarization of neutrons may be determined by measuring the left-right scattering asymmetry from a suitable polarimeter [16]).

The cross section for elastic scattering of polarized neutrons is given by

$$\sigma(\theta_2) = \sigma^u(\theta_2)[1+P_1(\theta_1)P_2(\theta_2)\mathbf{n}_1 \cdot \mathbf{n}_2], \tag{1}$$

where $P_1(\theta_1)$ is the initial neutron polarization, θ_2 is the angle through which the neutrons are scattered, $\sigma^u(\theta_2)$ is the cross section for scattering of unpolarized neutrons, $P_2(\theta_2)$ is the polarization produced in an initially unpolarized beam of neutrons, and $\mathbf{n}_1$ and $\mathbf{n}_2$ are unit vectors normal to the reaction and scattering planes. The positive direction for $\mathbf{n}$ is given by $\mathbf{k}_{inc} \times \mathbf{k}_{out}$ where $\mathbf{k}_{inc}$ refers to the incident particle and $\mathbf{k}_{out}$ to the outgoing particle.

The geometry of the experiment is shown in fig. 1. If the reaction and scattering processes are taken to be coplanar it can be seen from eq. (1) that the right-left scattering asymmetry is given by

$$\frac{R}{L} \equiv \frac{\sigma(+\theta_2)}{\sigma(-\theta_2)} = \frac{1+P_1(\theta_1)\,P_2(\theta_2)}{1-P_1(\theta_1)\,P_2(\theta_2)}. \tag{2}$$

The polarization $P_2(\theta_2)$ can be calculated providing the phase shifts for the scattering of unpolarized neutrons from the polarimeter are known. Hence, the initial neutron polarization $P_1(\theta_1)$ may be determined from the measured value of R/L.

Helium was chosen for the polarimeter since the scattering phases were reasonably well known and since the analyzing efficiency was high over the entire energy range covered and was not a sensitive function of the neutron

energy. The polarization $P_2(\theta_2)$ was calculated from the phase shifts determined by Seagrave and by Clementel and Villi. The present status of the n—He^4 phase shifts is summarized in a review article by Hodgson [17]).

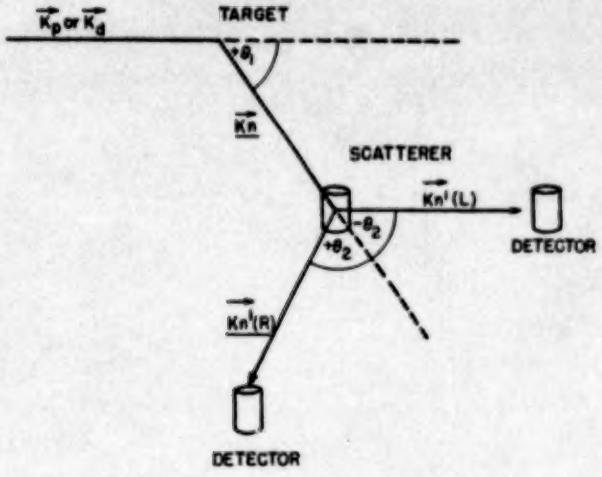

Fig. 1. Geometry of the experiment.

3. Experimental Details

The neutrons were produced with a pulsed beam ($\frac{1}{2}$ to 1 μA) from a Van de Graaff accelerator. A schematic diagram of the general experimental arrangement is shown in fig. 2. For the D(d, n)He^3 measurements the target consisted

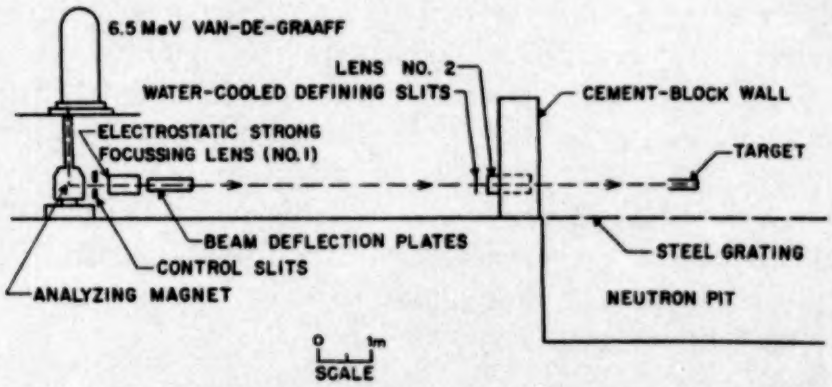

Fig. 2. Sketch of experimental area.

of a gas cell 3 cm long with a nickel entrance foil 0.63 to 1.27 μm in thickness. The target pressure was approximately $\frac{1}{2}$ atm. For the Li^7(p, n)Be^7 measurements the target was natural metallic lithium evaporated on a tantalum backing. The target thickness used varied from approximately 50 keV to 200 keV for 2 MeV incident protons.

Neutrons emitted from the target at an angle θ_1 passed through a collimator composed of paraffin and boric acid with lead and iron inlays. The collimator

shielded the counter and portions of the dewar not containing helium from the neutrons coming directly from the target. The collimator geometry is shown in fig. 3. The polarimeter subtended a solid angle of approximately 10^{-3} sr at the target. The boric acid at the rear of the collimator was used to reduce the back-

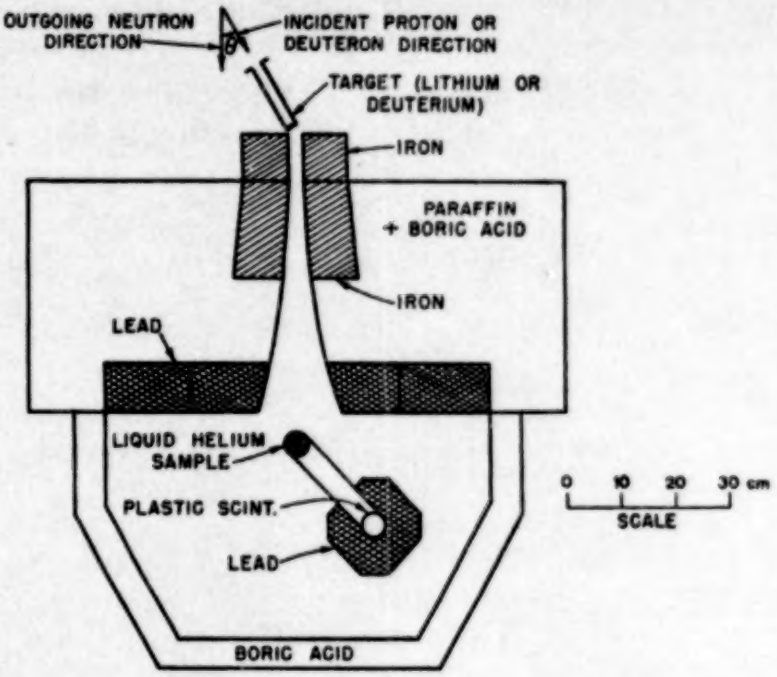

Fig. 3. The neutron shielding geometry.

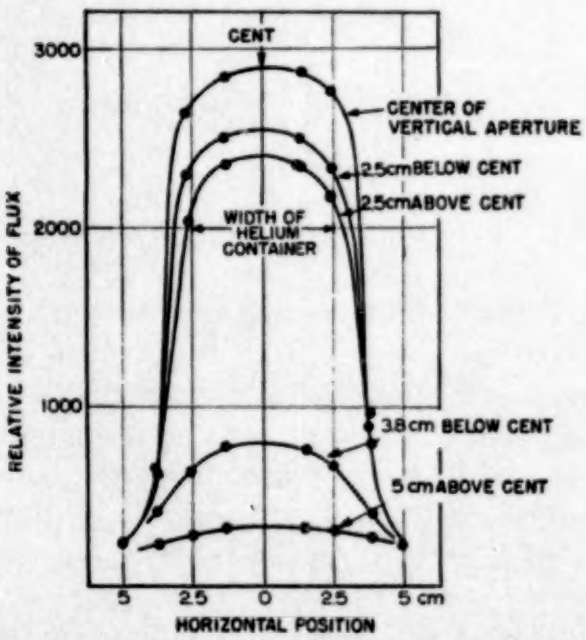

Fig. 4. Profile map of neutron flux at the rear of the collimator.

ground of high energy gamma rays arising from the capture of thermal neutrons in or near the counter. A second paraffin shield completely surrounding the target helped to reduce the amount of room scattering. The closed shielding made direct monitoring of the neutron beam very difficult so that the data were normalized on the basis of the integrated beam current. The data were taken in such a way that errors due to fluctuations in neutron yield were minimized. The neutron intensity distribution at the polarimeter is shown in fig. 4. This was measured often during the course of the experiment to ensure that no right-left asymmetries in the scattering were caused by an asymmetric

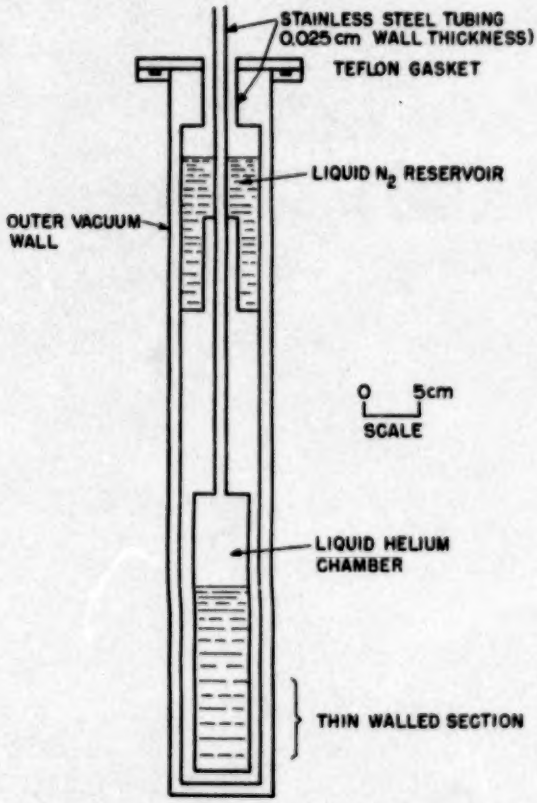

Fig. 5. Schematic diagram of liquid helium dewar.

beam distribution. Difficulties in ensuring symmetry were such that measurement of the angular distributions of the polarization P_1 were not made.

Liquid helium used as the polarimeter was contained in the dewar shown in fig. 5. The inner chamber containing the liquid helium was 5 cm in diameter with a wall thickness of 0.025 cm. Surrounding the helium chamber was a 0.01 cm copper heat shield at liquid nitrogen temperature and a 25 μm outer vacuum chamber wall. The evaporation rate of the liquid helium was 12 cm^3 per hour.

A block diagram of the fast neutron time-of-flight spectrometer is shown in fig. 6. The system is nearly identical to that described by Cranberg *et al.* [18,19]);

the main difference lies in the method of gating. With the present system it is possible to set an upper as well as a lower limit on the pulse heights counted. This method allows the rejection of high energy capture gamma ray pulses which are larger than the maximum pulse height from recoil protons. The neutron detector consisted of a cylinder of plastic scintillator (4.45 cm diameter and 7.62 cm long) and an RCA type 6342 photomultiplier. The axes of the detector and the helium chamber were parallel and 20 cm apart. The solid angle subtended at the polarimeter was about 0.06 sr.

There were several sources of background in the experiment. The largest background was neutrons scattered from the walls of the dewar. This ranged from 20 % to 40 % of the total counting rate. For subtraction of this background a dummy dewar was constructed which simulated the empty dewar to

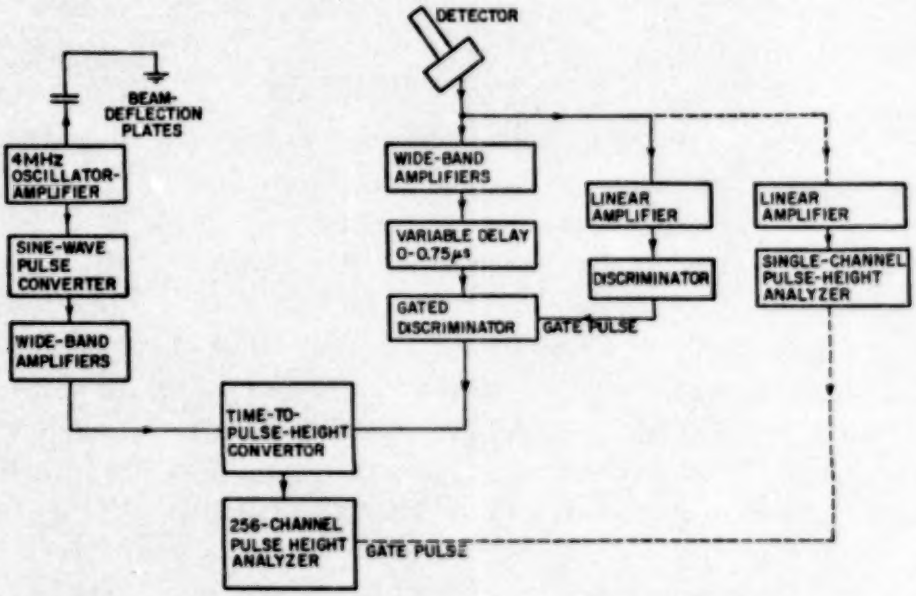

Fig. 6. Block diagram of electronics.

better than 5 %. A summary of the various background components for a typical run is shown in table 1. In general the total background ran from 40 to 60 % of the total counting rate with a few runs going as high as 75 %.

Asymmetries introduced by the apparatus were checked by frequent measurements of the right-left asymmetry at $\theta_1 = 0^0$. Since the polarization is zero at zero degrees there should be no asymmetry. Within the statistical accuracy of these measurements (1 to 2 %) no asymmetry was observed. The final polarization values were the average of points taken for θ_1 to the left and right of the charged particle beam. This procedure averages out systematic errors in the setting of θ_1. Measurements were also made for more than one value of θ_2.

Corrections were made to all of the data for the effects of multiple scattering in the sample, the finite geometry of the sample and detector and in-scattering

TABLE 1
Background components for a typical run

Source of background	Percentage of total counting rate
Neutrons scattered by dewar	25
Air scattered neutrons plus leak-through neutrons due to imperfect collimation	15
Time independent background	15
Total background	55

from the lead shield. The multiple scattering correction was made on the assumption that only singly and doubly scattered neutrons need be considered. A numerical integration was used to calculate the finite-geometry and in-scattering corrections.

3. Errors and Uncertainties

The errors given in tables 2 and 3 below include those arising from the statistical nature of the scattering process as well as an estimate of possible systematic errors introduced in calculating the multiple-scattering, in-scattering and finite geometry corrections to the data. Other systematic errors should be small since there was no left-right scattering asymmetry at $\theta_1 = 0°$ and consistent results were obtained for angles of observation to left and right of the incident beam and for different values of θ_2 with a fixed θ_1. The errors due to the uncertainties in the phase shifts for the scattering of neutrons by helium are difficult to assess. The values of the D-wave phase shifts are small ($< 1°$) in the energy region concerned and were assumed to be zero for lack of precise information. The calculated value of $P_2(\theta)$ can be quite sensitive to even a small amount of the D wave, especially where $P_2(\theta)$ is changing rapidly with angle. The $S_{\frac{1}{2}}$, $P_{\frac{1}{2}}$ and $P_{\frac{3}{2}}$ phase shifts are also uncertain by a few degrees. Again $P_2(\theta)$ can be quite sensitive to values chosen for these phase shifts in regions where $P_2(\theta)$ is changing rapidly.

Most of the measurements in the present work were made at angles where the polarization $P_2(\theta)$ was slowly varying in order to minimize the effects of phase shift uncertainties. The entire set of D(d, n)He^3 runs and most of the Li^7(p, n)Be^7 runs for proton energies above 5 MeV were made with $\theta_2 = 68°$(C.M.) where the polarization has a broad maximum. For the lowest energy Li^7(p, n)Be^7 runs the scattering angle was 90°(C.M.). At $E_p = 3$ MeV ($E_n \approx 1$ MeV) the polarization has a smooth maximum at this angle. As the energy is increased this maximum moves slowly back in angle and the scattering angle was shifted accordingly. Since the maxima in the polarization at back angles were always somewhat greater than at forward angles, it would have been desirable to work at angles greater than 90°. Unfortunately, the scattering cross section decreases

as the angle is increased and also as the energy is increased, and for neutron energies of 2.5 MeV and above it was necessary to go to forward scattering angles in order to obtain reasonable counting rates.

For neutrons in the energy range 1.8 to 2.3 MeV, the measurements had to be made at angles where the polarization is changing sharply. This was in the proton energy range 3.8 to 4.3 MeV, and it is in this region that the uncertainties in the n—He^4 phases would have the greatest effect on the experimental results.

4. Results and Discussion

4.1. $Li^7(p, n)Be^7$

Measurements were made for neutrons emitted at $\theta_1 = 50°$ in the laboratory system. This angle was chosen so that direct comparison could be made with

TABLE 2

Polarization of neutrons from the reaction $Li^7(p, n)Be^7$

E_p (MeV)	θ_1 (lab)	θ_2 (lab)	$P_2(\theta_2)$	$\frac{R}{L}$ †	P_1P_2 ††	P_1	Average
2.98	±50°	76°	0.87	1.770	0.350	0.402±0.077	
3.15	+50°	68°	0.57	1.29	0.156	0.274±0.045	0.299±0.037
	−50°	80°	0.79	1.55	0.266	0.337±0.053	
3.36	+50°	68°	0.43	1.22	0.120	0.279±0.065	0.354±0.060
	−50°	80°	0.68	1.57	0.271	0.398±0.052	
3.58	+50°	90°	0.69	1.445	0.225	0.326±0.043	0.356±0.072
	−50°	80°	0.47	1.483	0.240	0.511±0.091	
3.78	±50°	90°	0.55	1.443	0.214	0.390±0.036	
3.99	±50°	90°	0.39	1.310	0.161	0.412±0.038	
4.20	±50°	100°	0.62	1.413	0.228	0.369±0.051	0.343±0.049
	±50°	55°	−0.19	0.933	−0.051	0.267±0.074	
4.42	±50°	100°	0.61	1.381	0.212	0.347±0.040	0.354±0.034
	±50°	55°	−0.25	0.874	−0.093	0.371±0.062	
4.57	+50°	100°	0.59	1.234	0.126	0.214±0.083	0.274±0.048
	+50°	55°	−0.28	0.877	−0.084	0.300±0.056	
4.66	−50°	100°	0.57	1.32	0.163	0.286±0.060	
4.86	±50°	100°	0.54	1.206	0.120	0.222±0.054	0.172±0.035
	±50°	55°	−0.36	0.921	−0.056	0.155±0.049	
5.01	−50°	100°	0.53	1.11	0.066	0.125±0.080	0.099±0.033
	−50°	55°	−0.40	0.940	−0.038	0.095±0.033	
5.03	+50°	55°	−0.40	0.964	−0.022	0.054±0.029	
5.20	±50°	55°	−0.43	1.058	0.034	−0.078±0.022	−0.086±0.023
	+50°	100°	0.50	0.870	−0.090	−0.180±0.077	
5.39	+50°	55°	−0.46	1.12	0.070	−0.152±0.025	
5.58	−50°	55°	−0.49	1.22	0.117	−0.238±0.037	
5.78	−50°	55°	−0.52	1.33	0.169	−0.325±0.048	
5.98	−50°	55°	−0.55	1.4	0.127	−0.230±0.042	

† The values given here and in table 3 for R/L are the averages of R/L for θ_1 positive and L/R for θ_1 negative.

†† Correction has been made for the effects of the finite geometry of the scatterer and detector, in-scattering from the shielding material and multiple scattering in the sample.

the Wisconsin data. [11,13,14]). In order to get the best possible counting rates the time-of-flight system was operated with relatively poor time resolution (5 to 10 ns) and the lower discrimination level was set to discriminate against neutrons from the $Li^7(p, n)Be^{7*}$ reaction. Above 4 MeV this procedure was impossible. The flight times of the two groups are such that it is also rather difficult to differentiate between the ground state and first excited state by use of time-of-flight even with good time resolutions. Consequently, above 4 MeV both groups were detected, but with somewhat higher efficiency for the ground state group than for the first excited state group.

The results obtained are shown in table 2 and fig. 7. For several of the points the right-left asymmetry was measured at more than one value of θ_2. These angles were chosen so that the analyzer efficiency was positive for one angle and negative for the other. The asymmetry reversed itself for the two measurements so as to give a consistent value for the polarization of the incident neutrons.

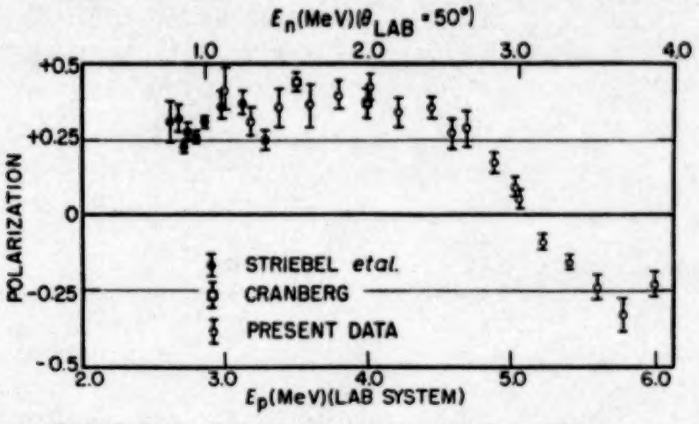

Fig. 7. $Li^7(p, n)Be^7$. Polarization of neutrons emitted at $50°_{lab}$ vs proton energy.

This fact provided another convincing proof that there were no large instrumental asymmetries.

The agreement between the Wisconsin data and the present data is quite good in the region around 3 MeV where the two experiments could be compared. The comparison between the two experiments, which used entirely different polarimeters, is evidence that no large errors are introduced by uncertainties in the values used for the efficiency of the helium polarimeter. It also, of course, implies that no serious errors exist in the choice of the phase shifts used for the calculation of the efficiency. This conclusion is in agreement with the results of Levintov *et al.* [8,9]). The recent measurements of Cranberg [15]) using a high pressure helium cell as a polarimeter are also in good agreement with the present results.

As was mentioned previously both the ground state and first excited state groups were detected above 4 MeV, although with somewhat different efficiencies. It was felt that it was worthwhile to extend the data to 6 MeV in order to achieve at least a qualitative idea of the behaviour of the polarization in this

region. The intensity of the excited state relative to the ground state is about 20 % or less at 50° up to incident proton energies of 4.0 MeV and the polarization is known to be small up to energies of 3.5 MeV [15]). If this behaviour continues at higher bombarding energies, the measurements are a fairly good representation of the polarization for the ground state alone up to 6 MeV.

The total yield of the ground and first excited states was measured by Willard *et al.* [21]) and a resonance was observed at a bombarding energy of 4.89 MeV with a width of approximately 400 keV. The rapid change of the polarization in this energy region suggests that the polarization may be strongly influenced by the resonance. This is in contrast to the behaviour observed at the 2.25 MeV resonance where the polarization remains essentially constant across the resonance.

4.2. D(d, n)He³

Polarization measurements for the D(d, n)He³ reaction were made at θ_1 (lab) = 40°. This angle corresponds roughly to the position of the theoretically predicted polarization maximum over the entire energy range covered. The results obtained are shown in table 3 and fig. 8. It was not possible to take data above $E_d = 4.5$ MeV because of the high background from the nickel

TABLE 3

Polarization of neutrons from the reaction D(d, n)He³

E_D (MeV)	θ_1 (lab)	θ_2 (lab)	$P_2(\theta_2)$	$\frac{R}{L}$ †	P_1P_2	P_1
2.0	±40°	±55°	−0.58	1.246	0.132	−0.227±0.035
2.5	±40°	±55°	−0.63	1.240	0.131	−0.208±0.037
3.0	+40°	±55°	−0.64	1.207	0.115	−0.179±0.029
3.5	±40°	±55°	−0.64	1.20	0.113	−0.176±0.022
4.0	±40°	±55°	−0.64	1.180	0.101	−0.158±0.022
4.5	±40°	±55°	−0.64	1.192	0.108	−0.169±0.015

† See table 2, footnote.

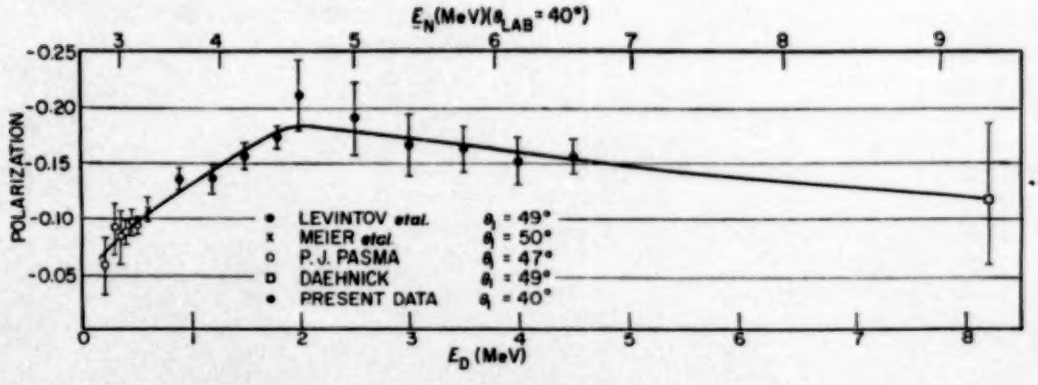

Fig. 8. D(d, n)He³. Polarization of neutrons emitted at 40°$_{lab}$ vs deuteron energy.

entrance foil in the gas target. Another difficulty in the measurement was the necessity to choose an angle θ_2, which compromised between the need of a high scattering cross section (forward angles) and a high polarimeter efficiency (back angles).

The data agree reasonably well with that of Levintov *et al.* [8,9]) although it is clear that the accuracy is not as good. The relatively poor accuracy in the present experiment is due to the problems of high time independent background associated with running a deuteron beam, and the difficulties of efficiently collimating high enrgy neutrons. There is evidence for a broad maximum in the polarization at about 2 MeV which could be the maximum predicted theoretically by Fierz.

The authors are grateful to Dr. R. E. Benenson, Mr. B. Tell, and Mr. H. Hess for their assistance during the experiment; to Professor W. W. Havens, Jr. and Dr. L. J. Lidofsky for many helpful discussions; and to Dr. W. A. W. Daehnick and Mr. P. R. Bevington for furnishing their results prior to publication.

References

1) R. J. Blin-Stoyle, Proc. Phys. Soc. A **64** (1951) 700; Proc. Phys. Soc. A **65** (1952) 949
2) M. Fierz, Helv. Phys. Acta **25** (1952) 629
3) See for example: W. B. Cheston, Phys. Rev. **96** (1954) 1590
4) R. K. Adair, Phys. Rev. **96** (1954) 709
5) Striebel, Darden and Haeberli, Nuclear Physics **6** (1958) 188
6) Meier, Scherrer and Trumpy, Helv. Phys. Acta **27** (1954) 577
7) McCormac, Steuer, Bond and Hereford, Phys. Rev. **104** (1954) 718
8) Levintov, Miller and Shamshev, Nuclear Physics **3** (1957) 221
9) Leventov, Miller, Tarumov and Shamshev, Nuclear Physics **3** (1957) 237
10) P. J. Pasma, Nuclear Physics **6** (1958) 141
11) W. A. W. Daehnick, Phys. Rev. **115** (1959) 1008
12) Adair, Darden and Fields, Phys. Rev. **96** (1954) 503
13) Willard, Bair and Kington, Phys. Rev. **95** (1954) 1359
14) A. Okazaki, Phys. Rev. **99** (1955) 55
15) L. Cranberg, Phys. Rev. **114** (1959) 174
16) A review of the theory is given by L. Wolfenstein, Annual Review of Nuclear Science **6** (1956) 43; see also J. V. Lepore, Phys. Rev. **79** (1950) 137
17) P. E. Hodgson, Phil. Mag. Suppl. **7** (1958) 1
18) Weber, Johnstone and Cranberg, Rev. Sci. Inst. **27** (1956) 166
19) L. Cranberg and J. S. Levin, Phys. Rev. **103** (1956) 343
20) Bevington, Mitchell, Rolland, Wilenzick and Lewis, Bull. Am. Phys. Soc. **4** (1959) 218; P. R. Bevington, private communication
21) Bair, Willard, Snyder, Hahn, Kington and Green, Phys. Rev. **85** (1952) 946

1.D.1

Nuclear Physics **17** (1960) 434—447; © *North-Holland Publishing Co., Amsterdam*

Not to be reproduced by photoprint or microfilm without written permission from the publisher

s-PARTICLE DOUBLETS IN CERTAIN LIGHT NUCLEI

O. M. BILANIUK

Dept. of Physics and Astronomy, University of Rochester, Rochester N.Y., USA †

and

J. B. FRENCH

Fysisch Laboratorium der Rijksuniversiteit, Utrecht, The Netherlands †

Received 15 March 1960

Abstract: The splitting of an s-particle doublet in B^{11} is examined to see what information it gives about the effective 1p-2s shell model interaction and it is concluded that the small splitting is explainable by an interaction whose spin dependence is primarily of $\mathbf{s}_1 \cdot \mathbf{s}_2 \mathbf{t}_1 \cdot \mathbf{t}_2$ nature. Certain other s-doublets of the "hole-particle" type are considered too and their small splitting appears to show that the spin dependence of the effective n-p interaction between inequivalent nucleons is weaker than normally assumed. A very simple procedure is used to evaluate the interaction energies.

1. Introduction

In a recent B^{10}(d, p) experiment by Bilaniuk and Hensel [1]) a pair of single-particle s levels were observed at 9.19 and 9.28 MeV as well as a single-particle d level at 8.93 MeV which has a measurable s admixture. The spins of the three levels are believed [2]) †† to be as in fig. 1.

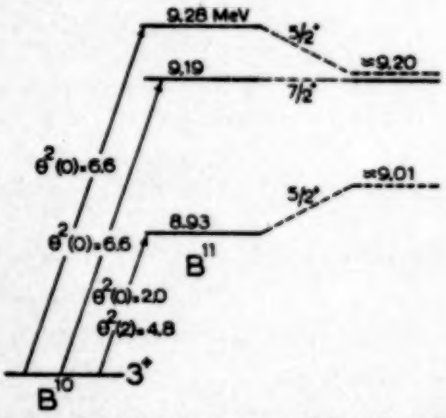

Fig. 1. The B^{11} single-particle levels with the observed $l = 0$ and $l = 2$ reduced widths (in an arbitrary unit) and the probable spins. The energies at the right are the "unperturbed" energies, the repulsive effect between the two $\frac{1}{2}^+$ levels being subtracted out.

† Work at the University of Rochester was supported in part by the Atomic Energy Commission. Work at Utrecht was done while the second-named author was Senior Post-Doctoral Fellow of the National Science Foundation on leave during 1959-60 from the University of Rochester.

†† Our conclusions would be essentially unaltered by a change in the assignments (all three levels must be $\frac{1}{2}^+$, $\frac{3}{2}^+$) as long as the upper two are assigned different spins.

By a "single particle" state we mean a state which is well described by a 2s or 1d particle coupled to the B^{10} ground state, this "weak coupling" model being that originally discussed by Lane [3]). As far as the s-levels are concerned we would expect this to be a very favourable case for the weak-coupling model since no excited B^{10} state below 5.5 MeV can contribute to the $\frac{7}{2}^+$ level and none below 3.6 MeV to the $\frac{5}{2}^+$ level. Besides this we shall see that the interaction energy of an s particle with a $T=0$ core can be written in a very direct and simple way and it then becomes worthwhile to consider whether the small observed doublet splitting tells us anything about the shell model 1p—2s interaction. We begin by considering the three B^{11} levels as an isolated system and afterwards consider in a simple way the effects which core excitation and single-particle s—d mixing can have on the validity of the weak-coupling model. We shall pay a little attention also to a few other interesting s-particle doublets.

2. The s-Doublet Splitting in B^{11}

The observed splitting is 90 keV but the two $\frac{5}{2}^+$ levels have been spread apart from their zero-order position by interaction between them. We need the zero-order splitting to compare directly with the calculated doublet splitting for the levels $\{\phi_0 \times 2s\}$ (where ϕ_0 is the ground state of B^{10}). If we write Ψ_1, Ψ_2 for the $\frac{5}{2}^+$ levels at 8.93 and 9.28 MeV respectively we have

$$\begin{aligned} \Psi_1 &= \alpha\{\phi_0 \times d\} + \beta\{\phi_0 \times s\}, \\ \Psi_2 &= -\beta\{\phi_0 \times d\} + \alpha\{\phi_0 \times s\}. \end{aligned} \tag{1}$$

Now directly from the $l=0$ relative reduced widths [4]) for the $\frac{5}{2}^+$ states (as shown in fig. 1) we have $|\alpha| = (6.6/8.6)^{\frac{1}{2}} = 0.88$, $|\beta| = (2.0/8.6)^{\frac{1}{2}} = 0.48$. The two wave functions together with the two known energy levels define the $\frac{5}{2}^+$ Hamiltonian matrix in the $\{\phi_0 \times l\}$ representation to be

$$H \approx \begin{pmatrix} 9.01 & \pm 0.15 \\ \pm 0.15 & 9.20 \end{pmatrix} \text{MeV}. \tag{2}$$

If we had instead compared the widths for the two lowest levels (the middle one being a pure s level) we would have found slightly different values †; in fact making a very generous allowance for the uncertainty in the wave functions ($\alpha^2 = 0.77 \pm 0.1$) we conclude that, for the zero-order s-doublet splitting Δ, defined as $E_{\frac{1}{2}}^{(0)} - E_{\frac{3}{2}}^{(0)}$, and the interaction matrix element between the two $\frac{5}{2}^+$ states, we have

$$\begin{aligned} &-45 \text{ keV} \leqq \Delta \leqq 25 \text{ keV}, \\ &|\langle\{\phi_0 \times s\} H \{\phi_0 \times d\}\rangle| \approx 140 \pm 20 \text{ keV}. \end{aligned} \tag{3}$$

† The corresponding 20 % discrepancy in the two determinations of the single-particle s width is within the range of fluctuation found for reduced widths in general. Note too that it is experimentally impossible to detect the $l=2$ admixture in the s levels.

We now calculate this splitting taking as a model that the wave functions are those of a 2s particle coupled to the ground state of B^{10} which in turn is described as belonging to the s^4p^6 configuration (or more simply p^6 since the s^4 shell is inert) and more specifically as the particular state found by means of a standard intermediate-coupling calculation. Physically then one assumes, as is justified by the B^{10} spectrum, that the spin-orbit interaction is so strong in B^{10} that the s-particle interaction cannot uncouple the orbital and spin angular momenta of the core. The doublet splitting then arises from a difference in the orientations of the s-particle with respect to the core.

For cases such as presently interest us, the interaction matrix element is given by

$$\langle\{\phi_a\times l_1\}H\{\phi_b\times l'_1\}\rangle = \langle\phi_a H\phi_a\rangle\delta_{ab}\delta_{l_1 l'_1} + \langle\phi_a(1\ldots n)\times l_1(n+1)|\sum_{i=1}^{n} H_{i,n+1}(1-P_{i,n+1})|\phi_b(1\ldots n)\times l'_1(n+1)\rangle. \quad (4)$$

Here ϕ_a, ϕ_b are two orthogonal states of the n-particle system and it is understood that the coupled particle l_1(or l'_1) is not equivalent to any particle in ϕ_a or ϕ_b. $\{\phi_a\times l\}$ is a completely antisymmetric state, the $\times$ denoting vector coupling. If $a = b$ and $l_1 = l'_1$, the first term on the right is simply the internal energy of the core (H of course being the n-particle Hamiltonian) and the second term, the interaction energy of the particle with the core, produces the splitting. For the rest of this section we shall be concerned with this interaction energy where the coupled particle is an s particle ($l_1 = l'_1 = 0$).

We evaluate the energy by a simple direct procedure. If ϕ belongs to l^n, closed shells being ignored, and if, as is conventionally assumed, the interaction is a central one †, we can use the fact that the two-particle system $\{l\times s\}$ has only four multiplets and thus, representing the l—s interaction by four independent two-body operators we can write by introducing the spin and isobaric spin operators ($\mathbf{s}^2 \equiv \mathbf{t}^2 \equiv \frac{3}{4}$),

$$H_{12}(1-P_{12}) = B_0+B_s\mathbf{s}_1\cdot\mathbf{s}_2+B_t\mathbf{t}_1\cdot\mathbf{t}_2+B_{st}\mathbf{s}_1\cdot\mathbf{s}_2\mathbf{t}_1\cdot\mathbf{t}_2. \quad (5)$$

We evaluate the quantities B by using

$$\langle(l\times s)|H_{12}(1-P_{12})|(l\times s)\rangle = \langle\{l\times s\}|H_{12}|\{l\times s\}\rangle,$$

which is simply the two-body multiplet energy. Writing this as ${}^{2T+1,2S+1}E$ we have four equations for the coefficients and solving these gives

$$\begin{pmatrix} 16B_0 \\ 4B_s \\ 4B_t \\ B_{st} \end{pmatrix} = \begin{pmatrix} 1 & 3 & 3 & 9 \\ -1 & 1 & -3 & 3 \\ -1 & -3 & 1 & 3 \\ 1 & -1 & -1 & 1 \end{pmatrix} \begin{pmatrix} {}^{11}E \\ {}^{13}E \\ {}^{31}E \\ {}^{33}E \end{pmatrix}. \quad (6)$$

† We can of course ignore the single-particle spin-orbit interaction and consider only the two-body interaction. It will appear later that the central-force assumption is not essential for the B^{11} case.

The first three terms of eq. (5) lead to an interaction operator in eq. (4) which can be summed over the core particles. For the special cases where $\langle\phi\mathbf{t}_i\phi\rangle$ or $\langle\phi\mathbf{s}_i\phi\rangle$ is independent of i, the fourth term can be summed too and we have then

$$\sum_{i=1}^{n} H_{i,n+1}(1-P_{i,n+1}) \equiv nB_0+B_s\mathbf{S}_1\cdot\mathbf{s}_{n+1} +B_t\mathbf{T}_1\cdot\mathbf{t}_{n+1}+\frac{B_{st}}{n}(\mathbf{S}_1\cdot\mathbf{s}_{n+1})(\mathbf{T}_1\cdot\mathbf{t}_{n+1}), \quad (7)$$

where $\mathbf{S}_1$ and $\mathbf{T}_1$ are spin and isobaric spin operators for the core. The principal cases in which eq. (7) is valid are those in which $T_1 = 0$ (the B_t, B_{st} terms then do not contribute), $S_1 = 0$, $T_1 = \frac{1}{2}n$, $S_1 = \frac{1}{2}n$ and of course the trivial ones where $n = 1$ or where $B_{st} = 0$. From now on we deal only with such cases.

The matrix element can now be evaluated by a Landé type argument; since the angular momentum coupling is defined by the scheme

$$[(\mathbf{L}_1\times\mathbf{S}_1)_{J_1}\times\mathbf{s}]_J, \quad \mathbf{S}_1 \equiv \frac{(\mathbf{S}_1\cdot\mathbf{J}_1)\mathbf{J}_1}{J_1(J_1+1)}$$

and then since

$$\mathbf{S}_1\cdot\mathbf{s}_{n+1} \equiv \frac{(\mathbf{J}_1^2+\mathbf{S}_1^2-\mathbf{L}_1^2)(\mathbf{J}^2-\mathbf{J}_1^2-\mathbf{s}_{n+1}^2)}{4J_1(J_1+1)}, \quad (8)$$
$$\mathbf{T}_1\cdot\mathbf{t}_{n+1} \equiv \tfrac{1}{2}(\mathbf{T}^2-\mathbf{T}_1^2-\mathbf{t}_{n+1}^2),$$

the interaction energy becomes

$$nB_0+\tfrac{1}{2}B_t\{T(T+1)-T_1(T_1+1)-\tfrac{3}{4}\} +\tfrac{1}{4}\left[B_s+\frac{B_{st}}{2n}\{T(T+1)-T_1(T_1+1)-\tfrac{3}{4}\}\right] \cdot[J(J+1)-J_1(J_1+1)-\tfrac{3}{4}]\left[1-\frac{\langle\mathbf{L}_1^2-\mathbf{S}_1^2\rangle}{J_1(J_1+1)}\right], \quad (9)$$

and of course $\{T(T+1)-T_1(T_1+1)-\frac{3}{4}\} = T_1, -(T_1+1)$ for $T = T_1+\frac{1}{2}, T_1-\frac{1}{2}$ respectively, and similarly for the J expression. In eq. (9), $\langle\mathbf{L}_1^2-\mathbf{S}_1^2\rangle$ is the expectation value in the core state of the indicated operator.

For the case $T_1 = 0$ the doublet splitting $\Delta \equiv E_{J_>}-E_{J_<}$ is a significant quantity and we have

$$\Delta = \frac{(2J_1+1)}{4}B_s\left\{1-\frac{\langle\mathbf{L}_1^2-\mathbf{S}_1^2\rangle}{J_1(J_1+1)}\right\}, \quad (10)$$

while rewriting the interaction energy for this case gives

$$E_{J_>} = nB_0+\frac{J_1\Delta}{(2J_1+1)}, \quad E_{J_<} = nB_0-\frac{(J_1+1)\Delta}{(2J_1+1)}. \quad (11)$$

The expectation value $\langle \mathbf{L}_1^2 - \mathbf{S}_1^2 \rangle$ is trivial to calculate if the core function is available in an LS representation. Using functions previously derived (defined by a Rosenfeld [5]) interaction with the Slater-integral ratio $L/K = 6$) we find for the B^{10} ground state $\langle \mathbf{L}_1^2 - \mathbf{S}_1^2 \rangle / [J_1(J_1+1)] = 0.49, 0.51, \frac{1}{3}$ for $\zeta = 3.8, 5.7, \infty$ where $\zeta \equiv a/K$ is the usual spin-orbit parameter and the value ∞ defines jj coupling. The result is rather insensitive to the spin-orbit parameter as it should be in any practical case when J_1 is large. Taking the jj value we then conclude that

$$\Delta = \tfrac{7}{6} B_s = -\tfrac{7}{24}\{^{11}E - {}^{13}E + 3\,{}^{31}E - 3\,{}^{33}E\}, \tag{12}$$

and inversely the experimental splitting determines a very small (essentially zero) value for this combination of the two-body 1p—2s multiplet energies. The splitting can of course be written simply in terms of the jj coupling two-body energies but this we leave for the next section.

If now we ignore the exchange interaction in eq. (4) (the exchange integral should be an order of magnitude smaller than the direct one) we see that the splitting will be proportional to the $\mathbf{s}_1 \cdot \mathbf{s}_2$ part of the interaction and will therefore vanish for an interaction such as Rosenfeld's [5]) which is proportional to $\mathbf{t}_1 \cdot \mathbf{t}_2$; the other interaction which has been conventionally used in p-shell spectroscopy, that of Inglis [6]), should produce a large splitting. Since the p—s energies calculated with a conventional interaction span an energy region of 10 MeV we expect then that a Rosenfeld-type interaction should give a "small" splitting, a few hundred kilovolts, while an Inglis-type interaction should give a "large" splitting of a few MeV. This is exemplified in table 1, which gives the energies for a Gaussian interaction.

TABLE 1

The p—s multiplet energies and interaction constants (in MeV) for a Gaussian interaction with $L/K = 6.6$ and $K = -1.1$ MeV.

	^{11}E	^{13}E	^{31}E	^{33}E	B_0	B_s	B_t	B_{st}
Rosenfeld	7.5	−5.5	−3.3	1.4	−0.41	0.27	2.5	17.7
Inglis	4.1	−5.5	−3.3	2.5	0.01	1.9	4.1	15.4

The experimental result of course favours the Rosenfeld-type interaction but still the 300 keV value calculated is much larger than the "very small" value experimentally found and we might ask whether a different interaction still compatible with the many p shell results could indeed give the observed zero splitting. For this purpose we observe that for a given radial dependence (adequately specified by the conventional L/K for p^2 and I_e/I_d, the ratio of the exchange and direct integrals, for ps) we can express the ps multiplet energies in terms of those for p^2. This simple operation then gives for $B_s = 0$ the

following equation for the p^2 multipet energies $^{2T+1,2S+1}L$:

$$[3\,^{33}\mathrm{P}-{}^{11}\mathrm{P}] = \frac{(1-3K/L)(1+I_e/I_d)}{(1+2K/L)(1-I_e/I_d)}[3\,^{31}\mathrm{S}-{}^{13}\mathrm{S}]. \tag{13}$$

The Gaussian interaction which we use as an example gives $K/L = 0.15$, $I_e/I_d = 0.14$ and any other reasonable radial dependence will give about the same results. Then since one knows that $^{31}\mathrm{S} \approx -5.5$ MeV, $^{13}\mathrm{S} \approx -9$ MeV, the condition is that $[3\times{}^{33}\mathrm{P}-{}^{11}\mathrm{P}] \approx -4.5$ MeV. This may be satisfied for example by $^{33}\mathrm{P} = 0$, $^{11}\mathrm{P} = 4.5$ MeV without disturbing any of the p shell results.

We conclude from all this that there may be a good reason for the B^{11} doublet splitting to be *small* (namely the interaction having a $\mathbf{t}_1 \cdot \mathbf{t}_2$ dependence) but that there seems no general reason why it has the *very small* value found, though the latter value is quite compatible with the p shell results. In fact, because of departures from the simple model (which we consider in the next section) it may be that the very small value has no particular significance. Besides this, of course, there seems no *a priori* reason why the effective central interaction valid for p^2 should be satisfactory for ps, though whether it is or not is a question of interest.

We obviously expect to find further s-doublets with "small" (though not necessarily "very small") splittings at higher excitations in B^{11} (according to eq. (11) since $\Delta \approx 0$ their position should in principle simply mirror the $T = 0$ spectrum of B^{10}), and similarly in other odd-mass nuclei throughout the p shell as discussed by Lane [3]). However, many of the possible cases which one thinks of are far less favourable than the present one because there are other low-lying core states which can contribute. As far as the absolute energy of the s levels is concerned we observe that the binding energy of the s levels to a $T_1 = 0$ core is simply nB_0. Then proceeding in the same way as Unna and Talmi [7]) but restricting ourselves to levels with a $T_1 = 0$ core and to cases where the excitation corrections should not be too large we could in principle determine B_0 from the known s level positions. Of course the s-particle binding does not display the characteristic difference found between the binding energy of a p particle to an $A = 4m$ and $A = (4m+2)\mathrm{p}^n$ core. The fact that the lowest s level is at 3 MeV in C^{13} while the B^{11} doublet is at 9 MeV simply reflects this difference.

3. Some Corrections

In this section we first consider briefly the circumstances under which we should expect the simple model used above to be satisfactory. We do this by calculating some corrections to it. These are of two types corresponding either to a mixing of the core states (in which, in the above case, the B^{10} core would be excited) or to a mixing of the single article states (in which the s particle would

be promoted to d). One such matrix element of the second class has already been empirically determined to be about 140 keV and we shall calculate it using explicit interactions. It is very convenient and obviously satisfactory to calculate the corrections in jj coupling and we first derive the jj analogues of equations (9—11).

The two-particle system $\{j\times s_{\frac{1}{2}}\}$ has four states and consequently, when dealing with the interaction of $s_{\frac{1}{2}}$ with j^n, we can write,

$$H_{12}(1-P_{12}) = B_0+B_j\mathbf{j}_1\cdot\mathbf{j}_2+B_t\mathbf{t}_1\cdot\mathbf{t}_2+B_{jt}(\mathbf{j}_1\cdot\mathbf{j}_2)(\mathbf{t}_1\cdot\mathbf{t}_2) \tag{14}$$

and then for the several cases $T_1 = 0, J_1 = 0, T_1 = \frac{1}{2}n, J_1 = nj, n = 1, B_{jt} = 0$ we have for the interaction energy and doublet splitting

$$\begin{aligned} E_J &= nB_0+\tfrac{1}{2}B_t\{T(T+1)-T_1(T_1+1)-\tfrac{3}{4}\} \\ &\quad +\tfrac{1}{2}\left[B_j+\frac{1}{2n}B_{jt}\{T(T+1)-T_1(T_1+1)-\tfrac{3}{4}\}\right][J(J+1)-J_1J_1+1)-\tfrac{3}{4}], \qquad (15) \\ \Delta &= \tfrac{1}{2}(2J_1+1)B_j, \end{aligned}$$

which then gives for the B^{11} doublet $\Delta = \frac{7}{2}B_j$.

The constants B are given in terms of the two-body jj energies $E_{TJ}(T = 0, 1; J = j\pm\frac{1}{2})$ by

$$(4j+2)\begin{pmatrix} B_0 \\ B_j \\ B_t \\ B_{jt} \end{pmatrix} = \begin{pmatrix} \frac{3}{2}(j+1) & \frac{3}{2}j & \frac{1}{2}(j+1) & \frac{1}{2}j \\ 3 & -3 & 1 & -1 \\ 2(j+1) & 2j & -2(j+1) & -2j \\ 4 & -4 & -4 & 4 \end{pmatrix}\begin{pmatrix} E_{1>} \\ E_{1<} \\ E_{0>} \\ E_{0<} \end{pmatrix}. \tag{16}$$

It is not necessary to assume here a central interaction since, unlike the LS case, every interaction is diagonal in the two-particle states. We can infer from this, since jj coupling is not a bad approximation for B^{10}, that our calculated B^{11} doublet splitting is likewise insensitive to the central-interaction assumption provided we express it in terms of the two-body jj energies. If we do have a central interaction given by eq. (5) the two sets of interaction constants of eqs. (5) and (14) are related by observing † that, if l, j are specified for a particle, a Landé argument gives

$$\mathbf{s} \equiv \frac{(\mathbf{s}\cdot\mathbf{j})\mathbf{j}}{j(j+1)} \equiv \frac{(-1)^{j-l-\frac{1}{2}}}{(2l+1)}\mathbf{j}. \tag{17}$$

† Or alternately from

$$E_{T,\,J=l}(j, s_{\frac{1}{2}}) = \tfrac{1}{2}(2l+1)^{-1}\{(2j+1)^{2T+1,1}L+(4l-2j+1)^{2T+1,3}L\},$$
$$E_{T,\,J\neq l}(j, s_{\frac{1}{2}}) = {}^{2T+1,3}L.$$

Then for two particles l_j and $s_{\frac{1}{2}}$, $(\mathbf{s}_1 \cdot \mathbf{s}_2) \equiv (2l+1)^{-1}(-1)^{j-l-\frac{1}{2}}(\mathbf{j}_1 \cdot \mathbf{j}_2)$ and thus we have †

$$\frac{B_j}{B_s} = \frac{B_{jt}}{B_{st}} = (2l+1)^{-1}(-1)^{j-l-\frac{1}{2}}, \tag{18}$$

while B_0, B_t have the same significance in the two forms. The equality of the two forms found for the B^{11} doublet splitting ($\Delta = \frac{7}{6}B_s = \frac{7}{2}B_j$) supplies an example of eq. (18).

Considering now the core-excitation corrections, and restricting ourselves to excitations inside the same configuration as the principal core state, we see that the first three terms of eq. (14) have no off-diagonal matrix elements at all and thus produce no first-order mixing of the core states. The fourth term of eq. (14) cannot admix two $T_1 = 0$ states. Thus, ignoring for the moment the single-particle s—d mixing, we conclude that the simple model of an s particle coupled to a $T_1 = 0$ core might be very good unless there is, not too far away, a $T'_1 = 1$, $J'_1 = J_1, J_1 \pm 1$ core state which may be admixed. In the case of the B^{11} doublet built on the B^{10} ground state there is no such state.

The doublet founded on the first excited B^{10} state ($T, J = 0, 1$) would be a quite different case since a (1, 0) state lies one MeV away. A more interesting quite analogous case would be the N^{15} doublet involving the N^{14} ground state where once again an excited $(T_1 J_1) = (1, 0)$ state can admix with the (0, 1) ground state. A simple calculation gives for the matrix element connecting the two states $\{s_{\frac{1}{2}} \times (p_{\frac{1}{2}})^2_{T=0,\, J=1}\}$ and $\{s_{\frac{1}{2}} \times (p_{\frac{1}{2}})^2_{T=1,\, J=0}\}$ the value $\frac{3}{8}B_{jt}$ and relating this to B_{st} by eq. (18) and using table 1 we have that our Gaussian interaction of either exchange nature would produce a value for $-\frac{1}{8}B_{st}$ of about 2 MeV. Since the two core states are only 2.4 MeV apart (which becomes 2.4 MeV$+ B_j - B_t$ when the s-particle interaction is added in) we obviously have the possibility of large admixtures and large distortion of the s-doublets splitting †† in N^{15}.

As far as the second type of admixing is concerned (the single particle s—d mixing), we guess that it is not usually important for the lower states. This is certainly demonstrated by the N^{15} calculations [8]) and also is consistent with the very small value (140 keV) found for the matrix element "measured" in the B^{11} experiment. A calculation of that matrix element, by the way, produces, with the Gaussian interaction the considerably larger value 800 keV for either exchange mixture. The reason for the disagreement is unclear but the fact that the measured matrix element is smaller reinforces the belief that s—d admixtures are in general small.

† For a coupled $p_{\frac{1}{2}}$ particle (l_j and $p_{\frac{1}{2}}$) the ratio is $-\frac{1}{3}(2l+1)^{-1}(-1)^{j-l-\frac{1}{2}}$.

†† Moreover it is very probably not reasonable to consider only the two $(p_{\frac{1}{2}})^2$ core states, as is shown by the elaborate calculations of Halbert [8]). A simple and reasonable treatment would use the *LS* form for the interaction and consider the first *three* core states, also however taking account of the effects due to the center-of-mass motion. The N^{15} example has been considered also by Unna and Talmi [7]) but using only the lowest *jj* configurations.

4. Hole-Particle s-Doublets

Doublets of this type occur in N^{16} (involving the first and third excited states) and as ground-state doublets in Al^{28} and P^{32}, the doublet splittings being respectively 270, −31, 77 keV. In each case there is strong evidence that the states are well described in jj coupling, the configurations being $\{j^{-1}\times s\}_{T=1}$ or $\{j\times s^{-1}\}_{T=1}$ with $j \equiv p_{\frac{1}{2}}$, $d_{\frac{5}{2}}$, and $d_{\frac{3}{2}}$ respectively. The N^{16} levels have been studied in detail by Elliott and Flowers [9]) using an explicit interaction and, among many other pieces of data, have been considered by Unna and Talmi [7]) in their determination of the $p_{\frac{1}{2}}$-$s_{\frac{1}{2}}$ interaction constants. The other doublets have been considered by Mayer and by Inglis as reported in Inglis' review article [6]).

As they stand our equations (15) do not apply in this case but on the other hand it is obvious, from the tensorial character of the separate terms, that if the particle-particle interaction is given by (14) with $n = 1$, then to within a mutiple of B_0, the hole-particle interaction is given by the same expression with the sign of B_{jt} changed †. Thus

$$\Delta(j^{\pm 1}\times s) = \tfrac{1}{2}(2j+1)(B_j \pm \tfrac{1}{4}B_{jt}). \tag{19}$$

The $\{p_{\frac{1}{2}}\times s_{\frac{1}{2}}\}$ doublet may be identified †† in the $A = 14$ nuclei and has $\Delta \approx -650$ keV. Comparing the $\{p_{\frac{1}{2}}\times s\}$ and $\{p_{\frac{1}{2}}^{-1}\times s\}$ doublets then shows that $B_{jt} < 0$ and $|B_{jt}| > 4B_j$; indeed taking both splittings seriously would give $B_j \approx -200$ keV, $B_{jt} \approx -1800$ keV. If instead we determine the constants from the four $\{p_{\frac{1}{2}}\times s_{\frac{1}{2}}\}$ energies [10]) we have $B_j \approx -280$ keV, $B_{jt} \approx -1400$ keV and, for N^{16}, $\Delta \approx +70$ keV. The constants which follow from the work of Unna and Talmi [7]) are $B_j = -270$ keV, $B_{jt} = -2060$ keV which fit both splittings quite well and should of course be regarded as the best values.

† Alternatively observe [6]) that the interaction which produces the splitting is simply the n−p interaction which is half the sum of the $T = 0$ and $T = 1$ interactions. Since then $\mathbf{t}_1 \cdot \mathbf{t}_2 \to -\frac{1}{4}$ we have from eq. (14) that

$$H_{12}(1-P_{12}) \to H_{12}^{n,p} = (B_0 - \tfrac{1}{4}B_t) + (B_j - \tfrac{1}{4}B_{jt})\mathbf{j}_1 \cdot \mathbf{j}_2;$$

this of course to be used without antisymmetrization between neutrons and protons. Eq. (19) now follows directly from this as do the more general equations for the interaction between an $s_{\frac{1}{2}}$ neutron and a $(j^m)_{J_1}$ proton core (the j-neutron subshell being filled), namely

$$E_J = m(B_0 - \tfrac{1}{4}B_t) + \tfrac{1}{2}(B_j - \tfrac{1}{4}B_{jt})[J(J+1) - J_1(J_1+1) - \tfrac{3}{4}],$$
$$\Delta = \tfrac{1}{2}(2J_1+1)(B_j - \tfrac{1}{4}B_{jt}).$$

Of course $\Delta[j(p)\times s_{\frac{1}{2}}(n)] = \Delta[j^{-1}(p)\times s_{\frac{1}{2}}(n)]$ (and it would be of interest to see whether P^{34} has the same ground-state doublet as P^{32}). If in the equations for E_J, we change the signs of B_t, B_{jt} we have the interaction of an $s_{\frac{1}{2}}$ neutron with an open *neutron* subshell, both proton subshells j, s being filled (or both empty). Finally the equations have obvious LS analogues.

†† We follow here the assignments made by Warburton and Pinkston [10]) which differ slightly from those used by Unna and Talmi [7]).

Our explicit interactions produce values for B_{jt} (see table 1 and eq. (18)) which have the correct sign but which are too large by a factor 3. They would produce an N^{16} splitting $\approx$ 1400 keV (Rosenfeld) or 640 keV (Inglis); these numbers would become 1000 keV and 500 keV with a Yukawa radial dependence. This appears to indicate that the shell model 1p—2s interaction has a weaker spin dependent n—p part than does the corresponding p^2 interaction. The same conclusion will come from the Al^{28} and P^{32} doublets.

The $B_s \approx 0$ value implied by the B^{11} doublet splitting would, if the interaction were central, imply that the N^{14} and $N^{16}\{p_{\frac{1}{2}}^{\pm 1} \times s_{\frac{1}{2}}\}$ splittings would be equal and opposite but it is hard to guess the significance of the deviation from this result which is observed. On the other hand if we knew the $\{p_{\frac{3}{2}}^{-1} \times s_{\frac{1}{2}}\}$ levels of N^{16} we might be able to decide (if the levels were not too broad) whether we have an effective *central* interaction; such an interaction would imply, via eq. (18),

$$\Delta(p_{\frac{3}{2}}^{-1} \times s_{\frac{1}{2}}) = -2\Delta(p_{\frac{1}{2}}^{-1} \times s_{\frac{1}{2}}), \tag{20}$$

and any major deviation not ascribable to interaction with nearby levels could be used to argue that the effective interaction has a non-central part.

The conventional interactions will give, for Al^{28} and P^{32}, doublet splittings of the correct sign but with far too large values. As discussed by Inglis [6]) the Majorana interaction, the dominant part of a conventional interaction, does not contribute to an n—p s-doublet † splitting but this is not sufficient to explain the smallness of the observed splittings. Formally, writing the interaction as $[A_W + A_B B_{12} + A_H H_{12} + A_M M_{12}]V(r_{12})$ where B, H, M are the exchange operators (and $H \equiv (-1)^{T+1}$), we find

$$\Delta = (-1)^{j-l-\frac{1}{2}} \frac{(2j+1)}{(2l+1)} \{A_B I_d - A_H I_e\}, \tag{21}$$

where I_d, I_e are the direct and exchange integrals for $V(r)$. The interaction of table 1 gives $I_d = -3.7$ MeV, $I_e = -0.85$ MeV if we maintain the same r_1 value (the single-particle radial function having the factor $\exp(-r^2/r_1^2)$) and then the calculated splittings, for Al^{28} and P^{32} respectively, are -1800, $+1200$ keV (Rosenfeld) or -900, $+600$ keV (Inglis). One actually expects that r_1 might decrease by 15 %, and there is evidence from the equivalent-particle spectra that the range of the effective interaction might increase by as much as 50 %, its strength at the same time decreasing. But these effects can scarcely change the splittings by as much as a factor two; in any case a large overall reduction in the radial integrals would be inconsistent with the $\{d_{\frac{3}{2}} \times s_{\frac{1}{2}}\}_{T=1}$ doublet †† splitting which is apparently [11]) larger than 1.2 MeV, and with the

† A descriptive alternative name for doublets, such as the hole-particle doublets with maximum isobaric spin, in which the splitting is due to the n—p interaction.

†† It would be worthwhile to locate the members of this doublet by the Si^{29}(d, p) experiment.

"absolute" n—p energies determined [12]) for the $\{d_{\frac{5}{2}} \times s_{\frac{1}{2}}\}$ nuclei to be about −1 MeV.

It seems then that the smallness of the n—p s-doublet splittings indicates a cancellation between the two terms of eq. (19) (or (21)) which is not given by the conventional interactions. Moreover if in eq. (21) we put $\Delta \approx 0$, $I_s/I_d = \frac{1}{4}$ and rewrite the equation in terms of the p^2 energies with $L/K = 6$ we find

$$(^{33}\mathrm{P} - {}^{11}\mathrm{P}) \approx 1.6\ (^{31}\mathrm{S} - {}^{13}\mathrm{S}) \approx 6\ \mathrm{MeV}. \tag{26}$$

This result is not compatible with binding-energy data in the p shell which demands $^{33}P \approx 0$ nor for that matter with the low-lying level structure of Li^8 which requires that the ^{11}P multiplet be at least 2—3 MeV above the ^{33}P.

One tends to conclude then that no central interaction compatible with the p-shell data will explain the smallness of the n—p splittings and that a different approach is required to explain them. Finally we note that a central interaction would give $\Delta(Al^{28}) = -\frac{3}{2}\Delta(P^{32})$ and this is satisfied in the sense that both splittings have an essentially zero value.

5. Final Remarks

Using very simple procedures we have looked into the information which certain s-doublet splittings give about the shell model interaction. It seems that B^{11} doublet splitting, which measures the average spin-dependent interaction between two nucleons (with a $(2T+1)$ weighting) is easily explainable by an interaction which also fits the many p-shell results. On the other hand the hole-particle splittings, which measure the spin-dependent n—p interaction, are too small to be thus explainable. Further information about levels of N^{16} (as well as † B^{12}) and Si^{30} would be helpful.

From the formal standpoint the reason why a simple technique has sufficed to evaluate the interaction energy is that, except for the double vector $\mathbf{s}_i \cdot \mathbf{t}_i$, the interaction operator is expressible in terms of simple vectors; this simplicity would be lost if the smaller of the two interacting j's were greater than $\frac{1}{2}$, for then of course tensor interactions of higher order would enter and the simple vector procedure would produce only sum rules for the energies; more important is the fact that a calculation would require more information about the core state. Note too that the interaction of a *group* of s particles with a core, as considered for example by Unna and Talmi [7]), can also be handled by the direct procedure.

One correction which has been ignored is that connected with the fact

† We expect, from eq. (18) that $\Delta(p_{\frac{3}{2}}^{-1} \times s_{\frac{1}{2}}) < 0$ and thus that the 1.67 MeV level in B^{12} (which is the first negative-parity level and has a large $l = 0$ reduced width to B^{11}) should be 2^-. Our further expectation that $\Delta(p_{\frac{3}{2}}^{-1} \times p_{\frac{1}{2}}) > 0$ is satisfied since the B^{12} ground-state spin is 1^+. (However, the B^{12} spectrum would not determine a value of this splitting satisfactory for use in eq. (20) because, as shown by the probable existence of more than two strong $l = 1$ transitions in $B^{11}(d, p)B^{12}$ jj coupling is not a sufficiently accurate approximation.) Observe too that the Y^{90} ground state doublet (apparently [13]) a $\{p_{\frac{1}{2}} \times d_{\frac{5}{2}}\}$ n—p doublet) has $\Delta > 0$ as we would expect. The level ordering of all the n—p doublets we have considered is in agreement with Nordheim's rules.

discussed by Elliott and Skyrme [14]), that the shell model functions for excited configurations may contain a part in which the centre of mass of the system has an orbital angular momentum. The way which they suggest to eliminate this difficulty, and which has been used on a few occasions, is to consider the entire function space of the states which are degenerate in the harmonic oscillator sense and to use the subspace of this in which the centre of mass is in an S state. It is physically not clear that this is always the most reasonable procedure [15]); for example if there is a strong spin-orbit coupling † it may be more economical of energy to bring the center of mass to rest by admixing in low states of an even more highly excited configuration. Besides this the procedure is opposed in spirit to the weak coupling model; it is clear that, when we have a particle weakly coupled to a core which is hard to excite, it should not be necessary to reconstruct the core function using a different set of basic states than are used when the particle is not present. It is possible in fact to consider a model in which the added particle is described with respect to the centre of mass of the core (instead of the entire system) and in which the summed interactions of the added particle with the core particles provided a one-body potential for the added particle. This is not quite the same as the conventional shell model but it seems easy in this case to treat the centre of mass problem and it is obvious that the formal procedures used above for handling the spin and isobaric spin dependence of the interaction can be used without change. It seems improbable then that the conclusions which we have drawn about the nature of the interaction will be modified by a reasonable treatment of the centre of mass effects though a closer study would seem to be desirable.

The authors are grateful to Dr. Elizabeth Baranger for discussions concerning the s-particle levels in the p shell region, to Dr. D. R. Inglis for comments about the n—p doublets and to Mr. C. H. Kim for checking some of the results.

Notes added in proof: (1) Professor D. H. Wilkinson, in a private communication, suggests that the 8.93 MeV level has negative parity, this result following from an analysis of a low-energy (d, p) experiment. If this be so the off-diagonal matrix element of eq. (3) should be ignored as well as the repulsive effect between the two levels shown in fig. 1, the s-doublet splitting of eq. (3) becoming then −90 keV. However, all the arguments and conclusions about the interaction would be unchanged.

(2) The n—p s-doublet splitting in certain heavier nuclei has recently been calculated by F. C. Barker (private communication and Nuclear Physics, in press), using an interaction (given by Elliott and Flowers [9])) which has a weakly spin-dependent n—p part. These calculations, which give small splittings

† Or if, for some other reason, the spacing between single-particle levels is less than that corresponding to their harmonic oscillator excitation.

in apparent agreement with experiment, reinforce the conclusion that the n—p interaction between inequivalent nucleons is indeed weakly spin-dependent, at least if one of the nucleons is in an s-orbit. The interaction used would, hwever, not fit the p^4 spectrum of Li^8.

References

1) O. M. Bilaniuk and J. C Hensel, Bull. Am. Phys. Soc. **3** (1958) 188
2) F. Ajzenberg-Selove and T. Lauritsen, Nuclear Physics **11** (1959) 1
3) A. M. Lane, unpublished manuscript (1955)
4) M. H. Macfarlane and J. B. French, University of Rochester N.Y.O. Report 2846, unpublished (1959)
5) L. Rosenfeld, Nuclear Forces (North-Holland Publishing Company, Amsterdam, 1948)
6) D. R. Inglis, Revs. Mod. Phys. **25** (1953) 390
7) I. Unna and I. Talmi, Phys. Rev. **112** (1958) 452
8) E. C. Halbert and J. B. French, Phys. Rev. **105** (1957) 1563
9) J. P. Elliott and B. H. Flowers, Proc. Roy. Soc. A **242** (1957) 57
10) E. K. Warburton and W. T. Pinkston, Princeton University N.Y.O. Report 2823, unpublished (1959)
11) P. M. Endt and C. M. Braams, Revs. Mod. Phys. **29** (1957) 683
12) S. Goldstein and I. Talmi, Phys. Rev. **105** (1957) 995
13) Bartholomew, Campion, Knowles and Manning, Nuclear Physics **10** (1959) 590
14) J. P. Elliott and T. H. R. Skyrme, Proc. Roy. Soc. A **232** (1955) 231
15) H. J. Lipkin, Phys. Rev. **110** (1958) 1395

2.F

Nuclear Physics **17** (1960) 448—467; © *North-Holland Publishing Co., Amsterdam*

Not to be reproduced by photoprint or microfilm without written permission from the publisher

L'ÉJECTION PAR INTERACTION DIRECTE DANS LA RÉACTION $Be^9(n, 2n)Be^8$

ROGER BALIAN et VINCENT P. GILLET

Centre d'Etudes Nucléaires de Saclay, Gif-sur Yvette (S & O)

Reçu le 8 février 1960

Abstract: Methods of direct interaction are applied to the study of ejection reactions, which end into a 3 particle channel. General expressions for cross sections are given. Application is made to the reaction $Be^9(n, 2n)Be^8$ up to 14 MeV, for which the contribution of the ejection process must be important, due to the low binding energy of the last nucleon of Be^9. Energies of 0.5 and 5 MeV for outgoing neutrons are found to be favoured. Contributions of various regions of interaction are separately analysed, and the reaction is found to take place mainly outside the core of Be^9. The cross section, calculated through ejection mechanism, together with compound nucleus results for low energy, agrees well with experimental data. If a break-up process is considered instead of the compound one, the agreement is less satisfactory.

1. Introduction

Les caractéristiques de la contribution du mécanisme d'interaction directe aux réactions nucléaires du type (p, 2p) et (n, 2n) d'une part, et du type (p, d) et (n, d) d'autre part, diffèrent sensiblement en raison de la composition de l'état final. Pour une réaction de pick-up, l'état final est en effet complètement caractérisé par l'énergie du noyau résiduel, par son impulsion de recul et par l'impulsion du deuteron émergent. La voie de sortie est donc une voie à deux fragments, et des modèles simples [1–3]) expliquent, de façon satisfaisante, les distributions angulaires et les ordres de grandeur des sections efficaces observées. Par contre, lorsque les deux nucléons de l'état final sont identiques, un paramètre supplémentaire devient nécessaire pour définir cet état. Il faut tenir compte de l'impulsion relative des deux nucléons émergents: la voie de sortie est en effet une voie à trois fragments †.

Si les particules de l'état final sont un neutron et un proton, il est également permis de penser qu'une partie de la réaction ouvre sur une voie à trois fragments. Nous dirons que la transition s'est effectuée par éjection pour distinguer ce mécanisme du pick-up. Le mécanisme d'éjection dans le cas considéré est d'autant plus compétitif avec le pick-up que l'énergie disponible pour la réaction est plus élevée.

† Si les deux particules finales sont deux neutrons, on ne doit pas envisager la possibilité d'une voie de sortie à deux fragments, comprenant le noyau résiduel et un di-neutron. Le temps de vie du di-neutron, noyau hypothétique instable constitué de deux neutrons, est en effet de l'ordre de grandeur du temps de traversée du potentiel nucléonique par le neutron incident.

L'éjection, qui est un mécanisme d'interaction directe, doit surtout être importante en dehors de la région des résonances. Les transitions vers une voie à trois fragments peuvent également mettre en jeu, à des énergies modérées, des mécanismes du type break-up [4]) et, à des énergies plus faibles, des mécanismes de noyau composé.

La probabilité de décomposition d'un noyau composé en trois fragments est très faible. Mais une transition faisant intervenir deux noyaux composés successifs, émettant chacun un nucléon, peut donner une contribution importante [5]) pour des énergies assez basses.

Les diverses possibilités de partage de l'énergie disponible entre les trois fragments de l'état final donnent lieu à la mesure d'une section efficace différentielle en angle et en énergie:

$$\frac{d\sigma(E, E_1)}{d\omega_1 d\omega_2 dE_1}$$

C'est le flux des fragments sortants 1 et 2 (supposés distincts) dans les angles solides $d\omega_1$ et $d\omega_2$ respectivement, pour une énergie de la particule 1 comprise entre E_1 et E_1+dE_1, ce flux étant rapporté à un courant unité du nucléon incident (d'énergie E). Cette définition s'étend aisément au cas où les fragments sortants 1 et 2 sont indiscernables.

Dans la sect. 2 nous donnons une expression formelle de la contribution des voies à trois fragments à l'amplitude de transition, ainsi que les expressions explicites au premier ordre des sections efficaces pour le mécanisme d'éjection, dans le cadre du modèle des couches pour le noyau et en décrivant les états individuels de diffusion par des ondes déformées par un puits complexe.

Nous étudions dans la sect. 3 l'exemple de la réaction $Be^9(n, 2n)$. La structure particulière du noyau de béryllium, due à la très faible énergie de liaison de son dernier nucléon, permet a priori de penser que le mécanisme d'éjection joue un rôle important dans cette transition, pour des énergies suffisantes. Après avoir rappelé la situation expérimentale actuelle et les résultats de la théorie du noyau composé et de la théorie du break-up, nous donnons les résultats du modèle précédent, pour des énergies du neutron incident inférieures à 15 MeV.

2. Formalisme Général

2.1. FORMES ASYMPTOTIQUES DES ÉTATS STATIONNAIRES DE COLLISION POUR LES VOIES À TROIS FRAGMENTS

Nous considérons les transitions entre une voie α à deux fragments et les voies β à trois fragments, pour un système d'énergie E régi par l'Hamiltonien $\mathscr{H}$. Les voies à deux fragments autres que la voie α sont désignées par γ.

Une particule incidente, d'impulsion relative $\hbar\mathbf{k}_\alpha$ par rapport au noyau cible, donne un état stationnaire de collision initié dans la voie α, représenté par la fonction propre $\Psi^{(+)}(\alpha, \mathbf{k}_\alpha)$ de l'opérateur $\mathscr{H}-E$, dont les formes asymptotiques

dans les voies α, β et γ sont respectivement les suivantes:

$$\Psi^{(\pm)}(\alpha, \mathbf{k}_\alpha) \sim \begin{cases} \varphi_\alpha \left\{ e^{i\mathbf{k}_\alpha \cdot \mathbf{r}_\alpha} + f_{\alpha\alpha}^{(\pm)}(\hat{\mathbf{r}}_\alpha) \dfrac{e^{\pm i k_\alpha r_\alpha}}{r_\alpha} \right\} & \text{pour } r_\alpha \to \infty, \quad (1.a) \\ \varphi_\beta \left\{ \displaystyle\int dk'_{\beta_1} f_{\alpha\beta}^{(\pm)}(\hat{\mathbf{r}}_{\beta_1}, \hat{\mathbf{r}}_{\beta_2}, k'_{\beta_1}) \frac{e^{\pm i(k'_{\beta_1} r_{\beta_1} + k'_{\beta_2} r_{\beta_2})}}{r_{\beta_1} r_{\beta_2}} \right\} & \text{pour } r_{\beta_1} \to \infty \text{ et } r_{\beta_2} \to \infty, \quad (1.b) \\ \varphi_\gamma \left\{ f_{\alpha\gamma}^{(\pm)}(\hat{\mathbf{r}}_\gamma) \dfrac{e^{\pm i k_\gamma r_\gamma}}{r_\gamma} \right\} & \text{pour } r_\gamma \to \infty. \quad (1.c) \end{cases}$$

Dans ces expressions (où on a donné également la forme de $\Psi^{(-)}$, état stationnaire avec ondes entrantes) φ_α, φ_β, φ_γ représentent les fonctions d'onde internes normalisées des fragments; $\mathbf{r}_\alpha$, $\hbar\mathbf{k}_\alpha$ et $\mathbf{r}_\gamma$, $\hbar\mathbf{k}_\gamma$ sont les coordonnées relatives et les impulsions des fragments dans les voies α et γ; de même, $\mathbf{r}_{\beta_1}$, $\hbar\mathbf{k}'_{\beta_1}$ et $\mathbf{r}_{\beta_2}$, $\hbar\mathbf{k}'_{\beta_2}$ sont les coordonnées relatives et les impulsions de deux des fragments par rapport au troisième. On suppose la masse de celui-ci assez grande par rapport aux masses m_{β_1} et m_{β_2} des deux autres pour négliger son recul. Avec cette hypothèse, l'énergie cinétique dans une voie β est

$$T_\beta = \tfrac{1}{2}\hbar^2 \left(\frac{k'^2_{\beta_1}}{m_{\beta_1}} + \frac{k'^2_{\beta_2}}{m_{\beta_2}} \right).$$

L'intégrale de l'expression (1b) exprime les diverses possibilités de partage de l'énergie entre les fragments 1 et 2; si ε_β est l'énergie du noyau résiduel, k'_{β_2} doit être liée à la variable d'intégration k'_{β_1} par la condition de conservation de l'énergie

$$T_\beta = E - \varepsilon_\beta.$$

Dans l'expression (1b), l'amplitude de transition $f_{\alpha\beta}^{(\pm)}(\hat{\mathbf{r}}_{\beta_1}, \hat{\mathbf{r}}_{\beta_2}, k'_{\beta_1})$ est une fonction de la direction des deux fragments émergents et de l'énergie cinétique emportée par chacun d'eux.

Pour un état stationnaire de collision dont la voie d'entrée est une voie β à trois fragments, les formes asymptotiques des fonctions propres $\Psi^{(\pm)}(\beta, \mathbf{k}_{\beta_1}, \mathbf{k}_{\beta_2})$ de l'Hamiltonien précédent $\mathscr{H}$ pour la même énergie E et pour des valeurs déterminées de $\mathbf{k}_{\beta_1}$ (et $\mathbf{k}_{\beta_2}$) sont respectivement les suivantes dans les voies α (ou γ) et β:

$$\Psi^{(\pm)}(\beta, \mathbf{k}_{\beta_1}, \mathbf{k}_{\beta_2}) \sim \varphi_\alpha \left\{ f_{\beta\alpha}^{(\pm)}(\hat{\mathbf{r}}_\alpha) \frac{e^{\pm i k_\alpha r_\alpha}}{r_\alpha} \right\} \qquad \text{pour } r_\alpha \to \infty, \quad (2.a)$$

$$\Psi^{(\pm)}(\beta, \mathbf{k}_{\beta_1}, \mathbf{k}_{\beta_2}) \sim \varphi_\beta \left\{ e^{i(\mathbf{k}_{\beta_1} \cdot \mathbf{r}_{\beta_1} + \mathbf{k}_{\beta_2} \cdot \mathbf{r}_{\beta_2})} + \int dk'_{\beta_1} f_{\beta\beta}^{(\pm)}(\hat{\mathbf{r}}_{\beta_1}, \hat{\mathbf{r}}_{\beta_2}, k'_{\beta_1}) \frac{e^{\pm i(k'_{\beta_1} r_{\beta_1} + k'_{\beta_2} r_{\beta_2})}}{r_{\beta_1} r_{\beta_2}} \right.$$

$$\left. + g_{\beta\beta}^{(\pm)} e^{i\mathbf{k}_{\beta_1} \cdot \mathbf{r}_{\beta_1}} \frac{e^{\pm i k_{\beta_2} r_{\beta_2}}}{r_{\beta_2}} + h_{\beta\beta}^{(\pm)} e^{i\mathbf{k}_{\beta_2} \cdot \mathbf{r}_{\beta_2}} \frac{e^{\pm i k_{\beta_1} r_{\beta_1}}}{r_{\beta_1}} \right\}$$

$$\text{pour } r_{\beta_1} \to \infty \text{ et } r_{\beta_2} \to \infty. \quad (2.b)$$

2.2. EXPRESSION DE L'AMPLITUDE DE TRANSITION

Si $\mathscr{V}$ représente une partie de $\mathscr{H}$ responsable de la transition $\alpha \to \beta$, on définit les fonctions propres $\tilde{\Psi}^{(\pm)}$ de l'Hamiltonien réduit $H = \mathscr{H} - \mathscr{V}$ pour l'énergie précédente E, ayant des comportements asymptotiques analogues à ceux des expressions (1) et (2).

En appliquant la formule de Green à l'identité

$$\langle \Psi^{(-)}(\beta, \mathbf{k}_{\beta_1}, \mathbf{k}_{\beta_2}) | \mathscr{V} | \tilde{\Psi}^{(+)}(\alpha, \mathbf{k}_\alpha) \rangle = \langle \Psi^{(-)}(\beta, \mathbf{k}_{\beta_1}, \mathbf{k}_{\beta_2}) | \mathscr{H} - \mathscr{H}^* | \tilde{\Psi}^{(+)}(\alpha, \mathbf{k}_\alpha) \rangle,$$

on obtient pour les voies à trois fragments l'analogue d'une relation bien connue dans le cas des voies à deux fragments [2, 6]):

$$\langle \Psi^{(-)}(\beta, \mathbf{k}_{\beta_1}, \mathbf{k}_{\beta_2}) | \mathscr{V} | \tilde{\Psi}^{(+)}(\alpha, \mathbf{k}_\alpha) \rangle = \frac{2\pi\hbar^2}{m_\alpha} f_{\beta\alpha}^{(-)*}(\hat{\mathbf{k}}_\alpha) - i \frac{16\pi^3\hbar^2}{m k_{\beta_1}} \bar{f}_{\alpha\beta}^{(+)}(\hat{\mathbf{k}}_{\beta_1}, \hat{\mathbf{k}}_{\beta_2}, k_{\beta_1}), \tag{3}$$

où

$$m = m_{\beta_1} = m_{\beta_2}.$$

En faisant $\mathscr{V} = 0$ dans la formule (3), on obtient la relation de réciprocité

$$i \frac{8\pi^2}{m k_{\beta_1}} f_{\alpha\beta}^{(+)}(\hat{\mathbf{k}}_{\beta_1}, \hat{\mathbf{k}}_{\beta_2}, k_{\beta_1}) = \frac{1}{m_\alpha} f_{\beta\alpha}^{(-)}(\hat{\mathbf{k}}_\alpha). \tag{4}$$

Le terme en $\bar{f}_{\alpha\beta}^{(+)}(\hat{\mathbf{k}}_{\beta_1}, \hat{\mathbf{k}}_{\beta_2}, k_{\beta_1})$ dans l'expression (3) représente les transitions $\alpha \to \beta$ induites par l'Hamiltonien réduit H. Si $\mathscr{V}$ est choisi de façon à représenter l'interaction du nucléon incident avec le nucléon éjecté, $\bar{f}_{\alpha\beta}^{(+)}(\hat{\mathbf{k}}_{\beta_1}, \hat{\mathbf{k}}_{\beta_2}, k_{\beta_1})$ contient en particulier la contribution à la transition $\alpha \to \beta$ du mécanisme par formation d'un noyau composé. Les largeurs pour l'émission simultanée de deux particules par un noyau composé sont très faibles. Il peut exister néanmoins à basse énergie un mécanisme mettant en jeu deux noyaux composés successifs et ne faisant intervenir que des voies à deux fragments. Si N représente le noyau initial, on a le schéma

$$(\mathrm{N}+\mathrm{n})+\mathrm{n} \to (\mathrm{N}+2\mathrm{n})^* \to (\mathrm{N}+\mathrm{n})^*+\mathrm{n} \to \mathrm{N}+2\mathrm{n}.$$

La contribution de ce mécanisme peut être importante pour des valeurs de k_{β_1} et k_{β_2} correspondant respectivement aux énergies de résonance des réactions ci-dessus. Si un mécanisme de ce type n'existe pas ou si la réaction a lieu à énergie suffisamment élevée (en dehors de la région des résonances séparées) on est en droit de faire l'approximation

$$\bar{f}_{\alpha\beta}^{(+)}(\hat{\mathbf{k}}_{\beta_1}, \hat{\mathbf{k}}_{\beta_2}, k_{\beta_1}) \approx 0. \tag{5}$$

2.3. DÉFINITION ET EXPRESSION GÉNÉRALE DE LA SECTION EFFICACE DIFFÉRENTIELLE EN ANGLE ET EN ÉNERGIE

Nous supposons, pour commencer, que les deux fragments émergents 1 et 2 de la voie de sortie β sont discernables. On mesure le flux des fragments de type

2 par exemple, dans l'angle solide $d\hat{\mathbf{k}}_{\beta_2}$ autour de la direction $\hat{\mathbf{k}}_{\beta_2}$, le reste du système étant dans un état quantique bien déterminé: entre autres, les fragments du type 1 ont leur impulsion comprise entre k_{β_1} et $k_{\beta_1}+dk_{\beta_1}$, dans l'angle solide $d\hat{\mathbf{k}}_{\beta_1}$ autour de la direction $\hat{\mathbf{k}}_{\beta_1}$. Soit $P(\mathbf{k}_{\beta_1}, \beta)dk_{\beta_1}$ le projecteur sur cet état et $J(\mathbf{r}_{\beta_2})$ l'opérateur courant radial pour les fragments 2 au point $\mathbf{r}_{\beta_2}$ où a lieu la mesure. Pour un courant incident donné I_α dans la voie α ($I_\alpha = \hbar k_\alpha/m_\alpha$), la section efficace différentielle est la valeur moyenne de $(P(\mathbf{k}_{\beta_1}, \beta)J(\mathbf{r}_{\beta_2})k_{\beta_2}^2)/I_\alpha$ sur la forme asymptotique (1.b) dans la voie β, de l'état stationnaire de collision $\Psi^{(+)}(\alpha, \mathbf{k}_\alpha)$. On obtient après simplification

$$\frac{d\sigma(\alpha, \mathbf{k}_\alpha \to \beta, \mathbf{k}_{\beta_1}, \mathbf{k}_{\beta_2})}{d\hat{\mathbf{k}}_{\beta_1} d\hat{\mathbf{k}}_{\beta_2} dk_{\beta_1}} = \pi \frac{m_\alpha}{k_\alpha} \frac{k_{\beta_2}}{m_{\beta_2}} |f_{\alpha\beta}^{(+)}(\hat{\mathbf{k}}_{\beta_1}, \hat{\mathbf{k}}_{\beta_2}, k_{\beta_1})|^2. \tag{6}$$

Si les fragments 1 et 2 sont indiscernables, il faut multiplier l'expression de droite par un facteur 2. Le compteur détecte en effet indifféremment les fragments 1 ou 2 dans l'angle solide $d\hat{\mathbf{k}}_{\beta_2}$, les fragments 2 ou 1 étant respectivement dans l'état $\mathbf{k}_{\beta_1}$. L'expression (1.b) est alors antisymétrique dans l'échange des deux coordonnées, ce qui s'exprime par

$$\frac{f_{\alpha\beta}^{(\pm)}(\hat{\mathbf{r}}_{\beta_1}, \hat{\mathbf{r}}_{\beta_2}, k_{\beta_1})}{k_{\beta_1}} = (-)^\sigma \frac{f_{\alpha\beta}^{(\pm)}(\hat{\mathbf{r}}_{\beta_2}, \hat{\mathbf{r}}_{\beta_1}, k_{\beta_1})}{k_{\beta_2}},$$

où σ est le spin total des deux particules sortantes.

En utilisant la relation fondamentale (3) et la relation de réciprocité (4) et avec l'approximation (5), la section efficace différentielle en angle et en énergie (E_1 étant l'énergie cinétique du fragment 1) s'exprime maintenant en fonction de l'interaction $\mathscr{V}$ (pour des fragments indiscernables) par

$$\frac{d\sigma(\alpha, \mathbf{k}_\alpha \to \beta_1, \mathbf{k}_{\beta_1}, \mathbf{k}_{\beta_2})}{d\hat{\mathbf{k}}_{\beta_1} d\hat{\mathbf{k}}_{\beta_2} dE_1} = \frac{k k_{\beta_1} k_{\beta_2} m^2}{8(2\pi)^5 \hbar^4 E} |\langle \Psi^{(-)}(\beta_1 \mathbf{k}_{\beta_1} \mathbf{k}_{\beta_2}) | \mathscr{V} | \tilde{\Psi}^{(+)}(\alpha, \mathbf{k}_\alpha) \rangle|^2. \tag{7.a}$$

Cette section efficace caractérise à la fois la corrélation angulaire des nucléons émis, et leur spectre d'énergie. On peut, en intégrant sur les angles, définir une section efficace différentielle en l'énergie de l'une des particules

$$\frac{d\sigma(\alpha, \mathbf{k}_\alpha \to \beta, k_\beta, k_{\beta_2})}{dE_1} = \int d\hat{\mathbf{k}}_{\beta_1} d\hat{\mathbf{k}}_{\beta_2} \frac{d\sigma(\alpha, \mathbf{k}_\alpha \to \beta, \mathbf{k}_{\beta_1} \mathbf{k}_{\beta_2})}{d\hat{\mathbf{k}}_{\beta_1} d\hat{\mathbf{k}}_{\beta_2} dE_1}. \tag{7.b}$$

Si E_F est l'énergie disponible dans l'état final, la section efficace totale vers la voie β est enfin égale à

$$\sigma(\alpha \mathbf{k}_\alpha \to \beta) = \int_0^\varepsilon dE_1 \frac{d\sigma}{dE_1}, \tag{7.c}$$

où $\varepsilon = \frac{1}{2}E_F$ si les fragments émergents sont indiscernables et $\varepsilon = E_F$ dans l'autre cas.

Lorsque (5) est vérifiée, l'expression (7.a) est exacte.

Pour calculer effectivement les expressions (7) on prend pour valeur approchée de la fonction propre inconnue Ψ une solution Ψ de H obtenue à l'aide de modèles particuliers. Les expressions (7) correspondent alors au premier ordre de la théorie des perturbations indépendante du temps dans le cadre de ces modèles.

2.4. EXPRESSIONS DES FONCTIONS D'ONDE

Pour le calcul explicite des sections efficaces d'éjection nous faisons appel aux approximations usuelles des ondes déformées par un puits complexe pour la description des états de diffusion, et du modèle des couches pour les états nucléaires [7]).

Dans ces conditions, si l'état du noyau initial (A nucléons) ne diffère de l'état du noyau final ($A-1$ nucléons) que par l'occupation d'un état individuel de particule, les autres états individuels occupés restant les mêmes †, l'élément de matrice dans (7.a) se simplifie: il suffit de prendre l'opérateur $\mathscr{V}$ entre les produits (antisymétrisés) des fonctions d'onde individuelles du projectile et de la particule éjectée dans l'état initial et dans l'état final.

Comme modèle du noyau initial, nous considérons le cas simple d'un cœur de spin $I = 0$, plus un nucléon de coordonnée spatiale $\mathbf{x}$ et de moment angulaire total $\mathbf{j} = \mathbf{l}+\mathbf{s}$. La fonction d'onde du nucléon lié en couplage spin-orbite s'écrit ††

$$|\psi_{lj}(x);\ lsjm^j\rangle = \sum_{m^l m^s} \langle lsm^l m^s|jm^j\rangle |lm^l\rangle |sm^s\rangle \psi_{lj}(x);$$

$|sm^s\rangle$ est l'état de spin et $|lm^l\rangle$ la partie angulaire de la fonction d'onde.

On pose

$$\Psi_{lj}(x) = \frac{\chi_{lj}(x)}{x}$$

La fonction radiale $\chi_{lj}(x)$ est solution de

$$-\frac{\hbar^2}{2m}\left\{\frac{\mathrm{d}^2}{\mathrm{d}x^2} - \frac{l(l+1)}{x^2}\right\}\chi_{lj} + \left\{\bar{V}(x) + \frac{\lambda\hbar^2}{4m^2C^2}\,\frac{1}{x}\,\frac{\mathrm{d}}{\mathrm{d}x}\bar{V}(x)\mathbf{l}\cdot\mathbf{s} - \varepsilon\right\}\chi_{lj} = 0. \quad (8)$$

Les paramètres du potentiel nucléaire moyen réel $\bar{V}(x)$, du type de Saxon [22]) par exemple, sont adaptés pour rendre compte de l'énergie de liaison effectivement observée ε ($\varepsilon < 0$). Nous avons introduit un couplage spin-orbite du type Thomas-Fermi, le paramètre λ étant adapté pour rendre compte de l'espacement expérimental des niveaux de même l. Pour un proton, on devrait ajouter un terme d'interaction coulombienne. La fonction $\chi_{lj}(x)$ satisfait de plus aux

† C'est le cas par exemple pour un noyau constitué d'une couche complète plus un nucléon.

†† Pour les définitions et les notations adoptées pour les divers coefficients géométriques de couplage, voir les références [8]) ou [9]).

conditions suivantes

$$\chi_{lJ}(0) = 0, \tag{9.a}$$

$$\chi_{lJ}(x) \sim e^{-\sqrt{\frac{2\varepsilon}{m}}x} \quad \text{pour } x \to \infty \tag{9.b}$$

$$\int_0^\infty |\chi_{lJ}(x)|^2 dx = 1. \tag{9.c}$$

Le nucléon incident a pour coordonnée spatiale $\mathbf{r}$, pour impulsion $\hbar\mathbf{k}$, et, en couplage spin-orbite, pour moment angulaire total $\mathbf{J} = \mathbf{L}+\mathbf{S}$. Pour les deux nucléons émergents on a de même $\mathbf{r}_1$ et $\mathbf{r}_2$, $\hbar\mathbf{k}_1$ et $\hbar\mathbf{k}_2$, $\mathbf{J}_1 = \mathbf{L}_1+\mathbf{S}_1$ et $\mathbf{J}_2 = \mathbf{L}_2+\mathbf{S}_2$. Le flux incident polarisé (M^S fixé) est décrit par une fonction d'onde de la forme

$$|\Phi^{(+)}(kr), M^S\rangle = \sum_{L,J} f(LS, JM^J)|LS, JM^J\rangle$$

La fonction $f(LS, JM^J)$ est déterminée par la condition de raccordement à l'infini avec le développement en ondes partielles de l'onde plane polarisée, ce qui donne

$$|\Phi^{(+)}(kr), M^S\rangle = 4\pi \sum i^L Y_L^{M^L *}(\hat{\mathbf{k}})\langle LSM^L M^S|JM^J\rangle\langle LSM^{L'} M^{S'}|JM^J\rangle \\ |LM^{L'}\rangle|SM^{S'}\rangle\Phi_{LJ}^{(+)}(kr),$$

où la sommation porte sur L, J, M^L, M^J, $M^{L'}$ et $M^{S'}$. On pose

$$\Phi_{LJ}^{(+)}(kr) = \frac{\varphi_{LJ}^{(+)}(kr)}{kr}.$$

La fonction radiale $\varphi_{LJ}^{(+)}(kr)$ est solution en couplage spin-orbite d'une équation du type (8), où $\varepsilon = \frac{1}{2}\hbar^2k^2/m$ ($\varepsilon > 0$), et où $\bar{V}(r)$ est maintenant complexe pour rendre compte des transitions hors de la voie d'entrée, ses paramètres étant déterminés par les expériences de diffusion élastique instantanée sur un noyau de A nucléons. La fonction radiale satisfait en outre aux conditions

$$\varphi_{LJ}^{(+)}(0) = 0 \tag{10.a}$$

$$\varphi_{LJ}^{(+)}(kr) \sim e^{i\delta_L}\sin(kr - \tfrac{1}{2}\pi L + \delta_L) \qquad \text{pour } kr \to \infty. \tag{10.b}$$

Pour les états de diffusion des nucléons émergents, les expressions utilisées sont analogues, les paramètres du puits complexe $\bar{V}$ étant maintenant adaptés pour rendre compte des expériences de diffusion élastique instantanée sur un noyau de $A-1$ nucléons, et les énergies positives ε_1 et ε_2 étant respectivement égales à $\frac{1}{2}\hbar^2k_1^2/m$ et $\frac{1}{2}\hbar^2k_2^2/m$. De plus, nous devons changer le signe de la partie imaginaire de $\bar{V}$, car nous nous intéressons, pour les nucléons émergents, à des solutions du type $\varphi^{(-)}$, équation (7.a), qui se déduisent de $\varphi^{(+)}$ par renverse-

ment du temps. Les $\varphi^{(-)}$ satisfaisant à l'équation conjuguée de (8) et aux conditions aux limites conjuguées de (10) sont les complexes conjugués de $\varphi^{(+)}$ et forment avec eux un système biorthogonal

$$\varphi_{LJ}^{(-)}(kr) = \varphi_{LJ}^{(+)*}(kr), \tag{12.a}$$

$$\int_0^\infty \mathrm{d}r\varphi_{LJ}^{(+)}(kr)\varphi_{LJ}^{(+)}(k'r) = 0 \quad \text{si } k \neq k'. \tag{12.b}$$

2.5. EXPRESSION DES SECTIONS EFFICACES

Nous donnons d'abord l'expression de l'amplitude de transition entrant dans la formule (7.a) pour les flux incidents et émergents polarisés (M^S, $M_1{}^S$ et $M_2{}^S$ fixés), dans le cas général d'une interaction $\mathscr{V}$ conservant le spin total $\mathbf{s}+\mathbf{S} = \mathbf{S}_1+\mathbf{S}_2$. Pour mettre en évidence les invariants de la transition, les fonctions des voies initiale et finale $|\tilde{\Psi}_{\text{in}}^{(+)}\rangle$ et $\langle\tilde{\Psi}_{\text{fin}}^{(-)}|$ sont exprimées dans la représentation du moment orbital de la voie $\boldsymbol{\lambda}$, du moment total de la voie $\boldsymbol{\nu}$ et du spin total de la voie $\boldsymbol{\sigma}$. La conservation de $\boldsymbol{\sigma}$ impose les règles de sélection

$$\mathbf{l}+\mathbf{L} = \mathbf{L}_1+\mathbf{L}_2 = \boldsymbol{\lambda}, \qquad \mathbf{j}+\mathbf{J} = \mathbf{J}_1+\mathbf{J}_2 = \boldsymbol{\nu}, \qquad \boldsymbol{\lambda}-\boldsymbol{\nu} = \boldsymbol{\sigma},$$

et l'amplitude de transition prend la forme

$$\begin{aligned}
&\langle\tilde{\Psi}^{(-)}(M_1{}^S M_2{}^S, \mathbf{k}_1\mathbf{k}_2)|\mathscr{V}|\tilde{\Psi}^{(+)}(m_j M^S, \mathbf{k})\rangle \\
&= (4\pi)^2 \sum i^{L-L_1-L_2}\{(2l+1)(2L+1)(2L_1+1)(2L_2+1)(2j+1)(2J_1+1)(2J_2+1)\}^{\frac{1}{2}}(2\sigma+1) \\
&Y_L^{M^L*}(\hat{\mathbf{k}})Y_{L_1}^{M_1{}^L}(\hat{\mathbf{k}}_1)Y_{L_2}^{M_2{}^L}(\hat{\mathbf{k}}_2)\langle lL00|\lambda 0\rangle\langle LSM^L M^S|JM^J\rangle \qquad (13) \\
&\langle L_1 S_1 M_1{}^L M^S|J_1 M_1{}^J\rangle\langle L_2 S_2 M_2{}^L M_2{}^S|J_2 M_2{}^J\rangle\langle jJ-m^j-M^J|\nu M^\nu\rangle\langle J_1 J_2-M_1{}^J-M_2{}^J|\nu M^\nu\rangle \\
&\begin{Bmatrix} l & j & s \\ L & J & S \\ \lambda & \nu & \sigma \end{Bmatrix}\begin{Bmatrix} L_1 & J_1 & S_1 \\ L_2 & J_2 & S_2 \\ \lambda & \nu & \sigma \end{Bmatrix}\langle\Phi_{L_1 J_1}^{(-)}(k_1 r)\Phi_{L_2 J_2}^{(-)}(k_2 x)|\mathscr{V}(|\mathbf{r}-\mathbf{x}|)|\Phi_{LJ}^{(+)}(kr)\Psi_{ij}(x)\rangle.
\end{aligned}$$

Comme l'interaction résiduelle $\mathscr{V}(|\mathbf{r}-\mathbf{x}|)$ responsable de la transition est à courte portée, on peut prendre pour la décrire un pseudo-potentiel à portée nulle

$$\mathscr{V}(\mathbf{r}-\mathbf{x}) = \frac{\hbar^2}{m} 4\pi a\delta(\mathbf{r}-\mathbf{x})$$

où a est un paramètre ayant la dimension d'une longueur de l'ordre de grandeur de la longueur de diffusion nucléon-nucléon. Dans ce cas, si les deux nucléons sont identiques, ils ne peuvent interagir que dans un état de spin total nul. On a la règle de sélection supplémentaire $\lambda = \nu$, l'amplitude de transition précédente se simplifiant d'une manière évidente.

La section efficace différentielle en angle et en énergie, lorsque les nucléons incidents et les noyaux cibles ne sont pas polarisés, et lorsqu'on n'observe pas la polarisation des produits finaux, est obtenue en portant (13) dans (7.a),

puis en moyennant et en sommant respectivement sur les états de polarisation initiaux et finaux:

$$\frac{d\sigma(\mathbf{k}\to\mathbf{k}_1,\mathbf{k}_2)}{d\hat{\mathbf{k}}_1 d\hat{\mathbf{k}}_2 dE_1}=\frac{kk_1k_2m^2}{8\pi^4\hbar^4E}\frac{1}{(2s+1)(2j+1)}\sum i^{L-L_1-L_2-\hat{L}+\hat{L}_1+\hat{L}_2}(-)^{-j+s+J+\hat{J}+\hat{J}_1-\hat{J}_2+\nu}$$

$$\cdot(2l+1)(2L+1)(2\hat{L}+1)(2L_1+1)(2\hat{L}_1+1)(2L_2+1)(2\hat{L}_2+1)(2j+1)(2J+1)$$

$$\cdot(2\hat{J}+1)(2J_1+1)(2\hat{J}_1+1)(2J_2+1)(2\hat{J}_2+1)(2\sigma+1)(2\hat{\sigma}+1)(2\lambda+1)(2\hat{\lambda}+1)$$

$$\cdot(2\nu+1)(2\hat{\nu}+1)\sqrt{(2\tau+1)(2\tau_1+1)(2\tau_2+1)}\begin{pmatrix}\tau_1&\tau_2&\tau\\-\mu_1&-\mu_2&-\mu\end{pmatrix}Y^{\mu}_{\tau}(\hat{\mathbf{k}})Y^{\mu_1}_{\tau_1}(\hat{\mathbf{k}}_1)Y^{\mu_2}_{\tau_2}(\hat{\mathbf{k}}_2)$$

$$\cdot\begin{pmatrix}l&L&\lambda\\0&0&0\end{pmatrix}\begin{pmatrix}l&\hat{L}&\hat{\lambda}\\0&0&0\end{pmatrix}\begin{pmatrix}L_1&L_2&\lambda\\0&0&0\end{pmatrix}\begin{pmatrix}\hat{L}_1&\hat{L}_2&\hat{\lambda}\\0&0&0\end{pmatrix}\begin{pmatrix}L&\hat{L}&\tau\\0&0&0\end{pmatrix}\begin{pmatrix}L_1&\hat{L}_1&\tau_1\\0&0&0\end{pmatrix}\begin{pmatrix}L_2&\hat{L}_2&\tau_2\\0&0&0\end{pmatrix}\begin{Bmatrix}J&\hat{J}&\tau\\\hat{\nu}&\nu&j\end{Bmatrix}\begin{Bmatrix}J&\hat{J}&\tau\\\hat{L}&L&S\end{Bmatrix}$$

$$\cdot\begin{Bmatrix}J_1&\hat{J}_1&\tau_1\\\hat{L}_1&L_1&S_1\end{Bmatrix}\begin{Bmatrix}J_2&\hat{J}_2&\tau_2\\\hat{L}_2&L_2&S_2\end{Bmatrix}\begin{Bmatrix}l&j&s\\L&J&S\\\lambda&\nu&\sigma\end{Bmatrix}\begin{Bmatrix}l&j&s\\\hat{L}&\hat{J}&S\\\hat{\lambda}&\hat{\nu}&\hat{\sigma}\end{Bmatrix}\begin{Bmatrix}L_1&J_1&S_1\\L_2&J_2&S_2\\\lambda&\nu&\sigma\end{Bmatrix}\begin{Bmatrix}\hat{L}_1&\hat{J}_1&S_1\\\hat{L}_2&\hat{J}_2&S_2\\\hat{\lambda}&\hat{\nu}&\hat{\sigma}\end{Bmatrix}\begin{Bmatrix}J_1&J_2&\nu\\\hat{J}_1&\hat{J}_2&\hat{\nu}\\\tau_1&\tau_2&\tau\end{Bmatrix}$$

$$\cdot A_{lLL_1L_2jJJ_1J_2}A^{*}_{l\hat{L}\hat{L}_1\hat{L}_2j\hat{J}\hat{J}_1\hat{J}_2}. \qquad (14)$$

La somme porte sur L, $\hat{L}$, L_1, $\hat{L}_1$, L_2, $\hat{L}_2$, J, $\hat{J}$, J_1, $\hat{J}_1$, J_2, $\hat{J}_2$, σ, $\hat{\sigma}$, λ, $\hat{\lambda}$, ν, ν, τ, τ_1, τ_2, μ, μ_1, μ_2.

Si on prend pour axe de référence la direction d'incidence on a

$$Y^{\mu}_{\tau}(0)=\sqrt{\frac{2\tau+1}{4\pi}}\delta_{\mu 0}\ \text{donc}\ \mu_1=-\mu_2.$$

Pour une interaction à portée nulle, l'élément de matrice réduit $A_{lLL_1L_2jJJ_1J_2}$ est égal à

$$\frac{\hbar^2}{m}4\pi a\frac{1}{kk_1k_2}\int\chi_{lj}(r)\varphi^{(+)}_{LJ}(kr)\varphi^{(+)}_{L_1J_1}(k_1r)\varphi^{(+)}_{L_2J_2}(k_2r)\frac{dr}{r^2}, \qquad (15)$$

en tenant compte de la relation (12.a). Dans ce cas, si les deux nucléons sont indiscernables, l'expression (14) se réduit à

$$\cdot\frac{d\sigma(\mathbf{k}\to\mathbf{k}_1,\mathbf{k}_2)}{d\hat{\mathbf{k}}_1 d\hat{\mathbf{k}}_2 dE_1}=\frac{kk_1k_2m^2}{8\pi^4\hbar^4E}\frac{1}{(2s+1)(2j+1)}\sum i^{L-L_1-L_2-\hat{L}+\hat{L}_1+\hat{L}_2}(-)^{-j+s+J+\hat{J}+\hat{J}_1-\hat{J}_2+\nu}$$

$$\cdot(2l+1)(2L+1)(2\hat{L}+1)(2L_1+1)(2\hat{L}_1+1)(2L_2+1)(2\hat{L}_2+1)(2j+1)(2J+1)$$

$$\cdot(2\hat{J}+1)(2J_1+1)(2\hat{J}_1+1)(2J_2+1)(3\hat{J}_2+1)\frac{(2\nu+1)(2\hat{\nu}+1)}{(2s+1)^2}$$

$$\cdot\sqrt{(2\tau+1)(2\tau_1+1)(2\tau_2+1)}\begin{pmatrix}\tau_1&\tau_2&\tau\\-\mu_1&-\mu_2&-\mu\end{pmatrix}Y^{\mu}_{\tau}(\hat{\mathbf{k}})Y^{\mu_1}_{\tau_1}(\hat{\mathbf{k}}_1)Y^{\mu_2}_{\tau_2}(\hat{\mathbf{k}}_2)$$

$$\cdot\begin{pmatrix}l&L&\lambda\\0&0&0\end{pmatrix}\begin{pmatrix}l&\hat{L}&\hat{\lambda}\\0&0&0\end{pmatrix}\begin{pmatrix}L_1&L_2&\lambda\\0&0&0\end{pmatrix}\begin{pmatrix}\hat{L}_1&\hat{L}_2&\hat{\lambda}\\0&0&0\end{pmatrix}\begin{pmatrix}L&\hat{L}&\tau\\0&0&0\end{pmatrix}\begin{pmatrix}L_1&\hat{L}_1&\tau_1\\0&0&0\end{pmatrix}\begin{pmatrix}L_2&\hat{L}_2&\tau_2\\0&0&0\end{pmatrix}\begin{Bmatrix}J&\hat{J}&\tau\\\hat{\nu}&\nu&j\end{Bmatrix}\begin{Bmatrix}J&\hat{J}&\tau\\\hat{L}&L&S\end{Bmatrix}$$

$$\cdot\begin{Bmatrix}J_1&\hat{J}_1&\tau_1\\\hat{L}_1&L_1&S_1\end{Bmatrix}\begin{Bmatrix}J_2&\hat{J}_2&\tau_2\\\hat{L}_2&L_2&S_2\end{Bmatrix}\begin{Bmatrix}l&j&s\\J&L&\nu\end{Bmatrix}\begin{Bmatrix}l&j&s\\\hat{J}&\hat{L}&\hat{\nu}\end{Bmatrix}\begin{Bmatrix}L_1&J_1&s\\J_2&L_2&\nu\end{Bmatrix}\begin{Bmatrix}\hat{L}_1&\hat{J}_1&s\\\hat{J}_2&\hat{L}_2&\hat{\nu}\end{Bmatrix}\begin{Bmatrix}J_1&J_2&\nu\\\hat{J}_1&\hat{J}_2&\hat{\nu}\\\tau_1&\tau_2&\tau\end{Bmatrix}A_{lLL_1L_2jJJ_1J_2}A^{*}_{l\hat{L}\hat{L}_1\hat{L}_2j\hat{J}\hat{J}_1\hat{J}_2}$$

où l'on a fait $s = S = S_1 = S_2$.

Enfin la section efficace différentielle en énergie (7.b) est dans le cas général d'une interaction quelconque,

$$\frac{d\sigma(k \to k_1, k_2)}{dE_1} = \frac{kk_1k_2m^2}{8\sqrt{2}\pi^2\hbar^4 E} \sum_{\substack{LL_1L_2 \\ JJ_1J_2\nu}} \frac{(2l+1)}{(2s+1)^3} (2L+1)(2L_1+1)(2L_2+1)(2J+1)$$

$$(2J_1+1)(2J_2+1)\left[\sum_{\lambda\sigma} (2\sigma+1)(2\lambda+1) \begin{pmatrix} l & L & \lambda \\ 0 & 0 & 0 \end{pmatrix} \begin{pmatrix} L_1 & L_2 & \lambda \\ 0 & 0 & 0 \end{pmatrix} \begin{Bmatrix} l & j & s \\ L & J & S \\ \lambda & \nu & \sigma \end{Bmatrix} \begin{Bmatrix} L_1 & J_1 & S_1 \\ L_2 & J_2 & S_2 \\ \lambda & \nu & \sigma \end{Bmatrix}\right]^2$$

$$|A_{lLL_1L_2jJJ_1J_2}|^2.$$

Dans le cas d'une interaction à portée nulle et de particules identiques cette expression se réduit à

$$\frac{d\sigma(k \to k_1, k_2)}{dE_1} = \frac{kk_1k_2m^2}{4\sqrt{2}\pi^2\hbar^4 E} \frac{1}{(2j+1)(2s+1)^3} \sum_{\substack{LL_1L_2 \\ JJ_1J_2\nu}} \frac{1}{2\nu+1} Z^2(ljLJ; s\nu)$$

$$Z_2(L_1J_1L_2J_2; s\nu)|A_{lLL_1L_2jJJ_1J_2}|^2. \quad (16)$$

3. Application à la Réaction $Be^9(n, 2n)Be^8$

3.1. SITUATION EXPÉRIMENTALE ET THÉORIQUE

La réaction $Be^9(n, 2n)$ jusqu'à 15 MeV a été étudiée par nombre d'expérimentateurs avec des méthodes parfois très différentes (entre autres, voir les références [10–14]). Les résultats ne sont pas toujours sans contradiction ainsi

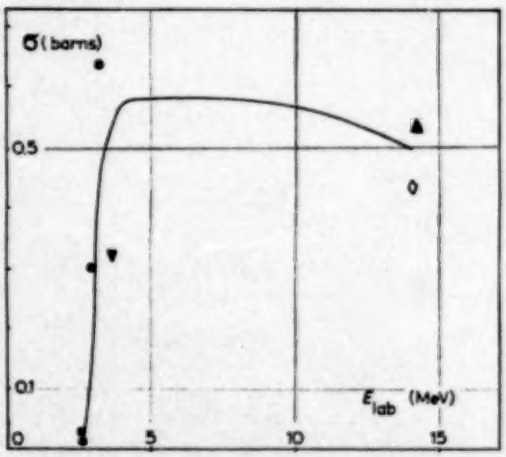

Fig. 1. La section efficace $Be^9(n, 2n)Be^8$ jusqu'à 15 MeV. La courbe interpolée à partir des points expérimentaux est extraite de la réf. [15]).

que les conclusions qu'on en tire. La figure 1 représente l'ensemble des résultats expérimentaux [15]) sur la section efficace $Be^9(n, 2n)$. On admet généralement que cette réaction peut se produire par l'intermédiaire de plusieurs mécanismes.

Le premier est la formation d'un noyau composé de Be^{10*} se désexcitant, soit par émission simultanée de deux neutrons (ce cas est en fait exclu, la largeur réduite correspondante étant très faible), soit par une désexcitation, conforme au schéma de la figure 2, passant par un niveau intermédiaire excité du Be^9. Ce

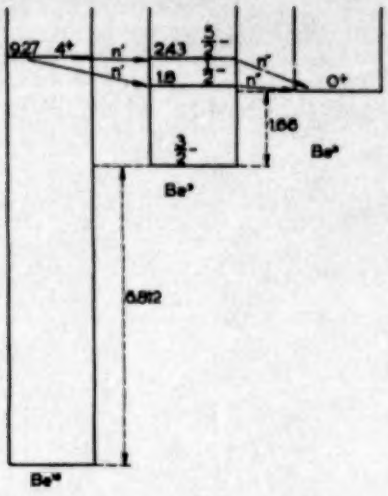

Fig. 2. Schéma de désexcitation du niveau Be^{10*} d'énergie 9.27 MeV. La voie de neutron est la seule ouverte pour la désexcitation des niveaux intermédiaires 2.43 MeV et 1.8 MeV du Be^9.

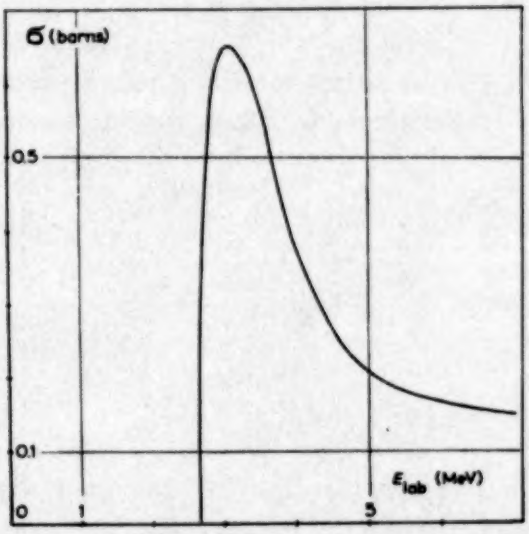

Fig. 3. La section efficace $Be^9(n, 2n)Be^8$ calculée dans l'hypothèse du passage par le niveau composé Be^{10*} de 9.27 MeV [4]. La courbe est calculée par la théorie de Breit-Wigner à un niveau, conformément au schéma de la figure 2 et elle est adaptée au point $E = 3.2$ MeV pour rendre compte du résultat expérimental $\sigma = 0.64$ b.

mécanisme est représenté par $Be^9(n)Be^{10*}(n')Be^{9*}(n'')Be^8$. La figure 3 représente la section efficace calculée [5]) dans cette hypothèse, à l'aide de la théorie à un niveau de Breit et Wigner, en donnant au niveau Be^{10*} de 9.27 MeV le spin

4 et la parité +, et en utilisant les largeurs expérimentales de la réf. [16]) et les spins attribués aux divers niveaux du Be^{9*} en couplage intermédiaire par Inglis [17]). Cette courbe est normée au point $E = 3.2$ MeV pour rendre compte du résultat expérimental $\sigma = 0.64$ b.

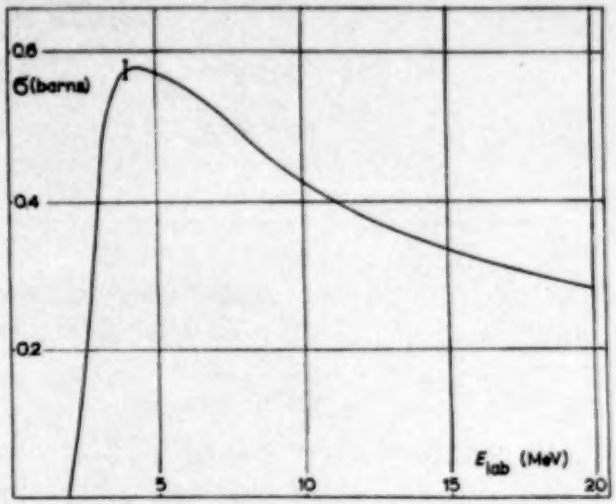

Fig. 4. La section efficace $Be^9(n, 2n)Be^8$ calculée par M. Sachs [4]) dans l'hypothèse d'un mécanisme de break-up.

M. Sachs [4]) a envisagé la possibilité d'une réaction $Be^9(n, 2n)$ par mécanisme de break-up. Ce modèle semi-empirique suppose qu'un équilibre thermodynamique s'établit dans un certain volume entre le nucléon incident, le nucléon lié et le cœur de Be^8 avant éclatement en trois fragments. Le modèle du break-up n'est valable que dans une région où les niveaux du noyau composé sont peu nombreux, et où l'énergie du nucléon incident est assez faible pour se répartir également entre les divers fragments. Avec un puits de Be^9 de 40 MeV, une région d'interaction sphéroïdale dont les axes sont des paramètres déterminés pour que la courbe calculée passe par le point mesuré [14]) à 4.07 MeV on obtient une section efficace (n, 2n) dont la dépendance en énergie est représentée sur la figure 4. La section efficace moyenne expérimentale prise sur le spectre Ra-Be est de 300 ± 100 mb [14]); l'intégration de la courbe de la figure 4 sur divers spectres expérimentaux [18]) donne les sections efficaces moyennes $\bar{\sigma}_{\text{break-up}}$ portées sur la première ligne du tableau 1. A titre de comparaison, nous avons aussi donné les valeurs qu'on obtient dans l'hypothèse du noyau composé.

Les autres mécanismes sont des mécanismes d'interaction directe. Tout d'abord le nucléon incident peut exciter directement le noyau de béryllium et le faire passer dans l'un des états excités du Be^{9*}, celui-ci se désexcitant ensuite par émission d'un deuxième neutron, conformément au schéma $Be^9(n, n')\ Be^{9*}(n'')Be^8$. Bien que l'on puisse penser que la composante de la fonction d'onde du Be^{9*} sur un état excité de particule individuelle soit faible, Marion *et al.* [11]) attribuent à ce mécanisme la moitié de la section efficace non

TABLEAU 1

La section efficace $Be^9(n, 2n)Be^8$ (exprimée en mb) moyennée sur le spectre des neutrons d'une source Ra-Be.

Selon le spectre expérimental de	Demers [21])	Houtermans et Teucher [20])	Schmidt-Rohr[19])
$\bar{\sigma}_{\text{break-up}}$ [4])	500	460	330
$\bar{\sigma}_{\text{composé}}$ [5])	220	230	180
$\bar{\sigma}_{\text{éjection + break-up}}$	530	500	540
$\bar{\sigma}_{\text{éjection + composé}}$	400	410	290
$\bar{\sigma}_{\text{mesurée}}$ [14])	300 ± 100		

élastique. L'existence de deux groupes d'énergie pour les neutrons sortants, l'énergie du projectile étant de 3.7 MeV, est également attribuée par Fowler *et al.* [18]) à un mécanisme de ce type.

Au delà de la région du seuil, où la théorie du noyau composé et celle du break-up rendent bien compte de la croissance rapide de la section efficace totale (n, 2n), il reste la possibilité de l'éjection du neutron lié par le neutron incident. Le noyau résiduel de Be^8 est dans l'état fondamental; les deux neutrons sortants sont en interaction (sans former d'état lié). La voie de sortie est à trois fragments et la réaction répond au schéma étudié plus haut.

3.2. L'ÉTAT $P_{\frac{1}{2}}$ DU Be^9

Le modèle simple d'un cœur de spin 0 autour duquel gravite le dernier nucléon est justifié dans le cas du Be^9 par la très faible énergie de liaison du dernier nucléon (1.66 MeV, la plus faible de la table des éléments) et, en conséquence, par la forte largeur expérimentale pour la réaction $Be^9(n, 2n)$. Le potentiel nucléaire moyen adopté dans l'équation (8) est du type de Saxon[22]) $\bar{V}(x) = -V_0/[1+\exp \alpha(x-R)]$. Ici R est le rayon classique $r_0 A^{\frac{1}{3}}$ ($r_0 = 1.3 \times 10^{-13}$ cm) et $\alpha = 1.45 \times 10^{13}$ cm^{-1}. La constante du couplage Thomas-Fermi λ est extrapolée des tables de A. A. Ross, R. D. Lawson et H. Mark [23]): $\lambda = 39.5$.

L'intégration de l'équation (8) est faite en considérant V_0 comme un paramètre, ajusté de manière que la solution se raccorde asymptotiquement avec l'exponentielle décroissante (9.b) correspondant à l'énergie de liaison observée. La valeur de V_0 obtenue ($V_0 = 28$ MeV) est faible comme on devait s'y attendre. Avec un puits carré de rayon R, on aurait eu $V_0 = 24$ MeV.

La figure 5 montre l'extension remarquable du carré de l'amplitude de la fonction radiale $\chi_{1\frac{1}{2}}(x) = x\Psi_{1\frac{1}{2}}(x)$. Cette extension est mise en évidence par le choix du rayon classique R du Be^9 comme unité sur l'axe des abscisses. Nous indiquons les contributions des différentes parties de cette courbe à la probabilité de présence totale. Nous voyons que la probabilité, pour que le dernier nucléon soit à l'intérieur du cœur n'est que de 0.31.

La très grande extension de l'état de particule indépendante $P_{\frac{1}{2}}$ du Be^9

justifie le modèle choisi pour décrire le noyau de Be^9; elle suggère l'importance du mécanisme d'interaction directe mais elle rend nécessaire l'utilisation d'un grand nombre d'ondes partielles pour décrire la diffusion de la particule incidente et, par conséquent, pour décrire la diffusion des deux particules émergentes.

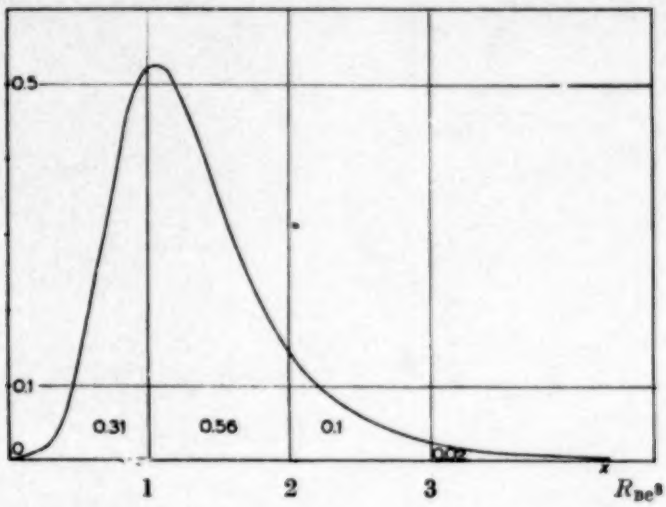

Fig. 5. Carré de l'amplitude de l'état $P_{\frac{3}{2}}$ du Be^9. L'équation (8) est intégrée en ajustant la profondeur du puits de Saxon pour obtenir l'énergie de liaison observée ($\varepsilon = 1.66$ MeV, C.M.). L'unité des abscisses est le rayon du cœur Be^8 et on a porté, dans les diverses régions indiquées, la probabilité de présence du dernier nucléon.

3.3. LES ÉTATS DE DIFFUSION

Les états décrivant la diffusion du nucléon incident par le puits de Be^9, et des nucléons émergents par le puits de Be^8 sont solutions de l'équation (8) avec les conditions aux limites (10.a) et (10.b), le potentiel choisi étant encore du type de Saxon avec $V_0 = V + iW$. Les valeurs utilisées pour les divers paramètres sont interpolées des tables de M. A. Melkanoff, J. S. Nodvik, D. S. Saxon et R. D. Woods [22]). On a calculé les fonctions d'ondes correspondant à des énergies du projectile égales à 2, 2.5, 3.2, 4, 6, 10 et 14 MeV, l'énergie disponible dans l'état final se partageant dans les rapports (0.5—0.5), (0.43—0.57), (0.17—0.83), (0.1—0.9) entre les deux nucléons émergents.

A titre d'exemple, nous donnons la forme des ondes radiales de diffusion, pour diverses énergies du nucléon incident et pour divers moments orbitaux, sur les figures 6a. Malgré le petit nombre des nucléons formant le cœur, on remarque la très forte atténuation à l'intérieur de celui-ci. Cette atténuation, coopérant avec la forme de la fonction liée, indique que l'interaction nucléon-nucléon sera surtout importante hors du cœur. La mauvaise convergence du développement en ondes partielles, conséquence de cette situation, oblige à prendre dans les sommations des moments orbitaux maximum élevés ($L_{max} = 7$ pour $E = 10$ et 14 MeV).

La contribution à l'absorption de la partie intérieure du puits complexe est

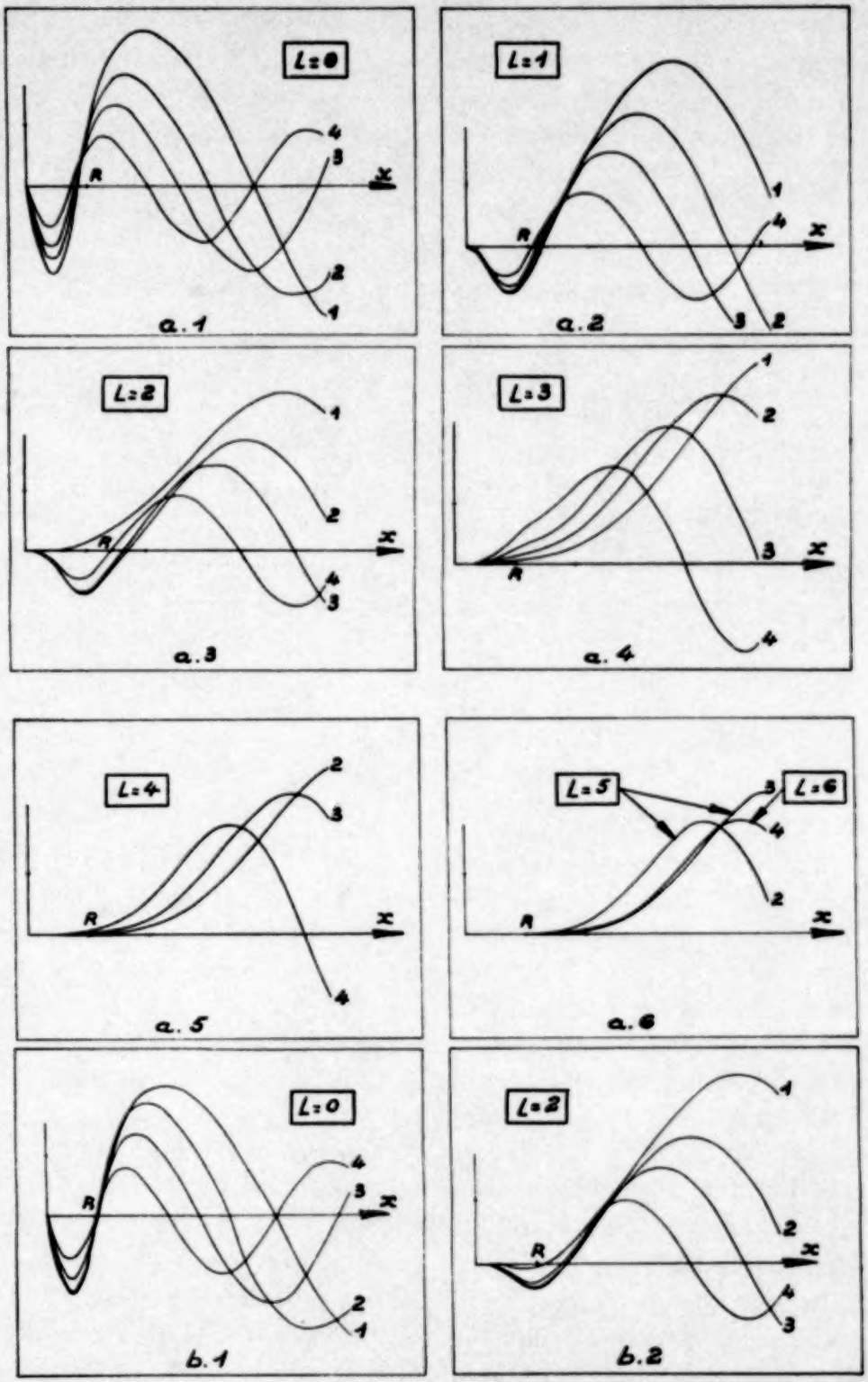

Fig. 6. États de diffusion élastique instantanée de neutrons par le Be^9, calculés avec le modèle optique, pour des énergies de 2.5 MeV (courbes 1), 4 MeV (courbes 2), 6 MeV (courbes 3), 10 MeV (courbes 4), et pour divers moments angulaires. On a représenté uniquement les états $J = L + \frac{1}{2}$. Les courbes a sont calculées avec un puits complexe dont les parties imaginaire et réelle ont toutes deux une forme de Saxon. Les courbes b sont calculées avec un puits dont la partie réelle est la même que précédemment mais dont la partie imaginaire s'annule à l'origine.

faible, comme il est bien connu; l'interaction du nucléon incident avec le noyau est surtout localisée „à la surface". Ce fait est mis en évidence sur les figures 6b où nous avons représenté quelques-unes des fonctions d'onde précédentes calculées avec un puits de Saxon dont la partie réelle est inchangée, mais dont la partie imaginaire est nulle à l'origine et maximum à la surface, ce maximum étant déterminé pour que la partie imaginaire du puits présente le même volume que précédemment. Par comparaison avec la figure 6a, nous voyons que l'atténuation dans le cœur est à peine modifiée.

3.4. RÉSULTATS ET COMPARAISONS

Nous avons porté sur la figure 7 les sections efficaces différentielles en énergie, calculées à l'aide des expressions (7.b) et (16), en fonction du mode de partage

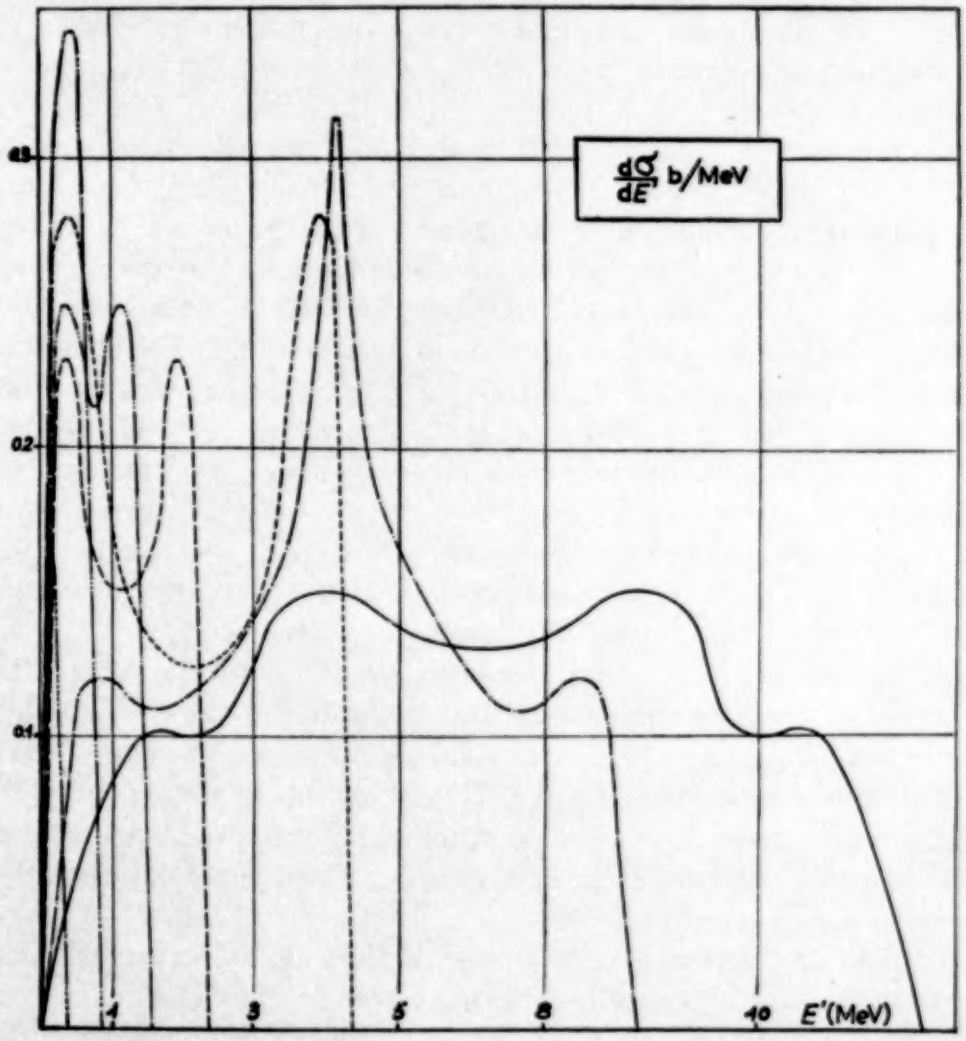

Fig. 7. Contributions du mécanisme d'éjection à la section efficace différentielle en énergie $d\sigma/dE'$ de la réaction $Be^9(n, 2n)Be^8$ pour diverses énergies E du projectile. On remarque le comportement résonant autour des énergies $E' = 0.5$ MeV et 5 MeV accompagné évidemment du pic symétrique par rapport à $\frac{1}{2}(E'-1.66)$.

de l'énergie et pour les diverses énergies d'incidence E_{inc} précédemment données. L'énergie E' emportée par l'un des neutrons sortants est portée sur l'axe des abscisses, l'autre neutron ayant l'énergie $E_{\text{inc}}-E'-1.66$ MeV. Ces courbes sont symétriques autour de $\frac{1}{2}(E_{\text{inc}}-1.66)$, nulles à l'origine et en $E' = E_{\text{inc}}-1.66$ comme il se doit. On remarque l'existence de deux „résonances" lorsque l'énergie de la réaction le permet, l'une autour de 0.5 MeV, l'autre autour de 5 MeV. Ces résonances sont d'autant moins bien définies que l'on monte en énergie. Jusqu'à environ 5 MeV, on a deux pics correspondant à la résonance de 0.5 MeV; de 5 à 10 MeV, nous avons trois pics, le pic médian correspondant à la résonance de 5 MeV. Au-dessus de 10 MeV la résonance de 0.5 MeV disparaît et il reste deux pics correspondant à la résonance de 5 MeV. Ces résultats sont à rapprocher de la détection de deux groupes en énergie pour les neutrons sortants par Fowler *et al.* [12]) et Marion *et al.* [11]). On doit, semble-t-il, les attribuer à des états de particule indépendante dans le puits moyen de Be^9, la résonance à 0.5 MeV correspondant ainsi à l'état métastable $P_{\frac{1}{2}}$.

La section efficace totale $n \to 2n$ par mécanisme d'éjection, définie par l'expression (7.b), est donnée à chaque énergie E par l'intégration jusqu'à $\frac{1}{2}E$ de la courbe correspondante de la figure 7. La dépendance en énergie de $\sigma_{\text{direct}}(n, 2n)$ est représentée sur la courbe de la figure 8. Les valeurs portées en ordonnées, en barns, sont celles obtenues avec la longueur de diffusion singulet expérimentale pour des nucléons libres $a = -2.43\ 10^{-12}$ cm. L'utilisation, pour l'interaction résiduelle $\mathscr{V}(|\mathbf{r}-\mathbf{x}|)$, du potentiel décrivant la diffusion nucléon-nucléon libre à basse énergie, est justifiée dans la mesure où l'interaction des deux neutrons a lieu loin des nucléons du cœur. Nous verrons plus loin que, grâce à la faible énergie de liaison du dernier nucléon du Be^9, c'est effectivement le cas. Ceci explique que la section efficace calculée a le bon ordre de grandeur, dans le domaine d'énergie où le modèle est valable, sans qu'on ait besoin d'adapter le paramètre de l'interaction résiduelle.

J. B. Marion, J. S. Levin et L. Cranberg [11]) ont mesuré la contribution du mécanisme direct aux énergies 3.50, 4.10 et 5.00 MeV. La section efficace était de 200 mb dans chaque cas, avec une tendance à croître avec l'énergie. La section efficace calculée continue à croître à 14 MeV, en raison du grand nombre d'ondes partielles qui interviennent et de l'extension de la fonction liée. Au-delà de cette énergie on peut s'attendre à une décroissance, le maximum des amplitudes de diffusion s'éloignant de l'origine.

Pour montrer l'importance de la contribution de la région extérieure au cœur dans les intégrales réduites (15) nous avons porté sur la figure 8 les sections efficaces calculées en integrant le produit des fonctions complexes radiales sur une partie de l'espace seulement. Les régions d'intégration sont définies sur le schéma de la figure 9. Ainsi les courbes α à ε de la figure 8 correspondent respectivement à la variation de la section efficace en fonction de

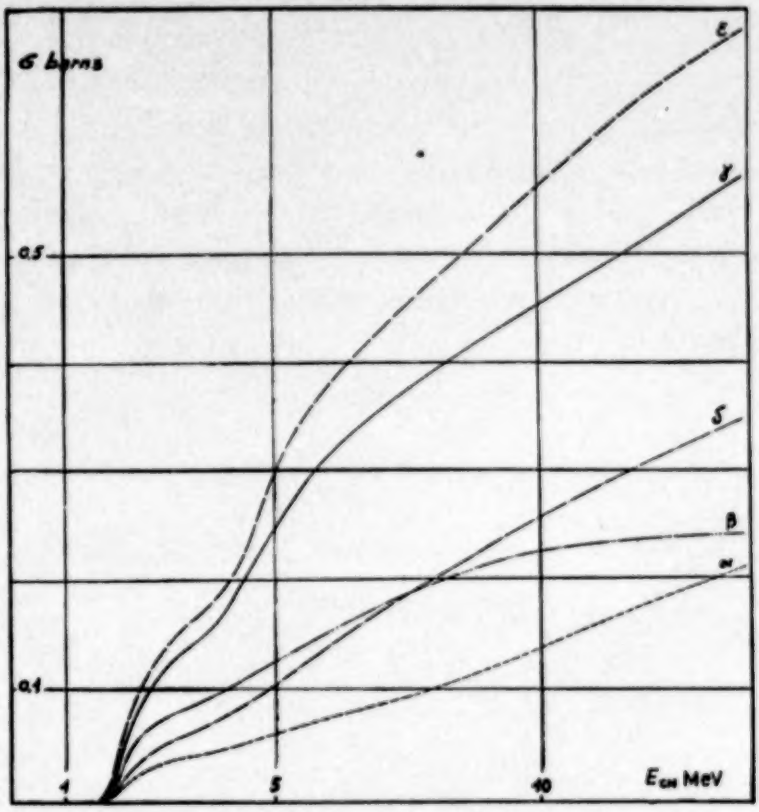

Fig. 8. Contributions au mécanisme d'éjection des régions définies sur la figure 9 dans le cas de la réaction $Be^9(n, 2n)Be^8$. Les courbes de section efficaces α à ε correspondent respectivement a une interaction nucléon-nucléon localisée dans le cœur (α), dans „la surface" (β) dans le cœur plus la surface (γ), dans la surface plus l'extérieur (δ), dans tout l'espace (ε).

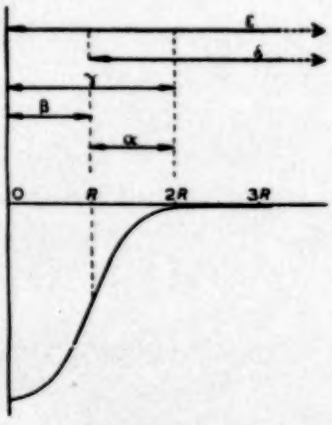

Fig. 9. Schéma des régions d'interaction dont les contributions sont analysées sur la figure 8.

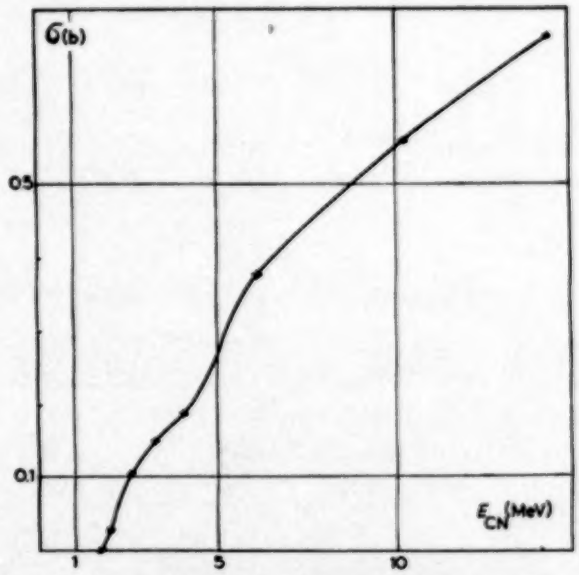

Fig. 10. Contribution du mécanisme d'éjection à la section efficace $Be^9(n, 2n)$. Les valeurs portées en ordonnées sont celles obtenues en prenant pour constante de couplage a dans (15) la longueur de diffusion nucléon-nucléon singulet ($a = -2.43 \times 10^{-13}$ cm).

l'énergie lorsque l'interaction a lieu uniquement dans le cœur (α), dans la surface (β), dans le cœur plus la surface (γ), dans la surface et à l'extérieur (δ) et dans tout l'espace (ε), cette dernière courbe étant celle de la figure 10; ces courbes ne sont évidemment pas additives puisque l'intégrale (15) intervient dans (19) sous forme du carré du module d'une quantité complexe. Nous voyons que la majeure partie de la contribution du mécanisme d'éjection à la réaction $Be^9(n, 2n)$ se fait par une interaction localisée principalement à la „surface" et à l'extérieur du noyau.

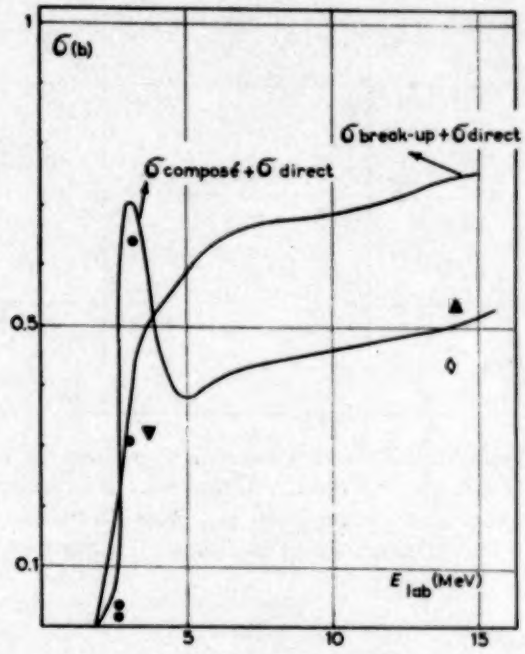

Fig. 11. La section efficace $Be^9(n, 2n)$ dans l'hypothèse d'une addition incohérente des mécanismes par noyau composé et par éjection (courbe 1) et des mécanismes par break-up et par éjection (courbe 2). Les courbes sont adaptées pour rendre compte le mieux possible des points expérimentaux (également portés sur la figure) dans l'hypothèse d'une interaction directe prépondérante à 15 MeV.

Dans l'ensemble du domaine d'énergie considéré, ni le mécanisme par formation d'un noyau composé (figure 3), ni le mécanisme direct par éjection (figure 10) ne permettent seuls d'expliquer la section efficace observée $Be^9(n, 2n)$ de la figure 1. La théorie du break-up de M. Sachs donne un résultat qualitatif plus satisfaisant (figure 4), mais nous savons que dans la région des résonances sa validité est douteuse. La situation physique réelle est évidemment constituée par l'interférence de plusieurs mécanismes, mais nous ne connaissons pas les phases relatives des amplitudes de transition correspondantes. A titre indicatif, nous avons néanmoins porté sur la figure 11 les courbes de section efficace $Be^9(n, 2n)$ qu'on obtiendrait dans l'hypothèse d'une addition incohérente des contributions éjection plus composé et éjection plus break-up. Nous avons adapté la courbe du mécanisme direct par éjection de la figure 10 pour qu'elle

rende compte entièrement des résultats expérimentaux à 15 MeV et nous lui avons ajouté, soit la courbe de la figure 3, soit la courbe de la figure 4, adaptées pour que la somme rende compte des résultats expérimentaux à basse énergie. Les sections efficaces moyennes sur le spectre des neutrons du Ra—Be obtenues avec les courbes de la figure 11 sont portées dans le tableau 1. Il semble qu'on doive exclure le mécanisme de break-up. D'une part, le seuil observé et l'énergie des produits de la réaction à très basse énergie [11, 12]) sont conformes au mécanisme de noyaux composés décrits par la figure 2. D'autre part, lorsqu'on tient compte du mécanisme d'éjection, en même temps que du break-up, la section efficace moyenne calculée est incompatible avec le résultat expérimental.

Les auteurs tiennent à remercier tout particulièrement les Professeurs C. Bloch, C. T. De Dominicis et A. Messiah pour de nombreuses suggestions et discussions. Ils remercient également Mademoiselle Nicole Castille ainsi que les Services de Calcul numérique du Centre d'Études Nucléaires de Saclay pour leur collaboration.

Bibliographie

1) S. T. Butler, Proc. Roy. Soc. A **208** (1951) 559
2) J. Horowitz, Physica **22** (1956) 969; Sup. 3 Nuovo Cimento **4** (1956) 1137
3) W. Tobocman et M. H. Kalos, Phys. Rev. **97** (1955) 132
4) M. Sachs, Phys. Rev. **103** (1956) 671
5) C. T. de Dominicis et V. P. Gillet, Rapport SPM — CEA No 309 (1958)
6) A. Messiah, Mécanique Quantique (Dunod, Paris, 1959) T. II, Ch. XIX—II
7) Levinson et M. K. Banerjee, Ann. Phys. **2** (1957) 471
8) A. R. Edmonds, Angular Momentum in Quantum Mechanics (Princeton Univ. Press, 1955)
9) A. Messiah, loc. cit. T. II, appendice C
10) Goldstein, N.D.A. (1957)
11) J. B. Marion, J. S. Levin et L. Cranberg, Phys. Rev. **114** (1959) 1584
12) J. L. Fowler, Hanna et Owen, Phys. Rev. **98** (1955) 249; Bull. Am. Phys. Soc. **29** (1954) 75
13) K. Winter, B. Torki et E. Remy, C. R. du Congrès Int. de Phys. Nucl. (Dunod, Paris, 1958) p. 561
14) M. Teucher, Z. Phys. **126** (1949) 410
15) D. J. Hughes et R. B. Schwartz, Neutron Cross Section, ACRL (1959)
16) F. Ajzenberg et T. Lauritsen, Rev. Mod. Phys. **27** (1955) 77
17) D. R. Inglis, Rev. Mod. Phys. **27** (1955) 76
18) W. N. Hess, Annals Physics **2** (1959) 115
19) U. Schmidt-Rohr, Z. Naturf. **8a** (1953) 670
20) F. G. Houtermans et M. Teucher, Z. Phys. **129** (1951) 365
21) P. Demers, U.S.A.E.C. report M.P. 204 (1948)
22) M. A. Melkanoff, J. S. Nodvik, D. S. Saxon et R. D. Woods, Phys. Rev. **106** (1957) 793
23) A. A. Ross, M. Mark et R. D. Lawson, Phys. Rev. **102** (1956) 1613

7.C

Nuclear Physics **17** (1960) 468—476; © *North-Holland Publishing Co., Amsterdam*

Not to be reproduced by photoprint or microfilm without written permission from the publisher

A POSSIBLE EXPLANATION OF THE HIGH ENERGY PEAKS IN PION-NUCLEON CROSS SECTIONS

W. KRÓLIKOWSKI

Institute of Theoretical Physics, University of Warsaw, and

Institute for Nuclear Research, Polish Academy of Sciences, Warsaw

Received 1 February 1960

Abstract: The motion of the core inside the nucleon is pointed out as the possible origin of the high energy maxima observed in pion-nucleon scattering. An effective range approach of the Chew-Low type leads to results which are not in contradiction with present experimental data.

1. Introduction

Within the last year, the existence of the second and third maxima in the π^-p total cross section and their resonance character have been rather well established [1, 2]). The most probable assignment of quantum numbers to resonant states producing these peaks seems to be $D_{\frac{3}{2},\frac{1}{2}}$ and $D_{\frac{5}{2},\frac{1}{2}}$ (we use the symbol L_{IJ}). Also in the π^+p total cross section a second maximum is observed and it is probably due to a $(\frac{5}{2}, \frac{3}{2})$ resonant state (perhaps $D_{\frac{3}{2},\frac{3}{2}}$). The above mentioned resonant states, beside the well known $P_{\frac{3}{2},\frac{1}{2}}$ resonant state causing the first maximum in both π^+p and π^-p total cross sections, are interpreted as some excited states of the nucleon and referred to as its isobars.

The mechanism of the $P_{\frac{3}{2},\frac{1}{2}}$ excitation of the nucleon has been explained to some extent by Chew and Low's effective range approach [3, 4]), and, on the other hand, by the old Pauli-Dancoff strong coupling procedure [5, 6]). In the first treatment the scattering transitions are discussed by the technique of dispersion relations without necessity of finding the structure of the intermediate $P_{\frac{3}{2},\frac{1}{2}}$ isobar state. In the second treatment this isobar is constructed by an approximate diagonalization of the Hamiltonian. Both treatments show that the $P_{\frac{3}{2},\frac{1}{2}}$ excitation of the nucleon is essentially due to the coupling of spin and isospin of the core to the pion cloud. The motion of the core inside the nucleon and, therefore, the coupling of this motion to the pion cloud are negligible in the $P_{\frac{3}{2},\frac{1}{2}}$ excited state, because the fixed-source approximation turns out to be rather adequate in this case. The interaction of the core with all pions having orbital angular momenta different from $l = 1$ is neglected in the fixed-source approximation, because pseudoscalar coupling is assumed.

In the present paper the motion of the core inside the nucleon is taken into account. To this end the pseudoscalar coupling of a slowly moving extended source (representing the core) to the pion field is used:

$$H^{N\pi} = \frac{f_0}{\mu}\boldsymbol{\sigma}\cdot\boldsymbol{\tau}_a \int \mathrm{d}_3 x \rho_0(|\mathbf{x}_0-\mathbf{x}|)\nabla\varphi_a(\mathbf{x}), \tag{1}$$

where $\mathbf{x}_0$ is the position of the centre of mass of the core (if we replace $\rho_0(|\mathbf{x}_0-\mathbf{x}|)$ by the Chew-Low cut off $\rho(|\mathbf{x}|)$, we go over to the conventional fixed-source interaction). In this way we include the coupling of the motion of the core to the pion cloud. The Hamiltonian (1) describes the interaction of the core with pions possessing all orbital angular momenta l, and not only $l = 1$. At this point a suggestion could be made that the higher excitations of the nucleon (probably D states) would be provided by the coupling of the motion of the core (inside the nucleon) to the pion cloud. This possible mechanism for the higher excitations of the nucleon would compete with a mechanism via pion-pion interaction suggested previously [7, 8]).

If we make use of the formulae

$$\varphi_a(\mathbf{x}) = \sum_{\mathbf{k}} \frac{1}{\sqrt{2\omega_k}}(a_{\mathbf{k}a}\mathrm{e}^{i\mathbf{k}\cdot\mathbf{x}} + a^*_{\mathbf{k}a}\mathrm{e}^{-i\mathbf{k}\cdot\mathbf{x}}), \quad \omega_k = \sqrt{k^2+\mu^2} \tag{2}$$

and

$$\rho_0(|\mathbf{x}|) = \sum_{\mathbf{k}} v_0(k)\mathrm{e}^{i\mathbf{k}\cdot\mathbf{x}}, \tag{3}$$

we can put the interaction (1) in the form

$$H^{N\pi} = \frac{f_0}{\mu}\boldsymbol{\sigma}\cdot\boldsymbol{\tau}_a \sum_{\mathbf{k}} \frac{v_0(k)}{\sqrt{2\omega_k}} i\mathbf{k}(a_{\mathbf{k}a}\mathrm{e}^{i\mathbf{k}\cdot\mathbf{x}_0} - a^*_{\mathbf{k}a}\mathrm{e}^{-i\mathbf{k}\cdot\mathbf{x}_0}). \tag{4}$$

The total Hamiltonian of the system under consideration looks as follows:

$$H = M_0 + \frac{\mathbf{p}_0^2}{2M_0} + H^\pi + H^{N\pi}, \tag{5}$$

where M_0 is the mass of the core, $\mathbf{p}_0$ the momentum of the core canonically conjugate to the position $\mathbf{x}_0$ of the centre of mass of the core, and where

$$H^\pi = \sum_{\mathbf{k}} \omega_k a^*_{\mathbf{k}a} a_{\mathbf{k}a} \tag{6}$$

is the pion field Hamiltonian.

2. Low's Equation

Let us denote by $\mathbf{p}$ and σ the momentum of the nucleon and its spin and isospin indices, by $\mathbf{k}$ and a the momentum of a pion and its isovector index.

Then, the S matrix for elastic scattering of a pion on the nucleon can be written as follows:

$$\langle \mathbf{p}'\sigma'\mathbf{k}'a'|S|\mathbf{p}\sigma\mathbf{k}a\rangle = \delta_{fi} - 2\pi i\delta(E_{p'}+\omega_{k'}-E_p-\omega_k)T_{\mathbf{p}\sigma\mathbf{k}a}(\mathbf{p}'\sigma'\mathbf{k}'a'), \quad (7)$$

where

$$T_{\mathbf{p}\sigma\mathbf{k}a}(\lambda) = \langle \phi_\lambda^- V_{\mathbf{k}a}\phi_{\mathbf{p}\sigma}\rangle. \quad (8)$$

Here, we have

$$V_{\mathbf{k}a} = [H^{N\pi}, a^*_{\mathbf{k}a}] = \frac{f_0}{\mu}\boldsymbol{\sigma}\cdot\boldsymbol{\tau}_a\frac{v_0(k)}{\sqrt{2\omega_k}}i\mathbf{k}e^{i\mathbf{k}\cdot\mathbf{x}} = V^*_{-\mathbf{k}a} \quad (9)$$

and

$$(E_\lambda - H)\phi_\lambda^- = 0, \quad (10)$$

and especially $\phi_{\mathbf{p}\sigma}$ describes states of the nucleon

$$(E_p - H)\phi_{\mathbf{p}\sigma} = 0, \quad E_p = M + \frac{\mathbf{p}^2}{2M}. \quad (11)$$

The transition matrix T satisfies the following Low equation:

$$T_{\mathbf{p}\sigma\mathbf{k}a}(\mathbf{p}'\sigma'\mathbf{k}'a') = \sum_\lambda\left[\frac{T^*_{\mathbf{p}'\sigma'\mathbf{k}'a'}(\lambda)T_{\mathbf{p}\sigma\mathbf{k}a}(\lambda)}{E_{p'}+\omega_{k'}-E_\lambda+i\varepsilon} + \frac{T^*_{\mathbf{p}'\sigma'-\mathbf{k}'a'}(\lambda)T_{\mathbf{p}\sigma-\mathbf{k}'a'}(\lambda)}{E_p-\omega_{k'}-E_\lambda-i\varepsilon}\right]. \quad (12)$$

Now, we made the essential assumption that the dependence of the transition amplitude on the momentum change of the nucleon is rather negligible in the energy region where the isobars can be formed. Till now, all known resonances lie below 2 GeV of pion kinetic energy (lab.). In this extended region recoils of the nucleon can already be quite considerable, but our assumption is that the transition amplitude depends on those recoils rather insignificantly. This assumption enables us to write down explicitly approximate partial wave dispersion relations. According to the assumption we shall treat the centre of mass of the nucleon (as a whole) as fixed in the laboratory system:

$$\mathbf{p} = \mathbf{p}_0 + (\text{momentum of the cloud}) \equiv 0, \quad E_p \equiv M \quad (13)$$

(then we shall write $\phi_{\mathbf{p}\sigma} = \phi_\sigma$). Making the approximation $\mathbf{p} \equiv 0$ we should simultaneously replace the source function $v_0(k)$ by a new one, $v(k)$, which could be interpreted for P wave scattering as Chew-Low cut off.

We separate now a Born term in the Low equation (12):

$$T_{\sigma\mathbf{k}a}(\sigma'\mathbf{k}'a') = T^B_{\sigma\mathbf{k}a}(\sigma'\mathbf{k}'a') + \sum_{\lambda\neq\sigma''}[\ ], \quad (14)$$

where

$$T^B_{\sigma\mathbf{k}a}(\sigma'\mathbf{k}'a') = \frac{1}{\omega_{k'}}\sum_{\sigma''}[\langle\phi_{\sigma'}V^*_{\mathbf{k}'a'}\phi_{\sigma''}\rangle\langle\phi_{\sigma''}V_{\mathbf{k}a}\phi_\sigma\rangle - \langle\phi_{\sigma'}V_{\mathbf{k}a}\phi_{\sigma''}\rangle\langle\phi_{\sigma''}V^*_{\mathbf{k}'a'}\phi_\sigma\rangle]. \quad (15)$$

Applying a usual argument of covariance we obtain

$$T^{B}_{\rho ka}(\sigma' \mathbf{k}' a') = \left(\frac{f_0}{\mu}\right)^2 \frac{v(k')v(k)}{\sqrt{4\omega_{k'}\omega_k}} Z^{\frac{1}{2}}(k'^2) Z^{\frac{1}{2}}(k^2) \frac{1}{\omega_{k'}} [(\boldsymbol{\sigma}\cdot\mathbf{k}')\tau_{a'}, (\boldsymbol{\sigma}\cdot\mathbf{k})\tau_a]_{\sigma'\sigma}, \quad (16)$$

where $0 < Z^{\frac{1}{2}}(k^2) < 1$ is an unknown function of k^2:

$$\langle \phi_{\sigma'} \sigma_i \tau_a e^{i\mathbf{k}\cdot\mathbf{x}_0} \phi_\sigma \rangle = \langle \phi_{\sigma'} \sigma_i \tau_a \cos(\mathbf{k}\cdot\mathbf{x}_0) \phi_\sigma \rangle = Z^{\frac{1}{2}}(k^2)(\sigma_i\tau_a)_{\sigma'\sigma}. \quad (17)$$

Let us remark that the Born term (16) contains the interaction with P-wave pions only.

If $r_{ef}/\lambda\!\!\!^{-} < 1$, where $\lambda\!\!\!^{-} = 1/k$ and r_{ef} is the effective radius of a sphere within which the centre of mass of the core remains, we can apply to $\exp(i\mathbf{k}\cdot\mathbf{x}_0)$ in formula (8) a kind of multipole expansion, choosing for convenience the origin of the laboratory system at the centre of mass of the nucleon (as a whole):

$$e^{i\mathbf{k}\cdot\mathbf{x}_0} = 1 + i\mathbf{k}\cdot\mathbf{x}_0 - \tfrac{1}{2}(\mathbf{k}\cdot\mathbf{x}_0)^2 + \ldots. \quad (18)$$

Then, for instance,

$$Z^{\frac{1}{2}}(k^2) = Z^{\frac{1}{2}}(0)(1 - \tfrac{1}{2} r_{ef}^2 k^2 + \ldots), \quad (19)$$

where $Z^{\frac{1}{2}}(0)$ can be identified with the renormalization factor for the coupling constant f_0.

3. Dispersion Relations

Applying formulae (8), (9) and (14), as well as the expansion (18), and retaining approximately in each partial wave only the lowest contributing power of $\mathbf{k}\cdot\mathbf{x}_0$, we decompose the transition amplitude into partial waves as follows:

$$\begin{aligned} T_{ka}(\mathbf{k}' a') &= \|T_{\sigma ka}(\sigma' \mathbf{k}' a')\| \\ &= -4\pi \frac{v(k')v(k)}{\sqrt{4\omega_{k'}\omega_k}} \sum_T P_T(a', a) \Big[\sum_J (4\pi k' k) P_J{}^{P}(\mathbf{k}', \mathbf{k}) h^{P}_{JT}(\omega) \quad (20) \\ &+ (4\pi k'^2 k^2) P^{S}(\mathbf{k}', \mathbf{k}) g_T{}^{S}(\omega) + \sum_J (4\pi k'^2 k^2) P_J{}^{D}(\mathbf{k}', \mathbf{k}) g^{D}_{JT}(\omega) + \ldots \Big], \end{aligned}$$

where P_J and P_T are projection operators given by

$$\begin{aligned} P^{S}(\mathbf{k}', \mathbf{k}) &= \frac{1}{4\pi}, \\ P^{P}{}_{\frac{1}{2}}(\mathbf{k}', \mathbf{k}) &= \frac{(\boldsymbol{\sigma}\cdot\mathbf{k}')(\boldsymbol{\sigma}\cdot\mathbf{k})}{4\pi k' k}, \\ P_{\frac{3}{2}}{}^{P}(\mathbf{k}', \mathbf{k}) &= \frac{3(\mathbf{k}'\cdot\mathbf{k}) - (\boldsymbol{\sigma}\cdot\mathbf{k}')(\boldsymbol{\sigma}\cdot\mathbf{k})}{4\pi k' k}, \quad (21) \\ P_{\frac{1}{2}}{}^{D}(\mathbf{k}', \mathbf{k}) &= \frac{3(\boldsymbol{\sigma}\cdot\mathbf{k}')(\boldsymbol{\sigma}\cdot\mathbf{k})(\mathbf{k}'\cdot\mathbf{k}) - (k'k)^2}{4\pi (k'k)^2}, \\ P_{\frac{3}{2}}{}^{D}(\mathbf{k}', \mathbf{k}) &= \frac{5(\mathbf{k}'\cdot\mathbf{k})^2 - 2(\boldsymbol{\sigma}\cdot\mathbf{k}')(\boldsymbol{\sigma}\cdot\mathbf{k})(\mathbf{k}'\cdot\mathbf{k}) - (k'k)^2}{\frac{8}{3}\pi (k'k)^2} \end{aligned}$$

and

$$P_{\frac{1}{2}}(a', a) = \tfrac{1}{3}\tau_{a'}\tau_a, \quad P_{\frac{3}{2}}(a', a) = \delta_{a'a} - \tfrac{1}{3}\tau_{a'}\tau_a. \tag{22}$$

These projection operators satisfy the relations

$$\int d\Omega_{\mathbf{k}''} P_{J'}^{L'}(\mathbf{k}', \mathbf{k}'') P_J^{\,L}(\mathbf{k}'', \mathbf{k}) = \delta_{J'J}\delta_{L'L} P_J^{\,L}(\mathbf{k}', \mathbf{k}) \tag{23}$$

and

$$\sum_{a''} P_{T'}(a', a'') P_T(a'', a) = \delta_{T'T} P_T(a', a). \tag{24}$$

They have the following crossing properties:

$$\sum_{J'} P_{J'}^{\mathrm{P}}(\mathbf{k}', \mathbf{k}) A_{J'J}^{\mathrm{P}} = P_J^{\,\mathrm{P}}(\mathbf{k}, \mathbf{k}'), \quad \sum_{J'} P_{J'}^{\mathrm{D}}(\mathbf{k}', \mathbf{k}) A_{J'J}^{\mathrm{D}} = P_J^{\,\mathrm{D}}(\mathbf{k}, \mathbf{k}') \tag{25}$$

and

$$\sum_{T'} P_{T'}(a', a) B_{T'T} = P_T(a, a'), \tag{26}$$

where

$$\left(A_{J'J}^{\mathrm{P}}\right) = \tfrac{1}{3}\begin{pmatrix} -1 & 4 \\ 2 & 1 \end{pmatrix}, \quad \left(A_{J'J}^{\mathrm{D}}\right) = \tfrac{1}{5}\begin{pmatrix} -1 & 6 \\ 4 & 1 \end{pmatrix} \quad \text{and} \quad \left(B_{T'T}\right) = \tfrac{1}{3}\begin{pmatrix} -1 & 4 \\ 2 & 1 \end{pmatrix}. \tag{27}$$

In terms of h and g functions the optical theorem can be written as follows:

$$\begin{aligned} \sigma_{JT}^{\mathrm{P}}(\omega) &= 4\pi k v^2(k) \ \ \mathrm{Im}\ h_{JT}^{\mathrm{P}}(\omega), \\ \sigma_T^{\,\mathrm{S}}(\omega) &= 4\pi k^3 v^2(k) \ \ \mathrm{Im}\ g_T^{\,\mathrm{S}}(\omega), \\ \sigma_{JT}^{\mathrm{D}}(\omega) &= 4\pi k^3 v^2(k) \ \ \mathrm{Im}\ g_{JT}^{\mathrm{D}}(\omega), \end{aligned} \tag{28}$$

where

$$\sigma_{JT}^{L}(\omega) = 2\pi\lambda\!\!\!^{-2}\,\mathrm{Re}\,[1 - S_{JT}^{L}(\omega)] = -\left(\frac{2\pi}{k}\right)^2 \mathrm{Im}\, T_{JT}^{L}(\omega) \tag{29}$$

are partial wave total cross sections. We have

$$\begin{aligned} T_{JT}^{\mathrm{P}}(\omega) &= -\frac{k^3 v^2(k)}{\pi} h_{JT}^{\mathrm{P}}(\omega), \\ T^{\mathrm{S}}{}_T(\omega) &= -\frac{k^5 v^2(k)}{\pi} g^{\mathrm{S}}{}_T(\omega), \\ T_{JT}^{\mathrm{D}}(\omega) &= -\frac{k^5 v^2(k)}{\pi} g_{JT}^{\mathrm{D}}(\omega). \end{aligned} \tag{30}$$

Partial wave amplitudes $T_{JT}^{L}(\omega)$ for elastic scattering are connected with complex phase shifts $\eta_{JT}^{L}(\omega)$ by the relations

$$T_{JT}^{L}(\omega) = -\frac{1}{\pi} \sin \eta_{JT}^{L}(\omega) e^{i\eta_{JT}^{L}(\omega)}. \tag{31}$$

Let us note that

$$\cot\ \eta^L_{JT}(\omega) = -\frac{1}{\pi}\frac{1}{T^L_{JT}(\omega)} + i. \tag{32}$$

Making use of (20) we can now decompose the Low equation (14) into partial waves and go over to the approximate partial wave dispersion relations. For the P-wave we obtain, of course, the well known Chew-Low dispersion relations

$$h^{\mathrm{P}}_{JT}(\omega) = \frac{\lambda^{\mathrm{P}}_{JT}}{\omega} + \frac{1}{(2\pi)^2}\int_{\mu}^{\infty} \mathrm{d}\omega' \frac{1}{k' v^2(k')}\left[\frac{\sigma^{\mathrm{P}}_{JT}(\omega')}{\omega' - (\omega + i\varepsilon)} + \sum_{J'T'} A^{\mathrm{P}}_{JJ'} B_{TT'} \frac{\sigma^{\mathrm{P}}_{J'T'}(\omega')}{\omega' + \omega}\right], \tag{33}$$

where

$$\lambda^{\mathrm{P}}_{JT} = \frac{2}{3}\frac{f^2}{4\pi\mu^2}\begin{cases} -4 & (J = \frac{1}{2}, T = \frac{1}{2}) \\ -1 & (J = \frac{1}{2}, T = \frac{3}{2}) \\ -1 & (J = \frac{3}{2}, T = \frac{1}{2}) \\ +2 & (J = \frac{3}{2}, T = \frac{3}{2}). \end{cases} \tag{34}$$

Here, $f = f_0 Z^{\frac{1}{2}}(0)$ is the renormalized coupling constant ($f^2/4\pi \approx 0.08$). For the S and D waves we get dispersion relations not containing inhomogeneous terms

$$g_T{}^{\mathrm{S}}(\omega) = \frac{1}{(2\pi)^2}\int_{\mu}^{\infty} \mathrm{d}\omega' \frac{1}{k'^3 v^2(k')}\left[\frac{\sigma^{\mathrm{S}}_{JT}(\omega')}{\omega' - (\omega + i\varepsilon)} + \sum_{T'} B_{TT'} \frac{\sigma^{\mathrm{S}}_{T'}(\omega')}{\omega' + \omega}\right] \tag{35}$$

and

$$g^{\mathrm{D}}_{JT}(\omega) = \frac{1}{(2\pi)^2}\int_{\mu}^{\infty} \mathrm{d}\omega' \frac{1}{k'^3 v^2(k')}\left[\frac{\sigma^{\mathrm{D}}_{JT}(\omega')}{\omega' - (\omega + i\varepsilon)} + \sum_{J'T'} A^{\mathrm{D}}_{JJ'} B_{TT'} \frac{\sigma^{\mathrm{D}}_{J'T'}(\omega')}{\omega' + \omega}\right]. \tag{36}$$

For the S wave, inhomogeneous terms do appear, if we add to the interaction (1) the term

$$\frac{f_0}{\mu}\gamma_5 \tau_a \int \mathrm{d}_3 x \rho_0(|\mathbf{x}_0 - \mathbf{x}|)\dot{\varphi}_a(\mathbf{x}), \tag{37}$$

completing it to full pseudovector coupling, or the term

$$\frac{\lambda_0}{M}\left[\int \mathrm{d}_3 x \rho_0(|\mathbf{x}_0 - \mathbf{x}|)\varphi_a(\mathbf{x})\right]^2, \tag{38}$$

which may be treated as a result of the Dyson-Foldy transition from the pseudoscalar to the pseudovector coupling. In contra-distinction to the S wave, the vanishing inhomogeneous terms in the D wave dispersion relations following from eq. (14) are in the zero-recoil limit a more general result (cf. also ref. [9])).

4. An Effective Range Approximation

In order to apply to the D wave scattering an effective range approximation of Chew-Low type we rewrite the dispersion relations (36) in an equivalent form:

$$g^{\mathrm{D}}_{JT}(\omega) = g^{\mathrm{D}}_{JT}(0) + \frac{1}{(2\pi)^2}\int_{\mu}^{\infty} \mathrm{d}\omega' \frac{\omega}{\omega'} \frac{1}{k'^3 v^2(k')} \left[\frac{\sigma^{\mathrm{D}}_{JT}(\omega')}{\omega' - (\omega + i\varepsilon)} - \sum_{J'T'} A^{\mathrm{D}}_{JJ'} B_{TT'} \frac{\sigma^{\mathrm{D}}_{J'T'}(\omega')}{\omega' + \omega}\right], \quad (39)$$

where

$$g^{\mathrm{D}}_{JT}(0) = \frac{1}{(2\pi)^2}\int_{\mu}^{\infty} \mathrm{d}\omega' \frac{1}{\omega' k'^3 v^2(k')} [\sigma^{\mathrm{D}}_{JT}(\omega') + \sum_{J'T'} A^{\mathrm{D}}_{JJ'} B_{TT'} \sigma^{\mathrm{D}}_{J'T'}(\omega')]. \quad (40)$$

By formulae (32) and (30) we have

$$\mathrm{Re}\cot \eta^{\mathrm{D}}_{JT}(\omega) = \frac{1}{k^5 v^2(k)} \mathrm{Re}\frac{1}{g^{\mathrm{D}}_{JT}(\omega)}. \quad (41)$$

Now, we write approximately

$$\frac{g^{\mathrm{D}}_{JT}(0)}{g^{\mathrm{D}}_{JT}(\omega)} \approx 1 - r^{\mathrm{D}}_{JT}\omega, \quad (42)$$

where by means of eq. (39) the effective ranges have the forms

$$r^{\mathrm{D}}_{JT} = -\left[\frac{\mathrm{d}}{\mathrm{d}\omega}\frac{g^{\mathrm{D}}_{JT}(0)}{g^{\mathrm{D}}_{JT}(\omega)}\right]_{\omega=0} = \frac{1}{(2\pi)^2 g^{\mathrm{D}}_{JT}(0)}\int_{\mu}^{\infty} \mathrm{d}\omega' \frac{1}{\omega'^2 k'^3 v^2(k')} [\sigma^{\mathrm{D}}_{JT}(\omega') - \sum_{J'T'} A^{\mathrm{D}}_{JJ'} B_{TT'} \sigma^{\mathrm{D}}_{J'T'}(\omega')]. \quad (43)$$

From eqs. (41) and (42) we obtain the following effective range formulae:

$$\mathrm{Re}\cot \eta^{\mathrm{D}}_{JT}(\omega) \approx \frac{1}{k^5 v^2(k) g^{\mathrm{D}}_{JT}(0)} (1 - r^{\mathrm{D}}_{JT}\omega). \quad (44)$$

Formulae (40) and (43) written down explicitly have the forms (we write $2J2T$ instead of JT)

$$\begin{aligned} g^{\mathrm{D}}_{31}(0) &= 16I_{31} - 4I_{33} - 6I_{51} + 24I_{53}, \\ g^{\mathrm{D}}_{33}(0) &= -2I_{31} + 14I_{33} + 12I_{51} + 6I_{53}, \\ g^{\mathrm{D}}_{51}(0) &= -4I_{31} + 16I_{33} + 14I_{51} + 4I_{53}, \\ g^{\mathrm{D}}_{53}(0) &= 8I_{31} + 4I_{33} + 2I_{51} + 16I_{53} > 0 \end{aligned} \quad (45)$$

and

$$\begin{aligned}
r_{31}^{\mathrm{D}} &= \frac{1}{g_{31}^{\mathrm{D}}(0)}\,(\ \ 14J_{31}+\ 4J_{33}+\ 6J_{51}-24J_{53}),\\
r_{33}^{\mathrm{D}} &= \frac{1}{g_{33}^{\mathrm{D}}(0)}\,(\ \ \ 2J_{31}+16J_{33}-12J_{51}-\ 6J_{53}),\\
r_{51}^{\mathrm{D}} &= \frac{1}{g_{51}^{\mathrm{D}}(0)}\,(\ \ \ 4J_{31}-16J_{33}+16J_{51}-\ 4J_{53}),\\
r_{53}^{\mathrm{D}} &= \frac{1}{g_{53}^{\mathrm{D}}(0)}\,(\ -8J_{31}-\ 4J_{33}-\ 2J_{51}+14J_{53}).
\end{aligned} \tag{46}$$

Here we use the notation

$$\begin{aligned}
I_{JT} &= \tfrac{1}{15}\frac{1}{(2\pi)^2}\int_{\mu}^{\infty}\mathrm{d}\omega\,\frac{\sigma_{JT}^{\mathrm{D}}(\omega)}{\omega k^3 v^2(k)} > 0,\\
J_{JT} &= \tfrac{1}{15}\frac{1}{(2\pi)^2}\int_{\mu}^{\infty}\mathrm{d}\omega\,\frac{\sigma_{JT}^{\mathrm{D}}(\omega)}{\omega^2 k^3 v^2(k)} > 0.
\end{aligned} \tag{47}$$

From eqs. (46) it follows that

$$g_{33}^{\mathrm{D}}(0)r_{33}^{\mathrm{D}} = -5g_{31}^{\mathrm{D}}(0)r_{31}^{\mathrm{D}}-9g_{53}^{\mathrm{D}}(0)r_{53}^{\mathrm{D}},\quad g_{51}^{\mathrm{D}}(0)r_{51}^{\mathrm{D}} = 6g_{31}^{\mathrm{D}}(0)r_{31}^{\mathrm{D}}+10g_{53}^{\mathrm{D}}(0)r_{53}^{\mathrm{D}}. \tag{48}$$

It is probable from the experimental point of view that the observed high energy peaks are due to $\mathrm{D}_{\frac{3}{2},\frac{1}{2}}$, $\mathrm{D}_{\frac{1}{2},\frac{1}{2}}$ and $\mathrm{D}_{\frac{3}{2},\frac{3}{2}}$ resonant states. In this case the integrals I_{33} and J_{33} would be much smaller than the remaining integrals, which would contain the resonance cross sections. On the other hand, it seems from the present, rather scarce, experimental data that all resonance integrals I as well as J should be nearly of the same order of magnitude. Then, it would follow from eqs. (45) that all $g_{JT}^{\mathrm{D}}(0)$ would be positive. In such a case it would be deduced from eq. (48) that r_{33}^{D} and r_{51}^{D} would be negative and positive respectively, if only r_{31}^{D} and r_{53}^{D} given by eq. (46) were positive. But the last possibility is not in contradiction with the present experimental data. More quantitative conclusions could be drawn, if results of a phase shift analysis were available.

We can see from this discussion that the case

$$r_{31}^{\mathrm{D}} > 0,\quad r_{33}^{\mathrm{D}} < 0,\quad r_{51}^{\mathrm{D}} > 0,\quad r_{53}^{\mathrm{D}} > 0 \tag{49}$$

is rather probable. In this case we might conclude that the theory would predict resonances in $\mathrm{D}_{\frac{3}{2},\frac{1}{2}}$, $\mathrm{D}_{\frac{1}{2},\frac{1}{2}}$, $\mathrm{D}_{\frac{3}{2},\frac{3}{2}}$ states (beside the well known resonance in the $\mathrm{P}_{\frac{3}{2},\frac{3}{2}}$ state).

It would be interesting to discuss the problem of these isobars of the nucleon also from the side of an approximate diagonalization of the Hamiltonian (5).

References

1) Piccioni, Report at the 1958 Annual International Conference on High Energy Physics at CERN (Geneva), Proceedings edited by B. Ferretti (1958)
2) Pontecorvo, Report at the 1959 Annual International Conference on High Energy Physics (Kiev)
3) G. F. Chew and F. E. Low, Phys. Rev. **101** (1956) 1570
4) G. E. Chew, M. L. Goldberger, F. E. Low and Y. Nambu, Phys. Rev. **106** (1957) 1337
5) W. Pauli and S. M. Dancoff, Phys. Rev. **62** (1942) 85
6) W. Królikowski, Bull. Acad. Polon. Sci. **6** (1958) 413
7) F. J. Dyson, Phys. Rev. **99** (1955) 1057;
G. Takeda, Phys. Rev. **100** (1955) 440;
A. N. Mitra, Phys. Rev. **108** (1957) 1083;
L. S. Rodberg, Phys. Rev. Lett. **3** (1959) 58
8) Wan-Non Wong and M. Ross, Phys. Rev. Lett. **3** (1959) 398
9) R. Oehme, Phys. Rev. **102** (1956) 1174

1.C:
1.D.1

Nuclear Physics **17** (1960) 477—485; © *North-Holland Publishing Co., Amsterdam*

Not to be reproduced by photoprint or microfilm without written permission from the publisher

SHORT-RANGE CORRELATIONS IN NUCLEAR WAVE FUNCTIONS

F. COESTER

Department of Physics and Astronomy, State University of Iowa, Iowa City, Iowa

and

H. KÜMMEL

Max Planck Institut für Chemie, Mainz, Germany †

Received 18 February 1960

Abstract: We assume that the ground state wave functions of a closed shell nucleus is approximated by a Slater determinant in the restricted region of configuration space where all internucleon distances are larger than a certain "healing distance". The remainder of the wave function is given in terms of a series of cluster functions. The overlap integral between the correct wave functions and the Slater determinant is small and depends on the higher cluster functions in a complicated manner. Nevertheless we can show that the one- and two-body density matrices are well approximated by expressions involving only the single-particle wave functions and the two-body cluster functions. The Schrödinger equation yields a coupled set of equations which determine the cluster functions as well as the single-particle wave functions.

1. Introduction

In any attempt to relate the nuclear shell model to the many-body problem with two-body forces the question arises whether the shell-model state Φ approximates the correct state vector Ψ in some sense or whether there is merely a certain correspondence [1]) between them. The overlap integral between the two wave functions is known to be small for large nuclei [2–4]). On the other hand there are good reasons to believe that the two functions approximate each other if all particles are sufficiently separated [5]). It is the purpose of this note to exploit the mathematical consequences of such a relation, and discuss a formalism which allows us to calculate corrections to the shell model wave functions by perturbation theory for separated particles while using different approximations where two or several particles are close to each other. The results of such a procedure must, of course, be related to the well-known selective summations of the perturbation series [2, 6–10]). We restrict ourselves to ground states of closed shell nuclei where we expect no long range correlations in the wave functions and non-degenerate perturbation theory is applicable. In the middle of the shell one must account for the well known collective features of the wave function as well as for the short range correlations. This problem will be dealt with a later paper. Nuclear matter is not an idealization of a closed shell nucleus.

† Work supported in part by the U. S. Atomic Energy Commission.

It corresponds more closely to a large nucleus in the middle of the shell. Pairing of nucleons near the Fermi surface gives rise to long range correlations which can be ignored, however, in calculating bulk effects such as the binding energy per particle.

2. The Structure of the Wave Functions

It will be useful for the following to review at the outset certain well known features of the perturbation theory for non-degenerate bound states. The Rayleigh-Schrödinger perturbation series for the state Ψ and the energy shift ΔE can be obtained by iterating the following exact equations:

$$Z^{-\frac{1}{2}}\Psi = \Phi + (1-\Lambda)(\mathscr{E}_0 - H_0)^{-1}(W-\Delta E)Z^{-\frac{1}{2}}\Psi, \tag{1}$$

$$\Delta E = (\Phi, WZ^{-\frac{1}{2}}\Psi), \tag{2}$$

$$Z = (\Phi, \Psi)^2, \tag{3}$$

where Φ is the zero order state satisfying the Schrödinger equation $(H_0-\mathscr{E}_0)\Phi = 0$ and $(\Phi, \Phi) = 1$. The projection operator Λ projects into the state Φ. Eqs. (1) and (2) follow from the Schrödinger equation

$$(H+W)\Psi = (\mathscr{E}_0+\Delta E)\Psi \tag{4}$$

and the coefficient Z is defined by eq. (3). Eqs. (1) and (2) yield a perturbation series for $Z^{-\frac{1}{2}}\Psi$ and for ΔE. The state vector Ψ itself can then be obtained from the condition $(\Psi, \Psi) = 1$.

We are interested in the case when H_0 is a shell model Hamiltonian and Φ is a shell model state, i.e. H_0 is additive in the nucleons and Φ is represented by a Slater determinant of single particle functions $\varphi_\nu(q)$. The letter q stands for the nucleon coordinates including charge- and spin coordinates. W is a two-body interaction. The state vector Ψ can then be expressed in the form

$$\Psi = Z^{\frac{1}{2}}\mathsf{F}\Phi, \tag{5}$$

where

$$\mathsf{F} = 1 + \sum_{k=1}^{A} \mathsf{F}_k, \tag{6}$$

with

$$\mathsf{F}_k = (k!)^{-2}\int dq_1 \ldots \int dq_k \sum_{\nu_1 \ldots \nu_k} c^\dagger(q_k) \ldots c^\dagger(q_1) (q_1 \ldots q_k|F_k|\nu_k \ldots \nu_1)c(\nu_1) \ldots c(\nu_k). \tag{7}$$

The operators $c(q)$ and $c^\dagger(q)$ respectively annihilate and create nucleons at the point q. They satisfy the usual commutation relations

$$\{c(q), c^\dagger(q')\} = \delta(q, q'). \tag{8}$$

The operator $c(\nu)$ destroys a nucleon in the state ν:

$$c(\nu) = \int dq\, c(q)\varphi_\nu^*(q). \tag{9}$$

The operator F_k by definition excites k nucleons from the zero order configuration into a superposition of excited configurations. The functions F_k therefore satisfy the orthogonality relation

$$\int dq_1 \varphi_\nu^*(q_1)(q_1 \ldots q_k|F_k|\nu_k \ldots \nu_1) = 0, \tag{10}$$

where $\varphi_\nu(q)$ is any of the A single particle functions which occur in Φ.

One might expect that for a weak interaction W the state Φ approximates Ψ in the norm. In other words one might expect

$$||\Psi - \Phi||^2 = 2(1 - Z^{\frac{1}{2}}) \ll 1. \tag{11}$$

Actually this is not the case for large systems [2-4]). For a Fermi gas of fixed density and a given interaction the constant Z tends to zero with increasing particle number A. This can easily be seen by examining the expression

$$Z^{-1} = 1 + \sum_k (k!)^{-2} \int dq_1 \ldots \int dq_k \sum_{\nu_1 \ldots \nu_k} |(q_1 \ldots q_k)|F_k|\nu_k \ldots \nu_1)|^2. \tag{12}$$

The functions F_k are antisymmetrized products of functions $(q_1 \ldots q_l|S_l|\nu_l \ldots \nu_1)$ such that the perturbation series for the S_l consists only of linked diagrams [12]) †. These functions have the property

$$(l!)^{-2} \int dq_1 \ldots \int dq_l \sum_{\nu_1 \ldots \nu_l} |(q_1 \ldots q_l|S_l|\nu_l \ldots \nu_1)|^2 \lesssim \eta^{l-1} A, \tag{13}$$

where η is some constant independent of A. In a Fermi gas with weak interaction we have $\eta \approx g^2(k_F r_0)^3$ where g is a "coupling constant" measuring the strength of the interaction and the Fermi momentum k_F is the reciprocal range of the linked functions. Similarly all integrals over linked functions in eq. (12) are proportional to A. The relation between the F_k and the S_l is most easily stated in operator form [12]):

$$\mathsf{F} = e^{\mathsf{S}}, \tag{14}$$

with

$$\mathsf{S} = \sum_{l=1}^{A} \mathsf{S}_l. \tag{15}$$

The operator S_l is related to the function S_l by a relation of the form (7). The functions S_l satisfy the orthogonality relation (10). For the right hand side of

† This expansion of the functions F in antisymmetrized products is analogous to the Ursell expansion of the density matrix. See ref. [11]).

eq. (12) one finds the following A-dependence of Z:

$$Z^{-1} = 1 + \sum_{p=2}^{A} \sum_{0<n\leq A/p} \frac{1}{n!} (C_p A)^n. \tag{16}$$

Only integrals over $S_{p'}$ with $p' \leqq p$ contribute to the coefficient C_p. For weak interactions we have $epC_p \ll 1$ and $\sum_p C_p$ converges to a constant C. Hence

$$Z \cong \mathrm{e}^{-CA}. \tag{17}$$

In general we may say that the parameter η defined by eq. (13) measures the strength as well as the range of the correlations in the wave function.

The following discussions are based on the assumption $\eta \ll 1$. This assumption may be verified in perturbation theory for reasonably weak interactions. It can be expected, however, to hold also where a perturbation expansion of the S_l is not valid. For hard core potentials the S-functions must cancel the products of single particle functions at the core surface and drop off with increasing separation of the particles. In addition to the assumption $\eta \ll 1$ we shall assume that the largest eigenvalue of the matrix

$$(l!)^{-1} \int \mathrm{d}q_1 \ldots \int \mathrm{d}q_l (q_1 \ldots q_l | S_l | \nu_l \ldots \nu_1)^* (q_1 \ldots q_l | S_l | \nu_l' \ldots \nu_1') \tag{18}$$

is of order η^{l-1} or smaller. If these assumptions are valid one can always make the integral

$$\int \mathrm{d}q \sum_{\nu} |(q|S_1|\nu)|^2$$

as small as desired by an appropriate choice of the single particle functions. Consider for instance

$$\Psi = Z_0^{\frac{1}{2}} \mathrm{e}^{S^{(0)}} \Phi^{(0)}, \tag{19}$$

with $S_1^{(0)} \neq 0$ and define the Slater determinant $\Phi^{(1)}$ by

$$\mathrm{e}^{S_1^{(0)}} \Phi^{(0)} = \text{const.}\, \Phi^{(1)}, \quad (\Phi^{(1)}, \Phi^{(1)}) = 1. \tag{20}$$

Like any other state, the state $\mathrm{e}^{S^{(0)} - S_1^{(0)}} \Phi^{(1)}$ may be represented in the form

$$\mathrm{e}^{S^{(0)} - S_1^{(0)}} \Phi^{(1)} = \text{const.}\, \mathrm{e}^{S^{(1)}} \Phi^{(1)}. \tag{21}$$

From this equation one can calculate $S_k^{(1)}$ in terms of the functions $S_p^{(0)}$ by expansion in powers of η. In zeroth order we have

$$(q_1|S_1^{(1)}|q_2) = \int \mathrm{d}q'_1 \int \mathrm{d}q'_2 \int \mathrm{d}q_3 \int \mathrm{d}q'_3 (q_1|1 - A^{(1)}|q'_1) \times (q'_3|A^{(1)}|q_3)(q'_2|A^{(1)}|q_2)(q'_1 q_3|S_2^{(0)}|q'_3 q'_2) \tag{22}$$

and

$$(q_1 q_2|S_2^{(1)}|q_3 q_4) = \int \mathrm{d}q'_1 \ldots \int \mathrm{d}q'_4 (q_1|1 - A^{(1)}|q'_1) \times (q_2|1 - A^{(1)}|q'_2)(q'_1 q'_2|S_2^{(0)}|q'_3 q'_4)(q'_3|A^{(1)}|q_3)(q'_4|A^{(1)}|q_4), \tag{23}$$

where

$$(q_1 q_2|S_2|q_3 q_4) \equiv \sum_{\nu_1 \nu_2} (q_1 q_2|S_2|\nu_2 \nu_1)\varphi^*_{\nu_2}(q_3)\varphi^*_{\nu_1}(q_4), \tag{24}$$

and

$$(q'|\Lambda^{(1)}|q) \equiv \sum_{\nu} \varphi_\nu{}^{(1)}(q')\varphi_\nu{}^{(1)*}(q). \tag{25}$$

If $S_1{}^{(1)}$ is not small enough the procedure can be repeated defining $\Phi^{(2)}$ by

$$e^{S_1{}^{(1)}}\Phi^{(1)} = \text{const.}\,\Phi^{(2)}. \tag{26}$$

In the following we shall therefore assume $S_1 = 0$. This assumption governs the choice of the single particle wave functions. It is a generalization of the Hartree-Fock condition.

In general our wave function $Z^{-\frac{1}{2}}\Psi$ is well approximated by the Slater determinant Φ if all nucleons are farther apart than a "healing distance" [5]) h which may be defined by

$$h \equiv \left(\eta\rho^{-1}\frac{3}{4\pi}\right)^{\frac{1}{3}}, \tag{27}$$

where ρ is the nucleon density. For smaller distances the corrections described by the cluster functions S_k may be large. Wave functions with such a structure have been widely used [13–18]). The "superposition wave function" of the form

$$\begin{aligned}\Psi_f(q_1 \ldots q_A) = \mathscr{A}_\nu[&(1+f_{\nu_1\nu_2}(q_1 q_2))(1+f_{\nu_1\nu_3}(q_1 q_3)) \ldots \\ &\times(1+f_{\nu_2\nu_3}(q_2 q_3)) \ldots (1+f_{\nu_{A-1}\nu_A}(q_{A-1}, q_A))\varphi_{\nu_1}(q_1) \ldots \varphi_{\nu_A}(q_A)]\end{aligned} \tag{28}$$

has these properties if the quantities f vanish outside the healing distance. The symbol $\mathscr{A}_\nu$ indicates antisymmetrization with respect to ν. It is therefore of interest to establish the relation between the functions f and our cluster functions S_k. These relations follow in a straightforward manner from eq. (28) and

$$\Psi_f = (\Phi, \Psi_f)e^{S_f}\Phi. \tag{29}$$

Simple explicit expressions are obtained by expansion in powers of η. The zero order term in S_{f1} vanishes. In first order we have

$$(q|S_{f1}^{(1)}|\nu) = \sum_{\nu'} \int dq' \int dq''(q|1-\Lambda|q')\varphi^*_{\nu'}(q'')\mathscr{A}_\nu f_{\nu\nu'}(q', q'')\varphi_\nu(q')\varphi_{\nu'}(q'') \tag{30}$$

where Λ is the projection into the occupied single particle states:

$$(q|\Lambda|q') = \sum_{\nu} \varphi_\nu(q)\varphi_\nu{}^*(q'). \tag{31}$$

Most authors [17–13]) assume only one function f independent of the single particle states. De Shalit and Weisskopf [18]) have state-dependent functions f

which satisfy the orthogonality relation

$$\int \mathrm{d}q' \varphi_\nu^*(q') f_{\nu_1\nu_2}(q', q)\varphi_{\nu_1}(q')\varphi_{\nu_2}(q) = 0. \tag{32}$$

In that case $S_{f1}^{(1)}$ vanishes and the first non-vanishing contribution to S_{f1} is of order η^2. The zero order term in S_{f2} is, as one should expect,

$$\begin{aligned}(q_1q_2|S_{f2}^{(0)}|\nu_2\nu_1) \\ = \int \mathrm{d}q'_1 \int \mathrm{d}q'_2 (q_1|1-\Lambda|q'_1)(q_2|1-\Lambda|q'_2)\mathscr{A}_\nu f_{\nu_1\nu_2}(q'_1q'_2)\varphi_{\nu_1}(q'_1)\varphi_{\nu_2}(q'_2)\end{aligned} \tag{33}$$

and to first order in η one finds

$$\begin{aligned}(q_1q_2|S_{f2}^{(1)}|\nu_2\nu_1) = \int \mathrm{d}q'_3 \sum_{\nu_3} \varphi_{\nu_3}^*(q'_3) \int \mathrm{d}q'_1 \int \mathrm{d}q'_2 (q_1|1-\Lambda|q'_1)(q_2|1-\Lambda|q'_2) \\ \times \mathscr{A}_\nu \{ f_{\nu_1\nu_2}(q'_1q'_3) f_{\nu_1\nu_3}(q'_1q'_2) f_{\nu_2\nu_3}(q'_2q'_3) + f_{\nu_1\nu_3}(q'_1q'_3) f_{\nu_2\nu_3}(q'_2q'_3) \\ + f_{\nu_1\nu_3}(q'_1q'_2) f_{\nu_1\nu_3}(q'_1q'_3) + f_{\nu_2\nu_3}(q'_2q'_3) f_{\nu_1\nu_3}(q'_1q'_2) \} \\ \times \varphi_{\nu_1}(q'_1)\varphi_{\nu_2}(q'_2)\varphi_{\nu_3}(q'_3).\end{aligned} \tag{34}$$

The last two terms between braces vanish if the orthogonality condition (32) is satisfied.

3. The Schrödinger Equation

In our representation the Schrödinger equation takes the form

$$H\mathrm{e}^{\mathsf{S}}\Phi = E\mathrm{e}^{\mathsf{S}}\Phi. \tag{35}$$

There follows an expression for the binding energy E:

$$E = (\Phi, \mathrm{e}^{-\mathsf{S}} H \mathrm{e}^{\mathsf{S}}\Phi) = (\Phi, (H+[H, \mathsf{S}_2])\Phi). \tag{36}$$

In the last step it is assumed that $\mathsf{S}_1 = 0$ and H contains only two body forces. There follows further from eq. (35) a set of coupled equations for the cluster functions:

$$(c(\nu_1) \ldots c(\nu_k)\Phi, a(q_1) \ldots a(q_k)\mathrm{e}^{-\mathsf{S}} H \mathrm{e}^{\mathsf{S}}\Phi) = 0, \tag{37}$$

where

$$a(q) = \int \mathrm{d}q' (q|1-\Lambda|q')c(q').$$

The perturbation solution of these equations for $H = H_0+W$ and $H_0\Phi = \mathscr{E}_0\Phi$ has been discussed elsewhere [12]). Even if this straightforward perturbation theory is not applicable expansion in powers of η provides a basis for a systematic approximation. In the lowest approximation the equations $k = 2$ and $k = 1$ are independent of S_3 and higher cluster functions. A hard core repulsion presents no serious difficulty provided the core radius is small compared to the average distance between particles. The equations $k = 2$ and $k = 1$ may be used with

the condition $S_1 = 0$ to determine the single particle functions φ_ν and the two-body cluster functions S_2. The equation is essentially the Bethe-Goldstone equation [19]). The Bethe-Goldstone wave functions are in our notation

$$(q_1 q_2|\psi|\nu_2\nu_1) = \mathscr{A}_{\nu}\varphi_{\nu_1}(q_1)\varphi_{\nu_2}(q_2)+(q_1 q_2|S_2|\nu_2\nu_1). \tag{38}$$

The equations (35) are equivalent to the system of equations for the functions

$$(q_1 \ldots q_k|\psi_k|\nu_k \ldots \nu_1) = (c(\nu_k) \ldots c(\nu_1)\Phi,\ c(q_1) \ldots c(q_k)Z^{-\frac{1}{2}}\Psi), \tag{39}$$

which have been discussed by Brenig [20]). The problem of finding approximate solutions for eqs. (37) will be treated in detail in a subsequent article.

4. The Density Matrices

While the energy formula (36) involves only S_2, the knowledge of higher cluster functions is necessary according to eq. (16) to obtain the normalized wave function. One might therefore suspect that our approximations are capable of giving approximate expressions for the energy only and not for the expectation values of other operators. Nevertheless we propose to show that approximate expressions for the density matrices can be obtained by expansion in powers of η.

The one-particle density matrix is defined by

$$\begin{aligned}(q|\rho|q') &= \int \mathrm{d}q_2 \ldots \int \mathrm{d}q_A\, \Psi(q_1 q_2 \ldots q_A)\Psi^*(q'_1 q_2 \ldots q_A)\\ &= A^{-1}(\Phi, \mathrm{e}^{S\dagger}\mathrm{e}^{S}\Phi)^{-1}(\Phi, \mathrm{e}^{S\dagger}c^\dagger(q')c(q)\mathrm{e}^{S}\Phi).\end{aligned} \tag{40}$$

In the evaluation of the ratio (40) the denominator will cancel out and a good approximation can be obtained which involves S_2 only.

It is convenient to define operators b by

$$\begin{aligned}b^\dagger(q) &= \int \mathrm{d}q'(q|\Lambda|q')c(q'),\\ b^\dagger(\nu) &= c(\nu).\end{aligned} \tag{41}$$

where Λ is the projection operator (31). The operator $b^\dagger(\nu)$ creates a "hole" in the state ν. To evaluate expression (40) we replace $c(q)$ everywhere by $a(q)+b^\dagger(q)$ and shift all annihilation operators to the right and creation operators to the left. The relevant relations are

$$c^\dagger(q')c(q) = (q|\Lambda|q')+a^\dagger(q')b^\dagger(q)+b(q')a(q)+a^\dagger(q')a(q)-b^\dagger(q)b(q') \tag{42}$$

and

$$a(q)\mathrm{e}^{S}\Phi = [a(q), S]\mathrm{e}^{S}\Phi, \quad b(q)\mathrm{e}^{S}\Phi = [b(q), S]\mathrm{e}^{S}\Phi. \tag{43}$$

There follows

$$\begin{aligned}(q|\rho|q') &= A^{-1}(q|\Lambda|q')\\ &+A^{-1}(\Phi, e^{S\dagger}e^{S}\Phi)^{-1}(\Phi, e^{S\dagger}([a(q'), S]^{\dagger}\{[b(q), S]^{\dagger}+[a(q), S]\}\\ &-\{[a(q), S]+[b(q), S]^{\dagger}\}[b(q'), S]\\ &+\{b(q'), [a(q)S]\}+\{[a(q'), S], b(q)\}^{\dagger})e^{S}\Phi).\end{aligned} \tag{44}$$

Re-ordering and successive application of eqs. (43) produces multiple integrals over linked products of the cluster functions S_k. The largest correlation correction to the density matrix $(q|\rho|q')$ come from terms which are bilinear in S_2. Let $(q|g_1|q')$ be defined by

$$(q|\rho|q') = A^{-1}((q|\Lambda|q')+(q|g_1|q')). \tag{45}$$

We find in first approximation for g_1

$$\begin{aligned}(q|g_1|q') &= \tfrac{1}{2}\int dq'' \sum_{\nu_1\nu_2}(qq''|S_2|\nu_2\nu_1)(q'q''|S_2|\nu_2\nu_1)^*\\ &-\tfrac{1}{2}\int dq_1\int dq_2 \sum_{\nu}(q_1q_2|S_2|\nu q')(q_1q_2|S_2|\nu q)^*,\end{aligned} \tag{46}$$

where

$$(q_1q_2|S_2|\nu q) \equiv \sum_{\nu'}(q_1q_2|S_2|\nu\nu')\varphi^*_{\nu'}(q). \tag{47}$$

We see that the order of magnitude of the correction to the one-particle density matrix may be measured by the integral

$$\int dq\int dq'|(q|g_1|q')|^2 \approx \eta^2 A. \tag{48}$$

Neglected terms contribute only higher powers of η. For the zero order term the corresponding expression is

$$\int dq\int dq'|(q|\Lambda|q)|^2 = \int dq(q|\Lambda|q) = A. \tag{49}$$

The same techniques may be used to calculate the two-particle density matrix:

$$\begin{aligned}(q_1q_2|\rho|q'_2q'_1) &= \int dq_3\ldots\int dq_A \Psi(q_1q_2\ldots q_A)\Psi^*(q'_1q'_2q_3\ldots q_A)\\ &= \frac{1}{A(A-1)}(\Phi, e^{S\dagger}e^{S}\Phi)^{-1}(\Phi, e^{S\dagger}c^{\dagger}(q'_2)c^{\dagger}(q'_1)c(q_1)c(q_2)e^{S}\Phi).\end{aligned} \tag{50}$$

Upon re-ordering the creation and annihilation operators we have

$$\begin{aligned}(q_1q_2|\rho|q'_2q'_1) = \frac{1}{A(A-1)}\{&\mathscr{A}(q_1|\Lambda|q'_1)(q_2|\Lambda|q'_2)\\ &+\mathscr{A}(q_1|\Lambda|q'_1)(q_2|g_1|q'_2)+(q_1q_2|g_2|q'_2q'_1)\}.\end{aligned} \tag{51}$$

The definition of g_2 is implied in this equation, neglecting all contributions involving higher cluster functions and higher powers of S_2 we find for g_2:

$$\begin{aligned}(q_1q_2|g_2|q'_2q'_1) = {} & (q_1q_2|S_2|q'_2q'_1)+(q'_1q'_2|S_2|q_2q_1)^* \\ & +\tfrac{1}{2}\int dq' \int dq''(q'q''|S_2|q'_2q'_1)(q'q''|S_2|q_2q_1)^* \\ & +\tfrac{1}{2}\sum_{\nu'\nu''}(q_1q_2|S_2|\nu''\nu')(q'_1q'_2|S_2|\nu''\nu')^* \\ & -\mathscr{A}\int dq \sum_{\nu}(qq_1|S_2|q'_2\nu)(qq'_1|S_2|q_2\nu)^*,\end{aligned} \tag{52}$$

where

$$(q_1q_2|S_2|q'_2q'_1) \equiv \sum_{\nu_2\nu_1}(q_1q_2|S_2|\nu_2\nu_1)\varphi^*_{\nu_2}(q'_2)\varphi^*_{\nu_1}(q_1). \tag{53}$$

The first two terms in eq. (50) give a contribution of order ηA to

$$\tfrac{1}{4}\int dq_1 \int dq_2 \int dq'_1 \int dq'_2 |(q_1q_2|g_2|q'_2q'_1)|^2. \tag{54}$$

The remaining terms give contributions of order $\eta^2 A$. The approximate density matrices (45) and (51) yield respectively approximations for the expectation values of one- and two-particle operators. Whether or not higher order correction terms are indeed negligible depends on the operators involved and must be examined in each case.

References

1) R. J. Eden, and N. C. Francis, Phys. Rev. **97** (1955) 1565
2) H. S. Bethe, Phys. Rev. **103** (1956) 1353; see in particular Sec. VI.
3) N. M. Hugenholtz, Physica **23** (1957) 481, 533
4) J. Hubbard, Proc. Roy. Soc. **240** (1957) 539
5) L. C. Gomes, J. D. Walecka and V. I. Weisskopf, Ann. of Phys. **3** (1958) 241
6) J. Goldstone, Proc. Roy. Soc. **239** (1957) 26
7) K. M. Watson, Phys. Rev. **103** (1956) 489
8) L. S. Rodberg, Ann. Phys. **2** (1957) 199
9) H. Kümmel, Nuovo Cim. **23** (1957) 1
10) W. Tobocman, Phys. Rev. **107** (1957) 203
11) U. P. Ursell, Proc. Camb. Phil. Soc. **23** (1927) 685;
    J. E. Mayer, J. Chem. Phys. **5** (1932) 67;
    B. Kahn and G. E. Uhlenbeck, Physica **5** (1938) 399
12) F. Coester, Nuclear Physics **7** (1958) 421
13) R. Jastrow, Proceedings of the Many-Body Symposium, Stevens Institute of Technology (1957)
14) F. Iwamoto and M. Yamada, Progm. Theor. Phys. **17** (1951) 543; 18 (1957) 345
15) V. J. Emery, Nuclear Physics **6** (1958) 585
16) G. Hartogh and H. A. Tolhoek, Physica **24** (1958) 721
17) J. W. Clark and E. Feenberg, Phys. Rev. **113** (1959) 388
18) A. De Shalit and V. F. Weisskopf, Ann. of Phys. **5** (1958) 282
19) H. A. Bethe and J. Goldstone, Proc. Roy. Soc. A **238** (1957) 551
20) W. Brenig, Nuclear Physics **4** (1957) 363

8.C

Nuclear Physics 17 (1960) 486—498; © *North-Holland Publishing Co., Amsterdam*

Not to be reproduced by photoprint or microfilm without written permission from the publisher

SOME REMARKS ON FIELDS WITH NEGATIVE PROPAGATORS IN QUANTUM FIELD THEORY

HAJIME SHIMODAIRA †

Dublin Institute for Advanced Studies

Received 29 February 1960

Abstract: The question of introducing a field ϕ which belongs to Hilbert space II is investitaged within the framework of quantum field theory. For this purpose a special model of the interaction Lagrangian, viz. $\psi^*\psi(\Box-\mu^2)\phi$, where ψ^*, ψ are ordinary field operators and μ is the mass of the ϕ field, is proposed, and we find that this leads to a self-consistent theory.

An extension that would be effective in eliminating divergences from the theory is also studied and it is shown that such an extension necessarily leads to the violation of the causality of the S-matrix. Since the only restriction is that ϕ be contained linearly in the interaction Lagrangian, this model serves to clarify the relation between the indefinite metric and the non-local interaction.

1. Introduction

It has been suggested that fields †† with propagators of negative sign might play an effective role in removing divergences from the theory of quantum fields [1–3]). From Lehmann's investigations such fields seem necessary in theory, in order to have sufficient inverse powers of the momentum in the propagator.

Though many attempts have been made to solve this problem, we have no satisfactory theory so far. The main reason for this is that, if we introduce an unphysical field, it is difficult to explain its invisible character or, in other words, to make the S-matrix unitary for the physical processes.

There have been two attempts to overcome this difficulty. One was proposed by Pauli and Villars [2]) using fields with negative propagators and letting the mass become infinite after calculation. The other was proposed by Bogoliubov *et al.* recently; this applied the projection operator Q to physical states and constructed the unitary S-matrix from the hermitian K-matrix $\tilde{K} = QKQ$.

It seems that these papers depend essentially on an artificial procedure. As long as we remain at this level, it is not clear what part of the present theory should suffer change, since these procedures have nothing to do with field theory.

It is, then, desirable to make a similar attempt in the framework of quantum field theory. In this paper we shall treat charged scalar fields ψ, ψ^* interacting

† On leave of absence from the Department of Physics, Nagoya University, Nagoya, Japan.

†† In this paper we shall call them unphysical fields. These field operators belong to Hilbert space II.

with neutral scalar fields ϕ, ϕ', where ϕ, ϕ' denote unphysical and ordinary fields respectively. We shall also postulate that the interaction Lagrangian contains the ϕ field only linearly, but with derivatives of any order.

Then we have generally

$$
\begin{aligned}
&L = \int [L_0(x) + L_1(x) + L_1'(x)]\mathrm{d}^4x, \\
&L_0(x) = -[\partial_\mu \hat{\psi}^* \partial_\mu \hat{\psi} + \kappa^2 \hat{\psi}^* \hat{\psi}] + \tfrac{1}{2}[\partial_\mu \hat{\phi} \partial_\mu \hat{\phi} + \mu^2 \hat{\phi} \hat{\phi}] - \tfrac{1}{2}[\partial_\mu \hat{\phi}' \partial_\mu \hat{\phi}' + \mu'^2 \hat{\phi}' \hat{\phi}'], \\
&L_1(x) = g \sum_i A_i(\partial) \hat{\psi}^* B_i(\partial) \hat{\psi} C_i(\partial) \hat{\phi}, \qquad (1) \\
&L'_1(x) = g'(\hat{\psi}^* \hat{\psi} \hat{\phi}'),
\end{aligned}
$$

where $A_i(\partial)$, $B_i(\partial)$ and $C_i(\partial)$ are any functions of derivative operators and $\hat{\psi}$, $\hat{\phi}$ are field operators in the Heisenberg representation. The sign of the second term in the free Lagrangian means that this field obeys the commutation relation with negative sign. We can obtain the S-matrix in the interaction representation by using the Yang-Feldmann method. To first order in g, we find

$$
S^{(1)} = \sum_n \frac{(-i)^n}{n!} \int \ldots \int \mathrm{d}^4x_1 \ldots \mathrm{d}^4x_n \mathrm{d}^4x P[\psi^* \psi \phi'(x_1), \ldots, \psi^* \psi \phi'(x_n), g \sum_i A_i(\partial) \psi^* B_i(\partial) \psi C_i(\partial) \phi(x)]. \qquad (2)
$$

As is easily seen, eq. (2) contains only one ϕ field, and it yields transitions from a physical state to an unphysical state unless

$$
g \sum_i A_i(\partial) \psi^* B_i(\partial) \psi C_i(\partial) \phi = 0. \qquad (3)
$$

Among the several possible ways of satisfying eq. (3), we shall choose †

$$
C(\partial) = f(\partial)(\Box - \mu^2). \qquad (4)
$$

If we substitute eq. (4) in eq. (1), it is expected that the ϕ field will not appear in initial and final states, but for intermediate states it gives some contribution because the energy-momentum relation of the free particle is satisfied only at $t \to \pm \infty$.

In section 2 we treat the simplest case $f(\partial) = 1$, $A(\partial) = B(\partial) = 1$, and it will be shown that unphysical processes never occur in this interaction. It will also be shown that this special model reduces to a non-linear interaction between the ψ fields, but, owing to the many derivatives, it is of no value in removing the divergence difficulty. If we want to go to cases in which ϕ is effective in eliminating the divergence which arises from the ϕ' field, we must take $f(\partial)$ in eq. (4) to be the second inverse power of ∂. This calculation is

† Refer to the argument given in section 5.

carried out in section 4, and we find that such an extension to the non-local case necessarily leads to the violation of either unitarity or causality. We note that the similar theory of Bogoliubov *et al.* [3]) is contained as a special case.

Section 3 is devoted to the examination of those terms in the S-matrix that give rise to difficulty, and it is shown there that the usual construction of the S-matrix in the P*-product form [5, 6]) is not correct in general, and that the additional terms violate causality in the non-local case.

2. Special model

2.1. THE CONSTRUCTION OF THE HAMILTONIAN

As the $L'_{\mathrm{I}}(x)$ in eq. (1) does not give rise to any difficulty on quantization, it is enough to study the rest of the Lagrangian. In this section we shall study the simple case of eq. (4), where we have the Hamiltonian in compact form:

$$\hat{L}_{\mathrm{I}}(x) = g\{\partial_\mu[\hat{\psi}^*\hat{\psi}(x)]\partial_\mu\hat{\phi}(x) + \mu^2\hat{\psi}^*(x)\hat{\psi}(x)\hat{\phi}(x)\}. \tag{5}$$

By partial integration we see that this is equivalent to a $(\Box-\mu^2)$-interaction. Using the quantization method given by Heisenberg-Pauli, we obtain the Hamiltonian in the Heisenberg representation

$$\begin{aligned}
\hat{H}(x) &= \hat{H}_0(x) + \hat{H}_{\mathrm{I}}(x), \\
\hat{H}_0(x) &= (\hat{\pi}_\psi\hat{\pi}_{\psi^*} + \nabla\hat{\psi}^*\nabla\hat{\psi} + \kappa^2\hat{\psi}^*\hat{\psi}) - \tfrac{1}{2}[\hat{\pi}_\phi{}^2 + (\nabla\hat{\phi})^2 + \mu^2\hat{\phi}^2] \\
H_{\mathrm{I}}(x) &= -g[(\hat{\pi}_\psi\,\hat{\psi} + \hat{\psi}^*\hat{\pi}_\psi)\hat{\pi}_\phi + \nabla(\hat{\psi}^*\hat{\psi})\nabla\hat{\phi} + \mu^2\hat{\psi}^*\hat{\psi}\hat{\phi}] \\
&\quad + \frac{g^2\hat{\psi}^*\hat{\psi}\hat{\pi}_\phi{}^2}{1+2g^2\hat{\psi}^*\hat{\psi}} - \frac{g^2(\hat{\pi}_\psi\psi + \hat{\pi}_{\psi^*}\hat{\psi}^*)^2}{2(1+2g^2\hat{\psi}^*\hat{\psi})} + \frac{2g^3\hat{\psi}^*\hat{\psi}(\hat{\pi}_\psi\hat{\psi} + \hat{\psi}^*\hat{\pi}_{\psi^*})\hat{\pi}_\phi}{1+2g^2\hat{\psi}^*\hat{\psi}},
\end{aligned} \tag{6}$$

where $(\hat{\pi}_\psi, \hat{\psi})$, $(\hat{\pi}_{\psi^*}, \hat{\psi}^*)$ and $(\hat{\pi}_\phi, \hat{\phi})$ are canonical variables. The interaction Hamiltonian in the interaction representation can be obtained from $\hat{H}_{\mathrm{I}}(x)$ in eq. (6) by transforming these canonical variables into the interaction representation.

2.2. THE INTRODUCTION OF THE INDEFINITE METRIC

It should be noted here that in the interaction representation

$$\dot{\phi} = i[H_0(t), \phi(t)] = -\pi_\phi, \tag{7}$$

provided that we use the usual commutation relation between canonical variables,

$$[\phi(\mathbf{x}, t), \pi_\phi(\mathbf{x}', t)] = i\delta(\mathbf{x}-\mathbf{x}'). \tag{8}$$

The minus sign in eq. (7), which comes from the different sign of the free Lagrangian of the ϕ field, expresses the fact that the propagator of the free ϕ particle is of opposite sign to the usual propagator.

If we expand ϕ, π_ϕ in terms of the creation and annihilation operators,

$$\begin{aligned}\phi(x) &= \frac{1}{(2\pi)^{\frac{3}{2}}}\int \frac{\mathrm{d}^3\mathbf{k}}{\sqrt{2k_0}}\{a(\mathbf{k})\mathrm{e}^{ikx}+a^*(\mathbf{k})\mathrm{e}^{-ikx}\},\\ \pi_\phi(x) &= \frac{1}{(2\pi)^{\frac{3}{2}}}\int i\sqrt{\frac{k_0}{2}}\,\mathrm{d}^3\mathbf{k}\{a(\mathbf{k})\mathrm{e}^{ikx}-a^*(\mathbf{k})\mathrm{e}^{-ikx}\},\end{aligned} \tag{9}$$

where $k_0 = \sqrt{\mathbf{k}^2+\mu^2}$, then, in order to obtain agreement with eq. (8), we must take the commutator of a, a^* as

$$[a(\mathbf{k}), a^*(\mathbf{k}')] = -\delta_{\mathbf{k},\mathbf{k}'}. \tag{10}$$

Though a, a^* are interchanged in the roles of creation and annihilation operators, in comparison with the ordinary case, we still have the same condition for the vacuum state, provided that it is the lowest energy state, as is shown in the following.

We note first

$$[H_0, a(\mathbf{k})] = [\sum_{\mathbf{k}'} k'_0\{a(\mathbf{k}')a^*(\mathbf{k}')+\tfrac{1}{2}\}, a(\mathbf{k})] = -k_0 a(\mathbf{k}), \tag{11}$$

and applying this to the vacuum state, we get

$$H_0 a(\mathbf{k})|\Psi_0) = (E_0-k_0)a(\mathbf{k})|\Psi_0), \tag{12}$$

where E_0 is the vacuum energy, and by requiring E_0 to be the minimum, we have

$$a(\mathbf{k})|\Psi_0) = 0. \tag{13}$$

E_0 is indeed $-\infty$, but after normalizing it to zero, we can define $a^*(\mathbf{k})|\Psi_0)$, $a^*(\mathbf{k})a^*(\mathbf{k}')|\Psi_0)$, etc. as one-particle state, two-particle state, etc., with positive energy.

There still remains the difficulty that the above-mentioned commutation relation leads to contradiction with the postulate of H_0 being hermitian †, and we are forced to introduce an indefinite metric. The simple and concrete way of doing this is the Gupta-Bleuler [7]) method in the case of quantum electrodynamics. Using this method, we shall understand all expectation values in this paper to be read as

$$\langle| \quad |\rangle = (|\eta \quad |) \tag{14}$$

where

$$\{\eta, a\} = \{\eta, a^*\} = 0 \quad \text{and} \quad \eta^2 = 1.$$

† As $[a(\mathbf{k})]^* = a^*(\mathbf{k})$, we have $(\Psi_0|a(\mathbf{k})a^*(\mathbf{k})|\Psi_0) = \Sigma_n|(\Psi_0|a(\mathbf{k})|\Psi_n)|^2 > 0$. But this is also equal to

$$(\Psi_0|[a(\mathbf{k}), a^*(\mathbf{k})]|\Psi_0) = -(\Psi_0|\Psi_0) < 0.$$

The contradiction mentioned above can be removed by using eq. (14), because $\Sigma_n|\langle\Psi_0|a(\mathbf{k})|\Psi_n\rangle|^2$ need not be positive by this definition. However, we must then consider negative probabilities.

2.3. THE *S*-MATRIX

We shall now show that all matrix elements between initial and final states actually vanish in this model, the initial state being constructed from physical particles only ($|\Psi_{\mathrm{p}}\rangle$) and the final state from both physical and unphysical particles ($a^* \ldots a^*|\Psi_{\mathrm{p}'}\rangle$).

The *S*-matrix is given by

$$S = \sum_n \frac{(-i)^n}{n!} \int_{-\infty}^{\infty} \ldots \int_{-\infty}^{\infty} \mathrm{P}[H_{\mathrm{I}}(x_1), \ldots, H_{\mathrm{I}}(x_n)] \mathrm{d}^4x_1 \ldots \mathrm{d}^4x_n, \tag{15}$$

where $H_{\mathrm{I}}(x)$ is given by eq. (6). The matrix element between the two states can be written as

$$\begin{aligned} M\ (\text{phys.} + \text{unphys.} \leftarrow \text{phys.}) &= \langle \Psi_{\mathrm{p}'}|a(\mathbf{k}_1) \ldots a(\mathbf{k}_m) S(\infty, -\infty)|\Psi_{\mathrm{p}}\rangle \\ &= \langle \Psi_{\mathrm{p}'}|a(\mathbf{k}_2) \ldots a(\mathbf{k}_m)[a(\mathbf{k}_1), S]|\Psi_{\mathrm{p}}\rangle \qquad (16) \\ &= (-i) \int \mathrm{d}^4x \langle \Psi_{\mathrm{p}'}|a(\mathbf{k}_2) \ldots a(\mathbf{k}_m) S(\infty, -\infty) S^{-1}(x, -\infty) \\ &\qquad [a(\mathbf{k}_1), H_{\mathrm{I}}(x)] S(x, -\infty)|\Psi_{\mathrm{p}}\rangle \end{aligned}$$

where $|\Psi_{\mathrm{p}}\rangle$, $|\Psi_{\mathrm{p}'}\rangle$ are the states at $t \to -\infty$, in the interaction representation.

After some calculation (given in the appendix), we get M in the Heisenberg representation

$$= (-i) \frac{1}{(2\pi)^{\frac{3}{2}}} \int \frac{(-g)}{\sqrt{2k_{1,0}}} \langle \Phi_{\mathrm{p}', k_2 \ldots k_m}|\hat{\psi}^* \hat{\psi}|\Phi_{\mathrm{p}}\rangle (-\partial_\mu \partial_\mu + \mu^2) \mathrm{e}^{-ik_1 x_1} \mathrm{d}^4x_1, \tag{17}$$

where

$$|\Phi_{\mathrm{p}', k_2 \ldots k_m}\rangle = S^{-1}(\infty, -\infty) a(\mathbf{k}_2) \ldots a(\mathbf{k}_m)|\Psi_{\mathrm{p}'}\rangle.$$

By repeated use of this procedure, we obtain at last

$$\begin{aligned} M = (-i)^m \frac{(-g)^m}{\{(2\pi)^{\frac{3}{2}}\}^m} \int \ldots \int & \frac{\mathrm{d}^4x_1 \ldots \mathrm{d}^4x_m}{\sqrt{2^m k_{1,0} k_{2,0} \ldots k_{m,0}}} \\ & \times \langle \Phi_{\mathrm{p}'}|\mathrm{P}[\hat{\psi}^* \hat{\psi}(x_1), \ldots, \hat{\psi}^* \hat{\psi}(x_m)]|\Phi_{\mathrm{p}}\rangle \qquad (18) \\ & \times (-\Box_1 + \mu^2) \ldots (-\Box_m + \mu^2) \mathrm{e}^{-ik_1 x_1 - \ldots - ik_m x_m}. \end{aligned}$$

These matrix elements vanish for $k_i^2 = \mu^2$, unless the P-bracket term has the factor $1/(k_i^2 + \mu^2)$.

To investigate this question, it is useful to rewrite the *S*-matrix as follows: from eq. (18),

$$\begin{aligned} S = \sum_n \frac{(-i)^n}{n!} \int \ldots \int & [\mathrm{P}^*\{-g\psi^*\psi(-\Box_1 + \mu^2)\phi(x_1), \ldots, -g\psi^*\psi(-\Box_n + \mu^2)\phi(x_n)\} \\ & + (\text{function of } \psi, \psi^* \text{ only})]\ \mathrm{d}^4x_1 \ldots \mathrm{d}^4x_n \\ \equiv \sum_n \frac{(-i)^n}{n!} g^n \int \ldots \int & [\mathrm{P}(\psi^*\psi, \ldots \psi^*\psi)(\Box_1 - \mu^2) \ldots (\Box_n - \mu^2) \mathrm{P}\{\phi(x_1) \ldots \phi(x_n)\} \qquad (19) \\ & + (\text{function of } \psi\psi^* \text{ only})]\ \mathrm{d}^4x_1 \ldots \mathrm{d}^4x_n. \end{aligned}$$

In this form, if we take the commutator $[a(\mathbf{k}_i), S]$, one ϕ operator must be emancipated from the P-product, because $[a(\mathbf{k}_i), \phi(x)]$ is a C-number. Applying the $(\Box - \mu^2)$-operator to $[a(\mathbf{k}_i), \phi(x)]$, we find it becomes zero for every order in g.

An alternative proof of the vanishing of the matrix elements is found in using the unitary transformation given by

$$U(\sigma) = \mathrm{e}^{-i\int_\sigma \partial'_\mu \phi(x')\psi^*(x')\psi(x')\,\mathrm{d}\sigma'_\mu}. \tag{21}$$

Then we get

$$U^{-1}(\sigma)H(x)U(\sigma) = H_0(x) + \mathscr{H}(x),$$
$$\mathscr{H}(x) = -\tfrac{1}{2}g^2\{\partial_\mu(\psi^*\psi)\partial_\mu(\psi^*\psi) + \mu^2(\psi^*\psi)^2\} + g^4\frac{[n_\mu\partial_\mu(\psi^*\psi)]^2\psi^*\psi}{1+2g^2\psi^*\psi}. \tag{22}$$

This is just the same Hamiltonian as is obtained by the S-matrix calculation of eq. (A.12). It means that, if we have no unphysical particle initially, we have no transition to an unphysical state. Therefore, in our model, if the S-matrix is unitary for the whole Hilbert space, it is also unitary for the sub-space which is constructed from physical states only. In any theory dealing with unphysical fields all ϕ operators in the S-matrix must be contracted and consequently the S-matrix reduces to a non-linear self-interaction as shown in eq. (22).

This interaction gives rise to divergent effects owing to high derivatives. Nevertheless it is worth noting that a non-linear self-interaction can contain the effect of an unphysical field.

3. Unitarity and Causality

The existence of a Hamiltonian which satisfies the integrability condition guarantees the unitarity and the causality of the S-matrix. However, we wish to investigate these properties in a direct way, which will serve to test the more extended interaction of the last section.

3.1. UNITARITY

The usual S-matrix constructed with the use of the P*-product is not unitary for many-derivative interaction. To see this, let us examine the following term of the S-matrix:

$$S' = \sum_n \frac{(-i)^n}{n!} g^n \int\ldots\int \mathrm{d}^4x_1 \ldots \mathrm{d}^4x_n \mathrm{P}^*[\partial_1 O(x_1)\partial_1\phi(x_1), \ldots, \partial_n O(x_n)\partial_n\phi(x_n)]$$
$$= \sum_n \frac{(-i)^n}{n!} g^n \int\ldots\int \mathrm{d}^4x_1 \ldots \mathrm{d}^4x_n \partial_1 \ldots \partial_n \mathrm{P}[O(x_1), \ldots, O(x_n)] \tag{23}$$
$$\times \partial_1 \ldots \partial_n \mathrm{P}[\phi(x_1), \ldots, \phi(x_n)],$$

where

$$O(x) = \psi^*(x)\psi(x).$$

The unitarity of the S-matrix up to order g^2 demands

$$S'^{(1)*} + S'^{(1)} = 0$$

and

$$S'^{(2)*} + S'^{(2)} + S'^{(1)*}S'^{(1)} = 0. \tag{24}$$

If we write $S'^{(2)}$ in the following form:

$$S'^{(2)} = \frac{(-i)^2}{2!}g^2\iint \mathrm{d}^4x\mathrm{d}^4x'\,(\partial_\mu\partial'_\nu\tfrac{1}{2}\{O(x), O(x')\} + \tfrac{1}{2}\varepsilon(x-x')[\partial_\mu O, \partial'_\nu O] + [\partial_\mu\partial'_\nu, \tfrac{1}{2}\varepsilon(x-x')][O(x), O(x')]) \text{ (same for } \phi), \tag{25}$$

and substitute this into eq. (24), then in the product all terms cancel except one †:

$$[\partial_\mu\partial'_\nu, \tfrac{1}{2}\varepsilon(x-x')][O(x), O(x')][\partial_\mu\partial'_\nu, \tfrac{1}{2}\varepsilon(x-x')][\phi(x), \phi(x')] = [\delta^4(x-x')]^2 2\psi^*(x)\psi(x). \tag{26}$$

As can be easily seen, this term is hermitian and has no corresponding term in $S'^{(1)*}S'^{(1)}$. We cannot interpret it as the usual normal dependent term, because such a term comes from the g^2 part of $-i\int H_I(x)\mathrm{d}^4x$ and it must be antihermitian.

This illustrates why eq. (23) is not unitary, and why direct calculation of eq. (A.11) yields the extra term of eq. (26).

3.2. CAUSALITY

In order to examine the causality of the S-matrix, it is convenient to accept the condition given by Bogoliubov [8]): "When every point in the four-dimensional region τ_A lies in the time-like domain to every point in another region τ_B, and $g_A(x)$, $g_B(x)$ are different from zero only in τ_A, τ_B respectively, the causality condition demands

$$S(g_A+g_B) = S(g_A)S(g_B)". \tag{27}$$

This is fulfilled by S' in eq. (23). The proof is obvious in the first order of g, and for the second order of g,

† This point was overlooked in many papers [5, 6]) in which the S-matrix was constructed from the P*-product alone after dropping the normal dependent terms in the Hamiltonian. This method is correct only for the lower order derivatives, or for the derivative interaction of the scalar field with the current.

$$S'^{(2)}(g_A+g_B)=\frac{(-i)^2}{2!}\iint \mathrm{P}^*[g_A(x)\partial_\mu O(x)\partial_\mu\phi(x)+g_B(x)\partial_\mu O(x)\partial_\mu\phi(x),$$
$$g_A(x')\partial'_\nu O(x')\partial'_\nu\phi(x')+g_B(x')\partial'_\nu O(x')\partial'_\nu\phi(x')]\mathrm{d}^4x\mathrm{d}^4x' \quad (28)$$
$$=\frac{(-i)^2}{2!}\iint \mathrm{P}^*[g_A(x)\partial_\mu O(x)\partial_\mu\phi(x),\, g_A(x')\partial_\nu O(x')\partial_\nu\phi(x')]\mathrm{d}^4x\mathrm{d}^4x'+(g_A\to g_B)$$
$$+\frac{(-i)^2}{2!}\iint 2\mathrm{P}^*[g_A(x)\partial_\mu O(x)\partial_\mu\phi(x),\, g_B(x')\partial'_\nu O(x')\partial'_\nu\phi(x')]\mathrm{d}^4x\mathrm{d}^4x'.$$

The first and second terms are just $S'^{(2)}(g_A)$, $S'^{(2)}(g_B)$, respectively, and the third term is

$$(-i)^2\iint g_A(x)g_B(x')\partial_\mu\partial'_\nu \mathrm{P}[O(x),O(x')]\partial_\mu\partial'_\nu \mathrm{P}[\phi(x),\phi(x')]\mathrm{d}^4x\mathrm{d}^4x' \quad (29)$$

where, if we remember the condition for g_A and g_B, the integrand is not zero only for a time-like region of $x-x'$. Therefore, we can drop the P-symbol, and eq. (29) becomes $S'^{(1)}(g_A)$, $S'^{(1)}(g_B)$.

In the same way we can prove that the causality condition is fulfilled for every order of g.

The other term in eq. (26) which should be subtracted from S' to make it unitary causes no trouble, because

$$\iint [g_A(x)+g_B(x)]^2[\delta(x-x')]^2\psi^*(x)\psi(x')\,\mathrm{d}^4x\mathrm{d}^4x'$$
$$=\iint [g_A{}^2(x)+g_B{}^2(x)]\,[\delta(x-x')]^2\psi^*(x)\psi(x)\,\mathrm{d}^4x\mathrm{d}^4x'; \quad (30)$$

the cross terms vanish owing to the δ-function: this corresponds to the fact that there is no first order term. Thus, the contact terms are causal too.

For the interaction with infinite derivatives, this is not the case: these contact terms increase so as to violate causality after the summing up. This will be discussed in the next section.

4. The generalization

If we expect the cancellation of the divergence to be due to the field ϕ', as we mentioned in section 1, we must take $f(\partial)$ in eq. (4) to be of the second inverse power in ∂. Thus we shall take the interaction Lagrangian as follows:

$$\hat{L}_1(x)=g\hat{\psi}^*(x)\hat{\psi}(x)\left\{\frac{\Box-\mu^2}{\Box-l^2}\right\}\hat{\phi}(x), \quad (31)$$

where for $\mu^2\neq l^2$, $\hat{L}_1(x)$ has derivatives of infinite order in the expansion of $\Box$ and is really a non-local interaction.

We cannot have the Hamiltonian in compact form, but we can obtain it by

the method of a perturbation expansion in g. This was done by Katayama [6]) and he obtained the S-matrix in the P-product form. We know, however, from the argument in section 3 that this is not unitary, and we must add some terms. Then we find

$$S = \sum_n \frac{(-i)^n}{n!} g^n \int \ldots \int [\mathrm{P}\{O(x_1) \ldots O(x_n)\} F(\Box_1) \ldots F(\Box_n) \times \mathrm{P}\{\phi(x_1) \ldots \phi(x_n)\} + C^{(n)}] \mathrm{d}^4 x_1 \ldots \mathrm{d}^4 x_n, \quad (32)$$

where

$$F(\Box) = \frac{\Box - \mu^2}{\Box - l^2}.$$

Though it is very difficult to determine $C^{(n)}$ for every n, we can conjecture from eq. (19) that for $\mu^2 \neq l^2$, the term $C^{(n)}$ is made up of ψ^*, ψ only, and that no ϕ appears. This is easily seen in second order of g. Then eq. (32) vanishes for unphysical processes, since any ϕ operators emancipated from the P-product give zero after the application of $F(\Box)$. Therefore the interaction Lagrangian in eq. (31) gives a consistent unphysical field theory in this sense.

The major difficulty arises with regard to causality. To see this we need to calculate the contact term up to order g^2.

From the unitarity of S in eq. (32) we find [6])

$$C^{(1)}(g) = 0,$$

$$-C^{(2)}(g) = \tfrac{1}{2}\varepsilon(x-x')[O(x), O(x')][F(\Box)F(\Box'), \tfrac{1}{2}\varepsilon(x-x')][\phi(x), \phi(x')]$$

$$= \tfrac{1}{2} i \varepsilon (x-x')[O(x), O(x')] F(\Box) \left\{ \frac{F(\Box) - F(\mu^2)}{\Box - \mu^2} \delta(x-x') \right\},$$

and after using the explicit form of $F(\Box)$, we get

$$C^{(2)}(g) = -\tfrac{1}{2} i \varepsilon (x-x') [O(x), O(x')] F(\Box) \left\{ \frac{1}{\Box - l^2} \delta(x-x') \right\}. \quad (33)$$

Substituting $C^{(2)}$ in eq. (32), we obtain an $S^{(2)}$ which agrees with that obtained by the Yang-Feldmann method.

It should be noted that this term has lost its meaning as a contact term, as the second bracket in eq. (33) has the form $\Delta_l(x-x')$ owing to the presence of $1/(\Box - l^2)$.

In the discussion in section 3 we found that both the P* terms and the contact terms were causal. In this case, however, $C^{(2)}(g)$ is no longer a function of $\delta(x-x')$, but can propagate as a particle of mass l. Moreover, we know it is hermitian. This means that such a term cannot have the character of the $\Delta_{(\mathrm{F})}$, $\Delta_{(\mathrm{ret})}$, $\Delta_{(\mathrm{ad})}$ functions, and in fact we find it equals $\Delta_l(x-x')$.

If we substitute $C^{(2)}(g)$ in eq. (32), and examine the causality condition of eq. (27), we obtain as the rest term

$$R(g_A, g_B) = -2\iint g_A(x) g_B(x') \left\{ -\tfrac{1}{2} i\varepsilon(x-x') [O(x), O(x')] \times \frac{\Box-\mu^2}{\Box-l^2} \bar{\Delta}_1(x-x') \right\} \mathrm{d}^4x \mathrm{d}^4x'. \quad (34)$$

If τ_A and τ_B are very small regions (we represent them by points x_A and x_B), and $\lambda \equiv (x_A{}^0-x_B{}^0)^2-(\mathbf{x}_A-\mathbf{x}_B)^2 \gg 0$, then

$$R(g_A, g_B) \approx g_A g_B i[O(x_A), O(x_B)] \frac{\Box-\mu^2}{\Box-l^2} l\lambda^{-\frac{1}{4}} J_1(l\lambda^{\frac{1}{2}}). \quad (35)$$

This never vanishes, even for macroscopic separation [9]) $\lambda \gg 0$, and referring to eq. (27) we can conclude that the ordinary multiplication law of the $S(t-t')$-matrix cannot be used in this case.

If we take $l = \mu$ after all the calculations have been performed, and include the L'_{I} interaction with $g' = g$, we have

$$S^{(2)}(g) = \frac{(-i)^2}{2!}\iint g^2[\mathrm{P}\{O(x), O(x')\}\mathrm{P}\{\phi(x), \phi(x')\} + iO(x)\bar{\Delta}_\mu(x-x')O(x')]. \quad (36)$$

This is similar to the expression given by Bogoliubov *et al.* [3]), and we know that their theory † is one of non-local interaction, and violates the causality condition [9]).

5. Summary and Discussion

We started our discussion by constructing a unitary S-matrix for physical processes, and we chose the interaction Lagrangian of eqs. (1) and (4). We might have chosen other solutions of eq. (3) such as $A(\partial) = A'(\partial)(\Box-\kappa^2)$ and $B(\partial) = B'(\partial)(\Box-\kappa^2)$, but under these choices the ϕ operators cannot be contracted perfectly, even in the second order of g, and this gives unphysical transitions. Therefore we may say that the choice of eq. (4) was also necessary.

By the argument of section 2 we found a theory with indefinite metric which was self-consistent at every point. It was, however, such that the unphysical particle could not propagate at all, and, after eliminating it, only the contact self-interactions of the physical field were left.

At the next stage we tried to extend the theory so as to effect the cancellation of the divergence. The acceptance of eq. (4) led us to non-local interaction, and

† In their theory, there are extra terms of the form $\Delta_\mu{}^+(x-x')$, due to the projection operator which separates ϕ^+ and ϕ^-. We, however, started from a Lagrangian which contained ϕ only linearly, and therefore this separation cannot occur. Anyway, this difference is not essential for the argument of causality

by choosing the form factor as $F(\partial) = (\Box-\mu^2)/(\Box-l^2)$ it is possible to avoid the unphysical processes, while it violates the causality inevitably.

It is usually said that the indefinite metric is equivalent to the non-local theory. The special model given in section 2 is opposed to this statement. It is our feeling that, in general, the condition for avoiding unphysical processes, together with the condition for compensation of the divergence, make it necessary to introduce non-local interaction. The violation of causality is due to the non-local interaction.

The negative probability may also be exploited in such problems as the nucleon current contribution to the anomalous magnetic moment. Then the model given in section 2 or its variant, the non-linear self-interaction like eq. (22), will be effective, though we must, of course, use the cut-off techniques, owing to the divergence of the expectation values calculated from eq. (22).

The author is grateful to Professor Y. Takahashi for helpful discussions.

Appendix

PROOF OF EQ. (6).

Applying the Heisenberg-Pauli quantization method to the system $L = L_0+L_1$ in eq. (5), we have

$$\hat{\pi}_\phi = -\dot{\hat{\phi}}-g\partial_t(\hat{\psi}^*\hat{\psi}), \quad \hat{\pi}_\psi = \dot{\hat{\psi}}^*-g\hat{\psi}^*\dot{\hat{\phi}}, \quad \hat{\pi}_{\psi^*} = \dot{\hat{\psi}}-g\hat{\psi}\dot{\hat{\phi}}, \tag{A.1}$$

and from these equations we obtain

$$\hat{\pi}_\psi\hat{\psi}+\hat{\psi}^*\hat{\pi}_{\psi^*} = \partial_t(\hat{\psi}^*\hat{\psi})-2g\hat{\psi}^*\hat{\psi}\dot{\hat{\phi}}. \tag{A.2}$$

Eqs. (A.1) and (A.2) can be solved for $\dot{\hat{\phi}}$, $\dot{\hat{\psi}}$, $\dot{\hat{\psi}}^*$, and yield

$$\begin{aligned}
\dot{\hat{\phi}} &= -\hat{\pi}_\phi + \frac{2g^2\hat{\psi}^*\hat{\psi}\hat{\pi}_\phi}{1+2g^2\hat{\psi}^*\hat{\psi}} - \frac{g(\hat{\pi}_\psi\hat{\psi}+\hat{\psi}^*\hat{\pi}_{\psi^*})}{1+2g^2\hat{\psi}^*\hat{\psi}}, \\
\dot{\hat{\psi}} &= \hat{\pi}_{\psi^*} - \frac{g\hat{\psi}\hat{\pi}_\phi}{1+2g^2\hat{\psi}^*\hat{\psi}} - \frac{g^2\hat{\psi}(\hat{\pi}_\psi\psi+\hat{\psi}^*\hat{\pi}_{\psi^*})}{1+2g^2\hat{\psi}^*\hat{\psi}},
\end{aligned} \tag{A.3}$$

with the complex conjugate form for $\dot{\hat{\psi}}^*$.

Substituting (A.3) in

$$\hat{H} = \dot{\hat{\psi}}^*\hat{\pi}_{\psi^*}+\hat{\pi}_\psi\dot{\hat{\psi}}+\hat{\pi}_\phi\dot{\hat{\phi}}-\hat{L}, \tag{A.4}$$

and after elementary calculations, we obtain eq. (6).

PROOF OF EQ. (17).

$$[a(\mathbf{k}), H_I(x)] = \frac{1}{\sqrt{2k_0}}\Big\{-g[(\pi_\psi\psi+\psi^*\pi_{\psi^*})ik_0+\nabla(\psi^*\psi)\cdot i\mathbf{k}+\mu^2(\psi^*\psi)] + \frac{2g^2\psi^*\psi\pi_\phi}{1+2g^2\psi^*\psi}ik_0+\frac{2g^3\psi^*\psi(\pi_\psi\psi+\psi^*\pi_{\psi^*})}{1+2g^2\psi^*\psi}ik_0\Big\}\times e^{-ikx}. \tag{A.5}$$

Therefore,

$$S^{-1}(x,-\infty)[a(\mathbf{k}), H_I(x)]S(x,-\infty) = \frac{1}{\sqrt{2k_0}}\Big\{-g[(\partial_t(\hat\psi^*\hat\psi)-2g\hat\psi^*\hat\psi\dot{\hat\phi})ik_0+\nabla(\hat\psi^*\hat\psi)\cdot i\mathbf{k}+\mu^2\hat\psi^*\hat\psi] + \Big[\frac{2g^2\hat\psi^*\hat\psi\{-\dot{\hat\phi}-g\partial_t(\hat\psi^*\hat\psi)\}}{1+2g^2\hat\psi^*\hat\psi}+\frac{2g^3\hat\psi^*\hat\psi\{\partial_t(\hat\psi^*\hat\psi)-2g\hat\psi^*\hat\psi\dot{\hat\phi}\}}{1+2g^2\hat\psi^*\hat\psi}\Big]ik_0\Big\}\times e^{-ikx}. \tag{A.6}$$

The two $\partial_t(\hat\psi^*\hat\psi)$ terms in the second bracket cancel, and so the second bracket yields $2g\hat\psi^*\hat\psi\dot{\hat\phi}ik_0$. Thus we get

$$\frac{1}{\sqrt{2k_0}}(-g)[\partial_\mu(\hat\psi^*\hat\psi)\partial_\mu e^{-ikx}+\mu^2\hat\psi^*\hat\psi e^{-ikx}],$$

and, after partial integration, we obtain eq. (17).

Now we shall calculate the S-matrix by the perturbation expansion in g. From eq. (15) we have

$$S^{(1)}(g) = (-i)(-g)\int[\partial_\mu(\psi^*\psi)\partial_\mu\phi+\mu^2\psi^*\psi\phi]d^4x = (-i)\int(-g)\psi^*\psi[-\partial_\mu\partial_\mu+\mu^2]\phi(x)d^4x = 0. \tag{A.7}$$

$$S^{(2)}(g)=\frac{(-i)^2}{2!}\iint(-g)^2P\{\partial_\mu(\psi^*\psi)\partial_\mu\phi+\mu^2\psi^*\psi\phi(x),\partial'_\nu(\psi^*\psi)\partial'_\nu\phi+\mu^2\psi^*\psi\phi(x')\}\times d^4xd^4x'-\int(-i)[g^2\psi^*\psi\dot\phi-\tfrac{1}{2}g^2\{\partial_t(\psi^*\psi)\}^2]d^4x \tag{A.8}$$

$$= \tfrac{1}{2}(-i)^2g^2\iint\{[P\{\partial_\mu(\psi^*\psi),\partial'_\nu(\psi^*\psi)\}P(\partial_\mu\phi,\partial'_\nu\phi) -2i\delta^4(x-x')\psi^*\psi\dot\phi^2+i\delta^4(x-x')\{\partial_t(\psi^*\psi)\}^2] + [\mu^2(P\{\partial_\mu(\psi^*\psi),\psi^*\psi\}P(\partial_\mu\phi,\phi)+P\{\psi^*\psi,\partial'_\nu(\psi^*\psi)\}P(\phi,\partial'_\nu\phi)) + \mu^4P(\psi^*\psi,\psi^*\psi)P(\phi,\phi)]\}d^4xd^4x'. \tag{A.9}$$

In the second bracket of eq. (A.9) the ∂-operators commute with the P-symbol.

The first term in the first bracket is

$$[\partial_\mu \partial'_\nu \mathrm{P}(\psi^*\psi, \psi^*\psi) - 2i\psi^*\psi\delta_{\mu 4}\delta_{\nu 4}\delta^4(x-x')][\partial_\mu \partial'_\nu \mathrm{P}(\phi, \phi) + i\delta_{\mu 4}\delta_{\nu 4}\delta^4(x-x')]$$
$$= \partial_\mu \partial'_\nu \mathrm{P}(\psi^*\psi, \psi^*\psi)\partial_\mu \partial'_\nu \mathrm{P}(\phi, \phi) + \mathrm{P}\{\partial_\mu(\psi^*\psi), \partial'_\nu(\psi^*\psi)\} i\delta_{\mu 4}\delta_{\nu 4}\delta^4(x-x') \quad \text{(A.10)}$$
$$- 2i\psi^*\psi\delta_{\mu 4}\delta_{\nu 4}\delta^4(x-x')\mathrm{P}(\partial_\mu\phi, \partial_\nu\phi') - (-2i)\psi^*\psi\delta_{\mu 4}\delta_{\nu 4} i\delta_{\mu 4}\delta_{\nu 4}[\delta^4(x-x')]^2.$$

The second and the third terms of eq. (A.10) compensate the second and third terms in the first bracket of eq. (A.9). Thus we have the contact term as well as the P*-product. Collecting from eq. (A.8) to (A.10), and integrating by parts, we find

$$S^{(2)}(g) = \frac{(-i)^2}{2!}(-g)^2 \iint [\mathrm{P}(\psi^*\psi, \psi^*\psi)(\Box - \mu^2)(\Box' - \mu^2)\mathrm{P}(\phi, \phi)$$
$$- 2\psi^*\psi[\delta^4(x-x')]^2]\mathrm{d}^4x\mathrm{d}^4x'. \quad \text{(A.11)}$$

Eq. (A.11) can be transformed into simpler form by calculating the $(\Box - \mu^2)$ term, and we obtain

$$S^{(2)}(g) = (-i)g^2 \int \psi^*\psi(x)(\Box - \mu^2)[\psi^*\psi(x)]\mathrm{d}^4x. \quad \text{(A.12)}$$

References

1) W. Heisenberg, Rev. Mod. Phys. **29** (1957) 269
2) W. Pauli and H. Villars, Rev. Mod. Phys. **21** (1949) 434
3) Bogoliubov, Medvedev and Polivanov, Sci. Trans. of the High Schools, Physico-Mathemat. Sciences **2** (1958) 137
4) H. Lehmann, Nuovo Cim. **11** (1954) 342
5) H. Umezawa and Y. Takahashi, Prog. Theor. Phys. **9** (1953) 14, 501
6) Y. Katayama, Prog. Theor. Phys. **10** (1953) 31
7) K. Bleuler, Helv. Phys. Acta **23** (1950) 567;
S. N. Gupta, Proc. Phys. Soc. A **63** (1950) 681
8) N. N. Bogoliubov and D. Y. Shirkov, Introduction to the theory of quantized fields (Interscience Publishers, New York, 1959)
9) D. A. Slanov and A. D. Sukhanov, Soviet Physics JETP **36** (9) (1959) 1044

1.C

Nuclear Physics 17 (1960) 499—515; © *North-Holland Publishing Co., Amsterdam*

Not to be reproduced by photoprint or microfilm without written permission from the publisher

ON THE PROBLEM OF REARRANGEMENT ENERGY OF NUCLEAR MATTER

P. MITTELSTAEDT

Max-Planck-Institut für Physik und Astrophysik, München

Received 2 March 1960

Abstract: The rearrangement energy of the nuclear many-body problem, which is important in the processes of separation, scattering and excitation of a particle, is investigated. To discuss the physical meaning of this quantity, a general definition, independent of perturbation theory, is given. The "model dependence" and other important properties can then be discussed in detail. Starting from this general formulations expressions for the rearrangement energy in the Brueckner two-particle approximation are derived, and the question of how the rearrangement energy can be determined experimentally is discussed.

1. Introduction

Numerous investigations involving a perturbation treatment of the nuclear many-body problem have shown, that, in addition to the kinetic and potential energy, the so-called rearrangement energy (r.e.) plays an important role in the processes of separation, scattering and excitation of a particle [1–4, 6]). To discuss the physical meaning of this quantity, we shall first give a general definition, independent of perturbation theory, of the r.e. involved in the various processes (section 2). However, we shall restrict these investigations to the case of systems of large numbers of nucleons A (nuclear matter), which are translation invariant. In this general formulation various important properties of the r.e. will become apparent, especially its "model-dependence" which is decisive for the question of the experimental measurability.

For treating the nuclear many-body problem it has been shown to be useful, especially as a starting point for perturbation calculations [5–8]), to represent the energy E_A of an A-particle system of Hamiltonian H_A and wave function Ψ_A not as an expectation value, but by means of a "model wave function" Φ_A, i.e. in the form

$$E_A = \langle \Phi_A | H_A | \Psi_A \rangle,$$

where Φ_A is an arbitrary A-particle function such that Ψ_A can be normalized by $\langle \Phi_A | \Psi_A \rangle = 1$. The separation of the total energy into a kinetic and a potential part is then model-dependent, i.e. depends on the model wave function used. In a similar way the r.e. mentioned above and its separation into a kinetic and a potential part depend on the model wave function.

By a special choice of model wave function Π_A it is possible to find a simple derivation of the perturbation theory given by Brueckner *et al.* [9–11]) or of the special case of the Hartree-Fock method [5]). The general expressions of section 2 for the r.e. will be reformulated in this perturbation theory in section 3. By comparison with the exact expressions for the r.e. it will be possible to discuss in detail the meaning of the Pauli principle and of the self-consistency requirement in the Brueckner method.

Using the results of sections 2 and 3 we shall investigate in sect. 4 the question of how the r.e. can be experimentally determined. In the exact formulations of sect. 2 it will become evident that on account of its model dependence the r.e. cannot be considered as the expectation value of an observable. For this reason the measurability of this quantity is very problematic.

2. General Formalism

In this section a few important processes of a many-body system will be discussed, for which the r.e. defined below plays an important role. We assume a system of A particles with the Hamiltonian

$$H_A = \sum_1^A T_i + \tfrac{1}{2} \sum_{i,k}^A v_{ik}, \tag{1}$$

the wave function Ψ_A and the energy E_A of the ground state, so that

$$(H_A - E_A)\Psi_A = 0.$$

Furthermore, for the calculation of the energy and the S-matrix it has been shown to be useful [1, 2]) to introduce a so-called model wave function Φ_A, i.e. a localized A-particle wave function of such a kind that Ψ_A can be normalized by $\langle \Phi_A | \Psi_A \rangle = 1$. The normalization will be carried out in a finite volume Ω_A, such that the density ρ of nuclear matter is $\rho = A/\Omega_A$. The energy can then be written in the form

$$E_A = \langle \Phi_A | H_A | \Psi_A \rangle_{\Omega_A}.$$

2.1. SEPARATION ENERGY

The separation energy, which is the energy necessary to separate a nucleon from an $(A+1)$-particle system, leaving the residual A-particle system in its ground state, is

$$-S = E_{A+1} - E_A.$$

From this relation and eq. (1) it follows that

$$\begin{aligned} -S = \langle \Phi_{A+1} | T_{A+1} | \Psi_{A+1} \rangle_{\Omega_{A+1}} &+ \sum_k^A \langle \Phi_{A+1} | v_{A+1,k} | \Psi_{A+1} \rangle_{\Omega_{A+1}} \\ &+ \sum_i^A \{ \langle \Phi_{A+1} | T_i | \Psi_{A+1} \rangle_{\Omega_{A+1}} - \langle \Phi_A | T_i | \Psi_A \rangle_{\Omega_A} \} \\ &+ \tfrac{1}{2} \sum_{i,k}^A \{ \langle \Phi_{A+1} | v_{ik} | \Psi_{A+1} \rangle_{\Omega_{A+1}} - \langle \Phi_A | v_{ik} | \Psi_A \rangle_{\Omega_A} \}. \end{aligned} \tag{2}$$

In a terminology which will be justified in a special case discussed below, we call

$$\langle \Phi_{A+1}|T_{A+1}|\Psi_{A+1}\rangle_{\Omega_{A+1}} = T$$

the kinetic energy and

$$\sum_i^A \langle \Phi_{A+1}|v_{A+1,i}|\Psi_{A+1}\rangle_{\Omega_{A+1}} = V \tag{3}$$

the potential energy of the separated particle. Furthermore,

$$\Delta_k = \sum_i^A \{\langle \Phi_{A+1}|T_i|\Psi_{A+1}\rangle_{\Omega_{A+1}} - \langle \Phi_A|T_i|\Psi_A\rangle_{\Omega_A}\} \tag{4}$$

will be called the kinetic r.e. and

$$\Delta_p = \tfrac{1}{2}\sum_{i,k}^A \{\langle \Phi_{A+1}|v_{ik}|\Psi_{A+1}\rangle_{\Omega_{A+1}} - \langle \Phi_A|v_{ik}|\Psi_A\rangle_{\Omega_A}\}$$

the potential r.e. From eqs. (4) and (5) it follows that Δ_k and Δ_p depend on the model wave functions Φ_A and Φ_{A+1}; for this reason we shall sometimes write $\Delta_k[\Phi_A]$ and $\Delta_p[\Phi_A]$.

For the special case of nuclear matter, i.e. for large particle numbers A, one may write S also in the form

$$-S = E_{A+1} - E_A = \frac{\mathrm{d}E}{\mathrm{d}A} = \left(\frac{\partial E}{\partial A}\right)_\Omega + \left(\frac{\partial E}{\partial \Omega}\right)_A \frac{\partial \Omega}{\partial A}. \tag{6}$$

Here, $\partial\Omega/\partial A$ is related to the density ρ by $1/\rho = \partial\Omega/\partial A$. In the equilibrium, we have $(\partial E/\partial\Omega)_A = 0$, and therefore the last term in eq. (6) vanishes and

$$-S = \left(\frac{\partial E}{\partial A}\right)_\Omega.$$

In the limit of large particle numbers A, eq. (2) can be rewritten with the help of eq. (6) as

$$-S = \langle \Phi_A|T_A|\Psi_A\rangle + \sum_k^A \langle \Phi_A|v_{Ak}|\Psi_A\rangle + \sum_i^A \frac{\mathrm{d}}{\mathrm{d}A}\langle \Phi_A|T_i|\Psi_A\rangle + \tfrac{1}{2}\sum_{i,k}^A \frac{\mathrm{d}}{\mathrm{d}A}\langle \Phi_A|v_{ik}|\Psi_A\rangle$$

and the r.e. as

$$\Delta = \sum_i^A \frac{\partial}{\partial A}\langle \Phi_A|T_i|\Psi_A\rangle + \tfrac{1}{2}\sum_{i,k}^A \frac{\partial}{\partial A}\langle \Phi_A|v_{ik}|\Psi_A\rangle + \frac{1}{\rho}\left\{\sum_i^A \frac{\partial}{\partial \Omega}\langle \Phi_A|T_i|\Psi_A\rangle + \tfrac{1}{2}\sum_{i,k}^A \frac{\partial}{\partial \Omega}\langle \Phi_A|v_{ik}|\Psi_A\rangle\right\}. \tag{7}$$

The last term of eq. (7) is equal to

$$\frac{1}{\rho}\frac{\partial}{\partial\Omega}\left\{\sum_i^A \langle\Phi_A|T_i|\Psi_A\rangle+\tfrac{1}{2}\sum_{i,k}^A\langle\Phi_A|v_{ik}|\Psi_A\rangle\right\}=\frac{1}{\rho}\frac{\partial E}{\partial\Omega}$$

and vanishes in the equilibrium. Therefore we get for the r.e.

$$\Delta=\sum_i^A\frac{\partial}{\partial A}\langle\Phi_A|T_i|\Psi_A\rangle+\tfrac{1}{2}\sum_{i,k}^A\frac{\partial}{\partial A}\langle\Phi_A|v_{ik}|\Psi_A\rangle. \tag{8}$$

The first term is the kinetic part, the second one the potential part of the r.e.

To illustrate in a special case the model dependence of $\Delta[\Phi_A]$, we rewrite eq. (8) in terms of differences instead of differentials and use the model wave function $\Phi_{A+1}=\Phi_A\varphi_F$, where $\varphi_F(x_{A+1})$ is a plane wave of momentum k_F (defined by $k_F^3=\frac{3}{2}\pi^2\rho$) †. For the potential energy (3) one obtains

$$V=\sum_k^A\langle\Phi_A\varphi_F|v_{A+1,k}|\Psi'_{A+1}\rangle \tag{9}$$

and for the r.e.

$$\Delta=\sum_i^A\{\langle\Phi_A\varphi_F|T_i|\Psi'_{A+1}\rangle_{\Omega_A}-\langle\Phi_A|T_i|\Psi_A\rangle_{\Omega_A}\}$$
$$+\tfrac{1}{2}\sum_{i,k}^A\{\langle\Phi_A\varphi_F|v_{ik}|\Psi'_{A+1}\rangle_{\Omega_A}-\langle\Phi_A|v_{ik}|\Psi_A\rangle_{\Omega_A}\},$$

where the wave functions Φ_A, φ_F, Ψ'_{A+1} are normalized in Ω_A so that

$$\langle\Phi_A\varphi_F|\Psi'_{A+1}\rangle=1.$$

Using the definition

$$\chi^F_{A+1}=\int_{\Omega_A}\varphi_F^*(x_{A+1})\Psi'_{A+1}\mathrm{d}x_{A+1}, \tag{10}$$

one obtains on account of the normalization conditions

$$\Delta=\langle\Phi_A|H_A|\chi^F_{A+1}-\Psi_A\rangle=\langle\Phi_A|H_A-E_A|\chi^F_{A+1}\rangle. \tag{11}$$

From this expression one can see that for the special model wave function $\Phi_A=\Psi_A$ the r.e. vanishes:

$$\Delta[\Psi_A]=\langle\Psi_A|H_A-E_A|\chi^F_{A+1}\rangle=0. \tag{12}$$

For many problems, especially as a starting point of perturbation calculations, it is convenient to use the special model wave function

$$\Phi_A=\Pi_A=\prod_k^A\varphi_k(x_k),$$

where $\varphi_k(x_k)$ are single-particle wave functions (plane waves) describing the

† The reason for this special choice of φ_F will become apparent later.

ground-state of an A-particle Fermi gas contained in the volume Ω_A. The density $\rho = A/\Omega_A$ of the nuclear matter is then related to the Fermi momentum k_F by $k_F^3 = \frac{3}{2}\pi^2\rho$. We now introduce the following notation.

$$\Pi_A^k = \prod_{i\neq k}^{A} \varphi_i, \qquad \Pi_A^{ik} = \prod_{j\neq i,k}^{A} \varphi_j, \tag{13}$$

$$\varphi_{ik} = \int_{\Omega_A} \Pi_A^{ik*} \Psi_A \frac{dx_1 \ldots dx_A}{dx_i dx_k}, \qquad \varphi_{ik}^F = \int_{\Omega_A} \Pi_A^{ik*} \varphi_F^* \Psi'_{A+1} \frac{dx_1 \ldots dx_{A+1}}{dx_i dx_k},$$

where Π_A^{ik}, φ_F and Ψ'_{A+1} are normalized in Ω_A. Taking into account the translation invariance of the nuclear matter we get for the kinetic part of eq. (8)

$$\sum_i^A \frac{\partial}{\partial A} \langle \Phi_A | T_i | \Psi_A \rangle = \sum_i^A \frac{\partial}{\partial A} \langle \varphi_i | T_i | \varphi_i \rangle = 0.$$

In this special case the r.e. therefore contains only contributions from the potential energy:

$$\Delta = \tfrac{1}{2} \sum_{i,k}^{A} \frac{\partial}{\partial A} \langle \Phi_A | v_{ik} | \Psi_A \rangle. \tag{14a}$$

If we write differences instead of differentials we get, according to eqs. (11) and (13),

$$\Delta = \tfrac{1}{2} \sum_{i,k}^{A} \{ \langle \Phi_A \varphi_F | v_{ik} | \Psi'_{A+1} \rangle_{\Omega_A} - \langle \Phi_A | v_{ik} | \Psi_A \rangle_{\Omega_A} \}$$

$$= \tfrac{1}{2} \sum_{i,k}^{A} \langle \varphi_i \varphi_k | v | \varphi_{ik}^F - \varphi_{ik} \rangle. \tag{14b}$$

In this model the terminology introduced above has a simple physical meaning:

$$\langle \Phi_A | T_A | \Psi_A \rangle = \frac{k_F^2}{2m}$$

is the kinetic energy and

$$\sum_k^A \langle \Phi_A | v_{Ak} | \Psi_A \rangle = \sum_k^A \langle \varphi_k \varphi_F | v_{Ak} | \varphi_{kF} \rangle = V(k_F)$$

the potential energy of the last occupied single-particle state ($k = k_F$).

2.2. ELASTIC SCATTERING

The elastic scattering of a particle with momentum $\mathbf{k}$ by an A-particle system can be described by

$$(H_A + T_r + v_r) \Psi_{Ak}^+ = (E_A + \varepsilon) \Psi_{Ak}^+. \tag{15}$$

Here T_r is the kinetic energy of the relative motion:

$$T_r |\mathbf{k}\rangle = \varepsilon |\mathbf{k}\rangle,$$

and $v_r = \sum_i^A v_{0i}$ the potential energy; Ψ^+_{Ak} is the scattering state, which contains asymptotically only outgoing waves †.

The S-matrix of this scattering process is

$$S_{kk'} = \delta(\mathbf{k}-\mathbf{k}') - 2\pi i \langle \Psi^+_{Ak} | \varepsilon - T_r | \Phi_A \varphi_{k'} \rangle \delta(\varepsilon - \varepsilon') \tag{16}$$

and is independent [6]) of the used model state Φ_A. Instead of this one often describes the scattering process by an "optical potential". This is defined as the single-particle potential W which satisfies the relation

$$W\psi^+_k = (\varepsilon - T_r)\psi^+_k,$$

where

$$\psi^+_k(x_0) = \int_{\Omega_A} \Phi_A^*(1, \ldots, A)\Psi^+_{Ak}(0, 1, \ldots, A)\mathrm{d}x_1 \ldots \mathrm{d}x_A.$$

Neglecting the non-hermitian part of W (i.e. the absorption), one obtains, on account of the homogeneity of nuclear matter, for Ψ^+_k a plane wave φ_q of momentum q:

$$T_r \psi^+_k = \frac{q^2}{2m}\psi^+_k, \tag{17}$$

and therefore for the optical potential

$$\langle \psi^+_k | W | \psi^+_k \rangle = W(q) = \varepsilon - \frac{q^2}{2m} = \frac{k^2}{2m} - \frac{q^2}{2m}.$$

On account of eq. (15) one obtains

$$W(q) = \langle \Phi_A | H_A - E_A | \chi_{Ak} \rangle_{\Omega_A} + \langle \psi^+_k \Phi_A | v_r | \Psi^+_{Ak} \rangle_{\Omega_A}, \tag{18}$$

with

$$\chi_{Ak} = \int_{\Omega_A} \psi^+_k(x_0)\Psi^+_{Ak}\mathrm{d}x_0.$$

The quantity

$$V(q) = \langle \psi^+_k \Phi_A | \sum_i^A v_{0i} | \Psi^+_{Ak} \rangle \tag{18a}$$

is the single-particle potential for a particle with momentum q and

$$\Delta(q) = \langle \Phi_A | H_A - E_A | \chi_{Ak} \rangle \tag{18b}$$

the r.e. for a particle with momentum q. In the same way as in eq. (12) one sees that for the special model wave function $\Phi_A = \Psi_A$ the r.e. vanishes.

In the limit $q \to k_F$ one obtains [12])

$$\lim_{q \to k_F} \Psi^+_{Ak} = \Psi'_{A+1},$$

† The states Ψ^+_{Ak} and $|\mathbf{k}\rangle$ will be normalized in the volume Ω_A in such a way that $\langle \Phi_A \varphi_0 | \Psi^+_{Ak} \rangle = 1$; cf. eq. (17).

and therefore

$$V(k_F) = \langle \varphi_F \Phi_A | \sum_i^A v_{0i} | \Psi'_{A+1} \rangle_{\Omega_A} \tag{19}$$

and

$$\Delta(k_F) = \langle \Phi_A | H_A - E_A | \chi^F_{A+1} \rangle_{\Omega_A}, \tag{20}$$

using the definition (10). The expressions (19) and (20) are equivalent to the expressions (9) and (11) which are important for the separation energy. If one chooses the model state $\Phi_{A+1} = \Phi_A \varphi_F$ the separation energy (5) yields

$$-S = \frac{k_F^2}{2m} + V(k_F) + \Delta(k_F), \tag{21}$$

recalling eqs. (9), (11), (19) and (20). Therefore the terms $V(k_F)$ and $\Delta(k_F)$ in eq. (29) are special cases of the general functions $V(q)$ and $\Delta(q)$ in eq. (18) for $q = k_F$.

For the perturbation methods which will be discussed in the next section, it is of interest to write the expressions $V(q)$ and $\Delta(q)$ considered here for the special model wave function $\Phi_A = \Pi_A$. The r.e. (18b) can be divided in the same way as in eq. (8) into the kinetic part

$$\langle \Pi_A | \sum_i^A T_i | \chi_{Ak} - \Psi_A \rangle = 0, \tag{22}$$

which vanishes in this model, and the remaining potential part

$$\tfrac{1}{2} \sum_{i,k}^A \langle \Pi_A | v_{ik} | \chi_{Ak} - \Psi_A \rangle.$$

Thus, with the definitions (13) and

$$\psi^q_{ij} = \int_{\Omega_A} \Pi_A^{ij*} \chi_{Ak} \frac{dx_1 \ldots dx_A}{dx_i dx_j},$$

$$\psi^q_{ik} = \int_{\Omega_A} \Pi_A^{i*} \varphi_q{}^* \Psi^+_{Ak} \frac{dx_0 \ldots dx_A}{dx_i dx_k},$$

it follows for the r.e.

$$\Delta(q) = \tfrac{1}{2} \sum_{i,k}^A \langle \varphi_i \varphi_k | v_{ik} | \psi^q_{ik} - \psi_{ik} \rangle. \tag{23}$$

For the single-particle potential $V(q)$ of eq. (18a) we get the expression

$$V(q) = \sum_i^A \langle \varphi_i \varphi_q | v | \psi^q_{iq} \rangle \tag{24}$$

and, with eq. (23), for the optical potential

$$W(q) = V(q) + \Delta(q).$$

2.3. SEPARATION OF AN ARBITRARY PARTICLE

We shall discuss here the separation process of an arbitrary particle from an $(A+1)$-particle system. In terms of the Fermi model Π_A one would call this the separation of a particle with momentum k smaller than the Fermi momentum k_F. To do this, we introduce the following notation: $\Pi_{A+1} = \varphi_s(x_s)\Pi^S_{A+1}$ is the Fermi model function of an $(A+1)$-particle system, Φ_{A+1} and Φ^S_{A+1} the Slater determinants formed by Π_{A+1} and Π^S_{A+1}, respectively. The wave functions are normalized in the volume Ω_{A+1}. The state of the true $(A+1)$-particle system, which corresponds to the free state Φ_{A+1}, will be called Ψ_{A+1} and the state which corresponds to the free state Φ^S_{A+1} will be called Ψ^S_{A+1}. The quantities E_{A+1} and E^S_{A+1} are the energy eigenvalues of these states:

$$(H_A - E^S_{A+1})\,\Psi^S_{A+1} = 0.$$

For the corresponding system without interaction we have

$$(H_A{}^0 - E^S_{A+1,0})\Phi^S_{A+1} = 0,$$

with

$$H_A{}^0 = \sum_1^A T_i, \quad H_A{}^1 = \tfrac{1}{2}\sum_{i,k}^A v_{ik}$$

and therefore

$$\Psi^S_{A+1} = \Phi^S_{A+1} + \frac{\mathrm{P}}{E^S_{A+1} - H_A{}^0} H_A{}^1 \Psi^S_{A+1},$$

with the normalization $\langle \Phi^S_{A+1} | \Psi^S_{A+1} \rangle = 1$; here, $P = 1 - |\Phi^S_{A+1}\rangle\langle\Phi^S_{A+1}|$ is a projection operator. For the separation process, which changes Ψ_{A+1} into Ψ^S_{A+1}, we therefore need the separation energy

$$-S(s) = E_{A+1} - E^S_{A+1}.$$

For the special model wave function

$$\Phi_{A+1} = \varphi_s(x_s)\Phi^S_{A+1},$$

we obtain

$$-S(s) = \frac{k_s^2}{2m} + \langle \Phi_{A+1} | \sum_{i \neq s}^{A+1} | v_{si} | \Psi_{A+1} \rangle + \langle \Phi^S_{A+1} | \sum_{i \neq s}^{A+1} T_i + \tfrac{1}{2} \sum_{i,k \neq s}^{A+1} v_{ik} | \chi^S_{A+1} - \Psi_{A+1} \rangle, \tag{25}$$

where

$$\chi^S_{A+1} = \int \mathrm{d}x_s \varphi_s^*(x_s) \Psi_{A+1}.$$

In the same way as in eqs. (12) and (22) the r.e. of the model function $\Phi^S_{A+1} = \Psi^S_{A+1}$ vanishes:

$$\Delta[\Psi^S_{A+1}] = \langle \Psi^S_{A+1} | H_A - E^S_{A+1} | \chi^S_{A+1} \rangle = 0.$$

For the Fermi-gas model there result a few simplifications. The kinetic part of the r.e. vanishes on account of the translation invariance:

$$\langle \Pi^{S}_{A+1} | \sum_{i \neq s}^{A+1} T_i | \chi^{S}_{A+1} - \Psi^{S}_{A+1} \rangle = 0.$$

For the potential part of the r.e. we obtain

$$\Delta[\Pi] = \tfrac{1}{2} \sum_{i,k \neq s}^{A+1} \langle \varphi_i \varphi_k | v | \chi^{S}_{ik} - \psi_{ik} \rangle,$$

using the definitions

$$\chi^{S}_{ik} = \int_{\Omega_{A+1}} \Pi^{i,k,s^*}_{A+1} \varphi_s^* \Psi_{A+1} \frac{dx_1 \ldots dx_{A+1}}{dx_i dx_k},$$

$$\psi^{S}_{ik} = \int_{\Omega_{A-1}} \Pi^{i,k,s^*}_{A+1} \Psi^{S}_{A+1} \frac{dx_1 \ldots dx_{A+1}}{dx_i dx_k}.$$

The separation energy has then the form

$$-S(s) = \frac{k_s^2}{2m} + \sum_{i \neq s}^{A+1} \langle \varphi_i \varphi_s | v | \psi_{is} \rangle + \tfrac{1}{2} \sum_{i,k \neq s}^{A+1} \langle \varphi_i \varphi_k | v | \chi^{S}_{ik} - \psi^{S}_{ik} \rangle. \tag{26}$$

In the framework of the Fermi model $k_s^2/2m$ can be interpreted as the kinetic energy of the removed particle, the second term in eq. (26) as its potential energy and the third term as the potential part of the r.e. for momentum $k = k_s$. Consequently the r.e. is now defined also for particles with momenta $k \leqq k_F$. In the special case $k = k_F$, eq. (26) goes over into the expression (21) for the minimum separation energy.

3. Formulations in perturbation theory

In this section we use the model wave function $\Phi_A = \Pi_A$ as this function is especially convenient as a starting point for the Brueckner two-particle approximation of the many-body problem and for the special case of the Hartree-Fock approximation. For the two-particle wave function we use the ansatz

$$\psi_{ik} = \int_{\Omega_A} \Pi^{ik*}_{A} \Psi_A \frac{dx_1 \ldots dx_A}{dx_i dx_k} = \left(1 + \frac{Pv}{e_{ik}}\right)^{-1} \varphi_{ik} = \Omega_{ik} \varphi_{ik}, \tag{27}$$

which follows from the Bethe-Goldstone equation. Here,

$$\varphi_{ik}(x_i, x_k) = \varphi_i(x_i)\varphi_k(x_k) - \varphi_i(x_k)\varphi_k(x_i);$$

P is the projection operator

$$P = \tfrac{1}{4} \sum_{i,k>F} |\varphi_{ik}\rangle\langle\varphi_{ik}| \tag{28}$$

and

$$e_{ik} = T_1 + T_2 + V_1 + V_2. \tag{29}$$

The quantity $e_{ik} = \varepsilon_i + \varepsilon_k$ is the sum of the single-particle energies, V_1, V_2 are single-particle operators of the form

$$V(k) = \sum_i^A \langle \varphi_i \varphi_k | v | \psi_{ik} \rangle, \tag{30}$$

depending on the momentum k, where ψ_{ik} is the two-particle function (27). From eqs. (29) and (30) it results that for nuclear matter the equation

$$e_{ik} \varphi_{ik} = 0 \tag{31}$$

is identically fulfilled, for the single-particle functions $\varphi_k(x)$ are plane waves.

3.1. SEPARATION ENERGY

To calculate in the two-particle approximation (27) the r.e. which appears in the separation energy, we start from eq. (14b):

$$\Delta(k_F) = \tfrac{1}{3} \sum_{i,k}^A \langle \varphi_i \varphi_k | v | \psi_{ik}^F - \psi_{ik} \rangle = \tfrac{1}{2} \sum_{i,k}^A \langle \varphi_i \varphi_k | v | \delta\psi \rangle,$$

where $\delta\psi$ is the change in the two-particle function when one goes from an $(A+1)$-particle system to an A-particle system, keeping the volume constant. On account of eq. (27) it follows that

$$\Delta(k_F) = -\tfrac{1}{2} \sum_{i,k}^A \langle \varphi_i \varphi_k | v \Omega \frac{\delta \mathrm{P}}{e} v + v \Omega \frac{\delta e}{e^2} \mathrm{P} v | \psi_{ik} \rangle. \tag{32}$$

By this means the variation of ψ_{ik} is reduced to the variation $\delta\mathrm{P}$ of P and the variation δe of e_{ik}. If one neglects the second term, which contains the variation of e_{ik} — this may sometimes be a good approximation — and takes into account that

$$\delta \mathrm{P} = \mathrm{P}' - \mathrm{P} = -\tfrac{1}{2} \sum_{i>F} |\varphi_{iF}\rangle\langle\varphi_{iF}|,$$

it follows that

$$\Delta(k_F) = \tfrac{1}{2} \sum_{\substack{i,k<F \\ j>F}} \frac{|\langle \varphi_i \varphi_k | v | \psi_{jF} \rangle|^2}{\varepsilon_j + \varepsilon_F - \varepsilon_i - \varepsilon_k}.$$

It is evident that this expression is $\geqq 0$. From the formulae (32) and (33) it becomes especially apparent that the separation of a particle produces a change in the projection operator P and consequently in the potential energy of the residual nucleus.

3.2. ELASTIC SCATTERING

For the calculation of the r.e. of the sacttering process of a particle with momentum q one has to investigate the expression (23). For the wave

functions ψ^q_{ik} and ψ_{ik} we use the two-particle approximation

$$\psi_{ik} = \left(1+\frac{\mathrm{P}v}{e}\right)^{-1} \varphi_{ik}, \qquad \psi^q_{ik} = \left(1+\frac{\mathrm{P}_q v}{e}\right)^{-1} \varphi_{ik},$$

where P_q differs from P by the state $|\mathbf{q}\rangle$. The differences between the two-particle wave functions above results from the difference of the projection operators P and P_q. Together with $\delta\psi = \psi^q_{ik} - \psi_{ik}$ and

$$\delta\mathrm{P} = \mathrm{P}_q - \mathrm{P} = -\tfrac{1}{2}\sum_{k>F} |\mathbf{qk}\rangle\langle\mathbf{qk}|,$$

it follows, corresponding to (34), that

$$\Delta(q) = \tfrac{1}{2}\sum_{\substack{i,k<F\\ j>F}}^{A} \frac{|\langle\varphi_i\varphi_k|v|\psi_{jq}\rangle|^2}{\varepsilon_j+\varepsilon_q-\varepsilon_i-\varepsilon_k}. \tag{35}$$

This expression is of interest inasmuch as the energy dependence of the r.e. can easily be calculated. This is important for the energy dependence of the optical potential [6])

$$W(q) = V(q)+\Delta(q).$$

Here the single-particle potential $V(q)$ is given by (24) as

$$V(q) = \sum_{i,k}^{A} \langle\varphi_i\varphi_q|v|\psi^q_{ik}\rangle. \tag{36}$$

3.3. THE SEPARATION ENERGY $S(s)$

The separation energy $S(s)$ of a particle with momentum $k_s < k_F$ is given by eq. (26). The r.e. of this process is

$$\Delta(S) = \tfrac{1}{2}\sum_{i,k}^{A} \langle\varphi_i\varphi_k|v|\chi^{\mathrm{S}}_{ik} - \psi^{\mathrm{S}}_{ik}\rangle.$$

Using again the two-particle approximation

$$\chi^{\mathrm{S}}_{ik} = \left(1+\frac{\mathrm{P}v}{e}\right)^{-1} \varphi_{ik}, \qquad \psi^{\mathrm{S}}_{ik} = \left(1+\frac{\mathrm{P}_s v}{e}\right)^{-1} \varphi_{ik}$$

together with $\delta\psi = \chi^{\mathrm{S}}_{ik} - \psi^{\mathrm{S}}_{ik}$ and

$$\delta\mathrm{P} = \mathrm{P}-\mathrm{P}_s = -\tfrac{1}{2}\sum_{i<F}^{A} |\varphi_{is}\rangle\langle\varphi_{is}|,$$

it follows, analogously to (35), that

$$\Delta(S) = \tfrac{1}{2}\sum_{\substack{i,k<F\\ j>F}}^{A} \frac{|\langle\varphi_i\varphi_k|v|\psi_{js}\rangle|^2}{\varepsilon_j+\varepsilon_s-\varepsilon_i-\varepsilon_k}. \tag{37}$$

With

$$V(s) = \sum_{i}^{A} \langle \varphi_i \varphi_s | v | \psi_{is} \rangle, \tag{38}$$

it follows for the separation energy

$$-S(s) = \frac{k_s^2}{2m} + V(k_s) + \Delta(k_s).$$

3.4. THE EXCITATION ENERGY

Using the results of the last two subsections 3.2 and 3.3 it is easy to estimate the energy needed to excite a particle from a state $|\mathbf{s}\rangle$ with $k_s \leqq k_F$ to a state $|\mathbf{q}\rangle$ with $q \geqq k_F$. To do this it is necessary to investigate on the one hand a A-particle system in the ground state with the energy E_A, and on the other hand the excited state which corresponds to the free-particle state in which the single-particle state $|\mathbf{q}\rangle$ is occupied and the state $|\mathbf{s}\rangle$ is unoccupied.

In the framework of the two-particle approximation discussed here the excitation energy is

$$S(s, q) = E_A(s, q) - E_A = \frac{q^2}{2m} - \frac{k_s^2}{2m} + \sum_{i<F}^{A} \langle \varphi_i \varphi_q | v | \psi_{iq} \rangle - \sum_{i}^{A} \langle \varphi_i \varphi_s | v | \psi'_{is} \rangle + \tfrac{1}{2} \sum_{i}^{A} \langle \varphi_i \varphi_k | v | \psi'_{ik} - \psi_{ik} \rangle,$$

with

$$\psi_{ik} = \left(1 + \frac{\mathrm{P}v}{e}\right)^{-1} \varphi_{ik}, \qquad \psi'_{ik} = \left(1 + \frac{\mathrm{P}'v}{e}\right)^{-1} \varphi_{ik}$$

and

$$\mathrm{P}' = \tfrac{1}{4} \sum_{i,k>F} |\varphi_{ik}\rangle\langle\varphi_{ik}| - \tfrac{1}{2} \sum_{i>F} |\varphi_{iq}\rangle\langle\varphi_{iq}| + \tfrac{1}{2} \sum_{i>F} \varphi_{is}\rangle\langle\varphi_{is}|.$$

On account of eqs. (36) and (38) we obtain

$$S(s, q) = \frac{q^2}{2m} - \frac{k_s^2}{2m} + V(q) - V(k_s) + \Delta(s, q)$$

where

$$\Delta(s, q) = \tfrac{1}{2} \sum_{i,k}^{A} \langle \varphi_i \varphi_k | v | \psi'_{ik} - \psi_{ik} \rangle$$

is the r.e. of the excitation process. Together with $\delta\psi = \psi'_{ik} - \psi_{ik}$ and

$$\delta\mathrm{P} = \mathrm{P}' - \mathrm{P} = \tfrac{1}{2} \sum_{i>F} |\varphi_{is}\rangle\langle\varphi_{is}| - \tfrac{1}{2} \sum_{i>F} |\varphi_{iq}\rangle\langle\varphi_{iq}|,$$

it follows, in the same way as in eqs. (35) and (37), that

$$\Delta(s, q) = \tfrac{1}{2} \sum_{\substack{i,k<F \\ j>F}} \frac{|\langle \varphi_i \varphi_k | v | \psi_{jq} \rangle|^2}{\varepsilon_j + \varepsilon_q - \varepsilon_i - \varepsilon_k} - \tfrac{1}{2} \sum_{\substack{i,k<F \\ j>F}} \frac{|\langle \varphi_i \varphi_k | v | \psi_{js} \rangle|^2}{\varepsilon_j + \varepsilon_s - \varepsilon_i - \varepsilon_k},$$

or

$$\Delta(s, q) = \Delta(q) - \Delta(s).$$

Therefore, the excitation energy is

$$S(s, q) = \frac{q^2}{2m} - \frac{k_s^2}{2m} + V(q) - V(ks) + \Delta(q) - \Delta(k_s),$$

so that $W(q) = V(q) + \Delta(q)$ is the single-particle potential which is relevant for the excitation process.

3.5. RELATIONS TO THE SELF-CONSISTENCY

The system of simultaneous equations (27)—(31) expresses what is usually called the self-consistency of the single-particle potential $V(k)$. In other words $V(k)$ depends on the same functions ψ_{ik} which can be calculated from $V(k)$ together with eq. (27). The further self-consistency condition (31) which is important for the calculation of the single-particle functions in finite systems, is identically fulfilled on account of the translation invariance of nuclear matter.

For the physical interpretation of the rearrangement effects these concepts are of interest in the following respect: from the expression (32) for the r.e. of the separation process (which will be discussed here as an example), it follows that $\Delta(k_F)$ derives from the fact that δP and δe are different from zero. The fact that $\delta P \neq 0$ is due to the exact consideration of the Pauli principle in the two-body approximation. The quantity δe, which is important for the second term, derives from the dependence of $V(k)$ on the wave function ψ_{ik} (what we have called the self-consistency). Therefore, one usually considers the r.e. as induced by two effects, the Pauli principle and the self-consistency [1–4]). However, such a formulation has a strict meaning only with respect to the Hartree-Fock approximation. In the Hartree-Fock theory the effect of the Pauli-principle is not taken into account in the manner described here. Therefore $\delta P = 0$ and the first term in eq. (32) vanishes. Furthermore in the Hartree-Fock method $\psi_{ik} = \varphi_{ik}$ and consequently there is no self-consistency condition to be satisfied, and therefore $\delta e = 0$. Hence in the framework of the Hartree-Fock method $\Delta(k_F) = 0$. In a more formal way this result follows directly when we use the expression (14a) and substitute $\psi_{ik} = \varphi_{ik}$. Then

$$\Delta(k_F) = \tfrac{1}{2} \sum_{i,k}^{A} \frac{\partial}{\partial A} \langle \varphi_i \varphi_k | v | \varphi_{ik} \rangle = 0,$$

for the function φ_{ik} does not depend explicitly on A. That is obviously not the case for finite systems, so that even in the Hartree-Fock method there results a r.e. different from zero.

By these considerations it is clear that the r.e. is in no way mainly induced by the Pauli-principle and the self-consistency. This is only the case in the

framework of the two-particle approximation, where the Bethe-Goldstone wave function depends on A only through the Pauli principle and self-consistency. The true two-particle wave function $\psi_{ik} = \int \Pi^{ik*} \Psi$ depends on A in a much more complicated manner than the Bethe-Goldstone function defined by eq. (27).

4. Comparison with experiment

In this section we shall discuss the question whether the r.e. is a measurable quantity or not. From the general expressions (8), (18b), (25) it follows that the r.e. is not the expectation value of a Hermitian operator. Therefore, the r.e. cannot be interpreted as an observable in the usual sense. The measurability of the r.e. is especially problematic on account of the fact that the r.e. depends strongly on the arbitrarily chosen model wave function Φ_A †.

On the other hand, numerical values of the r.e. have been given [2, 5-8]), which have been determined partially by comparison with experiment. However, this apparent contradiction can be removed if one takes into account that for a given model wave function the r.e. can be determined eventually by calculating backward from the experimental data: this has been done in the papers quoted above by assumption of the Fermi-model Π_A. Still, we shall see that this determination of Δ depends essentially on very special and rather unrealistic assumptions, which generally cannot be justified.

In the following we shall discuss two kinds of experiment for which the r.e. is important in the sense mentioned above: the elastic scattering in the approximation of the optical model and the inelastic scattering in the approximation of the direct interaction [13, 14]).

4.1. ELASTIC SCATTERING

The elastic scattering can be described by the S-matrix (16). As has been shown by Brenig [6]), this S-matrix as well the optical potential (18) are independent of the model wave function Φ_A. Therefore, these quantities can be determined directly from experiment. However, for the functions $V(q)$ and $\Delta(q)$ this is only the case under very special assumptions, as will be shown in the following.

We use the model wave function Π_A and assume that $V(k)$ can be written in the effective mass approximation as $V = V_0 + V_1 k^2/k_F^2$ and that $\Delta(k)$ is approximately independent of k, i.e. $\Delta(k) = \Delta_0$.

For the energy per particle which is known from experiment it then follows

† Of course, for a given model wave function the r.e. can be calculated backwards from a "maximal" observation, from which the wave function Ψ_A can be determined apart from a phase factor. However, this is not relevant for the present situation, in which only a few experimental results are known.

that

$$-\frac{E}{A}=\frac{3}{5}\frac{k_F^2}{2m}+\tfrac{1}{2}V_0+\tfrac{3}{10}V_1$$

and for the separation energy

$$-S=\frac{k_F^2}{2m}+V_0+V_1+\Delta_0.$$

Together with the experimental value of the optical potential at a given k_0,

$$W(k_0)=V_0+V_1\frac{k^2}{k_F^2}+\Delta_0,$$

it is possible to determine the parameters V_0, V_1 and the r.e. Δ from the experimental values of S, k_F and $W(k_0)$.

In this sense the r.e. which belongs to the model Π_A can be determined from experiment. However, this method depends essentially upon the rather unrealistic assumptions about $V(k)$ and $\Delta(k)$. For even if the function $W(k)$ is known from experiment for all values of k, and one makes the assumption $\Delta=\Delta_0+\Delta_1 k^2/k_F^2$ instead of $\Delta=\Delta_0$, it is no longer possible to determine the values of V_0, V_1, Δ_0, Δ_1 from experiment by means of the relations

$$-S=\frac{3}{5}\frac{k_F^2}{2m}+\tfrac{1}{2}V_0+\tfrac{3}{10}V_1=\frac{k_F^2}{2m}+V_0+V_1+\Delta_0+\Delta_1$$

and

$$W(k_0)=V_0+V_1\frac{k_0^2}{k_F^2}+\Delta_0+\Delta_1\frac{k_0^2}{k_F^2}.$$

The possibility to determine $V(k)$ and $\Delta(k)$ from the experimental data of E/A, S, ρ, $W(k_0)$, in the special case mentioned above, was brought about by the fact that the whole theory was characterised only by the 4 parameters V_0, V_1, Δ_0, k_F. If one wants to use an approximation that is better than the effective mass approximation for $V(k)$ and the zeroth order approximation for Δ, other experimental results on nuclear matter would have to be taken into account. But there are no such experimental data.

4.2. INELASTIC SCATTERING

Another process, which is well known from experiment and which seems to be very closely related to the problem of r.e., is the inelastic scattering of nucleons by complex nuclei. To describe this process we use the method of direct interaction [11, 14]). In other words we again use Π_A for the model state and assume that the incoming particle is scattered only by one single-particle in the interior of the nucleus. Here the kinetic and potential energy of the colliding particles

are to be determined by the single-particle energies corresponding to the model function Π_A. To calculate the cross sections by this method only the functions $V(k)$, $\Delta(k)$ and $W(k)$ discussed above are needed. Therefore, we shall investigate the question whether — at least in the direct interaction approximation — $\Delta(k)$ can be determined backwards from the experimental cross sections: we shall see that this is not the case.

Now $V(k)$ is as before the single particle potential (24) and $W(k)$ the corresponding optical potential. We call the momentum of the incoming particle $\mathbf{k}_1$ and that of the particle which is in the nuclear matter $\mathbf{k}_0$ ($k_0 \leqq k_F$). The energy of the incoming particle is

$$\varepsilon_1 = \frac{k_1^2}{2m} + W(k_1).$$

After the scattering process, which may be described by the corresponding S-matrix, the energy is

$$\varepsilon'_1 = \frac{k_1'^2}{2m} + W(k'_1),$$

If ε_0 and ε'_0 denote the energy of the collided particle before and after the collision, we obtain, on account of energy conservation,

$$\varepsilon_0 + \varepsilon_1 = \varepsilon'_0 + \varepsilon'_1.$$

The energy which is needed to excite a particle from state $|\mathbf{k}_0\rangle$ to the state $|\mathbf{k}'_0\rangle$ is, according to eq. (39),

$$S(k_0, k'_0) = \frac{k_0'^2}{2m} - \frac{k_0^2}{2m} + V(k'_0) - V(k_0) + \Delta(k'_0) - \Delta(k_0).$$

On the other hand the incoming particle loses the energy

$$\Delta\varepsilon = \frac{k_1^2}{2m} - \frac{k_1'^2}{2m} + W(k_1) - W(k'_1),$$

owing to the transition from the state $|\mathbf{k}_1\rangle$ to the state $|\mathbf{k}'_1\rangle$. On account of energy conservation $S(k_0, k'_0)$ and $\Delta\varepsilon$ are equal, and therefore

$$\frac{k_0^2}{2m} + \frac{k_1^2}{2m} + W(k_0) + W(k_1) = \frac{k_0'^2}{2m} + \frac{k_1'^2}{2m} + W(k'_0) + W(k'_1).$$

This relation means that the collision process of two particles described in the direct interaction approximation is the same as if the particles were moving in the potential $W(k)$. Therefore, in the description of the inelastic scattering the potentials $V(k)$ and $\Delta(k)$ are unimportant and only their sum, the optical potential $W(k)$, has a physical meaning. For this reason a determination of the

r.e. by analysing the inelastic scattering data in the direct interaction approximation is not possible.

The author is greately indebted to Dr. W. Brenig and Dr. G. Lüders for stimulating discussions.

References

1) K. A. Brueckner, Phys. Rev. **110** (1958) 597
2) P. Mittelstaedt, Nuclear Physics **8** (1958) 171
3) P. Mittelstaedt, Nuclear Physics **9** (1958/59) 116
4) D. J. Thouless, Phys. Rev. **112** (1958) 906
5) W. Brenig, Nuclear Physics **4** (1957) 363
6) W. Brenig, Nuclear Physics **13** (1959) 333
7) L. C. Gomes, J. D. Walecka and V. F. Weisskopf, Ann. Phys. **3** (1958) 241
8) R. J. Eden, Ann. Rev. Nucl. Science, **7** (1957) 1
9) K. A. Brueckner and J. L. Gammel, Phys. Rev. **109** (1958) 1023 further references may be found in this paper.
10) H. A. Bethe and J. Goldstone, Proc. Roy. Soc. A **238** (1957) 551
11) H. A. Bethe, Phys. Rev. **103** (1956) 1353
12) N. M. Hugenholz, Physica **23** (1957) 481
13) W. Heisenberg, Ber. Sächs. Akademie **89** (1957) 369
14) M. L. Goldberger, Phys. Rev. **74** (1948) 1269

8.B

Nuclear Physics **17** (1960) 516—528; © *North-Holland Publishing Co., Amsterdam*

Not to be reproduced by photoprint or microfilm without written permission from the publisher

SELECTION RULES IN STRONG INTERACTIONS

SEIBUN SASAKI

Institute of Physics, Faculty of Science, Kumamoto University, Kumamoto, Japan

Received 7 March 1960

Abstract: The invariances under P- and T-transformations in the electromagnetic and the mesonic interactions are discussed using the generalized Dirac equation obtained by assuming invariance only under the proper Lorentz transformation. It is shown that the existence of P- and T-invariance in the above interactions is based on the fact that the theories must be invariant under the extended gauge-like transformations. The strong mesonic interactions are found to be derivative. The "principle of the minimal electromagnetic interaction" and the assumption of the "global symmetry" for the strong mesonic interactions are naturally obtained from our standpoint.

1. Introduction

So far, the invariance under the transformations of parity inversion (P-transformation), charge conjugation (C-transformation) and time reversal (T-transformation) is believed to be confirmed experimentally for the electromagnetic interactions as well as for the strong ones. But for the weak interactions, the situation is quite different. It is proved pretty rigorously by various experiments that P- and T-invariance do not hold in the decay processes for which the weak interactions are responsible. Therefore, it seems reasonable to consider that all interactions are originally not invariant under P- and T-transformations and that the strong interactions are distinguished from the weak interactions by some additional conservation law or something similar. As an example, let us consider the case of quantum electrodynamics (Q.E.D.). Usually, Q.E.D. is built up under the assumption that the theory is invariant not only under proper Lorentz transformations but also under improper Lorentz transformations. But, from the above point of view, it seems unnecessary to retain the latter invariance. If the theory is required to be invariant only under the proper Lorentz transformations, we cannot consider the usual Dirac equation as the only possible form of linearization for the Klein-Gordon equation of motion [1, 2]), and we must therefore reconsider the properties of Q.E.D. under parity transformations from the new point of view. Lately, using the ordinary Dirac equation, S. N. Gupta [3]) pointed out that the invariance under P- and T-transformations in the electromagnetic interaction is due to the supplementary condition for the electromagnetic potential A_μ. His arguments, however, should be subjected to some modifications from our point of view.

Firstly, as we have assumed the invariance only under the proper Lorentz transformations, the Dirac equation itself must be reconsidered[1,2]), as it is so constructed that it may also be invariant under the improper Lorentz transformations. As the generalized Dirac equation thus obtained shows an effect of parity mixing for the fermion, we must examine the above arguments again for the generalized Q.E.D. in which, instead of the ordinary Dirac equation, the generalized one is used. As the additional conservation law, we can use the conservation law of the charge-current density. There are two types of interactions in Q.E.D., the vectorial interaction and the Pauli type interaction. The charge-current conservation law is able to remove the factor which is not invariant under P- and T-transformations from the vectorial interaction term. But, as this law has no such effect on the Pauli-term, and the presence of the latter interaction would accordingly cause effects arising from violation of P- and T-invariance, the Pauli-term should be excluded by some selection rule. In Q.E.D., this conservation law is intimately related with the property of invariance under the gauge transformations. The situation mentioned above can be reproduced by assuming the gauge invariance of the theory. In the section 3 of this paper, the role of the charge-current conservation law, the property of invariance under the gauge transformation and the selection rule for removing the Pauli-term are discussed in detail for Q.E.D., while section 2 is devoted to an outline of the generalization of the Dirac equation. It seems reasonable to consider that this selection rule offers the theoretical foundation for the "principle of the minimal electromagnetic interaction" [4]). For obtaining the selection rule satisfactorily, we have extended the concept of gauge transformation rather artificially, and have required the invariance of the theory under these extended gauge-like transformations. In general, to the requirement of this kind of invariance there corresponds one identical relation such as the charge-current conservation law in Q.E.D., and if this relation does not fit the physical experience, one must abandon the theory which gives rise to such a relation. In this way, the possibility of the wave function of the photon being pseudovector is excluded. To treat the electromagnetic field consistently with the fermion field and the interaction between them, we must introduce an artificial constant spinor, the physical meaning of which is not yet clear.

With only slight modifications, the selection rule obtained in Q.E.D. is also applicable to the pion-nucleon system. And further, if the assumption of the "global symmetry" [5]) is made, or rather if the coupling constants of the interactions $\Lambda\Sigma\pi$ and $\Sigma\Sigma\pi$ are equal, our selection rule is found to be applicable to all the strong interactions containing pions (the strong mesonic interactions). Conversely, by imposing our selection rule to the strong mesonic interactions, we are naturally led to the assumption of the global symmetry for them. The strong mesonic interactions, as well as the general case of the strong interactions of the Yukawa type containing iso-boson spin zero particles with strangeness

zero, are treated in section 4. It is found that the strong mesonic interactions are of derivative type.

Lately, S. Ozaki [2]) proposed a new selection rule. Though our selection rule is different from his, it seems remarkable that we can obtain the same results as those obtained by him.

As to the strong interactions, we assume charge independence and conservations of charge, strangeness and baryon number as well as invariance under the proper Lorentz transformations. The invariance under P- and T-transformations for the strong mesonic interactions is one of the results of our selection rule.

2. Generalization of the Dirac Equation

According to the general theory, we can rewrite the Klein-Gordon equation for the Dirac field $(\Box-\kappa^2)\psi=0$ into the form $\mathrm{d}(\partial)\Lambda(\partial)\psi=0$. Then, we obtain as the generalized Dirac equation

$$-\Lambda(\partial)\psi=(\mathrm{e}^{A\gamma_5}\gamma_\mu\partial_\mu+\kappa\mathrm{e}^{-B\gamma_5})\psi=0, \tag{1}$$

and, as the corresponding operator, the expression

$$\mathrm{d}(\partial)=-(\mathrm{e}^{A\gamma_5}\gamma_\mu\partial_\mu-\kappa\mathrm{e}^{B\gamma_5}). \tag{2}$$

The ordinary Dirac equation can be obtained by putting the arbitrary constants A and B equal to zero. The commutation relation for ψ takes the form

$$\{\psi_\alpha(x),\bar{\psi}_\beta(x')\}_+=-i(\mathrm{e}^{A\gamma_5}\gamma_\mu\partial_\mu-\kappa\mathrm{e}^{B\gamma_5})_{\alpha\beta}\Delta(x-x'),$$

where

$$\bar{\psi}=\psi^\dagger\exp(\tfrac{1}{2}\{(B+B^*)-(A-A^*)\}\gamma_5),\quad \psi^\dagger=\psi^*\gamma_4.$$

Now, let us consider the operator of the form $\mathrm{e}^{\alpha\gamma_5}$ (α is a c-number contant) such that the relations

$$\mathrm{e}^{\alpha\gamma_5}\gamma_\mu\mathrm{e}^{\alpha\gamma_5}=\gamma_\mu,\quad \mathrm{e}^{\alpha\gamma_5}\mathrm{e}^{A\gamma_5}\mathrm{e}^{-\alpha\gamma_5}=\mathrm{e}^{\alpha\gamma_5}\mathrm{e}^{-B\gamma_5}\mathrm{e}^{\alpha\gamma_5}$$

may hold. The first relation is identical and the second can be satisfied if we choose

$$\alpha=\tfrac{1}{2}(A+B).$$

Using this operator and introducing the new wave function φ defined by the relation

$$\psi=\mathrm{e}^{\alpha\gamma_5}\varphi, \tag{3}$$

the equation of motion for φ reduces to the form

$$(\gamma_\mu\partial_\mu+\kappa)\varphi=0.$$

This is just the ordinary Dirac equation. Moreover, the commutation relation for φ becomes

$$\{\varphi_\alpha(x), \varphi_\beta^\dagger(x')\}_+ = -i(\gamma_\mu\partial_\mu-\kappa)_{\alpha\beta}\Delta(x-x').$$

This is again the ordinary commutation relation for the ordinary Dirac field. Thus, so far as the free field is concerned, our formalism makes no effective difference from the ordinary theory, as it should be. The transformation (3) is that which reduces the generalized Dirac equation to the ordinary one. In the following, we shall call this transformation the "reducing transformation" and shall write it simply as R.T. It also shows that the wave function ψ obeying the generalized Dirac equation is a mixture of terms of opposite parities and the rate of mixing is determined by the constant α. The value of α can be chosen differently for the different fermions.

3. Electromagnetic Interactions

In this section, we shall consider the system of a nucleon and an electromagnetic field. The total Lagrangian of the system is, in general, written as [6])

$$\begin{aligned}
L &= L_N + L_{int} + L_R, \quad L_{int} = L_v + L_p, \\
L_N &= -\int \bar{N}(e^{A\gamma_5}\gamma_\mu\partial_\mu + \kappa e^{-B\gamma_5})N d^4x, \\
L_v &= ie\int \bar{N}e^{A\gamma_5}e^{-\delta\gamma_5}\gamma_\mu A_\mu \tfrac{1}{2}(1+\tau_3)N d^4x, \qquad (4) \\
L_p &= -\tfrac{1}{2}\frac{e'}{\kappa}\int \bar{N}e^{k\gamma_5}\sigma_{\mu\nu}F_{\mu\nu}\tfrac{1}{2}(1+\tau_3)N d^4x, \\
L_R &= -\tfrac{1}{4}\int F_{\mu\nu}F_{\mu\nu}d^4x,
\end{aligned}$$

where

$$\bar{N} = N^\dagger \exp\left(\tfrac{1}{2}\{(B+B^*)-(A-A^*)\}\gamma_5\right),$$

and N is the nucleon wave function obeying the generalized Dirac equation.

From the condition that the Lagrangian (4) must be Hermitian, we get the relations

$$\delta = \delta^*, \quad k = -B+is \qquad (5)$$

where s is an arbitrary real constant. The equations of motion obtained from the Lagrangian (4) are, using the relation (5),

$$\left\{\gamma_\mu(\partial_\mu - ie\tfrac{1}{2}(1+\tau_3)e^{\delta\gamma_5}A_\mu) + \tfrac{1}{2}\frac{e'}{\kappa}\tfrac{1}{2}(1+\tau_3)e^{-2\alpha\gamma_5}e^{is\gamma_5}\sigma_{\mu\nu}F_{\mu\nu} + \kappa e^{-2\alpha\gamma_5}\right\}N = 0, \qquad (6)$$

$$(\Box\delta_{\mu\nu}-\partial_\mu\partial_\nu)A_\nu = -j_\mu - J_\mu, \qquad (7)$$

where

$$j_\mu = ieN^\dagger e^{(\alpha+\alpha^*)\gamma_5}\gamma_\mu e^{\delta\gamma_5}\tfrac{1}{2}(1+\tau_3)N, \tag{8}$$

and

$$J_\mu = -\frac{e'}{\kappa}\partial_\nu(N^\dagger e^{(\alpha^*-\alpha)\gamma_5}e^{is\gamma_5}\sigma_{\mu\nu}N). \tag{9}$$

Applying the differential operator ∂_μ on both sides of eq. (7) and summing up with respect to the index μ, we find, since the left side and the second term of the right side vanish identically, that j_μ must satisfy the relation

$$\partial_\mu j_\mu = 0,$$

which exhibits the conservation law of the charge-current density. This relation must be consistent with eq. (6). By calculating the expression $\partial_\mu j_\mu$ directly from eq. (6), we find that the expression $\partial_\mu j_\mu$ vanishes if and only if the condition

$$\delta = 0 \tag{10}$$

is satisfied. As the relation $\partial_\mu J_\mu = 0$ holds identically, the charge-current conservation law cannot restrict the value of the constant s. Using the relations (5) and (10), and transforming the Lagrangian (4) by the R.T. (3), i.e.,

$$N = e^{\alpha\gamma_5}\mathring{N},$$

we get

$$\begin{aligned}
&L = L_{\mathrm{N}}^0 + L_{\mathrm{int}}^0 + L_{\mathrm{R}}^0, \quad L_{\mathrm{int}}^0 = L_{\mathrm{v}}^0 + L_{\mathrm{p}}^0,\\
&L_{\mathrm{v}}^0 = ie\int \mathring{N}^\dagger \gamma_\mu A_\mu \tfrac{1}{2}(1+\tau_3)\mathring{N}\mathrm{d}^4x,\\
&L_{\mathrm{p}}^0 = -\tfrac{1}{2}\frac{e'}{\kappa}\int \mathring{N}^\dagger e^{is\gamma_5}\sigma_{\mu\nu}F_{\mu\nu}\tfrac{1}{2}(1+\tau_3)\mathring{N}\mathrm{d}^4x,\\
&L_{\mathrm{N}}^0 = -\int \mathring{N}^\dagger(\gamma_\mu\partial_\mu + \kappa)\mathring{N}\mathrm{d}^4x,
\end{aligned} \tag{11}$$

where $\mathring{N}$ obeys the ordinary Dirac equation. It is apparent that the vectorial interaction is P- and T-invariant, but that the Pauli-term is not.

The same result can be obtained by requiring that the Lagrangian (4) must be invariant under the gauge transformations

$$\begin{aligned}
&A_\mu \to A'_\mu = A_\mu + \partial_\mu \Lambda,\\
&N \to N' = \exp\left(\tfrac{1}{2}ie\Lambda(1+\tau_3)\right)N.
\end{aligned} \tag{12}$$

In order to make the theory gauge invariant, we must take the value of δ equal to zero. If $\mathring{N}$ is substituted in place of N, these transformations also make the Lagrangian (11) invariant.

The condition $\delta = 0$ can also be obtained in the following manner. In the following, we consider the vectorial interaction and the Pauli-type one separately.

In the case when $e \neq 0$, $e' = 0$, let us introduce the apparent gauge-like transformations

$$\tfrac{1}{2}(1+\tau_3)A_\mu \to \tfrac{1}{2}(1+\tau_3)A_\mu + I\partial_\mu \Lambda, \quad N \to \mathrm{e}^{ie\Lambda}N, \tag{13}$$

where I denotes the unit matrix. Let us call this type of transformations the "extended gauge transformations". It is obvious that $L_{\mathrm{N}}+L_{\mathrm{int}}$ is invariant under the transformations (13) when and only when $\delta = 0$. To show that L_{R} is also invariant under the transformations (13), we must contrive some artificial treatment. Introducing the constant spinor ε having the property

$$\bar{\varepsilon}\tfrac{1}{2}(1+\tau_3)\varepsilon = 1, \quad \bar{\varepsilon}I\varepsilon = 1, \tag{14}$$

we write L_{R} as

$$\begin{aligned} L_{\mathrm{R}} &\to \bar{\varepsilon}L_{\mathrm{R}}\varepsilon \\ &= \bar{\varepsilon}\left(-\tfrac{1}{4}\int F_{\mu\nu}F_{\mu\nu}\mathrm{d}^4x\right)\varepsilon \\ &= \bar{\varepsilon}\left\{-\tfrac{1}{4}\int \tfrac{1}{2}(1+\tau_3)F_{\mu\nu}\tfrac{1}{2}(1+\tau_3)F_{\mu\nu}\mathrm{d}^4x\right\}\varepsilon. \end{aligned}$$

The above expression is easily found to be invariant under the transformations (13). There always exists such a constant spinor ε as defined above. Thus, by introducing the constant spinor ε into the theory, we find that there are two kinds of transformations under which Q.E.D. is invariant and both of them are intimately related with the conservation law of the charge-current density. Therefore, if we require the invariance of Q.E.D. under the transformations (13), we can obtain the condition $\delta = 0$. As was the case for the transformations (12), if $\mathring{N}$ is substituted in place of N, the transformations (13) also make the Lagrangian (11) invariant.

When $e = 0$, $e' \neq 0$, i.e., when there is only the Pauli-term, corresponding to the transformations (13), we introduce the transformations

$$\tfrac{1}{2}(1+\tau_3)\sigma_{\mu\nu}F_{\mu\nu} \to \tfrac{1}{2}(1+\tau_3)\sigma_{\mu\nu}F_{\mu\nu} + i\gamma_\mu\partial_\mu\Lambda, \quad \mathring{N} \to \mathrm{e}^{-i\frac{e'}{\kappa}\Lambda}\mathring{N}, \quad \Box\Lambda = 0. \tag{15}$$

It is easily found that the expression $L_{\mathrm{N}}^0 + L_{\mathrm{p}}^0$ is invariant under these transformations when and only when $s = 0$. To show that the free radiation part of the Lagrangian L_{R} is invariant under the above transformations, we shall examine the relation between $\bar{\varepsilon}\tfrac{1}{2}(1+\tau_3)\tfrac{1}{2}\sigma_{\mu\nu}F_{\mu\nu}\tfrac{1}{2}(1+\tau_3)\tfrac{1}{2}\sigma_{\lambda\rho}F_{\lambda\rho}\varepsilon$ and $F_{\mu\nu}F_{\mu\nu}$ where ε is a constant spinor satisfying the relation (14). The former is calculated as follows:

$$\bar{\varepsilon}\tfrac{1}{2}(1+\tau_3)\tfrac{1}{2}\sigma_{\mu\nu}F_{\mu\nu}\tfrac{1}{2}(1+\tau_3)\tfrac{1}{2}\sigma_{\lambda\rho}F_{\lambda\rho}\varepsilon$$
$$= \bar{\varepsilon}\tfrac{1}{2}(1+\tau_3)(\boldsymbol{\sigma}\cdot\mathbf{H}-i\boldsymbol{\alpha}\cdot\mathbf{E})(\boldsymbol{\sigma}\cdot\mathbf{H}-i\boldsymbol{\alpha}\cdot\mathbf{E})\varepsilon$$
$$= \bar{\varepsilon}\tfrac{1}{2}(1+\tau_3)\varepsilon(\mathbf{H}^2-\mathbf{E}^2)+i\bar{\varepsilon}\tfrac{1}{2}(1+\tau_3)\gamma_5\varepsilon(\mathbf{E}\cdot\mathbf{H}+\mathbf{H}\cdot\mathbf{E})$$
$$+\bar{\varepsilon}\tfrac{1}{2}(1+\tau_3)\boldsymbol{\alpha}\varepsilon\cdot(\mathbf{E}\times\mathbf{H}+\mathbf{H}\times\mathbf{E}).$$

As $\mathbf{E}$ is perpendicular to $\mathbf{H}$, the second term of the right side vanishes. The third term can be reduced to zero by the procedure

$$\int\boldsymbol{\alpha}\cdot(\mathbf{E}\times\mathbf{H}+\mathbf{H}\times\mathbf{E})\mathrm{d}^4x = \lim_{x'\to x}\boldsymbol{\alpha}\cdot\int(\mathbf{E}(x)\times\mathbf{H}(x')+\mathbf{H}(x')\times\mathbf{E}(x))\mathrm{d}^4x$$
$$= -8\pi i\lim_{x'\to x}\boldsymbol{\alpha}\cdot\boldsymbol{\nabla}'\int\delta(x-x')\mathrm{d}^4x$$
$$= 0.$$

Therefore, we can write L_{R} as follows:

$$L_{\mathrm{R}} = -\bar{\varepsilon}\tfrac{1}{8}\int\tfrac{1}{2}(1+\tau_3)\sigma_{\mu\nu}F_{\mu\nu}\sigma_{\lambda\rho}F_{\lambda\rho}\mathrm{d}^4x\varepsilon.$$

Applying the transformations (15), we get

$$L_{\mathrm{R}}\to-\bar{\varepsilon}\tfrac{1}{2}\int\{\tfrac{1}{2}(1+\tau_3)\tfrac{1}{2}\sigma_{\mu\nu}F_{\mu\nu}+i\gamma_\mu\partial_\mu\Lambda\}\{\tfrac{1}{2}(1+\tau_3)\tfrac{1}{2}\sigma_{\lambda\rho}F_{\lambda\rho}+i\gamma_\rho\partial_\rho\Lambda\}\mathrm{d}^4x\varepsilon$$
$$= \tfrac{1}{2}\int(\mathbf{E}^2-\mathbf{H}^2)\mathrm{d}^4x+\tfrac{1}{2}\bar{\varepsilon}\int(\gamma_\mu\partial_\mu\Lambda\gamma_\rho\partial_\rho\Lambda)\mathrm{d}^4x\varepsilon$$
$$-\bar{\varepsilon}\frac{i}{2}\int\tfrac{1}{2}(1+\tau_3)\{\tfrac{1}{2}\sigma_{\mu\nu}F_{\mu\nu}\gamma_\rho\partial_\rho\Lambda+\gamma_\rho\partial_\rho\Lambda\tfrac{1}{2}\sigma_{\mu\nu}F_{\mu\nu}\}\mathrm{d}^4x\varepsilon.$$

The second term of the right side vanishes owing to the condition on Λ, i.e., $\Box\Lambda=0$. The terms in the brackets in the third term of the right side can be calculated as

$$\tfrac{1}{2}\sigma_{\mu\nu}F_{\mu\nu}\gamma_\rho\partial_\rho\Lambda+\gamma_\rho\partial_\rho\Lambda\tfrac{1}{2}\sigma_{\mu\nu}F_{\mu\nu}$$
$$= (\boldsymbol{\sigma}\cdot\mathbf{H}-i\boldsymbol{\alpha}\cdot\mathbf{E})(\beta\partial_4\Lambda-i\beta\boldsymbol{\alpha}\cdot\boldsymbol{\nabla}\Lambda)+(\beta\partial_4\Lambda-i\beta\boldsymbol{\alpha}\cdot\boldsymbol{\nabla}\Lambda)(\boldsymbol{\sigma}\cdot\mathbf{H}-i\boldsymbol{\alpha}\mathbf{E})$$
$$= 2\beta\sigma_iH_i\partial_4\Lambda+2i\beta\gamma_5H_i\partial_i\Lambda+2\beta\alpha_i\alpha_kE_i\partial_k\Lambda.$$

Here, we used the relation $\sigma_i\alpha_k+\alpha_k\sigma_i=-2\gamma_5\delta_{ik}$. By integrating partially, as the second term vanishes because $\mathrm{div}\,\mathbf{H}=0$, we obtain

$$(2\beta\boldsymbol{\sigma}\cdot\partial_4\mathbf{H}+2\beta\alpha_i\alpha_k\partial_kE_i)\Lambda = 2i\beta\boldsymbol{\sigma}\cdot\left(\frac{\partial\mathbf{H}}{\partial t}+\mathrm{not}\,\mathbf{E}\right)\Lambda=0.$$

Thus, the transformed expression for L_{R} is shown to be invariant under the transformations (15). Accordingly, by requiring that the Lagrangian $L_{\mathrm{N}}^0+L_{\mathrm{p}}^0+L_{\mathrm{R}}$ must be invariant under the transformations (15), we can obtain the condition $s=0$ and hence, the P- and T-invariance of the theory is assured.

But these transformations cannot make the Lagrangian $L_N+L_p+L_R$ invariant. In order to make the part L_N+L_p of the Lagrangian invariant, they must be modified as

$$\begin{gathered} e^{(\alpha^*-\alpha)\gamma_5}\tfrac{1}{2}(1+\tau_3)\sigma_{\mu\nu}F_{\mu\nu} \to e^{(\alpha^*-\alpha)\gamma_5}\tfrac{1}{2}(1+\tau_3)\sigma_{\mu\nu}F_{\mu\nu}+ie^{(\alpha+\alpha^*)\gamma_5}\gamma_\mu\partial_\mu\Lambda, \\ N \to e^{-i\frac{\varepsilon'}{\kappa}\Lambda}N. \end{gathered} \tag{16}$$

As for L_R, if we impose upon the constant spinor ε the further condition $\bar{\varepsilon}\tfrac{1}{2}(1+\tau_3)\gamma_5\varepsilon = 0$, we can replace it by

$$L_R \to -\bar{\varepsilon}\tfrac{1}{8}\frac{1}{\cosh 2(\alpha^*-\alpha)}\int e^{2(\alpha^*-\alpha)\gamma_5}\tfrac{1}{2}(1+\tau_3)(\sigma_{\mu\nu}F_{\mu\nu})^2 d^4x\varepsilon,$$

in which we used the relation $e^{a\gamma_5} = \cosh a+\gamma_5\sinh a$. Here, we shall pay attention to the fact that, unlike the vectorial case, the transformations (15) and (16) have different forms unless $\alpha = 0$.

Now, it seems reasonable to postulate that quantum electrodynamics must be independent of the mixing ratio of parity for the fermion in all its aspects, especially, the extended gauge transformations which make the formalism invariant when only one of the vectorial and the Pauli-type interactions is present must be the same for any value of the mixing ratio for the fermion. In the following, we shall call this requirement the "equivalence requirement" and write it shortly as E.R. Hence, if we require that the interactions which do not satisfy the E.R. should be excluded, we can get rid of the Pauli-term from Q.E.D., and thus, we can conclude that the electromagnetic interaction can be obtained from the free Lagrangian by the replacement

$$\partial_\mu \to \partial_\mu - ie\tfrac{1}{2}(1+\tau_3)A_\mu, \tag{17}$$

which shows the "principle of the minimal electromagnetic interaction". This selection rule is found to be applicable to the cases of the strong mesonic interactions, as will be shown later.

At the end of this section, let us consider the possibility of the photon wave function A_μ being pseudovector. In this case, as the formalism is not invariant under the ordinary gauge transformations (12), we shall apply the extended gauge transformations (13) and require the invariance of the theory under the transformations

$$\tfrac{1}{2}(1+\tau_3)\gamma_5 A_\mu \to \tfrac{1}{2}(1+\tau_3)\gamma_5 A_\mu + I\partial_\mu\Lambda, \quad N \to e^{ie\Lambda}N.$$

However, the relation corresponding to this invariance becomes

$$\partial_\mu j_\mu^{\,p} = 2ie\kappa N^\dagger e^{(\alpha^*-\alpha)\gamma_5}\gamma_5\tfrac{1}{2}(1+\tau_3)N,$$

where

$$j_\mu^{\,p} = ieN^\dagger e^{(\alpha+\alpha^*)\gamma_5}\gamma_5\gamma_\mu\tfrac{1}{2}(1+\tau_3)N.$$

This is not the charge-current conservation law. Therefore, the possibility of the photon wave function A_μ being pseudovector must be excluded.

4. Strong Mesonic Interactions

4.1. PION-NUCLEON SYSTEM

The interactions between the pion and the nucleon have the form $\bar{N}O\boldsymbol{\tau}\cdot\boldsymbol{\pi}N$ where O denotes a suitable combination of γ-matrices. The total Lagrangian of the system is

$$\begin{aligned} L &= L_N + L_{N\pi} + L_\pi, \quad L_{N\pi} = L_{ps} + L_{pv}, \\ L_{ps} &= -ig_{ps}\int \bar{N}e^{\beta\gamma_5}\gamma_5\boldsymbol{\tau}\cdot\boldsymbol{\pi}N\,d^4x, \\ L_{pv} &= -ig_{pv}\int \bar{N}e^{\delta\gamma_5}\gamma_5\gamma_\mu\partial_\mu\boldsymbol{\tau}\cdot\boldsymbol{\pi}N\,d^4x, \\ L_\pi &= -\tfrac{1}{2}\int(\partial_\mu\boldsymbol{\pi}\cdot\partial_\mu\boldsymbol{\pi} + m^2\boldsymbol{\pi}\cdot\boldsymbol{\pi})\,d^4x, \end{aligned} \tag{18}$$

where N stands for the generalized nucleon wave function and m denotes the pion mass. As is in Q.E.D., the hermiticity conditions for $L_{N\pi}$ reduce to

$$\beta = -B + i\phi, \quad \delta = A + q$$

where both ϕ and q are real arbitrary constants. Transforming the nucleon wave function N to $\mathring{N}$ by the R.T. (3), we get

$$\begin{aligned} L = -\int\{&\mathring{N}^\dagger(\gamma_\mu\partial_\mu + \kappa)\mathring{N} + ig_{ps}\mathring{N}^\dagger e^{i\phi\gamma_5}\gamma_5\boldsymbol{\tau}\cdot\boldsymbol{\pi}\mathring{N} \\ &+ ig_{pv}\mathring{N}^\dagger e^{q\gamma_5}\gamma_5\gamma_\mu\partial_\mu\boldsymbol{\tau}\cdot\boldsymbol{\pi}\mathring{N}\}\,d^4x + L_\pi. \end{aligned} \tag{19}$$

This is not P- and T-invariant as it should be. In order to make it P- and T-invariant, we must have $\phi = q = 0$, but usually, as there is no property of the pion-nucleon system similar to the gauge invariance of Q.E.D., we cannot impose the above conditions.

Now we shall follow the case of Q.E.D., and require that the Lagrangian (19) be invariant under the transformations

$$\gamma_5\boldsymbol{\tau}\cdot\boldsymbol{\pi} \to \gamma_5\boldsymbol{\tau}\cdot\boldsymbol{\pi} + \Lambda I, \quad \mathring{N} \to e^{-ig_{pv}\Lambda}\mathring{N}, \quad \text{when } g_{ps} = 0,\ g_{pv} \neq 0; \tag{20}$$

$$\gamma_5\boldsymbol{\tau}\cdot\boldsymbol{\pi} \to \gamma_5\boldsymbol{\tau}\cdot\boldsymbol{\pi} + \gamma_\mu\partial_\mu\Lambda, \quad \mathring{N} \to e^{-ig_{ps}\Lambda}\mathring{N}, \quad \text{when } g_{ps} \neq 0,\ g_{pv} = 0; \tag{21}$$

where Λ is a c-number space-time scalar function obeying the relation

$$(\Box - m^2)\Lambda = 0.$$

As in Q.E.D., the pion part of the Lagrangian L_π is to be considered, introducing the constant spinor ε defined by the relations (14), as

$$\partial_\mu\pi\cdot\partial_\mu\pi+m^2\pi\cdot\pi$$
$$=\bar{\varepsilon}\{\partial_\mu\pi\cdot\partial_\mu\pi+m^2\pi\cdot\pi\}\varepsilon \tag{22}$$
$$=\bar{\varepsilon}\{\partial_\mu(\gamma_5\tau\cdot\pi)\partial_\mu(\gamma_5\tau\cdot\pi)+m^2(\gamma_5\tau\cdot\pi)(\gamma_5\tau\cdot\pi)\}\varepsilon.$$

The expression (22) is found to be invariant under the transformation (20) or (21). Requiring the above restrictions, we can get $p=0$ or $q=0$ in the same way as in Q.E.D., and are able to obtain the P- and T-invariant theory. In this case, however, there is no transformation under which both the direct and the derivative interactions remain invariant. Therefore, if one of them is allowed, the other should be abandoned.

Now, it is reasonable to impose the E.R. to the pion-nucleon system as was done in Q.E.D. For the pion-nucleon system, the E.R. takes the following form: for both the common theory using the ordinary Dirac equation and the generalized theory using the generalized Dirac equation, the formalism of the pion-nucleon system should be invariant under the same transformations. The derivative interaction is easily proved to satisfy the above requirement. As for the direct one, the transformations which make the generalized theory invariant must take the form

$$e^{(\alpha^*-\alpha)\gamma_5}\gamma_5\tau\cdot\pi\to e^{(\alpha^*-\alpha)\gamma_5}\gamma_5\tau\cdot\pi+e^{(\alpha+\alpha^*)\gamma_5}\gamma_\mu\partial_\mu\Lambda,\quad N\to e^{-ig_{p\Lambda}\Lambda}N.$$

It is apparent that these have a different form from that of the transformations (22). Hence, the direct interaction should be excluded so long as we postulate the E.R., and thus, we can say that the type of interaction for the pion-nucleon system is derivative.

4.2. GENERAL STRONG MESONIC INTERACTIONS

The allowed forms of interaction are, omitting γ-matrices,

$$g_1\bar{N}\tau\cdot\pi N, \tag{23-1}$$
$$g_2\{\bar{\Lambda}\Sigma\cdot\pi+\bar{\Sigma}\cdot\pi\Lambda\}, \tag{23-2}$$
$$g_3 i(\bar{\Sigma}\times\Sigma)\cdot\pi, \tag{23-3}$$
$$g_4\bar{\Xi}\tau\cdot\pi\Xi. \tag{23-4}$$

The interaction (23-4) can be treated in parallel with (23-1). The reducing transformations for Λ and Σ are

$$\Lambda=e^{\beta\gamma_5}\mathring{\Lambda},\quad \Sigma=e^{\delta\gamma_5}\mathring{\Sigma},$$

respectively. In this case, however, we cannot satisfy the E.R. unless $\beta=\delta$. As there seems to be no reason for the Λ- and Σ-particles to have equal mixing ratios of parity, we cannot put $\beta=\delta$ from the beginning. In order to satisfy the

E.R., the form of the interaction must be

$$\bar{B}\boldsymbol{\tau}\cdot\boldsymbol{\pi}B \tag{24}$$

where $\bar{B}$ denotes the iso-spinor baryon wave function obeying the generalized Dirac equation. Therefore, whether eqs. (23-2) and (23-3) satisfy the E.R. depends upon whether we can construct the form of interaction (24) from them. The assumption of the "global symmetry" shows the very possibility for this. We can conclude that, if the strong mesonic interactions satisfy the E.R., they must be written as

$$g_i\bar{B}_i\boldsymbol{\tau}\cdot\boldsymbol{\pi}B_i \quad (i=1,2,3,4),$$

where

$$B_1=N,\quad B_2=\frac{1}{\sqrt{2}}\begin{pmatrix}\Sigma_1-i\Sigma_2\\ \Lambda+\Sigma_3\end{pmatrix},\quad B_3=\frac{1}{\sqrt{2}}\begin{pmatrix}\Lambda-\Sigma_3\\ \Sigma_1+i\Sigma_2\end{pmatrix},\quad B^4=\Xi,$$

provided that $g_2=g_3$; or alternatively that if the strong mesonic interactions are globally symmetric, they satisfy the E.R. By repeating the same procedure as was used for the pion-nucleon system, we can show that the whole theory becomes P- and T-invariant. The types of interactions are, of course, derivative.

4.3. STRONG INTERACTIONS BETWEEN THE BARYONS AND THE ISO-BOSON SPIN ZERO PARTICLE WITH STRANGENESS ZERO

The treatment for the iso-vector boson is almost the same as for the case of the pion treated above. Let us write the wave function of the iso-vector spin 0 particle as $\mathbf{V}$. Then, the strong interactions between $\mathbf{V}$ and the baryons that satisfy the E.R. must have the form

$$g\bar{B}\Gamma\gamma\boldsymbol{\tau}\cdot\partial\mathbf{V}B,$$

where $\gamma\partial$ denotes 1 for the direct coupling and $\gamma_\mu\partial_\mu$ for the derivative coupling, and

$$\Gamma=\begin{cases}1 & \text{for even parity } \mathbf{V},\\ \gamma_5 & \text{for odd parity } \mathbf{V}.\end{cases}$$

Concerning the properties of the E.R., the matrices that appear in the above expression are classified into two groups:

$$\text{(1)}\quad \gamma_\mu,\quad \gamma_5\gamma_\mu,$$
$$\text{(2)}\quad 1,\quad \gamma_5.$$

When the ordinary Dirac equation is used, the formalism becomes invariant under the following transformations:

$$\text{for group (1): } \Gamma\boldsymbol{\tau}\cdot\mathbf{V}\to\Gamma\boldsymbol{\tau}\cdot\mathbf{V}+I\cdot\Lambda,\quad B\to e^{-ig\Lambda}B;$$
$$\text{for group (2): } \Gamma\boldsymbol{\tau}\cdot\mathbf{V}\to\Gamma\boldsymbol{\tau}\cdot\mathbf{V}+\gamma_\mu\partial_\mu\Lambda,\quad B\to e^{-ig\Lambda}B.$$

In the above expressions, the quantity Λ is a c-number space-time scalar function obeying the relation

$$(\Box - M^2)\Lambda = 0,$$

and the quantity M denotes the mass of the iso-vector spin 0 particle. As is easily seen, the second group does not satisfy the E.R., and must therefore be abandoned. Next, if the wave function of the iso-scalar spin 0 particle is S, the form of the interaction must be

$$g\bar{B}\Gamma\gamma\partial SB,$$

and can be treated in parallel with the iso-vector cases. Therefore, remembering that the derivative coupling of the scalar boson does not play a role in meson physics, we can conclude that if there exist in nature iso-boson (vector or scalar) particles with spin zero and strangeness zero, they must be pseudoscalar particles with derivative coupling. Thus, we arrive at the same result as that obtained by S. Ozaki [2]) from a different point of view.

In our case of strong interactions between the baryons and the iso-boson spin zero particle with strangeness zero, according to the existence of the proposed extended gauge invariance, it is found that the interaction terms can be obtained from the free Lagrangian for the baryon by the substitutions

$$\gamma_\mu\partial_\mu \to \gamma_\mu\partial_\mu + ig\Gamma\gamma_\mu\boldsymbol{\tau}\cdot\mathbf{V}$$

for the iso-vector spin 0 particle, and

$$\gamma_\mu\partial_\mu \to \gamma_\mu\partial_\mu + ig\Gamma\gamma_\mu S$$

for the iso-scalar spin 0 particle. This may be called the "principle of the minimal mesonic interaction", corresponding to the "principle of the minimal electromagnetic interaction".

4. Discussion

In this paper, we have considered the gauge invariance of Q.E.D. only as a mathematical latitude of the theory, leaving out any speculation concerning its nature. The requirement of gauge invariance is so strong that the form of the interaction is Q.E.D. is well determined even though the invariance of the theory is only required under the proper Lorentz transformations (except for the Pauli-term). [1-3, 7]) Following Q.E.D., after extending the concept of gauge invariance and requiring that the strong mesonic interactions be invariant under gauge-like transformations of extended form, we can restrict the strong mesonic interactions to be P- and T-invariant and further we can restrict them to be derivative interactions. The property of invariance under the new transformations must be interpreted as follows: in the strong interactions between the

baryons and the iso-boson spin 0 particle with strangeness zero, the expressions

$$\Gamma\gamma\boldsymbol{\tau}\cdot\mathbf{V} \quad \text{or} \quad \Gamma\gamma S(\tfrac{1}{2}(1\pm\tau_3)\gamma_\mu A_\mu)$$

are indefinite by a space-time scalar quantity. Of course, the ordinary gauge transformation in Q.E.D. can be included into this interpretation. We must introduce the constant spinor ε for treating the boson part of the Lagrangian, but unfortunately, its physical meaning is not clear.

As to the case of the K-particle, according to the conservation of strangeness, the strong K interactions of the Yukawa type necessarily contain three different particles and we cannot therefore treat them by the procedure mentioned above for the spin 0 particles with strangeness zero. If we assume that the formalism must reduce to the ordinary one by applying the R.T. to each of the fermions participating in the interaction, then, so long as the K-particle has pure parity, the mixing ratio of the parities of the fermions must be equal for all the baryons. However, if such an assumption as a compound model is correct for the K-particle, it seems unnecessary to assume that the K-particle has pure parity, and it may happen that the requirement itself that the theory must reduce to the ordinary one by the R.T. has to be reconsidered. Anyway, it seems to be difficult to find a solution in the case of the K-particle.

The author wishes to express his heartful thanks to Prof. S. Ozaki for his kind help and discussions.

References

1) S. Ozaki and S. Sasaki, Soryushiron Kenkyu **19** (1959) 589 (mimeographed in Japanese); S. Sasaki, Kumamoto Journal of Science **4** (1960) 176
2) S. Ozaki, Progr. Theor. Phys. **23** (1960) 221
3) S. N. Gupta, Canadian Journal of Physics **35** (1957) 1309
4) M. Gell-Mann, Nuovo Cim. Suppl. **4** (1956) 848
5) M. Gell-Mann, Phys. Rev. **106** (1957) 1296
6) S. Ozaki, Progr. Theor. Phys. **14** (1955) 511; Nuclear Physics **15** (1960) 501
7) V. G. Soloviev, Nuclear Physics **6** (1958) 618

8.B

Nuclear Physics **17** (1960) 529—547; © *North-Holland Publishing Co., Amsterdam*

Not to be reproduced by photoprint or microfilm without written permission from the publisher

DISCRIMINATION BETWEEN STRONG AND WEAK INTERACTIONS

YASUHISA MURAI

Department of Physics, Saitama University, Urawa, Japan

Received 15 March 1960

Abstract: A discrimination between strong and weak interactions will be made on the basis of a five-dimensional theory in which fermions are represented by eight-component spinors. The operators representing hyperonic charge and chirality are formed and it will be shown how strangeness, as derived from them, can give a measure of the strength of the interaction. The type of coupling is determined too, though this depends on the assignment of new characteristics to the particles.

1. Introduction

The present theory of strange particles is supported by two concepts: strangeness and isobaric spin. The isobaric spin has opened the way for introducing or rather discovering the concept of strangeness. Though the isobaric spin is very useful for analysing experimental data, it will be right to say that it is less fundamental than strangeness. Firstly this is because the validity of charge independence has not yet been confirmed experimentally except for the case of pion-nucleon interaction. Secondly, the validity of charge independence being assumed, we can let particles have values of isobaric spin different from those commonly adopted [1]). Thirdly, the inadequacy of charge independence has been suggested by some authors, in view of the failure to explain, e.g., mass differences within the Σ multiplet by the electromagnetic interaction [2]), or the K^+-nucleon scattering experiments [3]). On the contrary, the concept of strangeness is indispensable to allow for the existence of hyperons and heavy mesons. In this respect, the role played by strangeness is similar to that played by the conservation of baryon number. Therefore, when one tries to give a foundation to the theory of strange particles it will be natural to begin with unravelling the mystery of strangeness. The mathematical tool needed for this purpose has been published already [4]) in a paper which we shall quote as I hereafter. In order to make the basis of our theory clear we first re-explain the basic idea underlying our theory.

We use a five-dimensional space. The meaning of the fifth coordinate r is as follows. On the hypersurface $r = 0$, which is the usual Minkowski space, we regard the conformal group as the fundamental group of our theory. This group

consists of the inhomogeneous Lorentz transformations, dilatation (scale transformation), and the transformations which lead an inertial system to a uniformly accelerated one. The reason why we take this group as the fundamental group was explained in I in relation to the negligibility of the gravitation force, but we can also say that it is suggested by the fact that the Maxwellian equations and the Dirac equation for the neutrino are invariant under this group [5]). Although these transformations cannot be written as linear transformations among four variables, they can be so written if use is made of six homogeneous coordinates. We introduce r in such a way that it preserves the linearity of transformation and in the limit $r \to 0$ we get the above group. Then, as was shown in I, there is a unique way of introducing the new variable r. Owing to this extra variable the Dirac equation for a particle of non-vanishing mass becomes form invariant under our group and we can get rid of the conflict between extension of the physical group and the law of inertia; this is so because our group does not contain the aforementioned transformations (inertial system→ uniformly accelerated system) unless r is zero. This occurs since r is transformed in a compensatory way (cf. section 6). Thus, the transition from the Lorentz group to our group resembles that from the Galilei group to the Lorentz group. We may say that the latter was introduced to resolve difficulties related to the Maxwellian equations which are invariant under this group. Then, the Newtonian equation was required to be form invariant under this group and this was achieved by introducing time as a variable. In our case the introduction of a new variable is likewise necessary.

We do not try to quantize in the five-dimensional space but establish a correspondence between our formalism and the current one (sect. 2). The form of Lagrangian in the former is more limited by high symmetry than in the latter. Thus, starting from the Lagrangian in the five-dimensional space we can get the conventional Lagrangian in more or less fixed form. Though the internal part (a part which contains only r) had completely disappeared from the final field equations when we considered the free state in I, it plays a dominant role in fixing the type and the magnitude of the coupling constant of the interaction. Even for the free Lagrangian, if we consider the Lagrangian but not the field equations, the internal part gives rise to the density functions of Lehmann and others [6]). This is in accord with the general idea which motivated the present formalism explained in I. The idea was that we could extend the fundamental group if we confined ourselves to the investigation of phenomena which do not involve extremely high energies. If there is any truth in this approach, some features, which stem from the excluded region and manifest themselves in the region where the conventional theory is applicable, should be obtainable in some way or other. Perhaps the mass spectrum of elementary particles will be one of them. The free Lagrangian will be treated in sect. 3.

In sect. 4 we investigate various symmetries involved in our theory. It will be

shown among others that there are two operators which may be interpreted as chirality and hyperonic charge and that the free equation for the fermion admits the generalized Pauli transformation. Though there have been several attempts to relate the isobaric spin with the last mentioned transformation we shall not touch this point and rely on the isobaric spin with regard to charge multiplicity. We treat interaction among strongly interacting particles in sect. 5, where it will be shown that strong interaction can occur only when strangeness is conserved. We defer every detail of mathematics to the appendix.

2. Relation between the Lagrangian Densities in Our Formalism and in the Conventional One

All the equations we obtained in I can be derived from an action integral in the six-dimensional space through variation:

$$\delta \int L(\Psi(X), \Psi_\mu(X), X)\sqrt{G}\mathrm{d}^6X = 0. \tag{2.1}$$

The domain of integration is the manifold

$$G_{\mu\nu}X^\mu X^\nu = -1, \tag{2.2}$$

non-vanishing elements of $G_{\mu\nu}$ being $G_{11} = G_{22} = G_{33} = -G_{00} = -G_{56} = = -G_{65} = 1$ and $G = |G_{\mu\nu}|$. Eq. (2.2) shows that $G_{\mu\nu}$ is a covariant tensor of homogeneity -2. The quantity $\sqrt{G}\,\mathrm{d}^6X$ is a scalar of homogeneity zero. When L is of homogeneity zero, it can be written in terms of x^i and r (cf. eq. (A-1)):

$$L(\Psi(X), \Psi_\mu(X), X) = L'(\varphi(x, r), \varphi_a(x, r), r), \tag{2.3}$$

where φ_a represents $(\partial\varphi/\partial x^i, \partial\varphi/\partial r)$. (Cf. the appendix for the notation concerning indices.) Since $\sqrt{G}\,\mathrm{d}^6X = r^{-5}\mathrm{d}r\mathrm{d}^4x$, the action integral in eq. (2.1) turns out to be $\int L' r^{-5}\mathrm{d}r\mathrm{d}^4x$. Therefore, we may consider $\int L' r^{-5}\mathrm{d}r$ a Lagrangian density in the conventional formalism, i.e.,

$$\mathscr{L}(\varphi(x), \varphi_i(x)) = \int L'(\varphi(x, r), \varphi_a(x, r), r)r^{-5}\mathrm{d}r. \tag{2.4}$$

3. Free Lagrangians

3.1. THE REAL BOSON FIELD

Eq. (I, 4.6) can be deduced from

$$L = -\tfrac{1}{4}\mathring{M}^{\mu\nu}\Psi\mathring{M}_{\mu\nu}\Psi - \tfrac{1}{2}Q\,\Psi\Psi, \tag{3.1}$$

where Ψ is a scalar of homogeneity zero. In terms of x^i and r, L becomes

$$L' = -\tfrac{1}{2}r^2\left[\frac{\partial\varphi}{\partial x^i}\frac{\partial\varphi}{\partial x_i} + \frac{\partial\varphi}{\partial r}\frac{\partial\varphi}{\partial r} + \frac{Q}{r^2}\varphi\varphi\right], \tag{3.2}$$

where $\varphi(x, r) = \Psi(X)$. According to (I, 4.7) we put

$$\varphi(x, r) = r^2 \int \mathrm{d}m\, a(m) J_p(mr) \varphi_m(x), \tag{3.3}$$

where $p = \pm\sqrt{Q+4}$, and $\varphi_m(x)$ satisfies $(\Box - m^2)\varphi_m = 0$. Substituting from (3.3) into (3.2) and integrating with respect to r we get

$$\mathscr{L} = -\tfrac{1}{2}\int \frac{\mathrm{d}m}{m} a(m)^2 \left[\frac{\partial \varphi_m}{\partial x^i}\frac{\partial \varphi_m}{\partial x_i} - m^2 \varphi_m{}^2\right]. \tag{3.4}$$

If we define the average of φ_m by φ:

$$\int \frac{\mathrm{d}m}{m} a(m)^2 \varphi_m \varphi_m = \varphi\varphi \int \frac{\mathrm{d}m}{m} a(m)^2 = \varphi\varphi \int \frac{a(m)^2}{2m^2}\mathrm{d}m^2,$$

and replace $\varphi_m\varphi_m$ in the second term in (3.4) by $\varphi\varphi$, we get

$$\mathscr{L} = -\tfrac{1}{2} Z_3{}^{-1} \left(\frac{\partial \varphi}{\partial x^i}\frac{\partial \varphi}{\partial x_i} - m_0{}^2 \varphi\varphi\right), \tag{3.5}$$

where

$$Z_3{}^{-1} = \int \frac{a(m)^2}{2m}\mathrm{d}m^2, \quad \text{and} \quad m_0{}^2 = Z_3 \int \frac{a(m)^2}{2m} m^2 \mathrm{d}m^2. \tag{3.6}$$

Though we have used the common symbol Z_3 for the integral (3.6), this quantity has not the same meaning as the usual renormalization constant. This must be so since no interaction has yet been considered. But from the outset of our paper I we restricted the domain of applicability of our theory; thus, some features which spring out of the excluded high energy region will manifest themselves in the outer region most probably in an averaged form. Thus we consider Z_3 as a part of the real Z_3 which comes from the high energy virtual states, and the renormalized operator in this sense, $Z_3{}^{-\frac{1}{2}}\varphi$, is subject to the ordinary procedure of renormalization with cut-off. A similar situation will occur in the case of the fermion field. (We mention that these density functions were also obtained by Ingraham and Ford [7]) who considered the Green's function for a boson field on the basis of the extended physical group.)

3.2. THE FERMION FIELD

Eq. (I, 4.13) and the corresponding equation for the adjoint operator can be obtained from

$$L = \Psi^\dagger[\beta_7(i\beta_\mu\beta_\nu \overset{\leftrightarrow}{\underset{\circ}{M}}{}^{\mu\nu} - 5) + \tfrac{8}{9}R]\Psi, \tag{3.7}$$

where $\Psi^\dagger \overset{\leftrightarrow}{\underset{\circ}{M}} \Psi$ means $\frac{1}{2}[\Psi^\dagger(\overset{\circ}{M}\Psi) - (\overset{\circ}{M}\Psi^\dagger)\Psi]$ (cf. eq. (I, 4.11)); Ψ is a spinor of homogeneity 1 and $\Psi^\dagger = (i/\sqrt{2})\Psi^*\beta_0(\beta_5+\beta_6)\beta_7 (= i\Psi^*\eta_4\eta_6\eta_7)$ is of homogeneity -1. Now we introduce Ψ' instead of Ψ (cf. eq. (I, 4.6)), change variables

from X to x and r and write $\varphi(x,r)$ for $\Psi'(X)$. As an example we consider the case when Ψ is an eigenstate of β_7. Then according to eqs. (I, 4.21, 4.22) we write φ as follows:

$$\begin{aligned}\varphi &= \varphi_1+\varphi_2 = -\tfrac{1}{2}\beta_6\beta_5\varphi-\tfrac{1}{2}\beta_5\beta_6\varphi,\\ \varphi_1 &= \sqrt{l_0}\int \mathrm{d}m[a(m)J_p(mr)+b(m)J_{-p}(mr)]r^2\varphi_{m1}(x),\\ \varphi_2 &= \frac{1}{\sqrt{(2l_0)}}\int \mathrm{d}m[a(m)J_{p+1}(mr)+b(m)J_{-p-1}(mr)]r^3\varphi_{m2}(x),\end{aligned} \tag{3.8}$$

where $p = \pm\frac{4}{9}R-\frac{1}{2}$ according as $\beta_7\Psi = \pm\Psi$. When p is an even (odd) integer we get for $\mathscr{L}$ (cf. the appendix):

$$\begin{aligned}\mathscr{L} = \sqrt{2}\Big[&\int |a(m)|^2\left\{\varphi^\dagger_{m1}\left(\gamma\frac{\partial\varphi_{m1}}{\partial x}+m\varphi_{m2}\right)+\varphi^\dagger_{m2}\left(\gamma\frac{\partial\varphi_{m2}}{\partial x}+m\varphi_{m1}\right)\right\}\frac{\mathrm{d}m}{m}\\ &+\int |b(m)|^2\left\{\varphi^\dagger_{m1}\left(\gamma\frac{\partial\varphi_{m1}}{\partial x}-m\varphi_{m2}\right)+\varphi^\dagger_{m2}\left(\gamma\frac{\partial\varphi_{m2}}{\partial x}-m\varphi_{m1}\right)\right\}\frac{\mathrm{d}m}{m}\\ &\mp\int (\overline{b(m)}a(m)+b(m)\overline{a(m)})\left(\varphi^\dagger_{m1}\gamma\frac{\partial\varphi_{m1}}{\partial x}-\varphi^\dagger_{m2}\gamma\frac{\partial\varphi_{m2}}{\partial x}\right)\frac{\mathrm{d}m}{m}\Big].\end{aligned} \tag{3.9}$$

Since we may write $\varphi_{m1} = \frac{1}{2}(1\pm\gamma_5)\psi_m$, $\varphi_{m2} = \frac{1}{2}(1\mp\gamma_5)\psi_m$ according as $\beta_7\Psi = \pm\Psi$, we get $\mathscr{L}$ in the following form:

$$\begin{aligned}\mathscr{L} = \sqrt{2}\int\frac{\mathrm{d}m}{m}\,[\psi^\dagger_m\{(|a(m)|^2+|b(m)|^2)\mp(\overline{a(m)}b(m)+a(m)\overline{b(m)})\gamma_5\}\gamma\frac{\partial}{\partial x}\psi_m\\ +\psi^\dagger_m(|a(m)|^2-|b(m)|^2)m\psi_m],\end{aligned} \tag{3.10}$$

where the upper sign is taken for p even (odd) and $\beta_7 = +1(-1)$, and the lower sign for p even (odd) and $\beta_7 = -1(+1)$. It is to be remarked that a parity violating term is contained in (3.10). As was shown by Okabayashi [8]) the self field of a particle will also be influenced by parity non-conserving weak interactions and in that case the free Lagrangian is to be modified as (3.10) suggests. If we require the invariance by charge conjugation this term drops off. Eq. (3.10) without this term can be compared to the expression with density functions of Lehmann and others. Again as in the case of the boson field, if we replace Ψ_m by its average we get

$$\mathscr{L} = Z_2^{-1}\left(\psi^\dagger\gamma_i\frac{\partial\psi}{\partial x_i}+m_0\psi^\dagger\psi\right), \tag{3.11}$$

where Z_2 and m_0 are given by

$$Z_2^{-1} = \sqrt{2}\int\frac{\mathrm{d}m}{m}\,(|a(m)|^2+|b(m)|^2), \tag{3.12}$$

$$m_0 = Z_2\sqrt{2}\int \mathrm{d}m(|a(m)|^2-|b(m)|^2). \tag{3.12'}$$

Of course we have to interpret those relations as we did in the case of the boson field. Lehmann's ρ_1 and ρ_2 correspond to $(|a(m)|^2+|b(m)|^2)/\sqrt{2m^2}$ and $\sqrt{2}|b(m)|^2/m$, and the relation $0 \leqq \rho_2 \leqq 2m\rho_1$ is obvious.

In the following, when we deal with the interaction between elementary particles, we shall approximate $a(m)$ by the delta function (and put $b(m)$ equal to zero for the fermion field). At the same time, however, we have to change somewhat the integration with respect to r to get a convergent result. We shall integrate over r not to infinity but to some large R, or equivalently, for easier manipulation, we insert a convergent factor $e^{-\varepsilon r}$. In other words, we replace the delta function by $\pi^{-1}\varepsilon/(x^2+\varepsilon^2)$ with small but finite ε. Because of

$$\int e^{-\varepsilon r} J_n(mr) J_n(mr) r^2 dr \sim 1/(\pi\varepsilon m),$$

if we write

$$\varphi(x, r) = \sqrt{\varepsilon\pi M}\, r^2 J_p(Mr)\varphi(x),$$

in place of (3.3), $\mathscr{L}$ becomes

$$\mathscr{L} = \int e^{-\varepsilon r} L' r^{-5} dr = -\tfrac{1}{2}\left(\frac{\partial\varphi}{\partial x^i}\frac{\partial\varphi}{\partial x_i} - M^2\varphi^2\right).$$

4. Symmetries involved in Our Theory

In addition to 15 parameter transformations under which our theory is invariant it possesses further symmetries and they are quite interesting for the classification of elementary particles.

1) The free Lagrangian is invariant when Ψ representing a fermion field changes into $\beta_7\Psi$. As $\beta_7{}^2 = 1$, we may consider Ψ as an eigenstate belonging to eigenvalue $+1$ or -1 of β_7. The operator β_7 is written as $-\tau_3\gamma_5$ when the special representation (I, 4.24) is adopted for the β's. This operator is equivalent to Watanabe's chirality operator X [9]), Okabayashi's $\zeta_3\gamma_5$ [8]), and Finkelstein's X [10]). The correspondence becomes apparent when we consider the operator playing the role of hyperonic charge in the following. When Ψ satisfies $\beta\Psi_7 = \pm\Psi$, the function Ψ' takes the form

$$\Psi' = \sqrt{\frac{\pi m\varepsilon}{2^{\frac{3}{4}} l_0}}\begin{pmatrix} r^2\tfrac{1}{2}(1\mp\gamma_5)J_p(mr)\Psi \\ \sqrt{2}\, l_0 r^2\tfrac{1}{2}(1\pm\gamma_5)J_{p-1}(mr)\Psi \end{pmatrix},$$

$$p = \pm\tfrac{4}{9}R+\tfrac{1}{2}.$$

We may take the point of view that this transformation of Ψ corresponds to the total reflection $X^\mu \to -X^\mu$, which has nothing to do with x and r.

2) The free Lagrangian for the fermion field is also invariant when Ψ changes into $(\beta_\mu X^\mu)\Psi(\Psi^\dagger \to -\Psi^\dagger(\beta_\mu X^\mu))$. Though we cannot see it directly, we can easily check this property. Most simply we see the existence of this symmetry

from eq. (I, 4.25), where $\tau_1\varphi$ together with φ is also a solution of this equation. For Ψ', $(\beta_\mu X^\mu)$ can be written as $(l_0/r)\beta_6+(r/2l_0)\beta_5$ (cf. eq. (I, 4.15)). Since this replaces not only $\varphi_1(x)$ by $\varphi_2(x)$ but also the attached internal functions, it cannot be expressed solely by the quantities τ and γ as in the previous case. But roughly speaking this operator is equivalent to $i\tau_1$. For convenience we use the product $\beta_7(\beta_\mu X^\mu)$ instead of $(\beta^\mu X_\mu)$ itself: $\beta_7(\beta_\mu X^\mu)$ corresponds to $\tau_2\gamma_5$, roughly. This operator is essentially equivalent to the hyperonic charge operator, Watanabe's Λ, Okabayashi's $\zeta_2\gamma_5$, and Finkelstein's Q. In fact, $\beta_7(\beta_\mu X^\mu)$ anticommutes with β_7 and as $[\beta_7(\beta_\mu X^\mu)]^2=1$, Ψ can be an eigenfunction of this operator belonging to either $+1$ or -1. When Ψ belongs to the eigenvalue $+1(-1)$ of this operator, Ψ' takes the form

$$\Psi'=\sqrt{\frac{\varepsilon\pi m}{2^{\frac{1}{2}}l_0}}\begin{pmatrix} r^3(\pm\frac{1}{2}(1+\gamma_5)J_p+\frac{1}{2}(1-\gamma_5)J_{p+1})\Psi \\ \sqrt{2}l_0r^2(\frac{1}{2}(1+\gamma_5)J_p\mp\frac{1}{2}(1-\gamma_5)J_{p+1})\Psi\end{pmatrix},$$

where $p=\frac{4}{9}R-\frac{1}{2}$ is an integer. Signs are so determined that the free Lagrangian takes the form $\psi^\dagger\gamma(\partial\psi/\partial x)+m\psi^\dagger\psi$ but not $\psi^\dagger\gamma(\partial\psi/\partial x)-m\psi^\dagger\psi$.

The following transformation will not be used in the present paper, but for the sake of completeness we mention it briefly.

3) If we juxtapose the Lagrangian for particle and antiparticle, we see that the free Lagrangian is invariant under the transformation

$$\Psi\to a\Psi+b\beta_7\Psi^c,\qquad \Psi^c\to\bar{a}\Psi^c+\bar{b}\beta_7\Psi,\qquad (|a|^2+|b|^2=1),$$

which can be regarded as the generalized Pauli transformation [12]). Though the relation between this group and the rotations in isobaric spin space has been conjectured by several authors, the argument is not quite convincing; therefore in the spirit explained in the introduction, we shall leave this point untouched and use the isobaric spin for the description of charge multiplets for the present.

It will be noteworthy, however, that the three transformations mentioned in 1) and 2), i.e.,

$$\Psi\to T_1\Psi=\beta_7\Psi,\qquad T_2\Psi=i(\beta_\mu X^\mu)\Psi,\qquad T_3\Psi=\beta_7(\beta_\mu X^\mu)\Psi,$$

satisfy the familiar relations

$$T_1^2=T_2^2=T_3^2=1,\qquad T_1T_2=iT_3\ (\text{cycl.}).$$

Thus, if we adopt the baryon doublet scheme implied by the global symmetry, these transformations may be adequately interpreted as infinitesimal rotations in the isobaric spin space.

5. Interactions among Strongly Interacting Particles

In the following we study the interactions between elementary particles starting from the tentative assignment of a definite form of Ψ for each field.

The necessity might occur of changing the assignment when we proceed to the consideration of the Fermi interactions between particles including leptons, which we do not consider for the present.

As explained in sect. 4 the operator $\beta_7(\beta_\mu X^\mu)$ can be regarded as the hyperonic charge operator. Therefore, the following assignment will be natural for nucleon and Ξ particle:

$$\Psi_N = -\beta_7(\beta_\mu X^\mu)\Psi_N,$$
$$\Psi'_N = \tfrac{1}{2}\sqrt{\frac{\pi N\varepsilon}{2^{\frac{1}{2}}l_0}}\begin{pmatrix} r^3[-\frac{1}{2}(1+\gamma_5)J_0(Nr)+\frac{1}{2}(1-\gamma_5)J_1(Nr)]\psi_N \\ \sqrt{2}l_0r^2[\frac{1}{2}(1+\gamma_5)J_0(Nr)+\frac{1}{2}(1-\gamma_5)J_1(Nr)]\psi_N \end{pmatrix}; \quad (5.1)$$

$$\Psi_\Xi = +\beta_7(\beta_\mu X^\mu)\Psi_\Xi,$$
$$\Psi'_\Xi = \tfrac{1}{2}\sqrt{\frac{\pi\Xi\varepsilon}{2^{\frac{1}{2}}l_0}}\begin{pmatrix} r^3[\frac{1}{2}(1+\gamma_5)J_0(\Xi r)+\frac{1}{2}(1-\gamma_5)J_1(\Xi r)]\psi_\Xi \\ \sqrt{2}l_0r^2[\frac{1}{2}(1+\gamma_5)J_0(\Xi r)-\frac{1}{2}(1-\gamma_5)J_1(\Xi r)]\psi_\Xi \end{pmatrix}. \quad (5.2)$$

As to Λ and Σ particles, of which the hyperonic charge is zero, they will be eigenstates of β_7. We fix the form of Ψ' as follows:

$$\Psi_\Lambda = +\beta_7\Psi_\Lambda, \quad \Psi'_\Lambda = \sqrt{\frac{\pi\Lambda\varepsilon}{2^{\frac{3}{2}}l_0}}\begin{pmatrix} r^3\frac{1}{2}(1-\gamma_5)J_1(\Lambda r)\psi_\Lambda \\ \sqrt{2}l_0r^2\frac{1}{2}(1+\gamma_5)J_0(\Lambda r)\psi_\Lambda \end{pmatrix}, \quad (5.3)$$

$$\Psi_\Sigma = -\beta_7\Psi_\Sigma, \quad \Psi'_\Sigma = \sqrt{\frac{\pi\Sigma\varepsilon}{2^{\frac{3}{2}}l_0}}\begin{pmatrix} r^3\frac{1}{2}(1+\gamma_5)J_0(\Sigma r)\psi_\Sigma \\ -\sqrt{2}l_0r^2\frac{1}{2}(1-\gamma_5)J_1(\Sigma r)\psi_\Sigma \end{pmatrix}. \quad (5.4)$$

Firstly we form a Lagrangian for pion-baryon interaction. But before doing this, we have to examine the symmetries possessed by our theory. Once the interaction Lagrangians for every conceivable coupling between elementary particles were written down, the theory under consideration would accomplish its first object. As we predetermined the domain of applicability of our theory, some measure for it might be included in the formalism (as the presence of h distinguishes quantum mechanics from classical mechanics), and in view of the fact that only a universal constant of the dimension of a length is still missing, l_0 may be the right one for this purpose. Then it will be necessary that we should have no symmetry like dilatation.

Every infinitesimal transformation of our group can be written as

$$X'^\mu = X^\mu + \varepsilon_\nu{}^\mu X^\nu, \quad \varepsilon_{\mu\nu}+\varepsilon_{\nu\mu} = 0, \quad (5.5)$$

ε_{ij}, ε_{i6}, ε_{i5} and ε_{56} being related to the proper Lorentz transformations, translations, transformations connecting uniformly accelerated systems and dilatation, respectively. We have to take off ε_{56} so as to leave an invariant sub-algebra. For this purpose we have only to fix X^6, having an algebra spanned by ε_{ij} and ε_{i6}, i.e. ,the Lie algebra of the inhomogeneous Lorentz group. This means that we may insert β_5 or X^6 or $\partial/\partial X^5$ or any combination of these into an interaction

Lagrangian, which has to be a scalar if it is unaffected by this insertion. Of course we need not do so for every interaction Lagrangian. Perhaps one would be enough.

We assume only Yukawa interaction between fermions and bosons. And we further take it for granted that every boson appears in the interaction always coupled with the same matrix. This is the procedure adopted e.g., by, Watanabe [8]) and Okabayashi [7]).

We assign the following form for $\varphi'(x, r)$ of the pion:

$$\varphi'(x, r) = \sqrt{\pi m_\pi \varepsilon}\, r^2 J_0(m_\pi r)\varphi_\pi(x), \tag{5.6}$$

and demand that it appear in the Lagrangian together with

$$\beta X + \frac{\beta^6}{X^6}. \tag{5.7}$$

Table 1 shows how various matrices are simplified when they stand between $\Psi_1^\dagger$ and Ψ_2.

TABLE 1

Simplified forms taken by matrices

$\Psi_1^\dagger\Psi_2$	1	β_7	(βX)	β_5/X^6	$\beta_7\beta_5/X^6$	$\beta_7(\beta X)$	$\beta_5(\beta X)/X^6$	$\beta_7\beta_5(\beta X)/X^6$
$\bar{N}N$	1	0	0	β_5/X^6	-1	-1	0	β_5/X^6
$\bar{\Xi}\Xi$	1	0	0	β_5/X^6	$+1$	$+1$	0	$-\beta_5/X^6$
$\bar{N}\Xi$	0	β_7	β_7	β_5/X^6	$\beta_7\beta_5/X^6$	0	$-\beta_7\beta_5/X^6$	0
$\bar{\Xi}N$	0	β_7	$-\beta_7$	β_5/X^6	$\beta_7\beta_5/X^6$	0	$-\beta_7\beta_5/X^6$	0
$\bar{N}\Lambda$	1	1	1	β_5/X^6	$-\beta_5/X^6$	-1	β_5/X^6	β_5/X^6
$\bar{N}\Sigma$	1	-1	-1	β_5/X^6	β_5/X^6	-1	$-\beta_5/X^6$	β_5/X^6
$\bar{\Xi}\Lambda$	1	1	-1	β_5/X^6	$-\beta_5/X^6$	1	$-\beta_5/X^6$	$-\beta_5/X^6$
$\bar{\Xi}\Sigma$	1	-1	1	β_5/X^6	β_5/X^6	1	β_5/X^6	$-\beta_5/X^6$
$\bar{\Lambda}\Lambda$	1	1	0	0	0	0	$\beta_5(\beta X)/X^6$	$\beta_5(\beta X)/X^6$
$\bar{\Sigma}\Sigma$	1	-1	0	0	0	0	$\beta_5(\beta X)/X^6$	$-\beta_5(\beta X)/X^6$
$\bar{\Lambda}\Sigma$	0	0	(βX)	β_5/X^6	β_5/X^6	(βX)	0	0
$\bar{\Sigma}\Lambda$	0	0	(βX)	β_5/X^6	$-\beta_5/X^6$	$-(\beta X)$	0	0

The Lagrangian for pion-nucleon interaction, for example, is

$$L = G_\pi \Psi_N^\dagger \left(\beta_\mu X^\mu + \frac{\beta^6}{X^6}\right) \Psi_N \Phi_\pi. \tag{5.8}$$

Following the prescription in sect. 2, we get the conventional Lagrangian of the form

$$\mathscr{L} = \tfrac{1}{2} N (m_\pi \varepsilon^3 \pi^3)^{\frac{1}{2}} G_\pi \int \mathrm{e}^{-\varepsilon r} J_1(Nr) J_0(Nr) J_0(m_\pi r)\, r^2 \mathrm{d}r\, \psi_N^\dagger \gamma_5 \psi_N \varphi_\pi. \tag{5.9}$$

As is shown in the appendix,

$$\int J_1(Nr)J_0(Nr)J_0(m_\pi r)r^2 e^{-\varepsilon r}dr = \frac{\cos\alpha}{\pi N m_\pi{}^2 \sin^3\alpha} \quad (\cos\alpha = m_\pi/2N).$$

Thus we get $\mathscr{L} = g_\pi \psi_N^\dagger \gamma_5 \psi_N \varphi_\pi$ with

$$g_\pi = \tfrac{1}{2} G_\pi \left(\frac{\varepsilon^3\pi}{m_\pi{}^3}\right)^{\frac{1}{2}} \frac{\cos\alpha}{\sin^3\alpha} \approx G_\pi \frac{(\varepsilon^3\pi)^{\frac{1}{2}}}{4Nm_\pi{}^{\frac{1}{2}}}. \tag{5.10}$$

For the $\bar{\Xi}\,\Xi$–π and $\Lambda\Sigma$–π interactions we get a similar result; we have only to change N to Ξ or N to $\Lambda(=\Sigma)$. Because of (5.7), we see from table 1 that $\bar{\Sigma}\Sigma$–π does not occur and it seems that this does not cause any trouble. Rather, this gives a good account of the branching ratio of hyperon production by K^- absorption [12]). For the $\bar{\Lambda}\Sigma$–π interaction we assumed that the masses Λ and Σ are equal to get a parity conserving coupling. The mass splitting between Λ and Σ can also be caused by the lack of $\bar{\Sigma}\Sigma$–π interaction. In the other cases of pion interaction, for example $\bar{\Lambda}$N–π, the mass values of the three participating particles do not form sides of a triangle, the relevant integrals over r are negligible and the coupling constants are smaller than (5.10) by a factor ε/N, which may be assumed as small as 10^{-10}.

Next we consider the K meson interaction. We assume that the K meson has

$$\varphi(x, r) = \sqrt{\varepsilon\pi K}\, r^2 J_0(Kr)\varphi_K(x) \tag{5.11}$$

and appears in the interaction Lagrangian always together with

$$\beta X + \beta_7. \tag{5.12}$$

Unlike in the case of the pion, this satisfies

$$[\beta_7(\beta X),\ \beta_7 + (\beta X)] = -2(\beta_7 + (\beta X)). \tag{5.13}$$

Therefore, we can introduce the hyperonic charge operation defined by

$$\Psi \to \pm\beta_7(\beta X)\Psi, \tag{5.14}$$

and require that the K meson interaction be invariant under this transformation. We fix the sign of Ψ_N appearing in eq. (5.14) as being positive and assume for the other fields the following choice of signs:

$$\begin{aligned}
&\Psi_N \to \beta_7(\beta X)\Psi_N \quad (= -\Psi_N),\\
&\Psi_\Xi \to \beta_7(\beta X)\Psi_\Xi \quad (= +\Psi_\Xi),\\
&\Psi_\Lambda \to -\beta_7(\beta X)\Psi_\Lambda,\\
&\Psi_\Sigma \to -\beta_7(\beta X)\Psi_\Sigma,\\
&\Phi_K \to \Phi_K.
\end{aligned} \tag{5.15}$$

As a consequence of eq. (5.12), $\overline{\mathrm{K}}$ appears always together with

$$\beta X - \beta_7. \tag{5.16}$$

This satisfies

$$[\beta_7(\beta X),\ \beta_7 - (\beta X)] = 2(\beta_7 - (\beta X)). \tag{5.17}$$

Because of eq. (5.12), we see from table 1 that the interaction Lagrangian can be written only for $\overline{\mathrm{N}}\Lambda\mathrm{K}$, $\overline{\mathrm{N}}\Sigma\mathrm{K}$, $\overline{\Xi}\Lambda\overline{\mathrm{K}}$, $\overline{\Xi}\Sigma\overline{\mathrm{K}}$, $\overline{\mathrm{N}}\Xi\mathrm{K}$, $\bar{\Lambda}\Lambda\mathrm{K}$, $\overline{\Sigma}\Sigma\mathrm{K}$, $\bar{\Lambda}\Sigma\mathrm{K}$, $\overline{\Sigma}\Lambda\mathrm{K}$; of these, the requirement of invariance under (5.14) allows the first four but not the others. In the case of the $\overline{\mathrm{N}}\Lambda\mathrm{K}$ interaction we start from

$$L = G_{\mathrm{K}} \Psi_{\mathrm{N}}^{\dagger}(\beta X + \beta_7)\Psi_{\Lambda}\Phi_{\mathrm{K}}. \tag{5.18}$$

Following the prescribed procedure we get from this Lagrangian

$$\mathscr{L} = G_{\mathrm{K}} \sqrt{\frac{\pi^3 \varepsilon^3 \Lambda N K}{2}} \{[N\Lambda K]\psi_{\mathrm{N}}^{\dagger}\tfrac{1}{2}(1+\gamma_5)\psi_{\Lambda}\varphi_{\mathrm{K}} + [\Lambda N K]\psi_{\mathrm{N}}^{\dagger}\tfrac{1}{2}(1-\gamma_5)\psi_{\Lambda}\varphi_{\mathrm{K}}\},$$

where $[abc]$ denotes $\int \mathrm{e}^{-\varepsilon r} J_1(ar) J_0(br) J_0(cr) r^2 \mathrm{d}r$. If we assume $\Lambda : \mathrm{N} : \mathrm{K} \approx$ $\approx 2.34 : 1.84 : 0.97$, the Lagrangian $\mathscr{L}$ becomes

$$\mathscr{L} \approx \psi_{\mathrm{N}}^{\dagger}\gamma_5\psi_{\Lambda}\varphi_{\mathrm{K}} + 0.34\, \psi_{\mathrm{N}}^{\dagger}\psi_{\Lambda}\varphi_{\mathrm{K}}. \tag{5.19}$$

We get a similar result for the other K meson interactions.

Thus, as far as we consider a Yukawa interaction between baryons and K or π mesons, only those interactions which are at present regarded as strong have been singled out. We noted already the lack of $\overline{\Sigma}\Sigma - \pi$ interaction. The only thing which is different from what we usually assume is that K meson interactions come out to be parity violating. As a matter of fact, it has not yet been experimentally determined whether K meson interactions are parity conserving or not. It has to be noted, however, that this result depends on the assignment made in eqs. (5.1), (5.4), (5.6), (5.7), (5.11) and (5.12). It is also possible to get a parity conserving coupling for all the strong interactions. For this it is necessary either to assume half-integral values for orders of Bessel functions of fermion fields or to use the Y and Z scheme instead of Λ and Σ. But in the latter case we have to assume that all the masses of baryons are equal and the interactions we get possess so high a symmetry that they have to face Pais' objection [13]) and other criticisms levelled at the global symmetry [14]).

It will be interesting to note that a similar situation occurred in an attempt at relating the parity conserving property of strong interactions with other symmetry requirements: for pion interaction, charge symmetry together with the requirement of direct coupling and T invariance implied parity conservation [15]), but it was not possible to proceed along the same line in the case of K-baryon interaction [16]).

6. Concluding Remark

In the foregoing section we have shown that those interactions which preserve strangeness can be singled out from the others. Now we are in a position to say something about weak interactions. We saw that the interactions which did not come out as strong interactions had a coupling constant whose magnitude is smaller than that for the strong interaction by a factor ε/N or less. If this ratio were assumed to be around 10^{-7}—10^{-8}, this would give the right order of magnitude for weak interaction. But in that case the $\bar{N}\Lambda$–π interaction, for instance, would become a direct coupling and the ratio of scalar and pseudoscalar couplings would not have the right value to explain the observed up and down asymmetry. Therefore, we shall have to give up this possibility of deriving weak interactions, though we cannot absolutely deny the existence of a way out of this difficulty through different assignments of irreducible representations to each of the particles. In order to discard those redundant interactions, we have simply to give a sufficiently small value to ε, and then establish anew a recipe to construct the weak interaction Lagrangian. In view of the great success of the V—A coupling scheme, one way will be to assume Fermi interactions in addition to Yukawa interactions. As we have seen, Yukawa interactions afforded only strong interactions; thus, if Fermi interaction gives rise to every desired weak interaction, the present formalism will be provisonally completed. The formulation of Fermi interaction in 6-dimensional space has been investigated by Finkelstein [17]). But in our case it is allowed to use both X_μ and β_μ to form tensors, and his result cannot be used directly. It needs a separate consideration to proceed along this line. Perhaps it is to be noted that though we were forced to introduce the quantity l_0 with the dimension of a length, it has completely disappeared from the final expression so far. It is certain, however, that l_0 comes out in Fermi interaction when we form a four-fold product of J's.

With regard to the tremendous difference between strong and weak interactions, it would also be necessary to take different attitudes for the treatment of r, depending whether one is to deal with strong or weak interaction. We used throughout in the foregoing discussion free internal functions when we transcribed the 6-dimensional Lagrangian into the conventional one. It is conceivable that the internal functions are also distorted when particles decay. An abbreviated way of taking the distortion into account will be to use the second approximation for a's and b's, which were put equal to a delta function and zero, respectively, in the first approximation. In other words, in the first approximation we used the plane wave solution, the mass having a sharp value. When a particle decays, energy has a certain width and consequently the r-dependent part differs from the plane wave solution.

The conjecture that the r-dependent part of the function may be closely

related to the interaction springs from the following consideration. If the variable r were not introduced, the geodesic in the Minkowski space would have been a hyperbola, a trajectory of a particle moving with a constant acceleration, since the fundamental group has been extended. But once r is introduced, the geodesic becomes a straight line in the Minkowski space, transferring complicated time dependence to the behaviour of r. Since r increases with time in just the same way as the width of the wave packet, we can express the situation intuitively like this: though we have widened the class of equivalent observers, a free particle performs a rectilinear motion; a particle, however, has spherical extension and its radius increases with time, the envelope of the expanding sphere being described by hyperbolae. To make the analogy between the width of a wave packet and the variable r complete, we must consider the problem of measurement. When we observe the position of a particle represented by a wave packet, this shrinks to a delta function-like narrowness. Likewise, if the particle were described in our formalism, the magnitude of r should jump to a small value according to the precision of the measurement at the moment of observation. Otherwise it is hardly possible to imagine a particle whose extension increases constantly with time, irrespective of its interaction with environment. This means that the r-dependent internal function may undergo a large change when interaction takes place. Thus, it is most likely that the distortion of the r-dependent part gives rise to an appreciable influence upon the interaction formula when the transcription of 6-dimensional to 4-dimensional formalism is made. For the present we leave these problems to be the subject of separate investigation.

What we claim to be new and important among the results we obtained is that we could single out strong interactions. So far as we know there has been only a single attempt to differentiate the strong from the weak interaction. In fact Van Hove tried this using a simple model [18]). He showed that when the interaction Lagrangian is asymmetric with respect to the coupling constants, the renormalized coupling constant of the antisymmetric part becomes small (but not very small, if a reasonable cut off momentum is assumed) compared to that of the symmetric part. In our case the envisaged problem is much more realistic and the strong interactions we derived cover nearly all the desired ones.

Finally we add that Markov's theory [19]) has some bearing with ours. He also introduced a quantity a which plays a similar role as our r, and its geometrical meaning is quite similar. But the Dirac equation which he got, through a heuristic procedure, is different from ours. We want to emphasize that the Lagrangian densities appearing in eqs. (3.1) and (3.7) are nothing but invariants of our group as was shown in eq. (I, 4.3) with $M_{\mu\nu} = \overset{\circ}{M}_{\mu\nu}$, and eq. (I, 4.11).

Appendix

1. RELATION BETWEEN HOMOGENEOUS AND INHOMOGENEOUS COORDINATES

Most of the following relations are mere specialization of those given by Pauli long ago [20]; for the details see his paper. The variables x and r are related to the quantities X by (cf. I, sect. 3 and (I, 4.17))

$$\frac{X^i}{X^6}=\frac{x^i}{l_0}, \qquad \frac{X^5}{X^6}=\frac{x^2+r^2}{2l_0 r}, \qquad G_{\mu\nu}X^\mu X^\nu=-1,$$

or

$$X^i=\frac{x^i}{r}, \qquad X^5=\frac{x^2+r^2}{2l_0 r}, \quad X^6=\frac{l_0}{r}. \tag{A-1}$$

We use three kinds of suffices: $\lambda, \mu, \nu, \ldots = 1, 2, 3, 0, 5, 6$; $\alpha, \beta, \ldots = 1, 2, 3, 0, 5$; $i, j, k, \ldots = 1, 2, 3, 0$, $(x^5 = r)$.

From a six-vector A^μ we can form a five-vector and a scalar by the transformation matrix $\gamma_\mu^{\cdot\alpha} = \partial x^\alpha/\partial X^\mu$; we have

$$\mathscr{A}^\alpha = \gamma_\mu^{\cdot\alpha} A^\mu, \qquad \mathscr{A} = X_\mu A^\mu, \tag{A-2}$$

where

$$(\gamma_\mu^{\cdot\alpha}) = \begin{pmatrix} \frac{r}{l_0} & & & & & \frac{-rx^1}{l_0^2} \\ & \frac{r}{l_0} & & & & \frac{-rx^2}{l_0^2} \\ & & \frac{r}{l_0} & & & \frac{-rx^3}{l_0^2} \\ & & & \frac{r}{l_0} & & \frac{-rx^0}{l_0^2} \\ \frac{-x^1}{l_0} & \frac{-x^2}{l_0} & \frac{-x^3}{l_0} & \frac{x^0}{l_0} & 1 & \frac{x^2-r^2}{2l_0^2} \end{pmatrix}. \tag{A-3}$$

Similary, $\gamma^\mu_{\cdot\alpha}$ connects two kinds of covariant vectors,

$$\mathscr{A}_\alpha = \gamma^\mu_{\cdot\alpha} A_\mu, \qquad \mathscr{A} = X^\mu A_\mu, \tag{A-4}$$

where

$$(\gamma^\mu_{\cdot\alpha}) = \begin{pmatrix} \frac{l_0}{r} & & & & \frac{-x^1 l_0}{r^2} \\ & \frac{l_0}{r} & & & \frac{-x^2 l_0}{r^2} \\ & & \frac{l_0}{r} & & \frac{-x^3 l_0}{r^2} \\ & & & \frac{l_0}{r} & \frac{-x^0 l_0}{r^2} \\ \frac{x^1}{r} & \frac{x^2}{r} & \frac{x^3}{r} & \frac{-x^0}{r} & \frac{-x^2+r^2}{2r^2} \\ & & & & \frac{-l_0^2}{r^2} \end{pmatrix}. \tag{A-5}$$

The following relations hold among the matrices γ:

$$\gamma_{\mu}^{\ \alpha} X^{\mu} = 0, \quad \gamma^{\mu}_{\ \alpha} X_{\mu} = 0, \quad \gamma^{\mu}_{\ \alpha}\gamma_{\mu}^{\ \beta} = \delta_{\alpha}^{\ \beta}, \quad \gamma^{\mu}_{\ \alpha}\gamma_{\nu}^{\ \alpha} = \delta_{\nu}^{\ \mu} + X^{\mu}X_{\nu}, \tag{A-6}$$

and hence

$$A^{\mu} = \gamma^{\mu}_{\ \alpha}\mathscr{A}^{\alpha} - \mathscr{A}X^{\mu}, \qquad A_{\mu} = \gamma_{\mu}^{\ \alpha}\mathscr{A}_{\alpha} - \mathscr{A}X_{\mu}. \tag{A-7}$$

From

$$\mathscr{A}^{\alpha} = \gamma_{\mu}^{\ \alpha} A^{\mu} = G^{\mu\nu}\gamma_{\mu}^{\ \alpha} A_{\nu} = G^{\mu\nu}\gamma_{\mu}^{\ \alpha}\gamma_{\nu}^{\ \beta}\mathscr{A}_{\beta} = G^{\alpha\beta}\mathscr{A}_{\beta}, \tag{A-8}$$

we get $G^{\alpha\beta} = G^{\mu\nu}\gamma_{\mu}^{\ \alpha}\gamma_{\nu}^{\ \beta}$, and likewise, $G_{\alpha\beta} = G_{\mu\nu}\gamma^{\mu}_{\ \alpha}\gamma^{\nu}_{\ \beta}$. Here,

$$G_{\mu\nu} = \begin{pmatrix} 1 & & & & & \\ & 1 & & & & \\ & & 1 & & & \\ & & & -1 & & \\ & & & & 0 & -1 \\ & & & & -1 & 0 \end{pmatrix}, \quad G^{\alpha\beta} = \frac{r^2}{l_0^2}\begin{pmatrix} 1 & & & & \\ & 1 & & & \\ & & 1 & & \\ & & & -1 & \\ & & & & 1 \end{pmatrix}.$$

Examples:

$$\begin{aligned} \frac{\partial}{\partial X^i} &= r\frac{\partial}{\partial x^i} - x_i\frac{\partial}{\partial r} - \frac{nx_i}{r}, \quad \frac{\partial}{\partial X^5} = l_0\frac{\partial}{\partial r} + \frac{nl_0}{r}, \\ \frac{\partial}{\partial X^6} &= -\frac{rx^i}{l_0}\frac{\partial}{\partial x^i} + \frac{x^2-r^2}{2l_0}\frac{\partial}{\partial r} + \frac{n(x^2+r^2)}{2l_0 r}, \end{aligned} \tag{A-9}$$

where n is the degree of homogeneity of the operand.

If $A_{\mu} = \Psi^{\dagger}\beta_{\mu}\Psi$, we have

$$\begin{aligned} \mathscr{A}_i &= \frac{l_0}{r}\Psi^{\dagger}\beta_i\Psi + \frac{x_i}{r}\Psi^{\dagger}\beta_5\Psi, \\ \mathscr{A}_5 &= -\frac{l_0 x^i}{r^2}\Psi^{\dagger}\beta_i\Psi - \frac{x^2-r^2}{2r^2}\Psi^{\dagger}\beta_5\Psi - \frac{l_0^2}{r^2}\Psi^{\dagger}\beta_6\Psi, \\ \mathscr{A}_6 &= \frac{x^i}{r}\Psi^{\dagger}\beta_i\Psi + \frac{x^2+r^2}{2rl_0}\Psi^{\dagger}\beta_5\Psi + \frac{l_0}{r}\Psi^{\dagger}\beta_6\Psi. \end{aligned}$$

If use is made of $\Psi' = (1+\frac{1}{2}\beta_i x^i\beta_5)\Psi$ instead of Ψ, we can simplify these expressions as follows:

$$\mathscr{A}_i = \frac{l_0}{r}\Psi'^{\dagger}\beta_i\Psi', \ \mathscr{A}_5 = -\frac{l_0}{r}\Psi'^{\dagger}\left(\frac{l_0}{r}\beta_6 - \frac{r}{2l_0}\beta_5\right)\Psi', \ \mathscr{A}_6 = \Psi'^{\dagger}\left(\frac{l_0}{r}\beta_6 + \frac{r}{2l_0}\beta_5\right)\Psi'; \tag{A-10}$$

the corresponding contravariant vector is

$$\mathscr{A}^i = \frac{r}{l_0}\Psi'^\dagger\beta^i\Psi', \quad \mathscr{A}^5 = -\frac{r}{l_0}\Psi'^\dagger\left(\frac{l_0}{r}\beta_6 - \frac{r}{2l_0}\beta_5\right)\Psi'.$$

From eqs. (A-6) and (A-7) we get

$$A_\mu B^\mu = (\gamma_{\cdot\mu}^{\alpha}\mathscr{A}_\alpha - \mathscr{A}X_\mu)(\gamma^\mu_{\cdot\beta}\mathscr{B}^\beta - \mathscr{B}X^\mu) = \mathscr{A}_\alpha\mathscr{B}^\alpha - \mathscr{A}\mathscr{B}. \tag{A-11}$$

When $B^\mu = \partial\phi/\partial X_\eta$ (ϕ of homogeneity zero),

$$\mathscr{B}^\alpha = \left(\frac{r^2}{l_0}\frac{\partial\phi}{\partial x_i}, \quad \frac{r^2}{l_0}\frac{\partial\phi}{\partial r}\right) \quad \text{and} \quad \mathscr{B} = 0;$$

thus we have

$$\Psi^\dagger\beta_\mu\Psi\frac{\partial\phi}{\partial X_\mu} = r\Psi'^\dagger\beta_i\Psi'\frac{\partial\phi}{\partial x_i} - r\Psi'^\dagger\left(\frac{l_0}{r}\beta_6 - \frac{r}{2l_0}\beta_5\right)\Psi'\frac{\partial\phi}{\partial r}. \tag{A-12}$$

For the second rank tensor we have the following relations:

$$T_{\mu\nu} = \gamma_\mu^\alpha\gamma_\nu^\beta T_{\alpha\beta} - X_\mu\gamma_\nu^{\cdot\alpha}T_{(0)\alpha} - X_\nu\gamma_\mu^{\cdot\alpha}T_{\alpha(0)} + X_\mu X_\nu T_{(0)(0)}, \tag{A-13}$$

with

$$T_{\alpha\beta} = \gamma^\mu_{\cdot\alpha}\gamma^\nu_\beta T_{\mu\nu}, \quad T_{(0)\alpha} = X^\mu\gamma^\nu_{\cdot\alpha}T_{\mu\nu},$$
$$T_{\alpha(0)} = X^\nu\gamma^\mu_{\cdot\alpha}T_{\mu\nu}, \quad T_{(0)(0)} = X^\mu X^\nu T_{\mu\nu}.$$

For example from $\frac{1}{2}\Psi^\dagger(\beta_\mu\beta_\nu - \beta_\nu\beta_\mu)\Psi$ we obtain

$$\begin{aligned}
t_{ij} &= \frac{l_0^2}{r^2}\tfrac{1}{2}\Psi'^\dagger(\beta_i\beta_j - \beta_j\beta_i)\Psi', \quad t_{55} = t_{(0)(0)} = 0,\\
t_{i5} &= -\frac{l_0^2}{r^2}\Psi'^\dagger\beta_i\left(\frac{l_0}{r}\beta_6 - \frac{r}{2l_0}\beta_5\right)\Psi',\\
t_{i(0)} &= -t_{(0)i} = \frac{l_0}{r}\Psi'^\dagger\beta_i\left(\frac{l_0}{r}\beta_6 + \frac{r}{2l_0}\beta_5\right)\Psi',\\
t_{5(0)} &= -t_{(0)5} = \frac{l_0}{2r}\Psi'^\dagger(\beta_5\beta_6 - \beta_6\beta_5)\Psi'.
\end{aligned} \tag{A-14}$$

The suffices can be raised by $G^{\alpha\beta}$. A product of two tensors is

$$T_{\mu\nu}T'^{\mu\nu} = T_{\alpha\beta}T'^{\alpha\beta} - T_{(0)\alpha}T'^{(0)\alpha} - T_{\alpha(0)}T'^{\alpha(0)} + T_{(0)(0)}T'^{(0)(0)}. \tag{A-15}$$

2. DETAILS OF THE PASSAGE FROM (3.7) TO (3.9)

Eq. (3.7) can be written as

$$L = \tfrac{1}{2}\Psi^\dagger\left[2(\beta X)\left(\beta\frac{\vec{\partial}}{\partial X}\right) - 2\left(X\frac{\vec{\partial}}{\partial X}\right) - 5 + \tfrac{8}{9}R\beta_7\right]\beta_7\Psi$$
$$+\tfrac{1}{2}\Psi^\dagger\left[2\left(\beta\frac{\overleftarrow{\partial}}{\partial X}\right)(\beta X) - 2\left(\frac{\overleftarrow{\partial}}{\partial X}X\right) - 5 + \tfrac{8}{9}R\beta_7\right]\beta_7\Psi,$$

where $\Psi^\dagger\overleftarrow{\partial}/\partial X\Psi$ means $\partial\Psi^\dagger/\partial X\Psi$. Using eqs. (A-1) and (A-9) we can write

this in terms of Ψ' as follows (cf. eq. (I, 4.15)):

$$L = \Psi'^{\dagger}\beta_7\Big[\Big(l_0\beta_6+\frac{r^2}{2l_0}\beta_5\Big)\Big\{\beta_i\frac{\vec{\partial}}{\partial x_i}-\frac{l_0}{r}\beta_6\Big(\frac{\vec{\partial}}{\partial r}+\frac{n}{r}\Big)+\frac{1}{l_0}\beta_3\Big(\tfrac{1}{2}r\frac{\vec{\partial}}{\partial r}-\tfrac{1}{2}n-2\Big)\Big\}$$
$$-(n+\tfrac{5}{2}-\tfrac{4}{9}R\beta_7)\Big]\Psi'+\Psi'^{\dagger}\beta_7\Big[\Big\{\beta_i\frac{\overleftarrow{\partial}}{\partial x_i}-\Big(\frac{\overleftarrow{\partial}}{\partial r}+\frac{n'}{r}\Big)\frac{l_0}{r}\beta_6$$
$$+\Big(\tfrac{1}{2}\frac{\overleftarrow{\partial}}{\partial r}r-\tfrac{1}{2}n'-2\Big)\frac{1}{l_0}\beta_5\Big\}\Big(l_0\beta_6+\frac{r^2}{2l_0}\beta_5\Big)-(n'+\tfrac{5}{2}-\tfrac{4}{9}R\beta_7)\Big]\Psi'.$$

For simplicity, we use the representation of β matrices shown in eq. (I, 4.24) (for the relation between η's and β's see the expressions following eq. (I, 4.13)),

$$L=\Psi'\beta_7\begin{pmatrix} r\dfrac{\vec{\partial}}{\partial r}-\dfrac{5}{2}-\dfrac{4R}{9}\gamma_5 & \dfrac{r^2}{\sqrt{2}l_0}\gamma_i\dfrac{\vec{\partial}}{\partial x_i} \\ \sqrt{2}l_0\gamma_i\dfrac{\vec{\partial}}{\partial x_i} & -r\dfrac{\vec{\partial}}{\partial r}+\dfrac{3}{2}+\dfrac{4R}{9}\gamma_5 \end{pmatrix}\Psi'$$
$$+\Psi'^{\dagger}\beta_7\begin{pmatrix} -\dfrac{\overleftarrow{\partial}}{\partial r}r+\dfrac{3}{2}-\dfrac{4R}{9}\gamma_5 & -\dfrac{r^2}{\sqrt{2}l_0}\dfrac{\overleftarrow{\partial}}{\partial x_i}\gamma_i \\ -\sqrt{2}l_0\dfrac{\overleftarrow{\partial}}{\partial x_i}\gamma_i & \dfrac{\overleftarrow{\partial}}{\partial r}r-\dfrac{5}{2}+\dfrac{4R}{9}\gamma_5 \end{pmatrix}\Psi'. \quad \text{(A-16)}$$

When Ψ' is of the form

$$\Psi'=N\begin{pmatrix} \dfrac{r^3}{\sqrt{2l_0}}J_{-\frac{4R}{9}\gamma_5-\frac{1}{2}}\varphi_2 \\ r^2\sqrt{l_0}J_{\frac{4R}{9}\gamma_5-\frac{1}{2}}\varphi_2 \end{pmatrix},\quad \Psi'^{\dagger}\beta_7=N\begin{pmatrix} \sqrt{l_0}r^2\varphi_1^{\dagger}J_{-\frac{4R}{9}\gamma_5-\frac{1}{2}} \\ \dfrac{r^3}{\sqrt{2l_0}}\varphi_2^{\dagger}J_{\frac{4R}{9}\gamma_5+\frac{1}{2}} \end{pmatrix}, \quad \text{(A-17)}$$

where $\varphi_i^{\dagger}=\varphi_i^{*}\gamma_4$, eq. (A-16) becomes

$$L=(\varphi_1^{\dagger},\varphi_2^{\dagger})\begin{pmatrix} \dfrac{N^2}{\sqrt{2}}r^6J^2_{-\frac{4R}{9}\gamma_5-\frac{1}{2}}(mr) & \\ & \dfrac{N^2}{\sqrt{2}}r^6J^2_{\frac{4R}{9}\gamma_5+\frac{1}{2}}(mr) \end{pmatrix}\begin{pmatrix} m & \gamma_i\dfrac{\vec{\partial}}{\partial x_i} \\ \gamma_i\dfrac{\vec{\partial}}{\partial x_i} & m \end{pmatrix}\begin{pmatrix}\varphi_2\\ \varphi_1\end{pmatrix}$$
$$+(\varphi_1^{\dagger},\varphi_2^{\dagger})\begin{pmatrix} m & -\dfrac{\overleftarrow{\partial}}{\partial x_i}\gamma_i \\ -\dfrac{\overleftarrow{\partial}}{\partial x_i}\gamma_i & m \end{pmatrix}\begin{pmatrix} \dfrac{N^2}{\sqrt{2}}r^6J^2_{-\frac{4R}{9}\gamma_5+\frac{1}{2}}(mr) & \\ & \dfrac{N^2}{\sqrt{2}}r^6J^2_{\frac{4R}{9}\gamma_5-\frac{1}{2}}(mr) \end{pmatrix}\begin{pmatrix}\varphi_2\\ \varphi_1\end{pmatrix} \quad \text{(A-18)}$$

$$= A\varphi_1^{\dagger}\left(\gamma\frac{\partial\varphi_1}{\partial x}+m\varphi_2\right)+B\varphi_2^{\dagger}\left(\gamma\frac{\partial\varphi_2}{\partial x}+m\varphi_1\right)+A\left(-\frac{\partial\varphi_1^{\dagger}}{\partial x}\gamma+m\varphi_2^{\dagger}\right)\varphi_1$$

$$+B\left(-\frac{\partial\varphi_2^{\dagger}}{\partial x}\gamma+m\varphi_1^{\dagger}\right)\varphi_2. \quad \text{(A-18)}$$

If the sign of the order of the quantities J in eq. (A-17) is changed, the sign in front of m changes too. Thus Ψ' given by (3.8) leads (3.7) to (3.9).

3. EVALUATION OF $\int e^{-\varepsilon r}J_1(ar)J_1(br)J_1(cr)r^2dr$ AND $\int e^{-\varepsilon r}J_1(ar)J_0(br)J_0(cr)r^2dr$

To evaluate these integrals we proceed at first as follows:

$$\int_0^{\infty} e^{-\varepsilon r}J_1(ar)J_1(br)J_1(cr)r^2dr$$

$$= \frac{bc}{\pi}\int_0^{\pi} d\vartheta\lambda^{-1}\sin^2\vartheta\int dr e^{-\varepsilon r}J_1(ar)J_1(\lambda r)r^3 \quad (\lambda=\sqrt{b^2+c^2-2bc\cos\vartheta})$$

$$= 5!\,\frac{abc}{2\pi^2\varepsilon^6}\int d\vartheta\sin^2\vartheta\int d\phi\sin^2\phi\,{}_2F_1\left(3,\tfrac{7}{2};2;-\frac{\omega^2}{\varepsilon^2}\right)(\omega=\sqrt{a^2+\lambda^2-2a\lambda\cos\vartheta})$$

$$= 5!\,\frac{abc}{2\pi^2\varepsilon^6}\int d\vartheta d\phi\sin^2\vartheta\sin^2\phi\left(1+\frac{\omega^2}{\varepsilon^2}\right)^{-\frac{1}{2}}{}_2F_1\left(-1,-\tfrac{3}{2};2;-\frac{\omega^2}{\varepsilon^2}\right) \quad \text{(A-19)}$$

$$= \frac{15\varepsilon abc}{\pi^2}\int d\vartheta d\phi\sin^2\vartheta\sin^2\phi\,\frac{4\varepsilon^2-3\omega^2}{(\omega^2+\varepsilon^2)^{\frac{1}{2}}}.$$

When a, b and c form sides of a triangle, ω reaches zero and the main contribution comes from the integration around $\omega\approx 0$ (ε is assumed to be negligibly small compared to a, etc.). In this approximation, we may use the following expressions:

$$\omega^2\approx\xi^2+a^2\phi^2+a\xi\phi^2-\tfrac{1}{12}a^2\varphi^4, \qquad (\xi=\lambda-a),$$

$$\sin\vartheta\approx\sin\alpha\left[1+\frac{\xi s\cos\alpha}{bc\sin^2\alpha}+\tfrac{1}{2}\left(\frac{\cos\alpha}{bc\sin^2\alpha}-\frac{a^2}{b^2c^2\sin^4\alpha}\right)\xi^2\right], \quad \left(\cos\alpha=\frac{b^2+c^2-a^2}{2bc}\right),$$

and integrate over ϕ from 0 to ∞ and over ξ from $-\infty$ to $+\infty$. The result is

$$\int e^{-\varepsilon r}J_1(ar)J_1(br)J_1(cr)r^2dr=\frac{a}{\pi b^2c^2\sin^3\alpha}+0(\varepsilon). \quad \text{(A-20)}$$

As is easily seen from eq. (A-19), when a, b and c do not satisfy the triangular condition, the integral is proportional to ε.

The evaluation of $\int e^{-\varepsilon r}J_1(ar)J_0(br)J_0(cr)r^2dr$ is much simpler, as is seen from the following expression:

$$\int e^{-\varepsilon r}J_1(ar)J_0(br)J_0(cr)r^2dr=\frac{3\varepsilon}{\pi^2}\int d\vartheta d\phi\,\frac{a-\lambda\cos\phi}{(\omega^2+\varepsilon^2)^{\frac{1}{2}}}. \quad \text{(A-21)}$$

In this case we may write $\omega^2 \approx \xi^2+a^2\phi^2$, and $\sin\vartheta \approx \sin\alpha$ and the result comes out at once. We have

$$\int e^{-\varepsilon r} J_1(ar)J_0(br)J_0(cr)r^2 dr = \frac{a\cos\alpha}{\pi b^2 c^2 \sin^3\alpha} + O(\varepsilon). \qquad \text{(A-22)}$$

The quasi-discontinuous character of those integrals is not possessed by some others in which the sum of the three orders is even. For example,

$$\int e^{-\varepsilon r} J_0(ar)J_0(br)J_0(cr)r^2 dr = \pi^{-2}\int d\vartheta d\phi \frac{2\varepsilon^2-\omega^2}{(\omega^2+\varepsilon^2)^{\frac{1}{2}}},$$

and when a, b and c form sides of a triangle a term inversely proportional to ε vanishes; so that the leading term does not contain ε irrespective of whether the triangular condition is satisfied or not.

References

1) M. Gell-Mann, Phys. Rev. **106** (1957) 1296;
J. Tiomno, Nuov. Cim. **11** (1957) 69
2) M. Kato and G. Takeda, Prog. Theor. Phys. Suppl. **7** (1959) 35
3) C. Ceolin, V. De Santis and L. Taffara, Nuov. Cim. **12** (1959) 502
4) Y. Murai, Nuclear Physics **6** (1958) 489
5) E. Cunningham, Proc. Lond. Math. Soc. [2], **8** (1910) 77;
H. Bateman, Proc. Lond. Math. Soc. [2], **8** (1910) 223;
P. A M Dirac, Proc. Roy. Soc. A **167** (1938) 457;
A. H. Taub, Bull. Amer. Math. Soc. **44** (1938) 457
6) M. Gell-Mann and F. E. Low, Phys. Rev. **95** (1954) 1300;
H. Lehmann, Nuov. Cim. **11** (1954) 342;
G. Källen, Helv. Phys. Acta **25** (1952) 417
7) R. Ingraham and J. Ford, Phys. Rev. **106** (1957) 1324
8) T. Okabayashi, Prog. Theor. Phys. **20** (1958) 583
9) S. Watanabe, Phys. Rev. **106** (1957) 1306; Nuov. Cim. **6** (1957) 187
10) R. Finkelstein, Phys. Rev. **110** (1958) 1200
11) W. Pauli, Nuov. Cim. **6** (1957) 204
12) K. Kawarabayashi, Prog. Theor. Phys. **22** (1959) 451;
H. Miyazawa, T. Nakano and H. Umezawa, Prog. Theor. Phys. **22** (1959) 643
13) A. Pais, Phys. Rev. **110** (1958) 574
14) D. Amati and B. Vitale, Nuov. Cim. **9** (1958) 895;
B. D'Espagnat and J. Prentki, preprint
15) G. Feinberg, Phys. Rev. **108** (1957) 878;
V. G. Soloviev, Nuclear Physics **6** (1958) 618;
G. Feinberg and F. Gürsey, Phys. Rev. **114** (1959) 1153
16) V. G. Soloviev, Nuov. Cim. **13** (1959) 442
17) R. Finkelstein, Nuov. Cim. **1** (1955) 1104; Phys. Rev. **109** (1958) 1842
18) L. Van Hove, Physica **25** (1959) 365
19) M. Markov, Nuclear Physics **10** (1959) 140
20) W. Pauli, Ann. der Phys. **18** (1933) 305

4.A

Nuclear Physics **17** (1960) 548—562; © *North-Holland Publishing Co., Amsterdam*

Not to be reproduced by photoprint or microfilm without written permission from the publisher

INTERACTION OF BETA-DECAY AND SECOND FORBIDDEN SPECTRUM OF Cs^{137}

TOSHIO KATOH, SHUICHIRO YAMASAKI and YASUKAZU YOSHIZAWA

Department of Physics, Faculty of Science, Osaka University, Osaka, Japan

Received 18 March 1960

Abstract: We discuss the allowed as well as non-unique first forbidden β-spectra, and, in particular, the second forbidden spectrum of Cs^{137} taking account of parity non-conservation. Our analysis can be summarized in the following way:

(i) From the consideration of Fierz terms in allowed as well as forbidden transitions, we can treat the two combinations STP and VA separately. Though a linear combination of the five interactions is possible, no interference term between STP and VA exists.

(ii) In the discussion of non-unique first forbidden transitions the combination VA is more favourable than STP.

(iii) From the second forbidden spectrum of Cs^{137} we see that

$$\frac{\mathrm{Re}(C_X C_Y^* + C'_X C'^*_Y)}{|C_Y|^2 + |C'_Y|^2} \approx -\frac{|C_X|^2 + |C'_X|^2}{|C_Y|^2 + |C'_Y|^2}$$

where X and Y mean S and T, or V and A.

1. Introduction

The high energy component of the β-ray spectrum from Cs^{137} was carefully investigated first by Langer and Moffat [1]). This transition is supposed to take place between the ground states of Cs^{137} and Ba^{137}, whose spins have been measured and to which parities can be assigned from shell model configurations near neutron magic number 82, and it is classified as one of the second forbidden transitions. The measured value of log $ft(= 11.6)$ supports this view.

The measurement and analysis of the β-spectrum of this nucleus made recently by Yoshizawa [2]) have established a spectrum shape consistent with Langer's within experimental error. Recently Yamazaki *et al.* [3]) have carried out this experiment with sufficient caution against chamber scattering and the result agreed well with the two just noted. We may consider that these experimental results are reliable and the spectrum shape is well established. Yoshizawa measured accurately the maximum energy W_0^{L} of the low energy component (unique first forbidden transition) of the β-decay spectrum, and derived that of the high energy component W_0^{H}, by the relation $W_0^{\mathrm{H}} = W_0^{\mathrm{L}} + W_\gamma$, where W_γ is the γ-ray energy. Using this value for the analysis, he succeeded in eliminating the ambiguity of the spectrum shape coming from the maximum energy.

The suggestion made by Lee and Yang [4]) that parity is not conserved in weak interactions was confirmed by the experiment of Wu *et al.* [5]). Following studies [6]) in this field, the angular distribution of β-rays from polarized nuclei, the polarization of β-rays, the $\beta-\gamma$ polarization correlation, have confirmed the violation of parity conservation, and specific possibilities such as the two-component theory [7]) or the twin-component theory [8]) were proposed. On the other hand, the combination of ST interactions, long believed to be adequate, became doubtful, and another possibility VA turned out to be favoured by the experiments on Eu^{152} [9]) and He^6 [10]). Analyzing the spectrum of RaE, Fujita *et al.* [11]) obtained the result

$$\frac{C_S}{C'_S} = \frac{C_T}{C'_T}, \quad \frac{C_S}{C_T} \text{ real} \quad \text{or} \quad \frac{C_V}{C'_V} = \frac{C_A}{C'_A}, \quad \frac{C_V}{C_A} \text{ real.}$$

The previous analysis [2]) of the Cs^{137} spectrum was based on the parity conserving theory with the ST combination. We tried, therefore, to re-analyze the Cs^{137} spectrum from the standpoints of ST and VA combinations and parity conserving as well as non-conserving theories. For this purpose we begin with a general discussion of β-ray spectra.

2. General Discussion of Beta-Ray Spectra

The study of the spectrum shape of the β-decay, along with that of life times, $\beta-\nu$ and $\beta-\gamma$ angular correlation or recoil spectrum, has great importance for the determination of the interaction type in β-decay. Continued studies from the early 1930's brought great advances in experimental techniques, and the measurement of spectrum shapes as well as life times are the most reliable among those noted above.

With the recognition of parity violation, we have to determine an increased number of interaction constants, and experiments on the angular distribution of β-rays from polarized nuclei, the polarization of β-rays, the $\beta-\gamma$ circular polarization correlation, etc. are to be consulted. In this way it seemed at first sight that the information obtainable from spectrum shapes came to be less decisive. But the other experiment can hardly be said to be as precise and unambiguous as those relating to the spectra. In fact, if a careful analysis is made of many β-spectra, some of the plausible possibilities may be excluded and the violation of parity conservation as well as the question of time reversal invariance can be discussed. Especially, specific cases of forbidden spectra are expected to lead to interesting conclusions.

We discuss the relation between the interaction types and the spectrum shapes in detail.

2.1. ALLOWED SPECTRA

The spectra of allowed transitions have the allowed shape proposed by Fermi, i.e. the so-called Fierz term is always absent or at least very small. The interference term between two interactions X and Y carries a factor

$$\frac{\mathrm{Re}(C_{\mathrm{X}}C_{\mathrm{Y}}^{*}+C'_{\mathrm{X}}C'^{*}_{\mathrm{Y}})}{|C_{\mathrm{Y}}|^{2}+|C'_{\mathrm{Y}}|^{2}},$$

and its absence means only

$$\frac{C_{\mathrm{X}}}{C'_{\mathrm{X}}}=-\left(\frac{C'_{\mathrm{Y}}}{C_{\mathrm{Y}}}\right)^{*}.$$

Thus, coexistence of interactions SVTA cannot be excluded provided that the coupling constants are properly related in such a way that

$$\mathrm{Re}(C_{\mathrm{S}}C_{\mathrm{V}}^{*}+C'_{\mathrm{S}}C'^{*}_{\mathrm{V}})=0 \quad \text{and} \quad \mathrm{Re}(C_{\mathrm{T}}C_{\mathrm{A}}^{*}+C'_{\mathrm{T}}C'^{*}_{\mathrm{A}})=0.$$

2.2. UNIQUE FIRST FORBIDDEN SPECTRA

In the case of unique first forbidden transitions the shape factor depends on the electron and the neutrino momenta p and q, simply by $p^{2}+q^{2}$ and contains only T and A contributions. Such spectra in $\Delta I=2$ transitions with change of parity are the evidence for the existence of Gamow-Teller interactions. Furthermore, we conclude

$$\mathrm{Re}(C_{\mathrm{T}}C_{\mathrm{A}}^{*}+C'_{\mathrm{T}}C'^{*}_{\mathrm{A}})=0,$$

because otherwise the TA interference term with $1/W$ dependence upon the electron energy W would have been observed.

2.3. NON-UNIQUE FIRST FORBIDDEN SPECTRA

Non-unique first forbidden spectra have up to date been observed in many cases, most of them being of allowed shape. Following the theory of forbidden spectra of Konopinski and Uhlenbeck [12]), one arranges terms in the spectra in powers of $\alpha Z/2\rho(\approx 10)$, taking into account Feenberg's estimate [13]) for the matrix elements. When only the dominant term in $(\alpha Z/2\rho)^{2}$ is considered, it is found that combinations such as ST, VA and TP give allowed shape spectra in agreement with experiment, whereas other combinations SV, TA, SA, VT and AP lead to interference terms with $1/W$ energy dependence similar to the Fierz terms known in allowed transitions. These terms can be discarded if nuclear matrix elements happen to make them vanish, but all the observed allowed shape spectra cannot be explained in this way. The violation of parity conservation, however, opens the possibility of vanishing interference terms in SV, TA, SA.

VT and AP combinations. These considerations, when combined with those for allowed as well as unique first forbidden spectra, leave us with the two combinations STP and VA. As their coexistence, if any, must be such that interference terms do not appear, we can treat these combinations separately in discussing the spectrum.

Hitherto we have confined ourselves to the dominant term $\propto (\alpha Z/2\rho)^2$. Terms of order $\alpha Z/2\rho$ are known to lead to energy-dependent shape factors. In case of large electron maximum momentum, it is expected that this energy dependence comes to play an important role and a closer inspection is required of the correction factor $S^{(L)}_{n\mathrm{XY}}$, where X and Y represent interaction types, L is the rank of the tensor matrix and n is the degree of forbiddenness.

The leading term $\propto(\alpha Z/2\rho)^2$ in $S^{(0)}_{1\mathrm{VT}}$ $(= S^{(0)}_{1\mathrm{T}})$ is not energy dependent, but the next order term $\propto(\alpha Z/2\rho)$ carries a factor $\frac{2}{3}(2W-1/W-W_0)$. For $\alpha Z/2\rho \approx 10$ and the maximum energy $W_0 \approx 1$ MeV, the latter undergoes a variation with energy of about 30 %, which is fairly large. The factor $S^{(1)}_{1\mathrm{VT}}$ has a term of order $(\alpha Z/2\rho)^2$ with a factor $1/W$ which is not negligible in general, the next order terms $\propto \alpha Z/2\rho$ vary as $-\frac{2}{3}(W_0-1/W)$ and $-\frac{2}{3}(W_0/W-1)$, and the change with energy, though dependent on matrix elements, is about 10 %. The leading term $\propto (\alpha Z/2\rho)^2$ in $S^{(0)}_{1\mathrm{SA}}$, similarly to that in $S^{(0)}_{1\mathrm{VT}}$, is independent of energy, but the next order term undergoes a change of about 5 % with energy. The factor $S^{(1)}_{1\mathrm{SA}}$ has a term $\propto (\alpha Z/2\rho)^2/W$ and the change with energy amounts to about 30 %. The factor $S^{(0)}_{1\mathrm{AP}}$ has also a $(\alpha Z/2\rho)^2/W$ term.

As to the combinations STP and VA, no $1/W$ term is present in their leading terms. Thus, these combinations can be distinguished from the others (namely VT or SA) by the investigation of the energy spectrum of transitions with $\Delta J = 1$. The correction factors for the STP and VA combinations were given by Konopinski and Uhlenbeck [12]) as follows:

$$S^{(0)}_{1\mathrm{STP}} = S^{(0)}_{1\mathrm{TP}}$$

$$= G_{\mathrm{T}}{}^2 \left|\int \beta\boldsymbol{\sigma}\cdot\mathbf{r}\right|^2 \left[\left(\frac{\alpha Z}{2\rho} + iG_{\mathrm{PT}}\frac{\int\beta\gamma_5}{\int\beta\boldsymbol{\sigma}\cdot\mathbf{r}}\right)^2\right.$$

$$+\tfrac{2}{3}\left(2W-W_0-\frac{1}{W}\right)\left(\frac{\alpha Z}{2\rho}+iG_{\mathrm{PT}}\frac{\int\beta\gamma_5}{\int\beta\boldsymbol{\sigma}\cdot\mathbf{r}}\right)$$

$$\left.+\tfrac{1}{9}\left\{(W_0-W)^2+W^2-1-2(W_0-W)\left(W-\frac{1}{W}\right)\right\}\right],$$

$$S^{(1)}_{1STP} = S^{(0)}_{1ST}$$

$$= G_T{}^2 \left| \int \beta\sigma\times\mathbf{r} \right|^2 \left[\left\{ \frac{\int \beta\alpha}{\int \beta\sigma\times\mathbf{r}} - \frac{\alpha Z}{2\rho}\left(1 + iG_{ST}\frac{\int \beta\mathbf{r}}{\int \beta\sigma\times\mathbf{r}}\right)\right\}^2 \right.$$

$$- \tfrac{2}{3}\left(2W - W_0 - \frac{1}{W}\right)\left\{ \frac{\int \beta\alpha}{\int \beta\sigma\times\mathbf{r}} - \frac{\alpha Z}{2\rho}\left(1 + iG_{ST}\frac{\int \beta\mathbf{r}}{\int \beta\sigma\times\mathbf{r}}\right)\right\} iG_{ST}\frac{\int \beta\mathbf{r}}{\int \beta\sigma\times\mathbf{r}}$$

$$- \tfrac{2}{3}\left(W_0 - \frac{1}{W}\right)\left\{ \frac{\int \beta\alpha}{\int \beta\sigma\times\mathbf{r}} - \frac{\alpha Z}{2\rho}\left(1 + iG_{ST}\frac{\int \beta\mathbf{r}}{\int \beta\sigma\times\mathbf{r}}\right)\right\}$$

$$+ \tfrac{1}{9}\left\{3(W_0 - W)^2 + 3(W^2 - 1) - 2(W_0 - W)\left(W - \frac{1}{W}\right)\right\}\left(iG_{ST}\frac{\int \beta\mathbf{r}}{\int \beta\sigma\times\mathbf{r}}\right)^2$$

$$\left. + \tfrac{1}{18}\left\{3(W_0 - W)^2 + 3(W^2 - 1) + 4(W_0 - W)\left(W - \frac{1}{W}\right)\right\}\right],$$

$$S^{(2)}_{1STP} = S^{(0)}_{1T}$$

$$= G_T{}^2 \sum |B^{\beta}_{ij}|^2 \tfrac{1}{12}\{(W_0 - W)^2 + (W^2 - 1)\},$$

$$S^{(0)}_{1VA} = S^{(2)}_{1A}$$

$$= G_A{}^2 \left| \int \sigma\cdot\mathbf{r} \right|^2 \left[\left(\frac{\alpha Z}{2\rho} + i\frac{\int \gamma_5}{\int \sigma\cdot\mathbf{r}}\right)^2 + \tfrac{2}{3}\left(W_0 - \frac{1}{W}\right)\left(\frac{\alpha Z}{2\rho} + i\frac{\int \gamma_5}{\int \sigma\cdot\mathbf{r}}\right)\right.$$

$$\left. + \tfrac{1}{9}\left\{(W_0 - W)^2 + (W^2 - 1) + 2(W_0 - W)\left(W - \frac{1}{W}\right)\right\}\right],$$

$$S^{(1)}_{1VA} = G_A{}^2 \left| \int \sigma\times\mathbf{r} \right|^2 \left[\left\{ G_{VA}\frac{\int \alpha}{\int \sigma\times\mathbf{r}} - \frac{\alpha Z}{2\rho}\left(1 + iG_{VA}\frac{\int \mathbf{r}}{\int \sigma\times\mathbf{r}}\right)\right\}^2 \right.$$

$$- \tfrac{2}{3}\left(W_0 - \frac{1}{W}\right)\left\{ G_{VA}\frac{\int \alpha}{\int \sigma\times\mathbf{r}} - \frac{\alpha Z}{2\rho}\left(1 + iG_{VA}\frac{\int \mathbf{r}}{\int \sigma\times\mathbf{r}}\right)\right\} iG_{VA}\frac{\int \mathbf{r}}{\int \sigma\times\mathbf{r}}$$

$$-\tfrac{2}{3}\left(2W-W_0-\frac{1}{W}\right)\left\{G_{\mathrm{VA}}\frac{\int\boldsymbol{\alpha}}{\int\boldsymbol{\sigma}\times\mathbf{r}}-\frac{\alpha Z}{2\rho}\left(1+iG_{\mathrm{VA}}\frac{\int\mathbf{r}}{\int\boldsymbol{\sigma}\times\mathbf{r}}\right)\right\}$$

$$+\tfrac{1}{9}\left\{3(W_0-W)^2+3(W^2-1)+2(W_0-W)\left(W-\frac{1}{W}\right)\right\}\left(iG_{\mathrm{VA}}\frac{\int\mathbf{r}}{\int\boldsymbol{\sigma}\times\mathbf{r}}\right)^2$$

$$+\tfrac{1}{18}\left\{3(W_0-W)^2+3(W^2-1)-4(W_0-W)\left(W-\frac{1}{W}\right)\right\}\Bigg],$$

$$S^{(2)}_{\mathrm{1VA}}=S^{(2)}_{\mathrm{1A}}$$
$$=G_{\mathrm{V}}^2\,\Sigma|B_{ij}|^2\tfrac{1}{12}\{(W_0-W)^2+(W^2-1)\},$$

where

$$G_{\mathrm{X}}^2=|C_{\mathrm{X}}|^2+|C'_{\mathrm{X}}|^2 \quad\text{and}\quad G_{\mathrm{XY}}=\frac{\mathrm{Re}(C_{\mathrm{X}}C^*_{\mathrm{Y}}+C'_{\mathrm{X}}C'^*_{\mathrm{Y}})}{|C_{\mathrm{Y}}|^2+|C'_{\mathrm{Y}}|^2}.$$

The expression for $S^{(1)}_{\mathrm{1VA}}$ can be rearranged as follows:

$$S^{(1)}_{\mathrm{1VA}}=G_{\mathrm{V}}^2\left|\int\mathbf{r}\right|^2\Bigg[\left\{-\frac{i\int\boldsymbol{\alpha}}{\int\mathbf{r}}-\frac{\alpha Z}{2\rho}\left(1-iG_{\mathrm{AV}}\frac{\int\boldsymbol{\sigma}\times\mathbf{r}}{\int\mathbf{r}}\right)\right\}^2$$

$$-\tfrac{2}{3}\left(2W-W_0-\frac{1}{W}\right)\left\{-\frac{i\int\boldsymbol{\alpha}}{\int\mathbf{r}}-\frac{\alpha Z}{2\rho}\left(1-iG_{\mathrm{AV}}\frac{\int\boldsymbol{\sigma}\times\mathbf{r}}{\int\mathbf{r}}\right)\right\}\left(-iG_{\mathrm{AV}}\frac{\int\boldsymbol{\sigma}\times\mathbf{r}}{\int\mathbf{r}}\right)$$

$$-\tfrac{2}{3}\left(W_0-\frac{1}{W}\right)\left\{-\frac{i\int\boldsymbol{\alpha}}{\int\mathbf{r}}-\frac{\alpha Z}{2\rho}\left(1-iG_{\mathrm{AV}}\frac{\int\boldsymbol{\sigma}\times\mathbf{r}}{\int\mathbf{r}}\right)\right\}$$

$$+\tfrac{1}{9}\left\{3(W_0-W)^2+3(W^2-1)+2(W_0-W)\left(W-\frac{1}{W}\right)\right\}$$

$$+\tfrac{1}{18}\left\{3(W_0-W)^2+3(W^2-1)-4(W_0-W)\left(W-\frac{1}{W}\right)\right\}\left(-iG_{\mathrm{AV}}\frac{\int\boldsymbol{\sigma}\times\mathbf{r}}{\int\mathbf{r}}\right)^2\Bigg].$$

From this formula it is seen that the $(\alpha Z/2\rho)^2$ term is energy independent and that the $\alpha Z/2\rho$ terms have the same energy dependence as those of $S^{(1)}_{\mathrm{1STP}}$ so far as the matrix elements are treated as adjustable parameters. The difference between $S^{(1)}_{\mathrm{1STP}}$ and $S^{(1)}_{\mathrm{1VA}}$ is caused only by terms of order $(\alpha Z/2\rho)^0$ which contribute but little to the spectrum. The correction factors can deviate as far as 30 %

from the allowed shape for a typical maximum energy of about 1 MeV, and we may hope to observe considerable distortion of the spectrum by a careful measurement of the first forbidden transition with $\Delta J = 1$.

One observes similarly that the energy dependence is not the same for $S^{(0)}_{1STP}$ and $S^{(0)}_{1VA}$ in terms of order $\alpha Z/2\rho$, namely $2W - W_0 - 1/W$ for the former and $W_0 - 1/W$ for the latter. Therefore, if a closer examination of first forbidden transitions with $\Delta J = 0$ reveals all of them to have allowed shape spectra within the experimental error, one could choose the combination VA rather than STP. Especially, the 0—0 transition spectra, lacking the contributions from $S^{(1)}_{1XY}$, open another possibility of discriminating between the two alternatives TP and A. In this respect the recent experiments [14, 15]) on Pr^{144} are of great significance.

Up to now non-unique first forbidden spectra have been observed for a number of nuclei; most of them are listed in table 1. Almost all of them, with the clear exception of Sb^{124}, Eu^{150} and RaE, are reported to have allowed shape except for the low energy part. The spectrum of Re^{186} was found by precise measurement to deviate a little from the allowed spectrum. $\Delta J = 0$ transitions, including that of Pr^{144}, are known to agree with the allowed shape spectrum within an experimental uncertainty of about 10 %. The RaE analysis requires the coming into play of interference terms of ST or VA. We take these experimental results in favour of the VA combination. $\Delta J = 1$ transitions with maximum electron energy of about 1 MeV could have an energy dependence in excess of the experimental uncertainty. It seems quite difficult to explain these transitions with allowed shape spectra, and more precise measurements as well as a more careful analysis are desired.

2.4. NON-UNIQUE SECOND FORBIDDEN SPECTRA

The highest term $\propto (\alpha Z/2\rho)^2$ in the correction factor for the second forbidden spectrum depends on energy in contrast to the case of allowed and first forbidden transitions. The combinations SV, TA, SA and VT yield $(\alpha Z/2\rho)^2$ terms which have $1/W$ energy dependence, but the ST and the VA combinations do not give such terms. The correction factor for the ST combination can be written

$$S^{(2)}_{2ST} \approx \tfrac{1}{12} q^2 X_1^2 + \tfrac{1}{12} p^2 X_2^2,$$

where X_1 and X_2, as shown in the next section, represent linear combinations of the ratios of matrix elements, both of them being of order $\alpha Z/2\rho$. This correction factor is of the unique first forbidden type for $X_1^2 \approx X_2^2$, and takes small values in the high or low energy limit according as $X_1^2 \gg X_2^2$ or $X_1^2 \ll X_2^2$. As to the VA combination, the correction factor can be written similarly as for the ST combination:

$$S^{(2)}_{2VA} \approx \tfrac{1}{12} q^2 X_1'^2 + \tfrac{1}{12} p^2 X_2'^2,$$

and the discussion proceeds as above.

TABLE 1

Non-unique first forbidden spectra

Parent nucleus	Spins and parities		Maximum energy (MeV)	Log ft	Refs.
	initial	final			
K^{42}	2^-	2^+	1.99	7.44	[a]
As^{76}	2^-	2^+	2.41	8.2	[a]
Rb^{86}	2^-	2^+	0.68	7.8	[b]
Sb^{122}	2^-	2^+	1.42	7.6	[c]
Sb^{124}	3^-	2^+	2.32	10.5	[d]
I^{126}	2^-	2^+	0.865	7.9	[e]
	2^-	2^+	0.46	7.4	
Pr^{142}	2^-	2^+	0.586	7.8	[b]
Ce^{144}	0^+	0^-	0.30	7.5	[f]
Pr^{144}	0^-	0^+	2.97	6.5	[g]
Eu^{150}	1^-	0^+	1.07	$\geqq 6.5$	[h]
Tm^{170}	1^-	0^+	0.968	9.0	[b] [i]
	1^-	2^+	0.884	9.1	
Ta^{180}	1^-	0^+	0.705	6.8	[j]
	1^-	2^+	0.605	6.5	
Re^{186}	1^-	0^+	1.071	7.68	[k]
	1^-	2^+	0.934	8.0	
Bi^{210}(RaE)	1^-	0^+	1.17	8.0	[l]
Ce^{141}	$\frac{7}{2}^-$	$\frac{5}{2}^+$	0.574	7.8	[m]
	$\frac{7}{2}^-$	$\frac{7}{2}^+$	0.432	6.9	
Pr^{143}	$\frac{5}{2}^+$	$\frac{7}{2}^-$	0.929	7.6	[n]
Pm^{147}	$\frac{5}{2}^+$	$\frac{7}{2}^-$	0.223	7.4	[o]
W^{185}	$\frac{3}{2}^-$	$\frac{5}{2}^+$	0.428	7.5	[p]

[a] Pohm, Waddell and Jensen, Phys. Rev. **101** (1956) 1315
[b] Pohm, Lewis, Talboy and Jensen, Phys. Rev. **95** (1954) 1523
[c] M. J. Glaubman, Phys. Rev. **98** (1955) 645;
Farrelly, Koerts, Benczer, van Lieshout and Wu, Phys. Rev. **99** (1955) 1440;
J. Moreau, Compt. Rend. **239** (1954) 1130
[d] Langer, Lazer and Moffat, Phys. Rev. **91** (1953) 338;
J. Moreau, Compt. Rend. **239** (1954) 800;
T. Azuma, J. Phys. Soc. Japan **10** (1955) 167;
Zolotavin, Grigoryev and Abroyan, Izvestia Acad. Nauk S.S.S.R. Ser. Fiz. **20** (1956) 289
[e] Koerts, Macklin, Farrelly, van Lieshout and Wu, Phys. Rev. **98** (1955) 1230;
Marty, Langevin and Hubert, J. Phys. et Radium **14** (1953) 663
[f] L. Pullman and P. Axel, Phys. Rev. **102** (1956) 1366
[g] M. J. Laubitz, Proc. Phys. Soc. A **69** (1956) 786;
Graham, Geiger and Eastwood, Can. J. Phys. **36** (1958) 1084;
F. T. Porter and P. P. Day, Phys. Rev. **114** (1959) 1286
[h] Mack, Neuer and Pool, Phys. Rev. **91** (1953) 903
[i] Graham, Wolfson and Bell, Can. J. Phys. **30** (1952) 459
[j] Brown, Bendel, Shore and Becker, Phys. Rev. **84** (1951) 292
[k] Porter, Freedman, Novey and Wagner, Phys. Rev. **103** (1956) 921
[l] E. A. Plassmann and L. M. Langer, Phys. Rev. **96** (1954) 1593
[m] J. T. Jones, Jr., and E. N. Jensen, Phys. Rev. **97** (1955) 1031
[n] Feldman, Lidofsky, Macklin and Wu, Phys. Rev. **76** (1949) 1888;
Ter-Pogossian, Cook, Goodard and Robinson, Phys. Rev. **76** (1949) 909
[o] Langer, Motz and Price, Phys. Rev. **77** (1950) 798
[p] I. R. Williams and M. W. Johns, Nuovo Cimento **6** (1957) 18;
Dubey, Mandeville, Mukerji and Potnis, Phys. Rev. **106** (1957) 785

The ST and VA combinations give equivalent correction factors to the first order in $\alpha Z/2\rho$ and it is difficult, as in the case of $S^{(1)}_{1ST}$ and $S^{(1)}_{1VA}$, to distinguish between these combinations experimentally. As only few non-unique second forbidden spectra have hitherto been subjected to thorough investigation, we discuss in the next section the analysis of Cs^{137}. A similar analysis for RaE has been carried out by Fujita *et al.* [11]).

3. Correction Factor of Cs^{137} Spectrum

The β-transition from the Cs^{137} ground state to the Ba^{137} ground state is classified as of the non-unique second forbidden type. This is because the ground state spins have been measured to be $\frac{7}{2}$ and $\frac{3}{2}$, respectively, for Cs^{137} and Ba^{137}, and the shell model predicts even parities for the ground states of these nuclei.

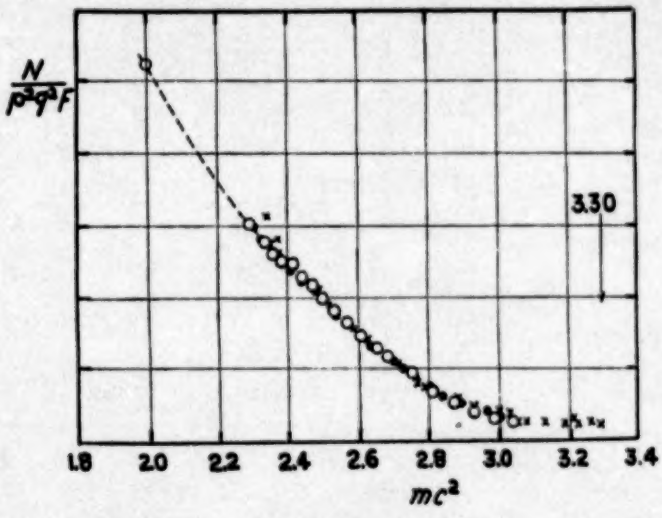

Fig. 1. Experimental correction factors of Cs^{137} second forbidden spectrum. Points indicated by × show the results of Langer and Moffat, ○ those of Yoshizawa and ● those of Yamazaki *et al.*

The maximum energy, though difficult to determine, was taken in the earlier paper [2]) as 1170 keV, which is the sum of the maximum energy (514 keV) of the lower component and the energy of the isomeric transition (662 keV). In this way the maximum energy was determined accurately, whereas many other analyses of forbidden spectra have been accompanied with ambiguities coming from the uncertainty of the maximum energies.

As is shown in fig. 1 the correction factor for Cs^{137} gives a strong distortion. From the discussion of the previous section we expect the p^2-contribution in the $(\alpha Z/2\rho)^2$ terms to be negligibly small, so that the contribution of the $\alpha Z/2\rho$ terms would be important in the vicinity of the maximum energy. The energy dependence of the latter contribution for ST is the same as for VA, similarly as in the case of the first forbidden spectra (sect. 2.3), and a difference should be looked for in the next order terms, but this is experimentally almost impossible to observe.

The correction factors for ST and VA combinations are given as follows:

$$S^{(2)}_{2ST} = G_T^2 \sum |T_{ij}{}^{\beta}|^2 \left[\frac{q^2}{12} X_1^2 + \frac{p^2}{12} X_2^2 + \frac{q^2}{6}\left(\frac{q}{5} - \frac{p^2}{3W}\right) X_1 Y \right.$$

$$+ \frac{p^2}{6}\left(\frac{q}{3} - \frac{p^2}{5W}\right) X_2 Y - \frac{q^2}{6}\left(\frac{q}{5} + \frac{p^2}{3W}\right) X_1 - \frac{p^2}{6}\left(\frac{q}{3} + \frac{p^2}{5W}\right) X_2$$

$$+ \left\{\tfrac{1}{120}(q^4 + p^4) + \tfrac{1}{36} q^2 p^2 - \tfrac{1}{90}\frac{qp^2}{W}(q^2 + p^2)\right\} Y^2$$

$$\left. + \tfrac{1}{180}(q^4 + p^4) + \tfrac{1}{54} q^2 p^2 + \tfrac{1}{90}\frac{qp^2}{W}(q^2 + p^2)\right],$$

$$S^{(2)}_{2VA} = G_A^2 \sum |T_{ij}|^2 \left[\frac{q^2}{12} X_1'^2 + \frac{p^2}{12} X_2'^2 - \frac{q^2}{6}\left(\frac{q}{5} + \frac{p^2}{3W}\right) X'_1 Y'_1 \right.$$

$$- \frac{p^2}{6}\left(\frac{q}{3} + \frac{p^2}{5W}\right) X'_2 Y' + \frac{q^2}{6}\left(\frac{q}{5} - \frac{p^2}{3W}\right) X_1 + \frac{p^2}{6}\left(\frac{q}{3} - \frac{p^2}{5W}\right) X'_2$$

$$+ \left\{\tfrac{1}{120}(q^4 + p^4) + \tfrac{1}{36} q^2 p^2 + \tfrac{1}{90}\frac{qp^2}{W}(q^2 + p^2)\right\} Y'^2$$

$$\left. + \left\{\tfrac{1}{180}(q^4 + p^4) + \tfrac{1}{54} q^2 p^2 - \tfrac{1}{90}\frac{qp^2}{W}(q^2 + p^2)\right\}\right],$$

where

$$X_1 = \frac{A^{\beta}_{ij}}{T^{\beta}_{ij}} - \frac{\alpha Z}{2\rho}\left(1 + 2iG_{ST}\frac{R^{\beta}_{ij}}{T^{\beta}_{ij}}\right),$$

$$X_2 = \frac{A^{\beta}_{ij}}{T^{\beta}_{ij}} - \tfrac{1}{2}\frac{\alpha Z}{2\rho}\left(1 + 2iG_{ST}\frac{R^{\beta}_{ij}}{T^{\beta}_{ij}}\right),$$

$$Y = 2iG_{ST}\frac{R^{\beta}_{ij}}{T^{\beta}_{ij}},$$

$$X'_1 = G_{VA}\frac{A_{ij}}{T_{ij}} - \frac{\alpha Z}{2\rho}\left(1 + 2iG_{VA}\frac{R_{ij}}{T_{ij}}\right),$$

$$X'_2 = G_{VA}\frac{A_{ij}}{T_{ij}} - \tfrac{1}{2}\frac{\alpha Z}{2\rho}\left(1 + 2iG_{VA}\frac{R_{ij}}{T_{ij}}\right),$$

$$Y' = 2iG_{VT}\frac{R_{ij}}{T_{ij}}.$$

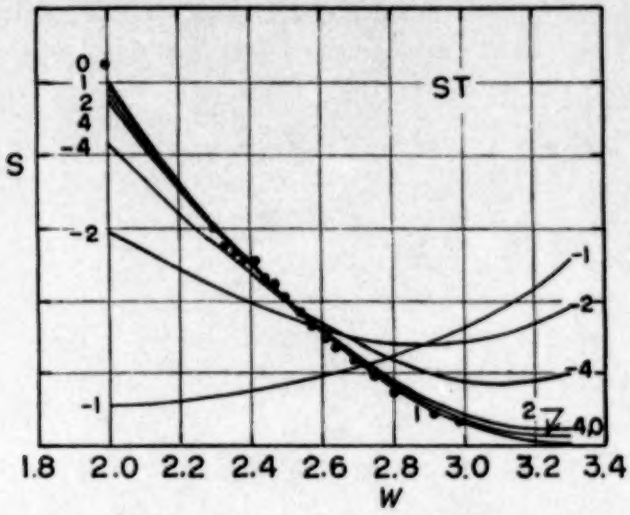

Fig. 2. Comparison of the calculated ST correction factors with the experimental ones. Points indicate the experimental results of Yoshizawa. For each choice of $2iR_{ij}^{\beta}/T_{ij}^{\beta}$ as indicated in the figure, the values of X_1 and X_2 are selected to make the theoretical curves approach the experimental points. These values are given in the following table:

$2iR_{ij}^{\beta}/T_{ij}^{\beta}$	4	2	1	0	−1	−2	−4
X_1	−2.86	−17.1	−11.3	−5.6	0.20	6.00	17.5
X_2	2.37	1.50	1.07	0.63	0.20	−0.23	−1.10

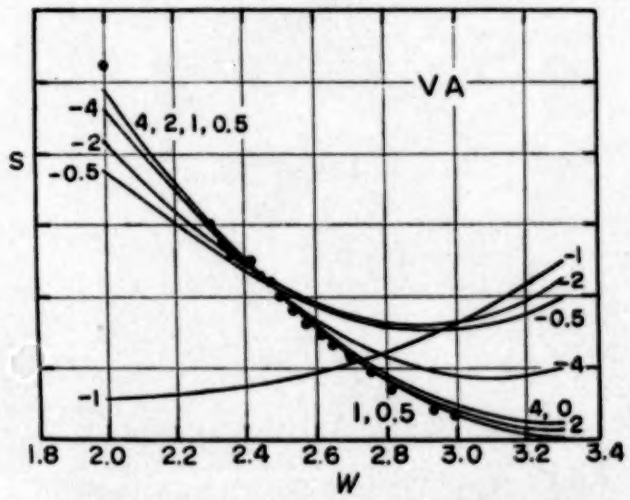

Fig. 3. Comparison of the calculated VA correction factors with the experimental ones. The selected values of X'_1 and X'_2 for each choice of $2iR_{ij}/T_{ij}$ are given in the following table:

$2iR_{ij}/T_{ij}$	4	2	1	0.5	0	−0.5	−1	−2	−4
X'_1	−27.7	−16.7	−11.2	−8.44	−5.69	−2.95	−0.20	5.29	16.3
X'_2	3.33	1.92	1.21	0.86	0.51	0.15	−0.20	−0.90	−2.32

In figs. 2 and 3 we compare the correction factors calculated from the above equations with the experimental result. Calculated curves correspond to the best fit values of X_1 and X_2 (X'_1 and X'_2) for each choice of Y (Y') which is shown in the figures. A good agreement is obtained between theory and experiment for $1 \geqq Y\ (Y') \geqq 0$, while no other value of Y (Y') leads to a satisfactory result outside this region.

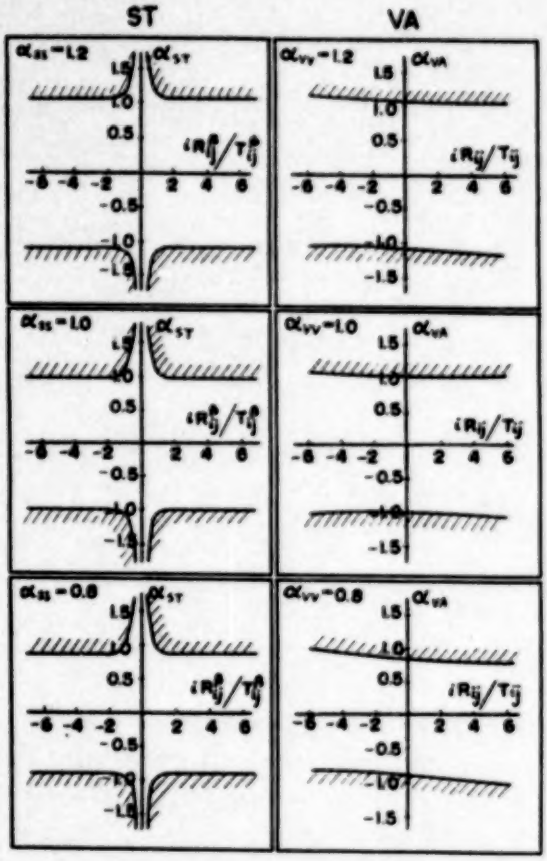

Fig. 4. The allowed values of G_{ST} and G_{VA} as functions of $2iR_{ij}^{\beta}/T_{ij}^{\beta}$ and $2iR_{ij}/T_{ij}$. The lines show the boundaries between allowed and forbidden region. The allowed values lie outside the region containing the origin.

In fig. 4 we show allowed values of G_{ST} or G_{VA} in terms of $2i\ R_{ij}^{\beta}/T_{ij}^{\beta}$ ($2i\ R_{ij}/T_{ij}$) for reasonable choices of G_S^2/G_T^2 or G_V^2/G_A^2. From experiments of super-allowed transitions [16]) the value of the latter ratio is estimated as 0.95 ± 0.20. The analysis is carried out for the values 0.8, 1.0 and 1.2, and it is concluded that $|G_{ST}| \approx G_S^2/G_T^2$ or $|G_{VA}| \approx G_V^2/G_A^2$. The estimated error due to both the experiment and the analysis is about 20 % but not conclusive.

4. Discussion

In the analysis of the second forbidden spectrum of Cs^{137}, it is seen that the correction factor is well explained in terms of the ST as well as the VA combina-

tion, and that G_{ST} (G_{VA}) cannot be small. This analysis was carried out by means of the Konopinski-Uhlenbeck theory and neglect was made of many effects due to the finite nuclear size, the finite de Broglie wave-length, the β-decay inside the nucleus and the screening by orbital electrons. The contributions from some of these effects are expected to be important for the spectrum in the vicinity of its upper limit, because cancellations took place among the main terms in the course of the calculation. Theoretical estimation of these effects is difficult, but they may amount to about 20 % according to Matumoto and Yamada [17]), and Rose *et al.* [18, 19]).

In the comparison of theoretical predictions with the observed spectrum, agreement was obtained only when

$$2iG_{ST}\frac{R^{\beta}_{ij}}{T^{\beta}_{ij}}>0 \quad \text{or} \quad 2iG_{VA}\frac{R_{ij}}{T_{ij}}>0.$$

The ratio of matrix elements can be calculated in the single particle shell model assuming $g_{\frac{7}{2}}$ and $d_{\frac{3}{2}}$ configurations for the ground states of Cs^{137} and Ba^{137}. We have

$$2i\frac{R^{\beta}_{ij}}{T^{\beta}_{ij}}=-1 \quad \text{or} \quad 2i\frac{R_{ij}}{T_{ij}}=-1,$$

hence

$$\frac{\mathrm{Re}(C_S{}^*C_T+C'_S C'^*_T)}{|C_T|^2+|C'_T|^2}<0 \quad \text{or} \quad \frac{\mathrm{Re}(C_V C_A{}^*+C'_V C'^*_A)}{|C_A|^2+|C'_A|^2}<0.$$

The ground state magnetic moments of these two nuclei, however, deviate from the Schmidt lines, implying the failure of the extreme single particle model. We should like, therefore, to estimate the ratio of the matrix elements in terms of the many particle shell model, assuming a closed neutron shell for Cs^{137} and a single particle configuration of the neutrons in Ba^{137}.

According to Klinkenberg [20]) the neutron shell $d_{\frac{3}{2}}$ and the proton shells $g_{\frac{7}{2}}$ and $d_{\frac{3}{2}}$ occur in nuclei near Cs^{137}. As the neutron configuration in Ba^{137} is $(d_{\frac{3}{2}})^{-1}$, namely one hole state from the closed shell 82, other configurations can be discarded.

The configurations consistent with spin and parity are given in table 2 with the seniority number v. The selection rule for the seniority number, besides those for spin and parity, restricts allowed cases of transitions between the configurations given in the table. The matrix elements R_{ij} and T_{ij} can be considered equal to R^{β}_{ij} and T^{β}_{ij}, respectively. The ratio $2R_{ij}/T_{ij}$ depends neither on the number of particles in the orbit relevant to the transition nor on the seniority number of the configuration. This is because each matrix element can be reduced to a single particle matrix element multiplied by a common statistical factor. Though the matrix elements depend on the radial parts of the wave

functions, the ratio $2R_{ij}/T_{ij}$ is independent of them and can easily be calculated in the shell model. We have

$$\frac{(\frac{1}{2}l_1 j_1 | 2R | \frac{1}{2}l_t j_t)}{(\frac{1}{2}l_1 j_1 | T | \frac{1}{2}l_t j_t)} = i\,\frac{\sqrt{2}}{3}\begin{Bmatrix} l_1 & l_t & 2 \\ j_1 & j_t & 2 \\ \frac{1}{2} & \frac{1}{2} & 0 \end{Bmatrix} \Big/ \begin{Bmatrix} l_1 & l_t & 2 \\ j_1 & j_t & 2 \\ \frac{1}{2} & \frac{1}{2} & 1 \end{Bmatrix},$$

$$\frac{(g_{\frac{7}{2}} | 2R | d_{\frac{3}{2}})}{(g_{\frac{7}{2}} | T | d_{\frac{3}{2}})} = i,$$

$$\frac{(d_{\frac{5}{2}} | 2R | d_{\frac{3}{2}})}{(d_{\frac{5}{2}} | T | d_{\frac{3}{2}})} = -\frac{2}{5}i.$$

TABLE 2

Configurations of Cs^{137} and Ba^{137}

$_{55}Cs^{137}_{82}$			$_{56}Ba^{137}_{81}$		
proton		neutron	proton		neutron
$(g_{\frac{7}{2}})^5_{\nu=1,3}$		full	$(g_{\frac{7}{2}})^6_{\nu=0,2}$		$(d_{\frac{3}{2}})^{-1}_{\nu=1}$
$(g_{\frac{7}{2}})^4_{\nu=0,2,4}$	$(d_{\frac{5}{2}})^1_{\nu=1}$		$(g_{\frac{7}{2}})^5_{\nu=1,3}$	$(d_{\frac{5}{2}})^1_{\nu=1}$	
$(g_{\frac{7}{2}})^3_{\nu=1,3}$	$(d_{\frac{5}{2}})^2_{\nu=0,2}$		$(g_{\frac{7}{2}})^4_{\nu=0,2,4}$	$(d_{\frac{5}{2}})^2_{\nu=0,2}$	
$(g_{\frac{7}{2}})^2_{\nu=0,2}$	$(d_{\frac{5}{2}})^3_{\nu=1,3}$		$(g_{\frac{7}{2}})^3_{\nu=1,3}$	$(d_{\frac{5}{2}})^3_{\nu=1,3}$	
$(g_{\frac{7}{2}})^1_{\nu=1}$	$(d_{\frac{5}{2}})^4_{\nu=0,2}$		$(g_{\frac{7}{2}})^2_{\nu=0,2}$	$(d_{\frac{5}{2}})^4_{\nu=0,2}$	
	$(d_{\frac{5}{2}})^5_{\nu=1}$		$(g_{\frac{7}{2}})^1_{\nu=1}$	$(d_{\frac{5}{2}})^5_{\nu=1}$	
				$(d_{\frac{5}{2}})^6_{\nu=0}$	

If a mixing of the configurations $d_{\frac{5}{2}}$ and $g_{\frac{7}{2}}$ is considered, the above argument fails and the ratio is no longer equal to a single particle value.

The $g_{\frac{7}{2}}$ orbit seems to be preferable to the $d_{\frac{5}{2}}$ orbit for the proton configuration of Cs^{137} in view of the shell model analysis for the magnetic moment of this nucleus [21, 22]). Of course a small amount of configuration mixing cannot change the sign of this ratio and within the validity of the shell model assignment of a $g_{\frac{7}{2}}$ configuration to the proton shell in Cs^{137} we can safely conclude

$$\frac{\mathrm{Re}(C_S C_T^* + C'_S C'^*_T)}{|C_T|^2 + |C'_T|^2} \approx -\frac{|C_S|^2 + |C'_S|^2}{|C_T|^2 + |C'_T|^2}$$

or

$$\frac{\mathrm{Re}(C_V C_A^* + C'_V C'^*_A)}{|C_V|^2 + |C'_V|^2} \approx -\frac{|C_V|^2 + |C'_V|^2}{|C_A|^2 + |C'_A|^2}.$$

The authors would like to express their thanks to Drs. J. Fujita, H. Takebe and Z. Matumoto for helpful discussions.

References

1) L. M. Langer and R. D. Moffat, Phys. Rev. **82** (1951) 635
2) Y. Yoshizawa, Nuclear Physics **5** (1958) 122
3) T. Yamazaki, H. Ikegami and M. Sakai, J. Phys. Soc. Japan **13** (1958) 1080
4) T. D. Lee and C. N. Yang, Phys. Rev. **104** (1956) 254
5) C. S. Wu, E. Ambler, R. W. Hayward, D. D. Hoppes and R. P. Hudson, Phys. Rev. **105** (1957) 1413
6) C. S. Wu, Revs. Mod. Phys. **31** (1959) 783
7) T. D. Lee and C. N. Yang, Phys. Rev. **105** (1957) 1671
8) M. G. Mayer and V. L. Telegdi, Phys. Rev. **107** (1957) 1445
9) M. Goldhaber, L. Grodzins and A. V. Sunyar, Phys. Rev. **109** (1958) 1015
10) Herrmannsfeldt, Burman, Stahelin, Allen and Braid, Phys. Rev. Letters **1** (1958) 61
11) J. Fujita, M. Yamada, Z. Matumoto and S. Nakamura, Prog. Theor. Phys. **20** (1958) 287
12) E. J. Konopinski and G. E. Uhlenbeck, Phys. Rev. **60** (1941) 308
13) T. Ahrens and E. Feenberg, Phys. Rev. **86** (1952) 64
14) R. L. Graham , J. S. Geiger and T. A. Eastwood, Can. J. Phys. **36** (1958) 1084
15) F. T. Porter and P. P. Day, Phys. Rev. **114** (1959) 1286
16) E. J. Konopinski, Revs. Mod. Phys. **27** (1955) 254
17) Z. Matumoto and M. Yamada, Prog. Theor. Phys. **19** (1958) 285
18) M. E. Rose and D. K. Holmes, ORNL-1022 (1951); Phys. Rev. **83** (1951) 90
19) M. E. Rose, C. L. Perry and N. M. Dismuke, ORNL-1459 (1953)
20) P. F. A. Klinkenberg, Revs. Mod. Phys. **24** (1952) 63
21) A. Arima and H. Horie, Prog. Theor. Phys. **11** (1954) 509; **12** (1954) 623
22) H. Noya, A. Arima and H. Horie, Suppl. Prog. Theor. Phys. no. 8 (1958) 33

2.C

Nuclear Physics **17** (1960) 563—585; © *North-Holland Publishing Co., Amsterdam*

Not to be reproduced by photoprint or microfilm without written permission from the publisher

THEORY OF RADIATIVE CAPTURE IN THE RESONANCE REGION

A. M. LANE and J. E. LYNN

Atomic Energy Research Estalishment, Harwell, England

Received 10 March 1960

Abstract: Starting from nuclear dispersion theory, a formalism is presented for the analysis of capture reaction cross sections at energies in the resonance region. Account is taken not only of capture through local resonances but also of "direct" or "potential" capture. The latter contributes to the cross section a smooth background with which resonances interfere. Estimates show that, in certain favourable cases, the direct capture can predominate. An important feature of direct capture (and also of the channel contribution to resonance capture) is that it tends to select final single particle states and so gives rise to anomalous groups in the photon spectrum.

1. Introduction

In previous papers [1, 2]) we have drawn attention to disagreement between compound nucleus theory and observed values of radiative capture cross sections in the high energy region (bombarding energies of 10 MeV or so) where resonances overlap. We saw that the observed cross sections are to be attributed to a "direct" radiative capture mechanism. Formally, from the point of view of dispersion theory, this component can be extracted by summing over distant levels in the dispersion series.

The present paper is concerned with similar matters in the low energy region where resonance levels are well spaced out. In this region, there is also disagreement with compound nucleus theory. One type of anomaly occurs in radiative capture in very light nuclei. Unlike heavier nuclei, these nuclei have very few final states, often only one, and the anomalies appear in the total capture cross section. The thermal cross section for Li^7 does not agree with that expected from nearby resonances. Thomas [3]) pointed out that the observed cross section could be fitted by taking into account the contribution to the dipole integral from the entrance channel. This contribution was recognized in earlier work on capture [4]) but has been ignored in analyzing the experimental data produced in recent years. More recently, anomalies have appeared in proton capture in light nuclei like O^{16} and Li^6. Attempts have been made [5]) to explain these in terms of channel contributions, and in terms of the presence of "single particle" levels in the energy level spectrum. The theory of the present paper has close connection with these ideas but is considerably more general. It applies to capture in any nucleus, and capture in light nuclei can be dealt with by appropriate specialisation of the theory.

In the next section, we present the basic dispersion formalism for radiative capture. It will be seen that, quite generally, terms occur in the scattering matrix element in addition to the usual dispersion sum. These arise from integration in the entrance channel and are largest for those final states which have strong channel components such as single particle states.

The distant terms in the dispersion sum can be taken into account if a model of the interaction between the incident particle and target nucleus (like the complex potential model) is assumed. This is done in section 3, where we show that the scattering matrix element for capture is composed of three parts, the conventional resonance part, an anomalous resonance part exhibiting selection rules, and a part for single particle capture in the nuclear potential.

2. Theory of Capture Mechanisms in the Resonance Region

2.1. DISPERSION FORMALISM FOR RADIATIVE CAPTURE

Suppose particles α' of spin $i_{\alpha'}$ are incident upon target nuclei β' of spin $i_{\beta'}$ with relative orbital angular momentum l'. Consider that the spin states are classified by coupling the intrinsic spins together to form the channel spin s':

$$\mathbf{s}' = \mathbf{i}_{\alpha'} + \mathbf{i}_{\beta'}$$

and by coupling this to l' to give the total spin J:

$$\mathbf{J} = \mathbf{s}' + \mathbf{l}'.$$

The wave-function $\Psi_{E(JM)}$ for the state of total energy E, spin J and component M takes on the following form in the "channel" $c' \equiv (\alpha'\beta's'l')$:

$$\Psi_{E(JM)} = v'^{\frac{1}{2}}(I_{c'}(k'r) - U^{(J)}_{c',c'} O_{c'}(k'r))\varphi_{c'(JM)}, \tag{1}$$

where $\varphi_{c'(JM)}$ is the channel function consisting of the intrinsic wave-functions of α' and β' coupled together to channel spin s' and this coupled to the angular functions $i^{l'} Y^{(l')}_m / r$ to give total spin J. Further, v' is the velocity in the channel and is related to the bombarding energy ε' and wave-number k' by

$$\varepsilon' = \tfrac{1}{2} M' v'^2 = \frac{\hbar^2 k'^2}{2M'}, \tag{2}$$

where M' is the reduced mass; $I_{c'}$ and $O_{c'}$ in eq. (1) are the spherical Bessel functions of the separation r between α' and β' that have the asymptotic forms †

$$I_{c'}(k'r) \to e^{-i(k'r - \frac{1}{2}l'\pi)}, \qquad O_{c'}(k'r) \to e^{+i(k'r - \frac{1}{2}l'\pi)}. \tag{3}$$

Finally, $U^{(J)}_{c',c'}$ in eq. (1) is the diagonal element of the scattering matrix for total spin J. In the resonance region where the mean level width $\langle \Gamma_\lambda \rangle$ is less

† Here and below, we quote channel wave-functions for uncharged particles. The extension to charged particles is straightforward.

than the mean level spacing $\langle D \rangle$, this quantity has the form

$$U^{(J)}_{c',c'} = e^{-2i\phi_{c'}}\left(1+i\sum_{\lambda}\frac{\Gamma_{\lambda c'}}{E_\lambda - E - \frac{1}{2}i\Gamma_\lambda}\right), \tag{4}$$

where the level shift Δ_λ has been dropped as irrelevant to the present discussion. In eq. (4), $\phi_{c'}$ is the hard-sphere scattering phase angle ($= -k'R$ for s-wave neutrons), E_λ and Γ_λ are the energy and total width of the level λ and $\Gamma_{\lambda c'}$ is the partial width of the level λ for the channel c' which is given by squaring:

$$\Gamma^{\frac{1}{2}}_{\lambda c'} \equiv (2P_{c'})^{\frac{1}{2}}\gamma_{\lambda c'}. \tag{5}$$

Here, $P_{c'}$ is the usual penetration factor and $\gamma_{\lambda c'}$ is the reduced width amplitude given by

$$\gamma_{\lambda c'} \equiv \left(\frac{\hbar^2}{2M'R}\right)^{\frac{1}{2}}\int X_{\lambda(JM)}\varphi^*_{c'(JM)}\,dS. \tag{6}$$

In this last equation, R is the interaction radius, $X_{\lambda(JM)}$ the wave-function of the compound state, dS indicates integration over all co-ordinates except that of radial distance of separation of α' and β' which is fixed at the value R.

Inside the radial separation R, the wave-function $\Psi_{E(JM)}$ may be expanded in the following form if $\langle \Gamma_\lambda \rangle \ll \langle D \rangle$:

$$\Psi_{E(JM)} = -i\hbar^{\frac{1}{2}}e^{-i\phi_{c'}}\sum_{\lambda}\frac{\Gamma^{\frac{1}{2}}_{\lambda c'}X_{\lambda(JM)}}{E_\lambda - E - \frac{1}{2}i\Gamma_\lambda}. \tag{7}$$

The cross-section for radiative capture of α' by β' to form the final bound state $\Psi_{f(J_fM_f)}$ has the form

$$\sigma_{\alpha'\beta',\gamma f} = \frac{\pi}{k'^2}\sum_{J}\frac{2J+1}{(2i_{\alpha'}+1)(2i_{\beta'}+1)}\sum_{s',l'}|U^{(J)}_{\gamma f,c'}|^2, \tag{8}$$

where $U^{(J)}_{\gamma f,c'}$ is the scattering matrix element given by

$$U^{(J)}_{\gamma f,c'} = \left(\frac{16\pi}{9\hbar}\right)^{\frac{1}{2}}k_\gamma^{\frac{1}{2}}\frac{(\Psi_{f(J_f)}||\mathscr{H}^{(1)}||\Psi_{E(J)})}{(2J+1)^{\frac{1}{2}}}. \tag{9}$$

The reduced matrix element has been introduced in accordance with the usual definition

$$\left(\frac{2J_f+1}{2J+1}\right)^{\frac{1}{2}}\sum_{M+q=M_f}(JM1q|J_fM_f)\int\Psi^*_{f(J_fM_f)}\mathscr{H}_q^{(1)}\Psi_{E(JM)},$$

where the integration is over all co-ordinates, the summation is to be performed for fixed M_f and $\mathscr{H}_q^{(1)}$ is the dipole operator of component q, and k_γ is the photon wave-number corresponding to photon energy ε_γ.

Substituting eq. (7) in eq. (9), the contribution of the region $r < R$ to

$U^{(J)}_{\gamma t, c'}$ is

$$-ie^{i\phi_{c'}} \sum_{\lambda} \frac{\Gamma^{\frac{1}{2}}_{\lambda c'} \Gamma^{\frac{1}{2}}_{\lambda \gamma t}}{E_\lambda - E - \frac{1}{2} i \Gamma_\lambda}, \tag{10}$$

where we have defined the photon width by

$$\Gamma^{\frac{1}{2}}_{\lambda \gamma t} = \left(\frac{16\pi}{9}\right)^{\frac{1}{2}} k_\gamma^{\frac{3}{2}} \frac{(\Psi_{t(J_t)} || \mathscr{H}^{(1)} || X_{\lambda(J)})}{(2J+1)^{\frac{1}{2}}}, \tag{11}$$

the integration being confined to the interior region $r < R$.

Now we consider the channel contribution to the integral in (9). It can easily be seen from eq. (1) and the definition of the various quantities involved that the second term in eq. (4) gives rise to a term in $U_{\gamma t, c'}$ of the form (10) and that this can be naturally included in (10) by adding to each $\Gamma^{\frac{1}{2}}_{\lambda \gamma t}$ of eq. (11) a term $\delta\Gamma^{\frac{1}{2}}_{\lambda \gamma t}$. This addition is defined just as (11) except that the integral in the matrix element is now taken in the channel ($r > R$) and $X_{\lambda(JM)}$ is extended into the channel as an outgoing wave:

$$X_{\lambda(JM)} \to [X_{\lambda(JM)}(r = R)] \frac{RO_{c'}(k'r)}{rO_{c'}(k'R)}.$$

It is to be noticed that this addition to the photon width amplitude is a complex number in general, but is essentially real when $P \ll 1$. The remainder of the channel contribution, which comes from the first term in (4) can be written out explicitly. To do this, first notice that the final state wave-function takes on the following form in the channel $c_t = (\alpha' \beta' s_t l_t)$:

$$\Psi_{t(J_t M_t)} = \left(\frac{2}{R}\right)^{\frac{1}{2}} \theta_{tc_t} \varphi_{c_t(J_t M_t)} \left(\frac{O_{c_t}(k_t r)}{O_{c_t}(k_t R)}\right). \tag{12}$$

Here we have used the relation (6) applied to $\psi_{t(J_t M_t)}$ and have introduced the dimensionless reduced width amplitude θ_{tc_t} by the definition

$$\theta_{tc_t} = \gamma_{tc_t} \left(\frac{\hbar^2}{MR^2}\right)^{-\frac{1}{2}}. \tag{13}$$

The outgoing wave $O_{c_t}(k_t r)$ has the form of a decreasing exponential for a bound final state, k_t being the wave-number corresponding to the binding energy ε_t of α' and β' in this state. The final form for the total scattering matrix element (9) is now a sum of three parts, viz. a resonant part, which contains an interior contribution and a channel contribution, and a non-resonant part corresponding to the channel integral from hard sphere scattering. We will now drop the labels $c'\gamma f$ and (J) on U for economy of notation and assume them to be understood in future. We have the following equations:

$$U = U(\text{res.})+U(\text{hard sph.}),$$

$$U(\text{res.}) = U(\text{int. res.})+U(\text{ch. res.})$$

$$= -ie^{-i\phi_{c'}} \sum_{\lambda} \frac{\Gamma_{\lambda c'}^{\frac{1}{2}}(\Gamma_{\lambda\gamma t}^{\frac{1}{2}}+(\delta\Gamma_{\lambda\gamma t})^{\frac{1}{2}})}{E_\lambda - E - \frac{1}{2}i\Gamma_\lambda}, \tag{14}$$

$$U(\text{hard sph.}) = \left(\frac{16\pi}{9\hbar v'}\right)^{\frac{1}{2}} k_\gamma^{\frac{3}{2}} \sum_{c_t} \theta_{tc_t} \frac{(r\varphi_{c_t(J_t)}||H^{(1)}||r\varphi_{c'(J)})}{(2J+1)^{\frac{1}{2}}} 2ik' R^{\frac{1}{2}} e I_{\text{HS}}^{(l'l_t)}, \tag{15}$$

where $I_{\text{HS}}^{(l'l_t)}$ is the dimensionless single particle integral corresponding to hard sphere scattering:

$$I_{\text{HS}}^{(l'l_t)} = \frac{\sqrt{2}}{R^3 e} \int \frac{O_{c_t}(k_t r)}{O_{c_t}(k_t R)} h^{(1)} \psi_{\text{HS}}(r) r \, dr; \tag{16}$$

$\psi_{\text{HS}}(r)$ is the hard sphere wave-function for incident energy ε':

$$\psi_{HS} = \frac{1}{2k'r}(I_{c'} - e^{-2i\phi_{c'}} O_{c'}). \tag{17}$$

The dipole operator $\mathscr{H}_q^{(1)}$ has been split into the angle-intrinsic spin part $H_q^{(1)}$ and the radial part (of dimensions of charge times length) $h^{(1)}$:

$$\mathscr{H}_q^{(1)} = h^{(1)} H_q^{(1)}. \tag{18}$$

For E1 transitions,

$$h^{(1)}(r) = \tilde{e}r, \quad H_q^{(1)} = Y_q^{(1)}(\Omega),$$

where $\tilde{e}$ is effective charge ($-Ze/A$ for neutrons, Ne/A for protons). With a little Racah algebra it is easily shown that the reduced matrix element in (15) is

$$\frac{(r\varphi_{c_t(J_t)}||H^{(1)}||r\varphi_{c'(J)})}{(2J+1)^{\frac{1}{2}}} = \left(\frac{3}{8\pi}\right)^{\frac{1}{2}} (-)^{+\frac{1}{2}(l'-l_t-1)+J_t-J} \frac{(l'+l_t+1)^{\frac{1}{2}}}{(2l'+1)^{\frac{1}{2}}} U(1l_t Js', l' J_t)\delta_{s',s_t}. \tag{19}$$

For M1 transitions (spin part) we have

$$h^{(1)}(r) = \frac{e\hbar}{2Mc}, \quad H_0^{(1)} = \left(\frac{3}{4\pi}\right)^{\frac{1}{2}} \left(\frac{\mu_{\alpha'}}{i_{\alpha'}} I_0(\alpha') + \frac{\mu_{\beta'}}{i_{\beta'}} I_0(\beta')\right),$$

where $I_0(\alpha')$, $I_0(\beta')$ are the intrinsic angular momentum operators for particles α', β' and $\mu_{\alpha'}$, $\mu_{\beta'}$ are their magnetic moments in Bohr magnetons ($e\hbar/2Mc$). The reduced matrix element for M1 transitions is

$$\frac{(r\varphi_{c_t(J_t)}||H^{(1)}||r\varphi_{c'(J')})}{(2J+1)^{\frac{1}{2}}} = \left(\frac{3}{4\pi}\right)^{\frac{1}{2}} U(1s_t Jl', s' J_t)\delta_{l'l_t}$$

$$\times \left[U(1i_{\alpha'}s'i_{\beta'}i_{\alpha'}s_t)\mu_{\alpha'}\left(\frac{i_{\alpha'}+1}{i_{\alpha'}}\right)^{\frac{1}{2}} + U(1i_{\beta'}s'i_{\alpha'}, i_{\beta'}s_t)(-)^{s'-s_t}\mu_{\beta'}\left(\frac{i_{\beta'}+1}{i_{\beta'}}\right)^{\frac{1}{2}}\right]. \tag{20}$$

It is to be emphasised that equations (14) and (15) are of general validity. The sum over levels λ can be split into two parts, viz. the contribution U (local res.) from "local" levels near the energy E, and that from "far-away" levels U (dist. res.). The former give rise to observed resonances. Interpretation of the latter can only be made by assuming specific models. Before introducing such models, we will make general estimates of the relative importance of the hard sphere parts (15) and "local" level parts (14) of U.

2.2. RATIO OF CHANNEL RESONANT PART TO INTERIOR RESONANT PART FOR "LOCAL" LEVELS

We shall consider the ratio U(ch. local res.)/U(int. local res.) near the level λ where it equals $\delta\Gamma^{\frac{1}{2}}_{\gamma\lambda f}{}^{-}/\Gamma^{\frac{1}{2}}_{\lambda\gamma f}$. For E1 radiation, the value of $\Gamma_{\lambda\gamma f}$ averaged over f ($\bar{\Gamma}_{\lambda\gamma f}$, say) for levels λ near the neutron binding energy has been deduced by fitting the observed values of total radiation widths of these levels [6]):

$$\frac{\bar{\Gamma}_{\lambda\gamma f}}{\langle D\rangle} = 3.3\times 10^{-10} A^{\frac{2}{3}}(\varepsilon_\gamma/1\ \mathrm{MeV})^3, \tag{21}$$

where $\langle D\rangle$ is the mean spacing of levels λ (of given spin J). From its definition (13) above, one can deduce that

$$\delta\Gamma^{\frac{1}{2}}_{\lambda\gamma f} \approx \left(\frac{16\pi}{9}\right)^{\frac{1}{2}}\left(\frac{\varepsilon_\gamma}{\hbar c}\right)^{\frac{3}{2}}\left(\frac{2}{R}\right)\theta_{fc_f}\theta_{\lambda c'}\left(\frac{3}{4\pi}\right)^{\frac{1}{2}}\frac{\bar{e}R}{k_f}, \tag{22}$$

where we have used (12) and (16) and assumed that the main variation in the integrand comes from the attenuation of $O_{c_f}(k_f r)$ in distance k_f^{-1}.

If the "strong interaction" model applies to the interaction between the incident particle and target, the corresponding average value of $\theta^2_{\lambda c'}$ is given by

$$\frac{\langle\theta^2_{\lambda c'}\rangle_{\mathrm{sl}}}{\langle D\rangle} = \frac{1}{\pi KR}\left(\frac{MR^2}{\hbar^2}\right) = 0.0075\, A^{\frac{1}{3}}(\mathrm{MeV})^{-1}, \tag{23}$$

where K is a nuclear wave-number corresponding to the nuclear potential depth 42 MeV, and R is set equal to $1.4\, A^{\frac{1}{3}}\times 10^{-13}$ cm. Referring $\theta^2_{\lambda c'}$ to this standard, we find from (22), (21):

$$\left|\frac{U(\text{ch. local res})}{U(\text{int local res})}\right|^2 = \frac{\delta\Gamma_{\lambda\gamma f}}{\bar{\Gamma}_{\lambda\gamma f}} = 3.5\,\frac{\theta^2_{fc_f}}{\varepsilon_f(\mathrm{MeV})A^{\frac{1}{3}}}\,\frac{\theta^2_{\lambda c'}}{\langle\theta^2_{\lambda c'}\rangle_{\mathrm{sl}}}\left(\frac{\bar{e}}{e}\right)^2. \tag{24}$$

Thus, for neutron capture in a state of average neutron width, a final state bound by 5 MeV in a nucleus of mass $A \approx 200$, the contribution to the partial level width from the channel will be about 10 times that from the interior if $\theta^2_{fc_f} \approx 1$ i.e. if the final state is a fairly pure single particle state. This condition is met by low lying shell model states.

These results have important implications for the integration of experimental

data on capture spectra at resonances. It is clear that the presence of final states that can be reached by the emission of dipole radiation and which have $\theta^2_{lc_f} \approx 1$ will cause anomalies in the spectrum. Conventional compound nucleus theory predicts that the photon spectrum has the form $\varepsilon_\gamma{}^3\rho(E_f)$, where ρ is the level density of final states f and ε_γ is the photon energy $(E-E_f)$. Our estimates show that one may occasionally expect to find groups superposed on the usual spectrum towards the high photon energy end where level density is low.

Let us now invoke the ideas of the intermediate model in which it is assumed that each single particle state is shared out between the actual states of a nucleus in a restricted energy region (only 2 MeV or so for bound states). From our estimates, it follows that if only a few states "share" the single particle state, this should produce an anomalous "bump" in the usual spectrum $\varepsilon_\gamma{}^3\rho(E_f)$. If many more states are concerned in the sharing no anomaly is expected. Since many thousands of final states often contribute to the total capture width, it follows that the total capture cross section is usually essentially unaffected by the channel resonant component. Exceptions may occur in lighter nuclei and those near closed shells where the number of final states may be much lower.

So far we have considered a state λ of average neutron width. Most states have widths below average. (The most probable width is zero!) Thus, at a typical resonance, the anomalies in the spectrum will be considerably less pronounced than at the resonance of average width just discussed. At energies between resonances however, the nearby levels of large neutron width will contribute more to the capture than those of small width and one can expect the anomalies to be in accord width the above estimates.

2.3. RATIO OF CHANNEL RESONANT PART FOR "LOCAL" LEVELS TO THE NON-RESONANT PART

This ratio in the vicinity of a level λ is, from eqs. (1), (4),

$$\frac{U(\text{ch. hard sph.})}{U(\text{ch. local res.})} \approx \frac{E_\lambda - E - \frac{1}{2}i\Gamma_\lambda}{Rk_f\gamma^2_{\lambda c'}}.$$

Using (23) and (13), this gives

$$\frac{|U(\text{ch. hard sph.})|^2}{|U(\text{ch. local res.})|^2} \approx \frac{(E_\lambda - E)^2 + \frac{1}{4}\Gamma_\lambda{}^2}{D^2} \frac{420}{\varepsilon_f(\text{MeV})} \left(\frac{\langle\theta^2_{\lambda c'}\rangle_{\text{sl}}}{\theta^2_{\lambda c'}}\right)^2 \qquad (25)$$

Thus it appears that the non-resonant part of U may exceed in magnitude the local resonant channel part at energies between levels. In the vicinity of reonances the resonant channel part dominates. Favourable situations for the non-resonant part to dominate occur in regions where the levels have widths for the incident particle channel that are smaller than average. Since the distribu-

tion function of level widths has a maximum at the value zero, such regions may occur fairly commonly.

2.4. RATIO OF INTERIOR RESONANT PART FOR LOCAL LEVELS TO THE HARD SPHERE NON-RESONANT PART

From the above ratios (24) and (25),

$$\frac{|U(\text{ch. hard sph.})|^2}{|U(\text{int. local res})|^2} \approx \left(\frac{E_\lambda - E}{D}\right)^2 \frac{2\times 10^5 \theta^2_{lc_l}}{\varepsilon_l^2 A^{\frac{1}{3}}} \left(\frac{\bar{e}}{e}\right)^2 \frac{\langle \theta^2_{\lambda c'} \rangle_{sl}}{\theta^2_{\lambda c'}}.$$

Considering the previous example of a target of mass 200 whose resonance neutron widths equal the strong coupling average and a final state binding of 5 MeV, the ratio attains a maximum value of $\approx 50\,\theta^2_{lc_l}$ at a distance $\approx \frac{1}{2}D$ from resonance λ. If the nearby levels have small neutron widths (and we recall that the most probable value of such widths is zero), the ratio will be correspondingly larger. It thus follows that any anomalies that occur in the photon spectrum taken at a resonance will be often considerably enhanced relative to the usual $\varepsilon_\gamma^3 \rho(E_l)$ background if the energy is taken away from resonance.

3. Introduction of Models for the Evaluation of the Contribution to U from Far-Away Levels

So far we have considered only the "local" terms in the dispersion sum (14). Now we turn our attention to the distant levels. In order to specify their contribution, one must introduce a model of the gross features of the interaction between the incident particle and target particles.

3.1. STRONG INTERACTION MODEL

One such model is the extreme "strong interaction" model which implies that there is no approciable free motion of the incident particle inside the target. Instead the particle experiences collisions as soon as it enters the target. This model is usually represented quantitatively as follows:

(i) all matrix elements like $\Gamma^{\frac{1}{2}}_{\lambda c'}$, $\Gamma^{\frac{1}{2}}_{\lambda \gamma f}$ have random signs, and therefore, the contribution of distant levels to U(int. res.) in (14) is zero.

(ii) the strength function for the incident particle is constant with energy so that the distant levels contribute zero to (4) and zero to U(ch. res.) in (14).

Thus the "strong interaction" model implies that distant levels can be ignored entirely. It follows that the above discussion of the different parts of the scattering matrix element is already adequate for this case; in particular after the subtraction of effects of local levels, the capture is simply that resulting from hard sphere scattering (15).

3.2. INTERMEDIATE INTERACTION MODEL

According to current ideas [7]) on the interaction between an incident nucleon and a nucleus, this is not strong enough to invalidate the idea of single particle motion in the nucleus. Here we just give a brief summary of the quantitative expression of these ideas.Suppose that the average potential between α' and β' is $V(r)$ and that we define a set of states $u_{N''l''}(r)Y^{(l'')}(\Omega)$ in this potential normalised thus:

$$\int_0^\infty \left(u_{N''l''}(r)\right)^2 r^2 \mathrm{d}r = 1. \tag{27}$$

Coupling these to states of internal excitation of the pair α', β', we have a complete set $u_{N''l''}(r\varphi_{c''(JM)})$ in which we can expand any of the proper states X_λ:

$$X_{\lambda(JM)} = \sum a^\lambda_{N''c''} u_{N''l''}(r\varphi_{c''(JM)}), \tag{28}$$

where the coefficients satisfy the normalisation condition $\sum_\lambda |a^\lambda_{Nc}|^2 = 1$. The intermediate model says that, when c'' corresponds to the incident channel c' (with α', β' in their ground states), the coefficient $\langle |a^\lambda_{N'c'}|^2 \rangle$ averaged over states λ near the energy ε' shows a peak at the energy $\varepsilon_{N'l'}$ of the state $u_{N'l'}$. This is often expressed quantitatively in the form

$$\frac{\langle |a^\lambda_{N'c'}|^2 \rangle}{\langle D \rangle} = \frac{-\dfrac{W}{\pi}}{(\varepsilon_{N'l'} - \varepsilon')^2 + (W)^2}, \tag{29}$$

where W is the "absorption potential" and is negative. We use the particular form (29) in what follows but it is to be stressed that the final results do not depend on this as long as the distribution has width W and is peaked at $\varepsilon_{N'l'}$. It is assumed that, when ε' is some distance from $\varepsilon_{N'l'}$, then the distribution falls off sufficiently quickly so that the distributions for different levels N' are essentially non-overlapping. It follows that the reduced width amplitude of a level λ near particle level N' is, from (6), (28):

$$\gamma_{\lambda c'} = \left(\frac{\hbar^2 R'}{2M'}\right)^{\frac{1}{2}} a^\lambda_{N'c'} u_{N'}(R'). \tag{30}$$

where we drop the subscript l' from $N'l'$ for brevity of notation. Taking the projection $v'^{\frac{1}{2}}(\Psi_{E(JM)}|r\varphi_{c'(JM)}) = 2ik'\psi(r)$ (say), we have from (7) (which is a good approximation when $\langle \Gamma_\lambda \rangle \ll \langle D \rangle$, and so will be at the low inter-resonance energies of interest to us):

$$\psi(r) = -\tfrac{1}{2}\left(\frac{\hbar^4 P_{c'} R}{M'^2 k'}\right)^{\frac{1}{2}} \mathrm{e}^{-i\phi_{c'}} \sum_{N'} \sum_{\lambda(N')} \frac{|a^\lambda_{N'c'}|^2 u_{N'}(R) u_{N'}(r)}{E_\lambda - E - \frac{1}{2}i\Gamma_\lambda}, \tag{31}$$

where $\lambda(N')$ means a summation over levels λ occurring near the level N'. If one averages over a small energy interval at E containing many levels λ,

using (29) gives

$$\langle\psi(r)\rangle = -\tfrac{1}{2}e^{-i\phi_c}\left(\frac{\hbar^4 P_{c'}R}{M'^2k'}\right)^{\frac{1}{2}}\sum_{N'}\frac{u_{N'}(R)u_{N'}(r)}{\varepsilon_{N'}-\varepsilon'+iW}. \tag{32}$$

(There should be a term $\frac{1}{2}i\Gamma_{N'}$ in the denominator, where $\Gamma_{N'}$ is the single particle width. Since $\Gamma_{N'}$ is small at low energies and $\ll W$, we drop this term). This average wave-function of the incident particle inside the undisturbed target nucleus is precisely that for the real potential V augmented by an imaginary part iW which is constant inside $r = R$. (For any other specified radial dependence of W, this same result can be reproduced if the form (29) is chosen appropriately.) This result, as embodied in (32) is vital in the consideration of "direct" radiative capture averaged over levels. For our present purposes, however, we are interested in such capture at a sharp energy ε'. There are two essential differences between $\psi(r)$ and $\langle\psi(r)\rangle$ as given by (32). First, there is a contribution to ψ from nearby levels which fluctuates with energy. However, we always keep explicit reference to these levels in the theory of section 2; at present we are interested in the contribution from far away levels, and we therefore ignore the local ones. Second, the imaginary part of the last term of (32), which comes from averaging over resonances, does not occur in ψ. From (29), (31),

$$\psi(r) = -\tfrac{1}{2}e^{-i\phi_c}\left(\frac{\hbar^4 P_{c'}R}{M'^2k'}\right)^{\frac{1}{2}}\sum_{N'}u_{N'}(R)u_{N'}(r)\frac{(\varepsilon_{N'}-\varepsilon')}{(\varepsilon_{N'}-\varepsilon')^2+(W)^2}, \tag{33}$$

the contributions of nearby levels being ignored. It follows by comparison of (32), (33) that $e^{i\phi_c}\psi(r)$ is equal to the real part of $e^{i\phi_c}\langle\psi(r)\rangle$ where $\langle\psi(r)\rangle$ is the wave-function of the complex potential.

The form of ψ in the channel is, from its definition and (1),

$$\psi(r) = \frac{1}{2ik'r}(I_{c'}-\overline{U}_{c',c'}O_{c'}), \tag{34}$$

where $\overline{U}_{c',c'}$ differs from $U_{c',c'}$ in that the contribution of nearby levels in (4) has been dropped. Taking the average of (34) over resonances and equating to (32) at $r = R$, one finds

$$\langle\overline{U}_{c',c'}\rangle = e^{2i\phi_c}\left(1+i\sum_{N'}\frac{\Gamma_{N'}}{\varepsilon_{N'}-\varepsilon'+iW}\right), \tag{35}$$

which is the scattering matrix element for the complex potential $(V+iW)$ as expected. At a sharp energy E, by joining (34) to (33) at $r = R$,

$$\overline{U}_{c',c'} = e^{-2i\phi_c}\left(1+i\sum_{N'}\frac{\Gamma_{N'}(\varepsilon_{N'}-\varepsilon')}{(\varepsilon_{N'}-\varepsilon')^2+W^2}\right). \tag{36}$$

The difference from (35) is that the summation term is the real part of that in (35). Eq. (35) corresponds to absorption of particles since $|\langle \bar{U}_{c'c'} \rangle| \neq 1$, but (36) corresponds to no absorption since $|\bar{U}_{c'c'}| \approx 1$. (The approximation sign only reflects the approximate nature of (36) which assumes $\langle \Gamma \rangle \ll D$. We could use a more exact form, then $|\bar{U}_{c'c'}|$ would equal 1 exactly). Inserting (35) and (36) separately into (34), we find that the above result that $\psi(r)$ equals the real part of $\langle \psi(r) \rangle$ holds in the channel region $r > R$ as well as $r < R$. (We have dropped the phase factors $e^{i\phi_{c'}}$ since $\phi_{c'}$ is very small at low energies). Thus, if the wave-function for the complex potential $V+iW$ is ψ_{V+iW} we have

$$\psi = \mathrm{Re}(\psi_{V+iW}). \tag{37}$$

Having seen how the far-away terms in the dispersion sum describe the motion of the incident particle in the nucleus, we can now take the previous equation

$$U = U(\text{res.}) + U(\text{hard sph.}), \tag{38}$$

divide U(res.) into local and distant terms:

$$U(\text{res.}) = U(\text{res. local}) + U(\text{res. dist.})$$

and incorporate the latter with U(hard sph.) to obtain the contribution from potential scattering:

$$U(\text{pot.}) = U(\text{hard sph.}) + U(\text{res. dist.}). \tag{39}$$

Thus, to summarise, the scattering matrix element is now the sum of a local resonance part and a potential part:

$$U = U(\text{res. local}) + U(\text{pot.}) \tag{40}$$

where the former is given by the local terms of (14) and the latter is given by expression (15) with the integral I_{HS} for hard sphere scattering replaced by

$$I_{\mathrm{HS}} \to \frac{1}{eR^{\frac{1}{2}}\theta_N} \int_0^\infty u_N(r) h^{(1)} \,\mathrm{Re}\,(\psi_{V+iW}) r^2 \mathrm{d}r. \tag{41}$$

We have introduced the dimensionless reduced width amplitude

$$\theta_N = (\tfrac{1}{2}R^3)^{\frac{1}{2}} u_N(r). \tag{42}$$

Since $u_N(r)$ and $h^{(1)}$ are real, we may write (41) as $\mathrm{Re}(I_{V+iW})$ where I_{V+iW} is the dimensionless integral corresponding to capture in the potential $V+iW$:

$$I_{V+iW} = \frac{1}{eR^{\frac{1}{2}}\theta_N} \int u_N^{(\mathrm{f})}(r) h^{(1)} \psi_{V+iW} \, r^2 \mathrm{d}r. \tag{43}$$

The superscript (f) on u_N denotes that, in the region $r > a'$, $u_N^{(\mathrm{f})}$ has the form of a decreasing exponential corresponding to the binding energy ε_t rather than the "natural" binding energy ε_N of the state N.

Finally it should be stressed that this derivation does not depend on the particular form (29). For any given absorption function $W(r)$, there is a corresponding form (29) and, if this is used, all the above results hold with ψ_{V+iW} as the solution for the potential $V+iW(r)$.

M1 *Transition* (spin part only), $h^{(1)} = e\hbar/2Mc$.

Since two radial solutions of the same l value in the same potential are orthogonal, (43) vanishes in first approximation for M1 transitions. There are non-zero correction terms from three sources:

(i) if a spin-orbit term occurs in the potential, the matrix element (43) will be non-zero for transitions $j = l+\frac{1}{2} \leftrightarrow j = l-\frac{1}{2}$. However, this correction is small and does not occur when $l = 0$;

(ii) the fact that $u_N^{(l)}$ occurring in (43) is not the same as u_N in the region $r > a$ means that there is a small non-zero correction to (43):

$$\mathrm{Re}\left(\frac{\hbar}{2Mc}\right)\frac{\sqrt{2}}{R^3}(\varepsilon_l-\varepsilon_N)\frac{\mathrm{d}}{\mathrm{d}\varepsilon_l}\int_R^\infty \frac{O(k_l r)}{O(k_l R)}\psi_{V+iW}\, r\,\mathrm{d}r; \tag{44}$$

(iii) Since u_N and ψ belong to potentials V and $V+iW$, u_N and ψ are not exactly orthogonal. The correction to (43) is easily shown to be

$$\mathrm{Re}\frac{iW\left(\frac{\hbar}{2Mc}\right)\frac{1}{\theta_N R^{\frac{1}{2}}}}{(\varepsilon'-\varepsilon_N)(\varepsilon'-\varepsilon_N-iW)}\frac{\hbar^2}{2M}\left(r\psi\frac{\mathrm{d}(u_N r)}{\mathrm{d}r}-u_N\frac{\mathrm{d}(\psi r)}{\mathrm{d}r}\right)_{r=R};$$

$u_N(R)$ can be obtained from (42). For s-wave neutrons we have from (32)

$$\psi(R) = \frac{\sum_{N'}\gamma_{N'}^2}{\varepsilon_{N'}-\varepsilon'+iW} = \frac{\bar{R}}{R}-1-i\pi s, \quad \left(\frac{\mathrm{d}}{\mathrm{d}r}(r\psi)\right)_{r=R} = -1, \tag{45}$$

where $\bar{R}$ is the average scattering length and s the strength function. For the slope of u_N at $r = R$,

$$\frac{\partial(ru_N)}{\partial r} = -k_N(ru_N),$$

where k_N is given by $\varepsilon_N = \hbar^2 k_N^2/2M$. The correction to (43) is thus

$$\frac{\hbar}{2Mc}\frac{\hbar^2\sqrt{2}}{2MR^3}\frac{W^2[(R-\bar{R})k_l-1]+W(\varepsilon'-\varepsilon_N)\pi sRk_N}{(\varepsilon'-\varepsilon_N)[(\varepsilon'-\varepsilon_N)^2+W^2]}. \tag{46}$$

Since $\pi s k_N R \approx 1$ and $\{(R-\bar{R})k_l-1\} \approx 1$, and in most cases $(\varepsilon'-\varepsilon_N)^2 \gg W^2$, $|\varepsilon'-\varepsilon_N| \gg \hbar^2/MR^2$, this is considerably less than the standard single particle value $\hbar/2McR$ obtained from (43) by setting $r\,u_N(r) = 1/R^{\frac{1}{2}}$ and $r\psi = R$.

For low energy neutrons, the integral I_{HS} in the hard sphere term (15) is $2ik'/k_l^2$. Thus the ratio of potential to hard sphere terms is, using (46);

$$\frac{U(\text{pot. M1})}{U(\text{hard sph. M1})} \approx \frac{W}{(\varepsilon_N)}. \tag{47}$$

For a binding energy ε_N of 5 MeV and $W \approx 2$ MeV this is ≈ 0.4. The smallness of U(pot. M1) may mean that this anomalous component in the spectrum of M1 radiation is in practice not discernible from the spectrum due to nearby resonances.

E1 *Transitions*, $h^{(1)} = \tilde{\varepsilon} r$.

For a realistic well shape with diffuse edge, the integral (43) cannot be evaluated analytically, but only numerically and this requires considerable labour. For the case of the square well V analytical evaluation can be made, both when the absorption W is concentrated at the surface $r = R$, and also when it is uniform inside $r = R$. For the square well one can proceed directly to the analytical formula from (43). It is, however, instructive first to transform the integral (43) to alternative form, and then to specialise to the square well. We give details of the transformation in the Appendix. Here we quote the results for the case of primary interest, capture from low energy s-wave incident neutrons ($\varepsilon' \approx 0$, $l' = 0$) to a bound p-wave orbit ($l = 1$)

Surface Absorption. Let us first define the positive dimensionless quantities $v(r)$, $w(r)$ by

$$v(r) = -V(r) \Big/ \frac{\hbar^2}{MR^2}, \qquad w(r) = -W(r) \Big/ \frac{\hbar^2}{MR^2} \tag{48}$$

and drop all labels on quantities in (43). For definiteness, for a general well-shape, R can be taken as the mid-point of the potential. Let us suppose that W is centred near the surface by assigning to it the form

$$W(r) = -\frac{W_0 R^2}{V_0}\left(\frac{1}{r}\frac{\partial V}{\partial r}\right), \tag{49}$$

where V_0 is the value of V in the centre of the nucleus. We may also define v_0 and w_0 and a new dimensionless quantity y:

$$v_0 = -V_0 \Big/ \frac{\hbar^2}{MR^2}, \qquad w_0 = -W_0 \Big/ \frac{\hbar^2}{MR^2}, \qquad y = k_{N1} R. \tag{50}$$

The integral (43) can be written as (see Appendix)

$$\int_0^\infty u\psi\, r^3 \mathrm{d}r = \frac{4R^2}{y^4}\left(\frac{iw_0 y^2}{2v_0} - 1\right)\int_0^\infty u\psi \frac{\partial v}{\partial r} r^2 \mathrm{d}r - \frac{4R^4 i w_0}{v_0 y^4}\left[\int_0^\infty \frac{\partial u}{\partial r}\frac{\partial v}{\partial r}\psi r\, \mathrm{d}r + 2\int_0^\infty u\psi \frac{\partial v}{\partial r}\, \mathrm{d}r\right]. \tag{51}$$

(Notice that we have dropped all subscripts on the wave-functions; in future they will be understood).

This applies to general well shape $v(r)$. In the case of a square well $\partial v/\partial r = -v_0\delta(r-R)$, and we have, therefore,

$$\int_0^\infty u\psi r^3\,\mathrm{d}r = 4\psi(R)u(R)\frac{R^4}{y^4}\left[v_0 - iw_0\left\{\tfrac{1}{2}y^2 - 2 - \left(\frac{r}{u}\frac{\partial u}{\partial r}\right)_R\right\}\right]. \tag{52}$$

For a state like u with $l = 1$ we have

$$\left(\frac{r}{ru}\frac{\partial(ru)}{\partial r}\right)_R = -\frac{y^2+y+1}{y+1}. \tag{53}$$

For a square well, $\psi(R)$ is given by

$$\psi(R) = \frac{\bar{R}}{R} - 1 - i\pi s = -\frac{\tan(p+iq)}{p+iq}, \tag{54}$$

where $p = \sqrt{(2v_0)}$, $q = \sqrt{(w_0^2/2v_0)}$. From (52), it follows that

$$\int_0^\infty u\psi r^3\,\mathrm{d}r = -\frac{2(2R^5)^{\frac{1}{2}}\theta_N p}{y^4}\frac{\tan(p+iq)}{p+iq}\left[p - iqy^2\frac{y+3}{y+1}\right], \tag{55}$$

$$\mathrm{Re}\int_0^\infty u\psi r^3\,\mathrm{d}r = -\frac{2(2R^5)^{\frac{1}{2}}\theta_N p}{y^4}\frac{p(p\sin 2p + q\sinh 2q) + qy^2\dfrac{y+3}{y+1}(p\sinh 2q - q\sin 2p)}{(p^2+q^2)(\cos 2p + \cosh 2q)}.$$

Anomalies are observed in the slow neutron capture spectrum near mass $A \approx 190$ and they are associated with the 3p state which is bound by about 5 MeV. The 3p state of the square well of depth 42 MeV is bound by this amount if $R = 7.26\times10^{-13}$ cm. With this choice, $y = 3.55$, $\hbar^2/MR^2 = 0.785$ MeV, and $v_0 = 53.5$, $p = 10.34$. If W_0 is chosen to be -2 MeV, then $w_0 = 2.52$, $q = 0.21$. Inserting these values in (54), (55), (43) we get

$$\begin{aligned}\psi(R) &= -\tfrac{1}{89}(10.1+4.1\,i),\\ \mathrm{Re}\int u\psi r^3\,\mathrm{d}r &= -0.18\,(2R^5)^{\frac{1}{2}}\theta_{Nl},\\ \mathrm{Re}\,I_{V+iW} &= -\sqrt{2}\left(\frac{\bar{e}}{e}\right)0.18.\end{aligned} \tag{56}$$

One can compare these values with that in the case when ψ corresponds to hard sphere scattering:

$$r\psi_{HS} = -r+R,$$

$$\int u\psi_{HS} r^3 \mathrm{d}r = -(2R^5)^{\frac{1}{2}}\theta_N \frac{1}{y^2}\frac{y+3}{y+1} = -0.11(2R^5)^{\frac{1}{2}}\theta_N, \tag{57}$$

$$\mathrm{Re}\, I_{HS} = -\sqrt{2}\left(\frac{\bar{e}}{e}\right)\frac{1}{y^2}\frac{y+3}{y+1} = -\sqrt{2}\left(\frac{\bar{e}}{e}\right)0.11.$$

Volume Absorption. If W is assumed to be uniformly distributed inside the radius R and zero outside, we have

$$\int u\psi r^3 \mathrm{d}r = -\frac{4R^2}{y^4}\int u\psi \frac{\partial v}{\partial r} r^2 \mathrm{d}r - \frac{16\, iwR^2}{y^4}\frac{(y^2+iw)}{(y^2+2iw)^2}\left[-\int u\psi \frac{\partial v}{\partial r} r^2 \mathrm{d}r\right.$$
$$\left. +\tfrac{1}{2}R^2\left\{\frac{\partial(ru)}{\partial r}\frac{\partial(r\psi)}{\partial r} + u\psi + \frac{u\partial(r\psi)}{\partial r} - \psi\frac{\partial(ru)}{\partial r} - r\psi\frac{\partial^2(ru)}{\partial r^2}\right\}_R\right] \tag{58}$$
$$+\frac{2iwR^4 u(R)}{y^4}\psi(R)\frac{y^2}{y^2+2iw}\left[-1+\frac{r}{r\psi}\frac{\partial(r\psi)}{\partial r} - \frac{r}{ru}\frac{\partial(ru)}{\partial r}\right]_R.$$

This can be applied to any well shape v. If the square shape is used, we may use the following relations:

$$\frac{\partial^2(ru)}{\partial r^2} = \frac{2M}{\hbar^2}\left(-\varepsilon_N + \frac{2}{r^2}\frac{\hbar^2}{2M} + V\right)ru, \qquad \frac{\partial(r\psi)}{\partial r} = -1, \tag{59}$$

along with (53) to show that

$$\mathrm{Re}\int u\psi r^3 \mathrm{d}r = \frac{2\theta_{Nl}(2R^5)^{\frac{1}{2}}}{y^4(y^2+2iw)^2}\left\{-iwy^4\frac{5+y}{1+y} + iwy^5\psi(R)\frac{4+y}{1+y}\right.$$
$$\left. +2w^2y^2\frac{3+y}{1+y} - 2w^2\psi(R)y^3\frac{2+y}{1+y} + 2y^4\psi(R)v\right\}. \tag{60}$$

(One can evaluate (58) either just inside or just outside $r = R$. The contribution from the integrals in (58) in the latter case is reproduced by the last term in (59) in the former.) Using form (54) for $\psi(R)$ and the same numerical values as in the above example one finds

$$\mathrm{Re}\int u\psi r^3 \mathrm{d}r = -0.15(2R^5)^{\frac{1}{2}}\theta_N, \qquad \mathrm{Re}\, I_{V+iW} = -0.15\sqrt{2}\left(\frac{\bar{e}}{e}\right), \tag{61}$$

which is quite close to the above value (56) obtained with the surface absorption.

No absorption. In the case when there is no absorption, from either (51) or (58) we get

$$\mathrm{Re}\int u\psi r^3 \mathrm{d}r = -\frac{4R^2}{y^4}\int u\psi \frac{\partial v}{\partial r} r^2 \mathrm{d}r. \tag{62}$$

In the case of a square well, from (52) or (60),

$$\mathrm{Re}\int u\psi r^3\,\mathrm{d}r = -2\theta_N(2R^5)^{\frac{1}{2}}\frac{p\tan p}{y^4}. \tag{63}$$

This gives $-0.17\,\theta_N(2R^5)^{\frac{1}{2}}$ in the numerical example.

Although the above numerical results for a square well may give a correct idea of the order of magnitude of the integrals I, they cannot be attributed any quantitative significance. The actual nuclear potential is not square but rounded. It is important to notice that the square well which we have used above gives the correct p-wave properties of nuclei $A \approx 190$, but quite the wrong s-wave properties. (The value of the argument $p = 10.34$, which is less than the value $\frac{7}{2}\pi$ which corresponds to the well-known s-wave state at zero energy near $A \approx 160$. Thus the s-wave properties implied by our square well correspond to mass ≈ 140). It is clear that realistic detailed estimates of I can be obtained only when a diffuse potential V is used.

Finally we notice that we have implicitly assumed that the potential V is velocity independent. In practice it is not, but there is no obvious reason why velocity dependence should seriously affect the values of the dipole integrals, and we therefore ignore this complication. (For the square well case, it is straightforward to modify the above expressions to include velocity dependence, but this leads to even more cumbersome formulae.)

3.3. CLOSED EXPRESSIONS FOR POTENTIAL CAPTURE CROSS SECTIONS

In observed cross-sections there is generally interference between the resonance and non-resonant (potential) capture. If the cross-section is integrated through resonance, the interference terms are removed to a good approximation, and the cross-section for the potential capture can be extracted by subtracting off the resonant part. It is of some interest therefore to give formulae for the potential capture alone.

E1 *Radiation.*

Inserting (15) in (8) and using formula (19) which applies to the case of E1 radiation, we find, for either hard sphere or potential capture,

$$\sigma_{\alpha'\beta',\gamma t} = \tfrac{8}{3}\pi e^2\frac{R^5}{\hbar v'}k_\gamma{}^3\sum_{l'l_t s}\frac{(2J_t+1)(l_t+l'+1)}{(2l_t+1)(2i_{\alpha'}+1)(2i_{\beta'}+1)}\theta_{tc_t}|I^{(l'l_t)}|^2, \tag{64}$$

after a little Racah algebra has been used.

The potential cross-section is given only roughly by this formula when a spin orbit force acts on the incident particle because the integrals I will then depend on J. For incident s-waves, the case of primary interest, this does not apply, and the formula (64) is correct.

Let us now accept the "intermediate model" and assume that a single particle orbit Nl_t is shared by states f in a limited energy region. If the region is first assumed to be so small ($\ll$ MeV) so that the various energy-dependent factors in (64) do not vary appreciably across it, then we may first sum over all states f for given J_t, s using

$$\sum_{f(J_t s)} \theta_{fc}^2 = \theta_N{}^2 \tag{65}$$

and then we may sum over J_t for fixed l_t, s, $\mathbf{J}_t = \mathbf{l}_t + \mathbf{s}$, and finally over s:

$$\sum \sigma_{\alpha'\beta',\gamma N} = \tfrac{8}{3}\pi e^2 \frac{R^5}{\hbar v'} k_\gamma{}^3 \sum (l_t + l' + 1)|\theta_N I^{(l' l_t)}|^2. \tag{66}$$

In practice however the factors k_γ and $I^{(l' l_t)}$ do vary appreciably across the width $2W_N$ of the state N, which may be ≈ 2 MeV. For this case consider the cross-section to all states f in a given small interval Δ. At binding energy ε, we may assume that, for given J_t, s,

$$\sum_{f(J_t s) \text{ in } \Delta} \theta_{fc}^2 = \Delta f(\varepsilon)\theta_N{}^2, \tag{67}$$

where $f(\varepsilon)$ is independent of J_t, s, satisfies

$$\int f(\varepsilon)\mathrm{d}\varepsilon = 1 \tag{68}$$

and has the form of a peak of width $2W_N$ centred at $\varepsilon = \varepsilon_N$, for instance (see (29))

$$\mathrm{f}(\varepsilon) = \frac{\dfrac{W}{\pi}}{(\varepsilon - \varepsilon_N)^2 + W^2}. \tag{69}$$

The cross-section to all states in the interval Δ is then

$$\sum_{f \text{ in } \Delta} \sigma_{\alpha'\beta',\gamma f} = \Delta \tfrac{8}{3}\pi e^2 \frac{R^5}{\hbar v'} f(\varepsilon_\gamma) k_\gamma{}^3 \sum (l_t + l' + 1)|\theta_N I^{(l' l_t)}|^2. \tag{70}$$

So far we have not allowed for the fact that the final state is usually split into spin orbit components $\mathbf{j} = \mathbf{l}_t + \mathbf{i}_{\alpha'}$. The appropriate modification of (66), (70) for radiation to just one j-component is obtained by multiplying by $2j+1/(2l+1)(2i_{\alpha'}+1)$.

M1 *Radiation.*

From (20), (15) and (8), the hard sphere or potential capture cross-section for M1 radiation is given, after carrying out the sums over J, s', by

$$\sigma_{\alpha'\beta',\gamma f}=\frac{16\pi R^5}{3\hbar v}k_\gamma{}^3e^2\sum_{s_f l'}\theta^2_{ic_f}|I^{(l'l')}|^2\frac{2J_f+1}{(2i_{\alpha'}+1)(2i_{\beta'}+1)}$$
$$\times\left[(\mu^2_{\alpha'})\left(\frac{i_{\alpha'}+1}{i_{\beta'}}\right)+(\mu^2_{\beta'})\left(\frac{i_{\beta'}+1}{i_{\beta'}}\right)+2\mu_{\alpha'}\mu_{\beta'}\sqrt{\left(\frac{i_{\alpha'}+1}{i_{\alpha'}}\right)\left(\frac{i_{\beta'}+1}{i_{\beta'}}\right)}\right. \quad (71)$$
$$\left.\times U(li_{\alpha'}i_{\beta'}s_f,i_{\alpha'}i_\beta)\right].$$

If this cross section is summed in a small energy interval Δ over the final states f that share a given particle state N, one finds, corresponding to (70),

$$\sum_{f\text{ in }\Delta}\sigma_{\alpha'\beta',\gamma f}=\Delta\frac{16\pi R^5}{3\hbar v}f(\varepsilon)k_\gamma{}^3e^2\sum_{l'}(2l'+1)|I^{(l'l')}0_N|^2\left\{\mu^2_{\alpha'}\left(\frac{i_{\alpha'}+1}{i_{\alpha'}}\right)+\mu^2_{\beta'}\left(\frac{i_{\beta'}+1}{i_{\beta'}}\right)\right\}. \quad (72)$$

4. The Contribution to U from Local Levels

We have now seen that we can extract channel elements from U which depend for their importance on the strength of single particle p-wave configurations in the final states. There still remains the possibility that the resonance (internal) capture may also depend appreciably on the nature of the final state. A hint of this comes from Cameron's claim [8]) that values of resonance total radiation widths depend on the proximity of s- and p-wave single-particle states.

Let us write the E1 matrix element between initial (resonance) state X_λ and final (bound) state ψ_f as $(f|\mathscr{H}|\lambda)$. If we neglect the $\varepsilon_\gamma{}^3$ factor for the moment, the total width will involve the quantity

$$Q=\sum_{\text{f (bound)}}|(f|\mathscr{H}|\lambda)|^2. \quad (73)$$

Now let us expand states f in terms of product states $\phi_{c'}u_{N'}$ where $\phi_{c'}$ are states of the target nucleus and $u_{N'}$ are single-particle states of the incident particle:

$$\psi_f=\sum_{c'N'}(f|c'N')\phi_{c'}u_{N'}; \quad (74)$$

then

$$Q=\sum_{cN,\,c'N'}(cN|\mathscr{H}|\lambda)(c'N'|\mathscr{H}|\lambda)\{\sum_{\text{f (bound)}}(f|cN)(f|c'N')\}. \quad (75)$$

According to the intermediate model [7]), for any given state cN, the coefficients $(f|cN)$ are appreciable for states f in a small energy range ($\approx$ 1 MeV) about the energy E_{cN}. It follows that the quantity Q is approximately given by

$$Q\approx\sum_{c'N'\text{ (bound)}}|(c'N'|\mathscr{H}|\lambda)|^2. \quad (76)$$

The operator $\mathscr{H}$ contains a part operating on the target particles ("core transitions") and a part operating on the incident particle ("particle transi-

tions"). We shall neglect the "core transitions" (the arguments given previously [1]) may provide partial justification for this). Since for given λ, c', the coefficients $(\lambda|c'N)$ are appreciable for only one particle state N, one can now write

$$Q \approx \sum_{c'N',\, N \text{ bound}} (\lambda|c'N)^2 |(N|\mathscr{H}|N')|^2. \tag{77}$$

Since the density of states c' increases strongly with excitation energy, the largest contribution to Q arises when N and N' are most strongly bound. It follows that the evaluation of this contribution depends critically on the excitation energy at which the summation over c is cut-off. (The same objection already applies to eq. (76)). The nature of this cut-off depends on the distribution function for the quantities $(f|c'N)^2$. Furthermore in the expression for the actual total radiation width the effective upper limit on states μ is not zero energy, but a negative energy, as a result of the E_γ^3 factor. This means that one cannot use the present considerations to make sensible predictions of the total radiation width.

However one may still enquire if single particle effects cause deviations from the predictions of statistical theory by proceeding as follows. Let us suppose that a low-lying bound state is approximately a pure state of the form $\psi_f \equiv \varphi_0 u_N$, so that the E1 matrix element between this state and the initial state λ is

$$(0N|\mathscr{H}|\lambda) = \sum_{c'N'} (0N|\mathscr{H}|c'N')(c'N'|\lambda) = \sum_{N'} (N|\mathscr{H}|N')(0N'|\lambda), \tag{78}$$

where we have again dropped terms corresponding to core transitions. Using the fact that, for given λ, $(0N'|\lambda)$ is appreciable for only one N', it follows that the partial width $\Gamma_{\lambda\gamma f}$ is given by

$$\Gamma_{\lambda\gamma f} = \Gamma_{N'\gamma N}(0N'|\lambda)^2 = \Gamma_{N'\gamma N}\left(\frac{\gamma_{\lambda c'}^2}{\langle\gamma_{\lambda c'}^2\rangle_{\mathrm{sl}}}\right)\left(\frac{\langle\gamma_{\lambda c'}^2\rangle_{\mathrm{sl}}}{\gamma_p{}^2}\right), \tag{79}$$

where $\Gamma_{N'\gamma N}$ is the single-particle radiation width, $\gamma_p{}^2$ is the single-particle reduced width $\hbar^2/MR^2$, $\gamma_{\lambda c'}^2$ is the reduced width of level λ, $\langle\gamma_{\lambda c'}^2\rangle_{\mathrm{sl}}$ is the average width of the "strong interaction" model given by

$$\frac{\langle\gamma_{\lambda c'}^2\rangle_{\mathrm{sl}}}{D} = \frac{1}{\pi KR}, \tag{80}$$

K being the wave-number of a nucleon of energy of about 42 MeV. If we estimate the single particle matrix element $\langle r\rangle$ by $\frac{3}{4}R$ (which follows if one assumes uniform radial wave functions), then

$$\Gamma_{N'\gamma N} \approx \tfrac{3}{8}e^2R^2\left(\frac{\varepsilon_\gamma}{\hbar c}\right)^3. \tag{81}$$

From eqs. (79), (80), (81), inserting some numerical values,

$$\Gamma_{\lambda\gamma f}(\text{meV}) \approx 0.25\times 10^{-6}[\varepsilon_\gamma(\text{MeV})]^3 A \left(\frac{\gamma^2_{\lambda c'}}{\langle\gamma_{\lambda c'}\rangle_{\text{SI}}}\right) D(\text{eV}). \tag{82}$$

This is to be compared with Cameron's formula [6]) deduced from fitting total radiation widths on the assumption that no single particle effects occur:

$$\Gamma_{\lambda\gamma f}(\text{meV}) \approx 3.3\times 10^{-7}[\varepsilon_\gamma(\text{MeV})]^3 A^{\frac{2}{3}} D(\text{eV}). \tag{83}$$

It can be seen that eq. (82) is larger than this standard by a factor of $0.8\ A^{\frac{1}{3}}\gamma^2_{\lambda c'}/\langle\gamma^2_{\lambda c'}\rangle_{\text{SI}}$ or about 4 for a level near $A \approx 180$ with roughly the average neutron width. It must be remembered that eq. (81) may be an incorrect estimate of the actual single particle width. Nevertheless it seems quite possible that transitions from strong resonances to final states of appreciable single-particle character may be enhanced above the usual statistical value.

It is of interest in connection with this point to make an interpretation of the imaginary part of the E1 matrix element for neutrons scattered by a complex potential. We have, from (14) and substituting (79),

$$U(\text{res.}) = -ie^{-i\phi_{c'}}(2P_{c'})^{\frac{1}{2}}\left(\frac{\hbar^2 R}{2M}\right)^{\frac{1}{2}} \sum_{N'} \Gamma_{N'\gamma N} u_{N'0}(R) \sum_\lambda \frac{(0N'|\lambda)^2}{E_\lambda - E - \frac{1}{2}i\Gamma_\lambda}. \tag{84}$$

This is similar, in its summation over N' and λ, to eq. (31), the factor $u_N(r)$ in the latter being included in the radial integral implicit in $\Gamma_{N'\gamma N}$. Averaging over a small energy interval at E containing many levels λ, results, as explained in connection with (32), in an E1 matrix calculated for the complex potential appropriate to the form taken for the neutron strength function. On dropping the factor $ie^{-i\phi_{c'}}$ the real part of this matrix element describes the potential capture. The imaginary part may be calculated directly from (14) without making the substitution (79), giving as its contribution to the capture cross section $\sigma_{\text{CP},\gamma}$ of neutrons scattered by a complex potential well

$$\sigma_{\text{CP},\gamma} - \sigma_{\text{POT},\gamma} = \pi^3 \lambda\!\!\!^{-2} \frac{\langle\Gamma_{\lambda c'}\rangle}{\langle D\rangle} \frac{\langle\Gamma_{\lambda\gamma f}\rangle}{\langle D\rangle}. \tag{85}$$

This relationship enables one to use the results of a computation of capture in such a well to evaluate the partial radiation width for a transition from a given resonance to a single-particle p-wave state.

5. Conclusions

It has been shown in this paper that, starting from nuclear dispersion theory, a formalism can be derived for the analysis of capture cross sections at energies in the resonance region. Such cross sections may include not only the effects of

capture through local resonances but also "direct" or "potential" capture with which resonances may interfere. Numerical estimates show that the potential capture, which tends to select final single-particle states in the radiative transition, may be of importance or even predominate in certain situations. Further estimates show that even the resonance contribution to capture leaving the final nucleus in a relatively pure single-particle state may be enhanced. This is particularly so if the resonance concerned has a large reduced neutron width. Such enhanced resonance capture contains a contribution to the matrix element from the channel region. This contribution is unimportant if the final state is not of an appropriate single-particle character.

Although some methods for the calculation of these effects have been presented in this paper we have not made any serious attempts at numerical calculation other than order of magnitude estimates. This will be done in the following paper where we attempt to analyse the available experimental data from neutron capture reactions [9]).

Appendix. The Transformation of Electric Dipole Integrals

In general, the integrand in the integral

$$\int_0^\infty u\psi r^3 \,\mathrm{d}r \tag{A1}$$

has appreciable values out to values of $r \gg R$. This integrand varies in sign and cancellations occur, especially in the region $r < R$ where u and ψ may have many nodes. For this reason, it is wrong, in general, to neglect the contribution to the integral from $r > R$. Because it is composed of fluctuating contributions from a large range of r, in order to discuss the magnitude of (A1) and make estimates it is desirable to transform it in such a way that this range is reduced and the fluctuations eliminated.

Let us first include the angular wave-functions Y_l, $Y_{l'}$ with u, ψ and consider

$$\int (uY_l)(\psi Y_{l'}) z \,\mathrm{d}\tau, \tag{A2}$$

where the integration is a volume one over all space $\mathrm{d}\tau = \mathrm{d}x\,\mathrm{d}y\,\mathrm{d}z$. Assuming that the potential is velocity independent,

$$Hz - zH = -\frac{\hbar^2}{m}\frac{\partial}{\partial z},$$

and then

$$(\varepsilon' - \varepsilon_N)\int (uY_l)\psi Y_{l'} z \,\mathrm{d}\tau = -\frac{\hbar^2}{m}\int (\psi Y_{l'})\frac{\partial}{\partial z}(uY_l)\mathrm{d}\tau + \int iW(uY_l)(\psi Y_{l'}) z \,\mathrm{d}\tau. \tag{A3}$$

From $(\partial/\partial zH - H\partial/\partial z) = \partial\partial/z(V+iW)$, one has

$$(\varepsilon-\varepsilon_N)\int(\psi Y_{l'})\frac{\partial}{\partial z}(uY_l)\mathrm{d}\tau = \int iW\psi Y_{l'}\frac{\partial}{\partial z}(uY_l)\mathrm{d}\tau - \int(uY_l)(\psi Y_{l'})\frac{\partial V}{\partial z}\mathrm{d}\tau. \quad \text{(A4)}$$

Combining these results one gets

$$(\varepsilon'-\varepsilon_N)^2\int(uY_l)(\psi Y_{l'})z\,\mathrm{d}\tau \quad \text{(A5)}$$
$$= \frac{\hbar^2}{m}\int(uY_l)(\psi Y_l)\frac{\partial V}{\partial z}\mathrm{d}\tau - \frac{\hbar^2}{m}\int iW\psi Y_{l'}\frac{\partial}{\partial z}(uY_l)\mathrm{d}\tau + (\varepsilon'-\varepsilon_N)\int iW(uY_l)(\psi Y_{l'})z\,\mathrm{d}\tau.$$

SURFACE ABSORPTION

We may concentrate the absorption potential W on the surface by the choice

$$W = -\frac{W_0R^2}{V_0}\frac{1}{r}\frac{\partial V}{\partial r} = -\frac{W_0R^2}{V_0}\frac{1}{z}\frac{\partial V}{\partial z}, \quad \text{(A6)}$$

where V_0 is the central value of V. From (A5) we then get

$$(\varepsilon'-\varepsilon_N)^2\int(uY_l)(\psi Y_{l'})z\,\mathrm{d}\tau = \left[\frac{\hbar^2}{m} - \frac{iW_0R^2}{V_0}(\varepsilon'-\varepsilon_N)\right]\int(uY_l)(\psi Y_{l'})\frac{\partial V}{\partial z}\mathrm{d}\tau$$
$$+\frac{iW_0}{V_0}\frac{\hbar^2R^2}{M}\int\frac{1}{r}\frac{\partial V}{\partial r}(\psi Y_{l'})\frac{\partial}{\partial z}(uY_l)\mathrm{d}\tau. \quad \text{(A7)}$$

VOLUME ABSORPTION

Let us suppose that W is constant over the volume $r < R$ and is zero outside. If the integrations in (A3), (A4) are restricted to the interior region I (say), they are replaced by

$$(\varepsilon'-\varepsilon_N-iW)I_1 = -\frac{\hbar^2}{m}I_2 - \frac{\hbar^2R^2}{2M}\int(zuY_l)\frac{\partial}{\partial r}(\psi Y_{l'}) - (\psi Y)\frac{\partial}{\partial z}(zuY_l)\mathrm{d}\Omega,$$
$$(\varepsilon'-\varepsilon_N-iW)I_2 = -\int(uY_l)(\psi Y_{l'})\frac{\partial V}{\partial z}\mathrm{d}\tau \quad \text{(A8)}$$
$$-\frac{\hbar^2R^2}{2M}\int\left[\frac{\partial(uY)}{\partial z}\frac{\partial\psi}{\partial r} - (\psi Y)\frac{\partial}{\partial r}\left(\frac{\partial u}{\partial z}\right)\right]\mathrm{d}\Omega,$$

where I_1 and I_2 are the integrals

$$I_1 = \int_{\mathrm{I}}(uY_l)(\psi Y_{l'})z\,\mathrm{d}\tau, \qquad I_2 = \int_{\mathrm{I}}\psi Y_{l'}\frac{\partial}{\partial z}(uY_l)\mathrm{d}\tau. \quad \text{(A9)}$$

The integrals in eq. (A8) are angular ones, the radial co-ordinates being fixed at

$r = R$. It is clear that the last two terms in (A5), which may be written as

$$iW\left[\frac{\hbar^2}{m}I_2+(\varepsilon'-\varepsilon_N)I_1\right],$$

may now be evaluated using (A8) for I_1 and I_2.

References

1) A. M. Lane, Nuclear Physics **11** (1959) 625
2) A. M. Lane and J. E. Lynn, Nuclear Physics **11** (1959) 646
3) R. G. Thomas, Phys. Rev. **84** (1951) 1061
4) G. Breit and F. L. Yost, Phys. Rev. **48** (1935) 203
5) G. M. Griffiths, Comptes rendus du congrès international de physique nucléaire, Paris 1958 (Dunod, Paris 1959) p. 447
6) A. G. W. Cameron, Can. J. Phys. **37** (1959) 322
7) A. M. Lane, R. G. Thomas and E. P. Wigner, Phys. Rev. **98** (1955) 693
8) A. G. W. Cameron, Proceedings of the international conference on the neutron interactions with the nucleus at Columbia University, New York, 1957 (U.S.A.E.C. TID-7547) p. 68
9) A. M. Lane and J. E. Lynn, Nuclear Physics **17** (1960) 586

2.C

Nuclear Physics **17** (1960) 586—608; © *North-Holland Publishing Co., Amsterdam*

Not to be reproduced by photoprint or microfilm without written permission from the publisher

ANOMALOUS RADIATIVE CAPTURE IN THE NEUTRON RESONANCE REGION: ANALYSIS OF THE EXPERIMENTAL DATA ON ELECTRIC DIPOLE TRANSITIONS

A. M. LANE and J. E. LYNN

Atomic Energy Research Establishment, Harwell, England

Received 10 March 1960

Abstract: The formalism of the preceding paper [1]) is used in a semi-quantitative attempt to analyze one of the most striking systematic features of low-energy neutron-capture γ-ray spectra, namely, the strong group of high energy transitions occurring in the spectra for nuclei below mass 208 and around mass 50. This is anomalous in the sense that it does not concur with our qualitative expectations from statistical theory. It is found that close to the giant resonance in the s-wave neutron strength function at $A \approx 50$ the anomaly appears to be associated with a selection rule operating in resonance capture while for lighter nuclei and for capture in some of the lead isotopes there is strong evidence that it is a consequence of "direct" or "potential" capture.

1. Introduction

A formalism for dealing with low energy neutron capture phenomena was set up in the preceding paper [1]). Numerical estimates based on this formalism showed that E1 transitions which involve final states having large admixtures of a single particle p-wave configuration may be enhanced in certain circumstances. In resonance capture there will be enhancement if the resonance has a particularly large neutron width. Such transitions should also occur in the nonresonant situation.

These conclusions are promising in attempting to explain the disagreement with statistical theory that is observed in low energy neutron capture. This does not occur in the total capture cross-section, which can usually be explained in terms of the nearby resonance levels of the compound nucleus, but in certain partial capture cross-sections and in the higher energy end of the photon spectrum. According to compound nucleus theory, the spectrum of primary photons from the decay of the compound state of excitation E^* has the form $\varepsilon_\gamma{}^3\rho(E^*-\varepsilon_\gamma)$, where ε_γ is the photon energy and $\rho(E^*-\varepsilon_\gamma)$ the level density of the compound nucleus at excitation $(E^*-\varepsilon_\gamma)$. Thus the spectrum is predicted to have a peak at a low photon energy (2 or 3 MeV) and then to fall off smoothly towards higher photon energies. If the secondary and the other cascade photons are included, it is clear that the prediction of smooth decrease above the peak is

preserved in the total spectrum, the rate of decrease being larger than in the primary spectrum alone.

It is the smooth decrease of the spectrum at the higher energies that is contradicted by some experimental results. As far as is known, the lower energy part of the observed spectra, which accounts for most of the total capture cross-section, agrees with the compound nucleus theory. At the higher energy end, however, anomalies appear. For instance, in nuclei with masses near $A = 190$, there is a "bump" occurring in the spectrum with an energy width of ≈ 1 MeV. As the mass increases, the bump moves systematically to higher energies and it seems beyond dispute that the bump is associated with the 3p neutron orbital that is filled at $N = 126$ (i.e. Pb^{208}). This connection has already been noticed [2]), but the question of the mechanism for the anomalous capture remains.

In the highest energy end of the photon spectra from neutron capture, one observes the discrete lines corresponding to the ground and low-lying excited states. Often these lines are anomalously strong, especially in the mass region $A \approx 50$. Also, certain selection rules seem to operate [3, 4]); these are unintelligible from the standpoint of compound nucleus theory except in terms of coincidental fluctuation of matrix elements.

In this paper a study of such experimental data will be made in the light of the theory of the preceding paper (henceforth referred to as I).

2. Analysis in Terms of the Strong Interaction Model

2.1. GENERAL REMARKS

The experimental data that are to be discussed have been taken from the compilations of Groshev *et al.* [5]) and of Bartholomew and Higgs [6]). It is first necessary to survey these data to discover how much is likely to be understandable on the basis of the theory of I. Nearly all the spectra in Groshev's compilation, down to intermediate nuclei at any rate, show a characteristic broad peak with a maximum at about 1 MeV (remembering that the intensity scale is multiplied by an instrumental factor — the momentum of the Compton electron — which is roughly proportional to energy) containing most of the primary, secondary, etc. transitions. The peak tails off towards the neutron separation energy of the compound nucleus but nearly always in this region there is a group of partially resolved γ-rays which almost certainly correspond to primary transitions to rather low-lying states. It is these groups which mainly concern us here. In the absence of any evidence to the contrary we shall assume that they are E1 transitions. The theory of I may be capable of giving a semi-quantitative explanation of these groups if the final states involved in the transitions contain an appreciable component of single-particle p-wave states. Now it is known that the $3p_{\frac{1}{2}}$ state is filled at Pb and that the 3p

TABLE 1

E1 capture spectra data for heavy nuclei

(1)	2(a)	2(b)	(2c)	2(d)	3(a)	3(b)	4(a)	4(b)
Pb^{208}	≈ 0.7	7.38	$\frac{1}{2}^-$	$0+(1)$ †	0.054	26	0.7	
Pb^{207}	≈ 0.025	6.73	0^+	$\frac{1}{2}-(\frac{1}{2})$ †	0.10	0.25	0.025	
Tl^{204}	4.2	5.6 ± 0.9	$\frac{1}{2}^+$		0.26	16	11.3	7.3×10^{-4}
Hg^{200}	930	5.4 ± 0.5	$\frac{1}{2}^-$		0.26	3.6×10^3	2500	
Au^{198}	27	5.4 ± 1.1	$\frac{3}{2}^+$		0.26	10^3	99	6.5×10^{-3}
Pt^{196}	1.8	5.5 ± 0.4	$\frac{1}{2}^-$		0.26	7	27	
Ir^{192}	107	5.5 ± 0.5	$\frac{3}{2}^+$		0.27	4×10^3	960	6.3×10^{-2}
W^{187}	2.9	5.2 ± 0.1	0^+		0.25	12	35	2.3×10^{-3}
W^{184}	1.0	6.9 ± 0.5	$\frac{1}{2}^-$		0.31	3.2	11	7.3×10^{-4}
W^{183}	1.5	6.0 ± 0.1	0^+		0.29	5.2	20	1.3×10^{-3}
Ta^{182}	1.1	5.5 ± 0.6	$\frac{7}{2}^+$		0.27	4.1	21	1.4×10^{-3}
Hf^{175}	10	5.0 ± 1.0	$\frac{7}{2}^-$		0.24	42	103	7.2×10^{-3}

Most of the data are taken from refs. [5, 6, 22]) where references to the experimental sources are given. The columns contain:

1. Compound nucleus
2. Description of anomalous transitions
   (a) Observed cross-section for anomalous region (b)
   (b) Mean binding energy of region and energy spread (MeV)
   (c) Spin i_β and parity of target
   (d) $J_t(s_t)$, i.e. total spin (channel spin) for final state when unique
3. Prediction of hard sphere capture cross-section
   (a) Predicted hard-sphere cross-section (b) (assuming $\theta_N^2 = 1$)
   (b) Ratio of observed to hard sphere cross-section
4. Prediction of capture from external contributions of local resonances together with hard-sphere capture
   (a) Total observed thermal capture cross-section (b)
   (b) Value of $\Sigma_\lambda(g_\lambda \gamma_{\lambda c}^2 \Gamma_{\lambda\gamma}/E_\lambda^2)$ extracted from 4(a)

† The orbital angular momentum in the final state has been established as $l_n = 1$ from (d, p) reactions.

state has zero binding energy at $A \approx 90$. There should thus be a steady diminution of the binding energy of states with strong p-wave components as A decreases from 208 to 90. A plot of the energies of the groups on the high energy tails of the capture γ-ray spectra reveals that the final states of these groups are only likely to contain strong p-wave components from about $A \approx 170$ to $A = 208$ among the heavier nuclei.

It appears from a study of the ground state spins of odd-neutron nuclei that the ground states may contain appreciable components of single-particle p-wave states from about $A \approx 77$ downwards. A plot of the binding of the strong groups in the Groshev spectra shows a fairly steady decrease from about $A \approx 77$ downwards in roughly the manner expected of the single particle 2p-state. Moreover, many of the final states involved in these groups show strong $l_n = 1$ patterns in deuteron stripping reactions. This group of data we have followed down to $A = 24$.

nuclei and comparison with theory

4(g)	4(h)	4(i)	4(j)	(4k)	4(l)	4(m)	4(n)
238	1	78		0.33		1.1	3.8 ††
4.91	2	1.9	0.12	0.39	6.2×10^{-3}	1.14	24
0.654		0.16	0.074	0.25	1.4×10^{-2}		†††
18.8	$\frac{1}{2}$	18	0.045	0.96	2.4×10^{-3}	5.2	0.56
7.6	1	0.33	0.073	0.043	3.1×10^{-4}		†††
4.14	$\frac{1}{2}$	0.20	0.050	0.048	5.8×10^{-4}		†††
4.28		0.53	0.064	0.12	9×10^{-4}	0.41	2.7
1.1		0.56	0.06	0.51	$\approx1.4\times10^{-2}$	1.1	9.1

(c) Observed thermal scattering cross-section (b)
(d) Observed coherent scattering cross-section (b)
(e) $\Sigma(\gamma^2_{\lambda c'}/E_\lambda)$ deduced from 4(c) and (d)
(f) Channel spin s' to which 4(e) applies
(The columns 4(c)—(f) only occur in table 3, and not in table 1 (because of lack of data)).
(g) Energy E_λ(eV) of known positive energy resonance that may be responsible for thermal capture
(h) Spin J_λ
(i) Reduced neutron width $\gamma^2_{\lambda c'}$(eV)
(j) Capture width $\Gamma_{\lambda\gamma}$ (eV)
(k) $\gamma^2_{\lambda c'}/E_\lambda$
(l) $(g_\lambda\gamma^2_{\lambda c'}\Gamma_{\lambda\gamma}/E_\lambda{}^2)$
(m) Predicted capture cross-section (with $\theta_N{}^2 = 1$) (b)
(n) Ratio of observed to predicted cross-sections

†† The large thermal capture indicates that unknown negative energy levels must be important.
††† The difference between columns 4(b) and 4(l) indicates that unknown levels must be important.

2.2. METHOD OF ANALYSIS FOR HEAVIER NUCLEI

In the first columns of table 1 we list the anomalous capture data for heavier nuclei. The other columns are concerned with theoretical calculations. It was shown in I that there are three contributions to the capture amplitude to any given final state: the potential, the resonance internal and the resonance channel capture. We shall compute these contributions in this section on the basis of the strong interaction model of nuclear reactions.

(a) *Potential capture*

Here we use computations of capture from hard sphere scattering. In I it was shown that this is the potential capture implied by the strong absorption model. The hard sphere cross-section σ(hard sph.) at the neutron energy ε' for capture to a final state of single neutron p-wave character ($l_t = 1$) is, from eqs. (66), (16) and (57) of I,

$$\sigma(\text{hard sph.}) = \frac{32\pi\tilde{e}^2}{3}\frac{R^5}{\hbar v'}k_\gamma{}^3\theta_N{}^2\frac{1}{y^4}\left(\frac{y+3}{y+1}\right)^2$$
$$= \frac{4\pi\tilde{e}^2\hbar^2\theta_N{}^2}{3Rv'M^3c^3}y^2\left(\frac{y+3}{y+1}\right)^2 \qquad (1)$$
$$= \frac{0.062}{R\sqrt{\varepsilon'}}\left(\frac{Z}{A}\right)^2\theta_N{}^2y^2\left(\frac{y+3}{y+1}\right)^2 \text{ barn},$$

where $\theta_N{}^2$ is the dimensionless reduced width of the final state, k_γ is the wave number of the emitted photon, v' is the velocity of the incident neutron, $\tilde{e}$ is the effective neutron charge, $y = k_{Nl}R$ (k_{Nl} being the wave number corresponding to the binding energy ε_{Nl} of the state Nl), R is the effective hard sphere radius (in 10^{-13} cm) and ε' is in eV. This result assumes that the energy spreading of the p-wave state (including spin-orbit splitting) amongst actual nuclear states is small. For a general spreading of these states, as given by the function $f(\varepsilon)$ described in (67) of I, the cross-section to a small energy interval Δ is

$$\sigma(\text{hard sph.}) = \Delta\frac{0.062}{R\sqrt{\varepsilon'}}\left(\frac{Z}{A}\right)^2\theta_N{}^2f(\varepsilon)y^2\left(\frac{y+3}{y+1}\right)^2 \text{ barn.} \qquad (2)$$

This is for the bombardment of a target β' of spin $i_{\beta'}$ by a neutron.

Equation (1) has been used to calculate $\sigma(\text{hard sph.})/\theta_N{}^2$ when the entry in table 1 is a group of transitions or $\sigma(\text{hard sph.})/\theta^2_{l,c_l}$ when the spin of the final state is unknown. In the latter case the use of equation (1) is an overestimate of course since (1) has been obtained by summing over all final spins J_f and channel spins s_f such that $\mathbf{J}_f = \mathbf{l}_f + \mathbf{s}_f$. When the spin of the final state is known $\sigma(\text{hard sph.})/\theta^2_{l,c_l}$ has been calculated by multiplying (1) by the statistical factor

$$\sum_{s'}\frac{(2J_f+1)}{6(2i_{\beta'}+1)}.$$

Here the sum over s' implies summing over only the incident channel spins consistent with $\mathbf{J}_f = \mathbf{s}' + \mathbf{l}_f$. The quantity $\sigma(\text{hard sph.})/\theta_N{}^2$ is given for $\varepsilon' = 0.025$ eV in column 3(a) of table 1, while $\sigma_{\text{obs}}\theta_N{}^2/\sigma(\text{hard sph.})$ is given in column 3(b). The cross-section $\sigma(\text{hard sph.})$ has been calculated using the value $R = 1.45\times10^{-13}A^{\frac{1}{3}}$ cm. for the radius of the hard sphere.

Since $\theta_N{}^2$ is of order 1, the entries in column 3(b) would all be ≈ 1 if the observed thermal capture were dominated by the direct hard sphere capture. In reality, the values are mostly much greater. Furthermore they fluctuate strongly, a fact which shows that local resonances strongly influence the observed cross-sections. Consequently we now try to estimate the effects of these resonances, concentrating first on the channel contributions.

(b) *Resonance channel capture*

The formula for the capture cross-section to a given final state f arising from the hard sphere and the resonance channel contributions is

$$\sigma_{\gamma f}^{(\mathrm{ch.})} = \frac{\pi}{k'^2} \sum_{s'} \frac{(2s'+1)}{2(2i_{\beta'}+1)} |U_{\gamma f, c'}^{(J=s')}(\text{ch. res.}) + U_{\gamma f, c'}^{(J=s')}(\text{hard sph.})|^2, \qquad (3)$$

where $U_{\gamma f, c'}$, the scattering matrix element, and its splitting into different components are defined in I. On evaluating U(ch. res.) from equations (9)—(13) and (19) of I, the E1 overlap integral being evaluated over the external region, we get

$$\sigma_{\alpha'\beta', \gamma f}^{(\mathrm{ch.})} = \frac{0.062}{R\sqrt{\varepsilon'}} \left(\frac{Z}{A}\right)^2 \theta_{\mathrm{I}c_f}^2 \sum_{s'} \frac{(2J_f+1)}{6(2i_{\beta'}+1)} \frac{1}{|1-\rho' R_{s'}|^2}$$
$$\times \left[y^2 \left(\frac{y+3}{y+1}\right)^2 + 2\mathscr{A}_{s'} \frac{y^3(y+1)(y+3)^2}{(y+1)^2} + (\mathscr{A}_{s'}+\mathscr{B}_{s'})^2 y^4 \left(\frac{y+2}{y+1}\right)^2 \right]. \qquad (4)$$

Here $R_{s'}$ is the function $(2\rho')^{-1}\sum_\lambda \Gamma_{\lambda c'}/(E_\lambda - E - \frac{1}{2}i\Gamma_\lambda)$ which occurs in I(4) and $\rho' = k'R$, where k' is the wave number of the bombarding neutron. The real and imaginary parts of this quantity are respectively

$$\mathscr{A}_{s'} = \frac{1}{2\rho'} \sum_\lambda \frac{\Gamma_{\lambda c'}(E_\lambda - E)}{(E_\lambda - E)^2 + (\frac{1}{2}\Gamma_\lambda)^2}, \qquad \mathscr{B}_{s'} = \frac{1}{2\rho'} \sum_\lambda \frac{\Gamma_{\lambda c'}\Gamma_\lambda}{(E_\lambda - E)^2 + (\frac{1}{2}\Gamma_\lambda)^2}.$$

If (4) is summed over all final states in the vicinity of the single-particle p-state N with $\mathbf{J}_f = \mathbf{s}' + \mathbf{l}$, the total channel capture cross-section becomes

$$\sigma(\mathrm{ch.}) = \frac{0.062}{R\sqrt{\varepsilon'}} \left(\frac{Z}{A}\right)^2 \theta_N^2 \sum_{s'} \frac{(2s'+1)}{2(2i_{\beta'}+1)} \frac{1}{|1-\rho' R_{s'}|^2}$$
$$\times \left[y^2 \left(\frac{y+3}{y+1}\right)^2 + 2\mathscr{A}_{s'} \frac{y^3(y+2)(y+1)}{(y+1)^2} + (\mathscr{A}_{s'}+\mathscr{B}_{s'})^2 y^4 \left(\frac{y+2}{y+1}\right)^2 \right]. \qquad (5)$$

In order to evaluate (4) or (5) in particular cases one has to know $\mathscr{A}_{s'}$ and $\mathscr{B}_{s'}$. In the case of thermal cross-section ($\varepsilon' = 0.025$ eV), since $\mathscr{A}_{s'}$ and $\mathscr{B}_{s'}$ are usually much less than unity,

$$|1-\rho' R_{s'}|^{-2} \approx 1.$$

There are a number of ways to obtain $\mathscr{A}_{s'}$ and $\mathscr{B}_{s'}$ from experimental data. The total thermal capture cross-section $\sigma_{\mathrm{th},\gamma}$ may be written

$$\sigma_{\mathrm{th},\gamma} = 18.1 \times 10^3 R \sum_{s'} \sum_\lambda \frac{(2s'+1)}{2(2i_{\beta'}+1)} \frac{\gamma_{\lambda c'}^2 \Gamma_{\lambda\gamma}}{E_\lambda^2}, \qquad (6)$$

provided all $|E_\lambda| \gg 0.025$ eV. Since Γ_λ is nearly always approximately equal to the total radiation width $\Gamma_{\lambda\gamma}$ at thermal energies, $\sigma_{\mathrm{th},\gamma}$ only differs from

$\mathscr{B}_{s'}$ by a constant and by spin weighting factors. These approximate to $\frac{1}{2}$ if $i_{p'}$ is large so that $\sigma_{\text{th},\gamma}$ gives an approximate measure of $\mathscr{B}_{s'}$. The quantity derived from $\sigma_{\text{th},\gamma}$ is listed in column 4(b) of table 1 (as $\sum_\lambda g_\lambda \gamma^2_{\lambda c'} \Gamma_{\lambda\gamma}/E_\lambda{}^2$). Often the thermal absorption cross-section is dominated by one or two positive energy resonances where widths (and perhaps spins) are well known from neutron spectroscopy measurements. In such a case the quantities $\mathscr{B}_{s'}$ and $\sum_\lambda g_\lambda \gamma^2_{\lambda c'} \Gamma_{\lambda\gamma}/E_\lambda{}^2$ can be evaluated directly. The second of these two quantities evaluated in this manner for one resonance is listed in column 4(l) of table 1 for comparison with that derived from the thermal value (column 4(b)). Agreement between the two values indicates that $\mathscr{A}_{s'}$ $(= \sum_\lambda \gamma^2_{\lambda c'}/E_\lambda)$ may be evaluated from the nearest positive energy resonances. It is nearly always found that $\mathscr{B}_{s'} \ll \mathscr{A}_{s'}$ and may be neglected in evaluating (4) or (5). The parameters of the nearest positive energy resonance are listed in columns 4(g) to 4(j) of table 1 and the value of $\mathscr{A}_{s'}$ derived from them in column 4(k). The quantity $\sigma(\text{ch})/\theta_N{}^2$ is given in column 4(m) and $\sigma_{\text{obs.}}\theta_N{}^2/\sigma(\text{ch})$ in column 4(n).

Comparing columns 3(a) and 4(m) it can be seen that, in the five cases where entries occur in 4(m), the effects of resonance channel capture are of the order of or larger than the hard-sphere capture. In two other cases (Hg and Ir), the large thermal capture cross-sections indicate that resonance effects must be relatively large. As mentioned earlier the importance of the resonance effects is indicated by the large values and fluctuations in column 3(b). It is gratifying to see this fact reproduced by the estimates of column 4(m), and in particular, to find that the fluctuations in column 4(n) are less than before.

(c) *Resonance internal capture*

The outstanding problem that remains is that of determining the importance of the resonance (internal) contribution to the capture groups. It may appear at first that this problem could be removed by dividing the cross-section for the anomalous region of the photon spectrum into two parts, a background obtained by extrapolating the smooth Maxwellian-type spectrum at lower photon energies, and the anomalous part itself. Then, assuming that the resonance (internal) capture gives a smooth spectrum, one would attempt to fit the background in terms of this, and the anomalous part in terms of the potential and resonance (channel) capture. There are two objections to this procedure. First there is the practical matter that the division of the observed spectra is very ambiguous. Second there is the possibility that the resonance (internal) capture does *not* give a Maxwellian spectrum but rather one exhibiting some selection rules like the spectra from channel and direct capture [1, 7]).

One can make estimates of the resonance (internal) cross-section only if one knows the number of final states in the anomalous region and the partial radiation widths to these states. In the absence of this knowledge, we quote in column 4 (table 2) values of the resonance (internal) cross-section for a typical

final state. This is estimated by multiplying the total thermal capture cross-sections of column 4(a) in table 1 by the ratio of the average partial radiation

TABLE 2

Resonance (internal) capture cross-section for typical final state

(1)	(2)	(3)	(4)	(5)	(6)
Hg^{200}	400	0.9	7	130	7
Au^{198}	190	0.08	0.08	350	12
Pt^{196}	200	0.5	0.12	15	2
Ir^{192}	440	0.03	0.4	300	8
W^{187}	300	0.3	0.25	12	3
W^{184}	66	0.07	0.02	50	2
W^{182}	220	0.3	0.12	14	3
Ta^{182}	64	0.015	0.006	180	7
Hf^{178}	48	0.01	0.015	600	8

Columns in the table are

1. Compound nucleus
2. Mean spacing $\bar{D}$(eV) of levels (reduced to spin zero by use of $\bar{D}_J = \bar{D}_0/(2J+1)$. Note, however, that the D implied in Cameron's formula (7) is D_J.
3. Mean partial radiation width $\bar{\Gamma}_{\lambda,\gamma f}$(MeV) from Cameron's formula (7).
4. Cross-section for capture (b) with primary transition to typical final state (from columns 4(a) and 4(j) of table 1 and column 3 of this table).
5. Inferred number of final states contributing to anomalous cross-section (from column 2(a) of table 1 and column 4 of this table).
6. Number of final states observed in capture γ-ray spectra.

width to the total radiation width. The latter is an observed quantity in most nuclei, whilst the former can be obtained from Cameron's [8]) formula

$$\Gamma_{\lambda\gamma f}(\text{MeV}) \approx 3.3\times 10^{-7}[\varepsilon_\gamma(\text{MeV})]^3 A^{\frac{2}{3}} D(\text{eV}). \qquad (7)$$

In order to estimate the resonance (internal) capture, one must multiply column 4 by the number of final states in the anomalous region. This depends on the nucleus, the excitation energy and extent of the region, and is difficult to estimate. In column 6 the observed number of final levels contributing to the anomalous region is stated, in order to provide a lower estimate. It can thus be seen that, in most cases, the presence of a reasonable number of levels is not sufficient to bring the entries in column 4 up to the order of those in column 4(m) of table 1. In other words, resonance (internal) capture appears not to be a significant contributor to the observed anomalous cross-section.

2.3 ANALYSIS OF DATA ON THE LIGHTER NUCLEI

Table 3 contains the data for the group of nuclei from As^{75} to Na^{24}. The data and calculated values are set down in the same way as in table 1 except that there are four extra columns inserted after column 4(b). These contain the

TABLE 3. E1 capture spectra: data for light nuclei and compa

1	2(a)	2(b)	2(c)	2(d)	3(a)	3(b)	4(a)	4(b)	4(c)	4(
As^{76}	0.3	6.8 ±0.5	$\frac{3}{2}^-$		0.31	0.97	4.3	3.9×10^{-4}	8.0	5.0
$Ga^{70,72}$	0.4	6.3 ±0.3	$\frac{3}{2}^-$		0.28	1.4	2.8	2.5×10^{-4}		
Zn^{69}	0.017	5.5 ±0.8	0^+		0.27	0.06	0.097	$\approx10^{-4}$		
	0.005	6.5		$\frac{1}{2}^-(\frac{1}{2})$ †	0.09	0.06				
Cu^{66}	0.33	7.0	$\frac{3}{2}^-$	1^+	0.08	4.1	2.2	2×10^{-4}		
	0.44	6.7			0.32	1.4				
Zn^{65}	0.16	7.8	0^+		0.40	0.4	0.44	4×10^{-5}		
Cu^{64}	1.1	7.91	$\frac{3}{2}^-$	1^+	0.09	12	4.5	4×10^{-4}		
	0.6	7.63		0^+	0.015	40				
	0.4	7.30		3^+	0.10	4				
Ni^{61}	1.0	7.82	0^+	$(\frac{1}{2})$	0.24	4.2	2.6	2.6×10^{-4}	1.0	
	1.3	7.2 ±0.5			0.36	3.6				
Ni^{59}	1.8	9.00	0^+	$\frac{3}{2}^-(\frac{1}{2})$	0.3	6	4.4		24	
	0.8	8.53		$\frac{3}{2}^-$	0.3	2.6				
	1.2	7.5 ±0.6			0.35	3.3				
Co^{60}	17	6.2 ±0.6	$\frac{7}{2}^-$		0.3	57	37		6.0	1
Fe^{58}	0.12	10.16	$\frac{1}{2}^-$	0^+ †	0.04	3	2.5			
Fe^{57}	0.95	7.64	0^+ †	$\frac{1}{2}^-(\frac{1}{2})$ †	0.13	7.3	2.7		12.8	
Mn^{56}	1.6	7.26	$\frac{5}{2}^-$	3^+	0.13	12	13.2	1.3×10^{-3}		
	1.9	7.1 ±0.05			0.33	5.8				
Fe^{55}	1.25	9.3	0^+	$\frac{3}{2}^-(\frac{1}{2})$ †	0.3	4.2	2.3			
Cr^{54}	1.5	9.72	$\frac{3}{2}^-$	0^+ †	0.017	90	18.2			
	4.4	8.88		2^+ †	0.16	27				
	1.9	8.5		†	0.37	5.1				
Cr^{53}	0.38	7.93	0^+	$\frac{3}{2}^-(\frac{1}{2})$ †	0.26	1.5	0.76			
	0.36	6.3 ±1.1			0.33	1.1				
V^{52}	0.29	7.3	$\frac{7}{2}^-$	2^+ †	0.033	8.8	5.0		5.1	
	2.5	6.2 ±1.0			0.29	8.6				
Ti^{50}	0.23	8.25	$\frac{7}{2}^-$	2^+	0.034	6.8	1.9			
Ti^{49}	3.3	6.75	0^+	$\frac{3}{2}^-(\frac{1}{2})$ †	0.20	16	8.3			
	2.4	6.41			0.30	8.				
Ti^{48}	0.034	10.62	$\frac{5}{2}^-$	2^+ †	0.11	0.31	1.7			
	0.05	8.34		4^+	0.09	0.56				
Sc^{46}	1.9	8.18	$\frac{7}{2}^-$		0.36	5.3	24		25	1
Ca^{41}	0.05	6.41	0^+	$\frac{3}{2}^-(\frac{1}{2})$ †	0.22	0.23	0.22		3.0	
	0.01	5.90		$\frac{1}{2}^-$ †	0.02	0.5				
	0.03	4.42		†						
K^{40}	0.21	5.73	$\frac{3}{2}^+$	†			1.94		2.2	
	0.06	5.65		†						
					0.29	1.4				
	0.05	5.25		†						
	0.09	5.02		†						
S^{33}	0.24	5.44	0^+	$\frac{3}{2}^-(\frac{1}{2})$ †	0.19	1.3	0.5		1.2	
	0.03	4.40		†						
	0.06	2.97		$\frac{1}{2}^-$ †	0.07	0.9				
P^{32}	0.07	3.9 ±0.8	$\frac{1}{2}^+$	†	0.22	0.32	0.2			
Si^{29}	0.04	3.55	0^+	$\frac{3}{2}^-(\frac{1}{2})$ †	0.14	0.29	0.08		2.4	
Mg^{25}	0.034	3.92	0^+	$\frac{3}{2}^-(\frac{1}{2})$ †	0.14	0.24	0.05		3.7	
	0.027	3.05		$\frac{1}{2}^-$ †	0.06	0.45				
Na^{24}	0.064	3.56	$\frac{3}{2}^+$	†	0.19	0.34	0.54		3.5	
	0.051	3.10		†	0.17	0.42				
	0.10	2.5 ±0.2		†	0.14	0.71				
	0.07	2.0 ±0.2		†	0.12	0.59				

† See footnote † below table 1.

i and comparison with theory. (See explanation below table 1)

(c)	4(d)	4(e)	4(f)	4(g)	4(h)	4(i)	4(j)	4(k)	4(l)	4(m)	4(n)
8.0	5.0	1.0	1	47		2.1		0.045	1.4×10^{-4}	1.9	0.16
		−0.65	2								
		−1.1	1							1.9	0.16
		0.58	2								
				≈100		≈2.3			3.6×10^{-5}		
				(both isotopes)							
				530	½	160		0.30	≈3 $\times10^{-4}$	0.84	0.02
										0.28	0.02
				227		0.36		0.0016	≈2 $\times10^{-5}$		
				2750	½	523		0.19	≈2 $\times10^{-5}$	1.0	0.16
				580		15		0.025	≈7 $\times10^{-6}$		
1.0		0.48		15×10^3	½	5.9 $\times10^3$		0.39		1.4	0.72
										2.1	0.62
		−1.5		5×10^3	½	1.7 $\times10^3$		0.35		3.1	0.44
										4.1	0.20
										4.9	0.25
6.0	1.0			132	4	198		0.67		1.4	12
2.8		−0.73	½							0.13	7.3
				337	2	591	0.5	1.75	≈1.2×10^{-3}	3.4	0.47
				2360	3	2900	0.5	1.23	≈1 $\times10^{-4}$		
										8.0	0.24
5.1	0.03(−)	2.4	3							1.6	0.18
		0.065	4							6.3	0.40
	17.5(+)	−3.02	3							8.1	0.23
		0	4								
		0.41	3							10	0.19
		−2.7	4								
1.0		≈0	½							0.22	0.23
										0.02	0.5
1.2	1.5	−0.32	1								
		0.66	2								
										1.0	0.41
1.2		0.33	½							0.5	4.8
										0.15	0.40
1.4		≈0	½							0.14	0.29
1.7		−0.3	½							0.05	0.7
										0.02	1.3
1.5	1.5	1.5	1	2850	1	4270		1.5		0.68	0.09
		−0.5	2							0.55	0.09
										0.38	0.26
										0.3	0.23

thermal elastic scattering cross-section $\sigma_{\text{th, sc.}}$ and the coherent thermal scattering cross-section $\sigma_{\text{th, coh.}}$. From these the quantities $\mathscr{A}_{s'}$ may be derived [9]) from the equations (with $a_{s'}$ for the thermal scattering length):

$$\sigma_{\text{th, sc.}} = 4\pi \sum_{s'} \frac{(2s'+1)}{2(2i_{\beta'}+1)} a_{s'}^2, \quad \sigma_{\text{th, coh.}} = 4\pi \left| \frac{2s'+1}{2(2i_{\beta'}+1)} a_{s'} \right|^2,$$
$$a_{s'} = R\left(1 - \sum_{\lambda} \frac{\gamma_{\lambda c'}^2}{E_\lambda}\right) = R(1-\mathscr{A}_{s'}). \tag{8}$$

In general two possible values for $\mathscr{A}_{s'}$ may be determined from these equations and it is not always possible to resolve the ambiguity. In such a case the alternatives are listed together with the corresponding calculations of σ(ch.). The fourth extra column contains the value of s' labelling $\mathscr{A}_{s'}$ calculated from (8).

In comparison with table 1, one sees that the inclusion of the resonance (channel) terms has less effect in the lighter nuclei. The last column of table 3 indicates that dominance of the resonance (internal) contribution to the cross-sections of the major transitions that we have studied appears to be the exception rather than the rule. This is probably because the resonances of these lighter nuclei are more widely spaced than in heavy nuclei and radiative capture as a whole is a less significant process than in the neutron reactions of heavy nuclei. The probability of finding a strong capture resonance close to the thermal energy is much smaller than amongst heavy nuclei. In Co^{60}, where there is a large resonance fairly close to thermal energy, $\sigma_{\text{obs}}\theta_N^2/\sigma^{(\text{ch.})}$ is large, viz. 12. Estimating the resonance (internal) capture in the same way as described for the heavier nuclei above one finds a cross-section of 0.3 b for a typical final state. The observed cross-section of 17 b is too high to be the sum of the cross-sections for a few final states.

3. Analysis in Terms of the Intermediate Coupling Model

3.1. GENERAL REMARKS

Further discussion of the experimental data requires the calculation of potential capture from the more realistic intermediate coupling model of nuclear reactions as discussed in I. In this model the neutron strength function shows strong peaking close to the single particle neutron levels corresponding to a real potential. The projection of the wave function of the neutron-nucleus system on the channel function, describing the coupling of the neutron and nucleus (in its ground state), gives rise to a wave function whose average over a small energy interval containing many levels is the wave function describing the interaction of a particle with a complex well. The real part of this wave function corresponds to ignoring the contribution of the local levels to the nuclear wave function at a sharp energy E, and gives the potential scattering cross-section. It is then necessary to calculate radial overlap integral of this part with a final

single particle wave function in the real part of the well in order to compute the potential capture cross-section.

It was pointed out in I that a square well is not expected to give a correct description of potential capture, for if its dimensions are adjusted to give the correct p-wave binding energy the s-wave scattering properties are not reproduced correctly. It is therefore necessary to compute potential capture using a diffuse well. A diffuse complex potential well which has been commonly used in the literature [10]) for discussion of neutron strength functions has the following form and parameters:

$$V(r) = \frac{V_0 + iW_0}{1 + \exp[(r-R)/a]},$$

where (9)

$$V_0 = -42 \text{ MeV}, \quad W_0 = -3.36 \text{ MeV},$$

$$R = 1.35\, A^{\frac{1}{3}} \times 10^{-13} \text{ cm}, \quad a = 0.58 \times 10^{-13} \text{ cm}.$$

This well gives a broad overall reproduction of the neutron strength functions experimentally observed as a function of A. It does not reproduce detail which is known to be a consequence of non-spherical shape of certain groups of nuclei[11]) or due to possible correlations of W_0 with nuclear shell closures [12]). Such details are not considered in this paper, however, and we have employed the above well for our computations. The real part of this well has been employed to calculate the bound p-wave properties. Here again spin-orbit coupling has been neglected. The appropriate wave functions, eigenvalues and radial overlap integrals were computed by numerical integration methods using an electronic computer.

3.2. COMPUTATIONS FOR HEAVIER NUCLEI

Figure 1 shows the eigenvalue of the 3p-state in the mass number range 130 to 208. For this same range the potential scattering cross-section, neutron strength function and potential capture cross-section are shown in figure 2. Noteworthy features of the potential capture curve are the two maxima corresponding roughly to the minimum and maximum in the potential scattering curve and the dip to zero just above the peak of the strength function curve. It is of interest to know how the potential capture cross-section depends on W_0. In figure 3 we show the potential capture cross-section for $W_0 = -0.5$, -3.36 and -10 MeV. The W_0 dependence is marked and it is interesting to see the zero value of potential capture shifted to higher values of A and beyond the region of interest as W_0 increases. There is a clear transition in this respect towards the strong absorption situation.

These results emphasize our conclusion of the previous section that the apparently anomalous behaviour of the thermal neutron capture γ-ray spectra between $A \approx 170$ and $A = 208$ cannot be explained as a potential capture

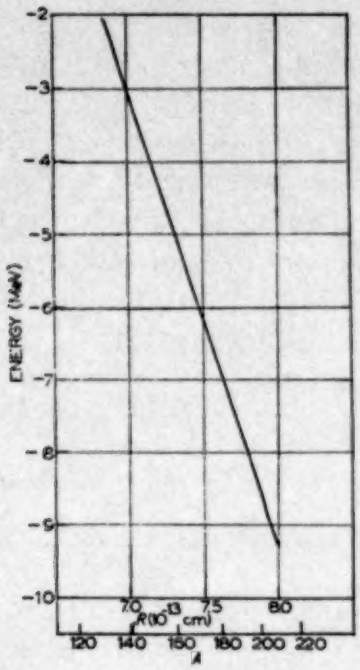

Fig. 1. The energy eigenvalue of the single-particle 3p-state calculated using the potential well form and parameters of eq. (9).

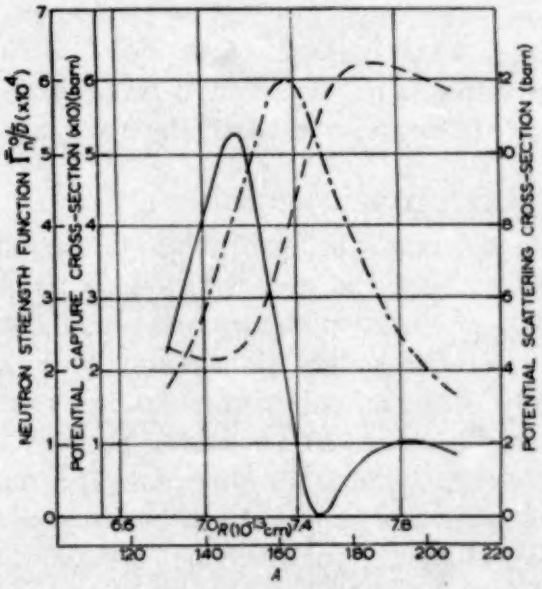

Fig. 2. The neutron strength function, potential scattering cross-section and potential capture cross-section associated with the 4s and 3p neutron orbitals. The neutron strength function is defined in the conventional way as $\bar{\Gamma}_n^0/\bar{D}$ where Γ_n^0 is resonance neutron width (in eV) divided by the square root of resonance energy (in eV) and $\bar{D}$ is the mean resonance spacing (of given spin and parity) in eV.

– – – – – – Neutron strength function; — — — — potential scattering cross-section; ———— potential capture cross-section

phenomena except possibly for some of the lead isotopes. For the most likely value of W_0 (≈ -3 MeV) the potential capture cross-section is a factor 2 to 3 below the hard sphere value which we have already found to be quite inadequate in this region.

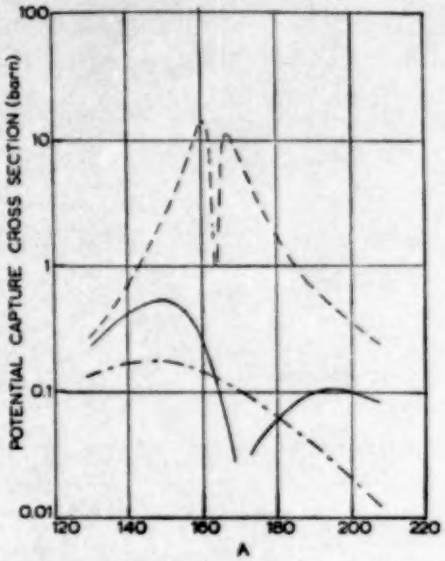

Fig. 3. The potential capture cross-section calculated for the well form (9) with different values of W_0.
– – – – – $W_0 = -0.5$ MeV; ——— $W_0 = -3.36$ MeV;
– – – – – – $W_0 = -10$ MeV.

The value of the partial radiation width $\Gamma_{\lambda\gamma l}$ at a resonance λ for the transition to a pure single particle p-wave state may also be derived from the complex potential well computation. It was explained in I how this quantity was asso-

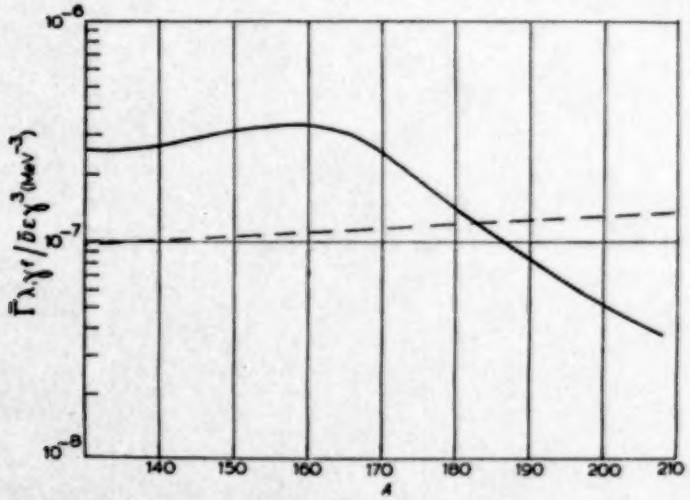

Fig. 4. The mean partial radiation width for the transition to a pure 3p-state. The full curve shows the quantity $\bar{\Gamma}_{\lambda\ \gamma l}/\bar{D}\varepsilon_\gamma^3$ as a function of mass number calculated for the well of the eq. (9). The dashed curve is ten times the same quantity as given by Cameron's formula [8]), eq. (7).

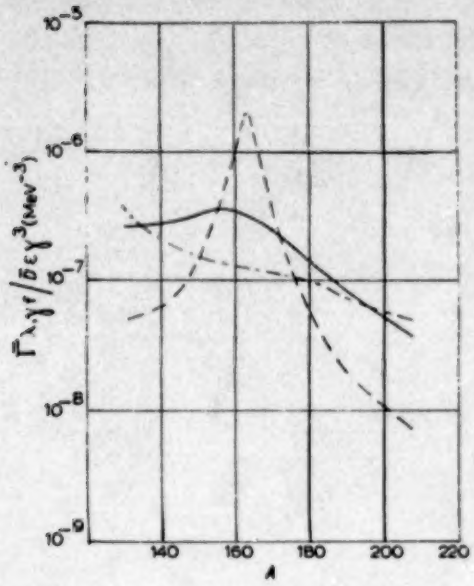

Fig. 5. $\bar{\Gamma}_{\lambda,\gamma f}/D\epsilon_\gamma{}^3$ calculated for the potential well form of eq. (9) with different values of W_0.
– – – – – $W_0 = -0.5$ MeV; ——— $W_0 = -3.36$ MeV;
– – – – – – – $W_0 = -10$ MeV.

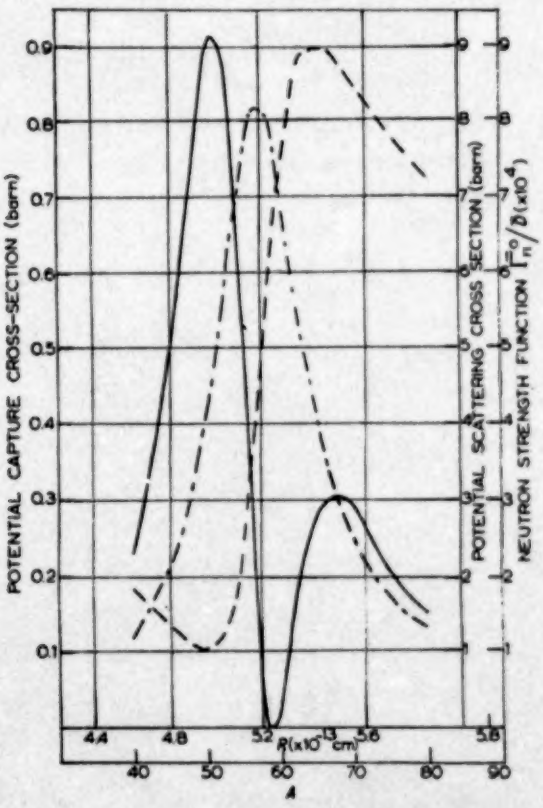

Fig. 6. The neutron strength function (– – – – – –), potential scattering cross-section (– – –) and potential capture cross-section (———) associated with the 3s and 2p neutron orbitals.

ciated with the radial overlap integral of the final state wave function and the imaginary part of the wave function corresponding to the interaction of an incident wave with a complex potential. For the well described by eq. (9) $\Gamma_{\lambda\gamma t}/D\varepsilon_\gamma{}^3$ for a resonance λ of average reduced neutron width is shown in fig. 4. Also shown is the curve of $\Gamma_{\lambda\gamma t}/D\varepsilon_\gamma{}^3$ as deduced by Cameron [8]) from a study of total radiation widths using statistical theory (eq. (7)). It is apparent that the former curve describing resonance capture to a pure p-wave state does favour transitions over the statistical theory deductions in the whole mass number range, espicially for resonances of large reduced neutron width, with which the strength of such a transition should be correlated. In fig. 5, $\Gamma_{\lambda\gamma t}/D\varepsilon_\gamma{}^3$ as obtained from the complex potential calculation is shown for a few values of W_0.

3.3. COMPUTATIONS FOR INTERMEDIATE NUCLEI

In fig. 6 the complex potential calculations are shown for the mass numbers around 50. The potential capture curve shows the same general features in relation to the strength function peak as in the higher mass number region but now has 2 to 3 times the amplitude. Before drawing conclusions from this figure it is necessary to point out that there is now some evidence from neutron

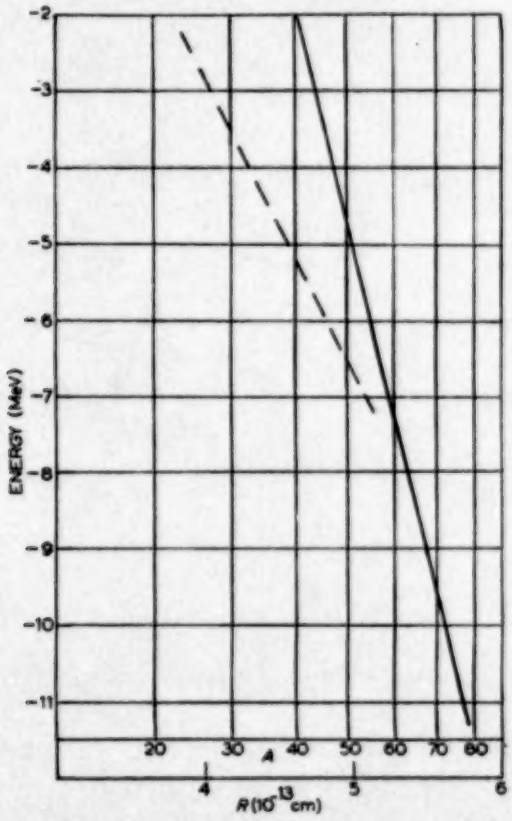

Fig. 7. The energy eigenvalue of the single-particle 2p-state calculated using the potential well form and parameters of eq. (9) (full curve). The dashed curve is approximately the eigenvalue experimentally observed in (d, p) reactions as a function of mass number. The discrepancy between the two curves is evidence that either the mass number-radius relationship ($R = 1.35A^{\frac{1}{3}} \times 10^{-13}$ cm) has been chosen wrongly or that $V_0(= -42$ MeV) should be slightly altered.

resonance studies that the strength function peak may be centred about mass 50 rather than 57 as shown here [13, 14]) and consequently the potential capture curve will be displaced to the left, or downwards in mass number. Further evidence for too small a radius or too shallow a potential having been chosen here is given by the p-wave state binding shown in fig. 7 together with a dashed curve which gives the approximate binding as inferred from deuteron stripping studies. Bearing these qualifications in mind then, we see from fig. 6 that some of our conclusions of section 2 about the data on light nuclei are substantiated. Between about mass number 65 and 75 there are apparently some cases where the strong high energy transitions may be the result of potential capture, the intermediate coupling calculation giving a result similar to the hard sphere calculation in this region. From approximately $A = 60$ down to 50 it appears that potential capture may well be small. On the other hand the average value of the width for a transition from a resonance to a single-particle p-wave state is enhanced above the statistical value of Cameron [8]) in this region (see fig. 8). Also the potential capture cross-section rises rapidly on either side of its minimum and the possibility of strong constructive resonance-potential capture interference in some cases cannot be ruled out.

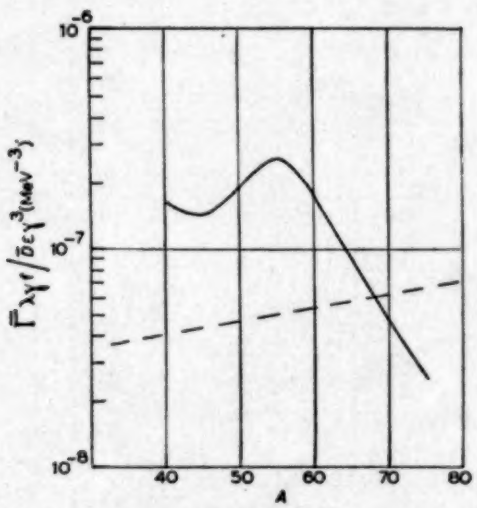

Fig. 8. $\bar{\Gamma}_{\lambda,\gamma f}/\bar{D}\varepsilon_\gamma^3$ calculated for the potential well (eq. (9)), where $\bar{\Gamma}_{\gamma,\lambda f}$ is the mean partial radiation width for the transition to pure 2p-state (full curve). The dashed curve is ten times Cameron's value deduced from statistical theory.

At still lower mass numbers, the intermediate coupling model calculation gives a value of the potential capture cross-section up to three times greater than the hard sphere value. It seems highly likely then that many of the cases below $A = 45$ are examples of potential capture.

4. Further Discussion of Special Cases

Further comments concerning some of the entries in tables 1 and 3 may be made here. Of particular interest are the cross-sections and γ-ray spectra of Pb^{206} and Pb^{207} with relation to the shell model theory of these nuclei (see fig. 9). Attention was already drawn several years ago [4]) to the existence of direct mechanism operating in the capture process in these nuclei. The capture γ-ray spectrum of Pb [5]) has one strong peak at maximum energy of 7.38 MeV ascribed to the ground state transition in Pb^{208}, a much smaller peak due to the ground state transition in Pb^{207}, a suggestion of a peak which is thought to be due to the transition to the 0.9 MeV excited state of Pb^{207} and a continuous

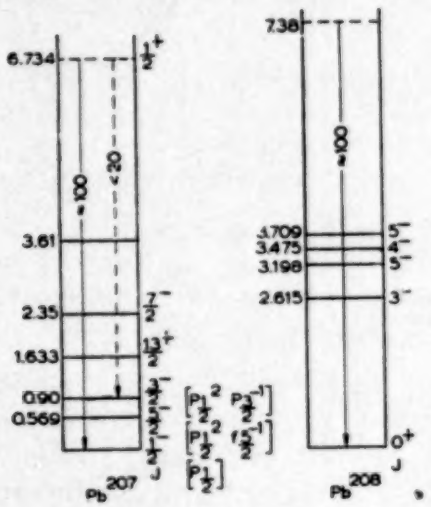

Fig. 9. Thermal capture spectra of $Pb^{206}(n, \gamma)Pb^{207}$ and $Pb^{207}(n, \gamma)Pb^{208}$.

spectrum of very low intensity down to zero energy. The ground state of Pb^{207} is considered to have a pure or nearly pure $(p_{\frac{1}{2}})^{-1}$ configuration based on the double closed shell ground state of Pb^{208}. Conversely, the ground state of Pb^{208} may be considered to have the nearly pure configuration of a single $p_{\frac{1}{2}}$ neutron in the field of Pb^{207} in its ground state. It follows that the transition to the ground state is the only intense E1 transition one would expect in any direct or channel mechanism of the capture of slow neutrons by Pb^{207} and it is the only such transition that is observed. The observed cross-section for the transition is much greater (a factor of about 12) than the order of magnitude value predicted by the channel-hard-sphere calculation (a factor 2 is inserted in the predicted cross-section because of the identity of the two $p_{\frac{1}{2}}$ particles in the final state).

A nearby negative energy level would explain this difference (by the channel resonance capture process). If such a level had a normal reduced neutron width, it would be bound by about 1 keV, which is fairly reasonable in view of level

spacings of the order of 10 keV which are known to occur in lead isotopes at about the binding energy.

In the case of capture in Pb^{206}, the intermediate coupling calculation indicates that the transition to the ground state should have a cross-section of about 0.03 b (including the spin weighting factor). This is to be compared with the experimental value of 0.025 b. The corresponding potential scattering cross-section is 11.7 b whilst the observed scattering cross-section of natural lead is 11.4 ± 0.1 b. There seems to be sufficient agreement here to indicate that this is certainly a case in which potential capture is being observed. True and Ford [15]) have given a shell-model theory of the lowest states of Pb^{206}. In the version of their theory which includes collective coupling they give the following eigenfunction for the Pb^{206} ground state:

$$\psi_{206} = 0.855(p_{\frac{1}{2}})_n^{-2} + 0.363(f_{\frac{5}{2}})_n^{-2} + 0.359(p_{\frac{3}{2}})_n^{-2} - 0.093(i_{\frac{13}{2}})_n^{-2}.$$

If the 0.90 MeV state in Pb^{207} is regarded as a pure $(p_{\frac{1}{2}})^{-1}$ state, this state may also be considered to contain a fraction 0.359 of the configuration $\psi_{206}(p_{\frac{3}{2}})_n^1$ while the ground state of Pb^{207}, $\psi_{208}(p_{\frac{1}{2}})_n^{-1}$ may be considered to contain a fraction 0.855 of the configuration $\psi_{206}(p_{\frac{1}{2}})_n^1$. A partial experimental confirmation of True and Ford's wave function has been given by the Pb^{206}(d, p)Pb^{207} reaction observed by McEllistrem *et al.* [16]) who find that the ratio of the cross-sections of the 0.9 MeV and ground states is 0.14 while the prediction of True and Ford's wave function is $(0.359/0.855)^2 = 0.18$ (apart from statistical factors). A similar application of the Pb^{206} wave function to the calculation of σ(hard sph.) would yield 0.3 for the ratio of the cross-sections of the 0.9 MeV and ground state of Pb^{207}. Groshev indicates [5]) that the observed ratio is of the order of or less than 0.2, so that there is qualitative agreement amongst the shell model, the (d, p) observations and the direct capture theory for Pb^{206}.

Amongst the lighter group of nuclei there are two examples which offer especially instructive evidence for channel capture. These are the spectra in the reactions $K^{39}(n, \gamma)K^{40}$ and $Ca^{40}(n, \gamma)Ca^{41}$.

The summed intensity of transitions to the states near 2.5 MeV in K^{40} is about 5 times that to the lower states (fig. 10) [17]). The upper and lower states are found from (d, p) stripping reactions to be $l_t = 1$ and $l_t = 3$ respectively. On grounds of spin, one might expect the upper states to be favoured by a factor of about 2 (all 4 states of $(d_{\frac{3}{2}})^{-1}(p_{\frac{3}{2}})$ can be produced by E1 radiation from the capturing states of spin 1, 2^+ but only 2 states of $(d_{\frac{3}{2}})^{-1}f_{\frac{7}{2}}$ can be produced). On the other hand, the E_γ^3 factor favours the lower states by a factor of 2 to 3. The observed dominance of the transitions to the upper state follows from the direct channel capture theory because the direct E1 transition is allowed in the s → p case but not in the s → f case. On the compound nucleus

theory one must appeal to fortuitous fluctuation of matrix elements to understand the result.

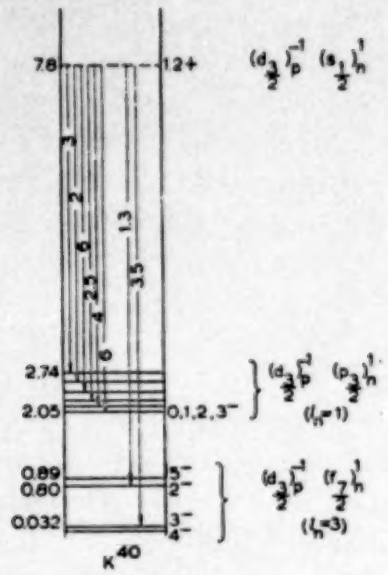

Fig. 10. Thermal capture spectrum of $K^{39}(n, \gamma)K^{40}$.

The final states associated with strong groups [18]) in $Ca^{40}(d, p)Ca^{41}$ are also associated with strong capture [19]) in $Ca^{40}(n, \gamma)Ca^{41}$. All the states of spin $\frac{1}{2}, \frac{3}{2}^-$ (those at 1.95, 2.47 and 3.95 MeV) come in this category. The states of spin $\frac{1}{2}, \frac{3}{2}^+$ show a striking similarity between the intensities of protons and gammas. (The 2.68 and 3.40 MeV states have strong groups, the 2.01 MeV state has a

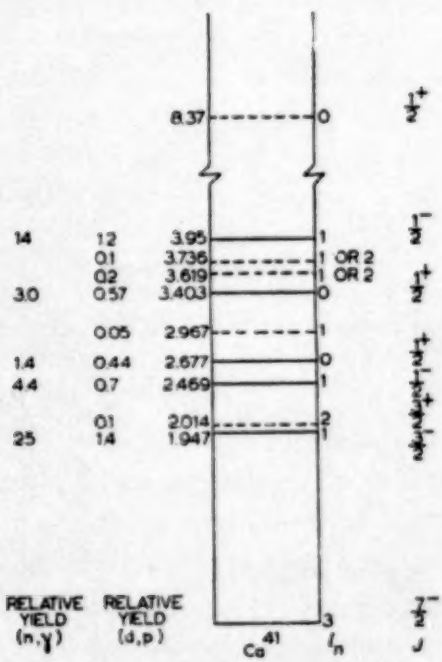

Fig. 11. Thermal capture spectrum of $Ca^{40}(n, \gamma)Ca^{41}$ and yield and stripping patterns of $Ca^{40}(d, p)Ca^{41}$.

weak one.) This suggests that, in certain cases at least, "direct" contributions to M1 transitions may be significant compared with the compound nucleus part. Further discussion of correlations between stripping reactions and neutron capture has been given by Bockelman [20]) and Groshev [2]).

In connection with capture by Ca^{40} it may be pointed out that the cross section here appears to be rather lower than indicated by the intermediate coupling calculation. This is in accordance with the fact that the observed scattering cross-section is 3 b — considerably greater than the value indicated by the complex potential model. There are two possible explanations here. One is the possibility of a bound level; this would raise the scattering cross-section and destructively interfere with the potential capture. The other is a possible reduction of W_0, the imaginary part of the complex potential, owing to the double shell closure Ca^{40}. This would tend to raise the potential scattering cross-section and correspondingly reduce the potential capture cross-section.

There is one case ($Mn^{55}(n, \gamma)Mn^{56}$) where the observation of capture γ-ray spectra [21]) at resonances may be of significance. The thermal neutron capture cross-section of Mn^{55} has been considered [22]) to be dominated by the contribution from the 337 eV neutron resonance of Mn^{55}. However, the ratio of the intensities of the 7.152 MeV and 7.046 MeV capture γ-rays in Mn^{55} measured at the 337 eV resonance (≈ 6) is strikingly different from the value of the same ratio measured at thermal energies (≈ 0.7). This could be explained by the presence of a negative energy resonance strongly influencing the thermal cross-section but there is no very strong evidence for this. On the other hand the difference may find a natural explanation in the channel capture theory without upsetting the present analysis of the total cross-section data [22]). The (d, p) spectrum shows relative intensities of 1 : 1 : 5 for final states corresponding to the 7.26, 7.15 and 7.05 MeV gamma-rays. Clearly a suitable admixture of interfering direct capture could change the ratio of 7.15 and 7.05 MeV lines from the resonance value of 6 : 1 to the observed value of 0.7 : 1.

5. Conclusions

Without making detailed analyses, it is easy to see that many features of capture cross-sections demand selection rules for their explanation, and cannot be understood in terms of the usual statistical theory. In nuclei of the mass range 170—210, the photon spectra reveal a clear tendency for transitions [2, 4]) to occur to those final states which share the single-particle $3p_{\frac{1}{2}}$ and $3p_{\frac{3}{2}}$ orbits. In the mass range 20—70, attention has been drawn previously to the fact that the relative intensities of photon groups are correlated to those of the proton groups of (d, p) reactions in selecting single-particle levels.

We have attempted to explain these selection rules by using the formalism developed in I to pick out components of the capture amplitude which clearly show selection by single particle p-wave components in the final state. We

have used as a standard, in order to compare our calculations with the predictions of statistical theory, the relation between an average partial radiation width and the level spacing of emitting states that was deduced by Cameron [8]) (see eq. (7)) from an analysis of total neutron radiation widths.

A complete analysis of the data would involve too many unknown factors at the present time. Hence we have adopted two approximate approaches in order to make order of magnitude calculations. The first approach has been to adopt the strong coupling or extreme compound nucleus picture of slow neutron interactions with nuclei whilst still assuming the existence of relatively pure single-particle states amongst the low-lying levels in the compound nucleus. The resonance internal contribution to the capture amplitude has then been ignored and our calculations have dealt only with the channel contribution to this amplitude which clearly selects only the single-particle p-wave components of the external wave functions of the final states. It was shown that this approach gave the right order of magnitude for the cross-sections of the anomalous groups in capture by the lead isotopes and many of the nuclei between $A = 20$ and $A = 70$. In many cases inclusion of the channel contribution to the wave function from known or inferred resonance levels was essential to obtain the correct magnitude.

In the second approach we have adopted the intermediate coupling or complex potential model. Here we have assumed the existence of a final state which is a pure single neutron p-wave state (and have neglected spin-orbit splitting); we have then calculated the potential capture cross-section to such a state which corresponds to capture at a neutron energy where the cross-section is negligibly affected by the local resonance levels, and also the average partial radiation width for the transition to the final state from a resonance. This radiation width includes both internal and channel contributions. The assumption of a pure single-particle final state is not necessary for the calculation of potential capture provided the answer is modified by the reduced width and spin statistical factors appropriate to an actual final state. These calculations give fair quantitative agreement for thermal neutron capture by Pb^{206} but it is apparent that for most of the nuclei between $A = 170$ and $A = 200$ neither the potential capture theory or even the resonance channel mechanism give the right order of magnitude of the observed anomalies. Further, the statistical theory standard set up by Cameron does not qualitatively explain the anomalies. On the other hand, the fact that our calculation of the partial radiation width to a single-particle p-wave state is an order of magnitude greater than Cameron's standard and even reproduces the maximum at $A = 160$ that Cameron discovered in later work [7]) suggest that an appreciable part of resonance capture occurs through coupling of a single s-wave neutron to a number of rather low-lying excited states of the target, in the initial state, and coupling of a single p-wave neutron to the same target states in the final state of the

compound nucleus. A similar suggestion has already been put forward by Cameron [7]).

In the group of nuclei from $A = 23$ to $A = 75$ there appear to be many examples in which the selection theory gives qualitative agreement with the observation. A few of the nuclei above mass number 60 are possibly affected in their capture properties by potential capture. Thermal capture in the group of nuclei from Sc^{45} to Co^{59} almost without exception has a large admixture of resonance capture but in a number of cases the channel mechanism gives the right order of magnitude. It is also encouraging that the average partial width for a transition to a p-wave state is calculated to be considerably greater than Cameron's standard in this region. Nuclei which are still lighter have cross-sections which are in qualitative agreement with our calculations of potential capture. It seems that, although we are unable to give a quantitative fit in detail to the capture data in this region, we have succeeded in qualitatively understanding the source of the observed selection rules.

We are grateful to Dr. G. A. Bartholomew for correspondence on the analysis of thermal capture data in the lighter mass region; also to Dr. A. G. W. Cameron for discussions of single-particle effects on the total capture widths.

References

1) A. M. Lane and J. E. Lynn, Nuclear Physics **17** (1960) 563
2) L. V. Groshev, A. M. Demidov, V. N. Lutsenko and V. I. Pelekhov, Proceedings of the Second International Conference on the Peaceful uses of Atomic Energy (United Nations, Geneva, 1958) Vol. **15**, p. 138
3) B. B. Kinsey and G. A. Bartholomew, Phys. Rev. **93** (1954) 1260
4) A. V. Shutko and D. F. Zaretskii, Soviet Physics JETP **2** (1956) 769
5) L. V. Groshev, A. M. Demidov, V. N. Lutsenko and V. I. Pelekhov, Atlas of γ-ray spectra from radiative capture of thermal neutrons, translated by J. B. Sykes (Pergamon, London, 1959)
6) G. A. Bartholomew and L. A. Higgs, Chalk River Report AECL 669 (1958)
7) A. G. W. Cameron, Proceedings of the International Conference on the Neutron Interactions with the Nucleus at Columbia University, New York, 1957 (U.S.A.E.C. TID-7547) p. 68
8) A. G. W. Cameron, Can. J. Phys. **37** (1959) 322
9) O. Halpern and M. H. Johnson, Phys. Rev. **55** (1939) 898
10) Feshbach, Porter and Campbell (unpublished)
11) D. Chase, L. Wilets and A. R. Edmonds, Phys. Rev. **110** (1958) 1080
12) A. M. Lane, J. E. Lynn, E. Melkonian and E. R. Rae, Phys. Rev. Letters **2** (1959) 424
13) F. W. K. Firk, J. E. Lynn and M. C. Moxon (to be published)
14) J. M. Leblanc, R. E. Coté and L. M. Bollinger, Nuclear Physics **14** (1959) 120
15) W. W. True and K. W. Ford, Phys. Rev. **109** (1958) 1675
16) McEllistrem, Martin, Miller and Sampson, Phys. Rev. **111** (1958) 1636
17) G. A. Bartholomew and B. B. Kinsey, Can. J. Phys. **31** (1953) 927
18) C. K. Bockelman and W. W. Buechner, Phys. Rev. **107** (1957) 1366
19) Adysevitch, Groshev, Demidov and Lutsenko, J. Nuclear Energy **3** (1956) 325
20) C. K. Bockelman, Nuclear Physics **13** (1959) 205
21) T. J. Kennett, L. M. Bollinger and R. T. Carpenter, Phys. Rev. Letters **1** (1958) 76
22) R. Krotkov, Can. J. Phys. **33** (1955) 622
23) D. J. Hughes and R. B. Schwarz, Neutron Cross Sections, BNL 325 (2nd edition, 1958)

7.C

Nuclear Physics **17** (1960) 609—613; © *North-Holland Publishing Co., Amsterdam*

Not to be reproduced by photoprint or microfilm without written permission from the publisher

ON THE CLOUD-CLOUD INTERACTION IN HIGH ENERGY INELASTIC NUCLEON-NUCLEON COLLISIONS

ANDRZEJ KRZYWICKI

Institute for Nuclear Research, Warsaw, Poland

Received 7 March 1960

Abstract: The role of the cloud-cloud interaction in the production of two pions in high-energy (several GeV) peripheral N-N collisions is examined. It is shown that the cloud-cloud interaction probably does not play any essential role in the process in question.

The experimental data on the high-energy (several GeV) inelastic nucleon-nucleon scattering are apparently inconsistent with the simple statistical theory [1]). These data show a sharp anisotropy of final nucleons in c.m.s. and an asymmetry in the distribution between final protons in p—n inelastic collisions. Also the momenta of nucleons are too large and those of pions too small if compared with the predictions of the statistical theory. In connection with these data the role of peripheral collisions has been examined and their importance is now commonly accepted. I. Tamm [2]) suggested a specific model of meson production in nucleon-nucleon collisions. According to Veksler's report in Kiev [1]) and to Dremin and Černiavski's paper [2]) the predictions of this model are in agreement with experiment. Tamm's idea consists of regarding peripheral collisions as due to one-meson exchange between two nucleons, which leads to the excitation of one or both nucleons. The isobars produced in this way decay afterwards into mesons and nucleons.

On the other hand experimental data on π-p inelastic scattering, especially the forward collimation of secondary pions support the idea of strong pion-pion interaction. The existence of such an interaction is now a subject of discussion [3]) Here, we shall not refer to the arguments for and against this hypothesis. We shall mention only the paper by D. Ito *et al.* [4]), who, using the simplest meson-meson interaction $\lambda\varphi^4$, made the calculations for the process $\pi+N \to 2\pi+N$ with the perturbation method. Treating by perturbation the pion-nucleon interaction can be partly justified by assuming a peripheral character of the process (as in Tamm's model). The calculation of the vertex corresponding to pion-pion interaction using perturbation method is of course a mathematical simplification. In spite of this defect the results obtained by Ito and others are more than qualitatively in agreement with experiment. In connection with their paper it is interesting to note the difference between the mechanisms of

production of even and odd numbers of mesons. The production of pions in $\pi-N$ collisions by means of interaction of the incident meson with only one virtual meson can occur in the case of production of an odd number of mesons, since the graph of the process, e.g. that shown in fig. 1, can only contain an odd number of external meson lines. If the production of an even number of pions were attributed to the interaction of the incident meson with the cloud of the target nucleon, we should be obliged to assume that it occurs in a more internal part of the nucleon. Another possibility consists e.g. in assuming that the interaction of the incident pion with a virtual one can produce the excitation of the nucleon (the possibility of such a process was noted by W. S. Barashenkov).

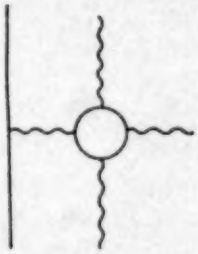

Fig. 1. An example of graph for the process in which the incident meson interacts with only one virtual meson.

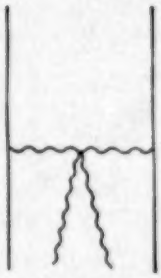

Fig. 2. Graph of the simplest interaction process between the pion clouds of two nucleons.

In connection with Tamm's model and the results of Ito *et al.* the question arises, what is the effect of the interaction between the pion clouds of two nucleons during their peripheral collision. We shall give in the following some preliminary results concerning this point. As in Tamm's model we shall assume that only one meson of the virtual meson cloud surrounding each nucleon participates in the interaction. The meson-meson interaction will be treated by perturbation method as in the paper of Ito *et al.* Let us limit ourselves to the simplest interaction $\lambda \sum_{ik}(\varphi^i)^2(\varphi^k)^2$ and to the case of two-meson production. In other words, we shall calculate the matrix element corresponding to the graph in fig. 2. The following notation is used (we work in c.m.s.):

p, E = momentum and energy of the incident nucleon;

p_1, E_1, p_2, E_2 = momenta and energies of the final nucleons;

$k_1, \omega_1, k_2, \omega_2$ = momenta and energies of the produced mesons;

θ_1, θ_2 = angles of deflection of the nucleons;

m, μ = nucleon and meson masses;

$\eta_1, \eta_2, \eta_{1'}, \eta_{2'}$ = iso-spinors corresponding to initial and final nucleons.

The probability of the examined transition is (the summation and averaging

over polarizations is performed)

$$P \propto \frac{g^4 \lambda^2 \delta_4(p_i - p_f - k_f)}{\omega_1 \omega_2 E_1 E_2 E^2}$$

$$[|X^{ik}|^2 A + |Y^{ik}|^2 B - \tfrac{1}{2}(X^{ik\dagger} Y^{ik} + Y^{ik\dagger} X^{ik}) C] \mathrm{d}_3 \mathrm{p}_1 \mathrm{d}_3 p_2 \mathrm{d}_3 k_1 \mathrm{d}_3 k_2, \qquad (1)$$

where

$$A = \frac{(m^2 + pp_1 \cos\theta_1 - EE_1)(m^2 + pp_2 \cos\theta_2 - EE_2)}{(-2m^2 - 2pp_1 \cos\theta_1 + 2EE_1 + \mu^2)^2 (-2m^2 - 2pp_2 \cos\theta_2 + 2EE_2 + \mu^2)^2},$$

$$B = \frac{(m^2 - pp_1 \cos\theta_1 - EE_1)(m^2 - pp_2 \cos\theta_2 - EE_2)}{(-2m^2 + 2pp_1 \cos\theta_1 + 2EE_1 + \mu^2)^2 (-2m^2 + 2pp_2 \cos\theta_2 + 2EE_2 + \mu^2)^2},$$

$$C = \frac{\{m^2(E - E_1)(E - E_2) + p^2 p_1 p_2 \sin\theta_1 \sin\theta_2\}}{(-2m^2 - 2pp_1 \cos\theta_1 + 2EE_1 + \mu^2)(-2m^2 + 2pp_1 \cos\theta_1 + 2EE_1 + \mu^2)}$$

$$\times \frac{1}{(-2m^2 - 2pp_2 \cos\theta_2 + 2EE_2 + \mu^2)(-2m^2 + 2pp_2 \cos\theta_2 + 2EE_2 + \mu^2)}.$$

The expression obtained for P gives a strongly anisotropic distribution of the final nucleons if the nucleon energy loss is not too large, showing that with the latter condition, the process in question corresponds really to a peripheral collision (the deflection of the nucleons is also small). To obtain a probability distribution depending on one angle only requires very cumbersome integrations. Therefore we shall not enter into detailed calculations and we shall give only a crude estimation of the anisotropy. Consider for simplicity p−p scattering. As will be shown later, in this case $X^{ik} = Y^{ik}$ and $P \propto A + B - C$. Since we assume $\Delta p/p$ to be not too large we can use the formula

$$\Delta E = \frac{p}{E} \Delta p - \frac{m^2}{2E^3} (\Delta p)^2,$$

where ΔE and Δp denote the energy and momentum loss of the nucleon. We obtain

$$A \approx \frac{\left[\frac{1}{2}\left(\frac{\Delta p_1}{E}\right)^2 + \frac{p}{m^2} p_1 (1 - \cos\theta_1)\right]\left[\frac{1}{2}\left(\frac{\Delta p_2}{E}\right)^2 + \frac{p}{m^2} p_2 (1 - \cos\theta_2)\right]}{\left[\left(\frac{\Delta p_1}{E}\right)^2 + \left(\frac{\mu}{m}\right)^2 + 2\frac{p}{m^2} p_1 (1 - \cos\theta_1)\right]^2 \left[\left(\frac{\Delta p_2}{E}\right)^2 + \left(\frac{\mu}{m}\right)^2 + 2\frac{p}{m^2} p_2 (1 - \cos\theta_2)\right]^2}$$

and similarly for B and C. The quantities p/m and p'/m are large compared with $(\Delta p_1/E)^2$, $(\Delta p_2/E)^2$ and $(\mu/m)^2$. Thus A is small, unless $\cos\theta_1$, $\cos\theta_2 \approx 1$ when it is large, being proportional to a small quantity divided by the square of a

small quantity. Similarly B reaches its maximum value when $\cos\theta_1$, $\cos\theta_2 = -1$ (one has $B(\theta_1, \theta_2) = A(\pi-\theta_1, \pi-\theta_2)$). The quantity C has a tendency to diminish the anisotropy, since it has also maxima at $\cos\theta_1$, $\cos\theta_2 = \pm 1$, but these maxima are considerably lower than those of A and B. Thus the anisotropy is due to the behaviour of A and B. As an illustration we shall compare the probability of an event with $\theta_1, \theta_2 = 0$ or π, with the probability of an event with $\theta_1, \theta_2 = \frac{1}{2}\pi$ (in order to simplify the expressions we put $p_1 = p_2 = p'$). We have

$$P \propto \left[\frac{\left(\frac{\Delta p}{E}\right)^2}{\left[\left(\frac{\Delta p}{E}\right)^2 + \left(\frac{\mu}{m}\right)^2\right]^2}\right]^2 + \frac{1}{\left(4\frac{p}{m}\frac{p'}{m}\right)^2} - \frac{4\left(\frac{\Delta E}{m}\right)^2}{\left[\left(\frac{\Delta p}{E}\right)^2 + \left(\frac{\mu}{m}\right)^2\right]^2 \left(4\frac{p}{m}\frac{p'}{m}\right)^2} \quad \text{for } \theta_1, \theta_2 = 0, \pi;$$

$$P \propto \frac{1}{\left(2\frac{p}{m}\frac{p'}{m}\right)^2} \quad \text{for } \theta_1, \theta_2 = \tfrac{1}{2}\pi.$$

To examine the dependence of the process in question on the isobaric spin we shall use the relation

$$\tau^i_{\alpha\beta}\tau^k_{\gamma\delta} = \tfrac{1}{2}\left[\delta^{ik}\delta_{\alpha\delta}\delta_{\gamma\beta} - i\sum_l \varepsilon_{ikl}(\delta_{\alpha\delta}\tau^l_{\gamma\beta} - \tau^l_{\alpha\delta}\delta_{\gamma\beta}) + \tau^i_{\alpha\delta}\tau^k_{\gamma\beta} + \tau^k_{\alpha\delta}\tau^i_{\gamma\beta} - \delta^{ik}\sum_l \tau^l_{\alpha\delta}\tau^l_{\gamma\beta}\right],$$

from which it follows that

$$\begin{aligned} X^{ik} &= \bar{\eta}_{1'}\bar{\eta}_{2'}\{\phi^{ik} - \delta^{ik}(1-\boldsymbol{\tau}_1\cdot\boldsymbol{\tau}_2)\}\eta_1\eta_2, \\ Y^{ik} &= \bar{\eta}_{1'}\bar{\eta}_{2'}\{\phi^{ik} + \tfrac{3}{2}\delta^{ik}(1-\boldsymbol{\tau}_1\cdot\boldsymbol{\tau}_2)\}\eta_1\eta_2, \\ \phi^{ik} &= \delta^{ik} + \tau_1{}^i\tau_2{}^k + \tau_1{}^k\tau_2{}^i \end{aligned} \tag{2}$$

(the superscripts of the τ matrices refer to the particles on whose wave functions they act).

We see that, when the initial or the final nucleons have identical charges, $X^{ik} = Y^{ik}$, since $(1-\boldsymbol{\tau}_1\cdot\boldsymbol{\tau}_2)$ acting on the triplet state gives zero. In this case P is invariant under the transformation

$$\theta_1, \theta_2 \to \pi-\theta_1, \pi-\theta_2$$

and we have forward-backward symmetry. When we have in both final and initial state differently charged particles a forward-backward asymmetry occurs. For simplicity, in examining this asymmetry, we sum over the charge states of produced mesons. Assume that the first (superscript 1,1′) nucleon is a proton and the second (superscript 2,2′) a neutron. In this case it follows from eq. (2) that

$$\sum_{ik}|Y^{ik}|^2 = \sum_{ik}|X^{ik}|^2 + 25 \quad > \quad \sum_{ik}|X^{ik}|^2 \quad \left(\sum_{ik}|X^{ik}|^2 = 11\right).$$

Thus the asymmetry produced by the discussed process is just the reverse of the experimentally observed one †). This shows that the contribution of the cloud-cloud interaction to the production of two mesons in peripheral nucleon-nucleon collisions is small ††.

I wish to express my gratitude to Prof. Z. Koba for his constant interest and for reading the manuscript.

† Z. Koba called my attention to the fact that as far as we consider the scattering due to the one-meson exchange with small momentum transfer this result is independent of the perturbation theory treatment of the nucleon-meson vertices. It seems to be a general feature of one-meson exchange that it leads to a small momentum exchange. We treat here these two conditions as independent only because it is difficult to say what is the influence on the angular distribution of taking the physical vertex instead of the simplest one. Koba's statement follows from the isobaric symmetry properties of the interaction. In fact at each meson-nucleon vertex the emission of the charged meson is more probable than the emission of the neutral one. Thus in the p−n case the more probable event occurring according to the mechanism in question is such that at each meson-nucleon vertex the corresponding nucleon changes its charge state. Since the momentum transfer is small the final protons will fly in opposite direction to the initial ones.

†† We hope that a more rigorous treatment of the pion-pion vertex will not change this conclusion. Our opinion is based on the agreement of the results of Ito *et al.* with experiment.

Note added in proof: The validity of our conclusion is limited by the fact that we use a special form of the pion-pion interaction Hamiltonian. One can show, however, that when incident and virtual pions interact predominantly in a S-state and when the pion-pion vertex depends weakly on energy this conclusion remains valid, unless the scattering in the $T = 2$ state is much stronger than that in the $T = 1$ state (T denotes the isospin of the two-pion system). When P-wave pion-pion scattering predominates the asymmetry is always opposite to the experimentally observed one.

References

1) V. I. Veksler, Report at the International Conference on High Energy Physics (Kiev, July 1959)
2) I. Tamm, unpublished;
I. M. Dremin and D. S. Černiavski, JETP **38** (1960) 229
3) See e.g., I. Sato, A. Takahashi and Y. Ueda, Prog. Theor. Phys. **22** (1959) 617;
Wen-Nong Wong and M. Ross, preprint
4) D. Ito, M. Yamazaki, T. Kobayashi and K. Mori, Prog. Theor. Phys. **22** (1959) 448

2.H

Nuclear Physics **17** (1960) 614—640; © *North-Holland Publishing Co., Amsterdam*

Not to be reproduced by photoprint or microfilm without written permission from the publisher

ALPHA-PARTICLE EXCITATION OF QUADRUPOLE AND OCTUPOLE SURFACE MODES IN Ti, Fe, Ni, Zn AND Sr

D. K. McDANIELS†, J. S. BLAIR, S. W. CHEN and G. W. FARWELL

Department of Physics, University of Washington, Seattle, Washington ††

Received 29 January 1960

Abstract: Angular distributions were obtained for elastic and inelastic scattering of 41 MeV alpha particles by Ti^{48}, Fe, Ni, Zn, Zn^{64} and Sr. In all targets excitation by inelastic scattering is strongest for the low-lying 2^+ levels, usually described in terms of quadrupole surface vibrations, and for the "anomalous" levels of somewhat higher excitation. The results for both elastic and inelastic scattering are analyzed in terms of a strong absorption diffraction scattering model. Parameters associated with collective interpretations of both types of levels are estimated and compared with values of the corresponding quantities derived from Coulomb excitation and electron scattering experiments. Reasonable agreement is obtained in the quadrupole excitation analyses. Strong support is given for 3^- assignments for the anomalous levels and for their interpretation in terms of surface octupole vibrations.

1. Introduction

Recent extensive experiments [1, 2]) on the inelastic scattering of 23 MeV protons by intermediate mass nuclei ($140 > A > 60$) have indicated strong excitation of levels lying less than 4 MeV above the ground state. There is good correlation between the levels strongly excited by protons and those excited by 43 MeV [3]), 30 MeV [4]) and 20 MeV [5]) alpha particles as well as by 21 MeV deuterons [6]). The strongly excited states may be classified into two groups: 1) levels near 1 MeV which are almost invariably those strongly excited in Coulomb excitation experiments; 2) An anomalous group generally with 2-4 MeV excitation energy.

The large cross sections for the first group may be attributed to excitation of quadrupole surface vibrations; this explanation has led Cohen and Rubin [2]) to suggest that the anomalous group is similarly reached through excitation of a collective mode of nuclear motion. Levinson [7]) and Lane and Pendlebury [8]) have suggested that such a collective excitation might be an octupole surface vibration. This suggestion is appealing for several reasons. First, until recently†††, the only state with known spin and parity in the anomalous group has been the 3^- level of Sr^{88} at 2.76 MeV. Second, according to hydrodynamic estimates the

† National Science Foundation Predoctoral Fellow.

†† Work supported in part by the U. S. Atomic Energy Commission.

††† Recent (α', γ) angular correlation experiments [9]) have indicated that $I = 3$ for the anomalous states in Ni^{58} and Ni^{60}.

ratio of octupole to quadrupole excitation energies $\hbar\omega_3/\hbar\omega_2$ is approximately [10]) 2 to 3; observed ratios are of the same order of magnitude. Third, observed angular distributions of protons which excite the anomalous levels are consistent with the simple Born approximation prediction for octupole vibrational excitation, although the assignment is far from unique [1]). The evidence for octupole excitation derived from proton experiments is summarized by Tamura and Choudhury [11]). Fourth, octupole vibrations have been observed previously in spheroidally deformed nuclei [12]).

The present experiments were undertaken in order to determine some properties of the strongly excited states of nuclei of intermediate mass as revealed by the angular distributions of inelastically scattered alpha particles of 41 MeV incident energy. Nuclei with $Z < 30$ were included particularly in this study to check the observation that anomalous excitations begins sharply at this point[2]); we find anomalous excitation by alpha particles for Z as low as 22. Our results lend strong support to the suggestion that the anomalous levels are characterized by surface octupole vibrations. We in find addition that a strong absorption diffraction model for both elastic and inelastic scattering [13]) successfully explains many features of the observed angular distributions.

2. Experimental Details

2.1. GENERAL

The experimental arrangement for measuring the angular distributions was similar to that used previously for lighter elements [14, 15]). The external beam of 41 MeV alpha particles from the University of Washington 152 cm cyclotron, focused and tightly defined in energy by a two-magnet external beam system, was used in conjunction with the 61 cm scattering chamber. Scattered particles were detected with a crystal-photomultiplier scintillation spectrometer. The beam passing through the target was monitored by measuring the charge collected on the Faraday cup system with a calibrated ballistic galvanometer.

2.2. TARGETS

Several criteria were kept in mind when choosing the target materials for the present study.

1) Only elements of even Z were considered since their major constituents have also even N; not only are even isotopes more amenable to theoretical treatment but also the level density is low, a major consideration when the energy resolution is of the order of 0.5 MeV. Fortunately two of the natural targets, Fe and Sr, are mainly composed of single isotopes, Fe^{56}(92 %) and Sr^{88}(83 %). Nearly pure Zn^{64}(98.5 %) and Ti^{48}(99 %) targets were also studied †.

† Isotopically enriched materials were obtained from the Isotopes Division of the Union Carbide Nuclear Company, Oak Ridge, Tennessee.

2) The lowest 2^+ levels of all the elements investigated, with the exception of Ti, possess electromagnetic properties consistent with the quadrupole vibration interpretation [12, 16]).

3) Sr was chosen particularly in order to provide a basis for comparison and interpretation of the results for the other elements, since electron inelastic scattering experiments have indicated that collective excitation is associated with the known 3^- level at 2.76 MeV [17]).

The zinc, nickel and iron targets were metal foils approximately 0.0008 cm thick. The Ti^{48} target was formed by the evaporation of $Ti^{48}O_2$ onto a thin ($\approx 20\ \mu g/cm^2$) VYNS film; this target was useful only at angles greater than 45°, since at smaller angles the inelastic alpha peaks for Ti^{48} were obscured by oxygen peaks. Strontium targets were formed by rolling strontium metal to about 0.0025 cm under a protective covering of *n*-decane to prevent oxidation.

2.3. DETECTOR SYSTEM

Reaction particles were detected with a scintillation spectrometer system consisting of aluminium absorber, collimator, CsI(Tl) crystal, Du Mont 6291 photomultiplier, preamplifier and amplifier, and 40-channel pulse height analyzer. Absorbers and crystals of various thicknesses were used. Discrimination against protons and deuterons was achieved by tailoring the aborber-crystal combination approximately to the range of elastically scattered alphas for a particular target and angular region. The function of the aborber was to improve the effective energy resolution by increasing the percentage difference between energies expended in the crystal by elastic and inelastic alpha groups; the upper limit to the amount of absorber used was set by the enhancement of pulses from particles other than alphas rather than by adverse effects of straggling in the absorber. Typical absorber thicknesses were, for nickel, 100 mg/cm² from 20° to 35° and 28 mg/cm² from 55° to 80°. Particle losses due to small-angle scattering in the absorber were shown to be negligible in the geometry used.

The absolute energy resolution obtained ranged from 1.6 % to 2.0 % (full width at half maximum, expressed in percent of actual alpha energy). Typical spectra are presented in figs. 1 and 2. Pulse heights were converted to excitation energies with the aid of calibrations obtained largely by observing alpha groups scattered elastically and inelastically by C^{12} at various angles.

The full angular acceptance of the counter system was 0.9°. Energy spectra were obtained for most targets at intervals of 1.8° from 18° to 75°. The angle of observation was known to $\pm 0.5°$ or less.

2.4. DETERMINATION OF ABSOLUTE CROSS SECTIONS

The measurement of an absolute cross section was made by normalizing counts in the appropriate peak to the deflection of a calibrated ballistic galvanometer which measured the charge collected on the Faraday cup system.

At times, especially for counts at small angles with very low beam intensities, normalization to a monitor scintillation counter at a fixed angle was used to provide better statistical accuracy.

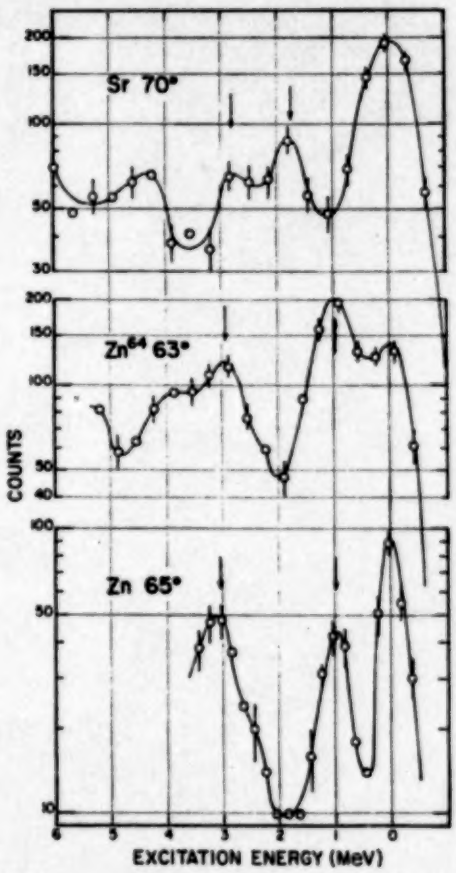

Fig. 1. Typical pulse height spectra of alpha particles scattered from targets of natural strontium (70°), Zn^{64}(63°) and natural zinc (65°). The detector was a single CsI(Tl) crystal mounted on a DuMont 6291 photomultiplier.

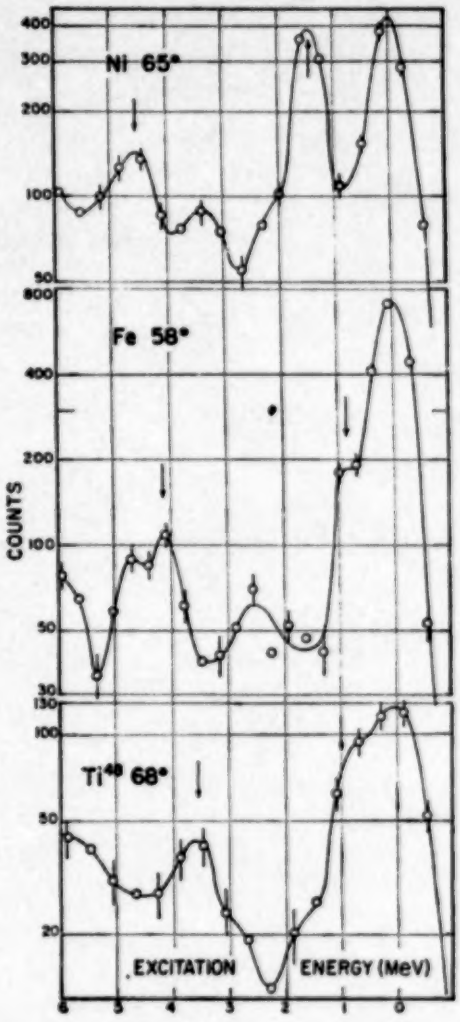

Fig. 2. Typical pulse height spectra of alpha particles scattered from targets of natural nickel (65°), natural iron (58°) and Ti^{48}(68°). The detector was a single CsI(Tl) crystal mounted on a DuMont 6291 photomultiplier.

In order to check the accuracy of the absolute cross sections the elastic scattering of gold was measured down to 6° to provide a direct comparison with the calculated Rutherford cross section. In order to eliminate possible systematic angular errors, the correct zero angle setting was determined by making observations on both sides of the incident beam and establishing the beam direction by symmetry. Fig. 3 compares the observed cross sections with the

calculated Rutherford cross sections; the agreement at small angles is very satisfactory. We conclude that errors in the beam integration and detector solid angle calculation are not significant compared to other errors.

Among the other errors the most significant are associated with the separation of a desired particle group from neighbouring particle groups and from a background continuum. As may be seen in figs. 1 and 2, the peaks of particular interest in the observed spectra (elastic peaks and those inelastic peaks indicated by arrows) are easily distinguished in some cases but not in others.

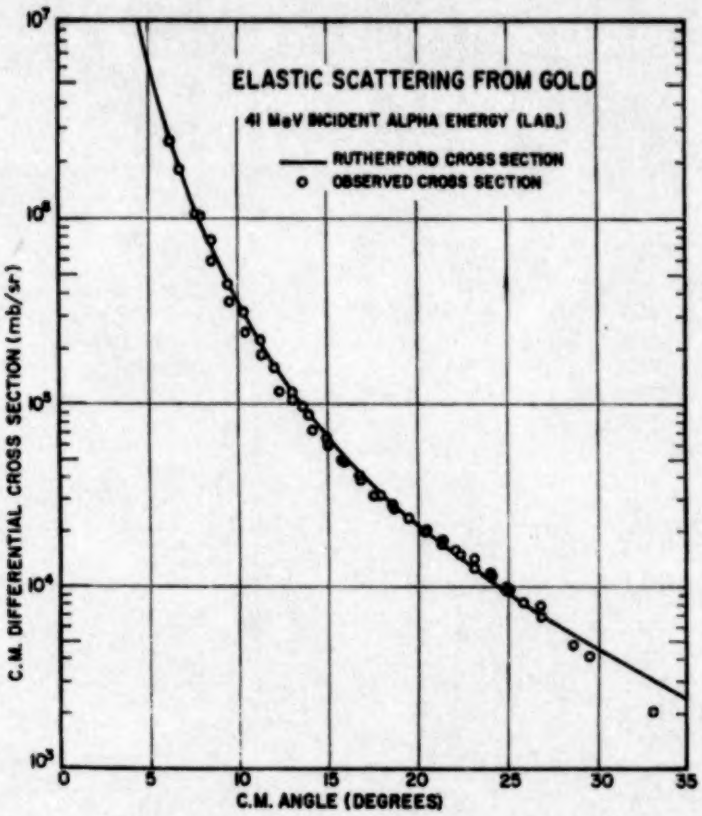

Fig. 3. Comparison of observed elastic scattering cross sections for 41 MeV alpha particles incident on a natural gold target with the calculated Rutherford cross sections at small angles to indicate the accuracy of the absolute cross section measurements.

(The spectral features for each element change rapidly with angle, however, and a peak which is barely distinguishable in one of the spectra shown may stand out clearly at a nearby angle.) The rather large errors shown in some regions of each angular distribution (sec. 3), particularly for the higher excited states, reflect these difficulties. Further, it must be remembered that groups appreciably closer than about 0.5 MeV in energy are simply not resolved by the detector system.

3. Results

3.1. ZINC

Available information concerning the energy levels and isotopic constitution of natural zinc is summarized in fig. 4. The Zn^{64} target contained 98.5 % Zn^{64}, 1.1 % Zn^{66}, 0.3 % Zn^{68} and negligible amounts of Zn^{67} and Zn^{70}.

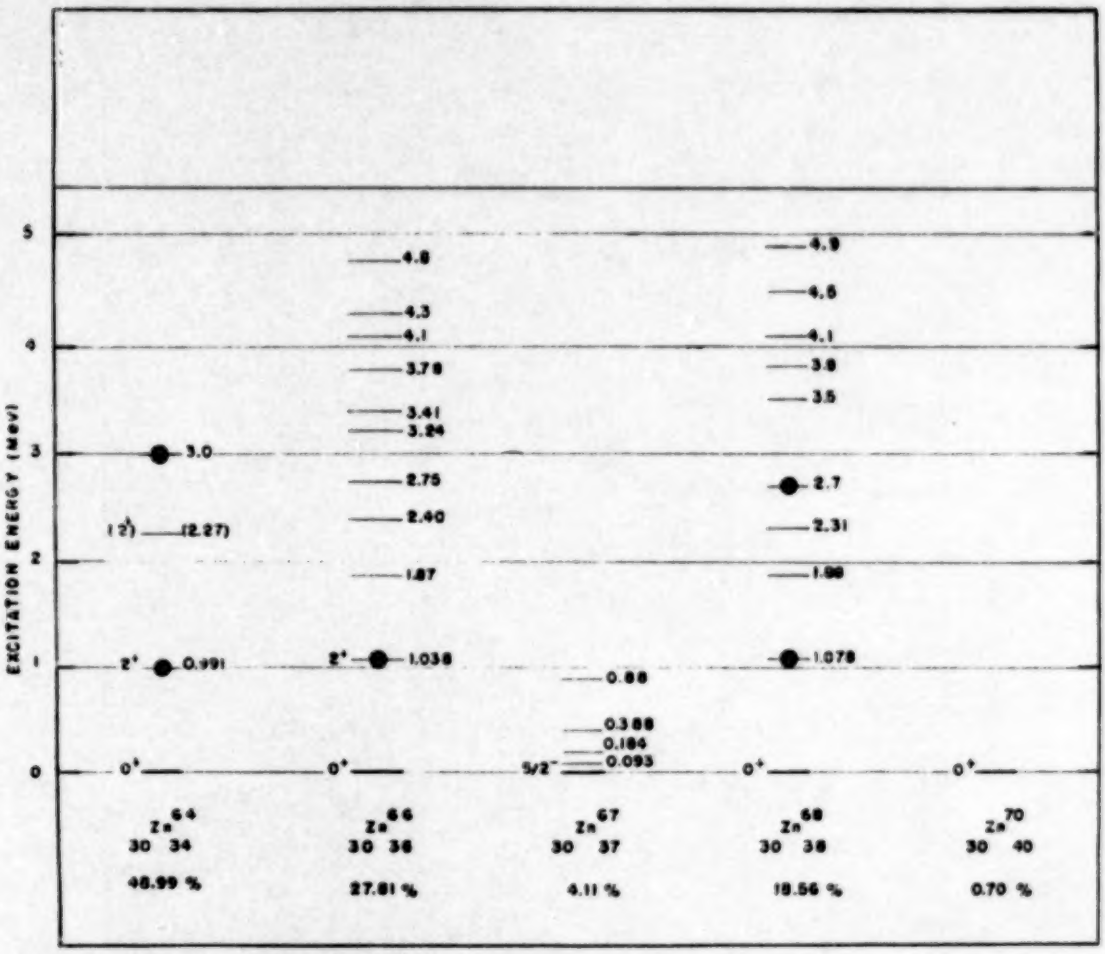

Fig. 4. Known states of Zn ($Z = 30$) up to 5 MeV excitation energy. Isotopic abundance, excitation energy, total angular momentum and parity are indicated (in parentheses where assignments are only probable). This chart summarizes the information contained in refs. [18]) and [19]). The energy levels of Zn^{68} are taken largely from ref. [2]) Levels strongly excited in elastic scattering of charged particles are indicated by solid black circles. The lowest 2^+ levels in the even isotopes have been strongly excited by protons [2, 20]) alpha particles [3, 5]) and deuterons [6]). The anomalous levels near 3 MeV also have been strongly excited by protons [2]), alpha particles [3, 5]) and deuterons [6]).

Typical alpha spectra for scattering from natural zinc and Zn^{64} targets were shown in fig. 1. These spectra have the same general features as those obtained by others through inelastic proton [2, 20]), alpha particle [3, 5]) and deuteron [6]) bombardment; there is strong excitation of the lowest 2^+ states as well as some states near 3 MeV. The measured excitation energy for the anomalous inelastic

group in natural zinc is 2.8 ± 0.1 MeV; this is actually probably made up of contributions from Zn^{64}(3.0 MeV; estimated here at 2.9 MeV from Zn^{64} data), Zn^{66}(2.75 MeV) and Zn^{68}(2.7 MeV).

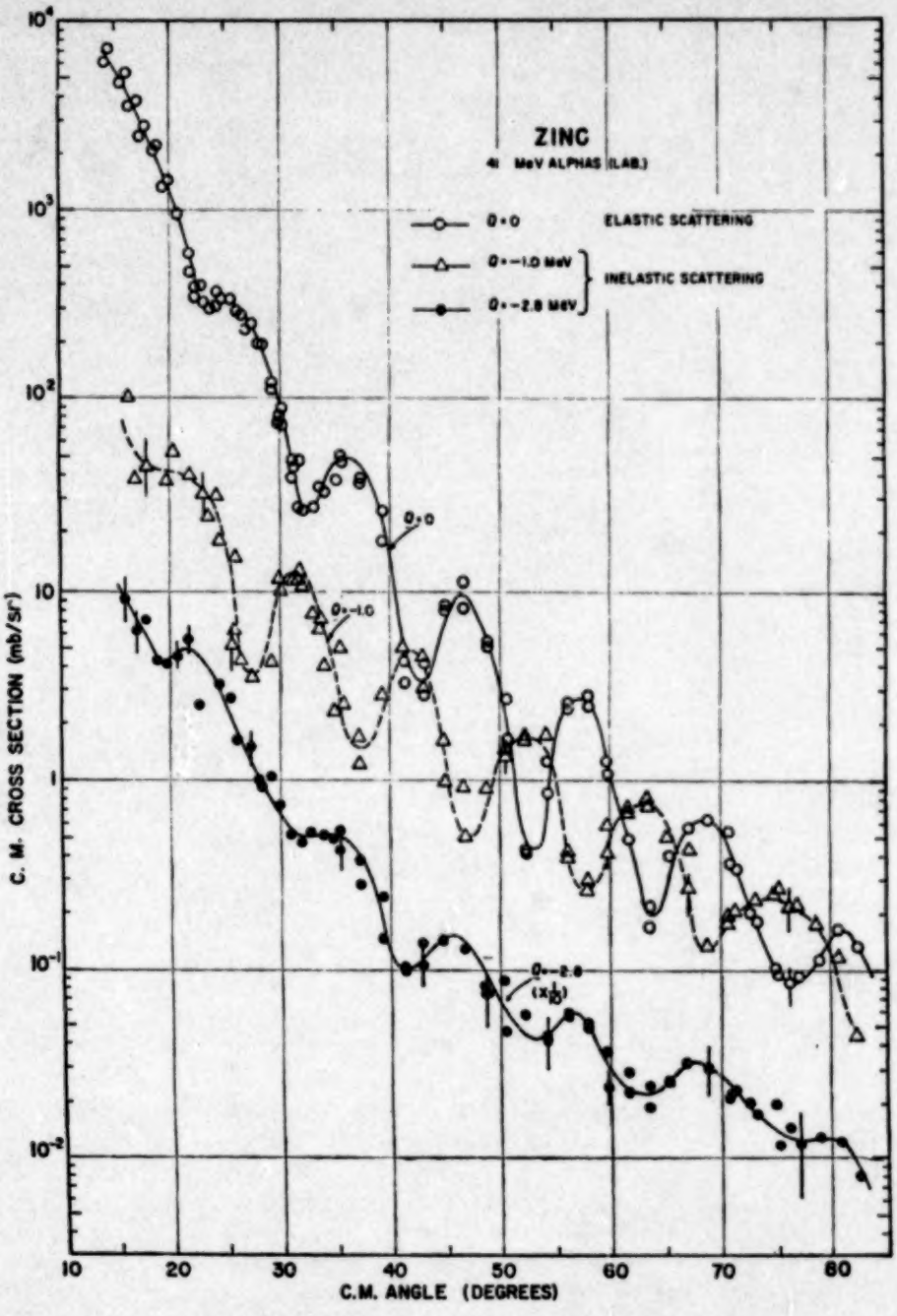

Fig. 5. Angular distributions for elastic and inelastic scattering of 41 MeV alpha particles by natural zinc. Experimental errors are shown for only a few representative points.

The differential cross sections for elastic scattering and inelastic scattering leading to the lowest 2^+ states and to the levels near 3 MeV are shown in fig. 5 for natural zinc and in fig. 6 for Zn^{64}. Angular distributions for the two targets

show great similarity. The only significant difference appears in the region of 15° to 35° (c.m.) for the anomalous groups; in this region the Zn^{64} spectra are generally sharper and allow more accurate estimates of the inelastic cross

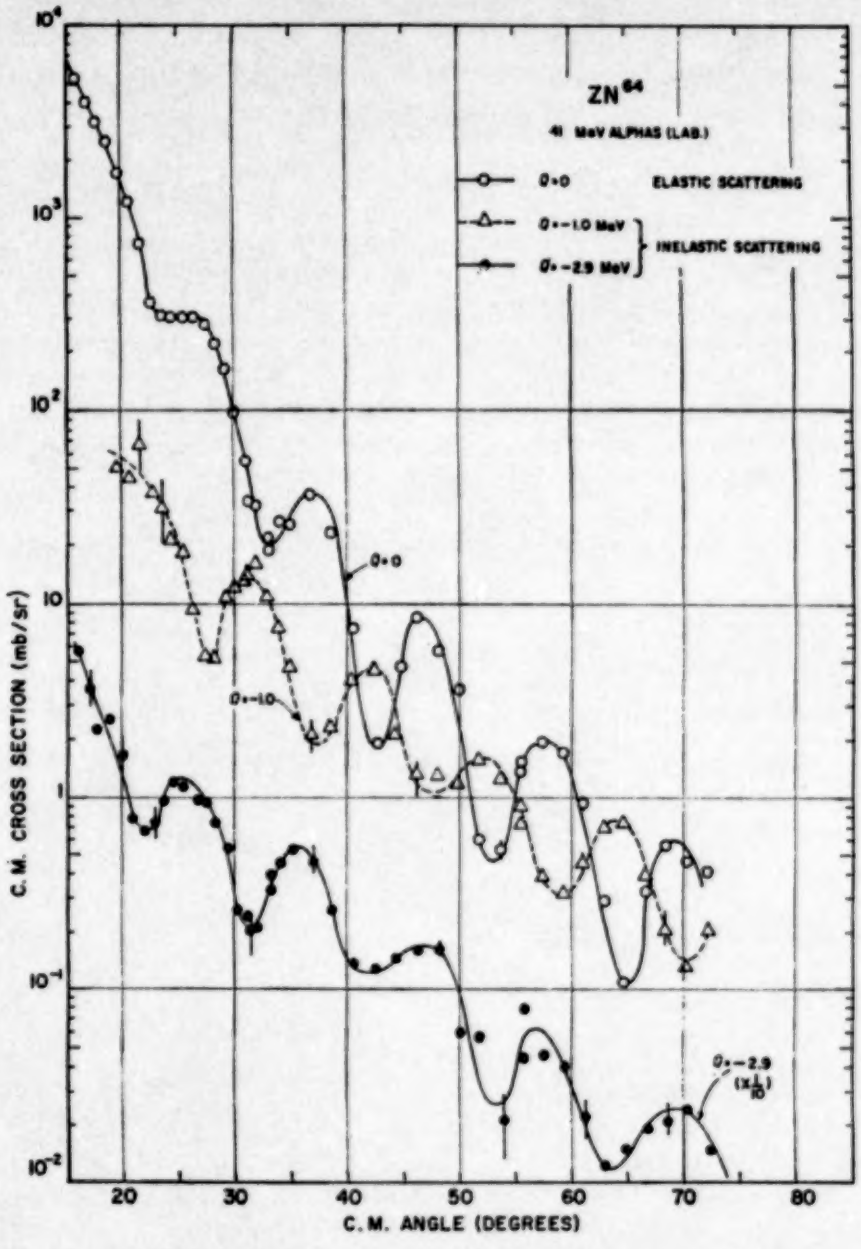

Fig. 6. Angular distributions for elastic and inelastic scattering of 41 MeV alpha particles by Zn^{64}.

sections. It also seems likely that the structure of the angular distribution for zinc in this region suffers from the presence of several contributions which are not precisely in phase.

In addition to these groups, a level in Zn with excitation energy of approximately 2.4 MeV was weakly excited; the angular distribution for alpha particles exciting this level was in phase with that for excitation of the 2^+ levels.

Scattering of 43 MeV alpha particles by natural zinc has been studied by Yntema, Zeidman and Raz [3]), who give angular distributions for elastic scattering and inelastic scattering with 3 MeV excitation. Their results are in good agreement with those shown in fig. 5, except that they find somewhat deeper minima and smaller cross sections at their largest angles for the inelastic group. The cross sections for 40 MeV alpha particles elastically scattered by the neighbouring element copper [21]) are somewhat higher at the maxima than our results for zinc.

3.2. NICKEL

Energy level data are summarized in fig. 7. A typical energy spectrum for alphas scattered from a natural nickel target was shown above in fig. 2. We

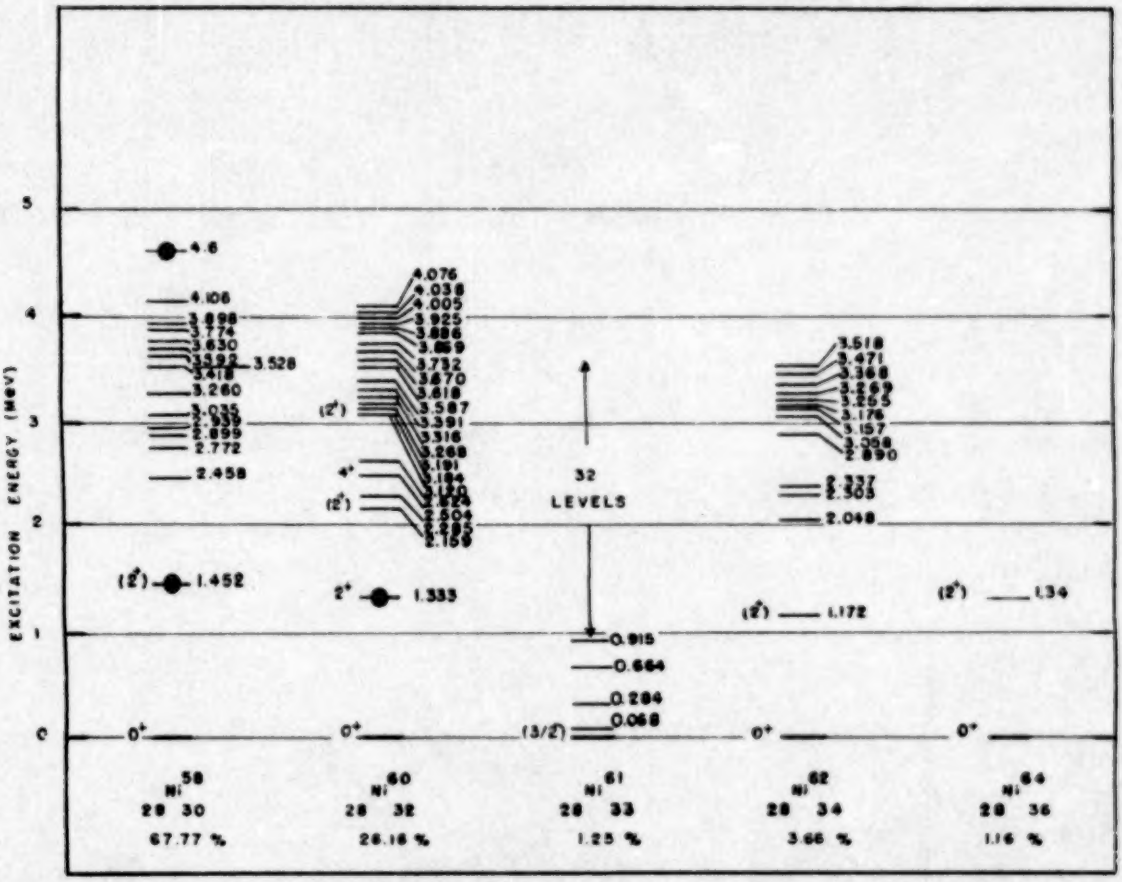

Fig. 7. Known states of nickel ($Z = 28$) to over 4 MeV. Excitation energies are chiefly from the work of the MIT-ONR generator group [22–24]). Angular momentum assignments are from ref. [18]). The lowest 2^+ levels of Ni^{58} and Ni^{60} have been strongly excited by protons [2, 20, 25]), alpha particles [3–5, 9]) and deuterons [6, 26]). The group near 4.6 MeV has been strongly excited by alpha particles [4, 5, 9]) and deuterons [6]).

find, again in accord with the work of others [2–6, 9, 20, 25, 26]), strong excitation of the first 2^+ levels and a level or group of levels with excitation energy of 4.6 MeV. There is weaker excitation of a group near 3.4 MeV.

The differential cross sections for elastic scattering and for inelastic scattering leading to the lowest 2^+ states and to the 4.6 MeV level or group of levels are presented in fig. 8.

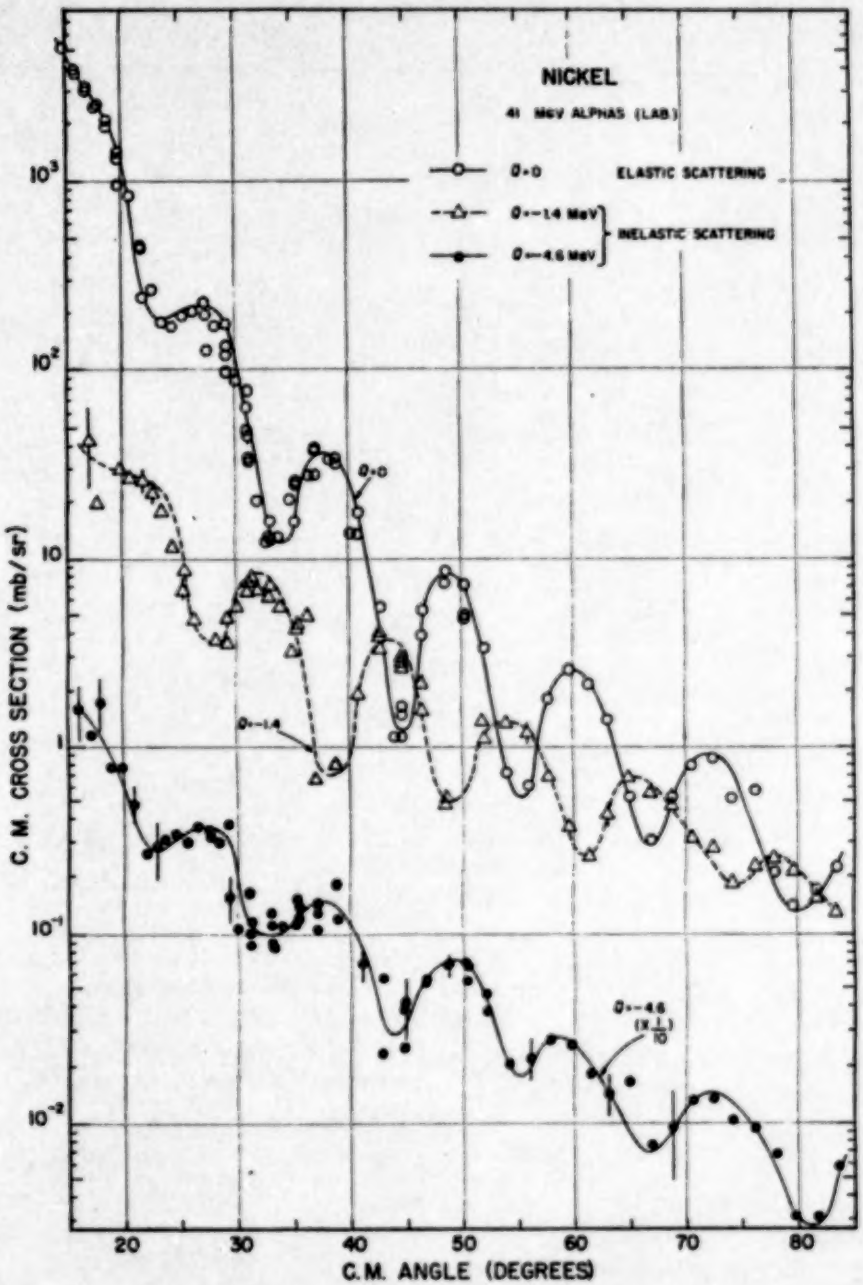

Fig. 8. Angular distributions for elastic and inelastic scattering of 41 MeV alpha particles by natural nickel. Experimental errors are shown for only a few representative points.

3.3. IRON

Energy level data are summarized in fig. 9. An energy spectrum for a target of natural iron was shown above in fig. 2. Isotopically enriched targets were not

prepared since natural iron is already 92 % Fe^{56}. The 2^+ level at 0.845 MeV and a level or group of levels at 4.2 MeV were strongly excited; other levels between 1 MeV and 4 MeV were observed at times but their excitation was usually weak.

Differential cross sections are given in fig. 10.

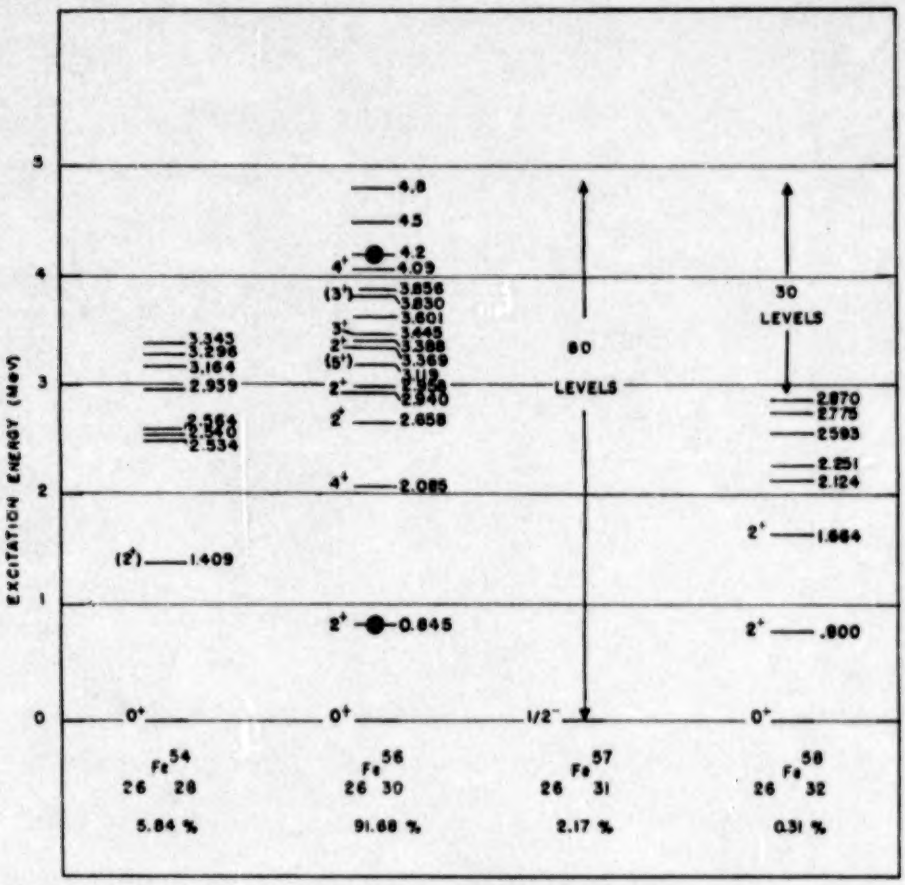

Fig. 9. Known states of iron ($Z = 26$) to 5 MeV. Excitation energies are chiefly from the work of the MIT-ONR generator group [27]). The angular momentum assignments are from refs. [18]) and [28]). The levels at 4.2, 4.5 and 4.8 MeV in Fe^{56} are according to Cohen and Rubin [2]). The lowest 2^+ level of Fe^{56} has been strongly excited by protons [2, 20, 25, 29]), while the group near 4.2 MeV has been excited by protons [2, 25]) and alpha particles [4]). The excitation energy shown in ref. [4]) is, however, about 5 MeV.)

3.4. TITANIUM

Energy level data are summarized in fig. 11. A typical energy spectrum for the Ti^{48} target (99.1 % Ti^{48}) was given above in fig. 2. The strongly excited levels are the groups near 1 MeV and 3.5 MeV.

It was possible to measure inelastic cross sections only in the range of scattering angles between 45° and 80°; these are presented, along with the elastic cross sections, in fig.12. There is excellent agreement between the elastic cross sections measured by Igo, Wegner and Eisberg [21]) and our results.

3.5. STRONTIUM

Energy level data are summarized in fig. 13. The 2^+ and 3^- levels of Sr^{88} at 1.85 and 2.76 MeV are clearly distinguishable in the alpha particle spectrum included in fig. 1.

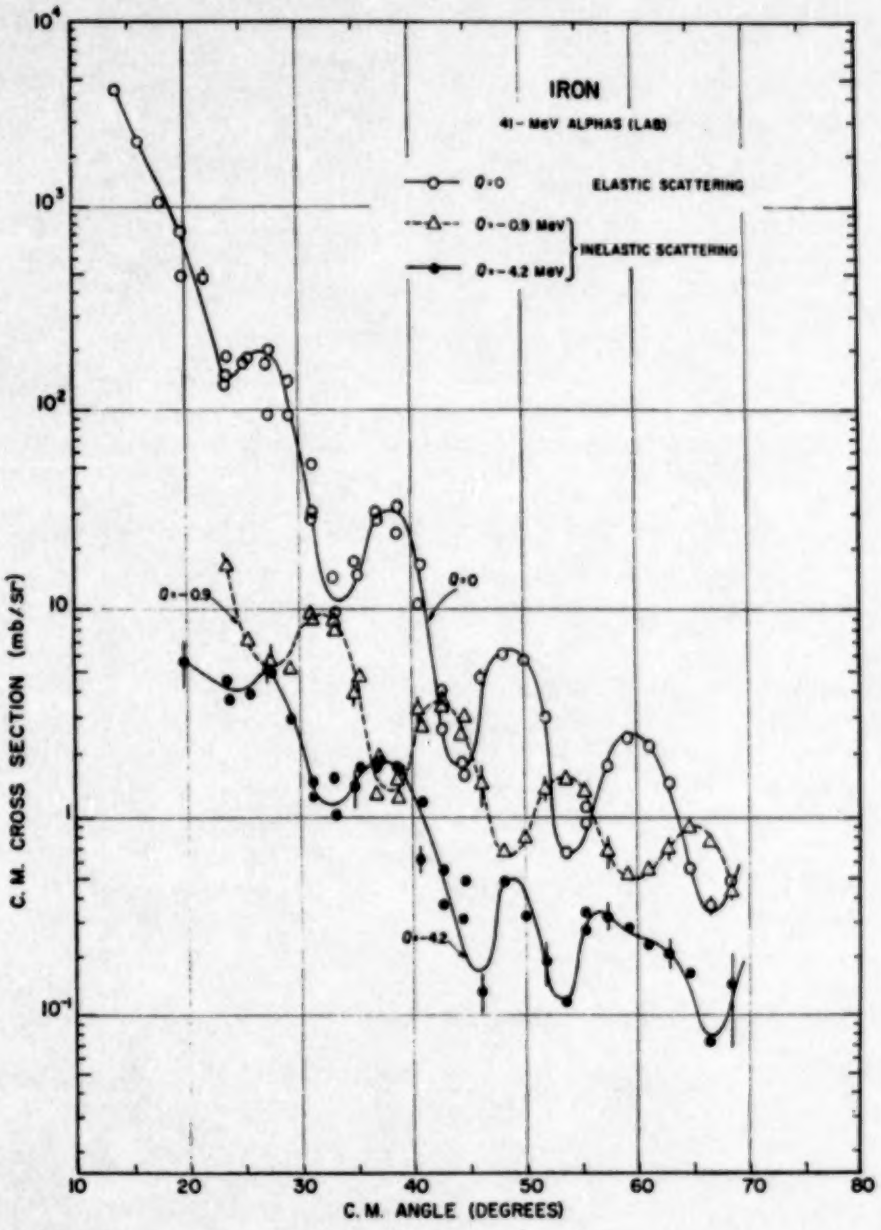

Fig. 10. Angular distributions for elastic and inelastic scattering of 41 MeV alpha particles by natural iron. Experimental errors are shown for only a few representative points.

Differential cross sections are shown in fig. 14. As in the case of Ti^{48}, oxygen contained in the target made it difficult to obtain inelastic cross sections at small angles.

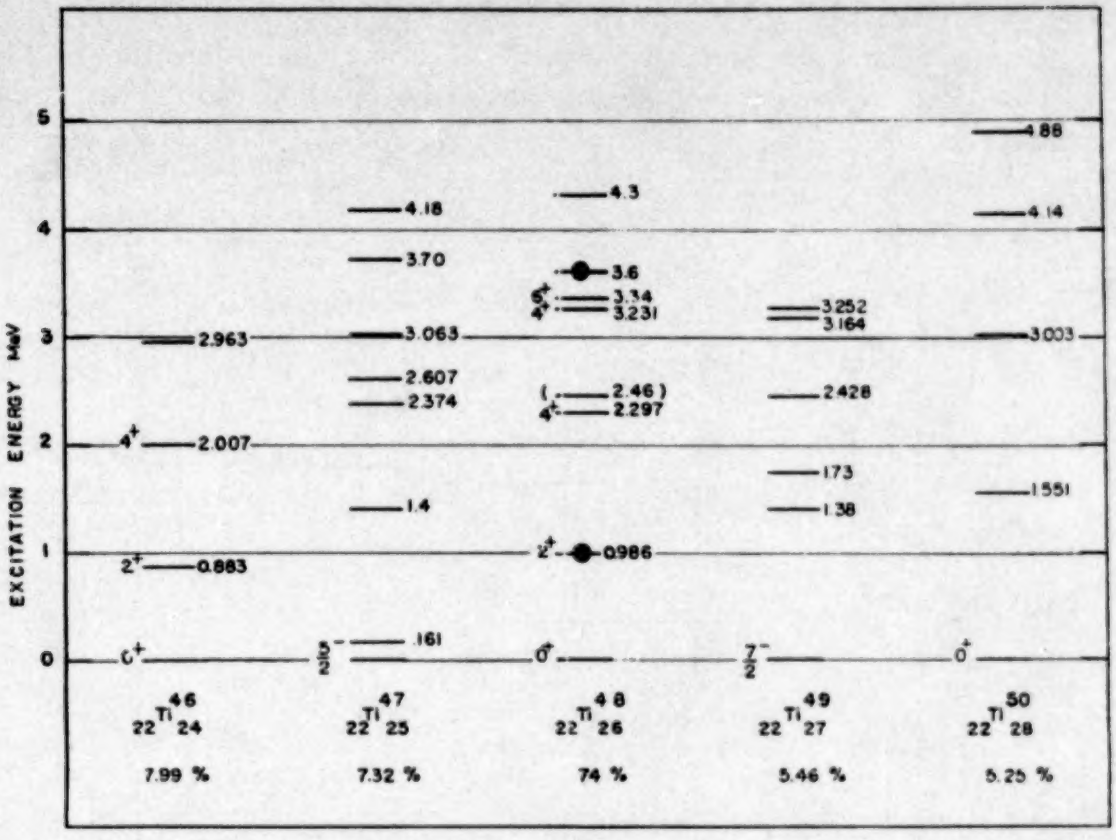

Fig. 11. Known states of natural titanium ($Z = 22$) up to 5 MeV excitation energy. This chart summarizes the results of the MIT-ONR generator group [30]) as well as the information contained in refs. [18]) and [19]). In addition, we include a state at 2.46 MeV, excited by 7 MeV protons [31]), which is attributed to Ti^{48}. The group near 1 MeV has been strongly excited by protons [25, 31]). It has been indicated [4]) that 30 MeV alpha particles produce considerable excitation at 1.3 MeV and 3.9 MeV. (Comparison between these energies, known levels and our own results suggests that the assignments of ref. [4]) have been slightly high and that the excitation corresponds to the level at 0.986 MeV and another near 3.6 MeV, tentatively assigned to Ti^{48}.)

4. Qualitative Conclusions

The angular distributions shown in figs. 5, 6, 8, 10, 12 and 14 exhibit striking similarities.

1) Regular and pronounced oscillations in both elastic and inelastic cross sections are observed whose periodicity increases with the mass number of the target. The results for Fe and Ni are almost interchangeable.

2) Average cross sections for anomalous excitations are lower than, but within one order of magnitude, of the corresponding cross sections for excitation of the 2^+ states.

3) For the five elements considered, the angular distribution of alpha particles exciting the lowest 2^+ levels is out of phase with the elastic scattering angular distribution. On the other hand, the angular distribution corresponding to the

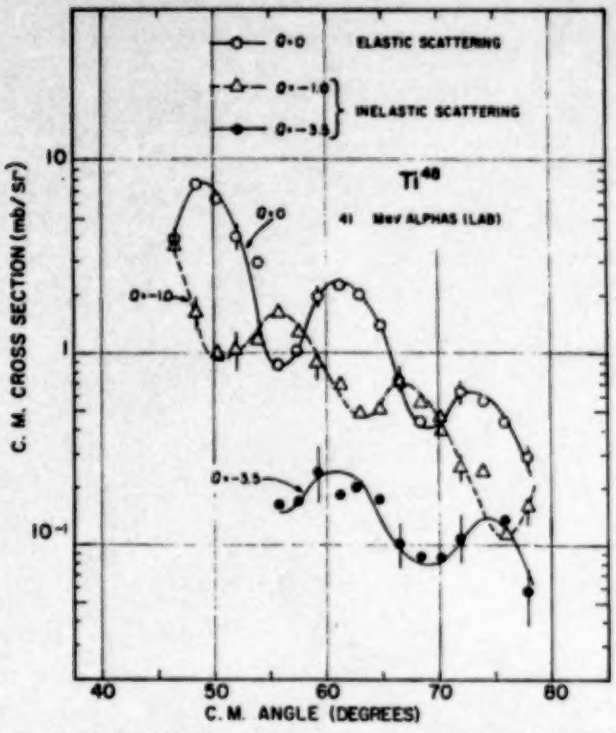

Fig. 12. Angular distributions for elastic and inelastic scattering of 41 MeV alpha particles by Ti^{48}. Experimental errors are shown for only a few representative points. Presence of oxygen in the target made the measurement of the cross sections at angles less than about 45° unfeasible because the energy resolution of the detector was inadequate to separate out the large elastic oxygen peak.

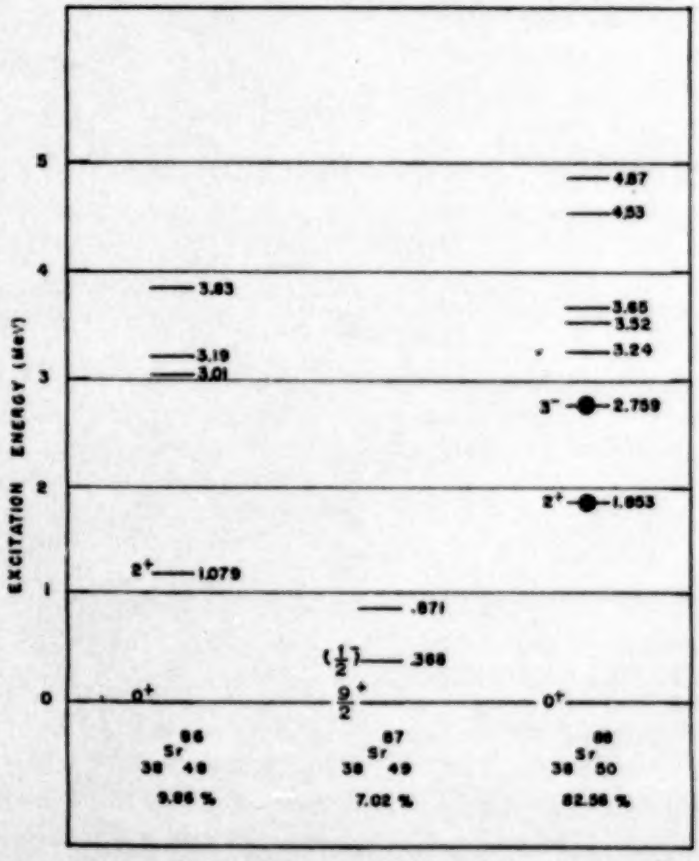

Fig. 13. Known states of natural Sr ($Z = 38$) up to 5 MeV excitation energy. This chart summarizes the information contained in refs. [18]) and [19]). The 2^+ and 3^- levels of Sr^{88} have been strongly excited by protons [2]) and electrons [17]).

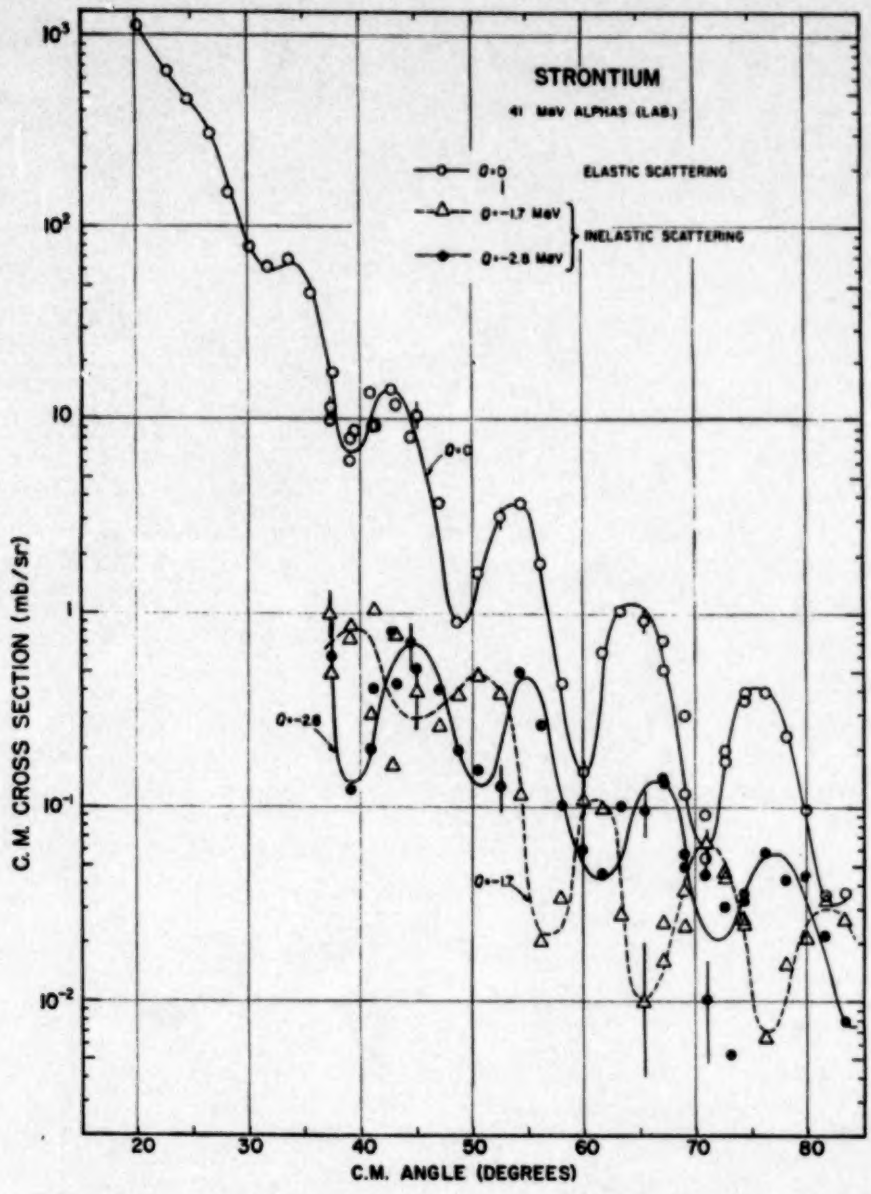

Fig. 14. Angular distributions for elastic and inelastic scattering of 41 MeV alpha particles by natural strontium. Experimental errors are shown for only a few representative points. Presence of oxygen in the target made the measurement of the cross sections at angles less than about 45° unfeasible because the energy resolution of the detector was inadequate to separate out the large elastic oxygen peak.

anomalous group is in phase with the elastic pattern. We believe this difference in phase relationships strongly suggests that all the contributing levels in the anomalous groups have odd parity; this conclusion is independent of the particular model assumed in analyzing the results (sec. 5).

The fact that the angular distributions for the anomalous levels are essentially as sharp as those corresponding to excitation of a single 2^+ level suggests that levels of differing character which also occur at or near these energies are not

strongly excited and that the levels which do contribute to the anomalous group are either single or similar in character. Our results are thus consistent with the statement that there is only one strongly excited odd-parity state in an even isotope; better energy resolution would be required, however, for a conclusive demonstration of its validity.

The present results therefore lend strong support to the Lane-Pendlebury-Levinson conjecture that the anomalous levels correspond to an octupole surface vibration, since this conjecture would lead to the following conclusions:

1) The properties of the octupole states should vary in a fairly continuous fashion through the periodic table. (The gross structure studies of the anomalous group by Cohen and Rubin have particularly suggested such a uniform variation [2]) and the present results add to the evidence.)

2) The properties of the octupole and quadrupole states should be related. (While the simple hydrodynamical model is not quantitatively reliable, it may provide some orientation concerning ratios of excitation energies and cross sections. These points are discussed further in sec. 5.)

3) For an even isotope in the Goldhaber-Weneser region [16]), there should be but a single surface octupole state, with $J = 3$ and odd parity, which is strongly excited through inelastic scattering.

5. Analysis: Strong Absorption Diffraction Scattering

5.1. GENERAL CONSIDERATIONS

Simple direct interaction theories have enjoyed considerable success in explaining inelastic alpha particle angular distributions [32–37]). All such theories, however, crucially employ the approximation that both incident and final unbound particies are well represented by plane waves over the entire nuclear surface region, an approximation which appears counter to the evidence for large nuclear attenuation [38, 39]), or equivalently, the success of "black nucleus" expressions for the elastic cross sections [14, 40]). A further difficulty is that different interaction radii must be assumed in order to fit the data for both elastic and inelastic scattering by a given target nucleide.

An alternative model, the inelastic diffraction mechanism, has been introduced by Drozdov [41]) to discuss inelastic neutron scattering from ellipsoidally deformed nuclei; this has been extended by Inopin [42]) to excitation of quadrupole vibrational states and generalized by one of the present authors [13]) to deformations of arbitrary multipolarity. In contrast to the plane wave assumption, one assumes that the nucleus is strongly absorbing within a radius which is a function of collective deformation coordinates α of the nuclear surface. Making further the adiabatic assumption, one obtains approximate expressions for the inelastic scattering amplitudes which are very similar to the analogous plane wave results.

Both the plane wave calculations (when employing only one value for the interaction radius, however) and the Drozdov diffraction mechanism yield the result that, beyond the initial maxima, the inelastic angular distributions associated with no parity change are out of phase with the elastic angular distribution, while those associated with a parity change are in phase with the elastic. The correspondence between these predictions and the present experiments as well as previous ones [13, 15]) suggests that this feature can be used as a tool for determining the parity of excited states, even when there are some disagreements between experiment and other predictions of the simple theories.

Detailed analysis of the present experiments will be made only in terms of the diffraction mechanism. Not the least of the virtues of this model is that, since an effective interaction radius will be determined from analysis of the elastic angular distribution, the only free parameters relating to the magnitude of the inelastic cross sections are the values of the collective matrix elements.

Simple expressions for elastic and inelastic scattering cross sections may be derived through use of the following assumptions and approximations:

1) the nucleus is considered to be strongly absorbing within the sharp radius

$$R(\theta, \Phi) = R_0(1+\sum_{l,m} \alpha_{lm} Y_{lm}),$$

where α_{lm} is a collective surface deformation parameter;

2) the scattered amplitude may be calculated in the adiabatic approximation;

3) the scattered amplitude is expanded only to terms linear in α_{lm};

4) the Fraunhover approximation is used to compute the scattered amplitude;

5) Coulomb effects are neglected.

The elastic scattering cross section in the centre of mass system is then the familiar result for scattering from a black sphere:

$$\frac{\mathrm{d}\sigma_{\mathrm{el}}}{\mathrm{d}\Omega} = \cos^2 \tfrac{1}{2}\theta (kR_0^2)^2 \left\{ \frac{J_1(2kR_0 \sin \tfrac{1}{2}\theta)}{2kR_0 \sin \tfrac{1}{2}\theta} \right\}^2, \qquad (1)$$

where k is the c.m. wave number and θ is the c.m. angle of scattering. The inelastic scattering cross section for quadrupole surface excitation of an even nucleus is [13, 42])

$$\frac{\mathrm{d}\sigma}{\mathrm{d}\Omega}(0 \to 2)$$

$$= \frac{5}{4\pi} \cos^2 \tfrac{1}{2}\theta (kR_0^2)^2 \left| \langle 2m | \alpha_{2m} | 00 \rangle \right|^2 \{ \tfrac{1}{4} J_0^2(2kR_0 \sin \tfrac{1}{2}\theta) + \tfrac{3}{4} J_2^2(2kR_0 \sin \tfrac{1}{2}\theta) \}. \qquad (2)$$

The inelastic scattering cross section for octupole surface excitation of an even nucleus is [13])

$$\frac{\mathrm{d}\sigma}{\mathrm{d}\Omega}(0 \to 3)$$

$$= \frac{7}{4\pi} \cos^2 \tfrac{1}{2}\theta (kR_0^2)^2 \left|\langle 3m|\alpha_{3m}|00\rangle\right|^2 \{\tfrac{3}{8} J_1^2(2kR_0 \sin \tfrac{1}{2}\theta) + \tfrac{5}{8} J_3^2(2kR_0 \sin \tfrac{1}{2}\theta)\}. \quad (3)$$

The argument of the Bessel functions corresponds to a shadow line which is a projection of the nuclear surface onto a plane containing the momentum transfer vector $\mathbf{K} \equiv \mathbf{k}_i - \mathbf{k}_f$, and perpendicular to the scattering plane †.
For consistency the obliquity factor $\cos^2 \frac{1}{2}\theta$ is included in both the elastic and inelastic scattering cross sections. It is convenient to characterize the collective matrix elements either by the surface tension parameter C_l which occurs in the weak coupling prediction $\left|\langle lm|\alpha_{lm}|00\rangle\right|^2 = \hbar\omega_l / 2C_l$, or by the equilibrium deformation parameter β_l which occurs in the strong coupling prediction $\left|\langle lm|\alpha_{lm}|00\rangle\right|^2 = \beta_l^2/(2l+1)$.

TABLE 1

Interaction radii R_0 obtained by diffraction analysis of elastic scattering data

Target	R_0 (10^{-13} cm)
Ti^{48}	6.51
Fe	6.88
Ni	6.83
Zn	7.08
Zn^{64}	7.10
Sr	7.44

The interaction radii R_0 are determined by matching the locations of the maxima and minima of eq. (1) to the experimental elastic scattering angular distributions. These radii are listed in table 1.

5.2. ELASTIC SCATTERING

Since the interaction radius is the only parameter contained in the expression for the elastic scattering cross section, it is instructive to compare the magnitudes of the experimental cross sections with eq. (1). As a typical example, the experimental and predicted elastic scattering cross sections for Ni are shown in fig. 15. For very small angles the experimental cross section rises considerably above the predicted cross section, due to the presence of the Coulomb field. Only for scattering angles in the neighbourhood of 30° does eq. (1) correctly estimate the magnitude of the elastic scattering cross sections for Ni and the other intermediate nuclei here under study.

The elastic scattering cross section may also be computed for the closely related sharp cutoff model, including the influence of the Coulomb field [43]).

† See ref. [13]) for a discussion of possible shadow line choices.

Such a calculation has been made for elastic scattering of 40 MeV alpha particles from the neighbouring element Cu($Z = 29$) and the results are compared with the present data. The computed sharp cutoff cross section is in good agreement with the rapidly increasing experimental cross section at small angles. However, it is about a factor of 2 larger than the Fraunhofer cross section at the larger angles; thus both the sharp cutoff and the Fraunhofer predictions fail to follow

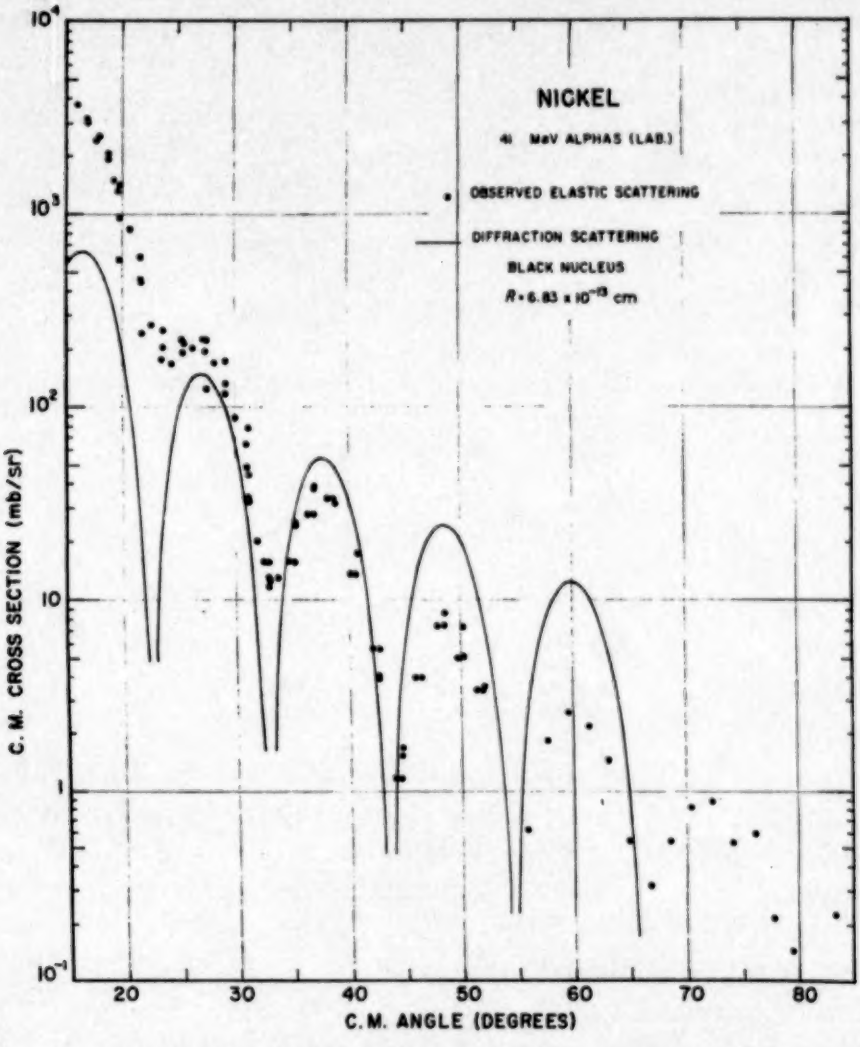

Fig. 15. Comparison of the observed angular distribution for elastic scattering of 41 MeV alpha particles by nickel with the predictions of the diffraction theory as given by eq. (1). The only adjustable parameter is the interaction radius R_0.

the rapidly dropping experimental cross sections at higher orders of the diffraction pattern. (This is a well-known ailment which can be remedied in optical model calculations by using a diffuse-edged potential [38, 39, 44]), or in strong absorption models by softening the transition from no absorption to complete absorption [45]).

In comparing the diffraction results with the sharp cutoff results we note also

that the interaction radii R_0 corresponding to eq. (1) are significantly smaller than the corresponding sharp cutoff Coulomb radii [40, 46]). This discrepancy is essentially removed if in eq. (1) we employ an effective wave number at the nuclear radius k_{eff} which takes into account the repulsive Coulomb potential:

$$k_{eff} = k(1-V(R_0)/E)^{\frac{1}{2}}.$$

5.3. INELASTIC SCATTERING

Application of the inelastic diffraction formulas (2) and (3) is here considered justifiable under the following conditions: 1) the inelastic scattering angular distribution must be appropriately phased with respect to the elastic scattering pattern (this is equivalent to the requirement that both the elastic and the inelastic scattering angular distributions be fitted using but one value of the interaction radius R_0); 2) the magnitudes of the observed elastic scattering cross sections should be correctly given by eq. (1) in the angular region in which it is desired to match the observed inelastic scattering cross sections. The first requirement is satisfied in all the present experiments; the second requirement is reasonably satisfied only in the neighbourhood of 30°.

Typical comparisons between the inelastic diffraction formula predictions of eqs. (2) and (3) and the experimental cross sections are made in figs. 16 and 17 for inelastic excitation of the lowest 2^+ and anomalous levels of Ni. Because of the limited angular range, it is not possible to match our data on Ti^{48} and Sr to the predicted magnitudes of the inelastic cross sections in an angular region where the latter can be reliably computed; rough estimates of the collective parameters of Sr and Ti^{48} have been made, however, through comparison to the cross sections for Zn^{64} and Ni at the larger angles and through use of the assumption that the scattered amplitudes at such angles are still linear in α_{lm}. Values of the collective parameters determined by fitting the observed inelastic cross sections to eqs. (2) and (3) are presented in tables 2 and 3.

TABLE 2

Parameters characteristic of the lowest 2^+ states. Column 2 gives the radius R_0 which results from analysis of the elastic scattering angular distributions in terms of the Fraunhofer spherical black nucleus cross section, eq. (1). Column 3 contains the scattering angle θ_n at which the magnitude of the experimental cross section is normalized to eq. (2). The resulting deformation parameter β_2 and surface tension C_2 are given in columns 4 and 5. Column 6 gives for comparison the corresponding electromagnetic parameter C_2(EM) as determined from electric quadrupole transition probabilities.

Nucleus	R_0 (10^{-13} cm)	θ_n	β_2	C_2 (MeV)	C_2(EM) (MeV)
Ti^{48}	6.51		≈0.15	≈120	82
Fe	6.88	32°	0.11	160	34
Ni	6.83	22°	0.15	160	88 (Ni^{60})
Zn	7.08	22°	0.19	70	
Zn^{64}	7.10	22°	0.19	70	59
Sr	7.44		≈0.08	≈800	220 (Sr^{88})

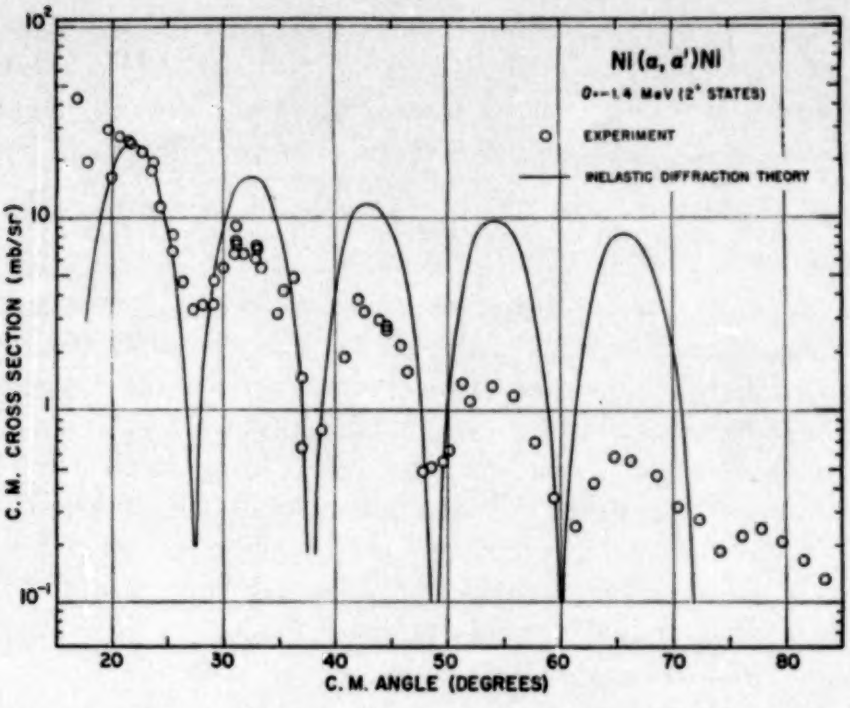

Fig. 16. Comparison between the strong absorption inelastic diffraction theory predictions of eq. (2) and the experimental cross sections for inelastic scattering with excitation of the lowest 2^+ states of nickel. The theoretical curve is normalized to experiment at 22° and corresponds to the value of the surface tension parameter C_2 given in table 2.

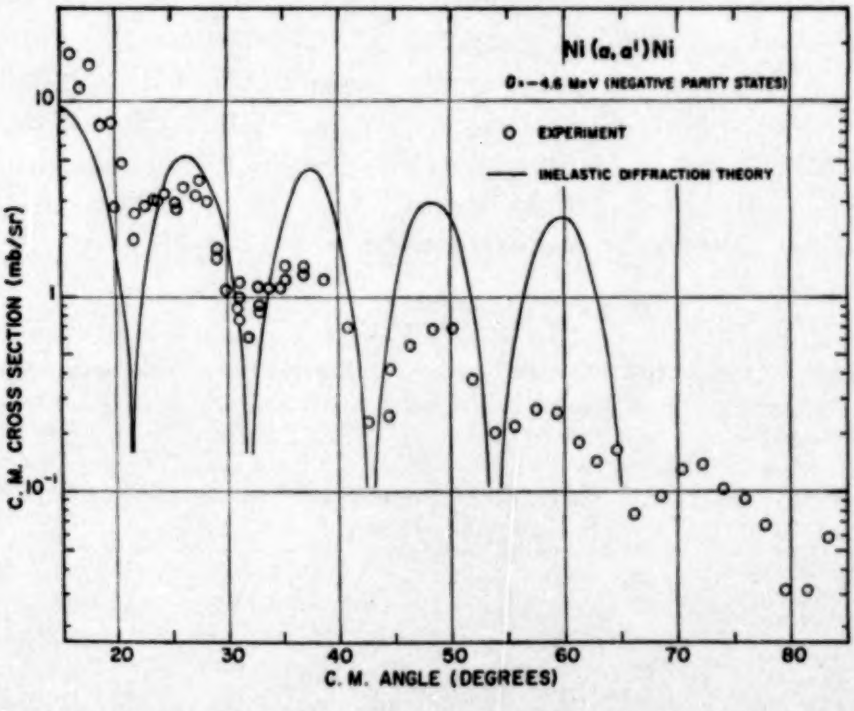

Fig. 17. Comparison between the strong absorption inelastic diffraction theory predictions of eq. (3) and the experimental cross sections for inelastic scattering with excitation of the anomalous level (or levels) of nickel. The theoretical curve is here normalized to make a compromise between a fit to experiment at 16° and a fit at 27°; the corresponding surface tension parameter C_3 is thus lower than that given in table 3.

TABLE 3

Parameters characteristic of the anomalous excited states. Column 2 gives the scattering angle θ_n at which the magnitude of the experimental cross section is normalized to eq. (3). The resulting surface tension C_2 and deformation parameter β_2 are listed in columns 3 and 4.

Nucleus	θ_n	C_2	β_2
Ti^{48}		≈ 2700	≈ 0.06
Fe	27.5°	2700	0.07
Ni	27°	4000	0.06
Zn^{64}	25°	900	0.10
Sr		≈ 2000	≈ 0.07

In view of the large Coulomb distortion of the cross sections at forward angles † and the rapid falloff below the sharp radius predictions at larger angles, not to mention the many approximations of the theory, it is not expected that the collective matrix elements should be given with precision by the diffraction scattering analysis of our results. (The difference between the values of β_2 for Ni and Fe given in table 2 should not be a matter of concern. The absence of reliable cross sections for excitation of the lowest 2^+ level in Fe near 22° made it necessary to match the theoretical cross section at the next maximum, which occurs at 32°. We note, however, that the cross sections for Ni and Fe are nearly identical at this angle as well as at larger angles.) Indeed, agreement with other estimates of squares of the matrix elements to within a factor of two should be regarded as excellent corroboration of the collective excitation hypothesis. In sec. 5.4. we turn to a consideration of other experiments which provide such estimates.

We should note first, however, that the collective deformation parameters α_{lm} corresponding to the values found for β_l are probably (as here defined) underestimates of the true nuclear deformation. The sharp radius $R(\Theta, \Phi)$ should be viewed as a sum of the interaction radii of an alpha particle and the nucleus, $R_\alpha + R_N(\Theta, \Phi)$, where it is the nuclear radius which is related to the deformation parameter:

$$R_N = R_{0N}(1 + \sum_{l,m} \alpha_{lm}^N Y_{lm}).$$

With this modified definition, we obtain the same diffraction formulas as before except that eqs. (2) and (3) are multiplied by the factor $(R_{0N}/R_0)^2$ and contain the true nuclear deformation parameter α_{lm}^N. The large interaction radii generally resulting from analyses of alpha particle scattering observations may be fitted with expressions of the form $R_0 = a + bA^{\frac{1}{3}}$, where the constant a is typically of the order [46]) of 2×10^{-13} cm. It is plausible to attribute a large

† Approximate formulas for quadrupole excitation which include Coulomb excitation are given in reference [13]), eqs. (5.8) and (5.9); these formulas, however, have merit only for small nuclear charge and very small angles, and thus are not applicable to the present experiments.

share of this constant to the radius of the alpha particle itself. If this is done in the present case, the resulting values of C_l^N are half those listed for C_l in tables 2 and 3.

5.4. OTHER ESTIMATES OF COLLECTIVE PARAMETERS

Evidence indicating collective transitions between the low-lying even-parity levels of light nuclei has been provided by Coulomb excitation experiments [12]) and studies of the systematics of gamma ray transitions [16]). The E2 transition probabilities between the ground and lowest 2^+ states of intermediate even nuclei are generally well above the single-particle estimates and accordingly have been interpreted in terms of the surface vibrations of a uniformly charged nucleus of radius $R(\mathrm{EM}) = 1.2A^{\frac{1}{3}} \times 10^{-13}$ cm. The lifetimes given in ref. [18]) have been used to compute the surface tension parameters $C_2(\mathrm{EM})$ given in table 2. (For Ni^{60} we have adopted the lifetime given by Metzer [47]) resulting from a nuclear resonance fluorescence experiment, while for Ti^{48} we have taken the lifetime determined from a Coulomb excitation experiment [48]).

The ratio of the collective estimate for the quadrupole transition probability to the corresponding single particle prediction is

$$\frac{B(\mathrm{E2}; 0 \to 2)}{B_{\mathrm{s.p.}}(2)} = 0.40[Z\beta_2(\mathrm{EM})]^2 = 1.00\,\frac{Z^2\hbar\omega_2}{C_2(\mathrm{EM})}\,; \tag{5}$$

this result applies under both uniform and non-uniform charge density assumptions [8, 49]). Inserting the quadrupole parameters of table 2 into eq. (5), we find that the collective to single particle ratio comfortably exceeds unity.

It is not at all obvious to us what is the appropriate quantitative relation between a deformed charge distribution and a deformed interaction radius. In view of this uncertainty and the ambiguities of the analyses, the agreement to within a factor of 4 between the electric and diffraction quadrupole surface tension parameters should be regarded as reasonable accord and strengthens our belief that the process of inelastic scattering is described correctly by the strong absorption diffraction model.

Electric octupole transition probabilities have been measured for two intermediate nuclei by means of inelastic scattering of high energy electrons [17]) and are also found to exceed the single particle estimates. When excitation of the 2.76 MeV 3^- level of Sr^{88} is interpreted in terms of the surface vibrations of a uniformly charged nucleus, the electromagnetic surface tension parameter $C_3(\mathrm{EM})$ is determined to be 210 MeV or equivalently $\beta_3^2(\mathrm{EM}) = 0.046$. Similarly in the excitation of the 3.73 MeV level of Ca^{40}, $C_3(\mathrm{EM}) = 75$ MeV or $\beta_3^2(\mathrm{EM}) = 0.175$. (Considering the vibrations to be those of the non-uniform charge density determined by electron scattering experiments, Lane and Pendlebury [8]) find values of $C_3(\mathrm{EM})$ which are a factor of 2 and 5, respectively, higher than those given above. The relevant moment of the non-uniform charge

density occurring in the electric octupole matrix element gives extra weight to the tail of the distribution so that the effective radius will exceed the mean radius; this difference in effective radii then leads to differing estimates of the surface tension parameter.)

The octupole surface parameters shown in table 3 are a factor of 10 larger than the values of C_3(EM) for Sr^{88} and Ca^{40} which result when a uniform charge density is assumed; the difference is less when a non-uniform charge density is employed and, indeed, Lane and Pendlebury [8]) estimate on theoretical grounds that C_3(EM) will be of the order of 1000 MeV for medium weight nuclei.

Should the magnitude of C_3(EM) turn out to be much larger than 1000 MeV for the intermediate nuclei, the question should be raised whether such values are consistent with a collective description. The ratio of the collective prediction for the octupole transition probability to the single particle estimate is

$$\frac{B(\mathrm{E3};\, 0 \to 3)}{B_{\mathrm{s.p.}}(3)} = 0.41[Z\beta_3(\mathrm{EM})]^2 = 1.43\,\frac{Z^2\hbar\omega_3}{C_3(\mathrm{EM})}\,, \tag{6}$$

when a uniform charge distribution is assumed. If the electric octupole oscillations are characterized by the octupole parameters given in table 2, then the ratios of collective to single-particle transition probability estimates are only slightly larger than unity.

However, as noted previously, since each interaction radius of table 1 should be considered as the sum of an alpha particle radius and a specifically nuclear radius, the values for C_2 and C_3 in tables 2 and 3 are probably overestimates by a factor of 2. Further, with a non-uniform charge density the ratio of collective to single-particle octupole transition probabilities should be more than 50 % greater than the uniform density prediction eq. (4) for intermediate mass nuclei [8]). We conclude that a collective description of the octupole excitations is reasonable, although the evidence is not as clear as in the case of the quadrupole excitations.

5.5. RESULTS OF OTHER RECENT SCATTERING EXPERIMENTS

We have mentioned previously other investigations of the anomalous levels by means of alpha particle scattering. Through arguments essentially equivalent to ours concerning the relative phases of angular distributions, Robison and Farwell [15]) conclude that $I = 3$ is the most plausible assignment for the 4.98 MeV level in S^{32}. Similarly, Yntema, Zeidman and Raz [3]) suggest $I = 3$ for the 3 MeV group in Zn. Crut and Wall [9]) come to the same conclusion regarding the anomalous states of Ni^{58} and Ni^{60}, basing their arguments on an $(\alpha, \alpha'\gamma)$ angular correlation experiment as well as on angular distributions. The cross sections for elastic scattering of alpha particles by Ag and Rh as well as those for inelastic scattering with excitation of a 2.5 MeV group in each of these elements have been measured by Yntema, Zeidman and Raz [3]). We note that

the inelastic scattering angular distribution for Rh is in phase with the elastic scattering pattern over a range of three maxima and minima; this observation again suggests the interpretation that the anomalous levels in these elements have parity opposite to that of the ground state and are similar in nature to those found in the lighter nuclei †.

There has been a preliminary report of the scattering of 21.6 MeV deuterons from Ni by Braid, Yntema and Zeidman [50]). The oscillations in the elastic scattering angular distributions are out of phase with those corresponding to excitation of the 1.45 MeV 2^+ state in Ni^{58} over 3 maxima and minima; the location of these maxima and minima are consistent with eqs. (1) and (2) where the interaction radius for deuterons is essentially the same as that appropriate to alpha particles. At corresponding orders of the diffraction patterns, the magnitudes of the deuteron and alpha particle cross sections should be in the ratio k_d^2/k_α^2. On the basis of our experiments with 41 MeV alpha particles, we would anticipate that the maximum in deuteron cross section at 40° would have the value 7 mb while that at 65° would be 1.7 mb. The observed deuteron cross sections at these points are 4.5 mb and 0.8 mb. Further comparisons of alpha particle and deuteron data are given in the paper which follows [51]).

The angular distributions of protons which are scattered elastically as well as with excitation of the first 2^+ levels have been reported for the elements Ti, Cr, Fe, Ni and Zn by the University of Tokyo cyclotron group [20, 25]) and for Fe by Schranck, Gugelot and Dayton [29]). We anticipate that inelastic cross sections computed either in the plane wave approximation [32–37]) or with the strong absorption diffraction model will have only qualitative relevance for bombardment by medium energy nucleons; for such projectiles the nucleus appears to be neither transparent nor black. Neither of the criteria for application of the inelastic diffraction model, which were stated above, are satisfied for these experiments; the elastic scattering cross section does not correspond to eq. (1) and the elastic and inelastic scattering oscillations are more nearly in than out of phase with one another. In addition, both elastic and inelastic cross sections increase rather than decrease with decreasing wave number k. Nonetheless for 14.1 MeV protons the maxima in the inelastic cross sections occurring near 40° and the minima near 70° do correspond to a reasonable value for an interaction radius, namely 5.5×10^{-13} cm. Naive application of eq. (2) to the forward maxima leads to values of $|\beta_2|$ which are approximately twice those

† *Note added in proof:* Measurements of elastic and inelastic scattering of 44.4 MeV alpha particles from isotopes of Zn have been reported by Beurtey, Catillon, Chaminade, Faraggi, Pahineau and Thirion [52]). Their observed angular distributions are consistent with our measurements and have been interpreted in terms of the diffraction scattering model. The magnitudes of their inelastic cross sections from Zn^{64} are, however, somewhat smaller than our results at corresponding maxima in the diffraction patterns. The above authors together with M. Crut and J. Saudinos (to be published) also have measured the inelastic scattering cross sections from Ni isotopes which are in general accord with our observations with the natural Ni target.

determined from the alpa particle experiments. Kikuchi, Kobayashi and Matsuda [25]) have also measured the inelastic scattering cross section for excitation of the 4.6 MeV level in Fe^{56}. The angular distribution for angles less than 90° suggests the broad forward double hump appropriate to octupole diffraction scattering, eq. (3). Application of this equation leads to $|\beta_3| \approx 0.17$, a value which is double that given in table 3.

The authors wish to thank Doctors J. L. Yntema, B. Zeidman, B. J. Raz, A. M. Lane and E. D. Pendlebury, and Professors C. A. Levinson, J. A. McIntyre and N. S. Wall for helpful discussion and communication of results prior to publication.

References

1) B. L. Cohen, Phys. Rev. **105** (1957) 1549
2) B. L. Cohen and A. G. Rubin, Phys. Rev. **111** (1958) 1568
3) Yntema, Zeidman and Raz (to be published)
4) D. R. Sweetman and N. S. Wall, C. R. Congr. Int. Phys. Nucl. (Dunod, Paris, 1959) 549
5) H. W. Fulbright, N. O. Lassen and N. O. Roy Poulsen, Mat. Fys. Medd. Dan. Vid. Selsk. **31**, No. 10 (1959)
6) J. L. Yntema and B. Zeidman, Phys. Rev. **114** (1959) 815
7) C. A. Levinson (private communication)
8) A. M. Lane and E. D. Pendlebury (to be published)
9) M. Crut and N. S. Wall, Phys. Rev. Lett. **3** (1959) 520
10) A. Bohr and B. R. Mottelson, Mat. Fys. Medd. Dan. Vid. Selsk. **26**, No. 14 (1952)
11) T. Tamura and D. C. Choudhury, Phys. Rev. **113** (1959) 552
12) Alder, Bohr, Huus, Mottelson and Winther, Rev. Mod. Phys. **28** (1956) 432
13) J. S. Blair, Phys. Rev. **115** (1959) 928
14) A. I. Yavin and G. W. Farwell, Nuclear Physics **12** (1959) 1
15) P. C. Robison and G. W. Farwell (to be published); results quoted in ref. [13])
16) G. Scharff-Goldhaber and J. Weneser, Phys. Rev. **98** (1955) 212
17) R. H. Helm, Phys. Rev. **104** (1956) 1466
18) Strominger, Hollander and Seaborg, Rev. Mod. Phys. **30** (1958) 585
19) Way, King, McGinnis and Van Lieshout, Nuclear Level Schemes, $A = 40-A = 92$, TJD-**5300** (U. S. Government Printing Office, Washington D.C., 1955)
20) Hu, Kikuchi, Kobayashi, Matsuda, Nagahara, Oda, Takuno, Takeda and Yamazaki, J. Phys. Soc. Jap. **14** (1959) 861
21) Igo, Wegner and Eisberg, Phys. Rev. **101** (1956) 1508
22) C. H. Paris, Annual Progress Report M.I.T. Laboratory for Nuclear Science (1956—'57) 138
23) M. Mazari and R. J. P. de Figueiredo, Annual Progress Report M.I.T. Laboratory for Nuclear Science (1956—'57) 141
24) C. H. Paris, Annual Progress Report M.I.T. Laboratory for Nuclear Science (1957—'58) 119
25) Kikuchi, Kobayashi and Matsuda, J. Phys. Soc. Jap. **14** (1959) 121
26) J. L. Yntema and B. Zeidman, Phys. Rev. Lett. **2** (1959) 309
27) A. Sperduto, Annual Progress Report M.I.T. Laboratory for Nuclear Science (1956—'57) 131, 152 and (1957—'58) 127
28) P. Kienle and R. E. Segel, Phys. Rev. **114** (1959) 1554
29) Schranck, Gugelot and Dayton, Phys. Rev. **96** (1954) 1156
30) J. E. Robertshaw, Progress Report M.I.T. Laboratory for Nuclear Science (31 Oct. 1958) 62
31) F. D. Seward, Phys. Rev. **114** (1959) 514

32) Austern, Butler and McManus, Phys. Rev. **92** (1953) 350
33) S. T. Butler, Phys. Rev. **106** (1957) 272
34) R. Huby and H. C. Newns, Phil. Mag. **42** (1951) 1442
35) S. Hayakawa and S. Yoshida, Prog. Theoret. Physics **14** (1955) 1
36) S. Hayakawa and S. Yoshida, Proc. Phys. Soc. A **68** (1955) 656
37) J. S. Blair and E. M. Henley, Phys. Rev. **112** (1958) 2029
38) G. Igo, and R. M. Thaler, Phys. Rev. **106** (1957) 126
39) W. B. Cheston and A. E. Glassgold, Phys. Rev. **106** (1957) 1215
40) J. S. Blair, Phys. Rev. **108** (1957) 827
41) S. I. Drozdov, JETP **28** (1955) 734, 736; translation: Soviet Phys. JETP **1** (1955) 591, 588
42) E. V. Inopin, JETP **31** (1956) 901; translation: Soviet Phys. JETP **4** (1957) 764
43) J. S. Blair, Phys. Rev. **95** (1954) 1218
44) G. Igo, Phys. Rev. Lett. **1** (1958) 72
45) McIntyre, Wang and Becker (to be published)
46) Kerlee, Blair and Farwell, Phys. Rev. **107** (1957) 1343
47) F. R. Metzger, Phys. Rev. **103** (1956) 983
48) G. M. Temmer and N. P. Heydenburg, Phys. Rev. **104** (1956) 967
49) L. J. Tassie, Aust. Jour. Phys. **9** (1956) 407
50) Braid, Yntema and Zeidman, Summary Report, Physics Division, Argonne National Laboratory ANL-**5955** (Dec. 1958—Jan. 1959) 15
51) Blair, Farwell and McDaniels, Nuclear Physics **17** (1960) 641
52) Beurtey *et al.*, Comptes Rendus **249** (1959) 2189

1.D.2:
2.L

Nuclear Physics **17** (1960) 641—654; © *North-Holland Publishing Co., Amsterdam*
Not to be reproduced by photoprint or microfilm without written permission from the publisher

DIFFRACTION ANALYSIS OF ELASTIC AND INELASTIC SCATTERING BY MAGNESIUM

J. S. BLAIR, G. W. FARWELL and D. K. McDANIELS †

Department of Physics, University of Washington, Seattle, Washington ††

Received 29 January 1960

Abstract: Angular distributions for elastic scattering by Mg and inelastic scattering proceeding to the 1.37 MeV 2^+ state in Mg^{24} have been measured for alpha particles of 41, 34 and 28 MeV incident energy and for deuterons of 21 MeV incident energy. These results as well as those obtained previously by other workers have been analyzed in terms of a diffraction scattering model. This model predicts that the elastic and inelastic differential cross sections, if divided by k^2, should each follow a single function of $2kR_0 \sin \frac{1}{2}\theta$ for all energies of the incident particles. Reasonable agreement between calculated and observed universal curves for alpha particle scattering lends support to this model. Normalization of the experimental and theoretical universal curves for inelastic scattering leads to a value for the absolute magnitude of the equilibrium deformation parameter $|\beta_2|$ of 0.24.

1. Introduction

The mechanism of inelastic diffraction scattering, introduced by Drozdov [1]) and Inopin [2]) to describe scattering from nuclei with quadrupole surface deformation, has been used to analyze the scattering of medium energy alpha particles and deuterons by light [3]) and intermediate [4]) mass nuclei. According to this mechanism, the dependence of both the elastic and the inelastic cross sections on the centre-of-mass wave number k is particularly simple. The differential cross sections are a product of two factors; one is proportional to k^2, while the other involves the squares of oscillating functions of the argument $2kR_0 \sin \frac{1}{2}\theta$, where R_0 is the interaction radius and θ is the centre-of-mass scattering angle.

Only one analysis of the dependence of experimental cross sections on k has been made up to this time. It was observed [3]) that the cross sections for elastic scattering of 24 MeV deuterons by Be^9 and similarly for inelastic scattering by Be^9 with excitation of the 2.43 MeV level [5]) were in at least qualitative accord with the parameters determined through analysis of the cross sections for scattering of 48 MeV alpha particles. The present work was undertaken in order to provide a more extensive test of the dependence upon k of both elastic and inelastic scattering cross sections, and especially to make the test for a case in which the inelastic scattering clearly results in collective excitation of the nucleus.

† National Science Foundation Predoctoral Fellow.

†† Work supported in part by the U. S. Atomic Energy Commission.

The target material, natural magnesium, was chosen for a number of reasons. The predominant isotope is Mg^{24}(78.6 %). The excitation of the 1.37 MeV 2^+ level in Mg^{24} has been studied previously by many groups employing a variety of projectiles and energies. In all cases the inelastic cross sections for alpha particles [6–10]) and deuterons [11–13]) show the regular oscillatory behaviour generic to a direct scattering mechanism. A model based on collective excitation is particularly appropriate to Mg^{24}; the low lying levels of this nucleide and its neighbours in the middle of the s–d shell exhibit rotational band structure [14, 15]) and the electric quadrupole transition probability between the 1.37 MeV and ground states is more than a factor of 10 larger than the Weisskopf-Moszkowski single particle estimate [16, 17]).

In the present experiments, the energy dependence of the elastic and inelastic ($Q = -1.37$ MeV) differential cross sections was studied by obtaining angular distributions for scattered alpha particles at incident energies of 41, 34 and 28 MeV. Scattering of 21 MeV deuterons was also studied. The results of these and of other similar experiments are analyzed here in terms of the simple diffraction model.

2. Experimental

The external beam system for the University of Washington 152 cm cyclotron has been discussed elsewhere [18]). The undegraded alpha particle beam has a maximum energy of about 41 MeV; the deuteron beam, about 21 MeV. A considerable reduction in energy can be obtained by passing the beam through absorbers. In order to avoid excessive reduction in beam intensity, the energy degradation was done by placing thin foil absorbers just ahead of the collimator system at the entrance to the 61 cm scattering chamber. The lowest energy for which usable beam intensity was available was 28 MeV. The incident beam energy was determined by measuring range in aluminium with the aid of a double proportional counter telescope. The target material was 0.00076 cm commercial magnesium foil. The detection system for alpha particles consisted of the same single crystal CsI(Tl) detector described previously [4]). Proper choice of crystal thickness and of aluminium absorbers in front of the detector provided discrimination against undesirable background in the alpha spectra. For the deuteron runs a double CsI(Tl) counter was used with the dE/dx and E crystal pulses in the desired energy intervals simultaneously gating each other; the desired energy intervals were obtained with single-channel differential pulse height analyzers. The resolution for the alpha particle counter was typically 2 % (with aluminium absorbers) of the full energy (full width at half maximum), while that for the deuterons was typically 4 % for the E crystal.

Typical pulse height spectra are shown in figs. 1 and 2 for alphas and deuterons, respectively. The principal error in the elastic scattering cross sections is

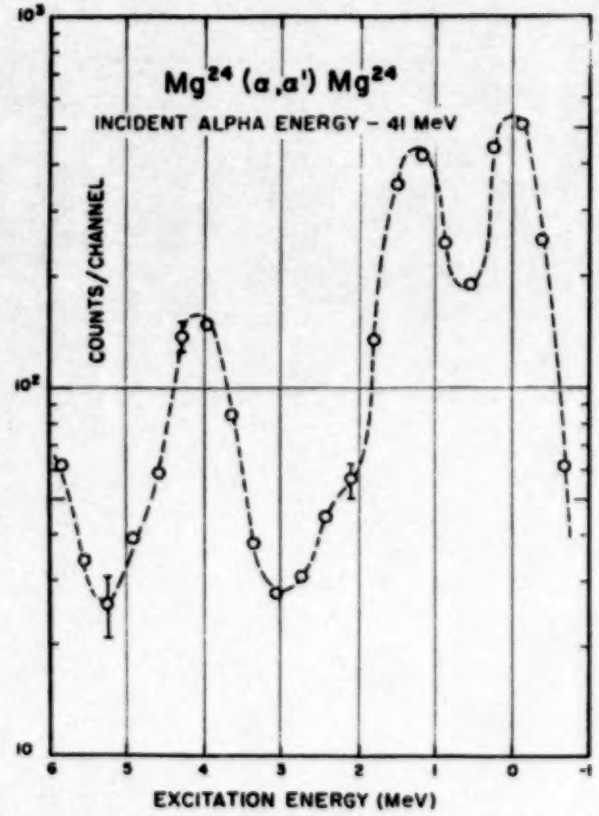

Fig. 1. Typical pulse height spectrum obtained with a CsI(Tl) detector for alpha particles of 41 MeV incident energy scattered by a 0.00076 cm natural Mg foil (78.6 % Mg^{24}) at an angle of 38°.

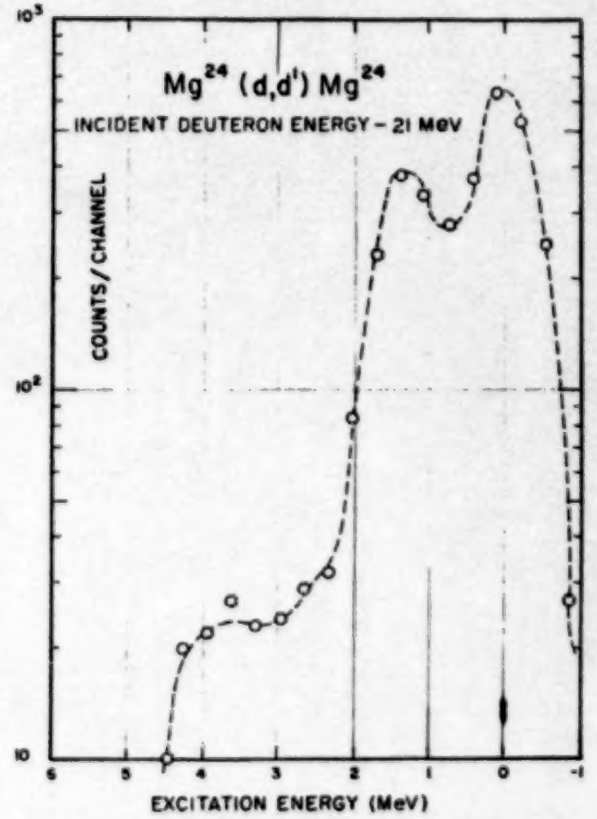

Fig. 2. Typical pulse height spectrum obtained with the CsI(Tl) E crystal in a two-component detector for deuterons of 21 MeV incident energy scattered by a 0.00076 cm natural Mg foil (78.6 % Mg^{24}) at an angle of 46°. Cross-gating of the E and dE/dx pulses from the double counter permits simultaneous display of only the elastic and first inelastic ($Q = -1.37$ MeV) groups.

due to the target density measurement ($\approx 3\,\%$); errors in the absolute inelastic cross sections are generally larger because of uncertainty in background subtraction. The error in the angle of the detector locating arms may be as large as 1° in certain runs.

3. Results

The experimental results for the alpha particle scattering are shown in figs. 3—5, in which angular distributions are presented for incident beam energies of 41, 34 and 28 MeV. The maximum error in the energy determination by the differential range proportional counter is estimated to be $\pm\frac{1}{4}$ MeV, assuming the revised range-energy data of Bichsel [19]) to be correct.

Fig. 6 shows the results for deuterons with an incident energy of 21 MeV scattered from Mg^{24}. The solid line for the elastic data is drawn through the

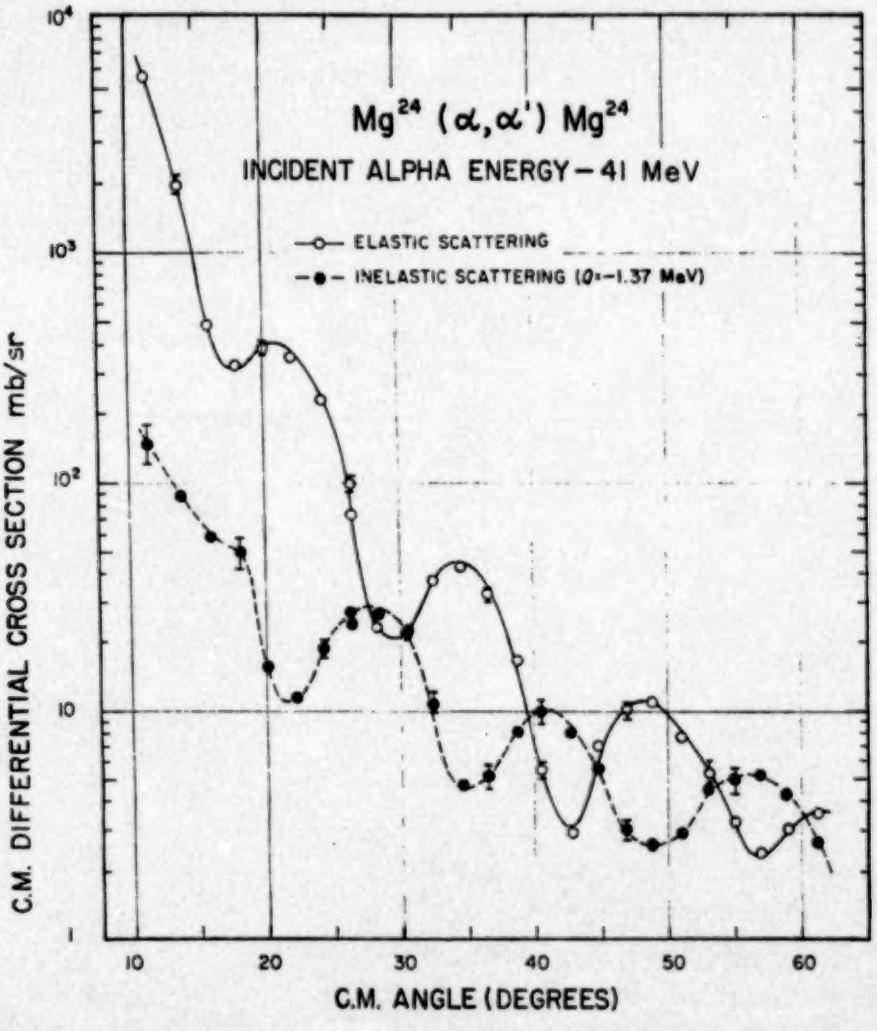

Fig. 3. Angular distributions for alpha particles of 41 MeV incident energy scattered by a 0.00076 cm Mg foil. Experimental errors are indicated for a few representative points.

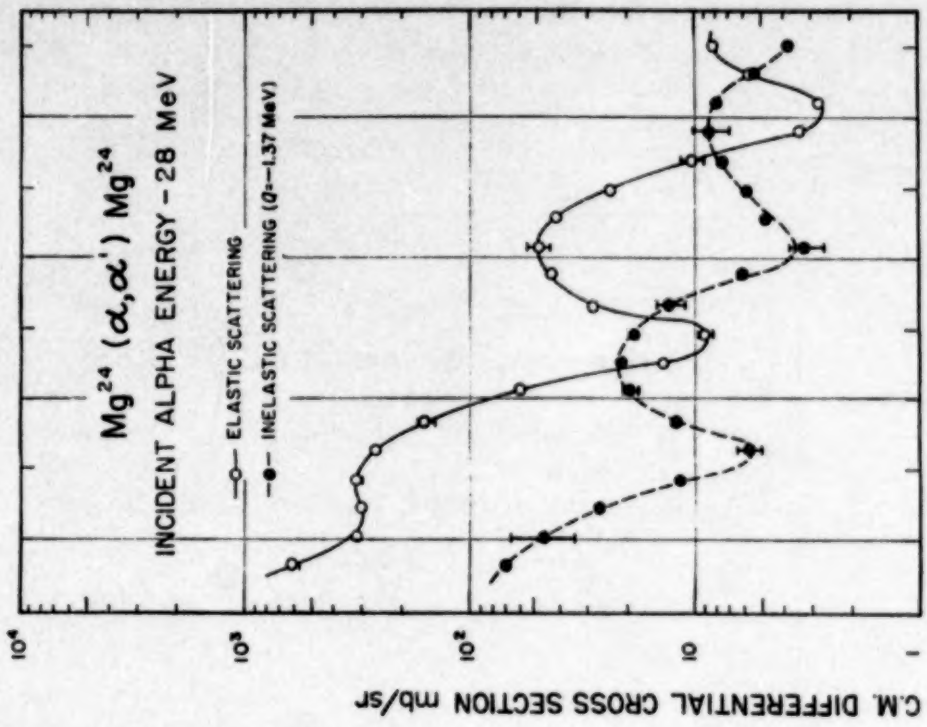

Fig. 5. Angular distributions for alpha particles of 28 MeV incident energy scattered by a 0.00076 cm Mg foil. Experimental errors are indicated for a few representative points.

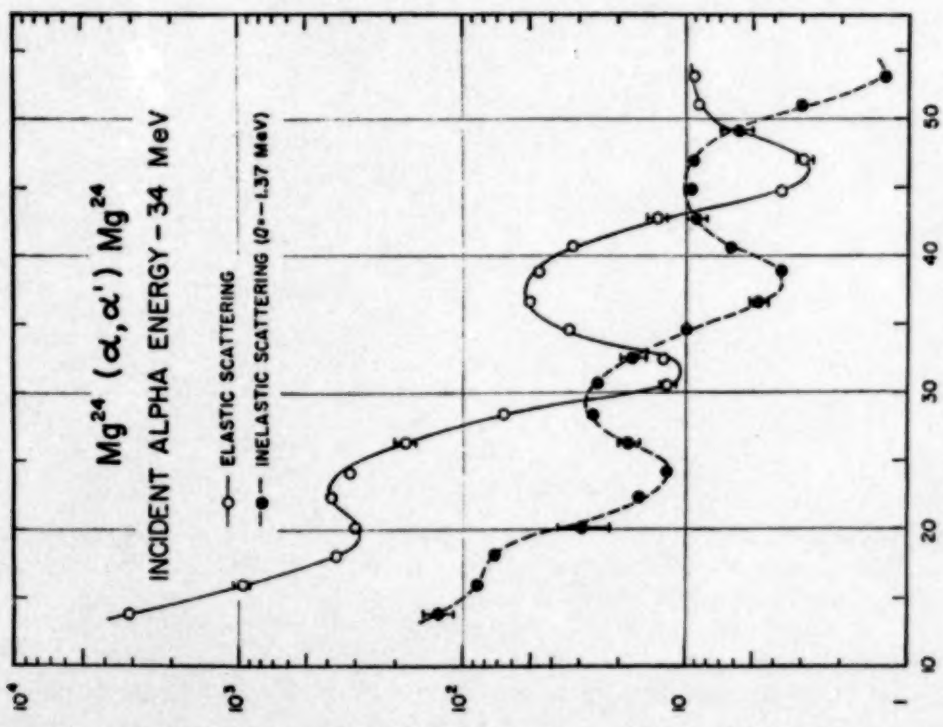

Fig. 4. Angular distributions for alpha particles of 34 MeV incident energy scattered by a 0.00076 cm Mg foil. Experimental errors are indicated for a few representative points.

present experimental points; the data of Yntema [20]) for deuterons of essentially the same energy are also shown for completeness. We note the good agreement, at the three diffraction peaks, between the elastic cross sections from the two different experiments, though there is some indication of an angular discrepancy of about one degree.

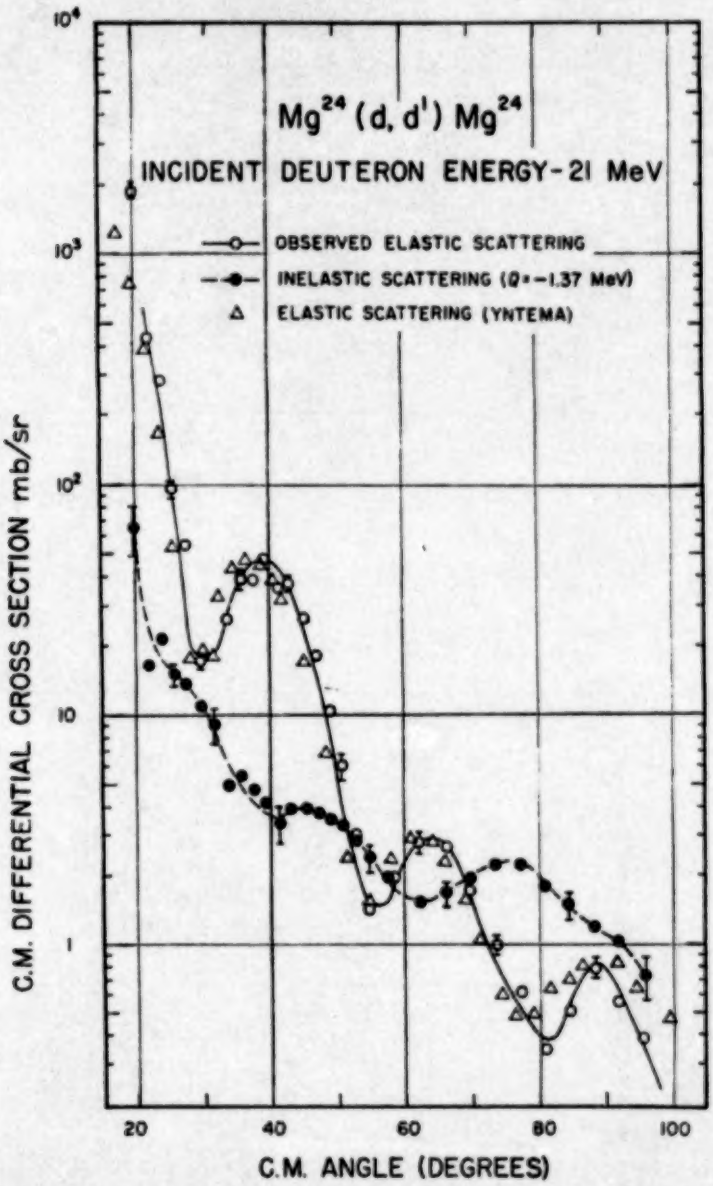

Fig. 6. Angular distributions for deuterons of 21 MeV incident energy scattered by a 0.00076 cm Mg foil. Experimental errors are indicated for a few representative points. The elastic scattering data of Yntema [20]) are included, although the curves are drawn as a best fit to the University of Washington data.

The elastic and inelastic differential cross sections have been previously measured by Gugelot and Rickey [6]); angular distributions (with arbitrary normalization) have been obtained by Shook [9]), using maximum energy alpha

particles from the University of Washington cyclotron. There is reasonable agreement between the results of these experiments and the present results with 41 MeV alpha particles.

4. Discussion

For the strong absorption diffraction model one may derive simple approximate expressions for the elastic and inelastic scattering cross sections. The elastic scattering cross section in the centre-of-mass system is the familiar black sphere result

$$\frac{\mathrm{d}\sigma_{\mathrm{el}}}{\mathrm{d}\Omega} = (kR_0^2)^2 \left[\frac{J_1(x)}{x}\right]^2, \tag{1}$$

where $x = 2kR_0 \sin \frac{1}{2}\theta$. The cross section for inelastic scattering from an even nucleus due to quadrupole surface deformation is [2, 3])

$$\frac{\mathrm{d}\sigma}{\mathrm{d}\Omega}(0 \to 2) = (kR_0^2)^2 \frac{\beta_2^2}{4\pi} \{\tfrac{1}{4}J_0^2(x) + \tfrac{3}{4}J_2^2(x)\} \tag{2}$$

where β_2 is the equilibrium deformation parameter. In the above formulas (in contrast to those employed in ref. [4])), we have not included the slowly varying obliquity factor; thus the angular dependence is entirely contained in the oscillating functions of the argument x.

According to the above predictions, both the elastic and inelastic cross sections measured for projectiles of differing wave number k should follow "universal" curves when divided by k^2 and plotted versus x. This is, of course, a necessary but not sufficient condition for the validity of the diffraction scattering expressions; universal curves also result should the observed cross sections be products of these factors and additional "form factors" which are functions of $2k \sin \frac{1}{2}\theta$. This latter situation is rather likely since eqs. (1) and (2) have been derived in the approximation that the nucleus is a sharp-edged absorbing object; we recall that in the plane wave Born approximation, the cross sections for scattering from a diffuse-edged potential can be expressed as products of the square well predictions and such form factors [16]).

In fig. 7 the observed elastic scattering cross sections divided by k^2 are plotted versus x. In addition to our own results with alpha particles of 41, 34 and 28 MeV incident energy we have included the results of alpha particle experiments performed by Vaughn [7]) (48 MeV), Watters [8]) (31.5 MeV) and Hu *et al.* [10]) (22.8 MeV). The radius used for all energies for the universal plot, $R_0 = 5.97 \times 10^{-13}$ cm, is an average of the radii determined by matching the observed locations of maxima and minima at a given energy to those predicted by eq. (1). These individual radii are given in table 1. A similar plot of the 21 MeV deuteron results is also shown in fig. 7; in this case a somewhat larger

radius, 6.31×10^{-13} cm, is used in order that the minima in both the deuteron and the alpha particle angular distributions occur at roughly the same value of x.

We note that the alpha particle results overlap particularly well at the first shoulder occurring near $x = 5$ and at the third maximum near $x = 11.4$.

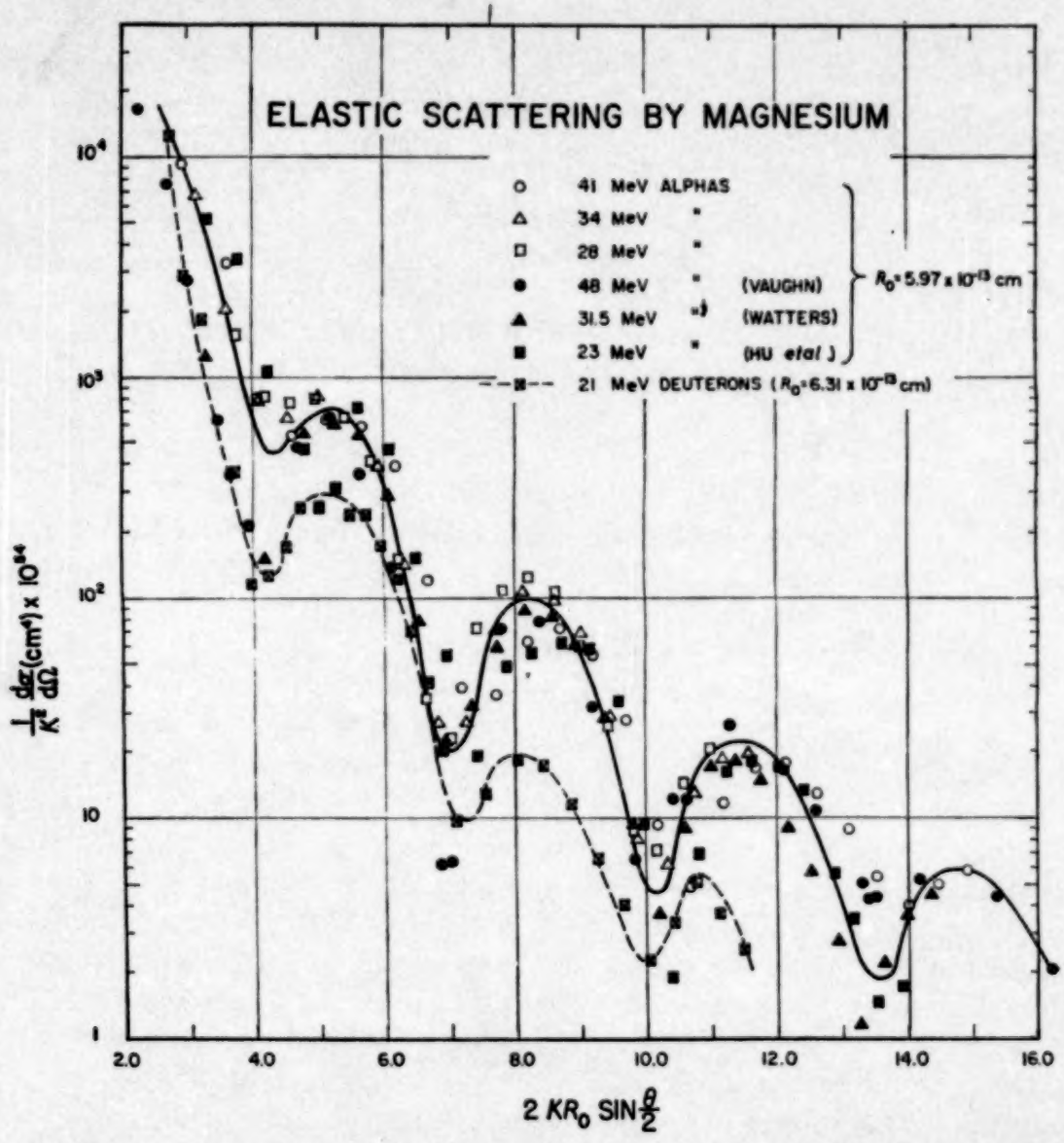

Fig. 7. The observed elastic scattering cross sections (for alpha particles of various energies incident on natural Mg), divided by k^2, plotted as a function of $x = 2kR_0 \sin \frac{1}{2}\theta$. Here, k, $d\sigma/d\Omega$ (obs) and θ are in the centre-of-mass system. The 21 MeV deuteron elastic data are plotted in the same manner for comparison.

There is considerable divergence, however, for $x < 4$; we believe that this may be attributed to (a) the varying importance of the Coulomb corrections to the scattered amplitude at small angles and (b) the experimental difficulties concomitant with the large and rapidly varying cross sections which occur at small

angles. A universal curve has been drawn to summarize the alpha particle results; the magnitude of the universal curve clearly has little meaning at small angles and at the minima but is a fair approximation at the maxima. On the

TABLE 1
Interaction radii

Group	Scattering Particle	Incident Energy (MeV)	Radius (10^{-13} cm)
Univ. of Wash.	d	21	6.31
Univ. of Wash.	α	41	5.98
Univ. of Wash.	α	34	5.87
Univ. of Wash.	α	28	5.98
Vaughn [7])	α	48	6.06
Watters [8])	α	31.5	5.90
Hu *et al.* [10])	α	22.8	6.02
	Average for alpha scattering 5.97		

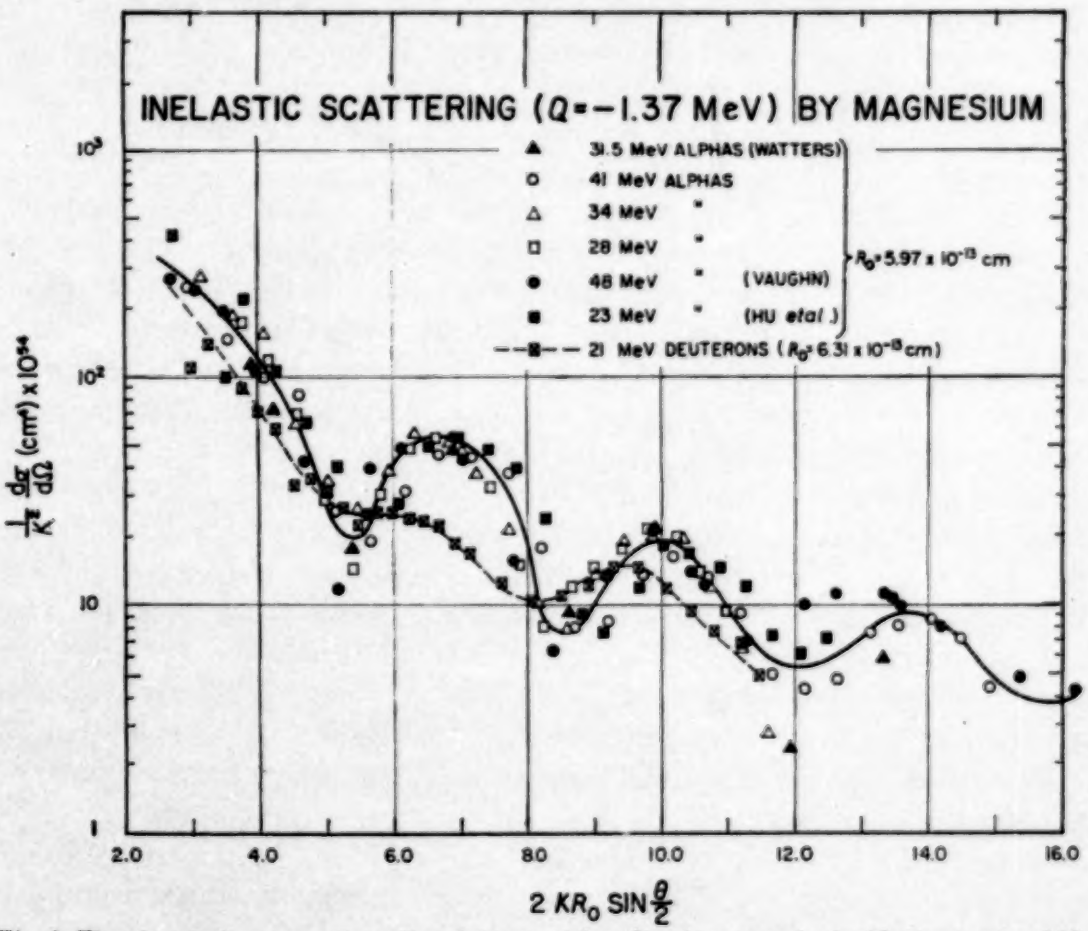

Fig. 8. The observed cross sections (for alpha particles of various energies incident on natural Mg) for inelastic scattering proceeding to the 1.37 MeV level in Mg^{24}, divided by k^2, plotted as a function of $x = 2kR_0 \sin \frac{1}{2}\theta$. Here, k, $d\sigma/d\Omega$(obs) and θ are in the centre-of-mass system. The 21 MeV deuteron inelastic data are plotted in the same manner for comparison.

other hand, even at the first maximum, the angular distribution for elastically scattered deuterons lies considerably below the universal curve for alpha particles.

A similar plot of the inelastic cross sections is given in fig. 8. The radii used (5.97×10^{-13} cm for alpha particle and 6.31×10^{-13} cm for deuteron scattering) are those determined from analysis of the elastic scattering angular distributions. The points corresponding to alpha particle scattering definitely cluster at the locations of theoretical maxima occurring at $x = 3.25$, 6.78 and 10.02, and there is little uncertainty in drawing a universal inelastic alpha particle scattering curve.

Again our deuteron results tend to lie beneath the alpha particle universal curve. The cross section for inelastic scattering of 15.1 MeV deuterons has been measured by Haffner [12]). If plotted in the manner of fig. 8 his results for $x < 4$ conform to our own deuteron measurements at 21 MeV; beyond the plateau near $x = 6$, his measurements of the cross section show little structure and tend to lie 30—50 % above our results. Hinds, Middleton and Parry [13]) have measured the cross section for inelastic scattering of 8.9 MeV deuterons. Their results, in contrast to the above deuteron results, are rather close to the theoretical curve for inelastic scattering which is discussed in a subsequent paragraph. The quantity $(1/k^2)\mathrm{d}\sigma/\mathrm{d}\Omega$ has a maximum value of 130×10^{-54} cm^4 between $x = 2.5$ and $x = 3.1$, a minimum value of 34×10^{-54} cm^4 at $x = 4.9$ and a second maximum 63×10^{-54} cm^4 near $x = 7$.

The universal curve corresponding to alpha particle scattering is compared to the predictions of eq. (1) in fig. 9. There is no arbitrary normalization of the theoretical to the experimental curves. The agreement between the diffraction formula and the universal curve is good at the first and second maxima occurring at $x = 5.14$ and $x = 8.42$, respectively. For the higher orders of the diffraction pattern one observes the typical result that the experimental curve drops below the prediction of a sharp-edged model†. The experimental results at small angles lie well above the predictions of eq. (1), a phenomenon which is not surprising inasmuch as the Coulomb interaction has been neglected in the derivation of eq. (1). At these small values of x, we also show the results of Vaughn [7]) at 48 MeV. Since the classical distance of closest approach for pure Coulomb scattering is proportional to $1/xk$ at small angles, we anticipate that for a given x the Coulomb corrections to the scattered amplitude are more easily reduced by nuclear absorption the higher the value of k. Closer agreement of the 48 MeV data with the diffraction prediction neglecting the Coulomb interaction bears this out.

The comparison between the universal curve for inelastic scattering and eq. (2) is also shown in fig. 9. The curves have been normalized at the maximum

† Recent work by McIntyre, Wang and Becker [21]) indicates that smoothing the transition between complete and no absorption in the sharp cutoff model will improve the agreement at the higher orders of the diffraction pattern of elastically scattered alpha particles.

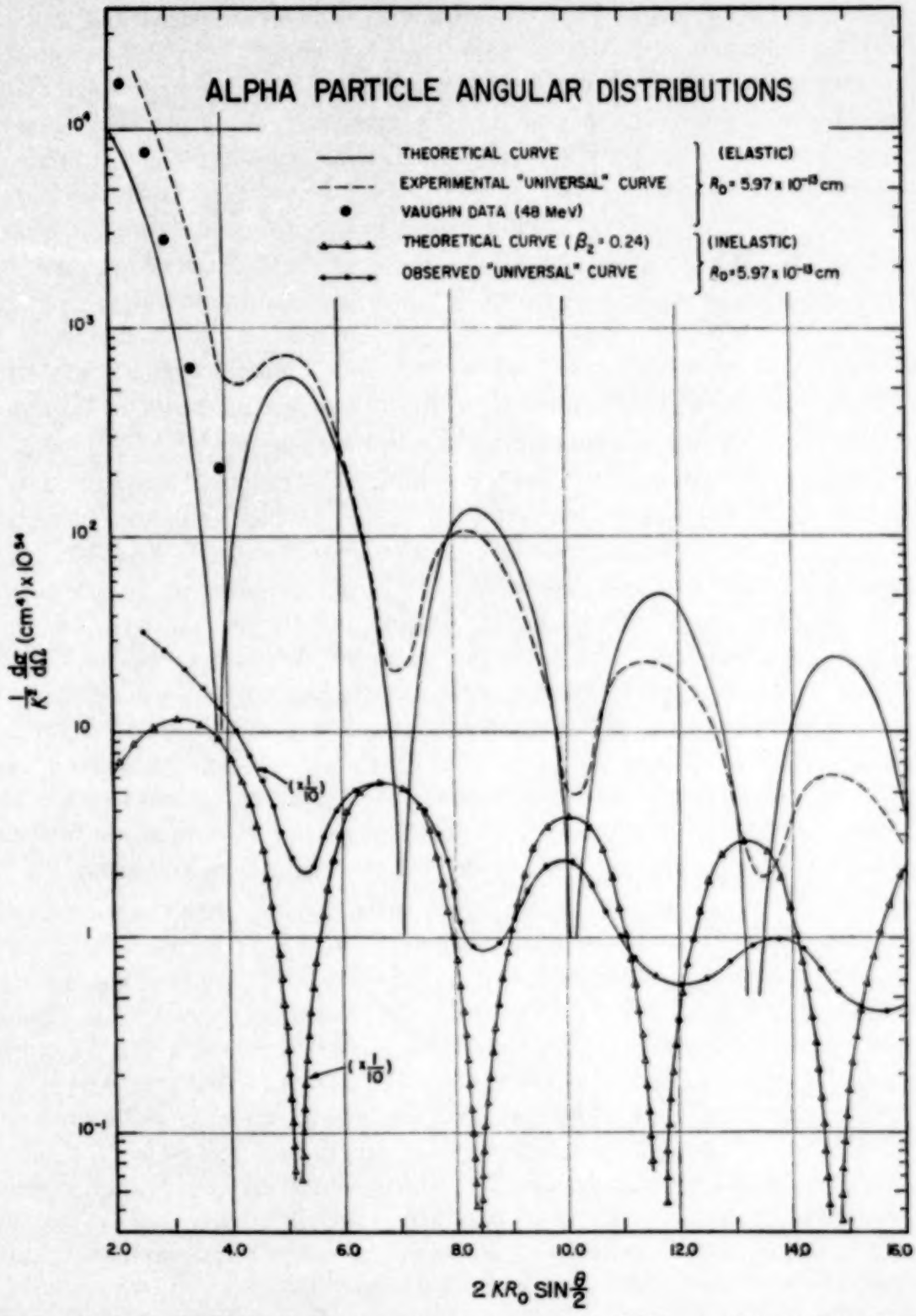

Fig. 9. Comparison of the universal curves for the scattering of alpha particles by Mg with the predictions of the diffraction model as given by eqs. (1) and (2). There is no arbitrary normalization of the experimental elastic data to the theoretical curve. The experimental universal curve for inelastic scattering has been normalized to the theoretical curve at the maximum which occurs at $2kR_0 \sin \frac{1}{2}\theta = 6.78$; this normalization leads to the value 0.24 for $|\beta_2|$, the absolute magnitude of the equilibrium deformation parameter.

which occurs at $x = 6.78$, since the elastic cross sections are rather well matched by the predictions of eq. (1) for values of the argument x in this region; this normalization leads to the value 0.24 for $|\beta_2|$, the absolute magnitude of the equilibrium deformation parameter. We again note that the experimental curve drops below the prediction of a sharp-edged model at the higher orders of the pattern. It is also observed that experimental results exceed the prediction of eq. (2) at small angles; this should not be surprising inasmuch as contributions to the scattered amplitude from Coulomb excitation have not been included in eq. (2). (See eq. (5.9) in ref. [3]) and accompanying discussion.)

Gugelot and Rickey [6]) have interpreted their results for alpha scattering (which are in essential agreement with our 41 MeV results) in terms of a simple model [22]) in which the following approximations are made: (a) the nuclear potential is represented by a square well; (b) the radius of this potential is related to deformation parameters in the same fashion as in the diffraction model; (c) both elastic and inelastic cross sections are calculated in the plane wave Born approximation. The value of $|\beta_2|$ corresponding to the theoretical curve in fig. 2 of their paper is 0.17, a value not greatly different from the value 0.24 which results from the diffraction analysis. We do not believe, though, that the plane wave Born approximation is applicable to this problem; of the many objections to this procedure, we believe the strongest is that it is contradictory to the known large nuclear absorption †. The similarity between their value of $|\beta_2|$ and ours can be understood by noting the near equivalence of the ratios of inelastic cross section to elastic cross section computed for both the plane wave Born approximation model and the diffraction model ††.

It is of interest to compare the present result for $|\beta_2|$ with electromagnetic estimates. The electric quadrupole transition probability between the ground and first excited 2^+ states of Mg^{24}, $B(E2, 0 \rightarrow 2)$, has been estimated to be $0.046\, e^2 \times 10^{-24}$ cm^2 from inelastic electron scattering experiments [16]) and $0.08\, e^2 \times 10^{-24}$ cm^2 from resonance fluorescence experiments [17]). When the equivalent uniform radius is taken to be [16]) $1.39\, A^{\frac{1}{3}} \times 10^{-13}$ cm, the strong coupling predictions [23]) for the electromagnetic deformation parameter $|\beta_2(EM)|$ are 0.43 and 0.56, respectively. We need not be surprised at the discrepancy between these values for $|\beta_2(EM)|$ and the value of $|\beta_2|$ which results from the diffraction analysis since the parameters are differently defined. As discussed in ref. [4]), the collective parameter from the diffraction analysis is probably an under-estimate since the interaction radius should be viewed as the sum of an alpha particle radius and a nuclear radius. For an alpha particle

† A fuller discussion of the applicability of the plane wave Born approximation to elastic alpha particle scattering is given in ref. [18]).

†† The analogy between the results of the plane wave Born approximation and the diffraction model is discussed in more detail in Sec. III of ref. [3]).

radius equal to 2×10^{-13} cm, the true nuclear deformation parameter would be 0.36, in closer accord with electromagnetic estimates.

The many experiments [24–29]) in which protons are scattered from Mg do not appear amenable to analysis with the simple diffraction model. We should also like to note that the strong absorption diffraction model does not appear to be able to explain experiments in which lower energy alpha particles are scattered by certain very light nuclei. Of targets other than Mg^{24}, C^{12} has been studied the most extensively. For alpha particles with 48 MeV [7]) or 41 MeV [18]) incident energy, the elastic scattering cross sections from C^{12} are in reasonable agreement with eq. (1) for an interaction radius $R_0 = 5.1\times10^{-13}$ cm. The angular distributions corresponding to excitation of the 4.43 MeV 2^+ state oscillate out of phase with those for elastic scattering; when matched to eq. (2) at forward angles they yield $|\beta_2| \approx 0.28$. But for the lower incident alpha particle energies 31.5 MeV [7]), 22.8 MeV [10]) and 18.0 MeV [30]), the elastic cross sections at corresponding maxima are either larger than or comparable to the values obtained at 48 and 41 MeV incident energy, in contradiction to the predicted energy dependence. At these lower energies, the magnitudes of inelastic cross sections show a similar inversion; for 18.0 MeV, even the usual phase relation between the elastic and inelastic angular distributions is not present.

5. Summary

Results for elastic scattering by Mg^{24} of alpha particles of energies from 23 to 48 MeV exhibit a considerable degree of consistency when analyzed in terms of a simple strong absorption diffraction model using identical interaction radii at all energies. The theoretical universal curve of $(1/k^2)\,d\sigma/d\Omega$ *versus* $2kR_0 \sin\frac{1}{2}\theta$ falls somewhat below the experimental universal curve at small angles, probably due to Coulomb effects; at large angles, the predicted diffraction maxima exceed the observed cross sections. Nevertheless, the clustering of the results for different energies about the best universal curve and the reasonable agreement between calculated and observed cross sections at the first and second diffraction maxima lend plausibility to the simple diffraction picture. Use of the best interaction radius for elastic scattering in the diffraction analysis of inelastic scattering of 23 to 41 MeV alphas leads likewise to a satisfactory universal curve. If experimental and theoretical universal curves for inelastic scattering are normalized in the region of best agreement for the elastic data, a reasonable value results for the equilibrium deformation parameter β_2 for Mg^{24}.

Deuteron results for both elastic and inelastic scattering at 21 MeV fall below the corresponding universal curves for alpha particles despite the larger interaction radius assumed in order to achieve the same periodicity in $2kR_0 \sin\frac{1}{2}\theta$.

References

1) S. I. Drozdov, JETP **28** (1955) 734, 736; translation: Soviet Phys. JETP **1** (1955) 791, 788
2) E. V. Inopin, JETP **31** (1956) 901; translation: Soviet Phys. JETP **4** (1957) 764
3) J. S. Blair, Phys. Rev. **115** (1959) 928
4) McDaniels, Blair, Chen and Farwell, Nuclear Physics **17** (1960) 614
5) R. G. Summers-Gill, Phys. Rev. **109** (1958) 1591
6) P. C. Gugelot and M. Rickey, Phys. Rev. **101** (1956) 1613
7) F. J. Vaughn, Ph. D. Thesis, U.C.R.L. Report 3174 (1955), unpublished
8) H. J. Watters, Phys. Rev. **103** (1956) 1763
9) G. B. Shook, Phys. Rev. **114** (1959) 310
10) Hu, Kato, Oda and Takeda, Jour. Phys. Soc. (Japan), **14** (1959) 539
11) J. R. Holt and C. T. Young, Nature **164** (1949) 1000
12) J. W. Haffner, Phys. Rev. **103** (1956) 1398
13) Hinds, Middleton and Parry, Proc. Phys. Soc. A **70** (1957) 900
14) A. E. Litherland *et al.*, Can. Journ. Phys. **36** (1958) 378
15) G. Rakavy, Nuclear Physics **4** (1957) 375
16) R. H. Helm, Phys. Rev. **104** (1956) 1466
17) S. Ofer and A. Schwarzschild, Phys. Rev. Lett. **3** (1959) 384
18) A. I. Yavin and G. W. Farwell, Nuclear Physics **12** (1959) 1
19) H. Bichsel, private communication (to be published)
20) J. L. Yntema, Phys. Rev. **113** (1959) 261
21) McIntyre, Wang and Becker (to be published)
22) S. Hayakawa and S. Yoshida, Proc. Phys. Soc. A **68** (1955) 656
23) Alder, Bohr, Huus, Mottelson and Winther, Revs. Mod. Phys. **28** (1956) 432
24) P. C. Gugelot and P. R. Phillips, Phys. Rev. **101** (1956) 1614
25) H. E. Gove and H. F. Stoddart, Phys. Rev. **86** (1952) 572
26) Baker, Dodd and Simmons, Phys. Rev. **85** (1952) 1051
27) G. E. Fischer, Phys. Rev. **96** (1954) 704
28) G. W. Greenlees and A. E. Souch, Proc. Phys. Soc. A **69** (1956) 686
29) Greenlees, Haywood, Kuo and Petravic, Proc. Phys. Soc. A **70** (1957) 331
30) Corelli, Bleuler and Tendam, Bull. Am. Phys. Soc. **2** (1957) 34

1.D.2:
2.L

Nuclear Physics **17** (1960) 655—683; © *North-Holland Publishing Co., Amsterdam*

Not to be reproduced by photoprint or microfilm without written permission from the publisher

THE ANOMALOUS INELASTIC SCATTERING OF ALPHA PARTICLES

M. CRUT †, D. R. SWEETMAN †† and N. S. WALL

Department of Physics and Laboratory for Nuclear Science, Massachusetts Institute of Technology, Cambridge, Massachusetts †††

Received 1 April 1960

Abstract: We report on a series of experiments establishing and identifying the properties of the so-called anomalous states in medium-weight nuclei. These excitation energies for states are about 4 MeV for nuclei with $Z \leqq 29$ and in the range of 2—3 MeV for nuclei with higher Z. From a combination of angular distribution and correlation data we have shown, and interpreted by means of inelastic diffraction scattering analysis, the anomalous states in several cases to be consistent with a 3^- interpretation. This lends credence to their collective interpretation. The difficulties with such analyses are discussed, and experimental matters are gone into in some detail.

1. Introduction

In numerous experiments, such as inelastic scattering of nucleons and alpha particles, transmutation through (d, p) or (α, p) reactions, or decay of radioactive nuclei, it has been found that, generally speaking, as one observes reactions leading to a more highly excited residual nucleus the spacing between the nuclear energy levels decreases. An essential characteristic of all such experiments is that the energies of the particles or photons involved are measured with a device, such as a magnetic analyzer for charged particles, which has an inherent resolution significantly less than the spacing between the levels of the nucleus under study.

From such experiments the determination of level density as a function of excitation energy simply reduces to counting the number of levels per unit energy. The results of such an analysis, as recently made by Ericson [1]), show that level density increases in the manner to be expected on the basis of various thermodynamic level density expressions [2, 2a]) ‡. Thermodynamic arguments do not, however, make specific predictions as to the absolute cross-section for the excitation of a given level, nor do they deal with fluctuations in the cross-section from level to level [3]). These arguments lead one to believe that, as

† On leave from C. E. N. Saclay.

†† Commonwealth Fund Fellow; now at AWRE, Aldermaston, England.

††† This work is supported in part through AEC Contract At (30—1) 2098, by funds provided by the U. S. Atomic Energy Commission, the Office of Naval Research and the Air Force Office of Scientific Research.

‡ Ref. [2a]) is a general review of the statistical theory and refers to many of the earlier expressions for level density.

nuclei are excited to higher and higher energy, and the resolution of the measuring device ΔE becomes large compared to the level spacing D the observed spectrum will essentially increase monotonically, since we are averaging over many levels and thereby cancelling fluctuations, until the Coulomb barrier (for charged particles) and the angular momentum barrier inhibit the emission of particles.

It is from this foundation that we are able to approach a definition of "anomalous" inelastic scattering, namely, that if one observes the spectrum of particles inelastically scattered from a medium or heavy weight nucleus, with a device having an instrumental energy resolution greater than the level spacing, any structure in this spectrum of width comparable to the experimental resolution is defined to be anomalous. Excluded from this definition are spectral peaks which can be attributed to single well resolved levels. This definition does not distinguish between an effect which might be called a fluctuation in level density (in principle determinable from a high resolution experiment) and a special interaction mechanism picking out a particular level or group of levels. Such a differentiation may in fact be somewhat artificial: the phenomenon which causes the fluctuation in level density may give to those affected levels a property permitting them to be readily excited in an inelastic scattering experiment. An operational definition such as the one we give causes, of course, some difficulty in making detailed comparisons between experimenters of the relative intensities of various components of the anomalous spectrum. However, no difficulty is experienced in comparing the excitation energies of the intense components of the spectrum.

In recent years, largely motivated by the original and interesting experiments of B. L. Cohen and his co-workers [4]) an increasing number of such low-resolution studies have been performed usually utilizing cyclotron beams and scintillation spectrometers or proportional counters. These experiments have involved protons [5]), deuterons [6]) and alpha particles [7]) at incident particle energies ranging from about 10 to 40 MeV. There have also been a series of (d, p) [8]) and (p, d) [9]) experiments; however, it has not been completely established whether the structure observed in the latter sets of experiments is related to that observed in the inelastic scattering experiments [10]).

In all the experiments referred to above the only information relative to the spins and parities of the anomalous states has come from angular distribution measurements. These measurements have been interpreted on the basis of one of the several variants of the direct interaction theory of Austern, Butler and McManus [7]) [11]) † or the more recent work of Blair [12]) which was stimulated by

† A rather complete review article has recently been written by N. Austern for the book Fast Neutron Physics [11]); this encompasses many of the earlier references and cites them. The (d, p) and (p, d) experiments have been interpreted by the stripping reaction theory first developed by S. T. Butler, which in fact formed the basis for the direct interaction theory (see the book by S. T. Butler and O. Hittmair [11]).

Drozdov [13]) and Inopin [14]). There were also some preliminary de-excitation gamma radiation experiments by Cohen and Rubin [4]) which at least indicated that the spins of some of the anomalous states were not 0^+.

The essential point in most of the early direct interaction calculations mentioned above is that the product of the momentum transferred in the reaction and an interaction radius evaluated at the first maximum of the observed angular distribution is approximately equal to the angular momentum transferred, or for a spin zero target nucleus, the angular momentum of the excited state. Experimentally it is quite frequently difficult to use angles small enough to locate the first maximum, and even if this is possible, there remains an ambiguity in the value of the interaction radius because it often differs from the nuclear radius $R = 1.3\,A^{\frac{1}{3}} \times 10^{-13}$ cm by a significant quantity, thereby introducing an uncertainty into the angular momentum interpretation. Blair [12]) has pointed out an alternative way of analyzing the data with which we shall deal in some detail later. There is still some question with his type of analysis because of the radius problem; however, our experiments support his analysis. One other problem associated with a direct interaction analysis, which seems to be very important for protons and judging by the data presented by Tobocman *et al.* [15]) also for deuterons, is the effect of the distortion of the incident plane waves. This causes the angular distributions to lose their simplicity of interpretation with respect to spectroscopic information. While this of course raises many other interesting questions [16,17]), it beclouds the issue when attempting to use such data to deduce spins. In particular the distortion causes the angular distributions to be diluted, and the characteristic diffraction structure, which is used to deduce the spin and parity, is lost. Though a detailed explanation has not yet been given, it is experimentally observed that inelastic alpha-particle angular distributions show much less of the distortion behaviour than protons. Furthermore, the short mean free path of alpha particles in nuclear matter compared to the protons restricts the reaction to the surface region, which should emphasize the diffraction-like behaviour.

Section 2 of this paper will present the inelastic alpha particle anomalous level structure, section 3 the angular distribution experiments, section 4 the gamma-ray correlation experiments and section 5 a discussion of the theoretical significance of these results.

2. Inelastic Alpha Particle Spectra

Following the discovery by Cohen [4]) of the anomalous levels we undertook a series of experiments to see if there were any similarities between inelastic proton and alpha scattering. One result of these experiments is to answer the question whether we were observing an effect which was a property of the nuclei investigated or a property of the particular interaction under study.

There is a need to answer such a question since the experiments on the inelastic scattering of alpha-particles and protons to discrete states of light nuclei do show marked differences [17]).

2.1. EXPERIMENTAL EQUIPMENT

In these first experiments the basic detector was a CsI(Tl) scintillation spectrometer preceded by a thin gas counter. This counter assembly was mounted external to a 10.2 cm diameter scattering chamber in such a way as to permit the counter angles to be varied continuously from about 30° to 130° from the incident beam direction. The scattered particles emerged through a 0.0013 cm thick mylar window.

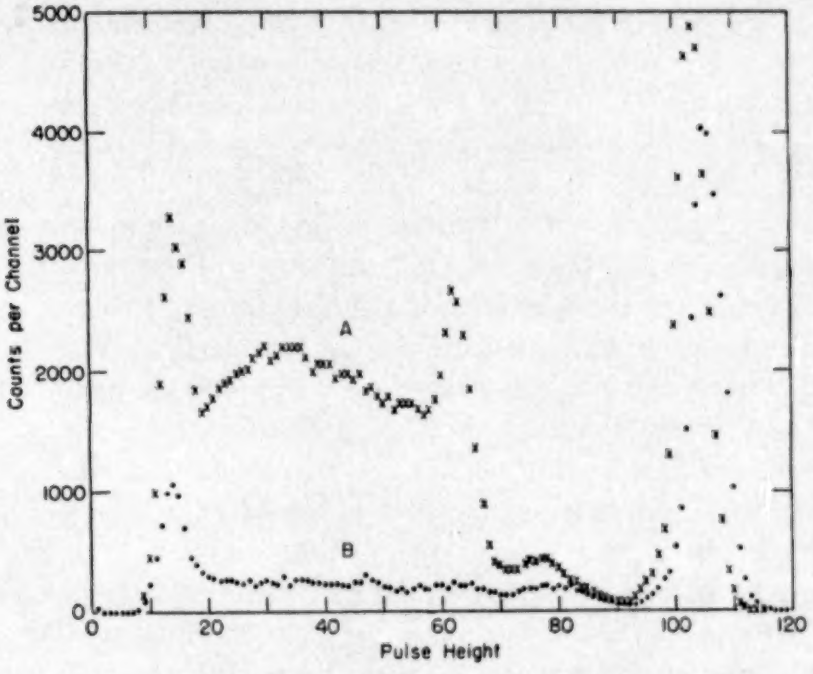

Fig. 1. Typical particle selection behaviour and energy resolution of the detector in the inelastic alpha-particle experiments.

The gas counter was about 1 cm in front of the scintillation crystal. The total thickness of this proportional counter including gas and windows, was equivalent to approximately 5 cm of air. This represents less than 10 % of the range of the elastically scattered alpha particles. The gas counter was operated with a mixture of Argon with 10 % Methane at atmospheric pressure. It was found that for most stable performance it was necessary to have the counting gas flowing continuously through the counter albeit at a low rate, of the order of 0.5 cm^3/sec. The collector electrode in the gas counter was mounted off centre so that it cast no shadow on the CsI(Tl) crystal behind it, producing spurious structure in the spectrum. To minimize pile-up effects the geometry of the two-counter assembly was such that every particle going through the gas counter struck the

CsI crystal. If this were not so, and more particles traversed the gas counter our counting rates would have been even lower than they were (some runs took several hours) because with 30 MeV alpha particles incident on a medium-A nucleus only a relatively small number of the emitted charged particles are scattered alpha particles. Fig. 1 illustrates the relative intensity of inelastic alpha particles to other charged particles in the particular case of the titanium reactions.

Fig. 1 also shows the typical resolution $\Delta E/E$, used in these experiments, approximately 4 %. The intense peak shown in spectrum A at about $\frac{2}{3}$ the energy of the elastic alpha particles corresponds to protons which have an energy great enough to go through the thin CsI crystal. This strong proton peak shows no sign of feeding through in spectrum B and thus shows the excellent performance of this counter as a particle selector. By using 7.5 MeV protons and 15 MeV deuterons from the cyclotron we were able to show that, at pulse heights in the CsI corresponding to those energies, there was essentially no ($< \frac{1}{2}$ %) feed-through when the counter was operated as described below. The defining

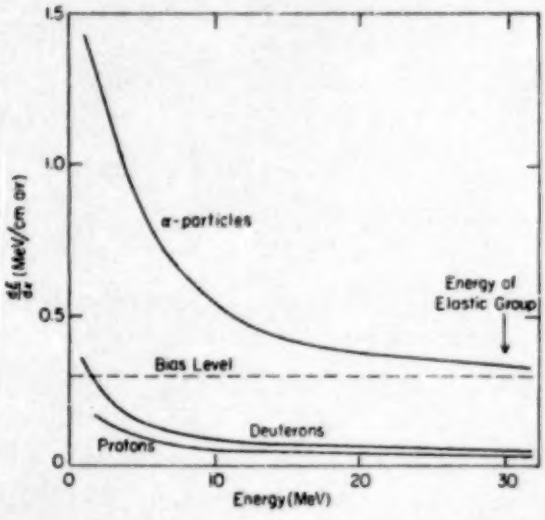

Fig. 2. Specific ionization vs. energy. The dotted line shows the minimum pulse height in the dE/dx counter necessary to identify an alpha particle.

aperture on the gas counter was approximately 0.32 cm diameter located about 6.4 cm away from the centre of the target and defined a solid angle of about 2×10^{-3} sr.

To identify alpha-particles use was made of the fact that the specific ionization as a function of energy in the energy range we are studying is dependent upon the type of particle. Fig. 2 shows the relative specific ionization for these particles as a function of energy. From this figure it is seen that by utilizing the fact that a thin proportional counter essentially measures the specific ionization, and requiring a signal in the proportional counter which corresponds to an

energy loss equal to or greater than the energy loss of the elastic alpha particles, we successfully discriminate against all protons or deuterons with energies greater than about 2 MeV. The resolution of the gas counter was relatively poor ($\approx$ 25 %) so that the significance of the spectra below alpha-particle energies of about 10 MeV is questionable. Fig. 3 is a block diagram of the electronic apparatus which enabled us to perform the particle identification. The main component of this scheme was an RCL 256-channel pulse-height analyzer †.

In operation the circuits were used in the following manner. The counters were set at some forward angle and detected the particles scattered from a thin Au target. Since this is predominantly elastic scattering a strong peak in the spectrum was observed corresponding to approximately 30 MeV alpha particles.

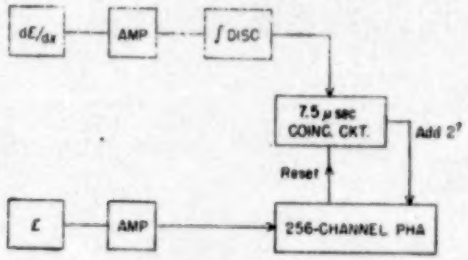

Fig. 3. Block diagram of electronics used in anomalous state experiments.

The gain of the amplifier was adjusted so that the elastic peak fell in the vicinity of channel 100 on the pulse-height analyzer. The bias of the integral discriminator on the output of the proportional counter (the dE/dx counter) was then raised until the peak nearly disappeared. From fig. 3 one can see that when an energy signal E enters the analyzer in coincidence with a signal from the integral discriminator the E signal is then displayed *not* in the first 2^7 channels of the pulse-height analyzer (PHA) but is converted to a binary digit corresponding to its energy plus 2^7. In other words those signals in coincidence with a signal from the integral discriminator are displayed in the upper half of the 256 channel PHA whereas those signals which are not in coincidence fall into the first 2^7 channels. The pulse heights of interest are then measured from either channel zero or channel 128, these two channels corresponding to zero pulses height in the E counter. Inasmuch as this PHA continuously displays the spectrum as it accumulates, it is only necessary to watch this display and adjust the

† Obtained from RCL, Chicago, Ill.; this analyzer is essentially the one described in ref. [18]). To utilize the RCL 256-channel PHA in the particle identification experiments described in section 2 several modifications were made. One of the first operations performed by an incoming pulse is to cause a univibrator to fire causing the address scaler to be reset to zero. We extract the reset signal and formed a coincidence between the trailing edge of this pulse and the dE/dx pulse. This assured that the add 2^7 pulse, which was the output of the coincidence circuit, came at the proper time. The add 2^7 signal was then applied through a diode to the appropriate grid in the address scaler. In other words the memory computer read an address signal corresponding to the pulse height plus 2^7 if there was an appropriate dE/dx signal.

bias on the integral discriminator so that the pulses corresponding to the elastically scattered alpha particles do not appear in the first 2^7 channels. To be certain that the integral discriminator was not set too high, we allowed a few percent of the elastically alpha particles to be counted in the first 2^7 channels. Since for almost all elements and angles of observation the elastically scattered alpha particles were easy to discern we had a continuous monitor on our proportional counter enabling us to make sure we were counting only particles with high specific ionization in the second 2^7 channels.

For all of the experiments referred to in this and the subsequent sections the same PHA was used, though in not the same manner. Also common to all of these experiments was the alpha particle beam produced by the MIT cyclotron, described in several papers [19, 20]). It is only necessary to mention that the beam spot was of the order of 1 cm^2 and that the intensity of the beam was of the order of 0.1 μA.

In all these experiments the relative intensity, at various angles, was determined by monitoring the incident beam with a scintillation counter which counted the number of alpha-particle elastically scattered through some fixed angle, usually 45°. No absolute measurements of the cross-section were made. In some cases, however, in which the elastic scattering cross-section is known, absolute values can be determined.

2.2. TREATMENT OF DATA

In experiments such as these, in which one has of the order of 10^4 individual data points, there is a serious question as to how these data should be treated. Specifically, it is necessary to convert the observed pulse-height spectrum to an energy spectrum. At the time these experiments were undertaken no computer program for analyzing the data was available. Now, however, such programs exist [21]). To deduce the excitation energy corresponding to the observed peaks it is necessary to make a number of empirical corrections and calculate, through the appropriate kinematical expression, the Q value for the reaction. Two important corrections are necessary to deduce the energy of the inelastically scattered alpha particle from the observed pulse height: This pulse height must be corrected for the non-linear response of the E detector [22]), and also for the energy loss in traversing the target, scattering chamber window and proportional counter. Rather than make these corrections for each peak of interest we constructed a calibration curve shown in fig. 4 incorporating both the effects mentioned. This curve was then checked by measuring the elastic and inelastic alpha particle spectrum from C^{12} and Au and comparing the observed pulse-height ratio to those expected on the basis of the known [23]) Q-values for the appropriate reactions. In fig. 4 are shown the calibration curves for three incident energies, 30, 27 and 24 MeV. The comparison with carbon was made assuming 30 MeV for the incident alpha particles energy. The data are seen to

be quite consistent with our assumed beam energy, target and counter thickness, and non-linearity assumptions concerning the response of CsI.

As can be seen from fig. 4 the calibration we made was in terms of the elastically scattered α particles. The reason for this is that the ratio of the energy of an outgoing alpha particle from a given level to that of the elastically scattered alpha particles is practically a constant, independent of angle and incident beam energy. Non-linearity of the detector, and kinematic considerations make the pulse-height ratio decrease only slightly with increasing Q-value and angle.

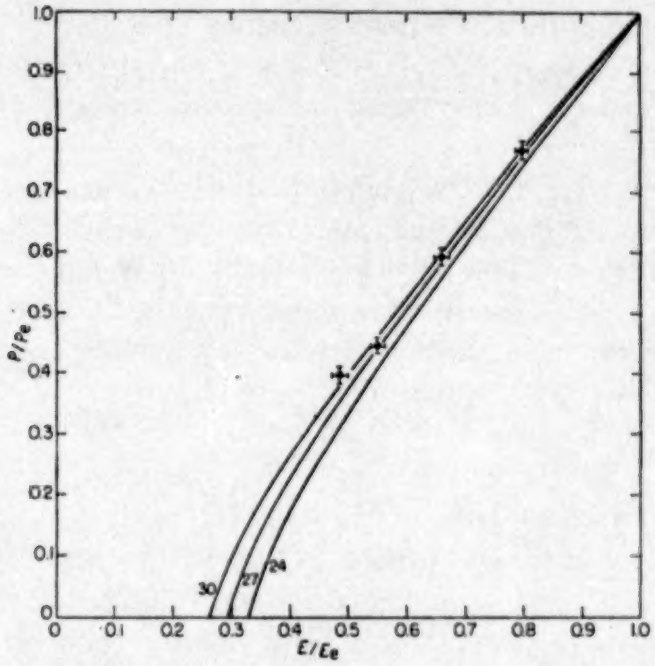

Fig. 4. Calibration curve of pulse height to energy relationship for the scheme used. The points illustrate the data for the scattering from carbon relative to Au elastic scattering.

In fig. 5 we have illustrated the data for Al, the lightest element studied. In this figure the spectra are plotted, at various angles, normalized to the elastic peak. The abscissa is plotted as the negative of the Q-value for inelastic scattering calculated for the most forward angle. It is seen that there is a shift of the order of only 10 % arising from kinematic corrections and non-linearity in this light nucleus. Fig. 6 shows similar data for one of the heavier nuclei studied, Cd, illustrating the fact that for the heavier nuclei the shift is negligible. Because of the large quantity of data to be processed we have presented our data only as shown in figs. 5 and 6. The energy of the outgoing particles from the anomalous states shifts in a manner understood as indicated above. The deduced Q-values have had all the kinematical, non-linear response, and absorption corrections applied to the appropriate pulse-height groups.

2.3. EXPERIMENTAL RESULTS

Figs. 5—9 show some of the experimental results for Al, Fe, Ni, Zr, and Cd. These curves do not present the experimental points but have been drawn in such a manner as to illustrate the characteristics of the spectra as a function of

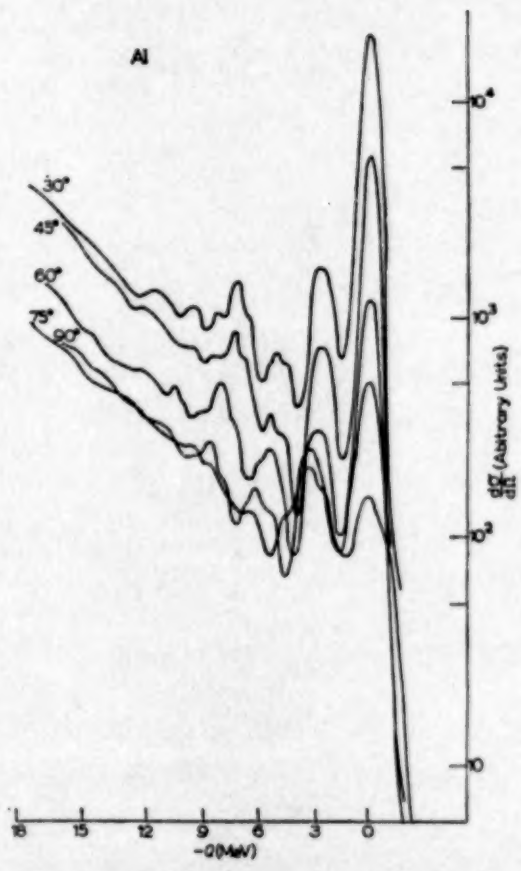

Fig. 5. Typical spectra as a function of excitation energy $(-Q)$ at various angles for Al.

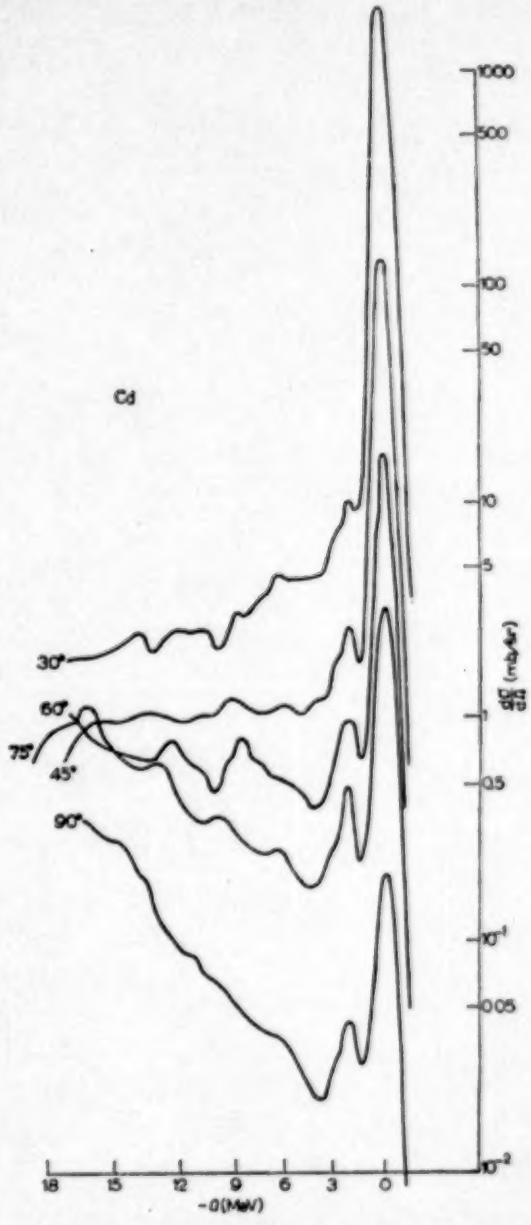

Fig. 6. Typical spectra as a function of excitation energy $(-Q)$ at various angles for Cd.

angle. The slow decrease of the peak location, relative to the elastic peak with increasing angle is seen in several of these curves. The energy scales are accurate to within only about 0.3 MeV and are drawn to correspond to the 30° spectrum in each case. The untreated data were illustrated in a paper by two of the present authors [7]).

As pointed out earlier no specific measurement was made of the differential cross sections. However, from elastic scattering data one can deduce such information [24]). This has been done in the Ni case and the absolute cross-sections are indicated. From other data [25, 26]) one can deduce that at 30° the elastic scattering from an element like Cd should be about 0.7 of Rutherford scattering.

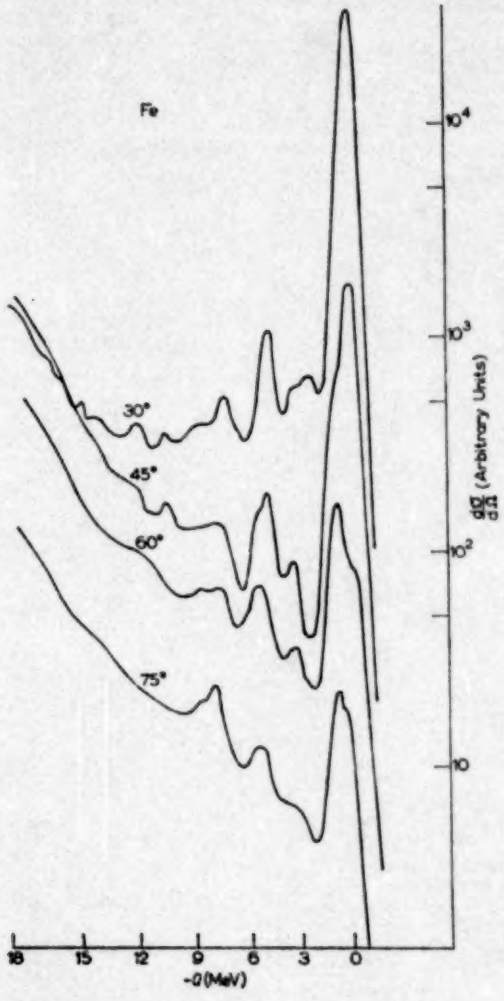

Fig. 7. Typical spectra as a function of excitation energy $(-Q)$ at various angles for Fe.

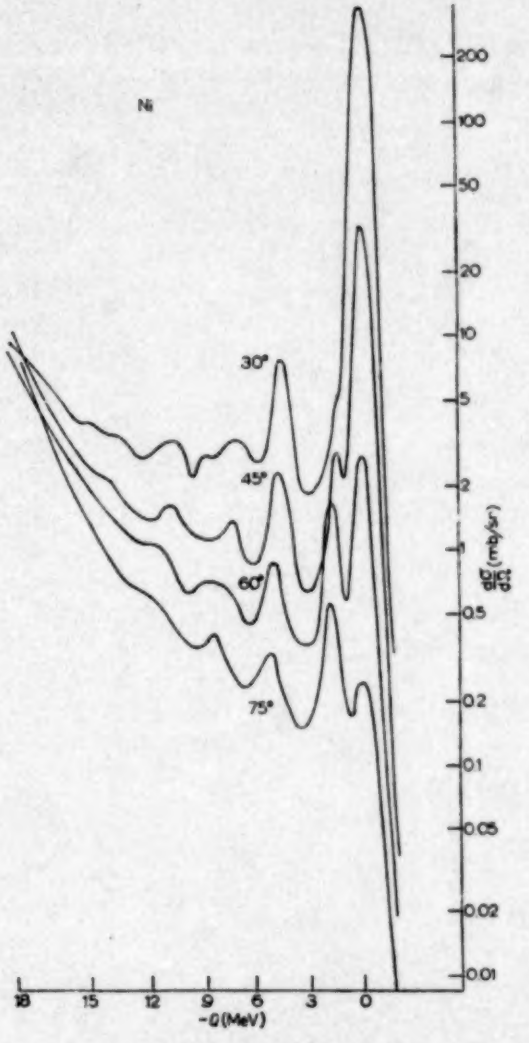

Fig. 8. Typical spectra as a function of excitation energy $(-Q)$ at various angles for Ni.

With this assumption the absolute cross-sections given in fig. 6 were also calculated.

In the case of Ni and Cd the strong anomalous state at 4.6 and 2.5 MeV respectively represent total cross-sections of 180 mb and 60 mb respectively with an accuracy of approximately ± 25 %. The other data illustrated have

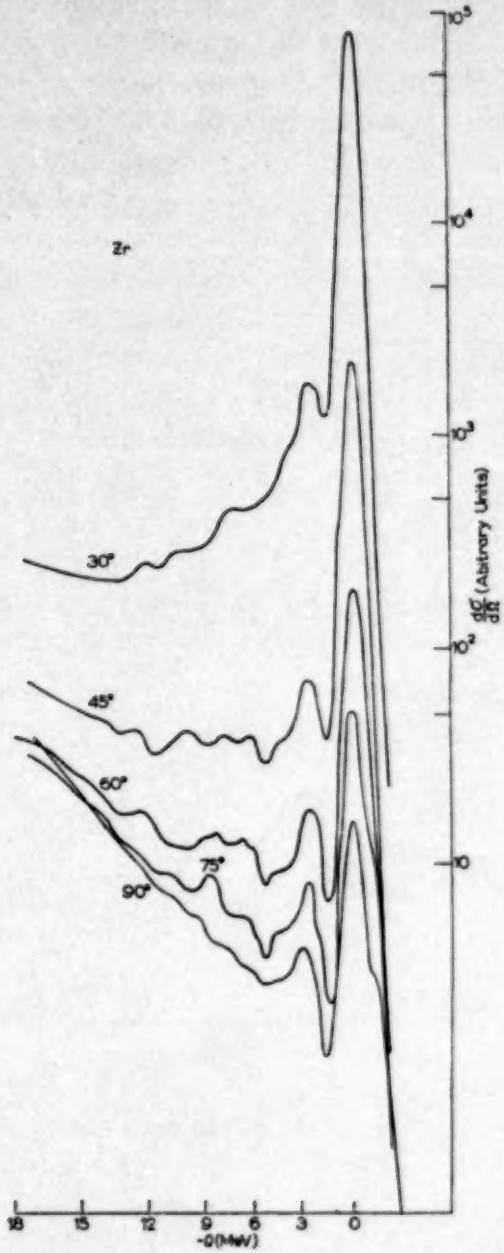

Fig. 9. Typical spectra as a function of excitation energy $(-Q)$ at various angles for Zr.

TABLE 1

Energy levels observed in the anomalous inelastic scattering

Al^{27}	2.69, 4.80, 6.87	Cu	1.10, 3.39, 5.51?
Ti	1.06, 3.38, 6.07	Se	2.98
V^{51}	2.23, 3.72, 6.82	Zr	2.52
Cr	3.60	Nb^{93}	2.40
Fe	1.34?, 2.55, 4.40, 6.82	Rh^{103}	2.15
Co^{59}	1.10, 4.10, 6.30?	Pd	2.12
Ni	1.43*, 4.37, 6.33, 10.2	Ag	2.28
Ni^{58}	1.45*, 4.60	Cd	2.12
Ni^{60}	1.33*, 4.15		

only the relative cross-sections indicated. Relative cross-sections for all these experiments are accurate to an estimated $\pm 10\,\%$.

Table 1 lists the various elements studied and the energies corresponding to the various groups we observed. Those energies marked by an asterisk may be associated with known levels or groups of two or three levels in the appropriate nuclei [27]) †. The accuracy of the energy measurements is ± 0.3 MeV.

Fig. 10 is a composite of all the experimental results drawn as an energy level diagram. This is only intended as a way to compare all the present experiments with each other, and is not an attempt to portray energy levels of the various nuclei. If one compares these results with the results of Cohen [4]), one sees a general agreement with respect to the location of the various anomalous states.

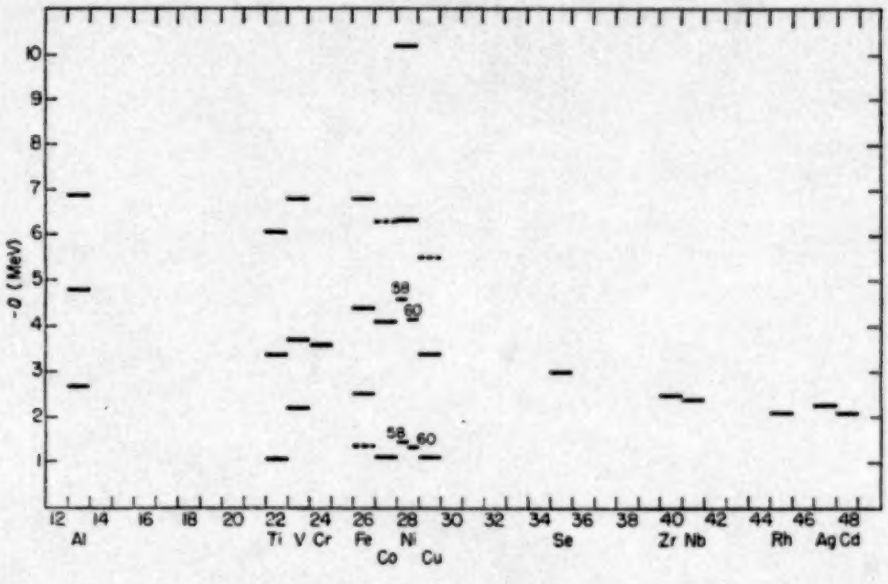

Fig. 10. Location of anomalous states observed in these experiments. Questionable states are shown as dotted lines. The notation on Ni refers to the particular isotope.

Because of the fact that the cross-sections are forward-peaked, one believes that they are representative of a direct excitation process. The details of such an interaction indicate that, if the anomalous state is indeed made up of several states, the Q-value comparisons of different experiments may not be significant, since, at a given momentum transfer (determined by incident energy and angle), the various contributions to the scattering may be different.

Quantitative comparisons of the relative intensity will not only suffer by the same token, but are further made difficult because of the different background causes in the various experiments.

† The various MIT-LNS progress reports of Prof. Buechner's group [28]) present a large number of energy levels for some of the nuclei studied in these experiments

3. Inelastic Scattering Angular Distributions

From the type of data shown in figs. 5—9 one can see that, generally speaking, the alpha particles leave the nucleus in a low state of excitation and come off predominantly in the forward direction. At higher excitation energies the alpha particles are more nearly isotropic. In fact, for some elements the cross-section in the 15—18 MeV excitation region seems isotropic to within about 20 %.

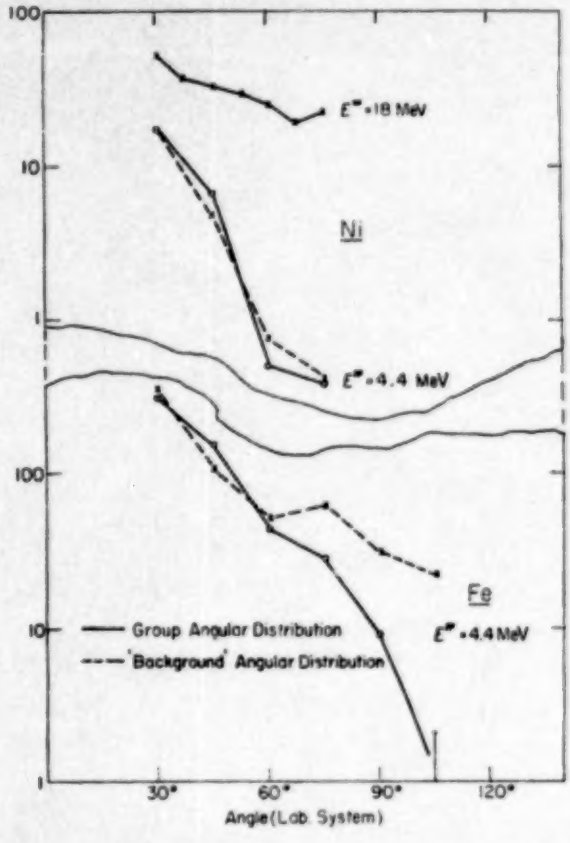

Fig. 11. Angular distribution for the anomalous states and background in Fe and Ni.

Fig. 11 illustrates that both the anomalous peak and the background below the peak are both strongly peaked forward. Further illustrated is the near isotropic nature of the high excitation energy data.

In a separate series of experiments a number of detailed angular distributions were measured. In these experiments we were able to utilize the known excitation energy of the anomalous states and selected elastically and inelastically scattered alpha particles by using a very thin ($\approx$ 0.051 cm) NaI(Tl) scintillation crystal. In a crystal of this thickness the largest size proton pulse corresponds to an energy loss of about 12 MeV. The alpha particles, corresponding to the excitation of the 4.5 MeV states in the Ni isotopes have an approximately 22 MeV energy loss in the crystal. Even allowing for the fact that the light output of NaI is less for alpha particles than protons [29]), one sees that the alpha

particles are clearly identified. With such a scheme for particle identification the angular distributions were readily obtained using the scattering chamber described in refs. [19, 20]).

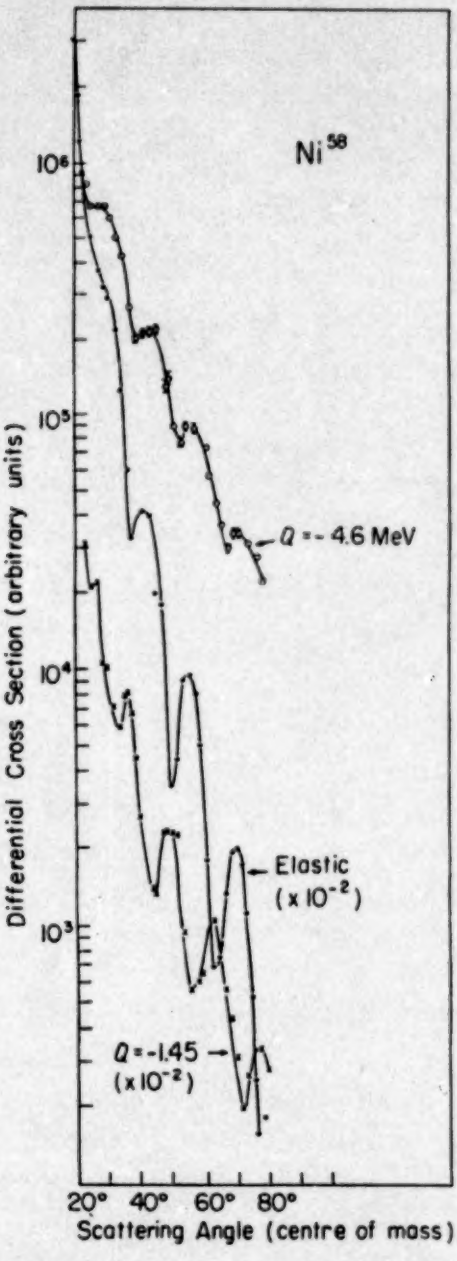

Fig. 12. The angular distribution for alpha particles scattered from Ni^{58} leaving it in the ground, first excited and anomalous states.

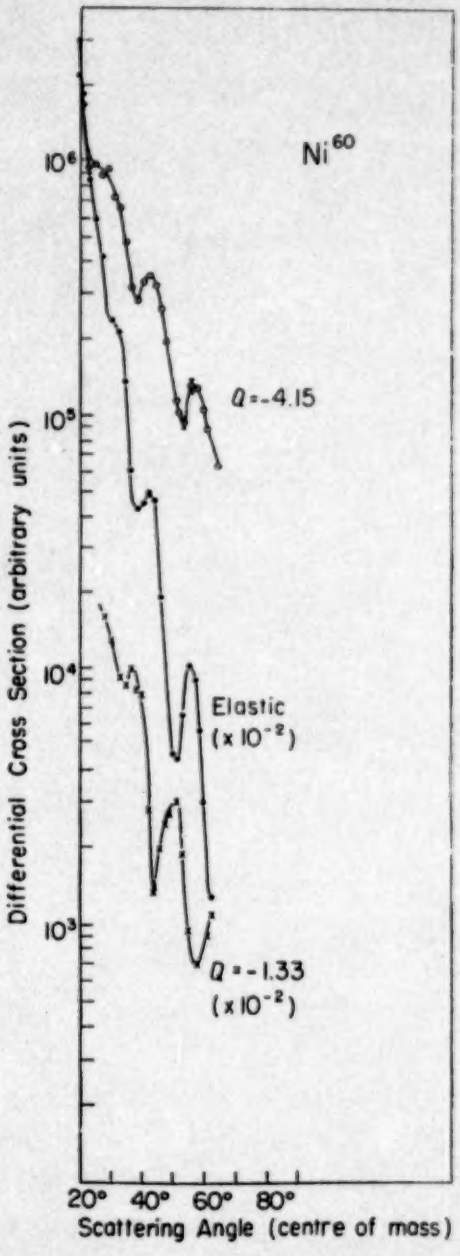

Fig. 13. The angular distribution for alpha particles scattered from Ni^{60} leaving it in the ground, first excited and anomalous states.

Detailed angular distributions were obtained in this manner for the scattering from Ni^{58}, Ni^{60}, Zr, Nb, Rh^{103} and Ag. These results are shown in figs. 12—17. In deriving these results from the experimental data it has been necessary to treat the data somewhat arbitrarily with respect to background. The inelastic

groups are sitting on a background which may vary with angle in a different manner from the anomalous peak. However, the data of fig. 11 show that, at least in these two cases, the background varies in a manner similar to the anom-

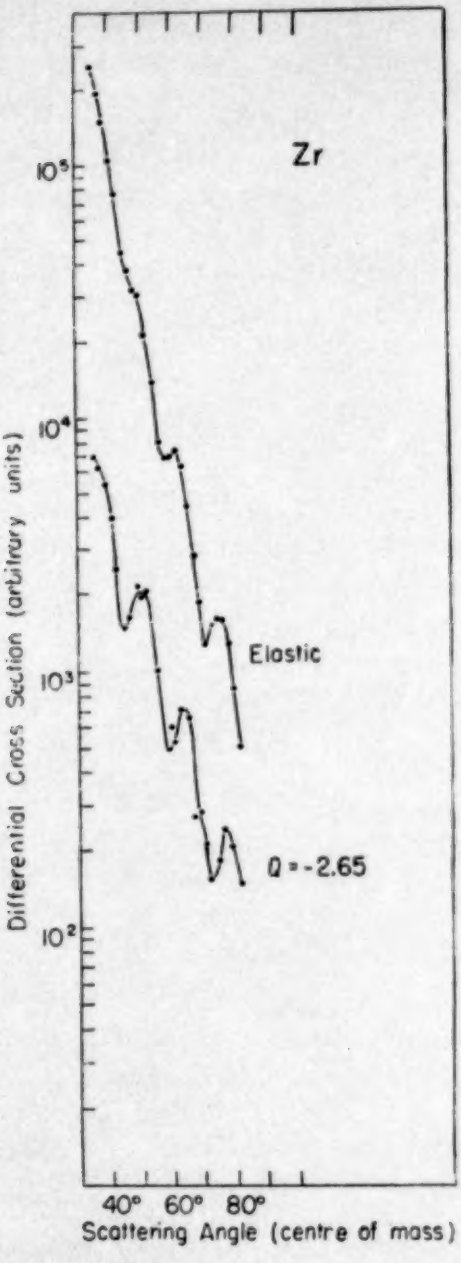

Fig. 14. The angular distribution of elastic and inelastic alpha particles from Zr.

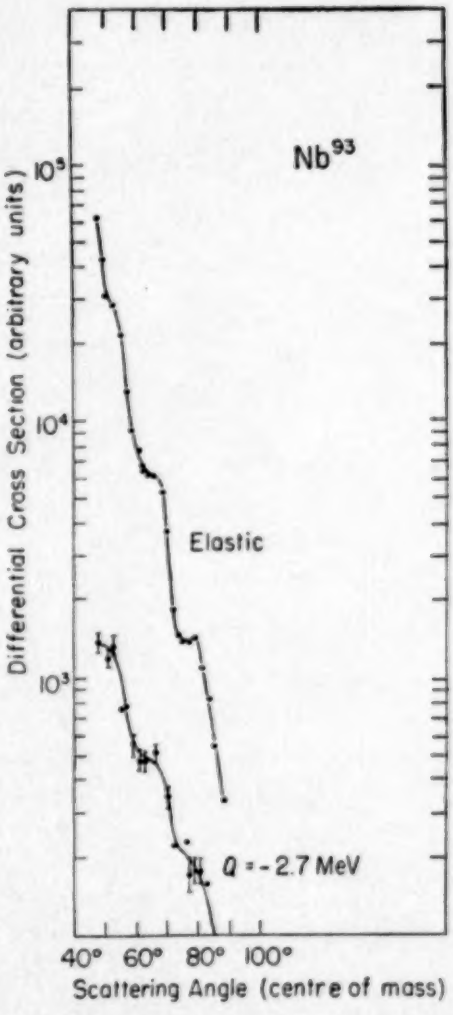

Fig. 15. The angular distribution of elastic and inelastic alpha particles from Nb.

alous peak. To subtract the background a curve was drawn on the observed spectrum representing the shape of an idealized peak; the area of the peak was measured and a contribution was subtracted due to an extrapolation of the part of the spectrum of lower energy than the group of interest, as well as the

contribution from the low energy side of the intense elastic peak. It is estimated that, even in the worst case, the background subtraction should not introduce an error of greater than $\pm 15\,\%$.

To interpret these experiments one is of course tempted to apply the various direct interaction theories. The basic problem is that all these theories predict structures which are much sharper and generally speaking do not drop off as

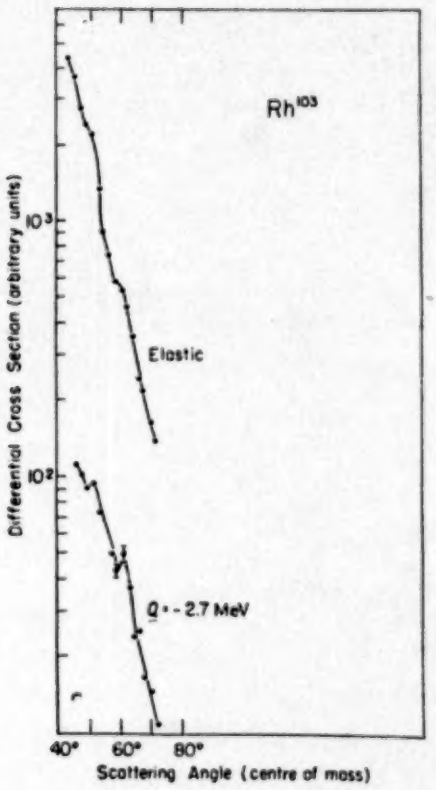

Fig. 16. The angular distribution of elastic and inelastic alpha particles from Rh.

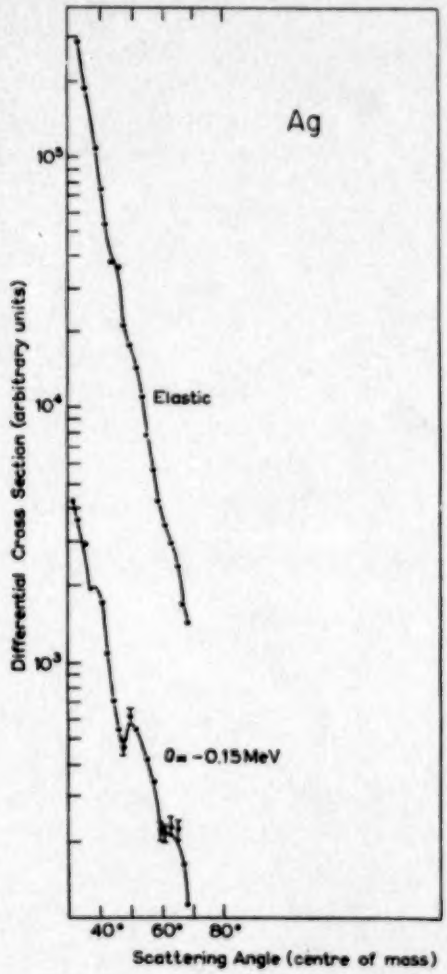

Fig. 17. The angular distribution of elastic and inelastic alpha particles from Ag.

rapidly as a function of angle as do the experimental results. The theoretically predicted maxima and minima have relative cross-sections which differ by a factor of the order of 10, and the envelope of the structure decreases by not much more than a factor of 10 over the range of angles with which we are dealing. The problem confronting us is therefore to see if there are any general characteristics of the data from which we can draw conclusions of physical significance without a detailed analysis. It is possible that a full scale distorted wave calculation along the lines of Levinson and Banerjee [16]) or an approximate

calculation similar to those of Glendenning [17]) might be profitable, but such calculations typically suffer from producing too much structure or requiring too many parameters to fit the data.

It appears from the recent analysis by Blair [12]) that one may in fact be able to deduce at least parity changes and a range of spin changes in the excitation process simply by comparing the location of maxima and minima of the angular distribution corresponding to the state in operation with those corresponding to the elastically scattered alpha particles. In the diffraction analysis he has shown that even parity states will have maxima which occur at the location of the elastic minima and for odd states the angular distributions are in phase with elastically scattered ones.

From figs. 14—17 it is rather obvious that at 30 MeV the elastic scattering is not a simple diffraction type scattering since except for Zr there is practically no structure. Therefore no comparisons of the type mentioned above are really possible. In the case of Zr, there is some structure in the elastic angular distribution but the anomalous state angular distribution seems to be neither in phase nor completely out of phase, but seems definitely correlated with the elastic one. This effect, however, may be a reflection of the fact that in the region of comparison the elastic scattering is still dominated by the Coulomb scattering, rather than by the diffraction scattering. This would cause the minima to appear at somewhat larger angles and the maxima to appear at somewhat smaller angles, assuming that the Coulomb scattering could be represented by an envelope of the diffraction scattering. Such behaviour may give some support to an interpretation of the data as showing that the anomalous state angular distribution is in phase with the elastic one, but cannot of course provide any rigorous justification for it. There is no a priori reason to assume that the Coulomb scattering should be an envelope to the diffraction scattering, and in fact there is experimental evidence which indicates otherwise [24]) †. We, therefore, believe that nothing conclusive can be deduced from the data shown in figs. 14—17 except to note that the locations of the maxima and minima are practically the same, and furthermore the relative intensity of the elastic to inelastic scattering is also practically the same, indicating, we believe, that these anomalous states in all the various nuclei are similar; although we are unable to deduce the spin or even the parity of these states unambiguously we believe them all to be the same.

Recent experiments by Yntema *et al.* [7]) and Thirion *et al.* [7]) have shown that the anomalous state in Zn^{64} at about 2.8 MeV, believed to be similar to the state at about 2.5 MeV which we have studied, can be interpreted either on a diffraction analysis or another version of the direct reaction calculations to be consistent with a spin and parity 3^-. One particularly interesting feature of the call

† In any correct calculation the scattering should be calculated as the square of the sums of the Coulomb and diffraction or general optical scattering amplitudes.

culation of Yntema *et al.* is that in addition to properly predicting the location of the maxima and minima they have an envelope which drops off rapidly enough to fit the relative heights of succeeding maxima †. These authors, however, point out that it is impossible to deduce the spins unambiguously from just the angular distributions. Their data for Ag and Rh do, however, show the inelastic scattering in phase with the elastic scattering, which, according to Blair [12]) or an equivalent Born approximation calculation, does favour the 3^- assignment for these states. It is not believed that the discrepancy in excitation energy between the present work and that of Yntema *et al.* is significant.

In the cases of Ni^{58} and Ni^{60} the situation is much less ambiguous. In both these cases the known first excited states of spin and parity 2^+ show strong diffraction-like behaviour which is out of phase with the elastic distributions, and the anomalous states show strong patterns in phase with the elastic. On the basis of the elastic scattering one deduces [24]) a radius of interaction of about 6.6×10^{-13} cm from the period of the oscillation. For the inelastic scattering the momentum transfer $\mathbf{k}_f-\mathbf{k}_i$ in the centre of mass differs by only about 3 % for the anomalous state and therefore the angles should be displaced less than 1.5° over the range covered in these experiments. The momentum transfers we are dealing with in these experiments are of the order of $3.2\times10^{+13}$ cm^{-1}. With so large momentum transfers the uncertainty in the interaction radius can be quite large if one uses the simple rule that $kR\approx l$ at the first maximum: for $l=2$ or 3, R can have the values 5.2×10^{-13} cm or 7.8×10^{-13} cm respectively and the first maximum may still occur at about 14°, the angle corresponding to that deduced from the elastic scattering radius [24]). Furthermore, the latter radius lies almost exactly midway between the two values given above. This is not surprising since, asymptotically, the diffraction analysis gives an angular distribution proportional to $\sin^2(qR\pm\frac{1}{4}\pi)$ and a Born approximation calculation gives an angular distribution proportional to $\sin^2(qR-\frac{1}{2}(l+1)\pi)$. In other words under either analysis the peak locations are $\frac{1}{2}\pi$ apart for $l=2$ or $l=3$, and furthermore for a given value the two calculations give peak locations also $\frac{1}{2}\pi$ apart.

4. Gamma Ray Measurements

4.1. INTRODUCTION

As indicated in the introduction and the previous section the inelastic scattering of alpha particles, as distinguished from protons, yields angular distributions which are rather simply interpreted on the basis of a plane wave Born approximation or Fraunhofer approximation calculation, except for the ambiguity in radius. As has been pointed out by Levinson and Banerjee [16]) the distortion of the incident wave by the nuclear potential, while possibly destroying

† Prof. Blair has pointed out in a private communication that the calculation of Yntema *et al.* should not be a simple multiplication by the free (α, p) or (p, α) cross-section of the Butler cross-section for large momentum transfers.

the simple Bessel function behaviour of the angular distribution, does not seem to disturb the angular correlation, except in that the axis of symmetry is shifted somewhat from the classical recoil direction. While these ideas have not been too widely tested [30, 31]), particularly for alpha particles [32]) it was felt valuable to undertake a study of the gamma radiation following the excitation of the anomalous states in a number of nuclei.

In this section we report on the de-excitation spectra of the anomalous states in Zr, Ag, Rh^{103} and as well as Ni^{58} and Ni^{60}. In the first three cases there was not sufficient structure in the gamma-ray spectrum to obtain a meaningful angular correlation. In the Ni isotopes, though the anomalous states showed no appreciable decay to the ground state, a line was observed corresponding to the decay to the well-known first excited states of each isotope. An earlier paper by two of the present authors presented the results of the Ni angular correlation [33]).

4.2. EXPERIMENTAL PROCEDURES AND TECHNIQUES

In all the present γ-ray experiments we used a 7.6×7.6 cm NaI scintillation spectrometer mounted on a Dumont 6363 photomultiplier. The particle counter used in the coincidence experiments was a 0.038 cm NaI crystal 3.8 cm in diameter covered with 0.0013 cm of Al foil on a lucite light pipe approximately 5 cm long coated with MgO. The full crystal gave an energy resolution of about 12 % and we therefore reduced the aperture to approximately 2 cm yielding a resolution of approximately 6 %. This crystal was mounted on RCA 6342 photomultiplier. The anode signals of both photomultipliers were each fed to a single Hewlett Packard Model 460 fast amplifier. The output signal of this amplifier was used to drive a Western Electric 404A pentode to saturation producing a limited pulse which was then shaped by a shorted delay line to produce a fairly square pulse about 16 μs wide and 3V high. This shaped pulse was then amplified by a factor 2 by a single tube EFP60 amplifier. The signals were then fed to a standard 6BN6 fast coincidence circuit [34]), with an overall resolving time of approximately 32 ns. This system was found to be stable over a period of several months to better than 2 ns. The particular resolving time chosen was intermediate between the width of the cyclotron beam bursts ($\approx$ 3 ns) and the period of the cyclotron oscillations (82 ns), since earlier measurements [35]) had shown the beam pulse to be very well contained ($\approx$ 99 %) in a time-interval of the order of 5 ns.

Slow signals derived from one of the photodynodes were inverted and amplified in Franklin Electronics Co. Linear Amplifiers which are of the double-differentiation type [36]) providing a rapid restoration of the baseline. This was particularly necessary in the γ-counter inasmuch as counting rates were typically 2×10^4 counts per second with a resulting pile-up ratio (overlap of successive pulses) of the order of 5 %. This much of the circuity is more or

less conventional and requires no particular further explanation. However, the remainder of the circuity, while not profound, does require some explanation.

Fig. 18 shows an overall block diagram of the circuity. There it is seen that the output of the α-counter was fed to a 20-channel pulse-height analyzer. It was possible to extract a signal from each of the 21 discriminators in this analyzer (similar to the Atomic Instrument Model 520) either singly or in groups of any of the channels. It was thus possible to obtain the three signals labelled A, B and C in fig. 18. Typically signal A might represent all those pulses falling in channels 6—10 encompassing the anomalous inelastic peak in Ni^{58}. Signal B would then represent channels 11—15 representing the well resolved first excited state, or some other part of the spectrum possibly below the energy of the inelastic state. Finally channels 16—20 would contain the

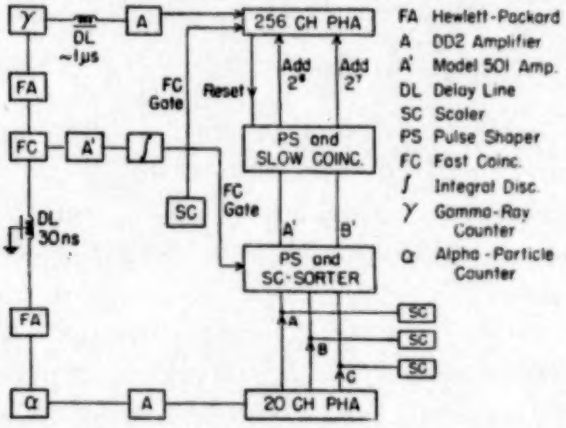

Fig. 18. Block diagram of coincidence analyzer and pulse sorter arrangement.

intense elastic peak and give rise to signal C. In other words these signals corresponded to signals which come from any alpha particle pulse height falling into one of the appropriate channels in the 20-channel analyzer to correspond to three areas of interest in the particle spectrum.

The signals A, B and C were then put into slow-coincidence ($\approx 5\mu s$) with a trigger pulse generated by the fast coincidence circuit and mixed in such a manner as to produce a signal in A′ when there was a signal A, a signal in B′ when there was a signal in B, and a signal in both A′ and B′ when there was signal in C. After describing the behaviour of the γ-counter we shall return to the utilization of signals A′ and B′.

The gain of the γ-ray counter was adjusted so that the entire γ-ray spectrum of interest occupied the first 64 channels of the PHA. In the coincidence experiments the analyzer was gated by an appropriately timed signal from the fast coincidence circuit (this accounts for the 1 μs delay line shown in fig. 18). As described in section 2 a reset signal was extracted from the analyzer. This signal was placed in slow coincidence (≈ 5 μs) with signals A′ and B′ and the

signals labelled add 2^6 and 2^7 respectively were introduced into the appropriate place of the address scaler.

The system then displays the γ-ray spectrum in fast coincidence with the particles corresponding, for example, to the anomalous inelastic group, the first excited group and the elastically scattered alpha particles in channels 65—128, 129—192 and 193—256 respectively. In channels 1—64 we have the γ-ray spectrum in fast coincidences with any other particle detected in the alpha counter. The value in this scheme over the use of a set of three window discriminators set on the various peaks, was simply that with this scheme we could observe the particle peaks continuously and detect any drift or malfunctioning rapidly. Inasmuch as our runs were typically several hours long it was necessary not to have to discard many data, which might have been necessary otherwise.

The reason for monotoring on the elastic peak is related to the fact that in addition to the fundamental modulation of cyclotron beam at 13.1 MHz caused by the phase grouping of the beam there are a number of other variable modulations at about 1 MHz, 150 kHz, 360 and 60 Hz. The first two of these latter modulations may arise from the non-uniform magnetic field in the cyclotron and plasma oscillations in the ion source [37]). The second two undoubtedly arise from inadequate filtering in the three-phase cyclotron oscillator power supply and unequal currents drawn in each of the three phases. Rather than attempting to track down the detailed cause of each of these modulations we thought it best to monitor the chance coincidence rate by measuring the gamma ray spectrum in coincidence with the elastically scattered alpha particles and correcting the inelastic data the product of the observed chance rate the ratio of the single rates in the group of interest to the elastic singles rate.

One further word on the coincidence analysis. If the beam pulses are contained in a short interval of time it can easily be shown that for a pulsed machine there is no increase in the chance rate if the resolving time of the coincidence circuit lies between the width of the beam pulse and the repetition period of the cyclotron. In fact, under these conditions the chance rate can be shown to be simply $N_1 N_2 T$ where N_1 and N_2 are the average singles rates and T is the time between successive beam pulses. Notice that this is independent of the resolving time of the circuit. Since the beam pulse was in fact of the order of 3 ns wide, to decrease the chance rate appreciably would have entailed going to resolving times of the order of 0.5 ns. With NaI for detecting the γ-rays we were studying ($\approx$ 3 MeV) this figure of 0.5 ns corresponds to about a 90 % coincidence efficiency [38]). The stability problems associated with such an operation, particularly when one considers the effects of the varying beam pulse distributions, essentially make such a scheme impractical.

To determine what fraction of the anomalous state decays directly to the ground state or any other state it is necessary to know the overall efficiency of the gamma-ray detector for that particular energy. In the experiments we are

reporting here we utilized two known decay schemes to calibrate our efficiency at appropriate energies. For our geometry and energies (γ rays from about 2—4.5 MeV) the efficiency is only a slowly varying function of energy, showing a decrease of less than 15 % from 2 to 4.5 MeV [39]).

At 2.753 MeV we were able to measure the efficiency of our detector easily by observing the decay of Na^{24} which decays by the emission of two coincident γ-rays very nearly 100 % of the time [40]). At 4.43 MeV we were able to utilize the fact that in the inelastic scattering of either alpha particles or protons the first excited state of C^{12} is strongly excited and decays by γ-radiation to the ground state very nearly 100 % of the time, internal pair formation being negligible [23]).

4.3. RESULTS

Figures 19—21 show the γ-ray spectrum arising from the de-excitation of the anomalous states in Rh^{103}, Ag and Zr. Utilizing the measured efficiency for our gamma-detector we were able to deduce branching ratios for the direct anomalous to ground state transitions of 0.3 ± 0.1, 0.2 ± 0.1 and 0.13 ± 0.05 for Rh, Ag and

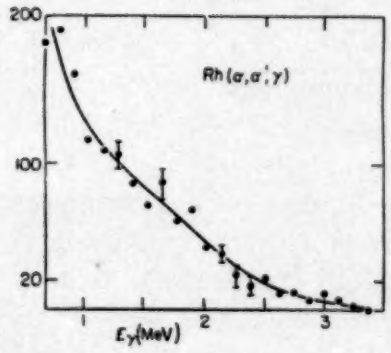

Fig. 19. The gamma-ray decay spectrum of the anomalous state in Rh^{103}.

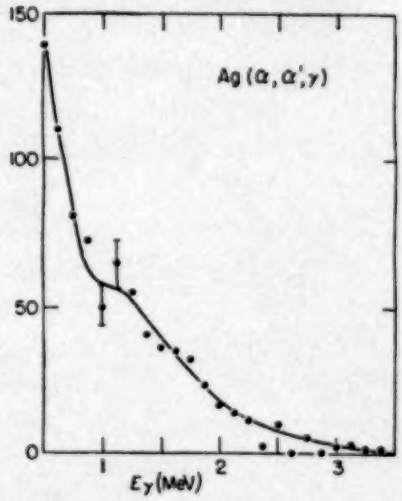

Fig. 20. The gamma-ray decay spectrum of the anomalous state in Ag.

Zr, respectively. The errors given here represent not only statistical errors, but also errors which arise in the estimate of the energy dependence of the NaI spectrometer and errors in the estimate of the background beneath the anomalous peak in the particle detector.

In estimating the branching ratio it is necessary to make some assumption about the expected nature of the spectrum to be able to know what fraction of the area under the entire spectrum can be attributed to the ground state transition. Knowing the energy resolution of our γ-detector for a mono-energetic γ-ray source we are able to utilize the same energy spread in determining

this area which implicitly assumes we are considering the anomalous state to be just one level. The actual energy widths used in evaluating the above numbers were of the order 0.4 MeV. On the other hand the width of the particle spectrum corresponding to the anomalous states is of the order of 1 MeV so that the numbers given above tend to be underestimated. However, for Rh and Ag the fact that the spectrum is monotonically decreasing, with no pronounced structure, particularly near the ground state, indicates that the anomalous state does not decay directly to the ground state, whether there are one or more levels in the 1 MeV wide peak representing the anomalous states. It is therefore believed that the numbers given above actually represent a reasonable evaluation of the branching ratio from the observed spectra.

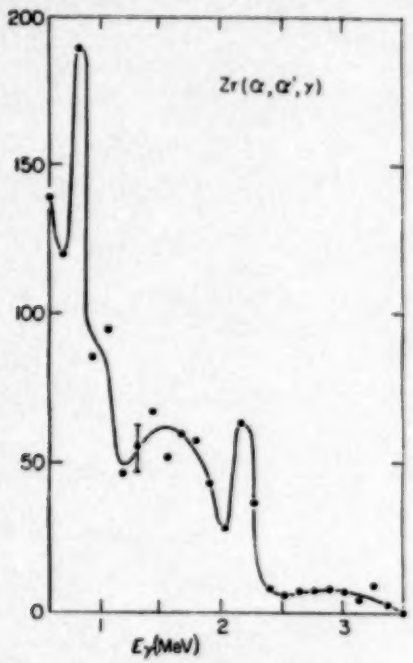

Fig. 21. The gamma-ray decay spectrum of the anomalous state in Zr.

For the case of Zr the situation is quite different. The known levels of Zr^{90}, the most abundant isotope, show four levels in the first 3 MeV excitation [40]). In addition to the levels reported by Sheline *et al.* [41]), a level at 2.76 MeV has also been reported by R. Day [42]). The fact that there are no states in the first 1.5 MeV of excitation means that any ground state transition would of course be well resolved. We do in fact see a weak peak at about 3 MeV, representing a ground state transition which occurs in 13 ± 5 % of the total number of anomalous excitations. However, a strong peak at 2.2 MeV, probably corresponding to the major components of the anomalous state decaying through the 2.13 and 2.32 MeV levels is observed 0.42 ± 0.15 of the time. In evaluating the branching ratios from Zr we have assumed that the anomalous state all arises

from the Zr^{90}. In all probability the state we observe is a mixture of the 2.76 state reported by Day in the inelastic neutron scattering experiments and the 2.182 and 2.315 MeV levels observed in the decay of Nb^{90}.

The low intensity of the ground state transitions in Zr, Rh and Ag prevented us from performing a decisive angular correlation experiment. However, this was not the situation in the case of the Ni isotopes. Typical spectra, as well as the angular correlation of the γ-rays from the anomalous state to the first excited state were given in an earlier note by two of the present authors [33]). There it was shown, rather conclusively, that the particular anomalous states at 4.5 and 4.15 MeV in Ni^{58} and Ni^{60}, respectively, could readily be interpreted as having angular momentum and parity $J^{\pi} = 3^{-}$. For completeness the angular correlations reported in ref. [33]) are given in fig. 22.

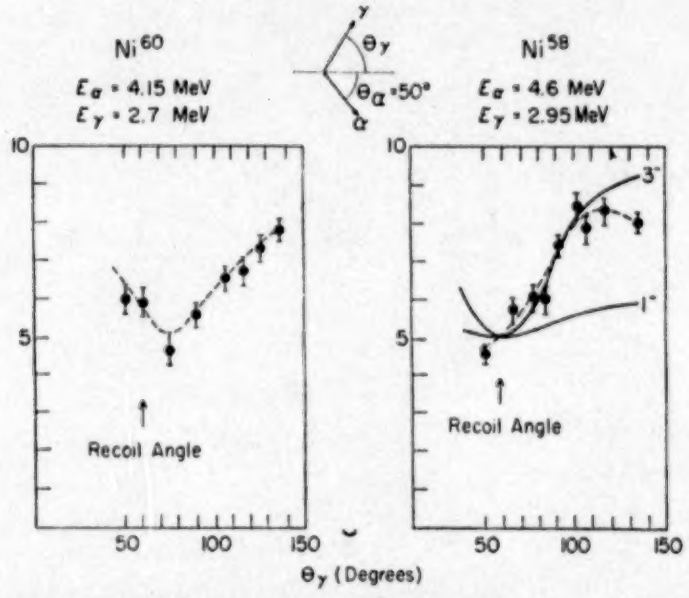

Fig. 22. The angular correlation of the gamma-rays from the anomalous inelastic states in Ni^{58} and Ni^{60} to the first excited states of the respective nuclei. The theoretic curves have had an appropriate angular resolution function folded into them.

5. Discussion

The results of the preceding sections can be summarized briefly by stating there is in nuclei with Z less than 30 a strong anomalous state at an excitation of 4—5 MeV. In two particular cases this state has unambiguously been shown to have a spin and parity 3^{-}. In heavier nuclei the strong anamalous state occurs at an energy of 2—3 MeV and the spin and parity have been shown to be consistent with the state also being 3^{-}. The fact that there is some small branching ratio of the γ-ray de-excitation in the Zr, Rh and Ag imply a spin change by one or more for the anomalous state to ground state transitions in these nuclei.

Recently several authors have indicated that a collective surface vibration of 3^- character could occur at the energies in the range of those observed for the anomalous scattering [43–45]). These authors have generally carried out their theoretical analyses for nuclei at or very near closed sub-shells or shells inasmuch as they were attempting to analyze vibrations of spherical nuclei, i.e. nuclei in the so-called Goldhaber-Weneser [46]) regions. It may be redundant to point out that to establish the nature (collective or single-particle) of a particular state experimentally it is necessary to correlate the energy, spin and parity as well as the transition probabilities, Coulomb excitation cross-sections, or generally speaking strength parameters †. From such data one can then deduce for example the collective parameters C_λ or B_λ or reduced widths compared to single-particle reduced widths.

In the present experiments our only information comes from a comparison of the angular distributions with the predictions of the theory of inelastic diffraction scattering [12]). By a comparison of the theoretical to experimental cross-sections we can find the quantities C_λ, the restoring force parameters for a vibration order λ. As can be seen in Blair's paper, and as we have found when trying to fit data to Blair's expressions the observed angular distribution drop off more rapidly than the predicted ones. For example, in the case of Ni^{58} the four maxima we observe at 28°, 45°, 56° and 71° have intensity ratios of 18.4: 5.9: 2.4 : 1 whereas the theoretical intensity ratios are 2.1 : 1.55 : 1.17 : 1. This discrepancy certainly arises to some degree from the small angle approximations of the theory even though for these comparisons we used the $2k \sin \frac{1}{2}\theta$ recipe to evaluate the momentum transfer. As a result of this disagreement we feel that the values deduced from a direct comparison tend to be over-estimates of the C_λ parameters. However, we can also compare the values for C_2 for the first excited state of deduction these experiments to the value observed in Coulomb excitation. If we make the comparison of theory and experiment at the 27° maximum in the angular distribution of the 1.45 MeV level in Ni^{58} we find $C_2 \approx 90$ MeV, whereas Alder *et al.* [47]) give 77 MeV††, and $C_3 \approx 1000$ MeV†††. A value for C_3 of this magnitude clearly involves collective frequencies comparable to single-particle frequencies. It then becomes questionable whether one can distinguish between collective motion and individual particle motion. On the other hand Araújo [44]) has shown that even if one drops

† From the following discussion in which we deduce the collective parameters C^3 and B^3, we can therefore estimate the lifetime of the states involved.

Note added in proof: There have recently been several measurements of the reduced matrix elements for the ground-state to 3^- state transitions by means of inelastic electron scattering [50]). One finds $B(E3)/B(E3)_{s.p.} \approx 5$. This is too close to the single-particle value to establish clearly the nature of the transitions.

†† The value deduced by Alder *et al.* [47]) may in fact be somewhat low since $B(E2)$ was derived from an experiment [48]) in which there could have been a contribution from other causes than Coulomb excitation.

††† See the note accompanying the Ni^{58} entry in table 2.

the adiabatic approximation the energy of the collective excitation can be written in the same form as for a simple collective vibration:

$$E = \tfrac{1}{2} \sum_{\lambda\mu n} (C_\lambda \alpha^2_{\lambda\mu n} + B_\lambda \dot{\alpha}^2_{\lambda\mu n}),$$

where $\lambda\mu$ is the order of the spherical harmonic describing the vibration and n the index describing the particular harmonic of the vibration frequency. In his calculations he finds C_3/C_3(hyd.) ≈ 1 for O^{16} and of the order of 2.7 for Si^{28}. For the case of Ni^{58} (Ni^{60} gives very nearly the same value) we find C_3/C_3(hyd.) ≈ 6. Lane and Pendelbury, still utilizing an adiabatic approximation find C_3/C_3(hyd.) ≈ 2 independent of the particular nucleus for the 4 cases O^{16}, Ca^{40}, Si^{88} and Pb^{208}. This again implies a danger of using the Blair theory to deduce precise quantitative data from inelastic scattering, a point made clearly also by McDaniels *et al.* [49]). One further point which should be mentioned is that Yntema *et al.* obtain a very fine fit to (α, α') angular distributions utilizing an improved form factor in a single particle description of the inelastic scattering.

In the case of Rh, Yntema's data [7]) can be interpreted in the light of the Blair model as well. If one accepts this interpretation and evaluates C_3 for the 2.5 MeV group we obtain a value of about 3000 MeV if we normalize the experiment to theory at the 32° maximum. Similarly Thirion *et al.* [7]) have studied the inelastic scattering from Zn^{64}. In this case they also have a first excited 2^+ state angular distribution from which we deduce a $C_2 \approx 50$ MeV. Alder *et al.* [47]) give 61 MeV for C_2 for the 1 MeV state in Zn^{64} as deduced from Coulomb excitation data. For the 2.9 MeV 3^- state we find their data give a $C_3 \approx 1500$ MeV. These values for C_3 are again extremely large and imply strong nucleon-surface coupling if not almost an individual particle nature to the states involved.

To recapitulate: for these various cases the Blair theory seems to be a reasonably good prescription for deducing the collective parameters when the states involved are clearly collective vibrations. However, there might be some question as to its validity when the states cannot be simply defined as vibrational.

It is obvious therefore that at present one cannot uniquely decide on the collective nature of the anomalous states for Z in the region greater than 30. As was mentioned in ref. [33]) Goodman has emphasized the single-particle nature of the anomalous states in the intermediate the heavy mass region of the periodic table. If in the case of the Ni isotopes the state involved a strong component of the p neutrons beyond the 28 closed shell, it is quite surprising that Chromium with only 28 neutrons also shows an anomalous state †.

To summarize, we find through Blair's analysis a collective state of spin and parity 3^- in the region of Ni which has a C_3 of a magnitude of the order of 10 times the hydrodynamic model C_3. Lane and Pendelbury's analysis of

† The authors would like to thank M. Banerjee for bringing up this point.

experimental data on the other hand yields values of the order of C_3/C_3(hyd.) ≈ 2. Their analysis, while not involving the uncertainties of the Blair analysis, are specifically for closed shell nuclei. However, they point out that their admittedly simplified theory of vibration—single-particle interaction would yield values of C_3 in the mid-region of the periodic table of the order of 1000 MeV. Table 2 presents a compilation of data pertinent to the question of interpreting the 3^- level observed in various nuclei on the basis of a collective model.

TABLE 2

Octupole parameters

Element	Energy (MeV)	C_3	Type of analysis †	Reference
O^{16}	6.13 ††	100	A	[a]
		650	B	[b]
		240 ± 120	C	[c]
Ne^{20}	7.2	370	B	[b]
Mg^{24}	6.3	3400	B	[b]
Si^{28}		276	A	[a]
S^{32}	4.98	350	B	[b]
Ca^{40}	4.48	1800	B	[b]
	3.73	370	C	[c]
Ni^{58}	4.5	1000 ± 200	B	[d]
		4000	B	[g]
Ni^{60}	4.15	1000 ± 200 ‡	B	[d]
Zn^{64}	2.9	≈1500	B	[e], [f]
		900	B	[g]
Sr^{88}	2.76	367	C	[c]
		≈2000	B	[g], [h]
Rh^{103}	2.5	3000	B	[h], [f]
Pb^{208}	2.61	1500 ± 750	C	[c]
Fe	4.2	2700	B	[g]
Ti	3.5	≈2700	B	[g]

† The symbol A refers to the analysis by Araújo [44]), who performed a detailed calculation with no parameters deduced directly from the level. Systematics would argue that this level in Si^{28} is probably the 4.61 MeV level. The symbol B refers to the Blair inelastic diffraction analysis given in ref. [12]). The symbol C refers to the analysis by Lane and Pendelbury [43]) of lifetime as determined from inelastic electron scattering or direct measurement.

†† In the calculations 6 MeV was used.

‡ The present analysis did not utilize the criterion given in ref. [49]) but normalized the data at the most forward (32°) maximum. Utilizing the 45° maximum we obtain a C_3 of 3500 MeV. We have attempted to deduce a minimum value for C_3 inasmuch as too high a value invalidates the adiabatic approximation.

[a]) See ref. [44]).

[b]) See ref. [12]).

[c]) See ref. [43]).

[d]) Present work.

[e]) Thirion *et al.*, Compt. Rend. **249** (1959) 2189.

[f]) These data have been analyzed by the present authors.

[g]) D. K. McDaniels *et al.*, to be published.

[h]) J. L. Yntema, B. Zeidman and B. J. Raz, to be published.

This table indicates the discrepancy between the various methods of interpreting the several types of experimental data.

It would appear, however, that particularly from Yntema's and Thirion's data the so-called "Cohen bumps", the anomalous states at 2.5 MeV, are, in fact, a collective 3^- surface vibration. However, it will be necessary to measure several more (α, α') angular distributions for Z in the region of 40—50 at energies greater than 40 MeV, or (e, e') angular distributions, to feel rather sure of this statement. Direct lifetime measurements at present seem impossible.

The authors would like to thank Professor Martin Deutsch for many interesting discussions on the experimental problems involved, particularly the complete utilization of the 256-channel PHA. They would also like to thank Prof. A. Kerman for a number of interesting conversations relative to collective nuclear properties.

One of the authors (D. R. S.) would like to thank the Commonwealth Fund for a grant during his stay at M.I.T. The French Atomic Energy Commission assisted in the support of one of the other authors (M. C.) during her visit to M.I.T., and their support is acknowledged.

We should also like to acknowledge the various conversations and prepublication information from Dr. J. L. Yntema and Professors J. S. Blair and G. W. Farwell. A particular debt of gratitude is due to Professor Blair for several valuable comments concerning the manuscript.

References

1) T. Ericson, Nuclear Physics **11** (1959) 481
2) A. G. W. Cameron, Can. J. of Physics, **36** (1958) 1040;
T. Ericson, Nuclear Physics **8** (1958) 265 and Nuclear Physics **6** (1957) 62;
N. Rosenzweig, Phys. Rev. **108** (1957) 817 and **105** (1955) 950;
2a) K. J. Le Couteur, in Nuclear Reactions, edited by P. Endt and M. Demeur (North-Holland Publishing Co. Amsterdam, 1959) Ch. VII
3) J. Blatt and V. Weisskopf, Theoretical Nuclear Physics (Wiley, New York, 1952) p. 367
4) B. L. Cohen and A. G. Rubin, Phys. Rev. **111** (1958) 1568;
B. L. Cohen, Phys. Rev. **105** (1957) 1549;
B. L. Cohen and S. W. Mosko, Phys. Rev. **106** (1957) 995
5) G. W. Greenless *et al.*, Proc. Phys. Soc. **71** (1958) 904;
Kikuchi, Kobayashi and Matsuda, J. Phys. Soc. Japan **14** (1959) 121
6) J. L. Yntema and B. Zeidman, Phys. Rev. **114** (1959) 815
7) J. L. Yntema, B. Zeidman and B. Raz, to be published
J. Thirion, Compt. Rend. **249** (1959) 2189 and private communication;
G. W. Farwell, private communication;
H. W. Fulbright, N. O. Lassen and N. O. Ray Poulsen, Mat. Fys. Medd. Dan. Vid. Selsk. **31** No. 10 (1959);
D. R. Sweetman and N. S. Wall, C. R. du Cong. Int. de Phys. Nucl. 1958, (Dunod, Paris, 1958) p. 547 brief (report of section 2 of the present paper)
8) B. L. Cohen, to be published;
J. P. Schiffer, L. L. Lee, Jr. and B. Zeidman, Phys. Rev. **115** (1959) 427;
R. A. Peck, Jr. and J. Lowe, Phys. Rev. **114** (1959) 847

9) B. L. Cohen and S. W. Mosko, Phys. Rev. **106** (1957) 995;
C. D. Goodman, Phys. Rev. Letters **3** (1959) 320
10) C. D. Goodman, ref. [9])
11) N. Austern, S. T. Butler and H. McManus, Phys. Rev. **92** (1953) 350;
Yntema, Zeidman and Raz, ref. [7]);
N. Austern, in Fast Neutron Physics, to be published;
S. T. Butler and O. Hittmair, Nuclear Stripping Reactions (Horovitz, Sidney, 1957)
12) J. S. Blair, Phys. Rev. **115** (1959) 928
13) S. L. Drozdov, JETP **28** (1955) 734, 736
14) E. V. Inopin, JETP **31** (1956)
15) W. Tobocman, Phys. Rev. **115** (1959) 98
16) C. Levinson and M. K. Banerjee, Annals of Physics **2** (1958) 471, **2** (1957) 499, **3** (1958) 67
17) N. K. Glendenning, Phys. Rev. **114** (1959) 1297
18) R. W. Schumann and J. McMahon, Rev. Sci. Instr. **27** (1956) 675
19) C. E. Hunting and N. S. Wall, Phys. Rev. **115** (1959) 956
20) H. Watters, Phys. Rev. **103** (1956) 1763
21) C. D. Goodman, private communication;
L. W. Swenson, to be published
22) D. R. Sweetman and A. E. Souch, Rev. Sci. Instr. **29** (1958) 794
23) F. Ajzenberg-Selove and T. Lauritsen, Nuclear Physics **11** (1959) 1
24) Swenson, Schindewolf and Wall, Nuclear Physics **6** (1958) 203
25) Wall, Rees and Ford, Phys. Rev. **97** (1955) 726
26) Igo, Wegner and Eisberg, Phys. Rev. **101** (1956) 1508
27) P. M. Endt and C. M. Braams, Rev. Mod. Phys. **29** (1957) 683
28) W. W. Buechner, private communication
29) Taylor *et al.*, Phys. Rev. **84** (1951) 1034
30) R. Sherr and W. F. Hornyak, Bull. Amer. Phys. Soc. **1** (1956) 97 (see also ref. [16]))
31) F. D. Seward, Phys. Rev. **114** (1959) 514;
H. A. Lackner, G. F. Dell and H. J. Hausman, Phys. Rev. **114** (1959) 560;
N. Hintz *et al.*, Progress Report (Univ. of Minnesota, 1958), unpublished
32) G. B. Shook, Phys. Rev. **114** (1959) 310
33) M. Crut and N. S. Wall, Phys. Rev. Letters **3** (1959) 520
34) J. Fisher and J. Marshall, Rev. Sci. Instr. **23** (1952) 417
35) L. W. Swenson, private communication
36) E. Fairstein, Rev. Sci. Instr. **27** (1956) 475
37) K. Boyer, private communication
38) R. E. Bell, in Beta and Gamma-Ray Spectroscopy, edited by K. Siegbahn (North-Holland Publishing Co., Amsterdam, 1955) Ch. XVIII
39) P. R. Bell, in Beta and Gamma-Ray Spectroscopy, edited by K. Siegbahn (North-Holland Publishing Co., Amsterdam, 1955) Ch. V
40) D. Strominger, J. M. Hollander and G. T. Seaborg, Rev. Mod. Phys. **30** (1958) 585
41) S. Bjørnholm, O. B. Nielsen and R. K. Sheline, Phys. Rev. **115** (1959) 1613
42) R. Day, Proceedings of the All-Union Conference on Nuclear Reactions at Low and Medium Energy (Izdat. Akad. Nauk. SSSR, Moscow, 1958)
43) A. M. Lane and E. D. Pendelbury, to be published
44) J. M. Araújo, Nuclear Physics **13** (1959) 360
45) T. Tamura and D. C. Choudhury, Phys. Rev. **113** (1959) 552
46) G. Scharff-Goldhaber and J. Weneser, Phys. Rev. **98** (1955) 212
47) Alder *et al.*, Rev. Mod. Phys. **28** (1956) 432
48) J. P. Schiffer, reported in ref. [45])
49) McDaniels, Blair, Chen and Farwell, Nuclear Physics **17** (1960) 614
50) Crannell, Helm, Kendall, Oeser and Yearian, Bull. Amer. Phys. Soc. **5** (1960) 270

1.D.2:
1.E.4

Nuclear Physics **17** (1960) 684—685; © *North-Holland Publishing Co., Amsterdam*
Not to be reproduced by photoprint or microfilm without written permission from the publisher

VIE MOYENNE DU PREMIER NIVEAU EXCITÉ DE ^{10}B

S. GORODETZKY, R. RICHERT, R. MANQUENOUILLE et A. KNIPPER
Institut de Recherches Nucléaires de Strasbourg

Reçu le 22 mars 1960

Abstract: The half life of the 720 keV state of ^{10}B has been measured by means of a fast time to amplitude converter. The abserved value is

$$T_{\frac{1}{2}} = (6.2 \pm 0.3) \times 10^{-10} \text{ sec.}$$

1. Introduction

La vie moyenne du premier niveau excité du ^{10}B à 720 keV a déjà fait l'objet de plusieurs déterminations [1–6]) en raison de son intérêt théorique (interaction de caractère collectif [7])). La possibilité de mettre le phénomène directement en évidence par la pente de la courbe de coincidences différées en coordonnées semi-logarithmiques nous a incités a reprendre la mesure pour en donner une valeur plus précise.

2. Mesure

Nous avons bombardé une cible de Be métallique de 0.1 mm d'épaisseur avec des protons accélérés a 1.2 MeV environ dans un accélérateur du type Cockcroft-Walton. Les rayonnements γ émis étaient détectés dans des scintillateurs plastiques NE 102 de hauteur 25 mm et de diamètre 20 mm; les photomultiplicateurs étaient des tubes 56 AVP de la Radiotechnique. Sur l'une des voies on n'admettait que la zone d'énergie correspondant aux électrons de recul les plus énergiques du rayonnement γ de 720 keV; sur l'autre voie une sélection d'énergie assez large était faite juste au-delà du maximum de la distribution Compton des rayonnements γ du ^{60}Co. Les coïncidences lentes correspondantes ouvraient la porte d'un analyseur multicanaux. Les coïncidences rapides étaient détectées dans un convertisseur temps-amplitude [8]) dont les impulsions de sortie étaient amplifiées avant d'etre envoyées à l'entrée de l'analyseur multicanaux. La figure montre la courbe de coïncidences différées obtenue. La pente de la droite en coordonnées semi-logarithmiques donne

$$T_{\frac{1}{2}} = (6.2 \pm 0.3) \times 10^{-10} \text{ sec.}$$

L'erreur calculée avec la méthode des moindres carrés tient compte de l'erreur statistique et de celle due au calibrage qui est la plus importante. La courbe de

résolution prompte relevée avec une source de ^{60}Co, dans les mêmes conditions de règlage montre sans ambiguité que cette pente est bien due à la vie moyenne du niveau excité étudié.

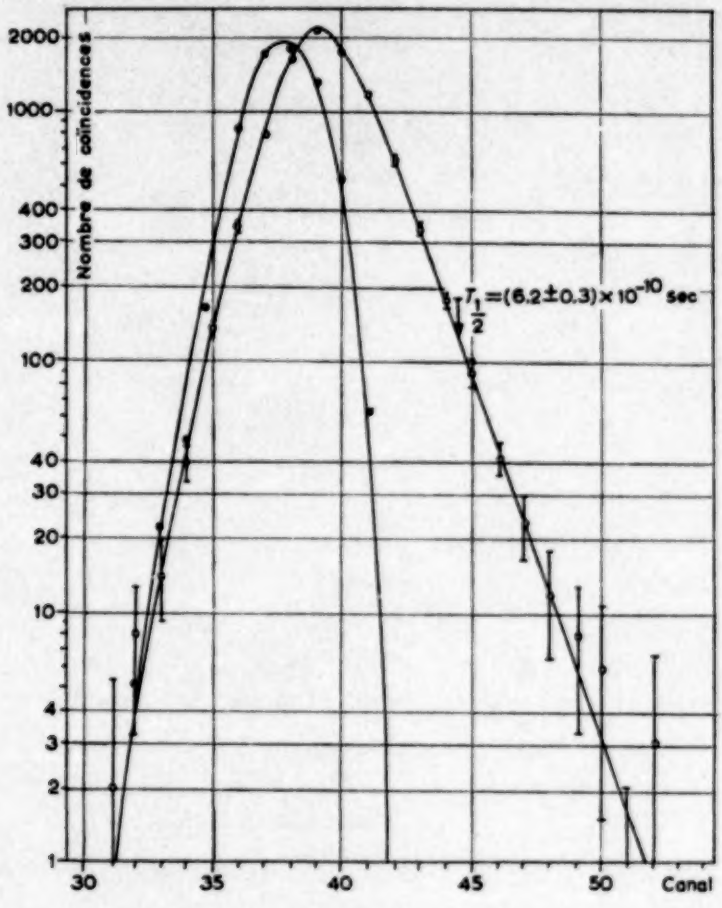

Fig. 1. Vie moyenne du premier niveau excité du ^{10}B. Largeur de canal 5.85×10^{-10} sec ($\pm2\%$).

Bibliographie

1) J. Thirion et V. L. Telegdi, Phys. Rev. **92** (1953) 1253
2) J. C. Severiens et S. S. Hanna, Phys. Rev. **104** (1956) 1612
3) S. D. Bloom, C. M. Turner et D. H. Wilkinson, Phys. Rev. **105** (1957) 232
4) S. Gorodetzky et A. Knipper, Journ. Phys. Rad. **19** (1958) 83;
A. Knipper, Thèse, Université de Strasbourg, Janvier 1958
5) R. E. Holland, F. J. Lynch and S. S. Hanna, Phys. Rev. **112** (1958) 903
6) M. Birk, G. Goldring and Y. Wolfson, Phys. Rev. **116** (1959) 731
7) D. H. Wilkinson, Proc. of the Rehovoth Conference on Nuclear Structure (1958)
8) S. Gorodetzky, R. Richert, R. Manquenouille et A. Knipper, Nuclear Instruments **7** (1960) 50

7.A

Nuclear Physics **17** (1960) 686—694; © *North-Holland Publishing Co., Amsterdam*

Not to be reproduced by photoprint or microfilm without written permission from the publisher

INVARIANCE AND THE *S*-MATRIX

S. KAMEFUCHI †

Imperial College of Science and Technology, London, England

and

Y. TAKAHASHI

Dublin Institute for Advanced Studies, Dublin, Ireland

Received 7 April 1960

Abstract: The transformation property of the state vector in the interaction picture is examined. The invariance condition is relaxed by requiring the invariance of the *S*-matrix only.

1. Introduction

In order to avoid the divergence difficulties inherent in local field theory, many authors have examined the possibility of a non-local field. However, when one tries to formulate such a theory starting from the Heisenberg picture, there immediately arises another type of difficulty in connection with quantization. Moreover, the theory sometimes even fails to remove the divergences [1]). In view of these circumstances, there has recently been another attempt to formulate the theory exclusively within the interaction picture [2]). It may be worthwhile to investigate in more detail the possibility of such a theory, in which we regard the interaction picture as the basis of the theory without recourse to any other picture.

As is well-known, when going over from classical to quantum theory, physical quantities are split into two independent elements, operator and state vector — the "dichotomy" of quantum theory. In so far as one is working only with the Heisenberg or Schrödinger picture, either operator or state vector can be regarded as something fixed and constant in time. On the contrary, in the interaction picture both are variable. Thus, when one wishes to introduce some transformation, there arises a certain freedom in prescribing the transformation property of the state vector, although the transformation property of the operator may in general be uniquely determined from an analogy with classical theory. Because of this fact, there appear some new features in the theory of the interaction picture. For instance, as we shall discuss later, even if the Schrödinger equation in the interaction picture is invariant under a certain transformation, this does not necessarily imply the invariance of all consequences of the theory.

† I. C. I. Research Fellow of University of London. Temporarily in Dublin.

The aim of this paper is to examine in detail the transformation properties of the state vector in the interaction picture, and thereby to discuss how the condition for invariance should be imposed. As one of the necessary conditions for invariance, we consider the transformation and invariance properties of the S-matrix.

2. The Invariance of the Schrödinger Equation in the Interaction Picture and the S-Matrix

We shall examine here the transformation property of the state vector in the interaction picture. As has been shown in previous papers [3]) the transformation property of the state vector in the interaction picture is determined uniquely, if the equation of motion for the operators in the Heisenberg picture is given. Our stand-point in this paper is that the Schrödinger equation in the interaction picture is given first, without recourse to the Heisenberg picture.

Let the interaction Hamiltonian in the interaction picture be $H(\tau)$, then the Schrödinger equation is

$$i\frac{\mathrm{d}}{\mathrm{d}\tau}\Psi(\tau) = H(\tau)\Psi(\tau). \tag{2.1}$$

We want to assign the transformation property of $\Psi(\tau)$ with respect to the transformation

$$H(\tau) \to H'(\tau) \equiv H(\tau)+K(\tau). \tag{2.2}$$

Here, we are assuming for simplicity that $H(\tau)$ does not depend explicitly on the parameter whose variation generates the above transformation, and also that K is an infinitesimal of the first order. The transformed state vector $\Psi'(\tau)$ satisfies a Schrödinger equation of the same form as that for $\Psi(\tau)$, if $\Psi'(\tau)$ is related to the original $\Psi(\tau)$ by

$$\Psi'(\tau) = \{I-iF(\tau)\}\Psi(\tau), \tag{2.3}$$

where

$$i\frac{\mathrm{d}}{\mathrm{d}\tau}F(\tau) = [H(\tau), F(\tau)]+iK(\tau). \tag{2.4}$$

The time-independent solution of (2.4) $-F^0$, where F^0 satisfies

$$[F^0, H(\tau)]+iK(\tau) = 0, \tag{2.5}$$

is the generator of the infinitesimal transformation (2.2) (see examples in section 3), which does not change the state vector at $\tau = -\infty$. The time-dependent solution of (2.4) is readily found to be

$$F(\tau) = U(\tau)\int_{-\infty}^{\tau}\mathrm{d}\tau' U^{-1}(\tau')K(\tau')U(\tau')U^{-1}(\tau), \tag{2.6}$$

which is, due to (2.5),

$$F(\tau) = -iU(\tau)\int_{-\infty}^{\tau} d\tau' U^{-1}(\tau')[H(\tau'), F^0]U(\tau')U^{-1}(\tau), \qquad (2.6')$$

where

$$i\frac{d}{d\tau}U(\tau) = H(\tau)U(\tau), \qquad U(-\infty) = I. \qquad (2.7)$$

Equation (2.6') holds also for a discrete transformation such as space reflection (see section 3).

The existence of the solution (2.6) means that the Schrödinger equation (2.1) is *always* invariant under an arbitrary transformation (2.2) of any given $H(\tau)$.

We shall now prove the following theorems.

(1) *The quantity (in the Heisenberg picture) defined by*

$$\mathbf{F}(\tau) \equiv U^{-1}(\tau)\{F^0+F(\tau)\}U(\tau) \qquad (2.8)$$

is independent of τ.

One has

$$\mathbf{F}(\tau) = U^{-1}(\tau)\{F^0+F(\tau)\}U(\tau)$$
$$= U^{-1}(\tau)F^0U(\tau) - i\int_{-\infty}^{\tau} d\tau' U^{-1}(\tau')[H(\tau'), F^0]U(\tau'). \qquad (2.9)$$

Therefore

$$i\frac{d}{d\tau}\mathbf{F}(\tau) = U^{-1}(\tau)\{[F^0, H(\tau)]+[H(\tau), F^0]\}U(\tau) = 0. \qquad (2.10)$$

Thus, $\mathbf{F}(\tau)$ can be regarded as a kind of generalization of the ordinary conserved quantity.

(2) $\mathbf{F}(\tau)$ *is equal to* F^0.

One first defines a quantity

$$\hat{F}(\tau) \equiv U^{-1}(\tau)F^0U(\tau), \qquad (2.11)$$

then

$$i\frac{d}{d\tau}\hat{F}(\tau) = U^{-1}(\tau)[F^0, H(\tau)]U(\tau) = -iU^{-1}(\tau)K(\tau)U(\tau). \qquad (2.12)$$

Integrating (2.12) from $-\infty$ to τ, one obtains

$$\hat{F}(\tau) = F^0 - \int_{-\infty}^{\tau} d\tau' U^{-1}(\tau')K(\tau')U(\tau'), \qquad (2.13)$$

where use has been made of

$$\hat{F}(-\infty) = F^0. \qquad (2.14)$$

Using the relations (2.6), (2.11) and (2.13), one arrives at

$$U^{-1}(\tau)F^0U(\tau) = -\int_{-\infty}^{\tau} d\tau' U^{-1}(\tau')K(\tau')U(\tau') + F^0, \qquad (2.15)$$

or

$$F^0 = U^{-1}(\tau)\{F^0+F(\tau)\}U(\tau). \qquad (2.15')$$

The comparison of (2.15′) and (2.8) gives immediately

$$\mathbf{F}(\tau) = F^0. \tag{2.16}$$

The existence of the Heisenberg operator $\mathbf{F}(\tau)$ for an arbitrary interaction corresponds to the invariance of the Schrödinger equation under (2.2) and (2.3). This result therefore clearly indicates that the invariance of the Schrödinger equation is not enough to secure the invariance of the whole theory.

For a time translation, the equation (2.15′) is

$$H_0 = U^{-1}(\tau)\{H_0+H(\tau)\}U(\tau), \tag{a}$$

which means that the total energy operator in the Heisenberg picture is the same as the free energy in the interaction picture. This seems strange at first glance. One must remember, however, that the S-matrix formalism is based on the assumption that there be no energy shift [4]). We assumed further that bound states can be ignored, that is, that $U(\tau)$ is unitary. Therefore the energy shift for a state Φ_α becomes

$$\Delta E_\alpha = (\Phi_\alpha, \mathbf{H}(\tau)-H_0\Phi_\alpha) = 0,$$

due to (a). This is consistent with the assumption. The effect of the energy shift is included in the interaction Hamiltonian $H(\tau)$ (the mass renormalization). In this case

$$F(\infty) = S\int_{-\infty}^{\infty} d\tau U^{-1}(\tau)\frac{dH(\tau)}{d\tau}U(\tau)S^{-1} = H(\infty)-SH(-\infty)S^{-1} \to 0 \text{ (adiabatically).}$$

Next we define the S-matrix by [4])

$$\Psi(\infty) = S\Psi(-\infty), \qquad \Psi'(\infty) = S'\Psi'(-\infty). \tag{2.17}$$

Since we have

$$\Psi'(-\infty) = \Psi(-\infty), \tag{2.18}$$

(the generator F^0 transforms only the field operators but not Ψ), the relation (2.3) yields

$$S' = \{I-iF(\infty)\}S,$$

or

$$\delta S \equiv S'-S = -iF(\infty)S = -iS\int_{-\infty}^{\infty} d\tau U^{-1}(\tau)K(\tau)U(\tau). \tag{2.19}$$

We now arrive at the following theorems.

(3) *The S-matrix is invariant under* (2.2), *if and only if*

$$\int_{-\infty}^{\infty} d\tau U^{-1}(\tau)K(\tau)U(\tau) = 0. \tag{2.20}$$

This is obvious from (2.19).

(4) *There exists a constant of collision associated with the transformation* (2.2), *if* (2.20) *holds.*

The proof is, from (2.15′),

$$[S, F^0] = F(\infty)S = S\int_{-\infty}^{\infty} d\tau U^{-1}(\tau)K(\tau)U(\tau) = 0. \tag{2.21}$$

The quantity $F^0[=\mathbf{F}(\tau)]$ is therefore a constant of collision, which can be diagonalized simultaneously with the S-matrix [5]), thus leading to selection rules.

The invariance condition (2.20) is less restrictive than the ordinary condition given usually in a differential form.

3. Examples

In order to make concrete the discussion in the previous section, we shall consider three well-known examples: the proper Lorentz transformation, the gauge transformation and the space reflection.

3.1. PROPER LORENTZ TRANSFORMATION

For an infinitesimal Lorentz transformation

$$x_\mu \to x'_\mu = (\delta_{\mu\nu}+\delta\omega_{\mu\nu})x_\nu, \qquad \delta\omega_{\mu\nu} = -\delta\omega_{\nu\mu}, \tag{3.1}$$

we have

$$K(\tau) = H'(\tau)-H(\tau) = \tfrac{1}{2}\delta\omega_{\mu\nu}\frac{\mathrm{d}M_{\mu\nu}(\tau)}{\mathrm{d}\tau}, \qquad F^0 = \tfrac{1}{2}\delta\omega_{\mu\nu}M^0_{\mu\nu}. \tag{3.2}$$

Here $M^0_{\mu\nu}$ is the angular momentum operator for free fields and

$$M_{\mu\nu}(\tau) \equiv \int \mathrm{d}^4x(n_\mu x_\nu - n_\nu x_\mu)\delta(nx+\tau)\mathscr{H}(x) \tag{3.3}$$

where the interaction Hamiltonian density $\mathscr{H}(x)$ is assumed to be an n_μ-independent scalar, n_μ being a time-like unit vector with $n_0 > 0$. In the case of quantum electrodynamics the interaction Hamiltonian density is

$$\mathscr{H}(x) = j_\lambda(x)A_\lambda(x) \tag{3.4}$$

and

$$[\mathscr{H}(x), \mathscr{H}(y)] = 0, \quad (x-y)^2 \geqq 0. \tag{3.5}$$

From (2.6) and (3.2), we have

$$\begin{aligned} F(\tau) &= \tfrac{1}{2}\delta\omega_{\mu\nu}U(\tau)\int_{-\infty}^{\tau}\mathrm{d}\tau' U^{-1}(\tau')\frac{\mathrm{d}M_{\mu\nu}(\tau')}{\mathrm{d}\tau'}U(\tau')U^{-1}(\tau) \\ &= \tfrac{1}{2}\delta\omega_{\mu\nu}M_{\mu\nu}(\tau)+\tfrac{1}{2}i\delta\omega_{\mu\nu}U(\tau)\int_{-\infty}^{\tau}\mathrm{d}\tau' U^{-1}(\tau')[M_{\mu\nu}(\tau'), H(\tau')]U(\tau')U^{-1}(\tau). \end{aligned} \tag{3.6}$$

The second term of (3.6) is zero on account of (3.5). We have, therefore,

$$F(\infty) = \lim_{\tau\to\infty}\tfrac{1}{2}\delta\omega_{\mu\nu}M_{\mu\nu}(\tau), \tag{3.7}$$

which vanishes adiabatically. The S-matrix is therefore *adiabatically* invariant.

3.2. GAUGE TRANSFORMATION IN QUANTUM ELECTRODYNAMICS

Consider an infinitesimal gauge transformation

$$A_\lambda(x) \to A_\lambda(x)-\partial_\lambda\delta\Lambda(x), \qquad \psi(x) \to \psi(x), \qquad \Box\delta\Lambda(x) = 0. \tag{3.8}$$

The interaction Hamiltonian transforms as

$$K(\tau) = H'(\tau) - H(\tau) = -\int \mathrm{d}^4x\,\delta(nx+\tau) j_\lambda(x)\partial_\lambda \Lambda(x) = \frac{\mathrm{d}}{\mathrm{d}\tau} G(\tau), \quad (3.9)$$

with

$$G(\tau) = \int \mathrm{d}^4x\,\delta(nx+\tau) n_\lambda j_\lambda(x)\delta\Lambda(x). \quad (3.10)$$

The equation (2.6) reads therefore

$$F(\tau) = U(\tau)\int_{-\infty}^{\tau} \mathrm{d}\tau' U^{-1}(\tau')\frac{\mathrm{d}G(\tau')}{\mathrm{d}\tau'} U(\tau')U^{-1}(\tau)$$

$$= G(\tau) + iU(\tau)\int_{-\infty}^{\tau} \mathrm{d}\tau' U^{-1}(\tau')[G(\tau'), H(\tau')]U(\tau')U^{-1}(\tau) = G(\tau), \quad (3.11)$$

since

$$[n_\lambda j_\lambda(x), j_\mu(y)] = 0, \qquad (x-y)^2 \geqq 0. \quad (3.12)$$

We have, therefore.

$$F(\infty) = \lim_{\tau\to\infty} G(\tau), \quad (3.13)$$

which is also adiabatically zero.

Incidentally, the quantity $G(\tau)$ in (3.10) is nothing but the Tomonaga-Schwinger unitary transformation for the infinitesimal gauge transformation [6]). The relation

$$G^0 = U^{-1}(\tau)\{G^0 + G(\tau)\}U(\tau) \quad (3.14)$$

is easily verified, with

$$G^0 = \int \mathrm{d}^4x\,\delta(nx+\tau)\{n_\mu\partial_\mu[\delta\Lambda(x)]\partial_\lambda A_\lambda(x) - [\delta\Lambda(x)]n_\mu\partial_\mu\partial_\lambda A_\lambda(x)\}. \quad (3.15)$$

Equation (3.14) means that, when written in terms of Heisenberg operators $\mathbf{A}_\mu(x) = U^{-1}(\tau)A_\mu(x)U(\tau)$, the operator G^0 takes the same form as (3.15).

3.3. SPACE REFLECTION

So far we have considered only the infinitesimal transformation of continuous groups. We shall now show that even in the case of a discrete transformation the arguments run almost parallel to the continuous case. As an example, let us consider space reflection.

Evidently,

$$F^0 = P^0, \quad (3.16)$$

where P^0 is the well-known parity operator for free fields, and is thus time-independent if the free field equations are invariant under the Lorentz transformation corresponding to space reflection. We shall also define $F(\tau)$ by the

same expression as (2.6'):

$$F(\tau) \equiv P(\tau) = -iU(\tau)\int_{-\infty}^{\tau} d\tau' U^{-1}(\tau')[H(\tau'), P^0]U(\tau')U^{-1}(\tau). \quad (3.17)$$

The transformation of the state vector (2.3) has now to be replaced by

$$\Psi'(\tau) = [P^0 + P(\tau)]\Psi(\tau). \quad (3.18)$$

Under this unitary transformation the Schrödinger equation remains invariant even if H contains so-called parity violating terms.

The "parity operator in the Heisenberg picture" $\mathbf{P}(\tau)$ is defined by (2.8), and is equal to the time-independent operator P^0 by virtue of the theorem (2). It is very interesting to see that $\mathbf{P}(\tau)$ thus defined is nothing but the operator which has recently been introduced by one of the present authors (S. K.) and Tiomno [7]) from quite a different consideration. They have shown that $\mathbf{P}(\tau)$ has many favourable features, for instance, that the vacuum and stable particle states have definite parities with respect to $\mathbf{P}(\tau)$, although this is not the case with the ordinary parity operator $U(\tau)P^0U^{-1}(\tau)$.

Note added in proof: An additional remark on the parity operator. Two state vectors combined by the relation (3.18) do not satisfy the initial condition (2.18). Thus, the relations (2.19)—(2.21) do not hold true for the parity operator defined by (3.16)—(3.18). However, we can introduce the operator in an alternative way, so that the new operator satisfies the above mentioned initial condition.

Let

$$H(\tau) \to H'(\tau) \quad (2.2a)$$

and

$$\Psi(\tau) \to \Psi'(\tau) = \mathfrak{p}(\tau)\Psi(\tau) \quad (3.3a)$$

be the transformations of the Hamiltonian and the state vector under space reflection. Then, (2.4) will be replaced by

$$i\frac{dP(\tau)}{d\tau} = H'(\tau)P(\tau) - P(\tau)H(\tau) \quad (2.4a)$$

The time independent solution of (2.4a) is identical with (3.16), for it satisfies

$$H' = P^0H(\tau)P^{0-1} \quad (2.5a)$$

On the other hand, the time dependent solution of the same equation, which satisfies the required condition

$$P(-\infty) = I \quad (2.18a)$$

is given by

$$P(\tau) = P_0U(\tau)P_0^{-1}U^{-1}(\tau) \quad (2.6a)$$

Thus, (2.19) is now replaced by

$$S' = P(\infty)S \tag{2.19a}$$

From (2.6a) and (2.19a) it follows that $S' = P_0 S P_0^{-1}$. Therefore, the condition for the invariance of the S-matrix is given by

$$[S, P^0] = 0 \tag{2.21a}$$

The parity operator in the Heisenberg picture $\mathbf{P}(\tau)$ is now defined by $\mathbf{P}(\tau) = U^{-1}(\tau) P_0^{-1} P(\tau) U(\tau)$, which is seen to be equal to P_0, and is therefore identical to that discussed at the end of section 2.

4. Discussion

We have shown in the preceding sections that under an arbitrary transformation (2.2) of H, the Schrödinger equation can always be kept invariant if we simultaneously make another transformation (2.3) of the state vector Ψ. Corresponding to this, there exists in the Heisenberg picture a formally conserved quantity $\mathbf{F}(\tau)$. On the other hand, we know that ordinary field theories in which the Lagrangian or Hamiltonian formalism is possible are, of course, not always invariant under a given transformation. Thus, what our result really means is simply that the condition for invariance of Schrödinger equations in the interaction picture is not at all sufficient to secure the invariance of the whole theory. Or, in other words, we may say that there is no definite criterion for invariance so long as we are concerned only with the interaction picture.

We should also remark that the quantity $\mathbf{F}(\tau)$ in general case is not a physical quantity of the ordinary kind: $\mathbf{F}(\tau)$, or $F(\tau)$, becomes a non-local quantity, which depends on all the past history. Moreover, although $\mathbf{F}$ is conserved in time, it does not lead to useful selection rules. Of course, we can prove that in cases of ordinary invariant theories which can be derived from invariant Lagrangians, $\mathbf{F}$ becomes a local quantity, which coincides with the ordinary expression for a constant of motion.

At first sight it may seem, therefore, that a possible criterion for invariance of the theory is to see whether $\mathbf{F}(\tau)$ is local or non-local. However, in the case of a non-local interaction, such a criterion is not valid at all, because of its inherent non-local character.

One necessary condition for invariance is to require the invariance of the S-matrix. The condition is given in integral form in (2.21), in contrast with the differential one in usual formalisms. Thus, it is obvious that our condition is weaker than those of usual local field theories. An example of this is the gauge transformation: For a general gauge function such that $\Box \Lambda \neq 0$, the Lagrangian of electrodynamics and the subsequent formalism in the interaction picture

are not invariant. It is evident, however, that our condition (3.13) is still fulfilled for this general gauge, if the interaction is adiabatically switched off at $\tau = \infty$.

In this paper we have started, as the basis of the theory, from the Schrödinger equation in the interaction picture. It is most desirable, however, to formulate the S-matrix theory more directly, by throwing away all the remnants of local field theory, and, instead, to demand that only some formal conditions be satisfied by the S-matrix.

One of the authors (S. K.) would like to thank Professor A. Salam and Professor J. L. Synge for their kind hospitality at their respective Institutes. This research was initiated while one of us (Y. T.) was temporarily in Zürich. He is greatly indebted to Professor W. Heitler, Dr. E. Arnous, and Mr. L. O'Raifeartaigh for their stimulating discussion and encouragement.

References

1) P. Kristensen and C Møller, Mat. Fys. Medd. Dan. Vid. Selsk. **27** No. 7 (1952)
2) E. Arnous and W. Heitler, Nuovo Cim. **11** (1959) 443;
E. Arnous, W. Heitler and Y. Takahashi, Nuovo Cim. in press
3) Y. Takahashi and H. Umezawa, Progr. Theor. Phys. **9** (1953) 14, 501;
H. Umezawa, Quantum field theory (North-Holland Publishing Company, Amsterdam, 1956)
4) J. M. Jauch and F. Rohrlich, Theory of photons and electrons (Addison-Wesley, Cambridge, Mass., 1955)
5) C. Møller, Mat. Fys. Medd. Dan. Vid. Selsk. **23**, No. 1 (1945); **22**, No. 19 (1946)
6) Z. Koba, T. Tati and S. Tomonaga, Progr. Theor. Phys. **2** (1947) 101;
Z. Koba, Y. Oisi and M. Sasaki, Progr. Theor. Phys. **3** (1948) 141, 229;
J. Schwinger, Phys. Rev. **74** (1948) 1439
7) S. Kamefuchi and J. Tiomno, to be published

1.D.1

Nuclear Physics **17** (1960) 695–698; © *North-Holland Publishing Co., Amsterdam*

Not to be reproduced by photoprint or microfilm without written permission from the publisher

THEORETICAL APPROACH TO THE LOW ENERGY SPECTRUM OF Mo^{93}

M. BOUTEN †

Interuniversitair Instituut voor Kernwetenschappen, Studiecentrum voor Kernenergie, Mol, Belgium

Received 12 April 1960

Abstract: The levels of Mo^{93} are calculated by considering three nucleons outside a spherical core. The interaction potential is taken to be of zero range. The level ordering is in good agreement with the experimental low-energy spectrum. The question whether Mo^{93m} has spin $\frac{21}{2}$ or $\frac{23}{2}$ seems to be settled in favour of the first value.

1. Introduction

The methods of atomic spectroscopy have been used by Pryce [1, 2]) and others [3]) for predicting the excited levels of nuclei with a few particles outside of closed shells. In order to get some definite results, however, it is necessary to know the main features of the spectrum because there are quite a few parameters which cannot be calculated accurately.

The nucleus Mo^{93} satisfies both these conditions approximately. If one considers all the nucleons inside the closed oscillator shell at $Z = 40$ and the closed shell at $N = 50$ as a spherical core, we are left with only three extra nucleons in a $(g_{\frac{9}{2}})^2 d_{\frac{5}{2}}$ configuration. This leads to spin values from $\frac{1}{2}$ to $\frac{21}{2}$ with positive parity. On the other hand, there exist quite a number of experimental data about the level scheme [4]) and especially the $\frac{21}{2}^+$ isomeric state at 2.428 MeV might allow some estimate of the strength of the interaction.

The isomerism in Mo^{93} is not explicable by a one-particle excitation as is for instance possible for the neighbouring Nb^{93}. Goldhaber [5]) speaks of "core-isomerism", which takes the neutron in a $g_{\frac{9}{2}}$ subshell while the core goes from $8^+ \rightarrow 4^+ \rightarrow 2^+ \rightarrow 0^+$. He does not, however, touch the question why the core does not pass through the 6^+ state which would naturally lie below the 8^+ state. According to him also, the spin of Mo^{93m} would be $\frac{23}{2}$, which necessitates putting the neutron in a $g_{\frac{7}{2}}$ rather than a $d_{\frac{5}{2}}$ subshell, although it seems obvious from the ground state spins of neighbouring odd-neutron nuclei that the $d_{\frac{5}{2}}$ subshell lies lower.

In order to calculate interaction energies between three particles in the $(g_{\frac{9}{2}})^2 d_{\frac{5}{2}}$ configuration, one needs a table of Racah-coefficients reaching as high as $\frac{21}{2}$ for the total spin. Such a table was calculated by Mr. L. Buyst [6]) of the Département de Mathématiques Appliquées of the C.E.N. at Mol.

† On leave from the Verschaffelt Laboratorium, University of Ghent.

2. Method of Calculation

For the configuration considered, it is generally possible to construct several orthogonal wave-functions with equal total spin. The antisymmetrization is easily taken into account if we first couple the two protons to even spin I_{12} and afterwards with the neutron to the total spin I. The different orthogonal wave-functions then correspond to different values of I_{12}. In this way, we get the interaction energies by diagonalizing the matrix

$$E_{ij} = \langle I_{12}^{(i)} I | V_{12} + V_{23} + V_{31} | I_{12}^{(j)} I \rangle. \tag{1}$$

Owing to the antisymmetry, eq. (1) can be rewritten as

$$E_{ij} = \langle I_{12}^{(i)} I | V_{12} | I_{12}^{(j)} I \rangle + 2 \langle I_{12}^{(i)} I | V_{23} | I_{12}^{(j)} I \rangle. \tag{2}$$

The first matrix-element is immediately reduced to a two-particle interaction energy. In order to reduce the second matrix-element, we make use of the expansion

$$|I_{12} I\rangle = \sum_{I_{23}} [(2I_{12}+1)(2I_{23}+1)]^{\frac{1}{2}} W(j_1 j_2 I j_3; I_{12} I_{23}) |I_{23} I\rangle,$$

where $W(j_1 j_2 I j_3; I_{12} I_{23})$ is a Racah coefficient. In this way eq. (2) becomes

$$E_{ij} = \langle I_{12}^{(i)} | V_{12} | I_{12}^{(j)} \rangle \delta_{ij} + 2 \sum_{I_{23}} [(2I_{12}^{(i)}+1)(2I_{12}^{(j)}+1)]^{\frac{1}{2}} (2I_{23}+1)$$
$$\times W(j_1 j_2 I j_3; I_{12}^{(i)} I_{23}) W(j_1 j_2 I j_3; I_{12}^{(j)} I_{23}) \langle I_{23} | V_{23} | I_{23} \rangle,$$

which reduces E_{ij} to the calculation of two-particle interaction energies.

The potential will be taken to be of zero range. This reduces the length of the calculation considerably and does presumably not change the order of the levels, as was indicated by Marty, Nataf and Prentki [7]); it is also to be remembered in

TABLE 1

Values of A_s and A_t for several types of interaction

Interaction		A_s A_t
proton-neutron	Rosenfeld	0.6 V_0 V_0
	Serber	V_0 V_0
proton-proton or neutron-neutron	Rosenfeld	0.6 V_0 0
	Serber	V_0 0

this connexion that the relative level spacing found from a zero-range potential has no physical meaning, while only the order of the levels is meaningful. In the calculation of the two-particle interaction energies, we follow Pryce [1]). If A_s and A_t are the strengths of the singlet and triplet force, respectively, this

energy can be calculated from $E = A_s Q a_s + A_t Q a_t = \varepsilon_s a_s + \varepsilon_t a_t$, where Q stands for 4π times the radial part and a_s and a_t represent the angular part of the matrix-element. For Rosenfeld and Serber interactions, one finds for A_s and A_t, when the potential is of zero range, the values given in table 1.
The values of a_s and a_t are calculated from simple formulas given by Pryce [1]).

3. Numerical results

Table 2 shows the interaction energies for the lowest configuration of Mo^{93}. The ratio $\frac{2}{3} : 1$ has been taken for $\varepsilon_s : \varepsilon_t$. This is the same ratio as was used by Pryce [1]) in Bi^{210} and corresponds roughly to the Rosenfeld mixture. The effect of changing the ratio was also considered by taking $\varepsilon_s : \varepsilon_t = 1 : 1$ which

TABLE 2

Interaction energies in units ε_t

$\varepsilon_s : \varepsilon_t = \frac{2}{3} : 1$ (Rosenfeld)	I	I	$\varepsilon_s : \varepsilon_t = 1 : 1$ (Serber)
0.775	$\frac{17}{2}$	$\frac{17}{2}$	1.047
1.040	$\frac{13}{2}$	$\frac{13}{2}$	1.283
1.293	$\frac{7}{2}$	$\frac{15}{2}$	1.675
1.495	$\frac{11}{2}$	$\frac{11}{2}$	1.710
1.509	$\frac{15}{2}$	$\frac{7}{2}$	1.735
1.545	$\frac{3}{2}$	$\frac{19}{2}$	1.851
1.625	$\frac{9}{2}$	$\frac{9}{2}$	2.052
1.713	$\frac{19}{2}$	$\frac{3}{2}$	2.081
1.795	$\frac{13}{2}$	$\frac{3}{2}$	2.232
1.819	$\frac{3}{2}$	$\frac{13}{2}$	2.248
1.972	$\frac{5}{2}$	$\frac{5}{2}$	2.308
1.993	$\frac{9}{2}$	$\frac{5}{2}$	2.417
2.164	$\frac{7}{2}$	$\frac{7}{2}$	2.508
2.305	$\frac{1}{2}$	$\frac{15}{2}$	2.576
2.409	$\frac{15}{2}$	$\frac{11}{2}$	2.789
2.545	$\frac{11}{2}$	$\frac{17}{2}$	2.800
2.655	$\frac{17}{2}$	$\frac{1}{2}$	2.835
2.746	$\frac{5}{2}$	$\frac{21}{2}$	2.914
2.804	$\frac{21}{2}$	$\frac{13}{2}$	3.050
2.830	$\frac{13}{2}$	$\frac{1}{2}$	3.597
3.072	$\frac{11}{2}$	$\frac{11}{2}$	3.793
3.412	$\frac{9}{2}$	$\frac{9}{2}$	3.966
3.721	$\frac{7}{2}$	$\frac{7}{2}$	4.484
5.627	$\frac{5}{2}$	$\frac{5}{2}$	7.460

corresponds roughly to a Serber interaction. As can be seen from the table, the order is practically not changed. The value of ε_t should be taken to be of the order of 0.85 MeV if we want the $\frac{21}{2}+$ level to coincide with the experimental level at 2.43 MeV. This value is a little greater than the one employed by Pryce [1]) in Bi^{210}.

4. Discussion

The level order found from the lowest configuration $(g_{\frac{9}{2}})^2 d_{\frac{5}{2}}$ is in very satisfactory agreement with the experimental spectrum: the possible assignments $\frac{7}{2}^+$ and $\frac{11}{2}^+$ to the levels at 1.35 and 2.02 MeV are compatible with the allowed β^+ transitions from the ground state of Tc^{93} with spin $\frac{9}{2}^+$. These assignments are, however, not certain, since other configurations may reach as low, like e.g. the $(g_{\frac{9}{2}})^2 g_{\frac{7}{2}}$ configuration, which also gives a low-lying $\frac{7}{2}^+$ level. Another configuration which might be needed to explain the $(\frac{1}{2}^-, \frac{3}{2}^-)$ level at 2.7 MeV is $(p_{\frac{1}{2}})^{-1}(g_{\frac{9}{2}})^3 d_{\frac{5}{2}}$.

A more definite result is obtained in explaining the nature of the isomeric state: as already observed by Pryce [1]) in Bi^{210}, levels with great spin-value may be very much depressed, inside the same configuration, by the interaction energy, and become isomeric. This type of isomerism is to be compared with that observed [8]) in the spectrum of Nb^{93}, which is due to the imbrication of different configurations. In order to know whether a similar case of isomerism might not be expected in Nb^{93}, we calculated the level ordering from the ground configuration $g_{\frac{9}{2}}(d_{\frac{5}{2}})^2$. The resulting sequence $\frac{9}{2}^+, \frac{5}{2}^+, \frac{11}{2}^+, \frac{7}{2}^+, \frac{13}{2}^+, \frac{17}{2}^+, \frac{15}{2}^+, \ldots$ does not provide such a case of isomerism.

Whether Goldhaber's proposal of a spin $\frac{23}{2}$ is justified or not, the interaction energy for this state in the $(g_{\frac{9}{2}})^2 g_{\frac{7}{2}}$ configuration was calculated to be 2.4803 ε_t. This is smaller than the value for the $\frac{21}{2}$ level which was 2.804 ε_t. Since, moreover, the $g_{\frac{7}{2}}$ subshell lies higher than the $d_{\frac{5}{2}}$ subshell, as known from Klinkenberg's scheme, the $\frac{21}{2}^+$ level falls below the $\frac{23}{2}^+$ level and this last one cannot be isomeric.

I wish to thank Prof. M. Demeur, who suggested the problem, for many helpful discussions, and Prof. J. Verhaeghe for his kind interest in this work. I would also like to thank Mr. J. Goens for the hospitality at the C.E.N. where this work was done.

References

1) M. H. L. Pryce, Proc. Phys. Soc. A **65** (1952) 772
2) M. H. L. Pryce, Nuclear Physics **2** (1956/57) 226
3) See e.g. J. P. Elliot and A. M. Lane, Hdb. der Phsy. **39**, p. 287, Ch. IV
4) Nuclear Data Sheets, C. L. McGinnis Editor
5) M. Goldhaber, Phys. Rev. **89** (1953) 1146
6) L. Buyst, Tables of Racah Coefficients (C.E.N., Mol, Belgium, 1960)
7) Marty, Nataf and Prentki, J. Phys. et Rad. **15** (1954) 1349
8) Nath, Rothman, Van Patter and Mandeville, Nuclear Physics **14** (1959) 78

10.D *Nuclear Physics* **17** (1960) 699; © *North-Holland Publishing Co., Amsterdam*

BOOK REVIEWS

O. KLEMPERER, *Electron Physics* (Butterworths Scientific Publications, London 1959. xi-248 p. 32s.6d).

The first part of this book treats electron motion in electric and magnetic fields, electron optics and various aspects of electron flow in the presence of space charge. The second part deals with some fundamental properties of the free electron, such as the electron mass, charge, spin and magnetic moment. The book is intended to serve as an undergraduate text for students having passed a general course in electricity and mechanics, but without knowledge of spcial relativity and wave mechanics. Some elements of these disciplines are, therefore, introduced underway. This approach necessarily brings up the question: is there presently a need for a textbook of this kind? In the opinion of the reviewer, the answer is no. The main subjects of the book are already covered adequately by many of the standard textbooks on electricity and magnetism and on atomic physics, and there seems no reason why, in an undergraduate physics program, the free electron, rather than the other particles of modern physics, should be honoured by a special course. On the other hand "Electron Physics" is hardly comprehensive enough to serve as a reference book for specialists in the field of electron optics and related subjects. The main virtue of the book is its emphasis on the historical side of the subject: a great number of the crucial and ingenious experiments related to the fundamental properties of the electron are discussed in detail and illustrated with excellent figures. Particularly valuable is the inclusion of several recent developments, such as for instance the beautiful electron interference experiments by Möllenstedt and Düker.

Ove Nathan

WOLFGANG RIEZLER, *Einführung in die Kernphysik*. Sechste, erweiterte Auflage. (R. Oldenbourg, München 1959. 381 p. DM 31.50)

The author has intended to give an introduction to nuclear physics, which is on the one hand fully scientific and comprehensive, and which on the other hand is easy to understand for young students as well as for others who, without being physicists, are interested in this field. The use of mathematics is kept to a minimum, and this is at the same time the great advantage and the drawback of the book. For example, when talking about α-decay the tunnel effect is explained and the formula for the barrier penetrability is given, but not its quantal deduction; the Fermi theory for β-decay is of course not given, but the author takes his starting point from the momentum distribution formula, mentions Kurie plots, ft-values, allowed transitions, Gamow-Teller and Fermi transitions, etc. In the reviewer's opinion, the advantage gained by the omission of the mathematical theories lies not so much in enabling mathematically untrained people to read the book, but in making it possible to mention a great many topics with much detail in a limited space. In fact, the book covers most of what can reasonably be expected, and also the most recent results of the experimental and theoretical investigations are included. The language is mostly concise and clear, and the illustrations are simple and instructive.

Only very few mistakes or misleading points can be found and they are unimportant. It might be mentioned, however, that in some places more figures would be helpful to the reader, for instance when deriving the formulae for deflection in electric and magnetic fields (p. 19), or when describing the photomultiplier tube (p. 232). Furthermore, although scintillation counters are thoroughly described, their use for γ-energy measurements is not mentioned.

At the end of the book are some very valuable tables listing the properties of the elementary particles, the elements, the stable and radioactive isotopes, as well as a nucleide chart.

N. O. Lassen

AUTHOR INDEX

ALEXANDER, K. F. und V. BREDEL, Erzeugung kurzlebiger Isomere durch Impulsaktivierung mit thermischen Neutronen 153

ALEXANDROV, I. P. and I. K. KIKOIN, I. V. Kurchatov (1930—1960) . . 177

ANDERSON, C. E., *see* QUINTON

BAICKER, J. A. and K. W. JONES, Polarization of neutrons from the reactions $Li^7(p, n)Be^7$ and $D(d, n)He^3$ 424

BAILEY, R. L., *see* SCHMITT

BALIAN, ROGER et VINCENT P. GILLET, L'éjection par interaction directe dans la réaction $Be^9(n, 2n)Be^8$ 448

BANERJEE, M. K. *see* NAGARAJAN

BARASHENKOV, V. S. and V. M. MALTSEV, Central and peripheral collisions of fast nucleons (II) 377

BARREAU, P., *see* BELLICARD

BELLICARD, J. B. et P. BARREAU, Mesures de diffusion élastique d'électrons de 28 MeV par les noyaux lourds. 141

BIAŁKOWSKI, GRZEGORZ and ANDRZEJ JUREWICZ, Non-adiabatic treatment of the scattering of K^+ mesons by nucleons 359

BILANIUK, O. M. and J. B. FRENCH, s-particle doublets in certain light nuclei 435

BLAIR, J. S., G. W. FARWELL and D. K. MCDANIELS, Diffraction analysis of elastic and inelastic scattering by magnesium 641

BLAIR, J. S., *see* MCDANIELS

BLATT, J. M., *see* DERRICK

BLOCK, R. C., *see* SCHMITT

BODMER, A. R., Neutron and proton densities in nuclei and the semi-empirical mass formula 388

BOUTEN, M., Theoretical approach to the low energy spectrum of Mo^{93} . 695

BREDEL, V., *see* ALEXANDER

BRITT, H. C., *see* QUINTON

BRODY, T. A., G. JACOB and M. MOSHINSKY, Matrix elements in nuclear shell theory 16

CHABAN, A. A., *see* DAVYDOV

CHEN, S. W., *see* MCDANIELS

COESTER, F. and H. KÜMMEL, Short-range correlations in nuclear wave functions. 477

COHEN, BERNARD L., and ROBERT E. PRICE, Location of the $3s_{\frac{1}{2}}$ single particle neutron level in various nuclei 129

CRUT, M., D. R. SWEETMAN and N. S. WALL, The anomalous inelastic scattering of alpha particles 655
DAVYDOV, A. S., N. S. RABOTNOV and A. A. CHABAN, Rotational energies and moments of inertia of non-axial nuclei 169
DEMEUR, M. et CH. JOACHAIN, Polarisation nucléaire dans l'atome mésique de deutérium 329
DERRICK, G. H. and J. M. BLATT, Tensor and $\mathbf{L} \cdot \mathbf{S}$ forces in the triton . 67
ERICSON, TORLEIF, Classical theory of compound nucleus reactions . . . 250
EVANS, LAWRENCE E., High energy theorem in quantum electrodynamics 163
FARWELL, G. W., *see* MCDANIELS
FARWELL, G. W., *see* BLAIR
FERGUSON, A. T. G., M. A. GRACE and J. O. NEWTON, Lifetime measurements on the first excited states of Mg^{25} and Al^{25} 1
FERGUSON, A. T. G., M. A. GRACE and J. O. NEWTON, The decay of the 136 keV level in Fe^{57} 9
FERGUSON, A. T. G., *see* MCCALLUM
FRENCH, J. B., *see* BILANIUK
GALANIN, A. D., A. F. GRASHIN, B. L. IOFFE and I. Ya. POMERANCHUK, Collision of nucleons with large angular momenta 181
GHOSH, ARUNDHATI and N. C. SIL, Neutron energy levels in a diffuse potential 264
GILLET, VINCENT P., *see* BALIAN
GORODETZKY, S., R. RICHERT, R. MANQUENOUILLE et A. KNIPPER, Vie moyenne du premier niveau excité de ^{10}B 684
GRACE, M. A., *see* FERGUSON
GRASHIN, A. F. and I. YU. KOBSAREV, On peripheral nucleon-nucleon interaction in the two-meson approximation 218
GRASHIN, A. F., *see* GALANIN
HORI, SHOICHI, On the interaction hamiltonian for the decay of Σ-hyperons 227
IOFFE, B. L., *see* GALANIN
JACOB, G., *see* BRODY
JOACHAIN, CH., *see* DEMEUR
JONES, K. W., *see* BAICKER
JUREWICZ, ANDRZEJ, *see* BIAŁKOWSKI
KAMEFUCHI, S. and Y. TAKAHASHI, Invariance and the S-matrix 686
KATOH, TOSHIO, SHUICHIRO YAMASAKI and YASUKAZU YOSHIZAWA, Interaction of beta-decay and second forbidden spectrum of Cs^{137} . . 548
KIKOIN, I. K., *see* ALEXANDROV
KNIPPER, A., *see* GORODETZKY
KNOX, W. J., *see* QUINTON
KOBSAREV, I. YU., *see* GRASHIN

KRÓLIKOWSKI, W., On the intrinsic Pauli principle 421
KRÓLIKOWSKI, W., A possible explanation of the high energy peaks in pion-nucleon cross sections 468
KRZYWICKI, ANDRZEJ, On the cloud-cloud interaction in high energy inelastic nucleon-nucleon collisions 609
KÜMMEL, H., *see* COESTER
LANE, A. M. and J. E. LYNN, Theory of radiative capture in the resonance region 563
LANE, A. M. and J. E. LYNN, Anomalous radiative capture in the neutron resonance region: analysis of the experimental data on electric dipole transitions 586
LOVAS, I., Annihilation of polarized positons in magnetized material . . 279
LUSTIG, HARRY, Resonance reactions with generalized one-level approximation 317
LYNN, J. E., *see* LANE
MALTSEV, V. M., *see* BARASHENKOV
MANI, G. S., *see* MCCALLUM
MANQUENOUILLE, R., *see* GORODETZKY
MCCALLUM, G. J., A. T. G. FERGUSON and G. S. MANI, A study of energy levels in Sc^{43}, Ti^{45}, V^{47}, V^{49}, V^{50} and Zn^{65} 116
MCCARTHY, I. E., and D. J. PROWSE, A model for the interpretation of K^--meson captures at rest in complex nuclei 96
MCDANIELS, D. K., J. S. BLAIR, S. W. CHEN and G. W. FARWELL, Alpha-particle excitation of quadrupole and octupole surface modes in Ti, Fe, Ni, Zn and Sr. 614
MCDANIELS, D. K., *see* BLAIR
MITTELSTAEDT, P., On the problem of rearrangement energy of nuclear matter 499
MOSHINSKY, M., *see* BRODY
MURAI, YASUHISA, Discrimination between strong and weak interactions 529
NAGARAJAN, M. A. and M. K. BANERJEE, Exchange effects in stripping reactions 341
NEWTON, J. O., *see* FERGUSON
PINAJIAN, J. J., The exchange transfer reaction $Al^{27}(N^{14}, Mg^{27})O^{14}$ . . . 44
POMERANCHUK, I. Ya., *see* GALANIN
PRICE, ROBERT E., *see* COHEN
PROWSE, D. J., *see* MCCARTHY
QUINTON, A. R., H. C. Britt, W. J. Knox and C. E. Anderson, The fission of gold by oxygen nuclei 74
RABOTNOV, N. S., *see* DAVYDOV
RAYSKI, JERZY, Interpretation of electrodynamics and baryon theory within a six-dimensional manifold 289

RICHERT, R., *see* GORODETZKY
ROLL, P. G. and F. E. STEIGERT, Energy loss of heavy ions in nickel, oxygen, and nuclear emulsion 54
ROSENBERG, LEONARD, *see* SPRUCH
SASAKI, SEIBUN, Selection rules in strong interactions 516
SAWICKI, J., Note on the spin-orbit part of the optical model potential . 89
SCHMITT, H. W., R. C. BLOCK and R. L. BAILEY, Total neutron cross section of B^{10} in the thermal neutron energy range 109
SHIMODAIRA, HAJIME, Some remarks on fields with negative propagators in quantum field theory 486
SIL, N. C., *see* GHOSH
SPRUCH, LARRY and LEONARD ROSENBERG, Upper bound on the neutron-deuteron doublet scattering length 30
STAUB, HANS. H. und HUBERT WINKLER, Absolutbestimmung des Schwellenwertes der Reaktion Li^7 (p, n) Be^7 271
STEIGERT, F. E., *see* ROLL
SWEETMAN, D. R., *see* CRUT
TAKAHASHI, Y., *see* KAMEFUCHI
WALL, N. S., *see* CRUT
WINKLER, HUBERT, *see* STAUB
YAMASAKI, SHUICHIRO, *see* KATOH
YOSHIZAWA, YASUKAZU, *see* KATOH
ZIEGLER, B., Gesamtabsorption von γ-Strahlen zwischen 10 und 30 MeV in leichten Kernen 238

SUBJECT INDEX

1. Nuclear Structure

1.B *Two- and three-body problems*

Upper bound on the neutron-deuteron doublet scattering length, Larry Spruch and Leonard Rosenberg 30
Tensor and **L** · **S** forces in the triton, G. H. Derrick and J. M. Blatt 67
On peripheral nucleon-nucleon interaction in the two-meson approximation, A. F. Grashin and I. Yu. Kobsarev 218

1.C *Many-particle systems*

A model for the interpretation of K^--meson captures at rest in complex nuclei, I. E. McCarthy and D. J. Prowse 96
Short-range correlations in nuclear wave functions, F. Coester and H. Kümmel 477
On the problem of rearrangement energy of nuclear matter, P. Mittelstaedt . 499

1.D *Nuclear models*

1.D.1 *Shell model*

Matrix elements in nuclear shell theory, T. A. Brody, G. Jacob and M. Moshinsky 16
Location of the $3s_{\frac{1}{2}}$ single particle neutron level in various nuclei, Bernard L. Cohen and Robert E. Price 129
Neutron energy levels in a diffuse potential, Arundhati Ghosh and N. C. Sil 264
s-Particle doublets in certain light nuclei, O. M. Bilaniuk and J. B. French 435
Short-range correlations in nuclear wave functions, F. Coester and H. Kümmel 477
Theoretical approach to the low energy spectrum of Mo^{93}, M. Bouten . . 695

1.D.2 *Collective model*

Lifetime measurements on the first excited states of Mg^{25} and Al^{25}, A. T. G. Ferguson, M. A. Grace and J. O. Newton 1
Rotational energies and moments of inertia of non-axial nuclei, A. S. Davydov, N. S. Rabotnov and A. A. Chaban. 169
Diffraction analysis of elastic and inelastic scattering by magnesium, J. S. Blair, G. W. Farwell and D. K. McDaniels 641
The anomalous inelastic scattering of alpha particles, M. Crut, D. R. Sweetman and N. S. Wall 655
Vie moyenne du premier niveau excité de ^{10}B, S. Gorodetzky, R. Richert, R. Manquenouille et A. Knipper. 684

1.E *Properties of nuclei*

1.E.1 *Energy levels*

A study of energy levels in Sc^{43}, Ti^{45}, V^{47}, V^{49}, V^{50}, and Zn^{65}, G. J. McCallum, A.T. G. Ferguson and G. S. Mani 116

1.E.2 *Binding energies; masses*

Neutron and proton densities in nuclei and the semi-empirical mass formula, A. R. Bodmer 388

1.E.4 *Transition probabilities; cross sections*

Lifetime measurements on the first excited states of Mg^{25} and Al^{25}, A. T. G. Ferguson, M. A. Grace and J. O. Newton 1
The decay of the 136 keV level in Fe^{57}, A. T. G. Ferguson, M. A. Grace and J. O. Newton 9
Erzeugung kurzlebiger Isomere durch Impulsaktivierung mit thermischen Neutronen, K. F. Alexander und V. Bredel. 153
Vie moyenne du premier niveau excité de ^{10}B, S. Gorodetzky, R. Richert, R. Manquenouille et A. Knipper. 684

1.E.5 *Nuclear radii; matter distributions*

Mesures de diffusion élastique d'électrons de 28 MeV par les noyaux lourds, J. B. Bellicard et P. Barreau. 141
Neutron and proton densities in nuclei and the semi-empirical mass formula, A. R. Bodmer 388

2. Nuclear Reactions

2.A *General properties*

2.A.1 *Cross-sections, energy relations*

Total neutron cross section of B^{10} in the thermal neutron energy range, H. W. Schmitt, R. C. Block and R. L. Bailey 109
A study of energy levels in Sc^{43}, Ti^{45}, V^{47}, V^{49}, V^{50} and Zn^{65}, G. J. McCallum, A. T. G. Ferguson and G. S. Mani 116
Absolutbestimmung des Schwellenwertes der Reaktion $Li^7(p, n)Be^7$, Hans H. Staub und Hubert Winkler 271

2.B *Angular distributions; correlations; polarization*

Polarization of neutrons from the reactions $Li^7(p, n)Be^7$ and $D(d, n)He^3$, J. A. Baiker and K. W. Jones 424

2.C *Resonance reactions; R-matrix theory*

Resonance reactions with generalized one-level approximation, Harry Lustig . 317
Theory of radiative capture in the resonance region, A. M. Lane and J. E. Lynn 563
Anomalous radiative capture in the neutron resonance region: Analysis of the experimental data on electric dipole transitions, A. M. Lane and J. E. Lynn . . 586

2.D *Statistical model*

Classical theory of compound nucleus reactions, Torleif Ericson 250

2.E *Optical model*

Note on the spin-orbit part of the optical model potential, J. Sawicki. 89

2.F *Direct interaction (other than stripping)*

The exchange transfer reaction $Al^{27}(N^{14}, Mg^{27})O^{14}$, J. J. Pinajian 44
L'éjection par interaction directe dans la réaction $Be^9(n, 2n)Be^8$, Roger Balian et Vincent P. Gillet 448

2.G *Stripping and pick-up*

Location of the $3s_{\frac{1}{2}}$ single particle neutron level in various nuclei, Bernard L. Cohen and Robert E. Price. 129
Exchange effects in stripping reactions, M. A. Nagarajan and M. K. Banerjee . 341

2.H *Coulomb excitation*

The decay of the 136 keV level in Fe^{57}, A. T. G. Ferguson, M. A. Grace and J. O. Newton 9

Alpha-particle excitation of quadrupole and octupole surface modes in Ti, Fe, Ni, Zn and Sr, D. K. McDaniels, J. S. Blair, S. W. Chen and G. W. Farwell . 614

2.I *Photonuclear processes*

Gesamtabsorption von γ-Strahlen zwischen 10 und 30 MeV in leichten Kernen, B. Ziegler 238

2.J *Fission and spallation*

The fission of gold by oxygen nuclei, A. R. Quinton, H. C. Britt, W. J. Knox and C. E. Anderson 74

2.L *Scattering processes (except two-nucleon system and meson scattering)*

Diffraction analysis of elastic and inelastic scattering by magnesium, J. S. Blair, G. W. Farwell and D. K. McDaniels 641

The anomalous inelastic scattering of alpha particles, M. Crut, D. R. Sweetman and N. S. Wall 655

3. Electromagnetic Radiation

3.C *Extranuclear effects*

Gesamtabsorption von γ-Strahlen zwischen 10 und 30 MeV in leichten Kernen, B. Ziegler 238

4. Beta Decay; Parity

4.A *General theory*

Interaction of beta-decay and second forbidden spectrum of Cs^{137}, Toshio Katoh, Shuichiro Yamasaki and Yasukazu Yoshizawa 548

6. Methods and Instruments

6.D *Tables and computational aids*

Matrix elements in nuclear shell theory, T. A. Brody, G. Jacob and M. Moshinsky 16

7. Quantum Field Theory

7.A *General*

Non-adiabatic treatment of the scattering of K^+ mesons by nucleons, Grzegorz Białkowski and Andrzej Jurewicz 359

Invariance and the S-matrix, S. Kamefuchi and Y. Takahashi 686

7.B *Quantum electrodynamics*

High energy theorem in quantum electrodynamics, Lawrence E. Evans . . . 163

Collision of nucleons with large angular momenta, A. D. Galanin, A. F. Grashin, B. L. Ioffe and I. Ya. Pomeranchuk 181

Annihilation of polarized positons in magnetized material, I. Lovas 279

Polarisation nucléaire dans l'atome mésique de deutérium, M. Demeur et Ch. Joachain 329

7.C *π-meson field (scattering and nuclear forces)*

On peripheral nucleon-nucleon interaction in the two-meson approximation, A. F. Grashin and I. Yu. Kobsarev 218
Central and peripheral collisions of fast nucleons (II), V. S. Barashenkov and V. M. Maltsev 377
A possible explanation of the high energy peaks in pion-nucleon cross sections, W. Królikowski 468
On the cloud-cloud interaction in high energy inelastic nucleon-nucleon collisions, Andrzej Krzywicki 609

8. Elementary Particles

8.B *Theory, interactions, transformation properties*

A model for the interpretation of K^--meson captures at rest in complex nuclei, I. E. McCarthy and D. J. Prowse 96
On the interaction Hamiltonian for the decay of Σ-hyperons, Shoichi Hori . 227
Non-adiabatic treatment of the scattering of K^+-mesons by nucleons, Grzegorz Białkowski and Andrzej Jurewicz 359
Selection rules in strong interactions, Seibun Sasaki 516
Discrimination between strong and weak interactions, Yasuhisa Murai 529

8.C *Fundamental theory of matter*

Interpretation of electrodynamics and baryon theory within a six-dimensional manifold, Jerzy Rayski 289
On the intrinsic Pauli principle, W. Królikowski 421
Some remarks on fields with negative propagators in quantum field theory, Hajime Shimodaira 486

9. Cosmic Radiation

9.B *Passage of particles through matter*

Energy loss of heavy ions in nickel, oxygen, and nuclear emulsion, P. G. Roll and F. E. Steigert 54

10. News Items

10.C *Obituaries*

I. V. Kurchatov (1903—1960), I. P. Alexandrov and I. K. Kikoin. . . . 177

10.D *Book Reviews*

M. Demeur, Aspects théoriques de la systématique des noyaux atomiques (1957) 175
G. Guében et J. Govaerts, La méthode d'analyse par activation en utilisant les neutrons d'une source Ra-Be. 175
J. Serpe, Les lois de conservation en physique des particules élémentaires (1959) 175
J. Géhéniau (Éditeur), Particules élémentaires (feuilles d'information) (1959) 175
M. Demeur, Développements théoriques récents en spectroscopie nucléaire (1959) 175
P. H. Margen, Nuclear reactor optimization (H. Abel-Larsen) 175
L. V. Groshev, A. M. Demidov, V. N. Lutsenko and V. I. Pelekhov, Atlas of spectra of gamma rays from radiative capture of thermal neutrons (B. R. Mottelson). 176

R. C. EXTERMANN (Editor) Radioisotopes in scientific research, vol. 1 (Hilde Levi) 339
FRIEDRICH MÜNZINGER, Atomkraft (O. Kofoed-Hansen) 339
S. T. BUTLER and H. MESSEL (Editors) From nucleus to universe (J. R.) . . . 339
RALPH T. OVERMAN and HERBERT M. CLARK, Radioisotope Techniques (O. Kofoed-Hansen) 340
Maritime Organic Moderated and Cooled Reactor (Jens J. Thiel) 340
O. KLEMPERER, Electron Physics (Ove Nathan) 699
WOLFGANG RIEZLER, Einführung in die Kernphysik (N. O. Lassen) . . . 699